CEMENT AND CONCRETE RESEARCH
CONTENTS OF VOLUME 14

1984 Volume 14, Number 1 January

M. PÉREZ, T. VÁZQUEZ and F. TRIVIÑO: Study of Stabilized Phases in High Alumina Cement Mortars. Part II. Effect of $CaCO_3$ Added to High Alumina Cement Mortar Subjected to Elevated Temperature Curing and Carbonation 1

L. HALICZ, Y. NATHAN and L. BEN-DOR: The Influence of P_2O_5 on Clinker Reactions 11

K.S. HARCHAND, VISHWAMITTER and K. CHANDRA: A Study of the Iron Phase and its Hydration Behaviour in High Alumina Cement 19

R. SH. MIKHAIL, A.M. MOUSA, S.A. ABO-EL-ENEIN and M.S. MARIE: Compressive Strength Versus Residual Porosity in Polymer Impregnated Cement Pastes 25

A. BENTUR and S. DIAMOND: Fracture of Glass Fiber Reinforced Cement 31

D.L. RAYMENT and E.E. LACHOWSKI: The Analysis of OPC Pastes: A Comparison Between Analytical Electron Microscopy and Electron Probe Microanalysis 43

D.W. HOFFMANN: Changes in Structure and Chemistry of Cement Mortars Stressed by a Sodium Chloride Solution 49

M. PÉREZ-MÉNDEZ, R.A. HOWIE and F.P. GLASSER: Ca_3SiO_5 and its Fluorine-Stabilized Aristotype: Synthesis, Stability and Postulated Structure of $Ca_{6-0.5x}Si_2O_{10-x}F_x$ 57

J.I. BHATTY and P.F.G. BANFILL: A Viscometric Method of Monitoring the Effect of Retarding Admixtures on the Setting of Cement Pastes 64

S.A. RODGER and D.D. DOUBLE: The Chemistry of Hydration of High Alumina Cement in the Presence of Accelerating and Retarding Admixtures 73

S.L. SARKAR and D.M. ROY: Important Experimental Prerequisites for Quantitative Clinker Phase Analysis by SEM-EDS 83

H.F.W. TAYLOR and D.E. NEWBURY: Calcium Hydroxide Distribution and Calcium Silicate Hydrate Composition in Tricalcium Silicate and β-Dicalcium Silicate Pastes 93

I. JAWED, J.F. YOUNG, A. GHOSE and J. SKALNY: Effect of Melt Composition on Tricalcium Silicate: Its Formation and Composition 99

M. COLLEPARDI, S. MONOSI, G. MORICONI and M. PAURI: Influence of Gluconate, Lignosulfonate or Glucose on the C_3A Hydration in the Presence of Gypsum with or without Lime 105

M.P.J. OLSEN: Mathematical Modeling of the Freezing Process of Concrete and Aggregates 113

Å. GRUDEMO: Variation with Solid-Phase Concentration of Composition, Structure and Strength of Cement Pastes at High Age 123

I. ODLER and S. ABDUL-MAULA: Possibilities of Quantitative Determination of the AFt-(Ettringite) and AFm-(Monosulphate) Phases in Hydrated Cement Pastes 133

Z.A. JUHÁSZ: Degree of Depolarisation, an Indicator for Water Bonding in Hydrated Cement Pastes 142

DISCUSSIONS

G.M. Idorn 145
S. Diamond 146
I. Odler 147
P.K. Mehta 149
S. Chatterji 151
P.K. Mehta 153
R.G. Blezard 154
G.M. Idorn and N. Thaulow 157

NEWS ITEMS 159

VOL. 14 984

1984 Vol. 14, Number 2 March

Editorial

M. PÉREZ MÉNDEZ and F. TRIVIÑO VÁZQUEZ: Study of the Strength Development by Stable Carbonated Phases in High Alumina Cement 161

K.S. HARCHAND, R. KUMAR, K. CHANDRA and VISHWAMITTAR: Mössbauer and X-Ray Investigations of of Some Portland Cements 170

K.H. JOST and B. ZIEMER: Relations Between the Crystal Structures of Calcium Silicates and Their Reactivity Against Water 177

C.R. WILDING, A. WALTER and D.D. DOUBLE: A Classification of Inorganic and Organic Admixtures by Conduction Calorimetry 185

S.L. SARKAR: X-Ray Mapping - A Supplementary Tool in Clinker Phase Characterization 195

P. CLASTRES, M. MURAT and A. BACHIORRINI: Hydration des Ciments Expansifs-Correlation entre l'Expansion et al Formation des Hydrates 199

N.B. MILESTONE: Identification of Concrete Admixtures by Differential Thermal Analysis in Oxygen 207

A.J. ZIELINSKI: Model for Tensile Fracture of Concrete at High Rates of Loading 215

N.J. CRAMMOND: Examination of Mortar Bars Containing Varying Percentages of Coarsely Crystalline Gypsum as Aggregate 225

J.J. BEAUDOIN and R.F. FELDMAN: Stresses and Strains in the Hardened Cement Paste - Water System 231

C. PLOWMAN and J.G. CABRERA: Mechanism and Kinetics of Hydration of C_3A and C_4AF, Extracted from Cement 238

J.L. GRANJU and J.C. MASO: Hardened Portland Cement Pastes, Modelisation of the Microstructure and Evolution Laws of Mechanical Properties. I. Basic Results 249

P.W. BROWN, E. FRANZ, G. FROHNSDORFF and H.F.W. TAYLOR: Analyses of the Aqueous Phase During Early C_3S Hydration 257

H.W. REINHARDT and H.A.W. CORNELISSEN: Post-Peak Cyclic Behaviour of Concrete in Uniaxial Tensile and Alternating Tensile and Compressive Loading 263

A.J. AINDOW, D.R. OAKLEY and B.A. PROCTOR: Comparison of the Weathering Behaviour of GRC with Predictions Made from Accelerated Ageing Tests 271

M. COLLEPARDI, S. MONOSI, G. MORICONI and M. PAURI: Combined Effect of Lignosulfonate and Carbonate of Pure Portland Clinker Compounds Hydration. V. Hydration of Dicalcium Silicate Alone and in the Presence of Tricalcium Aluminate 275

R.J. GRAY and C.D. JOHNSTON: The Effect of Matrix Composition on Fibre/Matrix Interfacial Bond Shear Strength in Fibre-Reinforced Mortar 285

M. GRUTZECK: Air Entrainment in Mortars and Concrete: The Effect of Superplasticizer/Salt Combinations 297

NEWS ITEMS 301

1984 Volume 14, Number 3 May

J.L. GRANJU and J.C. MASO: Hardened Portland Cement Pastes, Modelisation of the Micro-Structure and Evolution Laws of Mechanical Properties. II. Compressive Strength Law 303

A.D. JENSEN, S. CHATTERJI, P. CHRISTENSEN and N. THAULOW: Studies of Alkali-Silica Reaction - Part II. Effect of Air-Entrainment on Expansion 311

R.J. GRAY: Autogenous Healing of Fibre/Matrix Interfacial Bond in Fibre-Reinforced Mortar 315

C. TASHIRO and H. URUSHIMA: Strength Development and Pore Size Distribution of Cement Paste Cured with High Hydrostatic Pressure 318

S. SHIBATA, K. KISHI, K. ASAGA, M. DAIMON and P.R. SHRESTHA: Preparation and Hydration of β-C_2S without Stabilizer 323

R.L. DAY, P. CUFFARO and J.M. ILLSTON: The Effect of Rate of Drying on the Drying Creep of Hardened Cement Paste 329

VOL. 14 198

L.I. KNAB, H.N. WALKER, J.R. CLIFTON and E.R. FULLER, Jr: Fluorescent Thin Sections to Observe the Fracture Zone in Mortar 339

D.D. LASIČ and J. STEPIŠNIK: An Investigation of the Osmotic Model of Cement Curing by Ultrasonics 345

T. OHIGASHI: Fracture Energy of Glass Fiber Reinforced Cement Composites: Method of Determination 349

M.B. MARINHO and F.P. GLASSER: Polymorphism and Phase Changes in the Ferrite Phase of Cements Induced by Titanium Substitution 360

F.H. WITTMANN and I. GHEORGHITA: Fracture Toughness of Autoclaved Aerated Concrete 369

G. CORRADINI, G. SCOCCIA, R. VOLPE and S. TAVANO: Statistical Evaluation of Mechanical Properties of Superplasticized Concrete 375

G.I. ZHMOIDIN and A.K. CHATTERJEE: Conditions and Mechanism of Interconvertibility of Compounds $12CaO.7Al_2O_3$ and $5CaO.3Al_2O_3$ 386

M.T. BLANCO-VARELA, A. PALOMO and T. VAZQUEZ: Effect of Fluorspar on the Formation of Clinker Phases 397

G. GOSWAMI, S.K. MOHANTY and J.D. PANDA: Difference in Autoclave Expansions of Plant and Laboratory Ground Cements 407

I. MAKI and S. TAKAHASHI: Redistribution of Impurity during Recrystallization of Alite in Portland Cement Clinker 413

P. PARCEVAUX: Pore Size Distribution of Portland Cement Slurries at very Early Stages of Hydration (Influence of Curing Temperature and Pressure) 419

S. MINDESS: The Effect of Specimen Size on the Fracture Energy of Concrete 431

S.N. GHOSH, V.K. MATHUR and S.K. CHOPRA: Low Temperature OPC-Type Cement Containing Super-hydraulic C_2S Phase 437

D.M. ROY, G. VÁRADI, F.D. TAMÁS, G. PÁLYI and B. BARTHA: Application of GPC for the Analysis of the Oligomer Distribution of Naphtahlene-Based Superplasticizers 439

DISCUSSIONS
S.C. Kheok and C.F. Leung 443
O.A. Kayyali 445

NEW BOOKS 447

NEWS ITEMS 449

VOL.
14
984

1984 Volume 14, Number 4 July

G.J. McCARTHY: Characterization and Utilization of the By-Products of Coal Combustion and Gasification: Preface 453

S. DIAMOND: The Utilization of Flyash 455

G.M. IDORN and K.R. HENRIKSEN: State of the Art for Fly Ash Uses in Concrete 463

G.J. McCARTHY, K.D. SWANSON, L.P. KELLER and W.C. BLATTER: Mineralogy of Western Fly Ash 471

G.J. McCARTHY, L.P. KELLER, P.J. SCHIELDS, M.P. ELLESS and K.C. GALBREATH: Mineralogical Characterization of a Lignite Gasification Ash from a Low-BTU Fixed-Bed Gasifier. I. X-Ray Phase Analysis 479

R.J. STEVENSON: Mineralogical Characterization of a Lignite Gasification Ash from a Low-BTU Fixed-Bed Gasifier. II. Scanning Electron Microscope Phase Analysis 485

Y. HALSE, P.L. PRATT, J.A. DALZIEL and W.A. GUTTERIDGE: Development of Microstructure and Other Properties in Flyash OPC Systems 491

S. SCHLORHOLTZ, T. DEMIREL and J.M. PITT: An Examination of the ASTM Lime Pozzolanic Activity Test for Class C Fly Ashes 499

HE JUN-YUAN, B.E. SCHEETZ and D.M. ROY: Hydration of Fly Ash-Portland Cements 505

O.E. MANZ: Utilization of By-Products from Western Coal Combustion in the Manufacture of Mineral Wool and Other Ceramic Materials 513

WU XUEQUAN and D.M. ROY: Slag Cement Utilization: Rheological Properties and Related Characterization 521

S. SCHLORHOLTZ and T. DEMIREL: Quick Gypsum Lime Interactions in Stabilized Soil Basis for Concrete Highways 529

T. KITAMURA, R. MATSUO, Y. KOBAYASHI and S. KATOH: Bending Strength of Pulp Cement Board Composed of Separated Pulp from Municipal Solid Waste 533

J.L. GRANJU and J.C. MASO: Hardened Portland Cement Pastes, Modelisation of the Micro-Structure and Evolution Laws of Mechanical Properties. III. Elastic Modulus 539

H.G. MIDGLEY and J.M. ILLSTON: The Penetration of Chlorides into Hardened Cement Pastes 546

A. ZUK, M. WEJCHAN-JUDEK and L. BALEWSKI: Devices to Improving the Techniques of Preparing PIC 559

H.F.W. TAYLOR and D.E. NEWBURY: An Electron Microprobe Study of a Mature Cement Paste 565

C.M. HANSSON: Comments on Electrochemical Measurements of the Rate of Corrosion of Steel in Concrete 574

C.-L. HWANG and J.F. YOUNG: Drying Shrinkage of Portland Cement Pastes. I. Microcracking During Drying 585

R.W. CRAWFORD, C. McCULLOUGH, M. ANGUS, F.P. GLASSER and A.A. RAHMAN: Intrinsic Sorption Potential of Cement Components for ^{134}Cs 595

DISCUSSIONS
J. Bensted 601
B. Mather 603
M.D. Cohen 610

NEWS ITEMS 613

1984 Volume 14, Number 5 September

A. KRYSZTAFKIEWICZ and M. MAIK: Waste Cement Dusts as Activating Agents for Rubber Compounds ... 615

T. KNUDSEN: The Dispersion Model for Hydration of Portland Cement. I. General Concepts 622

S. NAGATAKI, E. SAKAI and T. TAKEUCHI: The Fluidity of Fly Ash-Cement Paste with Superplasticizer 631

J. PLANAS, H. CORRES, M. ELICES and R. CHUECA: Thermal Deformation of Loaded Concrete During Thermal Cycles from 20° to -165°C 639

H. UCHIKAWA, S. UCHIDA, K. OGAWA and S. HANEHARA: Influence of $CaSO_4.2H_2O$, $CaSO_4.1/2H_2O$ and $CaSO_4$ on the Initial Hydration of Clinker Having Different Burning Degree 645

K. LUKE and H.F.W. TAYLOR: Equilibria and Non-Equilibria in the Formation of Xonotlite and Truscottite 657

H. STADE and W. WIEKER: Observations on Silicate Gardens 663

S.E. COLEMAN and S. DIAMOND: Studies of Low Porosity Concretes Designed for Bridge Deck Applications: 1. Introductory Remarks, Mix Designs, Strength Development, and Rheological Characteristics 670

P. GALTIER et B. GUILHOT: Conductimetrie, Hydratation, Réactivite de l'Aluminate Monocalcique .. 679

Z. ZIEMER, B. ALTRICHTER and V. JESENAK: Effect of SO_3 on Formation and Hydraulic Reactivity of Belite 686

M. BUIL, A.M. PAILLÈRE and N. ROUSSEL: High Strength Mortars Containing Condensed Silica Fume .. 693

G. PASCALE and A. Di LEO: Assessment of Elastic Modulus of Concrete and Its Influence on Structural Design 705

S. LEONARD and A. BENTUR: Improvement of the Durability of Glass Fiber Reinforced Cement Using Blended Cement Matrix 717

B.H. HOWARD: Preliminary Data on QXRD Analysis of Portland Cement and Clinker Using CeO_2 as the Internal Standard 729

VOL
14
198

Y. XI and L.S. DENT GLASSER: Hydrothermal Study in the System Na_2O-CaO-SiO_2-H_2O at 200°C 741

G.M. IDORN: A Plea for Recognition of the Impact of Chemistry on the Durability of Concrete ... 749

A. MOR and P.K. MEHTA: Effect of Superplasticizing Admixtures on Cement Hydration 754

S. CHATTERJI: The Spacing Factor in Entrained Air-Bubbles. Has It Any Significance? 757

DISCUSSIONS
S. Chatterji 759
N.L. Thomas and J.D. Birchall 761
W.B. Butler 763
C.R. Wilding, A. Walter and D.D. Double 764

NEWS ITEMS 765

1984 Volume 14, Number 6 November

D. MONTGOMERY and S. DIAMOND: The Influence of Fly Ash Cenospheres on the Details of Cracking in Flyash-Bearing Cement Pastes 767

A. KRYSZTAFKIEWICZ and M. MAIK: Waste Cement Dusts as Fillers for Rubber Compounds 776

R.F. FELDMAN and J.J. BEAUDOIN: Mechanical Properties of Polymer Impregnation Cement Systems and the Effect of Moisture on Their Dimensional Stability 785

Z.P. BAZANT and J.-C. CHERN: Double-Power Logarithmic Law for Concrete Creep 793

H.W. DORNER: Mikrokalorimetrische Studie über die Eisbildung in Chloridhaltigem Zementstein 807

S. CHATTERJI and N.F. CLAUSSON-KAAS: Prevention of Alkali-Silica Expansion by using Slag-Portland Cement 816

J.D. LAZIĆ and V.B. LAZIĆ: Generalized Age-Adjusted Effective Modulus Method for Creep in Composite Beam Structures. Part I - Theory 819

V. RUNJE and A. BEZJAK: Kinetic Analysis of Extraction of Calcium Silicates with Methanolic Solution of Salicylic Acid. II. Extraction of Dicalcium Silicates 833

F.J. TANG and E.M. GARTNER: Formation of Soluble Anhydrite by Salicylic Acid Extraction of Calcium Silicosulfate 839

P.W. BROWN, K. GALUK and G. FROHNSDORFF: The Rate of Calcium Hydroxide Precipitation Measured by Electrical Conductance 843

C. GOTSIS and D.M. ROY: Parametric Analysis of the Heat Evolution during Hydration of a Cementitious Plug in a Borehole 847

K. FURTAK: Ein Verfahren zur Berechnung der Betonfestigkeit unter Schwellenden Belastungen 855

I. KAPRÁLIK, L. STEVULA, J. PETROVIC and F. HANIC: Study of the System CaO-SiO_2-CO_2-H_2O in Relation to Scawtite under Hydrothermal Conditions 866

A.R.N. EBERENDU and K.E. DAUGHERTY: The Quantitative Determination of Glass in Slag by Infrared Spectroscopy 873

I. SOROKA: The Determination of Setting Time of Portland Cement by the Vicat Test 884

B. MATHER: The Glass in Low Calcium Fly Ash 887

DISCUSSIONS
B. Mather 891
A.D. Jensen, S. Chatterji, P. Christensen and N. Thaulow 894

NEWS ITEMS 895

CONTENTS OF VOLUME 14 897
Key Word Subject Index 902
Author Index 905

SOFTWARE SURVEY SECTION I

VOL.
14
984

KEY WORD SUBJECT INDEX

ACCELERATED AGING 271
ACCELERATORS 73
ACTIVATORS 615
ADMIXTURES 185
ADVANTAGES 463
AERATED CONCRETE 369
AGE-ADJUSTED MODULUS METHOD 819
AGGREGATES 113, 225
AGGREGATION 64
AGING 123
AIR ENTRAINMENT 297, 311
ALITE 413
ALKALI-SILICA EXPANSION 816
ALKALI-SILICA REACTION 311
ANALYSES 257, 887
ANALYTICAL ELECTRON MICROSCOPY 43
ANHYDRITE 645
AQUEOUS PHASE 257
ASH 513
ATMOSPHERE 386
ATMOSPHERIC PRESSURE 318
AUTOCLAVE EXPANSION 407
AUTOCLAVING 369, 785

BELITE 686
BENDING STRENGTH 533
β-Ca_2SiO_4 323
BLAST FURNACE SLAGS 873
BLENDED CEMENTS 717
BOND 315
BONDING 142, 285
BY-PRODUCTS 513

CA 679
CA_2 679
C_4AF 238
CALCIUM SILICATE CARBONATE 866
CALCIUM SILICATES 177, 833
Ca SILICOSULFATE 839
$Ca(OH)_2$ 93, 491, 533
CeO_2 729
CH 843
C-S-H 323, 663
CAPILLARY POROSITY 249, 303
CARBONATE 275
CARBONATION 1, 161
C_3A 105, 238, 275
C_5A_3 386
$C_{12}A_7$ 386, 679

CS 595
C/S RATIO 663
C_2S 93, 275, 833
C_3S 57, 93, 99, 257
CEMENT 170, 491, 505, 533, 785
CEMENT COMPOSITES 349
CEMENT DUSTS 615
CEMENT HYDRATION 185, 622
CEMENT PASTES 25, 31, 43, 345, 539, 631
CENOSPHERES 767
CERAMICS 513
CHEMICAL ADMIXTURES 207
CHEMISTRY 49, 73, 485, 749
CHLORIDES 49, 546, 807
CLASS C 499
CLASSIFICATION 185
CLINKER 83, 413, 729
CLINKER FORMATION 397
CLINKER HYDRATION 645
CLINKER PHASES 195
CLINKER PHASES CHARACTERIZATION 195
CLINKER REACTIONS 11
CODES 705
COMPOSITION 123, 455
COMPOUNDS 595
COMPRESSIVE STRENGTH 855
COMPRESSIVE STRENGTH LAW 303
CONCENTRATION 546
CONCEPTS 622
CONCRETE 113, 639, 749
CONCRETE CYLINDER 847
CONCRETE PRACTICE 463
CONDUCTION CALORIMETRY 185
CONVERSION 386
CRACKING 767
CREEP 793, 819
CRYSTAL STRUCTURE 177
CYCLES 639
CYCLIC LOADING 263

DEGREE 754
DEPOLARIZATION 142
DESIGN 705
DIFFERENCES 407
DSC 807
DIMENSIONAL STABILITY 785
DISPERSION MODEL 622
DISTRIBUTION 93
DOUBLE-POWER LAW 793
DRYING CREEP 329
DRYING SHRINKAGE 585
DTA 133, 207
DURABILITY 521, 749

EARLY HYDRATION 257
EARLY STAGE 419
EDS 83
EFFECTS 749
ELASTIC MODULUS 539, 705
ELECTRICAL CONDUCTANCE 843
ELECTRICAL CONDUCTIVITY 679
ELECTROCHEMICAL PROCESSES 574
ELECTRON MICROPROBE 565
ENVIRONMENT 329
EQUILIBRIUM 657
ETTRINGITE 133
EVALUATION 499
EXPANSION 225, 311
EXPANSIVE CEMENTS 199
EXPERIMENTAL METHODS 83

FATIGUE 855
FERRITE 19
FERRITE PHASE 360
FIBERS 315
FILLERS 776
FLUIDITY 631
FLUORESCENCE 339
FLUORINE 57

VOL. 14 198

FLUORSPAR 397
FLY ASH 238, 463, 471, 491, 499, 505, 631, 767
FLYASH UTILIZATION 455
FORMATION 99, 686
FRACTURE 31, 339
FRACTURE ENERGY 215, 349, 431
FRACTURE TOUGHNESS 369
FREEZING 113, 807

GASIFIER ASH 479, 485
GEL STRUCTURE 249
GLASS 887
GLASS FIBER 31, 717
GLASS FIBER REINFORCEMENT 349
GLUCONATE 105
GLUCOSE 105
GPC 439
GRC 271
GRINDING 407
GYPSUM 105, 225, 529, 645

HARDENED CEMENT PASTE 231
HARDENING 345
HEATING 142
HEMIHYDRATE 645
HEXAGONAL STRUCTURE 57
HIGH ALUMINA CEMENTS 1, 19, 73, 161
HIGH LOADING RATE 215
HIGH STRENGTH 693
HYDRATED CEMENT 597
HYDRATION 1, 93, 105, 170, 177, 199, 238, 275, 323, 686, 679, 847
HYDRATION PRODUCTS 505
HYDRATION RATE 754
HYDROSTATIC PRESSURE 318
HYDROTHERMAL COMPATIBILITY 866
HYDROTHERMAL SYSTEM 741

IDENTIFICATION 207
IMAGES 485
IMPURITIES 177, 413, 499
INTERACTION 529
INTERFACE 315
INTERNAL STANDARD 873
IRON 19
IRREVERSIBILITY 329
IR SPECTROSCOPY 873

KINETICS 64, 99, 238, 474, 833

LABORATORY 407
LEVELING 271
LIGNITES 471, 479, 487
LIGNOSULFONATE 105, 275, 670
LIME 529
LIMITATIONS 884
Li SALTS 73
LOAD 639
LOW CALCIUM FLY ASH 887
LOW-POROSITY CONCRETES 670
LOW TEMPERATURE 639

MATRIX COMPOSITION 285
MATURE PASTE 565
MECHANISM 238
MELAMINE 297
MELT COMPOSITION 99
MELTING POINT 11
METHODS 43, 349
MICROANALYSIS 93
MICROCALORIMETRY 807
MICROCRACK 855
MICROCRACKING 585
MICROGRAPHS 559
MICROSTRUCTURE 249, 303, 339, 491, 539
MINERALOGY 471, 479
MINERAL WOOL 513
MODEL 215, 249, 303, 539
MODELING 113
MODULUS 375
MONOSULFATE 133
MORTARS 49, 315, 339, 693
MÖSSBAUER SPECTROSCOPY 19, 170

NAPHTHALENE 297, 439
NON-EQUILIBRIUM 657

OIL SHALE 11
OLIGOMER ANALYSIS 439
OPTICAL MICROSCOPY 585
OSMOTIC MODEL 345
OXYGEN 207

PARAMETRIC ANALYSIS 847
PARTICLE SIZE 622
PASTES 133, 318, 329, 546, 585, 767
PECTOLITE 741
PENETRATION 546
PERMEABILITY 546, 663
PERMITTIVITY 142
PHASE CHANGE 360
PHASES 1, 397
P_2O_5 11
PIC 559
PLANT 407
POLYMER IMPREGNATION 25, 785
POLYMERIZATION 559
POLYMINERAL PHASES 565
POLYMORPHISM 360
PORES 419
PORE STRUCTURE 318
PORE WATER 807
POROSITY 25
POZZOLANIC ACTIVITY TEST 499
POZZOLANS 170
PREPARATION 323
PREVENTION 816
PROFILES 49
PROPERTIES 455, 491, 559
PULL OUT 285, 315
PULP BOARD 533

QUANTITATIVE ANALYSIS 83, 729
QUANTITATIVE DETERMINATION 133
QUICK-SETTING CEMENTS 884

RATE 645, 843
REACTVITY 177, 679, 686, 741
RECRYSTALLIZATION 413
REDISTRIBUTION 413
REDUCTION 311
REINFORCEMENT 31, 717
RESIDUAL STRENGTH 263
RETARDATION 275

RETARDERS 64
RHEOLOGY 521, 670
RUBBER 615, 776

SALICYLIC ACID EXTRACTION 833, 839
SALT 297
SCAWTITE 866
SELF-HEALING 315
SEM 31, 83, 195, 485
SHRINKAGE 693
SILICA FUME 693
SILICATE GARDENS 663
SIZE DISTRIBUTION 419
SLAG 170, 816
SLAG CEMENTS 521
SLURRIES 419
NaCl 816
Na_2O-CaO-SiO_2 741
SOIL STABILIZATION 529
SOLUBLE ANHYDRITE 839
SPECIMEN GEOMETRY 369
SPECIMEN SIZE 431
STABILITY 161
STABILIZERS 386
STANDARD 729
STATISTICAL EVALUATION 375
STEEL FIBER 285
STRAIN 231
STRENGTH 25, 123, 161, 249, 271, 318, 375, 521, 670, 705
STRESS 231, 855
STRUCTURE 123
STRUCTURE FACTOR 231
SUBSTITUTION 360
SO_3 686
SULFATE-RESISTANT CEMENTS 225
SUPERPLASTICIZERS 297, 375, 439, 631, 754

TECHNIQUES 559
TECHNOLOGY 749
TEMPERATURE 225, 323, 397, 419
TEMPERATURE EFFECTS 1
TENSILE FRACTURE 215
TENSILE STRESS 263
TEST 297
THEORY 819
THERMAL DEFORMATION 639
THERMAL MODEL 847
THERMODYNAMICS 474
THICKENING 419
THIN SECTIONS 339
THIN-WALLED SPECIMENS 329
3-POINT TEST 431
Ti 360
TRANSITION 793
TRUSCOTTITE 657
TYPE "M" 199

ULTRASONIC TECHNIQUE 345
UNIAXIAL TEST 263
USES 463

VICAT TEST 884
VISCOMETRY 64

WASTE 615
WASTE CEMENT DUSTS 776
WATER 142, 231
W/C 345, 546
WATER CONTENT 375
WEATHERING 271
WESTERN REGIONS 471

X-RAY DIFFRACTION 19, 133, 170, 471, 479, 729
X-RAY MAPPING 195
XONOTLITE 657

ZETA POTENTIAL 631

VOL
14
198

AUTHOR INDEX

ABDUL-MAULA, S. 133
ABO-EL-ENEIN, S.A. 25
AINDOW, A.J. 271
ALTRICHTER, B. 686
ANGUS, M. 595
ASAGA, K. 323

BACHIORRINI, A. 199
BALEWSKI, L. 559
BANFILL, P.F.G. 64
BARTHA, B. 439
BAZANT, Z.P. 793
BEAUDOIN, J.J. 231, 785
BEN-DOR, L. 11
BENSTED, J. 601
BENTUR, A. 31, 717
BEZJAK, A. 833
BHATTY, J.I. 64
BIRCHALL, J.D. 761
BLANCO-VARELA, M.T. 397
BLATTER, W.C. 471
BLEZARD, R.G. 154
BROWN, P.W. 257, 843
BUIL, M. 693
BUTLER, W.B. 763

CABRERA, J.G. 238
CHANDRA, K. 19, 170
CHATTERJEE, A.K. 386
CHATTERJI, S. 151, 311, 757, 759, 816, 894
CHERN, J.-C. 793
CHOPRA, S.K. 437
CHRISTENSEN, P. 311
CHUECA, R. 639
CLASTRES, P. 199
CLAUSSON-KAAS, N.F. 816
CLIFTON, J.R. 339
COHEN, M.D. 610
COLEMAN, S.E. 670
COLLEPARDI, M. 105, 275
CORNELISSEN, H.A.W. 263
CORRADINI, G. 375
CORRES, H. 639
CRAMMOND, N.J. 225
CRAWFORD, R.W. 595
CUFFARO, P. 329

DAIMON, M. 323
DALZIEL, J.A. 491
DAUGHERTY, K.E. 873
DAY, R.L. 329
DEMIREL, T. 499, 529
DIAMOND, S. 31, 146, 455, 670, 767
Di LEO, A. 705
DORNER, H.W. 807
DOUBLE, D.D. 73, 185, 764

EBERENDU, A.R.N. 873
ELICES, M. 639
ELLESS, M.P. 479

FELDMAN, R.F. 231, 785
FRANZ, E. 257
FROHNSDORFF, G. 257, 843
FULLER, E.R., Jr. 339
FURTAK, K. 855

GALBREATH, K.C. 479
GALTIER, P. 679
GALUK, K. 843
GARDNER, N.J. 323
GARTNER, E.M. 839
GHEORGHITTA, I. 369
GHOSE, A. 99
GHOSH, S.N. 437
GLASSER, F.P. 57, 360, 585
GLASSER, L.S.D. 741
GOSWAMI, G. 407
GOTSIS, C. 847
GRANJU, J.L. 249, 303, 539
GRAY, R.J. 285, 315
GRUDEMO, Å. 123
GRUTZECK, M. 297
GUILHOT, B. 679
GUTTERIDGE, W.A. 491

HALICZ, L. 11
HALSE, Y. 491
HANEHARA, S. 645
HANIC, F. 866
HANSSON, C.M. 574
HARCHAND, K.S. 19, 170
HE, JUN-YUAN 505
HENRIKSEN, K.R. 463
HOFFMANN, D.W. 49
HOWARD, B.H. 729
HOWIE, R.A. 57
HWANG, C.-L. 585

IDORN, G.M. 145, 157, 463, 749
ILLSTON, J.M. 329, 546

JAWED, I. 99
JENSEN, A.D. 311, 894
JESENAK, V. 686
JOHNSTON, C.D. 285
JOST, K.H. 177
JUHÁSZ, Z.A. 142

KAPRÁLIK, I. 866
KATOH, S. 533
KAYYALI, O.A. 445
KELLER, L.P. 471, 479
KHEOK, S.C. 443
KISHI, K. 323
KITAMURA, T. 533
KNAB, L.I. 339
KNUDSEN, T. 622
KOBAYASHI, Y. 535
KRYSZTAFKIEWICZ, A. 615, 776
KUMAR, R. 170

LACHOWSKI, E.E. 43
LASIĆ, D.D. 345
LAZIĆ, J.D. 819
LAZIĆ, V.B. 819
LEONARD, S. 717
LEUNG, C.F. 443
LUKE, K. 657

MAIK, M. 615, 776
MAKI, I. 413
MANZ, O.E. 513
MARIE, M.S. 25
MARINHO, M.B. 360

OL.
14
984

MASO, J.C. 249, 303, 539
MATHER, B. 603, 887, 891
MATHUR, V.K. 437
MATSUO, R. 533
McCARTHY, G.J. 453, 471, 479
McCULLOUGH, C. 595
MEHTA, P.K. 149, 153, 754
MÉNDEZ, M.P. 161
MIDGLEY, H.G. 546
MIKHAIL, R. Sh. 25
MILESTONE, N.B. 207
MINDESS, S. 431
MOHANTY, S.K. 407
MONOSI, S. 105, 275
MONTGOMERY, D. 767
MOR, A. 754
MORICONI, G. 105, 275
MOUSA, A.M. 25
MURAT, M. 199

NAGATAKI, S. 631
NATHAN, Y. 11
NEWBURY, D.E. 93, 565

OAKLEY, D.R. 271
ODLER, I. 133, 147
OGAWA, K. 645
OHIGASHI, T. 349
OLSEN, M.P.J. 113

PAILLÈRE, A.M. 693
PALOMO, A. 397
PÁLYI, G. 439
PANDA, J.D. 407
PARCEVAUX, P. 419
PASCALE, G. 705
PAURI, M. 105, 275
PÉREZ, M. 1
PÉREZ-MENDEZ, M. 57, 161
PETROVIC, J. 866
PITT, J.M. 499
PLANAS, J. 639
PLOWMAN, C. 238
PRATT, P.L. 491
PROCTOR, B.A. 271

RAHMAN, A.A. 595
RAYMENT, D.L. 43
REINHARDT, H.W. 263
ROGER, S.A. 73
ROUSSEL, B. 693
ROY, D.M. 83, 439, 505, 521, 847
RUNJE, V. 833

SAKAI, E. 631
SARKAR, S.L. 83, 195
SCHEETZ, B.E. 505
SCHIELDS, P.J. 479
SCHLORHOLTZ, S. 499, 529
SCOCCIA, G. 375
SHIBATA, S. 323
SHRESTHA, P.R. 323
SKALNY, J. 99
SOROKA, I. 884
STADE, H. 663
STEPISNIK, J. 345
STEVENSON, R.J. 485
STEVULA, L. 866
SWANSON, K.D. 471

TAKAHASHI, S. 413
TAKEUCHI, T. 631
TAMÁS, F.D. 439
TANG, F.J. 839
TASHIRO, C. 318
TAVANO, S. 375
TAYLOR, H.F.W. 93, 257, 565, 657
THAULOW, N. 157, 311
THOMAS, N.L. 761
TRIVIÑO, F. 1

UCHIDA, S. 645
UCHIKAWA, H. 645
URUSHIMA, H. 318

VÁRADI, G. 439
VÁZQUEZ, F.T. 161
VÁZQUEZ, T. 1, 397
VISHWAMITTAR 19, 170
VOLPE, R. 375

WALKER, H.N. 339
WALTER, A. 185, 764
WEJCHAN-JUDEK, M. 559
WIEKER, W. 663
WILDING, C.R. 185, 764
WITTMANN, F.H. 369
WU, XUE-QUAN 521

XI, Y. 741

YOUNG, J.F. 99, 585

ZHMOIDIN, G.I. 386
ZIELINSKI, A.J. 215
ZIEMER, B. 177, 686
ZUK, A. 559

VOL. 14 1984

OL.
14
984

VOL.
14
1984

CEMENT and CONCRETE RESEARCH. Vol. 14, pp. 1-10, 1984. Printed in the USA.
0008-8846/84 $3.00 + 00. Copyright (c) 1984 Pergamon Press, Ltd.

STUDY OF STABILIZED PHASES IN HIGH ALUMINA CEMENT MORTARS

PART II

EFFECT OF $CaCO_3$ ADDED TO HIGH ALUMINA CEMENT MORTAR SUBJECTED TO ELEVATED TEMPERATURE CURING AND CARBONATION

M. Pérez, T. Vázquez and F. Triviño

Instituto Eduardo Torroja
Serrano Galvache s/n
Madrid - 33

(Refereed)
(Received July 19, 1982; in final form June 23, 1983)

OL.
14
984

ABSTRACT

The effects of adding ground limestone to high alumina cement mortar were studied. The hydration was carried out at 60°C to form the cubic hydrate C_3AH_6 directly, hence avoiding the conversion of CAH_{10} to C_3AH_6, and at 20°C. Other experiments involved subsequent carbonation with CO_2 and thermal treatment. The formation of stable carbonated phases was evident even at very early ages.

Introduction

Results of an attempt to stabilize 1:3 high alumina cement mortars against "conversion" by curing at 30°C and by subsequent carbonation with CO_2 and thermal treatment were described in Part I of the present paper (1). The formation of stable carbonated phases was shown. The addition of $CaCO_3$ to the anhydrous high alumina cement before mixing was investigated as a possible alternative way carrying out the carbonation process. The results will be discussed in this paper.

Experimental Procedure

1 x 1 x 6 cm specimens of a 1:3 mortar were prepared using a high alumina cement which had 20% by mass substituted by $CaCO_3$, analytical reagent grade. Both the carbonate and the anhydrous cement were previously mixed and homogenised. The W/C ratio used in all cases was 0.42. A summary of the curing conditions employed is given in Table I. IR spectroscopy and x-ray diffraction were used to identify the phases present in each case. They were used in a qualitative way and only relative intensities were considered.

Results

Figures 1 and 2 show the x-ray diffractogram and the IR spectrum, respectively, of the anhydrous (cement + $CaCO_3$) mixture.

Study of the Elevated Temperature Curing and Subsequent Carbonation of Specimens Containing $CaCO_3$

The specimens of 1:3 high alumina cement mortars with $CaCO_3$ were hydrated for 28 days at two different temperatures: 20°C used as a control and 60°C, to get the cubic phase; they were then carbonated for 3 days.

Hydration at 20°C

Table 1

Curing Conditions

β SPECIMENS WITH $CaCO_3$

	HYDRATION	
	T°C	AGE
1	20	28 days
2	60	28 days

δ SPECIMENS WITH $CaCO_3$

	HYDRATION		CARBONATION	
	T°C	AGE	T°C	AGE
A	20	28 days	20	3 days
			40	3 days
1	60	28 days	60	3 days
2				
B	60	6 hours	60	18 hours
			60	3 days
3			60	5 days
	60	24 hours	60	24 hours
			60	3 days
4			60	5 days
	80	3 hours	80	21 hours
			80	3 days
5			80	5 days
	80	24 hours	80	24 hours
			80	3 days
6			80	5 days

Figure 3 shows the IR spectra of the samples hydrated for 28 days at 20°C (Curve 1) and subsequently carbonated either at 20°C (Curve 2) or 60°C (Curve 3). Characteristic IR absorption bands of quartz from the mortar sand appear in all the spectra. The IR spectrum of quartz is given in fig. 14 of Part I (1).

Curve 1 proves that CAH_{10} if formed at 20°C. The spectrum shows a typical band of CAH_{10} at 3510 cm^{-1} due to OH^- valence vibrations and the band in the 1650-1600 cm^{-1} range due to H-O-H bending vibrations of this hydrate partially overlapped with the very intense ν_3-CO_3 band at 1435 cm^{-1}. In our opinion, the water in CAH_{10} is only weakly bonded to the rest of the molecule, so that the OH^- valence band appears wide and at higher frequency while the H-O-H deformation band appears also wide and at a lower frequency than normal values of ν_1 - OH, ν_3 - OH, and ν_2 - OH respectively. According to Rocchiccioli (2), water which is strongly bonded in a structure shows a higher frequency for the H-O-H deformation band and a lower frequency for the OH^- valence band. Bayerite (α -$Al(OH)_3$) can be detected by its typical absorption bands at 1025 cm^{-1} and 970 cm^{-1}. The calcium carbonate in the sample is present as calcite which coexists with calcium carboaluminate. The presence of carboaluminate is shown by the band at 422 cm^{-1} since it is the only one from this compound that is not masked. An alteration of the band corresponding to the ν_3-CO_3 vibration, 1500-1400 cm^{-1}, also seems to confirm the presence of carboaluminate. Hence, according to Vázquez et al. (3), we may say that the $CaCO_3$ addition to high alumina cement promotes the formation of carboaluminate.

VOL. 14 1984

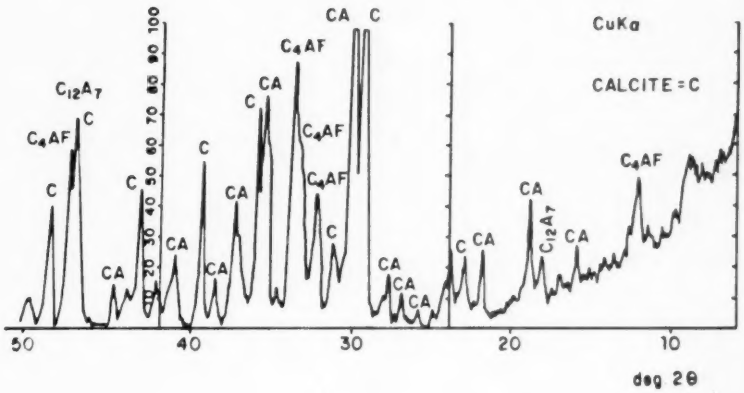

Fig. 1

X-ray Diffrac togram of the (High Alumina Cement+$CaCO_3$) Mixture.

Curve 2 in Figure 3 shows the IR spectrum of samples with $CaCO_3$ cured for 28 days at 20°C, and carbonated for 3 days at 20°C. The CO_2 treatment at 20°C of the sample with $CaCO_3$ cured at 20°C almost totally destroys the carboaluminate that had previously been formed during the hydration as shown by the considerable decrease in the band at 422 cm^{-1}. The presence of a large quantity of CAH_{10} proves that carbonation was not deep, probably due to the low temperature. The attack of CO_2 on the aluminates seems to favour the octahedral coordination of the aluminium, AlO_6, so that bands most altered by CO_2 treatment are those between 550-620 cm^{-1} and at 565 cm^{-1}; these are spectral regions in which Al-O vibrations usually appear, and more specifically where condensed AlO_6 groups absorb according to Tarte (4), and the proportion of these groups increases as the carbonation proceeds. This effect is favoured by elevated temperature since it is higher in samples carbonated at 60°C (Curve 3).

Differences in the absorption in the 680-600 cm^{-1} range are observed in Curve 2 of Figure 3 for the uncarbonated sample. It can be interpreted as a process involving crystal growth, as the bands appear much better defined, and an increase in the proportion of condensed AlO_6 groups. This is supported by the fact that the absorption between 860 and 830 cm^{-1} shows a higher relative intensity than that in curve 1 for the uncarbonated sample; this is interpreted as being caused by an increase in the quantity of condensed AlO_4 groups. Likewise, the interpretation given is confirmed by the decrease in

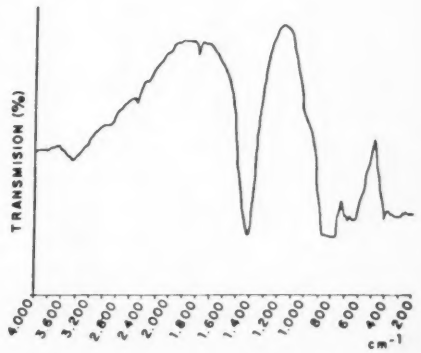

Fig. 2

IR Spectrum of the (High Alumina Cement + $CaCO_3$) Mixture.

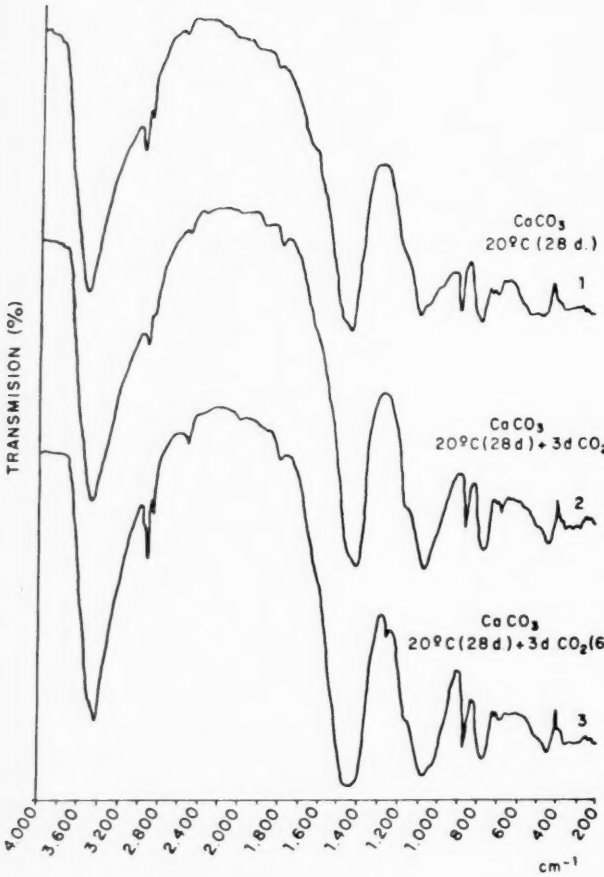

Fig. 3

IR Spectra of Specimens with $CaCO_3$ Hydrated for 28 Days at 20°C (Curve 1) and Carbonated for 3 Days at 20°C (Curve 2) or 60°C (Curve 3).

the characteristic absorption bands of isolated AlO_4 tetrahedra between 800 and 680 cm^{-1} (4). Important increases in the absorptions at 1080 cm^{-1} and 635 cm^{-1} are observed. These are interpreted as due to an increase in the α-alumina content.

Finally we conclude that carbonation causes structural alterations that, although not fully confirmed, can be summarized as follows: An increase in the quantity of calcium carbonate, mostly as calcite, when the carbonation takes place at 20°C, with a small quantity of aragonite forming from the cubic phase hydrate which might have formed during the hydration; a decrease in the quantity and ultimate disappearance of the previously-formed calcium carboaluminates; structural alterations in the aluminates interpreted as an increase in the quantities of condensed octahedral AlO_6 groups and condensed tetrahedral AlO_4 groups at the expense of isolated AlO_4 tetrahedra. The octahedrically-coordinated aluminium plays the role of lattice former and contributes to the development of mechanical strength, specially when in condensed units.

When the carbonation of the hexagonal phase, CAH_{10}, formed by curing at 20°C for 28 days, is performed at 60°C (Curve 3, Figure 3), neither C_3AH_6 nor gibbsite are detected. According to (3), this proves that the reaction

$$CAH_{10} \longrightarrow C_3AH_6 + AH_3$$

takes place only in a CO_2 free atmosphere. In our case $CaCO_3$, as well as the added CO_2, was present. Curve 3 shows a change in the band which appeared at

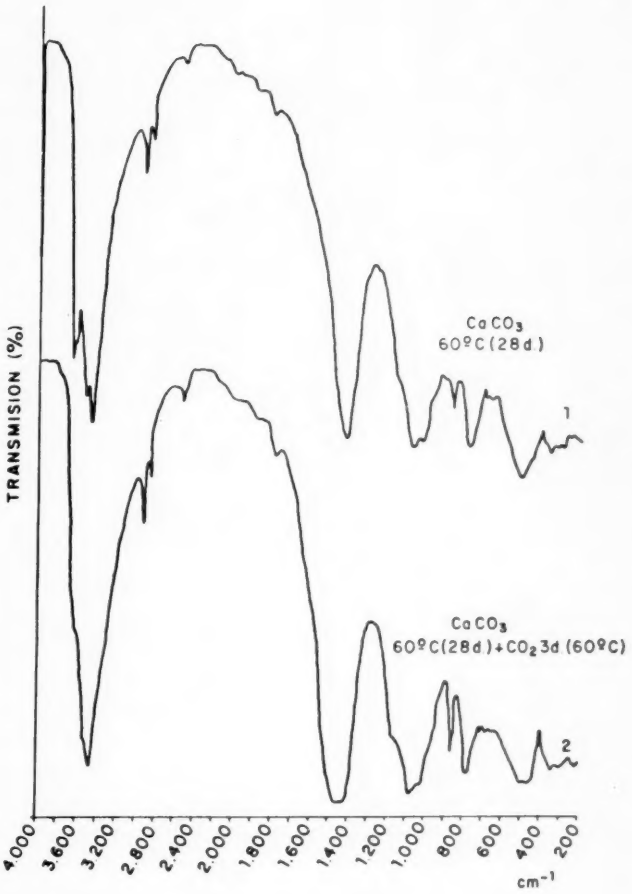

Fig. 4

IR Spectra of Specimens with $CaCO_3$ Hydrated for 28 Days at 60°C (Curve 1) and Carbonated for 3 Days at 60°C (Curve 2).

3510 cm^{-1} in the two previous cases, Curves 1 and 2. The sharp band which now appears at 3470 cm^{-1} suggests more strongly-bonded OH groups in the sample carbonated at 60°C. Further, a weak band observed at 3510 cm^{-1} is interpreted as due to the partial transformation of the water in CAH_{10} into another compound with different bonding of the water. Two shoulders are observed at 3665 and 3625 cm^{-1}, wavelengths characteristic of carboaluminates.

The band in Curve 3 between 1700 and 1600 cm^{-1} due to H-O-H bending vibrations appears diminished in intensity with respect to the sample carbonated at 20°C. This suggests that the molecular water initially present in hexagonal compounds ends up in another compound with more strongly-bonded water. The presence of bayerite seems to be confirmed by the absorption bands at 1025 and 970 cm^{-1}. The well-defined bands at 1480-1440 cm^{-1}, 875 cm^{-1} and 859 cm^{-1} are attributed to vaterite. An increase in the intensity of the band at 635 cm^{-1}, as compared to the sample carbonated at 20°C (3-2), is observed; this band is even stronger than that of the hydrated sample without carbonation. It suggests the presence of α - alumina.

Hydration at 60°C

When the high alumina cement mortar with $CaCO_3$ is hydrated at 60°C for 28 days (Fig. 4, Curve 1), C_3AH_6 is detected by the OH valence vibrations at 3670 cm^{-1} and by the vibrations between 600 and 500 cm^{-1} due to Al-O bonds. Aluminium hydroxide in the form of α - $Al(OH)_3$ is also detected by the typical absorp-

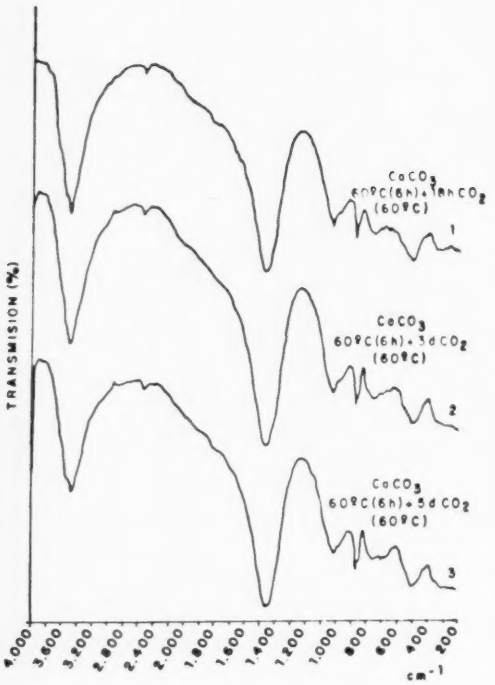

Fig. 5

IR Spectra of Specimens with $CaCO_3$ Hydrated for 6 Hours at 60°C and Carbonated at 60°C for: 18 Hours (Curve 1), 3 Days (Curve 2), and 5 Days (Curve 3).

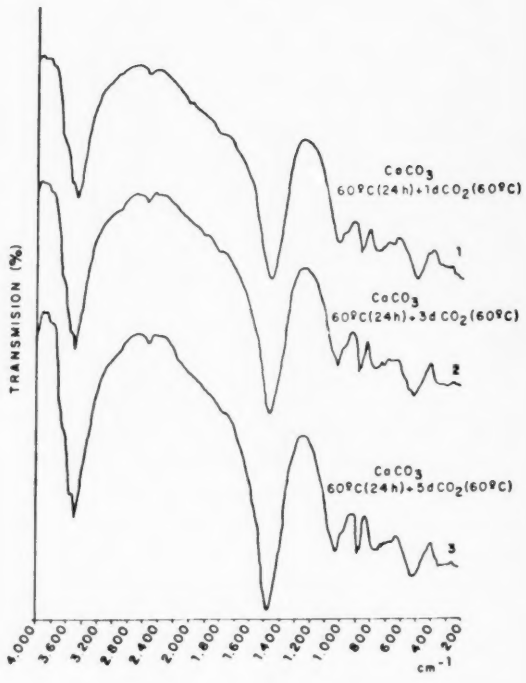

Fig. 6

IR Spectra of Specimens with $CaCO_3$ Hydrated for 24 Hours at 60°C and Carbonated at 60°C for: 24 Hours (Curve 1), 3 Days (Curve 2), and 5 Days (Curve 3).

tion bands at 3616, 3533, 3454, 3401, 1020 and 970 cm^{-1}. Carboaluminates with their characteristic band at 422 cm^{-1} also appear in this sample. The calcium carbonate is present mainly as calcite.

When the samples are exposed to CO_2 at 60°C for 3 days (Fig. 4, Curve 2), a deep carbonation of the hydrated cubic phase is observed. The quantity of C_3AH_6 decreases considerably although it does not disappear, probably because the time for carbonation is small compared to the time for hydration (28 days). Carboaluminates are not detected. This confirms that these compounds are intermediate states in the carbonation process, and they disappear as the reaction progresses. Therefore, we may conclude that carboaluminates are neither stable nor final phases in the high alumina cement carbonation process. The calcium carbonate is present as calcite and aragonite. The presence of aragonite is deduced from the shape of the absorption band between 1500 and 1400 cm^{-1} and it is confirmed by the absorption at 862 cm^{-1} typical of this compound.

VOL. 14 1984

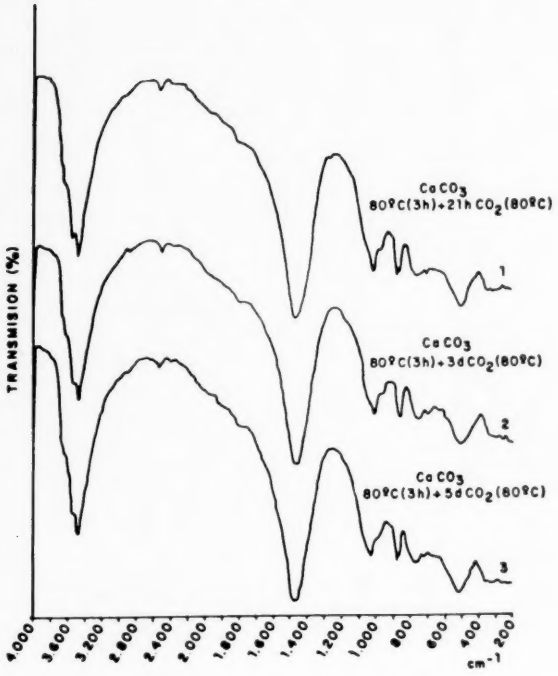

Fig. 7

IR Spectra of Specimens with $CaCO_3$ Hydrated for 3 Hours at 80°C and Carbonated at 80°C for: 21 Hours (Curve 1), 3 Days (Curve 2), and 5 Days (Curve 3)

The aluminium hydroxide found in Fig. 4, Curve 2, seems to be bayerite as in the previous case. However the relative intensities of its typical absorption bands seem to be decreased by the carbonation, as shown by comparison of the IR spectra. The intensity increase of the bands at 635 cm^{-1} and 520 cm^{-1} prove that the quantity of α-alumina is larger in the carbonated sample. The absorption of the latter is overlapped by the absorption of quartz at this frequency. The variation observed in the slope of the spectrum between 750 and 712 cm^{-1} is interpreted by Tarte (4) as an increase in the proportion of condensed tetrahedral AlO_4. Likewise, the diffuse absorption detected in the 660-620 cm^{-1} range is interpreted as due to a rise in the quantity of condensed octahedral AlO_6.

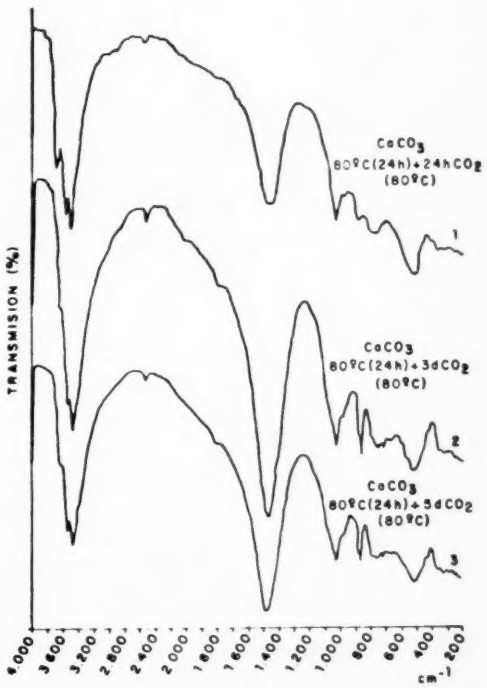

Fig. 8

IR Spectra of Specimens with $CaCO_3$ Hydrated for 24 Hours at 80°C and Carbonated at 80°C for: 24 Hours (Curve 1), 3 Days (Curve 2), and 5 Days (Curve 3).

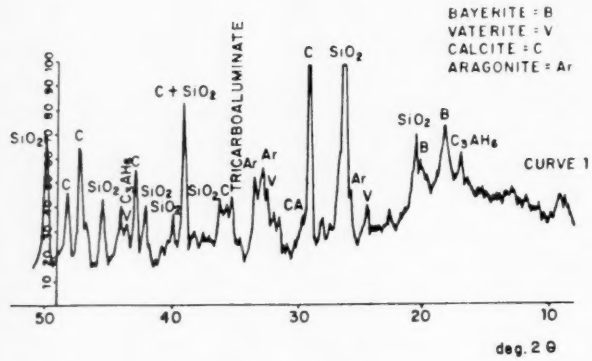

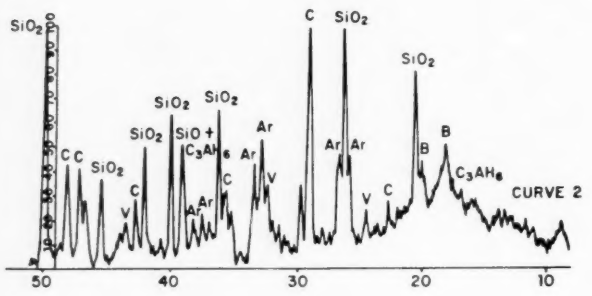

Fig. 9

X-ray Diffractogram of Specimens with $CaCO_3$ Hydrated for 6 Hours at 60ºC and Carbonated at 60ºC for: 18 Hours (Curve 1) and 5 Days (Curve 2)

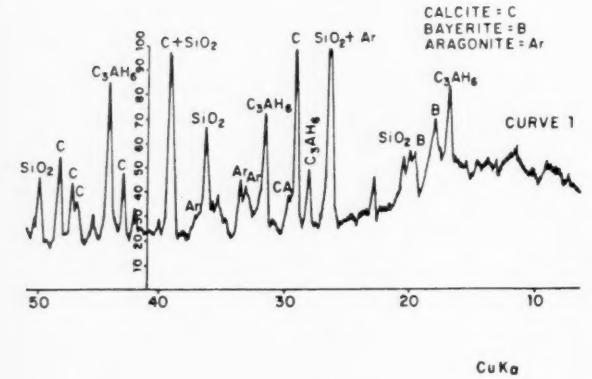

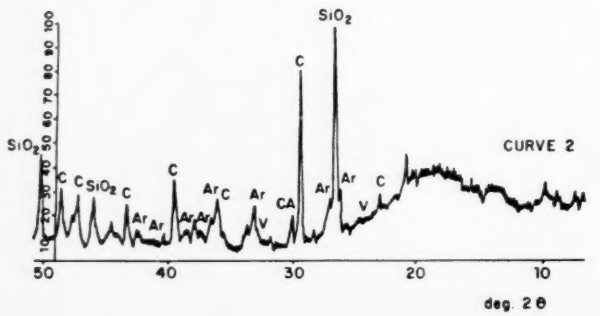

Fig. 10

X-ray Diffractograms of Specimens with $CaCO_3$ Hydrated for 24 Hours at 80ºC and Carbonated at 80ºC for: 1 Day (Curve 1) and 5 Days (Curve 2)

Table II

Compounds Formed

SPECIMENS WITH $CaCO_3$

	HYDRATION T°C	AGE	COMPOUNDS FORMED
1	20	28 days	CAH_{10} + $CaCO_3$ (calcite) + carboaluminate
2	60	28 days	C_3AH_6 + $CaCO_3$ (aragonite) + α-$Al(OH)_3$ (bayerite)

SPECIMENS WITH $CaCO_3$

	CURING HYDRATION T°C	AGE	CO_2 T°C	AGE	COMPOUNDS FORMED
1	20	28 days	20	3 days	$CaCO_3$ (calcite) + α-Al_2O_3 + α-$Al(OH)_3$ (bayerite)
			60	3 days	$CaCO_3$ (vaterite) + α-Al_2O_3 + α-$Al(OH)_3$ (bayerite)
2	60	28 days	60	3 days	$CaCO_3$ (aragonite) + α-Al_2O_3 + α-$Al(OH)_3$ (bayerite)
3	60	6 hours	60	18 hours	
			60	3 days	$CaCO_3$ (aragonite) + α-Al_2O_3 + α-$Al(OH)_3$ (bayerite)
			60	5 days	
4	60	24 hours	60	24 hours	
			60	3 days	$CaCO_3$ (aragonite) + α-Al_2O_3 + α-$Al(OH)_3$ (bayerite)
			60	5 days	
5	80	3 hours	80	21 hours	
			80	3 days	$CaCO_3$ (aragonite) + α-Al_2O_3 + α-$Al(OH)_3$ (bayerite)
			80	5 days	
6	80	24 hours	80	24 hours	
			80	3 days	$CaCO_3$ (aragonite) + α-Al_2O_3 + α-$Al(OH)_3$ (bayerite)
			80	5 days	

VOL. 14 984

Kinetics of Hydration and Carbonation Reactions of High Alumina Cement with $CaCO_3$

Specimens of high alumina cement mortar with $CaCO_3$ were cured at two temperatures, 60°C and 80°C, for short times. These were:

a) 6 hours at 60°C and subsequent carbonation for 18 hours (up to a total of 24 hours from the end of mixing), 3 days and 5 days.

b) 3 hours at 80°C with subsequent carbonation for 21 hours (up to a total of 24 hours from the end of mixing), 3 days and 5 days.

c) 24 hours for both 60°C and 80°C followed by CO_2 treatment for 1, 3 and 5 days.

Figures 5, 6, 7 and 8 show the IR spectra of all the samples cured in this way. The compounds present in all of them are the same as those which appeared in Fig. 4, Curve 2. We shall now consider only their hydration and carbonation kinetics at early ages as function of temperature and time.

The progress of the carbonation reaction can be deduced from the residual quantity of C_3AH_6 after the CO_2 treatment. At 24 hours after the end of mixing, specimens with $CaCO_3$ hydrated at 60°C for 6 hours (Fig. 5) and carbonated for 18 hours at the same temperature (Curve 1) show a lower quantity of C_3AH_6 than that which appears in samples hydrated for 24 hours at 60°C (Fig. 6) and afterwards carbonated for 24 more hours (Curve 1). The same effect is observed in comparing the IR spectra of specimens hydrated at 80°C for 3 hours (Fig. 7) and carbonated for 21 hours (Curve 1) and specimens hydrated at 80°C for 24 hours (Fig. 8) and carbonated 24 hours (Curve 1). The shorter hydration times show the better results from the point of view of obtaining carbonated phases.

The carbonation of high alumina cement mortars with $CaCO_3$ at 80°C causes the quantity of residual C_3AH_6 to be lower than those of the same age cured under

the same conditions at 60ºC. Both curing temperatures, 80ºC and 60ºC, give a practically total carbonation of the specimens after 3 days of treatment (Curves 3).

Figures 9 and 10 show the x-ray diffractograms of samples cured at 60ºC and 80ºC. They confirm everything that was deduced from the IR results. Table II summarizes the compounds formed with all the curing conditions studied.

Discussion

The rate of the carbonation reaction is higher in specimens with $CaCO_3$ than in those without carbonate (see part I) cured under the same conditions. This effect has the maximum importance when a large concrete mass is to be carbonated. This is because the CO_2 acts principally on the surface and the depth of its action will depend on its access to the inner part and, hence, on the concrete porosity. But if $CaCO_3$ is added to the anhydrous cement before mixing, the inner part is then carbonated causing an homogeneous distribution of the final stable phases. This effect, together with CO_2 addition from outside, leads to optimal results from the point of view of the phases formed and the very short curing times. The strength results obtained by the same authors (5) seem to confirm the good performance of high alumina cement cured in this way.

Conclusions

The results presented in the present paper suggest that the optimal way of curing a high alumina cement when a carbonated product is desired is:

a) Addition of $CaCO_3$ to the anhydrous high alumina cement before mixing to serve as a carbonating agent.

b) Carrying out the hydration and carbonation of high alumina cement at 80ºC

c) Hydration for 3 hours followed by exposure to CO_2 for 18 hours (or at most 3 days.

References

1. M. Pérez, T. Vázquez and F. Triviño, to be published in Cem. Conc. Res.

2. C. Rochiccioli, Chimie Analytique, 46, pp. 452 (1964).

3. T. Vázquez, F. Triviño and A. Ruiz de Gauna, Monografía del IETcc nº 334, Madrid (July 1976).

4. P. Tarte, Spectrochimica Acta, 23-A, 2127-2143 (1967) .

5. M. Pérez and F. Triviño, to be published in Cem. Concr. Res.

VOL 14 198

CEMENT and CONCRETE RESEARCH. Vol. 14, pp. 11-18, 1983. Printed in the USA.
0008-8846/84 $3.00 + 00. Copyright (c) 1984 Pergamon Press, Ltd.

THE INFLUENCE OF P_2O_5 ON CLINKER REACTIONS

L. Halicz* and Y. Nathan
Geological Survey of Israel

and

L. Ben-Dor
Department of Inorganic and Analytical Chemistry
Hebrew University, Jerusalem, Israel

VOL.
14
1984

(Communicated by C.D. Pomeroy)
(Received May 13, 1983)

ABSTRACT

Synthetic clinkers, similar to high-silica Portland Cement clinkers, were prepared from raw material containing at times more than 50% oil shale from Har-Tuv area (central Israel) to which phosphate rock and laboratory grade $CaCO_3$ and SiO_2 were added. Although some clinkers contained more than 3% P_2O_5, their mineralogical composition was satisfactory (50 to 60% C_3S). This result was obtained by taking into account in the SM formula the P_2O_5 concentrations. The resultant relatively high silica concentrations raise the melting point of the raw meal, causing a non-equilibrium state which allows the formation of C_3S and its preservation.

Introduction

The use of oil shale as raw material for the production of Portland cement is an attractive concept, since the organic part may serve as fuel while the inorganic part constitutes the raw material for the clinker. Furthermore this use of oil shale produces practically no waste and therefore does not present the usual ecological problem of how to cope with the spent shale. One of the obstacles to this use in Israel is the relatively high P_2O_5 content (1 to 5%) of the local Ghareb oil shales. These concentrations are higher than those now allowed in raw material used to produce Portland cement. This work was carried out with the aim of studying the influence of P_2O_5 on clinker reactions and avoid its detrimental effects in the manufacture of cement.

Many investigators have dealt with the influence of P_2O_5 on clinker minerals: Guye [1]; Vlkov and Tabakama [2]; Teoreanu and Tran van Huyrah

[3]; Salge and Thorman [4]; Rangarao [5] amongst others. Among the most important contributions to the subject are those from U.K. Building Research Station: Nurse [6]; Nurse et al. [7]; Welch and Gutt [8]; Gutt [9]; Gutt and Osborne [10]; Gutt and Smith [11]. They discovered that P_2O_5 (in the form of C_3P) forms a solid solution with C_2S thus stabilising it, and causing reduction in the concentration of C_3S with a corresponding increase in the free lime content. The importance of fluoride as mineralizer in the manufacture of phosphatic cement was elucidated and phase diagrams of the systems $2\ CaO.SiO_2 - 3\ CaO.P_2O_5$ and $2\ CaO.SiO_2 - 3\ CaO.P_2O_5 - CaO$ and others were published. Finally the effect of P_2O_5 on the hydraulicity of the calcium silicates was discussed.

Experimental

A composite sample of oil shale from the Har-Tuv area (L-30) with the following composition: CaO 37.8%; SiO_2 10.3%; Al_2O_3 4.2%; Fe_2O_3 1.6%; P_2O_5 1.3% was chosen for this study. One sample, prepared by adding laboratory grade $CaCO_3$ and SiO_2 to the composite sample in order to reach LSF ~ 1.0 and SM ~ 2.2, was then ignited to 1450°C in a vertical furnace. The sample was taken out at fixed intervals, ground and homogenised and returned to the furnace. A series of samples with increasing P_2O_5 content ranging from 1.9 to 5.0% after ignition, was prepared by adding phosphate rock (H.H. 203) which contains ~ 85% theoretical fluor-carbonate-apatite, the rest being mainly calcite. The LSF and SM were kept constant at ~ 1.0 and ~ 2.2 respectively.

The ignited products were chemically analysed. An NaOH melt was prepared for the determination of Si, Al, Fe, Mg, Ca and P. The analysis was carried out by ICP spectrometry. Some samples were analysed for F by the specific electrode method [12]. The resulting phases were determined by XRD amd were also studied by SEM and electron-probe.

Results

After ignition to 1450°C, the clinkers showed: a) A decrease in tricalcium silicate (alite) and an increase in dicalcium silicate (belite) relative to the phosphate concentration. This is, on the whole, in agreement with former results of Nurse [6] and Gutt [9]. It should be noted that the effect of P_2O_5 is appreciable only after its concentration is higher than 1% in the ignited product. b) A behaviour of the samples which indicates an increase of the molten-interstitial phase with increasing P_2O_5, suggesting its somewhat similarity in this respect to R_2O_3. Fig. 1 and Table 1 summarize the results of this experiment.

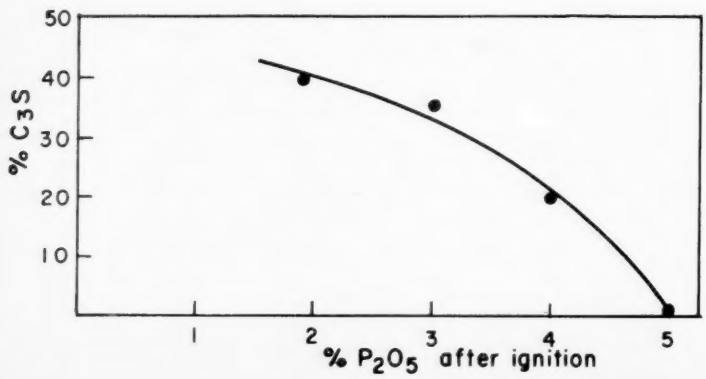

Fig. 1

VOL
14
198

Table 1. Alite (C_3S), Belite (C_2S) and P_2O_5 content in the clinkers

Sample	P_2O_5 % (after ignition)	C_3S %	Average* P_2O_5 % (in C_3S)	C_2S %	Average* P_2O_5 % (in C_2S)
L-33 (L-30 + 10% $CaCO_3$ + 2% SiO_2)	1.9	40	1.6	40	3.2
L-34 (L-30 + 8% $CaCO_3$ + 2% SiO_2 + 2% H.H.203)	3.0	35	n.d.**	45	n.d.
L-35 (L-30 + 6% $CaCO_3$ + 2% SiO_2 + 4% H.H.203)	4.0	20	n.d.	65	n.d.
L-36 (L-30 + 4% $CaCO_3$ + 2% SiO_2 + 6% H.H.203)	5.0	<5	-	85	5.7

* Average from several electron probe values collected from different grains.
** Not determined.

VOL. 14 1984

As can be seen from Table 1, the clinkers produced were unsatisfactory since they contain an unfavourable ratio of C_3S to C_2S. Portland cement should have at least 45% of C_3S. Adding $CaCO_3$ (LSF > 1) to the raw meal does not improve the results, on the contrary, it leads to the production of free lime. Addition of SiO_2 markedly improved the composition and since the behaviour of P_2O_5 appears to be similar to that of R_2O_3, it is suggested that a slightly different silica modulus be defined in the presence of P_2O_5 as follows:

$$SM' = \frac{SiO_2}{Al_2O_3 + Fe_2O_3 + P_2O_5}$$

It has previously been suggested by Gutt and Smith [11] that P_2O_5 be accounted for in the LSF formula. A second series of samples was thus prepared from L-30 in which SM' was kept constant at ~ 2.75 and LSF ~ 1.0. P_2O_5 ranged from 1.4 to 4.8% in the ignited products. Fig. 2 and Table 2 summarize the results of the second series.

The results of this experiment were satisfactory, viz., even at a level of 2.8% P_2O_5 in the ignited product, 62% C_3S were produced.

In all the products F was not detected.

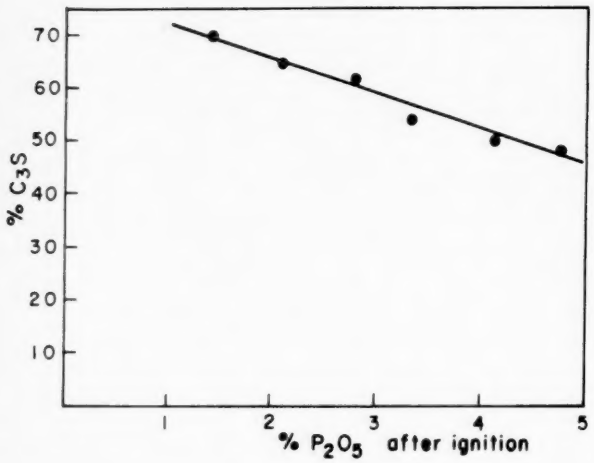

Fig. 2

Table 2. C_2S, C_3S and P_2O_5 content in the clinkers

Sample	P_2O_5 % (after ignition)	C_3S %	Average* P_2O_5 % (in C_3S)	C_2S %	Average* P_2O_5 % (in C_2S)
L-51-1 (L-30 + 9.2% SiO_2 + 43.3% $CaCO_3$)	1.4	70	1.3	20	3.0
L-51-2 (L-30 + 11.7% SiO_2 + 53% $CaCO_3$ + 3% H.H.203)	2.1	65	1.5	27	4.2
L-51-3 (L-30 + 14.7% SiO_2 + 65% $CaCO_3$ + 6% H.H.203)	2.8	62	1.6	28	5.3
L-51-4 (L-30 + 17.5% SiO_2 + 76% $CaCO_3$ + 9% H.H.203)	3.4	54	1.7	31	6.5
L-51-5 (L-30 + 23% SiO_2 + 98% $CaCO_3$ + 15% H.H.203)	4.2	50	1.6	43	8.5
L-51-6 (L-30 + 28.5% SiO_2 + 120% $CaCO_3$ + 21% H.H.203)	4.8	48	1.6	44	8.7

* Average from several electron probe values collected from different grains.

VOL. 14 1984

Discussion

It can be seen, from the second series of samples, that mineralogically acceptable clinkers can be produced with P_2O_5 concentrations up to 3.5% (where the original oil shale comprises about 50% of the sample). Preliminary tests of strength at the Israel Ceramic and Silicate Institute [13] gave encouraging results. Obviously more tests for this type of clinker are needed before any definite conclusions can be reached. It is to be noted that the P_2O_5 content of alite was more or less constant and homogeneous at 1.5%. On the other hand the amount of P_2O_5 in belite was in many cases different from grain to grain, it was also not homogeneous within the same grain; e.g. in sample L-51-5 it ranged from 3.3% to 16% (Fig. 3). In samples L-51-5 and L-51-6 some tricalcium phosphate grains almost non-reacted were found. A reduction in the amount of molten phase was also observed.

The concentrations of P_2O_5 found in alite were higher than those found by Gutt [9], viz. 0.5% in C_3S and are closer to those found by Schlaudt [14]: 1.1% and by Salge and Thorman [4]: up to 2.2%. These concentrations of P_2O_5 in C_3S probably explain why the influence of P_2O_5 on the clinker composition is evident only after it is higher than 1% in the clinker.

The concentrations of P_2O_5 in belite have a much larger variability and are related to the concentration of P_2O_5 in the raw material. Gutt [9] summarising earlier work showed that above 1500°C there is a complete solid solution between α-C_2S and $\bar{\alpha}$-C_3P, the so-called, super-α-tricalcium phosphate [15]. At temperatures of 500°C and below, C_2S may contain up to 35% C_3P (16% P_2O_5): α'-C_2S is the most common polymorph, α-C_2S and β-C_2S are also stable in certain ranges of temperature and P_2O_5 concentrations (see phase diagram of Nurse et al. [7]). It has been claimed that 2.5% P_2O_5 in cement mixes is the upper limit allowed for producing satisfactory cements [6]. This is based on Nurse's relation [6] that for each 1% P_2O_5 added to a cement mix C_3S is lowered by 9.9% and C_2S raised by 10.9%. Indeed this relation is correct and has been substantiated [16]; however it is correct only at equilibrium. Different C_3S and C_2S concentrations may be obtained from mixes with the same P_2O_5 contents; e.g., some of Gutt and Smith's results [11] which are summarized in Table 3 (based on their Tables 2, 5, 8 and 10). It is clearly seen from Tables 1, 2 and 3

Table 3. P_2O_5, SM, C_3S and C_2S content of some clinkers

RM No.*	Origin of the raw material	P_2O_5%	C_3S %	C_2S %	SM	SM'
9	West Africa	3.0	59	31	2.46	1.79
10	West Africa	3.5	54	33	2.43	1.69
7	West Africa	4.0	45	43	2.40	1.61
34	Uganda	2.95	38	40	1.42	1.14
31	Uganda	3.33	18	53	1.27	1.02

* Original numbers from Gutt and Smith [11].

(a)

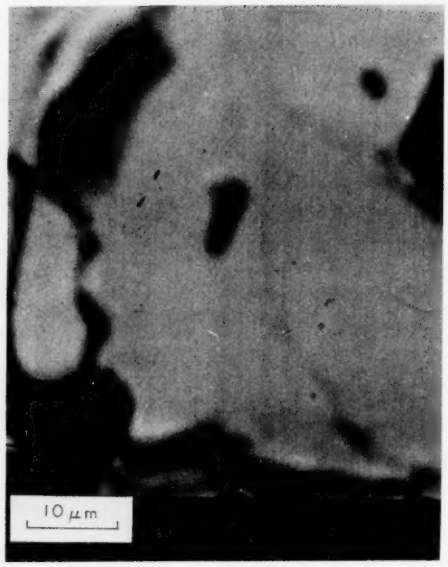

(b)

(c)

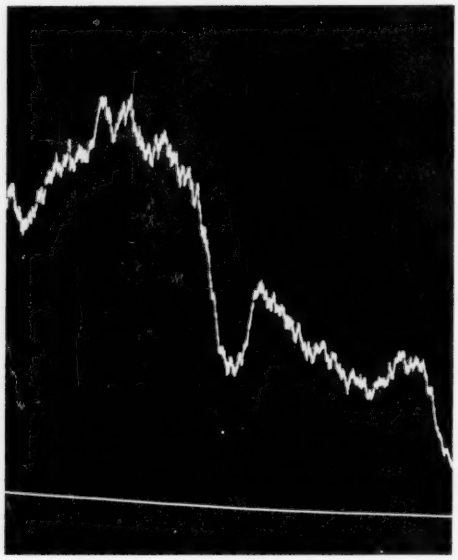

(d)

Fig. 3.

Electron-probe micrographs of a single C_2S grain

(a) Back-scattered electrons image (composition)
(b) Enlargement of detail in (a)
(c) X-ray (P K_α) distribution map of (a)
(d) X-ray (P K_α) line traverse in (c)

VOL
14
198

that although our results are very similar to those of Gutt and Smith [11], the SM is the key to the differences in C_3S and C_2S content in the clinker. We claim that the reason for these differences is non-equilibrium. Furthermore we suggest that the way to achieve non-equilibrium is by taking the P_2O_5 content into account in the calculation of the SM formula. The scarcity of the interstitial phase enhances non-equilibrium; some phosphate grains remain almost unreacted, some C_2S grains may contain up to 16% P_2O_5, while other grains may contain less than 2% and therefore transform into C_3S. To test this hypothesis one sample L-51-5 (Table 2) was heated and ground at periodical intervals during a long period (24 hours) to induce equilibrium. The mineralogy was examined by XRD at regular intervals. No significant change occurred within the first 11 hours. After 20 hours the concentration of C_3S dropped from 50% to 25% and after 24 hours to 17%. The results of these experiments: (a) support of the hypothesis of non-equilibrium and (b) show that this non-equilibrium does exist under the experimental conditions.

Conclusions

One of the effects of the presence of phosphate as carbonate-fluor-apatite in the raw material in the clinker reactions is to lower the melting point of the raw meal, thus increasing the liquid phase, and at times even causing a complete melt. This is probably due to two reasons, one the similarity in behaviour of P_2O_5 and R_2O_3 and second the probable catalytic influence of the fluorine which is part of the apatite. Taking into account the concentration of P_2O_5 in calculating the silica modulus (in other words increasing the silica concentration) solves this problem. This comparatively high silica concentration appears also to allow the use of raw meals higher in P_2O_5 (3%) than the suggested limit (2.25%, Nurse [6]). It should be stressed that these phosphate containing clinkers have been proved so far only to be mineralogically satisfactory and while preliminary tests of strength gave encouraging results, more work is needed before definite conclusions can be reached.

VOL. 14 1984

References

[1] Guye, F. Rev. Mater. Constr., 460, 7, 1954.

[2] Vlkov, V., Tabakama, N. Strit. Mat. Silic. Prom., 2, 6, 1967.

[3] Teoreanu, I., Tran van Huyrah. Rev. Roum. Chim., 15, 229, 1970.

[4] Salge, H., Thorman, P. Zement-Kalk-Gips, 26, 532, 1973.

[5] Rangarao, M.V. Cement (Bombay), 10, 6, 1977.

[6] Nurse, R.W. J. Appl. Chem., 2, 708, 1952.

[7] Nurse, R.W., Welch, J.H., Gutt, W. J. Chem. Soc., 220, 1077, 1959.

[8] Welch, J.H., Gutt, W. J. Chem. Soc., 222, 4442, 1961.

[9] Gutt, W. Nature (London), 197, 142, 1963.

[10] Gutt, W., Osborne, G.J. Trans. Br. Ceram. Soc., 69, 125, 1970.

[11] Gutt, W., Smith, M.A. U.K. Building Research Station, Current Paper 95/74, 1974.

[12] Thomas, J., Glass, H.D., White, W.A., Trandel, R.M. Clays and Clay Miner., 25, 278, 1977.

[13] Bentur, A., Ish-Shalom, M., Greenberg, T. Israel Ceramic and Silicate Institute, Research Report 1160 (in Hebrew), 1982.

[14] Schlaudt, C.M. Ph.D. Thesis, Pennsylvania State University, 1964.

[15] Nurse, R.W., Welch, J.H., Gutt, W. Nature 182, 1230, 1958.

[16] Gutt, W. U.K. Building Research Station, Current Paper 90/68, 1968.

Appendix

C_3S: $3CaO.SiO_2$

C_2S: $2CaO.SiO_2$

SM : Silica Modulus, $\frac{SiO_2}{Al_2O_3 + Fe_2O_3}$

LSF: Lime Saturation Factor, $LSF = \frac{CaO}{2.8SiO_2+1.65Al_2O_3+0.35Fe_2O_3}$

VOL
14
198

CEMENT and CONCRETE RESEARCH. Vol. 14, pp. 19-24, 1984. Printed in the USA.
0008-8846/84 $3.00 + 00. Copyright (c) 1984 Pergamon Press, Ltd.

A STUDY OF THE IRON PHASE AND ITS HYDRATION BEHAVIOUR IN HIGH ALUMINA CEMENT

K.S. Harchand, Vishwamitter* and K. Chandra
Department of Physics, University of Roorkee, Roorkee
247 667, India
*Department of Physics, Punjab University, Chandigarh
160 014, India

(Communicated by F.D. Tamás)
(Received May 17, 1983)

ABSTRACT

The Mössbauer spectroscopic investigations of dry sample of Indian high alumina cement (HAC) show that Fe_2O_3 occurs in the CF, CA and $C_2F_{1-x}A_x$ phases. The presence of CF component in this cement is being reported for the first time and its unambiguous detection has been made possible by the selectivity of Mössbauer spectroscopy. The spectra of hydrated HAC have been discussed in terms of hydration of the above mentioned compounds. The X-ray diffraction studies of dry as well as hydrated HAC are also included.

VOL. 14 1984

Introduction

The high alumina cement (HAC) is believed to be different from the portland cement and its main constituents are: CA and $C_{12}A_7$; and other compounds such as CA_2, β-C_2S, C_2AS, $C_2F_{1-x}A_x$ ($0.3 \leq x \leq 0.7$), C_6A_4MS and C_6A_4fS etc. The information in respect of composition and the hydration behaviour of the iron phase in this cement is very vague. In view of the selectivity of Mössbauer spectroscopy, this technique has been used by some workers (1-3) to study the iron phase in HAC. However, their studies have not helped in reducing the confusion. It was therefore decided to undertake the Mössbauer and X-ray diffraction investigation of HAC (dry as well as hydrated) and the findings are reported in this paper.

Experimental

The oxide composition, in mass percent, of the commercially supplied HAC, used in the present investigations is: CaO = 33, Al_2O_3 = 52, SiO_2 = 3, Fe_2O_3 = 5, MgO = 1, others = 6. It was hydrated at ambient temperature with distilled water, keeping initial water to cement ratio as 0.5 in four properly

sealed different tubes. After fixed intervals of time (1 day, 1 week, 2 weeks and 4 weeks), the hydrated cements from the tubes were vacuum dried and placed in a desiccator over silica gel. The fine powders of samples for X-ray diffraction and Mössbauer spectroscopic studies were prepared by grinding in a mortar.

The X-ray measurements on dry as well as hydrated samples were made at room temperature on PW 1140/90 Philips X-ray diffractometer using Cuk_{α} radiation.

The Mössbauer spectra have been recorded in the transmission geometry as described earlier (4,5) and analysed through computer fit on DEC-2050. These spectra, for dry and hydrated samples, are projected in Fig.1.

Results and Discussion

X-ray data

On the basis of the X-ray powder data available in the literature (6-8), various peaks in the diffractometer trace of dry HAC have been assigned as shown in Table 1.

This table includes the $CF_{1-x}A_x$ compound in addition to those listed earlier in the introduction. This assignment has been guided by our findings through Mössbauer spectroscopy, which are discussed in the next sub-section. As far as X-ray data are concerned, these alone are inadequate to give any unambiguous information about the iron-bearing compounds because the peaks corresponding to these are superimposed over those pertaining to CA and $C_{12}A_7$.

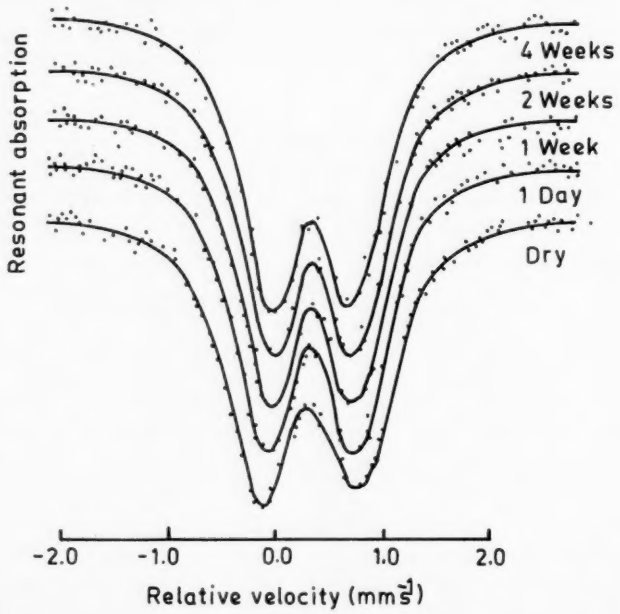

FIG.1

Mössbauer spectra of dry HAC and its hydrated samples

Table 1

The assignment of different X-ray peaks to the compounds in HAC

Bragg 2θ (in degrees)	Compound
24.0, 27.9	CA
29.2	C_2AS, C_6A_4MS
30.1, 31.1	CA
31.4	C_2AS, CA, C_6A_4MS
32.3	β-C_2S
33.3	$C_{12}A_7$, $CF_{1-x}A_x$, $C_2F_{1-x}A_x$
35.5	CA
35.8	CA, $CF_{1-x}A_x$
36.6	$C_{12}A_7$
37.4	CA, C_2AS
41.2	CA

A look on the traces for hydrated HAC samples showed that the peaks corresponding to CA alone almost disappear in one day. This is in accord with the fact that CA phase hydrates very quickly (9). However, the peaks at 2θ values 31.4° and 33.3° persist because the phases C_6A_4MS and $C_{12}A_7$ are known to be slow hydrating. The slow hydration of $C_{12}A_7$ is also supported by the fact that no peak is observed even in the cement hydrated for 4 weeks corresponding to 2θ = 31.0° due to C_2AH_8(H_8 H_2O), which is believed to be hydration product of $C_{12}A_7$. Various peaks in the traces for hydrated samples have been assigned as under (6,10).

C_3AH_6 : 20.6°, 26.6°, 28.5°, 32.0°, 39.3°, 44.6°

$C_3A\bar{C}H_{12}$($\bar{C}$=$CaCO_3$) : 23.4°, 31.4°

$Al(OH)_3$: 20.2°

C_4AH_{13} : 31.2°, 36.7°

C_2ASH_8: 31.2°, 36.1°

Once again, it is not possible to draw any unique conclusion about the hydration of iron bearing compounds from the X-ray data.

Mössbauer data

According to the available literature, ferric oxide present in HAC mainly occurs in $C_2F_{1-x}A_x$($0.3 \leq x \leq 0.7$) and can be distributed in CA and $C_{12}A_7$ phases. Therefore, it was anticipated that the Mössbauer spectrum of dry HAC would be broadened due to large number of Fe sites but qualitatively it should be similar to the spectra of other cements which have $C_2F_{1-x}A_x$ as the iron containing phase. However, it has been found that this spectrum is distinctly different from those for ordinary portland cement (OPC), portland pozzolana cement (PPC), portland slag cement (PSC) and sulphate

resisting portland cement (SRC) obtained in this laboratory (4,5). This observation is further corroborated by the difference in the spectra of HAC and SRC at 21 K: the HAC does not show ordering effect whereas it is very clear in SRC, even though Fe_2O_3 content of HAC is more than that of SRC (Fig.2).

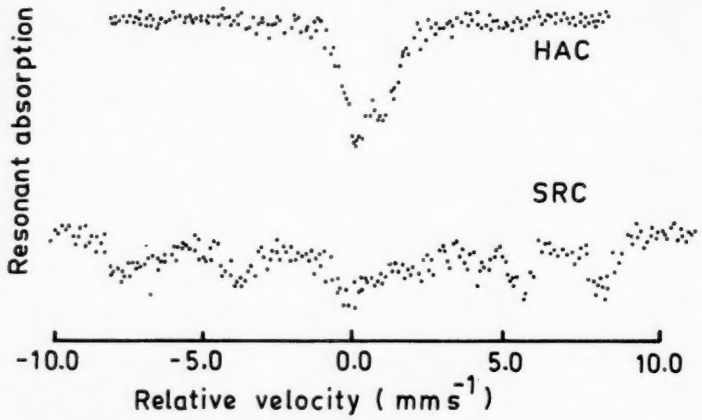

FIG.2
Mössbauer spectra of dry HAC and SRC at 21 K.

Instead, the envelope of HAC spectrum at room temperature closely resembled the spectrum of CF reported by Hudson and Whitfield (11) and those of the $CF_{1-x}A_x$ series, later on, recorded in this laboratory. A detailed study (12) of $CF_{1-x}A_x$ system revealed that for non-zero x there are two phases of CF and CA, which co-exist and that Fe and Al are distributed in CA and CF phases, respectively.

In view of the above comments we were led to believe that CF is the major iron-containing phase in HAC. In addition, Fe also occurs in CA, $C_2F_{1-x}A_x$ and other phases. Now the number of Fe sites in CF, CA and $C_2F_{1-x}A_x$ are 2,6 and 2, respectively, and all these are non-cubic. But fitting such a large number of doublet patterns in a spectrum covering small span of velocity is not advisable. Therefore, the analysis of the spectrum of dry HAC has been carried out in terms of lesser number of sites and a good fit is obtained by assuming four different Fe sites. The parameters so obtained are listed in Table 2. A comparison of these parameters with those for the compound CF (11, 12), CA (12) and the phase $C_2F_{1-x}A_x$ (4,5) in the cement, together with the fact that the behaviour of the compound in the cements is different from that in pure state, shows that the first two sites can be assigned to CF, the third site to $C_2F_{1-x}A_x$ and the fourth site to CA phases. The distribution of Fe in the six sites of CA and its presence in small quantity in the phase $C_{12}A_7$ leads to broaden the Lorentzian lines.

Table 2

The Mössbauer parameters of dry and hydrated HAC*

Sample	Isomer shift (w.r.t.iron) mms^{-1}			Quadrupole splitting mms^{-1}			Percent relative Intensities			Line width mms^{-1}
	δ_1	δ_2	δ_3	ΔE_1	ΔE_2	ΔE_3	I_1	I_2	I_3	Γ
Dry	0.31	0.31	0.23	1.03	0.70	1.54	29	29	21	0.57
1 Day	0.32	0.31	0.22	1.03	0.59	1.52	41	44	15	0.49
1 Week	0.33	0.31	0.25	0.98	0.55	1.52	40	46	14	0.47
2 Weeks	0.33	0.31	0.24	1.00	0.58	1.54	37	50	13	0.49
4 Weeks	0.33	0.31	0.22	1.04	0.57	1.60	37	55	8	0.50

*Parameters for the fourth site corresponding to CA in dry cement are δ_4= 0.21 mms^{-1}, ΔE_4= 0.53 mms^{-1} and intensity I_3= 21 percent whereas this site is absent in hydrated cement.

In order to facilitate the resolution of the spectra of hydrated HAC, the Mössbauer spectra of the CF, Fe : CA (Fe substituted CA) and $C_2F_{0.5}A_{0.5}$ compound hydrated for different intervals have been recorded and the parameters derived from the computer fit are given in Table 3.

Table 3

Mössbauer parameters of various iron bearing phases hydrated for different intervals of time

Sample	Isomer shift (w.r.t.iron) mms^{-1}		Quadrupole splitting mms^{-1}		Percent relative Intensities		Line width mms^{-1}
	δ_1	δ_2	ΔE_1	ΔE_2	I_1	I_2	Γ
CF (1 Week)	0.35	0.35	0.73	0.34	48	52	0.42
Fe : CA (2 Days)	0.32	0.23	0.82	0.43	63	37	0.48
$C_2F_{0.5}A_{0.5}$ (4 Weeks)	0.36	0.34	1.01	0.65	10	90	0.53

The isomer shift and quadrupole splitting values for the two sites of hydrated CF are very close to the corresponding magnitudes for dry CF (11,12). This implies that hydration of CF proceeds very slowly and that there is no significant change in one week. Since CA phase hydrates very fast, as shown by the X-ray diffractometer traces also, and our Fe : CA system does contain CF phase, we can only say that hydration of CA leads to formation of such compounds whose Mössbauer spectra can be fitted into two components with the parameters listed in Table 3. In the case of $C_2F_{0.5}A_{0.5}$, hydrated for four weeks, the major product has δ = 0.34 mms^{-1} and ΔE= 0.65 mms^{-1}.

In view of the above observations regarding the nature of the Mössbauer parameters for the hydrates of pure compounds, the spectra for the hydrated HAC samples have been analysed in terms of three doublet patterns and the resulting parameters are also included in Table 2. While interpreting these data, it has been kept in mind that parameters for various phases and their hydrates in the cement are modified as compared to those for pure ones.

Since $C_2F_{1-x}A_x$ is a slow hydrating phase (13), its hydration in the cement may not be complete in four weeks. The third site in the hydrated HAC should be due to unhydrated $C_2F_{1-x}A_x$ and decrease in its intensity down the column is expected on its slow hydration with time. The hydrated phase appears to contribute to the second site (qualified by the parameters δ_2 and ΔE_2) as the parameters for hydrated $C_2F_{0.5}A_{0.5}$ are close to these. As more and more $C_2F_{1-x}A_x$ is hydrated, I_2 goes on increasing. In the case of CF sites, it is expected that the parameters in hydrates should also be close to those in the dry cement, as has been observed for the hydrated pure CF compound. Accordingly, it is concluded that the site assigned to the parameters δ_1 and ΔE_1 in dry powder continues to contribute to first site and that with parameters δ_2 and ΔE_2 to the second site. Lastly, the hydration of the CA phase seems to contribute to the two sites labelled with subscripts 1 and 2, making effective contribution of about 13% to the first site. The decrease in the intensity of the first site with time of hydration is attributed to the fact that slow hydration of CF may lead to some increase in intensity of the site with lower quadrupole splitting at the cost of the site with higher quadrupole splitting.

Acknowledgements

We are grateful to the Associated Cement Companies Ltd., Thane(India) for making available the HAC sample.

References

1. F. Wittmann, F. Pobell and W. Wiedemann, Z. Angew Physik, 19, 281 (1965).
2. P.Pascual and C. Lupiani, Rev.Chim. Minerale 16, 174(1979).
3. C.L.Honeybourne, Cem. Concrete Research 10, 35(1980).
4. K.S. Harchand, Vishwamittar and K. Chandra, Cem. Concrete Research 10, 243 (1980).
5. K.S.Harchand, R.Kumar, Vishwamittar and K.Chandra,Int.Conf. on the Applications of Mössbauer Effect, Jaipur,India,1981. Proc.of the Indian National Science Academy p.296(1982).
6. H.F.W. Taylor, The Chemistry of Cements, Vol.2, Academic Press, London, p.347(1964).
7. B.F. Decker and J.S. Kasper, Acta. Cryst.10, 332 (1957).
8. ASTM X-ray Diffraction Files, No.20-199.
9. H.F.W. Taylor, The Chemistry of Cements, Vol.1, Academic Press, London, p.13(1964).
10. ASTM X-ray Diffraction Files, No.19-210.
11. A. Hudson and H.J. Whitfield, J.Chem. Soc.(A),376 (1967).
12. K.S.Harchand and K. Chandra, Cem.Concrete Research(Accepted for publication).
13. J.F. Young, Cement Production and Use(Proc. Engg. Found. Conf.)1, 117(1979).

VOL 14 198

CEMENT and CONCRETE RESEARCH. Vol. 14, pp. 25-30, 1984. Printed in the USA.
0008-8846/84 $3.00 + 00. Copyright (c) 1984 Pergamon Press, Ltd.

COMPRESSIVE STRENGTH VERSUS RESIDUAL POROSITY IN POLYMER IMPREGNATED CEMENT PASTES

R.Sh.Mikhail, A.M.Mousa, S.A.Abo-El-Enein and M.S.Marie

Department of Chemistry, Faculty of Science, Ain Shams University Abbassia, Cairo, Egypt

(Communicated by F.D. Tamás)
(Received May 20; in final form June 13, 1983)

VOL. 14 1984

ABSTRACT

Impregnated cement pastes were prepared from fine cement of Blaine area 600 m^2/kg using various initial W/C ratios in the range 0.25-0.70, cured for various durations, and by using styrene or methyl methacrylate, which were polymerized *in situ* by thermal treatment. The polymer effect on compressive strength was found to be variable and depends on pore size. Upon impregnation, low porosity samples show measurable reduction in zero strength porosity, whereas high porosity samples show measurable reduction in the strength at zero porosity. Enhancment of compressive strength takes place at an optimum range of porosity and gel/space ratio.

INTRODUCTION

Polymer impregnated concretes provide definite advantages over conventional concretes. The first investigations of impregnated polymer concrete tried mainly to increase the quantity of absorbed and polymerised monomer because this gave a greater decrease in the original porosity of concrete and a subsequent improvement in physico-mechanical properties. However, the technical considerations reported by Auskern (1) revealed that pore impregnation with polymers, even when complete, does not give the same strengths that theoretically could be reached by a cement paste without pores. Munoz, Escalona and Ramos (2) also showed that in order to develop true composite action a minimum amount of polymer inside the specimen is required. This critical amount depends on the characteristics of the polymer.

Contrary to prevailing opinion (3) and in agreement to what is stated by Auskern (1) and by Rio and Biagini (4) our experience confirms the non-equivalence between the solid fraction of the cement paste and polymer on mechanical characteristics of impregnated concretes. Recent studies revealed additional factors

which affect the mechanical properties of polymer impregnated concrete, such as the pore structure of the solid matrix, the degree of polymerization and average molecular weight of the polymer inside different size pores (5), and the distribution of the polymer inside the porous matrix in concrete (6). The present investigation reports some recent studies on polymer-impregnated cement pastes concerning the various factors affecting the compressive strength of the impregnated pastes, namely the residual porosity and the gel/space ratio. It will become evident that the nature of the polymer or its state of polymerization inside the pores can not be overlooked in such studies

EXPERIMENTAL

The cement was the same one used in a previous investigation (7). It was ground to a Blaine area 600 m^2/kg. The monomers were styrene (S) and methyl methacrylate (MMA), using benzoyl peroxide as an initiator. Impregnation was carried out by evacuating the sample then pressurizing the monomer under nitrogen at 1 atmosphere, using the same technique described earlier (7). Samples IB, IIB, IIIB, IVB and VB will indicate pastes mixed with 0.25, 0.30, 0.40, o.50 and 0.70 W/C respectively, and the impregnated samples will carry the letter S or M beside the notation to indicate impregnation with polystyrene or polymethyl methacrylate respectively

The porosity (ϵ) as well as the residual porosity (ϵ_r) for the impregnated samples were obtained from the water loss at 110 °C after water imbibition.

RESULTS AND DISCUSSIONS

A. Zero strength porosity and strength at zero porosity:-

In a semi-empirical model derived by Auskern (1), it was assumed that the strength of the composite is a function of the volume of cement paste and the final porosity of the sample, i.e. its residual porosity. According to this model the final strength of the composite is independent of the mechanical properties of the polymer. On the other hand, Bell et al. (8), in their work on polymer impregnated water saturated samples, have indicated that the polymer had a bigger effeect in reducing compressive strength than an equivalent volume fraction of pores. Our results indicate that the polymer effect is variable and depends on the pore size.

In the present investigation the variation of compressive strength with porosity in the control samples (ϵ) and with the residual porosity in the impregnated samples (ϵ_r) has been studied for all samples investigated and typical set of data are present in Figs 1 and 2 for BM samples and for the BS samples , respectively.

Fig.1 shows that the curve which represents the variation of compressive strength with porosity (ϵ) for the control samples, runs almost parallel to curve 1 which represents the variation of compressive strength with residual porosity (ϵ_r) for the same samples after impregnation, This parallelism however, holds only for samples I, II, III and IV BM mixed with W/C ratios 0.25, o.30, o.40 and 0.50, while for samples V BM mixed with W/C ratio 0.7, curve 2 was obtained which obviously has a totally different trend than curve 1. At the highest W/C ratio polymer loading has a much decreased effect in reducing strength with porosity.

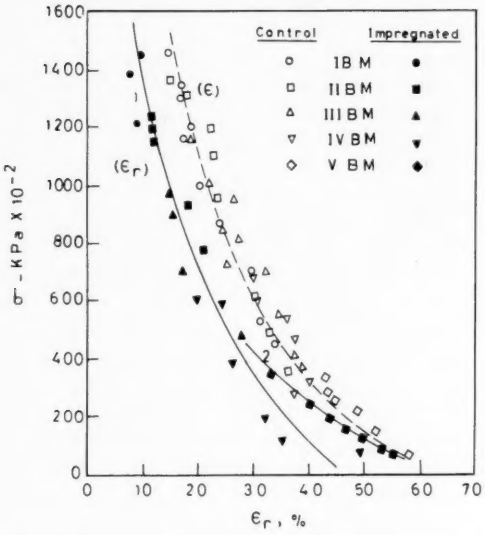

FIG. 1

Variation of σ (kPa) with (ϵ_r), % for the BM samples.

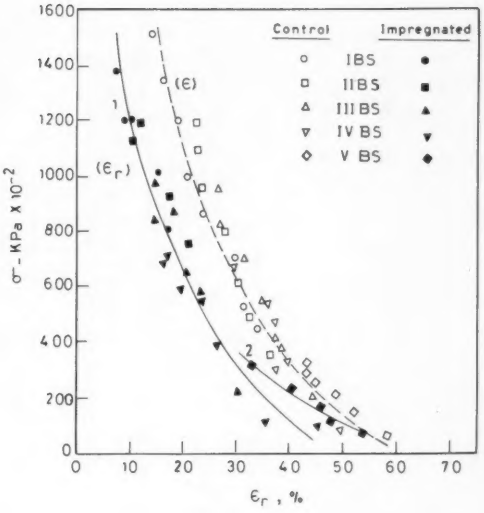

FIG. 2

Variation of σ (kPa) with (ϵ_r),% for the BS samples.

Using poly styrene instead of polymethyl methacrylate as an impregnant (Fig. 2), reproduces the same phenomenon except that curves 1 and 2 are not as perfectly parallel as they are in Fig.1, indicating that the polymer in this case (poly styrene), has some additional effect at all W/C ratios, but this effect is magnified at the highest W/C ratio used. In both figures , however, the near parallelism between the curves for the control samples and for the impregnated samples indicates that porosity is still a main factor affecting the strength. Curve 2 indicates also that the effect of polymer is variable in different size pores.

The data could be correlated by using the semi-empirical relation derived by Schiller (9), namely

$$\sigma = D \ln \frac{\epsilon_o}{\epsilon} \quad \ldots\ldots\ldots\ldots\ldots\ldots (1)$$

Where σ is the compressive strength, ϵ is the porosity of the hardened cement paste, ϵ_o is the zero strength porosity, and D is a constant , which represents the slope of the straight line obtained by plotting σ vs $\ln\epsilon$. Changes in this slope not only indicate changes in zero strength porosity, but also changes in the values of strength at zero porosity. This equation was used by Roy et al (10) and by Roy and Gouda (11,12) to correlate their data obtained on "hot" and other pressed samples. In this investigation results obtained indicate the following:-

1. Impregnation with MMA for samples mixed with W/C ratios up to 0.5 leads to reduction in the value of zero strength porosity, while for the samples mixed with W/C ratio 0.7 impregnation shows no reduction in this value. On the other hand , samples mixed with W/C ratios up to 0.5 shows a slight reduction in the value

of strength at zero porosity below that of the unimpregnated (control) samples (430 MPa), while the sample mixed with W/C ratio 0.7 shows upon impregnation a drastic reduction in the value of strength at zero porosity to reach 225 MPa.

2. Impregnation with S leads almost to the same effect as impregnation with MMA. Thus for samples of W/C ratios less than 0.5, there is a noticeable reduction in the value of the zero strength porosity upon impregnation , while above W/C ratio 0.5 there is no reduction in the same value. However for samples mixed with low W/C ratios the effect of impregnation on reducing the values of strength at zero porosity is more obvious than by using MMA and the strength at zero porosity for low W/C ratios samples impregnated with S was reduced from 430 MPa to become 300 MPa, while for the leaner sample mixed with W/C ratio 0.7, the value is further reduced to 210 MPa.

These results indicate that impregnation of the low-porosity samples leads to a measurable reduction in the zero strength porosity but to a slight reduction in the strength at zero porosity. On the other hand impregnation of higher porosity samples leads to no change in the zero strength porosity but to measurable reduction in the strength at zero porosity.

B. Relative compressive strength-residual porosity:-
The results presented in the previous section show that polymer impregnation leads to variable effects in low porosity and in high porosity samples. These results also show that residual porosity is still a main factor influencing the strength of the impregnated pastes. It would be of interest therefore, to present plots of relative compressive strength vs residual porosity, to show the influence of porosity (space) in affecting the compressive strength of the composite obtained by impregnation. These plots are shown in Figs. 3 and 4 for samples impregnated with PMMA and PS respectively. Relative compressive strength denotes the compressive strength of the impregnated samples to the control samples prepared under identical conditions. The results show that the relative compressive strength values increase as the residual porosities increase . This improvement in strength is the more pronounced the lower the W/C ratio of the sample, and impregnation with PMMA has a bigger effect on improving compressive ttrength than PS. However this improvement of compressive strength with residual porosity continues only up to a certain critical value of residual porosity then a retrogression in the relative strength values is noticed to take place giving a pronounced maximum in the relative compressive strength-residual porosity relationship. This behaviour is more obvious for the leaner samples. This trend is most probably related to the state of the polymer inside pores, and that the gain in strength with porosity (the ascending branch in the relationship) is due to polymerization into higher molecular weight polymer, a mechanism which is sterically assisted (5), while beyond a certain value of porosity the predominance of wide pores and voids , incompletely filled by the polymer, causes such retrogression. The distribution of the polymer along the pore and void surfaces will be a subject of a forth comming publication(6).

C. Relative compressive strength-Gel/space ratio:-
In comparing the change in relative strength, not as a function of the porosity (space) available , but as a function

VOL. 14 1984

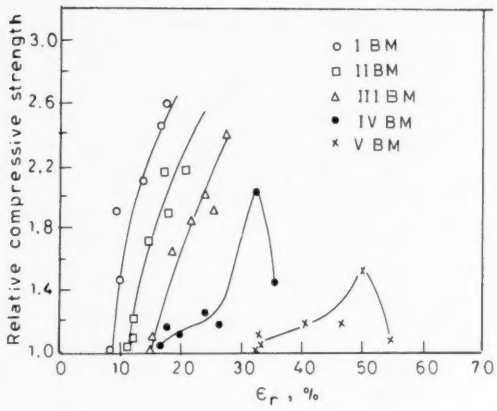

FIG.3

Variation of relative compressive strength with ϵ_r, % for the BM samples.

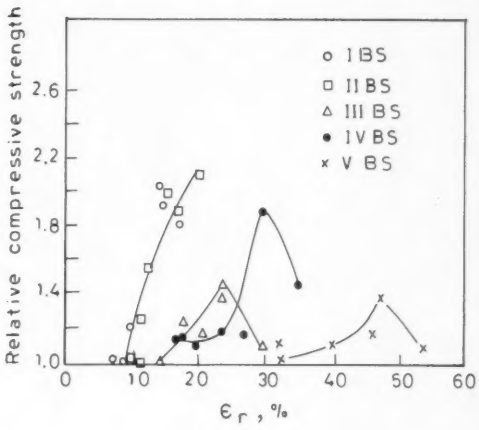

FIG.4

Variation of relative compressive strength with ϵ_r % for the BS samples.

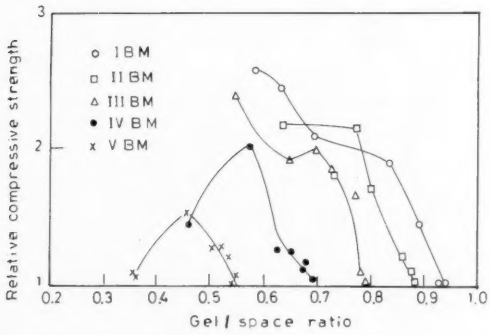

FIG.5

Variation of relative compressive strength with the Gel/space ratio for the BM samples.

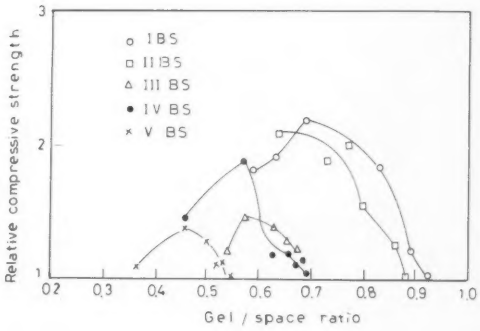

FIG.6

Variation of relative comressive strength with the Gel/space ratio for the BS samples.

of the solid to space available, known as the gel/space ratio, the relations shown in Figs. 5 and 6 were obtained .
Figures 5 and 6 are self-explanatory and they show in a clear way that the enhancement of compressive strength due to polymer impregnation is strongly operating at an optimum range of gel/space ratio, and that this range is the wider the lower the W/C ratio. Below this optimum range there is an ascending branch along which the voids and wide pores become filled with hydration products and the pore size is reduced, and beyond this optimum range , there is a descending branch along which the pore size is further reduced due to the accumulation of more hydration products.
There is obviously a certain range of optimum pore size along which polymer impregnation becomes benificial for improving compr-

essive strength. The state of the polymer inside pores is obviously different from that in bulk (5).

Conclusions

1. In polymer-impregnated hardened cement pastes, the polymer effect on compressive strength is variable and depends on the pore size.
2. Impregnation of low-porosity samples leads to a measurable reduction in the zero strength porosity but to a slight reduction in the strength of zero porosity.
3. Impregnation of high-porosity samples leads to almost no change in the zero strength porosity but to measurable reduction in the strength at zero porosity.
4. The enhancement of compressive strength due to polymer impregnation is strongly operating at an optimum range of pore size. The state of the polymer in this pore size range is expected to be the most favorable for improving the strength and is expected to be different from that in bulk polymerization.

References

(1) A.Auskern,"A model for the Strength of Cement-polymer Systems" Brookhaven National Laboratory, Upton, N.Y.,
(2) A. Munoz-Escalona and C.Ramos, Cement and Concrete Res. 6, 273 (1976)
(3) J.T. Dikeon et al "Concrete-Polymer Materials" Fourth Topical Report, MML 50328 and USER rec-Erc- 72-10, Jand. 1972.
(4) A. Rio and S. Biagini, "Recent Progress in the field of Polymer Impregnated Concretes", Proceedings of the First International Congress on Polymer Concretes" . The concrete society, UK, 1975, p. 17.
(5) R.Sh. Mikhail, A.M. Mousa, S.A. Abo-El-Enein, M.S. Marie, Cement and Concrete Res., Accepted for publication.
(6) R.Sh. Mikhail et al to be published; M.S. Marie, Ph.D. Thesis, Ain Shams University, 1982.
(7) R.Sh. Mikhail, S.A. Abo-El-Enein, A.M. Mousa and M.S. Marie Preprints, "Polymers in Concrete" Third International Congress on Polymers in Concrete, Koriyama, Japan, May 1981, Vol II p. 729
(8) R.L. Bell and R.G. Dingley, Proceedings of the first International Congress on Polymer Concretes, p. 162-167 1975.
(9) K.K. Schiller, Cement and Concrete Res., 1, 419 1971.
(10) D.M. Roy, G.R. Gouda and A. Bobrowsky, Cement and Concrete Res., 2, 349 1972.
(11) D.M. Roy and G.R. Gouda, Proc. 6 th, Int. Cong. Chem. Cement, Moscow, Vol. II, Book I, 310 1971.
(12)D.M.Roy and G.R. Gouda, J.Amer. Ceram. Soc. 56, 549 1973.

VOL. 14 1984

CEMENT and CONCRETE RESEARCH. Vol. 14, pp. 31-42, 1984. Printed in the USA.
0008-8846/84 $3.00 + 00. Copyright (c) 1984 Pergamon Press, Ltd.

FRACTURE OF GLASS FIBER REINFORCED CEMENT

A. Bentur(*) and S. Diamond
School of Civil Engineering, Purdue University
West Lafayette, IN 47907

(Communicated by A.J. Majumdar)
(Received May 23, 1983)

ABSTRACT

Fracture patterns produced when a crack advancing from a notch in cement paste intersected a Cem FIL-2 glass fiber strand placed perpendicular to it were studied. The specimens were small notched compact tension specimens that could be wedge loaded in the scanning electron microscope chamber using a wet cell. Four distinct cracking patterns were identified. In most cases the fiber caused a shift in the crack path and in some specimens, microcracking and separation of the crack into 2 to 4 branches were observed. The filaments maintained their continuity and bridged over the crack. Similar tests with E-glass fibers after accelerated curing revealed brittle behavior in which the crack path was straight and many filaments were broken.

Introduction

The incorporation of fibers in hydrated portland cement paste produces a composite of tensile strength and ductility significantly greater than that of a hardened cement paste (hcp) matrix.

Present understanding and modelling of the properties of these composites is not in an entirely satisfactory state. It is clear from the original investigations of Romauldi et al (1,2) that the fibers act as crack arrestors, and that shear stresses developed at the fiber-hcp interfaces tend to close the cracks in the vicinity of the fiber; hence the importance of fiber spacing as a fundamental parameter. Some investigators (3,4) have not found the expected inverse proportionality between first-crack stress and fiber spacing; others (5,6) have proposed alternative methods of calculation for the spacing factor. In one such proposal (6) the interfacial bond stress is used in addition to geometric parameters to calculate an "effective" spacing factor.

A fairly comprehensive model by Aveston et al (7-9) is based on an assumed multiple cracking process in which the matrix is viewed as being subdivided by multiple cracking into a series of blocks; the quantitative

(*) On sabbatical leave from the Technion, Israel Institute of Technology, Haifa, Israel

predictions of the model depend very much on the specifics of the fiber-hcp interaction assumed. Aveston et al assumed frictional stress transfer at a constant shear stress; Laws et al (10,11) subsequently extended the treatment to non-uniform interfacial shear stresses. Initial elastic stress transfer is assumed but allowance for frictional stress transfer after bond failure is also provided; such failure is expected in the highly-stressed zone around the fiber at the location of crack intersection with it.

These models provide some basis for interpreting the significance of pull-out tests of individual fibers (12-16), and emphasize the importance of the microstructure of the interfacial hcp region surrounding the fibers (16-20). In a recent review (21) the complexity of the actual bond and the need to consider the simultaneous contributions of elastic and frictional bonds was stressed.

The role of the interface is of special importance in glass-reinforced cement (GRC) products, where significant changes occur on weathering or water curing (18-20). There is a progressive secondary deposition of hydration products, mainly CH* between individual filaments in the strands of the glass fibers, at least partly reducing the ductility of the composite, and degradational changes in the surface of the glass fibers themselves may contribute to weakening. Both effects may influence the properties of the composites and result in significant loss of ductility and some loss of strength. The mechanics of such changes have been discussed by Stucke and Majumdar (18) in terms of loss of compliance at the interface as compared to air-cured GRC, where energy can be absorbed at the interfacial zones by subsidiary cracking and pull-out. Such changes have been incorporated in a fracture mechanics treatment of GRC by Nair (22).

Fracture mechanics has been applied to fiber-reinforced cement composites (5,23). This area has recently been reviewed by Mindess (24), who emphasized that linear elastic fracture mechanics parameters for hcp are not very sensitive to the incorporation of fibers, and therefore do not provide a useful means for characterizing such systems.

The analytical approaches so far discussed, e.g. crack arrest, multiple fracture, and G_c calculation (on the basis of energy required for stripping and debonding the fibers) have assumed the existence of straight finite crack growth. Optical microscopic studies such as those of Swamy (25) and Chan and Patterson (26) of the cracks produced in slow crack growth ahead of a notch, indicated the development of a complex crack pattern of fine branching cracks, with discontinuities near the fibers and some crushing of material inside large cracks. It is obvious that the assumption of straight, finite crack growth is a gross oversimplification. The real cracking behavior undoubtedly reflects microstructural variations in different systems, as well as differences in loading patterns and rates.

The foregoing emphasizes the need for detailed microstructural investigation of the processes occurring during fracture of fiber reinforced cement composites.

Recently a system was developed by Mindess and Diamond (27-30) for studying the details of crack propagation using a wedge-loaded specimen with the loading carried out within a scanning electron microscope (SEM). The specimen could be studied without prior evacuation and coating in a wet environment within the SEM chamber (30). In the present work this system was

* Cement chemistry notation is used: C = CaO; S = SiO_2; A = Al_2O_3; F = Fe_2O_3; H = H_2O

VOL
14
198

applied to the study of fracture patterns produced when a crack advancing from a notch intersects a glass fiber strand placed perpendicular to it, with the primary aim of classifying, documenting, and understanding the various effects produced.

The systems studied were primarily hcp incorporating strands of alkali resistant (AR) glass fibers cured in water for up to 14 days. Some preliminary work is also reported on pastes incorporating E-glass fiber strands subjected to accelerated deterioration conditions (90°C in water for 11 hours) prior to testing.

Experimental

Loading Arrangement

The experimental arrangement described by Mindess and Diamond (27) was used in the present study. This employs a small notched compact tension specimen, as shown in Fig. 1, which is wedge-loaded within the chamber of the ISI Super III-A SEM.

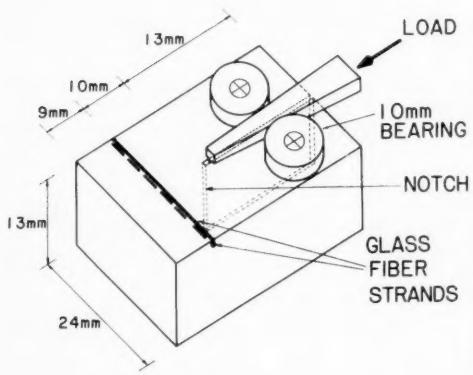

FIG. 1

Description of specimen and loading arrangement.

In the present work a modified loading scheme was developed to take into account that only the interaction of the propagating crack with a fiber at the upper surface of the specimen can be observed. A plane stress loading condition on a very thin specimen only slightly thicker than the glass fiber strand would be ideal, but such a specimen would be extremely difficult to cast and manipulate. The more practical alternative chosen here was to apply the wedge load only at the exposed face of the specimen, where the glass fiber strand is prepositioned. Two glass fiber strands, each composed of 208 filaments, were placed one above the other, as shown in Fig. 1. The tensile field is greatest at the top of the specimen and diminishes with depth. While this arrangement is by no means ideal it has been shown in preliminary testing to be effective, reproducible, and well suited to the qualitative study contemplated.

Specimen Condition and SEM Observation

The SEM observations were made using the wet environmental cell and the Robinson detector system described by Diamond et al (30). The pressure in the cell was maintained at 0.4 torr, with the air pumped into the cell being passed through two successive bubblers. This permitted testing of uncoated specimens that were in the saturated surface dry (SSD) condition; the elimination of the necessity for drying of specimens is of prime importance in hcp systems that may shrink and develop microcracks due to loss of water.

Use of the wet cell with air-dry (AD) uncoated specimens was found to improve resolution considerably. This was of particular importance in observation of the microstructural details present in the hcp interfacial zones around the fine (10 μm) glass filaments. Therefore the tests included

observations of companion SSD and AD specimens that were cured in water for similar time periods.

Specimen Preparation and Curing

The portland cement used was ASTM Type I cement of 3300 Blaine fineness. Its chemical composition is as follows: SiO_2 - 21.5%; Al_2O_3 - 5.4%; Fe_2O_3 - 2.3%; CaO - 55.2%; MgO - 1.22%; SO_3 - 2.97%; K_2O - 0.78%, Na_2O - 0.10%; L.O.I. - 0.80%.

Pastes were prepared at water:cement ratio 0.35 by a special mixing procedure involving shaking in an evacuated container after removal of dissolved air from the water; this procedure minimizes air bubble incorporation. In all cases the specimens were cast in molds of the dimensions given in Fig. 1, with 13 mm long and about 0.6 mm wide notches being cast into the specimens.

As previously indicated, most of the work was done on paste specimens incorporating AR glass fiber strands. These were Cem-FIL 2 fibers (Pilkington Bros., Ltd) arranged in strands. The compact tension paste specimens incorporated two prepositioned strands placed at about 0.2 mm above the bottom of the mold, with the paste being cast around and above it. Compaction was then secured on a vibrating table. The specimens were then cured for 1 day in a closed chamber positioned over a free water surface, demolded, and cured subsequently in saturated limewater.

Four specific curing regimes were followed. SSD specimens were cured in limewater for 3 or for 13 days after demolding and tested on the 4th or 14th day. Specimens designed for AD testing were cured in water for the same periods followed by air drying for 1 day in laboratory air. A total of 25 specimens of these different types were tested.

A day before the end of the water curing period the specimens were briefly removed from the limewater container and the lower surface of each (where the glass fiber strands had been prepositioned) was wet ground with No. 240 grit until the filaments were exposed. Further brief polishing was accomplished with No. 600 and then No. 1200 grit, and the samples were washed and returned to the curing chamber.

In addition to the Cem-FIL 2 specimens, several specimens were prepared using E-glass fiber strands obtained from PPG Industries. These specimens were prepared in the same way except for the curing regime. After demolding, these specimens were cured for 3 days in limewater and then immersed in water maintained at 90°C for either 3 hours or for 11 hours. They were subsequently cooled to room temperature in water, polished as described previously, and air dried for 1 day.

Results

Hardened Cement Paste Incorporating Cem-FIL 2 Glass Fiber Strands

Observations Prior to Loading

The typical appearance of the filaments on the ground and polished surface of specimens with two strands of Cem-FIL 2 fibers prior to loading is shown in Fig. 2a. The spacing between most of the filaments was about 3 μm or less, too small to admit most cement grains, and comparatively little material was found between individual filaments. The surfaces of the filaments tended to be clean, except for occasional particles such as that shown

VOL
14
198

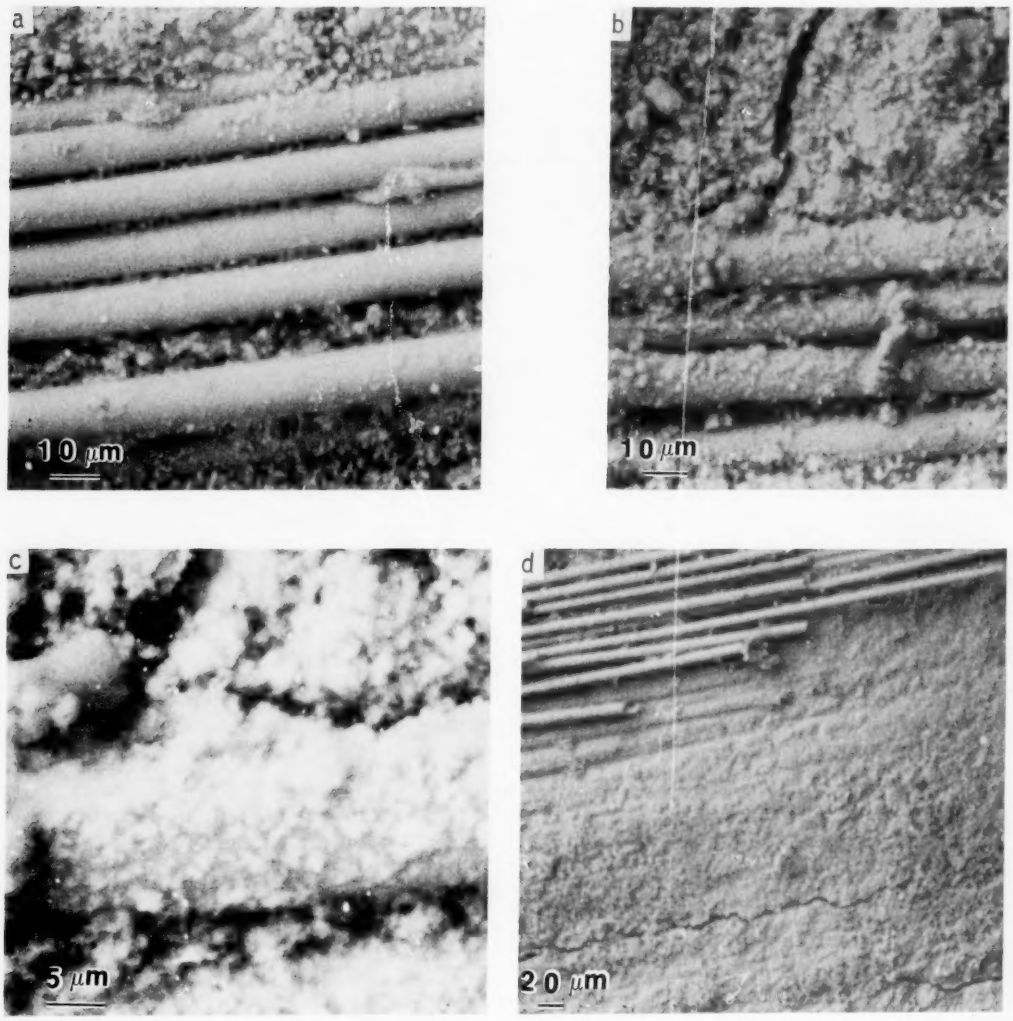

FIG. 2

The surface (before loading) of an air dry specimen, cured for 3 days in water. (a) Zone with no shrinkage crack. (b), (c), Perpendicular shrinkage crack. (d) Parallel shrinkage crack.

in Fig. 2b. It was not possible to tell from such micrographs whether these are hydration products or grit particles that were not washed off in specimen preparation. These characteristics are similar to those reported by Stucke and Majumdar (18) and Cohen and Diamond (20) for fibers embedded in cement matrix that was hydrated for short time periods of several weeks.

Narrow shrinkage cracks were observed on the surface of about half the specimens prepared for fracture testing, especially those that were air dried after only 4 days of curing (Fig. 2b & c). Such cracks were observed in 5 of 6 specimens air dried after 4 days; in 5 of 8 specimens air dried after 14 days; in 2 of 4 specimens examined SSD after 4 days; and in only

1 of 7 specimens examined SSD after 14 days. The width of these cracks was typically less than 3 μm, and most of them were perpendicular to long axis of the filament, and disappeared a few tenths of a millimeter away from it. Typically about 4 such cracks occurred in a specimen. Sometimes local debonding could be observed in the vicinity of the cracks, the separation taking place not at the filament-hcp interface but slightly away from it, as seen in Fig. 2c. In no case was adhesive debonding observed at the filament-hcp interface itself, and there was always contact between matrix particles and the outer filaments in the strands. The appearance of a typical interface on the polished surface is shown in Fig 2a; no apparent defects can be seen.

The perpendicular shrinkage cracks may be the result of restraint exercised in the axial direction by the filaments, which would generate tensile stresses in the nearby hcp tending to shrink in this direction; such tensile stresses could produce the local tensile failures observed.

Shrinkage cracks parallel to the axis of the filaments were found only in 2 of the many specimens observed; one of them is illustrated in Fig. 2d. Also evident in Fig. 2d is the fact that in this specimen, the polishing process was taken far enough so that some of the filaments on the surface were cut through. Such filament damage was restricted to the surface filament or filaments only, and the underlying filaments, in the 208-filament strand should have remained intact.

Loading Cracks

The crack produced by the wedge-loading arrangement, and specifically the effects on it produced by the presence of the glass filaments constitute the basic focus of this study.

A typical load-time plot as obtained in these trials is shown in Fig. 3. The load rapidly builds up to an initial peak, whose value ranges from about 20 to 30 N. Coincident with the attainment of the peak load the crack appears and propagates rapidly past the glass fiber strand. The advance of the wedge is stopped for observation (stage 1) then resumed, halted again for observation (stage 2) and resumed until the maximum possible movement of the wedge has been accomplished (stage 3). The crack depth at the first stage of loading was much greater than that of the filaments in the strand placed below the surface. By the third stage of loading the crack depth reached the bottom of the specimen.

The crack path observed after the first loading stage was initiated at the tip of the notch, traversed toward the glass fiber strand in its path, deviated and shifted on intersecting the glass fiber strand, and then continued to run to the edge of the specimen. None of the filaments were broken in this process. The additional movement of the wedge in stages 2 and 3 resulted in widening of the cracks, but the filaments maintained their continuity and mechanically bridged the underlying cracks.

The nature of the crack that propagated from the notch was similar to that described by Diamond and Mindess (28). On a macroscale it seemed to run straight, but at higher levels of magnification, a zig zag pattern could be observed. When it approached the glass fiber strand its width was in the range of 10 to 25 μm.

The interaction of the crack with the glass fiber strand often changed its propagation path, causing it to shift from its original course. In some cases microcracks could be observed around the crack-glass fiber strand

VOL
14
198

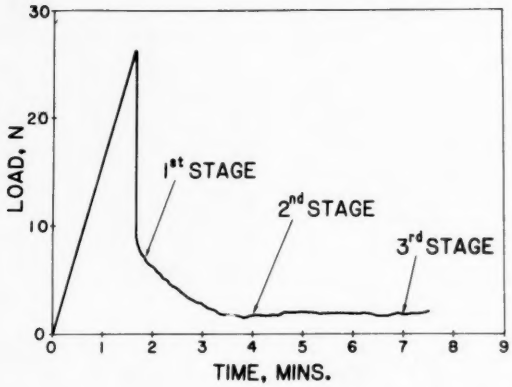

FIG. 3

Typical load-time curve.

intersection zone. The cracking modes in the vicinity of the fiber were variable, and four different patterns were recognized. They were labeled as Types I, II, III and IV, and are shown schematically in Fig. 4. Out of 25 specimens tested the number of each cracking pattern were 1, 5, 16 and 3 for Types I, II, III and IV respectively. Although the number of tests is too small for reliable statistical analysis these numbers indicate that Type III tends to be most common, while Type I is probably rare. The numbers do not show a clear cut trend with age, moisture content or presence of shrinkage cracks prior to loading. Type III fracture, for example, was observed with all types of specimens.

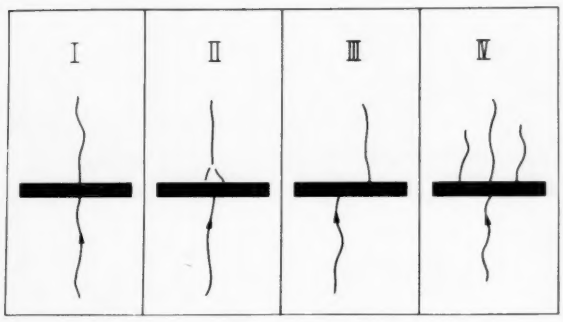

FIG. 4

The four cracking patterns observed at the intersection of the propagating crack and the glass fiber strand.

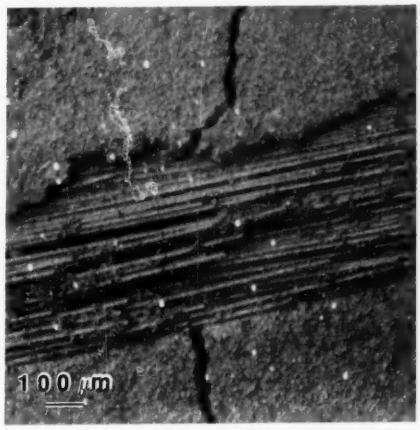

FIG. 5

Type I cracking pattern observed after the 1st loading stage of AD specimen cured for 13 days in water.

Type I Cracking:

A Type I crack is shown in Fig 5. The direction of crack propagation in all the micrographs is from the bottom upward. The crack path was hardly affected by the presence of the glass fiber strand. Only a slight change in the orientation could be observed. The bridging effect of the fiber is clearly seen here.

Although there is an apparent discontinuity in the observed crack, it should be appreciated that only the upper specimen surface is observed, and it is likely that below it continuity is maintained. It is interesting to note that no significant fiber-cement debonding could be observed, debonding occurring only at a local region to the right of the approaching crack. This

is typical of all the other fracture modes, and will be described in more detail subsequently.

Type II Cracking

In the Type II cracking pattern the path beyond the glass fiber strand seemed to be a straight continuation of the crack course before it, but discontinuities and microcracks were observed at the zone of intersection with the glass fiber strand. Typical micrographs are shown in Fig 6a, b, & c.

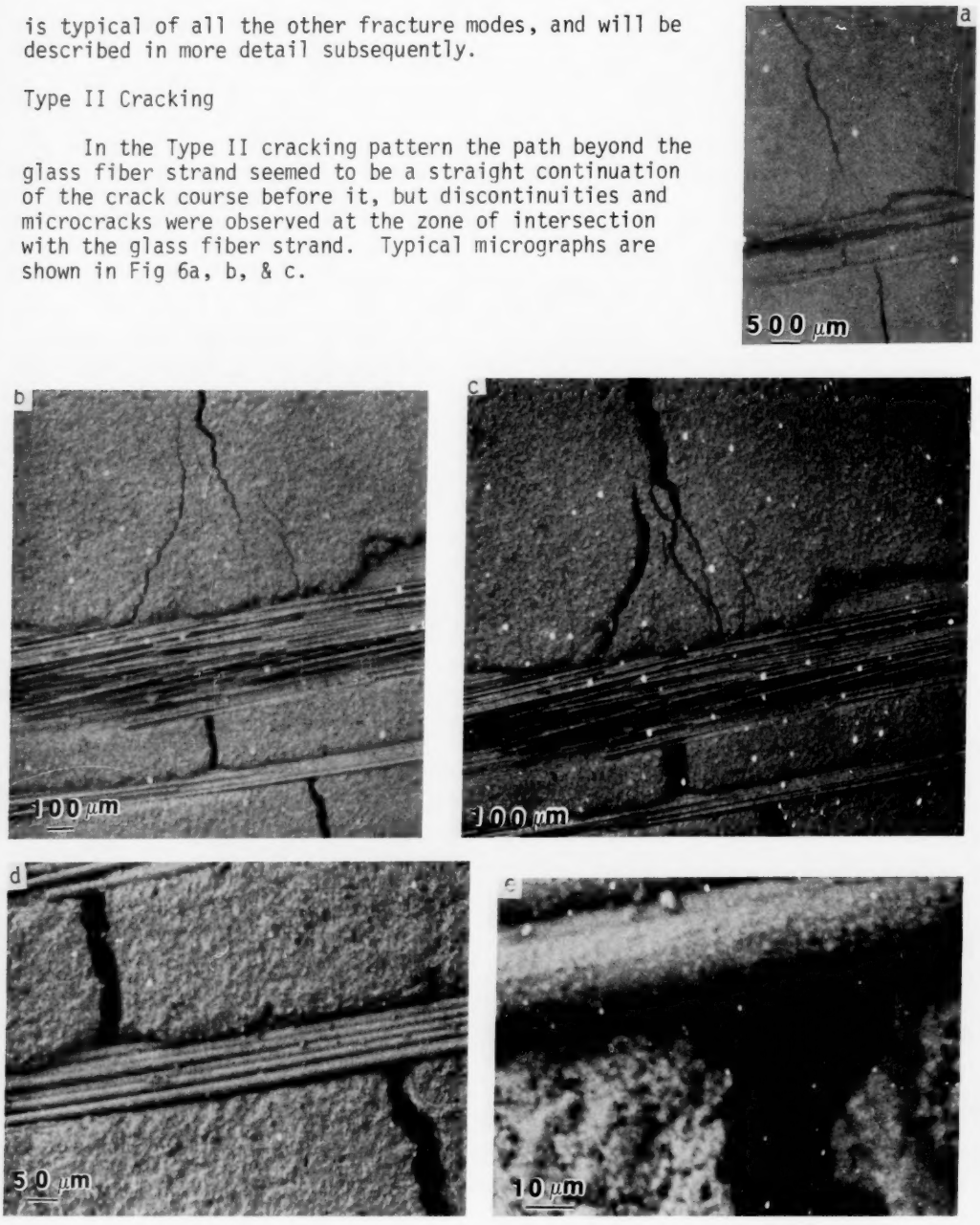

FIG. 6

Type II cracking pattern observed in AD specimen cured for 13 days in water. (a), (b), 1st loading stage, (c) 3rd stage of loading, (d) Intersection of the crack propagating from the notch with the glass fiber strand, 1st loading stage, (e) Debonding at the intersection of the crack propagating from the notch with the outer filament in the strand.

VOL
14
198

In examining the region of intersection of the crack with the glass fiber strand, no debonding beyond the first fiber is detected (Fig. 6d), but in front of it some local glass filament-cement separation, to the left of the crack, is observed (Fig. 6d & e). This is indicative of local adhesive failure. The separation is complete, without any contact between the matrix particles and the outer filaments; such as is typical for the specimens before cracking (Fig. 2a). It should be emphasized that this region is limited: To the right of the crack, or at a distance of more than about 0.5 mm to the left of it, the interface is unaffected and looks like that of unloaded specimens (Fig. 2a). This is characteristic in all of the cracking patterns.

The microcracks beyond the glass fiber strand (Fig. 6b) are seen to converge into one main crack that propagates further.

Loading to the 3rd stage resulted in widening of the cracks (Fig. 6c), including the smaller microcracks, but no significant debonding beyond that present in the 1st stage was usually observed. This is typical also for the other cracking patterns, and in most cases the width of the main cracks near the glass fiber strand was 70 to 150 μm in the 3rd loading stage. Nevertheless, in all cases the fibers maintained their continuity, and were able to bridge over the crack.

Type III Cracking:

Typical Type III cracking patterns are shown in Fig. 7. The crack running beyond the glass fiber strand was approximately parallel to the crack path approaching the fiber, but shifted by 0.5 to 2 mm. In the specimen in Fig. 7, the cracks passed through impressions of filaments that were removed accidentally from the matrix surface during polishing. On the surface there does not seem to be a continuity between the two branches. Some debonding could be observed at the intersection of the crack and the outer filaments, but it seemed to be limited to the zone near the crack, and it did not extend beyond the region between the points of intersection of the two crack branches and the glass fiber strand. The nature of the debonding was similar to that discussed in the previous section.

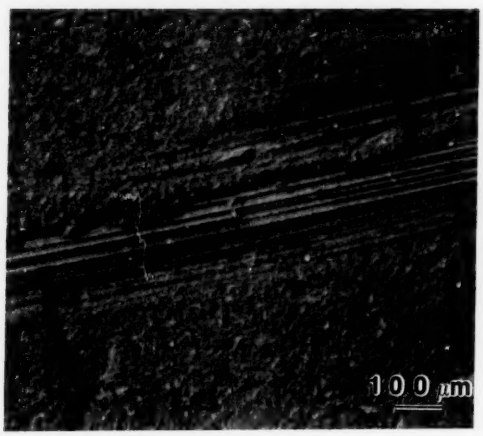

FIG. 7

Type III cracking observed in SSD specimen cured for 13 days in water, 1st loading stage.

Type IV Cracking:

In this case, too, the presence of the glass fiber strand caused a discontinuity in the observed crack. Here, however, the extension of the crack beyond the glass fiber strand was not in the form of a single crack but rather as 2 to 4 cracks with generally parallel orientation (Fig. 8a & b). The width of each of these cracks was smaller than that of the crack between the notch and the glass fiber strand. Debonding around the outer filaments of the strand was similar to that discussed previously. Again, loading to the 3rd stage resulted in widening of all the cracks. Most of the cracks beyond the glass fiber strand propagated to the edge of the specimen,

but one of them was usually significantly wider than the others.

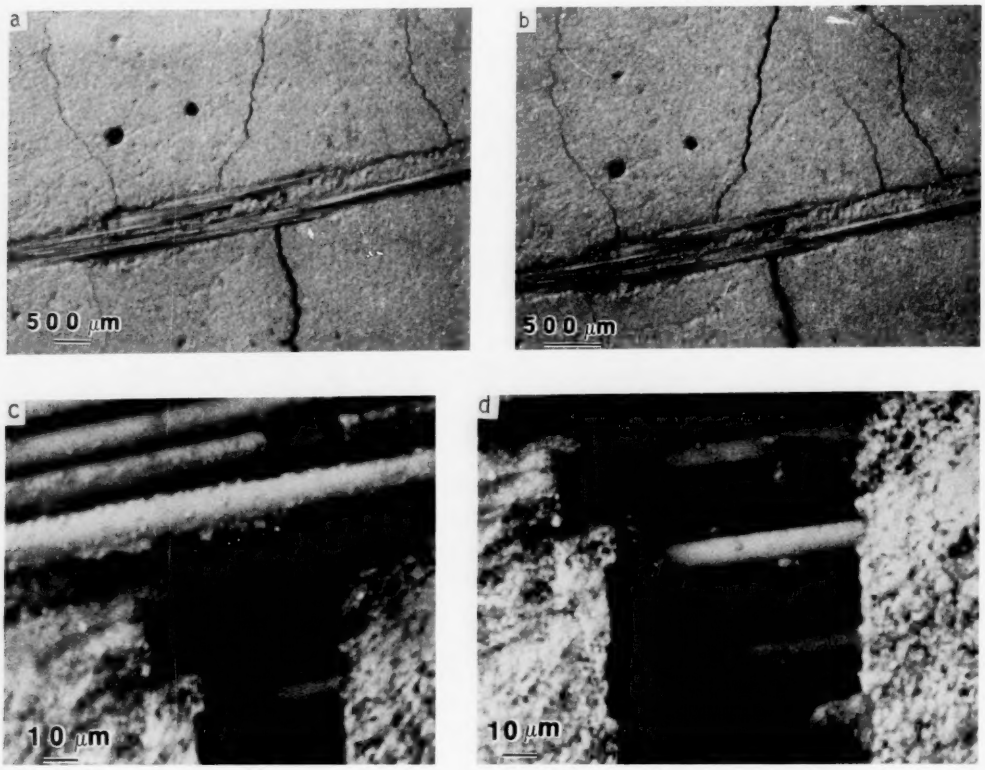

FIG. 8

Type IV cracking pattern observed in AD specimen cured for 3 days in water. (a) 1st loading stage, (b) 3rd loading stage, (c) 1st loading stage showing filaments bridging the crack, (d) The same field as (c) but at the 3rd loading stage.

Observations could sometimes be made of filaments beneath the exposed specimen surface, which were revealed during the opening of the crack. Typical micrographs showing such filaments are presented in Figs. 8c & d. They indicate that the filaments are pulled out as the crack is widened, but that they maintain their continuity and continue to bridge over the crack. It is interesting to note the "clean" surfaces of the filaments, which show hardly any hydration products bonded to them. The walls of the crack surrounding the fiber seems to remain intact and there is no sign of crumbling or any other damage to the matrix which makes up the crack wall.

Cement Reinforced With E Glass Fiber Strands.

Treatment in 90°C water for three hours did not result in any appreciable change in the cracking pattern. The two specimens tested showed a type III fracture. However, after 11 hours in hot water indications of brittle fracture could clearly be observed. The crack was not deviated or shifted by the glass fiber strand (Fig. 9a) and in its propagation it broke many of the filaments (Figs. 9b). These characteristics were observed in both of the specimens that were tested.

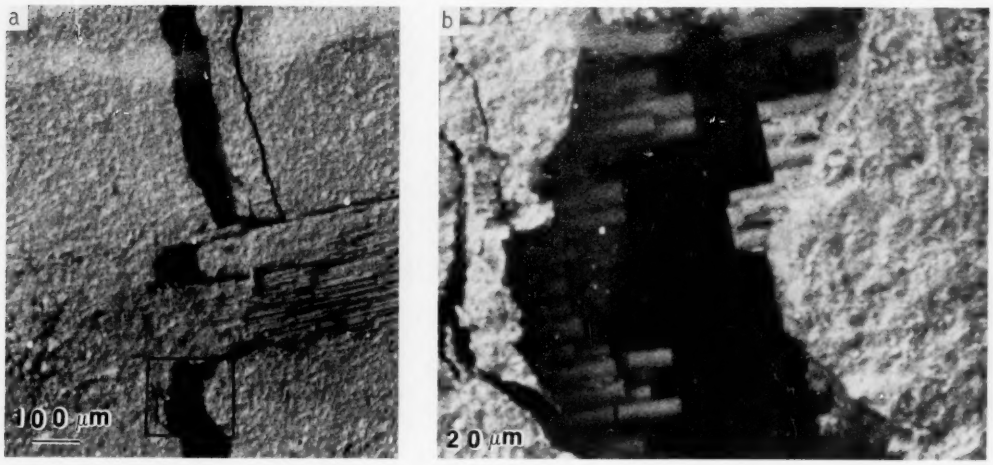

FIG. 9

Brittle fracture in AD E-glass GRC cured for 3 days in water and then aged at 90°C in water for 11 hours, (a) General appearance of the fracture at the 3rd loading stage, (b) Lower field of (a) at higher magnification.

VOL. 14 1984

Conclusions

The observations presented in this paper indicate that the effect of the glass fiber strand is usually to block the path of the crack and cause it to shift laterally about 0.5 to 2.5 mm. Sometimes two or more cracks are obtained beyond the glass fiber strand and these also are shifted laterally. No apparent continuity is observed between the different crack branches. These observations are similar in nature to those reported by Swamy (25) and Patterson and Chan (26), and indicate that models which assume the propagation of a single straight crack, and bridging by fibers which are being pulled out, are oversimplified. The energy dissipated in the shifting and branching of the crack may contribute significantly to the toughness of the composite, and this must be taken into account.

The pull-out process is more complex than the process usually modelled and tested in a simple pull-out test arrangement. The present observations indicate that there is a region of debonding which extends between the branches of the passing crack. The debonding observed is not symmetrical with respect to the glass fiber strand axis, and usually only one side of the glass fiber strand-cement interface is debonded. Such asymmetry may indicate that there is some bending of the glass fiber strand occurring in addition to pull-out. Stucke and Majumdar (18) considered such bending in the discussion of the embrittlement of GRC.

The fact that the interface beyond the cracking zone remains intact even after the cracks are opened to a width of 100 μm or more, suggests that frictional bond can develop in these regions, as predicted by many models. The "clean" surfaces of glass filaments that have been pulled out indicates adhesive failure, and suggests that the chemical bonding was not effective.

The nature of brittle fracture in this type of test was demonstrated for E glass reinforced cement which was exposed to accelerated deterioration conditions. Here the crack course is not shifted, and many of the filaments break during crack propagation.

References

1. J.P. Romualdi and G.B. Batson, J. Eng. Mech. Div., Proc. ASCE, 89, 147 (1963).
2. J.P. Romualdi and J.A. Mandel, J. Amer. Concr. Inst. 61, 657 (1964).
3. C.D. Johnston and R.A. Coleman, pp. 177-194 in "Fiber Reinforced Concrete" ACI publications SP-44, Detroit, 1974.
4. J. Edgington, D.J. Hannant and R.I.T. Williams, Current Paper CP69/74, Building Research Establishment, Garston, 1974.
5. S.R. Parimi and J.K.S. Rao, pp. 79-92 in "Fiber Reinfroced Concrete" ACI publications SP-44, Detroit 1974.
6. R.N. Swamy, P.S. Mangat and C.V.S.K. Rao, ibid pp. 1-28.
7. J. Aveston, G.A. Copper and A. Kelly, pp. 15-26 in "The Properties of Fiber Composites" Proc. Conf. of National Physical Laboratory, IPC Science and Technology Press Ltd. (1971).
8. J. Aveston, R.A. Mercer and J.M. Sillwood, pp. 93-103 in "Composites Standards Testing and Design" Proc. Conf. of National Physical Laboratory, IPC Science and Technology Press (1974).
9. J. Aveston and A. Kelly, J. Mater. Sci. 8 352 (1973).
10. V. Laws, P. Lawrence and R.W. Nurse, J. Phys. D: Appl. Phys. 6 523 (1973).
11. V. Laws, Composites, 13, 145 (1982).
12. A.E. Naaman, and S.P. Shah, pp. 171-178 in "Fibre Reinforced Cement and Concrete", A. Neville (Ed.) Proc. RILEM Symp., The Construction Press (1975).
13. R.C. DeVekey and A.J. Majumdar, Mag. Concr. Res. 20, 229 (1968).
14. G.H. Tattersall and C.R. Urbanowicz, Mag. Concr. Res. 20, 105 (1974).
15. D.J. Pinchin and D. Tabor, Cem. Concr. Res. 8, 139 (1978).
16. M.N. Al Khalaf and C.L. Page, Cem. Concr. Res. 9, 197 (1979).
17. D.J. Pinchin and D. Tabor, Cem. Concr. Res. 8, 15 (1978).
18. M.S. Stucke and A.J. Majumdar, J. Mater. Sci. 11 1019 (1976).
19. A.C. Jaras and K.L. Litherland, pp. 327-334 in "Fibre Reinforced Cement and Concrete" A. Neville (Ed.) Proc. RILEM Symp. The Construction Press (1975).
20. E.B. Cohen and S. Diamond, pp. 315-325, ibid.
21. P. Bartos, Int. J. Cem. Comp. 3, 159 (1981).
22. N.G. Nair, pp. 81-93 in "Fibre Reinforced Cement and Concrete" A. Neville (Ed.) Proc. RILEM Symp. The Construction Press. (1975).
23. J.P. Romualdi, pp. 190-201 in "The Structure of Concrete" Proc. Int. Conf. A.E. Brooks and K. Newman (Ed.) London, 1965. Cement and Concrete Association, London (1968).
24. S. Mindess, Int. J. Cem. Comp. 2 3, (1980).
25. R.N. Swamy, Int. J. Cem. Comp. 2, 43 (1980).
26. W.A. Patterson and H.C. Chan, Composites, 6, 102 (1975).
27. S. Mindess and S. Diamond, Cem. Concr. Res. 10, 509 (1980).
28. S. Diamond and S. Mindess, pp. VI-114 -VI-119 in Vol. III, Proc. 7th Int. Cong. Chem. of Cem., Paris (1980).
29. S. Mindess and S. Diamond, Materials and Structures, 15, 107 (1982).
30. S. Diamond, S. Mindess and J. Lovell, Cem. Concr. Res. 13, 107 (1983).
31. B.D. Barnes, S. Diamond and W.L. Dolch, Cem. Concr. Res., 8, 233 (1978).

VOL
14
198

CEMENT and CONCRETE RESEARCH. Vol. 14, pp. 43-48, 1984. Printed in the USA.
0008-8846/84 $3.00 + 00. Pergamon Press, Ltd.

THE ANALYSIS OF OPC PASTES: A COMPARISON BETWEEN ANALYTICAL ELECTRON MICROSCOPY AND ELECTRON PROBE MICROANALYSIS

D L Rayment
Building Research Establishment, Garston, Watford WD2 7JR, England

and

E E Lachowski
University of Aberdeen, Department of Chemistry, Meston Walk, Old Aberdeen AB9 2UE, Scotland

(Refereed)
(Received May 24; in final form Aug. 9, 1983)

VOL. 14 1984

ABSTRACT

The chemical compositions of two 5 year-old OPC pastes with w/c 0.3 and 0.6 have been investigated by Analytical Electron Microscopy and Electron Probe Microanalysis. Comparison of the distributions of Ca/Si ratios of C-S-H obtained by the two methods gave good agreement, although Microprobe analyses of bulk samples may contain contributions from regions other than C-S-H.

Introduction

Two types of electron probe instrument are commonly used in the quantitative chemical analysis of cement hydrates. Both rely on the analysis of the characteristic x-rays produced when the samples are bombarded with electrons of moderate energy (5-100 keV), but differ in the samples used. In electron probe microanalysis (EPMA) methods (which here include both electron microprobes and scanning electron microscopes with x-ray analysers), bulk samples are used, and there is no transmission of the probe through the specimen. In analytical electron microscopy (AEM), a very high proportion of the probe is transmitted through thin or particulate samples, and a normal transmission image is obtained. In both methods wavelength and energy-dispersive spectrometers, or a combination of the two can be used. They are very well described by S J B Reed(1).

The volumes occupied by the phases present in set cements can be less than the minimum volume analysed by electron probe instruments, so that the results obtained will depend on the ratio of the volume of the specified phase to that of the analysed volume. Procedures to minimise the effects of beam spreading in EPMA's have been described(2,3). The volume analysed by AEM is very much smaller than by EPMA. Nevertheless, the present results, obtained from pastes of two w/c ratios by AEM and EPMA, showed marked similarities.

Experimental

A Kratos Cora AEM with a Link Systems energy-dispersive x-ray analyser was used for the transmission analyses. The take-off angle from the specimen to the detector was 50°. No measurement of beam current was possible.

The EPMA used was a Cambridge Instrument Company Microscan 9, which has two computer-controlled wavelength-dispersive spectrometers with a take-off angle of 75°.

The main operating parameters of the instruments are given in Table 1.

The cement used has been described previously(4). Specimens were prepared for the EPMA by vacuum potting 20 mm dia. x 8 mm right prisms of the pastes in Araldite. These were then coarse ground on carborundum stone and polished on diamond laps to 0.25 µm, mineral oil was used as the lubricant. A coating of 20 nm of carbon (measured with an oscillating crystal balance) was applied to ensure electrical conductivity. All samples were vacuum-stored during and after preparation.

The following pairs of elements were analysed in the order given; S and Mg, Ca and Al and Fe and Si. Elemental compositions in terms of wt % were corrected for inter-element effects using methods by Sweatman and Long(5), and Heinrich(6), and then recalculated to give compositions relative to 10 oxygen atoms(7).

Since the specimen preparation is essentially non-destructive, analyses can be referred to the morphology. Fig 1 is a typical view of the 0.3 w/c paste, showing clearly visible unhydrated clinker grains. Fig 2 shows a clinker grain surrounded by C-S-H. There are two distinct hydrate regions, an inner surrounding the clinker and an outer surrounding the inner(4,8). These two regions were analysed separately.

Specimens for the AEM were prepared from the same batch of cylinders as were used for the EPMA. Coarse fragments were drilled from the centres of the cylinders. These were ground under iso-propyl alcohol in an agate mortar. The resulting slurry was then dispersed ultra-sonically in excess iso-propyl alcohol. The specimen was sampled by touching the surface of the suspension with a copper grid bearing a carbon film. The sample was analysed as soon as the grid had dried. On removal from the microscope, the sample was discarded(9). The morphological relationship between the

TABLE 1

Analysis Parameters

Parameter		AEM	EPMA
Accelerating voltage		80 kV	10 kV
Probe current		Not known	3 nA
Count rate for Ca Kα	Max	1260 cs^{-1}*	577 cs^{-1}
	Min	323 cs^{-1}	428 cs^{-1}
Count rate for Si Kα	Max	371 cs^{-1}	115 cs^{-1}
	Min	110 cs^{-1}	73 cs^{-1}
Counting time per element		60 sec	10 or 15 sec
Total counting time		60 sec	70 or 100 sec**

* For 'CSH' material over 7-11 channels.
** Six elements, allowing for spectrometer settling.

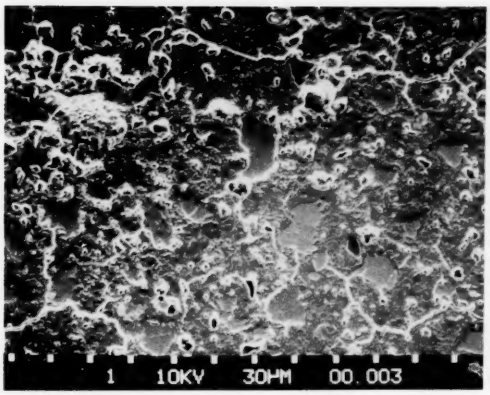

FIG 1
5 yr 0.3 w/c paste, 30 μm between blocks, EPMA micrograph

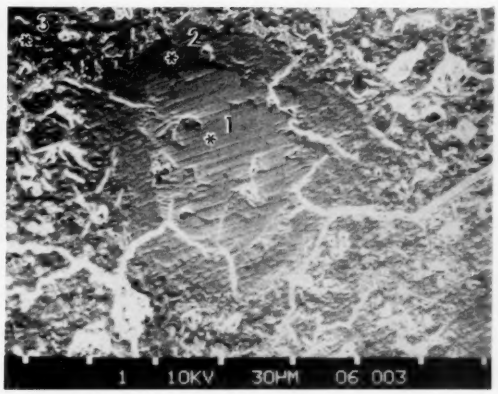

FIG 2
5 yr 0.6 w/c paste, 1 - unhydrated, 2 - inner hydrate, 3 - outer hydrate.

various phases is destroyed, so inner and outer hydrates cannot be distinguished.

Only particles which were shown by the absence of electron diffraction patterns to be amorphous were analysed. X-rays with energies up to 20 keV were collected and atomic ratios were obtained from peak areas by the Cliff-Lorimer technique(10). The probe diameter and shape could be adjusted to cover particular particles or regions of larger particles. Typically, circular beams with diameters of about 0.12 μm, and elliptical ones approximately 0.3 x 0.12 μm were used.

Physical Differences

The major difference between these two instruments that can affect the analytical results is the volume in which x-rays are generated. In the EPMA those electrons not back-scattered from the target are absorbed within it, and diffuse away from the impact area. This results in the production of x-rays from an area with a greater diameter than the original probe. Estimates of beam spread have been made(3). At 10 kV a spread of 0.65 μm and a penetration of 1.7 μm for a density of 2100 kg m^{-3} are likely in a C-S-H -type material. With a probe diameter of 0.35 μm the estimated effective volume of x-ray production is a teardrop shape of $\simeq$ 0.8 μm^3.

The situation is different in the AEM. In order to meet the thin film criterion, the material analysed is very much thinner than the depth of complete diffusion(11), and the bulk of the electrons are deflected only a few degrees before leaving the specimen. Thus, the volume of x-ray production is approximately that of a prism of cross-sectional area equal to that of the beam, and length equal to the thickness of the specimen. With a typical specimen thickness of 100 nm and an elliptical spot 0.3 x 0.12 μm, the volume of x-ray production is 2.5 x 10^{-3} μm^3. Therefore, the analysed volumes are at least two orders of magnitude greater in the EPMA than in the AEM.

Results

As this paper is intended to compare the AEM and EPMA, the main emphasis will be placed on Ca/Si ratios, although the Al, Mg, S and Fe results from

the EPMA will also be considered. The results for these cements from earlier EPMA analyses have been published(7).

(a) 0.6 w/c paste
Fig 3(a) shows the histogram of the Ca/Si ratios obtained with the AEM. The peak shape is reasonably normal, with a modal Ca/Si value of 1.75. The results from the inner hydrate analyses (Fig 3(b)) show a modal value at Ca/Si = 1.75, the same as for the AEM analyses. The modal value for the outer hydrate Fig 3(c) is higher, at Ca/Si = 2.05. This higher value may be attributed to a higher Al content and correspondingly lower Si content in the outer hydrate than in the inner. The Ca content of the inner hydrate is significantly greater than that of the outer. The compositions are Ca = 2.60 ± 0.08, Si = 1.49 ± 0.06 and Al = 0.20 ± 0.06, 93 results; and Ca = 2.46 ± 0.06, Si = 1.15 ± 0.09 and Al = 0.33 ± 0.08, 47 results. These values are the means ± 95% C.L, of the values within the mode ± 0.3 of the Ca/(Si + Al) distribution.

The histograms of the EPMA analyses of both the outer and inner hydrates have an extended distribution towards high Ca/Si values. This may be caused by three factors; the effect of probe overspill into regions of high Ca concentration such as clinker grains or CH; the presence of areas of low Si concentration, as detected in the outer hydrate; and the analysis of phases other than C-S-H.

Compositions with high Ca/Si ratios were assigned to AFm, AFt or CH phases according to the criteria established by Lachowski et al.(9). In the outer hydrate (73 results), 2 analyses correspond to AFm, 2 to AFt and 7 to CH. For the inner hydrate, 1 analysis corresponds to AFm and 6 to CH. In addition, 1 may be ascribed to C_3S.

Fig 3(b) also has a minor peak (8 results) with a centroid at Ca/Si = 1.35. These compositions all had low Ca concentrations. A single result from the AEM analyses was found in this position.

Two results from the AEM analyses lying between 2.1 and 2.3 occupy a position close to the EPMA outer hydrate peak.

(b) 0.3 w/c paste
The AEM analyses (Fig 4(a)) show a marked difference between this paste and the one with w/c 0.6. The distribution of results is much wider. The centroid of the major peak of the AEM analyses is at Ca/Si = 1.85. A peak at this position occurs in the EPMA outer hydrate analyses (Fig 4(c)). The inner hydrate EPMA results (Fig 4(b)) also shows a bimodal distribution with centroids at 1.75 and 1.95. Statistical analysis ('t' and 'F' tests) of the results in the centroids shows that the bimodularity is caused by a significant difference in Si content; no differences were found in the other elements. The ratio Ca/(Si + Al) gives a unimodal histogram. Since both these Ca/Si peaks fall within the AEM spread, the analyses in this region are considered to be equivalent.

The compositions of the hydrates are: inner, Ca = 3.0 ± 0.1, Si = 1.47 ± 0.09, Al = 0.20 ± 0.08, 38 results; outer, Ca = 2.90 ± 0.09, Si = 1.24 ± 0.07, Al = 0.34 ± 0.09, 77 results.

Of the non-C-S-H phases in the inner hydrate (58 results), 3 correspond to CH and 3 to C_3S. In the outer hydrate (128 results), 3 correspond to CH, 2 to C_3S, 8 to AFm and 1 to AFt.

VOL
14
198

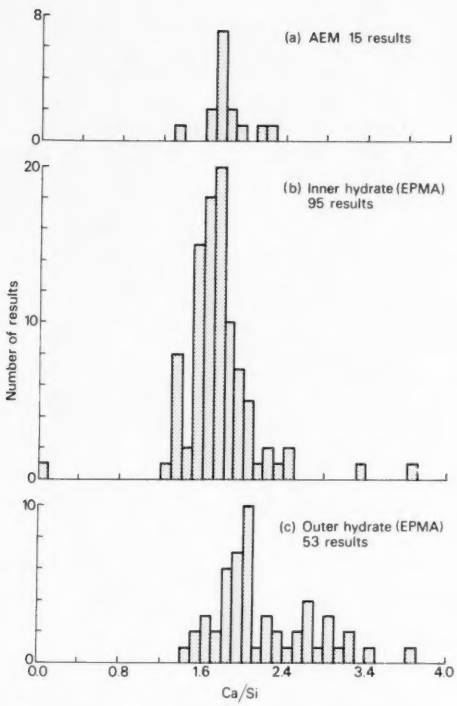

FIG 3
5 yr, 0.6 w/c OPC Paste

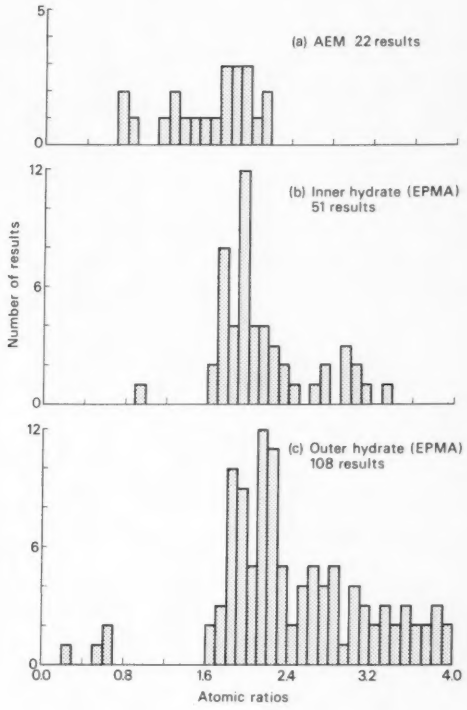

FIG 4
5 yr, 0.3 w/c OPC Paste

Discussion

In the AEM analyses areas containing crystalline material were avoided. Therefore no crystalline CH with a volume greater than the minimum detection limit for electron diffraction (estimated at between 1 and 5 x 10^{-3} μm^3) was analysed. The modal value from the EPMA inner hydrate analyses exactly matched that from the AEM. Therefore at 10 kV, the majority of EPMA inner hydrate analyses contained the same small (if any) proportion of CH as the AEM analyses.

The EPMA outer hydrate analyses showed a higher Ca/Si modal value than the inner or the AEM values for both pastes. These were caused by a reduced Si proportion, the Ca proportion being either less (0.6 w/c) or the same (0.3 w/c) as the inner hydrate value. In the AEM analyses only two results for each paste had this higher Ca/Si ratio. Although these results had some of the highest Al levels a high Al level did not necessarily give a low Si value. More AEM results are needed to give a clear picture of this high Ca/Si region.

In the outer hydrate analyses the topography makes the recognition of the various phases difficult. This is mirrored in the extended Ca/Si distribution . There are proportionately more high Ca/Si ratios than in the inner hydrates. These results, selected on the basis of having (Ca+Mg)/(Si+S+Al+Fe) values outside the major peak, and not belonging to AFm, AFt or CH phases, were distributed as follows; 0.6 w/c inner, 0%; outer, 15%; 0.3 w/c inner 10%, outer, 19%. (The relatively large number of high

Ca-analyses in the 0.3 w/c inner hydrate does not necessarily mean that more Ca was present than in the 0.6 w/c inner hydrate. The zone of inner hydrate is narrow in the low w/c paste, and it is difficult to analyse exclusively within it.) Although less CH (1.5% of results) was found in the 0.3 w/c paste than in the 0.6 w/c paste (9.5% of results), there were proportionately more high-Ca results in the lower w/c paste than in the higher. Two possibilities may account for this, either separately or together. As there is more unhydrated clinker in the 0.3 w/c paste, there is a greater chance of inadvertent analysis of C_3S. Two C_3S grains were analysed in this paste (1.5% of the analyses), whereas none were found in the other. Alternatively, the effect may have been caused by the presence of regions of microcrystalline CH, as seen by Groves(12). These regions are apparently not so widespread, at least at w/c ratios down to 0.3, that analyses of C-S-H only cannot be made. With higher accelerating voltages, however, the risk of analysing non-C-S-H regions will be greater.

Conclusions

In the case of the inner hydrate EPMA analyses and the AEM analyses an exact concurrence is obtained between the modal Ca/Si values. This is not the case where individual(13) or mean values(4,14) are compared.

The outer hydrate EPMA analyses show a higher Ca/Si modal value due to a reduced Si proportion. No conclusive evidence has been found from the AEM analyses to support this picture of any compositional difference between inner and outer hydrate.

In the EPMA results proportionately more high Ca/Si results are found in the 0.3 w/c paste than in the 0.6 w/c. These results are caused by the analysis of C-S-H intermixed with high Ca phases and may be evidence for an increasing amount of microcrystalline CH with decreasing w/c.

References

1 S J B Read. Electron Microprobe Analysis, Cambridge University Press, 1975.
2 S Chatterji. Cem. Concr. Res. 10, 783 (1980).
3 D L Rayment and A J Majumdar. Proc. 7th. International Congress on the Chemistry of Cement, vol. II, 2/64, Paris, 1980.
4 M S Stucke and A J Majumdar. In Hydraulic Cement Pastes: their Structure and Properties, Cement and Concrete Association, Slough, 1976.
5 T R Sweatman and J V P Long. J. Petrol. 10, 322 (1969).
6 K F J Heinrich. Quantitative Electron Probe Microanalysis: Nat. Bur. Stands. Spec. Publ. 298 (1968).
7 D L Rayment and A J Majumdar. Cem. Concr. Res. 12, 753 (1982).
8 S Diamond. In Hydraulic Cement Pastes: their Structure and Properties, Cement and Concrete Association, Slough, 1976.
9 E E Lachowski, K Mohan, H F Taylor and A E Moore. J. Am. Ceram. Soc., 63, 447 (1980).
10 G Lorimer, S A Al-Salman and G Cliff. Proc. Inst. Phys. Electron Microscopy and Analyses Group Conf., Glasgow, 1977 (EMAG 77).
11 V E Cosslett, Brit. J. Appl. Phys., 15, 107, 1964.
12 C W Groves, Cem. Concr. Res. 11, 713 (1981)
13 S Diamond, Cem. Concr. Res. 2, 617 (1972).
14 E E Lachowski, K Mohan, H F Taylor, C D Lawrence and A E Moore. J. Am. Ceram. Soc., 64, 319 (1981).

VOL. 14 1984

CEMENT and CONCRETE RESEARCH. Vol. 14, pp. 49-56, 1984. Printed in the USA.
0008-8846/84 $3.00 + .00. Copyright (c) 1984 Pergamon Press, Ltd.

CHANGES IN STRUCTURE AND CHEMISTRY OF CEMENT MORTARS STRESSED BY A SODIUM CHLORIDE SOLUTION

Dirk W. H o f f m a n n
Bundesanstalt für Materialprüfung(BAM)
Unter den Eichen 87
D - 1000 B e r l i n 45

(Communicated by M. Regourd)
(Received May 26, 1983)

OL.
14
984

ABSTRACT Cement mortars, one-sidedly stressed by a sodium chloride solution of 20 % for 140 days, show a marked area at a distance from the surface of nearly 30 mm. Its position is reflected in concentration profiles of the water soluble and nitric acid soluble parts of chloride, sulphate, sodium, potassium,and aluminium, in the mineral content as well as in the pore size distribution. This could serve as the starting point for deteriorations caused by cycles of freezing and thawing in connection with deicing salts, because destroying mechanisms could easily attack here.
Further studies must be carried out and the observation of stressed cement mortars and concretes has to be intensified to get a better insight into the principles and the mechanisms of such processes.

Introduction

Because of numerous damages to structural materials containing portland cement which are caused by deicing salts it is becoming necessary to clarify the reaction mechanisms happening there. Opinions about the attack of solutions of deicing salts on concrete vary greatly. There are two main points of view. One of them is concerned with the damages to the reinforcement caused by chlorides whereby only the portion of the latter present at the depth where such steel is situated is of interest. Although steel in concrete is quite well protected against corrosion because of the high pH-value of the pore solution an amount of only 0.035 % calcium chloride in a saturated solution of calcium hydroxide (pH-value > 12) is sufficient for the deterioration of the protecting layer (9). Also, the "magic" limit of 0.4 % chloride (related to the weight of the binding agent), experimentally found by Richartz (10), has to be mentioned, too, because below this value no further corrosion takes place. But other

authors (2, 7, 17) suppose that the agency of such solutions in the case of mortars stressed by cycles of freezing and thawing and the damages caused by these actions are only of a physical nature, because the free energy of NaCl on one hand and that of the contents of the mortar on the other are below chemical reaction threshholds. One can generally say that the heat of fusion of the melting ice is responsible for the deterioration. It is withdrawn from the mortar beneath, produces a rapid cooling (temperature shock) which causes freezing of the pore solution in such areas where the chloride content is low and consequently the freezing point reduction is diminished (6). The fact that newly formed transformation products take part in the reactions between deicing salt and hydrated contents of the portland cement , causing changes in the pore space there, has been left out of consideration till now. It is well known that, if chloride penetrates into mortar, $Ca(OH)_2$ is leached out (3, 12, 18) making the mortar porous and susceptible to subsequent actions of frost. The diffusion of $Ca(OH)_2$ out of the mortar is greater when using sodium chloride than magnesium sulphate, calcium chloride or distilled water. Besides this the formation of Friedel's salt $3\ CaO.Al_2O_3.CaCl_2.10\ H_2O$ is certain (10). According to Ben Yair's (1) statement, sodium chloride reacts with $Ca(OH)_2$ forming $CaCl_2$ before the precipitation of this salt. Additionally the cation exerts an influence on the amount of chloride which can be bound chemically (14). If there are high concentrations of alkali in the mortar, as in the case of a stress by a NaCl solution, the conversion of ettringite into monosulphate is forced (4), involving changes in the structure. Just recently Stockhausen et al. (13) have suggested that in the pore space of hardened cement pastes different "modifications" of water are present, showing the phase transformation of water into ice at different temperatures. Thereby the so-called bulk-water is found in pores having radii greater than 100 nm which exists out of the range of surface forces. The water filling pores with radii greater than 10 nm is deposited there because of capillary condensation. The freezing point declines with decreasing pore diameters so that water freezes in coarse pores first. The research of Efes (5) also shows changes in the pore structure caused by chloride influence. According to him a 6 or 12 month exposition to a sodium chloride solution causes a decrease in the total and gel pore volume and an increase in the amount of capillary pores. In this paper only a small part of these complex processes resulting from the combined influence of frost and deicing salts is broached. Tests on cylindrical specimens consisting of portland cement mortar under one-sided stress from deicing salt solutions resulted in concentration profiles of chloride, sulphate, sodium, potassium, and aluminium. After the extraction of the pulverized parts of the cylinders with water, the resulting soluble contents should make statements about the distribution of hydration and reaction products possible. Thereby X-ray diffraction analyses serve to identify the mineral contents. Specific values of the pore size distribution are used as well.

VOL.
14
198

Experimental

In the tests a portland cement PZ 45 F was used, which potential composition according to Bogue (2) was as follows:

TABLE 1

Potential Composition of the Portland Cement

mineral phase	content in % (related to the mass of the cement)
C_3S	67.5
C_2S	8.0
C_3A	9.0
C_4AF	7.3
C_2F	-
$CaSO_4$	4.9
alkali oxides	1.1
CaO + residue	2.0
total content	100.0

The aggregates of the mortar consisted of "Normsand", which is described in DIN 1164 (5). The water/cement ratio runs up to 0.5, causing an open porosity of 15.7 %. Cylindrically formed cement mortar specimens with diameters of 65 mm and lengths of 100 mm, which were sealed all around except on one of the front surfaces, were stressed by a sodium chloride solution of 20 % for 140 days. At intervals the solution was replaced. Afterwards the specimens were cut in discs of 5 mm thickness perpendicular to their longitudinal direction and then dried at a temperature of 50 °C till mass constancy was reached. Then the material was pulverized and examined.

Results

Chloride, Sulphate, Sodium, Potassium, and Aluminium Distribution

Figure 1 shows the concentration profiles of the water soluble amounts of chloride, sodium,and potassium.

It can be seen that, when using the described kind and duration of stress, a high chloride content is found near the surface (nearly 1.2 % related to the mass of the mortar, corresponding to 5.4 % of the mass of the binding agent). At a distance from the surface of 30 mm the values fall below the Richartz's limit of 0.4 %. At a greater depth there are not any alterations. The sodium distribution corresponds with that of chloride. Especially near the surface the Na/Cl ratio is no longer that of the former NaCl solution. A chloride excess is nearly always present. At a depth of 30 mm a concentration is reached which does not change

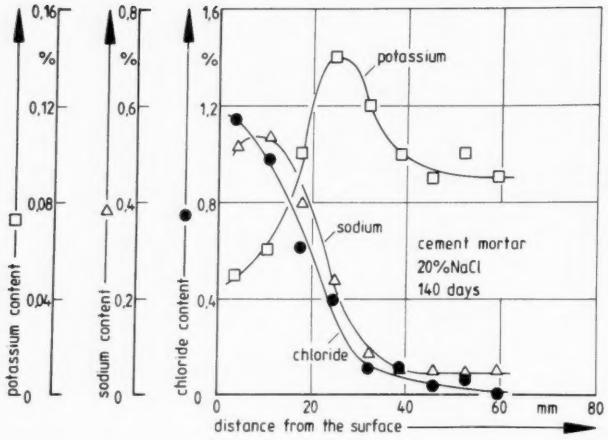

FIG. 1

Concentration Profiles of the Water Soluble Amounts of Chloride, Sodium and Potassium

any more. The potassium distribution runs nearly contrary to this. It shows, at the same depth, a maximum, where the aforementioned elements have reached constant values. The distributions of the water soluble and nitric acid soluble amounts of aluminium are shown in Figure 2. The run of curves has some typical characteristics. Thus the water soluble portion increases from 0 % to about 0.2 % and then decreases to the original value. Where there is a maximum, the total amount of aluminium is at the minimum. Thus a marked area also exists here, at the same depth as observed in the case of the other quoted elements. Iron is not present in the water soluble part. The concentration profile of the total amount of the binding agent shows no trend. The curve of the sulphate content (expressed as SO_3) is similar (Figure 3). The values increase with rising distance, having a broadened maximum, beginning at a depth of 30 mm.

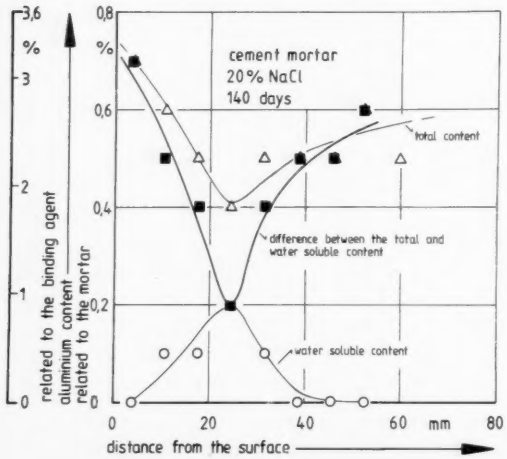

FIG. 2

Distribution of the Water and the HNO_3 Soluble Amount of Aluminium

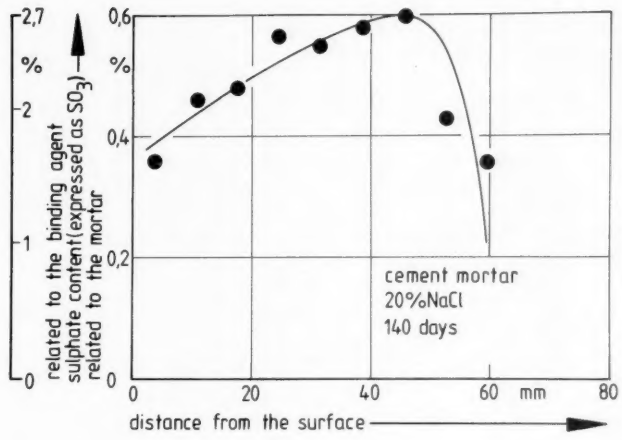

FIG. 3

Concentration Profile of the Water Soluble Amount of Sulphate

Distribution of Mineral Phases

In Table 2 the graduation of intensities of characteristic X-ray peaks of mineral phases, either newly formed or changed in their concentration, are plotted.

TABLE 2

Distribution of Mineral Phases of Cement Mortars after Stressing by a Solution of 20 % NaCl

mineral phases	distance from the surface (in mm)					
	0 - 7	7 - 14	14 - 21	21 - 28	28 - 35	35 - 42
monosulphate-like phases	X	-	-	-	-	-
Friedel's salt	XXX	XX	XXX	X	-	-
$Ca(OH)_2$	X	XX	XX	XXX	XXX	XXX
NaCl	XXX	XX	X	-	-	-
$CaCl_2 \cdot 4H_2O$	X	XX	X	X(?)	-	-
Hydrogarnet (?)	X	X	X	X	X	X

It seems that changes in the mineral content of this specimen take place only in the first 30 mm. Next to the surface small amounts of monosulphate-like phases are observed. Ettringite could not be

identified. According to (4) a high alkali concentration of the pore solution causes a forced transformation of ettringite into monosulphate.
Friedel's salt 3 $CaO.Al_2O_3.CaCl_2.10\ H_2O$ is also found up to a depth from the surface of nearly 30 mm. Portlandite $Ca(OH)_2$ shows extraction phenomena near the surface and does not change its concentration at the same depth. Sodium chloride, crystallized out of the pore solution, is visible up to 20 mm from the surface. Calcium chloride is also found. Perhaps it is a result of the reaction of NaCl with $Ca(OH)_2$, whereby the latter is formed before the crystallization of Friedel's salt.
Hydrogarnet C_3AH_6 - the stable phase of calcium aluminate hydrate - could not be identified for definite.
The described results are in accordance with thermogravimetric analyses.

Pore Size Distribution

To determine pore size parameters by means of the porosity-meter-test it was necessary to examine fragments from the same depth as the powdered material. The distribution curves give some criteria, for instance the median of the pore size distribution, the amount of pores with diameters smaller than 5 µm (microporosity) and such with radii smaller than 30 nm (gel pore volume). The median - borrowed from the pore size parameters of Trask (15) - can serve as a reference point. It is interpreted as the pore radius at a pore volume of 50 %. Considering that in the case of freeze-thaw stress smaller pores cause a greater deterioration of stone than coarser ones, the microporosity, described by Honeyborne and Harris (8), is used, too. The pores showing radii smaller than 30 nm characterize the gel pore volume, insofar as it is included in the porosity-meter test. In Figure 4 the above described parameters are plotted versus the distance from the surface. Here one can see contrary curves in the case of microporosity and gel pore volume. The increase of the former is connected to a decrease of the latter. At a depth of 30 mm the microporosity shows a maximum (increase from 92 % to 96 % of the total pore volume), whereas the gel pores show a minimum (decrease from 18 % to 16 %). The curve of the median of the pore size distribution presents a marked area at the same place, characterized by a pore radius of about 80 nm.

Discussion

By means of concentration profiles of the water soluble contents of chloride, sulphate, sodium, potassium, and aluminium as well as changes in the mineral content and the pore size distribution it is possible to find a marked area at a depth of nearly 30 mm. This area is characterized by the fact that, from here on, the amounts of chloride and sodium do not show any decrease and that here, potassium and aluminium are at a maximum, whereas the total amount of the latter is at a minimum at the same depth. The mineral phases sodium chloride and Friedel's salt are only identifiable up to this distance from the surface. Here portlandite reaches a value higher than at the surface, but constant. The amount of pores with diameters smaller than 5 µm, which is a crit-

VOL
14
198

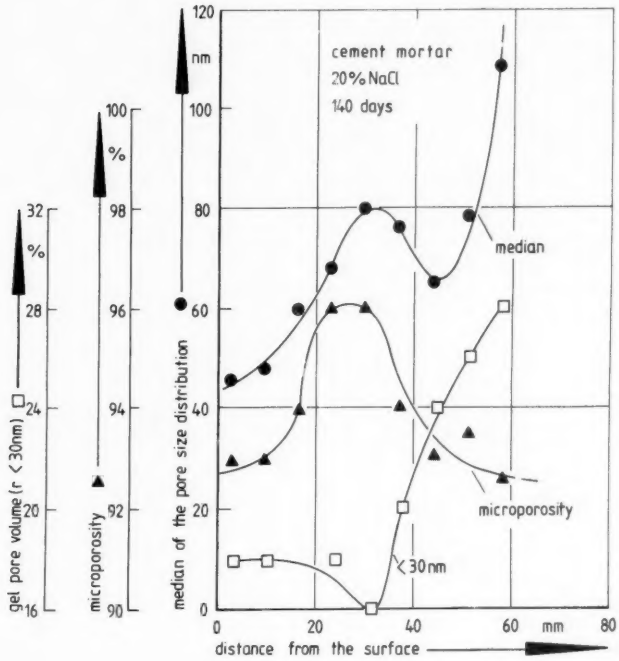

FIG. 4

Profiles of Characteristic Parameters of the Pore Size Distribution

ical measurement for the resistance of natural stones, presents a maximum of about 96 % of the total pore volume whereas the gel pores show a minimum. The changes in the content of the gel pores can be attributed to the formation of new mineral phases in this area, because the relatively stable Friedel's salt, monosulphate as well as other complex minerals containing chloride crystallize here, which happens at the expense of the amount of gel pores, a fact which is described by Efes (5).
A coarsening of pores, shown by the increase of the microporosity, is interpreted by Ushiyama and Goto (16) as a diffusion of portlandite out of the mortar contrary to the penetration of chloride. This is possible, because Schimmelwitz (11), as well as other authors (12, 18), has found an increased leaching of $Ca(OH)_2$ out of hardened cement pastes when using an alkali chloride solution. The distribution of the portlandite content, found in the described specimens, also gives reason to believe this.
The pore size at which the median shows a maximum (r = 80 nm) is in the field of radii about 100 nm, where the transformation of two different "modifications" of water happens (13). In the case of radii greater than 100 nm the so-called bulk-water exists, whereas pores with radii smaller than 100 nm are filled with water, which is precipitated there because of capillary condensation. A statement about whether the observed phenomena or the diffusion processes actually produce an attenuation of the cohesion of the structure which could serve as the starting point

of freeze-thaw deteriorations, is not yet possible. But similar marked areas which are found at different distances from the surface because of various kinds as well as diverse durations of stress, are proved by element distributions and local differences in the specific surface of many cement mortars and concretes.

Literature

1. M. Ben Yair, Cem. Concr. Res. 4, 405-416 (1974).
2. R.H. Bogue, The Chemistry of Portland Cement, 2nd Ed., Reinhold Publ. Corp., 793 pp., N.Y. (1976).
3. T.R. Cantor, C.P. Kneeter, Materials Performance, 28-32 (May 1977).
4. S. Chatterji, Cem. Concr. Res. 8, 461-467 (1978).
5. DIN 1164, part 7, 4 pp. (1970).
6. W. Dosch, H. zur Strassen, Zement-Kalk-Gips 9, 392-401 (1967).
7. Y. Efes, Cem. Concr. Res. 10, 231-242 (1980).
8. B. Harnik, Z. Rösli, Schweizerische Bauzeitung 93, 3-7 (1975).
9. E. Hartmann, Zement-Kalk-Gips 10, 265-281 and 314-323 (1957).
10. D.B. Honeyborne, P.B. Harris, Proc. Tenth Symp. Colston Res. Soc. Bristol 24/03-27/03/1958, Butterworth's Sci. Publ., 343-365, London (1958).
11. M. Poster, D. Keucher, Baustoffindustrie 17, No. B2, 4-7 (1974).
12. W. Richartz, Zement-Kalk-Gips 22, 447-456 (1969).
13. P. Schimmelwitz, Doctor Thesis, TH Darmstadt, 23-27 (1963).
14. A. Steopoe, Tonindustrie-Ztg. 59, 765-768 (1935).
15. N. Stockhausen, H. Dorner, B. Zeck, M.J. Setzer, Cem. Concr. Res. 8, 783-794 (1979).
16. E.M. Theissing, P. v. Hest-Wardenier, G. de Wind, Cem. Concr. Res. 8, 683-692 (1978).
17. P.D. Trask, Origin and Environment of Source Sediments of Petroleum, Houston Gulf Publ. Co., 323 pp. (1932).
18. H. Ushiyama, S. Goto, Sixth Intl. Congr. on the Chem. of Cem., Suppl. Paper, Sect. II, 23 pp., Moscow (1974).
19. K. Walz, R. Springenschmid, beton 11, 507-512 (1962).
20. B. Wenger, beton 2, 52-54 (1978).

VOL. 14 1984

CEMENT and CONCRETE RESEARCH. Vol. 14, pp. 57-63, 1984. Printed in the USA.
0008-8846/84 $3.00 + 00. Copyright (c) 1984 Pergamon Press, Ltd.

Ca_3SiO_5 AND ITS FLUORINE-STABILIZED ARISTOTYPE : SYNTHESIS, STABILITY AND POSTULATED STRUCTURE OF $Ca_{6-0.5x}Si_2O_{10-x}F_x$.

M. Pérez-Méndez, R.A. Howie and F.P. Glasser

Department of Chemistry, University of Aberdeen,
Meston Walk, Old Aberdeen AB9 2UE, Scotland UK.

(Communicated by D.M. Roy)
(Received May 31, 1983)

ABSTRACT

Single crystal structural studies disclose hexagonal symmetry, a = 7.099 ± 0.003 Å, c = 5.687 ± 0.002 Å. The structure has been refined in space groups $P6_3mc$ and finally in $P6_3/mmc$. The ideal cell contents are $Ca_6Si_2O_{10}$; any fluorine present is postulated to substitute randomly for oxygen with concommitant Ca omission. The close structural relations between this phase and Ca_3SiO_5 are described.

Introduction

The incorporation of fluorine in cement raw materials may have a considerable effect on the clinker mineralogy. In the present paper, we are concerned particularly with the specific interactions between calcium silicates and F^-. These should in theory be revealed by studies of phase formation and stability in the CaO-SiO_2-CaF_2 system. However, the literature reveals considerable disagreement on phase formation and mineral equilibria.

Bereczky (1) examined this system and described two ternary phases occurring at high CaO contents, which he designated phases A and B. It is generally accepted that phase B has the $Ca_5Si_2O_8F_2$ composition and is structurally the fluorine analogue of calciochondrodite, $Ca_5Si_2O_8(OH)_2$: its stability relations in the CaO-SiO_2-CaF_2 system were explored by Gutt and Osborne (2). However, the identity of phase A has been more difficult to establish. Bereczky believed it had the composition (in wt. %) 80 C_3S - 20 CaF_2. Murkerji studied portions of the system CaO-SiO_2-CaF_2 without finding a primary phase field for phase A (3) although subsequent investigators have apparently succeeded in delineating a primary phase field (4,5). From these studies, phase A appeared to be stable only over a short range of temperatures, between 1113°C and 1185°C, above which it melted incongruently to C_3S, C_2S and liquid. As deduced in these latter studies, it had the composition $Ca_{12}Si_4O_{19}F_2$. Evidence for its composition included crystallographic data: its supposed orthorhombic cell contained one formula unit, which gave a calculated density similar to that of the observed density of a chemically purified extract containing mainly phase A. However, Gutt and Osborne (6) had independently arrived at the formula $Ca_{10}Si_3O_{15}F_2$,

although their formulation of its composition did not benefit from the application of any crystallographic restrictions. However, their powder data-40 reflections, unindexed - agree well with those reported in (5). Subsequently Gilioli *et al* (7) synthesized phase A and determined its composition; F was determined by a classical bulk chemical method, using a concentrate of phase A purified prior to analysis by chemical extraction, while Ca and Si were determined on individual crystals by microprobe. Combining these results, they give the formula as $Ca_{21}Si_7O_{33}F_4$.

A further source of difficulty concerning phase A has been the inability of previous investigators to obtain a phase-pure preparation by direct synthesis, regardless of which formula is assumed correctly to represent phase A. Most investigators have attributed synthesis difficulties to the rather short range of thermal stability of phase A; for example, in reference (7) it is noted that not only were low yields obtained even in experiments of 24 d duration at 1150°C, but that a phase-pure fraction, obtained by chemical extraction, decomposed completely during the 4 minutes required to heat it in a quench furnace from 20° to 1150°C. Thus, while the stability and composition of phase B appear to be well-established, both the status of phase A as a stable phase in this system and its exact composition are uncertain.

Experimental

Two batches used for the synthesis of phase A were prepared from analytical reagent grades of $CaCO_3$ and CaF_2 and a pure SiO_2 containing *ca* 0.1% total impurity. The batches had the calculated compositions (wt %): (I) 45.95 C_2S, 42.67 CaF_2, 11.48 CaO and (II) 48.41 C_2S, 39.19 CaF_2, 12.61 CaO. After blending in an agate mortar, *ca* 10 - 20 g portions were heated in Pt crucibles in an electric muffle in air for 24 h at 1130°. X-ray diffraction showed the product to consist of a mixture of Phase A, together with CaF_2, CaO and γC_2S. The yield, especially of phase A, tended to decline with longer heating times in both batches, while at the same time the free lime content increased. This may be associated with loss of F, which is appreciably volatile at the synthesis temperature.

Single crystals of Phase A were grown in a vertical tube quenching furnace by heating a sample contained in Pt or enclosed in welded stainless steel capsules protected against oxidation by a SiO_2 sheath. The temperature was cycled between 1130 and 1140°C, finally cooling to 1130°C at $1°C\ h^{-1}$. Substantial yields of phase A were obtained, but the preparations were never phase-pure. Phase A crystals were eventually obtained from the samples contained in Pt by handpicking under a petrographic microscope. The phase A crystals occurring in mixtures were identified by their characteristic morphology, low optical birefringence and extinction angles.

A set of single-crystal precession photographs were obtained to determine the symmetry, which was subsequently also verified by selected area electron diffraction. Single-crystal intensity data were obtained using a Nicolet P3 four-circle single crystal diffractometer.

Results

Precession photographs obtained with Mo K_α radiation disclosed hexagonal symmetry. The systematic absences ($h\,h\,l$ present for $l = 2n$) indicate possible space groups $P6_3mc$ (no. 186) or $P6_3/mmc$ (no. 194). Intensity data were collected for 102 independent reflections appropriate to the apparent hexagonal symmetry ($^1/_{12}$ of reciprocal space) using graphite-monochromated MoK_α radiation. Reflections out to 50° (2θ) were measured by the θ/2θ scan

technique. The cell dimensions, refined against the angular settings for reflections close to $2\theta = 20^0$, were $a = 7.099(3)$, $c = 5.687(2)$ Å. A powder pattern (Table 1) gives satisfactory agreement between observed and calculated values when refined using these cell dimensions. The sample used to obtain this pattern was slightly impure and reflections due to impurity phases, principally CaF_2 and CaO, have been deleted.

Table 1. Powder Data for $Ca_{6-0\cdot5x}Si_2O_{10-x}F_x$

hkl	*d*	(Å)	I	*hkl*	*d*	(Å)	I
010	6.117	(48)	9	130	1.7038	(51)	20
001	5.678	(89)	3	032	1.6639	(27)	5
011	4.171	(76)	3	131	1.6340	(33)	4
110	3.548	(50)	4	023	1.6146	(39)	25
020	3.073	(74)	41	040	1.5359	(70)	4
002	2.842	(45)	100	222	1.5055	(57)	26
021	2.703	(04)	72	041	1.4845	(38)	11
012	2.583	(82)	7	123	1.4691	(92)	3
120	2.324	(24)	19	132	1.4629	(25)	3
112	2.201	(197)	11	004	1.4222	(22)	4
121	2.149	(51)	11	230	1.4104	(04)	2
022	2.090	(88)	30	033	1.3919	(19)	3
030	2.053	(49)	4	014	1.3857	(57)	5
031	1.928	(28)	70	231	1.3688	(90)	4
003	1.897	(96)	5	042	1.3529	(22)	3
013	1.812	(12)	3	140	1.3416	(16)	2
122	1.800	(00)	7	114	1.3202	(199)	1
220	1.775	(75)	22	141	1.3060	(58)	2

Hexagonal, $a = 7.099$, $c = 5.689$. Values in ( ) are the last significant figures of the calculated spacings. Data obtained with monochromated CuK_α radiation, $\lambda_{eff.} = 1.54179$ Å.

The programme "Multan" yielded positions for atoms initially in the space group $P6_3/mmc$ of the form 2x, x, ¼ (6-fold, x = 0.1584) and $^2/_3$ $^1/_3$ $^3/_4$ (2-fold) respectively. It seemed logical to place Si in the two-fold and Ca in the six-fold positions, giving cell contents Ca_6 Si_2 .... . Possible anion positions were calculated assuming the presence of SiX_4 tetrahedra and, in order to accommodate these, a change in symmetry to $P6_3mc$. This gives x(1) positions of the type 2x, x, z (x = 0.204, z = 0.827, 6 fold) and x (2) in positions of the type $^2/_3$ $^1/_3$, z (z = 0.423, 2 fold). These occupancies complete the SiO_4 tetrahedra and, with the addition of two X atoms designated x(3) at 0,0,z (z ∿ 0.5, two fold), also complete the Ca coordination. The structure refined to R = 15%, and provides satisfactory bond distances, except for some irregularity in the Si-O distances and angles. However, the symmetry will permit only ten anions which must balance the twenty cation changes; hence the only anion distribution which will give a charge balance is attained when all anions are oxygens, *i.e.*, the compound does not contain fluorine. The ideal cell contents are, therefore, fluorine-free and, moreover, chemically identical to Ca_3SiO_5. We return to this point subsequently. There is, however, some ambiguity about the orientation of the SiO_4 tetrahedra (the direction of the Si-O(2) bond along the three-fold axis at x = $^2/_3$ and y = $^1/_3$. Complete disorder in this respect allows refinement in the space groups $P6_3/mmc$ with O(1) on 12k and O(2) in 4f (both atoms with half occupancy). This disordered model allows further refinement to R = 12% but still produces some unsatisfactory Si-O distances and angles: however, the disordered model does not remove the necessity imposed by the cation content of having all oxygen anions. The refinement was completed by adjusting Si and O to produce satisfactory bond angles and distances, a procedure which did not markedly worsen the R factor; Table 2 lists positional and bond parameters for this version of the structure, for which R = 15.9%.

Table 1. Atomic Coordinates and e s d's.

Atom	x	y	z
Ca(1)	0.31372(32)	0.15685(37)	0.25
O(1)	0.41839(170)	0.20920(159)	0.8440(21)
Si(0)	0.66667	0.33333	0.75
O(2)	0.66667	0.33333	0.46666(411)
O(3)	0	0	0.5

Bond distances and e s d's.

Bond	Distance (Å)	Bond	Distance (Å)
Ca(10-O(2)	2.495(012)	Si(1)-(1)	1.619(012)
Ca(1)-O(3)	2.396(002)	Si(1)-O(2)	1.606(023)
Ca(1)-O(1)	2.398(012)	Si(1)-O(1)	1.619(012)
Ca(1)-O(3)	2.396(002)	Si(1)-O(1)	1.619(010)
Ca(1)-O(1)	2.379(010)		
Ca(1)-O(1)	2.379(013)		

The (001) and (110) projections of the crystal structure are shown in Figs. 1 and 2 respectively. Phase A may be described as a columnar structure in which the structural units are linked into a framework. One prominent columnar unit consists of infinite chains containing Ca and those oxygens which are not also bonded to Si. These form chains of face-linked Ca-O octahedra extending parallel to *c*, containing widely-spaced and therefore isolated SiO_4 groups. The oxygens of the tetrahedra provide

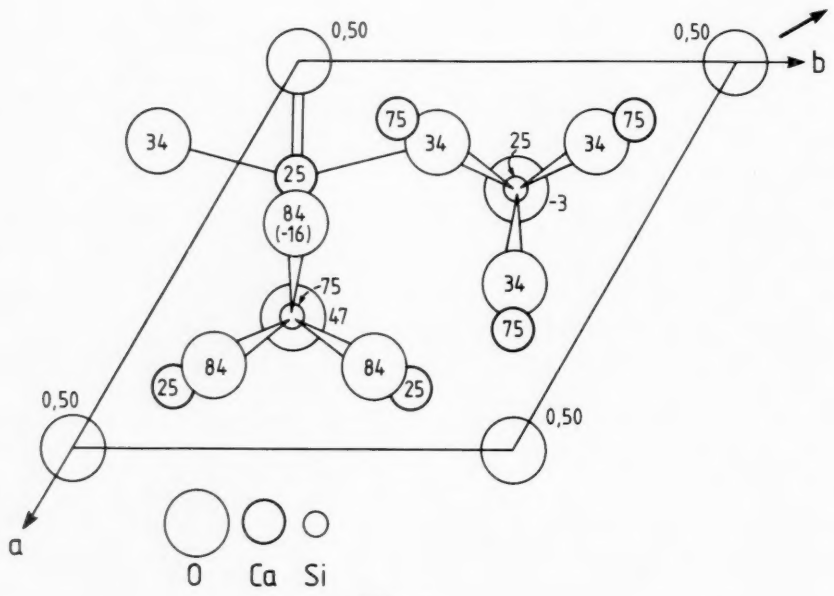

FIG. 1

Crystal structure of phase A projected on (001). Atom heights are shown as units of 0.01 z/c.

a second set of CaO-bonds rather longer than those which comprise the chains. Each Ca-O chain is surrounded by six columns containing isolated SiO_4 groups, while each column containing SiO_4 tetrahedra is in turn surrounded by three symmetrically-disposed chains of Ca-O octahedra.

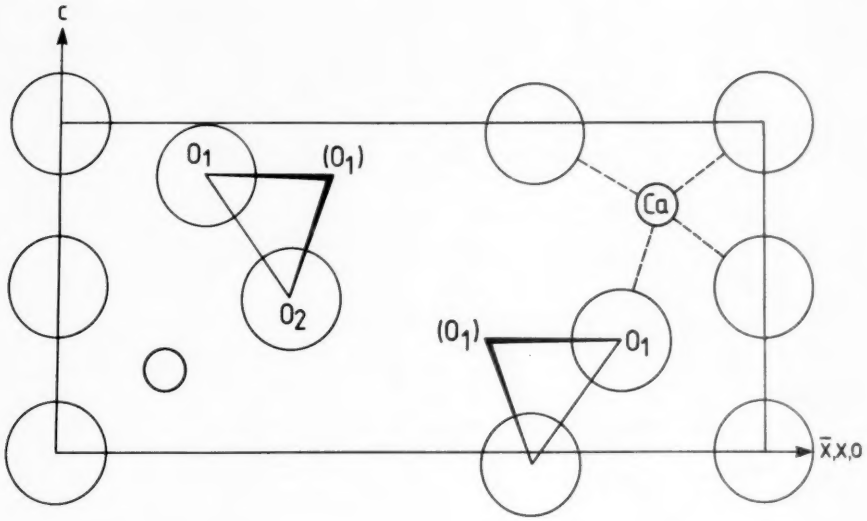

FIG. 2

Crystal structure of phase A projected on (110). The trace of the plane of this projection is shown in Fig. 1 by an arrow (upper right). Si atoms, at the centres of tetrahedra, are not shown and only Ca and O atoms actually on the plane are shown as circles.

Discussion

The crystal structure proposed for phase A may be compared with that of Ca_3SiO_5, since the idealized compositions of both phases are believed to be identical. In the C_3S structure (8) short chains each containing 3 linked Ca-O octahedra develop such that each octahedra has a three-fold axis parallel to *c*. These short chains are, however, interrupted by a regular translational motion every $^1/_3$ of a unit cell such that the topmost octahedra of each column shares corners with the three octahedra at the bottom of columns in the layer above. Dent Glasser (9), comparing the structure of Ca_3SiO_5 with those of Cd_3SiO_5 and Sr_3SiO_5, pointed out with respect to Ca_3SiO_5 that "if this arrangement is repeated regularly, rhombohedral symmetry is produced. It is suggested that the lower symmetries observed in Ca_3SiO_5 and its solid solutions are produced by slight changes in the stacking arrangement *or the introduction of columns of octahedra of different length* (italics ours) ..... such modifications may be produced by the introduction of small quantities of cations having different coordination requirements".

These speculations anticipate in several ways features observed in the present structure. In this instance, however, the substituents which alter the symmetry happen to be anions, not cations, and moreover the symmetry is not reduced but is instead enhanced by the simpler stacking pattern of octahedra in phase A, relative to C_3S. Thus, phase A is the *aristotype* structure *i.e.*, the simplest structure of its kind, while rhombohedral C_3S, together with the other stacking sequences envisioned in (9) but not yet represented by real examples, are *hettotypes* i.e., more complicated structures derivative from the ideal.

Several detailed features of the aristotype structure remain to be explored. While electron diffraction results confirm the hexagonal symmetry, they also disclose the existence of a superstructure which is not apparent by X-ray diffraction. These features, and their implications concerning the crystal structure and defect content of phase A, will be described in a subsequent paper (10). The defects may provide structural sites for fluoride ions.

Most reliable chemical analyses of phase A show that its Ca/Si ratio is 3.0, in agreement with the crystal structure analysis. It would appear from comparison of powder data that all descriptions relate to essentially the same phase. But the postulated crystal structure indicates that the idealized composition of phase A is C_3S, thereby implying that the likely level of fluorine substitution in real crystals is quite low while on the other hand, all published estimates of the fluorine content show sufficient fluorine to suggest that it is an essential constituent. Estimates of the oxygen : fluorine ratio do, however, vary widely from 7.5 (6) to 8.25 (7) and 9.5 or 10.0 (4,5) and (1) respectively. Thus the weight of published analyses appear to indicate that phase A has a substantial fluorine content although none of the analyses made on real crystals are satisfactory inasmuch as they yield unit cell contents which are commensurate with the known symmetry, cell size and density of phase A. Since the bulk compositions of mixtures used in the syntheses of phase A contain more F than the supposed composition of phase A itself, it is likely that these analyses somewhat overestimate the real F content of the crystals. Thus, although electrostatic valence considerations would rule out the presence of essential fluorine in the crystal structure some fluorine might occur, for example, substituted for oxygen with concomitant cation defects. We have preferred to indicate the possibility of some fluorine substitution in the formula, although the mechanism by which this occurs is not yet established and the quantitative extent of such substitution less than hitherto deduced from analyses.

The question arises: if the fluorine content of phase A is significantly lower than the previously - published estimates, why is phase A not more widely encountered in fluorine-fluxed cement compositions containing small amounts of fluorine (*e.g.* 0.5 - 1%)? One possible reason, we believe, lies in the origin of phase A which has not, to our knowledge, been observed to form except by crystallization from undercooled melts preferably those rich in F^-. Once formed, it does not survive even brief annealing at any subsolidus temperatures. It is possible therefore that its occurrence in the system CaO-SiO_2-CaF_2 is metastable, and that the primary phase field shown in (4,5) is instead a region in which compositions, initially all liquid or nearly so, devitrify to yield phase A upon quenching. But its suspected metastability, at least under some conditions, need not necessarily detract from its importance in the clinkering cycle. Metastable crystallizations are suspected to occur regularly in cement clinker systems; for example, much of the C_3A developed during clinker cooling is believed to form by crystallization from undercooled melts and, on that account, may exhibit solid solution compositions which cannot be achieved under equilibrium conditions (11). Nevertheless, phase A has a composition close to that of C_3S, and when fluoride-fluxed compositions are heated to temperatures such that a fluorine-rich liquid phase is developed, the possibility that phase A may crystallize during cooling - partly to the exclusion of C_3S - cannot be overlooked. Since phase A exhibits much less hydraulic activity than C_3S, the modifying effect of fluorine on the phase composition is obviously an important factor governing the proportioning of fluoride-containing clinker compositions.

VOL
14
198

Another interesting question raised originally in (9) concerns the possibility that other hettotypes of C_3S exist. These may not be immediately recognizable as such from their powder patterns and we hope to be able to undertake a more systematic search for other hettotypes.

Acknowledgement

This work was undertaken with financial assistance from the British Council which enable one of us (M.P.M.) to visit Aberdeen. Their support is gratefully acknowledge as well as the cooperation of the Instituto Eduardo Torroja for granting her leave of absence.

References

1. E. Bereczky, Epitöangag 16 (12), 441 (1964).
2. W. Gutt and G.J. Osborne, Trans. Brit. Ceram. Soc. 65 (9),521 (1966).
3. J. Mukerji, J. Am. Ceram. Soc. 48, 210-213 (1965).
4. S. Akaiwa, G. Sudoh and M. Tanaka, Rev. 20th Gen. Mtg. Cement Assoc. Japan (Engl. Abstr.), 34-38 (1966).
5. M. Tanaka, G. Sudoh and S. Akaiwa, Proc. 5th Intl. Symp. on the Chemistry of Cement (Tokyo), Vol. 1, 122-135, (Cement Assoc. Japan, Tokyo) (1969).
6. W. Gutt and G.J. Osborne, Trans. Brit. Ceram. Soc. 67,125-133 (1968).
7. C. Gilioli, F. Massazza and M. Pezzuoli, Cem. Concr. Res. 9, 295-302 (1979).
8. J.W. Jeffery, Acta Crystallog. 5, 26 (1952).
9. L.S. Dent Glasser, Acta. Crystallog. 18, 455-457 (1965).
10. M. Pérez-Mendez, J.A. Gard and F.P. Glasser (in preparation).
11. K.S. Han, J.A. Gard and F.P. Glasser, Cement and Concr. Res. 11, 79 - 84 (1981).

OL.
14
984

CEMENT and CONCRETE RESEARCH. Vol. 14, pp. 64-72, 1984. Printed in the USA.
0008-8846/84 $3.00 + 00. Copyright (c) 1984 Pergamon Press, Ltd.

A VISCOMETRIC METHOD OF MONITORING THE EFFECT OF RETARDING ADMIXTURES ON THE SETTING OF CEMENT PASTES

J.I.Bhatty and P.F.G. Banfill
Department of Building Engineering, University of Liverpool
Liverpool L69 3BX, U.K.

(Communicated by S. Diamond)
(Received May 31, 1983)

ABSTRACT

The effect of retarders on the rheological behaviour of fresh cement pastes has been studied, using rotational viscometry. Cement pastes subjected to continuous shear undergo reaggregation, indicated by the initial build up section of the torque-time curve. It is followed by a dormant period where the paste is at equilibrium which ends when setting starts and the final build up phase begins. The delay time and the kinetics of the final phase depend on the concentration of admixture and nature of the cement. The rates of build up in the initial and final build up sections of the torque-time curve are independent of retarder concentration but vary with the cement. The correlation between these results and those obtained with the Vicat test for the initial setting time of cement paste is discussed.

VOL. 14 1984

Introduction

Organic retarding admixtures are of great interest in concrete technology, giving prolonged setting time and workability retention without significantly affecting the long term mechanical properties (1). Evaluation of their mode of action and efficiency has been carried out by a variety of methods - electrical, thermal, chemical and mechanical. The latter category includes such well established tests as the Vicat penetrometer and the automated penetration devices of Bombled (2) and Forrester (3). Since setting can be viewed as the formation of a solid from a mobile suspension, the transformation should be amenable to study using conventional rheological techniques. This paper describes a rheological method based on a rotational viscometer which has been used to monitor the effect of various admixtures in cement pastes.

The Rheology of Cement Paste

In recent years, many workers have studied the rheological properties of cement pastes, with and without admixtures (4-13). Their investigations have generally been restricted to studying the behaviour of cement paste during the early periods of hydration either by the determination of flow

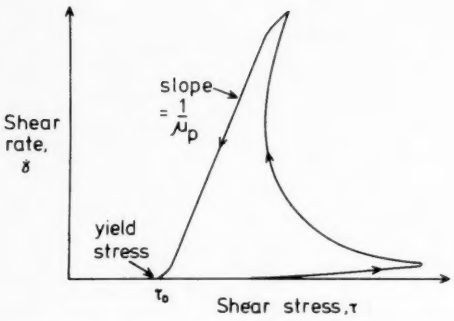

FIG.1
Flow curve of typical cement paste

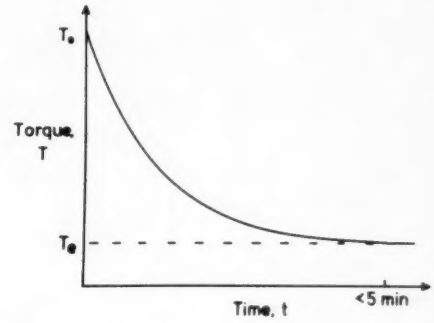

FIG.2
Structural breakdown of cement paste under continuous steady shear

curves at changing shear rates (Fig.1) or studying the time dependent rheological behaviour of the cement paste at a constant shear rate (Fig.2). Various flow curve shapes have been noted (10) while the time dependent behaviour, first investigated by Tattersall (11), has recently been reviewed in detail (15).

Fresh cement pastes undergo structural breakdown when subjected to shear which is indicated by decay in the torque on a rotating impeller with time according to an exponential relationship:

$$T - T_e = K.\exp(-Bt) \qquad (1)$$

At the equilibrium value of torque, T_e, the structure in the paste is either broken down to a fully dispersed state or the rates of breakage and of reforming are equal. Subsequently the apparent viscosity of the paste increases as setting starts and the structure builds up, increasing the torque on the impeller.

It has been suggested that retarding admixtures could delay this buildup region in the cement paste and in preliminary work, Banfill (14) found that the increase of torque, $T-T_{min}$, with time, t, followed a relationship of the form:

$$T - T_{min} = At^b \qquad (2)$$

The effect of retarding admixture appeared to be to change the value of A while b remained constant.

Experimental Details

Pastes of various commercially available cements, with the compositions given in Table 1, were prepared with a fixed w/c ratio of 0.35 by weight. 100 grams of cement was first mixed with 90% of the necessary deionized water using a Gallenkamp propellor turbine mixer rotating at 2500 rpm, until the paste was completely homogenized. The remaining 10% of the mixing water containing the required amount of admixture was then added while the paste was still being stirred. The stirring was stopped when this addition was complete after a total time of 4-6 minutes depending on the cement. The paste was then placed in the viscometer cup and the impeller lowered into position. The motor was then switched on and the measurements started.

TABLE 1
Chemical and Physical Properties of the Cements

CEMENT	A (high alkali)	B (low alkali)	C (high C_3A)	D (low C_3A)
SiO_2 (%)	19.9	18.7	20.5	19.8
CaO	65.4	63.6	65.7	64.6
Al_2O_3	4.8	5.6	5.8	3.6
Fe_2O_3	3.3	3.7	2.2	5.0
SO_3	2.3	2.5	2.7	2.3
Na_2O	0.36	0.08	0.20	0.24
K_2O	0.87	0.52	0.61	0.36
Specific surface (m^2/kg)	344	340	332	385
w/c for standard consistence	0.28	0.256	0.26	0.285

This mixing sequence had two advantages: (i) it produced a "fully broken paste" which gave no further breakdown in the viscometer, enabling the build up of structure to be seen right from the start of the experiment; (ii) it was expected that this mixing sequence would give an optimum retarding effect as the gypsum in the cement pre-mixed with water for few minutes would make a self retarding ettringite skin and leave a larger amount of retarder to adsorb on $Ca(OH_2)$ nuclei and on silicate materials (16). The mixing times to achieve a fully broken down paste varied from 3 to 6 minutes according to the cement.

The viscometric investigation of the cement pastes was carried out in a Haake Rotovisco RV2 viscometer with MK500 torque measuring head. All the experiments were done with a helical impeller in a serrated cylinder (Fig.3), and the behaviour of the pastes was directly recorded in the form of torque-time plots at a steady speed of 450 or 512 rpm (corresponding to an average shear rate of 187-213 sec^{-1}), using the electrical output for the torque dynamometer. It has previously been found that continuous shearing with this impeller prevents sedimentation during the experiment (17).

For reference information, conventional Vicat initial set time tests were carried out according to the procedure of B.S. 4550 (18) but with a mixing sequence similar to that adopted for the rheological tests. 400 grams of cement were mixed by hand with 90% of the mixing water for 3½ minutes after which the remaining 10%, containing the appropriate amount of admixture, was added and mixed for a further 1½ minutes before placing in the Vicat

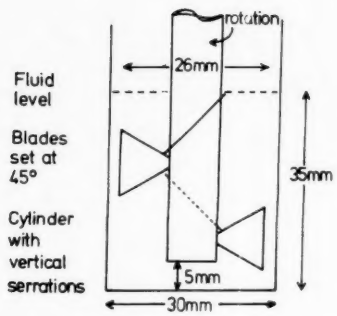

FIG.3
The helical impeller/serrated cylindrical viscometer geometry.

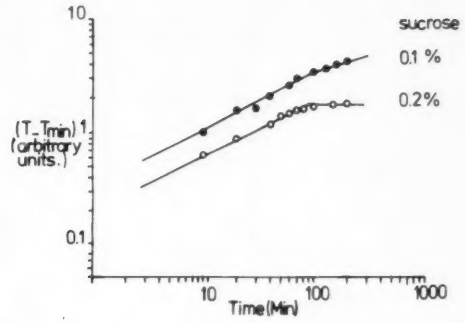

FIG.4
The increase in torque with time in the early stages of buildup.

mould. The water/cement ratio used in these tests was that needed to give a paste of standard consistence, as defined by B.S. 4550 and was different for each cement, as given in Table 1.

The retarders used were the sugars glucose, maltose and sucrose, all of analytical grade, and were used in concentrations of 0.05, 0.1 and 0.2% by weight of cement.

All experiments were carried out under thermostatically controlled conditions at 20 $\pm$ 1°C.

Results

Banfill's preliminary studies (14) implied that if a fully broken down paste were subjected to continuous shear the torque on the rotating impeller would increase smoothly right from the start of shearing, since the act of breaking down the structure in the paste by vigorous mixing would remove the structural breakdown part of the torque-time relationship. However, as shown in the example of Fig.4 the plot of log $(T-T_{min})$ against log t is indeed linear but shows a transition to a second region of reduced slope. This well defined and reproducible behaviour was found to be independent of the presence and concentration of sugar, but varied with cement. That the time of this transition, in the region of 100 minutes, is within the timescale of the induction or dormant period in the hydration of cement suggested that if shearing were further prolonged effects due to the end of the induction period would be detected.

Accordingly the next set of experiments were extended to 1000 or more minutes, the time limit being set by the maximum torque available on the viscometer. Only sucrose was used in this part of the work and Figs. 5 and 6 show the effect of concentration on the increase of torque with time. The parameters of the power law expression for the buildup of structure, equation (2), can be calculated from the data of Fig.6 and are presented in Table 2.

The increase in torque with time falls into three phases, which become more distinct as the concentration of sucrose increases: an initial build up phase of decreasing rate, an intermediate phase whose length increases with the concentration of sucrose and a final build up phase which shows contin-

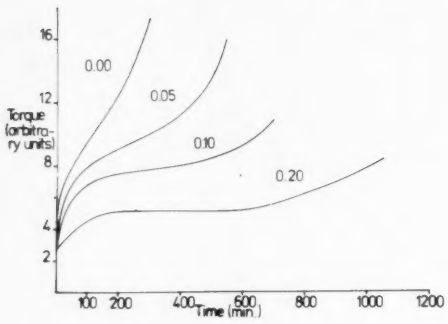

FIG.5
Extended torque-time plots for pastes of Cement C containing sucrose at various concentrations (% by weight of cement).

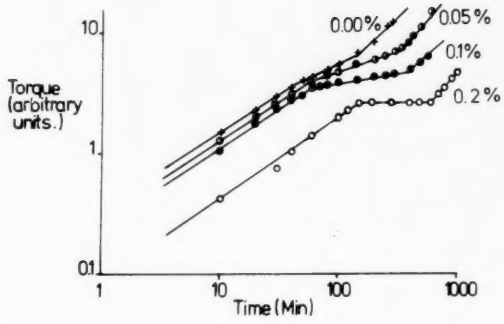

FIG.6
Data of Fig.5 plotted on logarithmic scales.

TABLE 2
Effect of sucrose concentration on parameters of equation (2) for Cement C paste. Shearing speed 512 rpm.

Phase	Parameter	Sucrose concentration % 0	0.05	0.1	0.2
I	A	0.35	0.28	0.24	0.09
	b	0.64	0.65	0.66	0.67
II	A	0.70	1.05	1.82	2.71
	b	0.45	0.33	0.16	0
III	A	0.07	0.01	0.02	0.002
	b	0.91	1.11	0.97	1.12

uous acceleration to the end of the experiment. Table 2 shows that the power law exponent, b, in phase III is 1.5 times that in phase I, but in both phases is independent of sucrose concentration. Both parameters depend on concentration in phase II, while the "length" of phase II makes parameter A of phase III strongly dependent on concentration.

A further parameter of potential use is the delay time, defined as the elapsed time from the start of the experiment to the transition between phases II and III. This implies that the onset of phase III marks the end of the induction period and the start of the main phase of hydration and avoids the complexities of the effects of the first two phases. It might be expected to correlate in some way with the setting time as determined by the Vicat test. Table 3 and Fig. 7 show that a linear relationship with a correlation coefficient of 0.95 exists.

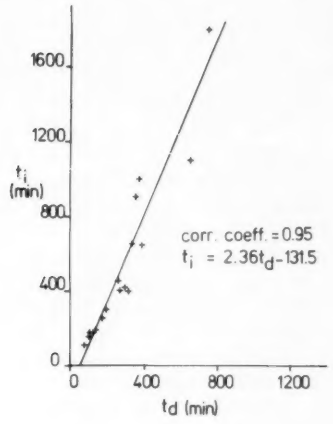

Fig.7
Correlation of Vicat initial setting time (t_i) and delay time (t_d) determined in viscometer.

TABLE 3
Effect of sucrose concentration on initial setting time (t_i) and delay time (t_d)

Cement	Times in minutes	Sucrose concentration %			
		0	0.05	0.1	0.2
A	t_i	170	420	1000	1800
	t_d	100	290	370	750
B	t_i	150	300	400	650
	t_d	100	190	265	330
C	t_i	185	400	650	1100
	t_d	130	310	385	600
D	t_i	110	250	450	900
	t_d	70	170	260	350

Discussion

Interpretation of results

The results confirm that changes in the rheology of cement pastes with time certainly occur, but the observed effects are complex. By appropriate calibration the torque data for the rotating impeller can be converted to apparent viscosity so that the results show that apparent viscosity increases with time. For cement paste this can be due to an increase in yield value and/or plastic viscosity (Fig.1). Other work suggests that the change in yield value is greater than the change in plastic viscosity (15).

Application of the special preparation technique used in this work has prevented the shear breakdown of flocculation structure from obscuring the build up of hydration structure in the early stages of reaction, but it has revealed fresh complexities. Apparent viscosity increases at a decreasing rate for an initial period, which is followed by a dormant period of relatively constant viscosity whose length depends on the concentration of retarder. The end of the dormant period is shown by the apparent viscosity again starting to increase, but this time at an increasing rate (Fig.5). This behaviour shows marked similarity to the stages of the hydration of cement as demonstrated by conduction calorimetry, where a pre-induction stage of decelerating reaction is followed by the induction period of very slow reaction and a post induction stage of accelerating reaction.

According to a recently proposed model (19), the initial reactions between cement and water produce a mixed calcium sulphoaluminate and silicate gel layer around the grains. This layer retards hydration during the dormant period and hydration can only restart when the gel is ruptured and reactants come into contact. As the gel layer is selectively impermeable to silicate ion, osmotic pressure builds up inside the skin until rupture occurs and extruded hydrosilicate combines with Ca^{2+} in solution to form the secondary outgrowths of calcium silicate hydrate. In these terms the observed initial increase in apparent viscosity (phase I) would appear to be due to removal of water from the paste combined with changing morphology which increases the resistance to flow of individual particles. Phase II would correspond to the dormant period in the hydration and the final increase in apparent viscosity (phase III) would be due to entanglement of the outgrowths which eventually interlock to give a solid mass.

VOL.
14
198

Closer scrutiny of the results casts some doubt on this interpretation as it is difficult to explain the effect of admixtures on the three sections of the increasing viscosity graph (Fig.5). The relationship between torque and time for a cement paste (equation 2) is entirely empirical, obtained by curve fitting, and there is at present no theoretical basis for it. However, we suggest that the exponent b can be described as a 'mechanism' parameter such that similar processes have the same values of b and wide variations in b indicate different mechanisms. The constant A is interpreted as a 'rate' parameter.

Thus the fact that admixture changes the value of A but not of b in phase III is taken to indicate that the same process is occurring, but at a different rate. Similarly the difference between the b values for phases I and III suggest that different processes are occurring in these phases.

The build up kinetics in the first phase of reaction are independent of admixture type and concentration. Since it is well known that retarders interact with the aluminate phases which react rapidly with water (16), this independence suggests that phase I of the build up is not due to chemical reaction. Also the initial chemical reactions are substantially complete within a few minutes of mixing and certainly within the time taken to load the paste into the viscometer. The first build up phase is more likely to be a physical process such as reaggregation or flocculation from the highly dispersed state in which the paste is prepared. However, further tests are necessary to confirm this.

Phases II and III of the structure build up are affected by concentration of admixture and clearly reflect chemical processes. In commercial cements

gypsum is added to prevent flash set due to the rapid hydration of tricalcium aluminate, and the dormant period lasts until sulphate is exhausted or until the hydration of tricalcium silicate restarts. Bensted concluded that only the latter process was responsible for setting provided that the tricalcium aluminate was adequately retarded (20).

The action of sugars is to extend the dormant period and slow down the subsequent hydration reaction. Without speculating on the mechanism, which is still controversial, it need only be noted that the effect of sucrose on phase II and III reflects this effect.

The correlation of delay time and Vicat initial setting time is further evidence in favour of this interpretation. If the delay time marks the end of the dormant period a further time interval would be expected before the hydration structure in the paste builds up enough to reach the arbitrary condition of penetration resistance. Therefore the delay time is always shorter than the Vicat initial setting time. In addition the length of the further time interval to setting depends on the rate of hydration subsequent to the delay time, which in turn is affected by the retarding admixture concentration. The twofold effect of sucrose noted above therefore results in the linear correlation between delay time and Vicat initial setting time, of which the latter is about 2.5 times the former.

OL.
14
984

Potential usefulness of the method

While the full details of the mechanisms underlying the changes in rheology described here are not yet fully worked out, the potential of the method has been shown. The delay time, marking the end of the dormant period and the start of the main stage of hydration, correlates with the initial setting time of the Vicat test and could be used alone as a criterion of setting for studies of the effect of set retarders. Inspection of Tables 2 and 3 shows a broad negative correlation between the parameter A of phase III of the build up of structure and the initial setting time so that this parameter, which relates to the position on the time axis of this phase of the torque-time plot, could also be used as a criterion of setting. Since both parameters are derived from kinetic data which are not sensitive to paste composition the preparation method need not be so rigorously defined as in the Vicat test and the results are consequently more reproducible.

Conclusions

1) The viscometric technique described is capable of monitoring the setting process in cement pastes.
2) The apparent viscosity of a cement paste which has been prepared by vigorous stirring to break down the floc structure increases in three phases which are interpreted as corresponding to (I) initial reaggregation, (II) dormant period, (III) hydration.
3) The transition from phase II to III occurs after a delay time which is shorter than the Vicat initial setting time but correlates linearly with it.
4) Phase I appears to be independent of the presence of retarders, but the kinetics of phases II and III depend on retarder concentration and can be used to judge the relative efficiencies of different retarding admixtures.

Acknowledgements

The authors are grateful to the Science and Engineering Research Council for the financial support of this work.

References

1. Rixom, M.R., Chemical Admixtures for Concrete. Spon, London 1978.
2. Bombled, J.P., Rev. Mater. Construct. (673), 256-277, 1970.
3. Forrester, J.A., Private Communication.
4. Daimon, M., Roy, D.M., Cem. Concr. Res. 9, 103-112, 1979.
5. Roy, D.M., Asaga, K., Cem. Concr. Res. 9, 731-739, 1979.
6. Asaga, K., Roy, D.M., Cem. Concr. Res. 10, 287-295, 1980.
7. Roy, D.M., Asaga, K., Cem. Concr. Res. 10, 337-344, 1980.
8. Jones, T.E.R., Taylor, S., Silic. Ind. 43, 83-88, 1978.
9. Banfill, P.F.G., Mag. Concr. Res. 33, 37-47, 1981.
10. Banfill, P.F.G., Saunders, D.C., Cem. Concr. Res. 11, 363-370, 1981.
11. Tattersall, G.H., Brit. J. Appl. Phys. 6, 165-167, 1955.
12. Tattersall, G.H., Dimond, C.R., Hydraulic Cement Pastes: Proc. Conf. University Sheffield, Slough, C. & C.A., 118-133, 1976.
13. Lapasin, R., Lougo, V., Rajgelj, S., Cem. Concr. Res. 9, 309-318, 1979.
14. Banfill, P.F.G., Proc. 7th. Int. Congr. Chemistry of Cement, IV, 324-328, Paris, 1980.
15. Tattersall, G.H., Banfill, P.F.G., The Rheology of Fresh Concrete, Pitman, London, 1983.
16. Bruere, G.M., Nature 199, 32-33, 1963.
17. Bhatty, J.I., Banfill, P.F.G., Cem. Concr. Res. 13, 69-78, 1982.
18. B.S.4550: Part 3: Section 3.6: 1978, Methods of testing cement: Test for setting times. B.S.I. London, 1978.
19. Birchall, J.D., Howard, A.J., Double, D.D., Cem.Concr.Res. 10, 145-155, 1980.
20. Bensted, J., Silic.Ind. 45, 115-20, 1980.

VOL. 14 1984

CEMENT and CONCRETE RESEARCH. Vol. 14, pp. 73-82, 1984. Printed in the USA.
0008-8846/84 $3.00 + 00. Copyright (c) 1984 Pergamon Press, Ltd.

THE CHEMISTRY OF HYDRATION OF HIGH ALUMINA CEMENT IN THE PRESENCE OF ACCELERATING AND RETARDING ADMIXTURES

S.A. Rodger and D.D. Double
University of Oxford
Department of Metallurgy and Science of Materials
Parks Road, Oxford, OX1 3PH, England

(Communicated by H.F.W. Taylor)
(Received May 31, 1983)

DL.
14
984

ABSTRACT

The effect of accelerators, and in particular lithium salts and citric acid solutions, on the setting time of high alumina cement has been studied using calorimetry, solution analysis and X-ray diffraction techniques. Results are discussed with respect to the ternary $CaO-Al_2O_3-H_2O$ solubility diagram. It appears that there is a nucleation barrier to the precipitation of the main products of hydration, CAH_{10} and C_2AH_8 and that lithium salts function as accelerators by precipitation of a lithium aluminate hydrate which acts as a heterogeneous nucleation substrate. It is suggested that retardation by citric acid is due to the precipitation of protective gel coatings around the cement grains which impede hydrolysis or inhibit growth of the hydration products.

Introduction

High alumina cement (HAC), which was originally developed for its sulphate resisting properties, has an important practical advantage in its rapid hardening characteristics (1). The principal hydraulic constituent in HAC clinker is monocalcium aluminate and the hydration process is usually represented as (2):

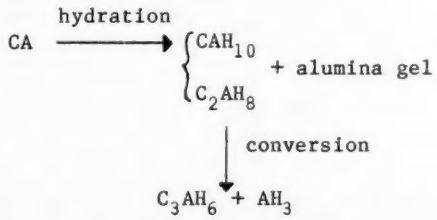

In contrast to Portland cement where the major cohesive hydration product is colloidal C-S-H gel (~60% by volume) with lesser amounts of crystalline calcium hydroxide and aluminate hydrates, the hardening of HAC is associated with the formation of an interlocking structure of crystalline aluminate hydrates, principally CAH_{10} but also C_2AH_8. The proportions of CAH_{10} and C_2AH_8 depend on the temperature of hydration. Quantities of alumina gel contribute to the consolidation of the microstructure, the gel having a tendency to age to crystalline forms in mature pastes (viz. gibbsite AH_3). The hydrates CAH_{10} and C_2AH_8, which have hexagonal crystal structures, are metastable with respect to 'conversion' to the cubic hydrate C_3AH_6, a process accelerated in warm and moist conditions (1-4). The microstructural changes associated with conversion involve not only a change in crystal structure and morphology of the hydrates but also a contraction in volume of solids with a resultant increase in porosity in the hardened paste. This can lead to very dramatic decreases in strength and durability and is the source of much-publicised problems that have been encountered in the past in the structural use of HAC concretes (3).

Because of the problems associated with conversion, there are now legal restrictions on the structural use of HAC concretes in many countries. Nevertheless, the cement still finds wide application for refractory purposes and also in grouts/concretes designed for anchoring or rapid repair work. In these latter applications, the use of admixtures to control the setting and hardening has been found desirable.

To a large extent, the practical use of accelerating and retarding admixtures for HAC is on an empirical basis and is not well documented in the literature. Robson (1) states that in general alkaline compounds tend to accelerate the set of HAC whilst acidic compounds retard. Thus dilute solutions of sodium or potassium hydroxide and organic bases such as triethanolamine are accelerators whilst hydrochloric and acetic acid act as set retarders. Solutions of glycols, glycerine, sugars and casein are reported to have a regarding effect. Citric acid is used commercially as a retarder for HAC and Young (5) has suggested that some hydroxycarboxylic acids have the advantageous effect of stabilising the hexagonal calcium aluminate hydrates with respect to conversion to the cubic hydrate. Lithium carbonate has been found to be a very effective accelerator for HAC, the degree of acceleration increasing with the amount of the salt added to the gauging water (6). In chemical terms, the mode of action of these admixtures is not well understood.

This paper describes a study of various admixtures for HAC with the object of assessing their effect as accelerators or retarders. In order to characterise their chemical interaction during hydration of the cement, lithium salts (accelerators) and citric acid (retarder) have been examined in some detail using calorimetry, solution analysis and X-ray diffraction methods.

Experimental Methods

(a) Materials

The cement used was a commercial Lafarge Ciment Fondu with the following oxide compositions:

CaO:	38.5%	FeO:	4.0	Mn_2O_3:	0.1
Al_2O_3:	39.0	TiO_2:	2.5	P_2O_5:	0.2
SiO_2:	4.5	MgO:	0.4	SO_3:	0.15
Fe_2O_3:	10.0	Na_2O:	0.1	Traces:	0.35

The major clinker phase was monocalcium aluminate (~70%) with minor phases including $C_{12}A_7$, C_4AF and C_2S. The admixtures used were Analar grade reagents, dissolved in freshly distilled water prior to mixing with the cement.

(b) Calorimetry

A simple adiabatic method was used to monitor the hydration process. Cement paste samples (w/c = 0.5) were contained in pyrex tubes surrounded by a thermally insulated container. The temperature rise as a function of time was measured by means of a chromel-alumel thermocouple embedded in the paste.

(c) Solution analysis

Cement slurries (w/c = 1.5) were mixed by means of a magnetic stirrer for prescribed time intervals and then rapidly filtered to extract the aqueous solution. Mixing and filtering was carried out in plastic apparatus (to avoid contamination by silica from glassware) under an atmosphere of nitrogen to prevent atmospheric carbonation. The ambient temperature was 22±2°C. After filtration, aliquot portions of the solution were immediately analysed for the following ions:

Calcium:	EDTA titration after complexing Fe and Al with ethanolamine.
Aluminium:	colorimetric analysis of solochrome cyanine R complex and by atomic absorption spectrophotometry.
Silicon:	colorimetric analysis of molybdenum blue complex.
Iron:	colorimetric analysis of thioglycollic acid complex.
Chloride:	colorimetric analysis of ferric thiocyanate complex.
Lithium:	atomic emission spectrophotometry.
Hydroxyl:	acid-base titration, using HCL and phenolphthalein indicator.
Citrate:	colorimetric analysis of acetic anhydride and pyridine citrate complex.

Details of the mixing and filtering system and the procedures for analysis may be found in previous publications (7, 8).

(d) X-ray diffraction

Samples of hardened cement cured for 2 days at room temperature were finely ground and diffractometer traces were obtained with a Philips PW10/50 goniometer system using Cu K_α radiation.

RESULTS

(a) Adiabatic calorimetry

Temperature versus time profiles for an untreated cement control sample and samples treated with equimolar amounts of various lithium salts (w/c = 0.5 with solutions 0.05M with respect to Li^+ in the admixtures) and citric acid are shown in Figure 1. In the control sample, the temperature of the paste remained roughly constant at room temperature for a period up to 6½ hours and then showed a rapid rise, the paste soon becoming too hot to touch and finally generating steam. During the initial latent period the paste remained in a fairly plastic condition the final temperature rise being associated with an observable hardening reaction. In a number of control samples the time of the temperature rise was fairly reproducible occurring between 6 - 7 hours after mixing.

The very pronounced accelerating effect of the lithium salt admixtures is evident in the heat evolution profiles. In cement samples treated with different lithium salts the temperature rise occurred very soon after mixing (in some cases beginning almost immediately) reaching a maximum within 20 - 30 mins, with a rapid stiffening and hardening of the paste. Each lithium salt tested proved to be effective as an accelerator with only slight variations in final set time.

In contrast, the citric acid admixture produced a very distinct retarding action. The latent period was extended to about 17 hours after mixing, the paste remaining in a plastic condition during this time. Eventually a temperature rise was recorded and the paste hardened. It is notable that lithium citrate, in common with other lithium salts, showed an accelerating effect.

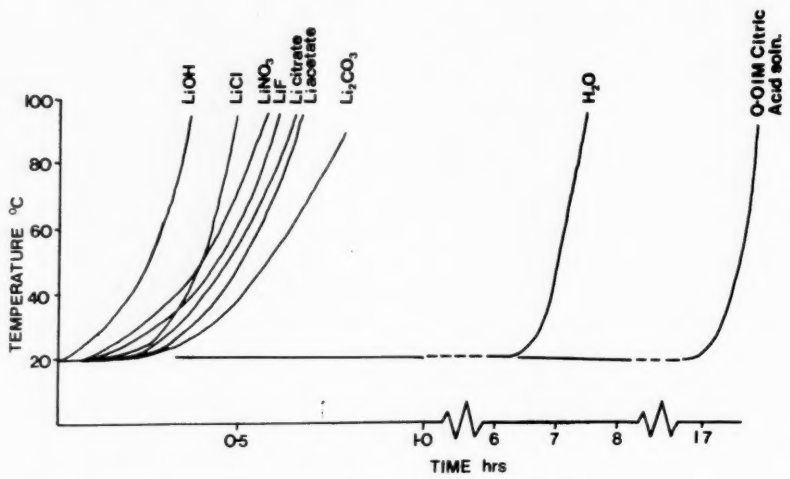

FIG. 1
Temperature versus time profiles for cement samples treated with various lithium salts, water and citric acid.

To test whether other metal cations had a similar effect to that of lithium a range of chloride salts of univalent, divalent and trivalent cations were investigated. The results are shown in Figure 2, which records the position of the maximum temperature rise from calorimetry traces. It is evident that none of the metal cations tested had an accelerating effect comparable to that of lithium. Lanthanum and magnesium chlorides showed some accelerating tendency whilst zinc, copper, mercury and manganese chlorides showed a distinct retarding effect. Both calcium chloride and strontium chloride which are set accelerators for Portland cement show a retarding effect with HAC.

(b) Solution Analysis

To investigate the chemistry of hydration of HAC in the presence of lithium chloride and citric acid admixtures comprehensive analyses were carried out of the solutions extracted from cement slurries (w/c = 1.5) at various time intervals after mixing. The results are shown in Figures 3(a), (b) and (c). In the untreated control sample (Figure 3(a)), calcium, aluminium and hydroxyl levels rise very rapidly within the first 10 minutes after mixing, reach a maximum after about 75 minutes and then gradually decline at similar rates over a longer time period. The CaO/Al_2O_3 ratio in solution is initially around 1 - 1.3 but decreases later. The iron and silicon levels in solution remain very low (generally 10^{-2}mm) during the six hour period.

Comparing this with the sample treated with lithium chloride (Figure 3(b)) it is evident that there are considerable changes in the solution chemistry. The Ca^{++} and OH^- levels reach about the same values as in the control sample during

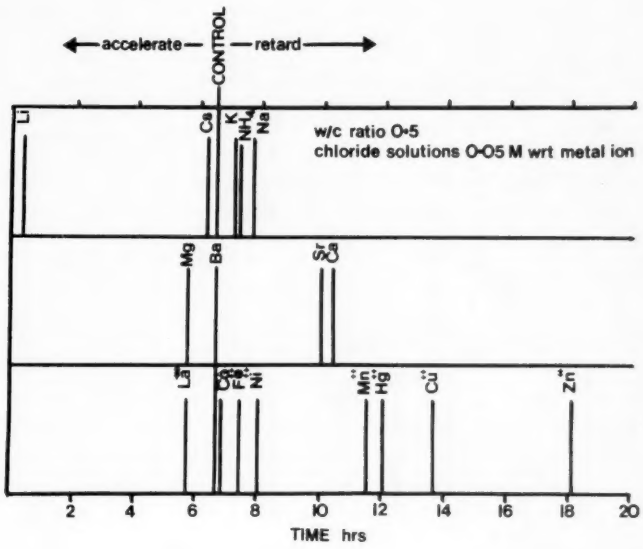

FIG. 2
Positions of maximum temperature use for cement samples treated with a variety of chloride solutions.

VOL.
14
984

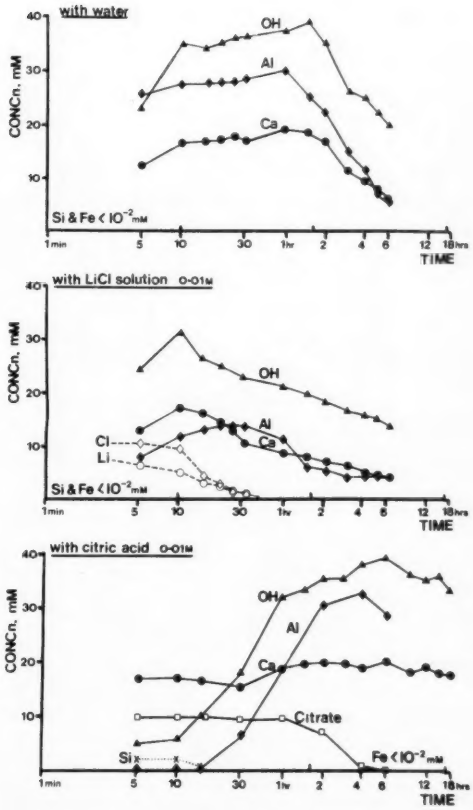

FIG. 3
Concentration versus time curves for solutions filtered from cement pastes made with
(a) Water
(b) Lithium chloride solution
(c) Citric acid solution

the first 10 minutes, but thereafter decrease much more rapidly. Notably, the aluminium levels in solution are depressed during the 6 hour period and do not reach the maximum value found in the control system. Lithium and chloride levels also drop very rapidly, becoming hardly detectable after about ½ hour. Silicon and iron concentrations again remain neglibibly low.

A more complex situation occurs in the cement sample treated with citric acid (Figure 3(c)). As one might expect from the addition of acid, the OH^- levels in solution are initially depressed but these gradually re-establish themselves to roughly the same values occurring at the maximum in the control. An interesting feature is that within detection limits, aluminium does not appear in solution until after the first ¼ hour, the concentration rising steadily thereafter reaching a maximum at about 30mM. During this period there is a transient appearance of silicon in concentrations substantially greater than observed hitherto. Throughout the period of observation, the Ca^{++} concentration in solution remains roughly constant at about 20mM. The citrate admixture remains in solution for the first hour and thereafter decreases slowly over the next four hours.

(c) X-ray Diffraction

Figure 4 shows the diffractometer traces obtained from (a) the anhydrous cement clinker, (b) a hydrated cement paste made with distilled water and (c) a cement paste hydrated in a 10mM solution of lithium chloride. Comparison of 4(a) and (b) shows, in addition to the peaks associated with the anhydrous clinker phases, the appearance of peaks from the hexagonal hydrate CAH_{10}. Smaller peaks from hexagonal C_2AH_8 are just detectable. As discussed in the introductory section, these are the expected hydration products of HAC under normal conditions. The samples were hydrated at room temperature and there was no sign of conversion to the cubic hydrate C_3AH_6. In the sample treated with LiCl (figure 4(c)) significant differences are evident. The diffraction peaks indicate that the main crystalline hydration product is now C_2AH_8 with only a small amount of CAH_{10} present. In addition extra diffraction peaks appear which are identifiable on the ASTM index with a lithium hydro-meta-aluminate LiH $(AlO_2)_2.5H_2O$. A diffractometer trace was also obtained from a cement sample treated with

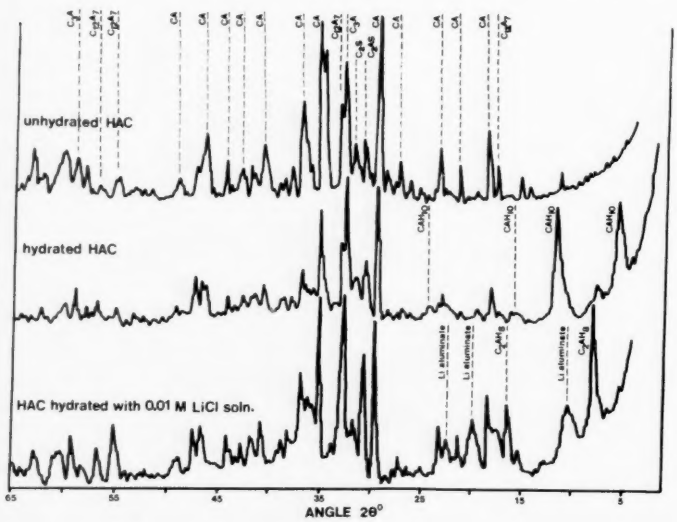

FIG. 4
X-ray diffraction traces obtained from
(a) unhydrated HAC
(b) hydrated HAC
(c) HAC hydrated with lithium chloride solution

citric acid solution but this was not significantly different from the control sample in Figure 4(b). CAH_{10} was the main hydration product and there was no evidence of any new crystalline hydrate phases.

Discussion

Lithium chloride admixture has been shown to produce changes in the chemistry of hydration of HAC and in the nature of the hydration products. It is relevant to consider the solution chemistry data (Figs. 3(a) and (b)) in terms of the solubility diagram for the ternary $CaO-Al_2O_3-H_2O$ system. Figure 5 illustrates the form of the solubility diagram at room temperature, plotted on orthogonal axes. The lines AB, BC, CD and DE indicate the solubility limits for solutions in contact with the crystalline phases CAH_{10}, C_2AH_8, C_4AH_{13} and calcium hydroxide respectively. The solubility limit for alumina gel/hydrous alumina (AH_x) is variable and is given approximately by the line OA. For clarity, the solubility limits of the stable cubic hydrate C_3AH_6 have not been included in the diagram. This omission is not important in this discussion since we are primarily concerned with the formation of the hexagonal calcium aluminate hydrates and not the conversion reaction. It is worth bearing in mind, however, that Figure 5 represents the metastable form of the solubility diagram. These solubility limits have been determined experimentally by a number of researchers (9 - 11). To obtain a comprehensive picture of the solubility relationships in this system, Figure 5 has been drawn to include two and three phase regions beyond the solubility limits. Three phase regions (two solid hydrates + solution) are represented by the triangular shaded areas. Two phase regions (one solid hydrate + solution) are represented by areas drawn with parallel lines. In the latter case, these 'tie-lines' are inclined at angles determined by the C/A ratio of the particular hydrate involved. The points A, B, C and D represent invariant points (according to the Gibbs phase rule) giving the compositions of solutions that can be in equilibrium with two hydrate phases simultaneously.

VOL.
14
984

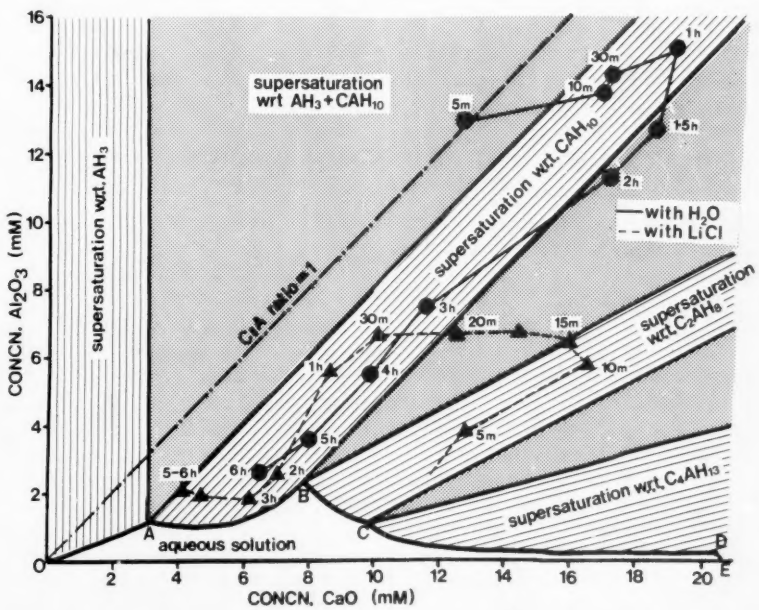

FIG. 5
The ternary $CaO-Al_2O_3-H_2O$ solubility diagram.

In applying the solubility diagram to the hydration of HAC, two processes have to be considered. The first is the hydrolysis of the anhydrous cement clinker which releases lime and alumina into aqueous solution. The second involves the removal of lime and alumina from solution by nucleation and growth of the hydration products when the solubility limits are exceeded. In general, the aqueous chemistry (starting from pure water at the origin 0) will be determined by both processes occuring simultaneously.

Superimposed on the solubility diagram of Figure 5 are the solution analyses from Figures 3(a) and (b). In the control sample the immediately noticeable feature is the very high degree of supersaturation which is reached in the solution within a few minutes of mixing and which persists for a period of several hours. As remarked upon by Barret et al (12), this 'latent' period of supersaturation is a characteristic feature of the hydration of HAC and implies that there is a nucleation barrier to the formation of the hydration products. As shown in Figure 5, at 5 minutes after mixing, the solution composition lies in the region of supersaturation with respect to both CAH10 and aluminium hydroxide. The C/A ratios in solution ≈1 indicating that initial hydration mainly involves the congruent dissolution of the CA phase in the cement. The slow drift in the solution composition within the first hour towards higher lime contents probably indicates the beginning of precipitation of hydrated alumina. After one hour, the solution composition lies in the two-phase regions of supersaturation with respect to CAH_{10}. At this point, the lime and alumina concentrations start to decrease, the solution composition moving in a direction approximately parallel to the CAH_{10} tie-lines and finally after 6 hours approaching the solubility limit of the CAH_{10} phase (the line AB). This relief of supersaturation clearly is associated with the nucleation and growth of the CAH_{10} hydrate. At 1½ and 2 hours there is a slight 'overshoot' of the solution composition into the region of supersaturation with respect to CAH_{10} and C_2AH_8 which could lead to some precipitation of C_2AH_8. This pattern of events is entirely consistent with the X-ray analysis (Figure 4) which shows that CAH10 is the predominant crystalline hydration product with smaller amounts of C_2AH_8.

Referring to the sample hydrated in LiCl solution, two main differences in the aqueous chemistry are evident: (a) everything happens much more quickly and (b) the degree of supersaturation is not as great as in the control sample, the composition being depressed towards lower aluminate concentrations. The fact that X-ray diffraction shows quantities of lithium aluminate in the hydration products suggests that preferential precipitation of the aluminate by Li^+ is responsible for these changes.

The following sequence of events is likely. The aluminate released into solution by hydrolysis of the cement is immediately precipitated as lithium aluminate. Referring to Figure 5, this means that the solution composition moves from the origin 0 along the abscissa towards increasing CaO concentrations. Aluminate is free to enter solution by continued hydration of the cement only when all the lithium has been removed by precipitation, a situation reached in this case when the lime concentration reaches 10mM (10mM of Li^+ combining with an equimolar quantity of Al_2O_3). Subsequently, as more lime enters solution with alumina the solubility limit is crossed but with the important difference in relation to the control sample that this occurs in a differnt region of the solubility diagram. The first measured analysis, at 5 minutes, shows this to be in the region of supersaturation with respect to the C_2AH_8 hydrate. If precipitation of C_2AH_8 were the only process to occur at this stage, the solution composition would move in a direction parallel to the C_2AH_8 tie-lines towards the solubility limit BC. In fact, as Figure 5 shows,

VOL. 14 1984

the solution composition moves horizontally towards lower lime concentrations over the period 10 -30 minutes. This implies that the effect of precipitation of C_2AH_8 is partly offset by the release of more lime and alumina into solution by continued hydration of the cement. The result is that the solution composition eventually moves over into the region of supersaturation with respect of the CAH_{10} hydrate. Thus the initial precipitation of C_2AH_8 is followed by a later precipitation of CAH_{10}, the solution composition finally approaching the solubility limit AB over a period of 3 - 6 hours. The end result, as evidenced by the X-ray diffraction data in Figure 4, is that the proportion of C_2AH_8 in the hydration products is substantially increased relative to that of CAH_{10}.

It still has to be established why the hydration of HAC is accelerated by the Li salt admixture. This is almost certainly related to the difficulty in nucleation of the calcium aluminate hydrates. As has been seen, this gives rise to very high degrees of supersaturation in solution during an initial 'latent' period which can extend for several hours. The hardening reaction only occurs following the nucleation and growth of an interlocking structure of hydration products. The importance of the nucleation barrier is highlighted by previously reported observations (1) that the hardening of HAC can be accelerated by the addition of pre-hydrated cement to the initial mix.

rne possible explanation is that the addition of the lithium salt changes the solution chemistry in such a way as to favour the formation of C_2AH_8 rather than CAH_{10} and that the former hydrate is easier to nucleate. To test this hypothesis samples of HAC were hydrated in solutions of 10mM calcium hydroxide. As expected, X-ray diffraction showed quantities of C_2AH_8 in the hydration products but the hydration reaction (as monitored by calorimetry) was accelerated only to a very limited extent. An alternative explanation is that the formation of lithium aluminate promotes the nucleation of the calcium aluminate hydrates. That is, lithium aluminate acts as a heterogeneous nucleation substrate. This explanation appears to be the correct one since in experiments where dried powdered lithium aluminate (synthetically prepared in the laboratory using a method described by Dobbins et al (13)) was added to the initial cement mix, a very marked acceleration of hydration was observed.

With regard to retardation by citric acid it is tempting to conclude that, if Li salts accelerate by promoting nucelation, then citric acid retards by inhibiting nucleation. However, solution chemistry measurements do not support this hypothesis. Neither are there grounds for supposing that retardation results from the inhibition of hydration by adsorption of the citrate radical directly on to the cement clinker surface as has been postulated (16). Interpretation of the solution chemistry is made difficult by the known propensity for citric acid to form soluble complexes with both calcium and aluminate in neutral and alkaline solution (14, 15). This prevents any useful conclusions being drawn from the $CaO-Al_2O_3-H_2O$ solubility diagram. Citrate can also be precipitated as the highly insoluble calcium salt. Preferential complexation of lime by citric acid is likely, in terms of the solubility diagram, to promote precipitation of alumina gel at early stages.

Our tentative conclusion based on the solution chemistry data are (a) that the presence of citric acid in solution initially promotes precipitation of alumina gel by preferential complexation of calcium (hence almost negligible quantities of aluminate in solution during the first 10 - 15 minutes of hydration) and (b) that the citrate is finally precipitated with the calcium aluminate hydrates (hence decreasing concentrations of citrate in solution over the 1-6 hour period). The precipitates are probably in amorphous gel form since X-ray diffraction shows no new crystalline phases. Retardation may thus be seen as resulting from the precipitation of protective gel coatings around the cement

grains which impede hydrolysis or alternatively inhibit growth of the hydration products.

Acknowledgements

The authors acknowledge financial support from the Science and Engineering Research Council. They express appreciation to researchers at AERE Harwell for carrying out X-ray diffraction analyses and in the Inorganic Chemistry Laboratory of the University of Oxford for carrying out solution analyses for aluminium.

References

1. T D Robson, High Alumina Cements and Concretes, Wiley, London (1962).
2. F M Lea, The Chemistry of Cement and Concrete, Edward Arnold Ltd, London (1976).
3. A M Neville, High Alumina Cement Concrete, Construction Press, Lancaster, England (1975).
4. C Bradbury, P M Callaway and D D Double, J. Mat. Sci. &n Eng. 23, 43 (1976).
5. J F Young, J. Am. Ceram. Soc. 53, 65 (1970).
6. Anon, Cemento Armato, 35, No. 7, 131 (1938).
7. N L Thomas, D A Jameson, D D Double, Cem. & Concr. Res. 11, 143 (1981).
8. N L Thomas & D D Double, Cem. & Concr. Res. 11, 675 (1981).
9. A Percival, F G Butler, H F W Taylor, Proc. 4th Int. Symp. Chem. Cem. (1960), Washington.
10. L S Wells and E T Carlson, J. Res. Nat. Bur. Stand. 57, 6 (Dec 1956).
11. L S Wells, W F Clarke and H F McMurdie, J. Res. Nat. Bur. Stand. 30, 367 (1943).
12. P Barret, D Ménétrier and D Bertrandie, Cem. & Conc. Res. 4, 545 (1974).
13. J T Dobbins and J P Sanders, J. Am. Soc. 54, 178 (1932).
14. A E Martell and M Calvin, Chemistry of the Metal Chelate Compounds, Prentic-Hall Inc, New York (1952).
15. G E F Lundel and J J Hoffman, Outlines & Methods of Chemical Analyses, J Wiley and Sons Inc, New York (1938).
16. W G Hansen, Proc. Third Intern. Symp. Chem. of Cements, London, England, 1952, 598.

VOL
14
198

CEMENT and CONCRETE RESEARCH. Vol. 14, pp. 83-92, 1984. Printed in the USA.
0008-8846/84 $3.00 + 00. Copyright (c) 1984 Pergamon Press, Ltd.

IMPORTANT EXPERIMENTAL PREREQUISITES FOR QUANTITATIVE CLINKER PHASE ANALYSIS BY SEM-EDS

S.L. Sarkar[1] and D.M. Roy
Materials Research Laboratory
The Pennsylvania State University
University Park, PA 16802 USA

(Communicated by S. Diamond)
(Received June 9; in final form Aug. 19, 1983)

VOL. 14 1984

ABSTRACT

The state of the art of quantitative analysis of phases in Portland cement clinkers lies in the selection of the optimal experimental conditions. The important parameters, such as acceleration potential, probe size, sample preparation and software handling are discussed.

INTRODUCTION

Electron-column instruments (EMPA, TEM, SEM and STEM) attached with wavelength dispersive (WD) or energy dispersive (ED) spectrometers, have been in use for the analysis of materials for over a decade. Their application in quantitative analysis of cementitious phases though has been somewhat limited (1,2). Interest in the microchemical study of Portland cement clinkers, lies not only in the principal elements Ca, Si, Al and Fe, but also in the minor elements (Na, Mg, S, P, K and Ti) present as accidental or intentional impurities in the phases. These impurities give an indication as to the anionic and cationic substitutions, the nature of solid solutions, inter- and intra-granular effects such as overgrowths, inclusions, and compositional variations, if any, within the grain itself.

The state of the art of quantitative analysis rests predominantly on the optimal experimental conditions. Selection of the correct beam voltage, probe diameter, sample preparation, etc., determine whether the analysis would turn out satisfactory.

For the present set of experiments, an ISI DS-130 dual screen/dual stage STEM attached to a Kevex Micro X.700 analytical EDS (with a dual floppy disc drive), 64K microcomputer was used. Only the SEM part of the microscope, i.e., the lower stage, was used. The advantage of using this stage lies in the use of large specimens (up to 30 cm).

---

[1]Permanent Address: Department of Geology and Mineral Sciences, University of Ilorin, Ilorin, Nigeria.

EXPERIMENTAL

The resolution of the detector being used is the first important factor the user needs to take into consideration. The resolution is determined by measuring the number of channels in electron volts at FWHM of the MnKα peak (3). The lower the value, the better is the resolution, i.e., its capability of resolving the separation of peaks increases. This is an important consideration when low energy elemental peaks, such as Al, Mg and Na are included in the analysis. Normally a resolution of 160eV is capable of separating these peaks (5). The manufacturer's value for the present detector was 152eV. The authors, however, found the experimental value to be 156eV, using a spectrally pure Mn. Aging of the detector is liable to cause this amount of degradation in the resolution. The position of the detector should be as close as possible to the specimen, without damaging either of these. In our case the detector was positioned 6 mm from the specimen. Experiments on the acceleration potential (6) have shown that the measured intensity goes through a maximum and then drops. Our results which are in accordance with (6) are given in Table I.

TABLE I
Variation of Measured Intensity with Acceleration Potential. Sample - C_3S*

KV	Integrated Intensity	
20	1343	6247
30	326	6455
40	106	4698

*Cement chemists' notation: C=CaO, S=SiO_2, A=Al_2O_3, F=Fe_2O_3.

For all practical purposes an 'overvoltage ratio U' (acceleration potential E_o/absorption edge energy E_c) ≥ 2 should be used (7). Since in cementitious compounds Fe is usually the highest energy element present, with E_c = 7.11 keV, 20 kV was selected for analyses.

Most electron-column instruments suffer from inherent beam fluctuation and drift, though in some cases it may be negligible. A small amount of beam drift which is difficult to detect visually on the SEM screen, is liable to introduce an error of 1% or more in quantitative analysis. This is illustrated in Table II.

To monitor and subsequently minimize this drift, a spectrally pure graphite was placed on the specimen stub at exactly the same height as the specimen. The specimen current on the graphite was monitored at a regular interval, and any dirft (from the 3 nano-amps value used) was adjusted whenever necessary. The graphite in a way served as the internal standard for correcting the beam drift.

Analytical results are partly dependent on the size of probe diameter being used. It has long been established that electron bombardment creates a pear-shaped active zone directly underneath the area of electron impingement (8). The volume of this zone depends on the composition of the specimen. Nevertheless, it is larger than the actual probe diameter by a factor of at least 2. Hence, very large probe diameters (>1μm) should be avoided so that there is no inadvertent sampling of neighboring grains.

A series of intensity measurements taken on a pure C_2S sample showed that a probe size of 5000 Å gave concentration values closest (Table III) to the theoretical (Ca=46.54, Si=16.30 weight percent).

TABLE II
Effect of Beam Drift on Intensity and (Concentration)$^{+}$ of C_2S* at 20 kV.

Integrated Intensity before drift (Ideal Condition)		Integrated Intensity after drift			
Si	Ca	Si	Ca		
8021	18226	8925	16338		
Concentration Before Drift (weight percent)		Concentration After Drift (weight percent)		Theoretical Concentration (weight percent)	
Si	Ca	Si	Ca	Si	Ca
16.64	46.03	18.84	42.67	16.30	46.54

$^{+}$obtained from MAGIC V program

TABLE III

(See Page 88)

Modern SEMs normally have facilities for selecting different probe sizes. Care should be exercised in selecting the correct one. We selected a probe diameter of 5000Å for better counting statistics and its small active volume.

The data acquisition period should not be prolonged, as cements are not perfectly non-volatile materials, and very long counting time (continual electron bombardment) causes degeneration on the surface of the sample. Counting time $\leq$100 secs is recommended. In the particular system used, loss of mass was denoted by the appearance of dots on the CRT screen of the spectrometer. By studying the density of dots at the end of data collection, it can be ascertained whether loss of mass was high enough to warrant the rejection of data. Regular monitoring of the count rate will also indicate the degree of degeneration and beam drift if any, during the counting period. A sudden increase or drop of count rate is indicative of either of these two.

Window width or the number of channels, where each channel is 20eV wide, for characteristic x-radiation selection is another important criterion to be considered. The results of varying the width and its effect on x-ray detection is given in Table IV. Hence, a window width of 4 channels was found to be optimum for our analyses of clinkers.

Sensitivity setting defines how small a peak can be detected compared to the background around it. A series of tests was performed on a clinker to determine the optimum sensitivity of the system. The results are summarized in Table V. From Table V it is evident that a sensitivity value >1 will tend to mask the peaks of Al and Fe.

The background in energy dispersive X-ray analysis, often referred to as the 'bremsstrahlung' follows a path as shown in Fig. 1. Programs are available for fitting and subtracting the background profile. It is crucial that an appropriate fitting and subtraction be performed for quantitative analysis. Background subtraction will depend on the background fit. An example of this is given in Fig. 2. The fitting routine follows the number of

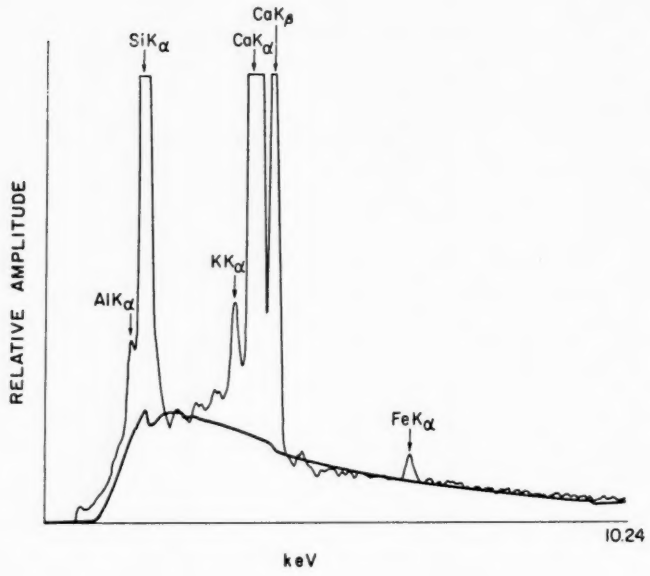

FIGURE 1
Spectrum of a clinker with its fitted background. The vertical scale has been expanded to illustrate the characteristic shape of the 'bremsstrahlung.'

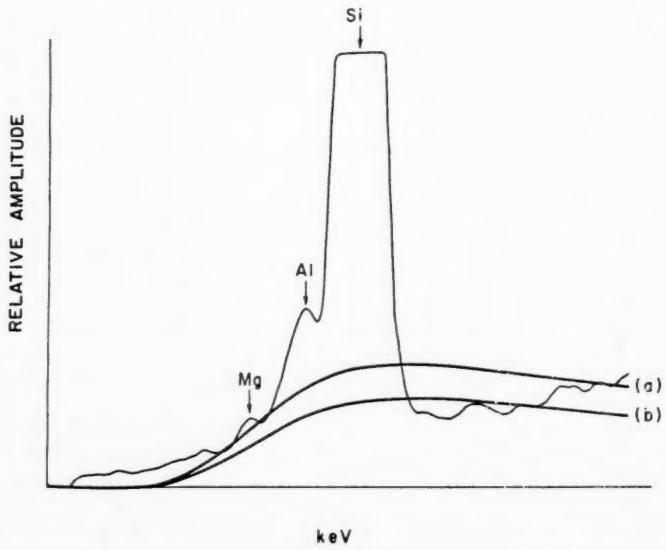

FIGURE 2
An example of background fitting with (a) 16 channels skipped and (b) 8 channels skipped. The former is seen to interface with substantial portions of Mg and Al peaks. The 'skip' in channels denotes the interval selected by the system to fit the background.

channels selected. If too many channels are skipped (e.g. 16), the background generated would tend to subtract substantial portions of the low Z elemental (Na, Mg, Al) peaks because of the unusual shape of the 'bremsstrahlung.'

The count rate should be maintained between 1,000-3,000 cps. A very high count rate tends to generate 'sum peaks' at twice the characteristic keV of the element (4). Too low a count rate, on the other hand, may be insufficient for the analysis of low Z elements, such as Na and Mg, which are expected to exist in low concentrations(<2% and <5% respectively) in clinker.

TABLE IV
Effect of Varying Window Width on the Detection of Characteristic X-ray Lines.

Window Width No. of Channels	X-ray Lines Detected Sample - C_3S*
1	$CaK\alpha_2$ 3.687 keV
2	$SiK\alpha_2$; $CaK\alpha_1$, $K\alpha_2$ 1.739, 3.691, 3.687 keV
4	$SiK\alpha_1$, $K\alpha_2$; $CaK\alpha_1$, $K\alpha_2$ 1.741, 1.739, 3.691, 3.687 keV
8	$SiK\alpha_1$, $K\alpha_2$; $CaK\alpha_1$, $K\alpha_2$, $KrLg_1$, $RbL\beta$, $SnL\beta_1$, $NpNg_2$ 1.741, 1.739, 3.691, 3.687, 1.734, 1.752, 3.662, 3.664

TABLE V
Capability of Characteristic X-ray Peak Detection with Varying Sensitivity

Sensitivity	X-ray Lines Detected. Sample - C_2S*
0.5	$AlK\alpha_1$, $K\alpha_2$, $SiK\alpha_1$, $CaK\alpha_1$, $K\alpha_2$, $K\beta_1$; $FeK\alpha_1$, $K\alpha_2$
1.0	$AlK\alpha_1$, $K\alpha_2$, $SiK\alpha_1$, $CaK\alpha_1$, $K\alpha_2$, $K\beta_1$; $FeK\alpha_1$, $K\alpha_2$
1.5	$SiK\alpha_1$, $CaKs_1$, $K\alpha_2$, $K\beta_1$
2.0	$SiK\alpha_1$, $CaK\alpha_1$, $K\alpha_2$, $K\beta_1$

Geometrical factors--tilt and take-off angles, and working distance are usually governed by the design of the instrument and ZAF correction program being used. The ISI DS 130 SEM and the MAGIC V ZAF program (9) dictates the use of 35 mm working distance, 0° tilt, 60° incidence angle and 74.3° X-ray emergence angle.

Standardization is critically important for quantitative micro-analysis. Wittry (10) and several other workers support the use of pure elemental standards for accurate quantitative EMPA, whereas another school of workers (11,12) favors standard compounds with compositions similar to the unknown being analysed. In case of cement analysis, it is not possible to obtain pure element standards for Na, Mg, P, S and K. Hence binary or ternary compounds of these elements in their purest forms need to be used as standards in place of pure elements. For our analyses four standards were used, namely (i) NBS

TABLE III
Variation of Intensity and (Concentration[+]) with Probe Size at 20 kV. Sample - C_2S*.

Probe Diameter (Å)	Integrated Intensity		Ratio Region 1.26-1.41 keV		Weight %*		Oxide %*		Precision 2σ	
	Si	Ca	Si	Ca	Si	Ca	Si	Ca	Si	Ca
5000	8021	18226	8.07	18.34	16.65	46.03	35.60	64.40	1.18	1.46
3300	5841	14335	9.80	24.05	15.78	47.34	33.76	66.24	1.31	1.69
1800	2350	6185	9.11	23.97	15.38	47.96	32.90	67.10	1.99	2.61
900	666	1575	10.25	24.23	15.62	47.59	33.41	66.59	3.94	5.12

[+]Obtained from MAGIC V program.

TABLE VI
Typical range of elemental composition of phases in clinker (weight percent).*

Authors	Program Used	Compound	Results												
			Ca	Si	Na	Mg	Al	P	S	K	Ti	V	Cr	Mn	Fe
Present	MAGIC V (9)	C_3S	52.70	10.57	Nil	0.56	0.55	Nil	0.18	Nil	Nil	---	---	Nil	0.95
		C_2S	45.54	15.49	Nil	0.25	0.53	Nil	0.21	0.33	Nil	---	---	Nil	0.63
		C_3A	46.32	1.86	Nil	0.48	12.96	Nil	Nil	1.12	Nil	---	---	Nil	3.54
		C_4AF	38.61	2.27	Nil	1.23	12.85	Nil	Nil	0.44	0.53	---	---	Nil	10.42
Ghose and Barnes (2)	FRAME (5)	C_3S	47.18 -52.63	9.76 -11.95	0.12 -0.40	0.09 -0.85	0.38 -2.96	0.03 -0.62	Nil -0.09	0.03 -0.14	0.02 -0.24	Nil -0.09	Nil -0.12	Nil -0.09	0.02 -1.16
		C_2S	43.25 -47.17	12.98 -15.64	0.12 -0.60	0.07 -0.42	0.37 -1.69	0.03 -0.44	Nil -0.14	0.10 -1.15	0.02 -0.23	Nil -0.10	Nil -0.18	Nil -0.12	0.03 -0.72
		Inter-stitial phase	29.69 -43.18	1.06 -7.73	0.11 -1.62	0.30 -6.92	7.97 -15.38	Nil -0.30	Nil -0.09	Nil -2.33	0.04 -0.90	Nil -0.11	Nil -0.07	Nil -0.30	1.56 -15.15
Barnes and Sarkar (1)	FRAME (5)	C_2S	39.60 -45.0	10.0 -14.7	Nil -Trace	Nil -0.42	0.24 -1.02	Trace -0.11	Nil -0.05	Nil -0.67	--- ---	--- ---	--- ---	--- ---	Nil Nil

*Each value is mean of approximately 20 values.

VOL. 14 1984

soda lime glass standard No. 621 containing Si, Ca, Mg, Na and K in their oxide forms, (ii) an FeS standard, (iii) an $AlPO_4$ compound and (iv) an NBS Waspaloy 1207-1 containing Mn, Cr, Ti in their elemental forms.

Either a pure element standard or a compound containing the elements of interest may be used, with precaution that the standard contains the element(s) in greater quantity than in the sample to be analysed.

Sample surface effects, in general, cannot be corrected for, and therefore a good flat, electrically conductive specimen surface is critically important for accurate analysis. Resin-impregnated polished and carbon coated clinker specimens have been successfully used in quantitative microanalysis (1,2,13). Polished clinker samples, however, introduce the difficulty of recognizing grains of different phases in the clinker. Ghose and Barnes (2) suggested a light ion-etching of the surface for a better delineation of grains. Ion-etching tends to introduce an overall irregularity of the surface, and is also a time-consuming process. We found selective chemical etching to be a rapid and convenient method of phase recognition, without destroying the planarity of the clinker surface. After polishing the clinker it was soaked in a solution of KOH and sucrose (KOSH) for 5 minutes (14). This leached out the C_3A and the C_4AF phases from the clinker (Fig. 3). A series of line profiles across the grains shows that reasonable flatness is maintained even after the KOSH treatment (Figs. 4a and b). After grain analyses of C_3S and C_2S, another polished sample of the same clinker was treated with maleic acid (15) for 10 minutes to remove the silicates. Once again, a line profile across the section shows that reasonable flatness is maintained (Fig. 5). Analyses of C_3A and C_4AF grains were then undertaken on the maleic acid treated sample. Owing to the much smaller size of C_3A and C_4AF grains (Fig. 5), there are limitations as to the precision of analysis of these grains.

OL.
14
984

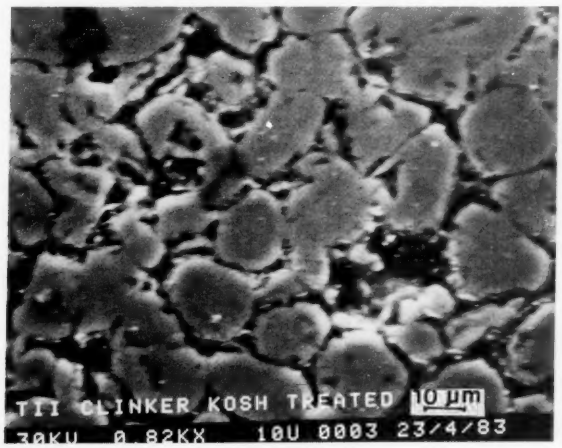

FIGURE 3
A clinker section polished and later etched in a solution of KOH and sucrose (14) to remove the interstitial phases (C_3A and C_4AF).

Finally, accurate quantitative microanalysis necessitates ZAF corrections on the data collected. Several standard correction programs are available (9,16,17,18) for implementing these corrections. Usually, the manufacturer supplies a suitable package program for the user. Table VI illustrates the results of three different clinkers obtained from two different ZAF correction programs, FRAME and MAGIC V.

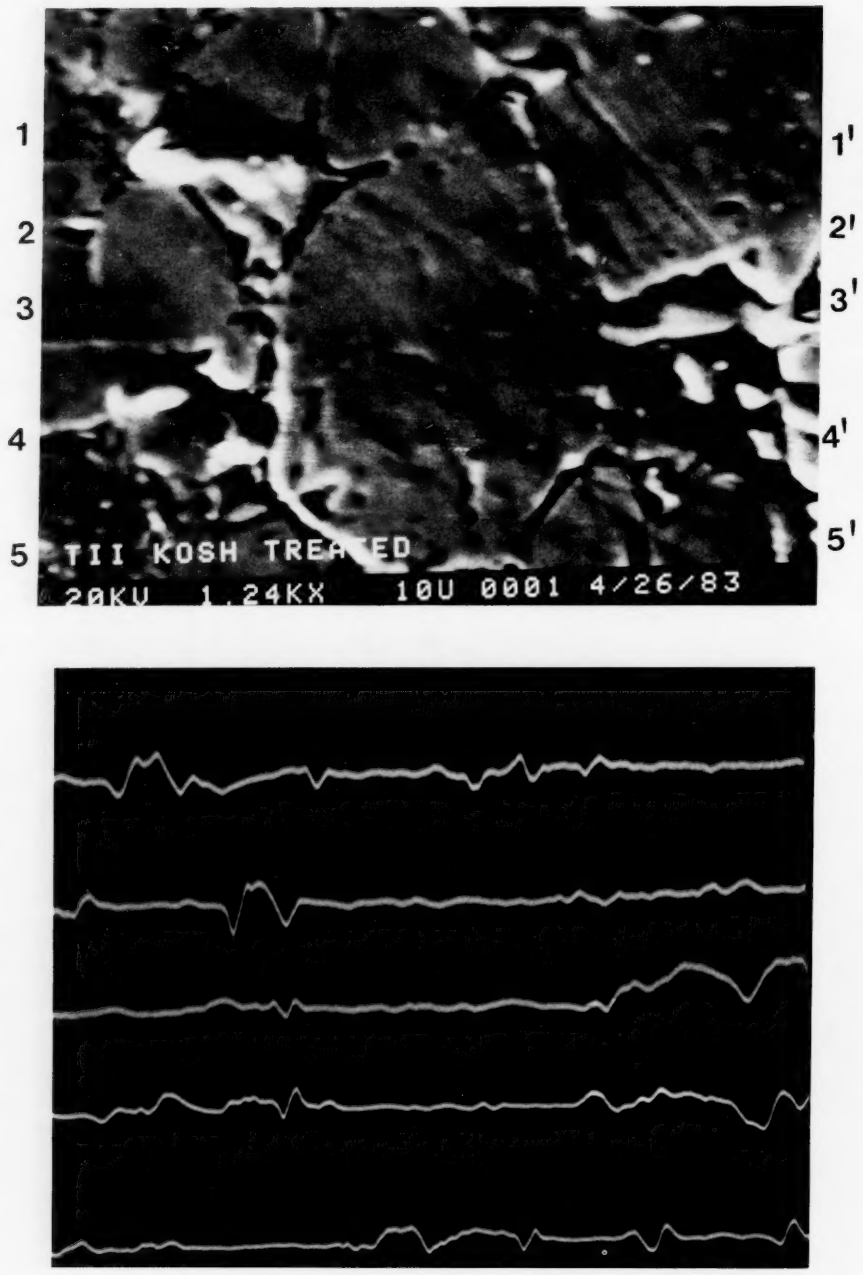

VOL.
14
1984

FIGURE 4
(a) A magnified view of the same clinker treated in KOSH.
(b) Line profiles along the large grain between 1-1', 2-2', 3-3', 4-4' and 5-5'.

CONCLUSIONS

It has been demonstrated that high level of accuracy can be obtained in an SEM-EDS analysis of cement clinker phases if the correct experimental conditions are selected. This is not fully routine, however, and workers attempting quantitative analysis of cement phases must devote some time in experimenting on the optimal experimental parameters for the particular instrument.

The advantages of etching have been reaffirmed. KOH and sucrose solutions removed the interstitial phase, allowing cleaner analysis of C_3S and C_2S grains. Similarly, removal of the silicate phases by leaching in a solution of maleic acid, allows cleaner analysis of the C_3A and C_4AF, in ech case reducing the chances of inadvertent sampling of neighboring grains. Recognition of grains thereby becomes much easier.

Limitations are imposed due to the effective beam size, and grains smaller than 2 μm cannot be analyzed. This imposes restrictions on the analyses particularly of the interstitial matrix. The present study has been successful in analysis of the silicates; and despite their small size has achieved resolution and analysis with moderate success of even the interstitial phases, C_3A and C_4AF.

ACKNOWLEDGEMENTS

One of the authors (SLS) wishes to acknowledge the financial assistance and leave from the University of Ilorin, which enabled him to participate in the research programme at the Materials Research Laboratory, The Pennsylvania State University. Thanks are also due to Dr. D.W. Strickler of the Materials Research Laboratory for his technical assistance, and to the Atlantic Cement Company for partial support, and supplying clinkers. This research was partially supported by the National Science Foundation under Grant No. NSFCPE-8112821.

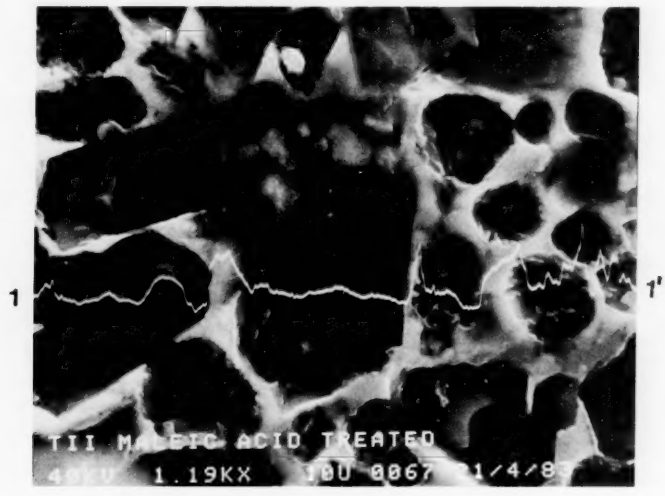

FIGURE 5
A different section from the same clinker, treated with maleic acid (15) to remove the silicates. A line profile across 1-1' indicate the planarity of the interstitial matrix. The depressed regions represent the C_3S and C_2S grains, whereas the elevated regions are composed of C_3A and C_4AF.

REFERENCES

1. P. Barnes, J.W. Jeffery and S.L. Sarkar, Cem. Concr. Res., 8, 559 (1978).
2. A. Ghose and P. Barnes, Cem. Concr. Res., 9, 747 (1979).
3. Kevex Manual, Kevex Corp., Calif., USA (1980).
4. Advances in Cement Technology, Ed. S.N. Ghosh, Pergamon Press, Ltd., U.K., 711 (1983).
5. J.C. Russ, Elemental X-Ray Anaysis of Materials, Edax Int. Inc., Illinois, USA (1972).
6. Edax Instruction Manual, Edax Int. Inc. (1973).
7. S.L. Sarkar, Ph.D. Thesis, University of London (1976).
8. D.R. Beaman and J.A. Isasi, Rev. Mat. Res. Stand., 11(11), 8, 11(12), 12 (1971).
9. J.W. Colby, Brit. J. App. Phys., 1, 685 (1968).
10. D.B. Wittry, ASTM Sp. Tech. Pub., No. 349, 128 (1963).
11. K. Keil and K. Fredriksson, J. Geophys. Res., 69, 348 (1964).
12. P.H. Ribbe and J.V. Smith, J. Geol., 74, 217 (1966).
13. M.S. Stucke and A.J. Majumdar, Cem. Concr. Res., 7, 711 (1977).
14. W.A. Gutteridge, Cem. Concr. Res., 9(3), 319 (1979).
15. A.A. Tabikh and R.J. Weht, Cem. Concr. Res., 1(3) 317 (1970).
16. A.E. Bence and A.L. Albee, J. Geol., 76, 382 (1968).
17. K.F.J. Heinrich and H. Yakowitz, Microchem. Acta., 182 (1968).
18. J.C. Russ, Proc. VI the Int. Conf. X-ray Optics and Microanal., Tokyo, Paper No. 36 (1971).

VOL.
14
1984

CEMENT and CONCRETE RESEARCH. Vol. 14, pp. 93-98, 1984. Printed in the USA.
0008-8846/84 $3.00 + 00. Pergamon Press, Ltd.

CALCIUM HYDROXIDE DISTRIBUTION AND CALCIUM SILICATE HYDRATE COMPOSITION IN TRICALCIUM SILICATE AND β-DICALCIUM SILICATE PASTES

H.F.W. Taylor* and D.E. Newbury
National Bureau of Standards
Washington, D.C. 20234, USA

(Communicated by J. Skalny)
(Received June 10, 1983)

OL.
14
984

ABSTRACT

Pastes of tricalcium silicate (C_3S) and β-dicalcium silicate (C_2S) 23 years old were studied by electron probe microanalysis. In both cases, regions consisting entirely or largely of calcium hydroxide and of C-S-H were distinguished on a scale of 2 - 50 μm. The regions high in C-S-H accounted for 75 - 80 percent of the whole in the C_3S paste and about 96 percent in the C_2S paste; these values are much higher than those initially occupied by anhydrous starting materials. Within the high C-S-H areas, no compositional variation was detected that could have corresponded to the so-called inner and outer hydrates. The ratio of mean Ca to mean Si in the high C-S-H areas was found to be 1.72 for the C_3S paste and 1.78 for the C_2S paste with an exciting beam energy of 10 keV.

Introduction

Previous electron probe (EPMA) or scanning electron microscope (SEM) microanalyses of the calcium silicate hydrate (C-S-H) formed in tricalcium silicate (C_3S) pastes cured at ordinary temperatures have given Ca/Si ratios of 1.44 to 1.9 (1-9). Rayment and Majumdar (7) showed that the apparent Ca/Si ratio increases with the accelerating voltage of the electron probe, and attributed this to close admixture of the C-S-H with calcium hydroxide (CH) or unreacted C_3S. With an increase in voltage, the volume analyzed became larger, and the probability of analyzing C-S-H free from these other phases decreased. Fig. 1 shows that variation among the other results in the literature can largely be explained in the same way. Chatterji (8) also concluded that the C-S-H was intimately mixed with CH and estimated its Ca/Si ratio by extrapolating the high Si tail of the Si/Ca distribution to zero frequency. These interpretations of the data give Ca/Si ratios of 1.4 to 1.6. Analytical electron microscopy (AEM), in which a much smaller volume is analyzed, indicates marked compositional variation among particles but gives similar mean Ca/Si ratios (1.43 to 1.66) for C_3S pastes (10-11) and somewhat lower ones (1.34 to 1.41) for C_2S pastes (12).

*Permanent Address: Department of Chemistry, University of Aberdeen, Meston Walk, Old Aberdeen AB9 2UE, Scotland, UK.

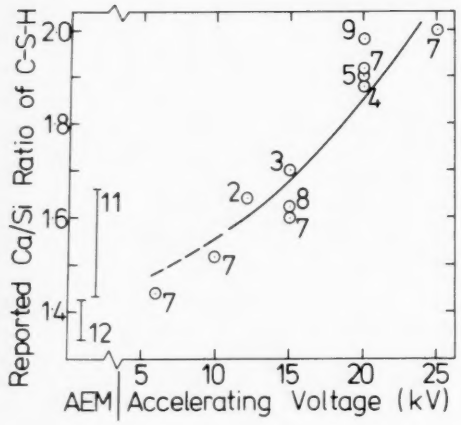

FIG. 1

Reported Ca/Si ratios of the C-S-H in calcium silicate pastes, plotted against the accelerating voltages used. Reference numbers as in text. Data are for C_3S pastes except for No. 12, which is for a β-C_2S paste.

No comparable EPMA or SEM data for β-C_2S pastes appear to have been reported. For C_3S pastes, there is uncertainty regarding the relations between composition and microstructure on the 2 to 50 µm scale, including, for example, whether the compositions of the so-called inner and outer products are different, or how the microstructure at this level is related to that of the fresh paste at the time when mixing was complete. The object of the present work was to obtain such information for mature C_3S and β-C_2S pastes.

Experimental

The pastes were prepared at the Portland Cement Association Research and Development Laboratories (13) and were 23 years old when examined. They had water/solids (w/s) ratios of 0.45 and had been stored moist at 25°C. The Blaine specific surfaces were 266 and 448 m^2kg^{-1} for the C_3S and C_2S pastes, respectively. The designations given by the Portland Cement Association were C80A-4525 for the C_3S paste and C85A-4525 for the C_2S paste. Those of the anhydrous starting materials from which the pastes had been prepared were B94 for the C_3S and B91 for the C_2S. X-ray diffraction for both pastes showed only CH and C-S-H, with no detectable unreacted starting materials.

Surfaces were prepared by cutting slices about 2 mm thick with a diamond saw and polishing, ultimately on a synthetic fiber cloth impregnated with 0.5 µm diamond from an aerosol spray. The surfaces were coated with layers of carbon 20 nm thick.

The specimens were examined in an electron microprobe equipped with an energy dispersive X-ray spectrometer (EDS). The take-off angle was 40°. For spot analyses, the accelerating voltage was 10 kV, the counting time 100 s, and the probe current 1 na. As a standard, NBS standard glass K411 (SRM 1470) was used. Matrix corrections were applied by the use of the NBS theoretical correction procedure, FRAME C (14). The instrument could be programmed to analyze a series of spots at intervals of 1, 2 or 5 µm, either in a linear traverse or in a two-dimensional grid. The calibration was checked before every such series of analyses. In area scans, for greater excitation, the accelerating voltage was 15 kV and wavelength dispersive spectrometers were employed. Areas on the resulting micrographs were estimated by point counting and with a computer-controlled measuring device.

After a series of spot analyses, markings were normally observed on the specimen and dosage tests were carried out to find whether any systematic change in either atomic ratio or totals occurred during exposure to the beam. During times of up to 270 s, the totals decreased markedly but the Ca/Si ratio either remained constant within experimental error or tended to decrease; thus, in a test with successive exposures of 10, 20, 40 and 200 s, the totals

VOL. 14 1984

(weight fractions of $CaO + SiO_2$) were .726, .696, .617 and .551, and the Ca/Si atom ratios were 1.80, 2.06, 1.82 and 1.83. These results differ from those of Rayment and Majumdar (15), who found that Ca/Si tended to increase under similar conditions. In the present work, the use of the EDS permitted analysis at low beam currents (1 na), which may explain the difference in this observation on the influence of beam damage.

Results

X-Ray Area Scans

Secondary electron images of the C_3S paste (Fig. 2a) showed rough and smooth areas, which were visible also in the light microscope. X-ray area scans (Fig. 2b and c), supported by subsequent spot analyses, showed that the rough areas consisted largely of CH and the smooth ones largely of C-S-H. From the point counts and area measurements, the CH areas constituted 20-25 percent of the whole. They were discontinuous, tended to be elongated, and were typically 5-30 µm in longest dimension. The high C-S-H areas were continuous, and tended to be equidimensional and up to approximately 50 µm in longest dimension. Broadly similar results were obtained for the β-C_2S paste, but the high CH areas were much fewer in number and made up only about 4 percent of the whole. They tended to occur in clusters (Fig. 2d) and could be distinguished on X-ray area scans but not on secondary electron images or in the light microscope.

OL.
14
984

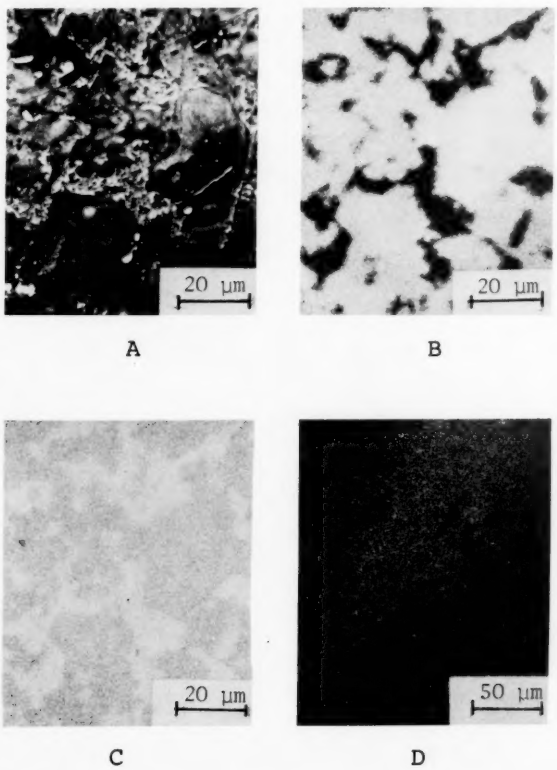

FIG. 2

Electron Microprobe Results.

(A) - (C) relate to the same area of the C_3S paste:
(A) Secondary Electron Image
(B) Si X-ray Image
(C) Ca X-ray Image.

(D) Si X-ray image for the β-C_2S paste.

In the X-ray images, light areas denote high concentrations of the specified elements.

Spot Analyses

The results are given in Fig. 3 and Table 1. For the C_3S paste, the 215 spot analyses were made in 7 separate traverses at 1 μm intervals, and their positions were biased towards the high C-S-H areas. For the β-C_2S pastes, the 418 spot analyses were made in 7 traverses, 3 grid scans and some extra points, at a mixture of 1, 2 and 5 μm intervals, and in positions selected at random. The frequency distributions of Ca/Si ratio (Fig. 3) were bimodal, with peaks corresponding to the high C-S-H and high CH areas. For the C_3S paste both peaks were well defined, but for the C_2S paste the high CH peak was only slightly above background. The poor definition is due partly to the low relative total area of the high CH areas, and partly to the fact that, within these areas, the Ca/Si ratios tended to be lower than in the case of the C_3S paste; the 80 points in this group for the C_3S paste included 40 with Ca/Si > 10, but of 70 such points for the C_2S paste, only 8 had Ca/Si > 10.

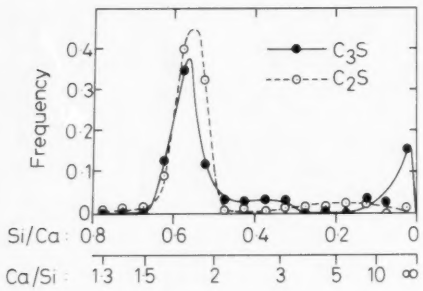

FIG. 3

Frequency distributions, for uniform intervals of Si/Ca ratio, for the atomic ratios in the C_3S paste (215 analyses) and the β-C_2S paste (418 analyses).

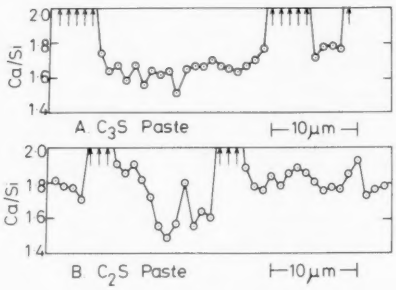

FIG. 4

Typical profiles of Ca/Si ratio, for (A) the C_3S paste and (B) the β-C_2S paste.

TABLE 1

Results of Electron Microprobe Analyses for C_3S and β-C_2S Pastes

Paste	Point Category*	No. of Points	Mean Mass Fractions $C_w(Ca)$	$C_w(Si)$	$C_w(\Sigma)$**	Atom Ratio Mean Ca/Mean Si
C_3S	All	215	.372	.099	.733	2.64
	High C-S-H	135	.315	.128	.716	1.72
	High CH	80	.470	.049	.762	6.75
C_2S	All	418	.347	.120	.744	2.02
	High C-S-H	348	.329	.130	.739	1.78
	High CH	70	.437	.075	.771	4.09

*High C-S-H and High CH defined as having Ca/Si > 2.1 and < 2.1, respectively.
**$C_w(\Sigma)$ = Mean $[C_w(CaO) + C_w(SiO_2)]$, where C_w denotes the weight fraction.

Within the high C-S-H areas, the variation in Ca/Si ratio appeared to be almost completely random; Fig. 4 shows results for two typical traverses. Apart from a slight tendency for the Ca/Si ratios to increase close to the boundaries with the high CH areas, there was no systematic difference between

the centers and the peripheral parts of the high C-S-H areas, though, very occasionally, regions were found in which Ca/Si was consistently low for distances of a few μm on the traverses, or over areas a few μm in each direction on the grid scans.

Discussion

Microstructure

The areas described here as high C-S-H and high CH do not agree with those initially occupied by anhydrous starting materials and water respectively, as calculated from the w/s ratios and densities, and therefore cannot be identified with the inner and outer products. For the C_3S paste, ignoring any entrapped or entrained air and any small change in the total volume during curing, the volume fraction initially occupied by water was 0.59, but that represented by the high CH areas, as found in the present experiments, was 0.20 - 0.25. For the C_2S paste, the corresponding values are 0.62 and 0.04, giving an even greater difference. On the other hand, the extents of the high CH areas agree well with those calculated for CH from the w/s ratio and the mean Ca/Si ratios of the high C-S-H areas. Taking the latter as 1.72 for the C_3S paste, the calculated volume fraction of the high CH areas is 0.24, while for the C_2S paste, assuming mean Ca/Si = 1.78 for the high C-S-H areas, the corresponding value is 0.06 . It is implicit in these calculations that the porosity resides entirely in the high C-S-H areas, and that the small amounts of Si in the high CH areas can be ignored.

OL.
14
984

At least for the C_3S paste, the high C-S-H areas are of such a size distribution that they could be centered on the larger grains of the anhydrous materials at the time of initial setting although there is no proof of this. The above volume comparisons require, however, that they also include substantial regions initially occupied by smaller anhydrous grains and by water. Together with the absence of any systematic difference in Ca/Si ratio between different parts of these areas, this implies that there is no difference between inner and outer products that can be detected by the methods used. Rayment and Majumdar (15) recently reached the same conclusion for mature cement pastes, though they found that a difference did exist for younger pastes. These results imply that substantial rearrangement of the microstructure occurs over a period of years.

Ca/Si Ratio of the C-S-H

The present results are compatible with the hypothesis (7,8) that the C-S-H has a Ca/Si ratio of about 1.5 and that higher values arise from admixture with CH on a scale somewhat below 1 μm. Some preliminary Monte Carlo calculations for interaction volumes (16) yielded results compatible with this view. For pure C-S-H, assumed to be of composition $C_{1.5}SH_{1.5}$ and density 2520 kg m^{-3}, nearly all the X-rays are generated within a region about 1 μm across and 1 μm deep. In order to determine the effect of incorporating fine scale CH into the C-S-H, a calculation was performed for a slab of CH with a width of 50 nm and of infinite extent, placed in a matrix of C-S-H. With the electron beam centered on the slab and parallel to its sides, the Ca/Si ratio was calculated to be 1.92. Note that in these calculations the effect of porosity was ignored.

This same hypothesis also explains the variation in observed Ca/Si ratio with accelerating voltage and the analytical electron microscope results, and is possibly the most satisfactory explanation of all the available data. However, the existence of CH closely admixed with the C-S-H has not been directly demonstrated except in the case of cement pastes of low w/c ratio

(17). There is also a problem in reconciling the hypothesis with most of the quantitative determinations of CH by thermal, X-ray diffraction or chemical extraction methods that have been reported in the literature. These tend to indicate Ca/Si ratios of the C-S-H similar to those found here for the high C-S-H areas, i.e., about 1.7 and 1.8 for the C_3S and C_2S pastes respectively.

Mass Fractions of the Elements

The mean totals [$C_w(\Sigma)$] found for the high CH points were 0.76-0.77 (Table 1), in good agreement with the theoretical value of 0.76 (= 56/74) for pure CH. For the high C-S-H areas, it is difficult to estimate the proper contribution from the water because of the uncertainty as to how much is retained under the conditions of the analysis, but the mass fraction is most unlikely to exceed ca. 0.16; this would mean totals of, at most, 0.86-0.90, well below theoretical. Plots of the observed totals of $CaO + SiO_2$ against Ca/Si for individual points in both C_3S and C_2S pastes showed positive correlations with the totals falling from about 0.8 at Ca/Si = 1.9 to about 0.6 at Ca/Si = 1.5. The reason for these low totals is not clear, but may lie in the high porosity associated with the C-S-H, perhaps due to the filling of pores near the surface with low atomic number impurities, such as organic material from specimen preparation. The decrease in total observed on prolonged exposure to the beam is consistent with this explanation.

Acknowledgments

One of us (H.F.W.T.) thanks the National Bureau of Standards, and more particularly Dr. G. Frohnsdorff (Building Materials Division, Center for Building Technology) and Dr. P.W. Brown (Cement Hydration Group), for the funding of this work and of the visits to NBS during which it was done, and for their interest and much helpful discussion. We thank also the Portland Cement Association for the specimens and Dr. C. Robbins for an XRD analysis.

References

1. D.M. Roy and M.W. Grutzeck, Proc. 5th. Int. Symp. Chem. Cement, Tokyo, 2, 301 (1968).
2. P. Terrier, ibid., p. 278.
3. M.W. Grutzeck and D.M. Roy, Nature (London) 223, 492 (1969).
4. S. Diamond, Cem. Concr. Res. 6, 413 (1976).
5. S. Goto, M. Daimon, G. Hosaka and R. Kondo, J. Amer. Ceram. Soc. 59, 281 (1976).
6. M.S. Stucke and A.J. Majumdar, Cem. Concr. Res. 7, 711 (1977).
7. D.L. Rayment and A.J. Majumdar, Proc. 7th. Int. Congr. Chem. Cements, Paris, 2, II-64 (1980).
8. S. Chatterji, Cem. Concr. Res. 10, 783 (1980).
9. K. Ogawa, H. Uchikawa and K. Takemoto, Cem. Concr. Res. 10, 683 (1980).
10. J.A. Gard, K. Mohan, H.F.W. Taylor and G. Cliff, J. Amer. Ceram. Soc. 63, 336 (1980).
11. E.E. Lachowski, K. Mohan, H.F.W. Taylor, C.D. Lawrence and A.E. Moore, J. Amer. Ceram. Soc. 64, 319 (1981).
12. K. Mohan and H.F.W. Taylor, J. Amer. Ceram. Soc. 64, 717 (1981).
13. D.L. Kantro, S. Brunauer and C.H. Weise, Advances in Chem. Series 33, 199 (1961); PCA Bull. 140.
14. R.L. Myklebust, C.E. Fiori and K.F.J. Heinrich, "FRAME C: A Compact Procedure for Quantitative Energy-Dispersive Electron-Probe X-Ray Analysis," National Bureau of Standards (U.S.) Technical Note 1106, Washington (1979).
15. D.L. Rayment and A.J. Majumdar, Cem. Concr. Res. 12, 753 (1982).
16. D.E. Newbury and R.L. Myklebust, Ultramicroscopy 3, 391 (1979).
17. G.W. Groves, Cem. Concr. Res. 11, 713 (1981).

VOL. 14 1984

CEMENT and CONCRETE RESEARCH. Vol. 14, pp. 99-104, 1984. Printed in the USA.
0008-8846/84 $3.00 + 00. Copyright (c) 1984 Pergamon Press, Ltd.

EFFECT OF MELT COMPOSITION ON TRICALCIUM SILICATE: ITS FORMATION AND COMPOSITION

I. Jawed,* J.F. Young,† A. Ghose,† and J. Skalny*

* Martin Marietta Laboratories, Baltimore, Maryland
† University of Illinois, Urbana, Illinois

(Communicated by D.M. Roy)
(Received June 13, 1983)

VOL. 14 984

ABSTRACT

This study describes the effect of several clinker melt phases on the kinetics of tricalcium silicate (C_3S) formation. At a given burning temperature, a maximum amount of C_3S was apparently formed for a given melt. The iron-rich melt phases promoted the consumption of lime and the rate of formation of C_3S in the order $C_2F > C_4AF > C_6A_2F > C_3A$. Results of the microprobe analyses of C_3S and melt phases suggest that iron and alumina entered the C_3S lattice during clinkering. Silica also apparently entered the melt phase, although conclusive evidence could not be obtained.

I. INTRODUCTION

The presence of even small amounts of liquid phase is known to increase the rate of reactions between solids. This is especially important in heterogeneous systems, such as mixtures of raw materials used in cement production, in which the reactivity depends on the composition, proportions, particle size, and other properties of the reactants. The properties of the liquid phase formed are also of great importance[1,2]: composition, viscosity and surface tension, for example, which are all temperature-dependent and interrelated. The above parameters determine the rate of ionic diffusion between the reactants, formation of nuclei, and the crystal growth processes; together, these processes control the overall kinetics of reactions.

The liquid phase formed during Portland cement clinker formation is composed primarily of calcium aluminates and ferrites, with dissolved lesser amounts of CaO, MgO, SiO_2, and alkalies. The effects of aluminum, iron and other oxides on the burnability of clinker and clinker materials have been studied recently by several authors.[3-7] It is known that an increase in the iron oxide to alumina ratio of the kiln feed increases the rate of tricalcium silicate formation. However, the real composition of the interstitial phase at the beginning of C_3S formation (1300°C) is unknown as it changes with variables such as kiln feed composition. Thus, it is not clear if it is the Al_2O_3/Fe_2O_3 ratio of raw feed or the actual melt composition which has the largest effect. Furthermore, although it is well known that tricalcium silicate contains elements

that form the liquid phase, the exact relationship between liquid phase composition and tricalcium silicate microcomposition has not been investigated.

Here we report preliminary results of a study designed to look at the influence of the liquid phase on the kinetics of formation of tricalcium silicate, its composition, and reactivity.

II. EXPERIMENTAL

To assess the effect of melt composition on the kinetics of tricalcium silicate formation, several melt phases were prepared separately. These were then finely ground and blended with mixtures of $3CaO + SiO_2$ in varying amounts. The formulations were compacted by isostatic pressing (35,000 psi) and then clinkered at 1450°C or 1550°C for periods up to 180 minutes in an electric furnace (Rapid Temperature Furnace, CM Inc., Bloomfield, New Jersey). The maximum temperatures were reached in less than 30 minutes, and it was assumed that in this short time the reaction between melt and calcium silicates did not occur. After the desired burning period, samples were cooled to 1250°C and then air-quenched at room temperature. Free lime was determined by an improved analytical method,[8] while C_3S was determined by quantitative X-ray diffraction as previously described.[9] Melting temperatures of the fluxes were determined using a Leitz Heating Microscope. Microanalyses were performed using a JEOLCO 50x electron microprobe or JEOL JSM 35C scanning electron microscope with energy dispersive spectroscopic capabilities. In both cases, an in-house computer program was used for ZAF corrections and calculations of composition from the raw data.

III. RESULTS AND DISCUSSIONS

A. KINETICS OF FORMATION

Data presented in Table 1 show that consumption of calcium oxide is a function of three variables: burning time, amount of liquid phase, and composition of liquid phase. In addition, the burning temperature was confirmed as a fourth variable (Fig. 1). Residual free lime is usually taken as a measure of tricalcium silicate formation and this was checked by the direct determination of tricalcium silicate which was found to be monoclinic. Some results are presented in Fig. 2 confirming the relationship. The following observations can be made:

- At a given temperature and time a maximum amount of C_3S is apparently formed for a given melt (Fig. 2). Increasing the melt content does not form greater amounts of C_3S. This behavior has been reported previously.[9,10]

- As expected, increasing the burning temperature accelerates the formation of C_3S. Even the iron-free melt causes rapid consumption of free lime at 1550°C.

- The iron-rich melts promote the consumption of lime and the rate of formation of tricalcium silicate. The order is approximately in line with the proportion of iron oxide, i.e., C_2F > C_4AF > C_6A_2F > C_3A. However, the alumina-free melt, C_2F, was only slightly more effective than C_4AF. This finding suggests that the A/F ratio in the raw feed is not only controlling the amount of liquid phase,[3] but also its reactivity with regard to forming C_3S.

- The maximum levels of C_3S reached varied with different melts. This suggests that some of the silica must enter the melt phase as would be expected from microanalyses of cements.[11,12] Attempts to confirm this are described in the next section.

Table 1

Kinetics of Free Lime Consumption at 1450°C in the Presence of Various Melt Compositions

Burning Time (min)	% Melt Added	% Residual Free Lime			
		C_3A	C_6A_2F	C_4AF	C_2F
30	1.0	9.4	8.9	8.0	6.3
	2.5	7.6	7.2	6.2	4.2
	5.0	3.9	3.0	2.3	0.6
	7.5	2.2	1.0	0.3	0.2
	10.0	1.1	0.5	0.2	0.1
60	1.0	6.3	5.1	5.8	5.1
	2.5	5.4	4.8	5.3	2.5
	5.0	2.1	0.5	0.4	0.1
	7.5	0.8	0.3	0.1	0.2
	10.0	0.4	0.2	0.1	0.1

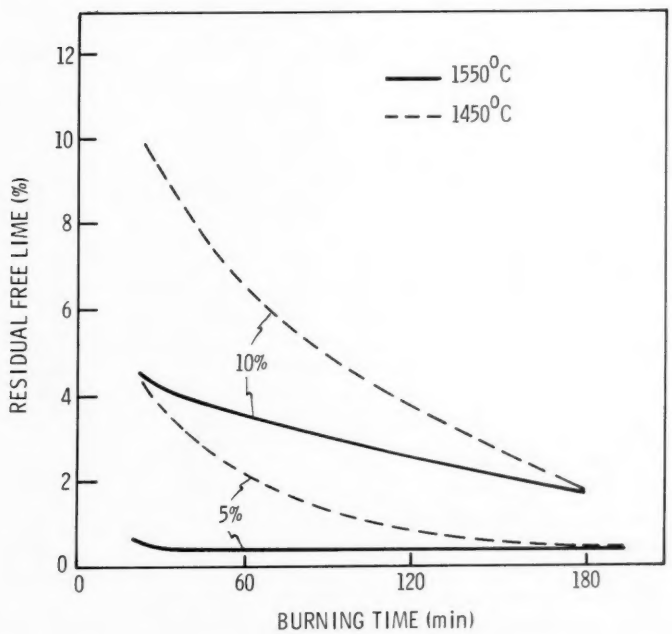

Fig. 1. Effect of burning temperature and time on the consumption of CaO.

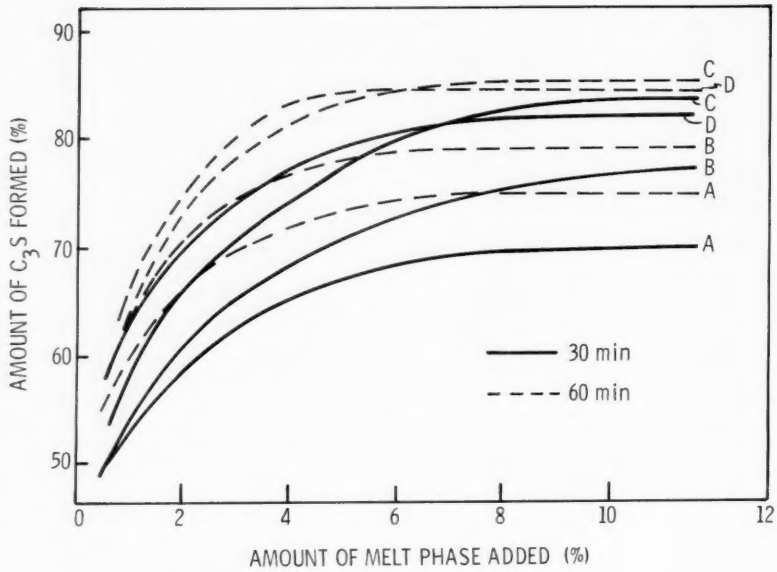

Fig. 2. Formation of C_3S as a function of melt composition, melt addition, and firing time at 1450°C (A=C_3A; B=C_6A_2F; C=C_4AF; D=C_2F).

B. MICROANALYSES OF C_3S AND MELT PHASE

Three samples were chosen for microprobe analyses of individual C_3S grains. All samples contained 10% of melt phase and were fired at 1450°C for 60 min. The results are shown in Table 2. It can be seen that the C_3S grains incorporate small amounts of alumina and iron oxide. The levels reflect the composition of the melt phase and are similar to values determined for actual cements.[11,12] The values appear to be close to the solid solution limits for C_3S.[13]

One might expect therefore that some silica would be contained in the melt phase, as suggested above. Microanalyses showed the presence of silica (5-10%) in the melt phase which surrounded the C_3S grains. However, because of the small width of the melt boundaries and the spread of the electrons within the material, at least part of that silica can be attributed to the adjacent C_3S grains. If all the silica is assumed to come from the C_3S then microanalyses give the following results: $C_4AF = C_4A_{1\cdot22}F_{1\cdot15}$ and $C_2F = C_2F_{1\cdot11}$. The analysis of C_6A_2F gave only $C_6A_{2\cdot07}F_{0\cdot65}$. These calculations give C/(A+F) ratios less than 2, but if about 2-3 wt % silica is assumed to be in the melt phase[11,12] then the ratio becomes much closer to 2. An attempt was made to obtain bulk analyses of the melt phase by dissolving the C_3S grain in methanolic salicyclic acid solution. Again, although residual silica was determined, quantitative dissolution of the C_3S apparently did not occur. It was noted that neither the melting point nor the lattice parameters of the melt phases had apparently changed after firing. Thus, it can be concluded that if silica does enter the melt phase its concentration remains fairly small and does not significantly affect the bulk properties

Table 2

Microprobe Analyses of Various C_3S Preparations

Melt Phase Present	No. of† Grains Analyzed	Method of Analysis††	Average Oxide Analyses (wt %)*				
			CaO	SiO_2	Al_2O_3	Fe_2O_3	TOTAL
C_6A_2F	7(2)	MP	70.66 (1.32)	24.23 (1.60)	1.37 (0.48)	1.07 (0.32)	97.18+ (3.08)
	6(2)	MP	71.01 (1.22)	24.84 (0.97)	1.46 (0.57)	1.10 (0.35)	98.43 (1.58)
	4(0)	SEM	71.52 (0.38)	24.02 (0.62)	0.97 (0.13)	0.86 (0.08)	97.38 (1.09)
C_4AF	7(0)	MP	69.71 (2.32)	23.99 (1.37)	0.85 (0.25)	1.17 (0.18)	96.08 (2.83)
	5(2)	SEM	72.24 (0.33)	25.00 (0.25)	0.90 (0.20)	1.15 (0.06)	99.02 (1.04)
C_2F	10(1)	MP	71.06 (0.76)	25.01 (0.73)	0.18 (0.18)	1.52 (0.43)	97.76 (1.40)
	4(0)	SEM	71.72 (0.85)	24.27 (0.69)	0.00	1.40 (0.16)	97.39 (1.25)

* Standard deviations in parentheses.
† The number of grains in parentheses were identified as C_2S and thus not included in the analysis.
†† MP = microprobe, SEM = SEM-EDS system.
\+ Except for one sample all totals exceeded 97%

of the melt. Methods are being explored to compare the reactivity of C_3S prepared under different conditions.

IV. CONCLUSIONS

Increasing the iron content of the melt phase up to about C_4AF composition increases the rate of formation of tricalcium silicate. The amount of melt phase as well as the time and temperature of clinkering also affect the kinetics of C_3S formation. Iron and alumina enter the C_3S lattice during clinkering in amounts reflecting their relative concentrations in the melt. Silica also apparently enters the melt phase, although conclusive evidence could not be obtained.

V. ACKNOWLEDGEMENTS

This work was supported by the National Science Foundation grant number CME 79-02665. Experimental assistance by L. Newman is gratefully acknowledged.

VI. REFERENCES

1. Y.M. Butt, V.V. Timashaev, and A.P. Ozokin, Prin. Paper, Proc. 6th Int. Cong. Chem. Cement, Moscow, 1974.
2. V.M. Viswanathan and S.N. Ghosh, in: Advances in Cement Technology, S.N. Ghosh, ed., p. 188 (Pergamon Press, 1983).
3. R.M. Harath Banda and F.P. Glasser, Cem. Concr. Res. 8, 319 (1978).
4. N.H. Christensen, O.L. Jepsen, and V. Johansen, Cem. Concr. Res. 8, 693 (1978).
5. N.H. Christensen and V. Johansen, in: Cement Production and Use, J. Skalny, ed., Proc. Eng. Found. Conf., publication number 79-08, p. 55 (New York, 1979).
6. W.A. Klemm, ibid, p. 71.
7. R. Bucchi, World Cem. Technol. 12, 210 (1981).
8. M.P. Javellana and I. Jawed, Cem. Concr. Res. 12, 399 (1982).
9. J. Skalny, K.H. Holub, and W.A. Klemm, Il Cemento 75, 351 (1978).
10. W.A. Klemm, I. Jawed, and K.J. Holub, Cem. Concr. Res. 9, 489 (1979).
11. M. Kristmann, Cem. Concr. Res. 8, 93 (1978).
12. A. Ghose and P. Barnes, Cem. Concr. Res. 9, 747 (1979).
13. A. Guinier and M. Regourd, Proc. 5th Int. Symp. Chem. Cement, Tokyo, 1968, Vol. I, p. 1, Cement Assoc. Japan, Tokyo, 1969.

VOL
14
198

CEMENT and CONCRETE RESEARCH. Vol. 14, pp. 105-112, 1984. Printed in the USA.
0008-8846/84 $3.00 + 00. Copyright (c) 1984 Pergamon Press, Ltd.

INFLUENCE OF GLUCONATE, LIGNOSULFONATE OR GLUCOSE ON THE C_3A HYDRATION IN THE PRESENCE OF GYPSUM WITH OR WITHOUT LIME

Mario Collepardi, Saveria Monosi, Giacomo Moriconi and Marco Pauri
Department of Materials and Earth Sciences
University of Ancona, Ancona, Italy

(Communicated by J. Skalny)
(Received June 20, 1983)

VOL.
14
984

ABSTRACT

The influence of gluconate, lignosulfonate or glucose at 0.1-0.3% dosages on the C_3A hydration in the presence of gypsum with or without lime has been examined. In the presence of lime all the admixtures at 0.3% dosage stabilize ettringite and retard its conversion to monosulfate; only 0.3% glucose retards gypsum consumption and ettringite production. In the absence of lime stabilization of ettringite by admixtures at 0.3% addition appears to be much less effective; no admixture is able to retard the ettringite production or gypsum disappearance. At 0.1% addition, the influence of admixtures seems to be negligible except when glucose is used in the presence of lime: in this case, the conversion of ettringite into monosulfate is retarded.

Introduction

Gluconate, lignosulfonate and glucose are the most widely used raw materials in the production of water-reducing admixtures for concrete. They also retard the early hydration of portland cement. As C_3A* affects setting and early hydration of portland cement, many works have been devoted to the influence of water-reducing admixtures on C_3A hydration. Most work has been devoted to the influence of these admixtures (generally at relatively high dosages in comparison with those used in practice), on the hydration of pure C_3A without lime and/or gypsum (1-12). However, C_3A in a cement will react with an aqueous solution saturated with CH, produced by C_3S hydration, and

* $A = Al_2O_3$; $C = CaO$; $S = S_iO_2$; $\overline{S} = SO_3$; $H = H_2O$; $\overline{C} = CO_2$

$CaSO_4 \cdot 2H_2O$. Therefore, it is very surprising that the effect of water-reducing admixtures on the C_3A-$C\bar{S}H_2$-CH-H_2O system has not been adequately studied. Only the effect of commercial lignosulfonate on this system has been examined (1, 13). Moreover, as these admixtures strongly retard the C_3S hydration (14), the aqueous solution in contact with C_3A in a cement could be saturated with gypsum but not with lime for a certain period of time. Thus, it should be useful examine also the effect of these admixtures on the C_3A-$C\bar{S}H_2$-H_2O system. Again, very few papers (2, 15), only concerning lignosulfonate, have been devoted to this subject.

The purpose of the present work is to study the effect of gluconate, lignosulphonate or glucose on C_3A hydration in the C_3A-$C\bar{S}H_2$-H_2O system in the presence or absence of lime.

The hydration of C_3A in this system occurs in three successive stages (13).

Stage I C_3A reacts with H_2O and $C\bar{S}H_2$ producing ettringite according to equation [1]

$$C_3A + 3C\bar{S}H_2 + 26\ H_2O \longrightarrow C_3A \cdot 3C\bar{S} \cdot H_{32} \qquad [1]$$

Stage II When $C\bar{S}H_2$ has been consumed, the transformation of ettringite into monosulfate occurs according to equation [2]

$$2C_3A + C_3A \cdot 3C\bar{S} \cdot H_{32} + 4H_2O \longrightarrow 3\ C_3A \cdot C\bar{S} \cdot H_{12} \qquad [2]$$

Stage III The remainder of the C_3A reacts with $Ca(OH)_2$ and monosulfate to form a solid solution, according to equation [3] and the rest combines with CH and H_2O forming C_4AH_{19} according to equation [4]

$$C_3A + xCH + (1-x)\left[C_3A \cdot C\bar{S} \cdot H_{12}\right] + 12xH_2O \longrightarrow C_3A \cdot xCH \cdot (1-x)C\bar{S} \cdot H_{12} \qquad [3]$$

$$C_3A + CH + 18H_2O \longrightarrow C_4AH_{19} \qquad [4]$$

Experimental

Tricalcium aluminate, quartz (S), sodium gluconate (NG), purified sodium lignosulfonate (NLS) and glucose (G) are the same as those used in a previous work (16). Calcium hydroxyde and gypsum were dry-mixes with the above materials in the proportions shown in Table I.

Hydration of pastes with and without admixtures (0.1 and 0.3% by weight of C_3A) was carried out at 20° C with a water solid ratio of 0.50. At hydration times from 30 min to 7 days DTG analysis was carried out as it was described in a previous paper (16). In some cases XRD analysis has been carried out.

TABLE I

Proportions of Anhydrous Mixes

C_3A	CH	$C\bar{S}H_2$	S	NG	NLS	G
50	–	10	40	–	–	–
50	10	10	30	–	–	–
50	–	10	39.95	0.05	–	–
50	10	10	29.95	0.05	–	–
50	–	10	38.85	0.15	–	–
50	10	10	28.85	0.15	–	–
50	–	10	39.95	–	0.05	–
50	10	10	29.95	–	0.05	–
50	–	10	38.85	–	0.15	–
50	10	10	28.85	–	0.15	–
50	–	10	39.95	–		0.05
50	10	10	29.95	–	–	0.05
50	–	10	38.85	–	–	0.15
50	10	10	28.85	–	–	0.15

Results and Discussion

Figure 1 shows the DTG curves of the hydration products for the C_3A-$C\bar{S}H_2$ system in the absence of admixtures, without and with CH. The specimens exhibit varions peaks which can be attributed as follows. The DTG peak at about 150° C with a shoulder on the right side is assigned to a stepwise thermal decomposition of $C\bar{S}H_2$ into $C\bar{S}H_{\frac{1}{2}}$ and $C\bar{S}$. The peak at about 120° C is attributed to the dehydration of ettringite ($C_3A \cdot C\bar{S} \cdot H_{32}$), whereas the peaks at about 200° C and 280° C are attributed to the thermal dehydration of the monosulfate. The peaks at about 500° C and 800° C are assigned to $C\bar{H}$ and $CaCO_3$ respectively. The disappearance of gypsum and the formation of ettringite (Stage I, e.q. [1]) and its conversion to monosulfate (Stage 2, e.q. [2]) are processes which occur more rapidly in the absence (Fig. 1A) than in the presence of CH (Fig. 1B). These data agree with XRD results showing that the C_3A disappearance in the presence of $C\bar{S}H_2$ was retarded by addition of CH. These results confirm the data obtained by Mehta (17) and the Forsen's results quoted by Taylor (18) indicating that CH addition retards the hydration of C_3A in the

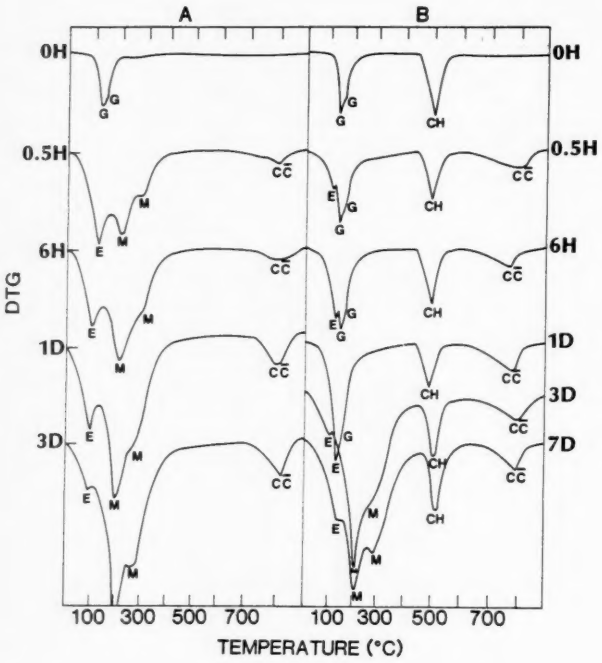

FIG. 1

DTG curves of the C_3A-$C\bar{S}H_2$-H system without (A) and with (B) CH. G = Gypsum; E = Ettringite; M = Monosulfate; CH - Calcium Hydroxide; $c\bar{c}$ = calcium carbonate.

presence of gypsum. According to Mehta, "colloidal" ettringite is produced in the presence of CH which would retard the C_3A hydration in a more efficient way (17).

In the system studied in the present work, $C\bar{S}H_2$ disappears in less than 0.5 hr in the absence of CH, and in more than 1 day in the presence of CH. However, preliminary tests showed that using different batches of C_3A, gypsum combines with H and C_3A with different reactions rates, possibly because of differences in the reactivity of C_3A. This means that the results obtained in different laboratories using different batches of C_3A may be quite different, even if an equal composition of the mixes is used. Therefore, the effects of water-reducing admixtures on the C_3A-$C\bar{S}H_2$ or C_3A-$C\bar{S}H_2$-CH systems obtained by different authors should be compared in relationship with the specific reference mixes without admixtures used by different researchers. The peak at 800° C is present also in the specimens without CH and it increases with the amount of monosulfate. It is confirmed that hexagonal aluminate hydrates are particularly reactive with CO_2 (16).

Figure 2 shows the DTG curves of the hydration products of C_3A in the presence of 0.3% NG and gypsum without (Fig. 2A) and with (Fig. 2B) CH. As no significant effect has been found in the presence of 0.1% NG the results are not shown here.

In the absence of CH, it seems that 0.3% gluconate slightly accelerates the ettringite production (equation [1]) during the first 30 min (Fig. 1A and 2A) whereas the subsequent conversion of ettringite into monosulfate (equation [2]) is retarded.

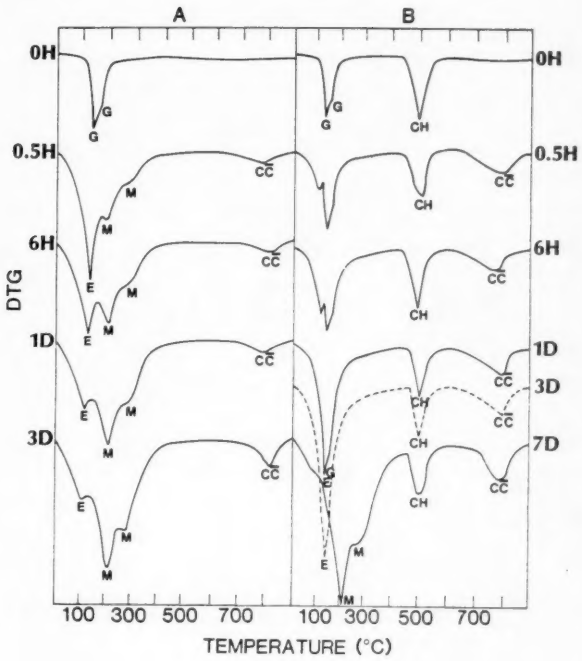

FIG. 2

DTG curves of the C_3A-$C\bar{S}H_2$-H system in the presence of 0.3% sodium gluconate without (A) and with (B) CH.

In the presence of CH, the rates of ettringite production and gypsum disappearance between 0 and 24 hours are not substantially modified by 0.3% NG addition (Fig. 1B and 2B). The type of ettringite produced in the presence of CH, seems to protect the C_3A particles from hydration so efficiently that the NG effect becomes negligible. However, even in the presence of CH, ettringite appears to be stabilized by NG addition so that its conversion to monosulfate after 1 day is significantly retarded. This would indicate that after 1 day C_3A disappears more rapidly in the reference mix than in the mix with NG according to the reaction [2] . For instance, at 3 days ettringite appears still to be the only hydration product in the presence of NG (Fig. 2B), whereas in the reference mix without admixture monosulfate is the predominant phase (Fig. 1B).

The stabilization of ettringite by organic products has been ascribed to the penetration of organic molecules into the intercolumnar region of ettringite crystal structure (19).

Figure 3 shows the DTG curves hydrated in the presence of 0.3% NLS and gypsum without (Fig. 3A) and with (Fig. 3B) CH. No significant effect has been found using 0.1% NLS; therefore the DTG curves of the hydration products in the presence of 0.1% NLS are not shown here.

In the absence of CH, 0.3% NLS does not affects the ettringite production; conversion of ettringite into monosulfate (Fig. 1A and 3A) appears to be retarded only to a negligible extent. So it seems that NG retards the C_3A hydration in the presence of $C\bar{S}H_2$ more remarkably than NLS does (Fig. 2A and 3A). Similar results have been obtained for the hydration of C_3A without gypsum (16). Massazza and Costa (15) and Chatterji (2) found that lignosulfonate acts as a

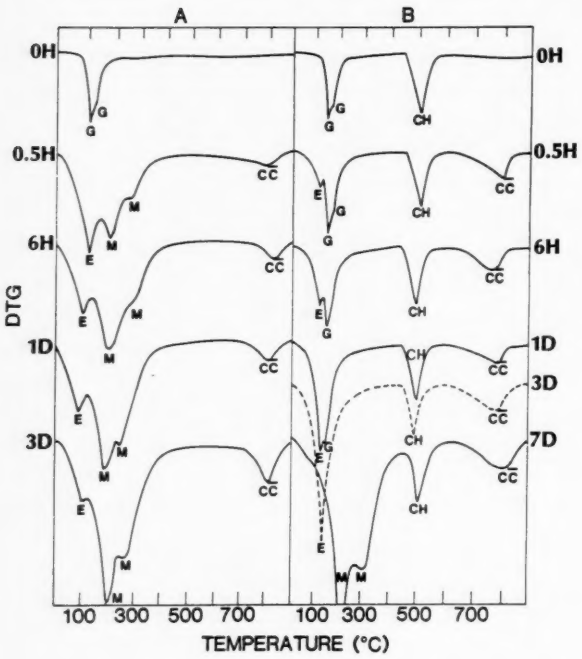

FIG. 3

DTG curves of the C_3A-$C\bar{S}H_2$-H system in the presence of 0.3% sodium lignosulfonate without (A) and with (B) $\bar{C}H$.

retarder for the hydration of C_3A in the presence of $C\bar{S}H_2$ and in the absence of CH. However, they worked in quite different experimental conditions. Massazza and Costa (15) worked with the same $C\bar{S}H_2/C_3A$ and H/C_3A ratios as those used in the present work. Moreover, the kinetics of the reactions (ettringite production and its conversion into monosulfate) in their reference mix without lignosulfonate is very similar to that of the present work. However, they used a much higher dosage (1% by weight of C_3A) of sodium purified lignosulfonate and this can explain why they found a significant retarding effect for lignosulfonate. Chatterji (2) worked with the same $C\bar{S}H_2/C_3A$ ratio as that of our work and a lower H/C_3A (= 0.6) ratio than that of the present work. He found that lignosulfonate significantly retards gypsum consumption, ettringite production and its conversion into monosulfate even with relatively low admixture dosages similar to those used in the present work. However, his C_3A-$C\bar{S}H_2$ system without admixture appears to be remarkably less reactive than that of the present work as, for instance, gypsum is still present at 1 day. Moreover, Chatterji used unrefined calcium lignosulfonate containing reducing sugars and organic acids which could be responsible for the retarding effect at low lignosulfonate dosage (0.2 – 0.4%).

In the presence of both CH and $C\bar{S}H_2$, 0.3% NLS affects the C_3A hydration (Fig. 3B) to the same extent as NG does (Fig. 2B): the rate of ettringite production during the first day is not substantially modified, whereas the transformation of ettringite into monosulfate after 1 day is significantly retarded. Similar results have been obtained by Seligmann and Greening (13) and Young (1) although they used higher dosages of commercial calcium lignosulfonate.

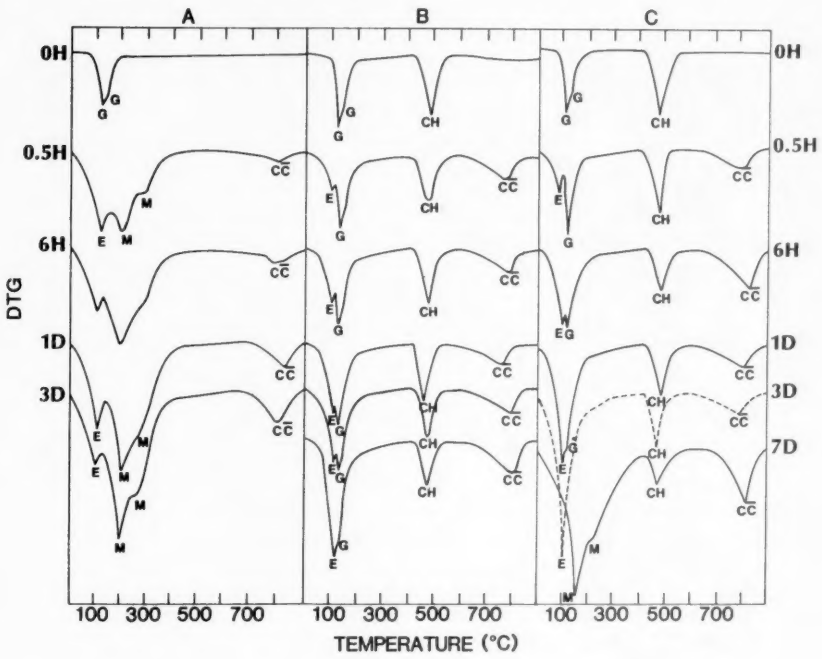

FIG. 4

DTG curves of the C_3A-CSH_2-H system in the presence of glucose without and with CH. (A = without CH and with 0.3% G; B = with CH and 0.3% G; C = with CH and 0.1% G).

Figure 4 shows the hydration products of C_3A in the presence of G and gypsum without (Fig. 4A) and with (Fig. 4B and C) lime.

In the absence of CH, 0.3% G does not changes significantly the ettringite production; the transformation of ettringite into monosulfate appears to be retarded to a negligible extent (Fig. 1A and 4A). Similar results have been obtained using 0.1% G.

In the presence of CH, 0.3% G remarkably retards the ettringite production and gypsum disappearance (Fig. 4B). Consequentely, the transformation of ettringite into monosulfate is delayed. For instance, at 3 days monosulfate is the predominant hydration product phase in the C_3A-CSH_2-CH-H system without admixture (Fig. 1B), whereas ettringite and gypsum are still present in the presence of 0.3% G (Fig. 4B). In the presence of a lower dosage (0.1%) of glucose, ettringite only is present at 3 days (Fig. 4C). At 7 days, monosulfate is not yet present when a high dosage (0.3%) of glucose is used (Fig. 4B), whereas it becomes the predominant phase in the presence of a lower amount (0.1%) of glucose (Fig. 4C).

Conclusions

At 0.1% addition, the effect of gluconate and lignosulfonate on the C_3A hydration in the presence of gypsum appears to be negligible, whether lime is present or not. At 0.1% dosage, glucose retards the conversion of ettringite into monosulfate only in the presence of lime.

At 0.3% addition, in the absence of lime all the admixtures retard the conversion of ettringite into monosulfate to a small extent; no retardation in the ettringite production or gypsum consumption is caused by all the admixtures.

At 0.3% addition, in the presence of lime all the admixtures stabilize ettringite and retard its conversion; only 0.3% glucose retards ettringite production and gypsum disappearance.

References

1. J.F. Young, Magazine of Concrete Research 14, 137-42 (1962).
2. S. Chatterji, Indian Concrete Journal 41, 151-60 (1967).
3. E.D. Ciach and E.G. Swenson, Cement and Concrete Research 1, 143-58 (1971).
4. V.S. Ramachandran and R.F. Feldman, Matèriaux et Constructions 5, 67-76 (1972).
5. N.B. Milestone, Cement and Concrete Research 6, 89-102 (1976).
6. N.B. Milestone, Cement and Concrete Research 7, 45-54 (1977).
7. V.S. Ramachandran, Zement-Kalk-Gips 31, 206-10 (1978).
8. M. Collepardi, M. Corradi, G. Baldini and M. Pauri, VII International Symposium on Cement Chemistry, Vol. IV, 524-28 (1980).
9. V.S. Ramachandran, VII International Symposium on Cement Chemistry, Vol. IV, 535-40 (1980).
10. M. Pauri, G. Baldini and M. Collepardi, Cement and Concrete Research 12, 271-77 (1982).
11. M. Pauri, G. Ferrari and M. Collepardi, Cement and Concrete Research 13, 61-68 (1983).
12. V. Lorprayoon and D.R. Rossington, Cement and Concrete Research 11, 267-277 (1981).
13. P. Seligmann and N.R. Greening, Highway Research Record, Highway Research Board No. 62, 80-105 (1964).
14. N.B. Milestone, Journal of American Ceramic Society 62, 321-24 (1979).
15. F. Massazza and U. Costa, VII International Symposium on Cement Chemistry, Vol. IV, 529-34 (1980).
16. S. Monosi, G. Moriconi, M. Pauri and M. Collepardi, Cement and Concrete Research 13, 568-574 (1983).
17. P.K. Mehta, Journal of American Ceramic Society 56, 315-19 (1973).
18. H.F.W. Taylor, The Chemistry of Cement, Vol. I, 317-18, Academic Press, Inc. New York (1964).
19. J.F. Young, Transportation Research Record, No. 564, 1-9 (1976).

VOL
14
198

CEMENT and CONCRETE RESEARCH. Vol. 14, pp. 113-122, 1984. Printed in the USA.
0008-8846/84 $3.00 + 00. Copyright (c) 1984 Pergamon Press, Ltd.

MATHEMATICAL MODELING OF THE FREEZING PROCESS OF CONCRETE AND AGGREGATES

Mikael P. J. Olsen
Texas A&M University
College Station, Texas 77843

(Communicated by G. Fagerlund)
(Received June 22, 1983)

VOL.
14
984

ABSTRACT

A two dimensional finite element computer model for predicting frost penetration in saturated porous materials is presented. Based on available second order parabolic differential equations for predicting temperature and moisture content, and equations relating freezing temperature and water potential, the finite element model predicts temperature, water and ice content, frost penetration, and generated pore water pressures as a function of freezing time and given boundary conditions. Comparison of models results with available experimental data for mature cement pastes rendered reasonable agreement between the model and data.

Introduction

The problem of determining the acceptability of aggregates for use in portland cement concrete and the durability of concrete which is subjected to freezing and thawing, cyclic wetting and drying, and other forms of climatic exposure is of continued concern to material engineers world wide. Phoenomena like D-cracking and scaling in concrete and heaving in soils are all known to be partly of fully caused by a combination of moisture movement and freezing of the water in the pore space.

Existing testing procedures for freeze-thaw durability can be grouped in two general categories:

1. Tests based on environmental simulation
2. Tests based on aggregate properties

In some instances an interaction or combination of the two test categories may exist (1). The two test categories are, however, either lengthy to perform or excludes important variables influencing the freeze-thaw durability (2). In order to improve the prediction of freeze-thaw durability of concrete and aggregates a mathematical model has been constructed. The model predicts temperature, water and ice

content, frost penetration, and generated pore water pressures as a function of freezing time. As assumptions the model have saturated condition of the materials and confined freezing.

Model Development

The mathematical model of the freezing of aggregates and concrete was developed based on a finite element formulation of the following two second order parabolic differential equations for predicting moisture content and temperature (3, 4):

$$\frac{\partial \theta}{\partial t} = \nabla D_T \nabla T + \nabla (D_\theta \nabla \theta) + \frac{K_\theta}{dz} - \frac{\rho_i}{\rho} \frac{\partial \phi}{\partial t} \quad (1)$$

$$c \frac{\partial T}{\partial t} = \nabla \lambda \nabla T + L \frac{\partial \phi}{\partial t} \quad (2)$$

The procedure used to solve Equations 1 and 2 is similar to that described References 5-8. (Symbols used in all equations are defined in Appendix I). It should be noted that numerical problems might occur if the moisture content during freezing is too close to saturation. This is caused by the slope, $\partial\theta/\partial P$, in Equation 3 being indefinite at that point. A way to eliminate this problem is to use

$$D_\theta = \frac{K_\theta}{\partial \theta / \partial P} \quad (3)$$

Darcy's equation directly (Equation 4):

$$\frac{\partial \theta}{\partial t} = \nabla D_T \nabla T + \nabla (K_s \nabla P) - \frac{\rho_i}{\rho} \frac{\partial \phi}{\partial t} \quad (4)$$

In solving Equations 1 and 2 the equations are coupled in the following manner. The water content calculated by Equation 1 are related to temperatures calculated by Equation 2. The specific relationship that makes the coupling possible is given by a temperature - water content curve which in turn has been produced from a combination of a temperature suction curve and a moisture characteristic curve. These relations are discussed further in the following section. The iterative solution scheme proceeds during a time step as follows:

1. Solve for temperature at grid point
2. Solve for water contents at grid point
3. Compute ice contents at grid points
4. Calculate values of λ, c, L, D_θ, D_T at grid points
5. Select time interval for the next time step

After calculating temperatures, the moisture and ice contents are also calculated and compared to the values computed using Equation 1. The final values of moisture and ice contents are those which are the highest and lowest respectively indicating the limitation of either the amount of ice to be formed or the possible amount of water movement towards the ice front.

Temperature-Water Content Relationships

Since porous materials like concrete and aggregates generally contain a wide distribution of pore sizes, not all pore water freezes at a given temperature. This is due to a lowering of the freezing temperature with a decrease in pore size, a concept well known as the freezing point depression (9, 10). Then, knowing the relationship

VOL. 14 1984

between freezing temperature and unfrozen water content becomes important in the estimation of the amount of ice formed in a porous material. Experimental results of the relationship exists for soils (3), cement paste (11) and other porous building materials (13), but the author has been unsuccessful in finding experimental data specifically for aggregates alone. In addition, experiments to find the unfrozen water content are often lengthy to perform. Other methods of determining the relationship are therefore desirable.

Fagerlund (14) has summarized the theoretical equations available to determine the freezing point depression for both saturated and unsaturated porous materials. The equations in the saturated condition are:

$$P = \frac{-RT\rho \ln (p/p_0)}{M} \tag{5}$$

$$\log_{10} (p/p_0) = \frac{1.1489T}{273.1 + T} + 1.33 \times 10^{-5} T^2$$

$$-9.084 \times 10^{-8} T^3 \tag{6}$$

Equation 5 relates the freezing temperature, T, with the suction, P, using the relative vapor pressure which is calculated by means of Equation 6. This last equation is a semi-empirical relationship given by Washburn (15). It assumes that the ice and the evaporable water are in equilibrium. It is further assumed that this is the only capillary condensed water, and no surface adsorbates in the pore system. For the freezing process of porous building materials the later assumption is reasonable in that the assumption is valid for $p/p_0 > 0.80$ corresponding to a freezing temperature of about -25°C (-13 °F).

In the computer program the unfrozen water content is found from tabulated values of either suction versus water content or relative humidity (vapor pressure) versus water content provided by the user. These tables should be easy to produce by simple sorption - desorption experiments or by use of the literature, thus making the estimation of unfrozen and frozen water content as a function of both time and temperature more easy and quick through use of the program.

Hydraulic Properties

Since drying shrinkage is often taking place in underlaying or surrounding areas near the primary freezing front in soils (16) the freezing process in porous materials can be viewed as a drying process. Furthermore, the technique of freeze-drying as a means of eliminating moisture from coffee beans and other products further justifies the comparison. The need for determining the change in both hydraulic conductivity and moisture diffusivity is then apparent.

Elzeftawy and Dempsey (17) have established methods for determining these theoretically as well as practically and their findings have been used in the model. The conductivities are obtained by dividing the moisture content-suction relation into n equal water content increments, obtaining the suction, P, at the midpoint of each increment, and calculating the conductivity using the equation:

$$K(\theta)_i = \frac{K_s}{K_{sc}} \frac{\sigma^2}{2\eta\rho^2 g} \left(0.15 \frac{\Delta\varepsilon_1}{P_1^2} + \sum_{j=2}^{i} \frac{\Delta\varepsilon_j}{P_j^2}\right) \qquad (7)$$

$$i = 1, 2, 3, \ldots, n$$

The first term, $0.15\,\Delta\varepsilon_1/P_1^2$, in the parantheses is taking the nonlinearity of the first part of the K_θ versus moisture content relationship into account, and has been determined experimentally (18).

With the unsaturated hydraulic conductivity known, the moisture diffusivity, D_θ, can be calculated using the definition of moisture diffusivity:

$$D_\theta = \frac{K_\theta}{\partial\theta/\partial P} \qquad (8)$$

and the suction versus water content data.

Philip and de Vries (19) have discussed the second term present in Equation (1), the thermal moisture diffusivity, D_T. According to Philip and De Vries (19) D_T can be found from the following expression:

$$D_T = K_\theta \gamma P \qquad (9)$$

where:

$$\gamma = \frac{1}{\sigma} \frac{\partial\sigma}{\partial T} \qquad (10)$$

is called the thermal coefficient. In the model Equation 10 has been combined with the following temperature dependency of the surface tension, σ, given by Dorsey (20):

$$\sigma(T) = (1 - aT - bT^2)\ 75.64 \qquad (11)$$

Inserting Equation 11 into Equation 10 then gives:

$$\gamma(T) = \frac{a + 2bT}{aT + bT^2 - 1} \qquad (12)$$

In accordance with Dorsey (20) the values for the constants a and b have been set equal to 1.839×10^{-3} and 3.97×10^{-6} respectively representing the temperature interval 0 to -40°C (32 to -40°F).

Thermal Properties

In order to solve Equation 2 the thermal conductivity, heat capacity, and latent heat of fusion of the porous material must be known.

Although the definition of thermal conductivity is simple it becomes more complex during freezing when trying to estimate it based on known values in the nonfrozen stage. Since the material is composed of solid, water and ice, the effective thermal conductivity is a function of the contributions of each individual thermal conductivity on a volumetric basis:

$$\lambda = \frac{\lambda_w\theta + \lambda_i\phi + \lambda_s}{1.0 + \theta + \phi} \qquad (13)$$

VOL. 14 1984

Both the thermal conductivity for water, λ_w , and ice, λ_i , are temperature dependent (20). The following equations have therefore been developed using information from Dorsey (20):

$$\lambda_w = 5.87 \times 10^{-3} (1.0 + 2.81 \times 10^{-3} (T-20.0)), \text{ T in } ^\circ C \quad (14)$$

$$\lambda_i = 0.0, \; T \geq 0^\circ C \quad (15)$$

$$\lambda_i = 2.24 \times 10^{-2} - 8.0 \times 10^{-5} T, \; -10^\circ C \leq T < 0^\circ C \quad (16)$$

$$\lambda_i = 2.32 \times 10^{-2} - 1.15 \times 10^{-4} (T + 10.0), \; T < -10^\circ C \quad (17)$$

Kersten (21) has separated the heat capacity into an unfrozen an frozen part:

$$C_u = \frac{100\, C_m + 1.0\, w}{100 + w} \quad (18)$$

$$C_i = \frac{100\, C_m + 0.50\, w}{100 + w} \quad (19)$$

For the 2° F temperature interval between 30 and 32° F Dempsey and Thompson (22) used a freezing heat capacity:

$$C_f = \frac{144\, w \gamma_d}{200\, \gamma_t}, \text{ in BTU/lb-F} \quad (20)$$

The reason for the use of Equation 20 is, that in a finite element solution scheme (or finite difference solution scheme) the predicted freezing time of the moisture is larger than the actual experimental value in cases when only Equation 2 is used to predict the freezing process. A revised form of Equation 2 is implied instead in which the latent heat of fusion term, $L\, \partial\phi/\partial t$, is elimated. Since, however, the latent heat of fusion is equal to:

$$L = \frac{144\, w\, \gamma_d}{100}, \text{ in BTU/ft}^3 \quad (21)$$

Equation 20 incooperates this important parameter.

In the model a more direct expression has been used based on Equations 18 and 19. An effective heat capacity is calculated using the following equation:

$$c = \frac{c_m + 0.05\phi + 1.00\theta}{1.0 + \theta + \phi} \quad (22)$$

where ϕ and θ are dimensionless (cm^3/cm^3). To facilitate the slower release of heat with time (and thus a faster freezing time) the latent heat of fusion has been made a function of the instantaneous volumetric water content, rather than the total gravimetric water content stated in Equations 20 and 21. After the necessary rearrangements of Equation 21, the following version of the equation becomes:

$$L = \frac{144\, \theta\, \gamma_w}{1.09} \quad (23)$$

where the constant 1.09 takes into account the change in volume when water freezes.

In the area of soil freezing, the latent heat of fusion has previously been regarded as a constant. From reference 20, however, the latent heat of fusion is found to be temperature dependent,

decreasing significantly with a decrease in temperature from about 144 BTU/lb-F at 32° F to about 133 BTU/lb-F at 23°F. The following equations were therefore introduced in the model:

$$L = 333.6 + 5.02T, \quad -5<T\leqq 0°C \tag{24}$$
$$L = 308.5 + 4.74\ (T+5.0), \quad -10\leqq T\leqq 0°C \tag{25}$$
$$L = 284.8 + 4.64\ (T+10), \quad -15<T\leqq -10°C \tag{26}$$
$$L = 261.6 + 4.04\ (T+15), \quad -20<T\leqq -15°C \tag{27}$$
$$L = 241.4 + 3.3\ (T+20), \quad T<-20°C \tag{28}$$

Freezing Pressure

Among the most important factors influencing freezing of soils and other porous materials is the freezing pressure. There are reasons to believe that the negative pore water pressure (suction), created during the drying process when the liquid water is transformed to solid ice, plays a major role in predicting the total pressure generated (9, 22, 23, 24, 25, 26). Works by Powers (27, 28) indicated the possible existence of sufficient hydraulic pressures generated by the movement of an ice front in connection with the 9 percent increase in volume when water is freezing. As proven by Litvan (29) the 9 percent increase in volume does not explain the freeing mechanism completely in that other non-expansive adsorbates still causes expulsion of pore liquid. The 9 percent volume increase must, however, add to the existing pressure, and further increase it.

In the model then, the total freezing pressure is estimated from essential two components, one being the total negative pore water pressure generated by the removal of liquid water, P_s , the other an elastic accomodation pressure caused by the formation of ice, P_c, equal to (30):

$$P_c = \frac{0.09\theta E}{3(1-2\mu)} \tag{29}$$

Thus:

$$P = P_s + \frac{0.09\theta E}{3(1-2\mu)} \tag{30}$$

In the output from the program both components, P_s and P_c, are listed.

Model Output and Capabilities

The computer model can deliver the following output variables at selected geometric points as a function of time:

1. Temperature
2. Water and ice content
3. Ice, suction, and total pore water pressure

To illustrate the capabilities and application of the model, Figure 1 shows the predicted frozen water content as a function of freezing temperature for two mature cement paste samples. Experimental data, indicated by the solid and broken lines, are given by Powers and Brownyard (26). The circles and squares represent values from the computer output of the mathematical model. Known parameters were substituted into the model based on values given in the literature. As can be seen, a quite reasonable agreement between the model and the experimental values is present.

VOL. 14 1984

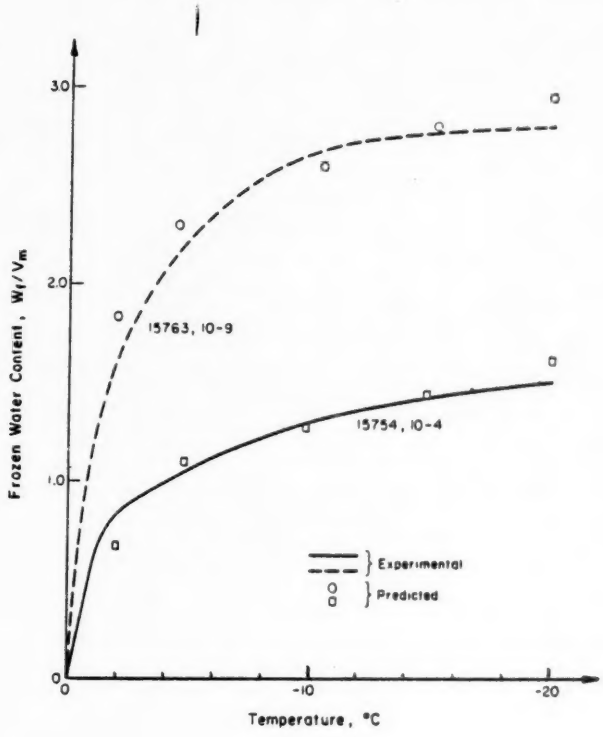

FIG. 1

Comparison of Experimental and Predicted Frozen Water Contents in Cement Paste Samples During Freezing. For Samples 15763, 10-9 and 15754, 10-4 V_m is 0.038 and 0.049 respectively.

After selecting appropriate values for the input parameters the model can be used to analyze the influence and effect any of the parameters have on the freezing process. For example the influence of changing the desorption characteristics of an aggregate (i.e. changing the pore structure) can be of importance in selecting and improving aggregates. Since the literature contains quite a few values for the thermal parameters of aggregates and cement paste the freeze-thaw interaction between these two materials can furthermore be studied. Based on simple measurements of hydraulic conductivity and sorption characteristics rather than the lengthy freeze-thaw experiments, faster results can be obtained in the decision process of accepting or rejecting aggregates through the use of this model.

Acknowledgment

This Study was conducted as part of the Illinois Cooperative Highway Research Program Project IHR-413, D-cracking in Portland Cement Concrete Pavements, by the staff of the Department of Civil Engineering in the Engineering Experiment Station, University of Illinois, under the sponsorship of the Illinois Department of

Transportation (Division of Highways) and the Federal Highway Administration, U.S. Department of Transportation.

Special thanks are extended to Dr. Barry J. Dempsey for his continued support and helpful suggestions during the course of this study.

Appendix I

Identification of symbols

C_f = Mass heat capacity of freezing material, BTU/lb-F

C_i = Mass heat capacity of frozen material, BTU/lb-F

C_m = Mass heat capacity of dry material, BTU/lb-F

C_u = Mass heat capacity of unfrozen material, BTU/lb-F

c = Volumetric heat capacity, cal/cm^3-C

c_m = Volumetric heat capacity of dry material, cal/cm^3-C

D_T = Thermal moisture diffusivity, cm^2/sec-C

D_θ = Isothermal moisture diffusivity, cm^2/sec-C

E = Modulus of elasticity, MPa

g = Acceleration due to gravity, cm/sec^2

K_s = Saturated hydraulic conductivity, cm/sec

K_{sc} = Calculated hydraulic conductivity, cm/sec

K_θ = Unsaturated hydraulic conductivity, cm/sec

L = Latent heat of fusion, cal/cm^3

M = Molar weight of water, g/mole

P = Pressure, MPa

P_c = Internal ice pressure or tensile strength required to increase volume of material sufficiently to accomodate expansion, MPa

p/p_o = Relative humidity

R = Gas constant, J/mole-C

T = Temperature, C, K, or F

t = Time, sec

V_m = Quantity of water required for a complete condenced layer on the solid, the layer being one molecule deep, g/g cement

w = Gravimetric water content, percent

z = Coordinate, cm

ϕ = Volumetric ice content, cm^3/cm^3

λ = Thermal conductivity, cal/cm-sec-C

λ_i = Thermal conductivity of ice, cal/cm-sec-C

VOL. 14 1984

λ_s = Thermal conductivity of solid, cal/cm-sec-C
λ_w = Thermal conductivity of water, cal/cm-sec-C
η = Viscosity of water, g/cm-sec
μ = Poisson's ratio
ρ = Density of water, g/cm^3
ρ_i = Density of ice, g/cm^3
γ = Thermal coefficient, C^{-1}
γ_d = Dry unit weight, lb/ft^3
γ_t = Total unit weight, lb/ft^3
θ = Volumetric water content, cm^3/cm^3
σ = Surface tension, dynes/cm
∇ = Differential operator

References

1. G. Fagerlund, RILEM, Materials and Structures 58, No. 10, 217-253 (1977).
2. S.R. Thompson, M.P.J. Olsen, B.J. Dempsey, Transportation Engineering Series No. 29, Illinois Cooperative Highway and Transportation Series, No. 187, Dept. of Civil Engineering, University of Illinois, Urbana-Champaign (June 1980).
3. G.S. Taylor and J.N. Luthin, Canadian Geotechnical Journal 14, No. 15, 548-555 (1978).
4. B.J. Dempsey, International Journal for Numerical and Analytical Methods in Geotechnics, No. 2, 19-34 (1978).
5. O.C. Zienkiewicz, The Finite Element Method, McGraw-Hill (1977).
6. G.F. Pinder and W.G. Gray, Finite Element Simulation in Surface and Subsurface Hydrology, Academic Press (1977).
7. Irwin Remson, G.M. Hornberger and F.J. Molz, Numerical Methods in Subsurface Hydrology, Wiley, 1971.
8. M.P.J. Olsen and B.J. Dempsey, Final Report, "Users Manual, Drainage 02", Report No. SSD-3-80, Federal Highway Administration, U.S. Dept. of Transportation, Washington, DC (1980).
9. D.H. Everett, Trans.Faraday Soc. 57, 1541-1551 (1961).
10. R.A. Helmuth, Proc. of the 4th Int. Symposium on the Chemistry of Cement, National Bureau of Standards Monograph 43, 2, 855-869 (1960).
11. Carl le Sage de Fontenay and Erik J. Sellevold, "Ice Formation in Hardened Cement Paste - I. Mature Water - Saturated Pastes," Durability of Building Materials and Components, ASTM STP 691, 439-454 (1980).
12. D.H. Bager and Erik J. Sellevold, "Ice Fromation in Hardened Cement Paste - II. Steam-Cured Pastes with Variable Moisture Content," Durability of Building Materials and Components, ASTM STP 691, 439-454 (1980).
13. G. Fagerlund, "Non-Freezable Water Contents of Porous Building Materials," Report No. 42, Division of Building Technology, Lund Institute of Technology, Lund, Sweden (1974).
14. G. Fagerlund, RILEM, Materials and Construction 33, No. 6, 215-225 (1973).
15. E.W. Washburn, Monthly Weather Review 52, 488-490 (1924); International Critical Tables 3, 210 (1928).
16. Stephen Taber, Journal of Geology 37, 428-461 (1929).
17. A. Elzeftawy and B.J. Dempsey, "A Method of Predicting Hydraulic Conductivity and Water Diffusivity for Pavement Subgrade Soils," Transportation

OL.
14
984

Engineering Series No. 16, Illinois Cooperative Highway and Transportation Series No. 164, Dept. of Civil Engg., Univ. of Illinois, Urbana-Champaign, (December 1976).
18. Donald J. Janssen and B.J. Dempsey, "Soil Water Properties of Subgrade Soils," Final Report, Transportation Engineering Series No. 27, Illinois Cooperative Highway and Transportation Series No. 184, Dept. of Civil Engg., Univ. of Illinois, Urbana-Champaign (April 1980).
19. J.R. Phillip and D.A. de Vries, Trans. American Geophysical Union 38, 222-232 (1957).
20. Ernest N. Dorsey, Properties of Ordinary Water-Substance, Haffner, New York (1968).
21. M.S. Kersten, "Thermal Properties of Soils," Bulletin No. 28, Univ. of Minnesota, Eng. Exp. Station, Minneapolis, MN (1949).
22. E. Penner, "Frost Heaving in Soils," Proc. Int. Conf. on Permafrost, Purdue University, 197-202 (1963).
23. D.H. Everett and J.M. Haynes, "Capillary Properties of Some Model Pore Systems with Special References of Frost Damage," RILEM Bulletin New Series, No. 27, 31-38 (1965).
24. P.J. Williams, "The Nature of Freezing Soil and Its Field Behavior," Norwegian Geotechnical Inst. Publication, No. 27, 20-119 (1967).
25. Raymond N. Yong, "Soil Suction Effects on Partial Soil Freezing," Highway Research Record 68, National Research Council, Washington, DC 31-42 (1965).
26. T.C. Powers and T.L. Brownyard, "Studies of the Physical Properties of Hardened Portland Cement Paste," Bulletin 22, Research Laboratories of the Portland Cement Association (March 1948).
27. T.C. Powers, ACI Proc. 41, 245-272 (1945).
28. T.C. Powers, ASTM Proc. 55, 1132-1155 (1955).
29. G.G. Litvan, American Creamic Society Journal 55, No. 1, 38-42 (1972).
30. George Verbeck and Robert Landgren, ASTM Proc. 60, 1063-1079 (1960).

VOL. 14 1984

CEMENT and CONCRETE RESEARCH. Vol. 14, pp. 123-132, 1984. Printed in the USA.
0008-8846/84 $3.00 + 00. Copyright (c) 1984 Pergamon Press, Ltd.

VARIATION WITH SOLID-PHASE CONCENTRATION OF COMPOSITION, STRUCTURE AND STRENGTH OF CEMENT PASTES AT HIGH AGE

Åke Grudemo
Cement and Concrete Research Institute
100 44, Stockholm 70, Sweden

(Communicated by G. Fagerlund)
(Received June 22, 1983)

OL.
14
984

ABSTRACT

Portland and white cement pastes of widely-variable water/cement ratios were studied after six years' hydration by means of quantitative X-ray diffractometric analysis of the CH and C-S-H gel contents. The results obtained have led to certain conclusions on the crystallinity and possible crystal structure of the gel. It was also observed that the flexural strength was considerably reduced for the cement pastes of lowest water/cement ratios.

Anomalous XD effects in old cement pastes

In a recent study of the state of crystallisation in the cement matrix of a very old concrete (1), the X-ray diffractometric (XD) effects from various particle-size fractions of the mortar were recorded and compared with those given by a number of pure cement pastes of different compositions, more or less fully-hydrated (moist-hydrated for 5 to 15 years). It was then noticed, in a series of white cement pastes of water/cement ratios (w_0) between 0.32 and 1.32 (stabilized by aerosil addition, maximum w_{ae} 0.05), that the peak heights for the 10·1 and 00·1 reflexions from CH varied with w_0 in essentially different ways. The 10·1 peaks were of almost constant height, as could be expected, with a low maximum for w_0 0.40 to 0.50, whereas the 00·1 peak heights increased continuously and considerably with w_0. The strongest gel peak at $2\Theta = 29^{0}3$ showed a similar increase. Since CH crystal orientation effects are out of the question, the XD samples being cut as 3 x Ø20 mm plates from longer cylinders, the reflexion at $2\Theta = 18^{0}0$ was interpreted as a CH 00·1 peak of about constant height superimposed by the basal reflexion from a C-S-H gel constituent, the content of which increases with w_0, for some reason.

In this context, the arrangement of crystal elements, silica chains in a frame of calcium ions, that could possibly satisfy the XD effects observed, was indicated, and a hypothetical structure of the C-S-H gel was given. Some slight evidence for the appearance of a double C-S-H fibre reflexion at about $2\Theta = 50^{0}$ was also presented.

However, because of the uncertainty of the XD data forming the basis of these theories (only one peak height per peak and material were observed), it seemed necessary to reinvestigate the matter more in detail.

The expected composition of fully-hydrated cement paste

The approximate composition of an average standard cement can be assumed to be $C_{2.75}S$, with alite:belite about 3:1. According to most of the sources of information, the C-S-H gel formed in the process of hydration has a C:S ratio of between 1.7 and 1.5. A simple calculation, disregarding the amounts of water fixed in the gel and in CH crystals, gives a CH content in the fully-reacted product of between 27 and 33 per cent, the rest being C-S-H-gel. A similar calculation for pure C_3S paste gives between 32 and 37 per cent.

In paste preparations with a higher water/cement ratio, it may be necessary to add high-surface silica (aerosil), in order to prevent excessive separation, up to 5 per cent or more of the cement weight. The effective C/S ratio would then decrease towards 2.3, and the content of CH formed would decrease to between 18 and 24 per cent, assuming that the C/S composition of the gel formed did not change.

XD intensities of cement hydration constituents

The CH contents of different cement pastes can be measured easily, provided that reliable comparison values for the XD peaks areas of pure CH substance can be obtained. As has been emphasized in various connections, certain precautions are necessary to prevent orientation of the CH crystal plates in the XD samples. For a chemically-pure sample with very small crystals the following values were observed.

TABLE 1.

XD intensity areas $Y_{hk\cdot l}$ and peak widths $B^{o}_{1/2}$ of CH peaks.

hk.l	$2\Theta^{o}$	$Y_{hk\cdot l}$ Si	$B^{o}1/2$
00·1	18.06	442	0.24
10·0	28.7	122	0.23
10·1	34.09	674	0.27
10·2	47.2	257	0.32
11·0	50.8	194	0.30
11·1	54 4	94	0.30

The Si unit of peak areas is (arbitrarily) determined by simultaneous measurement of the $28^{o}2$ to $28^{o}7$ total peak intensity of a standard sample of Si metal and assuming this to be 1 000 Si. The corresponding number of counts decreases slowly with time. For CH samples of other origin, the Y values can be generally smaller or larger by some per cents, depending on the crystal size and degree of crystallinity. Judging from the large and variable values of the peak widths (the normal value for well-crystallized substances with isometric crystals is $0^{o}10$ to $0^{o}12$) there are stacking faults of an unknown character in all types of CH crystals.

The peaks of pure cement gel are not so well defined. There is a rise in intensity extending from about 24^{o} to about 36^{o}, with a total intensity area of about 600 Si, and with a sharper peak at slightly above 29^{o}, and also

a rather sharp peak, not very high, at about 50°. There are no obvious differences in the appereances of these peaks in portland cement or pure silicate pastes, but possibly the intensity profile of the 29° peak is slightly more extended towards higher angles in the belite paste, as can be seen in FIG 1. The records in this figure are given by plates of C_3S or C_2S, preserved for about 15 years in lime solution, after which time most or all of the CH initially formed in the paste has migrated to the surface and formed a crystal layer which can be easily scraped off before XD examination.

Other C-S-H constituents resembling those present in cement pastes have been prepared by mixing cement with larger quantities of colloidal silica (aerosil) and shaking the mixture in suspension or ball-milling in a slurry, for times long enough to give complete hydration, and a C-S-H product free from CH (or nearly so). XD records from such preparations are shown in FIGs 2-3. The equivalent C/S ratios in these mixtures are 0.83 (as in tobermorite), 1.25 and 1.54 for the 61/39, 75/25, and 85/15 cement/silica mixes, respectively. The XD peaks given by the gel are in general similar to those given by old pastes of pure constituents, possibly with somewhat lower intensities for the 50° peak.

By counting squares in careful records from old C_3S and alite pastes, in the 28°0 to 31°0 and 49°0 to 51°4 ranges, deducting the overlapping CH reflexions and correcting to 100 per cent gel by applying a factor for CH content, obtained from the 34°1 CH reflexion, the following table for gel peak intensities has been obtained.

Small quantities of the anhydrous constituents in cement pastes, possibly still present after many years of hydration, can be best detected by the presence of the incompletely - resolved doublet at 32°2 and 32°6, with initial 100 per cent intensities of about 350 Si for alite, and 500 Si for belite. In belite pastes, weak indications of these peaks have occasionally

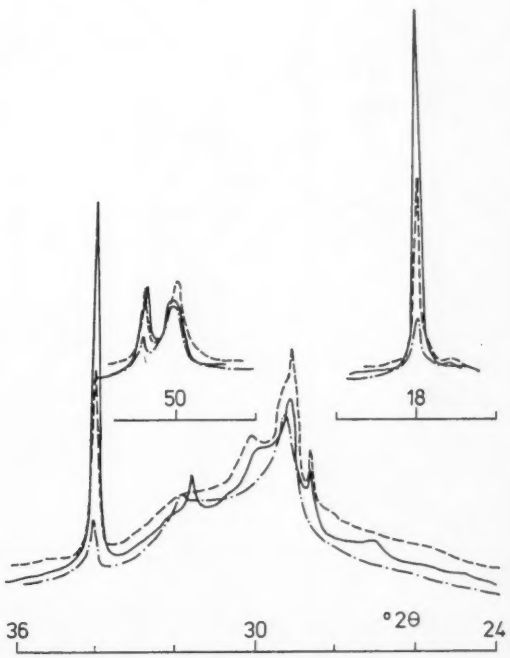

FIG 1 XD records of selected 2θ ranges for pastes, 15 years hydrated (CH partly removed), of C_3S 0.80 (——), C_3S 1.25 (– – –), and beta-C_2S 0.63 (—·—).

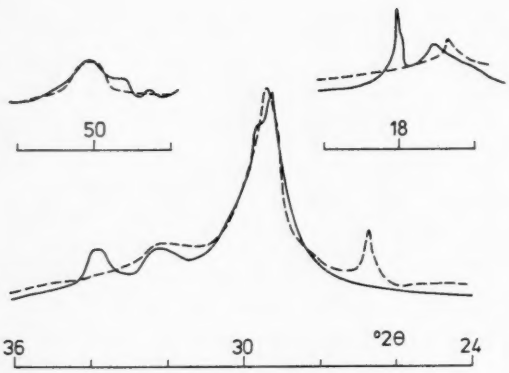

FIG 2 XD records of selected 2Θ ranges for 61/39 mixtures of cement/colloidal silica, hydrated by shaking in water suspension for 32 days (——) or in a ball-milled slurry for 27 days (– – –).

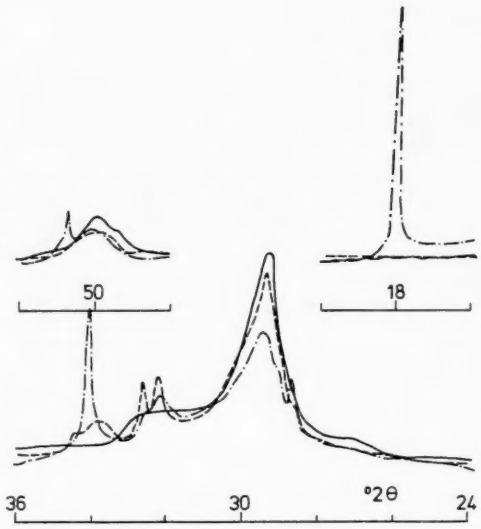

FIG 3 XD records of selected 2Θ ranges for mixtures of cement/colloidal silica, hydrated by ball-milling of 75/25 slurry for 15 days (——), or by paste-hydration for more than 3 months of 75/25 (– – –) and 85/15 (—·—).

been observed even after 15 years of hydration, and also ordinary pastes of the lowest w_o applied (0.32) contain a few per cent of unhydrated silicates even after long times.

A third hydration constituent is ettringite, $C_6A\bar{S}_3H_n$, which is known to very persistent in certain types of pastes, especially those low in alumi nate. THE XD pattern of ettringite contains a number of peaks (six) of about 200 Si intensity, the strongest being the $9^{o}08$ peak, 320 Si. This peak has been observed and accounted for in the data for the low-aluminate portland cement (Limhamn Standard) given below. Other ettringite peaks fall out-

TABLE 2

XD intensity areas for pure cement gels, more than 15 ys. old

Gel type	Y($28^{o}0$ to $31^{o}0$)Si	Y($49^{o}0$ to $51^{o}4$)Si	(CH)%
C_3S w_o 0.50	150	64	11.0
0.80	139	66	11.6
1.25	144	54	7.8
Alite w_o 0.50	145	63	2.0
1.25	146	51	0

side the ranges of CH and C-S-H gel peaks, and thus do not disturb the measurements of these.

Materials studied

The paste materials available for examination were white cement and standard portland cement pastes, of w_o in the series 0.32, 0.40, 0.50, 0.70, 1.00 and 1.32, with addition of w_{ae} = 0.05 (w_o-0.32), in order to prevent excessive separation. The clinker composition can be expected to be, for WhC (Aalborg): alite 85, belite 7, C_3A 8, Fss 0, and for PC (Limhamn): alite 65, belite 20, C_3A 3, Fss 12, + the usual addition of $C\bar{S}H_2$. The samples, in the form of 70 x Ø20 mm cylinders, were cured in water initially for some days, then wrapped tightly in moist plastic foil (to prevent too much CH crystals from forming on the surface), and cured moist in closed containers for more than 6 years.

Experimental procedures

The Ø20 cylinders were cut by a diamond saw in a number of plates, 3 mm thick. Three of these were used for counting of XD intensities (in order to get a reasonably-accurate average), and were therefore immersed in alcohol immediately after sawing, to prevent carbonation (traces of the strong (900 Si) CC - calcite peak at 29°40 can be very disturbing in the measurement of gel intensities). Three more plates were weighed moist and put in a heating cabinet at 65°C over saturated $MgCl_2$ solution (32% RH) in a desiccator. After a couple of weeks, they were again weighed, and the 65°C, 32% RH porosity was calculated as D(1). $\Delta W/W(1)$, assuming the density of the water removed to be 1.00 mg.mm^{-3}, and with D(1) determined beforehand by weighing and measuring the paste cylinders. The rest of the plates, six to twelve, were used for determining the concentric flexural strength B_c.

Solid-phase volumes

Porosity measurements were made only for the white cement pastes. The initial solid volume X_o can be calculated as $(1 + \rho w_o)^{-1}$, where ρ = average clinker density is assumed to be 3.1 mg.mm^{-3}. The final solid volume concentration is X = 1 - P, where P is the measured porosity. It turned out that the ratio of the final volume of the hydration products to the initial volume of the anhydrous cement, X/X_o, was about 1.6 for all the pastes, perhaps increasing slightly with w_o. A plot of the measured values X and D(1) can be drawn as a straight line, a shown in FIG 4.

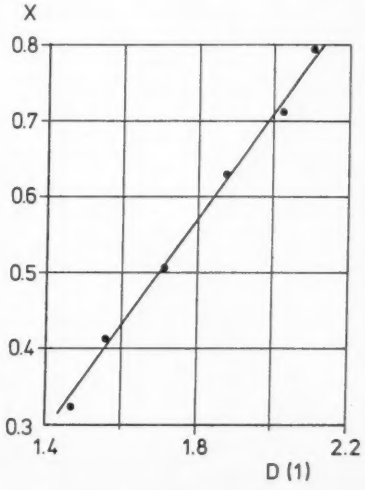

FIG 4 Relation between measured density D(1) and measured solid-phase concentration X (equilibrium at 65°C, 32% RH).

XD-data

The methods used for counting and evaluating XD intensities have been described previously (2). A few examples of XD traces recorded for the paste plates are shown in FIG 5. From these traces, suitable intervals were chosen, and total counts were measured for three plates per sample, as well as the associated background intensities. After deducting these, as well as possibly overlapping peaks, the reduced counts were transformed to Si units by comparison with the external Si standard, then further reduced to percentage values by dividing with the corresponding standard intensity values of the pure materials.

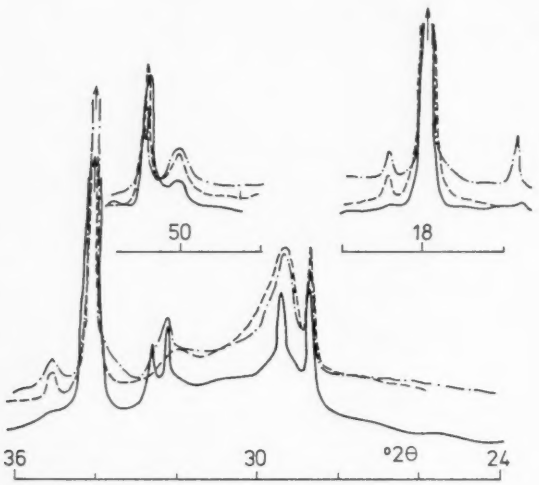

FIG 5 XD-records of selected 2θ ranges for pastes, 6 years hydrated, of white cement 0.32 (——) and 1.32 (– – –), and portland cement 1.32 (—·—).

The results are plotted in FIGs 6 and 7, as functions of X (for the white cement pastes) or X_0 (for the portland cement pastes).

Discussions of the cement paste phase composition

The expected phase composition of the cement pastes in hydration equilibrium would be about 30 to 35 per cent CH together with at C-S-H gel content above 60 per cent, with the CH content perhaps decreasing at the lowest w_0, depending on the presence of unhydrated material, and also falling off towards high w_0, where the influence of silica addition becomes noticeable. This level and shape of the CH content is also shown by the curve for the strongest reflexion 10·1, whereas the curve for the 10·2 reflexion comes out at a higher level, the curve for the 11·0 reflexion at a lower level, both, however, having the same shape as that of the 10·1 intensity. The reason for the variation in level is obscure, but has probably something to do with differences in crystallisation properties, the CH phase crystallising in cement paste being in general better crystallised (with sharper peaks) than the CH sample used as standard.

The apparent variation of the 00·1 (basal) reflexion is different. It is at an approximately correct level only at high X values, rising to a high maximum at w_0 1.00 and then decreasing at w_0 1.32. Such a variation can only be explained by the presence of an overlapping and nearly-coinciding peak from another substance of variable composition or crystallinity. It is

VOL 14 198

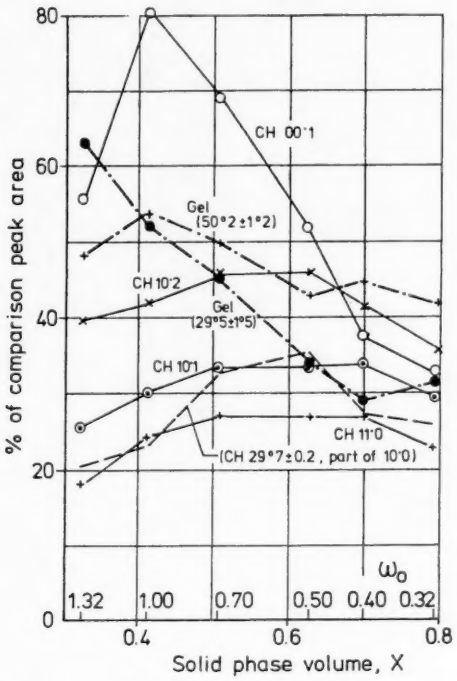

FIG 6 Contents of CH and gel in white cement pastes, from XD counts.

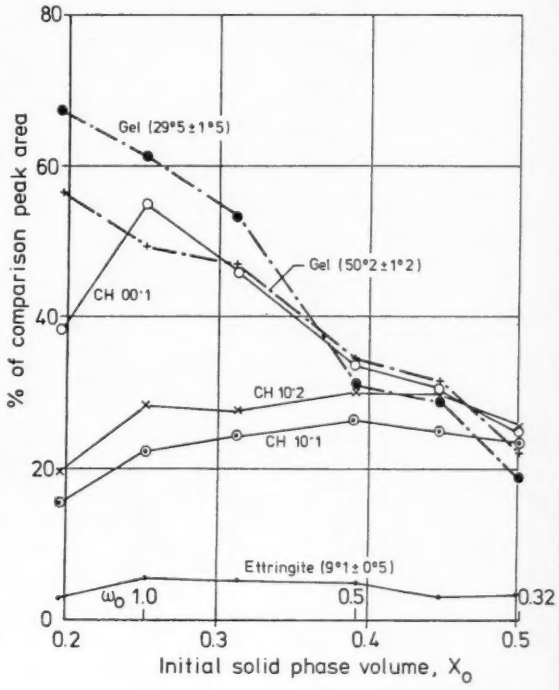

FIG 7 Contents of CH and gel in PC (Limhamn) pastes, from XD counts.

natural to assume that this additional intensity originates from a C-S-H gel constituent. However, it seems difficult to separate the relative contributions from CH and gel in this curve.

The gel contents calculated from the 29^0 and 50^0 intensity counts agree with the expected 60 per cent level only for the most porous pastes, and falls down to considerably lower values in the denser pastes, at least in the case of the more prominent 29^0 peaks. The values for the 50^0 peak are less certain, since their intensity areas mostly amount to less than 20 per cent of the areas actually counted. It is possible that the variation is associated with a gradual increase in crystallinity of the gel towards higher w_0 values. It is noticeable that a similar increase was not observed in the case of the standard substances (Table 2), nor was there any obvious contribution of gel intensity in the 00·1 peak given by the standard samples.

The white cement paste structures observed in SEM pictures may give some indication on the changes occurring with changing w_0 (FIG 8). The low porosity paste consists of irregular, structureless bodies of gel, mixed with stacks of CH plates. The high-porosity paste contains large quantities of extremely fibrous gel, and in addition some quantities of CH crystals (not shown).

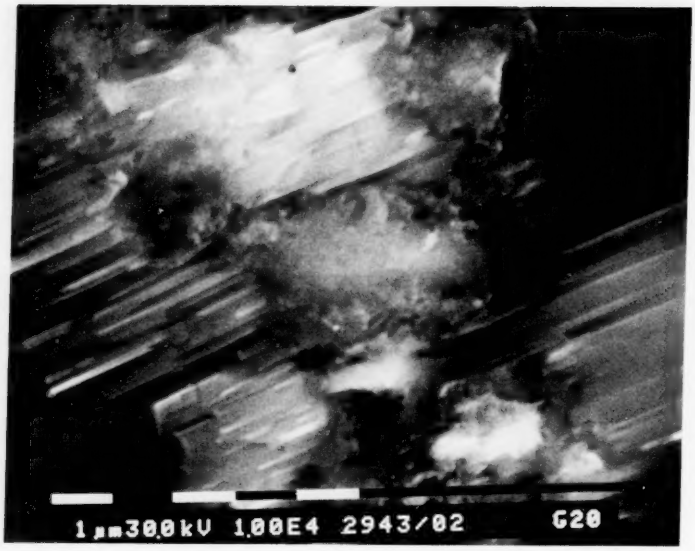

WhC ω_o 0.32 ~6 ys. 10 kX

VOL.
14
1984

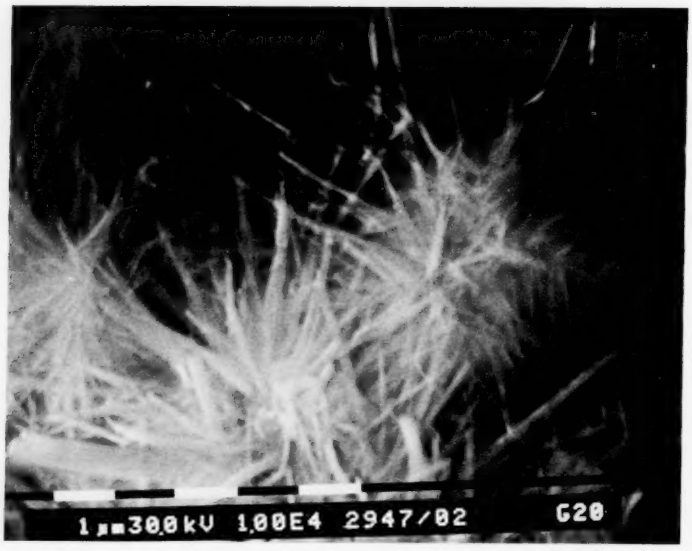

WhC ω_o 1.32 (ω_{ae} 0.05) ~6 ys. 10 kX

FIG 8 SEM micrographs of low-porosity and high-porosity white cement pastes.

Considerations on possible gel structures

In the report mentioned above (1), some suggestions were made on the accommodation of silica chain elements in the CH crystal structure. It was proposed that the general geometry of the orthohexagonal unit cell of CH could be maintained (FIG 9), even if half the Ca ions were replaced by Si (one or two per Ca replaced), with some type of silica chain running perpendicular to one set of 11·0 planes. It was also suggested that the gel peaks could be associated with a two-dimensional, face-centred cell of dimensions about 5.6x3.6 Å, as originally proposed by Taylor (3). However, it seems just as likely, that the cell dimensions associated with the gel peaks are truly one-dimensional, without any appreciable coordination in two-dimensional or three-dimensional crystal arrays. There is one repeat unit 4.9 Å of stacking of crystal planes or strips, incidentally coinciding with the 00·1 basal distance in the CH lattice, one repeat unit 3.05 Å (slightly contracted 10·0 - 3.11 Å distance in CH crystal) perpendicular to the silica chains, and one repeat unit 1.82 Å (slightly expanded 11·0 - 1.80 Å distance in CH crystal) in the direction of the silica chains.

One alternative for the suggested structure is shown in FIG 10, where a regular CH.CH layer is superimposed on a CH.SH-SH layer to an idealized structure of composition $C_{1.5}SH_n$. The structure of the silica complex (chain, dimer, monomer?) is only loosely indicated, and may vary within the layer, but the repeat units 4.9, 3.05, 1.82 Å(or multiples) are approximately constant. It is believed that the gel intensities observed may be explained in this way. The increases in gel peak intensities with increasing w_o would then be caused by an increasing degree of orderly arrangement of repeat units and cell contents. Further, the morphology would change from that of small, irregular flakes to that of long, thin needles.

OL.
14
984

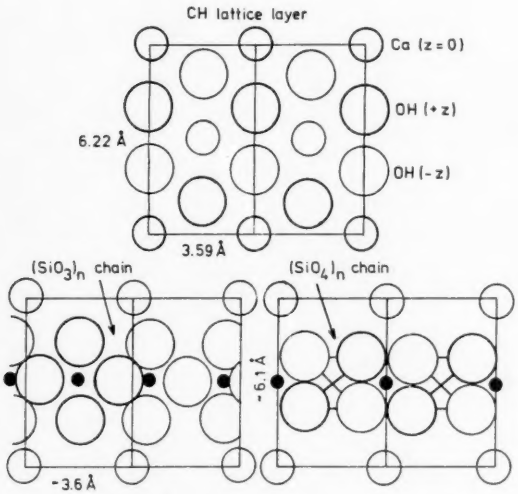

FIG 9 Structure of CH lattice layer, and of layers obtained by replacing $Ca(OH)_4$ rows by silica chain elements.

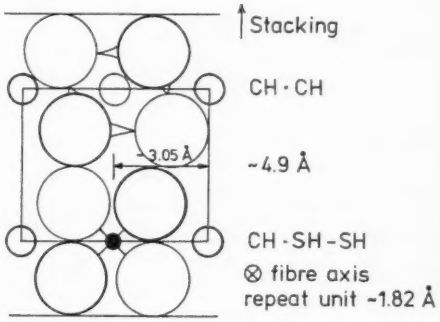

FIG 10 Hypothetical structure of gel (idealized), stacked layers of CH.CH and CH.SH-SH.

Strength tests

Although not really relevant in relation to the structures of cement hydration constituent, the flexural strength was determined simultaneously, for the sake of reference. The results turned out to be more interesting than anticipated.

The principle of measurement of B_c, concentric flexural strength, has been described previously (4), (5). Plates, 3 mm thick, are loaded to failure in bending between concentric rubber O-rings, 16.5 and 7.5 mm in diameter. The results are plotted against log X in FIG 11. The B_c strength increased rapidly with X up to about 20MPa for the PC 0.40 paste, and about 16 MPa for some of the WhC 0.40 plates, whereas others broke at a considerably lower level. The 0.32 plates were all disastrously weak, especially the PC 0.32 plates.

Inspection in a microscope revealed that the decrease in strength could be associated with the development of a system of very fine cracks running through the weakened plates, even in the saturated state. Decreases or irregularities of the tensile strength of pastes have been observed frequently in earlier studies (5), but not as radical as those shown in FIG 11. It is not known if compressive strength values are also influenced. The Vickers' hardness of the WhC pastes (H in FIG 11) does not show any sign of decrease.

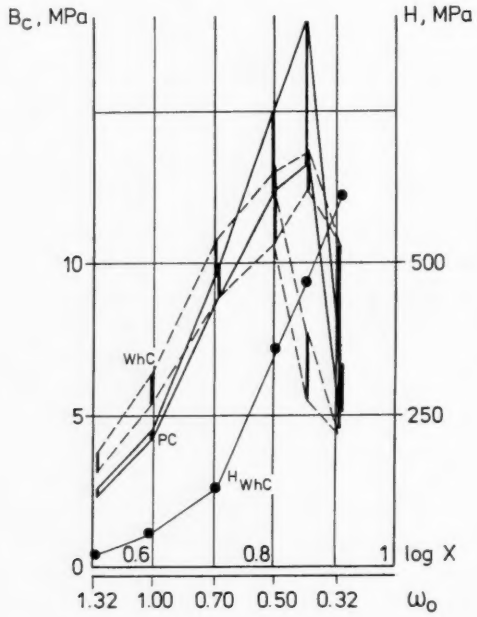

FIG 11 Flexural strength B_c and hardness H of the paste studied.

References

1. Grudemo, Å, "Nordic Concrete Research No. 1 (1982), 7.1-22."
2. Grudemo Å, "CBI Research 6:77, 1-101.
3. Taylor H F W, "J Chem Soc (London), 1950, 3682.
4. Grudemo Å, "CBI Research 8:79, 1-130.
5. Grudemo Å, "Cem Concr Res 9, 19 (1979).

CEMENT and CONCRETE RESEARCH. Vol. 14, pp. 133-141, 1984. Printed in the USA.
0008-8846/84 $3.00 + 00. Copyright (c) 1984 Pergamon Press, Ltd.

POSSIBILITIES OF QUANTITATIVE DETERMINATION OF THE AFt-(ETTRINGITE) AND AFm-(MONOSULPHATE) PHASES IN HYDRATED CEMENT PASTES

I. Odler and S. Abdul-Maula
Technical University Clausthal
3392 Clausthal-Zellerfeld
Federal Republic of Germany

(Refereed)
(Received March 23; in final form Nov. 21, 1983)

VOL. 14 1984

ABSTRACT

The possibilities to determine AFt-(ettringite) and AFm-(monosulphate) in hydrated cement pastes were studied by measuring the intensities of the pertinent DTA and XRD peaks on 4 synthetic AFt preparations, 5 synthetic AFm preparations and on a series of portland cement pastes of different composition and hydration time. For AFt determination the DTA method appears to be most suitable. AFm may be determined with any method at best semiquantitatively.

Introduction

The AFt-(ettringite) and AFm-(monosulphate) phases are regular constituents of hydrated portland cement pastes. The AFt phase is formed from the tricalcium aluminate and/or calcium aluminate ferrite phases of the clinker and calcium sulphate at the beginning of the hydration process and is instrumental in preventing the cement paste from quick setting. The formation of AFt is believed to be also responsible for expansion phenomena in most expansive cements and for crack formation in concrete structures made out of cements with excessive SO_3 contents or in those being in contact with ground waters containing large amounts of sulphates. The AFm phase is formed from AFt and additional tricalcium aluminate or calcium aluminate ferrite after depletion of free calcium sulphate in the system.

Very little has been published on the quantitative determination of the AFt- and AFm-phases in hydrated cements. Several investigators determined ettringite by differential thermal analysis (1,2,3) or by selective extraction (4,5). To our knowledge no method for quantitative determination of monosulphate in cement pastes has been published as yet. The present authors studied the possibility to determine the above phases by differential thermal analysis (DTA), by quantitative X-ray diffraction (QXRD) or by selective extraction. The obtained results are reported and discussed.

Experimental

Standard substances

The following standard substances were synthetized for further studies:

Ettringite-method I (Ettr.-I). A 1:3 molar blend of tricalcium aluminate ($3CaO.Al_2O_3$) and $CaSO_4.2H_2O$ was mixed with 50 wt % of water. The obtained paste was kept in a sealed plastic bag at room temperature for 40 days. The formed ettringite was ground with acetone, filtered and washed first with acetone and then ethyl ether and finally dryed at room temperature to a constant weight.

Ettringite-method II (Ettr.-II). A suspension of 0.02 mol $3CaO.Al_2O_3$ and 0.06 mol of $CaSO_4.2H_2O$ in 1 l H_2O was agitated for 72 hours at room temperature. The formed ettringite was isolated by filtering, washed on the filter with acetone and then with ethyl ether and finally dryed at room temperature to a constant weight.

Ettringite-method III (Ettr.-III). A suspension containing 0.02 mol of $Al_2(SO_4)_3.18H_2O$ and 0.12 mol $Ca(OH)_2$ in 1 l H_2O was agitated for 48 hours at room temperature. The formed ettringite was isolated in a similar way as employed in method Nr. II.

Ettringite-method IV (Ettr.-IV). The substance was prepared in a identical way as Ettr.-III however using an equimolar blend of $Al_2(SO_4)_3.18H_2O$ and $Fe_2(SO_4)_3.5H_2O$ rather than $Al_2(SO_4)_3.18H_2O$ alone. Thus the resultant AFt phase contained both Al^{+3} and Fe^{+3} ions in its crystalline lattice.

Monosulphate-method I (Mono.-I). A suspension of 0.02 mol $3CaO.Al_2O_3$ and 0.02 mol $CaSO_4.2H_2O$ in 1 l H_2O was agitated for 9 hours at room temperature. The reaction product that contained mainly monosulphate, beside small amounts of ettringite, was separated by filtering and washing on the filter first with acetone and then with ethyl ether. In order to remove ettringite the obtained material was suspended in a 3:1 ethylene glycol-methanol solution, agitated for 30 min., filtered, washed with methanol and ethyl ether.

Monosulphate-method II (Mono.-II). A suspension of 0.0033 mol Ettr.-II and 0.0066 mol $3CaO.Al_2O_3$ in 1 l H_2O was agitated for 2 days at room temperature. The reaction product was separated by filtering and washing on the filter with acetone and then with ethyl ether. The resulting material was suspended in a 3:1 ethylene glycol-methanol solution, agitated for 30 min., filtered, washed with methanol and ethyl ether and finally dried at room temperature.

Monosulphate-method III (Mono.-III). The product was synthetized in a similar way as Mono.-II, however using a suspension of 0.0033 mol Ettr.-II, 0.0033 mol tetracalcium aluminate ferrite ($4CaO.Al_2O_3.Fe_2O_3$) and 0.0066 mol $Ca(OH)_2$ in 1 l H_2O. The suspension was agitated for 7 days.

Monosulphate-method IV (Mono.-IV). The product was synthetized in a similar way as Mono.-II, however using Ettr.-IV rather than Ettr.-II as a starting material. The suspension was agitated for 3 days.

Monosulphate-method V (Mono-V). The product was synthetized in a similar way as Mono.-II, however using a suspension of 0.0033 mol Ettr.-IV, 0.0033 mol $4CaO.Al_2O_3.Fe_2O_3$ and 0.0066 mol $Ca(OH)_2$ in 1 l H_2O. The suspension was agitated for 5 days.

By the above procedures AFt and AFm phases free of any contaminants (as determined by XRD) were obtained. The theoretical oxidic composition of ettringite and monosulphate as well as that of the obtained products is shown in Table I.

VOL 14 198

Table I

Oxidic Composition (in wt %) of the Standard Substances Used

	CaO	Al_2O_3	Fe_2O_3	SO_3	H_2O
$6CaO.Al_2O_3.3SO_3.32H_2O$	26,82	8,13	-	19,14	45,91
Ettr.-I	26,9	8,2	-	19,2	45,6
Ettr.-II	27,0	8,1	-	19,3	45,5
Ettr.-III	26,7	8,4	-	19,6	45,2
Ettr.-IV	26,5	4,5	6,3	19,0	43,6
$4CaO.Al_2O_3.SO_3.12H_2O$	36,5	16,38	-	12,86	34,71
Mono.-I	36,6	16,3	-	12,2	34,9
Mono.-II	36,1	16,2	-	13,0	34,6
Mono.-III	31,0	10,0	10,2	11,2	37,7
Mono.-IV	35,0	14,3	6,2	9,0	35,5
Mono.-V	30,9	8,0	17,2	8,1	35,7

VOL. 14 1984

Determination of AFt by differential thermal analysis and X-ray diffraction

The DTA studies were performed using a Mettler-model 2000 apparatus (10°C/min, N_2).

Fig. 1 shows DTA curves of pure ettringite, monosulphate and of a portland cement paste (C_3A in cement = 9.7%) hydrated for different periods of time at room temperature. It can be seen that neither the gypsum nor the monosulphate peaks interfere with that of ettringite. On the other hand the determination of the exact area of the AFt peak in the cement paste becomes gradually more and more difficult as the hydration progresses due to the development of a broad endothermic area belonging to the CSH phase formed in the hydration of tricalcium and dicalcium silicate present in the cement.

Table II shows the intensities of the DTA peaks belonging to the four standard AFt preparations synthetized (average value of 5 measurements). It appears that the intensity of this peak is independent of the method of synthesis or on whether Al^{3+} ions in the crystalline lattice are partially substituted by Fe^{3+}. Table II also shows the intensities of AFt peaks determined in a series of portland cement pastes prepared out of laboratory-made cements of different clinker composition (all cements ground to 3000 ± 100 cm^2/g (Blaine) and containing 3.0% SO_3 as gypsum) and hydrated for various times at room temperature. All data in the table refer to identical amounts of sample and identical sensitivity of the DTA apparatus.

For determination of AFt in hydrated cement pastes by XRD the peaks d=9.73A and d=5.61A may be considered. Both peaks are relatively strong and do not coincide with peaks of other phases that may constitute the original nonhydrated cement or the hydration products. Table II shows the intensities of these two peaks as determined in the four synthetic AFt preparations and portland cement pastes. The measurements were performed using the step by step diffraction tracing technique (CuKα, 28 kV, 0.32 Amp., rotating sample holder, steps of

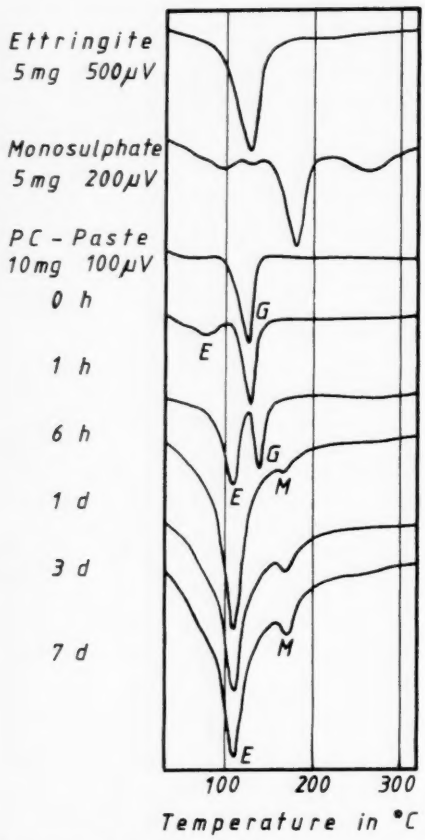

FIG. 1

DTA curves of pure ettringite monosulphate and of portland cement pastes hydrated for various times at room temperature (10°C/min., N_2).

2θ=0.02°, measuring time 40 sec/step). It appears that the intensities of these peaks were different in different AFt preparations and depended on the composition and the way of synthesis of the particular material. On the other hand, the mutual ratio of the intensities of the two main ettringite peaks - unlike their absolute intensities - remained constant in the different preparations studied. Due to the variations of the intensities of the XRD peaks, the ratio of the intensity of the XRD and DTA peak varied in different standard AFt preparations as well.

Expectedly the intensities of both the DTA and XRD peaks increased in the cement pastes studied with increasing content of the tricalcium aluminate phase and increasing hydration time. The ratio of the intensities of the XRD and DTA peaks was constant in different cement pastes and independent on hydration time, however decreased with increasing tricalcium aluminate and decreasing calcium aluminate ferrite content in the original cement. The ratio of the intensities of the two XRD peaks was constant in all cement pastes regardless of the kind of cement and time of hydration, however different from similar ratios found in the four standard ettringite preparations.

Determination of AFt by selective dissolution

According to (4) ettringite in hydrated cement pastes can be determined by dissolving it selectively in a 1:3 ethylene glycol-methanol solution and by calculating the amount of ettringite present on the basis of the amount of Al_2O_3 found in the solution.

Table III shows the solubility in the above solvent of a variety of phases that may be present in hydrated cement pastes (200 mg of substance in 300 ml solvent, stirring for 30 minutes at room temperature). The solvent dissolved ettringite almost quantitatively while the solubilities of other phases containing Al_2O_3, including AFm, were very low. Thus the solvent appears suitable to separate AFt from these phases with a fairly high selectivity.

Determination of AFm

Table IV shows the intensities of the DTA and XRD (d=8.92A) peaks found in the five standard AFm preparations (average values of 5 measurements). All data in the tables II and IV refer to the same amount of sample. It appears that the

Table II

Intensities or DTA and XRD Peaks (in Arbitrary Units) Determined in Standard AFt Preparations and in Portland Cement Pastes

Material		DTA	XRD_1 d=9.73A	XRD_2 d=5.61A	$\frac{XRD_1}{DTA}$	$\frac{XRD_1}{XRD_2}$
Ettr.-I		6790 ±195	3309 ±134	2280 ±127	0,487	1,45
Ettr.-II		6890 ±341	5907 ±121	3995 ± 99	0,857	1,48
Ettr.-III		6970 ±280	3633 ±234	2540 ±172	0,521	1,43
Ettr.-IV		7000 ±497	2469 ± 59	1665 ± 52	0,353	1,48
PC	1 h	-	-	-	-	-
C_3A=2,8% C_4AF=15,9%	3 h	58±3	38±9	-	0,655	-
SO_3=3 %	6 h	79±5	52±6	-	0,658	-
	12 h	-	70±6	33±3	-	2,12
	1 d	-	206±5	103±3	-	2,00
	3 d	-	240±6	115±5	-	2,09
PC	1 h	70±4	44±9	-	0,629	-
C_3A=7,2% C_4AF=11,9%	3 h	99±6	63±8	-	0,639	-
	6 h	123±5	76±3	-	0,618	-
SO_3=3 %	12 h	-	110±5	54±3	-	2,04
	1 d	-	218±7	112±5	-	1,95
	3 d	-	232±9	111±6	-	2,09
PC	1 h	78±5	46± 9	-	0,590	-
C_3A=9,7% C_4AF=8,4%	3 h	101±2	57± 8	-	0,564	-
SO_3=3 %	6 h	160±4	90±10	-	0,563	-
	12 h	-	168± 7	80±4	-	2,10
	1 d	-	249± 9	124±6	-	2,01
	3 d	-	187± 7	93±6	-	2,01
PC	1 h	131±9	65± 6	-	0,496	-
C_3A=15,9% C_4AF=3,1%	3 h	216±6	114± 7	-	0,528	-
SO_3= 3 %	12 h	-	203± 9	102±7	-	1,99
	1 d	-	89± 4	45±2	-	1,98
	3 d	-	72± 3	35±3	-	2,06
PC	1 h	346±10	156±18	-	0,451	-
C_3A=18,7% C_4AF=0%	6 h	-	227± 6	117±5	-	1,94
SO_3= 3 %	12 h	-	248± 9	130±8	-	1,91
	1 d	-	269±12	122±6	-	2,20
	3 d	-	299± 8	143±4	-	2,09

Table III
Solubilities of Different Phases in a 3:1 Ethylene Glycol-Methanol Solution

Substance	Solubility (%)
$3CaO.SiO_2$	1,6
β-$2CaO.SiO_2$	1,1
$3CaO.Al_2O_3$	3,4
$4CaO.Al_2O_3.Fe_2O_3$	0,3
$CaSO_4$	0,8
$CaSO_4.2H_2O$	69,6
$Ca(OH)_2$	68,4
$3CaO.SiO_2$ hydrat. 1 year	6,3
β-$2CaO.SiO_2$ hydrat. 1 year	2,0
$3CaO.Al_2O_3$ hydrat.	2,8
$4CaO.Al_2O_3.Fe_2O_3$ hydrat.	0,1
p-clinker hydrat. 12 h	1,2
AFt-I	97,1
AFt-II	98,4
AFt-III	97,8
AFt-IV	93,6
AFm-I	8,1
AFm-II	7,6
AFm-III	6,2
AFm-IV	6,9
AFm-V	5,1

Table IV
Intensities of the DTA and XRD Peaks (in Arbitrary Units) Determined in Standard AFm Preparations

Preparation	DTA	XRD
Mono.-I	1995 ± 182	24166 ± 2042
Mono.-II	1878 ± 125	25080 ± 2741
Mono.-III	967 ± 45	18800 ± 1033
Mono.-IV	1364 ± 130	15853 ± 1000
Mono.-V	968 ± 28	22626 ± 1038

VOL. 14 1984

intensities of DTA peaks belonging to different AFm preparation - unlike those belonging to different AFt preparations - varied in a wide range. Moreover, the intensities of the peaks belonging to AFm were significantly lower than those of AFt.

The intensities of the XRD peaks belonging to AFm were also different in different preparations, however these variations were by far less significant than those of the DTA peaks. The absolute intensities of the XRD peak belonging to AFm were significantly stronger than those of the AFt peaks.

Discussion

In the determination of AFt and AFm one has to keep in mind that both the oxidic composition and crystallinity of these phases, as they are present in hydrated cement pastes, may vary in a wide range. Thus, to obtain meaningful results the method employed for determining these phases must be unsensitive to such variations.

The DTA peak produced by AFt appears to be sharp and intensive enough to be used for quantitative measurements at least in pastes with low degrees of hydration and thus low contents of CSH-phase. For accurate quantitative determination of this phase on the basis of measuring the area of this peak, it is important to know whether and to what an extent the inetnsity of this peak is influenced by variations in oxidic composition and crystallinity of the Aft phase. The fact that synthetic AFt preparations of different composition and formed under very different experimental conditions produced consistently DTA peaks of identical intensities suggests a very low sensitivity of the DTA method to variations of this kind. Consequently this method seems to be well suitable for determining AFt in hydrated cement pastes especially at low degrees of hydration.

To obtain meaningful results by the DTA method a procedure gentle enough to preserve the entire fraction of bound water in the crystalline lattice of AFt has to be employed for stopping the hydration of the paste. In preliminary experiments using synthetic AFt and AFm preparations, it was proved that the "acetone-ethyl ether method" meets this requirement for both compounds. As the DTA method is highly unsensitive to variations of composition and crystallinity of AFt no special requirements are set as to the selection of the AFt preparation to be used as reference substance in quantitative determination of AFt in hydrated cement pastes.

In pastes with higher degrees of hydration the accuracy of AFt determination by DTA may be significantly impeded by the presence of the endothermic effect belonging to the CSH-phase. This difficulty may be overcomed to a great extent by placing a prehydrated, gypsum free cement, rather than an indifferent material into the reference sample holder of the DTA apparatus (Fig. 2).

Unlike the DTA peak, the intensity of the XRD peaks belonging to AFt is to a great extent sensitive to variation of oxidic composition and crystallinity of this material. Moreover, the fact that the ratio of the two main peaks belonging to AFt is different in cement pastes and synthetic preparations suggest that the structure of ettringite as formed in cement hydration is not identical with that present in ettringite preparations obtained artifically. Consequently, the selection of a proper reference substance, necessary for quantitative determination of AFt in cement pastes may cause insurmountable difficulties. In studies in which the XRD method is employed just for measuring the formation and decomposition of AFt in the course of hydration of a single cement, this difficulty may be overcomed to a certain degree by determining the absolute AFt content in a sample with low degree of hydration by DTA and by using the obtained values as a reference.

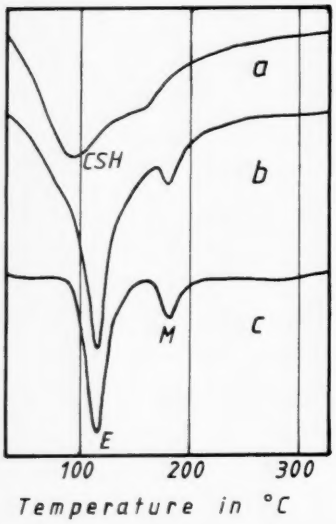

FIG. 2

a) of a ground portland clinker with no gypsum added, hydrated for 3 days
b) of portland cement made from the same clinker with 3% SO_3 (as gypsum) added
c) of the paste (b) using paste (a) as reference material

In the study of the extraction method the data of (4,5) according to which AFt is the only Al_2O_3-containing cement phases dissolvable in the ethylene glycol-methanol solvent, were confirmed. Nevertheless data on the AFt content in hydrated cement pastes obtained by this method must be taken with great caution due to the possible variations in the composition of this phase. In cement containing both Al_2O_3 and Fe_2O_3 more meaningful values may be obtained if the AFt content is calculated on the basis of the amount of dissolved Al_2O_3 + Fe_2O_3 rather than of Al_2O_3 alone.

The differences in the intensities of the DTA peaks found in different AFm preparations indicate - contrary to AFt - a great sensitivity of this method to composition and/or cyrstallinity variations of this phase. Moreover the thermoeffect due to AFm decomposition is significantly weaker than that of AFt and barely measurable in most cement pastes. For both reasons this method appears little suitable for quantitative determination of AFm in hydrated cements.

The intensity of the XRD peak at d=8.92A appears to be also dependent on composition and/or crystallinity variations of the particular material, however, in a much lesser extent. Moreover, the great intensity of this peak enables to detect even small amounts of AFm (down to about 1%) in hydrated cement pastes. For both reasons the XRD method appears to be suitable for at least semi-quantitative determination of the AFm phase in hydrated cements.

Conclusions

1. For quantitative determination of AFt in hydrated cement pastes, the DTA method appears to be the method of choice as the thermoeffect generated by AFt decomposition is highly unsensitive to variations of crystallinity and composition of this phase. The pertinent DTA peak does not coincide with those of gypsum and monosulphate however may be superposed by the thermoeffect caused by decomposition of the CSH phase.

2. The quantitative determination of AFt by X-ray diffraction is hampered by the fact that the intensity of the peaks suitable for quantitative measurements is sensitive to crystallinity and/or composition variations of this phase.

3. Out of different Al_2O_3 bearing phases AFt is dissolved with high selectivity in a 1:3 ethylene glycol-methanol solvent. Nevertheless, the determination of AFt on the basis of the amount of Al_2O_3 dissolved in this solvent may lead to erroneous results due to possible variations in the composition of the AFt phase.

4. For determination of AFm the XRD method appears to be more suitable

VOL 14 198

than DTA due to the lower sensitivity of the former method to composition and/or crystallinity variation of the AFt phase.

Acknowledgements

The financial support of this work by the Deutsche Forschungsgemeinschaft is gratefully acknowledged.

References

1. H.G. Migley and D. Rosama: Proc. 4th Internat. Symp. on the Chemistry of Cement, Washington, 181-217 (1968).
2. J. Millet, A. Bernard, R. Hommey and A. Poindefert: Bull. Liason Labo. P. et. Ch. 109, 91-96 (1980) (in French).
3. J. Millet, A. Bernard, R. Hommey and A. Poindefert: Analysis 9 (7), 311-317 (1981) (in French).
4. H. Raudoja and E. Djama: Issled. Stroit. No. 10, p. 37 (1969) (in Russian).
5. H. Uchikawa and S. Uchida: Cem. Concr. Res. 4, 821-834 (1974).

VOL.
14
1984

CEMENT and CONCRETE RESEARCH. Vol. 14, pp. 142-144, 1984. Printed in the USA.
0008-8846/84 $3.00 + 00. Copyright (c) 1984 Pergamon Press, Ltd.

NOTE

DEGREE OF DEPOLARISATION, AN INDICATOR FOR WATER BONDING IN HYDRATED CEMENT PASTES

Z. A. Juhász
University of Veszprém, Dept. of Silicate Chemistry, H-8201 Veszprém, POB 158, Hungary

(Communicated by F.D. Tamás)
(Received May 24, 1983)

ABSTRACT

Permittivity (dielectric constant), weight loss and shrinkage of hydrated cement pastes was measured after firing the samples up to 1000°C. The degree of depolarisation (DD) can be calculated from measured data. DD can be used as an indicator of water bonding in the cement paste.

A method has been developed for the determination of the bond form of water being fixed in hardened cement paste. The method is based on the measurement of permittivity (dielectric constant) of the paste having been heated to higher (up to 1000°C) temperatures prior to permittivity measurement.

A paste was made of the cement by mixing it with water, in the usual way. A plastic die was filled with the paste giving 5 mm high cement disks with 70 mm dia. After hardening and ignition at temperatures increasing by approximately 50°C steps, the permittivities of disk samples were measured at 25°C.

At the same time ignition losses /Δm/, bulk densitiy /ρ_T/, and density /ρ/ of powdered samples were also tested.

The analysis of experimental data has been made by the following train of thought:

It is presumable that permittivity changes after igniting samples at moderate temperatures /up to 400°C/ are caused mostly by the removal of water, having high dipole moment. /Obviously the change of dielectric properties may be caused by some other secondary changes of crystal structure following the removal of water, but for the time being these can be neglected/.

If the water were in simple mechanical mixture with the remaining silicate structure, the theoretical permittivity of the mixture would be given by the volume fraction of the two components /water and silicate frame/:

$$\varepsilon_{theor} = v_S \varepsilon_S + v_W \varepsilon_W$$

where v_S and v_W are the volume fractions of ignitition residue and leaving water, respectively /$v_S + v_W = 1$/, and ε_S and ε_W are the permittivity values of the same components. /ε_S is an experimentally measured value, and ε_W is the known permittivity of water at the temperature of experiment/.

However in reality it is erroneous to suppose the additivity because the apparent permittivity /ε/ of the hydrated cement is always smaller than the calculated value. This comes from the fact that the water was present as a more or less strongly bonded "gel water" rather than in the form "free water".

A value characterizing the strength of interaction could be calculated from this difference:

$$\Delta\varepsilon^{o} = \frac{\varepsilon_{theor} - \varepsilon}{\varepsilon_{theor}}$$

$\Delta\varepsilon^{o}$ can be considered as the "degree of depolarization" of silicate frame with respect to the water, since its value is determined first of all by the extent of decrease of directional polarization of the "free water". This decrease is caused by the /real/ bonding of water to the silicate frame.

VOL.
14
984

It should be noted that it is worthwhile to complement the experiment by measuring the linear shrinkage /Δ1/ during the calcination and by calculating the actual compactness from the sample size and density:

$$v_s = \frac{\rho_t}{\rho}$$

These latter, easily obtainable data can contribute to the interpretation of experimental results of permittivity.

An example shows the application of the method. ASTM type II. Hungarian-made portland cement was mixed with deionised water (w/c = 0.32) to make a paste. The paste was hardened in a water vapor saturated space for 28 days, after which interval hydration was stopped, desiccated for 24 hr., heated to various temperatures (up to 1000°C, in 50 C°steps), and apparent permittivity (ε), ignition loss (Δm) and linear shrinkage (Δ1) determined. Results are plotted in Fig. 1. as the mean of three parallel sets of experiments. (The relative error of the measurement is $\pm$ 6%).

The hardened cement paste is partly carbonated, therefore the ignition loss at high temperature is composed from H_2O and CO_2. However this fact has been disregarded. $\Delta\varepsilon^{o}$ and v_S values are shown on Figure 2, together with the v_S versus Δ1 relationship.

It is seen from the presented example that the increasing bon-

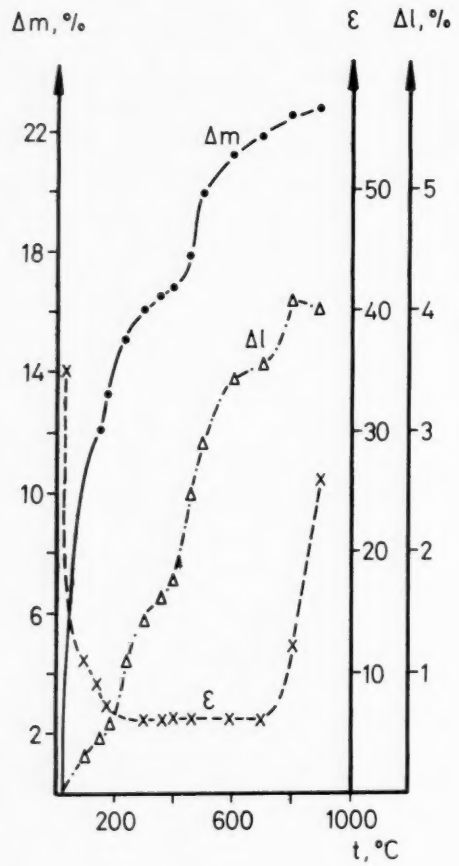

FIG. 1.

Δ m, Δl and ε values of portland cement past, in function of ignition temperature

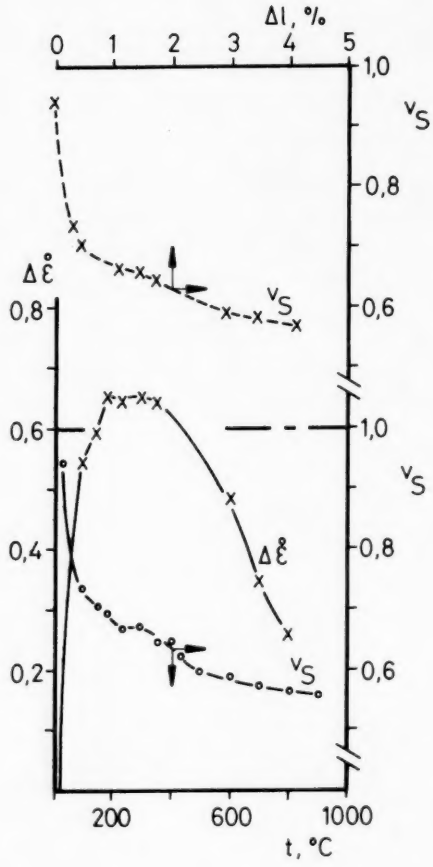

FIG. 2.

$\Delta\varepsilon^{\circ}$ and v_S vs. temperature and Δl vs. v_S plots

ding strength of water remained in the gel structure after increasing ignition temperature can be detected by the help of $\Delta\varepsilon^{\circ}$. Up to about 250°C, the change of $\Delta\varepsilon^{\circ}$ is nearly parallel with the ignition loss change.

A loosened, incompacted frame structure is left over by the removal of water between 25°C and 250°C, which is not followed by a strong shrinkage of the body /v_S versus Δl curve/.

Sudden changes of slopes and of curve shape and tendency are partly due to the changes in bonding form of water, or to internal morphological changes.

VOL. 14 1984

CEMENT and CONCRETE RESEARCH. Vol. 14, p. 145, 1984. Printed in the USA.
0008-8846/84 $3.00+00. Copyright (c) 1984 Pergamon Press, Ltd.

DISCUSSIONS

DISCUSSION OF THE PAPER "ON THE GLASS PRESENT IN LOW-CALCIUM AND IN HIGH-CALCIUM FLY ASHES" BY S.DIAMOND*

G. M. Idorn
G. M. Idorn Consult ApS
Tovesvej 14B, 2850 Naerum, DK

OL.
14
984

Professor Diamond's procurement of analytical data on the compositions and constitutions of fly ashes in the US is hopefully going to be widely appreciated.

The paper confirms, supplementary to previous studies that fly ashes are not as simple to characterize in generally valid terms as would be desirable for standard specification committees. The work of these might be facilitated by the creation of a system for fly ash characterisation. Even if a data file at present could only be introductory (maybe more than two types of glass in fly ashes will be identified - like more than two subspecies of C-S-H morphology in cement paste has appeared), it could be helpful for the evaluation of fly ash types.

The author's suspicion that a calcium aluminate glass in fly ash is more reactive than a siliceous structural glass is interesting and raises another issue of fly ash characterisation: "reactive to what and how?"

Those who work with fly ash the engineering ways need to have characterized the reactivity of the cement paste or mortar towards the fly ash species as well as "a specific" fly ash reactivity: And while some types of ash may be the best for autoclaved processing, other ones may be preferable for concreting of thin pavement slabs in cold weather, in dependence, for instance, of the alkali content of the concrete, the fineness of the cement or the simultaneous use of some chemical admixture or other.

The question to the author is: isn't it likely or at least possible that a variety of fly ash "subspecies" when adequately characterized, may become the basis for a variety of combinations with cements, other admixtures and processing technologies, with different, desirable product qualities as interesting downstream business opportunities?

*CCR 13, 459 (1983).

CEMENT and CONCRETE RESEARCH. Vol. 14, p. 146, 1984. Printed in the USA.
0008-8846/84 $3.00+00. Copyright (c) 1984 Pergamon Press, Ltd.

REPLY TO G.M.IDORN'S DISCUSSION OF THE PAPER "ON THE GLASS PRESENT IN LOW-CALCIUM AND IN HIGH-CALCIUM FLY ASHES"*

Sidney Diamond
School of Civil Engineering, Purdue University
West Lafayette, IN 47907, USA

I thank Dr. Idorn for his interesting comments.

At least certain synthetic calcium aluminate glasses, when finely divided, react rapidly with water and constitute an exceedingly self-hydraulic material; indeed the reaction may be so rapid that mixing with water cannot be completed before extensive heat evolution and hydration have taken place. Of course such glasses are not identical with the postulated calcium aluminate glasses in high-calcium flyashes, since the latter invariably contain significant amounts of silica, iron oxide, and other chemical components. Nevertheless, indications exist that they react in hydrated cement systems significantly more rapidly than the siliceous glasses found in low-calcium flyashes.

The possibility that different flyashes could usefully fall into different "subspecies" or "characterization groups" suitable for different specific end uses certainly exists. However, the economic realities underlying the utilization of flyash must always be kept in mind. As a low value, high bulk, commodity-type material, flyash can be economically transported only limited distances. Thus concrete or concrete product producers in a given area may only a few possible flyashes to choose from, or even only a single one.

Even when this is not the case, economic characterization groups may be hard to maintain. For example, flyash normally suitable for a specific end use may become unsuitable because a change in power plant boiler operation has caused a color change that renders the flyash unsuitable for the specific use.

Factors such as this may limit the practical applicability of flyash characterization groups; nevertheless, I do believe the idea is worth pursuing, and may indeed lead to "downstream business opportunities".

*CCR 13, 459 (1983).

VOL. 14 1984

CEMENT and CONCRETE RESEARCH. Vol. 14, pp. 147-148, 1984. Printed in the USA.
0008-8846/84 $3.00+00. Copyright (c) 1984 Pergamon Press, Ltd.

A DISCUSSION OF THE PAPER "MECHANISM OF SULFATE ATTACK ON PORTLAND CEMENT AND CONCRETE - ANOTHER LOOK" BY P.K. MEHTA*

by I. Odler
Technical University Clausthal
3392 Clausthal-Zellerfeld
Fed. Republic of Germany

The lack of a direct correlation between expansion and ettringite formation in sulfate attack, reported by Dr. Mehta, is in line with observations made in our laboratory. On portland cements containing elevated amounts of gypsum, expansion was observed both before and after the amount of ettringite present in the hydrating paste reached its maximum and an ettringite to monosulfate conversion got under way. Conversely in high iron cements no sulfate related expansion took place inspite of a significant ettringite formation in the hydration process. In the light of these and similar observations the classical theory, according to which the expansion in sulfate attack is directly related to ettringite formation, appears to be too simplistic. Thus, new theories to explain this phenomen must be welcomed, but also submitted to a critical scrutiny.

In his paper, Dr. Mehta forwarded a new theory to explain the mechanism of sulfate attack: According to it a precipitation of gypsum and a loss of strength and stiffness of the CSH-phase, due to an increased SO_4^{-2}- and decreased OH-ion concentration in the pore solution, are essential steps in the development of an expansion in the course of sulfate attack. According to the theory, only under the latter conditions ettringite crystals, which were formed earlier, become expansive and the cement paste expands and deteriorates.

If Dr. Mehta's theory were correct, a presence of gypsum and an absence of crystalline calcium hydroxide would have to be persistent findings in cement pastes destroyed by sulfate attack, which is not the case. It has to be also noted, that a simultaneous calcium sulfate precipitation and decrease of hydroxyl ion concentration, as postulated by the theory, may not occur in cement pastes, unless they are exposed to sulfuric acid solutions. In pastes exposed to calcium sulfate solutions no change of the pH-value takes place upon gypsum crystallization, while in those exposed to alkali metal sulfate solutions an eventual precipitation of gypsum is accompanied even with an increase of the hydroxyl ion concentration in the pore liquid (due to a simultaneous formation of alkali metal hydroxide).

* CCR 13, 401 (1983).

The assumed loss of adhesive ability of the CSH-phase and its central role in the development of expansion due to sulfates may be also questioned: In experiments on tricalcium silicate pastes an addition of calcium sulfate only resulted in strength losses of no more than 20 per cent, if any at all(1). If one assumes a similar effect of calcium sulfate on the CSH-phase of cement pastes it appears unlikely that strength changes of this order of magnitude would play a significant role in the development of sulfatic expansion.

In the light of existing experimental data "sulfate attack" appears to be a very complex phenomenon which, in our oppinion, probably cannot be interpreted by a single theory. Nevertheless, efforts to obtain a better understanding of this problem have to continue.

References

1. A. Bentur, J. Am. Ceram. Soc. 59, 210-213 (1967)

VOL
14
198

CEMENT and CONCRETE RESEARCH. Vol. 14, pp. 149-150, 1984. Printed in the USA.
0008-8846/84 $3.00+00. Copyright (c) 1984 Pergamon Press, Ltd.

A REPLY TO THE DISCUSSION OF "MECHANISM OF SULFATE ATTACK ON PORTLAND CEMENT CONCRETE - ANOTHER LOOK" BY I. ODLER

by P. K. Mehta
Department of Civil Engineering
University of California, Berkeley, CA 94720

The author appreciates the thoughtful comments of Professor Odler on the complex questions pertaining to mechanism of sulfate attack on portland cement concrete. It was not the intent of the author to propose a definite or comprehensive theory, but to draw the attention of researchers to certain experimental observations which make the current theories questionable, and to provide an opportunity for the advancement of new ideas. On further scrutiny some of these ideas may not prove to be sound, however they would have served their purpose if they help us arrive at a better understanding of the phenomenon.

Professor Odler agrees with the author that the expansions associated with the sulfate attack are not directly related to ettringite formation. However, he does not think that the loss of strength and stiffness due to gypsum formation plays an important role in sulfate-related expansions. The author would like to reiterate that the precipitation of gypsum and its presence in the deteriorated cement paste is not central to the proposed theory; it is only a symptom of the environment which has become supersaturated with respect to sulfate ions. It is speculated that the adhesive strength and stability of cement pastes, which derive their cementing property mainly from C-S-H, would be reduced when the hydroxyl ion concentration of the pure solution drops with simultaneous increase of the sulfate ion concentration. Thus, the presence of gypsum and depletion of calcium hydroxide need not be directly associated with the sulfate-related expansions. These are only indicative of the environmental change where the attractive forces normally present at the surface of C-S-H and ettringite particles would no longer be operative.

For precipitation of gypsum the presence of sulfuric acid, as suggested by Professor Odler, is not necessary. Alkali metal hydroxide formed as a result of attack by alkali sulfate solutions are known to gradually leach away from the pores, which then become saturated with the permeating sulfate solution. Not only this is observed from long-time laboratory tests but also from field tests. For instance, X-ray mineralogical examination of the specimens of deteriorated concrete from the Fort Peck dam in Montana, which had prolonged exposure to a natural water containing alkali sulfates, showed both gypsum

*CCR 13, 401 (1983).

and ettringite present.†

In regard to the specific value of the strength loss on sulfate attack, the author and his co-workers (6)* reported 40% loss of compressive strength in 90-day old alite pastes which contained 6% gypsum. It is possible that in the presence of sulfate ions the decrease in the stiffness of C-S-H, which would have a direct influence on the magnitude of expansion, is even greater.

---

†P. K. Mehta, "Discussion of the paper authored by T. J. Reading on Combating Sulfate Attack in Corps of Engineers Concrete Construction," J. Amer. Concr. Inst., V.73, No.4, pp. 237-238 (1976).

*CCR 13, 401-406 (1983).

VOL
14
198

CEMENT and CONCRETE RESEARCH. Vol. 14, pp. 151-152, 1984. Printed in the USA.
0008-8846/84 $3.00+0. Copyright (c) 1984 Pergamon Press, Ltd.

A DISCUSSION OF THE PAPER "MECHANISM OF SULFATE ATTACK ON PORTLAND CEMENT CONCRETE - ANOTHER LOOK" BY P.K. MEHTA*

S. Chatterji
Technological Institute
2630 Taastrup, Denmark

VOL. 14 984

In his paper Prof. Mehta has commented that the effect of gypsum formation on the sulfate attack has not been properly explained in the literature. As far as I know, Lea was the first to propose that gypsum formation may cause damage to Portland cement concrete and explained this on the assumption of a solid state conversion of $Ca(OH)_2$, present in the specimen, to gypsum (1). Since then it has been discussed many times. In 1968 an alternative explanation of the above damage was proposed in terms of the crystal growth pressure (2).

In this paper Mehta has also made two very interesting observations. These are that (i) the formation of even Type 2 ettringite by itself is not capable of causing an expansion (p. 404, par. 1); and (ii) ettringite can cause expansion only when the stiffness of the cement paste has already been lowered by something else (p. 406). However, these observations were already anticipated in 1963 (3). Rossetti et al have even shown that the expansivity of all types of ettringite is drastically reduced if a small restraining pressure is applied to them (4).

Mehta proposed that a "drop in the hydroxyl ions concentration and an increase in the sulfate ions concentration of the environment lowers the stiffness of the cement paste on one hand, and increases the water-adsorption capacity of the ettringite on the other hand" (p. 406) hence the expansion and damages. In this context the properties of K type expansive cement are of interest (5). It has been shown that a Type K expansive cement can expand over initial 14 days of hydration even though its strength increases at the same time period, i.e. expansion and an increase in the stiffness occur at the same time. The expansion has been attributed to ettringite formation. As Type K expansive cement specimens were in contact only with water neither SO_4 ion concentration in the environment could increase nor the hydroxyl ion

*CCR 13, 401 (1983).

concentration could decrease. Apparently neither of the two necessary conditions as proposed by Mehta were fulfilled by Type K cements. Prof. Mehta's comment on these results will be of general interest.

REFERENCES

1) Lea - Canadian J. Res. No. 27 B, 297, 1949.

2) Chatterji - Proc. Vth Intern. Symp. Chem. Cement, Tokyo 1968, III, 336.

3) Chatterji and Jeffery - Mag. Conc. Res. 15, 83, 1963.

4) Rosetti, Chiocchio and Paolini - Cem. and Conc. Res. 13, 23, 1983.

5) Mehta and Lesnikoff - ACI Special Publ. Sp 38, 89, 1973.

VOL
14
198

CEMENT and CONCRETE RESEARCH. Vol. 14, p. 153, 1984. Printed in the USA.
0008-8846/84 $3.00+00. Copyright (c) 1984 Pergamon Press, Ltd.

A REPLY TO THE DISCUSSION OF "MECHANISM OF SULFATE ATTACK ON PORTLAND CEMENT CONCRETE - ANOTHER LOOK" BY S. CHATTERJI*

By P. K. Mehta
Department of Civil Engineering
University of California, Berkeley 94720

VOL.
14
984

In regard to Dr. Chatterji's comments, the author agrees that many investigators including Lea have pointed out the detrimental effect on strength associated with gypsum formation during sulfate attack on portland cement concrete. In the earlier literature, however, the strength loss due to gypsum formation and the expansion due to ettringite formation are treated as isolated phenomena which have no effect on each other. This author feels that both the phenomena need to be considered together in order to appreciate and understand the complexity of sulfate-generated deteriorations in concrete. Therefore, it is suggested that a drop in the strength and stiffness (restraining capacity of the material) due to gypsum formation be seen as a necessary step for increasing the magnitude of expansion caused by ettringite. The concept is consistent with the experimental observations of the reverse phenomenon by many researchers, i.e. expansions associated with ettringite formation can be greatly reduced when restrained.

Dr. Chatterji's reference to the behavior of expansive cements offers the author another opportunity to reaffirm the important elements of the proposed hypothesis. Experience with commercial expansive cement concretes shows that, in general, the expansion associated with the formation of ettringite is over within 3 or at the most 7 days of moist curing, when the stiffness of the material is still very low. From reference (5) cited by Dr. Chatterji, the data show that after 7 days of hydration hardly any expansions were produced by the Type K, M, and S expansive cement pastes. In fact, in the case of Type K cement, more than two-thirds of the restrained expansion was completed within 3 days of hydration. Due to the high sulfate/hydroxyl ratio in the liquid phase, most of the ettringite formation and expansion had occurred during this period. The expansion continued for four days more (probably due to continuing water adsorption by ettringite), then stopped, possibly because the stiffness of the material increased beyond a certain level.

*CCR 13, 401 (1983).

CEMENT and CONCRETE RESEARCH. Vol. 14, pp. 154-156, 1984. Printed in the USA.
0008-8846/84 $3.00+00. Copyright (c) 1984 Pergamon Press, Ltd.

A DISCUSSION OF THE PAPER "EXAMINATION OF 136 YEARS OLD PORTLAND CEMENT CONCRETE" BY G.M. IDORN AND N. THAULOW*

R.G. Blezard
Blue Circle Cement (Technical Division)
Portland Street, Hull HU2 8JZ, England

There are a number of interesting points mentioned in this paper that have stimulated a re-examination of the concrete and the history of this concrete.

The paper by Idorn and Thaulow described a study of a hand sized piece of precast concrete from the remaining sections of the wall built in front of Portland Hall, Gravesend, Kent. A similar piece of concrete was examined earlier to identify the nature of the cement used. The observations were read as a paper to the Society of Chemical Industry (London, 17.5 1979) which was published (1) in 1981. The common link between the two specimens is that they were collected at the same occasion (8.9.77) by Mr. J. Figg.

There appeared to be a small controversy in the literature regarding the true date of the concrete. The evidence given by Francis (2) is very convincing, giving a date of between 1850-1851. Some references quoted 'about 1850'(3,4), which is probably the date to be quoted. Davis (5) gives a later date but this should be disregarded as the building work was abandoned within 18 months of starting due to the enormous cost involved in the project.

The concrete is from the decorative top of the boundary wall to the now demolished Portland Hall. The pre-cast top unit is well preserved and takes the shape of circles and fleurs-de-lys. This concrete is of fine quality and has shown good durability. It was a limestone aggregate (Kentish ragstone) and a miscellaneous fine aggregate. The main body of the wall, which was not sampled, has a flint aggregate and was in an inferior state of preservation and the concrete technology was not to the same standard as the decorative top.

The concrete specimen examined contained the relicts of entrained air, confirming Dr. Thaulow's observations. This does not necessarily infer that in 1850 a deliberate air entraining agent was added.

Exactly when air entrainment was first put to practical use is hard to say because initially it was an empirical observation and not deliberate addition. According to Power's (6) - 'the practice of deliberately entraining air bubbles in concrete was introduced in the mid-1930's.' It is more likely that air entrainment occurred by accident rather than design and that contamination from the mould release material (soap or fatty material) may be a more feasible thought.

*CCR 13, 739 (1983).

VOL
14
198

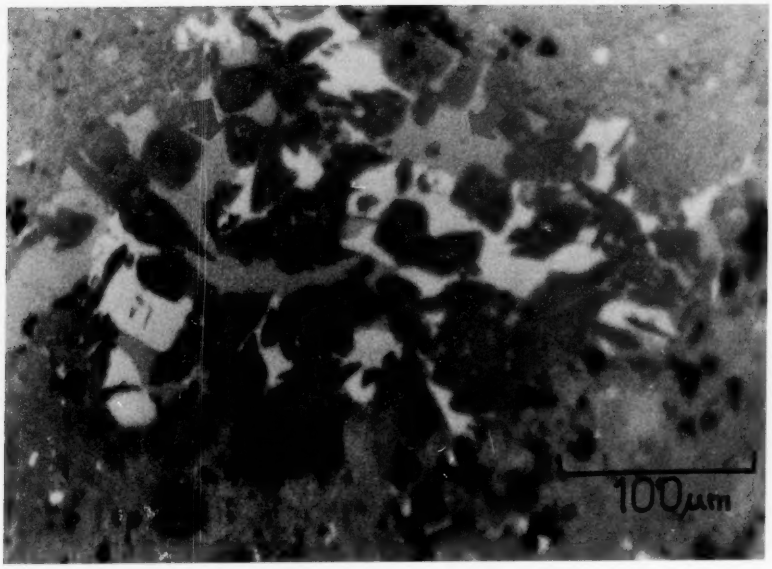

FIG. 1

Deformed belite - bulbous and cusp form in a matrix of C_3A and ferrite. The C_3A is marked with arrows. This form of belite is common in meso-Portland Cement.

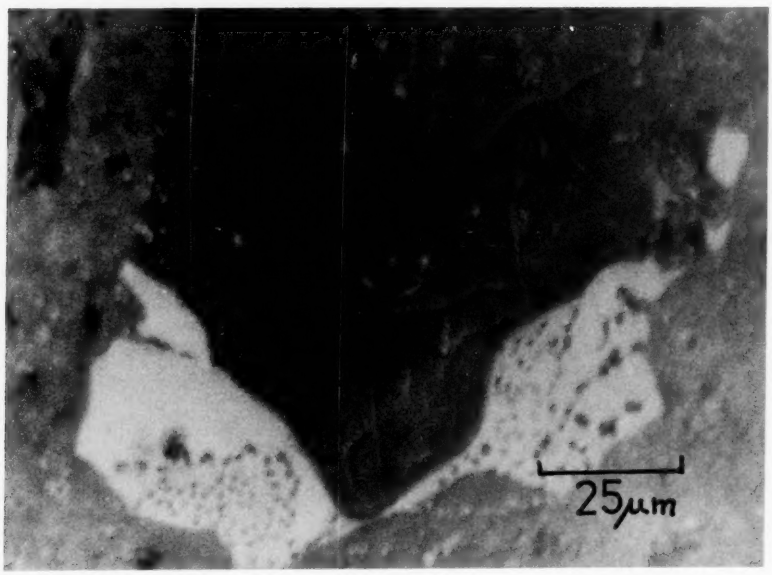

FIG. 2

Large deformed alite crystal typical of the slow heating and cooling cycle of the Aspdin kiln.

As the concrete was destined for use on Aspdin's own property, the cement was almost certainly made at Robins and Aspdin's plant at Northfleet which was about 1 1/2 miles away. The microstructure of the unhydrated regions in the concrete is typical of the meso-Portland cement made by Aspdin.

The concrete was heavily carbonated and there were regions of partially unhydrated clinker minerals. These regions were about 150-250 μm in size and this may be related to the coarse nature of the Aspdin cement. The coarse nature of Aspdin cement has been previously established (1). A study of photomicrographs taken in 1979 was, to an extent, in agreement with the findings of Idorn and Thaulow in so much that the ferrite phase (which was the major flux phase) was unhydrated. In contradiction to their views, C_3A was present as indicated in Figure 1. The crystal shapes of the silicate phases in meso-Portland cement are normally distorted (see Figure 2) because of the long residence times in processing.

In conclusion, these comments must not detract from the broad investigation, particularly in respect of durability and the work has been a valuable contribution.

References

1. R.G. Blezard, Chem. and Ind. 17, 630 (1981).
2. A.J. Francis, The Cement Industry 1796-1914: (A History), p. 118, (1977). David & Charles Ltd., Newton Abbot, England.
3. C.S. Stanley, Highlights in the History of Concrete, p. 15 (1979). C.&C.A., Slough, England.
4. Anonymous, Historic Concrete No. 67 Concrete, p. 16, June 1980.
5. A.C. Davis, A Hundred Years of Portland Cement (1824-1924) p. 69. Concrete Publications (1924) London.
6. T.C. Powers, The Properties of Fresh Concrete, p. 305 (1968). John Wiley, New York.

VOL
14
198

CEMENT and CONCRETE RESEARCH. Vol. 14, pp. 157-158, 1984. Printed in the USA.
0008-8846/84 $3.00+00. Copyright (c) 1984 Pergamon Press, Ltd.

A REPLY TO A DISCUSSION BY R.G. BLEZARD OF THE PAPER: "EXAMINATION OF 136 YEARS OLD PORTLAND CEMENT CONCRETE"*

G.M. Idorn
G.M. Idorn Consult ApS
14 B, Tovesvej, 2850-
Nærum, DK

N. Thaulow
Technological Institute
Gregersensvej, 2630-
Tåstrup, DK

VOL.
14
984

We are grateful for R.G. Blezard's comments to our examination of the W. Aspdin concrete specimen and wish to acknowledge the comprehensive descriptions of historic concrete in Great Britain in recent years. The supplementary data to our brief outline of the origin of the specimen are appreciated as placing the examination more adequately in the broader context.

The aim of our limited study was to ascertain phenomena in the microscopic structure of the concrete which could help to explain the reasons for its remarkable durability, taking its origin into consideration. We chose thin section petrography as a method we frequently use for comparable studies of insufficient durability of modern concrete.

We did wish to emphasize that the W. Aspdin concrete (like much surviving ancient and historic concrete) has been made very dense in such ways that its denseness has increased in the course of time. This has much more to say for modern cement and concrete technology than we could elaborate on in our paper.

We shall reply to the author's specific comments as follows:

1. The specimen we examined was only carbonated to depths of about 5 mm. This suggests that one should not accept much larger rates of carbonation in modern concrete as inevitable or acceptable - but also today make the concrete as dense as 130-140 years ago.

2. We did not mean to imply that air-entrainment has been applied deliberately as a precedence of the more recent discovery of its beneficial effects regarding frost resistance of concrete. But the air-void system is there and as it appears it can only have had its origin in the presence in the fresh concrete of a solute in the liquid phase which has decreased the surface tension and formed well distributed, genuinely entrained air.

The application of "tailored" admixtures (usually organic) to mortars and concrete for improvement of workability has been known since ancient times.

We think it is very likely that W. Aspdin and his masons knew such inherited means for making the fresh concrete adequate for mixing, placing and compac-

*CCR 13, 739 (1983).

tion considering their primitive means for doing this by the aid of mechanical energy.

3. We do not see the finding by the author of unhydrated C_3A in another piece of W. Aspdin concrete as contradictory to our limited observations. We simply did not see it. This was one reason why we dwelled upon the abundance of unhydrated C_4AF. We think that these observations together suggest a critical attitude to modern Portland cements, high in C_4AF, as far as their cementitious value goes, compared with ordinary Portland cement and blended cements. Seen together with the author's finding of unhydrated C_3A we are close to conclude that the conventional C_3A/C_4AF conceptions encompass myths of simplicity which ought to be dispelled for the benefit of assurance of the long-term durability of modern concrete.

We do also acknowledge the author's observation as a reminder that the use of several available examination methods in combination is usually advantageous in studies of the complex microstructure and behaviour of field concrete.

VOL
14
198

CEMENT and CONCRETE RESEARCH. Vol. 14, pp. 159-160, 1984. Printed in the USA.
0008-8846/84 $3.00+00. Copyright (c) 1984 Pergamon Press, Ltd.

NEWS ITEMS

Spring Meeting of the AMERICAN CONCRETE INSTITUTE, Hyatt Regency Hotel, Phoenix, AZ. Information: Convention Coordinator, ACI, P.O. Box 19150, Detroit, MI 48219 USA. — March 4-9, 1984

Symposium on NONDESTRUCTIVE TEST METHODS FOR CONCRETE STRENGTH, during the ACI Annual Meeting, Hyatt Regency, Phoenix, AZ. Information: Dr. H.S. Lew, Chairman, ACI Committee 228, National Bureau of Standards, Building 226, Room B162, Washington, DC 20234 USA. — March 4-9, 1984

6th International Conference on CEMENT MICROSCOPY, Mariott Hotel, Albuquerque, New Mexico. Information: Arturo G. Nisperos, Materials Service Corporation, 901 N. Sangamon St., Chicago, IL 60622 USA. — March 26-29, 1984

86th Annual Meeting of the AMERICAN CERAMIC SOCIETY, David L. Lawrence Convention Center, Pittsburgh, PA. Information: ACS, 65 Ceramic Drive, Columbus, OH 43214 USA. — April 29 - May 3, 1984

39th Symposium on FAILURE MECHANISMS IN HIGH PERFORMANCE MATERIALS, National Bureau of Standards, Gaithersburg, MD. Information: Dr. J.G. Early, Metallurgy Division, Room A153, Building 223, National Bureau of Standards, Washington, DC 20234 USA. — May 1-3, 1984

International Conference on CONCRETE UNDER MULTIAXIAL CONDITIONS, Université Paul Sabatier, Toulouse, France. Information: M. Lorrain, Conference Secretariat, I.N.S.A., Département de Génie Civil, 31077 Toulouse Cedex, France. — May 22-24, 1984

A Symposium on BLENDED CEMENTS, sponsored by Committee C-1, Cement, of ASTM, in Denver, CO. Information: Kathy Greene, ASTM, 1916 Race Street, Philadelphia, PA 19103 USA. — June 1984

International Conference on IN SITU/NONDESTRUCTIVE TESTING OF CONCRETE AND EVALUATION OF CONCRETE STRUCTURES, Ottawa, Canada. Information: V. Mohan Malhotra, CANMET, 405 Rochester Street, Ottawa, Ontario, Canada K1A 0G1. — Oct. 2-5, 1984

International Conference on TALL BUILDINGS, Shangri-la Hotel, Singapore, sponsored by the Council of the Institution of Engineers, Singapore. Information: The Chairman, ICTBS 84, 10, Anson Road, #14-06, International Plaza, Republic of Singapore (0207). — Oct. 22-26, 1984

NEWS ITEMS

CALL FOR PAPERS

The 14th Conference on *SILICATE SCIENCE AND THE SILICATE INDUSTRIES* will be held in Budapest, MAY 1985. The purpose of the conference is to discuss actual problems in the field of the silicate industries and silicate science by the personal meeting of internationally appreciated experts. Papers are requested on the following topics: Multi-disciplinary aspects in the silicate sciences; and quality control in the silicate industries. These topics will be discussed in the following sections: Glass; Concrete; Cement; Structural Ceramics and Insulating Materials; Rock Products; Ceramic Whitewares; and Refractories.

Authors are requested to contact the Conference Committee for further information: Scientific Society of the Silicate Industry, "SILICONF - COMMITTEE," H-1368 Budapest, P.O.B. 240, Hungary. Cable Address: SILICONF, Budapest.

ERRATUM

"Recycled Concrete and Silica Fume Make Calcium Silicate Bricks," by T.C. Hansen and H. Narud, Vol. 13, No. 5, pp. 626-630, 1983.

Page 627, Line 23 from top reads: ... analysis proved that the finely ground crusher fines contained 19 percent of calcium hydroxide.

It should read: ... analysis proved that the finely ground crusher fines contained 4 percent of calcium hydroxide.

VOL 14 198

U.S. Postal Mail

STATEMENT OF OWNERSHIP, MANAGEMENT AND CIRCULATION
(Required by 39 U.S.C. 3685)

1. TITLE OF PUBLICATION	4. PUBLICATION NO.	2. DATE OF FILING
CEMENT AND CONCRETE RESEARCH	0 0 0 8 8 8 4 6	10/1/83
3. FREQUENCY OF ISSUE	**A. NO. OF ISSUES PUBLISHED ANNUALLY**	**B. ANNUAL SUBSCRIPTION PRICE**
Bimonthly	6	$160.00

4. COMPLETE MAILING ADDRESS OF KNOWN OFFICE OF PUBLICATION (Street, City, County, State and ZIP Code) (Not printers)
Fairview Park, Elmsford, NY 10523

5. COMPLETE MAILING ADDRESS OF THE HEADQUARTERS OR GENERAL BUSINESS OFFICES OF THE PUBLISHERS (Not printers)
Fairview Park, Elmsford, NY 10523

6. FULL NAMES AND COMPLETE MAILING ADDRESS OF PUBLISHER, EDITOR, AND MANAGING EDITOR (This item MUST NOT be blank)

PUBLISHER (Name and Complete Mailing Address)
Pergamon Press, Fairview Park, Elmsford, NY 10523

EDITOR (Name and Complete Mailing Address)
Della M. Roy, Pennsylvania State Univ., University Park, PA 16802

MANAGING EDITOR (Name and Complete Mailing Address)
Kathleen Mourant, Pennsylvania State Univ., University Park, PA 16802

7. OWNER (If owned by a corporation, its name and address must be stated and also immediately thereunder the names and addresses of stockholders owning or holding 1 percent or more of total amount of stock. If not owned by a corporation, the names and addresses of the individual owners must be given. If owned by a partnership or other unincorporated firm, its name and address, as well as that of each individual must be given. If the publication is published by a nonprofit organization, its name and address must be stated.) (Item must be completed)

FULL NAME	COMPLETE MAILING ADDRESS
Pergamon Press Ltd	Headington Hill Hall, Oxford, England
Pergamon Press Inc	Fairview Park, Elmsford, NY 10523

8. KNOWN BONDHOLDERS, MORTGAGEES, AND OTHER SECURITY HOLDERS OWNING OR HOLDING 1 PERCENT OR MORE OF TOTAL AMOUNT OF BONDS, MORTGAGES OR OTHER SECURITIES (If there are none, so state)

FULL NAME	COMPLETE MAILING ADDRESS
Robert Maxwell	Headington Hill Hall, Oxford, England

9. FOR COMPLETION BY NONPROFIT ORGANIZATIONS AUTHORIZED TO MAIL AT SPECIAL RATES (Section 411.3, DMM only)
The purpose, function, and nonprofit status of this organization and the exempt status for Federal income tax purposes: (Check one)

☐ (1) HAS NOT CHANGED DURING PRECEDING 12 MONTHS ☐ (2) HAS CHANGED DURING PRECEDING 12 MONTHS (If changed, publisher must submit explanation of change with this statement.)

10. EXTENT AND NATURE OF CIRCULATION	AVERAGE NO. COPIES EACH ISSUE DURING PRECEDING 12 MONTHS	ACTUAL NO. COPIES OF SINGLE ISSUE PUBLISHED NEAREST TO FILING DATE
A. TOTAL NO. COPIES (Net Press Run)	1568	1575 Vol. 13(5)
B. PAID CIRCULATION 1. SALES THROUGH DEALERS AND CARRIERS, STREET VENDORS AND COUNTER SALES	----	----
2. MAIL SUBSCRIPTION	989	966
C. TOTAL PAID CIRCULATION (Sum of 10B1 and 10B2)	989	966
D. FREE DISTRIBUTION BY MAIL, CARRIER OR OTHER MEANS SAMPLES, COMPLIMENTARY, AND OTHER FREE COPIES	64	65
E. TOTAL DISTRIBUTION (Sum of C and D)	1053	1031
F. COPIES NOT DISTRIBUTED 1. OFFICE USE, LEFT OVER, UNACCOUNTED, SPOILED AFTER PRINTING	515	544
2. RETURN FROM NEWS AGENTS	----	----
G. TOTAL (Sum of E, F1 and 2 - should equal net press run shown in A)	1568	1575

11. I certify that the statements made by me above are correct and complete

SIGNATURE AND TITLE OF EDITOR, PUBLISHER, BUSINESS MANAGER, OR OWNER: James P. Alford sr prod mgr

PS Form 3526 July 1981 (See instruction on reverse)

CEMENT and CONCRETE RESEARCH. Vol. 14, pp.i, 1984. Printed in the USA.
0008-8846/84 $3.00 + .00 Copyright (c) 1984 Pergamon Press, Ltd.

EDITORIAL

It is planned to introduce a new Software Survey Section to CEMENT and CONCRETE RESEARCH to encourage the open exchange of information on software programs unique to our professional field. With the rapid penetration of computers into academic and industrial institutions has come a parallel increase in the number of scientists and researchers designing their own software. The existence of much of this software remains unknown to even those of us who could most benefit from its use. We believe that it is of vital importance to our readers that such information be made available. We believe also that a professional journal is the best place to share such information. Your contribution would be most welcome.

VOL.
14
1984

The questionnaire on the following pages is designed to assist you in reporting on software that you may have developed or be in the process of developing. By completing this form, your information will reach thousands of your colleagues who may benefit from your work and may possibly offer suggestions for further enhancements to your software. Please complete the enclosed form and return it to:

Kathleen S. Mourant
Assistant Editor
CEMENT and CONCRETE RESEARCH
Materials Research Laboratory
University Park, PA 16802 USA

We do not intend to review or comment on the contents of the questionnaire. It will be published as is in order to expedite the information cycle process. We welcome any comments you may have.

VOL.
14
1984

CEMENT and CONCRETE RESEARCH

SOFTWARE DESCRIPTION FORM

Title of Software Package: _____

_____

_____

It is: [ ] Application Program [ ] Utility [ ] Other _____

Specific Area _____ (e.g. Thermodynamics, Phase Analysis)

Software developed for [name of computer(s)] _____
in [language(s)] _____ to run under [operating system]
_____ and is available in the following media:

[ ] Floppy Disk/Diskette Specify:
Size _____ Density _____ [ ] Single sided [ ] Dual sided

[ ] Magnetic Tape Specify:
Size _____ Density _____ Character set _____

Distributed by: _____

Minimum Hardware Configuration Required: _____

Required Memory: _____

User Training Required: [ ] Yes [ ] No

Documentation:
[ ] None [ ] Minimal [ ] Self-documenting [ ] Extensive External Documentation

Source Code Available: [ ] Yes [ ] No

Level of Development:
[ ] Design Complete [ ] Coding Complete [ ] Fully Operational
[ ] Collaboration would be welcome

Is Software being used currently? [ ] Yes [ ] No
If yes, how long? _____
If yes, how many sites? _____

Contributor is available for user inquiries: [ ] Yes [ ] No

(over)

Pergamon Press, Inc.,
Maxwell House, Fairview Park, Elmsford, N.Y. 10523 • Headington Hill Hall, Oxford OX3 0BW, England

OL.
14
984

Description of what Software does [200 words]:

VOL
14
198

Potential Users:_____

Fields of Interest:_____

Name of Contributor:_____

Institution:_____

Address:_____

_____

Telephone Number:_____

Reference No. [Assigned by Journal Editor]_____

[The information below is not for publication.]

Would you like to have your program:

Reviewed? [ ] Yes [ ] No [ ] Not at this time

Marketed and Distributed? [ ] Yes [ ] No [ ] Not at this time

Pergamon Press, Inc.,
Maxwell House, Fairview Park, Elmsford, N.Y. 10523 • Headington Hill Hall, Oxford OX3 0BW, England

CEMENT and CONCRETE RESEARCH. Vol. 14, pp. 161-169, 1984. Printed in the USA.
0008-8846/84 $3.00 + 00. Copyright (c) 1984 Pergamon Press, Ltd.

STUDY OF THE STRENGTH DEVELOPED BY STABLE CARBONATED PHASES IN HIGH ALUMINA CEMENT

M. Pérez Méndez and F. Triviño Vázquez

Instituto Eduardo Torroja
Serrano Galvache s/n
Madrid - 33

(Refereed)
(Received Jan. 20; in final form July 15, 1983)

ABSTRACT

The direct hydration of high alumina cement to the cubic phase, C_3AH_6, at temperatures above 30°C is proposed to avoid the conversion from CAH_{10} to C_3AH_6. The carbonation of C_3AH_6 with CO_2 between 20°C and 80°C causes an increase in strength which is higher at higher temperatures. It is caused by the presence of thermodynamically stable carbonated phases. The optimum hydration times are the minimum necessary to get C_3AH_6: 3 hours at 80°C and 6 hours at 60°C. Subsequent carbonation up to a total time of 24 hours after the end of mixing provides 90% of the strength obtained after 28 days of hydration at the same temperature, with the same compounds being formed. If $CaCO_3$ is added to the cement before mixing, the strengths are even higher than for specimens without it. The effect of a super-water-reducing admixture on strength has also been studied.

Introduction

The hydration of high alumina cement at temperatures up to 20°C leads to the formation of the metastable hexagonal hydrate, CAH_{10}. At temperatures higher than 30°C, this converts into the cubic hydrate, C_3AH_6, which is stable in the $CaO - Al_2O_3 - H_2O$ system. This conversion, which can be represented:

$$3\ CAH_{10} \xrightarrow{T \geq 30^{\circ}C} C_3AH_6 + 2\ AH_3 + 18\ H$$

is typical of this cement and is accompanied by losses in strength (1). For that reason, elevated temperatures are strictly forbidden in standards and codes governing high alumina cement use.

We have studied the hydration of 1:3 high alumina cement mortar at temperatures above 30°C (40°C, 60°C and 80°C) with the direct formation of C_3AH_6, thereby avoiding the conversion reaction. The effects of adding $CaCO_3$ to the

cement before mixing as well as treating with CO_2 after hydration have also been studied. In previous papers (2) (3), the chemical changes were studied. In the present paper, an evaluation of the flexural and compressive strengths obtained from different curing conditions is described.

Experimental Procedure

The high alumina cement used in all cases was an A-650 (4) whose chemical analysis is given in a previous paper (2). The aggregate employed was silica sand and distilled water was always used. Two types of mortar were prepared:

a) High alumina cement
Aggregate (C:A = 1:3)
Water (W/C = 0.42)

b) High alumina cement + 20% by mass of $CaCO_3$ (80 parts of cement + 20 parts of $CaCO_3$)
Aggregate (C:A = 1:3)
Water (W/C = 0.42)

Different conditions and times of curing were used for both mortars. The main variables for both the hydration and carbonation processes were the temperature and time. Two groups of hydration times were studied A) Long: 28 days, and B) Short: 3 hours at 80°C, and 6 hours at 60°C.

Effect of W/C Ratio on Strength in the Hydration at 80°C. A preliminary study of the strength variation with W/C ratio in the hydration with thermal treatment was carried out. For this purpose, 4 x 4 x 16 cm prisms were made using 1:3 high alumina cement mortar (type a), using W/C ratios of 0.46, 0.44 and 0.42. These values are between the critical value of 0.4 and the value of 0.5 given in the Spanish standard for mortar preparation (4). All the specimens were hydrated at 80°C for 24 hours before measuring their flexural and compressive strengths. Table 1 shows the results.

Table 1

Effect of W/C Ratio on 24 Hours Strengths for Mortars Hydrated at 80°C

W/C	R_f (MPa)	R_c (MPa)
0.46	6	36 (+)
0.44	6	38
0.42	7	44

(+) Each value is the average from at least 10 specimens.

Effect of a Super-Water-Reducer on the Hydration at 80°C. The addition of a super-water-reducer during mixing was studied in the proportions: 1%, 0.2% and 0.1%. This admixture, a naphthalenic resin, not only decreased the W/C ratio from 0.42 to 0.40 and 0.38, but also increased the workability and fluidity and reduced the porosity. After mixing, the specimens were hydrated at 80°C for 24 hours. Finally, their flexural and compressive strengths were measured. Table 2 gives the strengths for the three admixture proportions for each of two different W/C ratios: 0.40 and 0.38.

An increase in strength was observed as the W/C ratio decreased from 0.40 to 0.38, the highest value being that for the minimum W/C ratio with the minimum quantity of admixture proportions studied. This suggested the possibility of using lower W/C ratios with the admixture proportions studied.

VOL. 14 1984

Table 2

Flexural and Compressive Strengths (MPa) of Specimens with Super-Water-Reducer Hydrated at 80°C for 24 Hours

	W/C = 0.40			W/C = 0.38		
	1%	0.2%	0.1%	1%	0.2%	0.1%
R_f (MPa)	9	12	13	9	11	14
R_c (MPa)	43	50	53	54	52	66

Results

1 x 1 x 6 cm specimens were prepared using the two types of mortar previously described: with and without $CaCO_3$. A summary of flexural and compressive strengths (MPa) obtained for each curing condition is given in Table 3. Standard deviations are in brackets after each strength value.

OL.
14
984

Discussion

A. Strengths of Specimens Hydrated for Long Times (28 Days). Curing conditions α in Table 3 show the strength of specimens hydrated 28 days at 40°C, 60°C and 80°C compared with those hydrated at 20°C. The large values for specimens hydrated at 20°C are due to the presence of CAH_{10} as the principal hydrated phase which is well-known as giving the usual high strengths to high alumina cements: Temperatures above 30°C cause C_3AH_6 to appear as the principal phase. This was confirmed by infra-red (IR) spectroscopy and x-ray diffraction (XRD) (2). The strength given by this hydrate is lower than that given by CAH_{10}. This effect is shown by the value for hydration at 40°C as compared to that obtained at 20°C.

Further, a considerable increase in strength is observed when the hydration temperature is increased, although C_3AH_6 is obtained in all cases.

Fig. 1 shows the strengths of specimens hydrated at 40°C, 60°C and 80°C for 28 days. Curves fitted by linear regression to the average flexural and compressive strengths are shown together with the 95% confidence limits. In each case, extrapolations to 100°C are indicated by dotted lines and the equations of the curves $\bar{R} = f(T°C)$ are given. A hypothesis that the standard deviation varies linearly with temperature has been partially confirmed. However, further experimental work will be necessary to confirm the hypothesis and therefore, on this basis, to carry out a linear regression analysis of strength with temperature.

CO_2 treatment of the hydrated specimens for 3 days under curing conditions δ-A, causes an increase in strength with respect to the specimens which had only been hydrated. Two sets of carbonation temperatures were used:

Table 3

Summary of Flexural and Compressive Strength (MPa) (Standard Deviation) of High Alumina Cement Mortars for all Curing Conditions

α — SPECIMENS WITHOUT $CaCO_3$

HYDRATION ONLY

	T°C	AGE	R_f MPa	R_c MPa
1	20	28 days	14 (2.7)	85 (7.9)
2	40	28 days	11 (1.2)	58 (2.5)
3	60	28 days	14 (1.6)	70 (5.2)
4	80	28 days	17 (3.2)	80 (3.5)

β — SPECIMENS WITH $CaCO_3$

HYDRATION ONLY

	T°C	AGE	R_f MPa	R_c MPa
1	20	28 days	9.7 (3.0)	69 (21.3)
2	60	28 days	10 (1.1)	74 (4.6)

γ — A — HYDRATION AND CO_2 TREATMENT

	HYDRATION	CO_2	R_f MPa	R_c MPa
1	40°C 28days	20°C 3 days	13 (1.3)	76 (8.2)
		40°C 3 days	13 (1.5)	77 (10.3)
2	60°C 28days	20°C 3days	16 (1.4)	77 (4.1)
		60°C 3days	15 (2.0)	93 (3.9)
3	80°C 28days	20°C 3days	15 (1.6)	86 (7.0)
		80°C 3days	17 (4.0)	114 (14.3)

δ — A — HYDRATION AND CO_2 TREATMENT

	HYDRATION	CO_2	R_f MPa	R_c MPa
1	20°C 28 days	20°C 3days	12 (1.2)	79 (15.7)
		60°C 3days	12 (1.7)	82 (7.3)
2	60°C 28days	60°C 3days	16.5 (3.4)	97 (7.5)

B

4	60°C 6 hours	60°C 18 hours	14.6(3.0)	76 (5.8)
		60°C 3days	16 (4.2)	80 (6.1)
		60°C 5days	15 (2.2)	81 (6.1)
5	60°C 24hours	60°C 24 hours	14 (1.9)	74 (5.3)
		60°C 3 days	15 (1.2)	81.5 (7.1)
		60°C 5days	15.2 (1.5)	82 (7.7)
6	80°C 3 hours	80°C 21hours	11.4 (1.4)	69 (6.3)
		80°C 3 days	13.7 (1.1)	91.3 (4.6)
		80°C 5days	13 (0.9)	86 (6.0)
7	80°C 24hours	80°C 24 hours	12.8 (1.5)	72.5 (5.2)
		80°C 3days	13.2 (1.8)	88 (5.7)
		80°C 5days	17.8 (2.9)	93.2 (8.0)

B

3	60°C 6 hours	60°C 18 hours	13.7 (2.7)	64 (4.0)
		60°C 3 days	17 (2.0)	85 (5.4)
		60°C 5 days	15 (2.8)	79 (6.2)
4	60°C 24 hours	60°C 24hours	13 (2.5)	77 (4.3)
		60°C 3days	16 (1.5)	82 (5.5)
		60°C 5days	17.2 (1.4)	89.2 (5.6)
5	80°C 3hours	80°C 21hours	16.5 (1.2)	80 (6.1)
		80°C 3 days	20 (3.8)	90 (12.0)
		80°C 5days	18 (2.9)	96 (6.0)
6	80°C 24hours	80°C 24 hours	17.5 (3.8)	101.5 (6.1)
		80°C 3days	16.8 (2.6)	102.2 (11.8)
		80°C 5days	18.7 (5.0)	104.3 (11.3)

VOL. 14 1984

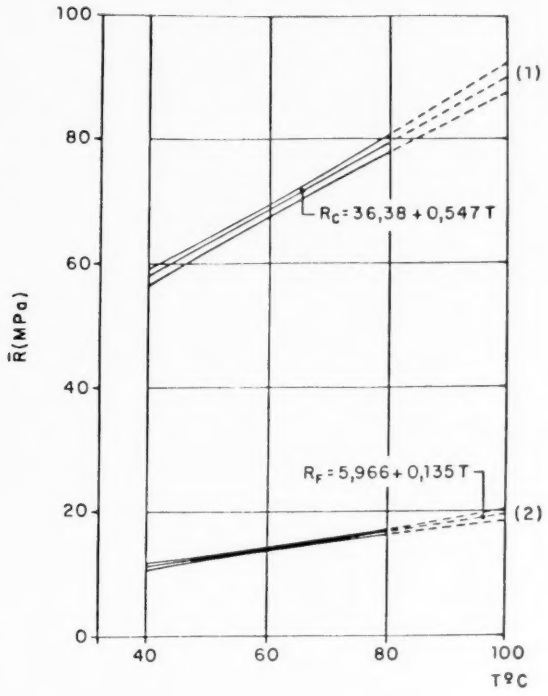

Fig. 1

Influence of the Hydration Temperature on the Flexural and Compressive Strength and Their 95% Confidence Limits for High Alumina Cement Mortars.

20°C (figure 2) and temperatures which were the same as the hydration temperature (40°C, 60°C and 80°C respectively) (fig. 3). Figure 2 shows that when the carbonation is performed at 20°C, the strength increases linearly with the hydration temperature. When the carbonation temperature is the same as that used during hydration, figure 3, the strength values are higher than when the CO_2 treatment was at 20°C and they increase linearly with the temperature used. The strength increase is interpreted as being due to the formation of carbonated phases according to:

$$3C_3AH_6 + 3CO_2 \longrightarrow \underset{\text{Aragonite}}{3CaCO_3} + \alpha\text{-}Al_2O_3 + 6H_2O$$

since this reaction is favoured at higher temperatures.

The compressive strength increases obtained when the carbonation is performed at 20°C with respect to the specimens which have only been hydrated are:

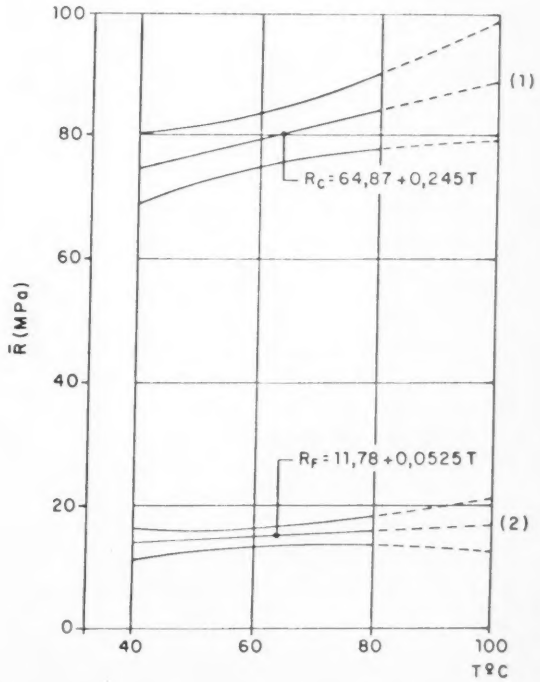

Fig. 2

Effect of CO_2 Treatment at 20°C on the Compressive and Flexural Strengths and Their 95% Confidence Limits for High Alumina Cement Mortars Hydrated for 28 Days at 40°C, 60°C and 80°C.

$$\triangle \bar{R}_c\ 40^{\circ}C = 76 - 58 = 18\ MPa$$
$$\triangle \bar{R}_c\ 60^{\circ}C = 77 - 70 = 7\ MPa$$
$$\triangle \bar{R}_c\ 80^{\circ}C = 86 - 80 = 6\ MPa$$

The smaller increases for samples hydrated at 80°C and 60°C as compared to those hydrated at 40°C, is interpreted as due to insufficient carbonation treatment - 3 days at 20°C - after hydration at 80°C and 60°C for such a long time, 28 days. This was confirmed by IR spectroscopy (2). If the carbonation takes place at the same temperature as the hydration, the increases in the average compressive strength values with respect to the specimens which have only been hydrated are:

$$\triangle \bar{R}_c\ 40^{\circ}C = 77 - 58 = 19\ MPa$$
$$\triangle \bar{R}_c\ 60^{\circ}C = 93 - 70 = 23\ MPa$$
$$\triangle \bar{R}_c\ 80^{\circ}C = 114 - 80 = 34\ MPa$$

The thermal treatment which accompanies the carbonation causes a much more pronounced increase in strength than that obtained at 20°C, the increase being higher as the temperature increases. The results are summarized in Table 4.

Table 4

Increase of Compressive Strength Due to CO_2 Treatment

Hydration Temperature T°C	Carbonation at 20°C $\triangle \bar{R}_c$ (MPa)	Carbonation at the Hydration Temperature $\triangle \bar{R}_c$ (MPa)
40	18	19
60	7	23
80	6	34

B. Strengths of Specimens Hydrated for Short Times. The hydration times used in this case were 3 hours at 80°C and 6 hours at 60°C; these were long enough to get C_3AH_6 as the principal hydrate. It can be seen in Table 3 that the curing conditions $\overline{\sigma}$-B, with short hydration times followed by carbonation for 1, 3 and 5 days, have similar strengths to those obtained after 28 days hydration and 3 days carbonation ($\overline{\sigma}$-A) at the same temperature.

After hydrating the specimens for 6 hours at 60°C and carbonating for 18 hours at the same temperature to a total age of 24 hours from the end of mixing, a

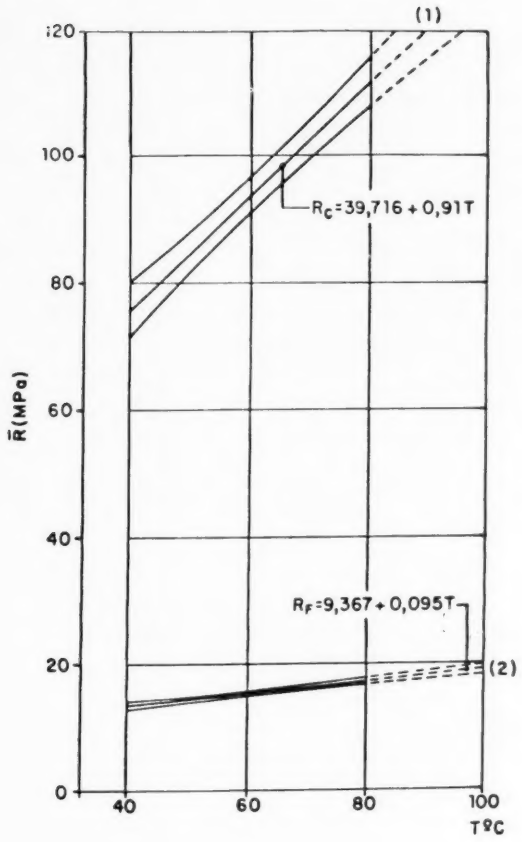

Fig. 3

Effect of CO_2 Treatment at the Same Temperature as that Used During the Hydration on the Strengths and Their 95% Confidence Limits for High Alumina Cement Mortars Hydrated at : 40°C, 60°C and 80°C.

$\bar{R}_c$ = 75 MPa is obtained. This is 81% of the value of 93 MPa, obtained for specimens hydrated for 28 days at 60°C and carbonated for 3 days at the same temperature. If the carbonation is continued for 3 days, the compressive strength reaches $\bar{R}_c$ = 80 MPa which is 86% of the value taken as the control (31 days of treatment). Carbonation for 5 days leads to a $\bar{R}$ = 81 MPa, which is 87% of the control. This implies a considerable saving in time and energy since a very good $\bar{R}_c$ is obtained only 24 hours after the end of mixing. This is 81% of the strength obtained in the control after 31 days. In both cases, the same compounds were formed (2).

If the specimens hydrated for 24 hours at 60°C are later carbonated at the same temperature for 24 hours, the compressive strength reaches the value $\bar{R}_c$ = 74 MPa which is 79% of the control. This fact, according to the IR and XRD data, suggests a slightly lower R than that obtained with specimens hydrated for 6 hours. Really, after treatment with CO_2 for 24 hours, more uncarbonated C_3AH_6 was found by IR and XRD in specimens hydrated for 24 hours than in those hydrated for 6 hours. In specimens hydrated for 6 hours at 60°C and carbonated for 18 hours, more of the cubic C_3AH_6 is transformed into the stable carbonated phases. Short hydration times let the next structural transformation, carbonation, occur more easily as the specimens are in a state we call "semiplastic", less rigid than for longer hydration times.

Carbonation for 3 days at 60°C of specimens hydrated for 24 hours at the same temperature results in an $\bar{R}_c$ = 81 MPa which is 88% of the control. The strength obtained after 5 days of carbonation was $\bar{R}_c$ = 82 MPa, (88%). When the specimens were hydrated at 80°C for 3 hours followed by carbonation for 21 hours at the

same temperature, for a total time of 24 hours, the R_c value obtained was 71 MPa (76%); a value of 91 MPa was reached after 3 days of carbonation (98%). For the specimens which were hydrated for 24 hours at 80°C, a value of $\bar{R}_c$ = 72 MPa was obtained after carbonation for 24 hours at the same temperature, 78% of the control; the value increased to 88 MPa after 3 days of carbonation (95%) and to 93 MPa after 5 days (100%).

Specimens with $CaCO_3$

In the studies carried out with specimens containing $CaCO_3$ mixed with the cement, comparatively higher values of the mechanical strengths were obtained than for specimens without $CaCO_3$

Table 5

Effect of $CaCO_3$ Addition to the Mortar on the Compressive Strength after a 28 Days Hydration

Curing Conditions	Specimens without $CaCO_3$ $\bar{R}_c$ (MPa)	Specimens with $CaCO_3$ $\bar{R}_c$ (MPa)
Hydration for 28 days at 60°C	70	74
Hydration for 28 days at 60°C and carbonation for 3 days at 60°C	93	97

The increase in strength produced by the $CaCO_3$, table 5, is interpreted as due to the compounds appearing in the specimens. IR and XRD showed them to be aragonite, alumina and bayerite (3). As for specimens without $CaCO_3$, the CO_2 treatment after the hydration caused an increase in strength. The value of the increase in the case of 60°C was:

$$\triangle \bar{R}_c = (97 - 74)\ \text{MPa} = 23\ \text{MPa}$$

This was an increase of 130% with respect to the $\bar{R}_c$ value obtained after 28 days of hydration.

The same argument as was made for specimens without $CaCO_3$ can be given for the curing conditions with short hydration times. They relate the optimal values obtained in the present paper with the minimum time needed. Table 6 shows the compressive strength for each case as a percentage of the value for the control (97 MPa).

VOL. 14 1984

Table 6

Compressive Strength Expressed as % of the Control for Each of the Curing Conditions δ -B

Curing Conditions		% with Respect to 97 MPa after 31 days
60°C (6 hours) + CO_2 (18 hours)	60°C	66%
+ CO_2 (3 days)	60°C	88%
+ CO_2 (5 days)	60°C	82%
60°C (24 hours)+ CO_2 (1 day)	60°C	79%
+ CO_2 (3 days)	60°C	85%
+ CO_2 (5 days)	60°C	92%
80°C (3 hours) + CO_2 (21 hours)	80°C	83%
+ CO_2 (3 days)	80°C	93%
+ CO_2 (5 days)	80°C	99%
80°C (24 hours)+ CO_2 (1 day)	80°C	105%
+ CO_2 (3 days)	80°C	105%
+ CO_2 (5 days)	80°C	108%

OL.
14
984

Conclusions

From the high strength values obtained after short times and the appearance of the same stable carbonated phases as were obtained after a longer curing of 31 days, we conclude that: Thermal treatment during the hydration and subsequent carbonation of the high alumina cement not only stabilizes the product, but also contributes significantly to its strength.

The addition of 20% by mass of $CaCO_3$ to the anhydrous cement before mixing constitutes the optimal case, as it improves the strength even at very early ages. After 24 hours of hydration at 80°C and 24 hours of carbonation at the same temperature, a compressive strength of 101 MPa was obtained with a 1:3 mortar of high alumina cement containing $CaCO_3$.

References

1. A.M. Neville, Proc. Inst. Civ. Engrs., 25, 287 (1963).
2. M. Pérez, T. Vázquez and F. Triviño, to be published in Cem. Concr. Res.
3. M. Pérez, T. Vázquez and F. Triviño, to be published in Cem. Concr. Res.
4. R.C.-75: "Pliego de Prescripciones Técnicas Generales para la Recepción de Cementos" (May 1975).

CEMENT and CONCRETE RESEARCH. Vol. 14, pp. 170-176, 1984. Printed in the USA.
0008-8846/84 $3.00+00. Copyright (c) 1984 Pergamon Press, Ltd.

MÖSSBAUER AND X-RAY INVESTIGATIONS OF SOME PORTLAND CEMENTS

K.S. Harchand, R. Kumar, and K. Chandra
Department of Physics, University of Roorkee
Roorkee 247 667, India

Vishwamittar
Department of Physics, Panjab University
Chandigarh 160 014, India

(Communicated by F.D. Tamás)
(Received May 24; in final form Dec. 5, 1984)

VOL.
14
1984

ABSTRACT

The Mössbauer spectroscopic and x-ray diffraction investigations have been carried out on a variety of ordinary portland, portland pozzolanic, portland slag and sulphate resisting portland cements, using dry as well as hydrated samples. The discussion of the Mössbauer parameters shows that Fe atoms occupying distorted octahedral and tetrahedral sites in the dry cements are hydrated to form ferrite monosulphate without producing $Fe(OH)_3$ and its gel; hydration of the slag cement proceeds much faster than other cements; and that the composition of the iron-bearing phase in the sulphate resisting portland cement, studied in detail, is close to C_4AF.

Introduction

The term portland cement (P.C.) is generally used to represent the group of cements consisting of ordinary portland cement (O.P.C), portland pozzolanic cement (P.P.C.), portland slag cement (P.S.C.), sulphate resisting portland cement (S.R.P.C.), etc. The main constituent compounds of these cements are: C_3S, β-C_2S, C_3A and $C_2F_{1-x}A_x$ with $0 \leq x \leq 0.67$. In addition, these cements also contain gypsum and small quantities of the oxides of Mg, Na, K, etc. It is believed that C_3S and C_3A contribute significantly to the hydration of cements; therefore these phases have been studied in more detail than the other two components (1). However, recently it has been realized that higher concentration of the ferrite phase ($C_2F_{1-x}A_x$) increases the strength and stability of cements (2-4) and attention has been paid to understand its role in the hydration process. Some of the workers (4-10) have carried out their investigations using the general techniques of conduction calorimetry, differential thermal analysis, infra-red spectroscopy, x-ray diffraction, electron probe analysis and electron microscopy, while others (11-14) have employed the iron-site selecting Mössbauer effect in their studies. The usefulness of selectivity of Mössbauer spectroscopy for iron in the compounds occurring in the cements is exemplified by the

Part of this work was presented at the International Conference on Applications of Mössbauer Effect held at Jaipur, India, in December 1981.

fact that Tamás and Vértes (11) used their experimental data to show that $Fe(OH)_3$ is not formed during the hydration of C_4AF and thereby obtained answer to the problem of its hydration mechanism. This aspect has recently been corroborated by the finding of Harchand, et al. (14), that neither $Fe(OH)_3$ nor its gel is produced in the hydration of $C_2F_{1-x}A_x$ phase in the cement. However, most of the Mössbauer spectroscopic work on the hydration of ferrite phase has been performed on pure compound and many workers (15) still seem to believe that $Fe(OH)_3$ is formed as a result of hydration of this system. Obviously, the study of hydration of $C_2F_{1-x}A_x$ continues to be a topic of interest. This is more so because the Mössbauer spectroscopic investigations on the hydration of $C_2F_{1-x}A_x$ in the cements, in the presence of other phases, have been very limited and essentially qualitative.

Realizing the importance of hydration of the ferrite phase in various cements and appreciating the difference in its behaviour in cements as compared to the pure state (14,16,17), a detailed investigation of this phase in a variety of dry as well as hydrated portland cements has been taken up through Mössbauer spectroscopy. The results of these findings together with the x-ray diffraction data, constitute the content of this article.

Experimental

The samples of O.P.C., P.P.C., P.S.C. and S.R.P.C. under report, were procured from different sources and their oxide composition, in mass percent, is listed in Table 1. The x-ray diffraction and Mössbauer spectroscopic studies of dry powders were carried out as described in an earlier communication (18). It turned out that the results for all the samples of O.P.C. are essentially identical among themselves and so is the situation in case of two samples of S.R.P.C. Therefore, the detailed studies were performed only on one sample of O.P.C. (labelled as O.P.C.5), one sample of S.R.P.C. (viz. S.R.P.C.2) and each of the samples of P.P.C. and P.S.C. For this purpose the hydration of the samples for different intervals of times was carried out as detailed in Ref. 18 and then x-ray diffraction as well as Mössbauer spectroscopic data were recorded at room temperature. The results of the Mössbauer spectroscopic study of O.P.C.5 and P.P.C. have been presented in Ref. 14. However, now we have been able to improve upon the fitting of the data reported earlier and are combining the main results for these two samples with the findings obtained from the detailed investigation of P.S.C. and S.R.P.C.2.

The computer fitted Mössbauer spectra of dry as well as hydrated samples

Table 1

Chemical Composition of Various Portland Cements, in Mass Percent

Sample	CaO	SiO_2	Al_2O_3	Fe_2O_3	SO_3	MGO	Others
OPC 1	60	20	5	4	2	4	5
OPC 2	59	21	6	3	2	2	7
OPC 3	63	24	5	2	3	1	2
OPC 4	63	22	6	3	1	1	4
OPC 5	59	21	7	3	2	3	5
PPC	52	18	6	4	2	3	15
PSC	45	26	15	1	2	4	7
SRPC 1	62	24	5	5	1	2	1
SRPC 2	65	20	4	5	2	-	4

for 4 weeks of the samples of OPC5, PPC, PSC and SRPC2 constitute the contents of Figure 1.

Results and Discussion

The peaks in the x-ray diffractometer traces of the dry samples have been assigned on the basis of available literature (19,20) to various components of cements as shown in Table 2. The values of 2θ differ by less than ±0.1° from one sample to another and the intensities of the peaks depend on the relative concentration of the constituent compounds. For example, almost zero intensity of peak at 33.0° for C_3A in S.R.P.C. implies that the concentration of this component in the cement is below the detectable limits.

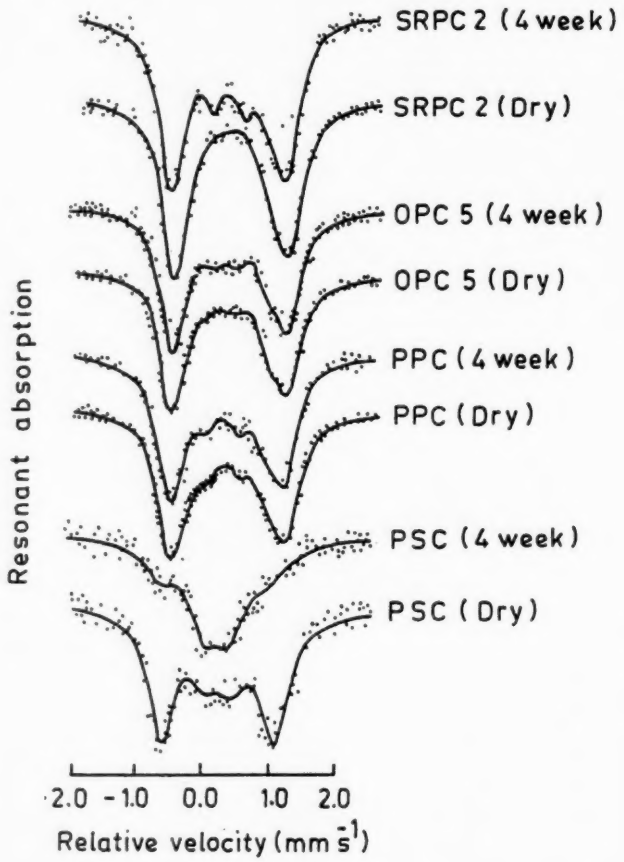

FIG. 1
Mössbauer spectra of dry and hydrated samples

In the case of hydrated OPC5, the intensity of the peaks corresponding to C_3S and β-C_2S decreases and that of the peaks at 29.5° due to C-S-H phase increases with time of hydration. The development of peaks at 23.1°, 34.4° and 41.1° indicates the production of ettringite whereas the peaks at 32.2°, 39.5°, 43.5°, 47.5°, etc. are due to $CaCO_3$ which is produced during hydration through some contact with atmospheric carbondioxide. The trace for hydrated PPC shows of increasing intensity at 20.9° and 26.8° in addition to those observed for OPC. These two peaks have been assigned to the hydration product CAS_2H_4. In both the cases there does not seem to be any peak corresponding to $Ca(OH)_2$ indicating that the amount of this compound if formed is below the detection limits.

The trace for 4-week hydrated SRPC2 is very clear and exhibits peaks of $Ca(OH)_2$ at Bragg 2θ angles 34.1°, 47.1° and 50.8° and those of C-S-H phase at 28.9° and 32.1°. However, the graph for 4-week hydrated PSC is relatively complex and additional peaks arising from the presence of C_3AH_6, C_4AH_{13} and ettringite are also observed (19,20).

The Mössbauer Data

The x-ray crystallographic work on the single crystals of $C_2F_{1-x}A_x$, for different values of x, has shown that Fe occupies octahedral and tetrahedral

Table 2

The Assignment of Different Peaks in the X-Ray Diffractometer Traces, to the Compounds Percent in Portland Cements

Compound	Bragg angle, 2θ (in degrees)
C_3S	29.3, 32.5, 34.3, 41.3, 51.7
β-C_2S	32.1, 32.5, 34,3, 41.3
C_3A	33.0, 26.6
$C_2F_{1-x}A_x$	33.8, 46.8
CA	30.0, 31.1
$K_{0.33}Na_{0.67}AlSiO_4$	29.6, 23.0
C_6A_4MS	31.1, 32.5
SiO_2	26.7, 20.8
Gypsum	29.3

sites, whose relative concentration varies with x (21). Therefore, it is reasonable to expect that Fe occupies similar sites in the cements also. Of course, the bonding of Fe is altered by the presence of other phases and this, in turn, distorts the octahedra and the tetrahedra. In addition to this, some of the iron phase may be converted into hydrate due to its contact with moisture. Accordingly, it is anticipated that the Mössbauer spectra of dry samples are composed of two or three doublets; the absence of third doublet implying absence of the hydrated phase.

In view of the above remarks, the analysis of the Mössbauer spectra of dry powders of various cement samples has been carried out in terms of two or three doublet patterns. The parameters derived through the computer fitting of these spectra are listed in Tables 3-6.

While executing the computer fit of the Mössbauer spectra for the hydrated cements, good fit was obtained with three doublets in all the cases except PSC where such a fitting led to inconsistent results. Rather, this spectrum had to be fitted in terms of two doublets. The reason for this departure seems to lie in the fact that the quality of the spectrum is very poor, in spite of 1.6×10^6 counts/channel, due to low Fe_2O_3 content (1%). The Mössbauer parameters for the hydrated samples are also included in Tables 3-6.

In the dry samples of OPC, PPC and SRPC the first doublet with higher values of isomer shift and quadrupole splitting seems to be due to Fe at the octahedral site, while the second doublet with smaller values of these parameters is due to the tetrahedral iron atoms. The third doublet with much smaller magnitude of quadrupole splitting is assigned to the hydrate of ferrite phase. This assumption is justified by the fact that intensity of the third site increases with time for which the cement has been hydrated. In the case of PSC, the first doublet pertains to the iron atoms distributed in both the octahedral and tetrahedral sites. The second site with lesser quadrupole splitting is that due to the hydration product.

A perusal of Tables 3-6 shows that the isomer shifts and quadrupole splittings do not change with the time of hydration. This is in contrast with the observation reported for the hydration of pure compound C_4AF, wherein quadrupole splitting decreases with time and finally becomes zero (11). The difference in

Table 3

Mössbauer Parameters for Dry Samples of Different OPC and the Hydrated Sample of OPC 5

Sample	Isomer shift (w.r.t. Fe) mms^{-1}			Quadrupole splitting mms^{-1}			Relative percent intensity			Line width mms^{-1}
	δ_1	δ_2	δ_3	Δ_1	Δ_2	Δ_3	I_1	I_2	I_3	Γ
OPC 1 (Dry)	0.37	0.15	0.25	1.72	1.57	0.42	60	29	11	0.37
OPC 2 (Dry)	0.35	0.14	0.23	1.73	1.61	0.42	55	28	17	0.40
OPC 3 (Dry)	0.34	0.13	0.24	1.72	1.61	0.40	54	27	19	0.45
OPC 4 (Dry)	0.35	0.14	0.25	1.71	1.60	0.35	57	29	14	0.40
OPC 5 (Dry)	0.34	0.11	0.24	1.70	1.59	0.40	59	32	9	0.40
OPC 5 (1 Day)	0.36	0.11	0.24	1.72	1.61	0.38	54	31	15	0.40
OPC 5 (1 Week)	0.35	0.12	0.27	1.71	1.63	0.44	52	30	18	0.40
OPC 5 (2 Weeks)	0.34	0.12	0.24	1.71	1.59	0.41	52	29	19	0.40
OPC 5 (4 Weeks)	0.35	0.11	0.22	1.69	1.56	0.36	53	31	16	0.39

the hydration of the ferrite phase in free state and in the cements is understandable because the pure ferrite phase forms cubic hydrates (11) whereas in the presence of gypsum, which is present in all the cements, it leads to the formation of ettringite which is finally converted into iron-substituted monosulphoaluminate (2,5,22).

In view of the comments made above, it may be concluded that the Fe atoms giving rise to the doublet with quadrupole splitting nearly 0.4 mms^{-1} belong to the Fe-substituted monosulphoaluminate. Furthermore, the Mössbauer parameters corresponding to the hydration product in all the samples are distinctly

Table 4

Mössbauer parameters for dry and hydrated PPC

Sample	Isomer shift (w.r.t. Fe) mms^{-1}			Quadrupole splitting mms^{-1}			Relative percent intensity			Line width mms^{-1}
	δ_1	δ_2	δ_3	ΔE_1	ΔE_2	ΔE_3	I_1	I_2	I_3	Γ
Dry	0.36	0.12	0.23	1.68	1.59	0.50	53	29	18	0.45
1 Day	0.36	0.11	0.23	1.70	1.59	0.47	52	28	20	0.43
1 Week	0.37	0.13	0.28	1.66	1.58	0.54	51	28	21	0.43
2 Weeks	0.35	0.12	0.26	1.66	1.55	0.53	49	27	24	0.44
4 Weeks	0.36	0.12	0.26	1.66	1.57	0.47	50	27	23	0.42

VOL 14 198

Table 5

Mössbauer Parameters for Dry and Hydrated PSC

Sample	Isomer shift (w.r.t. Fe) mms^{-1}		Quadrupole splitting mms^{-1}		Relative percent intensity		Line width mms^{-1}
	δ_1	δ_2	ΔE_1	ΔE_2	I_1	I_2	Γ
Dry	0.25	0.28	1.65	0.40	70	30	0.49
1 Day	0.26	0.25	1.59	0.37	62	38	0.53
1 Week	0.25	0.28	1.63	0.41	34	66	0.55
2 Weeks	0.25	0.28	1.54	0.45	29	71	0.56
4 Weeks	0.24	0.28	1.59	0.38	28	72	0.54

different from those of $Fe(OH)_3$ and its gel; for which the two parameters are $Fe(OH)_3$: δ = 0.25, ΔE = 0.72 and $Fe(OH)_3$ gel: δ = 0.45, ΔE = 0.75 mms^{-1} (23). Therefore, the formation of $Fe(OH)_3$ and its gel during the hydration process in various portland cements is ruled out. This conjecture is in agreement with that of Tamás and Vértes (11), but in contrast with the prediction of Teoreanu, et al. (15) for the hydration of C_4AF.

From Tables 3-6, it is obvious that the intensity of the third site increases with the time of hydration, at the cost of other two sites; in the case of PSC the intensity of second site increases while that of the first site decreases. This indicates that more and more ferrite monosulphate is being formed during the hydration of portland cements. A comparison of the rate of increase of intensities for ferrite monosulphate with time of hydration for various cements shows that the hydration is fastest in the case of PSC. This is due to the fact that this cement has low SO_3 content and lesser release of $Ca(OH)_2$ during hydration, as observed from the development of the peaks corresponding to

Table 6

Mössbauer Parameters for Dry Samples of SRPC 1 and SRPC 2 and the Hydrated Samples of SRPC 2

Sample	Isomer shift (w.r.t. Fe) mms^{-1}			Quadrupole splitting mms^{-1}			Relative percent intensity			Line width mms^{-1}
	δ_1	δ_2	δ_3	ΔE_1	ΔE_2	ΔE_3	1	2	3	Γ
SRPC 1 (Dry)	0.35	0.13	-	1.67	1.54	-	59	41	-	0.46
SRPC 2 (Dry)	0.34	0.16	-	1.67	1.52	-	67	33	-	0.46
SRPC 2 (1 Day)	0.33	0.15	0.27	1.65	1.50	0.37	61	31	8	0.44
SRPC 2 (1 Week)	0.34	0.15	0.32	1.64	1.54	0.42	54	26	20	0.44
SRPC 2 (2 Weeks)	0.34	0.16	0.33	1.64	1.52	0.39	54	26	20	0.46
SRPC 2 (4 Weeks)	0.35	0.14	0.31	1.64	1.58	0.44	50	27	23	0.42

$Ca(OH)_2$ in the X-ray diffractometer traces, and the presence of gypsum as well as $Ca(OH)_2$ retards the hydration of ferrite phase.

In the case of SRPC 2, the ratio of the intensities for octahedral and tetrahedral sites in the dry cement is found to be 2.04, which suggests that in this cement the ferrite phase is close to C_4AF (24). Furthermore, this intensity ratio remains fairly constant with hydration implying that both the sites have equal tendency for hydration. Similar type of behavior is also obtained in the case of OPC and PPC with hydration.

The ratio I_1/I_2 in various cements is different implying that the composition of the ferrite phase $C_2F_{1-x}A_x$ is not similar in all these cements which may be a consequence of the method of preparation and the proportion of materials used.

Acknowledgements

The cements used in these studies and their composition data were received from research sections of Associated Cement Companies, Ltd., India (OPC, PPC and PSC) and from Dr. J. Bensted, Blue Circle Industries Ltd., Kent (England) (SRPC2) and we are grateful to them for their kind gesture. K.S.H. acknowledges the grant of study leave by the Punjab Agricultural University, Ludhiana, and the financial assistance from Phys. Deptt. U.O.R. Roorkee.

References

1. J. Skalny, I. Jawed and H.F.W. Taylor, World Cement Technology 9, 183 (1978).
2. J.F. Young, Cement Production and Use (Proc. Eng. Found. Conf.) 1, 117 (1980).
3. J. Bensted, Seventh Int. Congress on the Chemistry of Cement 2, 1 (1980).
4. M. Fukuhara, S. Goto, K. Asaga, M. Diamon and R. Kondo, Cem. Conc. Res. 11, 407 (1981).
5. I. Jawed, S. Goto and R. Kondo, Cem. Conc. Res. 6, 441 (1976).
6. J. Bensted, Il Cemento 73, 45 (1976).
7. A.A. Klyusov, E.N. Lepnev, V.S. Bakshutov, V.V. Ilyukhin and V.N. Nikitin, Izv. Akad. Nauk SSSR Neorg. Meter. 13, 2070 (1977).
8. D.E. Rogers and L.P. Aldridge, Cem. Conc. Res. 7, 399 (1977).
9. A. Negro and L. Stafferi, Zement-Kalk-Gip 32, 83 (1979).
10. M. Collepardi, S. Monosi, G. Moriconi and M. Corradi, Cem. Conc. Res. 9, 431 (1979).
11. F.D. Tamás and A. Vértes, Cem. Conc. Res. 3, 575 (1973).
12. A. Vértes, M. Ranogajec-Komar and F.D. Tamás, Hung. J. Indus. Chem. 3, 339 (1975).
13. A. Vértes, M. Ranogajec-Komar and F.D. Tamás, Epitoanyag 27, 207 (1975).
14. K.S. Harchand, Vishwamittar and K. Chandra, Cem. Conc. Res. 10, 243 (1980).
15. I. Teoreanu, G. Filoti, C. Hritcu and L. Bucea, V. Spanu, S. Ciocanel and M. Ivascu, Cemento 76, 19 (1979).
16. F. Wittmann, F. Pobell and W. Wiedemann, Z. angew Phys. 19, 281 (1965).
17. P. Pascual, C. Lupiani, J. Sancho and J.M. Vara, An. Quim. 75, 3 (1979).
18. K.S. Harchand, Vishwamittar and K. Chandra, Cem. Conc. Res. 14, 19 (1984).
19. H.F.W. Taylor, The Chemistry of Cements, Vol. 2, Academic Press (London), p. 347 (1964).
20. ASTM X-ray Powder Diffraction File, No. 9-338,20-452.
21. D.K. Smith, Acta Cryst. 15, 1146 (1962).
22. J. Bensted, Cem. Conc. Res. 10, 719 (1980).
23. J.G. Stevens and V.E. Stevens (eds.), Mössbauer Effect Data Index, Plenum Press, New York (1966-68, 1983, 1975).
24. R.W. Grant, S. Geller, H. Weidersich, U. Gonser and L.D. Fullmer, J. Appl. Phys. 39, 1122 (1968).

VOL. 14 1984

CEMENT and CONCRETE RESEARCH. Vol. 14, pp. 177-184, 1984. Printed in the USA.
0008-8846/84 $3.00+00. Copyright (c) 1984 Pergamon Press, Ltd.

RELATIONS BETWEEN THE CRYSTAL STRUCTURES OF CALCIUM SILICATES AND THEIR REACTIVITY AGAINST WATER

K.H. Jost and B. Ziemer
Zentralinstitut für Anorganische Chemie der Akademie der Wissenschaften der DDR
1199 Berlin, Rudower Chaussee

(Communicated by W. Wieker)
(Received May 20; in final form Dec. 16, 1983)

ABSTRACT

In the crystal structures of all calcium silicates which are reacting with water, and only in these, there are infinite building units of CaO_x polyhedra linked by face-sharing. Resting on Pauling's rules on the stability of ionic compounds, a hypothesis is developed why this structural feature makes the reaction with water easier. The influence of thermal history of reactive phases and their content of foreign oxides on their reactivity is discussed.

Introduction

There are marked differences between the various anhydrous calcium silicates with respect to the rates of their reaction with water. While C_3S is reacting rapidly, other calcium silicates, e.g. γ-C_2S are nearly stable against water. The reason for these differences should be looked for in the arrangement of the atoms in the undisturbed crystals. Disturbances in the crystals formed, for instance by grinding or by substitutional disorder, only gradually influence the reactivity but cannot be their origin. Therefore, reactive phases are reactive with and without substitutional disorder, and unreactive ones do not become reactive by grinding or alloying.

In the past ten years the crystal structures of some calcium silicates have been determined for the first time or redetermined with higher accuracy, so that it is now worthwhile to ask again the question for the structural background of reactivity.

Features of the Crystal Structures of Reactive Phases

A survey of the crystalline phases in the system CaO-SiO_2 is given in Table 1. Accordingly, all reactive calcium silicates are monosilicates but this holds for the unreactive γ-C_2S too, whereas all calcium silicates with polymeric anions are unreactive.

From the crystal structures, it follows:

Bond lengths and angles in the SiO_4 tetrahedra have the usual values.

Table 1

Crystalline Phases in the System $CaO-SiO_2$

Phase	Reactive	Constitution	Remarks on the Crystal Structures and Literature
C_3S	yes	$Ca_3O[SiO_4]$	6 closely related modifications Structure of TI: (2)
C_2S	yes yes yes yes no	$Ca_2[SiO_4]$	α-C_2S : (3) α'H-C_2S : (3) α'L-C_2S : (4,5) β-C_2S : (6) γ-C_2S : (7)
C_3S_2 Rankinite	no	$Ca_3[Si_2O_7]$	(8)
C_3S_2 Kilchoanite	no	$Ca_6[(SiO_4)(Si_3O_{10})]$	(9) A closely related phase is C_8S_5
CS Cyclo-Wollastonite	no	$Ca_3[Si_3O_9]$	(10), OD-structure A high pressure phase is known (11)
CS Chain-Wollastonite	no	$(Ca[SiO_3])_x$	(12), OD-structure
A high pressure modification of C_2S is existing too, in which Si is octahedrally surrounded by oxygen (1).			

Therefore, in the monosilicates the tetrahedra show no striking distortions.

The Ca ions are surrounded by 6-10 oxygen atoms which form more or less distorted coordination polyhedra (Table 2). The average values of the (Ca-O) distances in the polyhedra naturally increase with increasing coordination number.

Holes by which entering of water could be made easy if these would be large enough and connected to tunnels cannot be found in any of these structures.

This survey of some structural features of calcium silicates already invalidates assumptions of the reasons of reactivity which were made at a time when the crystal structures were not known with sufficient accuracy (13,14,15,16). According to these assumptions:

- The CaO_x polyhedra in reactive phases should be more distorted than those in unreactive ones. That this is not true can easily be seen e.g. by comparison of the octahedra in C_3S and γ-C_2S.

- The (Ca-O) distances in the CaO_x polyhedra of reactive phases should be longer in average than those in unreactive ones. An example of the contrary: The average (Ca-O) distance in C_3S amounts to 2.42Å, in the far lower reactive β-C_2S this value is 2.50Å.

- Reactive phases should have holes in their structures. That this is not true has been said already. And in the example β-/γ-C_2S a simple comparison of the densities which are D_β = 3.33 and D_γ = 2.97 Mg/m^3 shows that in this case

Table 2

Coordination of Calcium by Oxygen

Phase	Number of Ca per unit cell with respect to coordination number and mean (Ca-O) distance			
C_3S TI	46	VI	with	2.41Å
	8	VII		2.51
α'_L-C_2S	4	VI	with	2.52Å
	4	VII		2.60
(Sr-stabilized)	12	VIII		2.51
	4	X		2.79
β-C_2S	4	VII	with	2.51Å
	4	VIII		2.49
γ-C_2S	8	VI	with	2.37Å
Rankinite	12	VII	with	2.46Å
Kilchoanite	20	VI	with	2.37Å
	4	VIII		2.51
Cyclo-Wollastonite	12	VIII	with	2.54Å
Chain-Wollastonite	12	VI	with	2.39Å

VOL. 14 1984

the structure of the reactive phase is the more densely packed one.

The conclusion from failing of these assumptions is that the structural reasons for the differences in reactivity do not rest on special features of small groups like single CaO_x polyhedra but on the way in which such groups are joined together in the crystal structure. In this respect now the pair

reactive β-C_2S / unreactive γ-C_2S

will be considered. This pair is very convenient for a comparison because the stochiometry of the counterparts is the same one and the coordination numbers of the Ca are not too different.

At first the common features: The CaO_x polyhedra are linked with the SiO_4 tetrahedra by common vertices as well as by common edges. The shortest distances between Ca and Si in β- and γ-C_2S are with 2.97 and 2.96Å, respectively, practically equal. The same holds for the shortest distances between Si atoms which amount to 4.11 and 4.06Å in β- and γ-C_2S, respectively.

Now the differences: They are inherent in the way in which the CaO_x polyhedra are joined together. Additional to common vertices and edges, neighboured CaO_x polyhedra in β- but not in γ-C_2S share faces too (Fig. 1).

According to one of Pauling's rules on the stability of ionic compounds, the transition from vertex- to edge- to face-sharing of neighboured polyhedra which is connected with an approach of the central atoms makes the respective compound increasingly unstable.

Therefore, now all crystal structures of calcium silicates were checked for face-sharing CaO_x polyhedra and, moreover, with respect to the environment of the Ca ions by other Ca ions. In order to have more structures of reactive phases available for comparison, the Sr- and Ba-monosilicates and the phase alinite, $Ca_{11}O_2Cl[(SiO_4)_3(AlO_4)]$, were included (17). The data according to Table 2 on the coordination of Ca in alinite are: 16 VI (5 oxygen atoms with 2.42 and 1 Cl with 3.27Å), 4 VI with 2.28Å, and 2 VIII with 2.52Å.

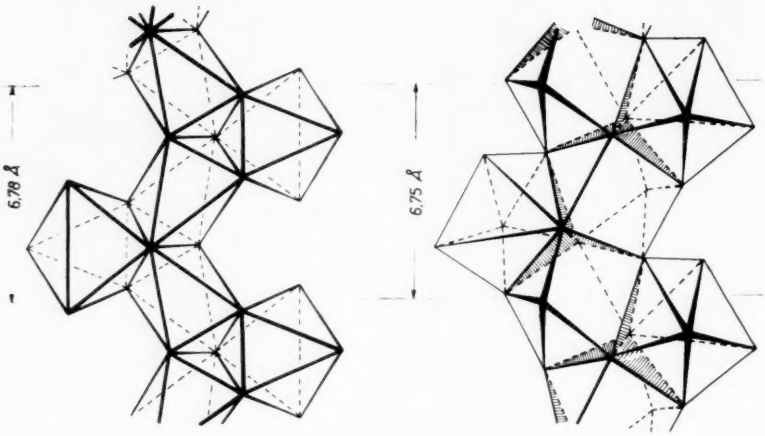

FIG. 1

Arrangement of the characteristic group of CaO_x polyhedra in the crystal structures of γ- and β-C_2S. Common faces are hatched.
Left: γ-C_2S Right: β-C_2S

The results of this check are compiled in Tables 3 and 4. The entries in these tables rest on the coordination of Ca by O as summarized in Table 2. The notations "high" and "low" for the reactivity rest on X-ray diffractometric determinations of the unreacted educt in the case of alinite (A.I. Boikova, IBAUSIL, 1982), C_3S (21), α'-C_2S (22), β-C_2S (22,23), γ-C_2S (23), $Ba_2[SiO_4]$ (24), on differential calorimetric measurements in the case of $Ba_3O[SiO_4]$ (G. Oliew, private communication, 1982) and Sr_3O $[SiO_4]$ (25).

In Table 3, it can be seen that the number of Ca neighbours of a Ca ion is higher and the average distance between neighboured Ca ions is lower for the reactive phases. But it can also be seen that these differences are only gradual.

The characteristic features of reactive phases can be seen in Table 4. Only in the reactive phases are there infinite building units of CaO_x polyhedra joined together not only by vertex- or edge-sharing, but also by face-sharing. The only exception of this rule is alinite in which CaO_x polyhedra are linked by shared faces only to finite groups, but these continue infinitely via common Cl^- vertices of CaO_5Cl octahedra. In the unreactive phase rankinite, there are also CaO_x polyhedra linked by common faces, but these are only forming pairs without continuation. In the structures of the three Sr- and Ba-silicates drawn in comparison and which are all reactive, there are also infinite building units of MeO_x polyhedra which are linked by face-sharing (Table 5).

Hypothesis on the Mechanism of the Reaction with Water

In the preceding part, structural features were deduced which mark out reactive over unreactive phases. Now it shall be tried to develop a hypothesis as to why these features are necessary for the reaction with water.

The Coulomb repulsion forces which act upon a Ca ion by its cation neighbours are balanced in the intact crystal. But as soon as its structure is disturbed, for instance by reaction with water, the tendency to follow these forces becomes larger the stronger the now uncompensated repulsion forces are.

In a calcium silicate crystal touched with water, Ca ions of the CaO_x polyhedra in the surface of the crystal may be exsolved at which OH^- and Si-OH will

Table 3

Neighbourhood Relations between Ca Ions. Neighbours are those Ca of which the CaO_x Polyhedra have common Oxygen Atoms.

Phase	Reactivity	Mean number of neighbours	Mean distance between neighboured Ca
Alinite	high	8.4	3.61Å
C_3S TI	high	7.8	3.47
α'_L-C_2S	low	7.7	3.69
β-C_2S	low	8.0	3.62
γ-C_2S	no	7.0	3.75
Rankinite	no	6.7	3.87
Kilchoanite	no	6.2	3.82
Cyclo-Wollastonite	no	6.0	3.97
Chain-Wollastonite	no	4.7	3.62

VOL.
14
1984

Table 4

Linking of CaO_x Polyhedra by Face-Sharing

Phase	Reactivity	Shared faces per polyhedron	Distances (in Å) between Ca's in shared polyhedra		Building units formed by face-shared polyhedra
			mean	range	
Alinite	high	2.2	3.25	3.08-3.60	clusters, connected by Cl^- to two systems of chains
C_3S TI	high	2.1	3.30	3.16-3.68	3-dimensional network
α'_L-C_2S	low	3.2	3.62	3.48-3.82	3-dimensional network
β-C_2S	low	3.0	3.50	3.43-3.56	spiro-chains
γ-C_2S	no	0	-	-------	--------
Rankinite	no	0.7	3.37	3.37	isolated pairs
Other Phases	no	0	-	-------	--------

be formed. In the CaO_x polyhedra behind those in the very surface, the repulsion forces are now no longer compensated. It remains a component directed into the original position of the exsolved Ca ion. If the empty and the occupied polyhedron share a face, the Ca ion will more easily follow this force than in the case of edge-sharing, and pass into the position of the formerly exsolved ion. The reason for this fact is that minor shifts of the atoms in the corners of a face than of the atoms limiting an edge are necessary to produce a hole of equal size between these atoms (Fig. 2).

Table 5

Linking of $Me^{II}O_x$ Polyhedra by Face-Sharing

Phase and coordination number of Me to oxygen	Reactivity	Shared faces per polyhedron	Mean distance between Me ions in shared polyhedra	Building units formed by face-shared polyhedra, literature
$Ba_2[SiO_4]$ 9.5	high	8.0	3.99Å	3-dimensional network (18)
$Ba_3O[SiO_4]$ 8.7	high	8.7	3.84	3-dimensional network (19)
$Sr_3O[SiO_4]$ 6.0	low	2.7	3.69	2-dimensional network (20)

In the new position, the Ca ion will be no longer fixed tightly because in this site the forces which the anions exert on it are partly shielded by protons. Thus it might leave the new site too and therefore the crystal at all. If the building units formed by face-shared CaO_x polyhedra are unlimited, this process will proceed. It is evident that 3-dimensional building units of this type are more effective than 2- or 1-dimensional ones.

Secondary Influences on Reactivity

It is known that the reactivity of reactive calcium silicates is influenced by kind and amount of the foreign oxides which they contain in solid solution and by their thermal history. Such influences are small in the case of C_3S, far more distinct in the case of C_2S and, therefore, the following remarks are referred to the latter.

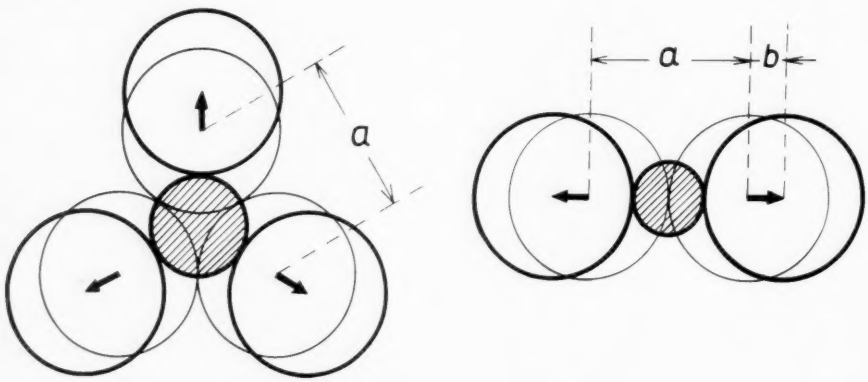

FIG. 2

Group of atoms forming an equilateral triangle of side length a and a line of length a. If these atoms move away from the centre of the triangle or line by an amount b, a void is formed (hatched). The diameter of the void is

$a(\frac{2}{3}\sqrt{3}-1) + 2b$ for the triangle

$2b$ for the line

Depending on the kind and amount of the foreign oxides which are solved in the C_2S crystals, the modifications α, α', or β may be stabilized. Moreover, in the case of α'-C_2S the foreign oxides give rise to various superstructures and modulations of the crystal structure (26), which also may influence the reactivity. An example: If one denotes the lattice parameters of α'_H-C_2S with a,b,c then $\alpha'_L C_2S$ generally has the lattice parameters a,b,3c (4,27), but with distinct contents of foreign oxide crystals with a unit cell of the size 4a,b,c (5) were observed.

The temperature at which a C_2S sample is fired and the rate with which it is cooled down may also influence the reactivity. The first one determines the highest possible concentrations of foreign oxides in solid solution and the multiplicity of twinning. The cooling rate determines the supersaturation, the size of twin areas, and probably the variance in the period of an eventually existing modulation.

Twinning results from the diminuation of the crystallographic symmetry at the transformations $\alpha \rightarrow \alpha' \rightarrow \beta$ according to hexagonal → orthorhombic → monoclinic. In the $\alpha'_H \rightarrow \alpha'_L$-transformation, a superstructure is formed. Generally, ordering to the superstructure begins in many parts of the crystal at the same time. When the growing superstructure areas meet together, with respect to their order, they will not always fit. They may be "out of phase." At high cooling rates, there is no time to correct such misfits by recrystallization. In Fig. 3, the processes of twinning and formation of domains are summarized.

An example of possible effects of supersaturation: If C_2S of composition $Ca_{1.8}Ba_{0.2}[SiO_4]$ is rapidly cooled down, one receives a very reactive α'-C_2S. If in contrast the same C_2S is cooled slowly, segregation into $Ca_{1.7}Ba_{0.3}[SiO_4]$ and $Ca_{1.9}Ba_{0.1}[SiO_4]$ takes place ($\alpha'_H + \alpha'_L$, ?) and the reactivity is far lower (28). In separate investigations, it was shown that for these differences in reactivity no effects of real structure were responsible.

An example of how twinning may operate on reactivity: When a C_2S with some foreign oxides in solid solution ("average belite" according to Table 9 in (29)) is cooled down from the stability range of the α'-modification, γ-C_2S is formed. When the same is done starting in the α-range, then β-C_2S is received. In the last mentioned case, 6-fold twinned β-C_2S crystals are formed in which the monocrystalline areas are obviously so small, that the probability to find an active

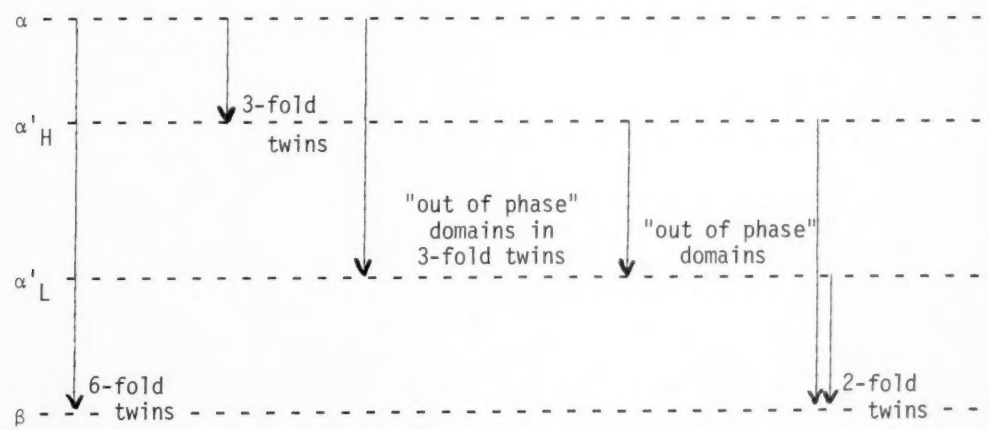

FIG. 3

Scheme of twinning and domain formation at the transformations of C_2S.

nucleus in them to allow for the $\beta \rightarrow \gamma$-transformation is low (30), whereas when only twofold twins are formed these areas seem to be large enough for the $\beta \rightarrow \gamma$-transformation.

On the Reactivity of Aluminates and Ferrites

Finally, the question whether the reactivity of the aluminate and ferrite phases in clinker may be explained by the same principles as those ones developed for the calcium silicates shall be considered. Obviously, these principles may be valid only in parts. In C_3A and $C_2(A,F)$ indeed there are 3- and 1- dimensional networks of CaO_x polyhedra linked by face-sharing, respectively (crystal structures in (31) and (32)). But in the reaction with water the cyclohexaaluminate and polyferritoaluminate anions take part also. That the latter point - AlO_4 or FeO_4 groups which are joined together by common vertices - is sufficient to make a phase reactive can be seen in the case of CA_2. In its structure there are no building units of face-shared CaO_x polyhedra, but there are infinite networks of vertex-shared AlO_4 tetrahedra (33)), and it is reactive (34).

Acknowledgements

In the calculations of interatomic distances and for limiting the coordination spheres, the programs CPA 12 (H. Schrauber) and WIRBER (W. Fischer) were used.

References

1. Lin-gun Liu. Phys. Chem. Minerals 3, 291 (1978).
2. N.I. Golovastikov, R.G. Matveeva & N.V. Below. Kristallografija 20, 721(1975).
3. S. Udagawa & K. Urabe. Semento Gijutsu Nempo 32, 35 (1978).
4. S. Udagawa, K. Urabe, T. Yano & M. Natsume. Semento Gijutsu Nempo 33, 35 (1979).
5. H. Saalfeld & K.H. Klaska, Z. Krist. 155, 65 (1981).
6. K.H. Jost, B. Ziemer & R. Seydel. Acta Cryst. B33, 1696 (1977).
7. R. Czaya. Acta Cryst. B27, 848 (1971).
8. Sh. Saburi et al. Mineralogical J. 8, 240 (1976).
9. H.F.W. Taylor. Mineral. Mag. 38, 26 (1971).
10. T. Yamanaka & H. Mori. Acta Cryst. B37, 1010 (1981).
11. F.J. Trojer. Z. Kristallogr. 130, 185 (1969).
12. F.J. Trojer. Z. Kristallogr. 127, 291 (1968).
13. J.W. Jeffery. Thesis, London: 1950.
14. C.M. Midgley. Acta Cryst. 5, 307 (1952).
15. H. O'Daniel. Zement, Kalk, Gips 10, 166 (1957).
16. D.K. Smith, A.J. Majumdar & F. Ordway. Acta Cryst. 18, 787 (1965).
17. V.V. Iljuchin, N.N. Nevskij & R.A. Chauri. Doklady Akad. Nauk SSR 237, 834 (1977).
18. H.P. Grosse & E. Tillmanns. Cryst. Struct. Comm. 3, 599 (1974).
19. E. Tillmanns & H.P. Grosse. Acta Cryst. B34, 649 (1978).
20. L.S. Dent-Glasser & F.P. Glasser. Acta Cryst. 18, 453 (1965).
21. I. Odler & J. Schüppstuhl. Cem. Concr. Res. 12, 13 (1982).
22. I. Jelenic, A. Bezjak & M. Bujan. Cem. Concr. Res. 8, 173 (1978).
23. J. Bensted. Cem. Concr. Res. 8, 73 (1978).
24. C. Tashiro, H. Yamada, T. Akiba & S. Navata. Cem. Concr. Res. 6, 633 (1976).
25. H. Schubert. Thesis, Berlin: 1974.
26. H. Saalfeld. Z. Krist. 133, 396 (1971).
27. H. Saalfeld. Amer. Miner. 60, 824 (1975).
28. B. Ziemer & G. Oliew. Silikattechnik 33, 176 (1982).
29. G. Yamaguchi & S. Takagi. Proc. V. Int. Symp. Chemistry of Cement, Tokyo, 1968, Vol. I, p. 210.
30. N. Yannaquis & A. Guinier. Bull. Soc. France Mineral. et Crist. 82, 126(1959).
31. P. Mondal & J.W. Jeffery. Acta Cryst. B31, 689 (1975).
32. A.A. Colville & S. Geller. Acta Cryst. B27, 2311 (1971).
33. V.I. Ponomarev, D.M. Cheiker & N.V. Belov. Kristallografija 15, 1140 (1970).
34. M. Jung. Proc. IV. Conf. on Refractory Concretes. Karlovy Vary, 1971.

VOL. 14 1984

CEMENT and CONCRETE RESEARCH. Vol. 14, pp. 185-194, 1984. Printed in the USA.
0008-8846/84 $3.00+00. Copyright (c) 1984 Pergamon Press, Ltd.

A CLASSIFICATION OF INORGANIC AND ORGANIC ADMIXTURES BY CONDUCTION CALORIMETRY

C R Wilding, A Walter and D D Double
Department of Metallurgy and Science of Materials
University of Oxford, Parks Rd, Oxford, OX1 3PH, England

(Communicated by C.D. Pomeroy)
(Received June 9, 1983)

Abstract

A wide range of inorganic and organic admixtures have been investigated using isothermal conduction calorimetry. The results are presented as a series of maximum rate of heat evolution ($\dot{Q}_{max}$) versus reciprocal to peak height ($1/t_{max}$) plots. Using equivalent molar concentrations of admixture under controlled conditions a comparative ranking system of inorganic and organic admixtures has been devised. Some general conclusions are drawn about the mechanism of action of accelerating and retarding admixtures.

Introduction

Heat liberation during the hydration of Portland cement containing accelerating and retarding admixtures has been studied previously by the use of conduction calorimetry. Stein (1) and Edwards and Angstadt (2) concluded that accelerators do not promote the hydration of the C_3A but predominantly accelerate hydration of the C_3S phase of Portland cement. Edwards and Angstadt (2) suggested that both cations and anions may be ranked according to their general effectiveness as accelerators for cement viz.

$$Ca^{2+} > Mg^{2+} > Li^{+} > Na^{+} > H_2O \gg Zn^{2+}$$

$$OH^{-} > Cl^{-} > Br^{-} > NO_3 > SO_4^{2+} \sim H_2O \gg CH_3CO_2^{-}$$

Murakami and Tanaka (3) used adiabatic calorimetry to rank various inorganic admixtures for cement and obtained the following sequence for anions:

$$Cl^{-} > S_2O_3^{2-} > SO_4^{2-} > NO_3$$

$$Cl^{-} > Br^{-} > I^{-}$$

and for cations as:

$$Ca^{2+} > Mg^{2+} > Na^{+}$$

Kondo et. al. (4) investigated the effect of chlorides and potassium salts on alite by conduction calorimetry. Kantro (5) undertook an extensive study of C_3S

hydration in the presence of various salts at equivalent molar concentrations and at different temperatures by means of conduction calorimetry. He examined variations in peak height and integrated heat as an indication of accelerated/retarded hydration. He divided admixtures into four groups in terms of those with anions that formed soluble/insoluble calcium salts and those with cations that formed hydroxides with greater or lower solubility than calcium hydroxide. Kantro found broad agreement in the ranking of cations with the work of Collepardi et al (6) who studied the rate of hydration of C_3S. Their results indicated that cations decreased in accelerating effect in the order:

$$Ca^{2+} > Sr^{2+} > Ba^{2+} > Li^{+} > Na^{+} > K^{+}.$$

Taplin (7) investigated the effect of a number of organic admixtures on the setting of Portland cement. The extent of the hydration was determined by a method which involved measuring the ignition loss of a paste previously dried in an atmosphere of steam at 125°C. He concluded that the hydroxycarboxylic groups appeared to be particularly active in producing retardation. Skalny and Young (8) reported that Milestone (unpublished data) using conduction calorimetry had obtained good qualitative agreement with Taplins findings.

Previte (9) studied the effect of various saccharide compounds using isothermal calorimetry. Previte in classifying the effectiveness of saccharides took the end of the induction period as an indication of the initial setting time. He showed that the set retardation efficiency was related to molecular weight and stability of the saccharide in the alkaline environment of hydrating cement. Thus for example, raffinose and sucrose were shown to be very effective retarders but fructose and ribose had a very minimal effect.

Yamamoto (10) investigated the effect of a large number of organic admixtures on the setting of Portland cement using the Procter needle penetration method. His conclusions were similar to those of Taplin (7).

A variety of different methods have been used to categorise admixtures, in some cases in terms of the physical process of setting (e.g. by Procter needle test), in others in terms of the chemical hydration rate (e.g. by calorimetry). Different parameters have been used to define the degree of acceleration or retardation and often a comparison between the relative effectiveness of the admixtures has been made difficult by the use of different conditions of hydration (different w/c ratios, different temperatures, weight percentage additions of admixtures rather than molar proportions, etc.).

In the present work a systematic survey of a wide range of admixtures is presented using conduction calorimetry as the quantitative basis, under controlled conditions which allows comparative assessments to be made. The purpose is to arrive at a pattern of effect between cations and anions in inorganic admixtures and between chemically similar groupings in organic admixtures which may provide insight into the way in which these admixtures modify the hydration chemistry and thus the setting and hardening of cement.

Experimental Methods

(a) Materials

Two samples of commercial Blue Circle OPC Northfleet were used which had the following Bogue compositions:

Cement A:	C_3S: 59.6%	C_2S: 11.8%	C_3A: 8.3%	C_4AF: 8.8%
Cement B:	C_3S: 54.1%	C_2S: 15.7%	C_3A: 9.1%	C_4AF: 9.7%

VOL
14
198

(b) Conduction Calorimetry

Heat evolution profiles from hydrating cement were obtained from a 'Calox' conduction calorimeter which had the facility to bring water into contact with the cement (after temperature equilibration) by suction under vacuum. The method gave a rapid and efficient mixing of cement and water and allowed heat evolution to be measured directly from time zero. The rate of heat evolution was determined by measuring the output voltage from thermoelectric sensors and subsequent calibration applying Tians equation (11). A water/cement ratio of 0.5 was used, the admixture being dissolved in distilled water prior to mixing with the cement. Hydration was carried out at 27°C.

(c) Presentation of results

The calorimetric curve for Portland cement has the characteristic shape shown in figure 1, with an initial exotherm within the first 10 minutes of hydration followed by an induction period lasting some 1½ - 3 hours. The acceleration stage after the induction period reaches a maximum after about 8 to 10 hours under normal conditions and thereafter decreases slowly.

Admixtures can affect the form of the curve in various ways. In general, an accelerator shortens the induction period and produces an earlier heat peak with a corresponding increase in height of the maximum rate of heat evolution. A retarder has the reverse effect (figure 2).

On the basis of calorimetry various methods have been used by other authors to categorise accelerators and retarders. These have involved measurements of the maximum rate of heat evolution ($\dot{Q}_{max}$) and measurement of total heat evolved i.e.

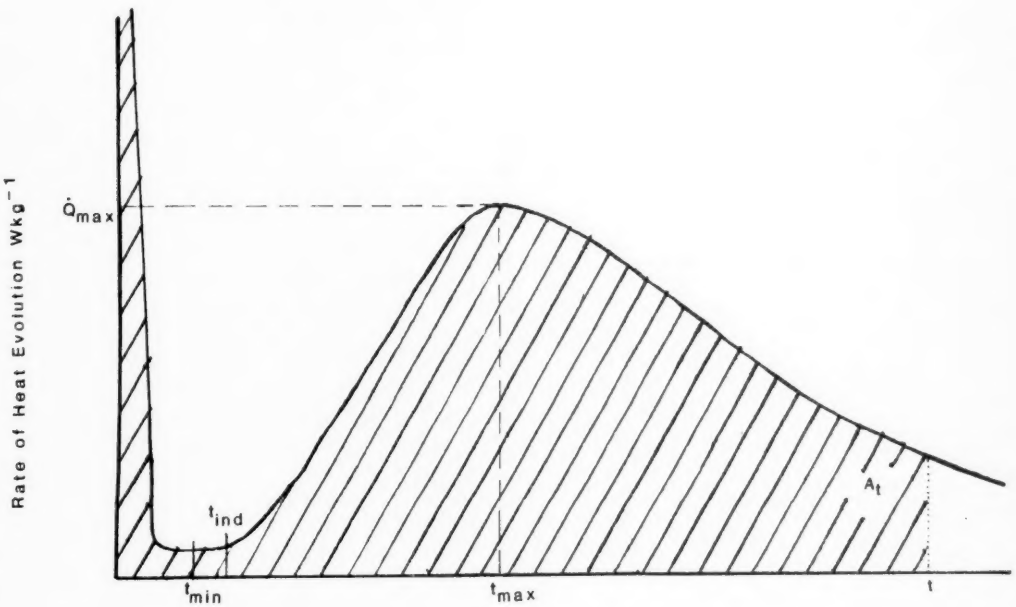

FIG. 1.

Characteristic calorimetric curve

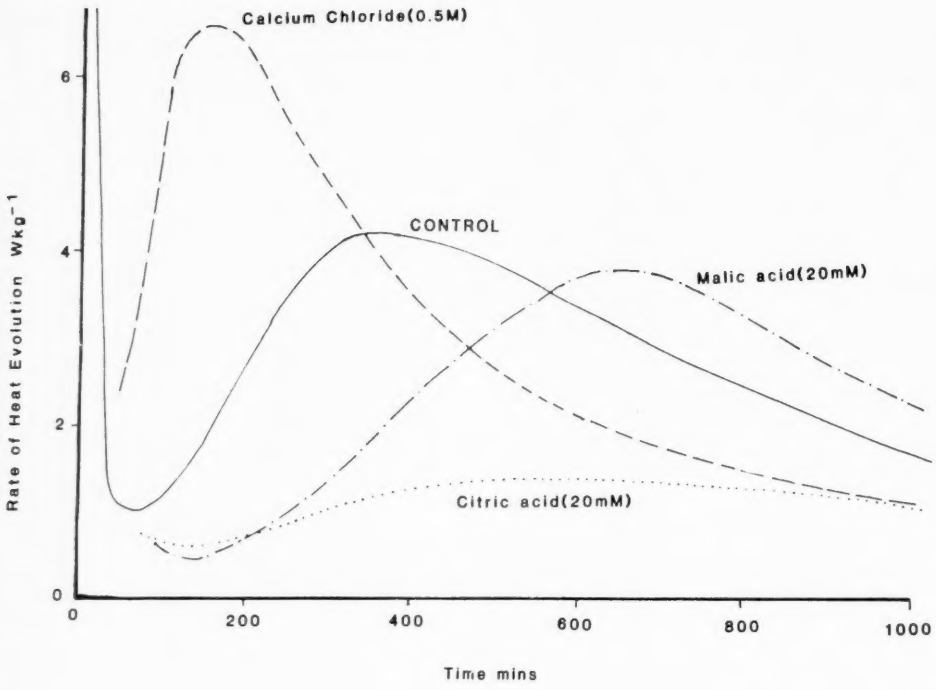

FIG. 2

Influence of admixtures on the calorimetric curve

the integrated area A_t. Also, measurement of time taken to reach the induction period minimum (t_{min}) and time to reach the maximum in the second isotherm (t_{max}).

In our studies we will present results as a series of graphs of the maximum rate of heat evolution ($\dot{Q}_{max}$) against the reciprocal of the time elapsed from the start of the experiment to the maximum in the second isotherm ($1/t_{max}$). This method of presentation allows the variations in the form of the second heat evolution (changes in time to peak height and maximum rate of heat evolution) to be clearly expressed. Since an accelerator tends to shorten the induction period and 'sharpen' the second heat peak accelerating admixtures can be expected to appear at greater values of $\dot{Q}_{max}$ and $1/t_{max}$. Retarders have the opposite effect. As will be shown in a subsequent paper kinetic laws expressing the rate of hydration of cement (Avrami equation) predict a proportional dependence between $\dot{Q}_{max}$ and $1/t_{max}$ (LeSueur and Double).

Results

Figure 3 shows the merits of this method of presentation. Admixtures are separated along a roughly diagonal relationship according to their accelerating (top right) or retarding (bottom left) capacity relative to the untreated controls. Calcium chloride is clearly shown as a good accelerator with an effectiveness that increases with concentration. In this work, the maximum amount of $CaCl_2$ used was 1M in aqueous solution which would correspond to 5.5 wt% relative to dry cement.

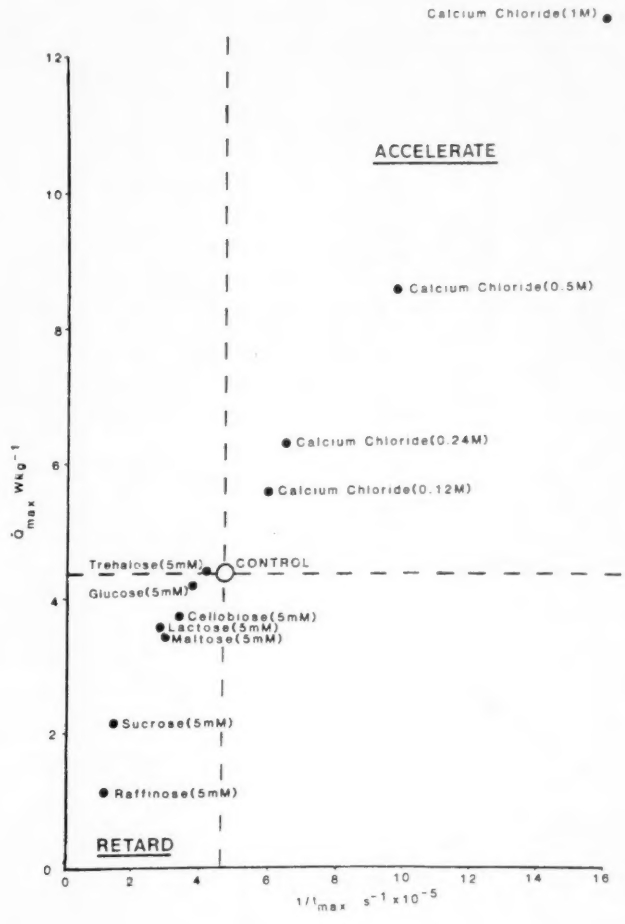

FIG. 3.
$\dot{Q}_{max}$ versus $1/t_{max}$ plot for calcium chloride and saccharide additions to OPC. (Cement A)

Amongst the saccharide admixtures, raffinose and sucrose appear as the most effective chemical retarders for cement, on an equivalent molar basis. Considerably smaller concentrations of the saccharides are required to produce significant retardation (compared with inorganic salts) and at 5mM concentration the retarding effectiveness of the saccharides may be represented in the following ranking order:

Raffinose $>$ Sucrose $\gg$ Maltose, Lactose $>$ Cellobiose $>$ Glucose $>$ Trehalose

In comparing inorganic salt admixtures, problems arise from the fact that both the cation and the anion may be effective to varying degrees in modifying the rate of hydration of cement. In order to rank cations and anions separately according to their accelerating or retarding strength, it is necessary to keep the concentration of the counter-ion constant. Thus, as figure 4 shows, the calorimetric system applied to cements treated with chlorides and nitrates (at concentrations of 1g ion/litre with respect to the anion) gives approximately the following ranking sequence for cations

$$\tfrac{1}{2}Ca^{++} > \tfrac{1}{2}Ni^{++} > \tfrac{1}{2}Ba^{++},\ \tfrac{1}{2}Mg^{++} > \tfrac{1}{3}Fe^{+++},\ \tfrac{1}{2}Cr^{++} > \tfrac{1}{2}Co^{++} > \tfrac{1}{3}La^{+++}$$
$$\gg NH_4^+,\ K^+ > Li^+ > Cs^+ > Na^+$$
$$\longleftarrow \text{acceleration}$$
$$\tfrac{1}{2}Cu^{++} > \tfrac{1}{2}Zn^{++} > \tfrac{1}{2}Pb^{++}$$
$$\text{retardation} \longrightarrow$$

In general, as can be seen from figure 4, for a given cation the chloride proves a more powerful accelerator than the nitrate. However, attempts to rank anions in a similar fashion are less successful. Figure 5, for example, shows the effect of varying the anion for a range of sodium salts and a range of cobalt salts at an equivalent anion concentration of 1 g ion/litre. The positions of the different anions are more closely bunched together in the plot of $\dot{Q}_{max}$ versus $1/t_{max}$ and the order of their effectiveness seems to depend on the identity of the cation.

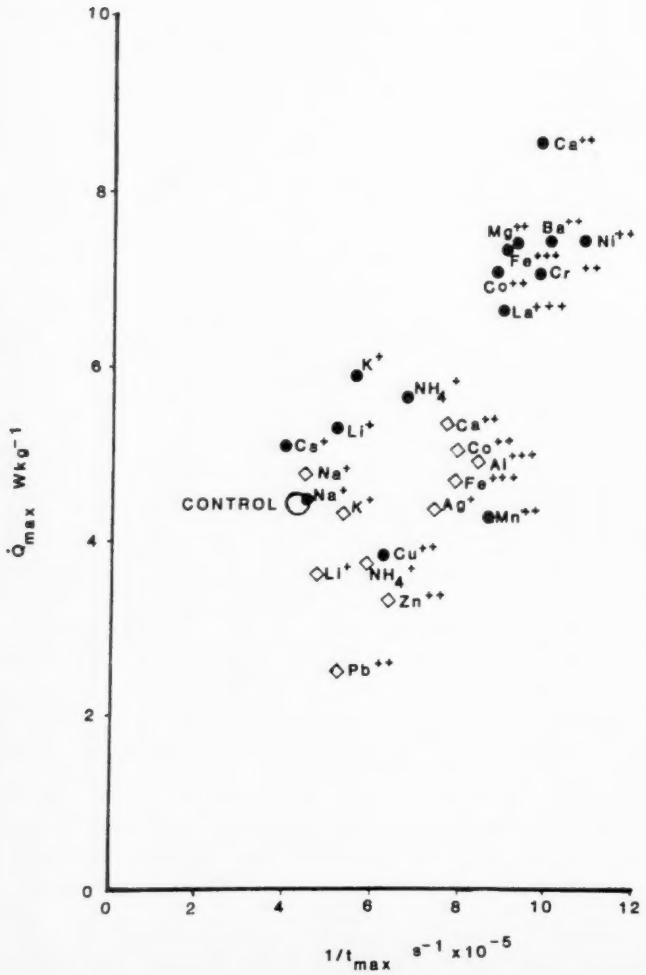

FIG. 4.
$\dot{Q}_{max}$ versus $1/t_{max}$ plots for cations at equivalent chloride and nitrate concentrations (1 g ion/litre). ● chlorides ◇ nitrates (Cement A).

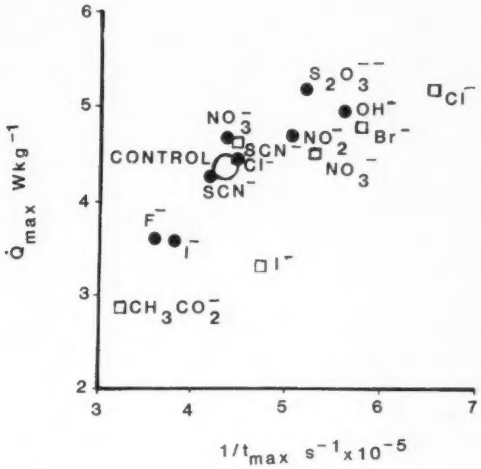

FIG. 5.
$\dot{Q}_{max}$ versus $1/t_{max}$ plots for (a) a range of sodium salts •(Cement A) (b) a range of cobalt salts □ (Cement B) at equivalent anion concentration of 1 g ion/litre.

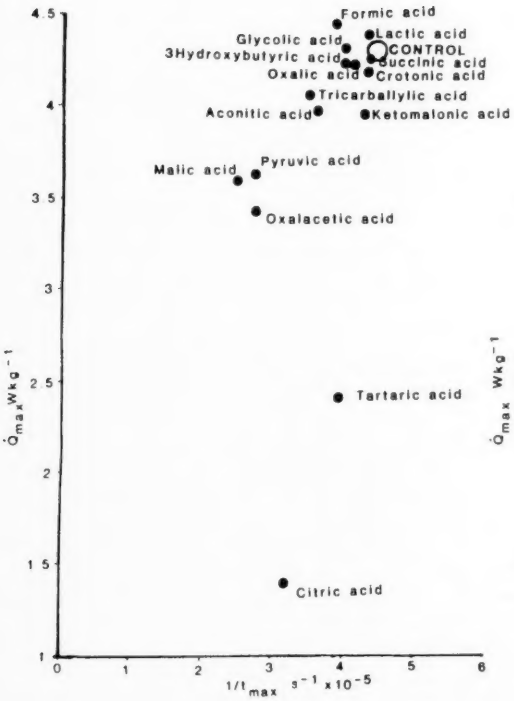

FIG. 6
$\dot{Q}_{max}$ versus $1/t_{max}$ plots for a range of aliphatic organic admixtures (Cement B)

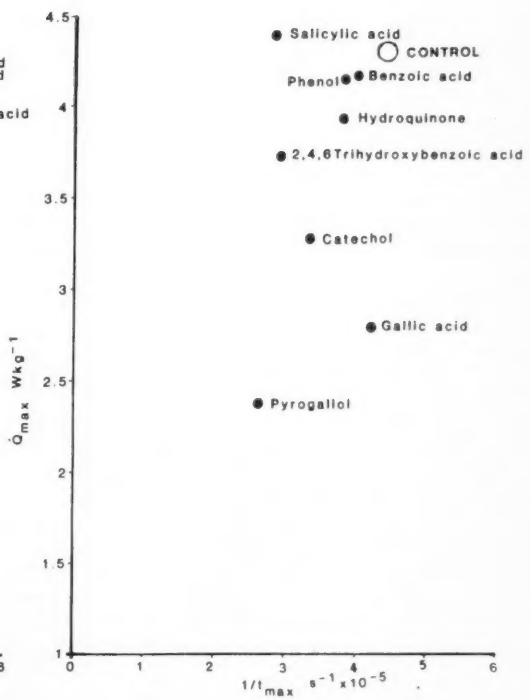

FIG. 7.
$\dot{Q}_{max}$ versus $1/t_{max}$ plots for a range of aromatic admixtures (Cement B)

Figures 6 and 7 show the same system applied to a range of aliphatic and aromatic admixtures used at a concentration of 20mM. The hydroxycarboxylic acids, citric acid and tartaric acid, stand out as powerful retarding agents whilst the lower molecular weight and simpler carboxylic acids such as oxalic acid and formic acid have relatively little effect. Amongst the aromatic admixtures a clear sequence of retarding effectiveness occurs from pyrogallol down to benzoic acid and phenol, the retarding power being associated with variations in the number and configuration of the hydroxyl and carboxylic groups around the benzene ring (see Appendix 1).

Discussion

In general, the method presented here of ranking inorganic salts according to their accelerating and retarding ability gives broadly similar ranking systems of the ionic constituents as those obtained by other researchers. The importance of calcium in the ranking system is evident but other polyvalent cations can have similar accelerating strength at appropriate concentrations. Monovalent and alkali metal cations seem only weakly effective. Attempts to rationalise the ranking system, for example in terms of the relative diffusivities of the ions (4) have generally proved inconclusive. For cations, problems arise in determining the configurations of the ionic species which in the highly alkaline environment of a cement paste (pH 12-13) will mostly be in a hydroxylated state in solution (viz $Ca(OH)^{+}$) or immediately precipitated as insoluble hydroxide. As discussed by Kantro (5) the relative solubilities of the hydroxides formed by the cations are likely to be an important factor. Studies of Pb and Zn salts show that retardation is associated with the precipitation of dense and impermeable coatings of hydroxide gel around the cement grains, Thomas et al (12), Arliguie et al (13). Double (14) has drawn attention to similarities in the ranking of ions in terms of their accelerating efficiency and the lyotropic ranking sequence of ions (the Hoffmeister series) which relates to the efficacy of flocculation of hydrophilic colloids by dissolved electrolytes. Essentially, the hydration of cement is seen as being controlled by diffusion of water and solute species through protective colloidal C-S-H gel coatings precipitated at very early stages around the cement grains. The rate of hydration depends on the permeability and cohesion of these coatings. Modification of the colloidal gel to a more open flocculated structure facilitates diffusion and accelerates hydration. Conversely, coagulation of the coating to a denser, less permeable and more adhesive layer results in retardation of hydration.

For the most part, organic admixtures act as retarders of cement hydration. In the aliphatic acids there is a general increase in retarding effectiveness with molecular weight but the important factor, as has been pointed out by previous researchers (see Skalny et al (8)), appears to be the presence of α- or β-hydroxycarboxylic configurations that are capable of strongly chelating a metal cation, such as Ca^{++}. In the aromatic admixtures the number and positioning of the hydroxyl groups is important (molecules with adjacent hydroxyl groups seem most effective as retarders) and again this can be related to their capacity for complexing calcium (15, 16). Saccharides are also capable of binding calcium, but in this case their chemistry in relation to cement hydration is complicated by their susceptibility towards degradation by alkaline hydrolysis. Sucrose and raffinose are relatively stable in this respect, and this factor is probably associated with their greater effectiveness as retarders for cement. Studies of the aqueous solution chemistry of cement have shown that abnormally high concentrations of silicon initially appear in solution with cements treated with retarders such as EDTA, citric acid and sucrose and this is associated with the preferential sequestration of calcium by the admixture (17). Additional factors such as the complexation of silicate (or aluminate) may also be important.

VOL. 14 1984

Citric acid and catechol, for example, in addition to their ability to complex calcium are also capable of complexing silica. This factor has been cited as the cause of promoted attack on silica glass in neutral and alkaline solutions containing dissolved organic species (18, 19). Although no complete explanation is available for the effect of organic admixtures, the general conclusions are that the chemistry of precipitation of C-S-H gel is altered by preferential complexation of Ca and/or silicon either in solution or by incorporation into the precipitated gel. The result is the formation of less permeable and more adhesive gel coatings around the cement grains, resulting in a retardation of hydration.

Acknowledgements

The authors gratefully acknowledge the Science and Engineering Research Council and Cormix Ltd for financial support. Thanks are also due to Miss S Rodger of the Dept of Metallurgy and Science of Materials, Oxford, for useful discussions.

References

1. H N Stein, J. Appl. Chem. 11, 474, 1961.
2. G C Edwards, R L Angstadt, J. Appl. Chem. 16, 166, 1966.
3. K Murakami, H Tanaka, Proc. 5th Int. Conf. on the Chemistry of Cement, II-2, 422, 1968.
4. R Kondo, M Daimon, E Sakai and H Ushiyama, J. Appl. Chem. Biotechnol. 27, 191, 1977.
5. D L Kantro, ASTM Jnl. of Test. and Eval. 312, 1975.
6. M Collepardi, G Rossi, M C Spiga, Annali di Chimica 61, No. 2, 137, 1971.
7. J H Taplin, Disc. of Paper by H E Vivian, Proc. Int. Symp. Chem. Cem. 3rd Washington DC (1960); Nat. Bur. Stand. (US) Monogr. 43, 924, 1962.
8. J Skalny, J F Young, Proc. 7th Int. Cong. Chem. Cem. Paris Vol I, 1980.
9. R W Previte, Cem. Concr. Res. 1, 301, 1971.
10. Y Yamamoto, Nat. Tech. Inf. Serv. Springfield, Virginia 22151, Report No. JHRP-51-72.
11. A Tian, Soc. Chim. de France, Vol. 33, No. 4, 1923.
12. N L Thomas, D A Jameson and D D Double, 1981, Cem & Concr Res, 11, 143.
13. G Arliguie, J P Ollivier and J Grandet, 1982, Cem & Concr Res, 12, 79.
14. D D Double, 1983, Proc Royal Soc Meeting for Discussion 'Technology in the 1990's - Developments in the Science and Technology of Hydraulic Cements (in press).
15. J A Rendleman, 1966, Adv Carbohydrate Chem, 21, 209.
16. S J Angyal, 1980, Chem Soc Rev, 4, 9.
17. N L Thomas and D D Double, 1983, Cem & Concr Res, 13, 391.
18. F M Ernsberger, 1959, J Amer Ceram Soc, 42, No. 8, 373.
19. F R Bacon and F C Raggon, 1959, J Amer Ceram Soc, 42, No. 4, 199.

OL.
14
984

Appendix 1

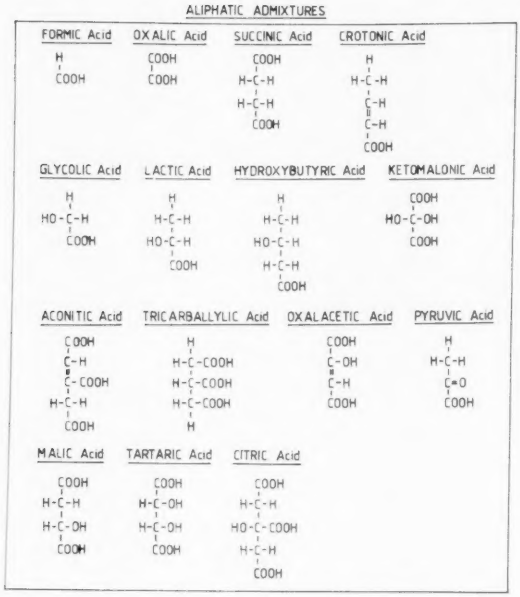

1A

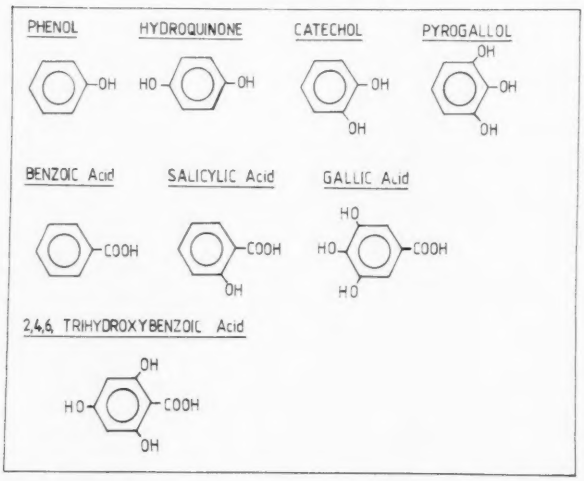

1B

VOL 14 198

CEMENT and CONCRETE RESEARCH. Vol. 14, pp. 195-198, 1984. Printed in the USA.
0008-8846/84 $3.00+00. Copyright (c) 1984 Pergamon Press, Ltd.

X-RAY MAPPING - A SUPPLEMENTARY TOOL IN CLINKER PHASE CHARACTERIZATION

S.L. Sarkar*
Department of Geology and Mineral Sciences
University of Ilorin
Ilorin, Nigeria

(Refereed)
(Received June 13, 1983)

VOL. 14 1984

ABSTRACT

X-ray mapping of selective elements under the SEM (fitted with an EDS), helps to establish the actual distribution and location of minor elements in a clinker. From these maps K-rich belite and MgO (periclase) grains were observed. The existence of alkali sulphate could also be established. The distribution of Ti was restricted to the alite lattice.

INTRODUCTION

X-ray mapping of selective elements was found particularly useful as a supplementary tool in the course of quantitative microanalysis of Portland cement clinkers by SEM-EDS. The electron probe is known for its lateral spread on impingement with the specimen being examined. In addition, the small size of grains (<5μm), especially the interstitial matrix phases in cement and clinker, is liable to generate spurious x-ray peaks of adjoining grains and/or inflate the existing peak heights.

METHOD

The principle and a suitable method of x-ray dot imaging under the SEM has been described earlier (1). Experience shows that the slower the scan rate (depending on the design of the instrument), the greater the density of x-ray dots. For the present series of x-ray maps on a JEOL 500 SEM, a scan rate of 500 secs was found acceptable for all the elements, except for Si and Ca. Owing to the high concentration of Si in comparison to the other minor elements mapped, a faster rate (250 secs) was adopted. This precludes to a large extent the possibility of imaging the x-ray dots arising from the high background.

*Study carried out at The Pennsylvania State University.

RESULTS AND DISCUSSION

The importance of this method in relation to the elemental distribution in a clinker is now briefly described.

A few interesting observations were made from the results of a series of quantitative analyses of clinkers:

(a) some belite grains appeared to contain high amounts of both K and S (up to 2%* and 1%*, respectively) whereas in others only K concentration was high. Concentration of K and S was noticeably lower in alite grains.

(b) on occasions the Mg content in the interstitial matrix, particularly the aluminoferrite phase) was rather high (up to 4%*).

(c) Ti was found to be concentrated (up to 1.5%*) only in the alite grains.

X-ray mapping of Si, Al, K, S, Mg and Ti were performed to ascertain whether K, S, Mg and Ti are genuine minor inclusions in the lattices, with Si and Al or Fe x-ray maps to assist in the process of distinguishing between the alite, belite and interstitial phases (Figs. 1a-f).

From the K and S maps (Figs. 1a, b) it can be established that some amount of K is definitely incorporated in a few belite lattices. These are the K-rich belites (2). These two maps (K and S) also indicate from their distribution pattern in the clinker the existence of some grains containing K, S and Ca (the x-ray map for Ca has not been included for the monotonous and fairly even nature of its distribution). These grains could be calcium langbeinite ($C_2K\bar{S}_3$)**, as suggested by (3) or syngenite, $CK\bar{S}_2H$ (4). According to Jawed and Skalny (3), there is a preferential formation of double alkali sulphate in the case of K. Taylor (4) suggested that long storage can lead to the formation of $KC\bar{S}_2H$.

Mg was found to be located in regions devoid of any other elements (Fig. 1c), suggesting that these are MgO crystals. This is interesting because Mg^{+2} is believed to replace Ca^{+2} in the alite lattice (2), but there is no evidence of preferential enrichment in alite from the x-ray map.

Ti is distributed in the alite grains (Fig. 1d). Since it is possible for Al^{+3} and Fe^{+3} to substitute for either Ca^{+2} or Si^{+4} in the alite lattice (2), it is likely that Ti^{+4} also replaces either Ca^{+2} or Si^{+4}.

CONCLUSIONS

From the x-ray maps of Si and Al at a slow scan rate, visual representation of the morphology of major phases in a clinker were obtained. Still slower scan rate yielded the distribution of some minor elements in the clinker. K was found to be incorporated in the lattice of some belite grains. K sulphate grains, whose exact composition could not be determined from empa were also located. Mg was present as MgO crystals, while Ti was distributed only in the alite lattice. It was observed that very little inadvertent inclusion of elements from neighboring grains occurred during the course of quantitative analysis, except for Mg in the aluminoferrite phase, and K and S in the belites, the former probably due to the small size of the grains. Other minor elements (Na and P) could not be mapped, though they were present in the clinker, because the low concentration of these elements (<1%) was below the detection capability of the mapping procedure.

---

*by weight percent

**cement chemists' notation: C=CaO. S=SiO_2 K=K_2O, $\bar{S}$=SO_3, H=H_2O

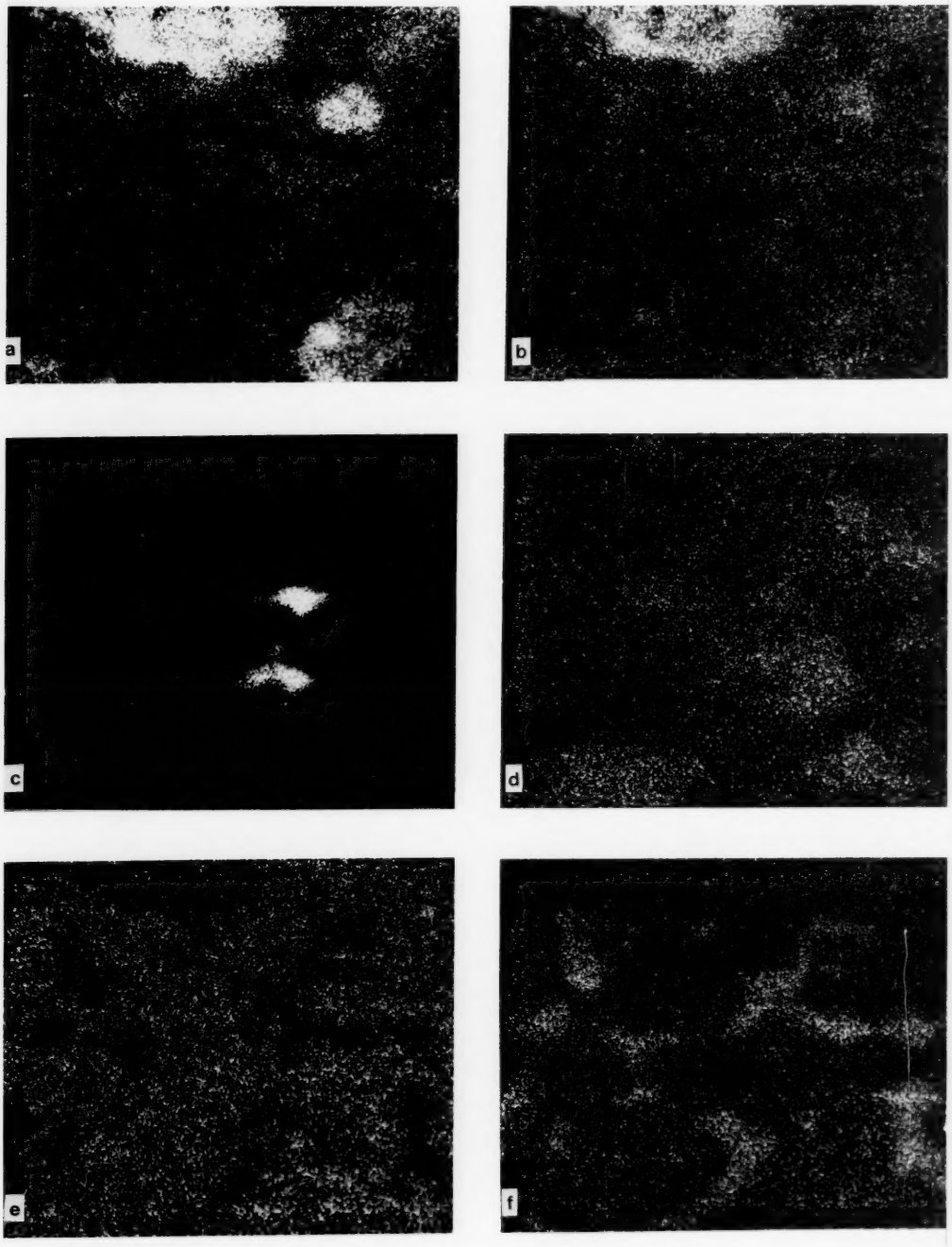

FIGURE 1
X-ray maps of some elements in a clinker. (a) K, (b) S, (c) Mg, (d) Ti, (e) Si, (f) Al. (e) and (f) were used to delineate the grain boundaries of different phases.

VOL.
14
984

ACKNOWLEDGEMENTS

The author wishes to thank Professor D.M. Roy, Materials Research Laboratory, The Pennsylvania State University, for allowing him the facilities, and to the University of Ilorin for financial assistance and leave. This work was supported by NSF grant CPE-8112821.

REFERENCES

1. P. Barnes, N.T. Moore and S.L. Sarkar, X-ray Spect., 1 (3), 145 (1978).
2. M. Regourd and A. Guinier, Proc. VIth Int. Conf. Chem. Cem., Moscow, USSR (1974).
3. I. Jawed and J. Skalny, Cem. Concr. Res., 7(6), 719 (1977).
4. W.C. Taylor, J. Res. NBS, 21, 315 (1938).

VOL
14
198

CEMENT and CONCRETE RESEARCH. Vol. 14, pp. 199-206, 1984. Printed in the USA.
0008-8846/84 $3.00+00. Copyright (c) 1984 Pergamon Press, Ltd.

HYDRATATION DES CIMENTS EXPANSIFS-CORRELATION ENTRE L'EXPANSION ET LA FORMATION DES HYDRATES.

P. CLASTRES, M. MURAT
Laboratoire des Bétons et Structures et Laboratoire de Chimie-Physique Appliquée et Environnement. Institut National des Sciences Appliquées de LYON. 69621 VILLEURBANNE CEDEX - FRANCE -
A. BACHIORRINI
Istituto di Chimica Generale e Applicata
Politecnico di TORINO - ITALIA -

VOL.
14
1984

(Communicated by M. Regourd)
(Received June 27, 1983)

ABSTRACT

The simultaneous study of both expansion and formation of hydrates up to 10,000 hours (≃ 400 days) during the hydration of two industrial "type M" expansive cements containing calcium sulfate as gypsum or anhydrite allows to point out that the expansion is delayed in the sample containing anhydrite and that only the expansion at short curing time (10-1,000 hours) can be attributed to the formation of colloïdal ettringite. The formation of monosulfoaluminate was never detected.

L'étude simultanée de l'expansion et de la formation des hydrates jusqu'à 10 000 heures (soit 400 jours environ) lors de l'hydratation de deux ciments expansifs industriels de type "M" contenant initialement le sulfate de calcium sous forme de gypse ou d'anhydrite permet de montrer que le gonflement est retardé dans l'échantillon contenant l'anhydrite et que l'attribution de l'expansion à la formation d'ettringite colloïdale ne peut concerner que les faibles échéances (10 à 1000 heures). A aucun moment n'a pu être mise en évidence la formation de monosulfoaluminate.

Introduction

Les résultats présentés ci-après ont été obtenus dans le cadre d'un travail plus général orienté vers l'étude du comportement mécanique du béton armé expansif, matériau pouvant être utilisé pour limiter, voire supprimer la fissuration du béton armé traditionnel.

Les théories concernant l'expansion des ciments expansifs sont nombreuses et contradictoires. En faisant un bilan rapide de l'étude bibliographique

(1 à 6), nous pouvons tirer quelques points d'accord et de nombreux points de désaccord, ce qui nécessitera, pour les éliminer, de nombreuses études complémentaires.

1. Quelques points d'accord :

Lors de l'hydratation des ciments expansifs, comme pour les ciments portland, l'ettringite est le premier hydrate à se former, et cela dès le malaxage.

Pour que l'ettringite formée soit "expansive", il est nécessaire que la phase liquide soit saturée en chaux.

L'expansion peut se poursuivre alors que la quantité d'ettringite cristalline formée (décelable par diffraction des rayons X) reste stable, voire diminue.

L'ettringite intervient dans la résistance de la pâte de ciment.

La "mécanique" de l'expansion des ciments à retrait compensé ou expansifs rencontre un large assentiment : il est nécessaire que l'ettringite ne se produise pas trop tôt car alors l'expansion se fait "à vide", la pâte de ciment étant trop déformable. L'expansion n'apparaît que lorsque la structure de la pâte a atteint un niveau suffisant de résistance mécanique.

Le type de conservation ou de cure du béton a une importance primordiale sur le taux d'expansion.

2. Les points de désaccord portent sur :

La nature de l'hydrate expansif : mono ou trisulfoaluminate.

Les conditions de formation de l'ettringite : hydratation avec ou sans dissolution préalable.

L'état de cristallisation de l'ettringite formée (ettringite cristalline ou amorphe) ainsi que la dimension des grains.

La cause de l'expansion : pression due à une transformation à l'état solide, à la croissance cristalline, à des forces osmotiques, à des forces de répulsion d'origine électrique.

De nombreux points restent donc à élucider dans le domaine des ciments expansifs. Les expérimentations rapportées ci-après sont une contribution, parmi d'autres, à une meilleure connaissance des phases hydratées formées et du processus d'expansion.

Etude de l'expansion de deux ciments expansifs

Nous avons utilisé pour nos essais, deux ciments à retrait compensé de type M produits en EUROPE (7), l'un en 1975 (CIMENT A), conservé dans des récipients étanches depuis, mais présentant les caractéristiques de l'éventement (hydratation de la chaux libre en $Ca(OH)_2$ et légère carbonatation de celle-ci - prise plus lente (8)), l'autre en 1981 (CIMENT B).

Ces deux ciments diffèrent du point de vue de leur composition minéralogique, essentiellement de part la présence de gypse dans le ciment A, d'anhydrite dans le ciment B.

Nous avons confectionné une pâte pure de rapport $\frac{E}{C} = 0,27$ par malaxage pendant cinq minutes dans un malaxeur de type RILEM puis nous avons avec cette pâte, réalisé en parallèle des essais d'expansion, de mesures de résistances mécaniques, d'analyse par diffraction X et A.T.D. afin de déterminer l'évolution des différentes phases en fonction du temps. Les éprouvettes de pâte pure ont été dans tous les cas conservées à 18°C sous l'eau.

VOL.
14
1984

1. Essais d'expansion :

Ils ont été effectués à l'aide d'aiguilles de LE CHATELIER de 0,5 mm d'épaisseur. C'est un essai d'expansion légèrement contrainte mais des travaux antérieurs ont montré que l'épaisseur de l'anneau n'affectait que la valeur de l'expansion et non l'évolution de l'expansion en fonction du temps (9).

Pour les deux ciments étudiés, les résultats sont obtenus par moyenne de trois mesures (Figure 1). On remarque que l'expansion du ciment A est nettement plus élevée en valeur absolue que celle du ciment B, pour les faibles valeurs du temps t d'hydratation. L'expansion du ciment A se stabilise par contre assez rapidement pour t = 600 h environ tandis qu'à partir de cette échéance, l'expansion du ciment B se met à croître très rapidement.

Des mesures d'expansion réalisées sur des éprouvettes de pâte pure de dimensions 4 x 4 x 16 cm à l'aide d'un rétractomètre (NFP 15 433) conduisent à un résultat similaire (Figure 2) avec cependant des valeurs d'expansion différentes, ce qui est lié à la forme et à la dimension des éprouvettes.

L'expansion moins importante du ciment B à court terme (jusqu'à 1000 h environ) doit être due à l'effet retardateur de l'anhydrite (comparativement à l'effet du gypse) dans la formation de l'ettringite, comme indiqué par OLDER et WONNEMANN (10).

2. Analyse par diffraction X :

Nous avons à des temps donnés, interrompu l'hydratation (sans contrainte) d'éprouvettes de mêmes dimensions que celles des essais d'expansion et conservées également sous l'eau. Le stoppage était réalisé par broyage, lavages successifs à l'éthanol puis à l'éther et enfin séchage à 40°C pendant deux heures selon le processus mis au point par A. BACHIORRINI et B. GUILHOT (11).

D'après les diagrammes obtenus, nous avons porté en fonction du temps, l'évolution des intensités relatives des pics correspondant à l'ettringite (2θ = 9,1° et 15,8° avec Cu Kα) au gypse (11,7° et 20,8°) ou à l'anhydrite

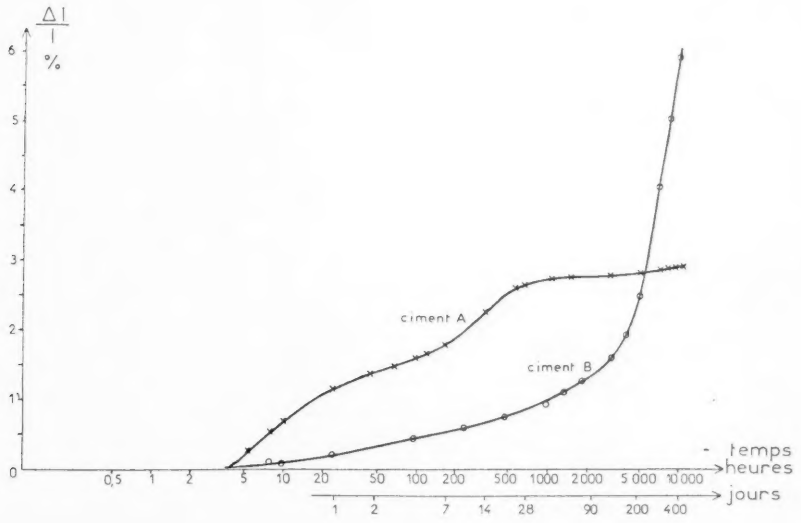

Figure 1 : Expansion mesurée avec les aiguilles de LE CHATELIER

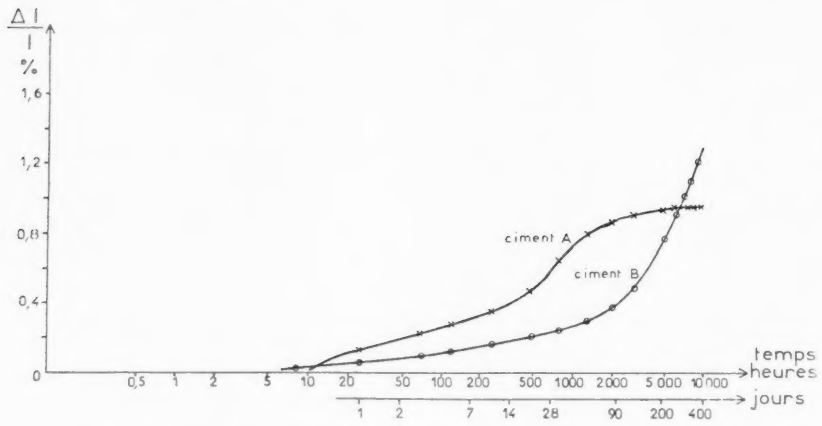

Figure 2 : Expansion sur éprouvettes 4 x 4 x 16 cm

(25,5°), à la chaux $Ca(OH)_2$ (18,1°) ainsi qu'au C_3S (29,5°). L'évaluation de ces intensités relatives a été faite à partir de la hauteur des pics correspondants.

La figure 3 fait apparaître pour le ciment A une stabilisation de la formation d'ettringite cristalline vers 7 jours, tandis que pour le ciment B, la formation d'ettringite cristalline se manifeste à nouveau vers 1800 h après un arrêt entre 10 h et 1800 h (Figure 4).

3. Analyse thermique différentielle :

Les mêmes échantillons, broyés et tamisés à 125 µ, ont été analysés par A.T.D. [essai sur 1,8 g ; vitesse de montée en température : 300°/h].

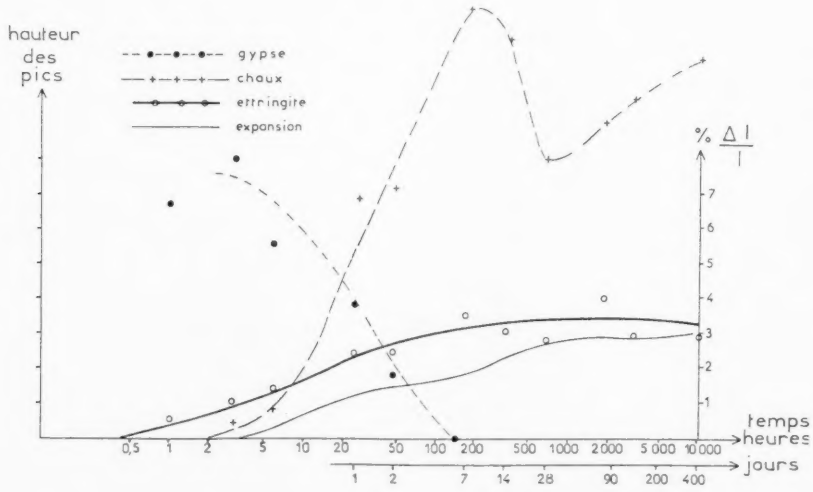

Figure 3 : Ciment A - hauteur des pics de diffraction X et expansion

VOL 14 198

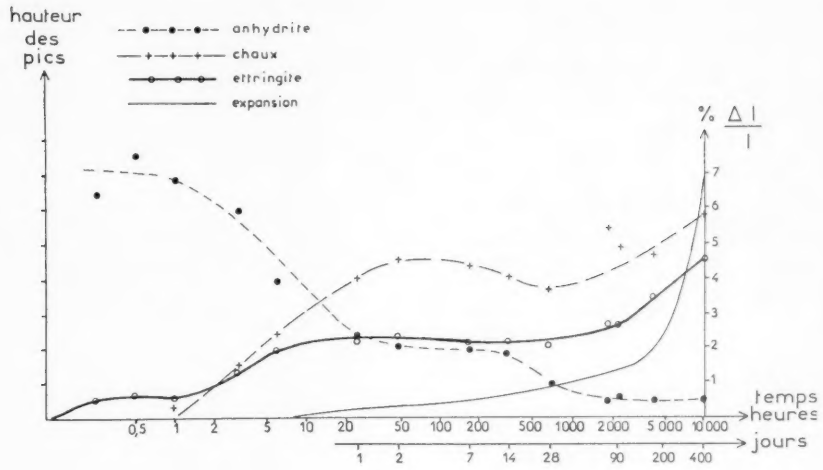

Figure 4 : Ciment B - hauteur des pics de diffraction X et expansion

Les diagrammes obtenus (Figures 5 et 6) font apparaître un pic d'ettringite vers 130-150°C dès le début de l'hydratation, un pic de **C-S-H** vers 110-130°C dès six heures, un pic de chaux vers 500-540°C à partir de trois heures et évidemment pour le ciment A, le double pic du gypse qui disparait vers quarante-huit heures. Notons qu'à aucun moment n'apparait le monosulfoaluminate. Pour le ciment A anhydre, la présence d'un faible pic à 480°C révèle une présence d'hydroxyde de calcium qui peut s'expliquer par un léger éventement du matériau.

Par ailleurs, les résultats non reportés ici obtenus sur des échantillons hydratés sous contrainte biaxiale ne présentent pas de différences significa-

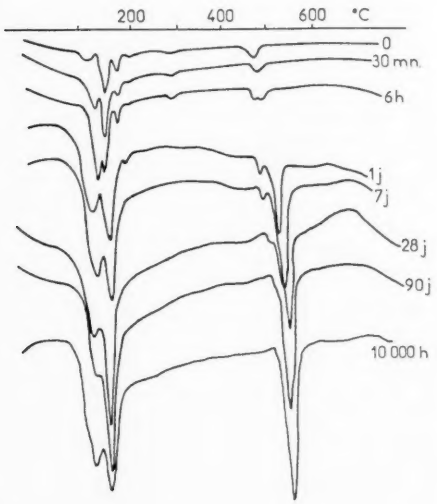

Figure 5 : Ciment A.-A.T.D.

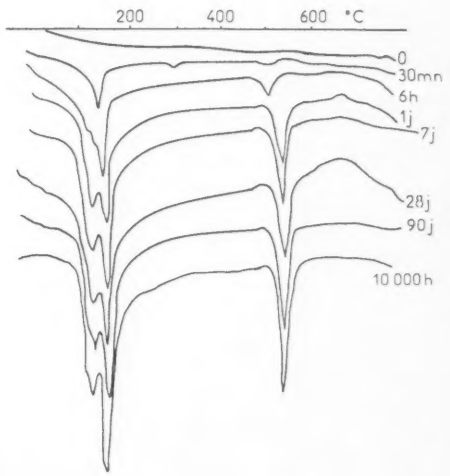

Figure 6 : Ciment B.-A.T.D.

tives avec les résultats ci-dessus correspondant à des échantillons très peu contraints.

L'étude comparative des hauteurs des différents pics A.T.D. en fonction du temps pour le ciment A (Figure 7) et pour le ciment B (Figure 8) permet de constater que l'intensité du pic A.T.D. de l'ettringite augmente constamment pour les deux ciments tant que l'expansion se poursuit et diminue même lors de la stabilisation de l'expansion du ciment A.

L'augmentation de la hauteur du pic A.T.D. de l'ettringite ne correspond pas nécessairement à un accroissement de la quantité d'ettringite formée, mais peut correspondre à un accroissement de la quantité d'eau de constitution de cet hydrate, et réciproquement.

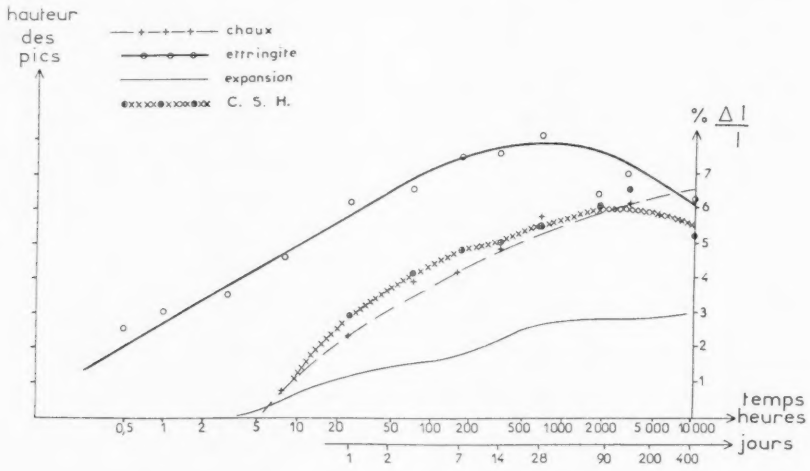

Figure 7 Ciment A : A.T.D. - Expansion

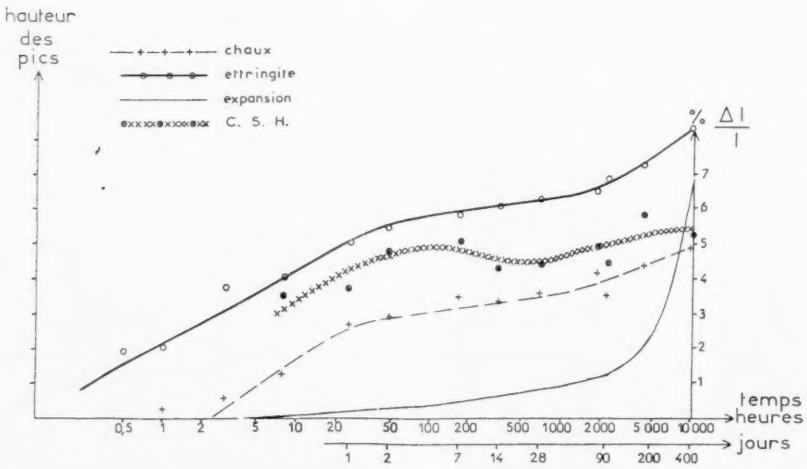

Figure 8.Ciment B : A.T.D. - Expansion

Conclusion

La discussion des différents résultats obtenus permet de tirer les conclusions suivantes :

a) il y a une bonne corrélation entre les courbes d'expansion et les variations de l'intensité du pic A.T.D. de l'ettringite.

b) à aucun moment la présence de monosulfoaluminate n'a pu être décelée. La formation d'ettringite est donc la seule cause de l'expansion de ces ciments.

c) pour le ciment A, la hauteur du pic de diffraction X de l'ettringite augmente jusqu'à environ 200 h alors que l'expansion se poursuit jusqu'à 600 h et que la réserve de gypse est épuisée.

d) pour le ciment B, la présence d'anhydrite limite l'expansion pour les faibles temps d'hydratation. Le pic de diffraction X de l'ettringite reste constant de 10 à 1800 h alors que la hauteur du pic A.T.D. correspondant à la déshydratation de cette phase augmente de 50 % et que l'expansion croît de façon non négligeable.

On peut donc considérer que dans le cas des deux ciments étudiés, c'est la formation et le gonflement de l'éttringite colloïdale (décelable par A.T.D. et non par diffraction X) qui semble être la principale cause de l'expansion macroscopique du matériau aux faibles échéances.

Mais les phénomènes d'expansion sont très variables selon le ciment utilisé. Ainsi, pour le ciment B contenant initialement le sulfate de calcium sous forme d'anhydrite, on ne peut utiliser l'hypothèse de formation d'ettringite colloïdale pour expliquer l'expansion importante qui se manifeste à partir de 1800 heures car parallèlement à ce phénomène d'expansion, la diffraction X met en évidence la formation d'ettringite cristallisée, ce qui entraîne des déformations très importantes. Seuls les phénomènes d'expansion à court terme ($t < 1800$ heures) seraient donc tributaires de la formation d'ettringite colloïdale.

Ces résultats permettent par ailleurs de constater l'influence de la nature du sulfate de calcium (gypse ou anhydrite) dans le ciment utilisé et en définitive de mieux préciser les rôles respectifs de la formation d'ettringite colloïdale et cristalline dans l'expansion des ciments étudiés ici.

BIBLIOGRAPHIE

1. P. CLASTRES and M. MURAT - Alluminati di Calcio/Aluminates de Calcium/Calcium Aluminates - Int. Seminary, TORINO (Italia), Sept. 12-14, 1982 - M. MURAT et al. Editors, 1983, p. 334-347.
2. Report of committee 223 of A.C.I. - A.C.I. Journal - p. 583-610 - (1970).
3. P.K. MEHTA, M. POLIVKA - 6ème Congrès de la Chimie des Ciments - Rapport principal - MOSCOU - (1974).
4. W. KURDOWSKI - Rapport principal - 7ème Congrès de la Chimie des Ciments - PARIS - (1980).
5. S. CHATTERJI - Calcium Aluminates - Int. Seminary, TORINO (Italia) - M. MURAT et al. Editors - 1983 - p. 325-333.
6. A. NEGRO, A. BACHIORRINI-C.C.R. 12 - p. 677-684 - (1982).
7. R. RABOT et R. MAGNAN - Annales de l'I.T.B.T.P. - 295-296 - p. 57-65 - (1972).

8. A. BONIN - 7ème Congrès int. de la Chimie des Ciments - PARIS II - p. 209-213 - (1980).
9. P. CLASTRES - Bull. Liaison Labo. Ponts et Chaussées 94 - p. 9-12 (1978).
10. I. OLDER et R. WONNEMANN - 7ème Congrès int. de la Chimie des Ciments - PARIS IV - p. 510-513 - (1980).
11. A. BACHIORRINI et B. GUILHOT - C.C.R. 12 - p. 559-567.

VOL.
14
1984

CEMENT and CONCRETE RESEARCH. Vol. 14, pp. 207-214, 1984. Printed in the USA.
0008-8846/84 $3.00+00. Copyright (c), 1984 Pergamon Press, Ltd.

IDENTIFICATION OF CONCRETE ADMIXTURES BY DIFFERENTIAL THERMAL ANALYSIS IN OXYGEN

N.B. Milestone*
Chemistry Division
DSIR, Private Bag
Petone, New Zealand

(Refereed)
(Received June 27, 1983)

ABSTRACT

It is often desirable to identify a concrete admixture uniquely before its use to avoid adverse reactions. Methods such as ir or uv spectroscopy only broadly classify the type of admixture while chemical analysis is difficult and results are often inconclusive, especially for admixtures containing lignosulphonates. The use of DTA under 250 kPa of O_2 provides a technique for identifying admixtures. Each admixture gives an unique pattern of exothermic peaks thus enabling its identification provided a known sample is available. Admixtures containing salts of hydroxycarboxylic acids show exotherms up to 700°C while those with free acids or sugars shown only exotherms in the range 200-400°C.

OL.
14
984

Introduction

Chemical admixtures are widely used in the concrete industry as aids for controlling the workability and setting of fresh concrete. They are usually supplied as solutions suitable for adding to the mixing water to enable an even distribution throughout the concrete. A large proportion of concrete admixtures, especially the water-reducing type, are based on sodium or calcium lignosulphonates - byproducts from the pulp and paper industry. Commercial lignosulphonates are usually not pure but contain a complex mixture of lignosulphonic acid salts as well as sugars, sugar acids and other hydroxy compounds.(1) Small proportions of these impurities (in particular sugars and sugar acids) have a marked effect on the hydration of cement compounds (2-6), and hence on the setting of concrete so that their content must be closely controlled. Changes in raw material sources for the admixture can made a profound difference in the behaviour of an admixture

* Present address: Development Finance Corporation, P.O. Box 3090, Wellington, New Zealand

due to small differences in the composition of the lignosulphonate.

Chemical analysis of complex materials such as concrete admixtures is difficult and very time consuming so that the quality of an admixture is usually measured in terms of its effect on the physical properties of concrete, e.g. setting times, workability and strength development.(7-8). Nevertheless, there are occasions when it is important to know whether an admixture to be currently used, is the same as the material that was used say six months earlier and so avoid the extra physical testing necessary to determine the optimum dose. Techniques such as IR and UV spectroscopy have been used (9-11) for identification purposes and can serve to identify the class to which an admixture belongs, but they are not suitable for positive identification of an individual admixture, which is often necessary if adverse results have been obtained. Gel chromatography,(12) thin layer chromatography(13) and high pressure liquid chromatography(14) have been used to characterize admixtures but all of these methods are still unable to identify an admixture uniquely.

This paper describes the use of DTA in oxygen to identify concrete admixtures both rapidly and uniquely.

Experimental

Twenty-one samples of water-reducing admixtures were obtained and analysed as part of an overall physical testing programme.(15) The admixtures studied can be broadly separated into four main classes based on the main chemical constituents.

Class 1. Admixtures based on lignosulphonates.
Class 2. Admixtures based on hydroxycarboxylic acids.
Class 3. Synthetic detergents.
Class 4. Admixtures based on synthetic condensed sulphonate systems.

Partial chemical analyses for these samples, which were carried out using a variety of methods developed for the programme, have been reported previously.(15) The chemical analyses from that report are reproduced in Table 1.

To enable reproducible results to be obtained for thermal analysis, the liquid admixtures were freeze-dried and stored over P_2O_5 before analysis. The admixtures from Class 3 analysed in the testing programme were still liquid when dried, so that only admixtures from classes 1, 2 and 4 were subjected to thermal analysis.

Twenty milligrams of admixture were interground with 200 milligrams of calcined alumina in a boron carbide mortar and pestle. Approximately 150 milligrams of the ground mixture was weighed into a platinum microcrucible which was placed in a ring sample holder (BR11) in a Stone thermoanalyser 202. The thermocouple used was Platinel 2. The furnace was placed over the sample followed by a pressure dome which was used to control the sample atmosphere and pressure up to 250 kPa. Oxygen was slowly admitted to the chamber and the whole system pressurized with oxygen to 250 kPa. Heating was then commenced at 10°C/min from room temperature to 950°C.

VOL. 14 198

TABLE 1

CHEMICAL ANALYSIS OF ADMIXTURES (from ref 15)

Admixture	pH	Solid content % w/v	Inorg. ash % w/v	Lignosulphonate mg/ml	Sugars (as glucose) mg/ml	Sugar acids (as sodium gluconate) mg/ml	Triethanolamine mg/ml	CaO mg/ml	Na_2O mg/ml
Class 1									
1	6.0	54	10	316	46	nd	7	56	17.3
2	4.5	53	6.5	352	122	nd	-	65	0.8
3	4.5	16	2.9	72	9	nd	6	9.1	5.8
4	6.5	36	8.1	260	19	nd	4	41	-
5	7.5	37	7.8	196	12	nd	57	35	3.1
6	6.0	41	10.7	288	19	nd	-	39	4.8
7	6.0	56	9.0	416	43	nd	-	78	3.4
8	6.5	48	9.4	314	21	nd	15	3.2	37
9	6.0	62	13.7	416	51	nd	-	0.42	42
10	5.5 (of 1% solution)	solid (11% moisture)	44mg/g	590mg/g	266mg/g	nd	-	nd	0.2mg/g
Class 2									
11	6.5	65	6.2	320	109	64	-	27	1.8
12	4.5	62	5.6	312	115	80	-	29	2.1
13	8.5	49	14.9	92	12.4	263	-	-	14
14	4.5	51	11.8	228	76	110	-	5.6	49
15	6.0	57	expanded	210	45	50	-	-	48
16	5.5	58	0.2	-	296	28	-	-	1.6
17	5.0	40	expanded	-	13.4	355	-	-	25
Class 3									
18	6.0	27*	nd	nd	nd	nd	nd	nd	nd
19	4.0	93*	nd	nd	nd	nd	nd	nd	nd

*final product was liquid or low melting wax

Class 4									
20	6.0	52	16.3	404*	2	nd	nd	10	3.5
21	8.0	solid (9.8% moisture)	26.7%w/w	769*mg/g	-	-	nd	-	133mg/g

*synthetic sulphonated material

Results and Discussion

DTA curves for the various samples are given in Figs 1 and 2. Some of the admixtures were extremely hygroscopic and the broad endotherm occurring between 100 and 200°C for these admixtures were due to evolution of the moisture absorbed during handling. Sample 17 was essentially a solution of sodium gluconate and the solid foamed so much on heating that it proved impossible to obtain a reproducible DTA curve.

The DTA curves for the various concrete admixtures are complex and no effort was made to assign the various exothermic peaks. When the samples were analysed under vacuum or in an inert atmosphere, the exothermic peaks were absent and only very small endothermic peaks were present so that the exothermic peaks are, as expected, due to a series of oxidation steps. Increasing the oxygen pressure to 400 kPa gave no appreciable difference in the DTA curves, while samples run in ambient air showed only small broad exothermic peaks, typical of slow oxidation steps.

Although the overall pattern for several of the admixutres is similar, no two samples gave exactly the same pattern. This pattern of peaks then provides a suitable identification method for admixtures. This is similar to the way in which the peaks in the "fingerprint" region of the IR spectrum are used for the identification of organic compounds. For many of these admixtures the IR spectra were very similar(15) and so are not suitable for identifying each admixture, although the different classes could usually be separated and the source of lignosulphonate identified.

The temperature of the final exotherm for many samples is higher than expected. Organic compounds have usually decomposed by 500°C in oxygen but temperatures up to 720°C were recorded for the final exotherm in some admixtures indicating unusual stability. For samples 10, 11, 12, 16 and 21 there is no major exotherm above 500°C. Samples 10, 11 and 12 contain only small amounts of organic acid salts other than lignosulphonic acid salts. Sample 21 is a melamine based admixture and sample 16 is essentially a sugar solution. Thus it appears that this high temperature exotherm is associated with salts of organic acids.

When samples 1, 2, 8, 14 and 15 were converted to the acid form by passing the diluted admixture through an ion exchange column in the hydrogen form before freeze drying, there were no exotherms above 500°C. The profile of the peaks below 500°C was also altered but as many of the free caboxylic acids are unstable, converting to cyclic lactones on drying, this change was not unexpected. Clearly the presence of sodium or calcium ions confers some exceptional stability to salts of and organic acid, the final breakdown being rapid giving the sharp peak. The expected inorganic products, sodium or calcium carbonate give endotherms on decomposition so the reaction must be oxidation of an organic species.

Further thermal analysis studies on a series of organic acids and their sodium and calcium salts(16) has shown that the

VOL
14
198

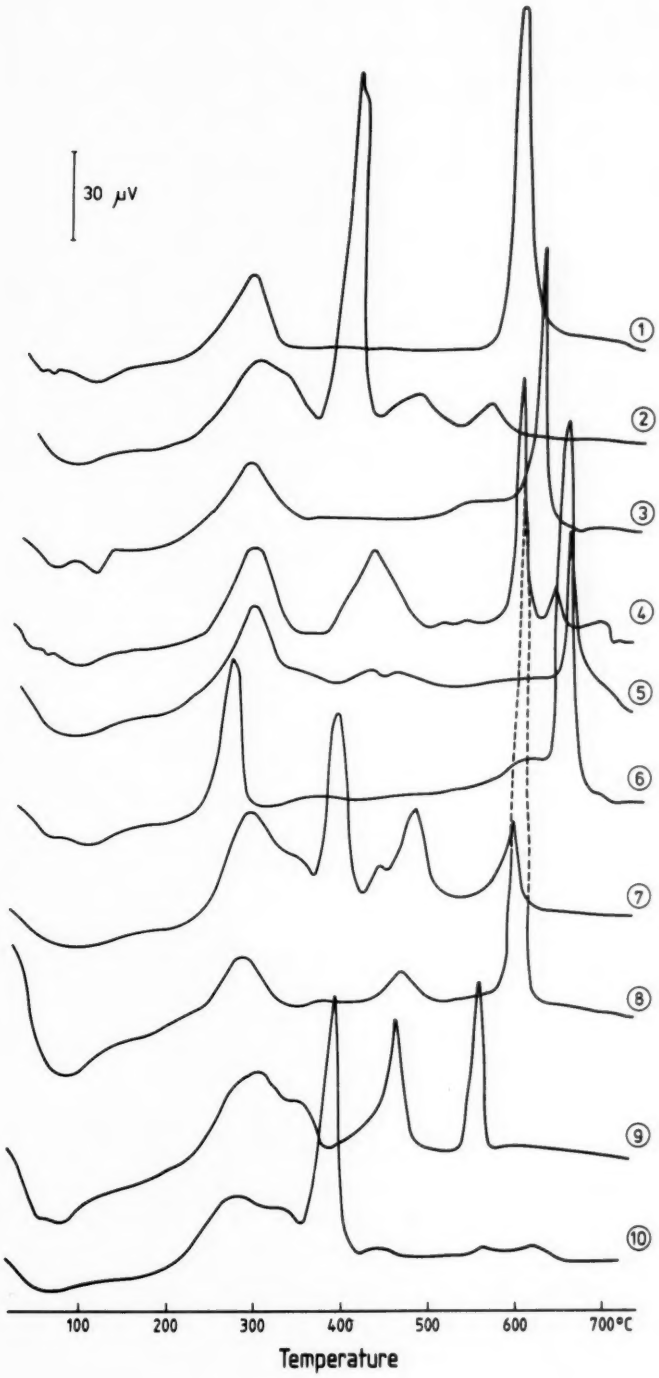

Figure 1. DTA Curves for Class 1 Admixtures.
(30 μv ≡ 0.67°C at 500°C)

VOL.
14
984

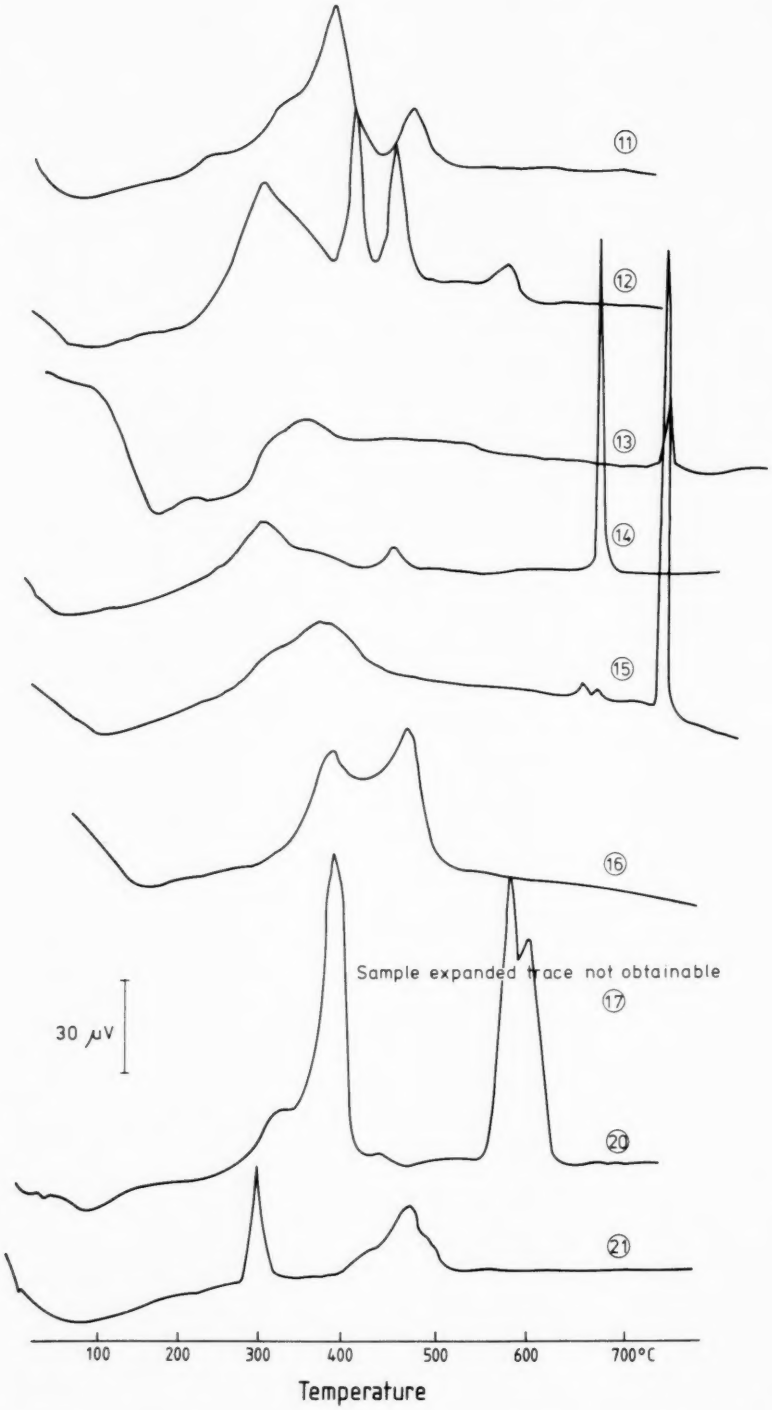

Figure 2. DTA Curves for Class 2 and Class 4 Admixtures. (30 μv ≡ 0.67°C at 500°C)

VOL.
14
1984

presence of a high temperature exotherm is common for many hydroxycarboxylic acid salts, but is absent in the pure acids. Further work is needed to elucidate this stable entity and its mechanism of breakdown.

This method has been used to confirm that two samples of supposedly identical admixtures were in fact different. On a major construction site, addition to a batch of concrete of an admixture from a drum received in a second shipment to the site, caused delays in setting time. The supplier was unable to distinguish readily between admixtures from the first and second shipments. The DTA method, using separate samples of known admixtures from the supplier as standards, was able to show that the drums in the second shipment had been incorrectly labelled and were actually a different admixture to the first shipment. The chemical formulation of the two admixtures was very similar and they could only be distinguished by a detailed chemical analysis.

Conclusion

DTA of concrete admixtures in an atmosphere of oxygen provides a method whereby the eighteen admixtures tested can be uniquely identified. Changes in raw materials or chemical formulation cause changes in peak profiles that can be readily detected using this method. These changes are not readily observed by other rapid screening methods such as IR or UV spectroscopy. Because properties such as setting times are affected by small changes to the hydroxycarboxylic acid fraction, close control of formulation is needed.

Exotherms in the range 500-700°C in the DTA curves are due to the presence of sodium or calcium salts of hydroxycarboxylic acids but do not occur above 500°C for the free acid form.

References

1. Y. Mouton, Bull. Liason Lab. Ponds. Chaux 1958 No. 58 pp 117-34.
2. N.B. Milestone, Cement Concr. Res., 7(1) 45-52 (1977).
3. N.B. Milestone, J. Amer. Ceram. Soc. 62 (7-8) 321-324 (1979).
4. J.F. Young, Proc 5th Int Symp Chem Cement Tokyo 1968 II 256-67.
6. W.C. Hansen, J. Materials, 5(4) 842-855 1970.
6. G.M. Bruere, Nature 212, 502-503 (1962).
7. N.Z. Standard 3113. Chemical Admixtures for Concrete 1979.
8. K.E. Fletcher and M.H. Roberts, Concrete 5, 142-148 and 175-179 (1971).
9. W.J. Halstead and B. Clarke, Nat. Acad. Sci. Nat Res. Council Pub 940. Highway Research Board Bull No. 310 33-35 (1962).
10. P. Diem and K. Krehl, Betonwerk and Fertigteil Technik 41 299 and 341 (1975).
11. B. Kroone, Mag. Conc. Res. 23 132-134 1971.
12. W.L. Dolch, "Analysis of Hardened Concrete for Admixture Content." Final Report Joint Highway Research Project. F HWA/IN/JHRP-80/5. NTIS PB81-132433.

OL.
14
984

13. M.H. Simatupang, Z. Kalk Gips. (10), 427-431 (1975).
14. F.W. Broker and M.H. Simatupang, Z. Kalk Gips. (8), 245-247, (1973).
15. N.B. Milestone, Report No. CD2262, Chemistry Division, DSIR, New Zealand, Dec. 1977.
16. D.E. Rogers, unpublished work.

Appendix

List of Admixtures Investigated

Name	Supplier
Darex WRDA	W R Grace
Daratard	"
Discon	Stipplecote Products Ltd
Eucon WR	Euclid Chemical Products
Eucon WR Retarding	" " "
Febflow Std	Jos Nathan Ltd
Febflow Retarding	"
Leadair R	Leadair Industries
Lissapol Z-N	ICI
Melment	Hoechst
Mighty 150	Chemiplas Agencies
Plastiment DSE	Sika
Plastiment N	"
Plastiment PHC	"
Plastiment VZ	"
Plastocrete CLK	"
Pozzolith 80	Embecon
Pozzolith 100 XR	"
Pozzolith 300N	"
Pozzolith 300R	"
Teric GN-9	ICI

VOL.
14
198

CEMENT and CONCRETE RESEARCH. Vol. 14, pp. 215-224, 1984. Printed in the USA.
0008-8846/84 $3.00+00. Copyright (c) 1984 Pergamon Press, Ltd.

MODEL FOR TENSILE FRACTURE OF CONCRETE AT HIGH RATES OF LOADING

A.J. Zieliński
Stevin Laboratory of Delft University of Technology
2628 CN Delft, Stevinweg 4, The Netherlands

(Communicated by F.H. Wittmann)
(Received July 5, 1983)

VOL.
14
984

ABSTRACT

Mechanisms of tensile fracture of concrete are described. A model is developed for an idealized material. The amount of simultaneous cracking and the path of each crack depend on the rate of stressing. The fracture energy and the tensile strength have been determined as functions of the rate of loading. The results of earlier experiments on concrete under impact tensile loading can be explained by this model.

Introduction

The theoretical work on modelling of behaviour and fracture of concrete materials at high rates of tensile loading presented here is a natural continuation of the earlier extensive experimental research program carried out in the Stevin Laboratory.

The Split Hopkinson Bar apparatus was applied for impact testing at stress rates ranging from 2,000 to 62,000 N/mm²s. The test method and the experimental results concerning the impact tensile strength, the impact fatigue tensile strength and the stress-strain behaviour of concrete materials under single and repeated impact tensile loading have already been reported and discussed in previous publications (1, 2, 3). The analysis of mechanisms of tensile fracture was conducted in order to explain the phenomena observed.

The aim of this research was to develop a model which gives a better insight into behaviour and fracture of concrete materials subjected to tension. The model should provide possibilities for studying the effects of loading rates, composition of concrete, properties of constituents and other parameters on fracture energy and strength of the material.

Mechanisms of Tensile Fracture

Concrete is a heterogeneous multiphase complex material consisting of aggregate particles of various sizes and irregular shape, which are dispersed and embedded in hardened cement paste. Air voids, interfacial bond microcracks and macrocracks within the cement matrix are inherent in this material due to manufacturing procedures and physico-chemical processes taking place during hardening of cement-based composites. Even hardened cement paste is actually a heterogeneous material if its microstructure is taken into consideration.

The microcracks are potential sources of fracture initiation, since at their tips local concentration of stresses occurs which can lead to extension of these microcracks under externally applied loading. Stiff aggregate particles embedded in the cement matrix also cause local stress concentrations in the zones around the particles (see Fig. 1) which may even be intensified by the presence of interfacial bond cracks.

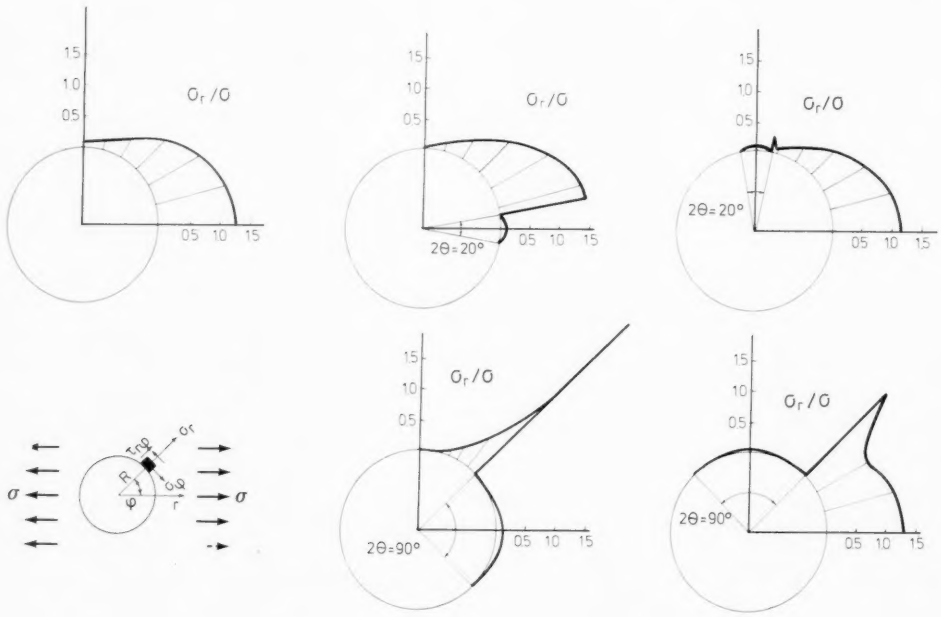

FIG. 1
Radial stresses along interfaces of a stiff bonded inclusion (4) and a partially debonded inclusion (5)

Once they have been initiated, the cracks may be arrested due to the heterogeneity of the material structure considered on both micro and macro level (see Figs. 2 and 3).

The growth of cracks can be arrested if the crack tip encounters material zones of either lower stress intensity or higher capacity to take up the local concentration of tensile stresses. Arrest due to blunting of the crack front may also occur.

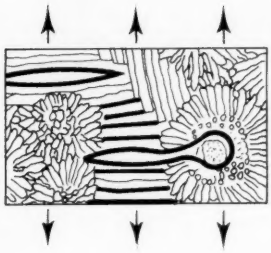

FIG. 2
Crack arrest at micro level (after (6))

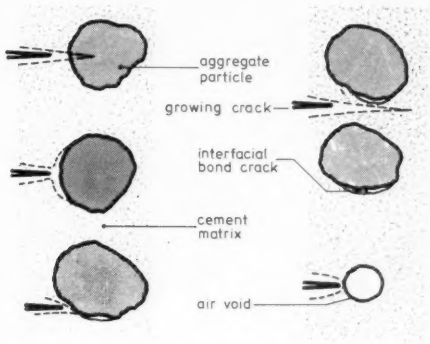

FIG. 3
Crack arrest at submacro level

The cracking process is not limited to the major crack only, but also includes extensive microcracking in the highly stressed crack tip zones.

The fracture process starts at the interfaces of aggregate particles, in zones situated perpendicularly with respect to the load direction.

Under very slowly increasing tensile loading the crack will grow along relatively weak interfaces between aggregate particles and the cement matrix and will then penetrate through the matrix, thus forming a continuous fracture. The fracture process is substantially limited to the weakest zone of the material, since in neighbouring zones redistribution of stresses and relaxation of material may take place under very slowly increasing tension.

Under impact loading conditions a great number of microcracks can be driven into extension at the same time, since the overall stress in the whole volume of material rapidly increases.

The time in which fracture oc curs is extremely short - a fraction of a millisecond - and the effect of strain relief in the zone around one growing crack may have no influence on the material response in the other zones of the material, this being due to inertia of elements, which delays the response of the material to the changed stress situation. In those other highly strained zones, extension of microcracks may be very strongly pronounced. The rapidly increasing tension will drive the cracks to very rapid extension.

They will be forced to develop along shorter paths of higher resistance, i.e., through tough aggre-

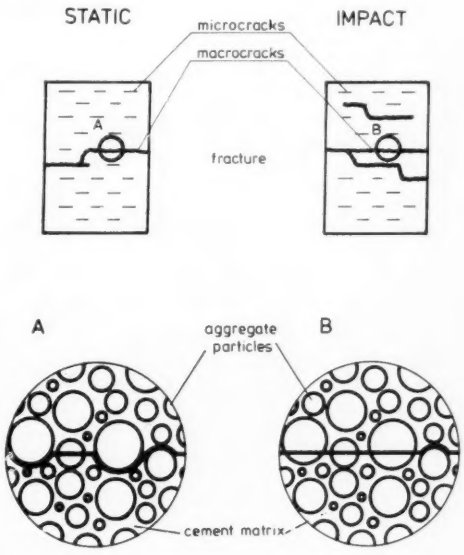

FIG. 4
Fundamental differences between static and impact tensile fracture

gate particles instead of growing around them. This is not only caused by high stresses in the material, but also due to the inertia of elements beside the surface of rapidly growing cracks.

Fig. 4 schematically shows differences with respect to the amount of simultaneous cracking and crack path under static and impact tensile loading, respectively.

Model

Idealization of Material and Crack Extension

The model developed is extensively described in (7). Concrete is idealized as a particulate composite consisting of spherical aggregate particles varying in size, dispersed and embedded within the cement matrix.

Fig. 5 shows an idealized concrete element fractured in tension.

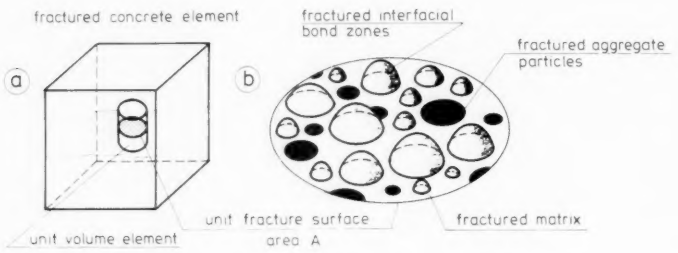

FIG. 5
The tensile fracture plane
a) macro level
b) submacro level (area A)

It is assumed that a unit area of fracture surface A is a plane surface as far as the macro scale is concerned. It is considered that undulations of the crack plane on a macro scale do not affect the mechanism of fracture of the composite material considered.

In this model it is assumed that a submacro level the plane section of the cracked surface is only formed within the matrix phase and partially by some fractured aggregate particles as shown in Fig. 5b.

Another part of the fracture surface is formed by spherical section areas as a result of interfacial bond fractures.

The fracture criterion determining whether a given aggregate particle will be fractured or whether the interface between the particle and the cement matrix will be fractured, involves two parameters. On the one hand, the position of the particle with regard to the xy crack plane (see Fig. 6) and, on the other hand, the rate of loading $\dot{\sigma}$ influencing the crack velocity v_c.

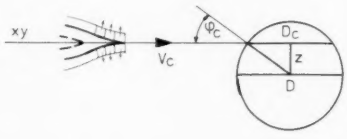

FIG. 6
Crack approaching an aggregate particle

It is assumed that the aggregate particle will be fractured if the angle between the xy crack plane and the normal to the surface of the aggregate particle at the

common point with the xy plane is smaller than a certain value φ_c.

Fig. 7 shows the ratio between the area of fractured surface of the idealized composite and the normal area A of the plane cross-section as a function of the critical angle φ_c. The area of fractured matrix A_m and the areas A_a^* and A_b^* of fractured aggregate and bond, respectively, varying with φ_c are determined with the aid of a statistical approach to the configuration of aggregate particles in the idealized composite.

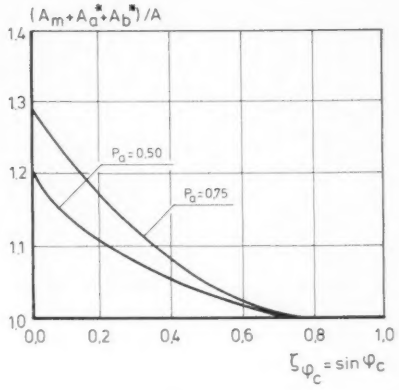

FIG. 7
Influence of φ_c upon the area of fractured surface for aggregate contents $p_a = 0.5$ and $p_a = 0.75$

Fig. 8 shows an approximated relationship between the critical angle φ_c and the rate of loading $\dot{\sigma}$. This relationship is determined under assumption that the velocity v_c of the growing crack increases with the increasing rate of loading, and so does the kinetic energy associated with the movement of material elements beside the surface of the extending crack. Those elements, once they have been accelerated will tend to move further in the same direction. The deviation of the crack from the original direction is therefore less probable for higher rates of loading, especially in particles situated quite symmetrically with respect to the xy crack plane.

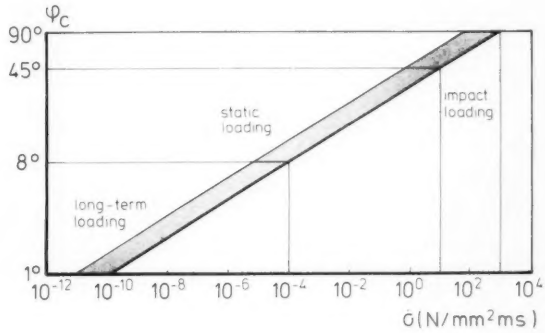

FIG. 8
Critical angle φ_c versus stress rate $\dot{\sigma}$

Fracture Energy

The energy absorbed during fracture of the particulate composite considered, is mainly associated with crack extension in the matrix phase, aggregate phase and interfacial bond phase. This energy U can be expressed as a sum of products of specific surface energies of the three phases mentioned (γ_m, γ_a, γ_b), with appropriate fractured areas of these phases (A_m, A_a^*, A_b^*) which concribute to the total fractured surface:

$$U = \alpha_c . U_c = 2\,\alpha_c (A_m . \gamma_m + A_a^* . \gamma_a + A_b^* . \gamma_b)$$

where:
- U_c = fracture energy associated with a single crack;
- α_c = multiple cracking coefficient;
- A_m, A_a^*, A_b^* = areas of fractured matrix, aggregate particles and bond respectively, corresponding to a single crack;
- γ_m, γ_a, γ_b = specific surface energies of matrix, aggregate and bond respectively.

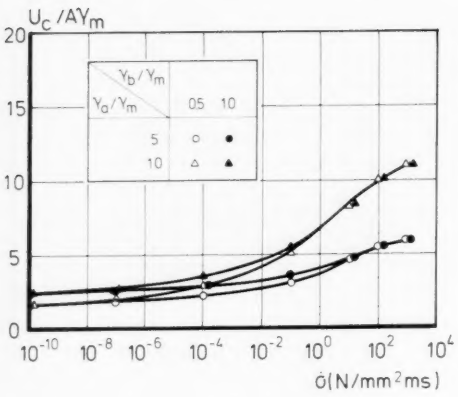

FIG. 9
$p_a = 0.5$

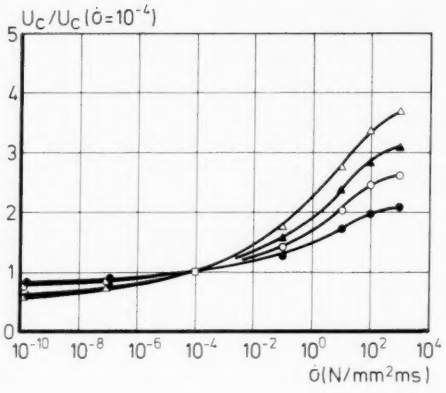

FIG. 11
$p_a = 0.5$

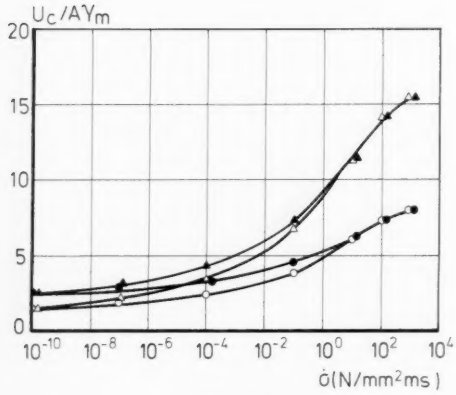

FIG. 10
$p_a = 0.75$

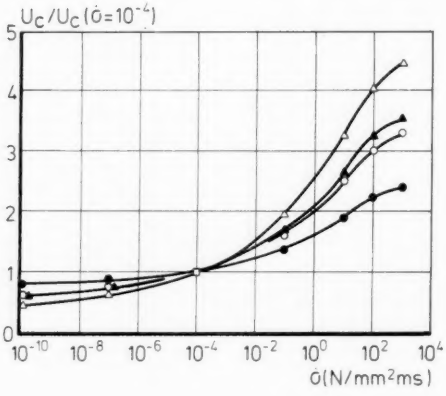

FIG. 12
$p_a = 0.75$

Figs. 9 and 10 show the influence of the rate of loading $\dot{\sigma}$ upon the fracture energy U_c expressed as a function of the nominal area A of the fractured cross-section and of the specific surface energy γ_m of matrix. In Figs. 11 and 12 the energy U_c is standardized to the energy U_c at a static stress rate of 10^{-4} N/mm²ms.

For normalweight concrete the specific surface energy of aggregate γ_a is about one order of magnitude greater than the specific surface energy of cement matrix γ_m, and the latter is approximately 2 times the specific surface energy of the bond phase γ_b. The aggregate content p_a usually varies between 0.5 and 0.75.

It is easy to see that the fracture energy U_c associated with a crack extension within a material of given surface energies γ_m, γ_a, γ_b increases with increasing stress rates. This increase is relatively small in the stress

rate range from 10^{-10} N/mm²ms to approximately 10^{-4} N/mm²ms. In the range from 10^{-4} N/mm²ms to 10^{2} N/mm²ms the increase of U_c is very strongly pronounced. It can be observed that in the lower stress rate range the fracture energy is mainly influenced by the ratio between the specific surface energies of the bond phase and the matrix (γ_b/γ_m). The fracture energy is higher in the case of a material with good interfacial bond ($\gamma_b/\gamma_m = 1$) than for one with poor bond ($\gamma_b/\gamma_m = 0.5$). The toughness of aggregate particles is less important at these low stress rates, since fractures of interfacial bond zones are dominant. At higher stress rates, however, the influence of the aggregate material becomes very important, since fewer bond fractures take place and more aggregate fractures may occur. Therefore, for high stress rates the fracture energy is much higher for material with a high ratio between specific surface energies of aggregate and matrix ($\gamma_a/\gamma_m = 10$) than for a material with less tough particles ($\gamma_a/\gamma_m = 5$). The effect of interfacial bond properties, expressed by the ratio γ_b/γ_m, is not pronounced at high stress rates. These effects are pronounced more strongly for the composite with higher aggregate content ($p_a = 0.75$).

Note that for the total amount of energy absorbed during fracture multiple cracking must be taken into account.

Tensile Strength

Tensile strength is a mechanical property which should be considered as being closely associated with fracture mechanisms of the material and the energy absorbed during the fracture process. The amount of absorbed energy corresponds with the area under complete σ-ε-curve.

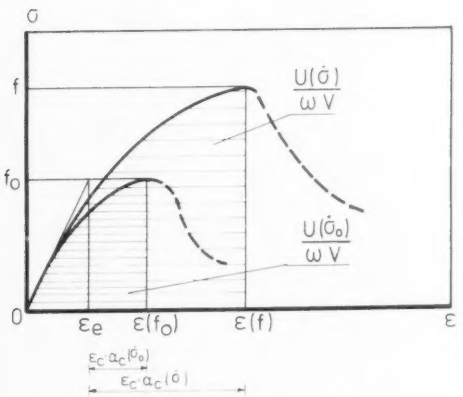

FIG. 13
Relationship between tensile strength, fracture energy and multiple cracking

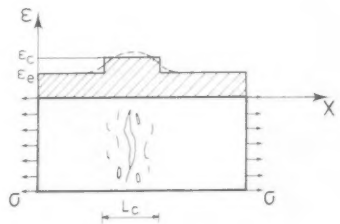

FIG. 14
Deformation of fracture zone

The tensile strength f can be expressed by means of the coefficient α_c of multiple cracking and the fracture energy U_c (see Figs. 13 and 14):

$$f = \frac{U}{\zeta.\omega.V.\varepsilon(f)} = \frac{\alpha_c.U_c}{\zeta.\omega.V(\varepsilon_e + \alpha_c.\varepsilon_c)}$$

where: ζ = shape factor of σ-ε-relationships;
ω = coefficient taking into account the descending branch of σ-ε-curves;

V = volume of stressed material;
ε_e = elastic strain;
ε_c = strain associated with a single fracture zone.

The effect of the loading rate upon the tensile strength may be determined with the aid of known static σ-ε-diagram and the effects of the rate of loading upon U_c and α_c:

$$\frac{f}{f_o} = \frac{f(\dot{\sigma})}{f(\dot{\sigma}_s)} = \frac{\alpha_c(\dot{\sigma}).U_c(\dot{\sigma})}{\alpha_c(\dot{\sigma}_o).U_c(\dot{\sigma}_o)} \cdot \frac{\varepsilon_e + \varepsilon_c.\alpha_c(\dot{\sigma}_o)}{\varepsilon_e + \varepsilon_c.\alpha_c(\dot{\sigma})}$$

This relationship is established assuming that the descending branch of σ-ε-curve may be determined with the aid of the known ascending branch (8), and that the shape of σ-ε-curve is not influenced by the rate of loading (3).

Comparison with Experimental Results

Generally, the experimental results (3) are in accordance with the model.

Under impact loading conditions much more energy is absorbed in the fracture process, the tensile strength is much higher, and the strain corresponding with the maximum stress is greater than under static loading - see Figs. 15, 16 and 17.

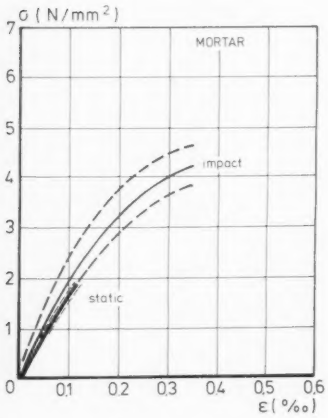

FIG. 15

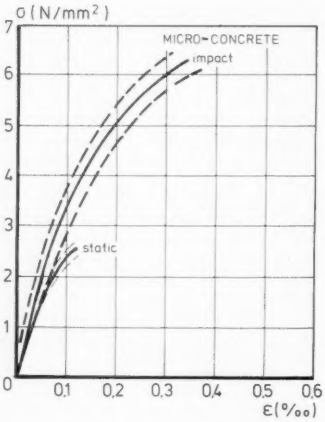

FIG. 16

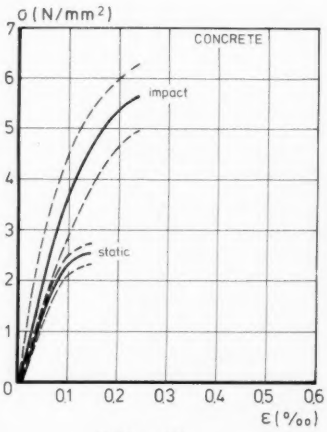

FIG. 17

Furthermore, it was observed that under impact loading some specimens fractured into three portions and fracture surfaces comprised more fractured aggregate particles. These facts support the fundamental mechanisms of tensile fracture - more extensive simultaneous cracking and fracturing tougher material zones at higher rates of loading - which have been considered in this model.

The experimental results obtained on mortar were used to determine the fracture energy and tensile strength of microconcrete and concrete according to the model (7). The same amount of multiple cracking was assumed for these three materials under static and impact loading, respectively.

The increase in fracture energy and tensile strength due to the presence of tough aggregate particles in microconcrete and concrete was in agreement with results of static tests.

The ratio between impact and static fracture energy of mortar was assumed to give a value of the ratio between impact and static coefficient of multiple cracking. Application of this value together with higher energy U_c associated with the presence of aggregate particles and rapid crack extension, led to theoretical values of the impact fracture energy and the impact tensile strength of microconcrete and concrete. Those values were higher than the values experimentally found. Some differences between the idealized fracture process considered in the model and the fracture of actual heterogeneous concrete materials may explain this fact.

It should be pointed out that the shape of aggregate particles may predetermine the way in which a fracture is most likely to occur - see Fig. 18.

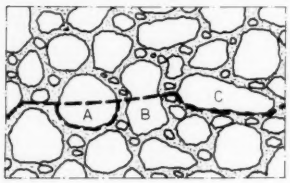

FIG. 18
Fracture modes
A. aggregate/bond
B. aggregate
C. bond

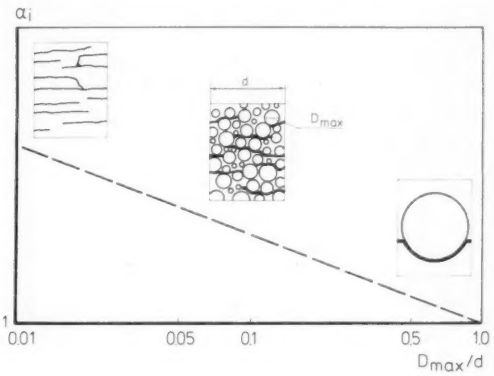

FIG. 19
Influence of relative heterogeneity of concrete upon the amount of cracking under impact tensile loading

Furthermore, the configuration of large aggregate particles may result in "prefactured planes" formed by bond cracks often situated underneath such particles. This can affect the amount of cracking (see Fig. 19) and crack paths due to externally applied tension.

The above indicates that both the fracture path of a single crack and the amount of multiple cracking in concrete may be less influenced by the high rate of loading than can be expected from the model developed for the idealized composite.

Nevertheless, the model proves to give good insight into mechanical behaviour and fracture processes of concrete materials at high rates of tensile loading.

The effects of mix composition, properties of constituents of concrete, curing conditions and other parameters upon fracture energy and tensile strength at various stress rates have been studied with the aid of this model (7) and are consistent with experimental evidence.

Conclusions

1. The mechanisms of extensive simultaneous cracking and fracturing tougher material zones are essential for the explanation of the behaviour of concrete materials at high rates of tensile loading.
2. The effect of high rates of loading upon the fracture energy and the tensile strength of concrete materials may be theoretically studied with the aid of the model presented here.

Acknowledgements

The theoretical research presented here has been made possible by the financial support received from the Foundation "Professor Bakkerfonds" and from the Foundation for Technical Sciences (STW Project DCT 11.0166). This support, and valuable discussions with Prof.Dr.-Ing. H.W. Reinhardt have been gratefully acknowledged by the author.

References

1. A.J. Zieliński, H.W. Reinhardt and H.A. Körmeling, "Experiments on concrete under uniaxial impact tensile loading", Materials and Structures (RILEM), No. 80, 1981, pp. 103-112.

2. A.J. Zieliński, H.W. Reinhardt and H.A. Körmeling, "Experiments on concrete under repeated uniaxial impact tensile loading", Materials and Structures (RILEM), No. 81, 1981, pp. 163-169.

3. A.J. Zieliński and H.W. Reinhardt, "Stress-strain behaviour of concrete and mortar at high rates of tensile loading", Cement and Concrete Research, No. 3, 1982, pp. 309-319.

4. N.I. Mushelishvili, "Some basic problems of the mathematical theory of elasticity", Noordhoff, 1953.

5. A.B. Perlman and G.C. Sih, "Elastostatic problems of curvi-linear cracks in bonded dissimilar materials", Int. Journal of Engineering Sciences, Vol. 5, 1967, pp. 845-867.

6. A. Grudemo, "Microcracks, fracture mechanism and strength of the cement paste matrix", Cement and Concrete Research, No. 1, 1979, pp. 19-34.

7. A.J. Zieliński, "Fracture of concrete and mortar under uniaxial impact tensile loading", Dissertation, Delft University Press, 1982.

8. K.E. Løland, "Continuous damage model for load-response estimation of concrete", Cement and Concrete Research, No. 3, 1980, pp. 395-402.

VOL
14
198

CEMENT and CONCRETE RESEARCH. Vol. 14, pp. 225-230, 1984. Printed in the USA.
0008-8846/84 $3.00+00. Pergamon Press, Ltd.

EXAMINATION OF MORTAR BARS CONTAINING VARYING PERCENTAGES OF COARSELY CRYSTALLINE GYPSUM AS AGGREGATE

N J Crammond
Building Research Establishment, Garston, Herts, UK.

(Communicated by H.F.W. Taylor)
(Received July 15, 1983)

VOL.
14
984

ABSTRACT

Contamination of aggregate sources by coarsely crystalline gypsum occurs frequently in the Middle East. Mortar bars were made which contained up to 5% gypsum (by weight of aggregate) in the form of aggregate pieces. The bars were made using three different cements of varying C_3A content and were stored at 20°C and 38°C. The results show that significant expansions do not occur within mortar bars if their total sulphate content lies below the present British Standard limit of 4% SO_3 by weight of cement. Sulphate Resisting Portland Cement (SRPC) can tolerate a higher level of contaminant gypsum than Ordinary Portland Cement (OPC). Temperature also effects the degree of expansion, especially in the case of high C_3A cement.

Introduction

In concretes, the presence of crystalline gypsum within the coarse and fine aggregate fractions is potentially deleterious. This type of deterioration, here described as internal sulphate attack, has been mentioned in the literature (1-5) and discussed in more detail in ref.(6). Petrographical evidence has shown that coarsely crystalline gypsum present as aggregate within a concrete or mortar reacts with the cement alkalis to form plates of portlandite, which concentrate in the first instance along the boundaries of the gypsum particles; once nucleated, larger crystals of $Ca(OH)_2$ grow inwards towards their centres. The conversion of gypsum into portlandite releases sulphate ions into the adjoining cement paste, initiating sulpho-aluminate formation. Ettringite formation by this mechanism was found to produce significant expansions in laboratory prepared mortar bars containing coarsely crystalline gypsum (6). These mortar bars were prepared using OPC or Rapid Hardening Portland Cement (RHPC) in accordance with the ASTM mortar bar test (7) and significant expansions were experienced by all the bars containing greater than 5% gypsum by weight of aggregate.

At present, the maximum amount of total sulphate permitted by BSI within a concrete is 4% SO_3 by weight of cement (8). The purpose of the present investigation is to determine the level of granular gypsum which can be

tolerated within an aggregate source. OPC and SRPC mortar bars containing 0%, 0.5%, 1.0%, 2.5% and 5.0% gypsum by weight of aggregate have been prepared. The bars are now one year old and this paper has been presented as an interim report. Measurement of the bars will continue and further experimentation has also been suggested. A mineralogical examination of a few selected bars was achieved using XRD and DTA analytical techniques.

Experimental Procedure

Fifty six mortar bars were prepared in accordance with the ASTM mortar bar test (7). The only variation was the use of a 1:2.75 cement:aggregate ratio (1:3 by volume) rather than 1:2.25. The cement content of the bars was 570 kg/m^3. Each aggregate size fraction (Table 1) contained crushed basalt mixed with varying percentages of coarsely crystalline gypsum. Five different levels of gypsum (0%, 0.5%, 1.0%, 2.5% and 5.0% by weight of aggregate) were incorporated into the series of mortar bars. The granular gyspum was received in a fairly pure form from British Gypsum and the basalt was quarried at Clee Hill, Shropshire.

The two aggregates were crushed separately, graded into the Standard fine aggregate fractions (Table 1) washed and then dried. Care had to be employed during the drying process of gypsum, as overheating causes dehydration to form hemihydrate or anhydrite. The five simulated aggregate mixes were mixed with three different cements of varying C_3A content. The w/c ratio was standardised at 0.4. The cement analyses and physical properties of each cement are listed in Table 2. Each mortar mix was used to prepare four bars, two of which were stored at 20°C and two at 38°C. The finished bars were maintained at a RH of 100% throughout their storage life.

The length changes experienced by each mortar bar were monitored using a dial gauge accurate to 0.0025 of a millimetre. The measurements were taken at least once a month.

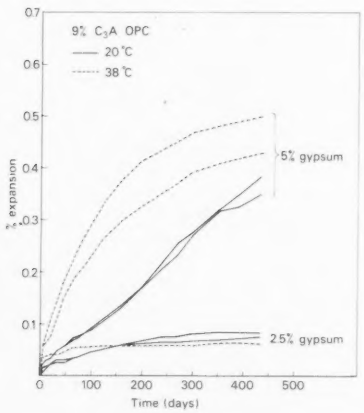

FIG. 1
Expansion curves for the 9% C_3A OPC mortar bars containing 2.5% and 5% gypsum by weight of aggregate

TABLE 1

Sieve Analysis of the Mortar Bar Aggregates

Passing (mm)	Retained (mm)	Weight percent
4.760	2.380	10
2.380	1.180	25
1.180	0.595	25
0.595	0.297	25
0.297	0.150	15

VOL. 14 198

TABLE 2

Chemical Analyses and Physical Properties of the Cements			
Chemical Analyses			
Cement	1	2	3
SiO_2	20.13	20.34	20.12
CaO	63.49	64.56	64.62
MgO	1.31	1.07	0.86
Al_2O_3	5.20	6.60	3.72
Fe_2O_3	2.77	2.10	5.37
TiO_2	0.28	0.28	0.35
P_2O_5	0.22	0.15	0.22
Mn_2O_3	0.03	0.02	0.06
Na_2O	0.21	0.37	0.28
K_2O	0.50	0.52	0.30
Cl^-	0.04	-	-
SO_3	2.77	2.51	2.06
SrO	0.16	0.06	-
BaO	0.01	0.02	-
LOI	1.93	1.22	1.84
Bogue Composition			
C_4AF	8.42	6.38	16.32
C_3A	9.10+	13.94+	0.78
C_3S	66.50	60.83	77.42
C_2S	7.9	12.75	0.00
Physical Properties			
Density (kg/m^3)	3.15	3.21	3.19
Specific Surface (m^2/kg)	334	360	404

+ XRD analysis showed both cubic and orthorhombic C_3A

Cement 1: 9% C_3A OPC
Cement 2: 14% C_3A OPC
Cement 3: SRPC

Results of the Mortar Bar Experiment and Mineralogical Examination

Figs. 1-3 give results for the bars containing 2.5% and 5% gypsum: none of the 0%, 0.5% and 1.0% mortar bars expanded within one year so these results are not shown. All the one year results have been plotted in Fig. 4.

OL.
14
984

The SRPC bars can accommodate 5% gypsum by weight of aggregate without experiencing significant expansion after one year. (The limit above which expansion becomes significant has been taken as 0.1% after 6 months as advised in the ASTM mortar bar test (7)). In the case of the OPC mortar bars, the threshold of permissible granular gypsum contamination lies somewhere between 2.5% and 5.0% by weight of aggregate. The difference between the two types of OPC bars is more noticeable at 20°C. At the lower temperature, the cement containing the larger amount of C_3A has expanded to a greater extent. In addition, the shapes of the curves at the two temperatures are different and are very similar to the results obtained by Richards (9).

The 9% C_3A OPC mortar bars containing 5% gypsum and stored at 20°C differed visually from the rest in that they were patchily covered with a fine grained white deposit. XRD and DTA analysis showed the deposit to contain a mixture of thaumasite and ettringite, with a greater abundance of the former. Thaumasite is isostructural with ettringite and is often associated with the products of sulphate attack. The centre samples of the four OPC bars comprising 5% gypsum by weight of aggregate and stored at both temperatures were also analysed using the above techniques. Gypsum and ettringite were the only sulphate minerals detected and the proportion of ettringite in each bar did not significantly alter as a result of temperature variation or C_3A content. Richards (9) obtained similar results.

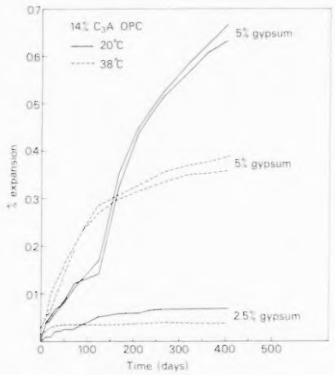

FIG. 2
Expansion curves for the 14% C_3A OPC mortar bars containing 2.5% and 5% gypsum by weight of aggregate

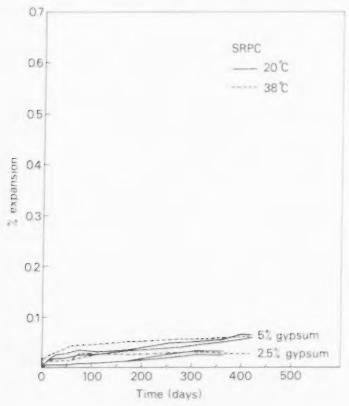

FIG. 3
Expansion curves for the SRPC mortar bars containing 2.5% and 5% gypsum by weight

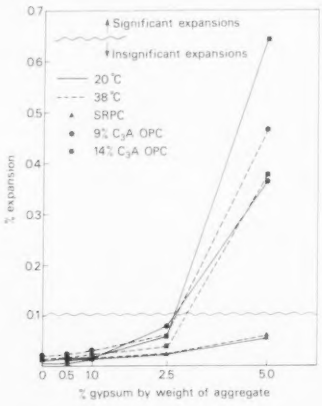

FIG. 4
Graph showing the % expansion of the different mortar bar types at one year

Discussion

Internal sulphate attack is greatly influenced by cement type. Therefore different 'total sulphate' limits can be tolerated depending on whether SRPC or OPC is used. The resistance of SRPC to internal sulphate attack is clearly dependant on the low C_3A content. Previous work (3,6) has shown that RHPC mortar bars containing aggregate gypsum are much superior in performance to equivalent bars made with OPC. Early strength development of the cement paste is the critical factor affecting the improved sulphate resistance of RHPC. Cubic C_3A, as opposed to the less stable orthorhombic variety (10), high specific surface and abundant C_3S all contribute to a high early strength. This is important with respect to internal sulphate attack because the aggregate sulphate is released into the cement paste during the initial period of hardening and strength development. The Ordinary Portland Cements in the present work have failed to build up enough resistance to ettringite precipitation during the early stages of hydration. The increased reactivity at lower temperatures in the case of the 14% C_3A OPC (Fig. 2) is independent of the amount of ettringite formed. Therefore, other factors, possibly related to the hydration characteristics of the high C_3A cement or to ettringite morphology must be responsible. Similar results were obtained by Richards (9) and as he immersed mortars in sulphate solutions, it follows that the effect of temperature is not characteristic of internal sulphate attack in particular but of sulphate attack in general.

VOL.
14
984

Where possible it would be beneficial to specify the concentrations of aggregate sulphate and cement sulphate separately as they influence potential reactivity in different ways. The higher the level of readily accessible crystalline gypsum within an aggregate source, the greater the expansion experienced by a concrete containing the aggregate. However, expansion is not necessarily proportional to the amount of sulphate originating from the cement paste. Retarder gypsum is incorporated into cement clinker to compensate for the quick setting properties of C_3A. Too much retarder sulphate will affect the setting time, strength and expansion of the cement. However, if the cement contains abundant C_3A or it is very fine grained, excess gypsum has to be added in order to maintain the early setting characteristics of the cement. The disadvantage of assessing a potentially reactive situation by the 'total sulphate' content of a mortar or concrete is clearly outlined in Table 3. The SRPC and 14% C_3A OPC bars have very similar sulphate concentrations but the difference in their expansion characteristics is considerable.

The amount of coarsely crystalline gypsum tolerated within an aggregate source should not be much greater than 2.5% by weight of aggregate in the case of OPC mortars. The limit is still not known for SRPC mortars but lies at a level of at least 5%. In the case of laboratory prepared mortar bars, the limit in BS 5328 of 4% total sulphate by weight of cement corresponds roughly to 1% gypsum by weight of aggregate (Table 3). This value lies well below the safety threshold for both types of cement. More work is needed in this field to establish the threshold of permissible aggregate gypsum contamination in construction concrete, where the aggregate/cement ratios will be greater.

Concrete constructions particularly above ground level may be able to tolerate a larger amount of aggregate sulphate than the mortar bars before they show significant expansions. Two of the main reasons are as follows:-

TABLE 3

Weight Percentages of Gypsum and SO_3					
1	2	3	4	5	6
0.0	0.00	0.00	2.77	2.51	2.06
0.5	1.37	0.63	3.40	3.14	2.69
1.0	2.75	1.26	4.03	3.77	3.32
2.5	6.87	3.16	5.93	5.67	5.22
5.0	13.75	6.32	9.10	8.83	8.38

1. Aggregate gypsum by weight of aggregate
2. Aggregate gypsum by weight of cement
3. Aggregate sulphate by weight of cement
4. Total sulphate by weight of cement for OPC with 9% C_3A
5. Total sulphate by weight of cement for OPC with 14% C_3A
6. Total sulphate by weight of cement for SRPC

(1) The mortar bars were kept constantly wet and water is an essential ingredient for internal sulphate attack.

(2) The mortar bars were constructed using pure gypsum whereas in many contaminated aggregate sources the gypsum may be locked away within larger fragments and therefore not readily available for reaction.

In the Middle East, incidences of internal sulphate attack are very infrequent compared with other durability problems such as reinforcement corrosion or seepage of sulphate-rich ground water through concrete structures. However, there is a definite need to monitor aggregate sources and to keep gypsum contamination under control. Work to date indicates that the current limit of 4% total sulphate by weight of cement in the concrete may be overcautious especially in cases where SRPC or RHPC are the cements used. Confirmation on this point is needed by further work with concrete specimens as opposed to mortar bars.

Acknowledgment

The work described has been carried out as part of the research programme of the Building Research Establishment of the Department of the Environment and this paper is published by permission of the Director.

References

1 P.G. Fookes and L. Collis, Concrete 9, 12 (1975).
2 W.J. French and A.B. Poole, Cem. and Conc. Res. 4, 925 (1974).
3 W.J. French and N.J. Crammond, Q.J. Eng. Geol. 13, 255 (1980).
4 M.A. Samarai, Mag. of Conc. Research 28, 130 (1976).
5 A.D. Buck, Proc. of Symposium, Energy and Resource Conservation in the Cement and Concrete Industry, CANMET, OTTAWA, (1976).
6 N.J. Crammond, PhD Thesis, London, (1980).
7 American Society for Testing Materials, Annual Book of ASTM Standards Part 14, Concrete and mineral aggregates, Easton, PA, USA, (1977).
8 British Standards Institution BS 5328, Methods for Specifying Concrete (1976).
9 J.D. Richards, Mag. of Conc. Research, 17, 69 (1965).
10 P.K.Mehta, 7th Int. Congress on the Chemistry of Cement, IV, 575 (1980).

VOL. 14 198

CEMENT and CONCRETE RESEARCH. Vol. 14, pp. 231-237, 1984. Printed in the USA.
0008-8846/84 $3.00+00. Copyright (c) 1984 Pergamon Press, Ltd.

STRESSES AND STRAINS IN THE HARDENED CEMENT PASTE - WATER SYSTEM

J.J. Beaudoin and R.F. Feldman
Research Officers
Division of Building Research
National Research Council Canada
Ottawa, Ontario K1A 0R6

(Communicated by M. Daimon)
(Received June 28, 1983)

OL.
14
984

ABSTRACT

The length change theory proposed by Flood and Heyding for microporous solids is applied to cement paste in considering the effect of porosity and compressibility on the solid phase. The theory is also used to estimate the dependence of modulus of elasticity on humidity and is in general agreement with experiment. Some insight into microstructural change and its effect on length change is provided by estimates of a structure factor, κ. For humidities up to 56%, values of κ are approximately constant, but major changes in structure occur at higher humidities.

Introduction

Hardened portland cement paste (HCP) - a term used to describe the rigid porous body, excluding any free or adsorbed water, formed when cement hydrates - is a multicomponent, microporous, moisture-sensitive material. Numerous studies have been conducted on the mechanical properties of HCP and the model proposed by Feldman and his co-workers (1,2) has been useful in explaining results, e.g., the dependence of modulus of elasticity (E) on humidity where increases in E with humidity were attributed to the stiffening effect of interlayer water.

Thermodynamic treatment of HCP length-change data is complicated because of irreversible processes that occur when the system is wetted. In addition to surface adsorption these processes include intercalation of water between sheets, swelling, agglomeration effects and possibly the effects of shear stresses in the solid material. Flood and Heyding used a thermodynamic approach (subsequently referred to as the F-H approach) to determine theoretically the length change isotherms for water vapor on carbon and for water vapor on porous glass (3). They derived a simple expression for length change as a function of porosity, compressibility of the solid, microstructure of the adsorbent, and amount of H_2O adsorbed. Their theory provides a possible means of assessing both irreversible effects on length changes of HCP and the assumption that these effects are due to exit and entry of interlayer water.

This paper describes the application of the F-H thermodynamic approach to the cement paste-water system and assesses the results based on the model for HCP developed by Feldman and his co-workers.

Length Change Isotherms

F-H Approach

Briefly, the F-H theory assumes that assemblies of volumes of pure adsorbable gas and assemblies of volumes of pure adsorbent can exist separately, in equilibrium with externally applied forces, in states thermodynamically identical to those in the adsorbent-adsorbate system. The conditions of reversibility and equilibrium lead to the following expression for the pressure of the pure adsorbate, p_a, in the pore volume V_a

$$p_a = \int_0^{p_1} \frac{\rho_a}{\rho_1} dp_1 = \overline{\left(\rho_a/\rho_1 \right)} \cdot p_1 = \alpha p_1$$

where ρ_a is the mean density of the substance in V_a, and p_1 and ρ_1 are the gas pressure and density of the gas surrounding the sample. The term, α, is the mean value of ρ_a/ρ_1 averaged over the pressure interval dp_1.

If $\phi = V_a/V_s$, where V_s is the non-porous solid volume, it may be shown that $p_s = (1 + \phi - \alpha\phi)p_1$, which is the pressure on the solid adsorbent in equilibrium with the surrounding gas at pressure p_1.

If the pressure on the solid adsorbent is uniform, the length change isotherm can be obtained from the equation

$$\frac{\delta \ell}{\ell} = \frac{1}{3} \beta \, (1 + \phi - \phi\alpha) dp_1 \qquad (1)$$

where β is the compressibility of the porous body.

Where solid pressures are not constant, κ, a small numerical factor dependent upon the structure of the porous solid, is introduced into eq. (1), i.e., the term in brackets becomes $(1 + \phi\kappa - \phi\kappa\alpha)$. κ, the ratio of the linear average pressures to volumetric average pressures, is generally independent of the nature of the adsorbate, but is a characteristic of the structure of the adsorbent. Flood and Heyding determined values of κ for various ideal models of pore structure, e.g., $\kappa = 1.0$ for a system of continuous non-intersecting straight capillaries, and $\kappa = 5.6$ for a system of continuous intersecting straight capillaries (3). If the shape of the average pore is not statistically independent of the surface free energy of the solid enclosing the average micropore, then κ will become a function of p_1. For large adsorptions $\alpha >> 1$ and

$$\frac{\delta \ell}{\ell} = \frac{1}{3} \beta \phi \kappa dp_a \qquad (2)$$

i.e., $\frac{\delta \ell}{\ell}$ becomes proportional to $\int_0^{p_1} \frac{\rho_a}{\rho_1} dp_1$

Porous Glass

The weight change isotherm for porous glass in the adsorption region is reversible and glass is considered to be relatively stable. Using the length

change data of Amberg and McIntosh (4), Flood and Heyding (3) were able to obtain good agreement between the calculated isotherm and experimental data, suggesting that eq. (2) is applicable to systems in which wetting and drying involve mainly reversible processes.

Hardened Cement Paste (HCP)

HCP-water isotherm. A brief comment on the HCP-water isotherm and on the assumptions made in using isotherm data to apply the F-H procedure follows. Along the adsorption branch of the HCP-water isotherm several reversible and irreversible effects occur. If relative humidity is reduced from a particular value on the adsorption curve, a scanning curve is obtained, for example, curves 1, 2, 3, Fig. 1. It has been argued that (to a first approximation) mainly reversible processes occur over a large part of the scanning curve. A "reversible" isotherm can be constructed by appropriate summation of reversible portions of the scanning curves. Details of this procedure have been published (5). It is assumed that irreversible effects can thus be separated from reversible ones. In addition, it is recognized that the reversible adsorption processes operative along each scanning curve are acting on a material that has changed since the previous scanning curve, i.e., the material is different for each of curves 1, 2, 3, Fig. 1. Thus, in transferring from curves 1 to 2 to 3, irreversible processes are operative. Application of the F-H procedure to the reversible isotherm assumes, however, that the irreversible changes in the solid material (interlayer penetration, etc.) do not affect the nature of the reversible adsorption processes occurring on the surface of the layers, and that surface energy changes are acting on a different material with different properties when positions are changed on the isotherm. It is assumed, then, that a step-by-step application of the F-H procedure along the reversible adsorption path is valid, even where intercalation of the layered silicate hydrate occurs; i.e., since the scanning isotherm is reversible, the F-H procedure is applicable. If scanning isotherms are irreversible, then changes have occurred in the porous system and the F-H procedure cannot be applied. Thus, the procedure may not be applicable when major changes in pore structure occur.

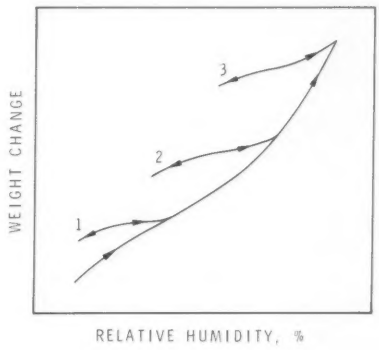

Figure 1

Schematic of primary adsorption curve with scanning curves

Application of F-H procedure to HCP. To apply eq. (2) to the HCP system it is necessary to evaluate the integral $\int_{o}^{p_1} \frac{\rho_a}{\rho_1} dp_1$. Consider the following:

For a cement paste with w/c = 0.50, porosity is approximately 26%. Therefore, $\phi = V_a / V_s = 0.351$. Assuming density of the non-porous solid = 2.2 g/cc, the mass/cc of the porous sample is 2.20 × 0.74 = 1.63 g/cc or 1 g of porous sample = 1/1.63 = 0.610 cc.

Thus V_a/g of sample = $0.260 \times 0.610 = 0.160$ cc

and $$\rho_a = \frac{\Delta W/W}{V_a} = 6.26 \frac{\Delta W}{W} \quad (3)$$

where $\Delta W/W$ = weight change per unit weight of sample. The mass of the gas in the void volume, V_a, is negligible in relation to the mass of the adsorbed phase. The density of the gas (water vapor) ρ_l is 18.34×10^{-6} g/cc at 21°C and 100% RH.

Data from weight and length change isotherms are taken from Feldman (5). Using scanning loops, these isotherms were separated into irreversible and reversible isotherms. The reversible isotherm is used in the following calculations:

A plot of $\frac{\rho_a}{\rho_l}$ versus ρ_l is given in Fig. 2; and the integral $\int_o^{p_1} \frac{\rho_a}{\rho_l} dp_l$ is evaluated graphically by determining the area under the curve. This provides a measure of $p_a = \alpha p_l$ = pressure of adsorbate. A curve of αp_l versus p_l (not presented) was constructed to assist in the calculations. Thus, eq. (2) can be fitted to the experimental length change data by assuming an appropriate value for $\beta\kappa$.

Figure 3 is a plot of length change versus vapor pressure, giving curves for eq. (2) and experimental values. A single average value of $\beta\kappa = 1.76 \times 10^{-4}$ MPa^{-1} was chosen to give a close fit between the experimental length change data and eq. (2).

Although this value of $\beta\kappa$ gives an approximation of the experimental data, $\beta\kappa$ varies with p and a more exact fit can be obtained by calculating $\beta\kappa$ at each data point. Values of $\beta\kappa$ at different humidities along the adsorption curve were calculated from eq. (2) using experimental values of $\delta\ell/\ell$. These values are given in Table 1.

Values of $\beta\kappa$ were also calculated for an HCP-water isotherm scanning curve over the range 56 to 11% RH. $\beta\kappa$ was approximately constant over that portion of the scanning curve (56 - 40% RH) used to construct the reversible isotherm. This supports the assumption that material properties are constant on the segment of each scanning curve used to construct the reversible isotherm.

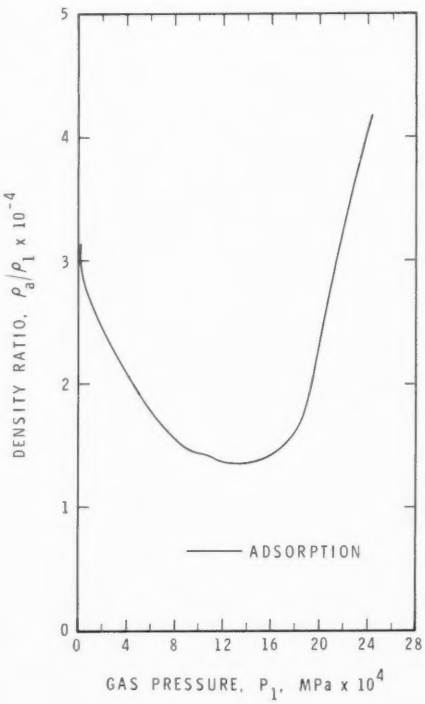

Figure 2

Ratio of adsorbate density to gas density versus gas pressure

VOL. 14 1984

TABLE 1

Calculation of compressibility and modulus of elasticity for HCP from adsorption data

RH %	$\frac{\delta \ell}{\ell} \times 100$	αp_1 MPa	$\beta\kappa$ $\times 10^{4}$ MPa^{-1}	β^* $\times 10^{4}$ MPa^{-1}	E $\times 10^{-5}$ MPa
10.3	0.016	6.67	2.06	1.08	0.167
12.7	0.018	7.88	1.96	1.03	0.176
15.4	0.020	9.18	1.85	0.97	0.186
18.5	0.022	10.74	1.76	0.92	0.196
24.1	0.026	12.99	1.70	0.89	0.202
27.8	0.030	14.28	1.79	0.94	0.192
31.1	0.032	15.84	1.73	0.91	0.199
34.0	0.033	16.93	1.68	0.88	0.206
37.4	0.035	18.09	1.65	0.86	0.209
42.7	0.037	20.13	1.56	0.82	0.221
45.3	0.039	20.67	1.60	0.84	0.216
48.5	0.040	21.90	1.56	0.82	0.221
51.5	0.041	22.71	1.52	0.80	0.226
53.6	0.042	23.46	1.52	0.80	0.226
56.6	0.043	24.48	1.49	0.78	0.230
62.2	0.047	26.04	1.57	0.82	0.219
66.9	0.052	27.54	1.60	0.84	0.216
72.5	0.057	29.85	1.63	0.85	0.245
88.0	0.080	36.72	1.85	0.97	0.265

* Calculation made using $\kappa = 1.91$

Values of β are calculated from $\beta\kappa$ values, assuming $\kappa = 1.91$. Choice of this κ value gives an initial value of β comparable to β calculated from the relation $\beta = \frac{3}{E}(1 - 2\upsilon)$, where υ is Poissons ratio of 0.20, as well as β determined by other methods (6). (Calculations of $\beta\kappa$ were also made using length change data for the porous glass-water system, but these are not tabulated.)

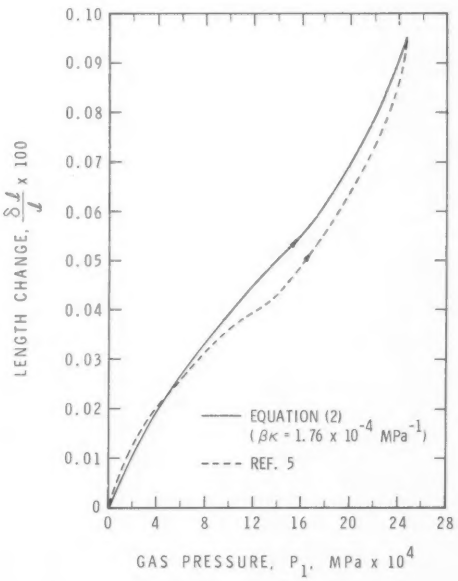

Figure 3

"Reversible" length change isotherm for portland cement paste, w/c = 0.50, experimental and theoretical

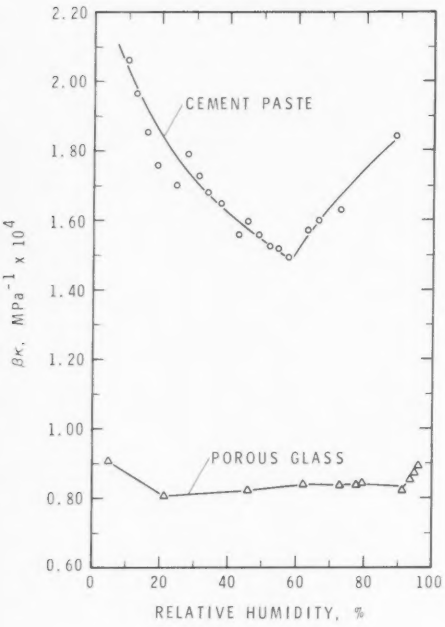

Figure 4

Dependence of βκ on relative humidity for cement paste and porous glass

Figure 4 is a plot of βκ for both HCP and porous glass. βκ for HCP is dependent on RH, whereas for porous glass it is independent of RH. It would be expected that porous glass would be stable, i.e., not undergo a material change as RH increases. Thus, the relatively constant value of βκ determined by the F-H procedure is appropriate. The dependence of βκ on RH is expected for HCP since the hydrated calcium silicates are unstable, i.e., C-S-H solids change as RH increases.

Figure 5 is a plot of E versus RH for HCP. One of the curves is a plot of the calculated E (determined by F-H procedure using $\kappa = 1.91$).

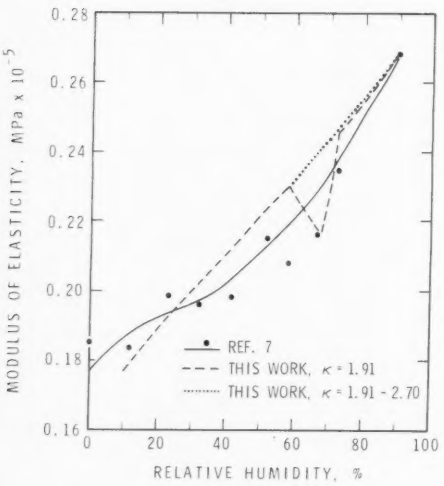

Figure 5

Modulus of elasticity versus relative humidity for cement paste, w/c = 0.50

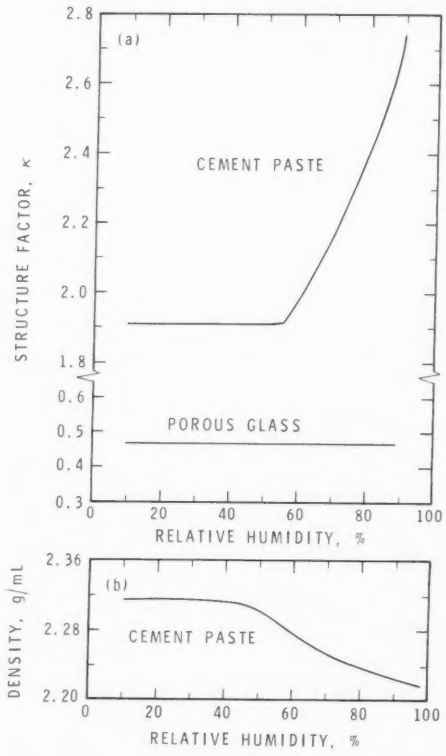

Figure 6

(a) Structure factor κ versus relative humidity
(b) Density of HCP exposed to various relative humidities and returned to 11% RH

Another curve is a plot of experimental values of E (7). On adsorption up to 56% RH, the two curves have a maximum difference in E (at any RH) of only 0.01×10^5 MPa, and E increases with RH. At higher humidities use of the structure factor $\kappa = 1.91$ gives decreasing values of E to 68% RH, followed by another increase in E as RH increases further. By adjusting κ at each humidity above 56% RH, however, (and determining a new value of β from $\beta\kappa$), the calculated value of E increases monotonically as the dashed curve (Fig. 5) is extended from 56 to 88% RH. The extended curve also gives values of E close to those determined by experiment.

Figure 6a is a plot of κ versus RH for HCP and porous glass. κ is constant for HCP up to 56% RH and is humidity-dependent thereafter. κ for porous glass is constant over the whole humidity range. Several irreversible changes take place in HCP at higher humidities. It is known, for example, that rewetting a dried sample above 50% RH significantly increases creep and drying shrinkage. It is in the high humidity range that the microstructure, and hence pore shape and/or contiguity, may be altered; for example, in Fig. 6b it is shown that absolute density (measured on samples of HCP exposed to various RH's and dried to 11% RH) is constant to about 42% RH and decreases thereafter. Experiments have shown that after wetting HCP to 42% RH, He gas is able to penetrate fully spaces previously vacated by water (8). It is noteworthy that each point on the curve in Fig. 6b represents the density of HCP that has been conditioned along each different scanning curve of the isotherm, since the material on each is different. The change in density at higher humidities suggests that microstructural changes, in addition to those occurring at lower humidities, occur (changes at lower humidities are attributed mainly to interlayer penetration). These changes appear to be reflected in the changing value of κ at higher humidities.

VOL.
14
984

Concluding Remarks

The Flood-Heyding length change theory for microporous adsorbents can be used to estimate the reversible length change isotherm for hardened cement paste and gives credence to the model of cement paste developed by Feldman and his co-workers. The theory is also in agreement with the observed humidity dependence of modulus of elasticity for the cement paste system. Although many of the irreversible microstructural changes resulting from wetting and drying of HCP are indeterminate, an appreciation of these effects can be obtained from estimates of the structure factor κ. Significant changes in the value of κ at humidities greater than 56% RH are concurrent with changes in the solid density of HCP.

References

1. R.F. Feldman and P.J. Sereda, Eng. J. 53, 53 (1970).
2. R.F. Feldman and V.S. Ramachandran, Cem. Concr. Res. 4, 155 (1974).
3. E.A. Flood and R.H. Heyding, Can. J. Chem. 32, 660 (1954).
4. C.H. Amberg and R. McIntosh, Can. J. Chem. 30, 1012 (1952).
5. R.F. Feldman, Proc. Vth Int. Symp. Chem. Cement, Tokyo, III-23, 53 (1968).
6. R.A. Helmuth and D.H. Turk, Proc. HRB, Spec. Rep. 90, 135 (1966).
7. V.S. Ramachandran, R.F. Feldman and J.J. Beaudoin, Concrete Science, Heyden & Son, Ltd., pp. 398 (1981).
8. R.F. Feldman, Cem. Concr. Res. 4, 1 (1973).

CEMENT and CONCRETE RESEARCH. Vol. 14, pp. 238-248, 1984. Printed in the USA.
0008-8846/84 $3.00+00. Copyright (c) 1984 Pergamon Press, Ltd.

MECHANISM AND KINETICS OF HYDRATION OF C_3A AND C_4AF, EXTRACTED FROM CEMENT.

C. Plowman and J.G. Cabrera

Department of Civil Engineering, The University of Leeds, Leeds LS2 9JT, England.

(Communicated by F.H. Wittmann)
(Received July 21, 1983)

ABSTRACT The early hydration of C_3A + C_4AF extracted from cement and mixes with quartz, gypsum and pulverised fuel ash (PFA) has been studied by x-ray diffraction. The investigation has shown that the hydration of both aluminates is essentially a mechanism which obeys a modified diffusion equation. The values obtained for the reaction rates show that the hydration of C_3A takes place at seven times the rate of hydration of C_4AF. PFA was shown to be a very effective retarder. A mechanism to explain retardation is also proposed.

VOL 14 198

Introduction

Addition of gypsum during the grinding process for the production of cement is the industrial accepted method for controlling flash setting which arises from the rapid hydration of cement. It is accepted that the main constituent of cement responsible for flash setting is C_3A, and that gypsum retards the hydration of this phase.

What is still a matter of controversy is the manner in which gypsum retards hydration; also there is very little information regarding the mechanism and kinetics of hydration of C_3A and C_4AF. The theories proposed to explain retardation of hydration can be broadly divided in two groups:

(a) The protective layer theory: researchers supporting this theory disagree mainly on the composition of the protective layer. Earlier work in the 1950's (1) advanced the idea that the protective layer consisted of a thin layer of ettringite formed around the aluminate particles. Later work (2,3,4) including the investigations of Collepardi et al (5) have supported this theory. Other investigators, notably Gupta, Chatterji and Jeffery (6) came to the conclusion that the impervious layer consists of C_4AH_n which is formed on the aluminate grains in the presence of CH and $C\bar{S}H_2$. They indicated that the thin C_4AH_n layer is overlaid with ettringite; when the ettringite cover becomes sufficiently thick, the mobility of the sulphate ion is restricted and thus the tetra-aluminate will be converted to monosulphate instead of ettringite.

(b) Incongruent dissolution of C_3A and C_4AF: Skalny and Tadros (7) studied the electrokinetic behaviour of C_3A and came to the conclusion that retardation of the hydration process is due to the formation of positively charged C_3A particles by adsorption of calcium, which reduces the active dissolution sites. They also suggested that $C\bar{S}H_2$ does not change the reaction path of the chemical processes which occur during hydration, but that adsorption of sulphate ions on the positively charged particles reduces still further the number of active sites. Forsen (8) postulated retardation to be due solely to sulphate, and his view was later supported by Feldman and Ramachandran (9). They suggested that it is the adsorption of sulphate ions on C_3A which is responsible for reduction of the rate of reaction. In the incongruent dissolution theories, the formation of ettringite is not related to the retardation effect.

More recently Birchall et al (10) have presented a mechanism based on the formation of an amorphous and gelatinous solid which acts as a continuous membrane around C_3A grains. This osmotic membrane allows water to diffuse inwards but stops the reaction proceeding until the intra-membrane pressure is sufficient to rupture the membrane. The manner in which the amorphous membrane is formed can then be explained either in terms of incongruent dissolution or in terms of a reaction of the type supported by Gupta et al (6).

Boikova et al (11) have recently studied the mechanism of hydration of C_3A. They have suggested that hydration of C_3A can be described by three distinct stages: the first stage is characterized by a rapid intense reaction lasting 10 to 12 minutes, the second stage distinguished by a retardation of the hydration process lasting up to 100 minutes and finally a long term third stage with very little hydration. Boikova et al applied to their studies the kinetic empirical equation developed by Kondo and Ueda (12) for the study of C_3S hydration. They limited their study to the second stage of the hydration of C_3A and, in the light of their results, suggested that the second stage of the hydration of C_3A is a diffusion controlled process.

A problem of practical importance is the effect of pozzolanic additives on the rate of hydration of C_3A and C_4AF since it is well known that the addition of pulverized fuel ash (PFA) to the constituents of concrete reduces the heat of hydration. Collepardi et al (13), investigating the effects of natural pozzolanas on the hydration of C_3A, confirmed the known effect of reduction of heat evolution during the hydration process but also suggested that in addition to the reaction between lime and pozzolanas, some other reaction between C_3A or its hydration products and the pozzolanas can occur. Cabrera and Plowman (14) have reported that pulverized fuel ash is an effective retarder of the hydration of C_3A and C_4AF. They have suggested that the mechanism of retardation of the hydration of the aluminate is probably similar to the mechanism which operates when gypsum is used as a retarding agent.

The object of the present paper is to present information obtained from an experimental study of hydration of C_3A and C_4AF using as retarders gypsum, quartz and PFA. The laboratory data is also used to study the mechanism of hydration and thus to determine quantitatively the rates of hydration of C_3A and C_4AF.

Materials

Most of the studies on the hydration of C_3A and C_4AF reported in the literature have used laboratory produced materials. However there are methods which can be used to isolate C_3A and C_4AF from ground cement clinker. The calcium silicate phases and calcium oxide can be extracted by using either a

TABLE 1

Chemical Composition of the Materials Used in the Investigation

Oxide	Pulverised Fuel Ash %	Ordinary Portland cement %	C_3A/C_4AF %
SiO_2	48.96	20.90	3.05
Al_2O_3	27.18	5.42	28.70
Fe_2O_3	10.85	2.70	11.33
CaO	1.57	64.90	48.90
MgO	1.30	2.23	3.52
K_2O	3.81	0.86	0.71
Na_2O	0.78	0.13	0.16
TiO_2	0.93	0.25	0.62
SO_3	1.25	2.68	0.15

maleic acid/methanol solution (15,16) or a salicylic acid/methanol solution (17,18). Anhydrite and other calcium sulphates can be removed with ammonium chloride solution (19).

During this investigation the aluminates were obtained using the maleic acid/methanol solution followed by the ammonium chloride solution. The products obtained at this stage cannot be hydrated. Both C_3A and C_4AF are passivated by the maleic acid, but they can be reactivated by ignition at a temperature high enough to destroy the maleic acid. This method will not remove all of the SiO_2 content of the cement, since some of this is in solid solution with the C_3A.

Table 1 shows the oxide composition of the final mixture of C_3A and C_4AF, and also the oxide composition of the original cement and that of the PFA used. The specific surface of the extracted material measured by the nitrogen adsorption method gave a value of $4.6 m^2/g$ with a mean particle diameter of approximately $2\mu m$.

The specific surface of the PFA was $1.1 m^2/g$ with a mean particle diameter of approximately $8\mu m$. Ground quartz, acid-washed, used as a diluting material had a maximum particle diameter of approximately $50\mu m$.

The hydration process was studied with five mixes, their composition is shown in Table 2. The mixes were hydrated using a constant water/solid ratio of 0.7. Mix 3 contained an amount of gypsum equivalent to a minimum addition of 2% to the original cement clinker which had approximately 25% content of C_3A and C_4AF. Mix 4 contains an amount of gypsum equivalent to the amount of sulphate present in the PFA.

TABLE 2

Composition of the Dry Mixes

Mix No.	$C_3A + C_4AF$ mg	Quartz mg	PFA mg	Gypsum mg
1	1000	-	-	-
2	700	300	-	-
3	700	300	-	56
4	700	300	-	8.1
5	700	-	300	-

Experimental Procedures

The course of hydrations was followed with a Philips APD-10 computer controlled diffractometer, with Cu Kα radiation at 45 kV, 55mA, 1° divergence and receiving slits, and a proportional detector fitted with a graphite monochromator. This was programmed to scan from 5° 2θ to 40° 2θ at 16° 2θ per minute, recycling after each scan. One scan was carried out every 2.5 minutes.

Samples were prepared by mixing rapidly but carefully the material to be hydrated with the appropriate amount of distilled, deionised and freshly boiled water. The resulting paste was mounted in a sample holder of an automatic sample changer and introduced to the nitrogen-flushed x-ray diffractometer. If the sample was not in the diffractometer within one minute of the commencement of mixing, the sample was discarded and the procedure was repeated. The sample was maintained in a nitrogen atmosphere during the period of x-ray scanning. An initial investigation carried out prior to the present experiments showed that unless carbon dioxide is excluded, carbonation is very rapid. The compound $C_3A.CaCo_3.12H_2O$ was observed after 5 minutes, and this almost completely suppressed the formation of hydration products for several hours. Comparison with external control samples showed that the rate of hydration was not affected by the sample remaining in the x-ray beam continuously.

As indicated before, the scanning speed necessary to follow the hydration process was very high. This precluded the possibility of quantitative analysis mainly due to relatively poor angular resolution, and to the reduced peak intensity (about 10%) resulting from the relatively long response time of the chart recorder. No attempt was made, therefore, to make an absolute measurement of the amount of a particular phase, but it was found to be perfectly feasible to measure the change in the intensity of a peak, even when quite a severe overlap exists.

Results and Discussion

Retardation Mechanism

It is assumed that peak intensity of the x-ray diffraction trace is proportional to the volume of the crystalline compound being studied, thus the

course of hydration can be followed by relating graphically the change in peak intensity with time of hydration. Figures 1, 2, 3 and 4 show the hydration-time relations for mixes 1, 2, 3 and 5. In general the amount of the aluminates decreases with time, this decrease is, as can be expected, very large for mix 1 and very small for mix 3. The detection of C_2AH_8/C_4AH_n and later on C_3AH_6 confirms the accepted view that the initial crystalline product of hydration is the hexagonal hydrate which converts to the stable cubic C_3AH_6. Breval (20) in a scanning electron microscope and x-ray diffraction study on the hydration of laboratory synthesised C_3A detected irregular flakes of C_2AH_8 and C_4AH_{13} after 6 minutes of hydration at 20°C. Hexagonal aggregates of C_2AH_8 and C_4AH_{13} as well as crystals of C_3AH_6 were only seen after 100 hours of hydration.

The development of hexagonal hydrates at 15 minutes can be seen for both the C_3A/C_4AF (mix 1), and the C_3A/C_4AF with PFA (mix 5), in figures 5 and 6.

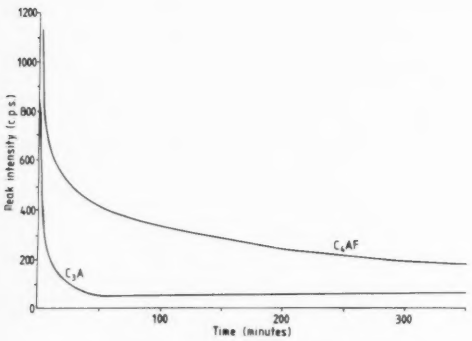

FIG. 1

Hydration-Time Relation for C_3A + C_4AF (mix 1)

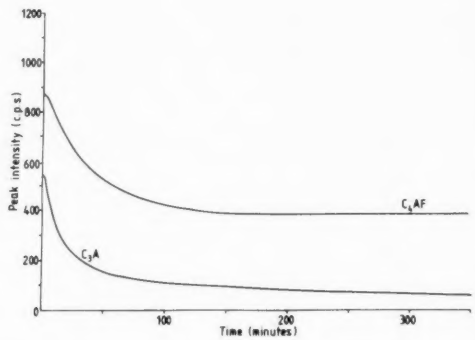

FIG 2

Hydration-Time Relation for C_3A + C_4AF + 30% quartz (mix 2)

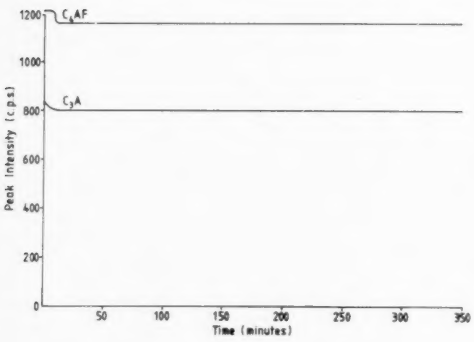

FIG 3

Hydration-Time Relation for C_3A + C_4AF + 30% quartz + 56 mg gypsum (mix 3)

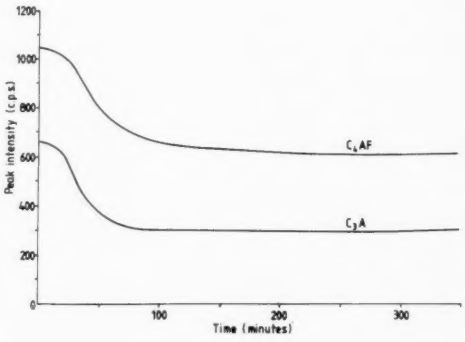

FIG 4

Hydration-Time Relation for C_3A + C_4AF + PFA (mix 5)

The most noticeable difference between the hydration-time relations is the time at which the stable cubic hydrates appear. For the pure C_3A + C_4AF the time is less than 15 minutes. This is interpreted as rapid conversion of the metastable lamellar form to the stable cubic form. It is thought that in the presence of water the conversion takes place at a rate which is reflected by the decrease in the volume of the aluminates. The reaction can then be written as:

$$2C_3A + H \rightarrow \{\begin{matrix} C_2AH_8 \\ C_4AH_n \end{matrix}\} \rightarrow 2C_3AH_6$$

The C_4AH_n phase is unstable in the presence of water but can be stabilised with decrease in the quantity of available water. Therefore the lamellar C_4AH_n which is formed around the aluminate grains can be viewed as a protective coating which, if not converted to the more permeable cubic packing will retard the hydration of the aluminates. In the case of mix 1, figure 5 shows that C_3AH_6 is detected very early, while in mix 5 (fig. 6) it appears later. In the case of mix 3 which contains 56mg of gypsum, C_3AH_6 is not detected for the duration of the experiment.

In the presence of gypsum or in the presence of sulphate and calcium ions (mix 5) the path of the reactions taking place can be simplified as follows:

$$4C_3A + H + \bar{S} \rightarrow \begin{cases} 3C_4AH_n(\bar{S}) \rightarrow 3C_4AH_{n-x}(\bar{S}) \\ + \\ AH_3 \end{cases}$$

$$4C_3A + H + \bar{S} \rightarrow C_3A3C\bar{S}31H \rightarrow C_3AC\bar{S}12H$$

The hydrates $C_4AH_n(\bar{S})$ and $C_4AH_{n-x}(\bar{S})$ are non-stoichiometric, and are considered to incorporate variable amounts of sulphate in the hexagonal structure. They are analogous to the compound described as "C_4AH_{13} containing essential carbonate" which has been reported in the literature (5). The degree of disorder introduced into the crystalline lattice by the incorporation of sulphates, inhibits recrystallisation to C_3AH_6.

The mechanism of retardation can be explained by the action of the protective coating created by the amorphous AH_3 and the lamellar $C_4AH_{n-x}(\bar{S})$ and not, as been proposed by many (2,3,4,5), by a protective layer composed of ettringite. It seems reasonable to suggest that the formation of ettringite results in a reduction of the amount of water available in the vicinity of the hydrating compounds and thus it reduces or retards the formation of the cubic C_3AH_6. This mechanism of retardation is similar to the mechanism proposed by Gupta et al (6) but it clarifies further the actual role of ettringite. The importance of postulating that ettringite acts as an inhibitor of water availability is that the mechanism of retardation can be generalized for inorganic and organic compounds. Young for example (21) has explained the effect of retardation of C_3A hydration by organic compounds, postulating that the conversion from C_4AH_n to C_3AH_6 is hindered by the organic compounds; Sakai et al (22) indicated that organic compounds retard C_3A hydration by preventing contact between water and C_3A, and showed that the effectiveness of the organic molecules in retarding hydration was related to their ability to repel water from the vicinity of the hydrating materials.

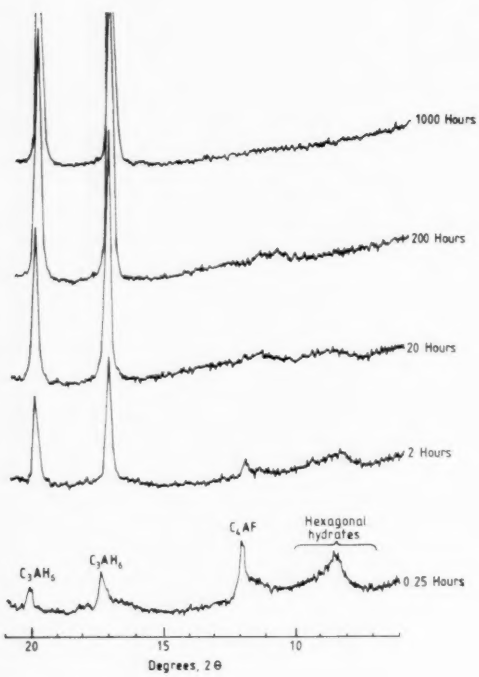

FIG 5

XRD traces for the hydration of $C_3A + C_4AF$ (mix 1)

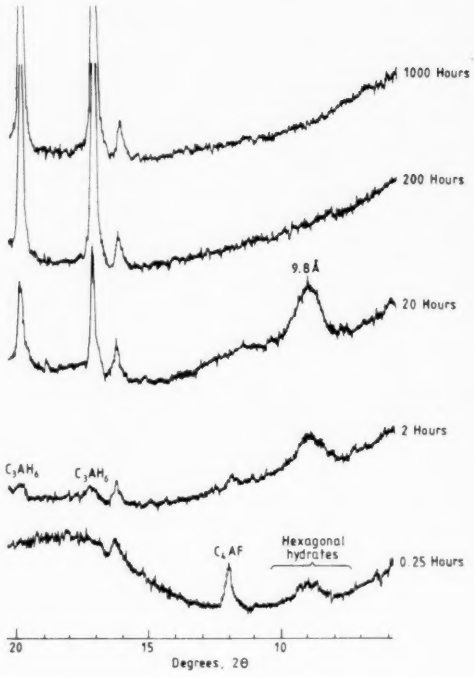

FIG 6

XRD traces for the hydration of $C_3A + C_4AF + PFA$ (mix 5)

Hydration Kinetics

The investigation in this paper was limited to the study of the mechanism and kinetics of hydration during the early part of hydration, i.e. during the initial 30 minutes. The authors of this paper agree with Boikova et al (11) with reference to the three distinct stages which may be observed during the hydration process, thus this study deals only with the first stage for which there has been no quantitative data available.

Various models for solid state reactions have been proposed to quantify the hydration processes in cement or its constituents (12,23). During these studies two possible mechanisms were investigated, the dissolution model (24) and the diffusion model originally suggested by Jander (25).

The experimental results did not fit the dissolution model but gave very close results with the values obtained using a modified diffusion equation, i.e.

$$(1 - (1-x)^{\frac{1}{3}})^2 = Kt - C$$

where:

$K = 2k/(0.5d)^2$

k = rate constant

d = diameter of reacting sphere

t = time of hydration

x = fraction which has reacted

C = empirical constant

The value of K can be taken as proportional to the rate constant and therefore when plotting time against the first term of the modified diffusion equation expressed as f(x), the slope of the straight line corresponds to the rate constant.

The lines obtained are shown in Figures 7 and 8. These lines were fitted by statistical analysis. The corresponding constants for the modified diffusion equation are shown in Table 3.

The values of K show clearly the extent of the differences in rate of hydration of the different systems (mix 3 is not shown here since the hydration is completely suppressed (Figure 3)). The influence of PFA on the rate of reaction of C_3A is far more effective than the one shown for a greater quantity of gypsum. In fact, the rate constant decreases approximately 7 times and hydration is practically suppressed during the initial 7 minutes. This finding is very significant from the point of view of using PFA materials for the production of blended cements.

TABLE 3

Numerical Values for the Constants of the Modified Diffusion Equation Obtained by Statistical Analysis

Mix No.	C_3A			C_4AF		
	K	C	*r^2	K	C	r^2
1	4.945×10^{-3}	-1.198×10^{-3}	0.95	8.072×10^{-4}	-1.511×10^{-3}	0.91
2	3.000×10^{-3}	6.000×10^{-3}	0.90	1.000×10^{-3}	3.000×10^{-3}	0.85
4	2.632×10^{-3}	1.000×10^{-2}	0.94	8.405×10^{-4}	1.000×10^{-2}	0.95
5	6.705×10^{-4}	4.680×10^{-3}	0.78	1.230×10^{-4}	1.030×10^{-3}	0.87

* r = coefficient of correlation
The significance level was for all cases < 0.001

The effect of quartz used as a diluent is one of reducing the rate and the commencement of hydration of C_3A, these changes are modest when compared with changes occasioned by PFA. It should be pointed out that this finding does not agree with the findings reported by Holten and Stein (26).

The rate constants for the hydration of C_4AF are, as can be seen in Figure 8, far smaller than for C_3A; this agrees with other findings but quantifies the extent of the differences, i.e., for pure C_3A the rate constant is approximately six times higher than for C_4AF.

On the strength of the statistical analysis which clearly shows the relation between the modified diffusion equation and the experimental data, it is proposed that the early stages of the hydration of $C_3A + C_4AF$ for the different mixes investigated follows a mechanism which can be described as diffusion. The study is continuing, to ascertain whether the other stages of the reaction follow the same mechanism using the same simple expressions or if they follow other models.

VOL. 14 1984

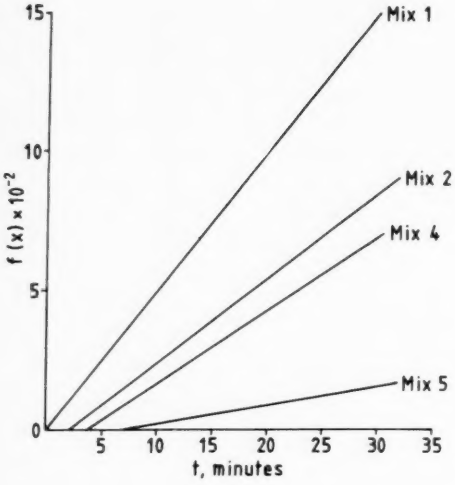

FIG 7
Relation Between the First Term of the Diffusion Equation f(x) and the Time of Reaction for C_3A

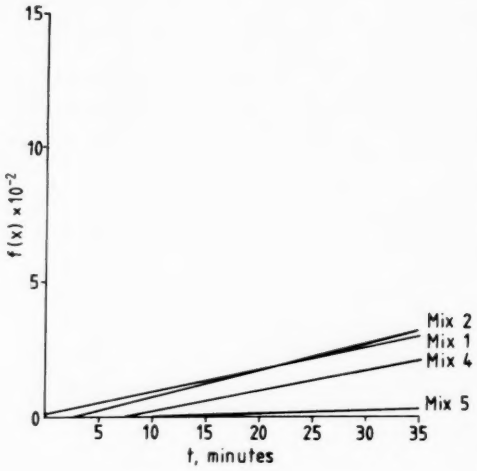

FIG 8
Relation Between the First Term of the Diffusion Equation f(x) and the Time of Reaction for C_4AF

The effectiveness of PFA as a retarder of the hydration of the aluminates can be explained by the extremely rapid release of both SO_3^{2-} and Ca^{2+} ions into solution. This has been reported elsewhere (27). Furthermore, the shape and surface properties of PFA are suitable to produce dispersion of the aluminates during the mixing process so that the distribution of SO_3^{2-} and Ca^{2+} ions is far more efficient than when using only equivalent quantities of gypsum in the solution as has been shown for mix 4 (Table 3).

Conclusions

1. This investigation has shown that the study of hydration during the initial stage can be carried out by an x-ray diffraction technique with an acceptable degree of accuracy. The use of $C_3A + C_4AF$ directly extracted from ordinary Portland cement is preferable to the use of synthetic materials.

2. The results obtained during this study indicate that the retardation of hydration occurs due to the formation of a protective coating consisting mainly of $C_4AH_{n-x}(\bar{S})$ which is stabilized by the incorporation of sulphate and the reduction of available water when ettringite is formed in the system. Stabilization of the hexagonal hydrates by deficiency of water in the vicinity of the hydrating system is a mechanism which has been invoked to explain the effect of organic retarders; thus it can be generalised to explain the retardation process.

3. The early stages of the hydration process, with a duration of approximately 30 minutes, obey a diffusion mechanism which can be quantified by a modified diffusion equation.

VOL
14
198

4. The rate constant for C_3A hydration is approximately six times larger than the rate constant for C_4AF.

5. PFA is shown to be a very effective retarder, in fact the rate constant for the mix containing PFA was approximately seven times smaller than the rate constant for the pure aluminates.

References

1. H.H. Steinour, Res. Dev. Labs. Portland Cement Assoc. Res. Dept. Bull. 98, 124, (1958)

2. N.N. Stein, Silicate Industry 28, 3, 41 (1963)

3. P. Seligmann and N.R. Greening, HRR. 62, 80 (1964)

4. H.E. Schwiete, U. Ludwig and P. Jaeger, Highway Research Board SR 90, 353 (1966)

5. M. Collepardi, G. Baldwin and M. Pauri, Jour. Am. Cer. Soc. 62, 33 (1979)

6. P. Gupta, S. Chatterji and J.W. Jeffery, Cement Technology 4, 4, 146 (1973)

7. J. Skalny and M.E. Tadros, Jour. Am. Cer. Soc. 60, 3-4, 174 (1977)

8. L. Forsen, Proc. of the Symposium on the Chemistry of Cement, Stockholm, Sweden 298 (1938)

9. R.F. Feldman and V.S. Ramachandran, Mag. of Conc. Res. 18, 57. 186 (1966)

10. J.D. Birchall, A.J. Howard and D.D. Double, Cem. Con. Res. 10, 2, 145 (1980)

11. A.I. Boikova, I. Domansky, V.A. Paramonova, G.P. Stavitskaja and V.M. Nikushchenco, Cem. Con. Res. 7, 247, (1977)

12. R. Kondo and S. Ueda, Proc. Vth Symp. on the Chemistry of Cements, p. 203 Tokyo (1969)

13. M. Collepardi, S. Monozi, G. Moriconi and M. Corradi, Cem. Con. Res. 9, 431, (1979)

14. J.G. Cabrera and C. Plowman, Proc. VIIth Int. Congr. Chem. Cem. 3, IV-85 Paris (1980)

15. J.E. Mandar, L.D. Adams and E.E. Larkin, Cem. Con. Res. 4, 533 (1974)

16. R. Tabikh and R. Weht, Cem. Con. Res. 1, 317 (1971)

17. S. Takashima, Rev. 12th Gen. Meeting, Cem. Ass. Japan, 12-13, Tokyo (1958)

18. W.A. Gutteridge, Cem. Con. Res. 9, 319 (1979)

19. K. Mather, Adv. X-ray Anal., 20, 41 (1977)

VOL.
14
1984

20. E. Breval, Cem. Con. Res. 6, 129 (1976)

21. J.F. Young, Jour. Amer. Cer. Soc. 53, 65 (1976)

22. E. Sakai, K. Raina, D. Asaga, S. Goto and R. Kondo, Cem. and Con. Res., 10, 311 (1980)

23. J.M. Pommersheim and J. Clifton, Cem. and Con. Res., 9 (1979)

24. E. Raask and M.C. Bhaskar, Cem. and Con. Res. 5, 363, (1975)

25. J.G. Cabrera and C.A. Nwakanma, Transp. Res. Rec. 702, 199 (1979)

26. C.L.M. Holten and H.N. Stein, Cem. and Con. Res., 7, 291 (1977)

27. J.G. Cabrera and C. Plowman, Proc. Int. Symp. Use of PFA in Concrete, 1, 111, Leeds, U.K. (1982)

VOL
14
198

CEMENT and CONCRETE RESEARCH. Vol. 14, pp. 249-256, 1984. Printed in the USA.
0008-8846/84 $3.00 + 00. Copyright (c) 1984 Pergamon Press, Ltd.

HARDENED PORTLAND CEMENT PASTES, MODELISATION OF THE MICRO-STRUCTURE AND EVOLUTION LAWS OF MECHANICAL PROPERTIES I- BASIC RESULTS

J.L. Granju and J.C. Maso
Laboratoire de Génie Civil
de l'Institut National des Sciences Appliquées
et de l'Université Paul Sabatier de Toulouse
(équipe de recherche associée au C.N.R.S. n°998)

(Communicated by M. Regourd)
(Received July 18, 1983)

VOL.
14
1984

ABSTRACT

This paper is the first of a series of three. For Portland cement pastes, it presents a model of the micro-structure and the associated compressive strength law which will be the base of the two following papers.

Model and strength law involve that the most important parameter influencing the strength is the capillary porosity. They allow to foresee the characteristic properties of the pastes of the first and of the second group. At last they give informations about the structure of the gel.

Introduction

This paper presents a model of the micro-structure of Portland cement pastes elaborated conjointly with a compressive strength law. It is in fact a compilation of results already published separatly (1)(2). Reminding them, arranged in order, is necessary for the good understanding of the following papers. In a second paper we will confirm the validity and the generality of both the model and the strength law proposed here. We will also benefit by new results to improve the model. At last, in a third paper, confident on the micro-structure model then confirmed, we will draw out the variation law of the elastic modulus and specify the evolutions of the parameters concerned.

The micro-structure model elaborated here derives, on the one hand from the mechanism of the growth of the hydrated material proposed by T.C. Powers (3), on the other hand from our previous, purely mechanical, results (1)(2).

Review

The mechanism of the growth of the hydrated material proposed by T.C. Powers may be reminded as following. Although T.C. Powers does not clearly refer to the notion of "hydrated grain" it is helpful to use it. We call "hydrated grain" the bulk volume obtained from a cement grain initialy anhydrous. It is made of a porous volume of hydrates, so called "gel", encapsuling an eventual

anhydrous part. In fact it does not exist "hydrated cement grains" but a bulk of eventual different anhydrous remainders of C_3S, C_2S, C_3A or C_4AF, gypsum and the porous agglomeration of various hydrates. Thus this notion of hydrated grain must be considered only in its lump, as the statistical image of the average grain, the agglomeration of which having the properties of the considered paste.

T.C. Powers has shown that the bulk volume V of the hydrated grain is larger than the volume V_o of the initial unhydrated grain. Hydration thus induces a swelling $K = V/V_o$ of the hydrated grain. For total hydration this swelling is maximum, it is the actual swelling of the hydrated material and will be noted as K_g; with Portland cements $K_g \simeq 2.2$. If the initial porosity of the paste is such as doubling the bulk volume of hydrated grains is not possible, hydration is definitively stopped as soon as all avaible voids are filled. The initial porosity which, for total hydration, allows the exact filling of all avaible voids is $n_{1p} = 1 - 1/K_g$. The initial porosity to account for is the one when the paste stiffens. In this study we characterize it by the coefficient $\Gamma = \frac{c}{c+e_1}$ with c = volume of mixing cement, e_1 = volume of water which would have been contained in the mixed paste if between this moment and the moment it stiffens there had been no bleeding nor evaporation. If n_1 is the initial porosity of the theoretical paste without bleeding nor evaporation, then $\Gamma = 1-n_1$. If we call e_o the mixing water, then $\gamma = \frac{c}{c+e_o} < \Gamma = \frac{c}{c+e_1}$. The difference $e_o - e_1$ having a large random component, the systematic determination of Γ cannot be dispensed with ; it is easy to do this, a posteriori, from a density measurement (4). The value corresponding to n_{1p} is $\Gamma_p = 1/K_g$.

So, after a hardening time long enough to be considered as infinite, if $\Gamma \leqslant \Gamma_p$ all pastes reach theoreticaly 100% hydration, if $\Gamma \gg \Gamma_p$ the hydration stops definitively while there is still some anhydrous matter. These last pastes are then characterized by a zero capillary porosity and hydration degrees decreasing when Γ increases according to the law : $m = \frac{1/\Gamma - 1}{K_g - 1}$.

The bulk of the hydrates formed keeps a very fine porosity, globaly constant and in the vicinity of 28%, the pore sizes vary between 20 and 100 A. From this T.C. Powers derived crystalisation characteristics for the dissolved hydrates, implying that they cannot precipitate inside pores narrower than 15 or 20 A. Due to the doubling of bulk volume, half of the hydrates have to migrate, while dissolved, toward the outside of the hydrated grain. This migration takes place through the porous mass of hydrates already created. As soon as the encountered pores are wider than 20 A the precipitation of CSH is possible. All gel pores wider than 20A (in theory) are thus unstable and bound to be filled, this implies a concentrical growth of the hydrated grains.

In gel, one should distinguish the gel porosity, 28%, the capillary porosity n made of the voids between hydrated grains and the total porosity wich is the combination of the previous two. From this, we derived two basic relations applicable to the general case of pastes hydrated m%. The corresponding swelling of the hydrated grains being K, the capillary porosity is completely represented by the product $K\Gamma$, since actually $n = 1-K\Gamma$; since the gel porosity is constant one might think that K_g is constant also, independant from the hydration degree. Hence the relation $m = \frac{K - 1}{K_g - 1}$

Experimental

Characteristics of the cement used : 55 MPa at 28 days

Chemical composition	SiO_2	Al_2O_3	Fe_2O_3	CaO	MgO	SO_3	ignition loss
	21%	5.2%	2.3%	64%	1.4%	3%	1.5%

Bogue composition	C_3S	C_2S	C_3A	C_4AF	Potassium and sodium sulfates
	54%	20%	10%	7%	0.8%

Blaine fineness 3400 cm^2/g

Curing of the pastes : immersion in water.

Testing characteristics : compression tests are performed at the stress rate of 30 MPa/mn on cylindrical testing samples (30 mm in diameter and 90 mm in height). If drying were necessary it was limited to surface drying and performed immediately before the compression test.

Results and proposed strength law

The results are presented on the figure 1. One clearly see that the Portland cement pastes must be separated into two groups of separate behaviour.

One also notes that, for the pastes of the first group and for the pastes of $\Gamma \leq \Gamma p$ hardened for an infinite time, the compressive strength is an exponential function of Γ. This exponential evolution can be parallelled to the strength law $R_C = R_o e^{-An}$ often fitting porous materials (5) with R_C = compressive strength, R_o = compressive strength of the same material at zero porosity and A being a coefficient, the value of which depending on the structure and micro-structure of the material. In the case of a sintered material it characterises the nature and quality of the contacts from grains to grains.

From this parallel and from the mechanism of the growth of the hydrated material proposed by T.C. Powers we concluded that for Portland cement pastes the porosity to account for is the capillary porosity. The compressive strength law can then be written $R_C = \frac{R_o}{eA} e^{AK\Gamma}$, with A : coefficient characterizing the nature and quality of the contacts between the hydrated grains. The more efficient they are, the smaller is A. R_o represents the compressive strength of the hydrated grains ; as the strength R_a of their anhydrous part and the strength R_g of their hydrated part are of the same magnitude (6) we stated that $R_o = {}^gCt = R_{cmax}$. R_{cmax} is the measured strength of pastes of $\Gamma \geq \Gamma_p$ hardened for an infinite time, they are expected to have a zero capillary porosity.

In the particular case of pastes of the first group and of pastes hardened for an infinite time with $\Gamma \leq \Gamma_p$ we have $AK = Ct = J$. A and K can be expressed as functions of hardening time t and written A(t) and K(t).

Micro-structure model and strength law

In the following pages the hydrated grain is schematized as a grain of C_3S or C_2S encapsuled in CSH, but all the numerical values connected with it account for the statistical incidence of compagnon anhydrous and hydrated materials.

Schematization of the micro-structure

A cement paste can be considered as an assembly of hydrated grains, comparable to a sintered material made of an assembly of grains more or less welded one to another. Its strength is function of the residual porosity between the

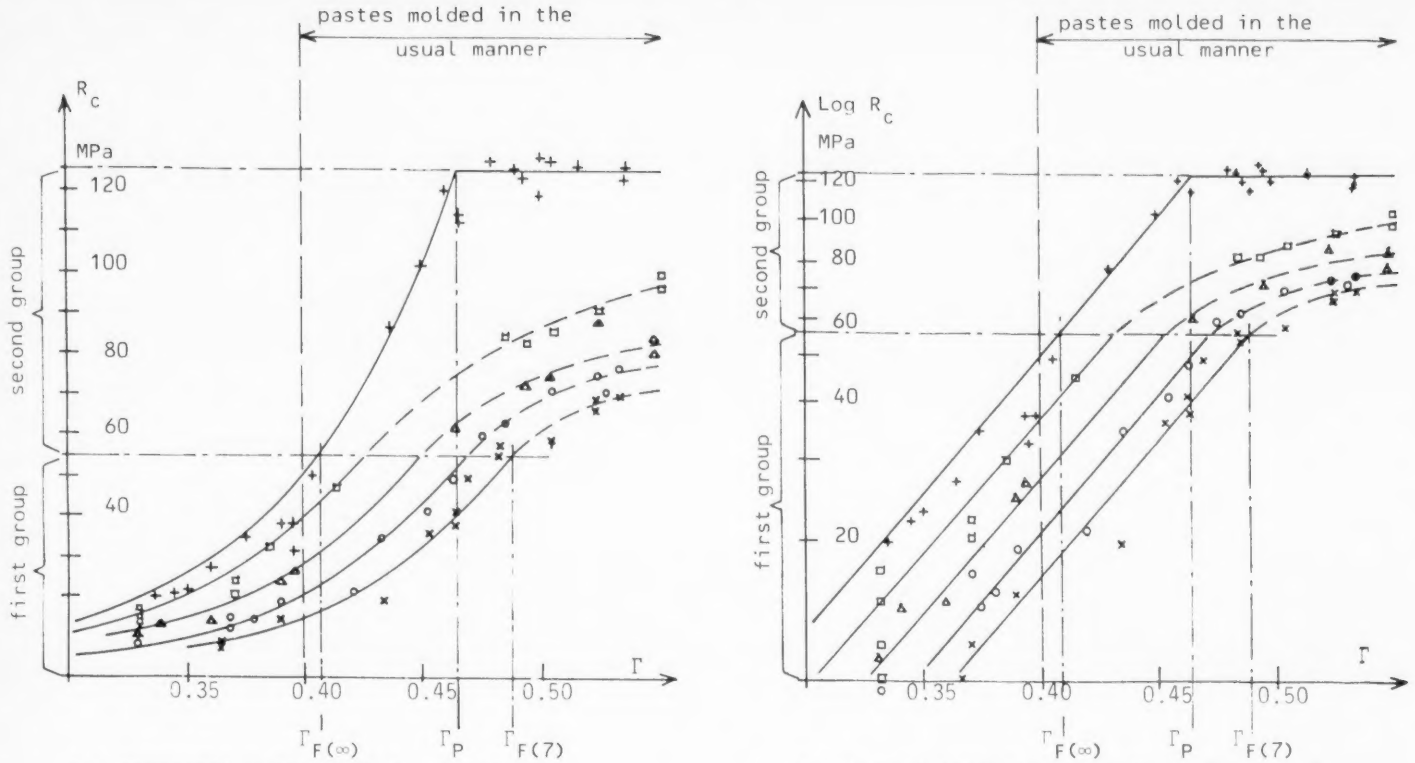

a - compressive strength R_c versus water-cement contents Γ^c

b - Log of compressive strength R_c versus water-cement contents Γ

hardening times : × 7 days ○ 14 days △ 28 days □ 56 days + infinite time (over 4 years)

FIG.1

Results previously found

VOL 14 1980

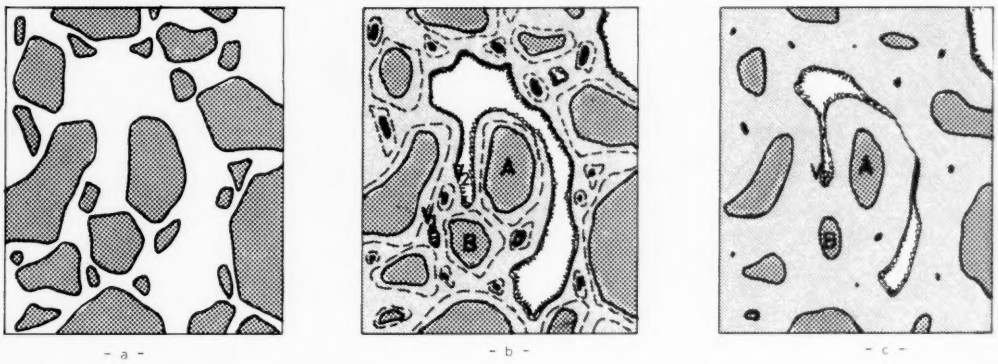

FIG.2 - Evolution of the micro-structure of a paste as hydration progresses

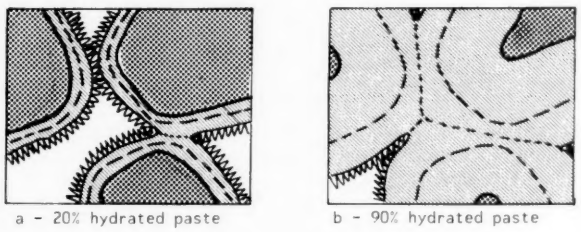

FIG.3 - Structure of the contact zone between "hydrated grains"

grains, i.e. capillary porosity n = 1 - KΓ, of the grain strength, considered as constant and equal to R_{cmax} and of the capacity to transmit stress from grain to grain, characterized by the coefficient A. This is greater as, on the one hand the peripheric layer of the grains, where contact is made, is stronger, and on the other hand, the contacts are less ponctual.

Evolution of the micro-structure and associated strength law (see figure 2)

From setting until the infinite time hardening, the micro-structure evoluates as follows.

First the hydrated grains develop in a concentric manner, they remain pseudomorphous with the initial anhydrous grains. All pastes of a same cement which are in this state get hydrated at the same rate. Then the hydrated grains are in mutual contact and the gel can develop only outside the contact zones. As long as most of hydrated grains are in the same situation as grain A of figure 2b, largely surrounded by capillary voids, the progression of water towards the surface of the anhydrous parts and the reciprocal progression of dissolved hydrates towards boundary of capillary woids where they will precipitate is not sensibly lengthened by the presence of the neighbouring grains. Each grain gets hydrated at the same rate as if there were no contact with the neighbouring grains. This is the first group : all pastes get hydrated at the same rate.

For a given hardening time t, they all have the same hydration degree m(t) and their strength is expressed by

$$R_c = \frac{R_{cmax}\, e^{A(t)\ k(t)\Gamma}}{e^{A(t)}} \quad \text{with } A(t).K(t) = \text{Constant} = J$$

The value of K, can be computed from the results of the mechanical tests only.

When, on the other hand most of grains are in the situation of B of figure 2b, the openings to capillary voids are limited and the seepage through the gel already formed is sensibly lengthened. More over, a slight increase of the solid volume , sufficient to fill the voids such as V_1 and V_2, causes an important lengthening in the seepage and slows down hydration. This is the second group, hydration is largely slowened when Γ or the hydration degree m increases. The strength law given before remains valid, but A and K are not functions of hardening time anymore and are not related by AK = Ct.

The boundary between first and second group is tied to a critical value Q_F of the ratio Q of the contact areas between hydrated grains to the peripheric areas of the hydrated grains.

At the time when the hydrated grains form a mutal contact they are pseudomorphous with the initial anhydrous grains, and the granular structures of all pastes formed from the same cement are similar. Since the porosity of a granular material depends only on the shape and the arrangement of its grains but not on their sizes, all these pastes show the same capillary porosity. Starting from similar conditions, the later growth of the hydrated grains remains uniform. Although nor pesudomorphous with the initial grains, their shapes evolve in similar fashion in all pastes. Thus, all through the hardening process, porosity and interlocking characteristics of the hydrated grains remain closely tied. Under those circonstances, for a given cement, the boundary between first and second group, which corresponds to a specific value Q_F of the Q ratio, is tied to a unique value n_F of the capillary porosity.

After an infinite hardening time,
- the pastes such as $\Gamma \leqslant \Gamma_p$ are 100% hydrated and their strength is :

$$R_c = \frac{R_{cmax}\, e^{A(\infty)\ K(\infty)\Gamma}}{e^{A(\infty)}} \quad \text{with } A(\infty) \cdot K(\infty) = J,$$

- the pastes such as $\Gamma \geqslant \Gamma_p$ all have the same zero capillary porosity associated with the same strength R_{cmax}, their hydration degrees decrease as Γ increases.

Structure of the hydrated grains (see figure 3)

Inside the mass of gel associated with hydrated grains each pore wider than 20 A is unstable and must be filled ; this results in a gel of very dense structure. In the vicinity of the capillary voids a very loose intertwinning of CSH needles takes place in the outer zone of the hydrated grains. This is the gel with acicular facies which appears often in fracture examination with a SEM. Its voids are quickly filled while other crystalites loosely intertwinned are formed outside.

While the hydration progresses, the contact zones between grains increase. The environmental conditions get further apart from those of a free surface of a hydrated grain, characterized by acicular gel, to approach those of

the inner core of the hydrated mass, associated with compact gel. Sketches a and b of figure 3 illustrate this process.

Our conclusion is that the major part of the gel of hydrated grains, outside as well as inside the boundaries of the initial anhydrous grains, is made of dense gel. The outer gel, with acicular facies, constitutes only a shallow peripheric rim, which remains durable only outside the contact zones between grains. The fact that R_0 remains constant versus the evolution of A(t), is consistent only with this description of the hydrated grains.

Such an image of the hydrated grains is confirmed by the observations of Dalgleish and al. (7) and of M.S. Stucke and A.J. Majumdar (8). The former noteced that in the contact zone between hydrated grains the acicular gel progressively turns to compact gel. The SEM pictures of the latter show that the rim of acicular gel remains too narrow to be else than the most external layer of the recently formed gel.

Structure of the contact zones between grains

In the second group, the contacts are of the type shown in figure 3b. They take place on very wide zones, and involve a compact gel. The transmission of stress from grains to grains takes place in the best conditions and the corresponding value of A must be minimum. The quality of the compact gel being constant and a characteristic of the cement used, in the second group one must have A = constant = smaller possible value = $A(\infty)$.

In the first group, the contacts between grains take place largely among outer gel. The fact that A(t) decreases when the hardening time increases shows that the quality of contacts, in pastes of similar granular structure, improves. Two explanations, not mutually exclusive, can be given. Firstly, while the hydration progresses, some components are used up and the composition of the interstitial liquid phase is modified. With the same effect, the ionic diffusion through a thickening mass of gel is slowened, the concentrations and concentration gradients of the dissolved hydrates in this same interstitial liquid are modified. One can think that this causes a modification of the structure of the outer gel, which is continually renewed. The SEM pictures of very old concretes, when they show the outer gel, indeed show a structure with very soft contours, apparently denser than those usually found after only a few days of hardening. Secondly, if two pastes of the first group with same capillary porosity are compared, the older one has a higher hydration degree, to which corresponds a larger K value and larger hydrated grains. As shown on figure 4, which sketches spherical hydrated grains, if the layer of

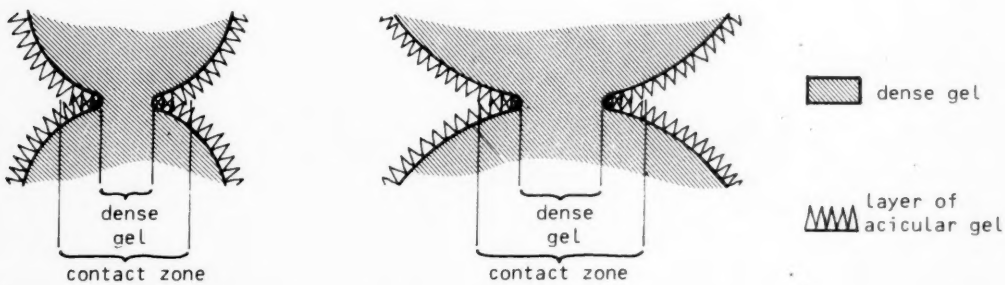

FIG. 4

outer gel keeps a constant thickness its influence in the contact between grains decreases when the grain diameter increases, this brings an improvement in the quality of contact and a decreases in A. This second concept also implies that in the first group, the contact zones being larger when Γ is larger, A decreases when Γ increases until it gradually reaches its minimum value in the second group.

Conclusion

The physical model proposed for the micro-structure of hardened Portland cement pastes is associated with the compressive strength law $R_c = R_o e^{-An}$ or $R_c = \frac{R_o}{e^A} e^{Ak\Gamma}$, R_o being constant and equal to R_{cmax}.

Both together allow to conclude that the essential parameter influencing the compressive strength of pastes is the capillary porosity n, linked to $K\Gamma$, K and m by a chain of reciprocal relations. The two groups of separate behaviour noticed when considering the compressive strength have the following characteristic properties :

- first group : at the same age all pastes have the same hydration degree
- second group : at the same age the hydration degree is a decreasing function of Γ
- the boundary between the two groups is characterized by a unique value n_F of the capillary porosity.

At last, the major part of the hydrates would be dense gel. The acicular gel (often observed on SEM pictures) would constitute only a shallow rim around the hydrated grain, its thickness would be roughly steady and it would remain only apart from the contact zone between grains.

The fact that the strength law accounts for all the strengths measured in our previous studies in a coherent manner tends to prove its validity.

Nevertheless to definitively prove this validity we have still to verify by direct measurement the actuallity of the conclusions proposed above and show that the strenght law is valid for any paste, including pastes of the second group.

This is the claim of the next paper.

References

1. J.L. Granju - Matériaux et Constructions - RILEM, 7, 37, pp 25-35, 1974.
2. J.L. Granju, J.C. Maso - CCR, 10, 5, pp 611-621, 1980.
3. T.C. Powers - PCA J. of Res. and Dev. Lab. - 3, 1, pp 47-56, 1961.
4. J.L. Granju, J.C. Maso - C.R. Acad. Sc. Paris - t.275 serie A, pp 81-84,1972.
5. E. Ryschkewitch - J. of the Am. Ceram. Soc. - 36, 65, 1953.
6. J.L. Granju, J.C. Maso - CCR-10, 6, pp 731-738, 1980.
7. B.J. Dalgleish, P.L. Pratt, R.T. Moss - CCR - 10, 5 , pp 665-676, 1980.
8. M.S. Stucke, A.J. Majumdar - CCR-7, 6, pp 711-718, 1977.

VOL. 14 1984

CEMENT and CONCRETE RESEARCH. Vol. 14, pp. 257-262, 1984. Printed in the USA.
0008-8846/84 $3.00 + 00. Pergamon Press, Ltd.

ANALYSES OF THE AQUEOUS PHASE DURING EARLY C_3S HYDRATION

Paul Wencil Brown, Ellen Franz, Geoffrey Frohnsdorff, and H. F. W. Taylor*

Center for Building Technology, National Bureau of Standards,
Washington, DC 20234
* University of Aberdeen, Aberdeen, Scotland

(Communicated by S. Diamond)
(Received June 10, 1983)

OL.
14
984

ABSTRACT

The concentrations of calcium and silica in solution during the first 4 hours of C_3S hydration were measured. The results of these analyses indicate that a solid calcium silicate hydrate forms within 30 seconds of the start of hydration and that an equilibrium between the solution and the solid hydrate is rapidly established. A strong dependence of the rate of early hydration on the w:C_3S ratio was observed, while the dependence on the surface area of the C_3S was minimal.

Introduction

Various studies have been undertaken in order to establish the solubility relationships in the $CaO-SiO_2-H_2O$ system under equilibrium conditions [1,2,3,4,5]. Similarly, a number of studies have addressed the time-dependent variations of the calcium and silica concentrations in solution during the course of tricalcium silicate hydration [6,7,8]. Still other studies have been performed in efforts to establish whether C_3S dissolution is congruent [6,7,9,10,11,12]. In general, the results of investigations carried out at temperatures below 50°C have shown:

(1) a solubility relationship exists between calcium and silica in solution and a hydrated solid phase of variable composition;
(2) during the first several hours of C_3S hydration, the calcium ion concentration in solution increases while the silica concentration in solution decreases;
(3) the calcium to silica ratios in solution vary depending on the water-to-C_3S ratio and the time of hydration at which the measurement is carried out.

However, no systematic study has been undertaken to establish the relevance of observations made at high w:C_3S ratios to those in pastes or to determine the rates at which equilibria are established during C_3S hydration.

Experimental

Triclinic tricalcium silicate having a Blaine fineness of 1986 cm^2/g or 3525 cm^2/g and a free lime content of 0.4 percent was hydrated at w:C_3S ratios of 20, 10, 5, 2, and 0.7 for periods up to 4 hours at a temperature of 24°C. In those experiments performed at w:C_3S ratios above 0.7, the slurries were stirred during the course of hydration. After predetermined lengths of hydration, the samples were filtered and the calcium and silica concentrations in solution immediately measured. The samples were initially filtered through blood serum filters to remove the bulk of solid material and subsequently through 0.2 μm filters to obtain the test solutions. The solution analyses were carried out using automated colorimetric methods. The colorimetric reagent used in the calcium analyses was cresol phthalein while ammonium molybdate and ascorbic acid were used in the analyses for silica. In order to minimize carbonation all the experiments were carried out in a glove box.

Results

Results typical of those obtained in this investigation are presented in Figs. 1-3. Fig. 1a shows the calcium concentration to increase rapidly during the first minute of hydration and to approach a linear rate of increase at longer times (see Fig. 2). This behavior appears to be independent of the w:C_3S ratio. The calcium concentrations in solution increase with a decreasing w:C_3S ratio; however, the total amount of calcium liberated increases with increasing w:C_3S ratio. Fig. 1b shows the silica concentrations in solution to continuously decrease between 30 seconds and 10 minutes of hydration. However, both the concentrations of silica in solution and the total amounts of silica present in solution at any given time increase with increasing w:C_3S ratio.

Fig. 3 plots the calcium and silica concentrations in solution during the first four hours of hydration at a w:C_3S ratio of 0.7. The calcium concentration in solution increases rapidly for about the first ten minutes as saturation with respect of calcium hydroxide is approached. The calcium concentration increases at an approximately linear rate for the next two hours until a maximum near 1.5 times saturation is reached. After reaching a maximum, the calcium concentration then slowly decreases as the result of $Ca(OH)_2$ precipitation. The silica concentration in solution decreases from 4.5 μmol/ℓ after three minutes of hydration reaching a minimum of 0.5 μmol/ℓ at the point where the calcium concentration is highest. The silica concentration then appears to increase slightly but remains below 1 μmol/ℓ.

Discussion

Figs. 1 and 3 indicate the formation of a hydrated solid to initiate by precipitation from solution within 30 seconds of hydration. This hydrate forms at the expense of silica in solution; thus initial hydrate formation occurs at least in part by a through-solution mechanism. Fig. 3 suggests that a solubility relationship between calcium and silica in solution and a hydrated solid is rapidly established and that the relationship obtains past the end of the induction period as defined in terms of the onset of $Ca(OH)_2$ precipitation.

When the pairs of calcium and silica concentration data obtained for various w:C_3S ratios at times ranging from 30 seconds to 4 hours are plotted against each other, a well defined solubility curve is the result (Fig. 4). For reference, the equilibrium data of Flint and Wells (1), Roller and Ervin (2), and Fujii and Kondo (5), are plotted on this curve. The solubility

VOL. 14 1984

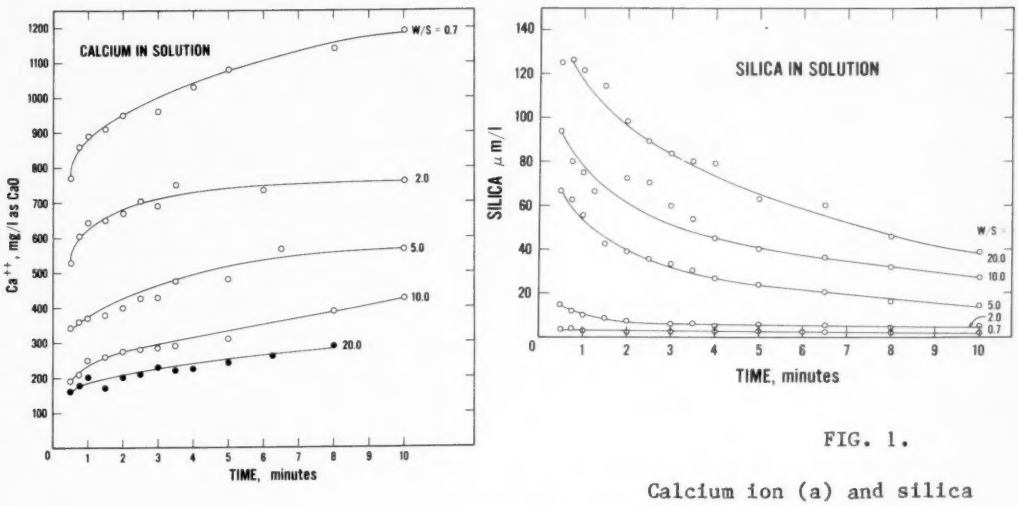

FIG. 1.

Calcium ion (a) and silica (b) concentrations in solution during the first 10 minutes of hydration of C_3S (3525 cm^2/g) at w:C_3S ratios ranging from 0.7 to 20. Stirring was used at w:C_3S ratios above 0.7.

OL.
14
984

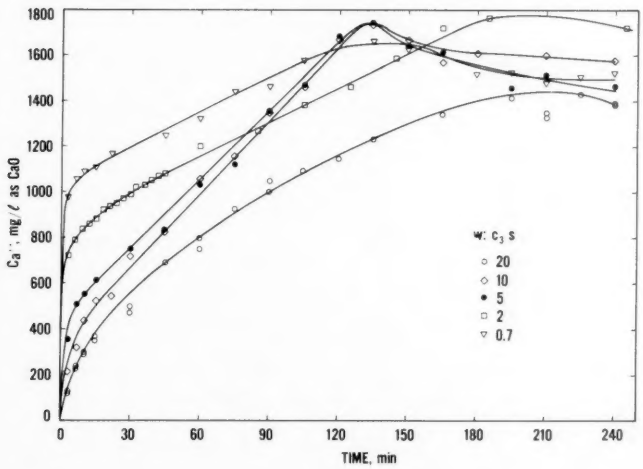

FIG. 2.

Calcium ion concentrations in solution during the first 4 hours of hydration at various w:C_3S ratios.

relationship calculated by Halstead and Lawrence (3): $[Ca(OH)_2]^{1.9}\ [SiO_2] = 3.4$ (concentrations in m M/ℓ) is also plotted; and, with this exception, the data are in good agreement. Fig. 4 indicates that equilibrium between the solution and a hydrated solid is established within the first 30 seconds of C_3S hydration and is maintained as hydration proceeds. In addition, this equilibrium relationship extends metastably beyond calcium hydroxide saturation. Viewing the equilibrium portion of this curve as representing a portion of the $CaO-SiO_2-H_2O$ ternary diagram, the various phase fields have been indicated. The invariant point, A, was determined to occur at a calcium ion concentration of 1260 mg/ℓ, as CaO (22.5 mM/ℓ). This was done by filtering a slightly supersaturated solution (≈1400 mg/ℓ as CaO) obtained by hydrating C_3S, seeding it with solid $Ca(OH)_2$ to promote precipitation, and

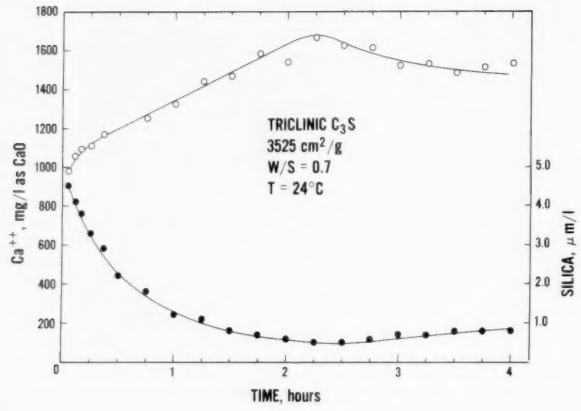

FIG. 3.

Calcium ion and silica concentrations in solution during the first 4 hours of hydration at a w:C_3S ratio of 0.7.

measuring the calcium ion concentration in solution after stirring for 16 hours and refiltering. This experiment was carried out in triplicate and the measured concentration values were 1245, 1265, and 1270 mg/ℓ as CaO. The saturation concentration of $Ca(OH)_2$ in water at 24°C, point B, was taken to be 1135 mg/ℓ as CaO by interpolation of the data of Hedin [13].

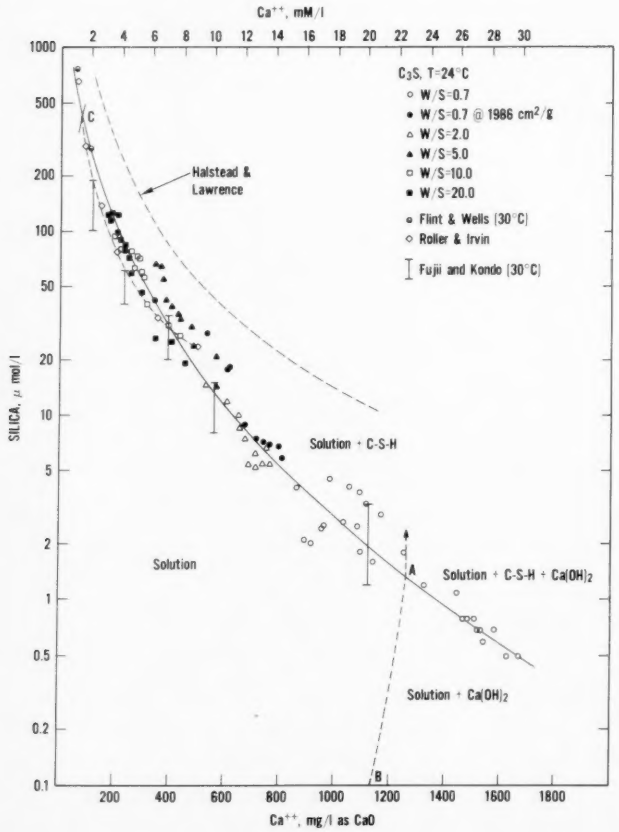

FIG. 4

Solubility curve for C-S-H. Data points were obtained for C_3S hydration times ranging from 30 seconds to 4 hours at water-to-C_3S ratios from 0.7 to 20. The line of congruent dissolution crosses the curve at point C. Point A represents the solubility of $Ca(OH)_2$ in the presence of a solution saturated in silica.

VOL 14 198

Fig. 4 also shows that C_3S dissolution is congruent. The line of congruent dissolution crosses the phase boundary at point C. However, the composition of the solution departs rapidly from congruency due to the formation of a hydrated solid having a C/S ratio less than 3. For example, the C/S ratio of the solution after 30 seconds of hydration at a w:C_3S ratio of 20 is about 23.

In order to compare the effects of the w:C_3S ratio on the rate of early hydration, the percentages of reaction at the various w:C_3S ratios were plotted against time for the first several hours. The percentage of reaction was calculated from the calcium ion concentrations in solution based on a materials balance for calcium predicated on the assumption that calcium hydroxide has not precipitated. This analysis is not valid after calcium hydroxide precipitation initiates. As Fig. 4 shows the dissolved silica can be neglected except at very low calcium ion concentrations.

$$\% \text{ Reaction} = \frac{\text{mass of CaO in solution at time, t}}{\text{hypothetical mass of CaO liberated to solution for complete reaction}} \times 100$$

$$= \frac{\text{mass of CaO in soln at time, t}}{\text{mass of CaO in } C_3S - \text{mass of CaO incorporated in C-S-H}} \times 100$$

$$= \frac{[\text{conc } Ca^{++} \text{ in soln, g/l as CaO}]\,[\text{vol.soln,}\ell]}{3\left(\frac{\text{wt } C_3S(g)}{228}\right) \times 56 - (C/S)\left(\frac{\text{wt } C_3S(g)}{228}\right) \times 56} \times 100$$

$$= 407.1\ \frac{[\text{conc } Ca^{++}][\text{vol.soln}]}{(3 - C/S)\ (\text{wt } C_3S)}$$

However, $\left(\frac{\text{vol.soln,}\ell}{\text{wt } C_3S,\ g}\right) = (w/C_3S) \times 10^{-3}$. Thus,

$$\% \text{ Reaction} = \frac{(w/C_3S)\ (\text{conc } Ca^{++},\ g/\ell \text{ as CaO})}{2.46\ (3-C/S)}$$

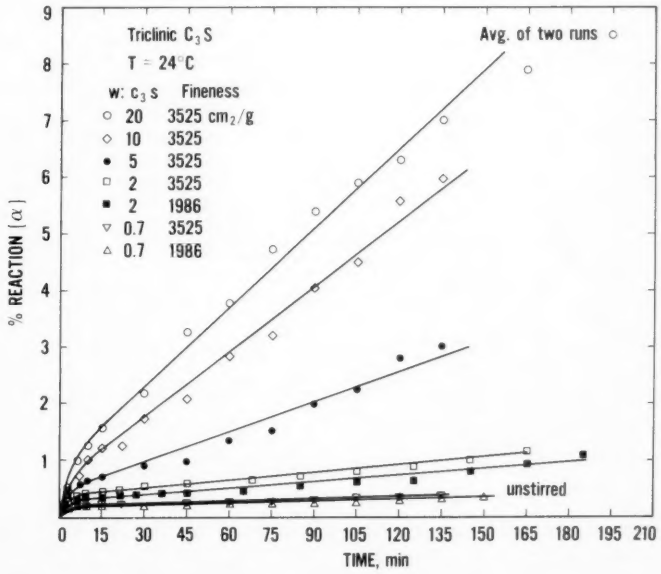

FIG. 5

The percentage of early C_3S hydration (α) calculated from a mass balance on calcium as functions of the w:C_3S ratio and fineness.

The C/S ratio of the solid formed was assumed to vary from 1 to 1.7 depending on the calcium ion concentration in solution according to the curve of Taylor [14].

Fig. 5 plots the percentage of C_3S reacted (α) against time for the various w:C_3S ratios investigated. The upper limit to α when calculated in this way is governed by the amount of $Ca(OH)_2$ that can be accomodated in solution without precipitation. Assuming this maximum $Ca(OH)_2$ concentration to be 1.5 times saturation (~1800 mg/ℓ as CaO) and assuming that the C:S ratio for the C-S-H in equilibrium with such a solution is 1.7, this calulation should apply for values of α ranging up to 0.45% at w:C_3S of 0.7 and to 11% at w:C_3S of 20.

The curves in Fig. 5 show the same general features, namely an initial rapid rise in α over the first minutes of hydration with the rate of increase thereafter approximating linearity. During the initial rapid increase in α, dissolution of C_3S may be rate controlling. However, this hypothesis does not appear to be tenable during the next several hours. Fig. 5 indicates $d\alpha/dt$ for a given w:C_3S ratio to remain approximately constant during this period with the rate being independent of the specific surface area of the C_3S for the two finenesses used. The interpretation of these results is uncertain, but a rate dependence involving the formation of a diffusion barrier of constant permeability is not indicated, and the data fit to the equations of Jander [16] and Ginstling and Brounstein [17] was poor.

Summary and Conclusions

Equilibrium between hydrated calcium silicate and the aqueous phase is rapidly established during C_3S hydration. This equilibrium extends metastably beyond $Ca(OH)_2$ saturation. The rate of early hydration shows a strong dependence on the w:C_3S ratio. In addition, the rate of hydration after the first few minutes does not appear to depend on the surface area of the C_3S. This rate dependence is inconsistent with the formation of a diffusion barrier of constant permeability.

References

1. E. P. Flint and L. S. Wells, NBS J. Res. 12, 751 (1934).
2. P. S. Roller and G. Ervin, Jr., J. Am. Chem. Soc. 62, 461 (1940).
3. P. E. Halstead and C. D. Lawrence, Proc. IV Intl. Sym. Chem. Cement 1, 321, Washington, D.C., 1960.
4. S. A. Greenberg, T. N. Chang, and E. Anderson, J. Phys. Chem. 64, 1151 (1960).
5. K. Kujii and W. Kondo, J. Chem. Soc. Dalton Trans. 645 (1981).
6. K. Fujii and W. Kondo, V Intl. Sym. Chem. Cement V II, 362, Tokyo, 1968.
7. P. Fierens and J. P. Verhaegen, Cem. Concr. Res. 10, 521 (1980).
8. N. L. Thomas and D. D. Double, Cem. Concr. Res. 11, 675 (1981).
9. S. Brunauer and S. A. Greenberg, Proc. IV Intl. Sym. Chem. Cement 1, 135, Washington, D.C., 1960.
10. M. E. Tadros, J. Skalny, and R. S. Kalyoncu, J. Am. Ceram. Soc. 59, 344 (1976).
11. J. F. Young, H. S. Tong, and R. L. Berger, J. Am. Ceram. Soc. 60, 1931 (1977).
12. P. Barret and D. Ménétrier, Cem. Concr. Res. 10, 521 (1980).
13. R. Hedin, Sven. Forskn. Cem. Betong. K. Tek. Hoegsk. Stockholm No. 33 (1962).
14. H. F. W. Taylor, J. Chem. Soc. 3682 (1950).
15. K. Laidler, Chemical Kinetics, McGraw Hill, N.Y. (1965).
16. W. Jander, Z. anorg. allgem. Chem. 163, 1 (1927).
17. A. M. Ginstling and B. I. Brounshtein, J. Appl. Chem. USSR 23, 1327 (1950).

VOL. 14 198

CEMENT and CONCRETE RESEARCH. Vol. 14, pp. 263-270, 1984. Printed in the USA.
0008-8846/84 $3.00+00. Copyright (c) 1984 Pergamon Press, Ltd.

POST-PEAK CYCLIC BEHAVIOUR OF CONCRETE IN UNIAXIAL TENSILE AND ALTERNATING TENSILE AND COMPRESSIVE LOADING

H.W. Reinhardt, H.A.W. Cornelissen
Stevin Laboratory of Delft University of Technology
2628 CN Delft, Stevinweg 4, The Netherlands

(Communicated by F.H. Wittmann)
(Received Aug. 2, 1983)

VOL.
14
984

ABSTRACT

Deformation controlled uniaxial tests have been carried out on cylindrical concrete specimens in order to establish the complete stress-deformation curve in tensile loading. Furthermore, cyclic tests have been performed under three types of loading: cycling from a tensile low stress, cycling from a compressive lower stress, and cycling between a lower and an upper stress to the envelope curve, respectively. The results seem to show that the tensile envelope curve is unique and the residual strength is the more affected the lower the stress at unloading is.

Introduction

During the last two decades, the attention paid to the mechanical properties of concrete has been continuously growing and the scope of advanced theoretical and experimental treatment has been extended. There are many reasons for this: engineering practice has been challenged by new types of structures, like offshore platforms, wind and wave energy converters, floating structures; materials engineers are asked for new types of high quality concrete; on the other hand, numerical analytical methods are rapidly developing and fracture mechanics has been established as a reliable discipline in safety assessment. Most of these developments did not start in the field of concrete and concrete structures, but rather in metal engineering. However, the methods proved to be applicable to concrete provided that the material models are appropriate and available (1, 2). Unfortunately, there is still a lack of understanding and of modelling of behaviour.

For instance fatigue of concrete under tensile and tensile-compressive loading, the knowledge of which is essential for the design and safety analysis of floating structures and energy converters (3). The approach of fatigue behaviour is rather empirical by means of S-N-curves (4) and Goodman diagrams than by fundamental considerations. Extrapolation to other conditions and interpretation of unexpected results is difficult; for instance, the fact that load reversals cause much more reduction in strength than repeated tensile or compressive loadings (5).

In a current research project, fatigue of concrete is studied and an attempt will be made to model fatigue in terms of crack growth (6). An essential parameter of the model will be the stress-strain curve of concrete under cyclic loading which should be used to describe the softening process near crack tips.

This paper will provide information on the stress-strain curve whereas the modelling will be published later. Probably this information can serve more fields than fatigue only, i.e. all problems which depend on the uniaxial strength of concrete. This is the reason for early publication.

Testing Program

Scope

On one type of concrete three variables have been investigated with regard to the complete stress-strain curve: the way of loading, the lower stress and the rate of deformation. There were three types of loading:
- monotonically increasing strain (deformation) beyond the peak stress;
- cycling to the envelope curve;
- cycling at a lower stress range after passing the peak stress.

The lower stress was tensile or compressive between 0.1 f_{ct} and 1.0 f_{ct} (f_{ct} tensile strength of concrete) whereas the upper stress in the last type of loading varied between 0.55 f_{ct} and 0.85 f_{ct}. An illustration of the type of loading is given in fig. 1. The applied rates of deformation were 0.4, 2, and 4 µm/s, during loading and unloading.

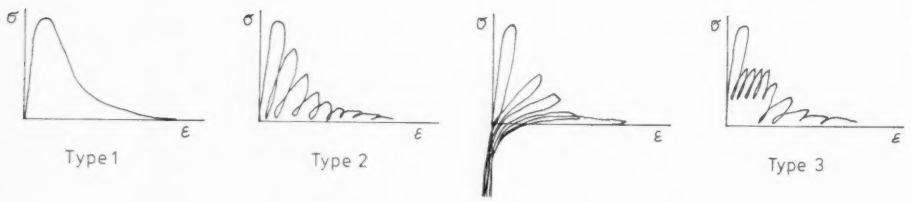

FIG. 1
Types of loading

Specimens

Tapered cylindrical specimens with a smaller diameter of 120 mm and 300 mm high were cast vertically in steel molds. 3 days before testing a saw cut of 5 mm deep and wide was made in the middle of the cylinder, in this way ascertaining that cracking would occur at a predetermined place. The 16% reduction in cross-section proved to be sufficient. During curing and during testing the specimens were sealed with a plastic foil and wetted with a wet sponge between concrete and foil. According to nonlinear fracture mechanics (7) the saw cut did not decrease the strength of the concrete compared to the strength which was determined on full cylinders.

Concrete mix and 28 days properties are given in table 1. The aggregate was quartzitic with rounded shape. Uniaxial tensile strength and Young's modulus under tension were received from the main testing program. On the days of testing which varied between 28 and 35 days after casting the tensile strength was 2.25 till 3.25 N/mm^2 and Young's modulus 30100 till 38300 N/mm^2 depending on age and rate of deformation.

TABLE 1
Concrete Mix and Properties

Type of cement	: Portland type B (medium rapid)
Cement content	: 325 kg/m^3
Sand /4 mm	: 878 kg/m^3
Gravel 4/16 mm	: 1064 kg/m^3
w/c-ratio	: 0.50
air content of fresh concrete	: 2.4%
density of fresh concrete	: 2360 kg/m^3
cube strength (150 mm cubes)	: f_{cc} = 45.4 N/mm^2, c.v. = 1,4%
splitting tensile strength	: f_{spl}= 2.9 N/mm^2, c.v. = 3.3%

Loading and Measuring Equipment

The tests were carried out on a displacement controlled electro-hydraulic loading equipment with two prestressed swivel heads between which the actuator, the load and the specimen glued to loading platens were arranged in series. The actuator can act in two directions with a capacity of 100 kN. The control of load and displacement was as follows: across the saw cut three LVDT's were attached to the concrete with a measuring length of 25 mm under 120 degress between each other. The signals were averaged and fed into a variable-gain amplifier and compared to the signal of the steering unit. In this way a constant deformation rate was achieved. For the first type of experiments this control was sufficient and the test could proceed until the measuring range of the LVDT's was reached (1 mm). At this moment the specimen already completely failed. For the second type of experiments two more conditions were defined: the point of deformation reversal and the lower stress. Both were force conditions. If the load dropped by a certain amount ΔF during deforming the steering unit generated a signal to the variable-gain amplifier to change the deformation direction and the specimen started to unload. The value of ΔF was generally 0.32 kN. The unloading continued until the lower stress was reached where once again the deformation direction changed. The third type of experiments had two upper stress conditions and a lower stress condition. The first loading cycle was the same as in the second type. The second loading cycle went on until a certain upper stress was reached where the deformation direction changed. Cycling between lower and upper stress took place until the upper stress could no longer be applied. The control procedure then switched to the second type of loading, i.e. ΔF was obeyed. The signal accuracy of lower and upper force corresponded with 0.16 kN.

Apart from the LVDT's mentioned, there were two more which were attached opposite to each other and which measured the total elongation of the specimen. All signals were stored on a seven track tape recorder and processed with the laboratory computer. A load displacement curve was plotted on a x-y-recorder during the test.

During the test program it turned out that the maximum deformation rate, where stable fracture occurred, was 4 µm/s. Higher rates caused immediate failure after the maximum stress had been reached.

Experimental Results

The primary results are force-displacement curves for the three loading types. From these, Young's modulus E and the tensile strength f_{ct} could be determined. E is the stress at one third of the tensile strength divided by the appropriate strain while f_{ct} is the ultimate stress of the stress-strain curve. From the same diagram also the strain ε_o at maximum stress could be

taken. Table 2 shows the results of the three quantities in relation to deformation rate. The number of samples n are 16, 28, and 13, resp., for the three strain rates. The variation of the deformation rate was not large enough to show a significant influence on E and ε_o. As f_{ct} is concerned a power relation could be established with a coefficient of correlation of 0.73.

TABLE 2
Youngs's modulus, tensile strength and strain at $\sigma = f_{ct}$

def. rate		E, N/mm^2		f_{ct}, N/mm^2		ε_o, µstrain	
µm/s	n	$\bar{x}$	c.v.[1]	$\bar{x}$	c.v.	$\bar{x}$	c.v.
0.4	16	34 700	8.4	2.56	8.1	111	13.9
2.0	28	34 800	7.9	2.87	7.0	109	16.2
4.1	13	34 400	4.9	2.92	4.6	117	9.4

1) coefficient of variation in %

The following five figures show typical results from the three types of loading. To start with, fig. 2 gives a stress-deformation curve for monotonically increasing deformation. After a rather linear ascending part the line bends to reach the top value and to descend steeply and furtheron more slowly. Similar results have already been reported by Petersson (7) and Mazars (8). Fig. 3 represents a cyclic stress-deformation curve for a tensile lower stress. The lines have several typical features: the loading and unloading stiffness decrease at each cycle, the irreversible deformation increases and the deformation increase per cycle increases (the upper stress is controlled and steers the unloading signal.

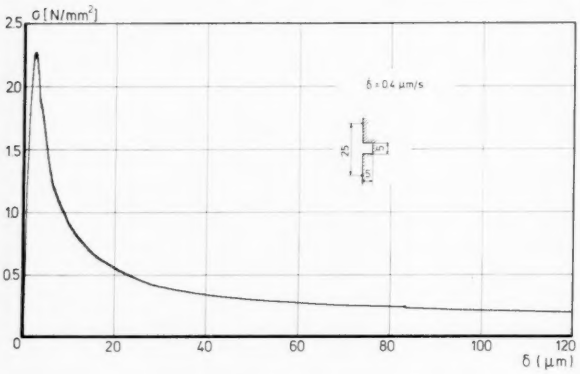

FIG. 2
Stress-Deformation Curve at Constant Rate of Deformation

The results of a test where the lower stress is compressive, is given in fig. 4. It shows the same features as fig. 3 with a more pronounced decrease of stiffness.

The amount of irreversible deformation is less increasing than in the previous case.

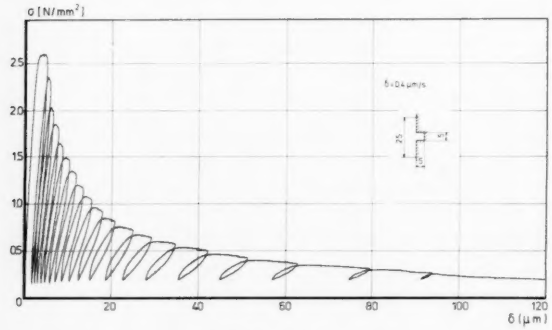

FIG. 3
Stress-Deformation Curve under Cyclic Tensile Loading

If the lower stress is a high compressive stress, fig. 5, the strain at compressive loading is also negative. However, after a certain number of cycles the irreversible strain at the lower stress has increased to the positive range. It is surprising how large the total deformation in one cycle

has become after a few cycles.

Before the third type of loading will be shown a few remarks will be made in regard to the general shape of the stress-deformation curve.

First, we should recall the type of measurements: the deformation as given in the previous figures, is the displacement of two points 10 mm above and below the saw cut. From experimental evidence, the saw cut is the place where the cracks starts to develop. Thus, the displacement contains the elastic deformation of the material between the two points and the exterior opening of the crack. So far nothing can be said about the shape of the cross-section of the crack. During cycling, the elastic portion diminishes while the crack opening prevails.

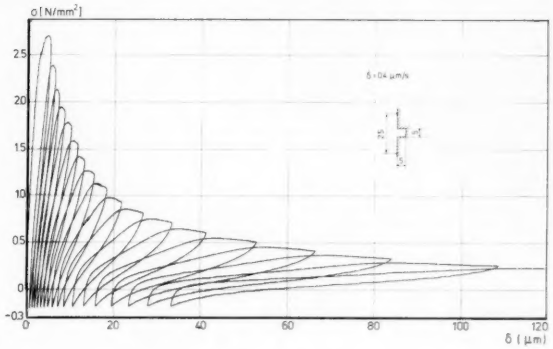

FIG. 4
Stress-Deformation Curve under Alternating Loading (Small Compressive Stress)

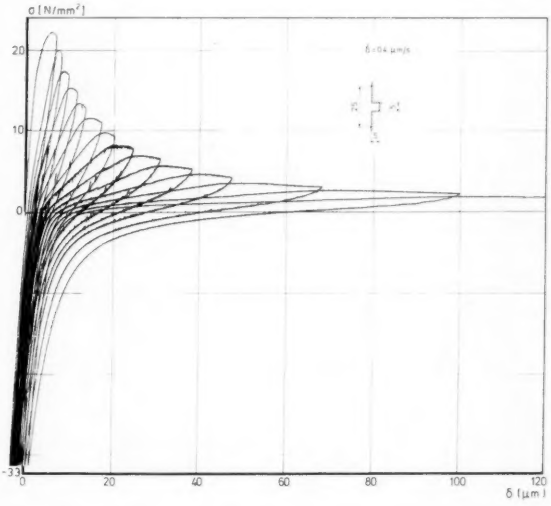

FIG. 5
Stress-Deformation Curve under Alternating Loading (Large Compressive Stress)

Following a cyclic stress-deformation curve various stages can be distinguished: elastic elongation, small crack opening, elastic unloading, crack closing. From the slope of the lines it can be said that in each cycle the cracked zone increases in the specimen and that the crack faces do not match any more. Some portions will be stressed in compression even if the remote average stress is tensile. When the average lower stress is compressive the crack faces are forced together, which is confirmed at reloading by a stiff, rather elastic behaviour.

In regard to the large absolute displacement as recorded in the alternating stress cycles a cracking zone should be assumed rather than a discrete crack. Because the elastic normal strain is not enough to explain the amount of elastic recovery the cracking zone may consist of voids which are interconnected by bridges, fig. 6.

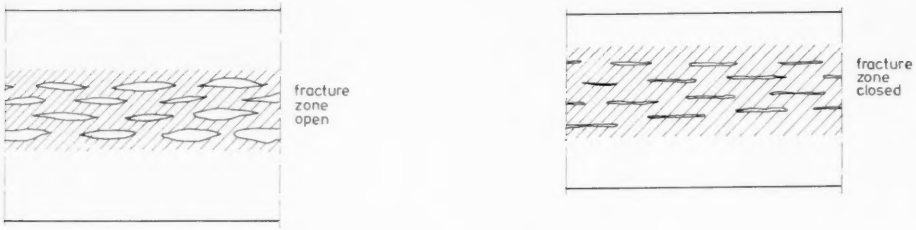

FIG. 6
Fracture Zone in Loaded and Unloaded State

These bridges undergo bending which leads to higher deformation than normal force would cause. This point needs more investigation before a rational model can be established.

The last figure 7 of this series shows results with cyclic loading between two fixed stress levels. It can be seen that during cycling the deformation increases gradually until the point is reached where the upper

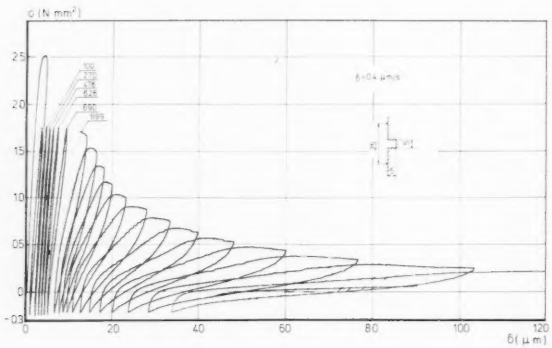

FIG. 7
Cyclic Loading between
Lower and Upper Stress

stress would lead to complete fracture. By proper load control, fracture is avoided and the test proceeds by following the descending branch of the stress-deformation curve.

Discussion of the Results

In this paragraph the shape of the stress-deformation curve will be examined in regard to the influence of loading history which can be expressed in terms of strain rate, lower stress and number of cycles. The first question to be answered is about the uniqueness of the stress-deformation envelope curve equivalent to the finding in compressive loading (9). For this purpose the stress-deformation envelope curves are compared at four points of the crack opening δ_c (defined as total deformation δ minus elastic deformation σ/E). Table 3 gives the results for the three types of loading (compare fig. 1). It should be pointed out that the values are averaged for all strain rates since no significant influence of the strain rate could be detected. The coefficient of variation within one strain rate is about the same as for all strain rates together.

It can be concluded from the table that the envelope curves are the same and that the scatter of the results is not much different, either. Admittedly, the scatter is rather great.

TABLE 3
Stress Ratios (σ/f_{ct}) versus Crack Opening for the Three Types of Loading

Type of loading	δ_c = 20		50		80		120 µm	
	$\bar{x}$	c.v.[1)]	$\bar{x}$	c.v.	$\bar{x}$	c.v.	$\bar{x}$	c.v.
1	0.39	15	0.21	21	0.14	30	0.10	36
2	0.38	14	0.21	16	0.13	22	0.10	28
3	0.38	18	0.20	14	0.13	18	0.10	23

1) coefficient of variation in %

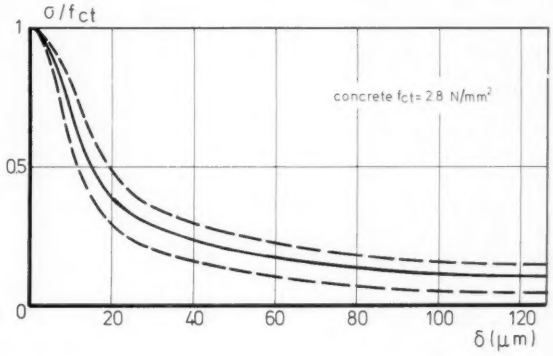

FIG. 8
Stress-Crack Opening Curve

Fig. 8 shows the average line and the 90% interval of all results of the crack opening in relation to the relative stress. For these types of experiments it may be stated that the envelope stress-deformation curve is unique, so not affected by the type of loading and the lower stress during cycling.

Another question is, whether a certain point of that line is reached after the same number of cycles. For that reason the force decrease within one cycle was determined. The cycle is defined to start in this case at the higher stress where the deformation is reversed and ends at the maximum stress reached again. It turned out that the force decrease was greater when the lower stress was lower (i.e. compressive). However, the scatter of these values was large so that this result can only be considered as an indication.

Conclusions

The purpose of this investigation was to establish complete stress-deformation curves for concrete in tension and alternating tension-compression. Therefore cylindrical specimens with a circumferential saw cut have been loaded with constant rate of deformation, the direction of which was controlled by predetermined stress values. It turned out that independently on loading history, the envelope of the stress-deformation curve is unique. Secondly it seems to be acceptable that the detrimental effect on strength is greater if the lower stress at unloading is lower (i.e. compressive).

During the first series much experience has been gained in experimental techniques. Tests which have already been started, are being performed on panels rather than cylinders with the intention to measure the strain distribution around the crack tip, the transverse shape of the crack and

VOL.
14
1984

the extension of microcracked zones in the specimen. These data are necessary for a quantitative modelling of the behaviour of concrete under fatigue loading.

References

1. IABSE Colloquium "Advanced Mechanics of Reinforced Concrete", Delft, 1981.

2. F.H. Wittmann, "Mechanisms of fracture of concrete", Advances in Fracture Res., 5th Intern. Conf. Fracture, Cannes, 1981, Vol. 4, pp. 1467-1487.

3. A.H. Tricklebank, W.I.J. Price and E.D. Hambly, "Implications of fatigue in the design of some concrete offshore structures", Proc. 3rd Intern. Conf. on Behaviour of Offshore Structures, BOSS '82, Cambridge, USA, 1982, Vol. 2, pp. 203-222.

4. T.T.C. Hsu, "Fatigue of plain concrete", ACI Journal 78(1981), no. 4, pp. 292-305.

5. H.A.W. Cornelissen and H.W. Reinhardt, "Fatigue of plain concrete in uniaxial tension and in alternating tension-compression loading", IABSE Colloquium Fatigue of Steel and Concrete Structures, Lausanne, 1982, pp. 273-282.

6. H.W. Reinhardt, "Ermüdung des Betons in Zusammenhang mit Offshore-Konstruktionen", Lecture 60th Birthday Prof. Weigler, Darmstadt, Institute of Technology, Oct. 22, 1982.

7. P.E. Petersson, "Crack growth and development of fracture zones in plain concrete and similar materials", Report TVBM-1006, Lund, Sweden, 1981.

8. J. Mazars, "Mechanical damage and fracture of concrete structures", Advances in Fracture Res., 5th Intern. Conf. Fracture, Cannes, 1981, Vol. 4, pp. 1499-1506.

9. D.C. Spooner and J.W. Dougill, "A quantitative assessment of damage sustained in concrete during compressive loading", Mag. Concrete Res. 27(1975), no. 92. pp. 151-160.

Acknowledgement

The authors would like to thank ir. A.J. Mutsaers and ing. G. Timmers for the assistance during the tests and the reduction of data. They gratefully acknowledge the valuable contribution by ir. H. Voorsluis in regard to the electronic control unit.

VOL
14
198

CEMENT and CONCRETE RESEARCH. Vol. 14, pp. 271-274, 1984. Printed in the USA.
0008-8846/84 $3.00+00. Copyright (c) 1984 Pergamon Press, Ltd.

COMPARISON OF THE WEATHERING BEHAVIOUR OF GRC WITH PREDICTIONS MADE FROM ACCELERATED AGEING TESTS

A. J. AINDOW, D. R. OAKLEY and B. A. PROCTOR
Pilkington Brothers PLC, R&D Laboratories, Lathom,
Nr. Ormskirk, Lancashire, United Kingdom.

(Communicated by A.J. Majumdar)
(Received Aug. 2, 1983)

ABSTRACT

Recent strength results from GRC materials exposed over 5 to 6 years in hot climates confirm, in real weathering conditions, the levelling of strength previously predicted from accelerated ageing tests.

VOL.
14
1984

Introduction

Glass fibre Reinforced Cement (GRC) is a relatively new material which has achieved widespread use in the construction industry over the last 10 to 12 years. An important factor contributing to the acceptance and specification of this new material was the development of a method of predicting the long term strength from accelerated ageing tests. The ageing procedures themselves, their interpretation and verification have been described in some detail by Litherland, Oakley and Proctor (Refs.1, 2).

The Prediction Method

Long term strength predictions were based on three main bodies of experimental data:-

(i) Measurements of the direct tensile strength of strands of alkali resistant glass fibre in cement environments after exposure to hot, wet, aggressive conditions.

(ii) Measurements of the strength of GRC composites after accelerated ageing in similar accelerated aggressive conditions.

(these two sets of experimental results giving knowledge of the extent, kinetics and temperature dependence of strength loss for both fibres and composites - Ref.1.)

(iii) Comparison of the above results with strength measurements on similar GRC composites after exposure to natural weathering over a number of years in different climates about the world.

The results of tests on the composites stored in artificial accelerated ageing conditions showed a consistent pattern of falling strength followed by a stable strength region. Composite strength changes in a variety of real climates showed similar patterns of behaviour in the initial falling strength region, with the same activation energy and temperature dependence as the accelerated tests. It was deduced from this that the same reaction governed strength loss in real and accelerated conditions, and that accelerated results could be used to predict the very long term behaviour in different climates (Refs.1, 2, 3, 4). Good correspondence was observed between predicted behaviour and actual weathering over 10 years in the UK as shown in Fig.1 (Ref.2).

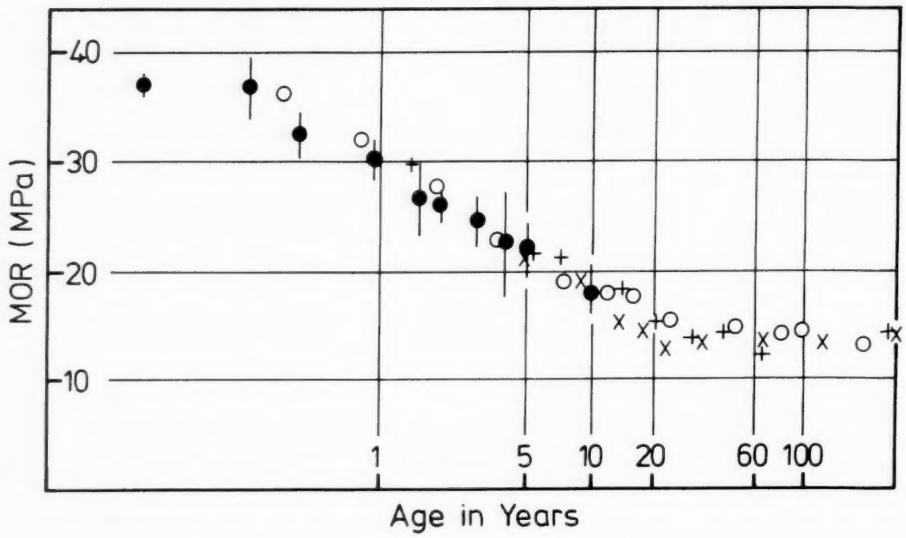

FIG.1

Strength retention of CemFIL GRC in UK weather (●) compared with predictions from accelerated ageing tests at 50°C (o), 60°C (+) and 80°C (x).

Further Confirmation of Method

Comparison of the real weathering and accelerated results given in Fig.1 shows that the method of prediction enabled the accelerated results to be positioned accurately in relation to real behaviour - also that the weathering behaviour, despite variations in conditions, followed the predicted initial falling strength behaviour very closely over 10 years. However, one critical point for long term prediction remained unconfirmed. That is whether the transition from falling strength to stable strength, seen in all the accelerated tests, would be reproduced in the cyclic and variable conditions of natural weathering?

It is clear from Fig.1 that this question would not be answered by results from cool/temperate weathering exposure for some 30 to 50 years. Recently however, additional results have become available from materials exposed over a number of years in warmer climates where changes occur significantly more quickly - as predicted in Ref.1. For the purposes of comparison, the data from these hot sites has been treated as if it were accelerated ageing data in relation to the cooler UK climate. It has been transposed to the appropriate age in the UK weather using the acceleration factors given in Table 1 which were calculated from the mean annual temperature of the site (Refs.1, 4). This treatment effectively averages and summarises the results from a number of climates and enables a consistent behaviour pattern to be deduced from the results presently available. The results are shown in Fig.2 and clearly indicate that the predicted transition from an initial falling strength behaviour to a stable strength region is occurring in real climatic conditions.

TABLE 1

Site	Mean Annual Temperature (°C)	Time equivalence to U.K.
United Kingdom	10.4	1
Arizona, U.S.	21.7	4.2
Innisfail, Australia	23.6	5.5
Cloncurry, Australia	26.2	7.3
Lagos, Nigeria	26.7	7.8
Bombay, India	27.6	8.4

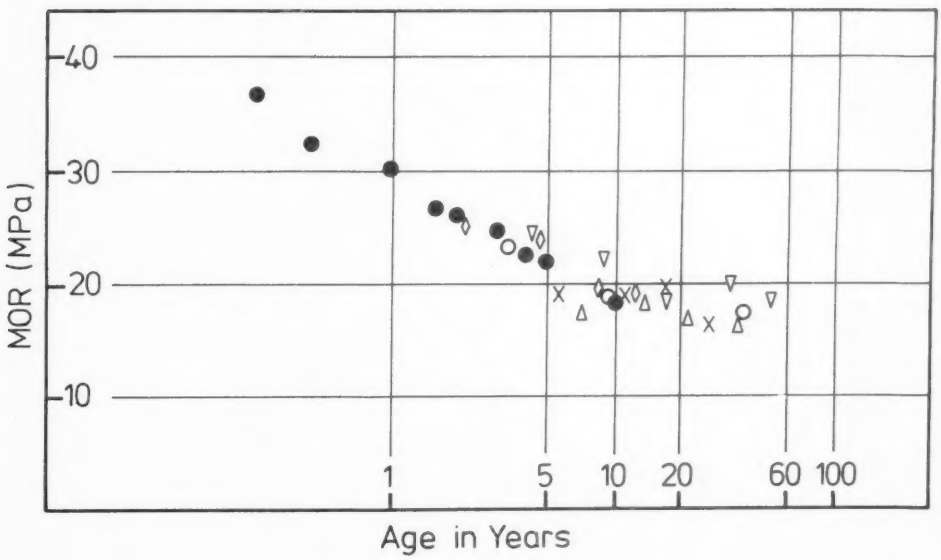

FIG.2

Strength retention of Cem-FIL GRC in UK weather (●) compared with predictions from real weather results obtained over several years in warmer climates, Arizona (◊), Innisfail (x), Cloncurry (△), Lagos (○) and Bombay (▽).

Conclusions

Strength tests on GRC composites weathered over 5 to 6 years in a number of hot climates have confirmed the levelling out of strength previously predicted from accelerated ageing tests in continuously hot wet conditions.

Acknowledgement

This paper is published with the permission of the Directors of Pilkington Brothers PLC and Mr. A. S. Robinson, Directors of Group Research and Development.

References

1. Litherland, K. L., Oakley, D. R. and Proctor, B. A., Cement & Concrete Research, Vol.11, pp.455-466, 1981.

2. Oakley, D. R., Litherland, K. L. and Proctor, B. A., Proceedings 2nd International Conference on Durability of Building Materials and Components, Gaithersburg, Maryland, USA, Sept. 1981, pp.225-231.

3. Proctor, B. A., Proceedings International Congress Glassfibre Reinforced Cement, "GRC in the 80's", Paris, Nov. 1981, ed. Vincent Blake, pp.50-67.

4. Proctor, B. A., Oakley, D. R., and Litherland, K. L., Composites, April 1982, pp.173-179.

VOL
14
198

CEMENT and CONCRETE RESEARCH. Vol. 14, pp. 275-284, 1984. Printed in the USA.
0008-8846/84 $3.00+00. Copyright (c) 1984 Pergamon Press, Ltd.

COMBINED EFFECT OF LIGNOSULFONATE AND CARBONATE ON PURE PORTLAND CLINKER COMPOUNDS HYDRATION. V. HYDRATION OF DICALCIUM SILICATE ALONE AND IN THE PRESENCE OF TRICALCIUM ALUMINATE

M. Collepardi, S. Monosi, G. Moriconi and M. Pauri
Department of Materials and Earth Sciences,
University of Ancona, Ancona, Italy

(Communicated by J. Skalny)
(Received Aug. 9, 1983)

VOL. 14 1984

ABSTRACT

The effect of sodium carbonate and/or sodium lignosulfonate on the hydration of C_2S alone and in the presence of C_3A has been examined by DTG and TG curves and by zeta potential measurements. The combined addition of sodium carbonate and lignosulfonate retards the C_2S hydration to a lower extent than that observed for the C_3S hydration. The retarding effect on the C_2S hydration is significantly lower in the presence of 20% C_3A. On the other hand, the early C_3A hydration is completely blocked by admixtures simultaneously added. Addition of 0.9% sodium carbonate without lignosulfonate blocks the early hydration of both C_3A and C_2S. This effect was not found in the C_3S-C_3A system.

Introduction

In previous papers the effect of lignosulfonate and/or carbonate on the hydration of C_4AF (1) C_3A (2,3) and C_3S with and without C_3A (4) has been studied. In the present paper the influence of these admixtures on the hydration of β-C_2S with and without C_3A is examined.

Experimental

Materials and Methods

β-dicalcium silicate was synthesized from reagent grade $CaCO_3$ and silica by heating the mixture in the proper molar ratio at 1500° C and using B_2O_3 (0.5%) as stabilizer for the β-form. The C_2S, with a free lime content lower than 0.4%, was ground to a Blaine fineness of about 3000 cm^2/g.

Tricalcium aluminate (C_3A) described in a previous paper (5) was used.

Reagent grade sodium carbonate (NC) and/or sodium lignosulfonate (lgs), said to be free of sugars or other carbohydrates, were dry-mixed with C_2S or C_2S and C_3A as shown in Table 1.

Paste Hydration

Hydration at 20° C of pastes with water/solid ratio of 0.5 was examined.

After a certain time (30 min - 28 days) the degree of hydration was evaluated by DTG and TG curves as it was described in a previous paper (4).

Zeta Potential Measurements on Suspensions

Zeta potential measurements were performed on suspensions using a Laser Zee Meter by Pen. Kem Inc. through electrophoretic measures in a fixed electric field, according to a methodology already described in a previous paper (4).

The suspensions were prepared by mixing 1 g of C_2S or C_2S-C_3A mixture and 100 ml of CH saturated water solution for 15 min. The concentrations of NC and lgs in the liquid phase have been changed from 0 to a maximum of 18 g/l. This value corresponds to the concentration of the admixture in the liquid phase of the paste experiment when 0.9% of admixture is used.

Table 1

Composition of Mixes

Mix	C_2S	C_3A	NC	lgs
A	100	—	—	—
B	100	—	0.300	—
C	100	—	—	0.300
D	100	—	0.300	0.300
A_1	80	20	—	—
B_1	80	20	0.300	—
C_1	80	20	—	0.300
D_1	80	20	0.300	0.300
$A_1 = A_2$	80	20	—	—
B_2	80	20	0.900	—
C_2	80	20	—	0.900
D_2	80	20	0.900	0.900

Results and Discussion

Influence of NC and lgs on C_2S Hydration

Figure 1 shows the DTG curves of the hydration products of C_2S with and without NC and/or lgs. When C_2S reacts with water without NC and lgs (Fig. 1A), C-S-H and CH are formed with a DTG peak at about 140° C and a sharper one at about 500° C respectively. A peak at about 750° C due to $CaCO_3$ is also observed.

The addition of NC (0.3%) to C_2S (Fig. 1B) does not cause any significant change.

In the presence of 0.3% of lgs (Fig. 1C) the C_2S hydration is completely blocked for at least 3 days. At 7 days the C_2S hydration starts, as small peaks

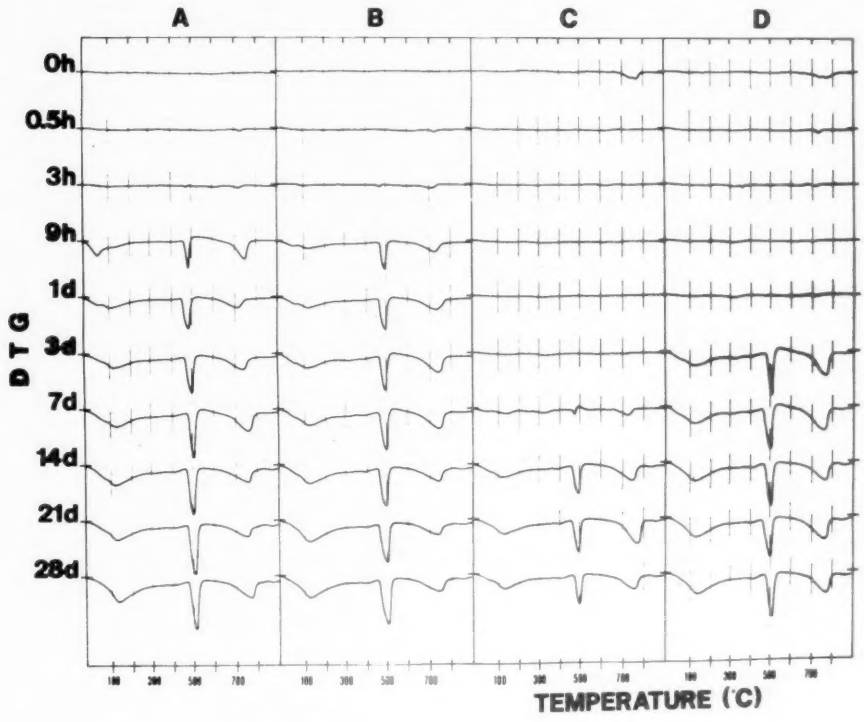

FIG. 1

DTG curves for C_2S pastes (See Table 1)

at about 140° C, 500° C and 750° C appear. Thus, it seems that lgs retards the C_2S hydration remarkably less than the C_3S hydration: in a previous paper it was found that 0.3% lgs completely blocked the C_3S hydration for at least 14 days. Similar results on the hydration of C_3S in the presence of lgs have been obtained by Young (6) and Ramachandran (7).

The combined addition of NC (0.3%) and lgs (0.3%) blocks the C_2S hydration for about 1 day (Fig. 1D). At 3 days C-S-H, CH and $CaCO_3$ peaks can be observed. Thus a combined addition of lgs and NC retards the C_2S hydration much less than lgs alone does (Fig. 1C and D). A similar effect was found also for the C_3S hydration (4). However, the combined addition of lgs and NC retard the C_2S hydration much less than that of the C_3S: 0.3% lgs and 0.3% NC simultaneously added completely block the hydration of C_3S for at least 7 days (4) and that of C_2S for about 1 day (Fig. 1D).

Figure 2 shows the percentage of CH including that transformed into $CaCO_3$ as a function of time for C_2S alone (control mix) and in the presence of 0.3% of additives. These data, based on TG curves, confirm that NC does not substantially change the C_2S hydration, whereas a combined addition of lgs and NC retards the C_2S hydration significantly less than lgs alone does.

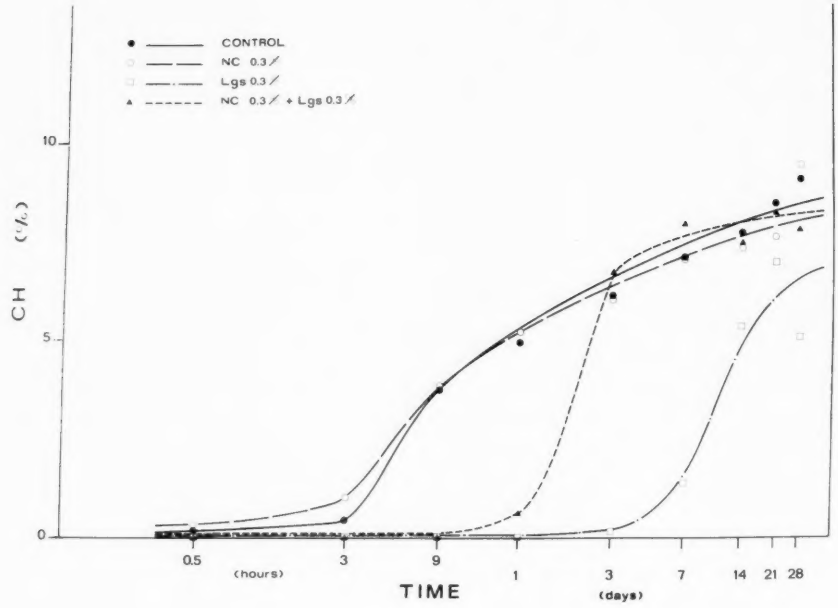

FIG. 2

Percentage of CH as a function of time for C_2S pastes.

In Fig. 3 the zeta potential as a function of NC and lgs concentration in the liquid phase is shown. The zeta potential value for C_2S without admixtures, even considering the relatively large scatter of the zeta potential of C_2S particles in the absence of admixtures, is about 0mV.

The addition of either NC or lgs lowers the zeta potential value. The latter seems to be a like more effective in the change of zeta potential, particularly at low concentrations.

When NC and lgs are simultaneously added, a minimum (-45mV) in the zeta potential curve is observed.

The concentration in the liquid phase of the admixtures corresponding to the minimum is about 4 g/l. Similar results have been obtained for the C_3S-water suspension (4).

Influence of NC and lgs on C_2S Hydration in the Presence of C_3A

Figures 4 and 5 show the DTG curves of C_2S-C_3A mixes hydrated for different periods of time and different dosages (0.3% and 0.9% respectively) of additives.

In the sample not containing admixtures (Fig. $4A_1$ and $5A_2$) four hydrated phases are observed: C-S-H (140° C), hexagonal hydroaluminates (190° C and 250° C), cubic hydrate (320° C) and CH (500° C). Within the first three hours of hydration only hexagonal hydroaluminates and traces of cubic hydrate can

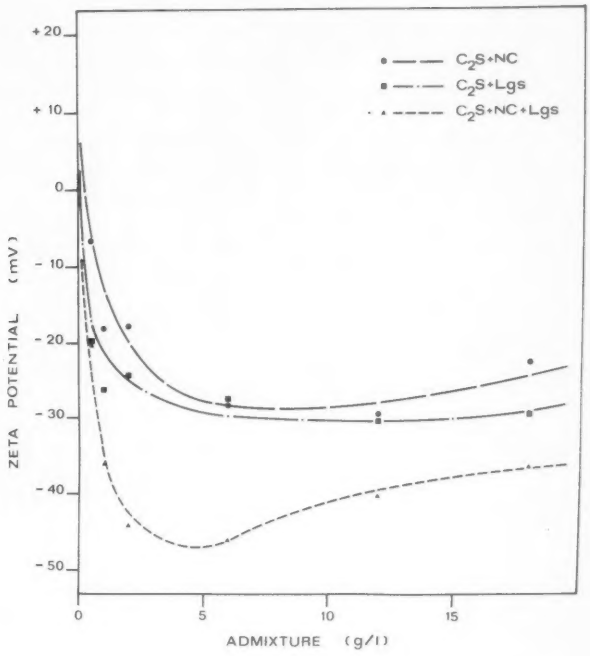

FIG. 3

Zeta potential of C_2S as a function of admixtures concentration in the liquid phase.

VOL.
14
984

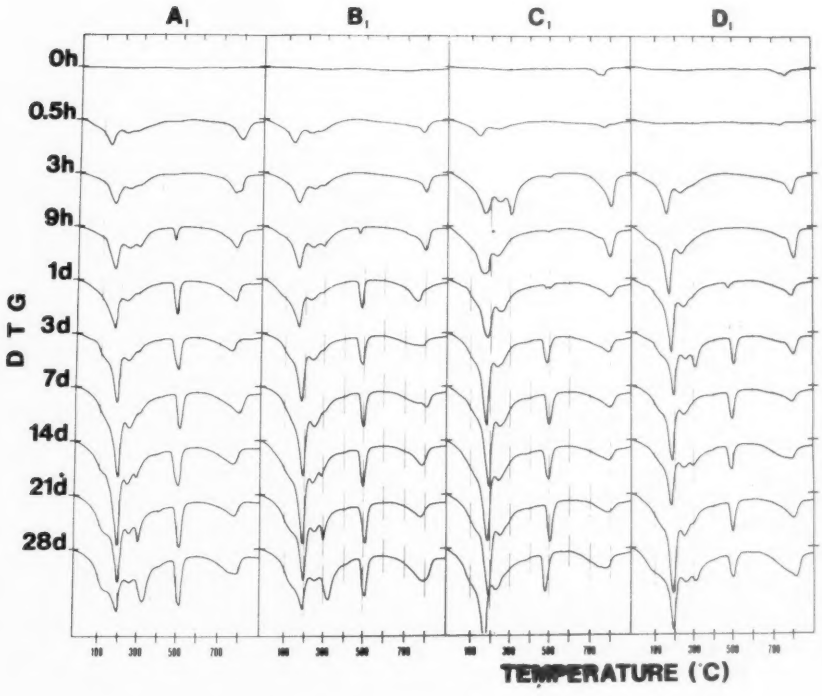

FIG. 4

DTG curves for C_2S-C_3A pastes with and without 0.3% of admixtures (See Table 1)

be detected. Calcium hydroxide is observed after 9 hours, whereas a shoulder at 140° C due to C-S-H can be detected at 3 days only. Calcium hydroxide is always accompained by calcium carbonate with a DTG peak at about 800° C.

The addition of 0.3% NC slightly retards the C_3A hydration (Fig. $4B_1$). At higher concentration of NC (0.9%) the C_3A hydration is stopped for at least 9 hours (Fig. $5B_2$).

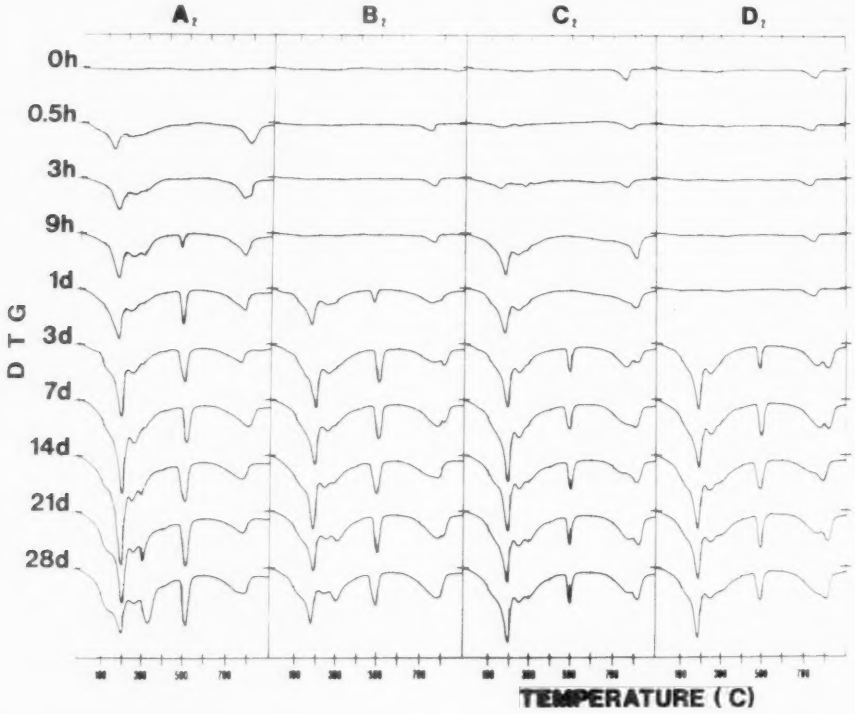

FIG. 5

DTG curves for C_2S-C_3A pastes with and without 0.9% of admixtures (See Table 1)

A high dosage of NC does not block the early C_3A hydration either in the C_3S-C_3A system (4) or in the C_3A-CH system (2). So, it seems that the initial blocking effect of 0.9% NC on the C_3A hydration in the C_2S-C_3A system (Fig. $5B_2$) is related to the absence of a CH saturated solution during the first hours, as also the early C_2S hydration is stopped (Fig. $5B_2$). In order to confirm this hypothesis, mixes E, F and G (Table 2) were hydrated at 20° C with a water/solid ratio of 0.50 in the presence of 0.9% NC. The DTG curves shown in Fig. 6 confirm the above hypothesis as the formation of hexagonal hydrates is blocked by 0.9% NC for about 9 hours only when C_3A hydrates without CH (Fig. 6E). Addition of lime to either C_3A (Fig. 6F) or C_2S-C_3A system

(Fig. 6G) removes the initial blocking effect caused by 0.9% NC. It seems that, in the absence of lime, high dosages of NC could cause precipitation of calcium carboaluminate and carbonate in form of a thin coating on the surface of C_3A and C_2S respectively, so blocking their early hydration. In the presence of CH, precipitation of $CaCO_3$ for the most part would occur in the CH saturated water phase without blocking the early C_3A hydration.

Table 2

Composition of Mixes E, F and G

Mix	C_3A	CH	C_2S	NC	S
E	20	—	—	0.9	80
F	20	4	—	0.9	76
G	20	4	76	0.9	76

The influence of 0.3% and 0.9% lgs on the hydration of C_2S-C_3A system is shown in Fig. $4C_1$ and $5C_2$ respectively. Addition of 0.3% lgs blocks the C_2S hydration within the first day, whereas hexagonal hydroaluminates can be detected within 30 minutes. In the presence of a higher dosage (0.9%), lgs does not seem to cause a significant stronger retarding effect on C_2S hydration, whereas the C_3A hydration appears to be retarded particularly within the first 3 hours.

Figures $4D_1$ and $5D_2$ show the DTG curves for the C_2S-C_3A system in the pre-

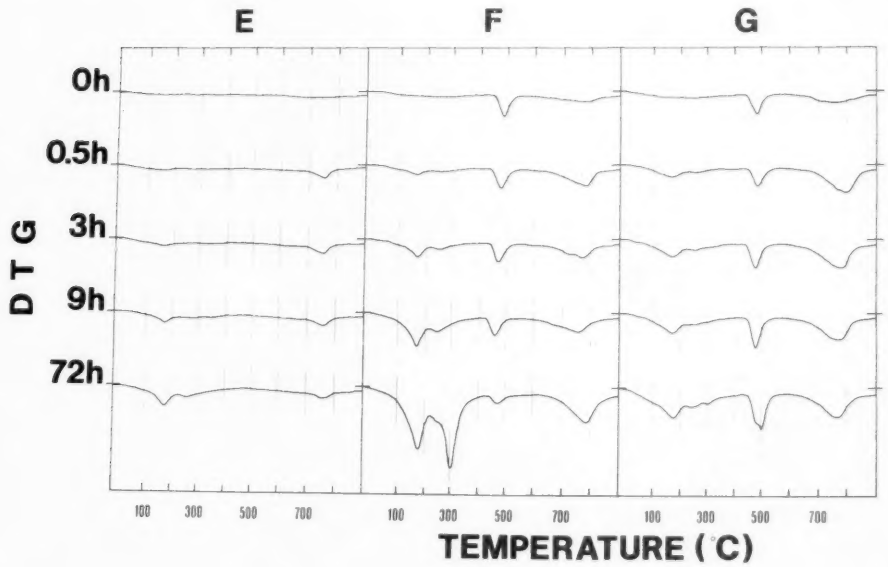

FIG. 6

DTG curves for C_3A pastes with 0.9% NC without CH (E), with CH (F) and in the presence of C_2S and CH (G) (See Table 2)

sence of both NC and lgs in percentages of 0.3% and 0.9% respectively. The combined addition of NC and lgs completely stops both C_2S and C_3A hydration for a certain period of time. The C_3A hydration is blocked for 0.5 hours with 0.3% NC and lgs (Fig. $4D_1$) and at least for 1 day with 0.9% of admixtures (Fig. $5D_2$). Moreover, the combined addition of admixtures retards the C_2S hydration (Figs. 7 and 8) to a higher extent than lgs alone does. At a given dosage of admixtures (0.3%), lgs or lgs and NC are much less effective in retarding the hydration of C_2S in the presence of C_3A (Fig. 7) than in the absence of C_3A (Fig. 2). Similar results were obtained in the C_3S-C_3A system. Hydrating C_3A strongly adsorbs lignosulfonate and may act as a sink for the admixtures (6,7), so that the lgs concentration in the aqueous phase decreases and the C_2S hydration is not retarded in the presence of C_3A to the same extent as in the absence of C_3A.

The combined addition of NC and lgs retards the C_2S hydration in the presence of C_3A to a greater extent than lgs alone does (Figs. 7 and 8) and this effect is different from that observed for the hydration of C_2S in the absence of C_3A (Fig. 2). Similar results were obtained examining the effect of lgs and NC on the hydration of C_3S or C_3S-C_3A mixture (4). As the combined addition of lgs and NC blocks the C_3A hydration for a longer time than that observed with lgs alone (Figs. $4C_1$-D_1 and $5C_2$-D_2), the concentration of lgs in the aqueous phase during the first hours is expected to be much higher when both NC and lgs are used. This hypothesis seems to be confirmed by the results obtained by Jawed et. al. (8). This effect results in a stronger retarding action of lgs and NC on the C_2S hydration than lgs alone (Figs. 7 and 8).

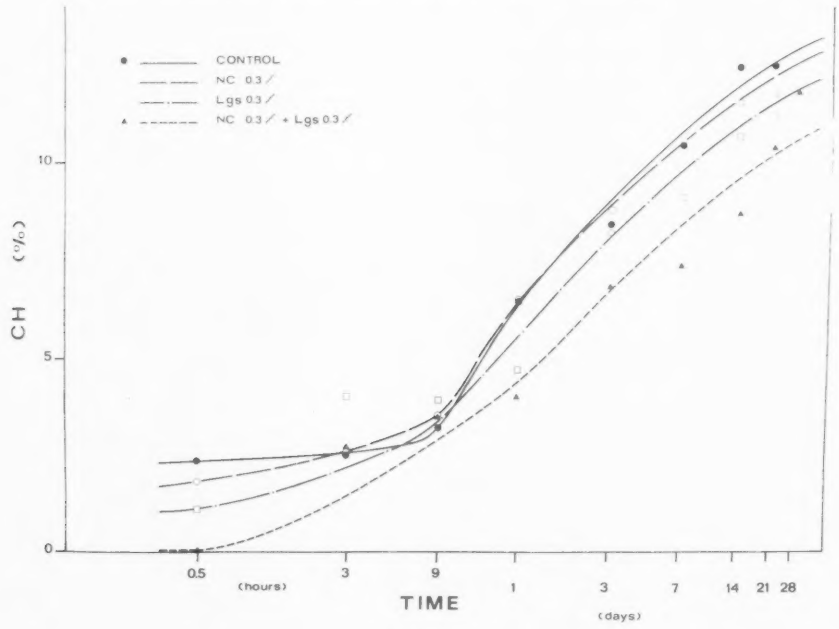

FIG. 7

Percentage of CH as a function of time for C_2S-C_3A pastes with 0.3% of admixtures

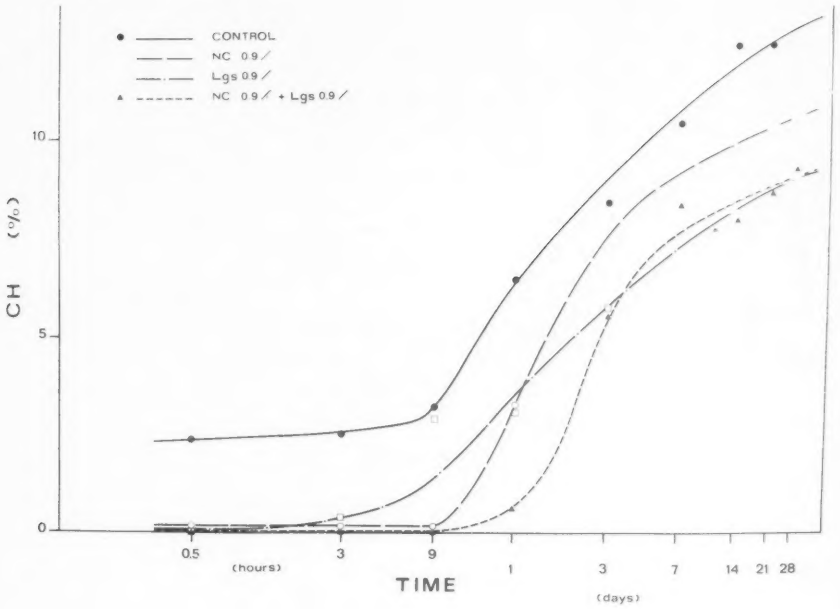

FIG. 8

Percentage of CH as a function of time for C_2S-C_3A pastes with 0.9% of admixtures

In Fig. 9 the influence of the admixtures on the zeta potential for the C_2S-C_3A system is shown. The effect is very similar to that discussed for the addition of NC and/or lgs to C_2S alone (Fig. 3). In particular it seems that also in the C_2S-C_3A system, as well as in the C_3S-C_3A one (4), there is a minimum in the zeta potential - concentration curve when NC and lgs are simultaneously added. Since no minimum has been observed for C_3A alone (2) it would seem that this minimum could be ascribed to the effect of NC and lgs on calcium silicates.

Conclusions

1. At a given dosage (0.3%), lgs alone retards the C_2S hydration in the absence of C_3A much more effectively than in the presence of C_3A (Figs. 2 and 7). This could be explained by the strong adsorption of lignosulfonate on hydrating C_3A, so that the lgs concentration is remarkably lower in the presence of C_3A.

2. Relatively high dosages of NC alone (0.9%) blocks the early hydration of both C_3A and C_2S (Fig. $5B_2$). This specific effect disappears in the presence of lime (Fig. 6) or when C_3S substitutes for C_2S (4).

3. The combined addition of lgs and NC blocks the early C_3A hydration. The higher the dosage of the admixtures, the longer the induction period (Figs. $4D_1$ and $5D_2$). The combined addition of NC and lgs retards the C_2S hydration much more effectively in the absence than in the presence of C_3A (Figs. 2 and

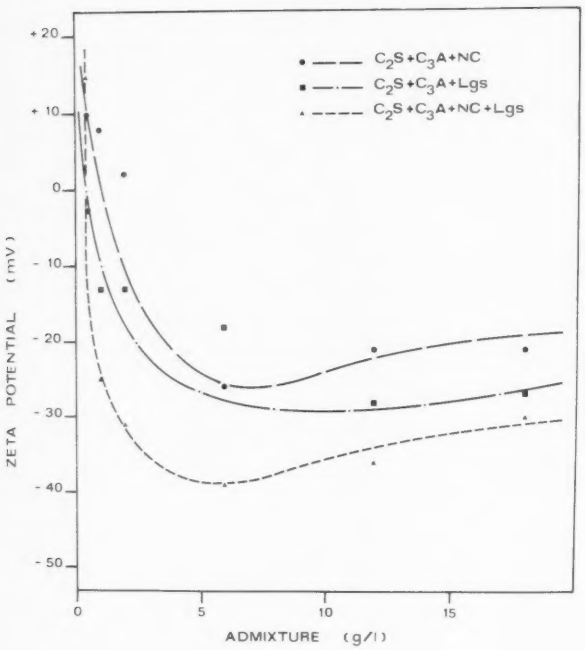

FIG. 9

Zeta potential of C_2S-C_3A as a function of admixtures concentration in the liquid phase.

7). The higher the dosage of lgs and NC simultaneously added, the longer is the induction period of the C_2S hydration in the presence of C_3A. Similar results were obtained in the C_3S-C_3A system (4).

4. In the absence of C_3A the combined addition of NC and lgs retards the C_2S hydration less effectively than lgs alone does (Fig. 2). The opposite is true in the presence of C_3A (Figs. 7 and 8). Similar results were obtained in the C_3S-C_3A system (4).

5. The effects caused by the combined addition of NC and lgs on the zeta potential of C_2S or C_2S-C_3A system are similar to the ones in the C_3S or C_3S-C_3A system, with the appearance of a minimum in the zeta potential - concentration curve.

6. The dispersion action and the completely blocking effect on the early C_3A hydration also in this case seem to be the determinant factors for the fluidifying effect caused by the combined addition of NC and lgs to a clinker Portland cement.

References

1. M. Collepardi, S. Monosi, G. Moriconi and M. Corradi, Cem. Conc. Res. 10, 455 (1980).
2. M. Pauri, G. Baldini and M. Collepardi, Cem. Conc. Res. 12, 271 (1982).
3. M. Pauri, G. Ferrari and M. Collepardi, Cem. Conc. Res. 13, 61 (1983).
4. S. Monosi, G. Moriconi and M. Collepardi, Cem. Conc. Res. 12, 425 (1982).
5. M. Collepardi, G. Baldini, M. Pauri and M. Corradi, Cem. Conc. Res. 8, 571 (1978).
6. J.F. Young, J. Am. Cer. Soc. 52, 44 (1969).
7. V.S. Ramachandran, Cem. Conc. Res. 2, 179 (1972).
8. I. Jawed, W. Klemm and J. Skalny, J. Am. Cer. Soc. 62, 461 (1979).

VOL 14 198

CEMENT and CONCRETE RESEARCH. Vol. 14, pp. 285-296, 1984. Printed in the USA.
0008-8846/84 $3.00+00. Copyright (c) 1984 Pergamon Press, Ltd.

THE EFFECT OF MATRIX COMPOSITION ON FIBRE/MATRIX INTERFACIAL BOND SHEAR STRENGTH IN FIBRE-REINFORCED MORTAR

R.J. Gray
Department of Civil Engineering
University of British Columbia, Vancouver, B.C., Canada, V6T 1W5

C.D. Johnston
Department of Civil Engineering
University of Calgary, Calgary, Alta., Canada, T2N 1N4

(Refereed)
(Received Aug. 16; in final form Oct. 3, 1983)

VOL.
14
984

ABSTRACT

The effects of factors associated with the composition of the matrix, i.e. curing conditions and time and mix proportions, on the shear strength of the interfacial bond between steel fibres and a cementitious mortar matrix have been examined experimentally using a single-fibre pull-out test technique. The experimental results indicate that bond shear strength increases significantly with an increase in matrix curing time and, for specimens with the fibre axis perpendicular to the direction of casting and compaction of the matrix, with a decrease in the proportion of water by weight in the matrix mortar. This latter effect is attributed to bleed water gain under the embedded fibre, as it is not observed in specimens with the fibre axis parallel to the direction of casting and compaction of the matrix. Furthermore, the results indicate that there is no correlation between interfacial bond shear strength and matrix mortar compressive strength.

Introduction

In comparison with other materials used as matrices in fibre-reinforced composites, e.g. plastics and metals, cementitious materials are heterogeneous and unstable. Consequently, the interfacial relationships responsible for fibre/matrix bonding in cement-based composites are more complex and not as well understood as those in other types.

As cementitious materials are particulate and porous in nature, the structure of the matrix, and hence the strength of the bond with the reinforcement, may vary considerably along the interface in an irregular way. Pores or voids in the matrix result in discontinuous interfacial contact, and therefore the effectively-bonded area is less than the nominal surface area of the reinforcement. These voids also act as stress concentrators, which lower the apparent strength of the interfacial bond.

Furthermore, chemical and physical changes occur in cementitious materials with time and the environmental conditions to which they are exposed during curing. These changes occur primarily in the hydrating cement paste, which is responsible for bonding with the reinforcement; chemical changes affect the chemical interaction and hence the adhesional bond with the reinforcement, whereas physical changes (expansion or contraction) affect the frictional resistance at the interface (1).

The strength of the fibre/matrix interfacial bond in cement-based composites is obviously dependent upon the physical and chemical composition of the matrix. It therefore follows that bond strength is affected by factors which affect the composition and strength of the matrix. An investigation which examines the influence of such factors, specifically (1) matrix curing conditions and time and (2) matrix mix proportions, on the apparent shear strength of the interfacial bond between brass-coated steel wire and a cementitious mortar matrix is described in this paper.

Review of Available Data

For the steel fibre-cement paste composite system, deVekey and Majumdar (2) reported that for plain wire pull-out specimens, curing under water for 28 days resulted in a lower average interfacial bond shear strength than curing in air at 100 percent relative humidity. The opposite effect was observed by Tattersall and Urbanowicz (3), whose results show that specimens cured under water have a higher average shear strength, at 7 days, than those cured in air at greater than 90 percent relative humidity. Harris et al. (4) found that, at 7 weeks, the dynamic frictional pull-out stresses for uncoated steel wires in a mortar matrix were higher in wet-cured specimens than in air-cured specimens.

Tattersall and Urbanowicz (3) also examined the effect of age and found that, for plain steel wire-cement paste specimens cured at 90 percent relative humidity, the apparent bond shear strength increased approximately 1.5 to 3.0 times between 7 and 28 days, depending upon the cleanness of the wire surface. However, den Boer (5) reports that the average shear strength of the bond between steel fibres and a mortar matrix showed little improvement with longer curing periods (up to 4 weeks), but he gives no indication of the curing conditions. Page et al. (6) similarly found little improvement in the tensile bond strength between mild steel and several cement pastes and mortars with an increase in curing time, in saturated air, between 7 and 28 days.

The effects of matrix mix proportions on the strength of the interfacial bond have been investigated to an even more limited extent than those of curing conditions and age. Tattersall and Urbanowicz (3) and Hughes and Fattuhi (7) tested pull-out specimens consisting of steel wire fibres in both cement paste and mortar matrices, but, as different water/cement ratios were used in each type of matrix in the two studies, it is not possible to separate the effect of the addition of the aggregate from that of the change in water/cement ratio. The results obtained by Tattersall and Urbanowicz for plain, cleaned wires show no difference between the mean values of the apparent bond shear strength for the cement paste (water/cement = 0.3) and the mortar (water/cement = 0.5, sand/cement = 3) matrices, but it is interesting to note that the variability in the test results for the mortar specimens is much larger than that for the cement paste specimens. Hughes and Fattuhi found that the mortar matrix (water/cement = 0.4, sand/ cement = 3) provided higher bond strengths than the cement paste (water/cement = 0.3) for most of the fibres used, which they attribute to the increased frictional resistance between the fibre and the matrix due to the aggregate. In a more thorough study covering a wide range of both water/cement and sand/cement ratios, Page et al. (6) found that for mixes of given water/cement ratio cured for 7 days or longer, aggregate content had an

VOL
14
198

insignificant effect on the tensile strength of the bond with mild steel.

Materials and Experimental Procedures

A single-fibre, single-sided pull-out test specimen and configuration, previously described by the authors (8), was used to determine the apparent fibre/matrix interfacial bond shear strength. The specimens were horizontally cast, i.e. with the embedded fibre perpendicular to the direction of casting and compaction of the matrix mortar, with an embedded fibre length of 50 mm. A brass-coated, high tensile steel wire, 0.38 mm in diameter, treated with trichlorethane and a water-based alkaline surface cleaner was used as the fibre. The mortar matrices consisted of a natural fine aggregate (FM = 2.73) and a normal Portland cement.

To examine the effects of curing conditions and time, three batches each of 16 pull-out specimens and 15 cylindrical compression specimens (50 mm long and 25 mm in diameter) were cast using a mortar with mix proportions sand:cement: water = 3.0:1.0:0.5. Approximately equal numbers of specimens from each batch were assigned to the two curing conditions — in water or in a fog room at approximately 100 percent relative humidity — and three test ages — 7, 28, or 90 days — to ensure that unavoidable differences between the batches did not interfere in a systematic manner with the factors being examined.

To examine the effects of matrix mix proportions, seven different mortar mixes, covering a range of water/cement ratios from 0.4 to 0.6 and sand/cement ratios from 2.0 to 4.0, were used. Eight pull-out and five compression specimens were cast from each mix, cured in water, and tested at 28 days.

VOL. 14 984

Experimental Results and Discussion

The results of the pull-out tests are reported in Tables 1 and 2 as the average interfacial bond shear strength. This average bond strength is calculated from the maximum pull-out load observed in the test and the nominal interfacial surface area between the fibre and the matrix using the following relationship, which assumes a uniform distribution of shear stress along the interface:

$$\tau_{ib,av} = \frac{P_{f,max}}{\pi d_f \ell_e}$$

where $\tau_{ib,av}$ = the average shear strength of the fibre/matrix interfacial bond,
$P_{f,max}$ = the maximum pull-out load,
d_f = the diameter of the fibre, and
ℓ_e = the embedded length of the fibre.

The test results were analyzed statistically to determine if the observed differences between the variances or the mean values for the sets of specimens at different levels of the variables being examined are significant. The difference between the variances was evaluated by the variance ratio or F-test and that between the means by the student's t-test; in all cases a double-sided test was employed. The observed difference is considered to be significant or highly significant if the probability of inferring that there is a real difference between the two sets of results when in fact the observed difference is due to chance only, is less than 5 percent or 1 percent respectively. However, given the inherently high variability of pull-out test results, as indicated by the coefficients of variation reported in Tables 1 and 2, some differences in means which are not statistically significant, may be important in confirming apparent trends in the data.

TABLE 1

Interfacial Bond and Compressive Strength Test Results for Different Curing Conditions and Times

Age, days			7		28		90	
Curing Conditions			Water	Fog Room	Water	Fog Room	Water	Fog Room
Average Interfacial Bond Shear Strength	mean,	MPa	1.01	0.99	1.23	1.41	2.11	---[1]
	standard deviation,	MPa	0.25	0.20	0.31	0.26	0.35	
	coefficient of variation,	%	25	21	25	18	16	
Compressive Strength	mean,	MPa	30.3	32.1	46.1	45.2	52.2	56.9
	standard deviation,	MPa	1.4	2.5	2.1	1.7	2.0	3.8
	coefficient of variation,	%	4.7	7.8	4.6	3.7	3.8	6.7

[1] unfit for testing due to fibre corrosion

TABLE 2

Interfacial Bond and Compressive Strength Test Results for Matrix Mortars With Different Mix Proportions

Mix Number	Mix Proportions				Average Interfacial Bond Shear Strength			Compressive Strength		
	Sand	Cement	Water	Flow[1] %	Mean MPa	Stand. Dev. MPa	Coeff. of Var. %	Mean MPa	Stand. Dev. MPa	Coeff. of Var. %
1	3.0	1.0	0.4	nm	1.41	0.47	34	52.2	1.7	3.2
2	2.0	1.0	0.4	122	1.20	0.25	21	62.2	1.0	1.7
3	4.0	1.0	0.5	nm	1.90	0.62	33	45.8	1.2	2.7
4	3.0	1.0	0.5	104	1.50	0.30	20	45.1	0.6	1.4
5	2.0	1.0	0.5	172+	1.00	0.18	18	51.9	1.3	2.5
6	4.0	1.0	0.6	64	1.14	0.35	31	30.6	0.9	3.0
7	3.0	1.0	0.6	172+	0.95	0.20	21	37.4	0.9	2.5

[1] ASTM Standard C109
nm = not measureable, i.e. fresh mortar crumbled during test
172+ = fresh mortar flowed off table during test

Curing Conditions and Time

The results of the pull-out and compression tests carried out in this series are summarized in Table 1, and the variation in the average bond strength with curing time for the two curing conditions is shown in Fig. 1. It should be noted that at 28 days, some, and at 90 days, all of the fog room cured pull-out specimens were unfit for testing as the portion of the fibre protruding from the matrix block was sufficiently corroded under these conditions that fibre failure occurred either before testing or at very low applied loads during testing.

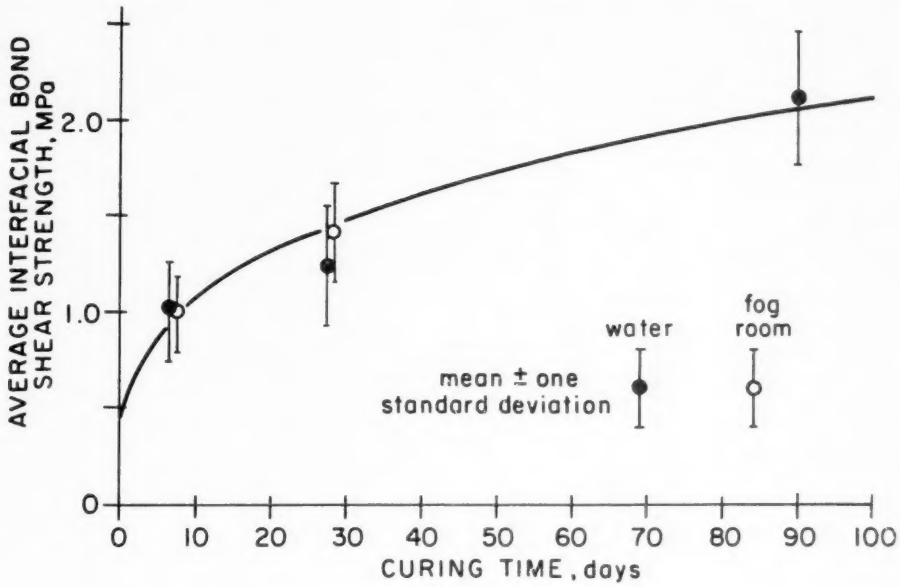

FIG. 1

Variation of Average Interfacial Bond Shear Strength With Matrix Curing Time

The mean values of the average bond strengths for the two curing conditions are the same at 7 days, but that of the fog room cured specimens is approximately 15 per cent higher at 28 days. However, the difference between the mean values at this later age is not statistically significant. It is apparent, therefore, that in comparison with standard fog room curing conditions, the extra moisture provided by water curing has no significant effect on the development of fibre/matrix interfacial bond shear strength up to an age of 28 days. These results are essentially in agreement with those obtained by deVekey and Majumdar (2) at 28 days, but differ from those obtained by Tattersall and Urbanowicz (3), for a cement paste matrix.

The compressive strength test results are similar in that the differences between the mean values for the two curing conditions are not statistically significant at 7 or 28 days. However, this difference is significant at 90 days, the strength of the fog room cured specimens being approximately 9 percent higher than that of the water cured specimens at this age.

The test data plotted in Fig. 1 clearly indicate an increase in the apparent shear strength of the interfacial bond with an increase in curing time. This increase is not statistically significant for the specimens cured in water between 7 and 28 days, but it is highly significant for the specimens cured in the fog room over this period and for the specimens cured in water between 28 and 90 days. Inspite of this inconsistency in the statistical significance of the test results, it is evident that increasing the curing time from 7 to 28 days and from 28 to 90 days produces a meaningful increase in fibre/matrix bond shear strength under both of the curing conditions examined.

Although the observed increases in apparent bond shear strength between 7 and 28 days are considerably less than that reported by Tattersall and Urbanowicz (3), they are somewhat greater than those reported by Page et al. (6) for tensile bond strengths. Furthermore, they are approximately the same as the increases in the compressive strength of the matrix over this period, which also differs from the results obtained by Page et al., and the increase in bond strength between 28 and 90 days is substantially greater than that in matrix compressive strength.

On the basis of their results, Page et al. (6) conclude that hydration of the cement in the zone of fibre/matrix interfacial contact effectively ceases, and hence the structure of the hydration products in this zone is relatively constant, after only a few days of curing. However, the results obtained in this investigation appear to contradict their conclusion, and suggest that hydration of the cement in the interfacial zone may continue to occur over the longer period characteristic of the bulk of the matrix, causing significant increases in bond strength with an increase in curing time. Alternatively, the discrepancy in findings may be associated with a dissimilarity in failure modes for the different types of specimens (tensile versus shear) and/or metallic surfaces (uncoated mild steel versus brass coated high tensile steel) (9), or with a difference in the test configuration, particularly the geometry of the steel/mortar interface and its orientation with respect to the direction of casting, compaction and curing of the matrix. The effect of the test configuration is discussed further in the following examination of the influence of mix proportions.

VOL
14
198

Matrix Mix Proportions

The pull-out and compression test results for this series of mixes are summarized in Table 2, and the variation in average interfacial bond shear strength with water/cement and sand/cement ratio is shown in Fig. 2(a) and (b) respectively.

The results plotted in Fig. 2(a) generally show a decrease in apparent bond strength with an increase in water/cement ratio, but the relationship is not as definite as that for the compressive strength of the matrix (see Table 2). This is perhaps due to the high variability in the pull-out test results, which may also be responsible for the seeming inconsistency in the statistical significance of the differences between the mean values of the apparent bond strength at different water/cement ratios. That is, whereas the difference between the mean bond strength values at water/cement ratios of 0.4 and 0.5 is not significant for a sand/cement ratio of either 2.0 or 3.0, the difference between these values at water/cement ratios of 0.5 and 0.6 is highly significant for a sand/cement ratio of both 3.0 and 4.0. These results indicate that for a constant sand/cement ratio, increasing the water/cement ratio from 0.4 to 0.5 does not produce a significant change in the apparent interfacial bond shear strength, but increasing it from 0.5 to 0.6 produces a significant decrease.

An increase in sand/cement ratio has the opposite effect on the apparent bond strength, however, as shown in Fig. 2(b). In this case, for a constant water/cement ratio, the bond strength increases as the sand/cement ratio increases. Although this trend is more consistent than that for water/cement ratio, the differences between the mean values for different sand/cement ratios, at a constant water/cement ratio, are generally not statistically significant, probably because of the large variability in the pull-out test results. The only exception is the difference between the mean values at sand/cement ratios of 2.0 and 3.0 for a water/cement ratio of 0.5, which is highly significant.

With one exception, the test results reported in Table 2 show a decrease in the compressive strength of the matrix mortar with an increase in the sand/

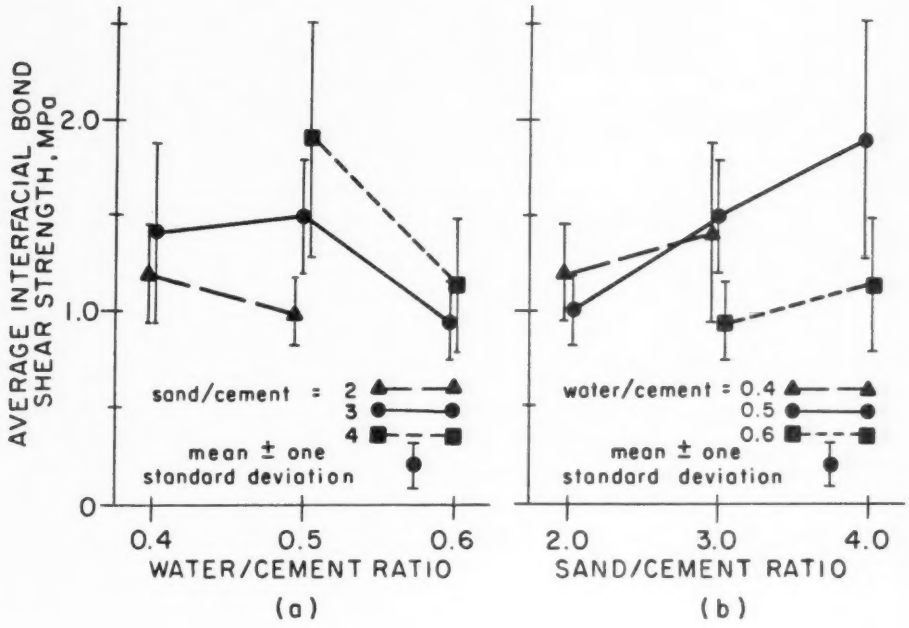

FIG. 2

Variation of Average Interfacial Bond Shear Strength With Matrix Mix Proportions

cement ratio at a constant water/cement ratio. A possible explanation for this behaviour, which has been previously noted (10) but is opposite to that observed for concretes, where increasing the aggregate/cement ratio generally produces an increase in the compressive strength (11), has been given by Ward (12). He notes that due to the high specific surface of fine aggregate, the material added to increase the sand/cement ratio increases the cement paste-aggregate surface bond area significantly. As crack propagation in mortars at loads near ultimate is primarily in the form of local bond failure, he suggests that the increase in total bond area leads to an increased rate of crack propagation in the higher sand/cement ratio mortars and therefore to a lower ultimate strength. In view of this obviously strong inverse dependence of matrix mortar compressive strength on sand/cement ratio and the specious interrelationship between matrix compressive strength and interfacial bond strength, the observed variation of bond shear strength with sand/cement ratio is perhaps surprising.

An attempt is made in Fig. 3 to show more clearly the effects of both water/cement and sand/cement ratio on the matrix mortar compressive strength and the apparent interfacial bond shear strength. The observed increases in strength with changes in these ratios, and the statistical significance of these increases, are represented diagrammatically in this figure. For compressive strength, only the increases between the diagonally related mixes are shown as these are all highly significant and therefore the effect of the two ratios, either separately or combined, is very clear, i.e. an increase in either or both ratios leads to a decrease in the compressive strength of the matrix mortar.

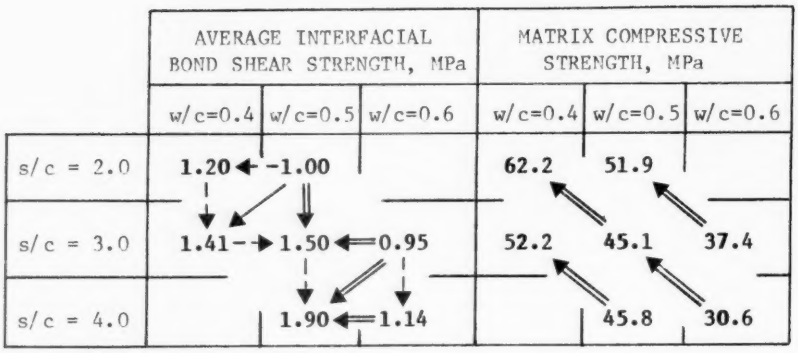

w/c = water/cement ratio
s/c = sand/cement ratio
– → = increase in strength, difference between means not significant
→ = increase in strength, difference between means significant
⟹ = increase in strength, difference between means highly significant

FIG. 3

Variation of Average Interfacial Bond Shear Strength and Matrix Compressive Strength With Matrix Mix Proportions

VOL. 14 198

For the apparent average interfacial bond shear strength, the relationships between all of the mixes are shown in Fig. 3 as the overall pattern is not as clearly defined as that for compressive strength. The diagonal relationship indicated in this figure confirms the trends observed in Fig. 2 and better illustrates the difference in the effect of sand/cement ratio on the two strengths. The results also suggest that some interaction between the effects of the two ratios on bond strength may be occurring, a reduction in water/cement ratio seeming to be more effective at the highest sand/cement ratio than at the lowest.

To examine the effects of the actual proportions of the materials in the matrix mortar on the shear strength of the bond in a more rigorous manner, a bivariate correlation analysis was carried out (13). Both the mean value and the standard deviation of the apparent bond strength were selected as dependent variables in the analysis, the latter to examine the effect of the independent variables, i.e. the proportions by weight of sand, cement, and water in the matrix mortar, on the observed variability in the pull-out test results. In addition, the flow and compressive strength of the matrix mortar mix were included in the analysis as both dependent and independent variables, and the water/cement and sand/cement ratios were included as independent variables only.

The important results of the analysis, presented in the form of a simple correlation matrix in Table 3, can be summarized as follows:

1. The mean value of bond strength is significantly correlated with the measured flow of the fresh mortar and the proportion of water in the mix.

2. The variability in the apparent bond strength is highly significantly correlated with the measured flow of the fresh mortar and the proportion of water in the mix.

3. The compressive strength of the matrix mortar is highly significantly correlated with the water/cement ratio.

TABLE 3

Simple Correlation Matrix

	Compressive Strength	Flow	Water/ Cement Ratio	Sand/ Cement Ratio	Mix Proportions		
					Sand	Cement	Water
Average Interfacial Bond Strength - Mean Value	0.120	-0.779[1]	-0.320	0.512	0.609	-0.454	-0.794[1]
Average Interfacial Bond Strength - Standard Deviation	0.045	-0.951[2]	-0.235	0.686	0.771	-0.615	-0.915[2]
Compressive Strength	1.00	0.032	-0.913[2]	-0.742	-0.632	0.801[1]	0.062
Flow		1.00	-0.321	-0.648	-0.759	0.576	0.968[2]

[1]Correlation significant ($P < 0.05$)
[2]Correlation highly significant ($P < 0.01$)

VOL. 14 984

4. The flow of the fresh matrix mortar is highly significantly correlated with the proportion of water in the mix.

It should be noted that the coefficients for the correlation between both the mean value and the standard deviation of the apparent bond strength and the compressive strength of the matrix mortar are small, indicating that the variables are essentially independent of each other, i.e. that there is no interrelationship between interfacial bond shear strength and matrix compressive strength. However, both the mean value and the standard deviation of the bond strength are significantly correlated with the measured flow of the fresh matrix mortar and the proportion of water in the mix. As these latter two variables are also significantly correlated, it is obvious that of those considered in the analysis, the principal variable affecting the apparent shear strength of the interfacial bond is the proportion of water in the matrix mortar.

The mean value and the standard deviation of the apparent bond shear strength, and the corresponding best-fit linear regression curves, are plotted against the proportion of water in the matrix mortar in Fig. 4. The linear regression coefficients are the same as the correlation coefficients given in Table 3, i.e. -0.794 for the mean value of the bond strength and -0.915 for the standard deviation. As shown in this figure, and indicated by the negative correlation/regression coefficients, both the mean value and the standard deviation of the apparent bond shear strength decrease with an increase in the proportion by weight of total mix water.

The detrimental effect of an increase in the water content of the matrix mortar on the apparent interfacial bond shear strength is almost certainly due to water gain, i.e. an accumulation of water, under the embedded fibre in these horizontally-cast specimens. This occurs as a result of the tendency of excess mix water to rise during and after consolidation. Water gain has been shown to have a weakening effect on the cement paste-aggregate bond in plain concrete (14, 15, 16) and the concrete-steel bond in reinforced concrete (14). The effect of this accumulation of water is to increase the water/cement ratio "locally" and hence to increase the porosity and decrease the strength of the

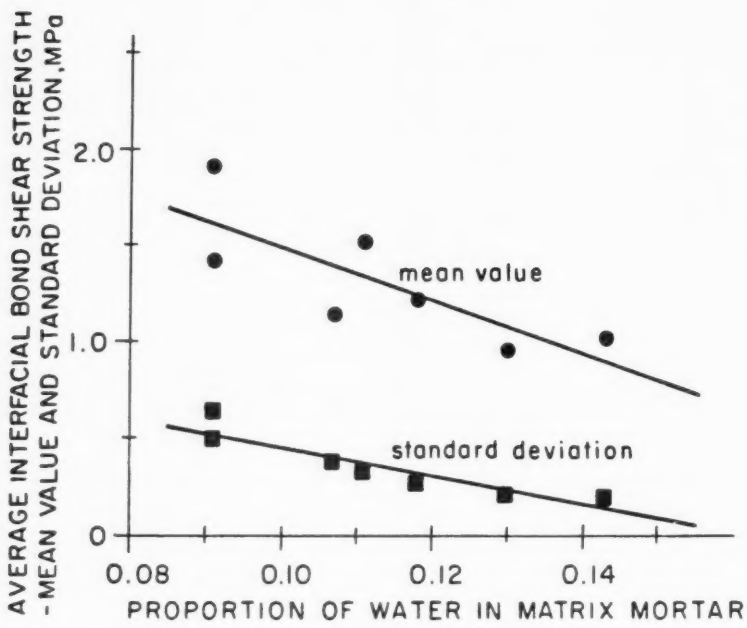

FIG. 4.

Variation of Average Interfacial Bond Shear Strength
With Proportion of Water In Matrix Mortar

cement paste immediately under the embedded fibre. The effective area as well as the adhesional and frictional resistance components of the interfacial bond are thereby reduced. Increasing the ratio of the surface area of the solids in the mix to the water by increasing the proportion of fine aggregate has been shown to reduce the effect of water gain (14) and this probably accounts for the observed increase in bond strength with an increase in the sand/cement ratio or the proportion of sand in the matrix mortar (as indicated by the corresponding positive correlation coefficients in Table 3). Further support for this supposition is provided by the observed effect of the orientation of the pull-out test specimens during casting on the apparent bond shear strength, previously reported by the authors (8). As shown in Fig. 5, the bond strength of specimens cast vertically, i.e. with the embedded fibre parallel to the direction of casting and consolidation of the matrix mortar, is higher than that for specimens cast horizontally from the same mix. The difference in apparent bond strength between the two specimen orientations is significant for the low sand/cement ratio mixes, but decreases as the sand/cement ratio increases or the proportion of water in the mix decreases.

For the vertically-cast specimens, an increase in the sand/cement ratio in the matrix mortar obviously results in a decrease in the apparent bond shear strength, although neither of the differences between the mean values for ratios of 2.0 and 3.0 or 3.0 and 4.0 are statistically significant. This variation in bond strength would seem to result from the change in the relative proportions of cement paste and aggregate in the matrix with the change in the sand/cement ratio — the proportion of the cement paste decreasing as this ratio increases

VOL
14
198

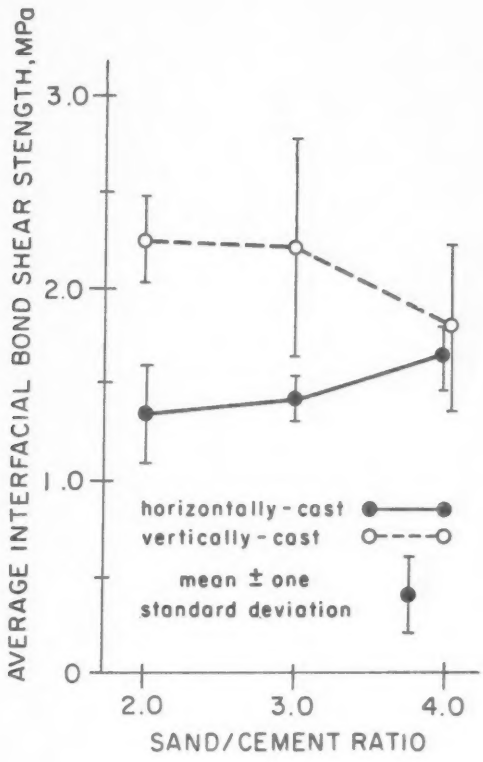

FIG. 5.

Variation of Average Interfacial Bond Shear Strength With Sand/Cement Ratio

VOL. 14 1984

and hence there being less paste in contact with the fibre along the interface. However, previous examination of the bonding between natural aggregates (17, 18) or mild steel (6, 9) and cementitious mortars, where an increase in the sand/cement ratio of the mortar has been observed to result in a decrease in the tensile strength of the aggregate- or steel-mortar interfacial bond, indicates that, in fact, the properties of the interface are independent of the aggregate content of the matrix mortar. In particular, Page et al. (6) found that the influence of the aggregate/cement ratio of the mortar on the tensile strength of the interfacial bond with mild steel was statistically insignificant and concluded that the interfacial zone of contact is aggregate-free and composed entirely of cement hydration products. The results of an examination of the microstructural features of the interfacial region by Al Khalaf and Page (9) and of the chemical composition of interfacial material by Pinchin and Tabor (19) support this conclusion.

Notwithstanding the above, the effect of water gain under the embedded fibre, and hence of the sand/cement ratio or the proportion of water in the matrix mortar, on apparent bond strength is clearly dominant in pull-out specimens cast horizontally. This has practical implications in that the largest volume usage of steel fibre reinforced concrete has been, and will probably continue to be, in pavements and similar applications (20) where the principal orientation of the fibres is two-dimensionally random in a plane perpendicular to the direction of bleed water movement.

Conclusions

1. The shear strength of the interfacial bond between a steel fibre and a cementitious mortar matrix, determined using a single-fibre, single-sided pull-out test technique, has been found to be affected by certain factors associated with the composition of the matrix mortar. In particular, a significant increase in bond strength occurs as a result of (1) an increase in curing time under moist curing conditions, and (2), in horizontally-cast specimens, a decrease in the proportion by weight of total mix water.

2. The observed improvement in interfacial bond shear strength with curing time suggests that hydration of the cement paste in the interfacial zone does not effectively cease after the initial few days of curing, but continues for some considerable time thereafter.

3. Accumulation of bleed water under the embedded fibre is believed to account for the decrease in bond strength with an increase in the proportion of mix water in specimens cast horizontally, even though the proportion of cement paste is also increasing. In contrast, results for vertically-cast specimens suggest that bond shear strength increases, although not significantly, with an increase in the proportion of mix water.

4. The results obtained in this investigation indicate that there is no correlation between interfacial bond shear strength and matrix mortar compressive strength.

Acknowledgements

The experimental work reported in this paper was carried out whilst the first author was a graduate student, under the supervision of the second, in the Department of Civil Engineering at The University of Calgary. The financial support provided by the Natural Sciences and Engineering Research Council of Canada and The University of Calgary is gratefully acknowledged.

References

1. D.J. Pinchin and D. Tabor, J. Mater. Sci., 13, 1261 (1978).
2. R.C. deVekey and A.J. Majumdar, Mag. Concr. Res., 20(65), 229 (1968).
3. G.H. Tattersall and C.R. Urbanowicz, Mag. Concr. Res., 26(87), 105 (1974).
4. B. Harris, J. Varlow and C.D. Ellis, Cem. Concr. Res., 2, 477 (1972).
5. L.J. den Boer, Proc. Conf. on Properties and Applications of Fibre Reinforced Concrete and Other Fibre Reinforced Building Materials, Delft University of Technology, 1974, p. 97.
6. C.L. Page, M.N. Al Khalaf and A.G.B. Ritchie, Cem. Concr. Res., 8, 481 (1978).
7. B.P. Hughes and N.I. Fattuhi, Mag. Concr. Res., 27(92), 161 (1975).
8. R.J. Gray and C.D. Johnston, Proc. RILEM Symp. on Testing and Test Methods of Fibre Cement Composites, The University of Sheffield, 1978, p. 317.
9. M.N. Al Khalaf and C.L. Page, Cem. Concr. Res., 9, 197 (1979).
10. H.J. Gilkey, Proc. ACI, 57(10), 1287 (1961).
11. B.G. Singh, Proc. ACI, 54(10), 897 (1958).
12. M.A. Ward, Ph.D. Thesis, University of London, 1964.
13. N.H. Nie, D.H. Bent and C.H. Hull, SPSS: Statistical Package for the Social Sciences, McGraw-Hill Book Company (1970).
14. B.P. Hughes and J.E. Ash, Concrete, 3, 494 (1969).
15. C.D. Johnston, Highway Res. Rec. No. 423, 11 (1973).
16. R.C. Fenwick and C.F.C. Sue, Mag. Concr. Res., 34(120), 139 (1982).
17. T.T.C. Hsu and F.O. Slate, Proc. ACI, 60(4), 465 (1963).
18. K.M. Alexander, Proc. ACI, 60(12), 1787 (1963).
19. D.J. Pinchin and D. Tabor, Cem. Concr. Res., 8, 15 (1978).
20. C.D. Johnston, Composites, 13, 113 (1982).

VOL
14
198

CEMENT and CONCRETE RESEARCH. Vol. 14, pp. 297-299, 1984. Printed in the USA.
0008-8846/84 $3.00+00. Copyright (c) 1984 Pergamon Press, Ltd.

NOTE

AIR ENTRAINMENT IN MORTARS AND CONCRETE: THE EFFECT OF SUPERPLASTICIZER/SALT COMBINATIONS

Michael Grutzeck
Materials Research Laboratory
The Pennsylvania State University
University Park, PA 16802

(Communicated by J. Skalny)
(Received Aug. 2, 1983)

VOL. 14 1984

Introduction

It has recently come to our attention that the use of salt-saturated solutions in mixing superplasticized mortars and concretes will sometimes lead to the entrainment of large quantities of air (in excess of 20%, often as high as 50%). This effect was unexpected and suggests a potential incompatibility between salt and superplasticizer. In an attempt to quantify the potential of various superplasticizers to entrain air when used in salt-containing mortars and concrete, the following test was developed. The concept is not entirely new (Dodson, 1981), but perhaps somewhat more quantitative.

Experimental

One hundred grams of water are added to a conventional laboratory Waring blendor. Superplasticizer (either dry or liquid) is then added to the water and blended at setting #4 for one minute. The level of foam generated is observed, relative to the original level of the solution. Observations are made immediately after mixing and again after one minute (to observe foam stability). Usually very little if any foaming occurs at this point. Next, 35g of salt (NaCl) are added to the original solution and once again the mixture is blended at #4 and the level of foam is measured. After these observations the solution is discarded and the process repeated for other combinations of ingredients.

In the present study, the brine compatibility of superplasticizers were evaluated. The two most common superplasticizers, a sulphonated naphthalene formaldehyde condensate and a sulphonated melamine formaldehyde condensate were studied. In each case three tests were carried out. In the first, the system contained only superplasticizer, water and salt. Foam production as a function of superplasticizer concentration was measured. In the second and third cases, the control of foaming was studied after adding either a phosphate-based (TBP or DBP) or silicone-based defoaming agent to the original solution.

Results

Results of testing a solid form of a sulfonated naphthalene formaldehyde condensate (SNFC) mixed with a saturated brine solution, with and without defoaming agents, are given in Figure 1. View (A) depicts foaming for various amounts of SNFC mixed with 100g H_2O and 35g of NaCl. Views (B) and (C) give the effect of the addition of either 0.5g of a phosphate or 1.0g of a 10% active silicone fluid to the original solution, respectively. The level of foam development was unexpected, but did explain why our mortars and concretes were entraining air on prolonged mixing.

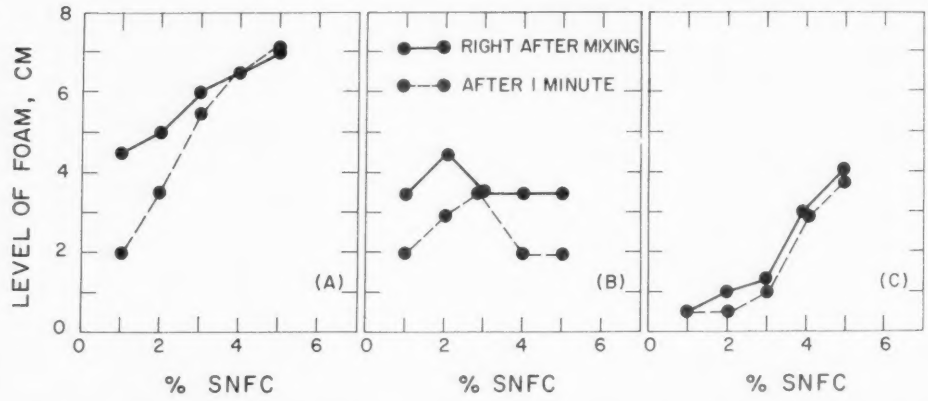

Figure 1. Sulphonated naphthalene formaldehyde condensate's (SNFC) tendency towards foam production when mixed with brine and various defoamers. View (A) 100g H_2O + 35g NaCl. View (B) 100g H_2O + 35g NaCl + 0.5g phosphate defoamer. View (C) 100g H_2O + 35g NaCl + 1.0g 10% silicone defoamer.

Repeating the same test, but substituting a 20% active liquid sulphonated melamine formadehyde condensate (SMFC) for the above superplasticizer gave the results shown in Figure 2. Again, view (A) depicts the level of foaming obtained with SMFC mixed with water and salt. Only relatively little foaming was observed. Views (B) and (C) indicate effective control of foaming by either type of defoamer.

Conclusions

Apparently some type of chemical interaction is taking place between the sulfonate formaldehyde napthalene condensate and the salt which produces a large amount of relatively stable foam. Defoamers are only partially effective in controlling the foam. In the case of the sulphonated melamine formaldehyde condensate, foaming is of little consequence and can be effectively controlled with a defoamer.

The described test is a simple one which allows one to quickly determine the potential for foaming. It allows one to sift through a complex matrix of potential combinations, reducing the number of full mortar or concrete mixtures needed for evaluation of suitability of potential mixtures.

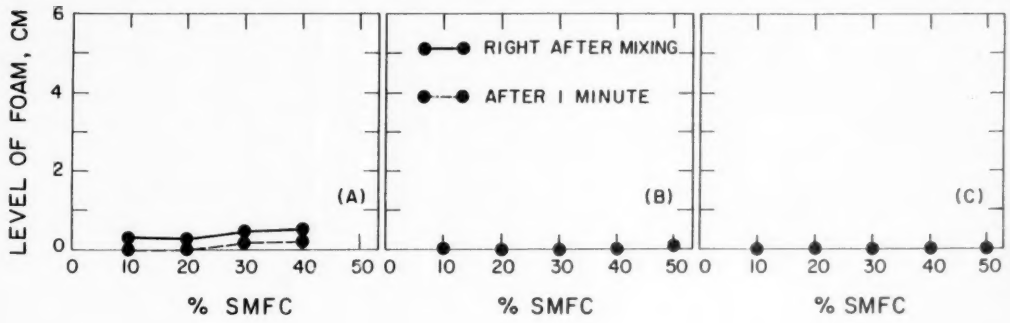

Figure 2. Sulphonated melamine formaldehyde condensate's (SMFC) tendency towards foam production when mixed with brine and various defoamers. View (A) 100g H_2O + 35g NaCl. View (B) 100g H_2O + 35g NaCl + 0.5g phosphate defoamer. View (C) 100g H_2O + 35g NaCl + 1.0g 10% silicone defoamer.

In the present situation we wanted to reduce air entrainment, but conversely, should one want to increase air entrainment, one might do so by adding some salt to the sulfonated naphthalene condensate mixtures.

VOL.
14
984

Acknowledgements

We are grateful to DOE for their support of this study. We would also like to thank Darlene Wolfe-Confer for her help in carrying out the described tests.

References

1. V. Dodson, personal communication. W.R. Grace and Company, Cambridge, MA (1981).

VOL.
14
1984

CEMENT and CONCRETE RESEARCH. Vol. 14, pp. 301-302, 1984. Printed in the USA.
0008-8846/84 $3.00+00. Copyright (c) 1984 Pergamon Press, Ltd.

NEWS ITEMS

6th International Conference on CEMENT MICROSCOPY, Mariott Hotel, Albuquerque, New Mexico. Information: Arturo G. Nisperos, Materials Service Corporation, 901 N. Sangamon St., Chicago, IL 60622 USA. — March 26-29, 1984

86th Annual Meeting of the AMERICAN CERAMIC SOCIETY, David L. Lawrence Convention Center, Pittsburgh, PA. Information: ACS, 65 Ceramic Drive, Columbus, OH 43214 USA. — April 29 - May 3, 1984

39th Symposium on FAILURE MECHANISMS IN HIGH PERFORMANCE MATERIALS, National Bureau of Standards, Gaithersburg, MD. Information: Dr. J.G. Early, Metallurgy Division, Room A153, Building 223, National Bureau of Standards, Washington, DC 20234 USA. — May 1-3, 1984

International Conference on CONCRETE UNDER MULTIAXIAL CONDITIONS, Université Paul Sabatier, Toulouse, France. Information: M. Lorrain, Conference Secretariat, I.N.S.A., Département de Génie Civil, 31077 Toulouse Cedex, France. — May 22-24, 1984

A Symposium on BLENDED CEMENTS, Sponsored by Committee C-1, Cement, of ASTM, in Denver, CO. Information: Kathy Greene, ASTM, 1916 Race Street, Philadelphia, PA 19103 USA. — June 1984

Third ASTM/CIB/RILEM International Conference on DURABILITY OF BUILDING MATERIALS AND COMPONENTS, Espoo, Finland. Information: Anneli Kaarresalo, Technical Research of Finland, Division of Building Technology, SF-02150 Espoo 15, Finland. — Aug. 12-15, 1984

International Symposia on CONCRETE PRESSURE AND STORAGE VESSELS, SEA STRUCTURES IN ARCTIC REGIONS, AND PREFABRICATION, Federation Internationale de la Procontrainte (FIP), Canadian Prestressed Concrete Institute, Calgary, Alberta, Canada. Information: FIP, c/o Genstar Structures, Ltd., 1000-1520 Fourth St., S.W., Calgary, Alberta T2R 1H5 Canada. — Aug. 25-31, 1984

Fourth International Congress on POLYMERS IN CONCRETE, Technische Holchschule Darmstadt, West Germany. Information: Prof. H. Schulz, Technische Hochschule Darmstadt, Kennwort; ICPIC 1984, Petersenstrasse 30, D-6100 Darmstadt, West Germany. — Sept. 19-21, 1984

OL.
14
984

NEWS ITEMS

International Conference on IN SITU/NONDESTRUCTIVE TESTING OF CONCRETE, by ACI, CANMET, National Bureau of Standards and the Canadian Society for Civil Engineering, Westin Hotel, Ottawa, Canada. Information: Harry S. Wilson, CANMET, 405 Rochester St., Ottawa, Ontario, Canada K1A 0G1. Oct. 2-5, 1984

International Conference on TALL BUILDINGS, Shangri-la Hotel, Singapore, sponsored by the Council of the Institution of Engineers, Singapore. Information: The Chairman, ICTBS 84, 10, Anson Road, #14-06, International Plaza, Republic of Singapore (0207). Oct. 22-26, 1984

ACI Convention, Grand Hyatt, New York, NY. Information: Ann K. Bruttel, Convention and Meetings Manager, ACI, P.O. Box 19140, Detroit, MI 48219 USA. Oct. 28 - Nov. 2, 1984

CALL FOR PAPERS

Materials Research Society Symposium on THE POTENTIAL FOR VERY HIGH STRENGTH CEMENT-BASED MATERIALS will be held in Boston, MA, November 26-30, 1984. The fourth in a series devoted to cementitious materials, it is concerned with the concretes with strengths in excess of 10,000 psi (70 MPa). The two-day symposium will have two sessions dealing with the fundamentals of achieving very high strength cement-based matrices. A further two sessions will be devoted to applications, both in civil engineering areas where cement and concrete have traditionally been used, and in new areas where formerly ceramics, metals, or reinforced plastics have been used. It is the aim of the symposium to explore the limits to high strength and examine the transition from a traditional structural material to a low temperature ceramic-type material. Both invited and contributed papers will be presented.

Papers are solicited for the following areas: 1) Microstructure - influence of hydration products, aggregates, and other solid phases on properties; 2) Porosity and pore size distrubutions - influence on properties; 3) Fracture - application of fracture theories, improvement of ductility; 4) Civil engineering applications - new processes, applications, concrete properties; and 6) Novel applications in areas not traditionally associated with cements and concretes - e.g., replacements for ceramics, metals, or plastics.

Abstracts and one- to two-page summaries must be received by Dr. J. Francis Young, 3209 Newmark Civil Engr. Lab., University of Illinois, 208 North Romine, Urbana, IL 61801, by June 15, 1984. Papers will be selected by the symposium co-chairman and authors will be notified of acceptance by July 30, 1984. Accepted papers will be published in full in a symposium volume, after being refereed. Authors must send two copies of the complete text to reach Dr. Young by Nov. 1, 1984 in order to have their paper included in the Proceedings. Write to Dr. Young to obtain the formats for the abstracts and for any additional information.

VOL
14
198

CEMENT and CONCRETE RESEARCH. Vol. 14, pp. 303-310, 1984. Printed in the USA.
0008-8846/84 $3.00+00. Copyright (c) 1984 Pergamon Press, Ltd.

HARDENED PORTLAND CEMENT PASTES, MODELISATION OF THE MICRO-STRUCTURE AND EVOLUTION LAWS OF MECHANICAL PROPERTIES II- COMPRESSIVE STRENGTH LAW

J.L. Granju and J.C. Maso
Laboratoire de Génie Civil
de l'Institut National des Sciences Appliquées
et de l'Université Paul Sabatier de Toulouse
(équipe de recherche associée au C.N.R.S. n°998)

(Communicated by M. Regourd)
(Received July 18, 1983)

VOL.
14
1984

ABSTRACT

The test results reported here confirm the validity and the generality of the compressive strength law and of the model of the micro-structure proposed for hardened Portland cement pastes in the first paper of this series (1).

The compressive strength obeys the law $R_c = R_o e^{-An}$ or $R_c = \frac{R_o}{e^A} e^{AK\Gamma}$.

It depends on the capillary porosity n, linked to the product $K\Gamma$ and to the hydration degree by a chain of reciprocal relations.

The main features of the model so confirmed are : the growth mode of the hydrated grains, the charactéristic patterns of the evolution of the capillary porosity and of the hydration degree for pastes of the first or the second group.

Introduction

In the first paper of this series (1) we proposed a physical model for the evolution of Portland cement pastes micro-structure and a strength law consistent with this model. They were derived, one from another, from the results of purely mechanical tests. Their mutual validity arises from their coherence associated with their capacity to account for the evolution of strength in all conceivable pastes.

The strength law is written $R_c = R_o e^{-An}$ or $R_c = \frac{R_o}{e^A} e^{AK\Gamma}$. The notations used here are those already used in the previous paper. We will just briefly remind them.

- R_c : compressive strength of the paste
- R_o : compressive strength of the hydrated grains
- n : capillary porosity = $1 - K\Gamma$, K being the swelling of hydrated grains associated with hydration and Γ being a coefficient characterizing the cement-water ratio in the paste when it stiffened.

- A : coefficient characterizing the nature and quality of the contacts from grains to grains.

The associated model of the micro-structure involves that the essential parameter influencing the compressive strength is the capillary porosity n, linked to the swelling K of the hydrated grains and to the hydration degree m by a reciprocal chain of relations. It appears that the pastes must be separated into two groups of separate behaviour, the first group : at the same age all pastes have the same hydration degree, and the second group : at the same age the hydration degree is a decreasing function of Γ. The boundary between the two groups is characterized by a unique value n_F of the capillary porosity.

The values of K_g, actual swelling of the gel, and of R_o, strength of the hydrated grains, would remain constant. The major part of the hydrates would be dense gel. The acicular gel (often observed on SEM pictures) would constitute only a shallow rim around the hydrated grain, its thickness would be roughly steady and it would remain only apart from the contact zones between grains. In the second group the coefficient A would quickly tend to its minimun value and remain steady.

These characteristic properties arise from deductions and have not yet been checked by direct measurements. Their verification is the aim of this second paper. That for, we developed an additional testing program with systematic measurement of the hydration degree m by a physico-chemical method. The results will verify directly every point involving the hydration degree. With K being derived from the hydration degree, hence not affected by the mechanical properties observed, if the strength still follows the given law for R_c it will prove the validity of the chain $m \leftrightarrow K \leftrightarrow n \leftrightarrow R_c$.

Experimental

The mixing cement-water ration is represented by $\gamma = \frac{c}{c+e}$ (c and e being the involved volumes of cement and water). γ is always smaller than Γ owing to water lost by bleeding. With the same cement as for the previous tests we decided to examine eight values of γ : 0.40 - 0.42 - ... 0.54 corresponding to the range of pastes molded in the usual manner and hardening times ranging from 4 days to several months.

Samples and their preparation

On the same day and under the same conditions a specimen (32 x 16 x 7 cm^3) is molded for each value of γ considered. In their mold, all of them are covered with a 1cm thick layer of water and lef overnight hardening in a room at 20°C. It is most important to make sure that during these first hours all speciments are exactly under the same conditions of temperature and ventilation. A specimen less ventilated showed a hydration degree quite higher than the others and many comparisons were then useless. The next day each specimen is removed from its mold and cut under raining water into as many prisms of 5 x 5 x 7 cm^3 as there will be different times of hardening. Their densities, from which Γ is derived, are measured by hydrostatic weightings. While all are immersed inside the same water tank at 20°C, it is take care that each of the prisms be surrounded in similar fashion by immersion water. Immediately before the mechanical test, from the concerned prisms, 10 cylindrical cores 20 mm in diameter and 60 mm high are drilled. Their ends are grinded. All this preparation takes place, of course, under raining water. From the cuttings of the cores, three samples of about 6 grams each, as representative as possible, are kept for determining the hydration degree.

Measurement of the strength R_c

The compression test is performed at a stress rate of 30 MPa/minute and the specimens are tested while wet. Their slenderness, at a value of 3, ensures that the measured strength is not altered by the plates restrain. Each value of R_c is obtained from the results of 10 sample tests.

Measurement of the hydration degree

This is based on the measurement of the quantity of non evaporable water. We followed a method established and tested by J.L. Gallias (2). Kept in water until the last minute, the sample, is surface dried and placed immediately in a stove at 115°C for 24 hours. Then it is weighted with an accuracy of 0.001g, calcinated in a kiln at 1000°C for 1 hour and weighted again. This technique avoiding crushing, eliminates an important factor of scattering and allows a much easier handling of the samples. Compared to another method (3) in which the sample is crushed and the evaporable water extracted at room temperature by acetone washing, the present method gave very similar results.

These measurements give the ratio E_h/C of the non evaporable water to the initialy anhydrous cement. The hydration degree is derived from the relation $m = \frac{E_h/C}{(E_h/C)_{100\%}}$, with $(E_h/C)_{100\%}$ being the water necessary for total hydration of one gram of cement.

The only measurable value of $(E_h/C)_{100\%}$ is actually $(E_h/C)_\infty$. For the cement and the method used, this value was established from a series of eight pastes of $\Gamma < \Gamma_p$ hardened in water between 4 and 15 years. This series of measures was made three times. The most frequent result was $(E_h/C)_\infty = 21{,}5\%$. Two paste blocks, sufficiently large and homogenous were selected to be used as standards of 100% hydration. These pastes were 10 years old.

From these bases, the test was conducted in the following manner : in order to avoid any shift in comparisons, at each step all the samples (3 for each value of Γ and for each standard) are processed together as well in the kiln as in stove and hydration degree is calculated by the formula $m = \frac{E_h/C}{(E_h/C)_{standard}}$. From practical experience it was found that, due to the very low level of acceptable inaccuracy in this study, this is still not enough to avoid all shift. Accordingly only the measurements from the same batch can be compared with complete confidence.

Results and discussions

The results are presented in figures 1, 2 and 3. We made several series of identical tests. In addition we tested a series of specimens from the same cement, water cured for 3.5 years ; they can be considered as hardened for an infinite time.

The strength tests are presented on scales of Log R_c and $K\Gamma$. The strength law is then written Log R_c = A.($K\Gamma$) + Log R_o - A ; if A = Ct the graph is made of straight lines going through the point Log R_c = Log R_o, $K\Gamma$ = 1.

Relationship $m \leftrightarrow K \leftrightarrow n \leftrightarrow R_c$

Pastes hardened for an infinite time (figure 1)

The pastes of $\Gamma \leqslant \Gamma_p$ are represented by the results of only one sample. In this range of values of Γ our previous results let foreseeing clearly what

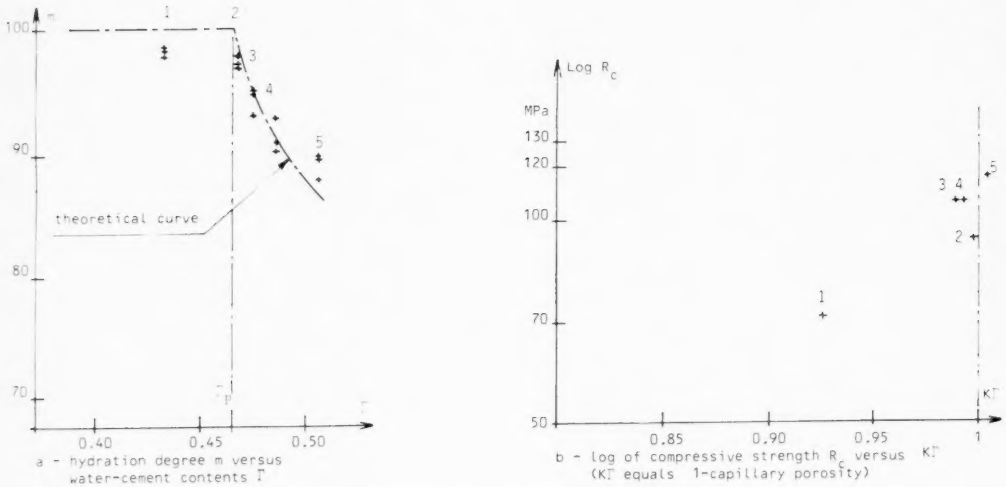

a - hydration degree m versus water-cement contents Γ

b - log of compressive strength R_c versus KΓ (KΓ equals 1-capillary porosity)

(corresponding numbers mark corresponding results)

FIG.1

Results of pastes hardened for an infinite time (3.5 years)

should be the evolutions of m and R_c, hence a unique point is enough to check them.

The results are in perfect agreement with what was expected. For $\Gamma \geqslant \Gamma_p$ the hydration degree decreases when Γ increases, the zero capillary porosity of all these pastes corresponds with KΓ = Ct = 1. For $\Gamma \leqslant \Gamma_p$ the hydration degree seems stabilized at 98.5% ≃ 100% ; the non-zero capillary porosity corresponds with KΓ ⩽ 1.

This confirms, for infinite hardening time, the validity of the calculation of m and K and the relation n = 1 - KΓ.

Pastes hardened for finite times (figures 2 and 3)

On the graphs Log R_c = f(KΓ) the experimental data are not scattered in the entire plane but gathered around the line of a simple curve, a straight line or parts of straight lines, as expected.

Our conclusion is that the value of the porosity used was realistic. According to the definition of K and its calculation from m and K_g, the porosity whose value n = 1 - KΓ is realistic can be nothing but the capillary porosity. On the other hand, the good agreement between experimental results and results expected theoreticaly confirms the validity of the relations m ⇔ K ⇔ n ⇔ R_c for finite hardening times.

Characteristic properties of the first and second groups

Figures 2 and 3 illustrating relation m = f(Γ) show clearly that the pastes can be separated into two groups whose characteristic properties are those expected for the first and second groups. In the second group ($\Gamma \geqslant \Gamma_F(t)$) it is found that the hydration degree decreases rapidly when Γ increases and in the first group ($\Gamma \leqslant \Gamma_F(t)$) the hydration degree seems steady ; it appears definitely constant when pastes of series 2 hardened for 4 to 7 days are

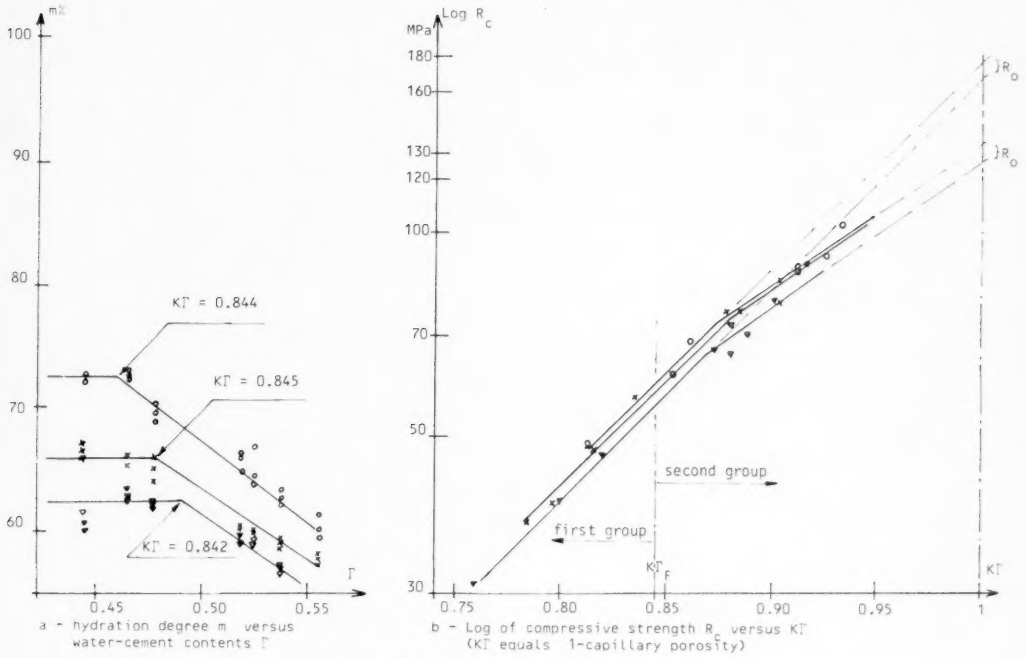

FIG.2 - Results of series 1

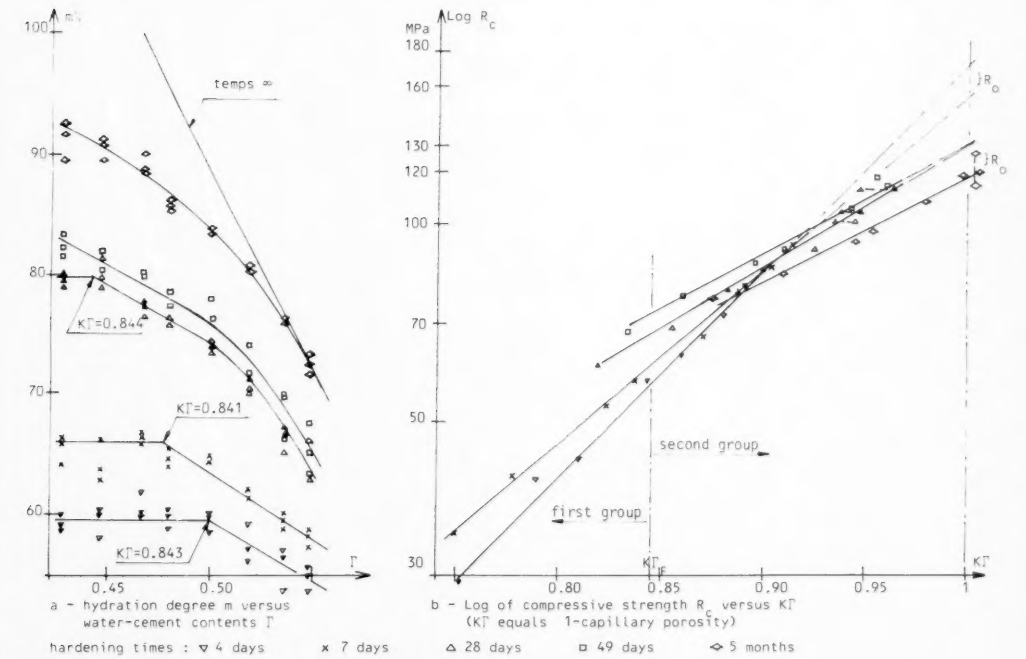

FIG.3 - Results of series 2

considered. The value of $K\Gamma$ associated with the boundary between the first and the second group and determined from the graphic data of figures 2a and 3a, is found to be constant, equal to $(K\Gamma)_F \simeq 0.85$. The corresponding value of capillary porosity is unique, $n_F \simeq 15\%$.

This confirms without any doubt the characteristics of the first and second groups which are the basis of the proposed model. Beyond that it confirms, for a given cement, the unicity of the relation capillary porosity $\leftrightarrow$ geometric characteristics of the hydrated grains assembly.

Value of A

It is represented by the slope of the curves Log $R_c = f(K\Gamma)$. The results agree in confirming that, in the first group for a given hardening time, A is constant. On the other hand, they oppose the following points, as the series 1 shows that A changes little with the hardening time and has a decreased value in the second group, the serie 2 shows that A decreases when the hardening time increases and that its value is not changed by going from the first to the second group.

Others series of tests not presented here as well as the results of F. Cuevas-Cancino (4) show that generally, the value of A is not changed by going from the first to the second group and decreases little when the hardening time increases.

This different behaviour observed between series 1 and 2 remains unexplained. It cannot be caused by a systematic measurement error on m in one of the cases because, for both series, the procedure was strictly identical. For each hardening time, all the samples were handled in a single batch. From one batch to another we were careful to systematically place all samples (same value of Γ) at the same location in the same stove and in the same kiln. One must conclude that this type of measurement, despite all the care taken to eliminate the scattering factors, cannot give a final answer regarding the changes of A. However it seems likely that in the first group A decreases when the hardening time increases but that its value steadies out quite fast, after two months, at its minimum value. In the second group, due to the range of the domaine of pastes made in classical fashion ($0.42 \leqslant \gamma \leqslant 0.55$) figure 3b shows that one can usualy consider A = Ct = A minimum.

Unicity of K_g and R_o

K_g is directly tied to the micro-structure of the hydrated paste as well as to its chemical composition. Thus it is very likely that any modification of $(E_h/C)_{100\%}$ be accompanied by a modification of K_g and vice-versa. S. Brunauer, J. Skalny, I. Odler and M. Yudenfreund (5) have shown that the computation of the hydration degree from the ratio $m = \frac{E_h/C}{(E_h/C)_\infty}$ is valid as soon as hardening time is longer than one day. This implies that for all hardening times concerned in this study $(E_h/C)_{100\%} \simeq Ct = (E_h/C)_\infty$, which in turn yields $K_g \simeq Ct = k_g(\infty)$. Our results do confirm this only for the paste $\Gamma = 0.55$ hardened for 5 months (figure 3). Indeed, if the values of K_g and $(E_h/C)_{100\%}$ used are realistic, for every paste with a zero capillary porosity we have $K\Gamma = 1$. This is confirmed for the pastes hardened for a infinite time since we used as a base $k_g = K_g(\infty)$ and $(E_h/C)_{100\%} = (E_h/C)_\infty$. This is also confirmed for the paste $\Gamma = 0.55$ hardened for 5 months ; it can be seen on the graph $m = f(\Gamma)$ of figure 3 that the paste has reached its final hydration degree corresponding

VOL. 14 1984

with a zero capillary porosity. The associated value of $K\Gamma$, read on the graph Log $R_c = f(K\Gamma)$, is actually equal to 1. More, considering finite times of hardening, the fact that testing two different series we found six times $K\Gamma_F$=Ct cannot be own to hazard. One can thus conclude that for hardening times longer than a few days K_g = Ct = $K_g(\infty)$.

If the values of K_g and $(E_h/C)_{100\%}$ are realistic, the ordinate corresponding to $K\Gamma = 1$ is R_o, readable on the curves Log $R_c = f(K\Gamma)$. The proposed model makes us expect R_o = Ct = R_{cmax}. Our results (figures 2b and 3b) show that, in spite of all experimental care, we do not find a unique value of R_o. On the one hand, for hardening times longer than 28 days, as expected, 110 MPa $\leqslant R_o \leqslant$ 130 MPa. On the other hand, for hardening times less than 14 days and for pastes of the first group R_o is much higher, especially for the younger pastes, 140 MPa $\leqslant R_o \leqslant$ 190 MPa ; to this high value of R_o corresponds a high value of A. If we accept the possibility of such a variation in R_o, it cannot be tied to hydration degree owing to a strength of the anhydrous part eventually higher than that of the gel. Indeed although the pastes hardened for an infinite time and with $\Gamma \geqslant \Gamma_p$ show hydration degrees which cover the entire range of hydration degrees observed with pastes of the first group between 4 days and infinite time, their measured strengths always are between 100 and 130 MPa. This higher value of R_o during the first days can be explained by the influence of ettringite, its large and long crystals bridge the grains over the mass of CSH. The associated contacts, necessarily less numerous, are consistent with a higher value of A. The portlandite in large crystals, more frequent when the hydration is not hindered, i.e. for young pastes and low values of Γ may have an effect in the same direction.

Second group

We have seen that the strength law applies to pastes of the second group. We also have noticed that the type of tests considered does not allow to obtain a final information about the value of A.

K_g being considered as constant, the value of K is entirely represented by the value of the hydration degree m. Its evolution as a function of Γ is shown in figures 2a and 3a. We will not go beyond this graphical representation and will not propose an empirical equation which would be simply a little translation of the observed results, without logical support.

Conclusion

The proposed strength law, under its general form $R_c = \frac{R_o e^{AK\Gamma}}{e^A}$, is confirmed for all hardening times and all values of Γ.

Are also confirmed the basic elements of the micro-structure model, they can be stated as follows :
- the essential parameter on which depends the compressive strength of APC pastes is capillary porosity,
- the capillary porosity is related biunivocally to the hydration degree by means of the swelling K of the hydrated grain and the initial composition Γ of the paste considered, i.e. $n \leftrightarrow K\Gamma \leftrightarrow K \leftrightarrow m$; the uniqueness of this relation is tied to the uniqueness of K_g and $(E_h/C)_{100\%}$,
- the characteristics of the first and the second groups are :
. first group : $m = f(t)$
. second group : $m = f(t,\Gamma)$
. boundary between the first and the second groups characterized by $n = Ct = n_F$.

These tests also have shown that it is interesting to measure systematically the hydration degree and to report the results of the mechanical tests on the graph Log $R_c = f(K\Gamma)$. This frees from considering the hydration rate, hence it makes possible to compare pastes which, at given age, have had different histories, this is the case of pastes of the second group. This method also allows finding, for each hardening time considered, the theoretical values of A and R_o.

At last, our results show that the proposed evolution of A and the unicity of $R_o = R_{cmax}$ must be shaded. But the scattering of the results, even reduced to its minimum, does not allow a final answer.

References

1. J.L. Granju, J.C. Maso - CCR 14, 249-256, 1984.
2. J.L. Gallias - Thèse U.P.S. Toulouse (France) n°805 - juillet 1982.
3. E. Papamichali - D.E.A. Dpt Génie Civil I.N.S.A. Toulouse - juillet 1980.
4. F. Cuevas-Cancino - D.E.A. Dpt Genie Civil I.N.S.A. Toulouse - juillet 1981.
5. S. Brunauer, J. Skalny, I. Odler, M. Yudenfreund - CCR - 3,pp 279,293, 1973.

VOL
14
198

CEMENT and CONCRETE RESEARCH. Vol. 14, pp. 311-314, 1984. Printed in the USA.
0008-8846/84 $3.00 + 00. Copyright (c) 1984 Pergamon Press, Ltd.

STUDIES OF ALKALI-SILICA REACTION - PART II
EFFECT OF AIR-ENTRAINMENT ON EXPANSION

A.D. Jensen, S. Chatterji, P. Christensen, N. Thaulow
Teknologisk Institute Tåstrup, Denmark

(Communicated by G.M. Idorn)
(Received Aug. 2; in final form Sept. 9, 1983)

VOL. 14 1984

ABSTRACT

From an extensive petrographic investigation of concrete samples suffering from alkali-silica reaction, it has been hypothesized that a deliberately introduced air-bubble system will reduce expansion due to alkali-silica reaction. The above hypothesis has been tested using mortar bars made from 35 sand types of differing degrees of alkali-silica reactivity. The results show that on the average the introduction of 4% air decreased the expansion by about 40%. A petrographic examination of mortar bars has shown that in the case of reactive sand the air-bubbles tend to get filled up by gel, but the air-bubbles remain empty in the case of unreactive sand. It has also been noted that this filling up of the air-bubbles will decrease their effectiveness in a freeze-thaw environment.

Introduction

From recent reports it will appear that alkali reactive aggregates are much more widely distributed than once thought. Damage to concrete structures due to alkali-aggregate reaction has been reported from countries such as England which was once thought to be free of reactive aggregates. This widespread reporting is partly due to the economic necessity of utilizing second-best quality local aggregates and to the increasing trend in fuel-saving practices of the cement plants which in turn has lead to a rising alkali content of cement. On occasions, considerable saving could be made if slightly reactive local aggregates could be utilized instead of imported, better quality aggregates; this is particularly so for fine aggregates, i.e. sand.

In the course of an extensive petrographic investigation of concrete cores taken from structures in Denmark, it has been observed that a reactive sand grain when present adjacent to an air-bubble may not cause any damage to its surroundings in spite of it being heavily reacted. It has also been observed that in such cases the air-bubbles are partly or fully filled with gel. From these observations it was hypothesized that a debliberately introduced air-bubble system, such as is used to improve the performance of concrete structures in a freeze-thaw environment, may reduce the expansion of structure undergoing an alkali-silica reaction.

In Part I of this series, attention has been drawn to the fact that the alkali-silica reaction may be accelerated by an increase in the alkali salt concentration. This increased alkali salt concentration may be achieved either by a migration from an external source or by an internal migration. An accelerated method has also been proposed both to detect the potential reactivity and to grade different aggregate samples in order of their potential expansivity (1).

The proposed method has been utilized to test the hypothesis of the reduction of alkali-silica expansion due to a deliberate introduction of air-bubbles. In this investigation the same 35 sand samples, which were investigated in Part I, have been utilized. In fact both the investigations were formulated and carried out simultaneously.

Materials and the Experimental Techniques

Sources of sand types varied from sea-dredges through land-based to tertiary sand sources. From each of these sources the sand fraction passing a 4 mm sieve was collected. Ordinary Portland cement of Danish origin was used to make mortar bars from the above sand types. A single lot of neutralized vinsol resin solution was used as an air-entraining agent.

Using the above materials, two batches of 1:3:cement:sand mortars were made from each of the sand types. In one of these batches sufficient vinsol resin was added to entrain about 10% air by volume. The effective water/cement ratios were 0.46 for the air-entrained mortar and 0.5 for the other. The air contents of both the batches were measured. From each of these mortars several 40x40x160 mm prisms were made, cured and treated for the measurement of their expansivity due to alkali-silica reactivity following the procedures already described (1). In this investigation length changes were measured up to 8 weeks by which time the major part of expansion had occurred. At the end of the expansion measurement selected prisms, both with or without air-entrainment, were used for petrographic examination.

Results and Discussions

The measurements of air contents showed that the mean air content of the air-entrained mortars was 9.3% with a standard deviation of 1.13; those of non-air-entrained mortars were 5.3% and 1.15, respectively. The petrographic examination showed that in the air-entrained mortars air was in the form of fine bubbles, and in the non-air-entrained mortars air was in the form of coarse air-voids. It has to be noted that in air-entrained mortars the number of air-bubbles, due to the smaller sizes, were higher and hence had a higher probability of finding themselves in the vicinity of reactive grains than in non-air-entrained mortars.

The expansion data of both air-entrained and plain mortar bars have been plotted in Fig. 1 along with the correlation line and the line of equality. Figure 1 indicates, and the correlation line confirms, that on the average the expansion of an air-entrained mortar is 0.65 times that of the plain mortar. In other words, the introduction of about 4% air has decreased, on the average, the expansion by about 40%. This decrease may on occasions allow for the use of a local slightly reactive sand instead of an imported non-reactive sand. In any case, air-entrainment may be used as an additional safeguard whenever alkali-reactivity of sand is suspected.

Figures 2 and 3 show the representative states of the air-voids in mortar bars made with non-expansive and expansive sand after their salt bath storage. Figure 2 shows that the air-voids of mortar made with a non-expansive sand remained empty; however, Fig. 3 shows that the air-voids of the mortar bar made with expansive sand is at least partly filled with a gel-like material. It is

VOL
14
198

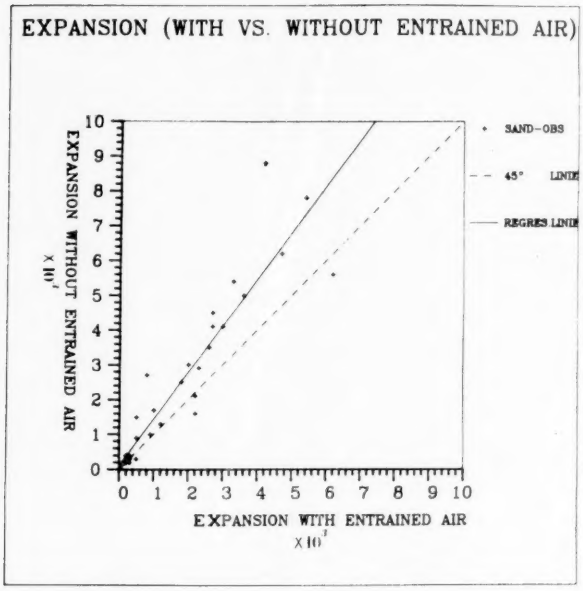

FIG. 1

Expansions of mortar bars with and without entrained air.

VOL.
14
984

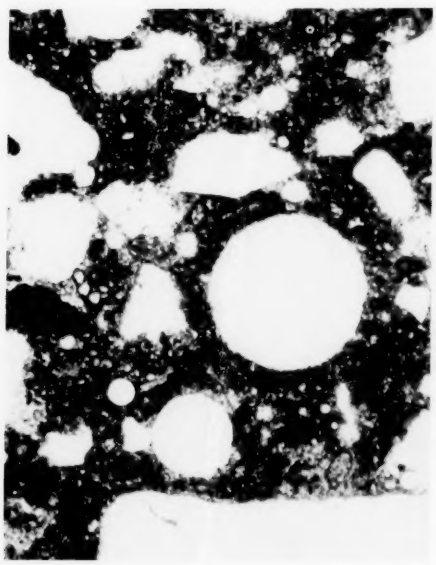

FIG. 2

Empty air-bubbles in a mortar made with an unreactive sand. (Mag x 63)

FIG. 3

A gel filled air-bubble. The aggregate near the air-bubble (arrowed) is a reactive flint grain. (Mag x 63)

reasonable to assume that the venting of the expansive gel in the air-voids will relieve a part of the expansive force and hence will cause less expansion and damage as has been found in the mortar bar expansion test.

It is perhaps in order to draw attention to another aspect of this filling-up of the air-voids. There is a general suspicion in Denmark that an entrained air-void system is not as effective, in a freeze-thaw condition, as has been claimed by workers of other countries. This suspicion seems to be well founded. Many of the Danish sand sources contain reactive particles. In air-entrained concrete made with reactive sand a part of the air-voids will tend to get filled up by a gel-like product whenever some alkali-silica reaction occurs. This filling-up will, of course, reduce space available for water to enter in a freeze-thaw condition and hence reduce the effectiveness of the entrained air-void system. It may be advisable to increase the entrained air-void from its usual value of about 5% when using an expansive sand; the actual increase needed will, of course, depend upon the expansivity of the sand and has to be determined experimentally. In this connection attention may be drawn to other pore filling processes. It is known that calcium hydroxide, ettringite, monosulphate, either singly or jointly, may form in voids (2,3). This filling up of air-voids will also reduce their efficiency.

References

1. A.D. Jensen, et al. Cement and Concrete Research 12, 641 (1982).
2. Bache, et al. Highway Research Board. Special Report No. 9 (1966).
3. P. Christensen, et al. Proc. 3rd Intern. Conf. Cement Microscopy, 298 (1981).

VOL.
14
1984

CEMENT and CONCRETE RESEARCH. Vol. 14, pp. 315-317, 1984. Printed in the USA.
0008-8846/84 $3.00+00. Copyright (c) 1984 Pergamon Press, Ltd.

AUTOGENOUS HEALING OF FIBRE/MATRIX INTERFACIAL BOND IN FIBRE-REINFORCED MORTAR

R.J. Gray
Department of Civil Engineering
The University of British Columbia, Vancouver, B.C., Canada, V6T 1W5

(Refereed)
(Received Aug. 16; in final form Oct. 3, 1983)

ABSTRACT

Autogenous or self-healing of the interfacial bond between steel fibres and a cementitious mortar matrix has been examined experimentally using water-cured, single-fibre pull-out specimens. The test results indicate that the extent of the interfacial bond healing which occurs is greater than that observed for fractured plain mortar or concrete similarly cured.

OL.
14
984

Introduction

Autogenous or self-healing has been found to occur in reinforced as well as plain cementitious materials. Munday et al. (1) in their paper on autogenous healing of different concretes note that Abrams first showed in 1913 that self-healing of bond failure in reinforced concrete can take place. Gilkey et al. (2) observed that bond test specimens subjected to moist curing conditions after being loaded to failure regained much of their initial bond resistance, and in some cases gave retest bond strengths exceeding those of the original test, whereas there was no bond recovery in specimens which were not exposed to moisture in the period between tests. Hannant and Keer (3) recently reported that cracks in polypropylene fibre-reinforced mortar specimens healed during exposure to natural weathering conditions, the fibres contributing to this process primarily by holding the cracked surfaces tightly together.

Autogenous healing of the fibre/matrix interfacial bond in steel fibre - cementitious mortar pull-out specimens was examined as part of a larger test program on the effect of matrix curing conditions and time on the development of interfacial bonding in this composite system, the results of which have been previously reported (4).

Experimental

Details of the materials, specimen types and dimensions, curing methods and times, and test procedures used have been presented previously (4). For the autogenous healing study, one pull-out and one compression specimen out of each of the three batches cast were selected from those cured in water and first tested at 7 and 28 days. The specimens were loaded in the normal manner at first, but the load was removed as soon as failure occurred rather than being continued past this point as for the other specimens. They were immediately reloaded at the same rate, and the load was again removed as soon as failure occurred for the second time. After testing, these specimens were returned to the curing container for storage until the next test age.

Results and Discussion

The test results for the autogenously healed pull-out and compression specimens have been "normalized" by dividing them by the appropriate mean value for all of the specimens first tested at 28 days (4) and are presented in this form in Table 1. A typical pull-out load versus time pattern for the interfacial bond test specimens is shown in Fig. 1.

TABLE 1

Normalized Autogenous Healing Test Results

	Mix Number	7 days		28 days		90 days
		Initial	Second	Initial	Second	Initial
Average Interfacial Bond Shear Strength	1	0.76	0.52	2.25	1.82	2.32
				1.41	1.58	>2.76
	2	0.93	0.63	1.19	0.75	2.47
				0.89	0.67	1.84
	3	0.89	0.59	1.84	1.77	2.69
				0.63	0.40	1.92
	average	0.86	0.58	1.76	1.45	2.49
				0.98	0.88	>2.17
Compressive Strength	1	0.68	0.63	0.96	0.85	0.86
				1.01	0.84	0.80
	2	0.70	0.64	0.95	0.80	0.80
				1.02	0.89	0.91
	3	0.63	0.57	0.84	0.75	0.77
				0.98	0.84	0.86
	average	0.67	0.61	0.92	0.80	0.81
				1.00	0.86	0.86

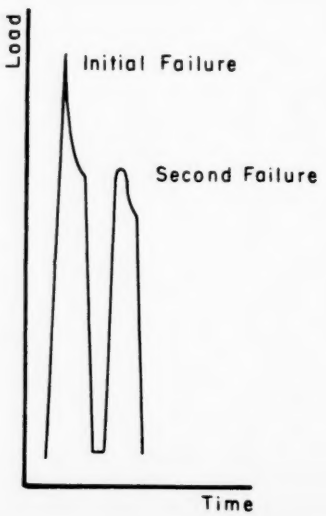

Fig. 1.

Typical Pull-out Versus Time Pattern for Autogenous Healing Test Specimens

In assessing the test results reported in Table 1, the extent of autogenous healing is properly gauged by comparing the "initial" strength value for a specimen at a given age with the "second" strength value at the prior age. These results show that at 28 days the average values (initial and second) of the apparent interfacial bond shear strength for the pull-out specimens first tested at 7 days and "healed" between 7 and 28 days are higher than those for "fresh" specimens first tested at 28 days. The apparent bond strength for these "7-day" specimens increased by a factor of approximately 3 (1.76/0.58) between 7 and 28 days, and further increased by a factor of approximately 1.7 (2.49/1.45) on healing between 28 and 90 days. At 90 days, these specimens had higher apparent strengths than those first tested at 90 days and than those first tested at 28 days and healed between 28 and 90 days, even though the apparent bond strength for these "28-day" specimens increased by approximately 2.5 (2.17/0.88). It is evident from these results that up to an age of 90 days, the increases in pull-out resistance that can be obtained as a consequence of autogenous healing in water-cured specimens are greater than the increases resulting from continuous curing under the same conditions.

The compressive strength specimens showed some healing between 7 and 28 days, but on average the healed specimens did not fully recover to the strength of the "fresh" specimens first tested at 28 days. Furthermore, for the specimens first tested at either 7 or 28 days, little or no healing took place between 28 and 90 days. These results are considerably different from those for the companion pull-out test specimens as well as from those reported by Munday et al. (1), who found that full recovery of compressive strength to values equal to or greater than those of corresponding fresh specimens is possible at these later test ages. It is thought that these discrepancies in the compressive strength test results are due to the lower degree of control exercised over the extent of fracturing in the specimens during the initial loading sequence.

OL.
14
984

Conclusions

Although the experimental data are limited, they do indicate that autogenous healing of the interfacial bond between steel fibres and a cementitious mortar matrix does occur under continued water curing conditions and that the extent of this healing is greater than that for fractured plain mortar or concrete.

Acknowledgements

The work reported in this paper was carried out whilst the author was a graduate student in the Department of Civil Engineering at The University of Calgary. The financial support provided by the Natural Sciences and Engineering Research Council of Canada and The University of Calgary is gratefully acknowledged.

References

1. J.G.L. Munday, C.M. Sangha and P.K. Dhir, Proc. First Aust. Conf. on Engineering Materials, The University of New South Wales, 1974, p. 177.
2. H.J. Gilkey, S.J. Chamberlin and R.W. Beal, Bulletin 147, Iowa Engng. Res. Stn., Iowa State College, 1940.
3. D.J. Hannant and J.G. Keer, Cem. Concr. Res., 13, 357 (1983).
4. R.J. Gray and C.D. Johnston, Cem. Concr. Res., 14, 285 (1984).

CEMENT and CONCRETE RESEARCH. Vol. 14, pp. 318-322, 1984. Printed in the USA.
0008-8846/84 $3.00+00. Copyright (c) 1984 Pergamon Press, Ltd.

STRENGTH DEVELOPMENT AND PORE SIZE DISTRIBUTION OF CEMENT PASTE CURED WITH HIGH HYDROSTATIC PRESSURE

C. Tashiro and H. Urushima
Faculty of Engineering, Yamaguchi University
Ube 755, Japan

(Communicated by D.M. Roy)
(Received Nov. 2, 1982; in final form Jan. 9, 1984)

ABSTRACT

Compressive strength, pore size distribution and total pore volume of cement pastes cured with high hydrostatic pressure were examined. Compressive strength (S) of paste cured with high hydrostatic pressure (P) is shown in the following formula: $S = a \cdot \log P + b$. Compressive strength of paste having total pore volume (V) is calculated from the following formula: $S = c \cdot V + S_o$. When hardened paste cured at atmospheric pressure is placed in high hydrostatic pressure, the larger the strength is, the larger the lowering it becomes.

VOL
14
198

Introduction

Low temperature-high hydrostatic pressure curing of cement and concrete has recently become important in connection with ocean disposal of industrial solid wastes solidified by cement or concrete, the development of artificial fishing reefs, and the exploitation of the continental shelf.

In the present study, strength development and pore size distribution of cement paste cured with hydrostatic pressure of 1, 50 and 450 kg/cm^2 were examined with varying ages. Cement paste cured with 1 kg/cm^2 was again cured with 450 kg/cm^2 at 20°C. Satisfactory results were then obtained on the strength development and pore size distribution.

Experimental Method

Preparation of the Test Specimen

An ordinary portland cement was used in the experiments. The water to cement ratio was 0.3. As shown in Fig. 1, the cement paste was set in a rubber sleeve with an inner diameter of 16 mm, and a wall thickness of 1 mm, having two steel disks at the bottom and top. The steel disk at the bottom was stuck to the rubber sleeve by gum arabic and the top-steel disk was free in order to liberate the air in the paste. The specimen was then put into a bombe and hydrostatic pressure raised at a rate of 30-50 kg/cm^2 per minute.

Curing was provided at a hydrostatic pressure of 1, 50 and 450kg/cm^2 for 3, 7, 14 and 28 days respectively. Some specimens were cured with 450 kg/cm^2 after 1 kg/cm^2 at 20°C.

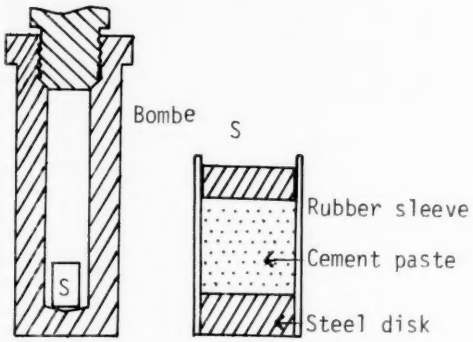

FIG. 1

Apparatus of hydrostatic pressure-curing.

Pore Size Distribution

The pore size distribution and total pore volume were measured by mercury porosimeter.

Results and Discussion

Strength Development

Figure 2 shows the relation between compressive strength and hydrostatic pressure with varying ages. The higher the hydrostatic pressure is, the larger it becomes. The following formula can be applied to the experimental data.

$$S = a \cdot \log P + b$$

Where S = compressive strength (kg/cm^2), P = hydrostatic pressure of curing (kg/cm^2), and a or b = constant representing age. The constants a, calculated with the above formula are 61, 33, 14 and 29, and b are 270, 401, 499 and 566 for ages of 3, 7, 14 and 28 days respectively.

Table 1 shows the compressive strength of pastes cured with 450 kg/cm^2-curing for 27, 21, and 1 day after 1 kg/cm^2-curing for 1, 7, and 27 days at 20°C respectively. It is clear that the longer 1 kg/cm^2-curing is, the smaller the strength after 450 kg/cm^2-curing becomes. Namely, in the case of 450 kg/cm^2-curing for 1 day after 1 kg/cm^2-curing for 27 days, the strength is decreased by 87% over that of 1 kg/cm^2-curing for 28 days. On the other hand, strength from 450 kg/cm^2-curing for 28 days is increased by about 127%.

Pore Size Distribution

The pore size distribution and total pore volume of cement pastes obtained from both curing of 450 and 1 kg/cm^2 are shown in Figs. 3 and 4 respectively.

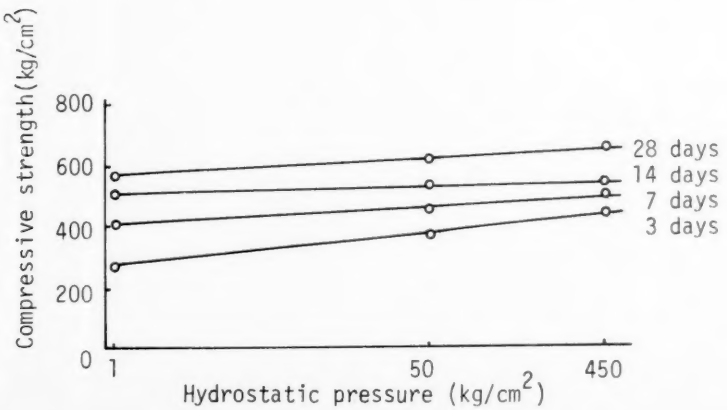

FIG. 2

Effect of hydrostatic pressure on compressive strength of pastes.

Table 1
Compressive strength of pastes cured with 450 kg/cm^2 after 1 kg/cm^2-curing.

Age (day)		Strength (kg/cm^2)	Total pore volume (cm^3/g)
Hydrostatic pressure 1	450 (kg/cm^2)		
0	28	647	0.087
1	27	632	0.092
7	21	528	0.086
27	1	508	0.104
28	0	583	0.096

The hydrostatic pressure of 450 kg/cm^2 shifts pore size distribution to a smaller size and total pore volume decreases. But, as with the 28-day paste, patterns of pore size distribution of both pastes are similar to each other, although the total pore volumes differ.

Total pore volume of pastes cured with 450 kg/cm^2 after 1 kg/cm^2-curing, is shown in Table 1. With the passage of curing time of 1 kg/cm^2-curing, strength decreases, but the total pore volume varies with the curing condition.

The Relation between Strength and Total Pore Volume

The results of pastes obtained from hydrostatic pressure of 450 and 1 kg/cm^2 are shown in Fig. 5. The following formula can be applied to the data.

$$S = c \cdot V + S_0$$

Where S = compressive strength (kg/cm^2), S_0 = compressive strength at zero porosity, V = total volume (cm^3/g), and c = constant.

The data shown agrees fundamentally with other experiments (1,2). It can therefore be presumed that compressive strength of cement pastes cured under various conditions are ultimately controlled by micropore or pore size distribution, even though obtained from pastes of hot-pressed, pressed and hydrostatic pressure. It also seems that the mechanism of hydration under high hydrostatic pressure is similar to that under ordinary conditions. Actually, the authors confirmed this by other experiments. The hydration of C_3S and C_2S under high hydrostatic pressure is faster than that under atmospheric pressure condition, and the hydration of cement paste or mortar under air-pressure is also faster (3,4). The hydration mechanism of these materials is similar to each other.

On the other hand, with pastes cured with 450 kg/cm^2 after 1 kg/cm^2-curing, the relation between strength and total pore volume is unlinear. It can be assumed that the micropore formed under 1 kg/cm^2-curing is destroyed by 450 kg/cm^2-curing and consequently, the pore becomes larger and the pore volume increases irregularly. Microcracks will be formed. It may be concluded that when cement paste cured with ordinary conditions is placed in high hydrostatic pressure, the stronger the strength at atmospheric conditions is, the larger the lowering of strength becomes.

Conclusion

The compressive strength development of pastes cured with hydrostatic pressure of 450, 50 and 1 kg/cm^2 were measured and pore size distribution of pastes

cured with 450 and 1 kg/cm^2 were examined. Strength and pore size distribution of pastes cured with 450 kg/cm^2 after curing of 1 kg/cm^2 were also measured. The conclusions are summarized as follows:

1) The relation between compressive strength and hydrostatic pressure of curing can be shown by the following formula:

$$S = a \cdot \log P + b$$

2) The relation between strength and total pore volume of pastes cured with 450 and 1 kg/cm^2 are shown by the following formula:

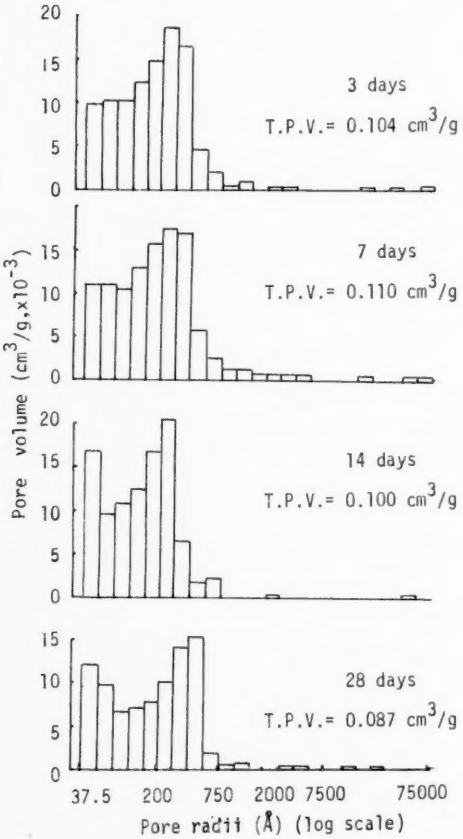

FIG. 3

Pore size distribution of pastes cured with hydrostatic pressure of 450 kg/cm^2.

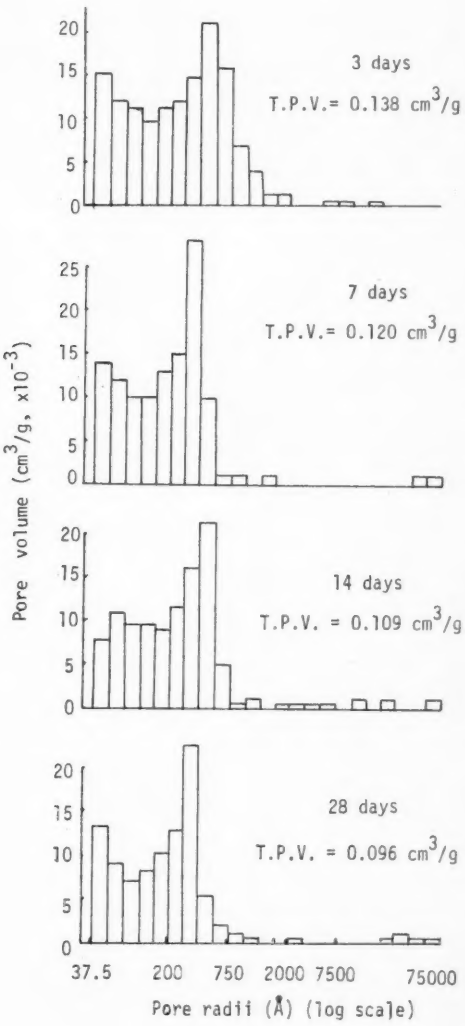

FIG. 4

Pore size distribution of pastes cured with hydrostatic pressure of 1 kg/cm^2.

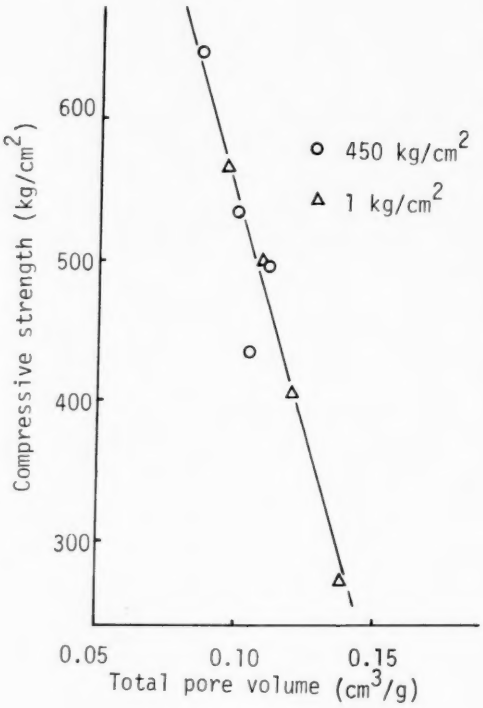

FIG. 5

Relation between compressive strength and total pore volume of pastes cured with hydrostatic pressures of 450 and 1 kg/cm^2.

$$S = c \cdot V + S_0$$

3) When the paste is placed in high hydrostatic pressure, the stronger the strength is at atmospheric condition, the larger the lowering of strength becomes. This is important from the viewpoint of effective ocean disposal.

Acknowledgement

The authors would like to express their thanks to Professor A. Yoshimota for his advice with this work.

References

1. D.M. Roy and G.R. Gouda, J. Am. Ceram. Soc. 56, 549 (1973).
2. H. Yamazaki, Proc. Japan Soc. Civil Engineers, 85, 15 (1962).
3. A. Yoshimota and C. Tashiro, Semento Gijutsu Nenpo, 30, 250 (1976).
4. C. Tashiro and K. Urushima, unpublished data.

VOL
14
198

CEMENT and CONCRETE RESEARCH. Vol. 14, pp. 323-328, 1984. Printed in the USA.
0008-8846/84 $3.00+00. Copyright (c) 1984 Pergamon Press, Ltd.

PREPARATION AND HYDRATION OF β-C_2S WITHOUT STABILIZER

S. Shibata, K. Kishi, K. Asaga and M. Daimon
Department of Inorganic Materials
Tokyo Institute of Technology
Ookayama, Meguro-ku, Tokyo 152, Japan

P. R. Shrestha
Department of Mines and Geology
His Majesty's Government
Lainchaur, Kathmandu, Nepal

(Communicated by J.P. Skalny)
(Received Sept. 9, 1983)

VOL.
14
984

ABSTRACT

The preparation method of β-C_2S without stabilizer, and their hydration characteristics were studied. β-C_2S is formed when γ-C_2S is heated at about 1000°C or about 1500°C. The hydration kinetics of β-C_2S produced from α′-C_2S is markedly different from that from α-phase. $Ca(OH)_2$ is hardly produced in the hydration of β-C_2S without stabilizer. Formed C-S-H has a composition of C/S ≃ 2.

Introduction

Dicalcium silicate (C_2S), occuring in five polymorphs ($\alpha, \alpha'_H, \alpha'_L, \beta, \gamma$), has very complicated characteristics. And most of the investigators have used various stabilizers, in order to study the hydration of high temperature modifications (1,2). B_2O_3 is the most popular stabilizer of β-C_2S (2-4). Pashohenko and Starchevskaya(5) and Fierens and Tirlocq(6) used B_2O_3 to prepare β-C_2S, and found that the hydraulic activity changed with tharmal hystory. But the nature of pure C_2S has not fully been studied.

Yamaguchi et al (7) proposed " γ reheating method " and " α air quenching method " for preparing β-C_2S without stabilizer. Korneev and Bygalia (8) synthesized β-C_2S by reheating γ-C_2S or by the addition of excess CaO. Yannaquis and Guinier (9) , and Chromý (10) found that the β-γ transformation was controlled by the particle size. Gawlicki (11) synthesized β-C_2S without stabilizer by restraining the crystal growth. Authors (12) discussed the relationship between the particle size and the β-γ transformation, after heating γ-C_2S at 1000-1400°C.

The present report deals with the preparation methods of β-C_2S without stabilizer, and their hydration characteristics.

Experimental procedure

The β-C_2S was synthesized by firing γ-C_2S. The γ-C_2S was prepared by heating a stoichiometric mixture of $CaCO_3$ and SiO_2 at 1500°C for 30 minutes, and cooled in air. The prepared γ-C_2S samples (5g baches of pressed pellets) were refired two times. The result of XRD showed that γ-C_2S was the only polymorph present.

High temperature XRD was measured in order to study phase transformations.

The γ-C_2S (0.5g baches of pressed pellets) were heated in platinum crucible in an electric furnace at various temperatures ; 1000°C, 1100°C, 1200 °C, 1300°C, 1400°C, 1500°C each for 10 minutes, 1 hour, 15 hours, 48 hours, and were quenched in water. The products were imediately washed with aceton to prevent hydration. The products were identified by XRD. And the ratios of β-C_2S/γ-C_2S were determined. The analisis required the construction of a calibration curve using synthesized pure γ-C_2S for the diffraction line of (1 3 0) and pure β-C_2S for that of (1 0 4).

The samples were heated at various temperatures ; 1000°C, 1100°C, 1200°C, 1300°C, 1400°C, 1500°C for 1 hour in order to study the hydration of β-C_2S without stabilizer. The samples were ground to the Blaine fineness about 0.5 m^2/g. The specipic surface area was determined by B.E.T. using Kr as adsobate.

The rate of heat liberation for 24 hours were determined by conduction calorimeter. For the conduction calorimeter measurement the samples were hydrated at W/C of 1 at 20°C.

The experiments of paste hydration were carried out at W/C ratio of 0.5 at 20°C for 7 days, 14 days, 28 days, 84 days and 168 days. The pastes hydrated were dried under the water vaper pressure of 3×10^{-2} mmHg, and identified by XRD. The loss on ignition at 1000°C was measureed by TG-DTA, and the amount of $Ca(OH)_2$ was determined by D.S.C..

Results

Measurement of high temperature XRD

When the γ-C_2S sample is heated at 10°C/min., the γ-α'_L transformation is observed to make slow progress at the temperature below 1000°C. There is no peak of γ-C_2S at 1000°C. It is necessary to heat above 1000°C in order to form the β-C_2S, otherwise it takes long time. The peak of α'_L just after the γ-α'_L transformation is sharp and there is no change in crystallinity with time and temperature. Difference in XRD pattern of α'_L and α'_H phase is not detected. The α'-α transformation makes rapid progress.

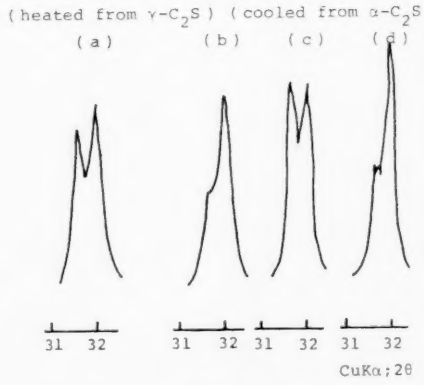

Fig. 1
XRD patterns of α'-phase at 1300°C.

XRD pattern of α' phase transformed from α phase is different from that heated from γ-C_2S. The main peaks $\begin{matrix}(2\,0\,0)\\(1\,1\,2)\\(0\,2\,2)\end{matrix}$ $(1\,3\,0)$ of α' phase at 1300 °C are illustrated in Fig. 1 ; (a) the sample heated from γ-C_2S, (b), (c), (d) the sample cooled from α phase. The main peaks of α'phase from α phase changes irregularly as seen in Fig. 1 - (b), (c), (d), while α' phase from γ phase shows a stable pattern as Fig. 1 - (a).

Change in the amount of β-C_2S with heating temperature and heating time

The ratios of the β-γtransformation were determined by XRD in the heated γ-C_2S samples. Figuar 2 presents the ratios of transformation with time for samples heated at 1000 °C, 1200°C, 1400°C and 1500°C. The amount of γ-C_2S is less in samples heated at 1000°C and 1500°C, and shows a little change with time, whereas in the case of sample heated at 1200°C γ-C_2S increases with time. The sample heated at 1200°C for 48 hours has maximum value than others. But the sample heated at 1400°C shows a different trend. The amount of γ-C_2S is maximum at 1 hour and decreases with time, and at 48 hours it is similar to that of heated at 1000°C. When the γ-C_2S are heated at 1000 °C or 1500°C, the β-C_2S is formed as a single phase.

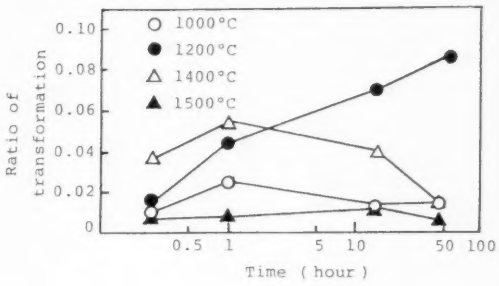

Fig. 2
Change in ratio of transformation, $\gamma/(\beta+\gamma)$,with heating time of γ-C_2S.

Table 1 shows the B.E.T. specific surface area and the Blaine fineness of the obtained β-C_2S. The Kr surface area of the sample heated at 1500°C is larger than those of 1000-1400°C, suggesting that its microstructure is different from the others.

Table 1

Specific surface area of samples for hydration experiments.

temperature (°C)	Kr surface area (m^2/g)	Blaine surface area (m^2/g)
1500	2.10	0.52
1400	1.49	0.53
1300	1.25	0.51
1200	1.15	0.45
1100	1.41	0.52
1000	1.59	0.49

Hydration during the early stage

The rate of heat liberation determined by conduction calorimeter are plotted against time in Fig. 3. It is observed that the rate of heat liberation for the sample heated at 1500°C is different from those of 1000-1400°C. The total calorific value of the sample heated at 1500°C for 24 hours is 40 J/g, whereas those of 1000-1400°C are 5-10 J/g. The heat liberation curve for the sample heated at 1500°C shows the broad peak at 6 hours after mixing. Those of 1000-1400°C show the small peaks at 1-2 hours and show very small heat liberation after 10 hours.

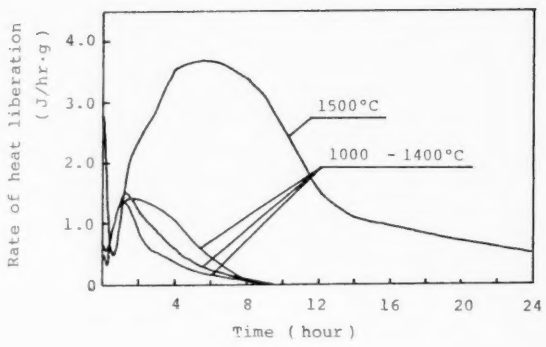

Fig. 3
Effect of the heating temperature on the heat liberation curve.

Hydration at later stages

The samples heated at 1000 °C and 1500°C are hydrated at W/C ratio of 0.5. The loss on ignition and the amount of $Ca(OH)_2$ of hydrated paste are plotted against time in Fig. 4. The loss on ignition is calculated on ignited base. Figure 4 shows the large difference between the hydration characteristics of 1000°C sample and 1500 °C sample.

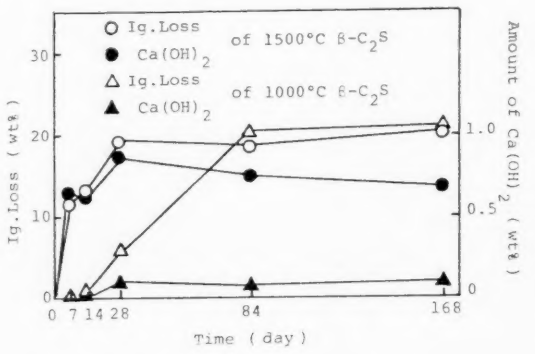

Fig. 4
Change in Ignition loss and amount of $Ca(OH)_2$ with the progress of β-C_2S hydration.

In the hydrated paste of the sample heated at 1500°C the loss on ignition increases actively up to 7 days, and is about 12%, however it becomes very slow after 28 days and is about 20% up to 168 days. In the case of 1000°C it makes a little change in the beginning, and after 14 days increases rapidly, and is about 20% up to 84 days. However it hardly increases after 84 days.

In the hydrated paste of both the samples heated at 1000°C and 1500°C, the amount of $Ca(OH)_2$ is very small, and is below 1% up to 168 days. In 1000°C sample, $Ca(OH)_2$ is hardly detected up to 14 days, and is about 0.1% up to 168 days.

Peak of β-C_2S remarkable decreases and a broad peak of C-S-H is shown in XRD pattern of the samples hydrated for 168 days. About 80% of β-C_2S have hydrated after 168 days in both cases.

Discussion

Preparation of β-C_2S without stabilizer

As above mentioned, when the γ-C_2S are heated at about 1000°C or at about 1500°C (above the α-α′ transformation temperature), the β-C_2S without admixture is formed as single phase.

When the γ-C_2S are heated at 1000-1400°C, the β-γ transformation depends on the particle size of β-C_2S. In the sample heated at 1000°C the amount of γ-C_2S is less on account of a little particle growth. The details are reported elsewhere (12).

The sample heated at 1500°C differs from those of 1000-1400°C, the amount of γ-C_2S is less and is not concerned with the heating time and the particle size. XRD pattern of α′ phase cooled from α phase is not stable, while that heated from γ phase shows stable pattern. Kr surface area (Table 1) of 1500°C sample is larger than others. This must be related to Groves's observation (13), on C_2S containing Cr_2O_3. Groves (13) reported that β-C_2S formed from α-C_2S had a complicated domain structure within an original α grain. Local elastic strains and in some cases dislocations are also present at twin domain interfaces.

VOL.
14
1984

Hydration of β-C_2S without stabilizer

Hydration kinetics of β-C_2S is affected by thermal history. The hydration of β-C_2S produced from α-C_2S proceeds actively at early stage, and becomes very slow at latter stage. In the case of β-C_2S formed α′ phase, it hydrates slowly in the beginning, but rapidly latter.

The amount of $Ca(OH)_2$ is very less in the hydrated pastes of both the samples heated at 1000°C and 1500°C. Fujii et al (3) reported that the C-S-H produced in the hydration of β-C_2S stabilized 0.2wt.% of B_2O_3 had a composition of C/S ratio =1.80. Kantro (4) mentioned that the C-S-H produced in the hydration of β-C_2S with a few stabilizer had cation/anion ratio of 1.83. In the hydration of β-C_2S without admixture in this study reacted about 80% after 168 days, and the amount of $Ca(OH)_2$ is below 1%. Therefore C/S ratio of produced C-S-H is nearly 2. The hydration of β-C_2S without impurity is markedly different from that of β-C_2S with stabilizer. Further detailed study must be carried out.

Conclusions

β-C_2S/γ-C_2S ratios were determined in the γ-C_2S samples heated at 1000-1500°C for 10 minutes-48 hours in order to establish a suitable method of preparation of β-C_2S without stabilizer. These samples were hydrated to know their hydraulic activities. Results obtained are as follows;

(1) β-C_2S without admixture is formed as a single phase, when γ-C_2S is heated at about 1000°C, or at about the α-α′ transformation temperature; about 1500°C.

(2) There is large difference between the hydration kinetics of β-C_2S formed from α′ phase and that from α phase.

(3) $Ca(OH)_2$ is hardly in the hydrate of β-C_2S without stabilizer. Produced C-S-H has a composition of C/S ≃ 2.

References

1. I.M. Pritts, K.E. Daughety, Cem. Concr. Res., 6, 783-796 (1976).
2. D.L. Kantro, C.H. Weise, J. Am. Ceram. Soc., 62, 621-626 (1979).
3. K. Fujii, W. Kondo, J. Am. Ceram. Soc., 62, 161-167 (1979).
4. D. Ménétrier, I. Jawed, T.S. Sun, J. Skalny, Cem. Concr. Res., 10, 425-432 (1980).
5. A.A. Pashohenco, E.A. Starchevskaya, U.P. Servin, Proc. 6th Intl. Cong. Chem. Cem. -Suppl. Paper - Section I-4-Moscow- (1974).
6. P. Fierens, J. Tiricoq, Cem. Concr. Res., 13, 41-48 (1983).
7. G. Yamaguchi, K. Suzuki, H. Miyabe, Semento Gijutsu Nenpo, 11, 28-31 (1957).
8. V.I. Korneev, E.B. Bygalina, Proc. 5th Intl. Symp. Chem. Cement, Tokyo 1968 Vol. I, 285-288 (1969).
9. N. Yannaquis, A. Guinier, Bull. Soc. franc. miner. et crist., 82, 126-136 (1959).
10. S. Chromý, Zement-Kalk-Gips, 23, 382-389 (1970).
11. M. Gawlicki, Proc. 7th Intl. Cong. Chem. Cement, Paris, Vol. II, 161-165 (1980).
12. S. Shibata, K. Kishi, K. Asaga, M. Daimon, Yogyo-Kyokai-Shi, to be submitted.
13. G.W. Groves, Cem. Concr. Res., 12, 619-624 (1982).

VOL.
14
198

CEMENT and CONCRETE RESEARCH. Vol. 14, pp. 329-338, 1984. Printed in the USA.
0008-8846/84 $3.00+00. Copyright (c) 1984 Pergamon Press, Ltd.

THE EFFECT OF RATE OF DRYING ON THE DRYING CREEP OF HARDENED CEMENT PASTE

R.L. Day[@], P. Cuffaro[*] and J.M. Illston[*]
[@]Dept. of Civil Engg., Univ. of Calgary, Alberta, Canada
*The Hatfield Polytechnic, Hatfield, Herts., U.K.

(Communicated by C.D. Pomeroy)
(Received Sept. 19, 1983)

VOL.
14
984

ABSTRACT

Tests were performed on miniature, thin-wall, hardened cement paste specimens; specimens under load were dried at various rates, re-wet and then unloaded. Deformation was monitored throughout. Appropriate control specimens for shrinkage/swelling, basic creep and weight change were also tested. Relationships between moisture loss, shrinkage and wetting creep were obtained. It was found that, like shrinkage, the magnitude of drying creep is independent of rate of drying. Also, drying creep bears a linear relationship to concomitant shrinkage over a wide range; similarly, wetting creep is linearly related to swelling. Drying creep and wetting creep are completely irrecoverable. Discussion centres about the significance of the results with respect to the prediction of creep strains when environmental conditions change; results suggest it may be possible to develop prediction equations which are not overly complicated.

Introduction

Recently, tests have been reported on the shrinkage behaviour of small, hardened cement paste (hcp) specimens when dried from 100 to 53% relative humidity at various rates (1). There, it was found that the magnitude of shrinkage strains when specimens reached equilibrium at 53% rh were indepedent of the rate of drying; it was concluded that small specimens can be used to examine the unrestrained response of the material and that if specimens are dried or wet while under load, the extra creep component which is observed -- 'drying creep' (e_{dc}) or 'wetting creep' (e_{wc}) -- is a property of the material; it is not due to spurious influences (such as microcracking) caused by internal moisture gradients.

Figure 1 shows a typical test to determine drying creep. Drying creep at time t_2, $e_{dc}=e_d-e_{bc}-e_s$ where e_d= total time dependent strain during the moisture change, e_{bc}= basic creep which occurs in a non-drying control specimen during the time of moisture change, and e_s= the concomitant shrinkage which occurs in a non-loaded control specimen. An analogous situation exists for wetting creep: $e_{wc}=e_w$(total strain during wetting)-e_{bc}(basic creep)-e_{sw} (swelling).

A relationship has been identified between the magnitude of excess strain (Δe, see Fig. 1) which occurs after the humidity change and the magnitude of concomitant shrinkage or swelling strain in a companion unloaded specimen (2,3). Gamble and Parrott (3) tested concrete, and obtained an excellent linear relationship between Δe and shrinkage or swelling. Since $e_{dc}=\Delta e-e_s$, a similar linear relationship exists between shrinkage and drying creep (or between swelling and wetting creep).

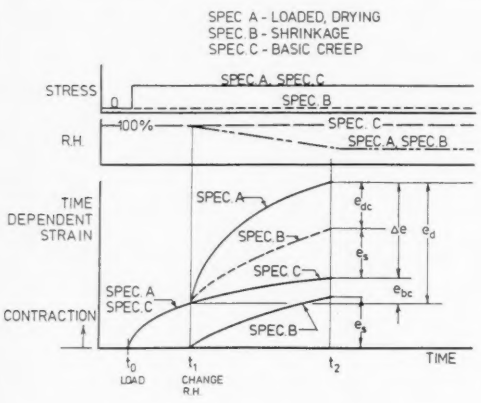

FIG. 1
Definition of Strain Components

These results are important from a practical viewpoint in that drying creep may be predictable from known shrinkage behaviour. They also infer that there may be a common, fundamental, process which relates drying creep, shrinkage and basic creep.

Because the trends which have been reported are important from both the fundamental and practical viewpoints, it was decided to study further the relationship between shrinkage and drying creep. In a parallel investigation to that described in (1), the effect of rate of drying on the magnitude of drying creep was examined. Because small hcp specimens were tested, the connection between shrinkage and drying creep could be investigated over a much greater deformation range than that established by Gamble and Parrott (3), who tested concrete. The test programme was also extended to examine the wetting creep vs. swelling relationship.

Experimentation

Miniature, thin-wall, hardened cement paste specimens were subjected to various regimes of loading, drying and wetting. The test programme is outlined in Figure 2.

The humidity reduction was always between 100 and 53% rh, but specimens were dried at different rates for each of tests 1, 2A and 3. In test 2B specimens were subjected to a second humidity cycle before they were unloaded; otherwise, this test was identical to test 2A.

For each test, 9 specimens were used. Three were loaded and immediate and time dependent strains were monitored. Three control specimens remained unloaded and shrinkage and swelling strains were measured. Three others were used to measure weight changes during the drying and wetting cycles. In general, results which are given in this paper are the means of three replicates.

The magnitude of basic creep is required in order that drying creep can be determined from the total strain curve (Fig. 1), so a fourth test (not shown in Fig. 2) was performed to measure the basic creep response of saturated specimens. Five specimens were loaded at 75 days of age and basic creep measurements were taken; to determine the development of irrecoverable creep with time, the 5 specimens were unloaded individually after periods under load of 7, 21, 35, 50 and 64 days. After unloading, recovery was monitored for at least 7 days; recovery was assumed to be complete when the strain rate dropped below 10×10^{-6}/day.

VOL. 14 1984

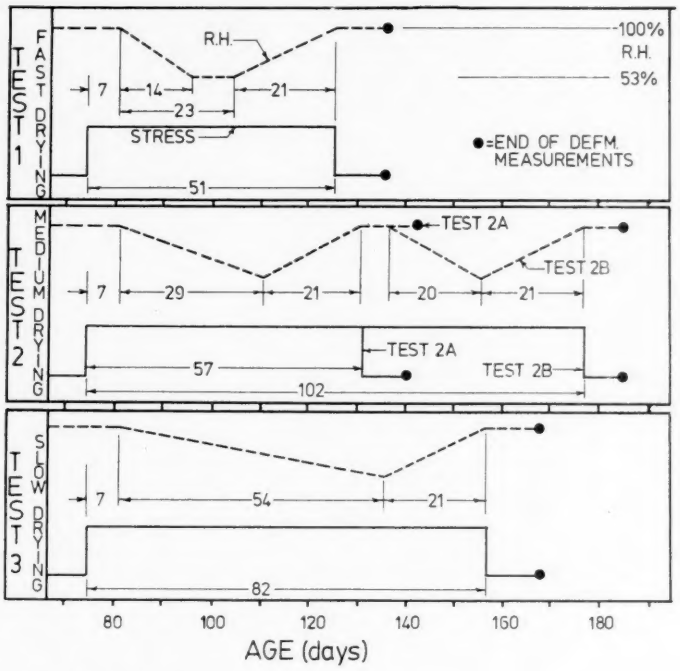

FIG. 2
Test Programme

Test details

Materials, equipment and test procedures have been described in detail elsewhere (1,4,5); a summary of the key aspects of experimentation is given below.

Specimens: 100 mm long, thin-wall, slotted hcp specimens were used; the cross-sectional dimensions of these specimens are shown in Figure 3. They were prepared from larger slabs by cutting with a diamond-impregnated saw blade.

Slabs were cast with an original water-cement ratio of 0.47; distilled water and ordinary portland cement were used. To produce a homogeneous product, the slabs were slowly rotated during hardening. After demoulding, during cutting and during storage until the start of tests at age 75 days, specimens were kept in saturated limewater.

Load application: Specimens were loaded by means of miniature, hydraulically controlled, creep-rigs (4). These rigs allowed the application of a constant axial compressive load; at the same time, their small size permitted a simple and economical design of the humidity control system.

All specimens were loaded to an applied stress of 11.6 MPa, corresponding to a stress/strength ratio of 0.3. Load application was rapid; 10 seconds after the start of loading was defined as the point at which creep strain commenced.

Deformation measurement: Invar rods (3 mm diameter) were attached to the ends of the specimens which were to be loaded. Since the creep-rig was designed to provide access holes

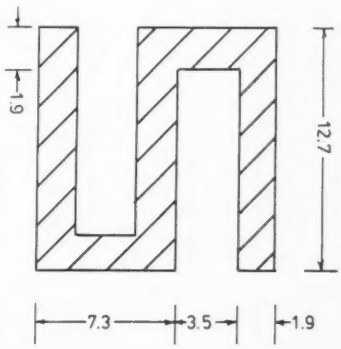

FIG. 3
Cross-section of slotted hcp specimen

through which the rods could freely pass, deformation was measured by monitoring the change in distance between the ends of the two rods (4). Each specimen for shrinkage/swelling was mounted in its own comparator; the change in length of each specimen was measured directly from its ends.

Transducers were used to measure deformation; they were accurate to 5 micro-strain. Each specimen had its own transducer.

Environmental control: For each test, the nine specimens were assembled in a single glass chamber. Soda-lime was placed in the chamber to prevent carbonation. Appropriate relative humidity and temperature probes were used to monitor environmental changes.

A dynamic method of relative humidity control was adopted; air, after being bubbled through a drying agent, was pumped through the chamber and then was returned to the drying agent for re-conditioning.

The medium drying rate (test 2A and 2B) was accomplished simply by changing the drying agent from water (i.e. no drying) to a saturated magnesium nitrate solution to give, at equilibrium, a relative humidity of 53%.

Slow drying (test 3) was similar to medium drying, but the concentration of the magnesium nitrate solution was increased in increments from zero at the start of the test to full saturation at the end, when the 53% rh equilibrium point was attained. The rate of increase of the concentration of the salt solution could be varied to suit the required drying rate.

For fast drying (test 1), the initial 70% of the expected water loss (between 100 and 53% rh) was very rapidly removed from the specimens by passing the circulating air through phosphorous pentoxide and silica gel. At the appropriate time, these drying agents were exchanged for a saturated magnesium nitrate solution. At this point, the rate of drying slowed substantially and the specimens tended towards their final 53% rh equilibrium moisture content.

All specimens were rewet by circulating saturated water vapour through the tanks. This is different from the tests reported in reference 1 where specimens were placed directly over water. The period of rewetting was fixed at 21 days.

Temperature was held constant at 24±1°C throughout the programme.

Results and Discussion

Figure 4 shows the moisture loss vs. time curves for the three drying rates which were used. Similar tests on slotted specimens, but dried at different rates, have been reported (1); these results are also included in Figure 4 for comparison. Figure 4 and inset show that for the drying creep analysis an even wider range of drying rates than for the drying shrinkage analysis (1) was achieved.

In the material to follow, deformation is expressed as micro-strain (μ); moisture content and moisture change are expressed as a percentage of the total evaporable water content of a saturated sample. The three drying rates which were used are denoted FD (fast drying), MD (medium drying) and SD (slow drying).

Shrinkage/Swelling Behaviour of Control Specimens

Table 1 summarises the equilibrium shrinkage strains for slotted specimens when dried from 100 to 53% rh. Despite a wide range of drying rates, differences in e_s are not large; the present results support the conclusion that the magnitude of shrinkage is independent of rate of drying (1).

Despite differences in age at the start of drying between specimens used here

VOL. 14 1984

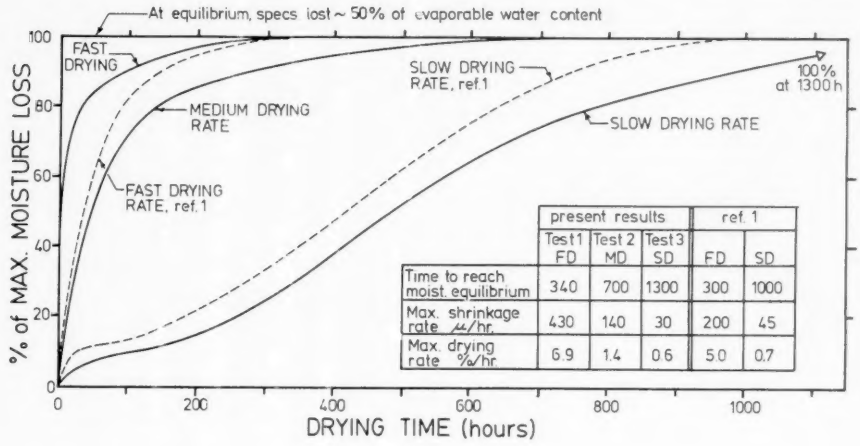

	present results			ref. 1	
	Test 1 FD	Test 2 MD	Test 3 SD	FD	SD
Time to reach moist. equilibrium	340	700	1300	300	1000
Max. shrinkage rate μ/hr.	430	140	30	200	45
Max. drying rate %/hr.	6.9	1.4	0.6	5.0	0.7

FIG. 4
Moisture Loss vs Drying Time (slotted hcp specimens)

OL.
14
984

TABLE 1
Drying Rate vs Equilibrium Shrinkage Strain

	Max. Shrinkage Rate μ/hour	Total Shrink. to 53% rh	% Irrecoverable Strain
Fast Drying	430	4520	32.5
Medium Drying	140	3430	25.4
Slow Drying	30	3960	35.1
Fast Drying, ref. 1	200	3980	24.4
Slow Drying, ref. 1	45	4240	32.0

(82 days old) and similar slotted specimens used in reference 1 (150 days old), the variation in shrinkage is quite small; the coefficient of variation for e_s is 10%, with a mean value of 4030μ .

Figure 5 shows the shrinkage and swelling vs moisture loss relationships for the fast and slow drying rates. These curves are typical of all tests both here and in reference (1) insofar as an approximate bi-linear relationship exists for both drying and wetting.

Note that for slow drying (and also for medium drying) 21 days resaturation was not sufficient to obtain equilibrium at 100% rh. Previous longer term tests (1) indicated that swelling could be assumed to be complete when all but 2% of the initial moisture loss had been regained. Therefore, to obtain a value for irrecoverable shrinkage (e_{irr}), swelling results were extrapolated to 2% moisture loss.

First drying creep

Figure 6 shows the total deformation curves for fast and slow drying. The

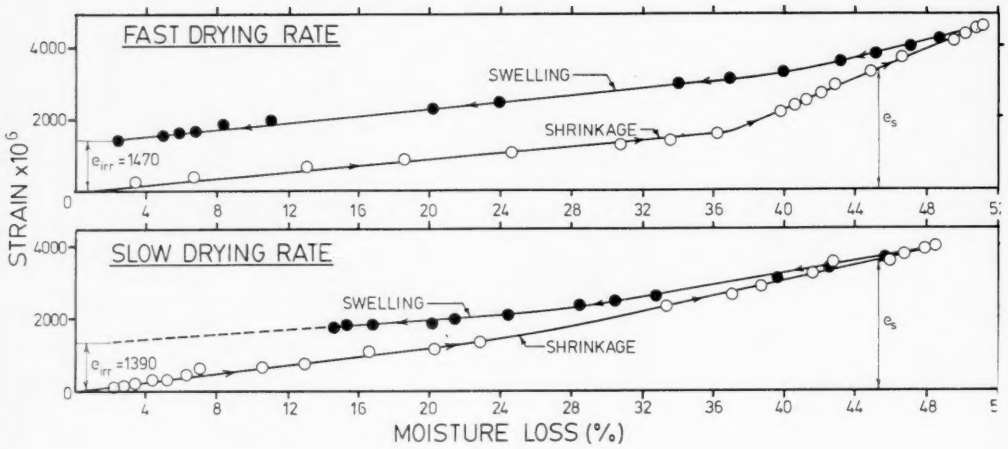

FIG. 5
Shrinkage and Swelling vs Moisture Change

VOL.
14
1984

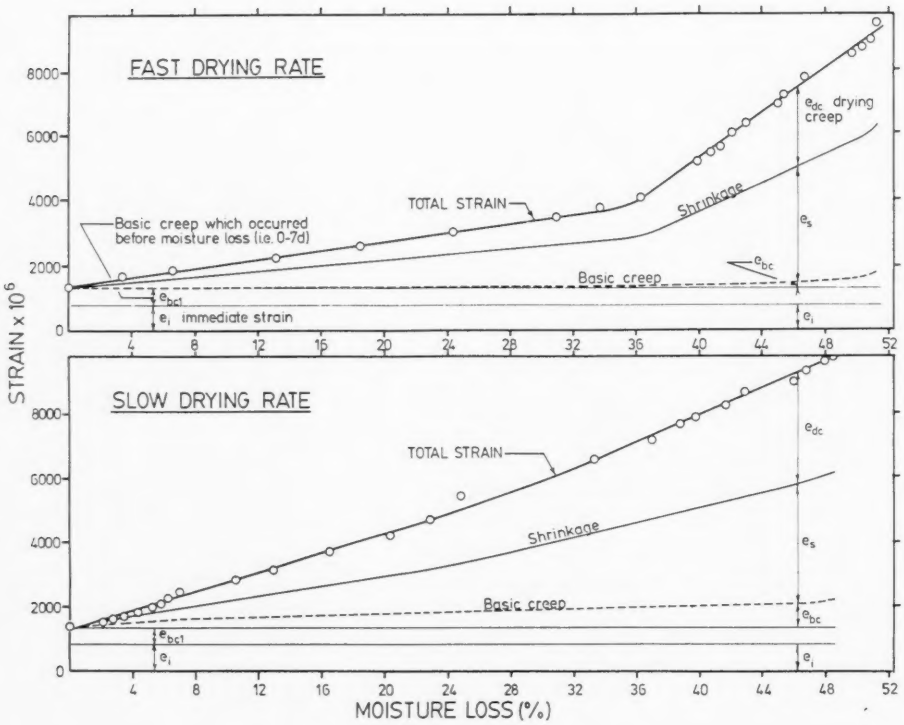

FIG. 6
Total Strain vs Moisture Loss

magnitude of drying creep can be extracted if total strain is divided into its components as shown in the figure -- $e_t=e_{dc}+e_s+e_{bc}+e_{bcl}+e_i$. Wetting creep can be obtained in a similar manner to drying creep. For the three drying rates, the drying and wetting creep vs. moisture change is shown in Figure 7.

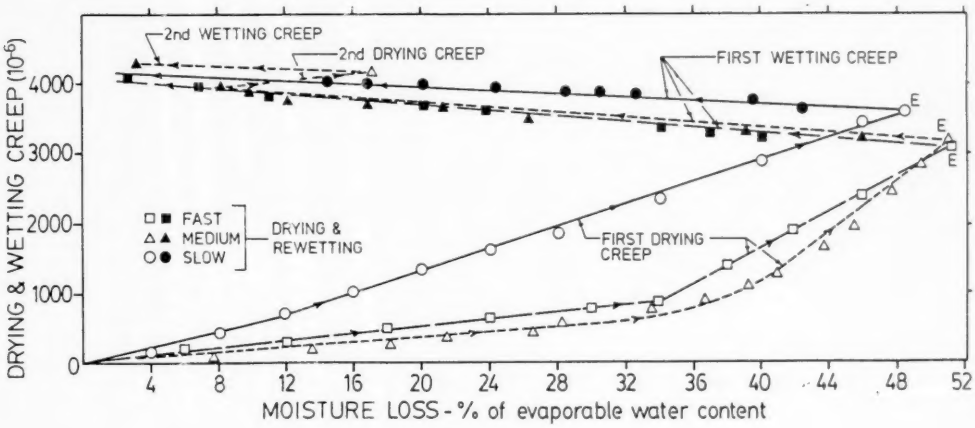

FIG. 7
Drying and Wetting Creep vs Moisture Change

VOL.
14
984

An important aspect of these results is that the equilibrium value for drying creep (pts. marked 'E' on Fig. 7) is approximately independent of the rate of drying; the coefficient of variation among the three tests is 7%, with a mean value of 3300μ (FD=3140, MD=3200, SD=3580).

In many respects, first drying creep is similar to shrinkage. The same bi-linear behaviour is observed as moisture is lost. Also, as with shrinkage, the final value of e_{dc} only depends upon the final relative humidity and not upon test conditions. Like shrinkage, the manner in which drying creep develops as moisture is lost does depend upon the test conditions (such as drying rate).

Observations that shrinkage and drying creep appeared to be qualitatively similar led Gamble and Parrott (3) to tests which showed a linear relationship between these two strains. Because concrete was tested, however, the largest shrinkage strains which they observed were in the region of 500μ.

Figure 8 shows that for hcp, an approximate linear relationship is obeyed over a much greater range. The slopes of the lines, however, depend upon the rate of drying. Nevertheless, the regression correlation coefficient is very high.

The linearity of this relationship should be qualified to some extent. In the very early stages of drying, drying creep was very small even though significant shrinkage had occurred; this explains why the lines shown in Fig. 8 have negative intercepts. Apparently, the emptying of the largest pores in the material is not important to drying creep even though this loss does produce significant shrinkage.

First Wetting Creep Following Drying Creep, Humidity Cycling

Figure 7 shows the wetting creep which occurred after first drying under load. For all cases, wetting creep followed an excellent linear relationship with moisture gain.

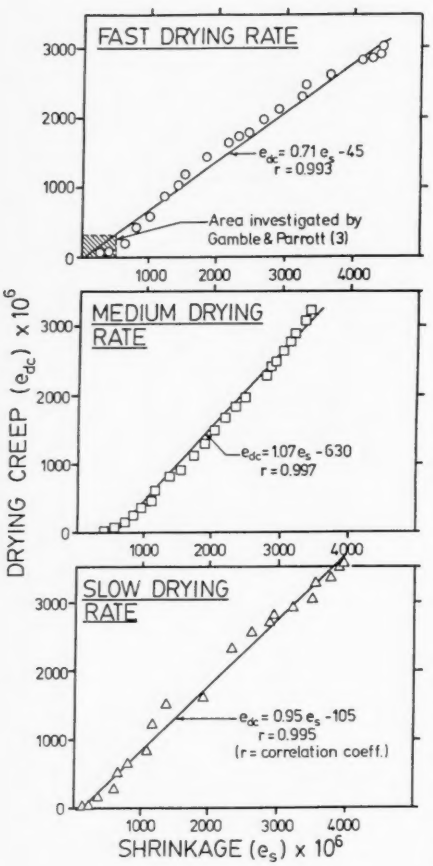
FAST DRYING RATE
e_{dc} = 0.71 e_s -45
r = 0.993
Area investigated by Gamble & Parrott (3)
MEDIUM DRYING RATE
e_{dc} = 1.07 e_s - 630
r = 0.997
SLOW DRYING RATE
e_{dc} = 0.95 e_s -105
r = 0.995
(r = correlation coeff.)
DRYING CREEP (e_{dc}) x 10^6
SHRINKAGE (e_s) x 10^6

FIG. 8
Shrinkage vs Drying Creep

The sum of wetting and drying creep appears to converge on a single value of about 4200μ; those specimens which showed the largest drying creep (slow drying) exhibited the smallest wetting creep. The total for all tests was about the same. Also note that on second drying and wetting (test 2B) very little further drying or wetting creep occurred.

These results indicate that for a given drying/wetting step (here, 100-53-100% rh), for a given material, and for a given applied stress, there is a threshold (or ultimate) value for drying + wetting creep; this value is approximately independent of the rate of drying or wetting, or the number of drying/wetting cycles. Although this has been stated several times by others in the past, the phenomenon needs further emphasis because of its practical significance; prediction of ultimate values for deformation when concrete is dried and wet while under load may be quite straightforward.

In Figure 9 the wetting creep vs swelling relationship is given. As with the drying creep-shrinkage behaviour, there is a period of swelling during which very little, if any, wetting creep occurs. After about 1000μ of swelling with no concomitant swelling creep, swelling and wetting creep increase in proportion to one another; all results conform approximately to the same linear relationship.

Prediction of Creep Strains

An important aim of research of the type described in this paper is to assist in the development of predictive equations for creep when the environment changes. Clearly, these equations should be as simple as possible, while at the same time maintaining reasonable accuracy.

Here, the results indicate that simple relationships do exist. It is especially significant that the linearity between shrinkage and drying creep and between swelling and wetting creep, suggested by Gamble and Parrott (3), is confirmed. Because of this linearity, equations which relate the strains have been developed (3); here, these equations take the forms $e_{dc}=k_d \cdot \sigma \cdot e_s$ and $e_{wc}=k_w \cdot \sigma \cdot e_{sw}$, where σ is the applied stress and k_d and k_w are constants for a given material. Gamble and Parrott used their results and those of others in the literature to show that k_d is linearly related to water-cement ratio; Figure 10 shows that the values for k_d from the present results (extracted from Fig. 8) are consistent with this relationship. k_d is dependent on drying rate; however, this dependence is not large, and for practical purposes it may be acceptable to use a mean k_d for all tests.

The other aspects of the results which may help to produce simplified equations for creep are that shrinkage, drying creep and drying + wetting creep for a given humidity step are effectively independent of rate of drying or wetting. Ultimate values for these components may be determinable without the annoyance

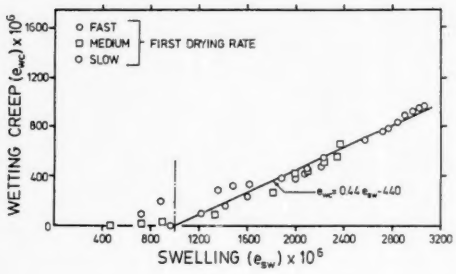

FIG. 9
Swelling vs Wetting Creep

FIG. 10
Relationship between w/c Ratio
and Coefficient k

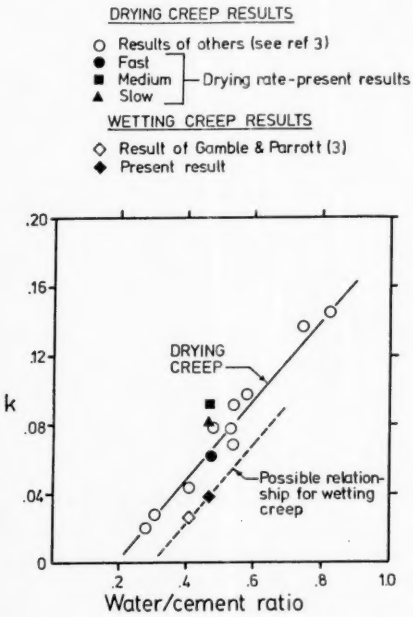

of having to monitor weight changes with time.

It has been suggested (6,1) that for practical purposes it may be valid to assume a unique relationship between moisture loss and shrinkage. The question arises, however, as to the size of error which is practically acceptable. For slotted hcp specimens, the range of shrinkage strains for a given moisture loss can be as large as 1800μ. An assumed best-fit curve could then be in error by 900μ. This error may be acceptable if, as here, the total expected strain is large. In hcp, drying while under load, a total strain approaching 10000μ is not uncommon, and 900μ may then be an acceptable margin. For concrete, the size of all strains would probably be similarly reduced and the percentage error can be expected to be much the same.

The Irrecoverable Nature of Drying and Wetting Creep

The total irrecoverable strains which were exhibited by the loaded specimens at the completion of testing were: FD=6480μ, MD=5860μ and SD=7040μ.

Table 2 shows that if drying creep and wetting creep are assumed to be completely irrecoverable, then total irrecoverable strain can be predicted from the magnitude of the components which were observed. The differences between the predicted values and the true values is very small. The conclusion is that drying creep and wetting creep can indeed be assumed to be completely irrecoverable.

This conclusion is different from that of Gamble and Parrott (3) who observed a recoverable component of drying creep. The disparity may be due to the fact that they tested concrete, while here hcp was tested; strain energy stored in aggregate during an extended period under load may play a significant role in determining recovery behaviour and the magnitude of recoverable creep strains.

Conclusions

Tests were performed on miniature hcp specimens to determine the effect of rate of drying on drying creep; one material, one stress level, one relative humidity step and three drying rates were used. Relationships between moisture loss, shrinkage and drying creep and between moisture gain, swelling and wetting creep were examined.

TABLE 2
Prediction of Irrecoverable Creep
results in μ; negative strain = expansion

	Fast Dry	Medium Dry	Slow Dry
Total observed irrecoverable strain	6480	5860	7040
Breakdown:			
Observed irrecoverable immediate strain	100	-60	160
Observed irrecov. shrinkage strain (from tests on unloaded companions)	1470	870	1390
Observed irrecov. basic creep (flow) during the time under load (Test 4)	740	800	1040*
Drying creep	3140	3200	3580
Wetting creep	960	860**	560**
Total irrecoverable strain predicted	6410	5670	6730
% difference from observed value	1.1%	3.2%	4.4%

*determined by a short extrapolation of the flow curve
**extrapolation to equilibrium at 2% irrecov. moisture loss (explained in text)

For these tests, it was found that like shrinkage, the magnitudes of drying creep and of drying + wetting creep were independent of the rate of drying. Drying creep bears a linear relationship to concomitant shrinkage; similarly, wetting creep is linearly related to swelling. In this regard, the results support the conclusions made by Gamble and Parrott (3).

The results also show that both drying creep and wetting creep are completely irrecoverable. Also, there appears to be a threshold or ultimate value for irrecoverable strain which cannot be exceeded, and is independent of rate of drying or the number of drying/wetting cycles.

The results are regarded as important with respect to the prediction of creep strains when environmental conditions change. They suggest that equations may not have to be overly complicated to produce predictions of acceptable accuracy.

Acknowledgements

Thanks are extended to the Science and Engineering Research Council (U.K.) and the Natural Sciences and Engineering Research Council (Canada) for support.

References

1. Day, R.L. and Illston, J.M., Cem. Concr. Res., V 13, No 1, pp 7-17, 1983
2. Ali, I. and Kesler, C.E., Symp. on Creep of Concrete, Detroit, A.C.I. Publ. SP-9, pp 35-63, 1964
3. Gamble, B.R. and Parrott, L.J., Mag. Concr. Res., V 30, No 104, Sept. 1978
4. Day, R.L., Mag. Concr. Res., V 34, No 120, pp 146-154, Sept. 1982
5. Cuffaro, P., M. Phil thesis, The Hatfield Polytechnic, 1983
6. Parrott, L.J. and Young, J.F., in 'Fundamental Research of Creep and Shrinkage of Concrete', ed. F.H. Wittmann, Martinus Nijhoff Publ., pp 35-48, 1982

VOL 14 198

CEMENT and CONCRETE RESEARCH. Vol. 14, pp. 339-344, 1984. Printed in the USA.
0008-8846/84 $3.00+00. Pergamon Press, Ltd.

FLUORESCENT THIN SECTIONS TO OBSERVE THE FRACTURE ZONE IN MORTAR

L.I. Knab
National Bureau of Standards, Washington, D.C., U.S.A.

H.N. Walker
Virginia Highway and Transportation Research Council,
Charlottesville, VA, U.S.A.

J.R. Clifton and E.R. Fuller, Jr.
National Bureau of Standards, Washington, D.C., U.S.A.

VOL.
14
984

(Communicated by R.E. Philleo)
(Received Sept. 23, 1983)

ABSTRACT

There have been relatively few studies of the microstructural details of the fracture zone of propagating cracks in mortars and concretes. The lack of information about the details has hindered the development and validation of fracture mechanics theories based on the micromechanisms of cracking. This report deals with the use of fluorescent thin sections to observe the microstructural details of the fracture zone. A mortar is used to illustrate the technique. It is concluded that the fluorescent thin section technique has the potential of providing a valuable new source of information on the microstructural details of the fracture zone in mortars and concretes, both near the surface and in the interior of specimens.

Background

Cracking mechanisms in concrete and mortar have been a subject of research interest for many years, particularly with the recent developments in the theories of fracture of brittle materials. Various methods have been used to model the cracking mechanisms (e.g. (1-4)). Modeling can require assumptions concerning the nature of the fracture zone and microstructural details surrounding a propagating crack, such as (a) area (volume) and shape of damaged material around and in front of the crack, (b) crack width (distance from one crack wall to the other), and (c) whether aggregate interlock or partial pullout causes the adjacent crack walls to interact and transfer stress. Despite the large amount of research on the application of fracture mechanics concepts and theories to concrete, there have been few published studies on the observation of the microstructural details of the fracture zone of propagating cracks (e.g. (5-7)). This lack of information has hindered the development and validation of fracture mechanics theories based on the micromechanics of cracking.

Recently Mindess and Diamond (5), using a special scanning electron microscopy technique, observed the microstructural details surrounding a load-induced propagating crack as seen on one surface of a small mortar compact tension specimen. The present study was performed to develop a method to enhance the microstructural details of the fracture zone in the interior of a specimen. Techniques using impregnation have been available (e.g. (8)). Of the known impregnation techniques, the use of epoxy containing a fluorescent dye appeared to have the most potential for enhancing the visibility of the cracking details of the fracture zone in the specimen interior. This report deals with the use of fluorescent thin sections to observe the microstructural details of the fracture zone. Mortar is used to illustrate the technique.

Technique

Fluorescent thin sections have been used to study certain microstructural characteristics of concrete, including hydration characteristics and air entrainment (9,10) and the relationship of porosity to compressive strength (11). The research reported here is the first known study of applying the technique to observe the microstructural details of the fracture zone surrounding a propagating crack. Thin sections, about 15 micrometers thick, were cut and ground from specimens which had been impregnated with an epoxy containing a fluorescent dye. In the vicinity of the crack, the fluorescent epoxy filled the cracks, voids, and areas having a high concentration of larger capillary pores. Under the excitation of ultraviolet light, the dye becomes a light emitter, making discernible details that would otherwise not be observed. Some of the crack details discernible at rather low magnification (50X) measure only two or three micrometers from one crack wall to the other. Because of fluorescence, these crack details are visible regardless of the angle that the plane of the crack wall makes with the plane of the thin section. Using illumination with visible light, the crack walls would have to be exactly parallel to the transmitted light to be visible. The equipment and processes used to impregnate the specimens and prepare thin sections have been documented (12).

Specimen Preparation and Testing

A mortar specimen was made from ASTM Type I portland cement using a standard graded (ASTM C778-80a, (13)) rounded Ottawa quartz sand, with the maximum aggregate size of 0.6 mm (100 percent passing No. 16 sieve and 2 percent retained on No. 30 sieve). The mixture proportions by weight were 1 part cement to 0.58 parts water and 3 parts sand. A crack was propagated in a double cantilever beam specimen, measuring 17 mm in thickness, 76 mm in width and 133 mm in length. A chevron notch (figure 1), about 60 mm in length, was cut through the 17 mm thickness with a saw blade having a 0.34 mm thickness. After moist curing at room temperature for 24 days, the specimen was gradually wedge loaded such that a crack propagated from the notch tip, but not completely to the bottom of the specimen (figure 1). After testing, the specimen was air dried at room temperature for 22 days and then impregnated with an epoxy containing a fluorescent dye.

Thin Section Results

Two thin sections were cut and ground so that their planes were approximately perpendicular to the through thickness dimension of the specimen (17 mm). The thin sections were about 1 mm inside the "front" (exposed-finished surface when cast) and "back" (surface in contact with the mold when cast)

VOL
14
198

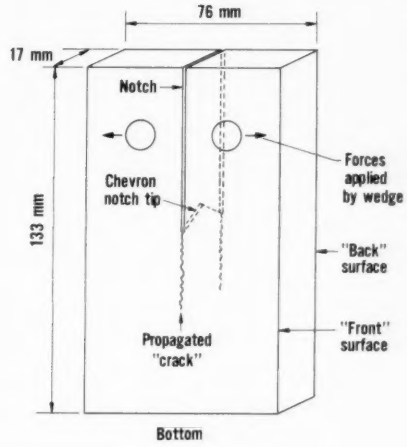

FIG. 1.

Schematic of double cantilever beam mortar specimen and propagated crack.

faces (figure 1) of the specimen. Each thin section contained a portion of the notch tip and about 28 mm of the crack pattern. An overall map of the crack portion contained on the thin section near the "back" face is shown in figure 2. This crack map is a tracing from a collage of many pictures taken of the thin section. It is noted that surface effects due to volumetric changes (e.g. shrinkage) may have influenced the cracking pattern shown in Figure 2. Further research is needed on these surface effects. Figure 3 shows the details of the crack pattern around the notch tip near the "back" face, including crack branching and tortuosity, and the apparent preference for cracks to propagate around the sand grains, at the interface between the sand and the cement hydration products. The effect of voids on crack propagation requires further study, including an analysis of the distribution of the number and size of voids. The crack walls were generally sharply defined. Figure 4, taken from the thin section near the "front" face and at a higher magnification than figure 3, illustrates typical instances of sharply defined crack walls (arrows A and C) and an atypical instance of where crack walls are not as sharply defined (arrow B), probably due to an area having a high concentration of larger capillary pores. In most cases, only those portions of sand grains located on the crack walls appeared to have their interface with the cement hydration products clearly disrupted (e.g. figures 3 and 4). The observed results appear to correlate with many of the trends that Mindess and Diamond observed for surface cracking of mortar using scanning electron microscopy (5).

Summary and Conclusions

Preliminary findings show that fluorescent thin sections can enhance observations of the cracking processes in mortar, including the path, shape, orientation, and width (distance from one crack wall to the other) of cracks. Also, the effects of aggregates, voids, and larger capillary pores on crack propagation can be studied. Crack widths of two or three micrometers can usually be discerned; although larger capillaries can be detected, the details of their structure are not easily discerned. Three dimensional (stereological) aspects of cracking can be studied by taking a series of thin sections through the specimen thickness at separations as small as about 1 mm. The use of fluorescent thin sections has the potential of providing a valuable new source of information on the microstructural details of the fracture zone for mortars and concretes, both near the surface and in the interior of specimens.

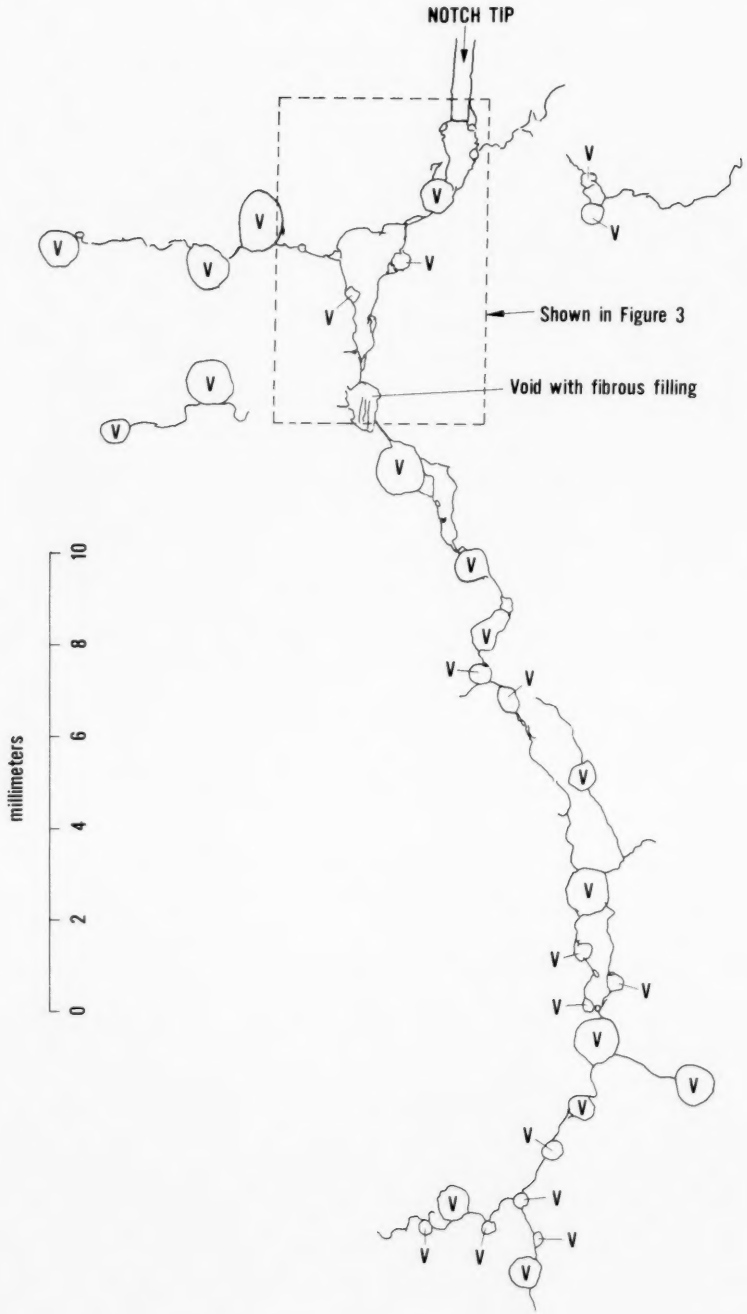

FIG. 2

Crack map obtained by tracing from a collage of pictures of thin section taken from "back" face. "V"=void. Only larger voids associated with the crack path are marked "V".

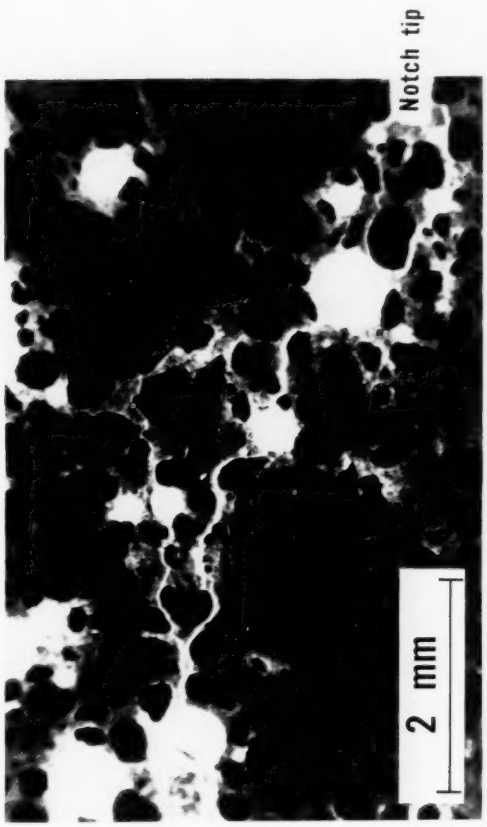

FIG. 3

Photomicrograph showing details of crack pattern around notch tip on thin section from "back" face (see Fig. 2).

VOL.
14
1984

Acknowledgment

The authors wish to acknowledge the expert work of Mr. B.F. Marshall, Virginia Highway and Transportation Research Council, in fabricating the fluorescent epoxy impregnated thin sections of mortar.

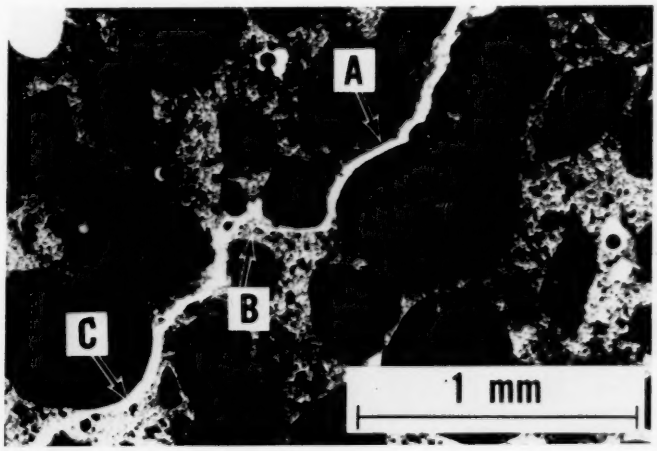

FIG. 4

Photomicrograph showing crack details on thin section from "front" face. Typical instances of sharply defined crack walls (arrows A and C) and an atypical instance of crack walls less sharply defined (arrow B) are shown.

References

1. Peterson, P.E., Cem. Conc. Res. 10, 78 (1980).
2. Wecharatana, M. and Shah, S.P., J. Structural Division 108, 1400 (1982).
3. Ingraffea, A.R. and Saouma, V., "Numerical Modeling of Discrete Crack Propagation in Reinforced and Plain Concrete," Application of Fracture Mechanics to Concrete Structures, Martinus Nijhoff Publishers (in press).
4. Bazant, Z.P. and Oh, B.H., Materials and Structures 16, 155 (1983).
5. Mindess, S. and Diamond, S., Materials and Structures 15, 107 (1982).
6. de Haas, H.M. and Stroeven, P., Crack Detection Techniques in Concrete Materials Research, Report 1-75-1, Delft University of Technology, The Netherlands (1975).
7. Cedolin, L., Poli, S.D., and Iori, I., Cem. Conc. Res. 13, 557 (1983).
8. Gardner, K.L., Can. J. Earth Sci. 17, 1104 (1980).
9. Wilk, W., Dobrolubov, G., and Romer, B., Transportation Research Board, TRR 504, 1 (1974).
10. Walker, H.N., Proc. 3rd Intl. Conf. on Cement Microscopy, 257 (1981).
11. Thaulow, N., et al., J. Nordic Concrete Federation, 2-4, 51 (1982).
12. Walker, H.N. and Marshall, B.F., Cement, Concrete, and Aggregates 1, 3 (1979).
13. ASTM C778-80a, "Standard Specification for Standard Sand," Part 13 (1981).

VOL
14
198

CEMENT and CONCRETE RESEARCH. Vol. 14, pp. 345-348, 1984. Printed in the USA.
0008-8846/84 $3.00+00. Copyright (c) 1984 Pergamon Press, Ltd.

AN INVESTIGATION OF THE OSMOTIC MODEL OF CEMENT CURING BY ULTRASONICS

D.D. Lasič and J. Stepišnik
J. Stefan Institute and Department of Physics
E. Kardelj University of Ljubljana
Ljubljana, Yugoslavia

(Communicated by D.M. Roy)
(Received April 6, 1983; in final form Jan. 23, 1984)

VOL. 14 1984

ABSTRACT

Ultrasonic measurements were performed in the samples with different water to cement ratios, at different temperatures, and in the samples with added retardants. The results could be qualitatively explained with the osmotic theory of the solidification of cement.

Introduction

According to the osmotic theory of the solidification of cement (1), the silicate grains form a gel coating in contact with water. The silicate begins to dissolve in the gel phase and the concentration of salts in the gel phase increases. The concentration difference of the salts in the liquid and in the gel phase produces the osmotic pressure and the water molecules penetrate into the gel phase. The surface of gel acts as a semipermeable membrane (1). When the necessary amount of water in the gel is reached, the coating bursts and the gel fibrils begin to grow. This is the end of the dormant period (2), and the thixotropy disappears. The crosslinking of the fibrils produces the hardness of the cement. With the application of this theory, the retardation and acceleration effects can be explained (2), using the simple approximation for the osmotic pressure $\pi = \Delta c\ R\ T$, where R is gas constant, T the temperature and c the concentration difference of salts in the gel coating and in the bulk liquid phase, $\Delta c = c_g - c_w$. The large and nonpolar molecules of retardants can be dissolved only in the bulk liquid phase and therefore the concentration difference is lowered: $\Delta c = c_g - (c_w + c_{ret})$. Lower osmotic pressure results in slower water penetration rate, growth and crosslinking; i.e. solidifying of fibrils is also slower. According to this model, the high efficiency of the retardants can be understood because the osmotic coefficients, i.e. the factor which determines the real activity of the solvent, is several orders of magnitude bigger in the bulk liquid phase as in the gel phase where there are severe restrictions of mobility and many additional interactions. The effect of the accelerators can be explained in the same way. Because of their ionic character, the cations are attracted by the negatively charged silicate surfaces and the concentration difference increases, $c = (c_g + c_{acc}) - c_w$ (3). However, the lower efficiency of the accelerators can be understood through the low values of the osmotic coefficients of the ions in the very viscous gel phase.

Recently the ultrasonic technique which measures the development of the shear modulus of elasticity in cement pastes has been introduced (4). The experiments show that even slight changes of sheer modulus during the cement hydration can be measured which makes this method appropriate for studies of cement hydration. The measurements are based on the sheer ultrasonic waves reflected from a hardening cement paste. The reflection coefficient r_o is determined by the relation

$$r_o = \frac{Z_2 - Z_1}{Z_2 + Z_1}$$

where the acoustic impedances (Z_1 and Z_2) are determined by the viscoelastic properties of the media. For the case of incident sheer waves, it is

$$Z = (\zeta(G + i\eta\omega))^{1/2}$$

where ζ is the mass density, G the sheer elastic modulus, η the viscosity, and ω the angular sonic frequency. Since the phase changes of the reflected waves during the hydration of cement pastes are very small (5), the imaginary part of the acoustic impedance can be neglected. A direct relation between the change of the reflection coefficient (in dB) and the sheer elastic modulus (5) is

$$y = -20 \log r_o = 17.376 \frac{(\zeta G)^{1/2}}{Z_1}$$

where Z_1 is the acoustic impedance of the buffer. This relation is valid as long as y is smaller than 5 dB.

Experimental

The measurements were performed at the frequency 16.5 MHz of acoustic waves using the quartz bar as a buffer. The cement paste was spread on the top of the bar in a 4 to 5 mm thick layer and covered with a glass cup with a defined humidity to prevent evaporation.

The time development of r_o was (1) followed in the samples with different water to cement ratios at different temperatures, and (ii) the retardation effects were studied in the samples with added saccharose and glucose (both 1% o). These molecules are chemically similar, only saccharose has a twice bigger molecular mass. If the permeability characteristics are also similar, the osmotic pressure decrease would be twice bigger in the sample with added glucose which would result in bigger retardation effect.

Results and Discussion

The time dependence of the reflection coefficient which is proportional to the cement hardness is shown in Fig. 1. The different curves correspond to different water to cement ratios and different temperatures. All the curves have a similar shape. The slope of the constant monotonic increase of the negative logarithm of the reflection coefficient with time, increases after the break. By the extrapolation of the second part of the curve to log r_o = 0, one defines the initiation time of hardening (t_H). This parameter is a function of temperature, but practically not of the w/c ratio. The hardening rate itself increases with decreasing w/c ratio. However, the hardening rate depends strongly on the temperature. In Figure 1, families with different w/c ratios at different temperatures can be distinguished. The hardening rate decreases with increasing w/c ratio. Overall, the families show a decrease in the hardening rate (dlog r_o/dt) with decreasing temperature.

The fact that t_H is a function of temperature but not of w/c ratio, can be

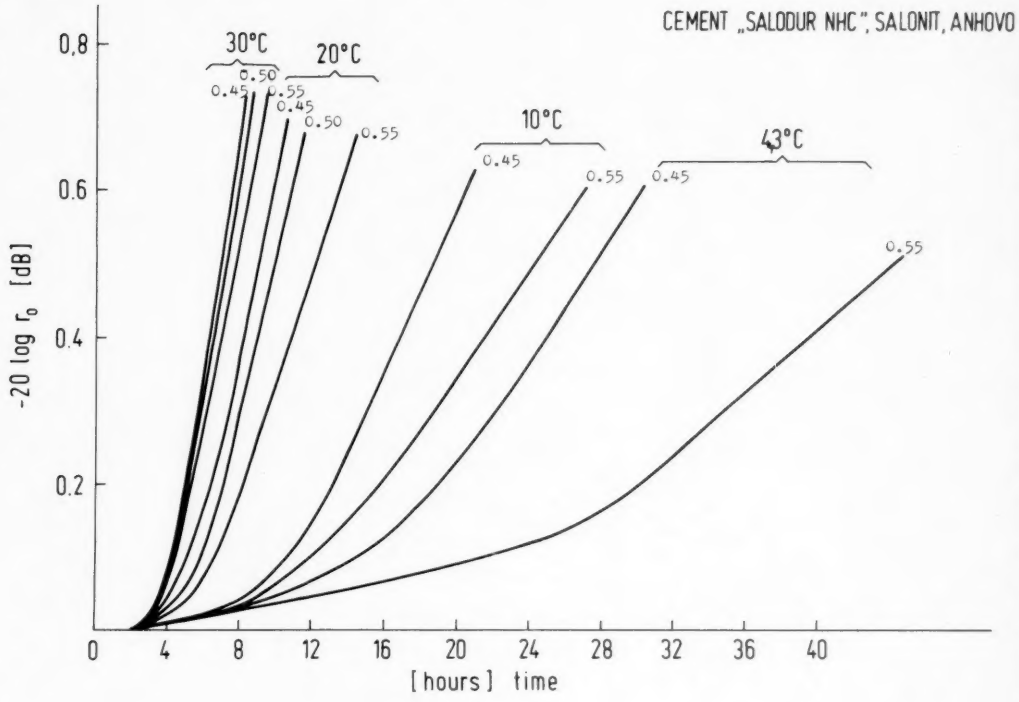

FIG. 1

Variation of the reflection coefficient during the initial stages of Portland PC 550 cement (by "salonit", Anhovo, Yugoslavia), at different temperatures and water to cement ratios.

explained with the osmotic model. The early stage - the gel coating formation and dissolution processes - is independent of the amount of water. Above some critical, minimal water content, the same amount of water is required for wetting the given grain surface. After the gel coatings are formed and the fibrils begin to grow, the samples with the smaller water content harden faster because the fibrils grow through the shorter distances to crosslink at low w/c ratios.

However, the hardening (dlog r_o/dt) as osmotic pressure itself, increases with temperature. In order to obtain some quantitative correlation, one should know more about the geometry of the growing fibrils as well as consider the temperature dependence of the solubilities, water permeability and diffusion coefficients. Probably all these factors contribute to the increase of t_H with decreasing temperature.

Figure 2 shows the effect of the retardants on the time dependence of the reflection coefficient. Retardants increase the t_H value. The "solidification rate," defined as (dlog r_o/dt), is for a sample without any additive 2.17, for a sample with added saccharose 3.13, and for glucose 3.7. The extrapolated t_H values 4, 15 and 20 hours respectively, indicate that glucose is a slightly stronger retardant than saccharose, which may be expected from the inverse proportionality of the osmotic pressure and molecular mass.

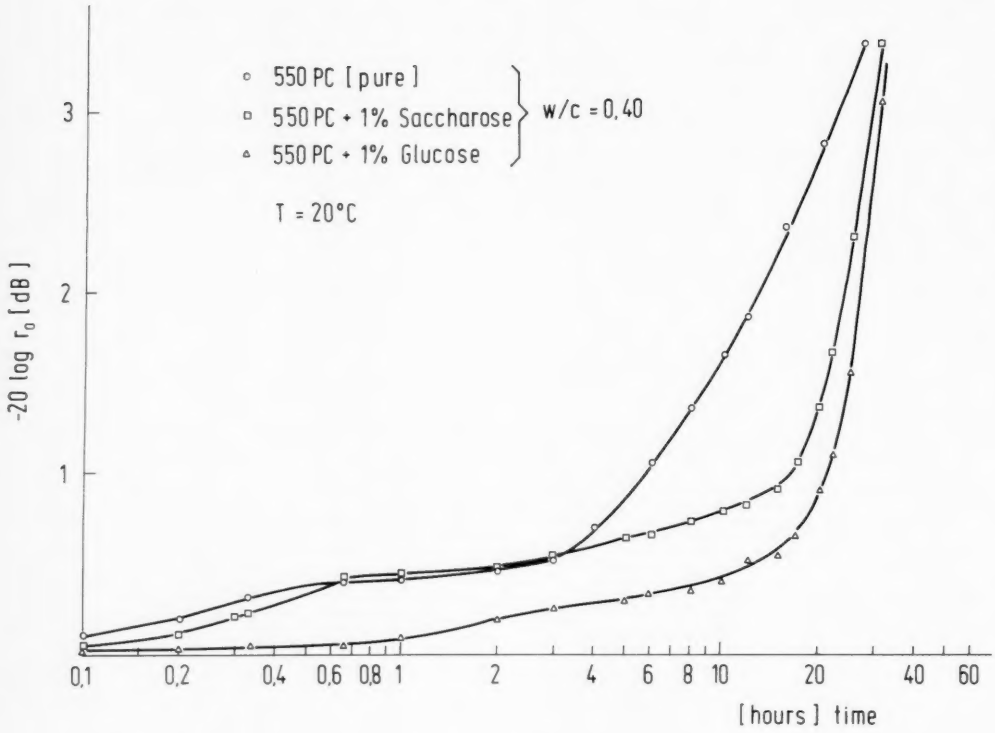

FIG. 2

Effect on cement hydration by addition of saccharose and glucose at 20°C and w/c = 0.4.

References

1. D.D. Double, A. Hellawell, Nature 261, 486 (1976).
2. D.D. Lasič, G. Lahajnar, R. Blinc, I. Kocuvan, Z. Naturforsch. 36a, 203 (1981).
3. P. Triereus, J.P. Verhagen, Cem. Conc. Res. 6, 103 (1976).
4. F.V. Lawrence, J.F. Young, R.L. Bergeer in Proc. of 6th intl. Congress on Chemistry of Cement, Moscow 1974, Vol. II, part I, p. 134-38.
5. J. Stepišnik, M. Lukac, I. Kocuvan, Cer. Bull. 60, 481 (1981).

VOL
14
198

CEMENT and CONCRETE RESEARCH. Vol. 14, pp. 349-359, 1984. Printed in the USA.
0008-8846;84 $3.00+00. Copyright (c) 1984 Pergamon Press, Ltd.

FRACTURE ENERGY OF GLASS FIBER REINFORCED CEMENT COMPOSITES: METHOD OF DETERMINATION

T. Ohigashi
Asahi Glass Co. Ltd. Research Center,
Hazawa-cho, Kanagawa-ku, Yokohama 221, Japan

(Refereed)
(Received March 1, 1983; in final form Jan. 23, 1984)

VOL.
14
984

ABSTRACT

Based on theoretical consideration, it has been found that the fracture energy is an useful index for the evaluation of fracture toughness of GRC (Glass Fiber Reinforced Cement Composites). The method for determination of the fracture energy was proposed in this paper. Fracture energy was obtained from the work required for the fracture, i.e. the area under the load-displacement curve in a tensile test. Two notches were introduced on both sides of the specimen surface in order to obtain a stable load-displacement curve, which is necessary in determining fracture energy. The determined value did not depend on the depth of the notches if they were appropriately deep. The value, therefore, represented a property of the material, while the impact strength and critical stress intensity factor (K_{IC}), which are widely used as the indices of the fracture energy and fracture toughness, respectively, are not considered to be the material's properties because of the great influence of the notch depth on the indices. This paper also discusses the suitability of the present method and the error factors caused in the measurement.

Introduction

The evaluation of the main properties of glass fiber reinforced cement composites (GRC) can be usually carried out by the flexural strength and the impact strength, from which the other properties are presumed. A characteristic of GRC consists in large fracture toughness. It is seen in the crack propagation that the reinforcing elements in the matrix already cracked can still keep resisting failure even under the increasing tensile strain. Large energy, therefore, is required for the fracture. This characteristic is generally seen in fiber reinforced composites. The fracture toughness index is usually measured with an Izod or Charpy-type impact testing machine and it means the energy absorbed by the test piece in the process of the dynamic

fracture. The value can also be evaluated from the work required for static fracture, e.g. the integral value of the load-deflection curve in the bend test. The values mentioned above, however, are sensitively affected either by the depth of the notch made on the specimen or by the size of the specimen (1, 2).

C.H. Henager (3) proposed a fracture toughness index (F.T.I.) obtained from the three-point bend test in which the span is 305 mm and the cross section of the specimen is 102 x 102 mm. It is given by the following equation:

$$F.T.I. = (S_1 + S_2)/S_1 \tag{1}$$

where S_1 is the area under the load-deflection curve obtained by the time that the crack begins and S_2 is the one obtained in the range from the deflection value at the crack initiation point to a constant deflection value of 1.9 mm. J.R. Rice (4) proposed a parameter called J-integral given by the following equation:

$$J = -\frac{1}{b} \cdot \frac{\partial u}{\partial a} \tag{2}$$

where b is the width of the specimen, U is the potential energy and a is the crack extension. G. Velazco, et. al (5), however, pointed out that the value obtained often depends on the notch depth and then cannot be considered a geometry-independent material fracture toughness parameter. In the field of fracture mechanics the critical stress intensity factor (6), K_{1C}, obtained in a three-point bend test, is also usually used for the evaluation of fracture toughness. It is written by:

$$K_{1C} = \frac{3Wl\sqrt{c}}{2bd^2} \cdot F\left(\frac{c}{d}\right) \tag{3}$$

where W is the failure load, l is the span, b is the width, d is the thickness, C is the notch depth of the specimen and F(c/d) is a function of c/d. G. Velazco, et.al (5) also reported that the K_{1C} for steel fiber reinforced cement depends on the initial notch depth. It is not considered, therefore, that the K_{1C} for GRC is independent of the specimen geometry and represents a material property. After all, it is not appropriate to evaluate the fracture toughness using the above equations (1), (2) and (3).

The following equation obtained from a combination of the Griffith's theory (7) and the definition of K_{1C} is then considered convenient for use:

$$K_{1C} = \sqrt{2\gamma E} \tag{4}$$

where γ is surface energy and E is Young's modulus (8). J.J. Gilman (9) or A. Kelly (10) shows that γ is approximately proportional to E in his theory. The combination of the theory and the equation (4) gives a relation that K_{1C} is also approximately proportional to γ. The comparison of the K_{1C} value, therefore, is given by the determination of γ if it is assumed that the material is homogeneous and isotropic elastic solid. The 2γ in the equation (4) is represented by G, which is often called strain energy release rate or fracture energy.

In paper (11) a method for the determination of 2γ(G) has already been proposed. It was calculated from the area under the load-deflection curve ob-

VOL. 14 1984

tained in a stable three-point bend test by using the specimen with the deep and shallow notches on the compressive and tensile stress sides, respectively. But this method is not always suitable for the thinner specimen since it is, in practice, difficult and troublesome to give a deep notch to the specimen. The method, also, makes an error in measuring the deflection because of the plastic deformation on the load-point if the specimen is not as rigid as GRC. Furthermore, the deeper notch is less desirable for achieving a maximum fracture area and a good averaging process over coarse microstructures such as GRC and hence a better reproducibility of the measured values. In order to overcome the disadvantages, a tensile test method which is able to decrease the ratio of the notch depth to the specimen thickness was investigated. The present paper describes the method of determining the 2γ (G) which depends seriously on K_{1C} and discusses the errors caused by the measurement.

Experimental

Preparation of Specimen

A commercial rapid hardening portland cement, Kimitsu Sand and glass fiber were used for preparing the GRC. The chemical composition and the physical properties of the cement are summarized in Tables 1 and 2. The diameter distribution of the sand is shown in Table 3.

OL.
14
984

TABLE 1

Chemical Composition of Rapid Hardening Portland Cement (wt%).

Ig.loss	Insol.	SiO_2	Al_2O_3	Fe_2O_3	CaO	MgO	SO_3
1.0	0.2	21.0	4.8	2.7	66.0	1.1	2.6

An alkali-resistant glass fiber roving containing more than 7 mol% ZrO_2 was used as the reinforcing element. The roving consisted of 32 strands, all of which consisted of 204 filaments of 14.5 μm in average diameter. The filaments were bundled with a size. The sand to cement and the water to cement ratios of the mortar matrix for GRC were 0.5 and 0.33, respectively. Water reducing agent of 1 wt% was added to cement. After the roving was chopped to the 37 mm long strands with a chopper gun, they were immediately sprayed together with mortar onto a flat sheet mould (600 x 1200 mm). The content of strands was controlled to be nominally 5 wt% of the green sheet of GRC. After spraying, the sheet surface was finished by using a trowel. The green sheet were cured in moist air at 20°C for 3 months and the trowel-finished surface was then ground to obtain the flat surface. The GRC specimens thus prepared had random and two-dimensional orientation of strands.

Testing Procedure

The tensile test method proposed here was compared with the bend test method presented in paper (11). The tensile test geometry is illustrated in Fig. 1. The specimen size was 10~15 (thickness) by 40 by 150 ~ 400 mm. Two notches were made at the center of both surfaces of the specimen as shown in Fig. 1. Fig. 2 shows an example of the tensile stress-elongation curve

TABLE 2

Physical Properties of Rapid Hardening Portland Cement (wt%).

Specific Gravity			3.13
Finess	Residue 88 μ (%)		0.5
	Blaine (cm^2/g)		4260
Setting Time	Amount of Water (%)		28.7
	Initial Setting (hr-min)		2 - 38
	Final Setting (hr-min)		3 - 58
	Flow (JIS) (mm)		259
Strength (N/mm^2)	Flexural Strength	1 day	3.03
		3 days	5.25
		7 days	6.55
		28 days	8.04
	Compressive Strength	1 day	11.9
		3 days	24.2
		7 days	34.3
		28 days	47.3

TABLE 3

Grain Size Distribution of Kimitsu Sand.

Diameter of Sand (mm)	2.0~1.2	1.2~0.6	0.6 ~ 0.3	0.3 ~ 0.15	0.15 ~ 0
Weight (%)	8.0	17.0	45.5	24.5	5.0

obtained when the tensile load was given to the notched specimen. The curve indicates that the fracture mode in the tensile test is not catastrophic but stable because of the presence of the reinforcing elements and the notches, and that since the elastic energy stored in both specimen and testing machine in the tensile test gradually decreases with decreasing tensile load (stress) until it becomes zero, all the above elastic energy is consumed for

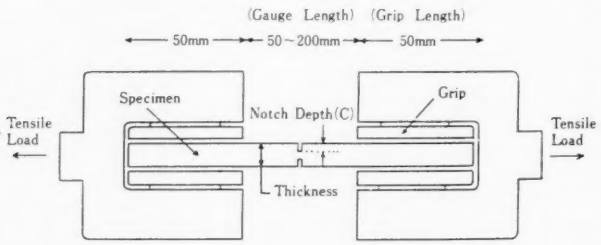

FIG. 1

Tensile test geometry of the notched specimen.

the fracture of the specimen. The area under the curve, therefore, means the work done by the testing machine for the fracture. The surface energy, γ_t, can be then given by:

$$\gamma_t = \frac{Ut}{2A_t} = \frac{Ut}{2(d - 2c)\cdot b} \quad (5)$$

where Ut is the work done by the testing machine for the fracture, A_t is the apparent cross-sectional area of the fracture portion in the tensile test, d is the thickness, b is the width and c is the notch depth of the specimen.

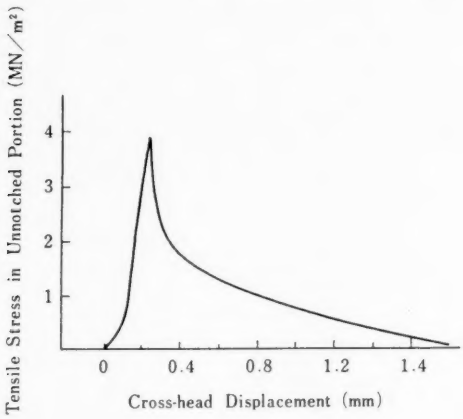

FIG. 2

Stress-elongation curve of the notched specimen in the tensile test.

Since the A_t is the apparent area for heterogeneous material such as GRC, the γ_t obtained is the effective fracture energy (often reffered to as work of fracture).

In order to confirm the validity of the measurement of γ_t, the fracture energy was measured by the three-point bend test (11) using the notched specimen. The test geometry is illustrated in Fig. 3. The load-deflection curve is shown in Fig. 4. The area under the curve is the energy consumed by the specimen during the fracture. The work of fracture obtained from the bend test, γ_b, is then given by:

$$\gamma_b = \frac{U_b}{2A_b} = \frac{U_b}{2(d-c_1-c_2)\cdot b} \quad (6)$$

where U_b is the work done by the bend test machine for the fracture, A_b is the apparent cross-sectional area of the fracture portion in the bend test and c_1 and c_2 are the notch depths.

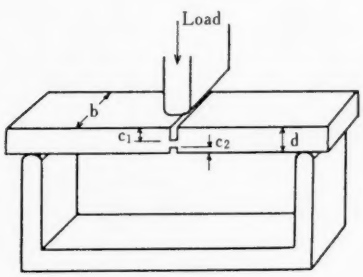

FIG. 3

Bend test geometry of the notched specimen.

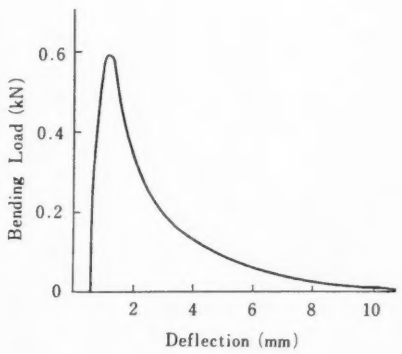

FIG. 4

Load-deflection curve of the notched specimen.

Results

The effect of the notch depth on the fracture energy, $2\gamma t$, was first investigated by the tensile test. The results are listed in Table 4. When the ratio of the total notch depth to the specimen thickness (2c/d) was not less than 0.4, the notch depth did not depend on the γt, while the γt for the unnotched specimen became approximately 1.6 times as large as that for the notched specimen. The results obtained under various gauge length conditions are listed in Table 5, which showed that the γt was not influenced by the gauge length of the specimen considering the standard deviation. The effect of the cross-head speed in the tensile test is listed in Table 6, which showed that the γt also was not affected by the cross-head speed.

The result shown in Table 7 is the fracture energy (work of fracture), γb, measured in the bend test in order to confirm the suitability of the tensile method. The good agreement of the γt with the γb showed that the present method is valid and suitable for measuring the fracture energy of GRC.

TABLE 4

Relation between Notch Depth and Fracture Energy.

Total Notch Depth [2c] (mm)	Thickness of Fracture Portion [d-2c] (mm)	Fracture Energy ($2\gamma t$) Mean (KJ/m^2)	Standard Deviation (KJ/m^2)	Number of Specimens
8	2	6.41	2.50	8
6	4	6.47	1.20	9
4	6	6.61	0.91	8
0	10	10.6	1.81	8

Specimen Size: 10 x 40 x 200 mm, Gauge Length: 100 mm,
Cross-head Speed: 0.5 mm/min.

TABLE 5

Relation between Gauge Length and Fracture Energy.

Specimen Size Thickness [d] (mm)	Width [b] (mm)	Length [L] (mm)	Gauge Length (mm)	Fracture Energy ($2\gamma t$) Mean (KJ/m^2)	Standard Deviation (KJ/m^2)	Number of Specimens
15	40	150	50	6.33	1.30	10
10	40	200	100	6.61	0.91	8
15	40	250	150	6.51	2.02	7
15	40	400	200	6.03	1.34	7

Cross-head Speed: 0.5 mm/min, Thickness of Fracture Portion [d-2c]: 6 mm

TABLE 6

Relation between Cross-head Speed and Fracture Energy.

Cross-head Speed (mm/min)	Fracture Energy ($2\gamma t$) Mean (KJ/m^2)	Standard Deviation (KJ/m^2)	Number of Specimens
0.5	6.33	1.30	10
2.0	6.15	0.85	9
7.5	6.43	0.94	7

Specimen Size: 15 x 40 x 150 mm, Gauge Length: 50 mm,
Thickness of Fracture Portion [d-2c]: 6 mm.

TABLE 7

Fracture Energy Obtained from Bend Test Method.

Specimen Size [d x b x L] (mm) (mm) (mm)	Thickness of Fracture Portion $[d - c_1 - c_2]$ (mm)	Fracture Energy ($2\gamma b$) Mean (KJ/m^2)	Standard Deviation (KJ/m^2)	Number of Specimens
25 x 40 x 150	4	6.48	0.89	10

C_1 : 20 mm, C_2 : 1 mm, Cross-head Speed: 0.5 mm/min, Span [1]: 135 mm.

Error Factors

The error factors in the measurement of the γt are discussed.

Notch Effect

As shown in Table 4 the γt of the unnotched specimen is approximately 1.6 times larger than that of the notched one. The reason is considered as follows. When the tensile load increases, a crack is initiated on the weakest portion of the specimen and then opened. The further increase in the crack opening, however, is prevented by the reinforcing elements. Another crack is then initiated on the other weaker portion of the specimen. The size of the crack thus increases with increasing tensile load (12). The formation of many cracks is considered to give larger fracture energy to the unnotched specimen than to the notched one. These cracks could be observed by the naked eye. For an accurate measurement, it is indispensable that there is no growth of the crack on the unnotched portion of the notched specimen in the tensile test. The acoustic emission (AE) count of both notched and unnotched specimens (8 x 20 x 150 mm^3) was then measured to investigate the crack initiation and growth under varing stress. Fig. 5 (a) shows the AE total counts of the event number, the AE total counts including the ring-down of the transducer and the tensile stress versus the cross-head displacement for the unnotched specimen in the tensile test. As shown in Fig. 5 (a), if the stress is

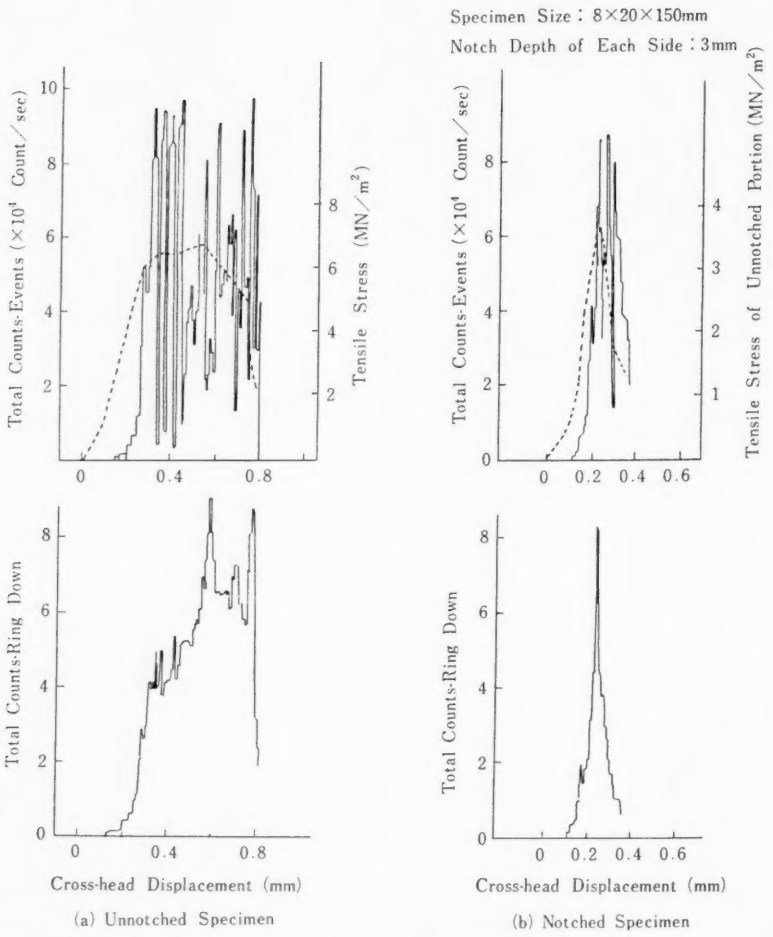
Specimen Size : 8×20×150mm
Notch Depth of Each Side : 3mm
Total Counts-Events (×10⁴ Count/sec)
Tensile Stress (MN/m²)
Tensile Stress of Unnotched Portion (MN/m²)
Total Counts-Ring Down
Cross-head Displacement (mm)
(a) Unnotched Specimen
(b) Notched Specimen

FIG. 5

Total counts of the acoustic emission (solid line) and the tensile stress (dotted line).

less than 5 MN/m^2, the AE counts of the event number and the ring-down were so low that the crack formation is considered negligible.

On the other hand, when the notched specimen illustrated in Fig. 1 is subjected to the tensile test, the stress of the notched portion will be a few times higher than that of the unnotched portion because of the higher stress concentration and the smaller cross-sectional area of the specimen. Fig. 5(b) shows the AE counts and the stress of the unnotched portion of the notched specimen. As shown in Fig. 5 (b), because of the notch effect the AE counts of the notched specimen was very high even under the low tensile stress (e.g. 3 MN/m^2) applied to the unnotched portion. However, such a low stress did not lead to any AE counts (i.e. crack formation) without the notch as shown in Fig. 5 (a). From the results shown in Fig. 5, it was proved that the crack formation does not occur in any unnotched portion of the notched specimen in

the tensile test although it occurs in the notched portion. This is also confirmed from the results listed in Table 5. If the crack had been formed on the unnotched portion, the increase in the gauge length of the specimen should result in the increase in the γt value.

Slip of Grip

It should be revealed that there is no slip between the specimen and the grip in the tensile test since it results in the overestimation of the γt value. A tensile load test was then repeated using the unnotched specimen (11.6 x 40 x 200 mm^3) in order to find out the slip in the grips. The results are illustrated in Fig. 6. As the stress first increased from the point A to B, the elongation, caused mainly by the elastic deformation of both specimen and testing machine, linearly increased. After the shift of the chart paper in the recorder from the point B to C, the curve CD was obtained when the stress or the elongation was decreased to zero. Since the length BC was equal to the DA and the curve AB was able to superposed upon the DC, no hysteresis was found in the stress-elongation curve. After the shift of the chart paper from D to E, the same experiments were repeated until the points W, X, Y and Z were obtained as shown in Fig. 6. As the elongation increased, a little hysteresis occured because of a little play of the testing machine, but the length XY was equal to the WZ if the stress is less than 5 MN/m^2. Since, as shown in Fig. 5 (b), the stress of more than 4 MN/m^2 was not required in the present tensile test method owing to the notch effect, it was found from Fig. 6 that the plastic deformation of both specimen and testing machine during the test was so small as to be unable to detect it from the recorder chart. It is then concluded the error is not caused by the slip and friction between the specimen and the grip or by the plastic deformation of the unnotched portion for the notched specimen.

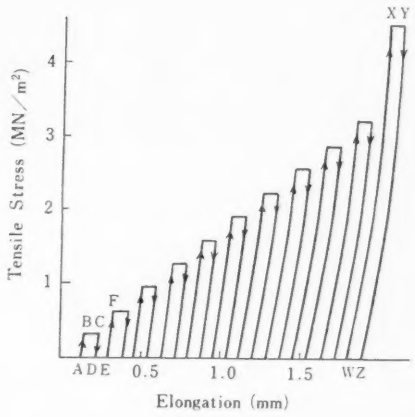

FIG. 6

Tensile stress vs. cross-head displacement of an unnotched specimen.

Irregularity of Fracture Surface

When the specimen was observed after the test, the broken or pulled-out strands stuck straight out on the fractured surface as shown in Fig. 7. In practice it is, therefore, difficult to measure the fracture surface area accurately although the fractured surface of the matrix portion is flat. Since, in the present method, the fractured surface is expressed by the term, $2(d-2c)\cdot b$, in Eq. (5), it is inevitable that a little difference is caused between the above term and the real fractured surface. Since the GRC also is an inhomogeneous material containing strands, aggregates and cement paste, the Ut value in Eq. (5) involves the energy caused by the pull-out or break of the strands as well as the fracture of the matrix. The γt value obtained from Eq. (5), therefore, should be considered the effective fracture energy.

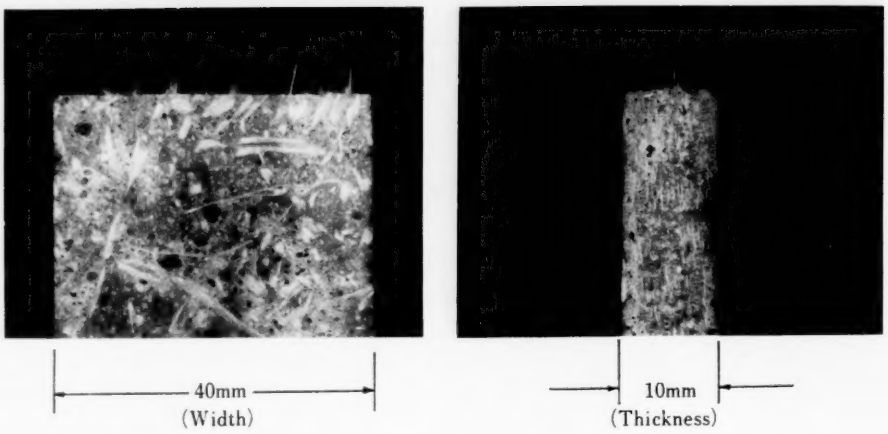

FIG. 7

Fractured surface of the notched specimen observed after the tensile test.

Summary

For some homogeneous materials the fracture toughness, usually called stress intensity factor (K_{1C}), was shown to be proportional to the fracture energy on the basis of the theoretical equations reported in some papers before. It was considered from this relation that the fracture energy of GRC (Glass Fiber Reinforced Cement) is an useful index of the fracture toughness. The determination method was then proposed for the estimation of the GRC fracture toughness. The fracture energy was measured by the tensile test method using the specimen with the two notches of the same depth on both sides. Since the value obtained was not influenced by the notch depth if the ratio of the notch to thickness (2c/d) was not less than 4/10, it was found that the measured value can represent the GRC material property. The suitability of the value thus obtained was confirmed by the close agreement with the value (Table 7) obtained from the bend test method (11) reported before. The ratio of the total notch depth to the specimen thickness in the present method was able to be smaller than that in the bend test one. The ratio of not less than 4/10, however, was necessary for obtaining the accurate value. The shallower notch (the larger fracture area) gives the better averaging process over coarse microstructures such as those of GRC and does not easily make the microcracks on the notched surface during the preparation of the specimen before the testing. The present method, then, is more desirable for the relatively thin specimen because of the shallower notch than the bend test method. It is also considered that this method can be applied not only to GRC but also to the relatively unrigid and brittle matrix composites which will have the plastic deformation at the load points of the specimen in the three-point bend test.

Acknowledgements

The author wishes to thank Dr. H. Ohta for his kind co-operation in measuring the acoustic emission, also Asahi Glass Company, Ltd. for permission to publish this paper.

VOL.
14
1984

References

(1) J. Nakayama, H. Abe and R.C. Bradt, J. Am. Ceram. Soc. 64 [11] 671-5 (1981).

(2) P.E. Petersson, Cement and Concrete Research 10 [1] 91-101 (1980).

(3) C.H. Hanager, A Thoughness Index of Fiber Concrete, Int. Symp. Testing and Test Methods of Fiber Cement Composites, Sheffield (England) 79-86 (1978).

(4) J.R. Rice, J. Appl. Mech., ASME 35 379 (1968).

(5) G. Velazco, K. Visalvanich and S.P. Shah, Cement and Concrete Research 10, 41, (1980).

(6) W.F. Brown, Jr and J.E. Srawley, ASTM STP 410 Philadelphia (1967).

(7) A.A. Griffith, Phil. Trans. Roy. Soc. A 211, 163 (1920).

(8) R.W. Hertzverg "Deform. and Frat. Mech. of Eng. Mater." Wiley & Sons 273 (1976).

(9) J.J. Gilman, Phys. Chem. of Ceramics", ed. by C. Klingsberg, Gordon & Breach, 240 (1963).

(10) A. Kelly, "Strong Solids", Clarendon Press (1966).

(11) T. Ohigashi, Measurement of effective fracture energy of glass fiber reinforced cement, Int. Symp. Testing and Test Methods of Fiber Cement Composites, Sheffield (England) p67 (1978).

(12) J. Aveston, R.A. Mercer and J.M. sillwood, "The mechanism of fiber reinforcement of cement and concrete", National Physical Laboratory Report, No. SI, No. 91/11/98, Part I (Jan. 1975); Part II, DMA 228 (Feb. 1976).

OL.
14
984

CEMENT and CONCRETE RESEARCH. Vol. 14, pp. 360-368, 1984. Printed in the USA.
0008-8846/84 $3.00+00. Copyright (c) 1984 Pergamon Press, Ltd.

POLYMORPHISM AND PHASE CHANGES IN THE FERRITE PHASE OF CEMENTS INDUCED BY TITANIUM SUBSTITUTION

M.B. Marinho and F.P. Glasser

Department of Chemistry, University of Aberdeen
Meston Walk, Old Aberdeen AB9 2UE, Scotland, UK

(Communicated by M. Regourd)
(Received Aug. 22, 1983)

ABSTRACT

The introduction of TiO_2 at 1-10% levels into the crystal structure of the ferrite phase, nominally $Ca_2(Fe_{2-x}Al_{2x})O_5$, has been studied experimentally by X-ray and electron diffraction. Ti^{4+} substitutes in ferrite mainly in octahedral sites, replacing Fe^{3+}. Charge compensation is maintained by adding extra oxygens. At low Ti contents, typically 1 - 9%, the oxygen distributions are random and the crystal structure extensively disordered in the *b* direction. However, at higher Ti contents, an ordered superstructure with a *b* axis periodicity of ~18.6 Å develops. This phase represents a different stacking arrangement than in C_4AF and has the ideal composition $Ca_5(Fe_{4-x}Al_x)TiO_{13}$. The appearance of powder X-ray diffraction patterns are interpreted in terms of the crystallographic changes.

VOL. 14 198

Introduction

The ferrite phase of cements comprises a range of solid solutions whose major-element substitution has the general formula $Ca_2Fe_{2-2x}Al_{2x}O_5$ where x ranges between zero and ~0.7 at 1 bar pressure (1); at very high pressures, x may attain the limiting value of 1.0 (2). The solid solutions high in iron exhibit a complex magnetic structure (3). With increasing Al substitution, a symmetry change also occurs amongst the orthorhombic solid solutions from primitive to body-centred. This change occurs gradually with increasing numerical values of x and is essentially complete at x = 0.33 (4). The effects of other substituents on the crystal chemistry and reactivity are less well known although it has long been known that the ferrite phase may preferentially concentrate many chemical impurities originally present in the clinker raw materials. Titanium is a notable example. The Ti content of a bulk clinker batch may be low, on the order of 0.2 - 0.4%, but microprobe analyses disclose that it is strongly fractionated into the ferrite phase during clinker cooling, so that the ferrite frequently contains 2 - 3% or more Ti (5). This Ti is believed to be present overwhelmingly as Ti^{4+}.

Kimura and Muan (6) studied phase equilibria in the system CaO-TiO_2-Fe-O and report that up to 2.5 wt % TiO_2 went into solid solution with C_2F at 1400°C. They determined that the mechanism of Ti substitution primarily

involved replacement of $2Fe^{3+}$ by $2Ti^{4+}$ with concomitant addition of O^{2-} ions. Thus the Ti-bearing solid solutions have a variable oxygen stoichiometry measured in terms of the number of oxide ions per unit cell. This behaviour is unusual amongst clinker phases; C_3S and C_2S form limited solid solutions incorporating ions with dissimilar charges (e.g., Fe^{3+}) but charge balance is apparently obtained by some mechanism which leaves the oxygen stoichiometry essentially unchanged.

Knöfel (7) studied the limit of Ti substitution in C_4AF and found that solid solutions extend to ∿18 wt % TiO_2 at 1400°C. The limit of solid solution was marked by the development of excess free lime. Systematic changes in the appearance of X-ray powder patterns were noted; these correlated with increasing Ti content, but the nature and cause of the changes remained unexplained.

Studies of phase formation in the system $CaTiO_3$-$Ca_2Fe_2O_5$ have also been made by high resolution electron microscopy and X-ray powder diffraction (8). The results obtained are somewhat at variance with those in (6) especially with respect to the limits of solid solution. Moreover, a series of discrete phases were found having a common substructure unit. Each phase had a range of stoichiometry, but all had the general formula $A_nM_nO_{3n-1}$ ($n = 2$ for $Ca_2Fe_2O_5$). Phase formation was also observed to occur at or close to n values equal to 2.5, 2.67, 3.0 and 4.0. Thus, at $n = 3$, a discrete phase having the formula $Ca_3(Fe_2Ti)O_8$ was encountered. It was suggested from lattice imaging studies that at $n > 2.0$, anions and defects associated with the increasing introduction of Ti were disordered but that phase formation at $n \sim 2.5$ was conditioned partly by ordering of oxygens and defects, thereby introducing lattice periodicities longer than those observed in C_2F itself. Although these studies relate mainly to high levels of Ti substitution relative to those encountered in clinker, they are nevertheless relevant, as will be shown.

The title study was initiated for three reasons: (i) the role of Ti substitution is interesting in its own right (ii) the relation between defect structures and reactivity has attracted much interest and the ferrites offer an example which might usefully be studied in more detail and (iii) changes in lattice periodicities arising from minor element substitution could alter the x-ray intensities of the ferrite, thereby affecting calibrations for quantitative phase determination by X-ray methods.

Experimental

Ferrite solid solutions were prepared from mechanical mixtures of 'AnalaR' $CaCO_3$, Merck reagent Fe_2O_3, 'Cera' Al_2O_3 and a chemically-pure rutile, prepared by ignition of anatase pulp. Most of the work was done on the compositions listed in Table 1. These were calculated to lie on several joins in the CaO-Al_2O_3-Fe_2O_3-TiO_2 system notably on compositions in the series $Ca_2Fe_{2-2x}Ti_{2x}O_{5+x}$ and $Ca_4Al_{2-2x}Fe_{2-2x}Ti_{4x}O_{10+2x}$. Additionally, compositions were prepared at $C_4A_{0.268}F_{1.518}T_{0.428}$, $C_4A_{0.538}F_{1.254}T_{0.416}$, $C_4A_{0.809}F_{0.989}T_{0.404}$ and $C_4A_{0.991}F_{0.811}T_{0.396}$: these contain uniformly about 6.5 wt % TiO_2, and were calculated to provide additional data on the effect of changing A/F ratios.

The preparations were placed in Pt crucibles and decarbonated by heating in air at 800-900°C. Subsequent reaction leading to homogeneous solid solution formation was achieved by pressing the decarbonated precursors into pellets and firing these on Pt foil in air at various temperatures between 1260° and 1325°C. The course of sintering was monitored by preparing

TABLE 1

Compositions of Ti-substituted Ferrites

Solid Solution Formula*	x	CaO	Al_2O_3	Fe_2O_3	TiO_2
$C_2F_{0.99}T_{0.02}$	0.010	41.26	-	58.16	0.59
$C_2F_{0.96}T_{0.08}$	0.040	41.26	-	56.39	2.35
$C_2F_{0.901}T_{0.193}$	0.097	41.32	-	53.00	5.68
$C_4A_{0.97}F_{0.97}T_{0.12}$	0.03	45.99	20.28	31.76	1.97
$C_4A_{0.90}F_{0.90}T_{0.40}$	0.10	45.61	18.70	29.23	6.50

* These formulae are written in cement chemical nomenclature where F = Fe_2O_3, etc. Thus values of x given in the text formulae for Al and Fe should be divided by two to arrive at the subscript numbers given here.

polished sections as firing at too high a temperature can result in partial melting.

Results

X-ray powder data

$Ca_2Fe_{2-2x}Ti_{2x}O_{5+x}$ solid solutions. The most conspicuous effect of Ti substitution is the disappearance from the X-ray powder pattern of all reflections having $h + k + l \neq 2n$. This process appears by X-ray to have been completed by 2.35% TiO_2. It is associated with a change in crystal symmetry from primitive at the C_2F composition to body-centred at higher Ti contents. Apparently Ti substitution, together with concomitant introduction of additional anions, relieves the distortion which, in the absence of Ti, lowers the symmetry to primitive. Amongst the main reflections - those which have $h + k + l = 2n$ and which in general, occur throughout the series - only minor variations in intensities occur. Table 2 shows the measured peak heights, determined by counting at the centre of the peak while using monochromated CuK_α radiation. The data observed for pure C_2F give rather better agreement with the calculated intensities than those recorded in the JCPDF (Card 19 - 222). The only other intensity variation with solid solution which may have statistical significance is 020, which passes through

TABLE 2

Intensity Data for $Ca_2Fe_{2-2x}Ti_{2x}O_{5+x}$ Solid Solutions

	C_2F	C_2F	C_2F	Solid solutions, % TiO_2			
hkl	(19 - 222)	calc.	obs.	0.59	1.18	2.35	5.28
002	70	37	28	32	34	30	28
200	70	44	41	40	42	36	37
202	70	34	32	33	32	26	27
020	40	14	12	25	17	16	17
161	40	12	11	16	15	11	11
143	40	15	15	15	-	11	11
341	40	12	19	10	-	10	11

a maximum intensity at 0.59% TiO_2. The effect of Ti substitution on the lattice parameters of the ferrite phase are negligible. Table 3 compares data in the literature with our measurements on pure C_2F and on Ti solid solutions: the cell parameters shown were obtained from least-squares refinement of all measurable reflections in the range up to 60° 2θ (CuK_α); the last significant figures of the estimated standard deviation are also given.

TABLE 3

Cell Parameters of Ferrites (Å)

	$Ca_2Fe_2O_5$		$Ca_2Fe_{2-2x}Ti_{2x}O_{5+x}$	
Parameter	Card 19 - 222	This Study	x = 0.04	x = 0.097
a	5.598	5.597 (3)	5.594 (2)	5.595 (3)
b	14.754	14.742 (8)	14.743 (4)	14.751 (6)
c	5.427	5.431 (4)	5.438 (2)	5.438 (4)

$Ca_4Al_{2-2x}Fe_{2-2x}Ti_{4x}O_{10+x}$ Solid Solutions. No gross changes were observed in the positions or relative intensities of reflections in the powder patterns as a function of Ti content at less than 1% TiO_2, but with increasing Ti content, many of the reflections became progressively broadened and more diffuse. Batches of Ti substituted ferrites were annealed for up to 21 d at 1200°, 1240°, and 1280°C without improving the sharpness of the X-ray reflections, even though the crystallite size was increased markedly by prolonged annealing. The chemical homogeneity of solid solutions on a scale of 10^3 nm was checked using CORA, a transmission electron microscope designed for chemical analyses. But even at this scale, the solid solution crystallites were chemically homogeneous within the limits of error imposed by counting statistics which, in chemical terms, mean that two standard deviations correspond to ±1 - 2% for both Al and Fe and ±0.2 - .3% TiO_2, relative to Ca used as an internal standard.

Obtaining consistent X-ray intensity measurements for C_4AF as well as its Ti - containing solid solutions presents some experimental difficulties. Some measurements, including a comparison between experimental and calculated

TABLE 4

X-Ray Intensity Data for C_4AF and $Ca_4Al_{2-2x}Fe_{2-2x}Ti_{4x}O_{10+2x}$

Reflection	Taylor†		This study, observed at TiO_2 =		
Index.	Calc.	Obs.	0.0%	1.99%	6.5% wt %
141	100	100	100	100	100
200	36	25	18	29	38
002	48	35	40	31	48
020	46	45	45	52	15
161	25	35	19	24	13
202	43	35	14	32	44
080	17	45	38	25	-

†Personal communication (H.F.W. Taylor): submitted to the Powder Diffraction File.

values, are shown in Table 4. The reasons for the poorer agreement relative to those obtained for C_2F are not obvious, but it is probable that they arise in part from the better crystallite morphology relative to C_2F, which tends to induce preferred orientation, as well as the increasingly diffuse nature of the powder pattern of the Ti-substituted solid solutions, which increases the uncertainty of either peak-height or peak-area measurements. On account of the diffuse nature of many of the patterns, no attempts were made to determine quantitatively the variations in cell parameters with Ti substitution. But any changes must be very small.

The structural position of Ti was inferred from CORA analyses of crystals containing Aℓ, Fe and Ti. Table 5 summarizes the results of analyses made on 38 crystals from one batch having the bulk composition $C_4A_{0.90}F_{0.90}T_{0.40}$. If the octahedral and tetrahedral M^{3+} sites were equally substituted by Ti^{4+}, the A/F ratio would be expected to remain equal to 1.0. Its decrease, to a mean value of 0.961 ± 0.088, is marginally significant, and it is probable that Ti exhibits a preference for those octahedral sites which in C_4AF would be occupied by Fe; Fe : Ti substitution therefore causes the A/F ratio to decrease below unity.

TABLE 5

Analyses of $C_4A_{0.9}F_{0.9}T_{0.4}$ Preparation

Aℓ/Fe ratios	Number of Crystals.	
> 1.06	3	8
1.05 - 1.00	5	
0.96 - 1.00	10	30
0.90 - 0.95	17	
< 0.89	3	

Electron Diffraction

$Ca_2Fe_{2-2x}Ti_{2x}O_{5+x}$ solid solutions. Fig. 1 compares the electron diffraction patterns obtained from C_2F with those obtained from Ti substituted solids solutions containing 2.35 and 5.68 wt % TiO_2. All patterns were obtained in the same orientation (010 projection). Reflections indicating primitive symmetry are plainly visible in the rows parallel to b; the reflections are sharp and distinct. However, at 2.35% TiO_2, the corresponding reflections, while still visible, have become weakened and diffuse. At 5.68% TiO_2, only a few reflections having $h + k + l = 2n + 1$ persist and these are largely confined to a region close to the a^* axis and, moreover, they are not only extremely weak but diffuse as well. Thus, by electron diffraction, the transition to body-centred symmetry is essentially complete at 5.68% TiO_2 whereas by powder X-ray diffraction it appears to be complete at much lower TiO_2 contents. This apparent discrepancy can be resolved by noting that electron diffraction is much more sensitive towards the presence of weak reflections than is X-ray diffraction.

$Ca_4Al_{2-2x}Fe_{2-2x}Ti_{4x}O_{10+2x}$. Electron diffraction measurements on solid solutions in this series in the range of Ti contents between 0 and 12.8% TiO_2 reveal that the structures fall into three groups. These groups can be explained with the aid of selected electron micrographs shown in Fig. 2, which are not in identical orientations, but all have the crystallographic b^* direction arranged horizontally, which is sufficient to illustrate the salient features. At the C_4AF composition, the pattern is body-centred, with a 14 Å b axis repeat; moreover, all reflections are sharp. At 3.3% TiO_2 the pattern has become notably more diffuse, with individual reflections forming conspicuous streaks of diffracted radiation $\| b^*$. The disorder along b^* increases progessively with increasing Ti content until at 9.7% TiO_2, the pattern is dominated by continuous streaks on which are superimposed reflections characteristic of more crystalline domains having a different b axis periodicity, ∿18.6 Å instead of ∿14 Å as in C_4AF. At still higher Ti

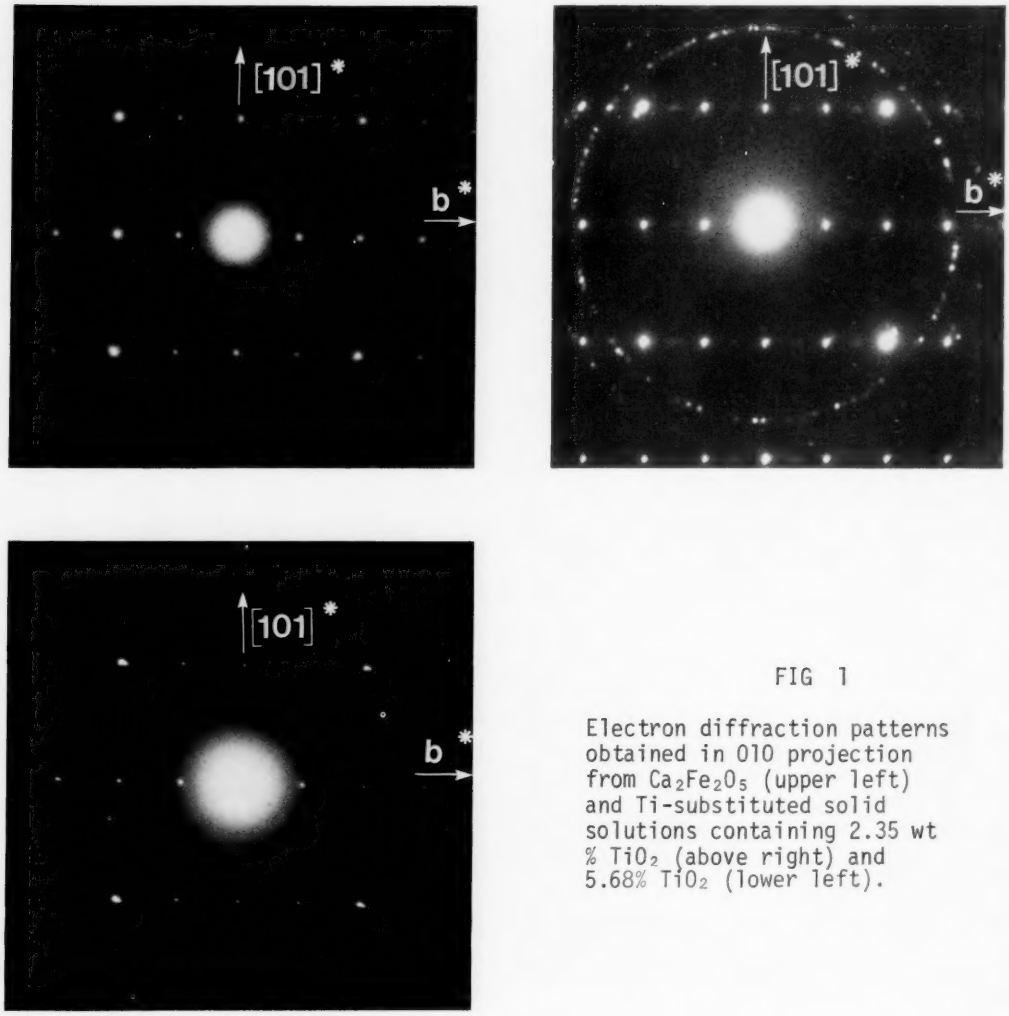

FIG 1

Electron diffraction patterns obtained in 010 projection from $Ca_2Fe_2O_5$ (upper left) and Ti-substituted solid solutions containing 2.35 wt % TiO_2 (above right) and 5.68% TiO_2 (lower left).

contents, 12.8 wt % TiO_2 in this instance, the pattern is again sharp and only the 18.6 Å domains persist. In the intermediate range of compositions lying roughly between 3 and 10% TiO_2 no amount of annealing at 1100 - 1200°C was sufficient to eliminate the b^* axis disorder, which, it is concluded, arises from random interstratification of the two types of repeating units.

Discussion

Data on several joins extending between $CaTiO_3$ and ferrite solid solutions can be combined to give a consistent explanation of the effects of introducing Ti into the lattice of the solid solutions. Ti is soluble in ferrites in preference to either forming a separate Ti phase - *e.g.* rutile - or dissolving in the host lattices of C_3S, C_2S or C_3A. The solid solution in ferrite is, however, accompanied by a series of complex changes with respect both to the symmetry and order or disorder of the solid solution. Fig. 3 correlates some of these changes. The primitive symmetry exhibited by $Ca_2Fe_2O_5$ and a

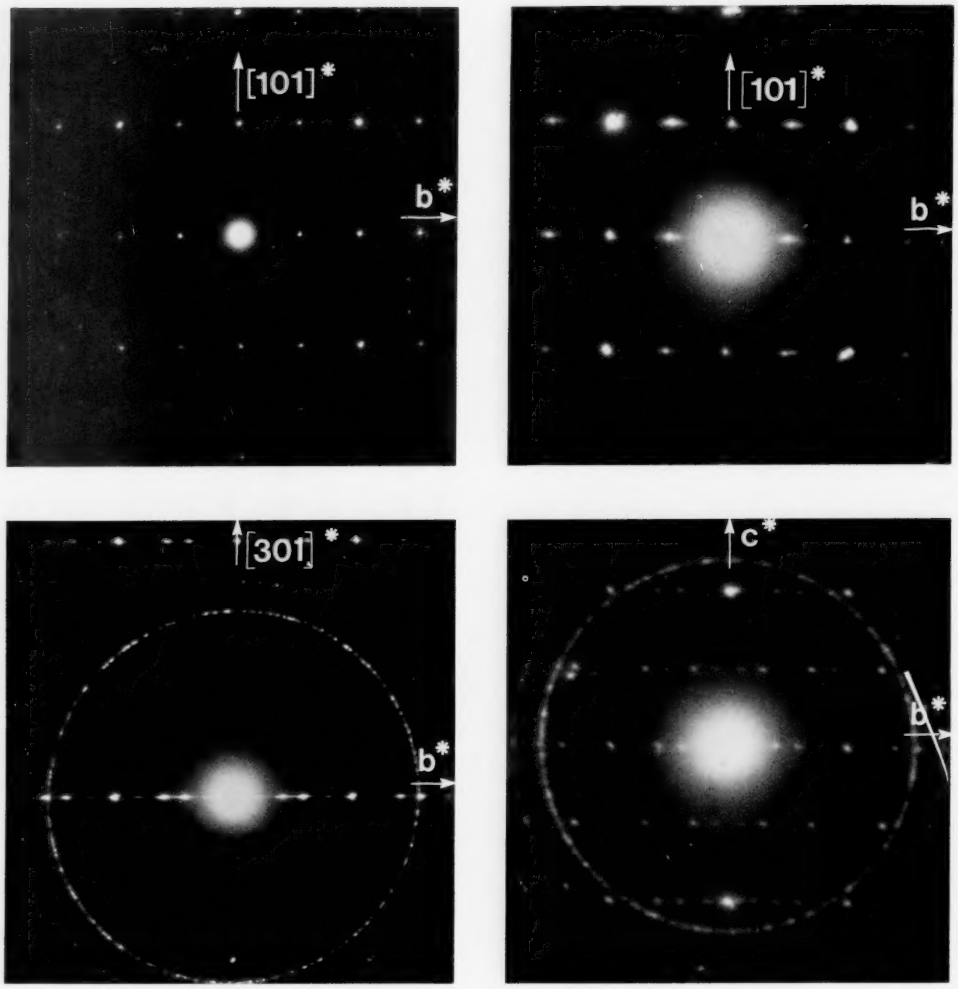

FIG 2

Electron diffraction patterns of C_4AF and Ti-substituted C_4AF solid solutions. All patterns have b* horizontal. Upper left, C_4AF (101 vertical); upper right, 3.3% TiO_2 (101 vertical); lower left, 9.7% TiO_2 (301 vertical) and lower right 12.8% TiO_2 (c* vertical), showing 18.6 Å b* repeat.

range of Aℓ containing solutions may be terminated either by addition of more Aℓ or even more effectively, by additions of Ti. Thus, the region of primitive solid solutions having a *b* axis repeat of 14 Å is confined to the high iron, low titanium regions. The symmetry transition between primitive and body-centred occurs gradually, over a range of compositions, and its location depends in part on the sensitivity of the techniques used towards

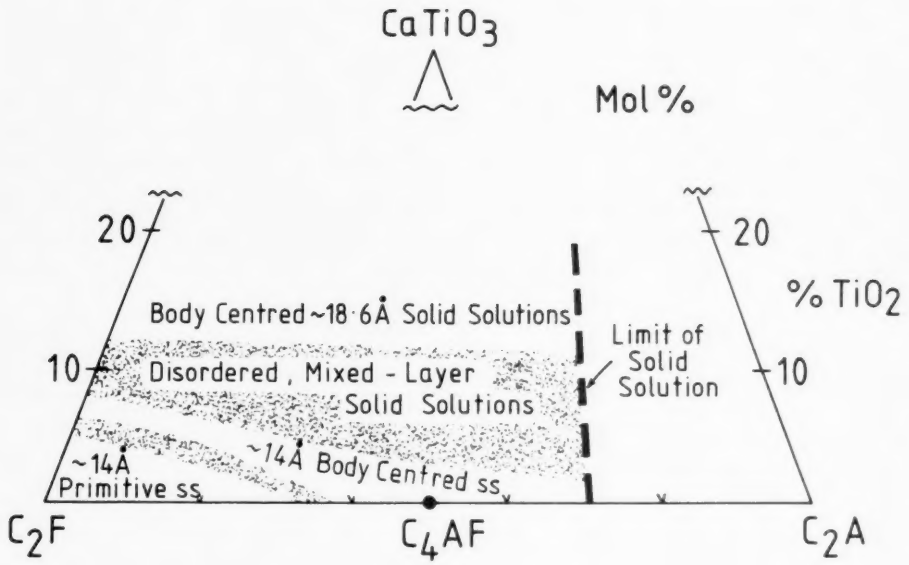

FIG. 3

Diagram showing phase formation in ferrite solid solutions containing Ti. The regions of phase formation are from annealing experiments made at 1000° - 1200°C. The vertical axis scale is exaggerated to show more clearly the phase boundaries at low TiO_2 contents.

the presence or absence of very weak reflections; electron-diffraction is more sensitive in this respect than X-ray powder diffraction. An extensive range of 14 Å body-centred solid solutions is encountered at higher Ti contents, but with increasing Ti contents, the solid solutions become progressively more disordered. The disordered region marks a transition to a new structure type, characterized by having a *b* axis repeat of 18.6 Å. The chemical analyses of numerous single crystals of this phase reveal a type formula very close to that of the $Ca_5Fe_4TiO_{13}$ phase (after allowing for extensive Aℓ for Fe substitution) encountered amongst Ti-substituted $Ca_2Fe_2O_5$ solid solutions by Grenier, *et al.* (8). Moreover, the *b* axis repeats at ∿18.6 Å are essentially identical. In this view, the structure of the crystals at $Ca_5Fe_2A\ell_2TiO_{13}$ containing about 12.8% TiO_2 may be compared with that of C_4AF in terms of the stacking of alternate tetrahedral-octahedral layers perpendicular to *b*. In C_4AF, the pseudo repeat is |OTO|OTO|··· (∿7 Å) whereas in $Ca_5Fe_2A\ell_2TiO_{13}$, it is |OTOTOO|OTOTOO| ····· giving rise to the observed 18.6 Å spacing. The ratio of octahedral : tetrahedral sites remains constant at 2:1, but the more complex repeating sequence leading to clustering of the remaining vacant oxygen sites and a longer *b* axis periodicity, is promoted by increasing Ti content. The sequences are sufficiently similar to permit the disordered stacking arrangements encountered in the range of Ti contents between C_4AF and $Ca_5Fe_2A\ell_2TiO_{13}$. Indeed, the $Ca_5Fe_2A\ell_2TiO_{13}$ composition prepared in the course of this study always contained a substantial proportion of disordered regions, hence superstructure reflections characteristics of the longer *b* axis repeat are not found in the powder X-ray patterns.

The consequences of these discoveries concerning the effect of Ti on the polymorphism of ferrite solid solutions are, briefly, (i) that the diffraction efficiency of disordered solid solutions is markedly affected, relative to synthetic Ti-free ferrites, and it may be necessary to take this into account when assessing the results of quantitative X-ray diffraction of cement clinkers, (ii) an understanding of the relationships between reactivity towards water of the anhydrous phases and their defect contents, and of the dependence of the defect content on chemical substitution, is somewhat advanced by the present study, which highlights the important role of Ti in controlling structural changes as well as the oxygen stoichiometry of the ferrite solid solutions.

Acknowledgement

M.B. Marinho thanks the Brazilian Government through the C.N.P.q. for financial support in this work.

References

1. A.J. Majumdar, Trans. Brit. Ceram. Soc. 64, 105 (1965).
2. P.S. Aggarwal, J.A. Gard, F.P. Glasser and G.M. Biggar, Cement Concr. Res. 2, 291 (1972).
3. A.A. Colville and S. Geller, Acta Cryst. B28, 3196 (1972).
4. D.K. Smith, Acta Cryst. 15, 1146 (1962).
5. D. Knöfel, Zem-Kal-Gips. 30, 191 (1977).
6. S. Kimura and A. Muan, Am. Mineralogist 56, 1332 (1971).
7. D. Knöfel, Zem-Kalk-Gips, 32, 35 (1979).
8. J.C. Grenier, G. Schiffmached, P. Caro, M. Pouchard and P. Hagenmüller, J. Solid State Chem. 20, 365 (1977).

VOL
14
198

CEMENT and CONCRETE RESEARCH. Vol. 14, pp. 369-374, 1984. Printed in the USA.
0008-8846/84 $3.00+00. Copyright (c) 1984 Pergamon Press, Ltd.

FRACTURE TOUGHNESS OF AUTOCLAVED AERATED CONCRETE

F.H. Wittmann and I. Gheorghita
Laboratory for Building Materials
Swiss Federal Institute of Technology, Lausanne

(Communicated by Z.P. Bazant)
(Received Sept. 29, 1983)

VOL.
14
1984

ABSTRACT

So far, few experiments to determine fracture toughness of autoclaved aerated concrete have been reported in the literature. Tests on three different types of autoclaved aerated concrete using six different specimen geometries have been carried out. Four of the six specimen geometries chosen lead to nearly identical results for K_{IC}. The two other types of specimen were used to determine fracture energy G_f. K_{IC} increases with compressive strength of the material. Fracture energy is about one tenth of the corresponding value of normal concrete. The influence of rate of loading on K_{IC} can be expressed by means of a power law. These results suggest that linear elastic fracture mechanics is a suitable approximation for the calculation of crack propagation in autoclaved aerated concrete.

Introduction

Autoclaved aerated concrete is a lightweight structural material with interesting thermal properties and it is widely used nowadays. Strength and deformation of this comparatively new building material have been studied by many authors. The characteristic mechanical behaviour can be explained on the basis of the particular porous structure of the material semi-quantitatively. Most recent results, and in particular the influence of moisture content on material properties, have been compiled in the proceedings of an International Conference /1/. There is a comprehensive bibliography on research on autoclaved aerated concrete /2/ published in addition in this volume.

It has been proved that fracture mechanics is a powerful tool in structural engeneering. There are different approaches to overcome limitations of linear elastic fracture mechanics as applied to normal concrete structures /3/. So far fracture mechanics parameters for autoclaved aerated concrete have not been determined and published. It can be assumed a priori that crack propagation in autoclaved aerated concrete is significantly less complicated as compared to the degradation of the composite structure of concrete under load. Therefore it seems to be a promising approach to apply fracture mechanics to study crack propagation in structural elements or in

masonry built with autoclaved aerated concrete blocks. In this contribution results of an experimental investigation to determine fracture toughness of three different types of autoclaved aerated concrete will be presented.

Experimental procedure

It is well known that experimental values of fracture toughness can depend significantly on specimen geometry. To make sure that we really determine material properties we have chosen different geometries, i.e. two ring beams tested under compression, three different prismatic beams tested under three point bending, and a compact tension (CT) specimen.

The ring beams had an outer radius of 93 mm. In the following we will call ring beam A the one with an inner radius of 53 mm and ring beam B the one with an inner radius of 28 mm. The thickness B of both ring beams has been chosen to be 35 mm. The length of the sawn notch was 8 mm and 25 mm for ring beam A and ring beam B respectively. The exact meaning of the symbols used can be seen in FIG. 1a.

It has been shown that fracture toughness of the ring beam can be determined if the ultimate load P is known by using the following equation /4/ :

$$K_{IC} = \frac{YP}{B\sqrt{R_o}} \qquad (1)$$

In this equation Y is a parameter which depends on geometry. In our case Y is approximately 3.4 and 1.5 for ring beam A and B, respectively.

The beam A for the three point bending test had a height W of 150 mm, a thickness B of 35 mm, a length L of 570 mm, and a sawn notch a with a length of 30 mm. For beams B and C the dimensions were as follows : W = 95 mm, B = 95 mm, and L = 570 mm (see FIG. 1b). The sawn notch has been 47.5 mm and 31.6 mm for beam B and beam C respectively.

In measuring the failure load P, K_{IC} can be determined by means of the following equation /5/ :

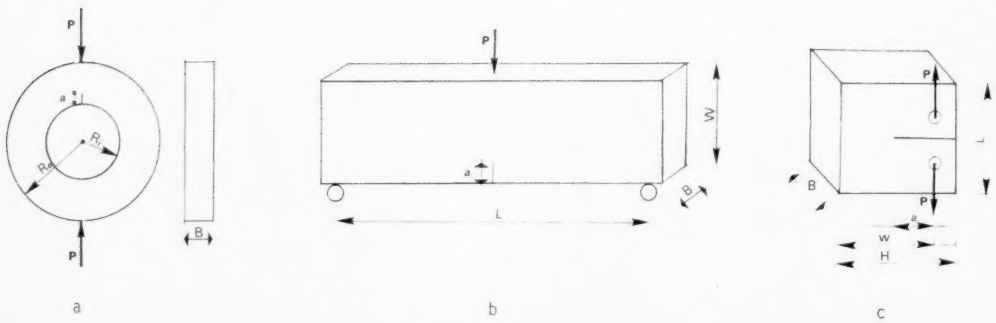

FIG. 1 : Sketch of the different specimens used to determine fracture toughness.

$$K_{IC} = \frac{3\ L\ \sqrt{a}}{2\ B\ W^2}\ P\ Y\ (\frac{a}{W}) \qquad (2)$$

where $Y\ (\frac{a}{W})$ has the following meaning :

$$Y\ (\frac{a}{W}) = 1.93 - 3.07\ (\frac{a}{W}) + 14.53\ (\frac{a}{W})^2 - 25.11\ (\frac{a}{W})^3 + 25.8\ (\frac{a}{W})^4 \qquad (3)$$

From identical blocks, CT specimens have been sawn. The dimensions have been chosen according to ASTM recommendations /6/. This leads to the following specimen geometry : B = 62.5, W = 125, H = 156, and a = 60 mm. For the exact meaning of the symbols used we refer to FIG. 1c.

After having measured the ultimate tensile load of the CT specimen, K_{IC} can be determined by means of the following equation /6/ :

$$K_{IC} = \frac{P\ \sqrt{a}}{W\ B}\ Y\ (\frac{a}{W}) \qquad (4)$$

where $Y\ (\frac{a}{W})$ stands for

$$Y\ (\frac{a}{W}) = 29.6 - 185.5\ (\frac{a}{W}) + 655.7\ (\frac{a}{W})^2 - 1017\ (\frac{a}{W})^3 + 638.9\ (\frac{a}{W})^4 \qquad (5)$$

Compression and tension tests at low rate of loading have been carried out in a conventional screw-driven universal testing machine with a constant preselected speed of the crosshead. Tests at high rate of loading have been carried out in a special high speed testing machine.

All specimens have been sawn from blocks coming from one factory. Three different types of material have been tested, i.e. a lightweight L, a normal N and a high strength S.

The compressive and tensile strength as well as the modulus of elasticity of the three different types of material are given in TABLE I. Compressive strength and modulus of elasticity have been determined in a conventional way. Tensile strength has been determined in a centrifuge.

TABLE I

Compressive strength, tensile strength, and modulus of elasticity for the three different types of auto claved aerated concrete examined in this study.

Type of material	Compressive strength (N/mm^2)	Tensile strength (N/mm^2)	Modulus of elasticity (N/mm^2)
L	2.23	0.27	1200
N	3.12	0.43	1500
S	4.45	0.47	1700

Results

All experimental results, obtained with a crosshead speed of 1 mm/min and by using different specimen geometries, are compiled in TABLE II. Each value indicated in the Table is the average of three to nine individual tests. In the last column, the overall mean value for the three different quality classes is given.

In order to study the influence of rate of loading on fracture toughness of aerated concrete, additional tests have been carried out at higher rate of loading. The range chosen covers impact loading conditions. In this test, series specimens of beam type A have been used exclusively. All tests have been run on normal strength aerated concrete. Results are shown in FIG. 2. K_{IC} as well as the rate of loading have been plotted on log. scales.

Conclusions

Altogether, six different specimen geometries have been used to determine fracture toughness. The experimental values obtained do not depend significantly on specimen geometry. Beams B and C give slightly lower values. This geometry is not really meant for tests to determine K_{IC}. It has been included in this study for reasons of comparison, because it is proposed to determine fracture energy of concrete /7/.

The stress-crack opening diagram for the CT specimens is nearly linear up to the ultimate load. Therefore this test is considered to be valid in the case of autoclaved aerated concrete.

TABLE II

K_{IC} as determined with different specimen geometries for three different types of autoclaved aerated concrete. All values are given in $MN/m^{3/2}$.

Type of material	Ring A	Ring B	Beam A	Beam B	Beam C	CT	Mean value
L	0.059 ± 0.011	0.052 ± 0.007	0.049 ± 0.001	0.043 ± 0.0031	0.044 ± 0.0035	--	0.050
N	0.078 ± 0.004	0.077 ± 0.005	0.063 ± 0.007	0.046 ± 0.0045	0.053 ± 0.0048	0.0606 ± 0.004	0.063
S	0.10 ± 0.0012	0.093 ± 0.005	0.083 ± 0.0032	0.071 ± 0.0018	0.065 ± 0.004	--	0.082

If the overall mean values of fracture toughness as determined for the three different types of aerated concrete are plotted as function of

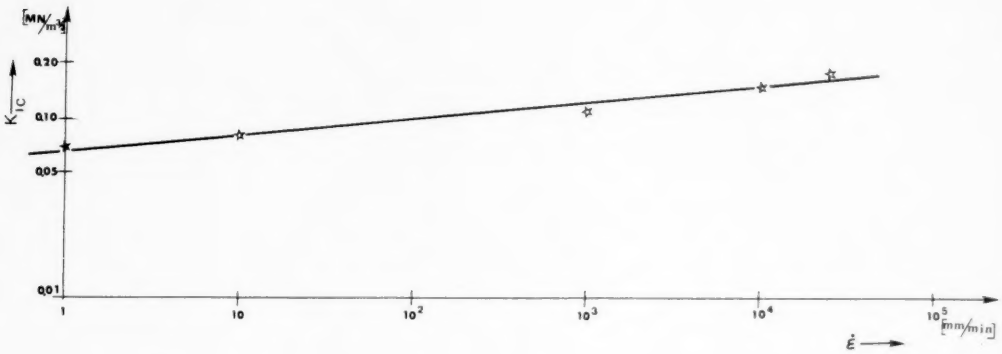

FIG. 2 : Fracture toughness as function of rate of loading.

compressive strength f_c, one obtains a linear relationship. This is shown in FIG. 3.

From the total force-displacement diagram of beams B and C, the fracture energy G_f can be determined following a procedure suggested by Hillerborg, Modéer, and Petersson /7/. The results are shown in TABLE III. From this Table it is evident that fracture energy of aerated concrete is about 1/10 of fracture energy of normal concrete.

As shown in FIG. 2 the influence of rate of loading $\dot{\varepsilon}$ on fracture tougness can be represented by a power law :

$$\frac{K_{IC}}{K_{IC}^{0}} = \left(\frac{\dot{\varepsilon}}{\dot{\varepsilon}_0}\right) \qquad (6)$$

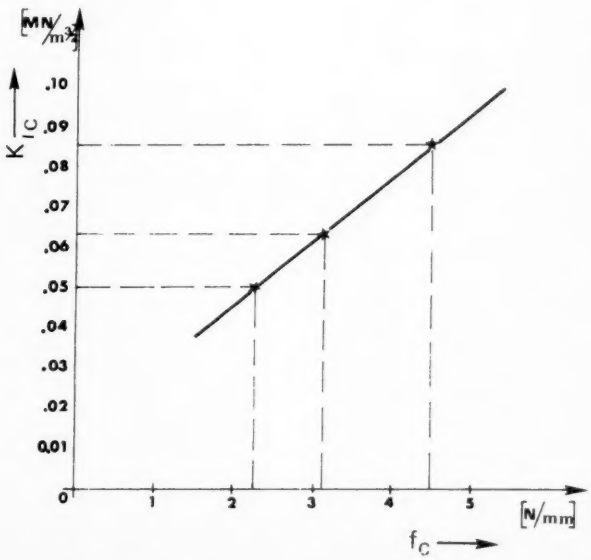

FIG. 3 : Fracture toughness as function of compressive strength.

TABLE III

Material	G_f N/m
Type L	6.07
Type N	7.83
Type S	10.17
concrete	110

Fracture energy G_f for three different types of aerated concrete compared to a characteristic value of normal concrete.

In this equation K^0_{IC} stands for the fracture toughness as measured at reference rate of loading $\dot{\varepsilon}_0$, and m is a material parameter.

This result can be compared with the predictions of a stochastic model originally developed to describe the influence of the rate of loading on the strength of concrete /8/.

On a special aerated concrete made with slate waste, G_c has been determined as function of density /9/. For a density of 600 kg/m^3 a value of 0.055 MN/m^3/^{2} is calculated from their results. This value corresponds reasonably well with our findings given in Table II.

VOL. 14 1984

References

/1/ WITTMANN, F.H. (Editor), Autoclaved Aerated Concrete, Moisture and Properties, Elsevier, 1983.
/2/ HOUST, Y., WITTMANN, F.H., Bibliography on Autoclaved Aerated Concrete, pp. 325-369, in Ref. 1.
/3/ WITTMANN, F.H. (Editor), Fracture Mechanics of Concrete, Elsevier, 1983.
/4/ AHMAD, J. ASHBAUGH, N.E., Constant K_I Crack Propagation Test Specimens, Int. Journal of Fracture 19, 115-129 (1982).
/5/ BROWN, W.F.,STRAWLEY, J.E., ASTM Special Technical Publication 410, p. 13 (1969).
/6/ ASTM, Proposed Method of Test for Plane - Strain Fracture Toughness of Metallic Materials, ASTM Standards Part 31, 1099-1114 (1969).
/7/ HILLERBORG, A., MODEER, M., PETERSSON, P.E., Analysis of Crack Formation and Crack Growth in Concrete by Means of Fracture Mechanics and Finite Elements, Cement and Concrete Research, 6, 773-782 (1976).
/8/ MIHASHI, H., WITTMANN, F.H., Stochastic Approach to Study the Influence of Rate of Loading on Strength of Concrete, Heron (The Netherlands) 25, No. 3 (1980).
/9/ EDEN, N.B., MANTHORPE, A.R., MIELL, S.A., SZYMANEK, P.H., WATSON, K.L., Autoclaved Aerated Concrete from Slate Waste - Part 1: Some Property/Density Relationships, The International Journal of Lightweight Concrete 2, 95-100 (1980).

CEMENT and CONCRETE RESEARCH. Vol. 14, pp. 375-385, 1984. Printed in the USA.
0008-8846/84 $3.00+00. Copyright (c) 1984 Pergamon Press, Ltd.

STATISTICAL EVALUATION OF MECHANICAL PROPERTIES OF SUPERPLASTICIZED CONCRETE

G. Corradini, G. Scoccia, R. Volpe
Istituto di Chimica Applicata e Industriale, Università dell'Aquila (Italy)

S. Tavano
RUREDIL S.p.A., S. Donato Milanese (Italy)

(Communicated by F. Massazza)
(Received Oct. 7, 1983)

OL.
14
984

ABSTRACT

The paper discusses the statistical evaluation of the effects of cement content, water content and superplasticizer dosage on 3 day and 28 day compressive strength and the modulus of elasticity of a superplasticized concrete.

Introduction

Superplasticized concretes have been studied from a number of Authors (1-3).

The statistical approach is an interesting way to evaluate the physical and mechanical behaviour of a superplasticized concrete. The statistical approach must intervene not only to design the tests, but also to interprete the obtained results and define mathematical models, both on empirical and physical bases (4, 5).

In this paper we report the statistical evaluation of the effects of factors such as cement content (C), water content (W) and superplasticizer dosage (S) on 3 day and 28 day compressive strength, and the secant modulus of elasticity of a superplasticized concrete.

The present work has been performed on the basis of a factorial experiment (6). It is well known that the main advantages of a factorial design are:

- where there are no interactions among the factors, the factorial design gives the maximum efficiency in the estimation of the effects;
- when interactions exist, their nature being unknown, a factorial design is necessary to avoid misleading conclusions;
- in the factorial design the effect of a factor is estimated at several levels of the other factors and the conclusions hold over a wide range of conditions;
- by using this type of experiment it is possible to determine the most economic way of designing a set of experiments in order to obtain the required information.

Experimental part

The following materials were used:

Cement: Portland cement "425" (D.M. 3.6.1968, G.U. n. 180 17.7.1968)

Aggregates: alluvial aggregates, with maximum size 30 mm, furnished by the TEGES S.p.A. (L'Aquila). To make the mixture grading 3 fractions of aggregate were used. Two aggregate mixtures were employed respectively for the cement content 275 and 350 and 425 kg/m^3 of aggregate. This was done in order to mantain the undersize percentage to 0.25 mm (including the cement) within the range established by the Standards (DIN 1045, UNI 7163/79) (7).

Water: drinking water was used. The content was related to cubic metre of dry-surface saturated aggregate.

Superplasticizer: a commercial superplasticizer, "Fluiment", was employed, composed of an aqueous solution containing 37% in weigth of active substance, resulting from the mixing of a sulphonated melamine-formaldheyde condensate and a sulphonated naphthalene-formaldheyde condensate.

To carry out the factorial design cement content, water content and superplasticizer dosage have been considered at 3, 4 and 4 levels respectively; the tests were repeated twice. In particular, levels C_1= 275, C_2= 350 and C_3= 425 kg/m^3 of aggregate were chosen for cement content; for water content the levels were W_1=130, W_2= 150, W_3= 170 and W_4= 190 kg per cubic metre of aggregate; while for superplasticizer dosage the levels were S_1= 0, S_2= 0.5, S_3= 1.0 and S_4=1.5% by wt. of cement.

The considered factor variations cover the very wide fields of applications ranging from precasting industry to common work-yarde.

In order to carry out the above-mentioned programme of factorial experiment, it was necessary to make 3x4x4x2=96 mixtures.

The mixing of the constituents composing the various concrete mixtures was carried out by a laboratory pan mixer with a vertical axis. The concrete mixtures were manufactured in a room conditioned at 24±2°C and 70% RH.

Steel moulds were employed in the preparation of specimens, and the concrete was compacted so as to obtain the maximum density. The fluid and medium-consistent concretes were manually compacted by means of standardized rod. In case of low-workability concretes, the compacting of the specimens was obtained by means of a plate vibrator (SIMBI electromagnetic vibrator, 6000 vivrations per minute).

Four cubic and two prismatic specimens were made from each mixture, according to the Standard UNI 6130, and successively cured in a room conditioned at 20°C and 98% RH. Their demoulding took place 24 h after casting (UNI 6129).

Compressive strength was measured after 3 and 28 days, according to the Standard UNI 6132, by means of a 300 t hydraulic press.

The secant modulus of elasticity was measured after 28 days, at a peak load proof equal to 1/3 of 28 day compressive strength, according to the Standard UNI 6556, by means of a 300 t hydraulic press, connecting the strain gauge for the reading of strains with a HBM automatical data processing gearbox, model UPH 3200.

Results

The obtained results for 3 day compressive strength, 28 day compressive strength, 3 day compressive strength expressed as percentage of 28 day compressive strength and secant modulus of elasticity are reported, respectively, in tables n. 1, 2, 3 and 4.

Table 1
Experimental results: 3 day compressive strength (kg/cm^2)

		W_1			W_2			W_3			W_4		
		C_1	C_2	C_3	C_1	C_2	C_3	C_1	C_2	C_3	C_1	C_2	C_3
I_1	S_1	209	351	554	204	279	376	144	216	293	97	218	274
	S_2	259	331	524	210	362	374	179	248	334	115	206	268
	S_3	267	347	531	177	302	398	172	283	346	131	211	269
	S_4	268	384	464	184	335	390	159	281	358	124	225	239
I_2	S_1	211	356	575	208	266	379	127	213	295	83	207	277
	S_2	267	311	520	225	419	338	177	244	293	126	206	280
	S_3	268	333	530	161	299	355	172	284	377	139	208	243
	S_4	270	391	438	199	350	359	170	264	355	177	223	240

VOL.
14
1984

Table 2
Experimental results: 28 day Compressive strength (kg/cm^2)

		W_1			W_2			W_3			W_4		
		C_1	C_2	C_3	C_1	C_2	C_3	C_1	C_2	C_3	C_1	C_2	C_3
I_1	S_1	465	639	724	400	527	627	351	470	553	276	430	526
	S_2	462	624	718	410	533	601	381	459	539	258	438	488
	S_3	471	601	699	403	504	603	338	472	540	291	449	499
	S_4	470	640	703	404	507	600	305	468	551	274	450	478
I_2	S_1	474	657	737	413	541	646	330	481	548	249	400	536
	S_2	468	617	737	448	590	527	367	470	496	279	442	463
	S_3	470	570	687	375	534	547	331	457	565	310	441	486
	S_4	469	656	686	441	545	567	320	468	554	260	456	471

Table 3
Experimental results: 3 day compressive strength as percentage of 28 day compressive strength.

		W_1			W_2			W_3			W_4		
		C_1	C_2	C_3	C_1	C_2	C_3	C_1	C_2	C_3	C_1	C_2	C_3
I_1	S_1	44.9	54.9	76.5	51.0	52.9	60.0	41.0	46.0	53.0	35.1	50.7	52.1
	S_2	56.1	53.0	73.0	51.2	67.9	62.2	47.0	54.0	62.0	44.6	47.0	54.9
	S_3	56.7	57.7	76.0	43.9	59.9	66.0	50.9	60.0	64.1	45.0	47.0	53.9
	S_4	57.0	60.0	66.0	45.6	66.1	65.0	52.1	60.0	65.0	45.3	50.0	50.0
I_2	S_1	44.5	54.2	78.0	50.3	49.2	58.7	38.5	44.3	53.8	33.3	51.7	51.7
	S_2	57.0	50.4	70.6	50.2	71.0	61.8	48.0	51.9	59.1	45.2	46.6	60.5
	S_3	57.0	58.4	77.1	42.9	55.9	64.9	52.0	62.1	66.7	44.8	47.2	50.0
	S_4	57.6	59.6	63.8	45.1	64.2	63.3	53.1	56.4	64.1	45.0	48.9	50.9

Table 4
Experimental results: secant modulus of elasticity (t/cm^2)

		W_1			W_2			W_3			W_4		
		C_1	C_2	C_3	C_1	C_2	C_3	C_1	C_2	C_3	C_1	C_2	C_3
I_1	S_1	396	418	399	349	393	412	326	388	389	305	370	360
	S_2	378	420	430	355	397	427	276	357	406	300	345	368
	S_3	364	405	422	355	354	424	350	356	374	281	372	352
	S_4	376	400	429	380	391	381	314	365	380	320	346	370
I_2	S_1	367	416	424	353	389	415	322	384	377	303	376	352
	S_2	386	418	434	361	393	435	367	351	400	296	343	366
	S_3	354	399	438	357	352	418	370	351	364	289	380	360
	S_4	372	401	417	384	383	377	318	379	376	336	350	376

The first step in the interpretation of the results was to verify if the main effects and interactions of the various factors were estimated at an acceptable significance level (6). For this end an analysis of variance was performed to determine whether the relationships were significant at a level of significance $\alpha = 0.01$ (6 ,8) . The results of this analysis are shown in table n. 5.

Table 5
Analysis of variance.

Source of variation	3 day compressive strength		28 day compressive strength		secant modulus of elasticity	
	$F_{calc.}$	$F_{theor.}$ $\alpha=0.01$	$F_{calc.}$	$F_{theor.}$ $\alpha=0.01$	$F_{calc.}$	$F_{theor.}$ $\alpha=0.01$
C	1056.33	5.10	1038.34	5.10	182.86	5.10
W	498.68	4.24	504.49	4.24	133.47	4.24
S	5.38	4.24	4.20	4.24	4.32	4.24
CW	29.19	3.22	5.77	3.22	3.66	3.22
CS	8.72	3.22	5.14	3.22	4.76	3.22
WS	7.65	2.82	2.79	2.82	2.85	2.82
CWS	3.48	2.36	2.16	2.36	3.67	2.36

As can be observed by comparing the statistical F-values, all the effects, both the main ones and the interactions among them, are statistically significant at levels of significance $\alpha<0.01$. For this reason, it was not necessary to ticken the mesh of the levels of these factors and then to perform other tests.

The figures 1, 2 and 3 show the main effects of the factors C, W and S on 3 day compressive strength, 28 day compressive strength and secant modulus of elasticity.

The abscissae of the graphs cover, with the same space, the fields of variation experimented for the various factors. Each of the curves of the three figures represents the main effect of a factor when the effect of the two other factors is "averaged". Each curve was obtained by interpolating 3 day compressive strength or 28 day compressive strength or secant modulus of elasticity values, indicated in the figures with a dot, corresponding to the number of levels at which each factor was considered. Each of these values is in

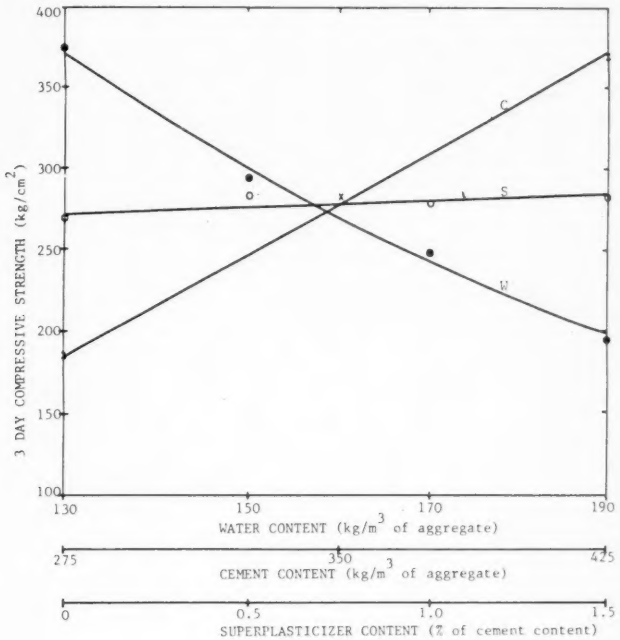

FIG. 1

Main effects of the factors C, W and S on 3 day compressive strength.

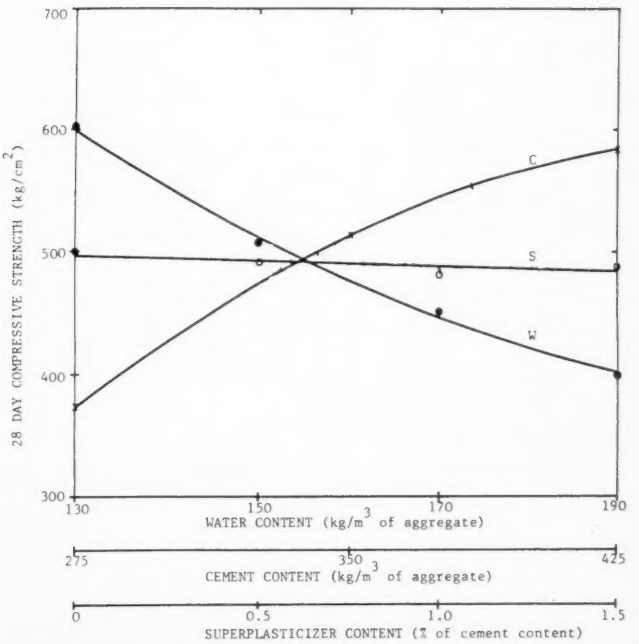

FIG. 2

Main effects of the factors C, W and S on 28 day compressive strength.

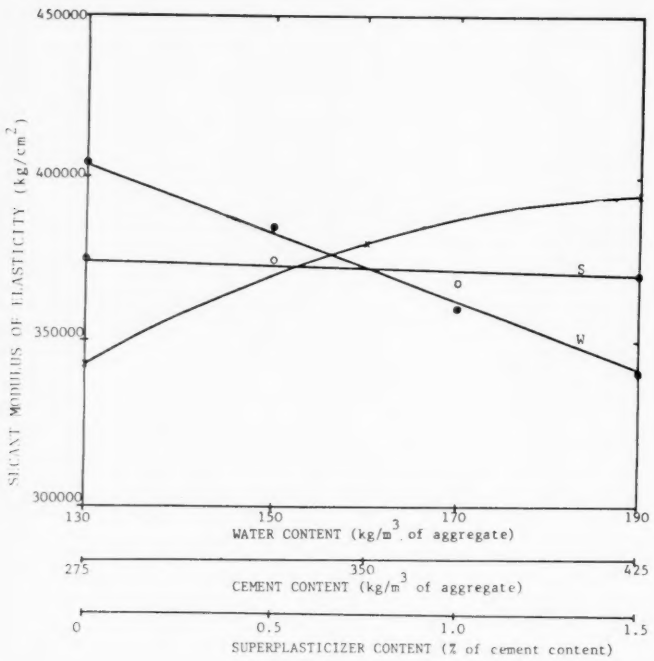

FIG. 3

Main effects of the factors C, W and S on the secant modulus of elasticity.

turn the average of a number of experimental values equal to the product of the number of the factor levels, including the iterates and excluding the factors whose effect is represented.

Thus, in the case of curves which represent the main effects of water content and superplasticizer dosage, each point, indicated by a dot, is the average of 4x3x2=24 experimental values, and, in the case of the cement content, of 4x4x2=32 experimental values.

The curves representing, in each figure, the shapes of the main effects have been obtained by interpolating the experimental mean values by means of the least squares criterion.

Examining the three figures we can note:

1 - 3 day compressive strength increases linearly with an increase in cement content while 28 day compressive strength and secant modulus of elasticity increase with parabolic shapes.

2 - 3 day and 28 day compressive strength decrease parabolically when water content increases, while the secant modulus of elasticity decreases almost linearly.

3 - Adding a superplasticizer practically does not bring sensible variations to 3 day and 28 day compressive strength and secant modulus of elasticity; only a slight positive influence on 3 day compressive strength and a slight negative influence on 28 day compressive strength, is noted.

4 - The shapes of the effects of the considered factors on the 3 measured properties, are similar enough, as it is intuitable, because of the relations between the compressive strengths and the secant modulus of elasticity.

In the interpretation of the graphs representing the effect of each single

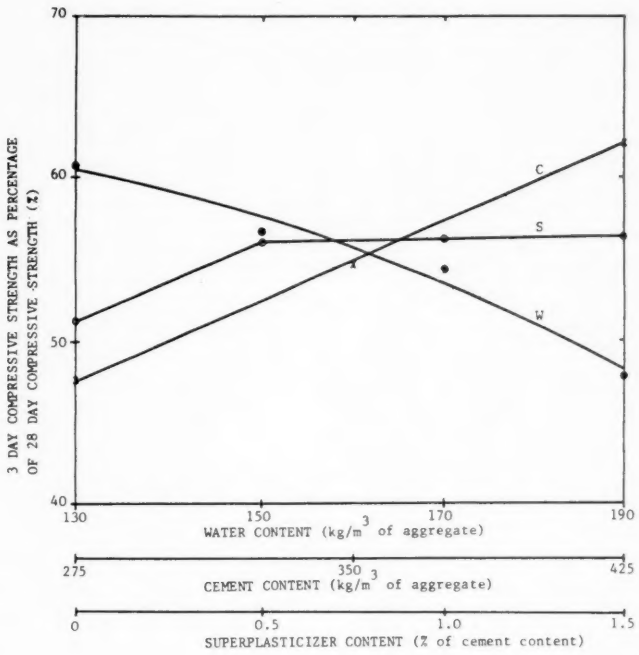

FIG. 4

Main effects of the factors C, W and S on 3 day compressive strength expressed as percentage of 28 day compressive strength.

factor, it must be born in mind that the effects of the two other factors are "averaged".

In fig. 4 the effects of the factors C, W and S on 3 day compressive strength expressed as percentage of 28 day compressive strength (see table 4) are reporetd with the same criteria.

The examination of fig. 4 shows that:

1 - the percentage increases linearly when cement content increases;
2 - the percentage decreases parabolically when water content increases;
3 - as regard to the main effect of superplasticizer dosage, we can note how the values of the percentage are practically the same in correspondence of $0.5 \leq S = 1.5$, while there is a difference in correspondence of S=0.

In order to see if the difference between the mean values of 3 day compressive strength expressed as percentage of 28 day compressive strength in correspondence of S=0 and $0.5 \leq S = 1.5$ is significant, a comparison by means of t-Student test was performed.

Comparing the two classes of experimental results, corresponding to S=0 and $0.5 \leq S=1.5$, a value of t=2.494 is obtained. This value is greater than $t_{0.01}(2.372)$. Therefore the above-mentioned difference is very significative.

In order to master this aspect and as examining table 3 it can be noted that the difference between the values of 3 day compressive strength, expressed as percentage of 28 day compressive strength, for S=0 and $0.5 \leq S=1.5$, changes as cement content changes, in fig. 5 the curves, showing the shapes of the percentage in function of superplasticizer dosage, are reported. Each curve has, as its parameter, cement content; the effect of water content is "averaged".

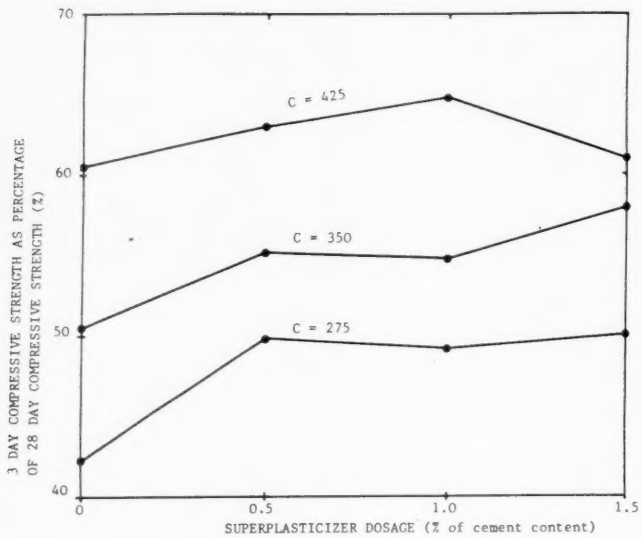

FIG. 5

Influence of superplasticizer dosage and cement content on 3 day compressive strength, expressed as percentage of 28 day compressive strength.

Examining fig. 5, it is evident that there is an interaction between the factors C and S in regard to 3 day compressive strength expressed as percentage of 28 day compressive strength.

To quantify the significance of this interaction, a comparison, by means of t-Student test, between the means of the percentages relating to S=0 and $0.5 \leq S=1.5$ connected with C=275 kg/m^3 of aggregate, was made.

A value of t equal to 3.306 was obtained. This value is greater than $t_{0.005}(2.750)$. Therefore the difference between the means of the values of 3 day compressive strength as percentage of 28 day compressive strength with S=0 and $0.5 \leq S=1.5$ is very significant.

The significativity of this difference gradually decreases as cement content increases; it become significative enough (t=2.288 corresponding to a confidence level $\alpha = 0.025 - t_{0.025}=2.042$) connected with C=350 kg/m^3 of aggregate and nul with C=425 kg/m^3 of aggregate.

To confirm all that above said, other tests were carried out, taking into account cement contents out off the range experimented variation field. In particular the contents C_0=225 and C_4=475 kg/m^3 of aggregate were considered.

The C_0 cement contents were considered at levels of water content W_1=130 and W_2=150 kg per cubic metre of aggregate, while the C_4 cement contents at levels W_3=170 and W_4=190 kg per cubic metre of aggregate.

The tests were carried out following the same above-mentioned criteria.

The results are reported in table 6, where:

R_3= 3 day compressive strength;

R_{28}= 28 day compressive strength;

% = 3 day compressive strength as percentage of 28 day compressive strength.

First of all we have verified if the main effect of superplasticizer dosage on R_3, R_{28} and 3 day compressive strength expressed as percentage of 28

VOL. 14 1984

Table 6

Experimental results of the additional tests.

		C_0						C_4					
		W_1			W_2			W_3			W_4		
		R_3	R_{28}	%	R_3	R_{28}	%	R_3	R_{28}	%	R_3	R_{28}	%
I_1	S_1	171	428	40.0	154	351	43.9	358	551	65.0	309	567	54.5
	S_2	176	379	46.4	155	375	41.3	369	584	63.2	318	540	58.9
	S_3	184	398	46.2	152	361	42.0	409	593	69.0	338	571	59.2
	S_4	151	352	43.3	133	332	40.2	362	601	60.2	319	586	54.4
I_2	S_1	149	412	36.2	144	343	42.0	358	540	66.3	313	564	55 5
	S_2	180	381	47.2	167	385	43.4	367	593	61.9	311	516	60.3
	S_3	178	397	44.8	148	357	41.4	398	587	67.8	336	540	62.2
	S_4	171	388	44.2	134	328	40.9	379	612	61.9	315	551	57.2

day compressive strength was altered by these results in comparison to what reported in figs 1, 2 and 4. The results shown in table 6 confirm entirely the shapes and the conclusions previously obtained.

Then we have estimated the significativity of the difference between R_3 as percentage of R_{28} in correspondence of superplasticizer dosages equal to S=0 and $0.5 \leq S \leq 1.5$ taking into account, also, the results of further tests.

We have obtained a t value equal to 2.336 corresponding to a significance level $\alpha < 0.025$ ($t_{0.025}=1.980$; $t_{0.01}=2.358$) confirming the significativity of the above-said difference.

A comparison between R_3 expressed as percentage of R_{28} in correspondence of C_0 and C_4 cement contents was, also, carried out.

A value of t equal to 1.939, corresponding to a significance level $\alpha<0.05$ ($t_{0.05}=1.761$), was obtained for C_0, while a value of t equal to 0.385 was obtained for C_4, making nul the significativity.

A lot of works have been published about the mechanism of action of superplasticizer (1 , 13,14) ; in these works some hypothesis, which still leave many doubts and perplexities, are reported.

The obtained results, could confirm, in a different way (that is in statistical manner), what some Authors (2 , 9, 10, 11) have supposed, that is the mechanism of action of a superplasticizer containing melamine resins is related to the formation os insoluble calcium salts of the melamine solphonated which are deposited on the cement granules.

The formation of these compounds bucks to the agglomeration of the cementitious particles, promoting a better dispersion of them in the aqueous medium. To this mechanisme is added to one, due to the sulphonated naphthalene-formaldheyde condensate that, though they don't give rise to insoluble calcium salts, fix around the cement granules charging them negatively with a consequent reciprocal electrical repulsion.

Moreover, the molecules of the polyelectrolyte, in relation to their right sizes which are determined by a correct grade of condensation during the process of syntesis, wrapping up the cement granule, determine a further impediment of physical nature, but not electrical one, to agglomeration. This impediment helps, in a significant manner, to disperse the cementitious particles.

As we have noted from numerous experimental tests and literature (12), this barrier around the cement granules can cause delays in the hydration more or less marked in function of the chemical nature of superplasticizer, of the length of hydrophobe chain, and, naturally, of its dosage.

Nevertheless, with a correct molecular weight (it should be around 20000 for melamine derivates (9) and around 1500 for naphtalene sulphonated compounds (12)), this delay is normally restricted at level of the setting time of the cement paste, so obtaining an increase of strengths, already at brief curing, as noted during our 3 day tests.

These increases of 3 day compressive strengths expressed as percentage of 28 day compressive strength, can be explained supponing a more uniform hydration of the cement paste homogeneously dispersed from the superplasticizer.

In fact, as we can note from fig. 5 and from the results shown in tables 3 and 6, a further acceleration of 3 day strength is compensated by the barrier effect that retards ulteriorly the reaction of hydration, increasing the dosage of the superplasticizer, that is $0.5 < S < 1.5$.

Further-more, as it can be noted from fig. 5, the dispersing effect results more marked in correspondence of lowest cement contents.

To conclude, the reaching of a determined value of mechanical strength at brief curings in a superplasticized concrete, is regulated, moreover, by the balancing of two phenomena: a better dispersion of cementitious particles which has an accelerating action and the barrier effect, function of the superplasticizer type and its dosage, which has, on the contrary, a delaying effect.

VOL
14
198

Conclusions

Examining the results we can draw the following conclusions:

1 - the influence of superplasticizer on 3 day compressive strength, 28 day compressive strength and secant modulus of elasticity is practically nul; only a slight positive influence on 3 day compressive strength and a slight negative influence on 28 day compressive strength is noted.

2 - If 3 day compressive strength is expressed as percentage of 28 day compressive strength, we can note how the difference between the means of the values with $S=0$ and $0.5 \leq S=1.5$ is significant.

3 - The above-mentioned difference (point 2) depends on the level of cement content and its significance decreases as cement content increases.

4 - The statistical way of inquiry adopted would seem to confirm the hypothesis of the dispersing effect of superplasticizers containing melamine resins.

5 - The adopted method of experimentation and elaboration of the data confers a high confidence level on the obtained results. Besides these results constitute a valid basis for the definition of mathematical models of the behaviour of a superplasticized concrete.

Notation

C	cement content
C_i	ith level of cement content
$F_{calc.}$	calculated F-value
$F_{theor.}$	theoretical statistical F-value

I_i	ith level of iterate
R_3	3 day compressive strength
R_{28}	28 day compressive strength
S	superplasticizer dosage
S_i	ith level of superplasticizer dosage
t_i	t-Student value at confidence level i
W	water content
W_i	ith level of water content
α	confidence level

References

1. Superplasticizers in concrete, ACI Publication SP-62, Detroit (1979).
2. F. Massazza, M. Testolin, Il Cemento, 3, 73 (1980).
3. M. Collepardi, Scienza e tecnologia del calcestruzzo, 346, Hoepli, Milano (1980).
4. G. Corradini, G. Scoccia, R. Volpe, M. Bastianoni, Il Cemento, 3, 127 (1979).
5. G. Corradini, G. Scoccia, R. Volpe, M. Bastianoni, Il Cemento, 1 (1982).
6. O.L. Davies, P. Goldsmith, Statistical methods in research and production, 247, ICI (1972).
7. A. Meyer, Experiences in the use of superplasticizers in Germany, Superplasticizers in concrete, ACI Publication SP-62/2, Detroit (1979).
8. D.M. Himmelblau, Process analysis by statistical methods, John Wiley, New York (1968).
9. A. Aignesberger, Th. Rey, W. Schrämli, Zement-Kalk-Gips, 7, 297 (1969).
10. A. Rauen, Cem. Concr. Res., 1, 57 (1976).
11. J. Bonzel, E. Siebel, Beton, 1, 2 (1974).
12. R. Kondo, M. Daimon, E. Sakai, Il Cemento, 3, 225 (1978).
13. F. Massazza, Admixtures in concrete. Advances in cement technology, Pergamon Press (1983).
14. Developments in the use of superplasticizers, ACI Special Publication SP-68 (1981).

OL.
14
984

CEMENT and CONCRETE RESEARCH. Vol. 14, pp. 386-396, 1984. Printed in the USA.
0008-8846/84 $3.00+00. Copyright (c) 1984 Pergamon Press, Ltd.

CONDITIONS AND MECHANISM OF INTERCONVERTIBILITY OF COMPOUNDS $12CaO.7Al_2O_3$ AND $5CaO.3Al_2O_3$

G.I. Zhmoidin
Baikov Institute of Metallurgy
Academy of Sciences, Moscow, USSR

and

A.K. Chatterjee
The Associated Cement Companies, Ltd.
Central Research Station
Thane, Maharashtra 400604, India

VOL. 14 1984

(Communicated by D.M. Roy)
(Received May 5, 1983; in final form March 6, 1984)

ABSTRACT

Based on a critical analysis of the data reported in the literature and our own experimental studies relating to the melt and glass formation from compositions corresponding to $12CaO.7Al_2O_3$ under various atmospheric conditions, the liquid structure of the melt phase and conditions for stabilization of $12CaO.7Al_2O_3$ and $5CaO.3Al_2O_3$ in crystalline state have been highlighted. The role of "stabilizers" like O^{2-}, F^-, Cl^-, S^{2-} for the crystalline structure of $12CaO.7Al_2O_3$, effect of temperature and atmosphere on melt structure and properties, and conditions favouring the appearance of $12CaO.7Al_2O_3$ and $5CaO.Al_2O_3$ crystalline phases from the given melt have been specifically dealt with.

Introduction

The calcium aluminates $12CaO.7Al_2O_3(C_{12}A_7)$ and $5CaO.3Al_2O_3(C_5A_3)$ are of immense practical significance in the fields of cement technology and metallurgy. While all the initial crystallochemical and structural studies (1-5) of these two aluminates revealed that they are two distinct phases having well-defined structure and stoichiometry, the conditions of their interconvertibility or individual stability were not firmly established. Further, the metallurgical studies relating to the melts of these compositions had methodological variations resulting in divergent data. In addition, there has been limited effort to correlate the melt properties and structure of these aluminates with their characteristics in glassy and crystalline states. The present paper is an attempt to fill up some of these gaps in the existing perception of these two compounds with special reference to the conditions of their interconvertibility.

Crystallochemical Characteristics

The crystal symmetry of $C_{12}A_7$ is reported to be T_d^6 ($I\bar{4}3$ d) (3). The unit cell is made up of 4 molecules having the formula $Ca_{24}Al_{28}O_{66}$, in which 64 atoms of oxygen are accounted for and the balance two are located "statistically." Because of this structural peculiarity, the following specific features have been observed for $C_{12}A_7$ (7-16).

(a) It is zeolitic in nature, having the capacity to absorb up to 1.3% H_2O from the furnace atmosphere of normal humidity at 950°-1350°C with the formation of $C_{11}A_7Ca(OH)_2$, which is accompanied with contraction of unit cell and increases in density.

(b) It can also form derivatives like $C_{11}A_7CaCl_2$, $C_{11}A_7CaF_2$ and $C_{11}A_7CaS$.

(c) The anhydrous $C_{12}A_7$ is stable with absorption of 0.07 - 0.10% excess oxygen (15) which is in agreement with the conditions found conducive for growth of $C_{12}A_7$ monocrystals (6).

The structural data furnished by different authors (3, 9-10, 17-20) on $C_{12}A_7$ and its various derivatives are summarized in Table 1.

Table 1

Structural Parameters of $C_{12}A_7$ Crystals and its Derivatives

Position of Peaks	Ref. (3)	Ref. (9,10)	Ref. (17)	Ref. (18)	Ref. (19,20)
48e(x,y,z)	O_2	-	-	O_1	O_1
24d(x,o, 1/4)	Ca	-	-	Ca,O_3	Ca_1,Ca_2
16c(x,x,x)	Al_1, O_1	-	-	O_2, Al	O_2, Al_2
12b(7/8, 0,1/4)	-	-	-	Al_2	F
12a(3/8, 0,1/4)	Al_2	-	-	-	Al_1
Symmetry	$I\bar{4}3d$	-	$I\bar{4}2d$	$I\bar{4}3d$	$I\bar{4}3d$
Crystal	$C_{12}A_7$	$C_{11}A_7$ $CaCl_2$	$C_{11}A_7$ $Ca(OH)_2$	$C_{12}A_7$	$C_{11}A_7$ CaF_2

On the other hand, the structural details of C_5A_3 are reported in (4,5). Its symmetry is $CmC2_1$ and the unit cell has 4 molecules ($Ca_{20}Al_{24}O_{56}$).

From the above crystallochemical data the following tentative observation can be made:

(a) $C_{12}A_7$ (with $I\bar{4}3d$, 2.69 g/cm) has a defect structure which helps in stabilizing its derivatives.

(b) Conditions of synthesis may alter the symmetry from $I\bar{4}3d$ to $I\bar{4}2d$. The anhydrous form is stable only under conditions of higher oxidation potential that ensures the presence of excess oxygen in the crystals.

(c) It is possible that under conditions of deficit oxygen $C_{12}A_7$ is unstable and C_5A_3 phase stabilizes with denser (3.03 g/cm^3) orthorhombic structure.

Characteristics of the Melt Phase

The transition of crystalline $C_{12}A_7$ into a melt phase is anomolous in the sense that its melting temperature ranges from 1380°C to 1415°C (14). The melt density (2.75 g/cm^3) is higher than the crystal density (2.68 - 2.69 g/cm^3) (21, 22). The viscosity variation of the melt at higher temperatures is also unusual (23); the activation energy of the viscous flow shows a sudden change at a transition temperature of 1500°C. Experimentally this effect is well reproducible near C/A = 0.91 - 0.99. When the temperature is brought down below 1500°C with samples having C/A = 0.99, the activation energy increased from 60 $\pm$ 4 to 108 $\pm$ 17 K-Cal/mole and with samples having C/A = 0.91 it increased from 45 $\pm$ 5 to 80 $\pm$ 8 K-Cal/mole.

Further, it has also been observed that $C_{12}A_7$ crystals that absorb 1.3% H_2O from the furnace atmosphere at 950°C - 1350°C shows reversibility in the gain and loss of weight before melting and the reversibility is lost on melting. After melting, crystals lose only 0.8% from 1.3% original weight increase (11), signifying that a substantial amount of water is retained in the melt. It has also been observed that the gas bubbles evolved from the crystals on melting are re-absorbed by the crystals on cooling (8).

Hypothetical Structural Model of the Melt Phase

The assumption of stability of Al-O network structure in calcium aluminate melts is well known and is based on the presence of similar network in crystalline substances. The increase in activation energy of the viscous flow of the melt below the transition temperature of 1500°C, as mentioned above, can be explained by complexing of network before crystallization. According to (24), this change in activation energy can be related to polymerization of Al-O anions of tetrasilicate type, which, in accordance with the theory of discrete anions of Bockris (25), is represented by a 4-layer packet of rings one lying on the other as schematically illustrated in Fig. 1. Similar structures have been experimentally observed in crystalline silicates (26).

The pre-crystallization complexing of calcium aluminate melt structure, described as a phase transformation of second order (27), in the present case may either be explained by change of co-ordination of Al atoms from 4 to 6 above 1500°C (24) or by ordering of network structure without change of co-ordination (28).

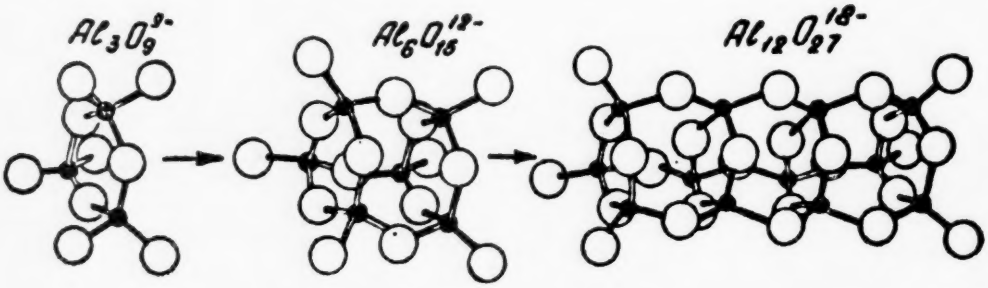

FIG. 1

Polymerization (after Bodkris) of flat three-chain Al-O rings of three-dimensional structures of di- and tetrasilicate type. The small and big circles represent aluminium cations and oxygen anions respectively. The four-chain rings polymerize in a similar way.

In the present case if the polymerization of the melt structure is presumed to proceed with the formation of three-dimensional n-layer packets of k-chain rings as depicted in Fig. 1, then in each packet having the general formula $Al_{kn}O(2kn + k)$ the stoichiometric ratio of O/Al is equal to $(2n + 1)/n$, which means that the stiochiometry is determined by the number of layers n in the packet, irrespective of the number of chains k in the ring. For the aluminate composition having 60 mole % CaO (i.e. 60 CaO.40 Al_2O_3) which shows the change in viscosity characteristics, we have O/Al = 2.25 and n = 4. Therefore, from pure geometric considerations, a tetra-anion is obtained. The simplest tetra-anion is represented by a 4-layer prism with a ring having k number of chains as the base. In 4- and 5- chain rings, the inside cavity (d_o = 1.6Å) does not exceed the size of oxygen atom but in 6-chain rings the cavity size increases to 2.8Å which matches with the size of oxygen atom (29). When the cavity size exceeds that of oxygen, the stability of such a structure will come down. In such a situation, the presence of larger anions that are capable of filling up such structural cavities helps to stabilize the structure.

In the present case of $C_{12}A_7$ melt the abrupt rise in activation energy of the viscous flow on cooling the melt below 1500°C apparently denotes gradual complexing of structure. This is facilitated by reduction in thermal shock with decrease in temperature and also by the presence of larger anions that are capable of filling up the structural cavities. A similar concept may explain the role of higher oxidation potential of the atmosphere for the growth of loose crystals of $C_{12}A_7$ instead of dense crystals of C_5A_3.

OL.
14
984

Experimental Verification of Melt Structure

Study of Melt Density

The melt density of $C_{12}A_7$ composition was studied in both reducing and oxidizing atmospheres. The first experiment was carried out under reducing conditions by using molybdenum crucibles in a furnace having graphite heating elements and argon atmosphere with oxidation potential of $P_{O_2} < 10^{-13}$ atm (the surface of molybdenum crucible became silver white on heating). The second experiment was carried out under oxidizing conditions in platinum crucibles, when the working chamber of the furnace was separated from the graphite heating element by an alumina tube, inside which argon or a mixture of argon with 20% O_2 was blown.

The sample used for the experiments was the melt of $C_{12}A_7$ composition, which was preliminary soaked at 1500°C for 7 hours under the reducing conditions and crystallized in the crucible and kept in air for 2 days. After using this sample in the first experiment, the same material, crystallized in a crucible and kept in air for a week, was utilized for the second experiment.

In both the experiments the measurements were carried out in accordance with the procedures given in (21,22) by dipping capillary tubes to depths of 0-4 and 4-10 mm (Fig. 2). The density measurements had an error of 0.2%. In both the experiments immediately on melting the surface layer was less dense than the rest of the melt volume. But under the oxidizing conditions the situation is maintained for a longer period than under the reducing conditions. Later, under the oxidizing conditions the density of the surface layer rose to 2.738 g/cm^3, while that of the surface layer under reducing conditions rose rapidly to 2.788 g/cm^3 exceeding the density of the inner layer by 0.04 - 0.12 g/cm^3 which is beyond the limits of experimental error. A high density at the surface layer as compared to the lower depths, compelled us to consider the melt as a dynamic mix of areas with varying density, forming as a result of deficit oxygen.

In the oxidizing experiment the drastic decrease in melt density in argon (below the density of the crystal) (Fig. 2) is explained by the evolution of

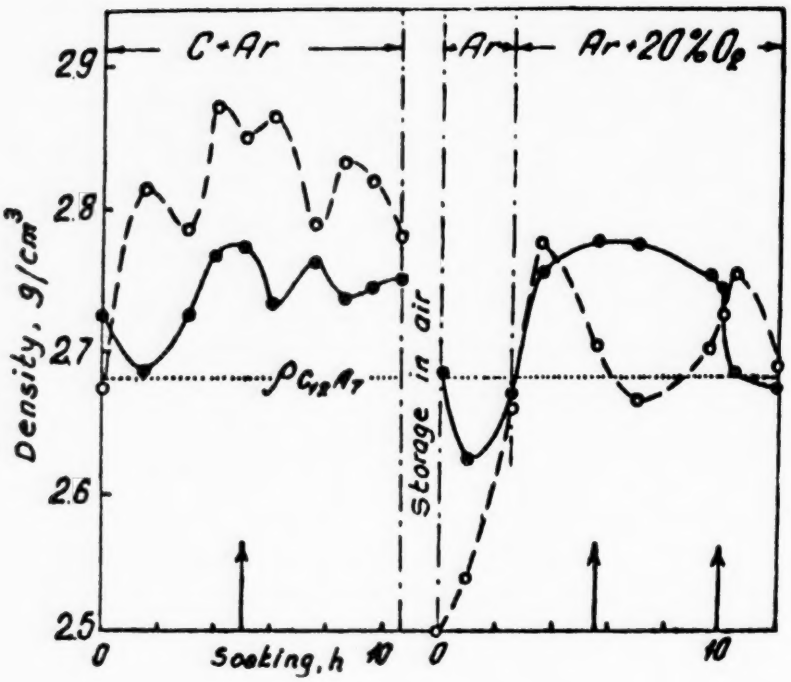

FIG. 2

Change in density of the $C_{12}A_7$ melt, when kept in different atmospheres. The solid lines show density of the layer at 4 - 10 mm depth and the dashed lines represent density of the surface layer (0 - 4 mm).

gases present in the crystals. It was only after 2-3 hours long soaking in argon that the melt came to a relative equilibrium: the densities at depth and at the surface were equilibrated, exceeding the density of the crystal and attaining an average value of 2.76 g/cm^3. However, after 2 hours feeding of argon-oxygen mixture to the furnace, the melt surface density again decreased to the crystal density and subsequently the density of deeper layers started decreasing. This process can be explained by the absorption of oxygen by the melt, which diffused from the surface without formation of bubbles due to the development of cellular structure areas in the melt, which were close in structure to crystalline $C_{12}A_7$.

Rapid crystallization of the melt under oxidizing conditions with subsequent melting (arrows in Fig. 2) resulted in a decrease in the melt density to the density values of the crystal. In the first case it happened only at the surface and in the second case, at lower depths. A similar operation under reducing conditions gave a substantially lower effect and the density of the melt never decreased to that of the crystal. It was consistently observed that the temperature variation with time of the experiment in the range of 1450°-1550°C affected the melt density less than the atmosphere or the soaking time. That is why the melt temperature measurements are not shown in Fig. 2.

VOL. 14 1984

Study of Glass Formation

The possibility of obtaining glass from the melt of $C_{12}A_7$ was first reported in (1,2) but the glass was studied later (3, 30). The glass was obtained under arbitrary conditions of melting in an oxygen flame with quenching of glass bead in water. It was established that the glass has higher density 2.87 - 2.91 g/cm^3 and refractive index 1.668 $\pm$ 0.005 than the corresponding crystal (2.69 g/cm^3 and 1.608).

While measuring the viscosity of $C_{12}A_7$ melt (23), an attempt was made to obtain glass at temperatures above and below 1500°C by congealing the melt on a water-cooled copper tube that ensured a rate of quenching of more than 300°/sec. From the melt kept in graphic crucibles at 1600°C a homogeneous transparent glass was easily obtained but below 1500°C the congealed layer was always microcrystalline.

The next attempt to obtain glass from temperature fields below 1500°C was made by using thin-walled hermetic platinum capsules (14), which raised the quenching rate to over 500°/sec. and eliminated the contact of melt with the furnace atmosphere. In samples quenched at 1380°C original unmelted crystals were present and in the temperature interval of 1380°-1415°C they co-existed with an isotropic substance having a refractive index of 1.634. Above 1415°C the original crystals were absent in the glass but right up to 1450°C quench crystals of $C_{12}A_7$ were regularly observed. The quench crystals could be easily differentiated from the original crystals by virtue of their cracked appearance. Only on quenching at temperatures above 1450°C a homogeneous glass with 1.671 refractive index was obtained. However, as in (30), the homogeneous glass showed x-ray diffraction lines corresponding to $C_{12}A_7$ phase.

A new experimental study, described below, was conducted to study the effect of furnace atmosphere and soaking time on the glass formation. At 1600°, 1550° and 1500°C, the soaking time was varied from 15 to 90 min. under three different atmospheric conditions: in open graphite crucibles, in graphite crucibles with screw-in lids and in platinum crucibles in air. The quenching rate in all the cases did not exceed 100°/min. In closed graphite crucibles the atmosphere was defined by the equilibrium with graphite ($P_{O_2} = 10^{-22}$ atm). In platinum crucibles in air P_{O_2} = 0.21 atm. With open graphite crucibles the atmosphere was of intermediate nature and corresponded to the conditions of viscosity measurements (23). The products were analyzed by optical microscopy and x-ray diffractometry. For single phase specimens the density was determined by hydrostatic weighing.

In open graphite crucibles (Table 2 and Fig. 3), even 15 min. soaking at temperatures above 1500°C is adequate to obtain a homogeneous glass with 1.670 refractive index and 2.96 - 2.98 g/cm^3 density. On quenching from 1500°C after soaking for up to 45 min. the melt crystallized into microstalline $C_{12}A_7$ (n = 1.609 and ρ = 2.64 - 2.74 g/cm^3) containing numerous inclusions of glass and C_5A_3. With further increase in soaking time it was possible to increase the glass fraction but it had a layered structure: the upper part of the column contained $C_{12}A_7$ crystallites, the lower part showed transparent glass and the intermediate portion consisted of a mixture of crystallites of $C_{12}A_7$ and C_5A_3 and glass. Along the graphite crucible walls the surface layer was that of glass saturated with gas bubbles and on the open surface there was a foamy layer of finely crystalline $C_{12}A_7$, which was never observed on heating the melt to 1600°C.

In closed graphite crucibles the homogeneous glass was obtained at lower temperatures with shorter soaking time. At 1500°C the homogeneous glass was obtained after 30 min. soaking time, but with soaking times up to 15 min. a double layer structure was observed for the glass.

Table 2

Glass Formation from Melts Kept in Open Graphite Crucibles

Temperature °C	Soaking time, t, for the melt			
	0.25	0.50	0.75	1.0
1600	Glass	Glass	-	Glass **
1550	Glass	Glass	-	Glass
1500	$C_{12}A_7$	$C_{12}A_7$	$C_{12}A_7$+ Glass	$C_{12}A_7$ + Glass
1500 *	$C_{12}A_7$ + Glass	Glass	-	Glass **

* Closed graphite crucible
** Steady crystallization of C_5A_3 on slow cooling

Two melts that gave homogeneous glass on quenching were cooled at the rate of 15°/min. for crystallization and C_5A_3 crystals were obtained with n = 1.683 and ρ = 3.03 g/cm^3 (open crucible, 1600°C, 1 hour soaking and closed crucible, 1500°C, 1 hour soaking). Further, C_5A_3 crystals, when melted in open crucibles and quenched after 15 min. soaking at 1500°C, coverted fo finely crystalline $C_{12}A_7$ but after being overheated at 1600°C for a short while and kept in an open crucible at 1500°C for 1 hour, $C_{12}A_7$ crystals reconverted to C_5A_3 (Fig. 3).

Slow cooling of the melt in air in platinum curcibles either from 1500°C or 1600°C always led to the appearance of $C_{12}A_7$ crystals.

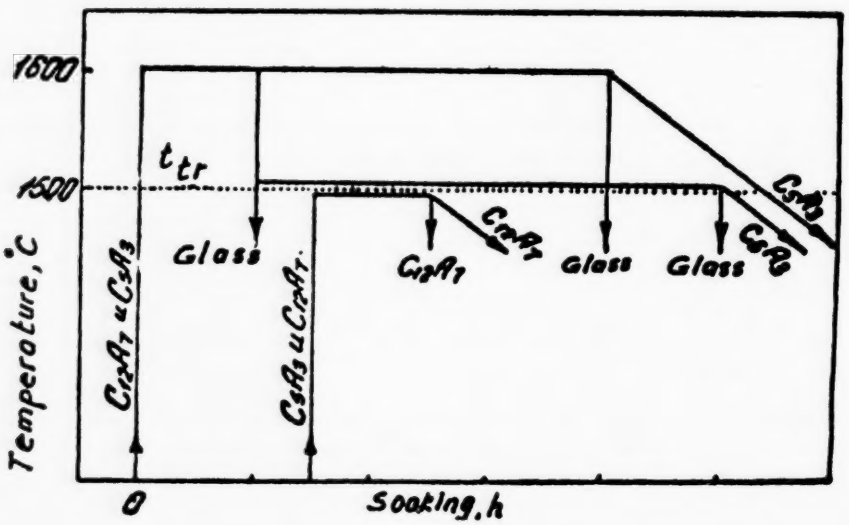

FIG. 3

Mutual transformations of $C_{12}A_7$, C_5A_3 and glass depending on the conditions of heat treatment of the specimens in open graphite crucibles.

Discussion of Results

A comparison of the results of the above mentioned combined study of the melt and glass formation with crystallochemical data confirms the earlier conclusion (21, 24, 31) regarding the double-structure nature of the melt that enables one to change the experimental conditions to crystallize either the cellular crystals of $C_{12}A_7$ or dense crystals of C_5A_3 or to quench it to a dense homogeneous glass. Based on the above-mentioned model of melt structure, the structural metamorphosis in the process of heating and melting of $C_{12}A_7$ crystals and the behaviour of the obtained melt on overheating and subsequent cooling are described below.

On heating the original $C_{12}A_7$ crystals before melting, gases are evolved from the loose zeolitic structure reversibly without destroying the crystal network. Only on approaching the melting temperature this network starts restructuring itself to denser structures of the type CA, C_3A and C_5A_3. This process, depending on the presence of microimpurities in the cavities of the original structure, leads to the melting of $C_{12}A_7$ crystals in the temperature interval of 1380° - 1415°C with intense gas evolution resulting in foaming of the melt. However, even after complete melting and removal of gas bubbles, the melt retains a part of "structural" gases in equilibrium with the furnace atmosphere, which enables the melt to retain a relict short-range order corresponding to the original $C_{12}A_7$ crystal. These micro-fields are the ready-made centres of crystallization and ensures a high growth rate of $C_{12}A_7$ crystals even with small super cooling as noticed by many investigators. At all rates of cooling of the melt these nucleii hinder the formation of a homogeneous glass and on quenching give a conglomerate of amorphous and finely crystalline areas having an intermediate refractive index. Even an otpically homogeneous glass gives x-ray diffraction lines corresponding to $C_{12}A_7$ phase.

VOL.
14
984

As a result of this peculiarity, the obtained melt is represented by a double-structure liquid consisting of microfields of "dense" and "cellular" structures. Their ratio depends on the external conditions and can be altered by removing from or adding to the melt stabilizing oxygen containing gases. Through removal of "structural" gases by raising the temperature, by applying vacuum or by holding the melt in reducing conditions, one may destroy the relict elements of $C_{12}A_7$ structure and obtain a homogeneous melt that can be quenched to a homogeneous glass or crystalline C_5A_3.

In order to obtain crystalline structure of $C_{12}A_7$ type from the melt, it is necessary to incorporate in it "modifiers" that are capable of initiating the development of nucleii for the "cellular" structure. This condition is fulfilled when the melt absorbs gases from the atmosphere (O_2, H_2O, CO_2, CO, SO_3) or when CaF_2, $CaCl_2$, CaS, $CaSO_4$, $CaCO_3$, etc., are added to the melt. In the first case $C_{12}A_7$ crystals, stabilized by gases, are crystallized and in the second case, one obtains derivatives of this compound.

Depending on the external conditions (viz., the composition of microimpurities, pressure, atmosphere, etc.) there is a temperature level, above which the "cellular" structural groups become metastable and decompose after a period of soaking, thus bringing the melt in equilibrium with the surrounding environment. In accordance with the concepts of Ubbelode (28), the temperature level of such structural transformation can occur below or above the melting temperature. A highly sensitive and simple method of detecting it, if it lies above the liquidus, is viscosimetry. This is indicated in Fig. 4, in which the transition temperature (t_{tr}) and liquidus temperature (t_l) obtained from the viscosimetric data (23) for sections C/A = 0.99 and 0.91 are juxtaposed with the section of the phase diagram $C_{12}A_7$ - CaS taken from Fig. 5. For the conditions of measurement (23) (open graphite crucibles), the transition temperature of 1500°C occurs

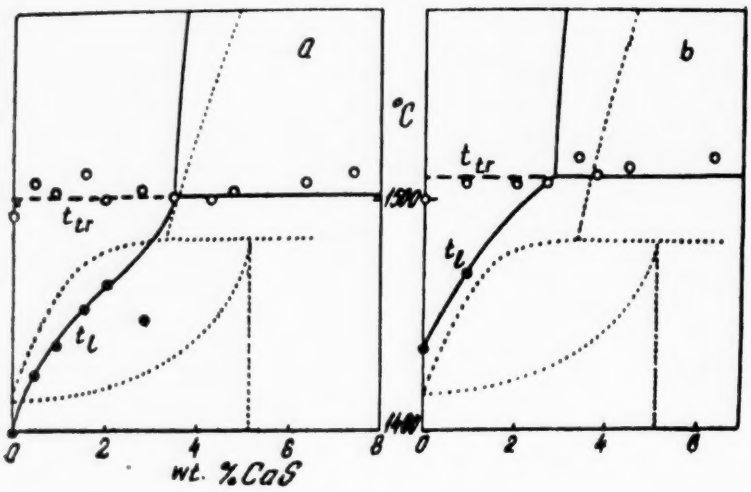

FIG. 4

Partial phase diagram of the system $CaO-Al_2O_3-CaS$ along lines CaO/Al_2O_3 = 0.99 (a) and 0.91 (b). The viscosimetric data (18) in solid lines are compared with the results of Fig. 5 (dotted lines).

above the liquidus t_l = 1415°C and agrees well with the results obrained from glass formation under the same conditions (Fig. 3). If the glass formation is carried out under more reducing conditions (closed graphite crucibles) the temperature is decreased and in oxidizing conditions (platinum crucibles in air) it is increased.

Other external conditions remaining the same, the stability of "cellular" structures, stabilized by gases, is lower than the structure of derivatives, stabilized by halogens and sulphur. It is evident from Fig. 5, the derivatives of this structure have a sharp melting point and possess all signs of being separate compounds, $C_{11}A_7CaF_2$ being a congruently melting one and $C_{11}A_7CaS$ being an incongruently melting type. Both these derivatives form a continuous solid solution series with the original compound. The physical characteristics of crystals of these compounds, as obtained by us, are given in Table 3.

The removal of stabilizing additives from $C_{12}A_7$ compound or its melt leads to densification of the structure with the formation of C_5A_3 and, in some cases, a mixture of C_5A_3, CA and C_3A. How to depict it in a phase diagram still remains problematic.

Table 3

Comparative Characteristics of Crystalline Phases

	Refractive Index	Density g/cm^3	Hardness H_B, kg/mm^2	Nature of melting
$C_{12}A_7$	1.608	2.683	1000	Anomalous
$C_{11}A_7CaF_2$	1.602	2.715	700	Congruent
$C_{11}A_7CaS$	1.643	2.619	1100	Incongruent

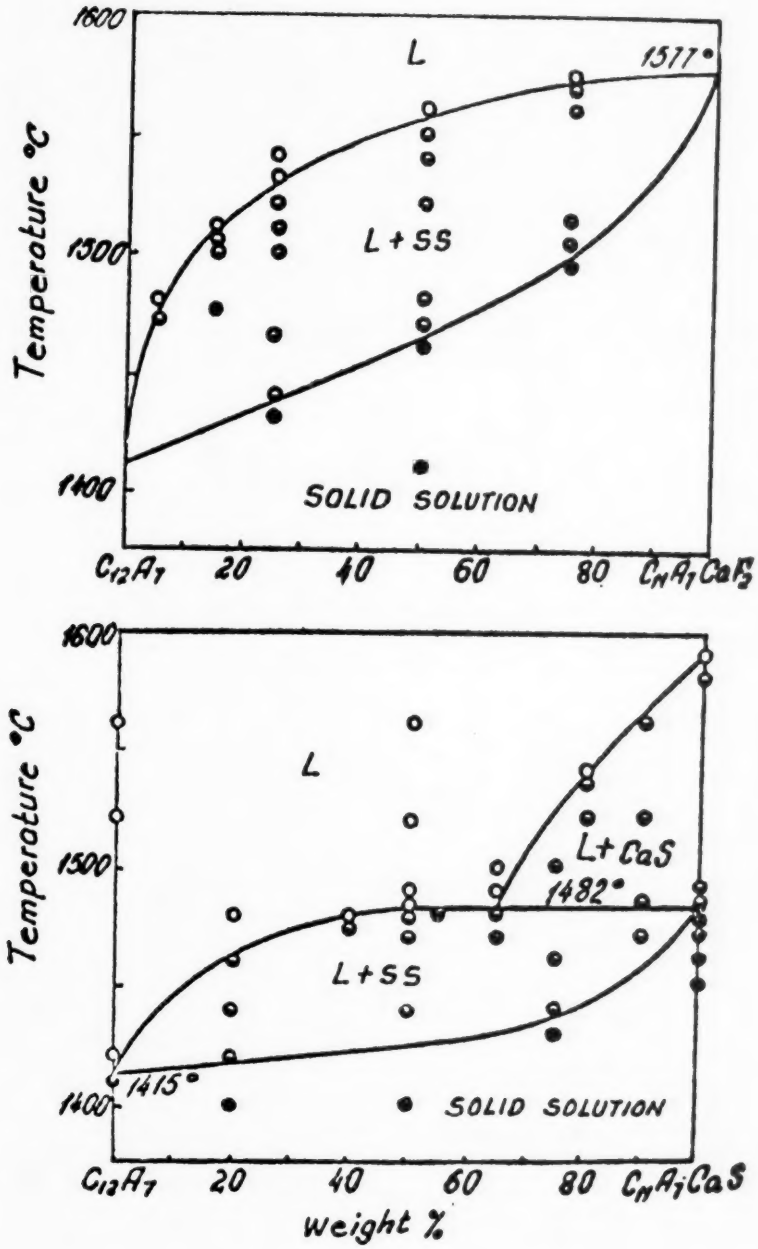

FIG. 5

Phase equilibrium diagrams of joins $C_{12}A_7$-$C_{11}A_7CaF_2$ and $C_{12}A_7$-$C_{11}A_7CaS$ obtained by quenching in hermetic platinum capsules.

Acknowledgements

The authors are thankful to Mr. G.S. Smirnov who took part in the study of phase equilibria, to Mrs. I.V. Ostrovskaya who carried out the phase analysis of glass and to Mr. V.N. Gladkii who conducted the experiments on the effect of atmosphere on the melt density.

References

1. E.S. Shepherd, G.A. Rankin, and F.E. Wright, Amer. J. Sci., 28, 293 (1909).
2. G.A. Rankin and F.E. Wright, Amer. J. Sci., 39, 1 (1915).
3. W. Buessem and A. Eitel, Z. Krist., 95, 175 (1936).
4. E. Aruja, Acta Cryst., 10, 337 (1957).
5. M.G. Vincent and J.W. Jeffrey, Acta Cryst., B34, 1422 (1978).
6. T. Yu. Chemikova and Yu. P. Udalov, Izv. Akad. Sci. USSR, Inorg. Mater, 10, 2191 (1974).
7. D.M. Roy and R. Roy, Chemistry of Cement, Proc. 4th Intl. Symp., Washington 1960, National Bureau of Standards 1, 307 (1962).
8. R.W. Nurse, ibid., 36.
9. J. Jeevaratnam, L.S. Dent Glasser and F.P. Glasser, Nature 194, 764 (1962).
10. J. Jeevaratnam, F.P. Glasser and L.S. Dent Glasser, J. Amer. Ceram. Soc., 47, 105 (1964).
11. R.W. Nurse, J.H. Welch and A.J. Majumdar, Trans. Brit. Ceram. Soc. 64, 323 (1965).
12. R.W. Nurse, J.H. Welch and A.J. Majumdar, Trans. Brit. Ceram. Soc. 64, 409 (1965).
13. R.W. Nurse, Proc. 5th Intl. Congress on Cement Chemistry, Tokyo, 1968.
14. G.S. Smirnov, A.K. Chatterjee, and G.I. Zhmoidin, J. Mater. Sci. 8, 1278 (1974).
15. J.A. Imlach, L.S. Dent Glasser and F.P. Glasser, Cem. Conc. Res. 1, 57 (1971).
16. G.S. Smirnov, G.I. Zhmoidin and A.K. Chatterjii, Vth All-Union Conference on Physico-Chemical Analysis, Synopsis of Papers, Moscow, 1976, p. 77.
17. H. Bartl, Neues Jahr. Min. Mh. 11, 404 (1969).
18. H. Bartl and T. Scheller, Neues Jahr, Min. Mh. 12, 547 (1970).
19. P.O. Williams, J. Amer. Ceram. Soc. 51, 531 (1968).
20. P.O. Williams, Acta Cryst. 29B, 1550 (1973).
21. G.I. Zhmoidin, Zh. Fiz. Khimii, 52, 18 (1978).
22. G.I. Zhmoidin, G.S. Smirnov and N.V. Gladkii, Isv. Akad. Nauk, SSSR, Neorg. Mater. 13, 352 (1977).
23. G.I. Zhmoidin in "Properties and Structure of Slag Melts," Nauka, Moscow, 1970, pp. 73-93.
24. G.I. Zhmoidin and I.S. Kulikov, Izv. Akad. Nauk, SSSR, Metally, 2, 42 (1965).
25. J.O'M. Bockris, J.D. Mackenzie and J.A. Kitchneer, Trans. Faraday Soc. 51, 1734 (1955).
26. Yu. I. Smolin, Yu. F. Shepelev and R.E. Pomes, Achievements in Physics and Chemsitry of Silicates, Nauska, Leningrad, 1978, pp. 62-84.
27. G.I. Zhmoidin - Synopsis of Scientific Communications, III All-Union Conference on Structure and Properties of Metallic and Slag Melts, Pt III, Sverdlovsk, 1978, pp. 41-44.
28. A. Ubbelode, Melting and Crystalline Structure, Mir, Moscow, 1969.
29. D. Breck, Zeolitic Molecular Sieves, Mir., Moscow, 1976.
30. S.A. Lindroth, Glastechn. Berichte, 23, 241 (1950).
31. G.I. Zhmoidin, G.S. Smirnov and V.N. Gladkii, Izv Akad. Nauk SSSR, Metally, 6, 71 (1976).

VOL
14
198

CEMENT and CONCRETE RESEARCH. Vol. 14, pp. 397-406, 1984. Printed in the USA.
0008-8846/84 $3.00+00. Copyright (c) 1984 Pergamon Press, Ltd.

EFFECT OF FLUORSPAR ON THE FORMATION OF CLINKER PHASES

M.T. Blanco-Varela, A. Palomo and T. Vázquez
Instituto Eduardo Torroja
Madrid 33, Spain

(Refereed)
(Received Feb. 3, 1983; in final form Jan. 26, 1984)

ABSTRACT

The evolution of the phases of a commercial clinker in relation to the time and temperature on the clinkerization has been studied. The influence on this evolution by the addition of a small quantity of fluorspar (∿ 0.2%) has been determined. The work was basically supported by a study carried out by IR spectroscopy.

VOL.
14
984

Introduction

The use of fluxes and mineralizers to facilitate the process of clinkerization goes back many years. Klemm and Skalny (1) did a good and complete review about fluxes and mineralizers. The concept of using such fluxes and mineralizers to burn normal raw mixes at a much lower temperature for the sole purpose of reducing the fuel requirements of the kiln, has begun to be seriously considered in the last few years. An effort to study these kinds of compounds has been made. Among these compounds, fluorides and silicofluorides have been studied more, although they have rarely survived commercially, owing to the rapid deterioration of refractory kiln linings and the effects on setting time and strength.

The possibility of reducing energy expenses in the clinkerization process by adding to the raw mix a small quantity of fluorspar (approximately 0.2%, since the initial criterion adopted is the weight relation $CaCO_3/CaF_2 = 400$), has been studied in this paper. For this purpose, the evolution of the silicates, aluminates and ferrites in function of time and temperature of clinkerization has been compared between samples with an addition of CaF_2, and with additive-free samples. The study has been basically led by the IR spectroscopy supplemented for the data obtained by XRD, DTA and TGA, optical microscopy and free (uncombined) lime analysis.

Experimental Procedure

The materials used were Spanish commercial raw mix, and a Spanish commercial fluorspar, of 97% purity. The composition of the raw mix was determined by chemical analyses and is given in Table I. Starting with this raw mix, which will hereafter be referred to as raw mix A (fluoride - free control samples), and of this same raw mix to which fluorspar has been added (∿0.2%), which will be referred to as raw mix B, the following operations were carried out:

Table I

L.I.	insol.	SiO_2	Al_2O_3	Fe_2O_3	CaO	MgO	SO_3	Na_2O	K_2O
33.90	0.20	14.13	4.14	1.76	43.45	1.81	0.50	0.23	0.63

- Study by DTA of the thermal behaviour of raw mixes A and B.

The curves of DTA, DTG and TG of raw mix A can be seen in Figure 1. These curves, which are very similar to those of raw mix B, have several thermal indications between 25 and 1450°C corresponding to chemical or physical transformations within the samples.

- Sixteen pellets from raw mix A and 16 from raw mix B were made up in a hydraulic press using a cylindrical mould of 2.5 cm inner diameter. Each pellet weighed ∿ 4 gr.

- With the object of knowing exactly what phenomena caused the thermal indications registered in the curves of DTA, DTG and TG, and the influence of fluorspar in these phenomena, a number of clinkerizations were carried out followed by air quenching on the pellets of raw mixes A and B.

The burning temperatures were 1160, 1200, 1250 and 1340°C respectively (temperatures before and after the thermic indications observed by thermal analyses). The heatings were carried out isothermically and the time in the furnace was 15, 20, 25 and 30 minutes for each sample.

- Once the samples underwent the thermal treatment their content of free lime was determined and they were also analyzed by XRD and IR spectroscopy with the object of obtaining information about their mineralogical composition and the variation of this with the temperature and the time of clinkerization. Likewise, the samples burned during the 30 minutes were submitted to treatment with methanol and salicylic acid (Takashima attack) with the object of separating the silicates and free lime from the aluminates and ferrites. In this way the evolution and composition of the "liquid phase" could be studied through XRD and IR spectroscopy.

Results

Studies were made of the behaviour of raw mixes A and B, subjected in the TA furnace to a programmed thermic treatment (V = 8°C/min.) up to a temperature of 1450°C. During the heating, an exothermic descent of the base line between 1160 and 1200°C, followed by a strong exothermic peak with a maximum of 1250°C, was observed in the DTA curve of the two raw mixes A and B (Fig. 1). This indicates that C_3S, C_2S, ferrites and aluminates are being produced. At 1290 and 1320°C two endothermic peaks, due to successive melting of compositions which reach invariant points, can be observed. During the cooling it can be seen in the DTA curve two exothermic peaks: the first at 1225°C is intense and is due to the solidification of the liquid phase which was formed during the heating, and the second at 1010°C is of little intensity and is due to the solidification of K_2SO_4 present in the raw mixes.

The clinkers proceeding from the TA were studied by XRD, IR spectroscopy and optical microscopy. By means of these techniques, better crystallization of the silicates and worse crystallization of the aluminates in the clinker with the addition of CaF_2, could be observed.

In order to know exactly what phenomena caused the thermal indications registered in the curve of DTA and the influence of fluorspar in these phenomena, the raw mixes were heated at the temperatures and durations mentioned in the

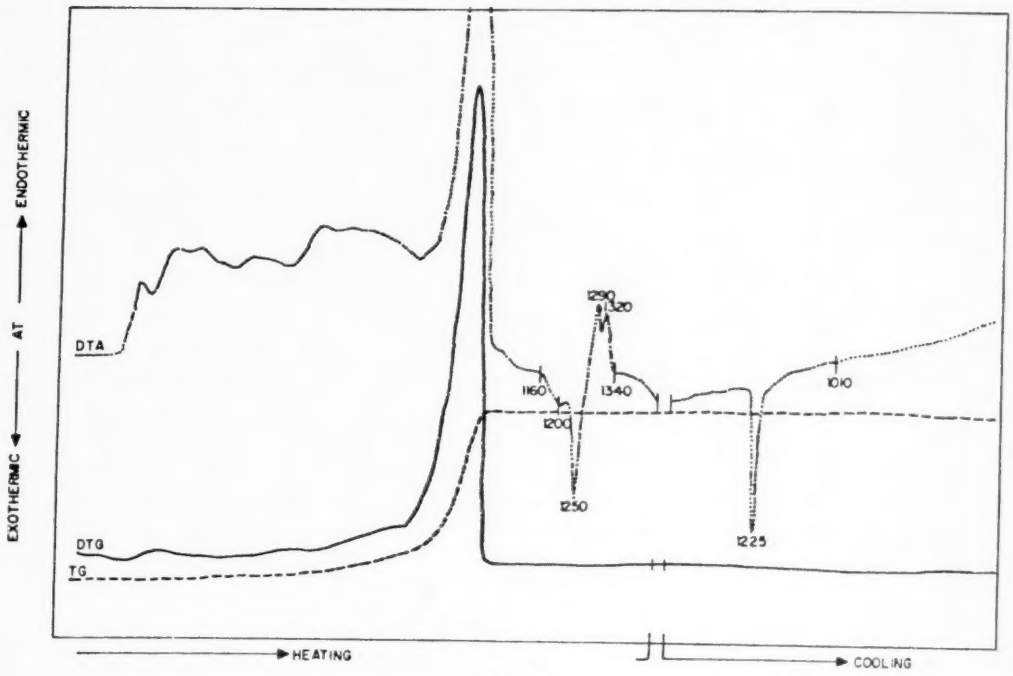

FIG. 1
DTA, DTG and TG curves of raw mix A.

experimental procedure and continuously quenched by air. The results of analyzing the clinkers proceeding from the quenchings by XRD (only those corresponding to the raw mixes which remained 30 minutes in the furnace), as well as the residue of the same, by subjecting them to the Takashima attack, are given in Table II. The analyses of these clinkers by IR spectroscopy (Figs. 2 and 3) agree with the results obtained by XRD and also contribute some other data of interest such as:

- In the spectra of the residue obtained by submitting the clinkers to the Takashima attack, the appearance of bands in 600-700 and 1100-1200 cm^{-1} characteristic of sulphates, were observed. These bands are identified as syngenite, K_2SO_4, ettringite, $CaSO_4.2H_2O$, etc. or mixtures of them. No interpretation has been made of the variations of these bands as to temperature, because there are serious doubts that the Takashima attack may in some way affect the sulphates, even facilitating their meteorization.

- The appearance of the characteristic bands of $C_{12}A_7$ in the spectra of the clinkers obtained at 1160 and 1200°C are observed; however, it is important to note that the IR spectrum of $C_{11}A_7CaF_2$ is very similar to that of $C_{12}A_7$, being hard to differentiate between them in samples like the ones studied. In these spectra bands were observed in 990, 940 and 920 cm^{-1}, which indicates vibrations of SiO_4^{4-} tetrahedra within the aluminates lattice. The spectrum of the fluoride-free clinker obtained at 1200°C has weak bands characteristic of cubic C_3A.

- In the spectrum of the fluoride-free clinker obtained at 1250°C, the disappearance of the characteristic absorptions of $C_{12}A_7$ is observed; however, $C_{12}A_7$ is detected in the clinker with the addition of CaF_2.

Table II
X-ray Data of Samples A and B Heated 30 Minutes
(Intensity of x-ray diffraction: xxx=strong; xx=moderate; x=weak; o=no signal)

		SAMPLES WITHOUT FLUORSPAR				SAMPLES WITH FLUORSPAR			
		CLINKERING TEMPERATURES (°C)							
		1160	1200	1250	1340	1160	1200	1250	1340
COMPOUNDS DETECTED	C_3S	o	x	xx	xxx	x	x	xx	xxx
	C_2S	x	xx	xxx	xx	x	xx	xx	xx
	FREE LIME	xxx	xxx	xx	x	xxx	xxx	xx	o
	C_3A	o	o	xx	xxx	o	o	xxx	xxx
	C_4AF	xx	xx	x	xxx	xx	xx	xx	xxx
	$C_{12}A_7$	xx	xx	o	o	xx	xxx	o	o
	C_2AS	xxx	xx	o	o	xx	x	o	o

NC_8A_3 and cubic C_3A is found in both clinkers, A and B, at this temperature (1250°C). A broad band in 970 cm^{-1} due to vibrations of SiO_4^{-4} deformed tetrahedra is also found.

- At 1340°C, NC_8A_3 and orthorhombic C_3A are observed in both clinkers, A and B. The two spectra have the absorption band of SiO_4^{4-} in 960-980 cm^{-1}. Between the two spectra there is little difference - the sharper bands are found in the fluoride-free sample.

- The ferritic phase increases its content in Al from 1160 to 1250°C, i.e., while the IR spectra of the samples quenched at 1160°C have the characteristic bands of C_4AF, the ones of the samples quenched at 1250°C have altered these bands. Even new bands appear. This means that the composition of the ferritic phase is between C_4AF and C_6A_2F. This phase is now less crystallized than before. At 1340°C the ferritic phase is C_4AF, but the crystallization is not as good as at 1160°C.

Table III shows the results of the analyses of free lime in the clinkers obtained after the quenchings.

Discussion

Evolution of the Silicates

Having analyzed the results provided by XRD and IR spectroscopy, it may be deduced that the influence of fluorspar on the formation of the silicate phases was as follows:

- According to the temperature at which the quenching took place, the stable polymorphic of C_2S changes. At 1160 and 1200°C, β-C_2S was found; at 1250°C,

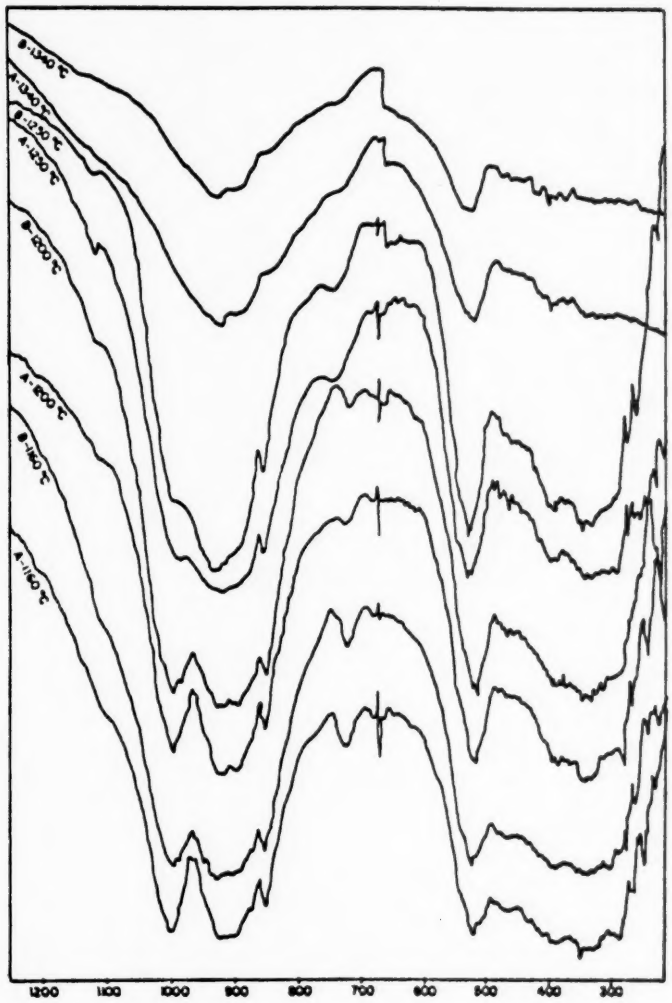

FIG. 2
IR spectra of clinkers A and B

a transition formed between β and α'-C_2S and at 1340°C the stable form is α'-C_2S. Due to displacements of the bands ν_3 SiO_4 in 990 and 850 cm^{-1} toward lower frequencies, α'-C_2S could be identified.

- The C_3S was detected in the raw mixes with fluorspar at 1160°C while in the fluoride-free samples, the C_3S was not detected until 1200°C. This fact diverges slightly from the affirmation of Gutt and Osborne (2) that when there is F^- in the system the lowest limit of the field of stability of C_3S is found at 1170°C. However, the fact agrees with Mukerjii (3) who says that the lowest limit of the field of stability of C_3S is 1107°C in the system C-S-CaF_2, although this author does not take in consideration the existence of $3C_3S.CaF_2$.

- The CaF_2 also increases the velocity of the formation of C_3S at any temperature (in the interval of those studied), a fact that is deduced by the greater intensity of the peaks of XRD and by the lessening of free lime. It agrees with the results of several authors (4,5,6).

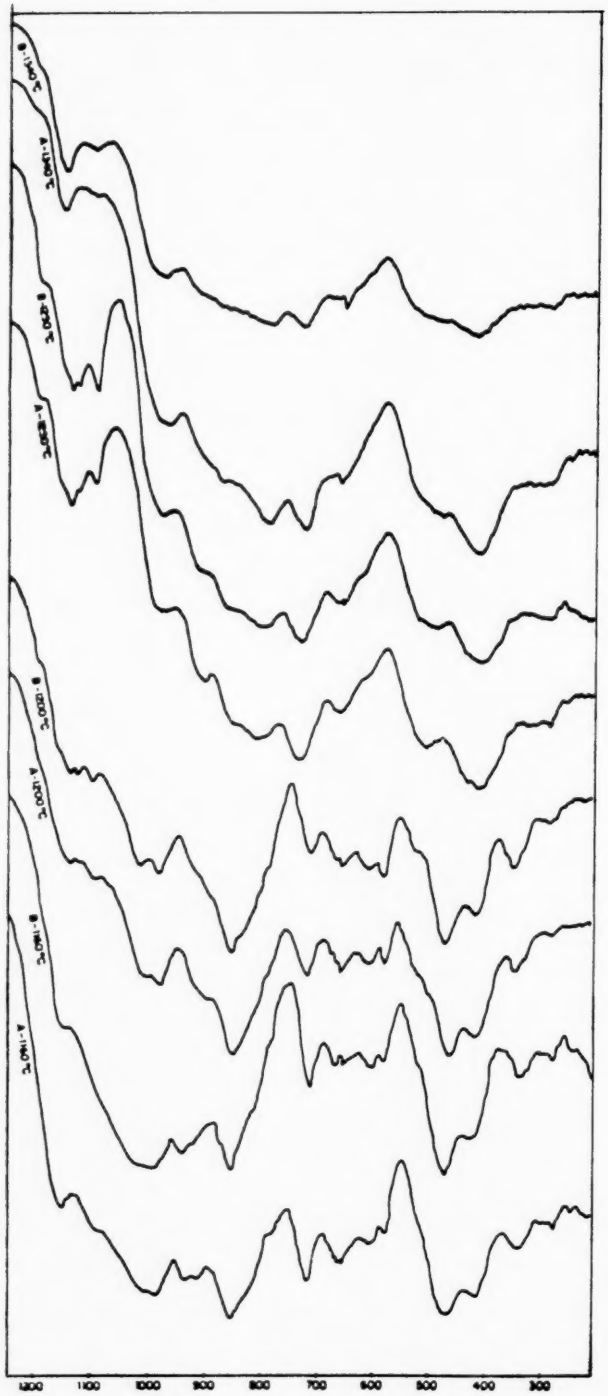

FIG. 3
IR spectra corresponding to the residue obtained when submitting clinkers A and B to the Takashima attack.

VOL. 14 1984

Table III
Results of the free lime analyses made in the clinkers A and B

		CLINKERING TEMPERATURES (°C)							
		1160		1200		1250		1340	
	AGE (minutes)	15	30	15	30	15	30	15	30
A	% FREE LIME	27.8	25.5	23.1	19.6	9.4	7.1	4.8	3.2
B	% FREE LIME	25.9	21.7	18.2	15.1	7.8	6.0	4.5	2.7

- Finally, the form of the bands of the IR spectra due to silicates indicates a greater structural order provoked by the F^-.

Evolution of the Liquid Phase

The evolution of the components of the so-called "liquid phase" with temperature and the presence or absence of fluorspar may be described in the following manner:

Ferritic phase. The ferritic phase may be considered as a solid solution of a general formula $C_2(A_{1-x}F_x)$ in which x may have values between 1 and 0.33. The formation of this phase may be from C_2F and later Fe substituted by Al. The structure is orthorhombic, having tetrahedral and octahedral coordinations. Initially the Al substitutes Fe in the tetrahedral coordination and later tetrahedrally and octahedrally. In this manner composites are formed according to the following sequence:

$$C_2F \xrightarrow{Al} C_6AF_2 \xrightarrow{Al} C_4AF \xrightarrow{Al} C_6A_2F$$

As the proportion of Al increases in the general formula of the ferritic phase $C_2(A_{1-x}F_x)$, the following are observed in the corresponding spectra (7):

1°. - Appearance of bands characteristic of AlO_4, i.e. absorptions in 780 and 830 cm^{-1} and perhaps bands characteristic of AlO_6 in 400-600cm^{-1}. Simultaneously, a lessening of the absorptions in 600-700 cm^{-1} (vibrations of FeO_4) and also in 400-450 and 300-400 cm^{-1} (vibrations of FeO_6) is observed.

2°. - As the substitution of Fe by Al increases, the intensity of the bands in 700-800 cm^{-1} increases and above all the intensity increases in 450 cm^{-1}. The outline of the bands varies progressively.

3°. - The bands vary toward higher frequencies as the proportion of Al increases.

On comparing the variations which, in the IR spectra, are experienced by the bands of adsorption corresponding to the ferritic phase when the temperature increases from 1160 to 1250°C it is deduced that initially at 1160°C there exists a ferritic phase with a composition like C_4AF and as the temperature increases, the phase reaches a composition compressed between C_4AF and C_6A_2F. It may be affirmed (from the form of the bands) that the ferritic phase is well crystallized at low temperatures (up to 1250°C).

On reaching 1340°C, the interstitial phase melted and on quenching there remained a ferritic phase very rich in Fe and a poorly crystallized and vitreous phase rich in Al.

Aluminates, C_3A: Pure C_3A is cubic with a parameter of unit element = 15.263 ± 0.003 Å. This compound admits oxides as impurities (up to certain proportions) in its lattice, which substitutes atoms of Al and/or Ca and which provokes variations in the size of the parameter of the lattice but which does not cause a change of symmetry from cubic to orthorhombic. Thus, the Al may be substituted by Fe (8,9) or Si (10) up to certain limits causing increases in the size of the unit element as in the case of Fe, or reductions in the case of Si. Naturally, for a correct balance of loads when it is the Si which replaces Al, there are two options: one atom of Si replaces two atoms of Al. In this way, the remaining one extra oxygen must be accommodated in the structure or 4 atoms of Al replaced by 3 of Si, a vacant hole thus remaining.

The Na_2O replaces the CaO, and as this replacement is taking place, the parameter "a" of the unit element slowly lessons until the concentration of Na_2O reaches 3%. From this moment, the C_3A, which is still cubic, changes to orthorhombic (10).

In the IR spectra of the residue obtained after submitting the fluoride-free clinkers to the Takashima attack, the appearance of the characteristic bands of C_3A was not observed in those samples heated below 1200°C. The spectum of the sample heated at 1200°C has weak bands which are characteristic of the ring Al_6O_{18} of the cubic C_3A. In the spectrum B (sample with fluoride) at this temperature, these absorptions do not exist.

At 1250°C, both spectra A and B have the absorptions of the cubic C_3A. Perhaps the effect of the fluoride in these samples is not a strong one, nevertheless a variation is observed in the band in 910 cm^{-1} which can be assigned to the vibrations stretching O-Al-O (11). It is also observed in the two spectra the appearance of a broad band in 970 cm^{-1} due to deformed tetrahedra SiO_4 which replaces AlO_4, also deformed within the structure of the cubic C_3A.

In the spectra of the samples heated to 1340°C, little bands, due to orthorhombic C_3A, are seen. This is due to the presence of impurities (for example Na^+) and the substitutions of SiO_4 - AlO_4 in the lattice of the C_3A.

NC_8A_3: The existence of NC_8A_3 in the clinkers is a function of two variables: content of Na_2O and speed of cooling. Suzukawa (12), in his studies of NC_8A_3 affirms that with the presence of an excess of Na_2O and rapid cooling, this composite is obtained, while if the cooling is slow, C_3A and Na_2SO_4 are obtained. In the opinion of this author, the NC_8A_3 contains some SiO_2 in its structure due to partial substitutions of lime-aluminium by sodium-silicon. Thus, in the clinkers of high temperature (1250 and 1340°C), since there already existed C_3A with SiO_4 in its lattice and the Na_2O was present, NC_8A_3 was formed, which on being subjected to rapid cooling remained stabilized as such and was not transformed into C_3A.

The lines of diffraction of NC_8A_3 are very similar to that of C_3A; thus the NC_8A_3 was identified as C_3A by XRD. However, in the IR spectra, the bands appearing in 865, 798, 725, 530, 520, and 400 cm^{-1} are interpreted as characteristic of NC_8A_3 (13).

C_2AS: The gehlenite is an intermediate compound within the process of clinkerization which is initially formed by solid state reactions. As the temperature is increased, gehlenite reacts to produce C_3A and C_2S (14). The content of gehlenite in the clinkers diminishes progressively when the temperature increases. At 1250°C gehlenite was not found. At 1160 and 1200°C, a higher

proportion of gehlenite was found in the fluoride-free samples, i.e. fluorides inhibit, partially at least, the formation of gehlenite. It was also observed that the $C_{12}A_7$ formed, increased as the gehlenite diminished (in those samples with CaF_2). This is probably because the addition of CaF_2 to the system extends the primary field of $C_{12}A_7$ ss (15).

$C_{12}A_7$ and $C_{11}A_7CaF_2$: As reported in the results, the IR spectra of our clinkers have the bands of the $C_{12}A_7$. We also found three bands in 990, 940 and 920 cm^{-1} which can be assigned to different vibrations of tetrahedra of SiO_4 within the structure of the aluminates. The highest frequency absorption is due to tetrahedra of SiO_4, probably deformed, which replaces tetrahedra of AlO_4, also deformed. This band in 990 cm^{-1} does not change either when the temperature changes or with the addition of CaF_2. However, the bands in 920 and 940 cm^{-1} change as the temperature increases and for the same temperature with the addition of CaF_2.

These facts are interpreted in the following manner:

The $C_{12}A_7$ can introduce within its lattice, tetrahedra of SiO_4 which replaces tetrahedra of AlO_4. It originates the absorptions in 990, 940 and 920 cm^{-1}. When there is fluoride in the system, the compound formed is the $C_{11}A_7CaF_2$ which prevents the tetrahedra of SiO_4 (those responsible for the vibrations in 940 and 920 cm^{-1}) to be icluded within its lattice.

To summarize the evolution of the aluminates, it can be said that at 1160 and 1200°C, the clinkers have a phase similar to $C_{12}A_7$; at 1250°C they have cubic C_3A and at 1340°C a phase like NC_8A_3 with orthorhombic structure.

All the phases mentioned are not pure ones. All have SiO_4 which replaces AlO_4. Of course, because of the correct balance of loads, the substitutions can be multiple ones, for example CaAl-NaSi giving in the case of the C_3A a phase like (16):

$$((Ca_{72-(n+m)})(Na_{(2n+m)})_{72+n}(Al_{48-m}Si_m)_{48}O_{144})$$

Han, et al. (16), considered that the multiple substitutions involve the formation of a solid solution in C_3A with this general formula:

$$((Ca)_{72-(n+m)}(Na_{(2n+m)}))_{72+n}((Al)_{48-(m-z)}(Si_{(m+3/4z)})_{48-1/4z})O_{144}$$

With regard to $C_{12}A_7$, Jeevaratnam, et al. say that $C_{12}A_7$ contains two reactive O^{2-} per cell which may be wholly or partly replaced by up to four univalent ions with only slight concomitant changes in cell size and density. Thus, by mean of the substitution of one of these O^{2-}, the $C_{11}A_7.CaF_2$ may be formed. In the samples under study, substitutions of SiO_4-AlO_4 within the lattice of the $C_{12}A_7$ are observed. These substitutions may be like Si X-CaAl (X=Na,K). It would produce a phase like $Ca_{12-n}Al_{14-n}Si_nX_nO_{33}$. The substitutions SiO_4-AlO_4 are not admitted in the lattice of the $C_{11}A_7CaF_2$ as easily as with the $C_{12}A_7$.

Finally, in the IR spectra of the samples heated at 1340°C, it is observed that the incorporation of strange ions within the lattice of C_3A produces a strong change in the symmetry of the rings Al_6O_{18}. It is explained as a change C_3-C_i. It agrees with Boikova, et al. (11).

Influence of the Time Clinkerization in the Speed of Reaction

All the thermic treatment applied to the samples under study were carried out at different times (15, 20, 25 and 30 minutes) with the object of studying the influence of the time of clinkerization in the velocity of the reactions. The results obtained on anlayzing all the clinkers by XRD, those obtained by analyses of the free lime given in Table III, and those obtained on analyzing the free lime at the temperatures already mentioned but during 5 and 10 minutes,

show that at low temperatures (up to 1200°C) the reactions are totally completed between the first 10 and 15 minutes of the reaction; at worst, the difference of the lime combined at 10 and 30 minutes, is in the order of 4%.

At high temperatures (1250 and 1340°C), when we compare the combined lime at 15 and at 30 minutes, the difference of 4% decreases by ∿2% in relative value. This 2% difference now has a greater importance since the lime must be totally combined. At a high temperature, the formation of phases is carried out in its majority during the first 15 minutes of reaction, although the effects on the samples of greater period in the furnace is more important than lower temperatures.

Conclusions

From this work, the following conclusions can be made:

1) Fluorspar, even when used in a small proportion, lowers the temperature of the formation of C_3S and increases the speed of the formation of the silicates.

2) Fluorspar stimulates the discomposition of the gehlenite favouring simultaneously the formation of $C_{11}A_7CaF_2$ between 1160 and 1200°C.

3) As the gehlenite decomposes in the presence of fluorspar between 1160 and 1200°C, C_2S, cubic C_3A and/or $C_{11}A_7CaF_2$ are formed.

4) Substitutions SiO_4-AlO_4 are admitted within the lattice of $C_{12}A_7$. These substitutions are partly prevented when substitutions $F^- - O^{2-}$ take place within the $C_{12}A_7$ to produce $C_{11}A_7CaF_2$. Thus be means of IR spectroscopy, it is possible to discern between $C_{12}A_7$ and $C_{11}A_7CaF_2$ in similar samples to those already studied.

5) An increase of the temperature from 1160°C until the formation of the liquid phase, produces in the ferritic phase of these clinkers, a progressive enrichment in aluminium. On passing the melting temperatures of the ferrites and aluminates and later cooling the clinker rapidly, a crystallization (poor) of a ferritic phase rich in Fe is produced.

6) The reactions are mainly produced before the first 15 minutes of keeping the samples inside the furnace.

7) It will be necessary to study the way of increasing the speed of reaction between 1160 and 1250°C and attempting to lower the temperature of formation of euthectics.

References

1. W.A. Klemm and J. Skalny, Cements Research Progress, 259-291 (1976).
2. W. Gutt and G.J. Osborne, Trans. Brit. Ceram. Soc. 69, 3, 125-129 (1970).
3. Mukerjii, Memoires Scientifiques, Rev. Metallurgh; IX, No. 11, 785-796 (1963).
4. W.A. Klemm, I. Jawed and K.L. Holub, Cem. Concr. Res. 9, 489-496 (1979).
5. S.G. Ampian and E.P. Flint, Am. Ceram. Soc. Bull. 52, 8, 604-620 (1973).
6. N.H. Christensen and V. Johansen, 7th Intl. Congress on the Chemistry of Cement, Vol. II, I.1-I.5, Paris (1980).
7. P. Tarte, Sil. Indust. Vol. 33, No. 11, p. 333 (1968).
8. A.J. Majumdar, Brit. Ceram. Soc. Vol. 64, No. 2, p. 105 (1965).
9. P. Tarte, Nature 207, N. 5000, 973 (1965).
10. M.A.E. Moore, Sil. Indust. Vol. 32, p. 87 (1967).
11. A.I. Boikova, A.I. Domansky, V.A. Paramonova, G.P. Stavitskaja and V.M. Nikushchenko, Cem. Concr. Res. 7, 483-492 (1977).
12. Y. Suzukawa, Zement Kalk Gips 9, 345, 390, 433 (1956).
13. T. Vázquez, Monografía No. 297, Instituto Eduardo Torroja de la Construcción y del Cemento. Madrid (España) (1971).
14. S. Chromy, VI Intern. Congress Chem. Cem. Sec.-III-III-8 Moscow (1984).
15. K. Asok Sarkar, D.M. Roy and R.M. Smart, 7th Intl. Congress of Chemistry of Cement, Vol. II I-195 I-201, Paris (1980).
16. K.S. Han, J.A. Garg and F.P. Glasser, Cem. Concr. Res. 11, 79-74 (1981).
17. J. Jeevaratnam, F.P. Glasser and L.S. Glasser, J. Am. Ceram. Soc. 47, 105-106 (1964).

VOL. 14 1984

CEMENT and CONCRETE RESEARCH. Vol. 14, pp. 407-412, 1984. Printed in the USA.
0008-8846/84 $3.00+00. Copyright (c) 1984 Pergamon Press, Ltd.

DIFFERENCE IN AUTOCLAVE EXPANSIONS OF PLANT AND LABORATORY GROUND CEMENTS

G. Goswami, S.K. Mohanty and J.D. Panda
Dalmia Institute of Scientific & Industrial Research
Rajgangpur-770017, India

(Communicated by D.M. Roy)
(Received May 13, 1983; in final form March 3, 1984)

ABSTRACT

In a cement plant, it was found that the cement ground in the laboratory mill showed higher autoclave expansion than the cement produced in the plant mill, although both of them were of the same specific surface (Blaine) area. DTA of the laboratory ground (autoclaved) cement showed only one endothermic peak corresponding to one dissociation temperature of $Mg(OH)_2$, while that of the plant cement showed two dissociation temperatures. It has been found that a wide range of particle size of periclase is responsible for two dissociation temperatures of $Mg(OH)_2$ produced in the autoclaved cement samples. It has also been established that periclase of narrower particle size range causes higher autoclave expansion than an equal amount of periclase of wider particle size range, although the latter may contain some coarser periclase than the former. Thus the difference in autoclave expansions of plant and laboratory ground cements is attributed to the difference in particle size ranges of the periclase present in the cement samples.

Introduction

The causes of unsoundness of cement and the influence of different parameters on the degree of autoclave expansion have been examined by a number of investigators (1-7). There seems to be a general acceptance among the researchers that high MgO and $3CaO$, Al_2O_3 (C_3A) contents of the clinker are the two most important factors for causing unsoundness of cement and parameters like fineness and mineralogical and chemical compositions of the raw mix, burning and cooling processes of the clinker and the fineness of the cement have significant influence on the resultant autoclave expansion. Although generally clinkers having MgO content of 3.5% or less are found to be sound, in certain exeptional cases, cement even with this level of MgO shows unsoundness. This aspect has also been examined by a number of workers (1,2,4,6). Another peculiar pehnomenon is that, sometimes cement ground in the laboratory ball mill shows higher autoclave expansion than the cement produced from the same clinker grinding in the plant mill at the same specific surface (Blaine) area. Recently, Dreizler (5) has reported that during his investigations, while the cement ground in a laboratory mill from pure portland cement clinker of high MgO content did not pass the

soundness test, he got mostly very low expansion values for the industrially produced cement. The aim of the present investigation is to examine this phenomenon of difference in autoclave expansions of laboratory- and plant-ground cements.

Experimental

Cement and clinker samples were collected from a plant, where the difference in autoclave expansions of laboratory ground cement and plant cement was reported. The plant has two kilns of almost equal capacity, one with planetary (Kiln-I) and the other with grate cooler (Kiln-II) systems. In the plant, clinkers from both the kilns are ground together. For laboratory prepared cement, clinkers were collected from the cooler mouth of each of the kilns. For a comparative study, clinkers produced on different days were taken for autoclave tests. Chemical composition with free lime % of different clinkers are shown in Table I. Laboratory cement was prepared by grinding in a small ball mill of the

Table I

Chemical Composition and Free Lime % of the Clinker Used

Clinkers for	Constituents (wt. %)					
	CaO	SiO_2	Al_2O_3	Fe_2O_3	MgO	Free CaO
Cement 1	64.0	22.6	5.1	2.3	4.8	1.6
Cement 2	64.7	22.0	5.2	2.4	4.8	2.0
Cement 3	63.0	22.8	5.4	2.8	4.9	1.0

of 450 x 450 mm, keeping clinker/gypsum ratio identical to that of the plant cement. The same gypsum was used in both the plant and laboratory-cements. Attempt was made to keep the specific surface (Blaine) area of the laboratory cement as near as possible to that of the plant cement.

Both laboratory ground and plant cement were autoclaved at a saturated vapour pressure of 21 $\pm$ 1 kg/cm^2, 215.7 $\pm$ 1.7°C for 3 hours. Expansion of the autoclaved samples was determined as per IS:4031 also tested by Le-Chatelier method. For a supplementary work, periclase (MgO) was ground to different fineness and then hydrated by autoclaving in the same condition as used for the cement samples. Combined DTA/TG of the autoclaved cement samples and hydrated periclase $Mg(OH)_2$ was carried out in the Netzsch Simultan Thermo Analysis, Model 429 with potentiometric recorder up to 1000°C. The rate of heating was kept constant at 10°C/minute. The weight of the sample taken for analysis in all cases, was 100 mg. The recorder speed and sensitivity were maintained identical in all cases.

Results

Autoclave expansions

In Table II, Blaine area and autoclave expansion of some of the cement samples tested during the investigation are shown. It is found that all the plant cement samples (Nos. 1.1, 2.1 and 3.1) show lower autoclave expansion (<0.8%, maximum autoclave expansion %, acceptable per IS:269, 1976) while all the cement samples ground in the laboratory ball mill from the same clinkers show higher autoclave expansion (>0.8%). In Table III, autoclave expansion of different cement compositions in addition to certain quantities of periclase of different particle size ranges are shown. It is found that in all compositions, addition of periclase of -63+45 micron size produces more autoclave expansion than that of equal amount of -90 micron size, which contains 41% grains above 63 micron size.

Table II

Autoclave Expansion and Corresponding DTA Characteristics

Sample No.	Fineness (Blaine area) cm^2/gm	Autoclave Expansion %	DTA peaks, T°C 410-420	460-75	510-20
Cement 1					
1.1 Plant	2714	0.37	P*	P	P
1.2 Lab (Kiln-I clinker)	2784	3.8	P		P
1.3 Lab (Kiln-II clinker)	2801	4.8	P		P
Cement 2					
2.1 Plant	2965	0.6	P	P	P
2.2 Lab	2881	4.6	P		P
Cement 3					
3.1 Plant	3840	0.78	P	P	P
3.2 Lab	3748	4.8	P		P

*P = Present

DTA/TG of the autoclaved samples

DTA/TG of a number of autoclaved plant and laboratory ground cement samples was conducted simultaneously. The DTA peak characteristics of some of the samples are summarized in Table I and are shown in Figs. 1 and 2. The plant cement samples are characterized by three endothermic peaks at (410-420°C), (460-475°C) and (510-520°C). The DTA curves of the corresponding laboratory cements do not record the endothermic peak at 460-475°C. The peak at 510-520°C is due to $Ca(OH)_2$ present in the sample (8). The other two peaks are identified to be of $Mg(OH)_2$ (9). The most significant feature in the DTA curves is the disappearance of the endothermic peak at 460-475°C in the laboratory ground cement and corresponding increase in volume of peak at lower temperature.

Table III

Autoclave Expansion in Presence of Periclase of Different Ranges of Particle Size
(-90 micron material contains 41% periclase of +63 micron)

Sample No.	Cement % OPC	Cement % HAC	Sand %	Additional periclase %	Size of additional periclase (in micron)	Autoclave expansion %
1.1	100	0	0	0	-	0.78
1.2	99.9	0	0	0.1	-90	8.77
1.3	99.9	0	0	0.1	-63+45	9.47
2.1	0	100	0	0	-	0.049
2.2	0	98.5	0	1.5	-90	0.104
2.3	0	98.5	0	1.5	-63+45	0.110
3.1	0	10	90	0	-	0.038
3.2	0	9.7	90	0.3	-90	0.093
3.3	0	9.7	90	0.3	-63+45	*

* Could not be measured as the bar got crumbled.

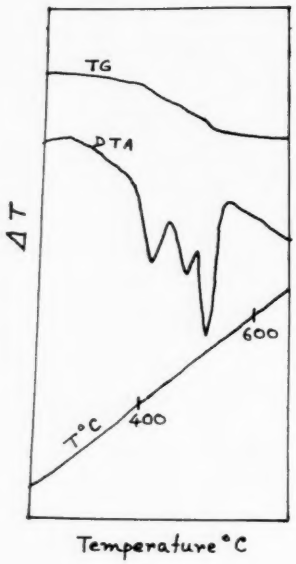

FIG. 1
DTA/TG curves of autoclaved plant cement.

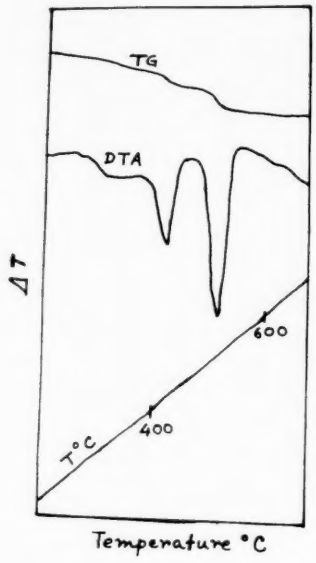

FIG. 2
DTA/TG curves of autoclaved laboratory ground cement.

VOL
14
198

DTA/TG of pure $Mg(OH)_2$

To examine the reason for the appearance of double endothermic peaks for $Mg(OH)_2$ in the autoclaved plant cement samples, a number of $Mg(OH)_2$ samples were prepared by autoclaving periclase of different particles sizes and then examined by DTA. It is found that DTA of $Mg(OH)_2$, prepared from +45 and -45 micron periclase shows endothermic peak at 440°C (Fig. 3) and 420°C (Fig. 4), respectively. But DTA of a sample prepared from periclase of two distinct particle sizes (equal amounts of -45+10 micron and -10 micron size) shows an endothermic peak at 435°C with a shouldering at 380°C (Fig. 5). From the DTA of these three $Mg(OH)_2$ samples, it is evident that $Mg(OH)_2$ samples produced from periclase of different particle sizes dehydrate and consequently produce endothermic peaks at different temperatures. Finer grains show endothermic peak at lower temperature than the coarser grains. $Mg(OH)_2$ produced from a mix of two grain sizes, shows two endothermic peaks.

Discussion

From Table I, the difference in autoclave expansions of plant and laboratory ground cement samples is quite evident. The laboratory cement samples prepared from both the kilns are unsound. Contrary to the general expectation, in the case of laboratory cement from the kiln I with planetary cooler, autoclave expansion is 20% less than that of the cement produced from the kiln II, with grate-cooler. No doubt, in general, there exists a relationship between clinker cooler system and content and grain size of periclase and from this aspect, grate-cooler is accepted to be preferable to the planetary cooler. But in many cases, it is not possible to locate any direct relationship between the soundness of the cement and the type of clinker cooler used (5). In fact, similar to the present findings Dreizler (7) also reported that one clinker cooled in a grate-cooler showed higher autoclave expansion than clinker cooled in a satellite cooler. Thus it is understandable that degree of autoclave expansion

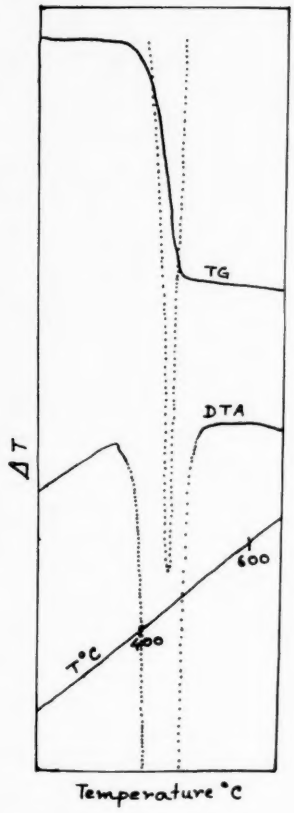

FIG. 3

DTA/TG curves of $Mg(OH)_2$ prepared from +45 micron periclase.

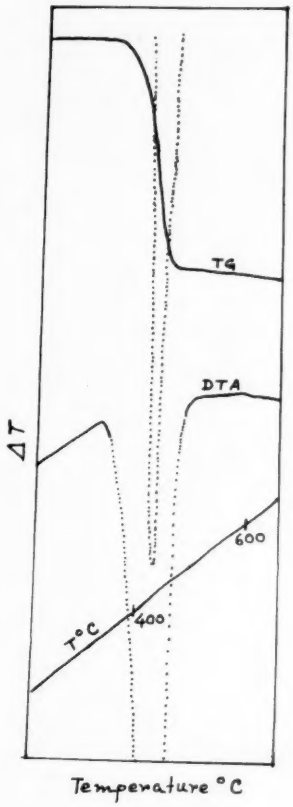

FIG. 4

DTA/TG curves of $Mg(OH)_2$ prepared from -45 micron periclase.

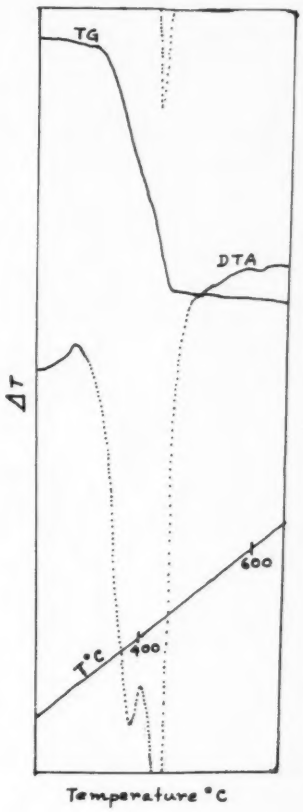

FIG. 5

DTA/TG curves of $Mg(OH)_2$ prepared from periclase of two particle sizes.

of cement can not be always directly connected with the cooling system and consequently to the temperature of the clinker at the discharge end of the kiln.

Le-Chatelier expansions of both the plant and laboratory ground cements are found to be the same (about 1 mm) and so, it is understandable that the difference in autoclave expansions is only due to the nature of the periclase content of the sample.

DTA curves of the autoclaved cement samples can be classified into two distinct groups, one for the plant cement with two endothermic peaks for $Mg(OH)_2$ and the other for the laboratory ground cement with only one endothermic peak. This suggests that autoclaved cement samples with two dissociation temperatures for $Mg(OH)_2$ produces less expansion than that with only one dissociation temperature, although both the samples are prepared from the same clinker. Thus, the disappearance of the endothermic peak at 460-475°C can be clearly correlated with the higher autoclave expansion of the laboratory ground cement.

From the DTA of the pure $Mg(OH)_2$ of controlled periclase size, it is found that periclase of limited grain size produces one peak, while a mix of two grain-sizes produces two peaks. It suggests that periclase in the plant cement with

two peaks in the DTA curve is of wider size range than that in the laboratory cement, which produces only one peak at lower temperature. It seems that in the laboratory mill coarser periclase gets reduced in size and then exists in a narrower range of particle size. But in the case of the plant mill, some coarser periclase remains as such even when the cement is ground to a Blaine area higher than that of laboratory cement and accordingly produces a wider range of particle size.

From Table III, it is found that in any cement composition, periclase of -63 +45 micron size produces higher autoclave expansion than the equal amount of periclase of -90 micron size although the latter contains 41% grains above 63 micron size. This shows clearly that periclase of narrower range of particle size produces higher autoclave expansion than the equal amount of periclase of wider range, although the latter may contain some coarser particles than the former. As the DTA of the laboratory ground (autoclaved) cement also shows a narrower range of periclase size than that of the plant cement, it is understandable that particle size range of the periclase is responsible for the difference in autoclave expansions of the two. In a somewhat similar investigation, Frigione and Marra (10) while examining the relationship between particle size distribution and compressive strength in portland cement, also demonstrated that volume of the hydrated product increased when the granulometric range decreased.

The fact that clinkers of the same production, ground at the same Blaine area in different tube mills, have sometimes different rates of hardening and consequently different michanical strengths is known and has been attributed to their difference in particle size distribution (10). This suggests that even the same type of mills may produce cement of different particle size ranges. Thus, it is conceivable that the changes in the width of granulometric ranges of periclase, leading to the difference in autoclave expansion of plant and laboratory ground cements, are caused by the effectiveness of the grinding mills only.

VOL
14
198

Conclusion

From the examination of the autoclaved samples of plant and laboratory ground portland cement, it is found that in determining the degree of autoclave expansion, grain size of periclase is a more important controlling factor than the overall Blaine area of the cement. Periclase of a narrower particle size range produces higher autoclave expansion than an equal amount of periclase of a wider particle size range. Cement from the same clinker and ground at the same Blaine area, but in different mills, may produce periclase of different granulometric ranges. Laboratory ground cement with a reduced range of particle size of periclase shows higher autoclave expansion than the plant cement produced from the same clinker and ground at the same Blaine area.

References

1. F. Gille, Zement-Kalk-Gips 5, 142 (1952).
2. G. Goggi, Zement-Kalk-Gips 11, 383 (1958).
3. A. Stahel and W. Schramli, Zement-Kalk-Gips 22, 407 (1969).
4. C. Schmitt-Henco, VI Intl. Symp. on Chemistry of Cement, Moscow, 110 (1974).
5. I.E. Dreizler, Proc. of 3rd Intl. Conf. on Cement Microscopy, Houston, Texas 33 (1981).
6. K.C. Narang, S.P. Ghosh and K.M. Sharma, Proc. of 3rd Intl. Conf. on Cement Microscopy, Houston, Texas, 140 (1981).
7. I.E. Dreizler and D. Knofel, Zement-Kalk-Gips, 35, 539 (1982).
8. H. Midgley, Cem. Concr. Res. 2, 77 (1979).
9. B.S. Neumann, Thermal Techniques in 'Physical Methods in Determinative Mineralogy', edited by J. Zussman, 2nd edition, Academic Press, London, 605 (1977).
10. G. Frigione and S. Marra, Cem. Concr. Res. 6, 113 (1976).

CEMENT and CONCRETE RESEARCH. Vol. 14, pp. 413-418, 1984. Printed in the USA.
0008-8846/84 $3.00+00. Copyright (c) 1984 Pergamon Press, Ltd.

REDISTRIBUTION OF IMPURITY DURING RECRYSTALLIZATION OF ALITE IN PORTLAND CEMENT CLINKER

I. Maki
Nagoya Institute of Technology
Gokiso-cho, Showa-ku, Nagoya, 466 Japan

S. Takahashi
Research and Development Laboratory
Cement Association of Japan
4-17-33, Toshima, Kita-ku, Tokyo, 114 Japan

VOL.
14
984

(Communicated by H.F.W. Taylor)
(Received Oct. 12, 1984)

ABSTRACT

The redistribution of impurity in alite during recrystallization has been confirmed by means of the electron probe microanalysis. Each of the main impurity components shows a significant decrease in content during recrystallization. This demonstrates that the growth velocity of alite exerts influence on the amount of the impurity taken up in alite in solid solution from the interstitial melt. Whether M_3 or M_1 occurs at ambient temperature depends on the cooling rate of clinker as well as the chemical composition of alite.

Introduction

The crystals of alite primarily formed in portland clinker from a raw mix generally show, if subjected to prolonged heating at high temperatures, a trend toward recrystallization. This trend is noticeable when the primarily formed crystals are small in size and the temperature of recrystallization exceeds *e.g.* 1500°C. Recrystallization is important in that it can cause significant changes in such characters of alite as the crystal size, size distribution, morphology, chemical composition and phase structure. In the previous study (1), we concluded the depletion of impurity during recrystallization from the resultant phase change of alite; *i.e.*, if the MgO content in clinker is selected at a certain proper level, the decrease in impurity content leads to a lowering of the crystal symmetry of alite, *e.g.* M_3 to T_2. The present study has been undertaken to confirm directly, by means of the electron probe microanalysis, the redistribution of impurity in alite during recrystallization.

Experimental

The clinker specimens employed in this investigation have been prepared in exactly the same way as in the previous study (1). The raw mix had the chemi-

cal composition: 22.94 SiO_2, 5.46 Al_2O_3, 3.04 Fe_2O_3, 66.56 CaO, 0.60 MgO, 0.40 SO_3, 0.40 Na_2O, 0.60 K_2O (in weight percent). As the starting raw materials were used limestone and clay ground to a residue of 8.0% on 240 mesh. The contents of SiO_2, Fe_2O_3, MgO and alkalies were adjusted by adding the corresponding chemical reagents. The SO_3 was added in the form of gypsum. The raw mix was fired at 1600°C, without any preliminary heat treatment, for a given period of time.

For EPMA studies, a HITACHI X 650 SEM was used in conjunction with a KEVEX 7000 Q energy dispersive analyzer. The spectral intensities obtained were compared with those of standard materials and converted to weight percentages by means of the standard ZAF correction routines.

Results

Figs.1(a) and 1(b) show, respectively, the distributions of the chemical composition of alite in the specimens fired for 5 and 120 min. Plotting the compositions in molar concentration also gave the distributions very similar to those in Fig.1. No distinction has been drawn, in preparing these figures, between Al and Fe ions as to their crystal-chemical behavior in the alite structure. Table 1 lists some of the chemical compositions determined.

In the specimen fired for 5 min the alite crystals are almost those which have been primarily formed from the raw mix. The nucleation and growth environment of the alite, very liable to wide local variations according to the inhomogeneity of the raw mix, must be primarily responsible for the scattering of the impurity contents shown in Fig.1(a). The recrystallization of alite,

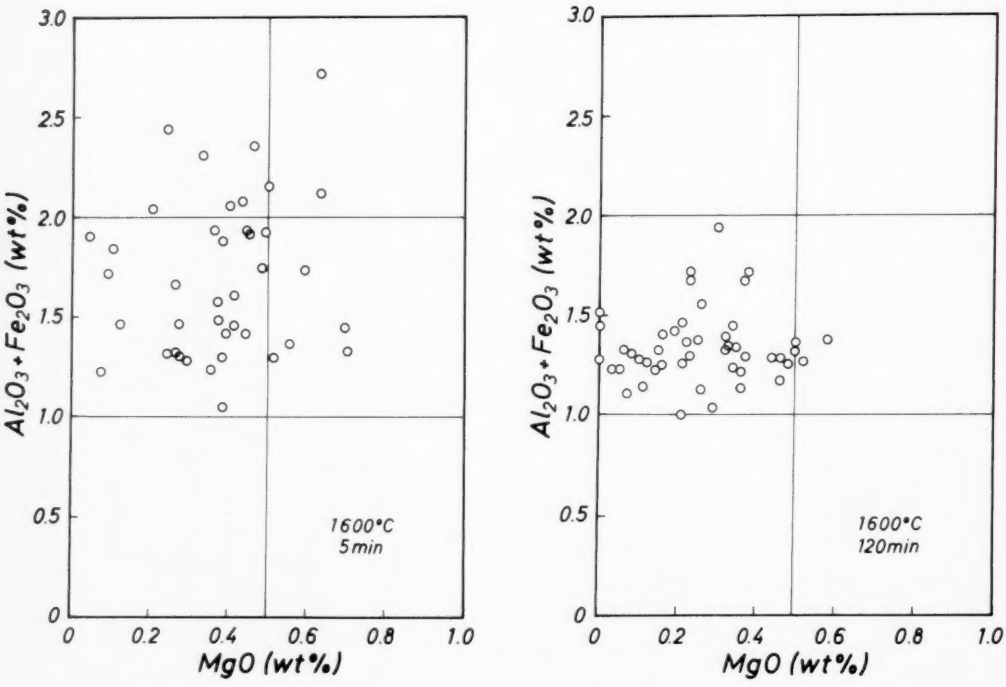

FIG. 1
Chemical compositions of alite as determined by EPMA in the specimens fired for (a) 5 and (b) 120 min.

TABLE 1 Chemical Composition of Alite

1600°C, 5 min						1600°C, 120 min					
SiO_2	Al_2O_3	Fe_2O_3	CaO	MgO	Total	SiO_2	Al_2O_3	Fe_2O_3	CaO	MgO	Total
25.75	1.09	0.58	72.86	0.26	100.54	26.29	0.86	0.50	69.18	0.22	97.05
26.12	0.80	0.52	72.17	0.24	99.85	25.75	0.75	0.57	68.72	0.15	95.94
25.90	1.10	0.62	70.48	0.09	98.19	26.02	0.89	0.50	68.00	0.16	95.57
26.72	0.98	0.44	71.42	0.39	99.95	26.19	0.67	0.46	68.17	0.36	95.85
25.81	1.26	0.66	70.39	0.45	98.57	26.30	0.78	0.47	69.08	0.48	97.11
26.02	0.90	0.40	70.23	0.51	98.06	25.89	0.82	0.58	69.18	0.16	96.63
25.24	1.37	0.56	69.73	0.49	97.39	26.35	0.80	0.48	71.97	0.46	100.06
26.38	0.88	0.59	69.95	0.12	97.92	27.60	0.82	0.54	69.33	0.50	98.79
26.62	0.98	0.47	70.81	0.69	99.57	27.44	0.91	0.46	70.51	0.58	99.90
25.52	1.32	0.57	69.94	0.38	97.73	27.10	0.73	0.50	70.63	0.34	99.30
25.80	0.82	0.42	69.72	0.35	97.11	26.08	0.79	0.51	69.87	0.07	97.32
25.74	1.56	0.80	69.33	0.46	97.89	25.85	0.67	0.59	70.53	0.12	97.76
25.49	0.66	0.57	72.41	0.07	99.20	26.46	0.95	0.47	72.08	0.19	100.15
25.48	1.08	0.77	70.87	0.10	98.30	26.05	0.80	0.47	71.85	0.10	99.27
25.22	1.13	0.78	72.19	0.04	99.36	25.96	0.68	0.54	70.46	0.14	97.78
25.46	1.53	0.92	71.50	0.24	99.65	24.91	0.63	0.33	70.39	0.21	96.47
26.19	0.99	0.50	71.89	0.37	99.94	25.72	0.97	0.47	68.55	0.00	95.71
26.28	0.91	0.51	70.41	0.44	98.55	26.74	0.68	0.54	71.12	0.03	99.11
25.90	0.87	0.50	70.56	0.55	98.38	26.83	0.87	0.59	70.76	0.21	99.26
26.38	0.97	0.64	71.24	0.41	99.64	26.88	0.89	0.48	68.54	0.25	97.04
25.51	1.62	1.10	71.41	0.63	100.27	27.04	0.70	0.42	71.44	0.26	99.86
25.18	1.30	0.86	70.16	0.50	98.00	26.34	0.59	0.51	70.99	0.07	98.50
26.17	1.16	0.78	70.64	0.44	99.19	27.13	0.87	0.63	68.34	0.00	96.97
26.55	0.73	0.60	71.39	0.70	99.97	26.96	0.92	0.63	69.10	0.26	97.87
25.51	1.28	0.93	70.20	0.33	98.25	26.73	0.69	0.34	68.20	0.29	96.25
25.56	0.97	0.61	70.72	0.37	98.23	26.75	0.68	0.64	69.75	0.32	98.14
25.83	0.81	0.47	70.15	0.29	97.55	25.87	0.66	0.58	68.86	0.16	96.13
25.84	1.25	0.69	69.59	0.36	97.73	25.69	0.82	0.50	71.06	0.06	98.13
25.05	1.36	0.76	69.83	0.63	97.63	27.19	0.85	0.46	69.31	0.50	98.31
25.92	0.83	0.47	70.73	0.38	98.33	26.06	0.94	0.40	68.50	0.33	96.23
26.48	0.94	0.52	69.94	0.41	98.29	26.24	0.81	0.52	70.84	0.35	98.76
28.14	1.20	0.54	69.05	0.59	99.52	25.69	0.81	0.48	70.95	0.23	98.16
26.68	0.65	0.40	71.06	0.38	99.17	26.09	0.82	0.62	71.13	0.34	99.00
26.33	0.86	0.47	70.12	0.26	98.04	26.28	0.92	0.47	70.41	0.16	98.24
25.53	1.42	0.64	69.12	0.40	97.11	26.33	0.90	0.49	67.78	0.32	95.82

in progress to a certain extent even within such a short period of time, can also influence the chemical composition and consequently contribute to the scattering of the impurity contents.

In spite of such a wide divergence in chemical composition, the alite in the specimen fired for 5 min is composed practically of M_3. According to the phase diagram for C_3S solid solutions, first given by Woermann *et al.* (2) and later revised by the authors (3) as regards its phase identification, the chemical compositions in Fig.1(a), rich in (Al_2O_3+ Fe_2O_3) and poor in MgO, are expected to produce M_1 rather than M_3 as the constituent phase of alite at ambient temperature. In commercial clinker, alite, despite its reasonably high (Al_2O_3+ Fe_2O_3) content, never occurs as M_3 if MgO is scarce in solid solution (4,5).

The conflict mentioned above can be solved by taking into account the cooling rate of clinker. A thin section of the specimen fired for 5 min was reheated under the microscope at the rate of 240°C/min up to 1150°C, when the alite exists as R, then cooled at a given rate down to 600°C and quenched. Quenching from 1150°C exclusively produces M_3 at ambient temperature. At 225°C/min are formed hybrid crystals in which M_1 is found in patches. With a decreasing cooling rate M_1 becomes more and more predominant within each crystal; and at a rate smaller than 70°C/min the alite crystals come to be made up uniformly of M_1. With the alite under consideration, therefore, its metastable occurrence as M_3 at ambient temperature is entirely due to the rapid cooling of clinker.

In accordance with this conclusion, the alite, when reheated, first undergoes the reversion to T_2 above 700°C and then the transition to M_1 at around 820°C (1). On the other hand, alite, if well-stabilized as M_3 with plenty

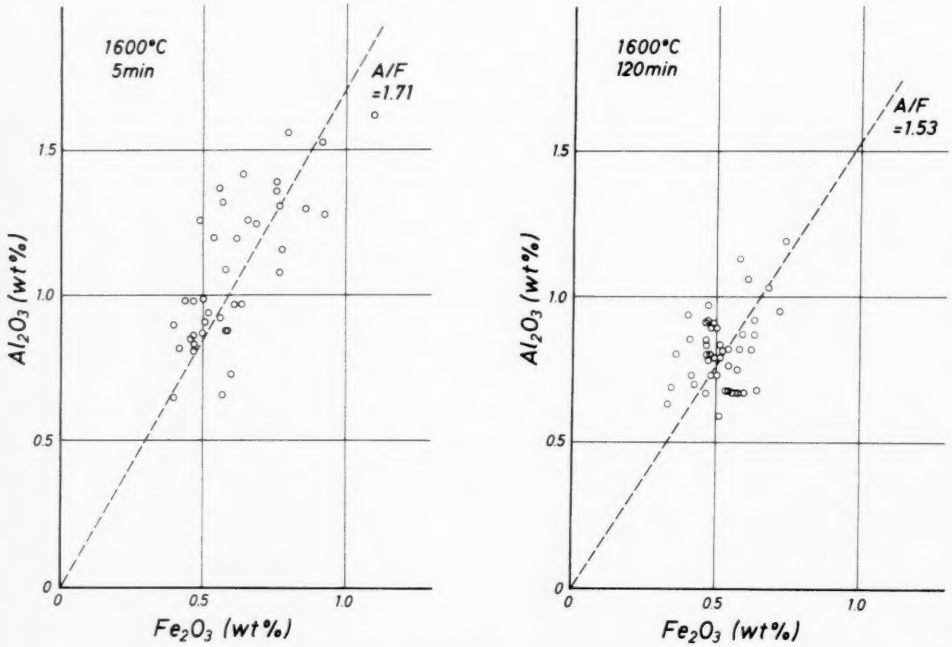

FIG. 2
Al_2O_3 *vs.* Fe_2O_3 in alite.

of MgO as well as Al_2O_3 and Fe_2O_3 in solid solution, gives no indication of phase change at all until the direct transition to R occurs above 1000°C.

According to Woermann *et al.* (6), the solubility limits of Al_2O_3 and Fe_2O_3 in C_3S are mutually dependent and restrict each other. Nevertheless, with the alite crystals primarily formed the amount of Al_2O_3 in solid solution often exceeds its equilibrium concentration determined separately from other components (1.0 wt % irrespective of temperature (6)). There seems to exist a trend that Fe ions enter into solid solution in parallel with Al ions (Fig.2).

Comparison of Figs.1(a) and 1(b) shows a significant decrease in impurity content due to recrystallization. MgO, Al_2O_3 and Fe_2O_3 have been decreased on the average by 35, 25 and 14 percent, respectively, with a corresponding decrease in the ratio of Al_2O_3/Fe_2O_3 from 1.71 to 1.53 (Fig.2). In Fig.1(b) the chemical compositions of alite lie in much more limited concentration ranges than in Fig.1(a). The impurity or solute concentration as given in Fig.1(b), too low to stabilize alite exclusively as M_3, produces T_2 predominantly at ambient temperature. During the intermediate stages of recrystallization, therefore, there occur in abundance hybrid crystals of alite consisting of both T_2 and M_3, as represented by the reverse zonation, which, however, eventually come to be made up uniformly of T_2 with duration of heating (1).

In spite of the foregoing it should be noted that a lowering of the impurity content does not necessarily lead to a phase change. To the metastable occurrence of M_3 at ambient temperature the presence of MgO in high concentration is most essential; so that with portland clinker rich in MgO, M_3 persists during the course of recrystallization despite a considerable decrease in both Al_2O_3 and Fe_2O_3 contents. In clinker containing 1.2 % of MgO, for example, alite can exist as M_3 even after firing for 120 min at 1600°C (1).

Discussion

A growing crystal, at any finite growth rate, can produce microsegregation in front of the advancing solid-liquid interface by rejecting impurity components. In a steady growth state it is the diffusion length D/f that determines the scale of diffusion segregation during crystal growth, where D is the appropriate diffusion constant and f the growth velocity. The interface segregation changes significantly the distribution of impurities between the solid and liquid and consequently affects the chemical composition of the crystal. The crystal growth of alite in clinker occurs in an essentially unsteady state under nonequilibrium conditions, so that the effective distribution or segregation coefficient cannot be expressed in a general form as a function of the growth velocity, diffusion boundary layer thickness, diffusion constant of the impurity ion concerned, growth direction and so on. Nevertheless there is experimental evidence which confirms, though qualitatively, the close dependence of the impurity content in alite on the growth rate from the interstitial melt (5).

With clinkering at 1600°C the precipitation of alite can generally be completed very quickly within a few minutes because of an extremely high degree of supersaturation resulting from the enhanced rate of dissolution of both CaO and C_2S into the interstitial melt. The consequent drop in supersaturation, together with the smallness of the grain size due to the very high nucleation rate, gives rise to an early onset of recrystallization. The degree of supersaturation remains so low during recrystallization that the growth rate of alite, as compared with that of the primary crystallization from the raw mix, is decreased drastically, say, by about two orders of magnitude. This wide difference in the growth rate manifests itself in a remarkable difference in the amount of impurity in solid solution. Thus the redis-

tribution of the impurity due to recrystallization demonstrates the very close dependence of the chemical composition of alite on its growth rate from the interstitial melt.

At a temperature as high as 1600°C part of the Fe ions in alite exist as ferrous ions, which are accomodated exclusively in the Ca-sites. The ferric ions, on the other hand, equally replace the tetrahedral sites as well as the Ca-sites (6). Fe_2O_3, as compared with Al_2O_3, shows a less decrease in content during recrystallization. This can be explained by assuming that in alite the Fe ions are distributed differently between the two distinct cation sites according to their valence state. In the specimen fired for 120 min the oxidation - reduction equilibrium of the Fe ions seems to have been almost reached as evidenced by the brownish tint of clinker.

Acknowledgment

Part of the support came from the Grant-in-Aid for Scientific Research from the Japanese Ministry of Education, Science and Culture (No.57430014).

References

1. I. Maki, H. Haba and S. Takahashi, Cement and Concrete Research 13, 689 (1983).
2. E. Woermann, W. Eysel and Th. Hahn, Zement-Kalk-Gips 22, 414 (1969).
3. I. Maki and K. Kato, Cement and Concrete Research 12, 93 (1982).
4. I. Maki, Il Cemento 76, 167 (1979).
5. I. Maki and K. Goto, Cement and Concrete Research 12, 301 (1982).
6. E. Woermann, W. Eysel and Th. Hahn, Zement-Kalk-Gips 22, 235 (1969).

VOL
14
198

CEMENT and CONCRETE RESEARCH. Vol. 14, pp. 419-430, 1984. Printed in the USA.
0008-8846/84 $3.00+00. Copyright (c) 1984 Pergamon Press, Ltd.

PORE SIZE DISTRIBUTION OF PORTLAND CEMENT SLURRIES AT VERY EARLY STAGES OF HYDRATION (INFLUENCE OF CURING TEMPERATURE AND PRESSURE)

P. PARCEVAUX
ETUDES ET FABRICATION DOWELL SCHLUMBERGER
Cementing Group
BP 90 - 42003 SAINT-ETIENNE (FRANCE)

(Communicated by M. Regourd)
(Received Oct. 24, 1983)

VOL.
14
1984

ABSTRACT

Pore size distribution of Portland cement pastes has been studied using helium picnometry and mercury porosimetry. Cement samples were hydrated under varying conditions of temperature and pressure and were investigated at very early stages of hydration : thickening, setting, and early hardening. The evolution of pore size distribution with time has been related to physical and chemical properties (compressive strength, shrinkage, and combined water). The interpretation has been based on the repartition between free pores of tubular shape and trapped pores of rounded shape, and a model is proposed for describing cement pore size distribution.

Introduction

Porosity and pore size distribution of hardened cement pastes have been widely investigated in the last ten years, as strong evidence of their influence on some cement mechanical properties has been demonstrated.

Total porosity has been measured through water or kerosene immersion (11) or through helium picnometry (8). Pore size distribution has been studied by gas adsorption (1, 7, 9) but pore size is then limited to a maximum diameter of 400 A°. At the opposite end of the range, wide pores (several microns) have been described using optical microscopy (12) but quantification is then difficult to achieve, the best technique being image analysis. Mercury porosimetry allows one to study pore size distribution over a wide range, from several tens of Angströms up to several tens of micrometers depending on the capability of the equipment used. The contact angle between mercury and cement has been experimentally studied in (2), and found to be dependent on the method of dehydration of the cement sample. Beaudoin (8) has pointed out some microsctructural limitations of mercury porosimetry like exclusion of mercury from too small pores and change in contact angle between mercury and surface. Winslow and Diamond (2) have defined some conditions to be taken in account for treatment

procedure, like mercury compressibility or mercury expansion upon heating. The minimum pore size accessible by liquid mercury is estimated at 20 Angströms (17), and some experimental data (16) show that matrix compressibility of a porous sample is negligible.

The total pore size distribution of hardened cement pastes, determined through the preceeding techniques, has been described as being composed of a threshold diameter (2) and several families of pores, macro or capillary porosity, micro or CSH gel porosity and mesoporosity (porosity between particulate hydration products). Macroporosity is found to be composed of pores wider than a few thousand of Angströms (2, 15) or wider than a few hundred of Angströms (6) and gel porosity composed of pores narrower than a few hundred Angströms. The effect of curing conditions on the pore size distribution of hardened cement pastes has been investigated. Auskern and Horn (6) have shown that curing under pressure increases the width of the pores, and Diamond (4) found the same tendency for curing at very low temperature (6°C) compared to a higher one (40°C). Bentur (9) found that when the curing temperature increases from 25 to 65°C, the macroporosity increases while the meso and microporosity decrease without any change in total porosity. He also stated that when the degree of hydration increases, macroporosity and total porosity decrease while mesoporosity increases. The relationships between pore size distribution and cement mechanical properties are still controversial but some researchers have demonstrated that total pore volume is correlated neither to flexural strength which can be associated to macroscopic pores (13), nor to permeability which is more related to pore size distribution (14). Furthermore, Sierra (15) has found that cement permeability is measurable only if the maximum pore diameter is wider than 0.13 microns.

Previous studies have been based upon the investigation of the total pore size distribution of cement samples, including pores which are trapped within the cement structure due to interconnexion through narrower ones. Furthermore, attention has been paid to hardened cement pastes only (after several days to several months of hydration) and most of the time with fairly smooth curing conditions (ambient temperature, low or atmospheric pressure). The purpose of this study has been to delve further into the investigation of pore interconnexion and to describe respectively the size distribution of free pores which contribute to cement permeability and the distribution of trapped pores which do not contribute to flow properties but nevertheless influence the cement mechanical properties. Furthermore, this investigation has been carried out on cement slurries at very young ages (from a few minutes to one day of hydration), and under various conditions of curing temperatures and pressures. High temperature and pressure conditions have been investigated to simulate the behaviour of a cement slurry used for cementing oil, gas or geothermal wells, application which have not been widely studied up to now, but which nevertheless require a large technical and scientific knowledge of cement physics and chemistry.

Experimental

Materials and Mixing

Only one cement slurry composition was used in order to allow easy comparison of various curing conditions and various stages of hydration : API Class G cement (Dyckerhoff Gulf type), in water at 44% by weight of cement, plus 1% of an organic superplasticizer and 0.5% of an antifoaming agent by weight of cement. The density of the slurry was 1.90.

Mixing was achieved following API procedure specification 10 using a high shear mixer of the Waring Blendor type. 600g of cement were first poured into 15 seconds in the correct volume of water with the impeller of the mixer rotating at 4000 rpm, and then high shear mixing was achieved with an impeller speed of 12000 rpm for 35 seconds.

VOL
14
198

Table I

CHEMICAL COMPOSITION OF DYCKERHOFF

API CLASS G CEMENT, GULF TYPE (% BY WEIGHT)

CHEMICAL ANALYSIS							POTENTIAL COMPOSITION (*)			
SiO_2	Al_2O_3	Fe_2O	CaO	Free lime	MgO	SO_3	C_3S	C_2S	C_3A	C_4AF
21.5	3.9	6.0	65.4	0.5-1.0	0.6	2.1	61	15	0	18

(*) according to Bogue's formula

Curing

After mixing each batch of cement, the slurry was agitated for 20 minutes at a given temperature (29, 55, 71 or 84°C) to allow initial maturation to take place, and then statically hydrated at the same temperature and at a given pressure (atmospheric or 4 MPa) in sealed cells located in a thermostated oven. Curing conditions are described for each system in Table II.

Cement hydration was continuously monitored by recording the internal cement slurry temperature.

Sampling

For each curing condition (i.e temperature, pressure), samples were taken at the following times of hydration : when cement temperature started to exceed the test temperature, then when cement temperature reached a maximum, and finally after 24 hours of curing. Each time, a cell was taken out of the oven, pressure was bled off when necessary and it was quickly cut into two cylindrical plugs, 5 cm in diameter by 5 cm in length. One plug was used for measurement of the cement compressive strength and water content by oven drying at 105°C for 24 hours. The second one was used for studying pore size distribution.

Preparation of Samples

Samples were dehydrated by freeze-drying. Small cuttings of about 0.1-0.3cm^3 were prepared and frozen in liquid freon (-40.8°C) continuously cooled by liquid nitrogen (-196°C). They were then transferred in liquid nitrogen, for a while, and the ice was sublimed under vacuum for about 24 hours. This technique has already been described (11) and allows one to properly prepare even very fragile samples without disturbing their microstructure.

Techniques of Measurement

Porosity measurements for each sample were determined using a mercury porosimeter (Autopore 9200) capable of intrusion pressures ranging from 0.007 to 407 MPa, and helium picnometer (model 1320) both from the Micromeritics Company. Mercury porosimetry was used to measure bulk density and pore size distribution and helium picnometry to measure skeletal density and then, total porosity. The surface tension for mercury was taken as the well established value of 484 dynes/cm. The contact angle was chosen at 117° according to (2) for oven dried samples and after having made sure that oven-drying and freeze drying led to the same contact angle. A correction was made for mercury compressibility, and an equilibrium time of 60 seconds was applied for each

VOL. 14 1984

Table II

TABLE OF SAMPLES

SAMPLE NUMBER	CURING TEMPERATURE (°C)	CURING PRESSURE (MPa)	SAMPLING TIME
1	29	atm.	T.T.
2	29	atm.	S.T.
3	29	atm.	24 H
4	55	atm.	T.T.
5	55	atm.	S.T.
6	55	atm.	24 H
7	71	atm.	T.T.
8	71	atm.	S.T.
9	71	atm.	24 H
10	84	atm.	S.T.
11	84	atm.	24 H
12	55	4.0	T.T.
13	55	4.0	S.T.
14	55	4.0	24 H
15	84	4.0	T.T.
16	84	4.0	S.T.
17	84	4.0	24 H

T.T. : thickening time S.T. : setting time

step of pressure. Experiments were run using 40 steps of increasing pressure, from 0.035 to 407 MPa, corresponding to diameters ranging between 25 microns and 21 Angströms, and total porosity given by helium picnometry was used to complete the curve on the smallest diameter side.

Theory of Pore Size Distribution Determination through Mercury Porosimetry

Mercury Porosimetry allows one to measure the entry pore sizes but not the real pore size, and hence interpretation of pore shape and pore interconnexion is difficult to achieve. But pore shape and interconnexion are responsible for trapped porosity which is the volume of mercury which stays in the pores of the sample when pressure is released, while the extruded volume corresponds to the free porosity. Figure 1 shows possible configurations of pores giving rise to trapped porosity.

Free and trapped porosity do not play the same role in the physical properties of a porous material. It is clear that permeability is related to free porosity only, while flexural strength is certainly related to trapped porosity and compressive strenth to both. Mercury porosimetry yields access to the distribution of free and trapped pores by running two intrusion-extrusion cycles of mercury on the same sample (10). The first intrusion curve is the distribution of total porosity, the second intrusion curve is the distribution of free porosity, and the difference between both intru-

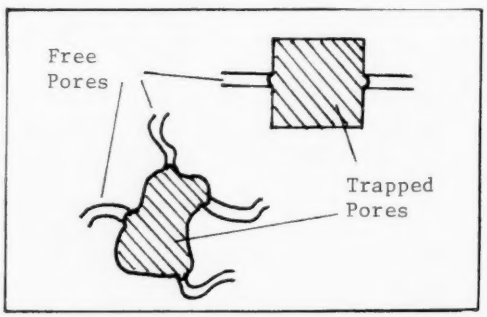

Figure 1
Example of Free Pores and Trapped Pores.

sion curves is the distribution of trapped porosity. Furthermore, as a first approximation, free pores can be assimilated to cylindrical tubes and trapped pores to rounded holes. The distribution of free porosity can then be considered as the distribution of the true pore-diameters and not only of the access pore diameters.

RESULTS

Cement Hydration and Bulk Properties

. Cement temperature curves have been used for monitoring cement hydration. They are presented in Figures 2 and 3. During the induction period, the cement temperature is constant. When cement hydration starts, the temperature increases up to a maximum value. The samples being located in an isothermal medium, as when a cement slurry is placed into a hole drilled in a subterranean formation, thermal exchange occurs between cement and the surrounding medium, and then, when the rate of hydration slows down, cement temperature decreases to its original value. Whatever the curing conditions (temperature and pressure), cement samples taken just after the beginning of hydration were like pastes of a high consistency, and we call this time the thickening time, while cement samples taken at the maximum temperature exhibited a rigid structure but with a low compressive strength and we call this time the setting time.

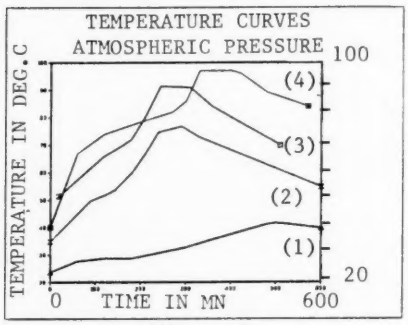

Figure 2

(1): 29 deg.C (3): 71 deg.C
(2): 55 deg.C (4): 84 deg.C

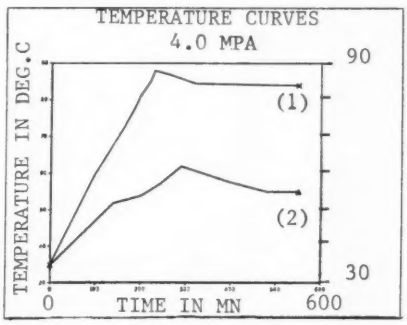

Figure 3

(1) : 84 deg.C
(2) : 55 deg.C

. For each sample examined, several properties were measured : compressive strength, water content, combined water, total porosity, free porosity, trapped porosity and chemical shrinkage. Combined water was determined using the formula : $Wc = (0.44 - W)/(1 + W)$, where 0.44 is the original water to cement ratio and W is the water content of the sample. Combined water, which is the amount of water which has been combined to form hydrates, is an indication of the degree of hydration of the cement sample. Cement chemical shrinkage due to hydration, S, was estimated using the relationship $S = \rho b.(N - W)$ where N is the total porosity, W the water content, and ρb the bulk density of the sample. Free porosity, experimentally determined down to a pore diameter of 20 A°, was linearly extrapolated to zero, as this extrapolation was found to be valid for total porosity by comparison with helium picnometry measurements. All these data are presented in Table III.

. At the time of thickening, the compressive strength is zero, whatever the curing conditions ; the combined water, which is already 6,5%, is not influenced by pressure but increases up to 9% when the curing temperature exceeds

TABLE III
BULK PROPERTIES OF CEMENT SAMPLES

SAMPLE NUMBER	COMPR. STRENGTH MPa	WATER CONTENT cc/g	COMBINED WATER %	TOTAL POROSITY cc/g	FREE POROSITY cc/g	TRAPPED POROSITY cc/g	SHRINKAGE %
1	0	0.3540	6.4	0.3520	0.2740	0.039	0
2	1.26	0.3226	8.9	0.3850	0.3220	0.059	9
3	13.24	0.3133	9.7	0.3650	0.2700	0.110	8
4	0	0.3586	6.0	0.3450	0.2830	0.023	0
5	0.70	0.3462	7.0	0.4150	0.3430	0.068	9
6	13.24	0.2741	13.0	0.2900	0.2100	0.120	3
7	0	0.3501	6.7				
8	1.82	0.3224	8.9	0.3300	0.2730	0.058	1
9	13.03	0.2766	12.8	0.2420	0.1450	0.070	0
10	1.02	0.2964	11.0	0.3600	0.2950	0.055	9
11	18.21	0.2364	16.5	0.2350	0.1400	0.085	0
12	0	0.3481	6.8	0.3075	0.2420	0.012	0
13	1.33	0.2628	14.0	0.2920	0.2350	0.020	5
14	25.84	<0.2628		0.3550	0.2450	0.107	12
15	0	0.3239	8.7				
16	2.24	0.2601	14.3	0.3080	0.2575	0.045	7
17		0.2065	19.3				

80°C; the total porosity does not depend on curing temperature but decreases with increasing pressure from 0.35 cc/g at atmospheric pressure to 0.31 cc/g at 4 MPa ; the free porosity represents 80% of total porosity, and chemical shrinkage is nil.

. At the time of setting, compressive strength does not depend on curing temperature but it doubles when pressure is applied. Combined water increases when temperature exceeds 80°C and when pressure is applied. It ranges between 7 and 14%. Total porosity decreases when temperature and pressure increase and free porosity is 83% of total porosity. Chemical shrinkage is high and does not depend on temperature but decreases when pressure is applied, from 9% at atmospheric pressure to 6% under 4.0 MPa.

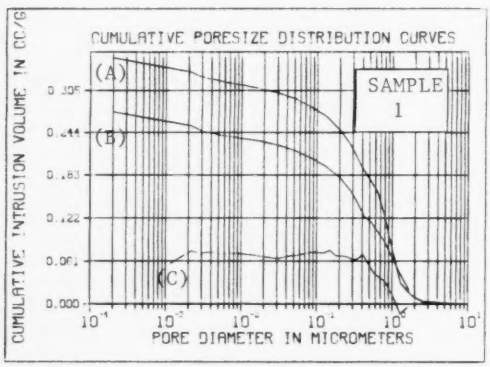

Figure 4
(A) Total pores (B) Free pores
(C) Trapped pores

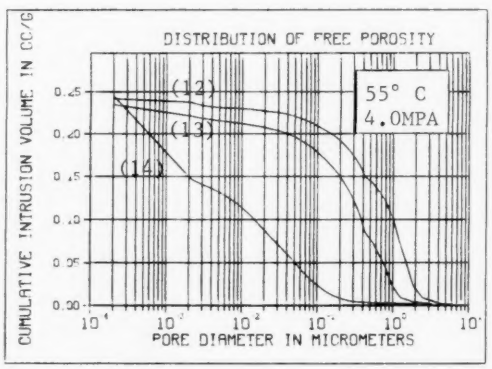

Figure 5
(12) Thickening (13) Setting
(14) 24 hours

. After 24 hours of hydration, all cement properties depend strongly upon curing conditions. Compressive strength increases when temperature exceeds 80°C. It also increases with increasing pressure, from 13 MPa when cured at atmospheric pressure up to 26 MPa when cured under 4.0 MPa. Combined water increases when temperature and pressure increase. It ranges between 10% to 19%. Total porosity decreases from 0.365 to 0.235 cc/g when temperature increases from 29°C to 84°C, but it increases when pressure is applied. Free porosity follows the same behaviour in absolute value but in percentage of total porosity, free porosity is independant upon pressure and decreases from 74% to 60% when temperature is increased.

Pore size Distribution

. On each cement sample, the total, free and trapped pore size distributions were determined using two cycles of mercury intrusion-extrusion plus helium picnometry. Some of the cumulative curves are presented in Figures 4 to 6, and examples of differentiated curves are presented in Figures 7 and 8. Each specific peak on a differentiated curve corresponds to a family of pores and the maximum of the peak is the mode of the family, or the most represented diameter in this family. The dispersion of pores around the mode in each family is then characterized by the width of the peak at mid height.

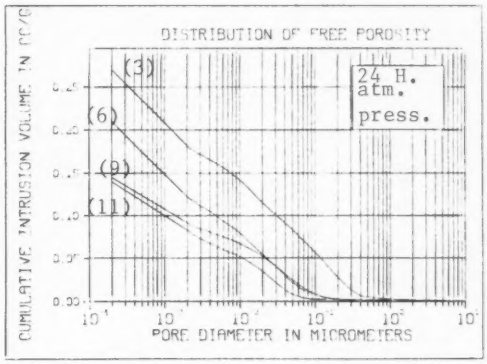

Figure 6

(3) 29°C (6) 55°C (9) 71°C
(11) 84°C

. The pore size distribution curves all exhibit the same shape :
(1) A flat or low slope linear region in the range of wide diameters.
(2) A threshold diameter below which intrusion proceeds at a high rate and which is determined by the diameter below which the differentiated volume starts increasing sharply.

Three families of pores more or less well distributed around modal diameters can be distinguished according to their size : (3) Macroporosity (4) Mesoporosity (5) Microporosity.

. Typical parameters of the distribution of trapped and free porosities are presented in Table IV. Free porosity, which can be considered as composed of tubular pores, is characterized through the values of threshold diameter, modal diameters and pore families. On the contrary, as the trapped porosity is composed of round shaped pores, only access pores diameters can be known but not the true pore diameters, then it has been characterized by the relative percentages of each family of pores only.

. The values of the families of pores depend essentially on the stage of hydration and not on curing conditions. Whatever the curing conditions, at the time of thickening, cement porosity is essentially composed of macro and mesoporosity, free porosity being composed of 50% macroporosity and 40% mesoporosity while trapped porosity is at 80% composed of macropores. At the time of setting, the main representative family of pores is the mesoporosity and the free porosity is composed of 25% macroporosity, 55% mesoporosity and 20% microporosity, while trapped porosity is composed of both macro and mesopores. After 24 hours of hydration, macroporosity has completely disappeared except for samples cured at the lowest temperature (29°C). Free porosity is then composed

OL.
14
984

TABLE IV
Distribution of Trapped Porosity

SAMPLE NUMBER	% OF TOTAL POROSITY	TRAPPED MACRO POROSITY %	TRAPPED MESO POROSITY %	TRAPPED MICRO POROSITY %
1	22	73	27	0
2	17	76	15	9
3	26	42	58	0
4	18	89	0	11
5	17	100	0	0
6	28	0	75	25
8	17	12	88	0
9	40	0	93	7
10	18	40	60	0
11	40	0	100	0
12	21	81	19	0
13	20	70	25	5
14	31	0	61	39
16	16	50	50	0

Distribution of Free Porosity

SAMPLE NUMBER	% OF TOTAL POROSITY	THRESHOLD DIAMETER µm	MACRO MODE µm	MACRO POROSITY %	MESO MODE µm	MESO POROSITY %	MAX. MICRO PORE µm	MICRO POROSITY %
1	78	2.6	0.90	44	0.40	42	0.010	14
2	83	2.0	0.88	26	0.39	52	0.006	18
3	74	0.44	0.13	37	0.016	22	0.005	41
4	84	2.4	0.90	51	0.39	41	0.012	8
5	83	2.0	0.87	27	0.39	53	0.014	20
6	72	0.22		0	0.012	43	0.007	57
8	83	2.0	0.83	17	0.40	62	0.001	21
9	60	0.20		0	0.038	52	0.006	48
10	82	3.0	0.83	27	0.39	54	0.015	19
11	60	0.12		0	0.024	39	0.007	61
12	79	2.5	1.15	62	0.39	33	0.008	5
13	80	1.6	0.87	32	0.39	60	0.006	8
14	69	0.20		0	0.057	56	0.0034	44
16	84	2.0	0.85	14	0.39	69	0.005	17

of 50% mesoporosity and 50% microporosity while trapped porosity is mainly composed of mesopores (60-100%).

. The threshold diameter is 2.5 microns at the time of thickening and decreases down to about 2.0 microns at the time of setting. But at this setting time the threshold diameter increases when the temperature exceeds 80°C and it decreases when the curing pressure increases. Modal diameters of macro and meso porosities are more or less identical at both thickening and setting times, whatever the curing conditions (macromode : 0.90 microns and mesomode : 0.40 microns).

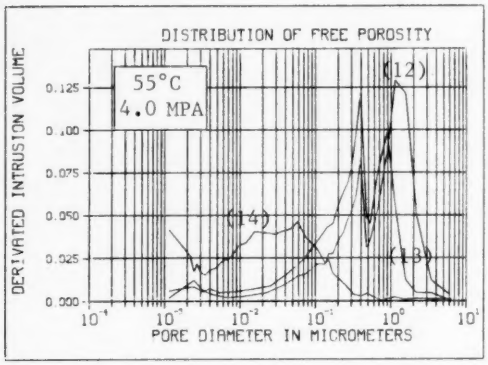

Figure 7
(12) Thickening (13) Setting
(14) 24 hours

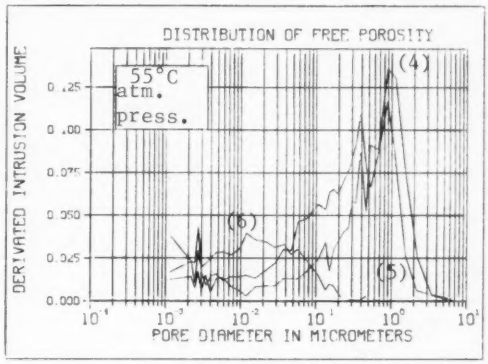

Figure 8
(4) Thickening (5) Setting
(6) 24 hours

After 24 hours of hydration, the threshold diameter is independant of pressure but it decreases when temperature increases, from 0.44 microns at 29°C to 0.12 microns at 84°C, while the modal diameter of mesoporosity increases when curing temperature and pressure increase, from 0.016 microns at 29°C and atmospheric pressure to 0.057 at 55°C and 4.0 MPa. In every case, the microporosity does not exhibit any particular mode and most of the time ranges between 0 and 0.01 microns.

VOL.
14
1984

DISCUSSION

. Thickening and setting time, as defined on the temperature curve of cement samples, are specific steps of the cement hydration which correspond to a given physical appearance of the cement. At the thickening time, cement properties are essentially independant of curing conditions. The influence of curing conditions starts being appreciated at the setting time and they become predominant during the hardening phase. Nevertheless, already since the thickening time, a change in combined water is observed when the curing temperature exceeds 80°C, which suggests that hydration proceeds almost identically for temperature up to 80°C but certainly faster and differently above 80°C. Investigation of cement hydration at high temperature must then be carried out especially for application to the cementation of deep or geothermal wells.

. Total porosity and chemical shrinkage are closely related to each other and to cement hydration since the total porosity must decrease when hydration proceeds, however, it also should increase with chemical shrinkage. Between the initial time of mixing and the thickening time, some hydration proceeds but no chemical shrinkage is noticed because cement structure is deformable, and so effectively the total porosity decreases. On the other hand, between the thickening and the setting times, hydration goes on and the cement gains a cohesive and less deformable structure, and then a high chemical shrinkage is observed. Consequently, the total porosity increases, the effect of shrinkage compensating for the effect of hydration. However, on the other hand, the curing pressure increases the deformability of the cement structure and when hydration is achieved under pressure, the value of chemical shrinkage is lower and total porosity does not change significantly. After the setting time, and when the cement hardens, total porosity decreases sharply while shrinkage becomes lower or even not visible. We are certainly observing plugging of some pores through a structural change of hydration products. Curing under pressure delays the appearance of shrinkage, which still occurs but at a later time, when the internal cohesion

of the cement is greater than the applied pressure.

. The total porosity of the cement samples can be divided into free porosity, composed of tubular well interconnected pores which participate in flow properties, and trapped porosity, composed of round pores interconnected through free pores. Free porosity follows exactly the behaviour of total porosity which indicates that the porosity generated by the chemical shrinkage during hydration is entirely composed of free porosity. Therefore up to the setting time, trapped porosity is only determined by the original distribution of cement grains in water and not by the cement hydration. During hardening, hydration still generates free pores but in the same time the formation of non-porous or microporous hydration products leads to a semi-plugging of some pores which drastically increases the amount of trapped porosity, and reduces the permeability of the sample.

.Regardless of the curing conditions and the stage of hydration, the pore size distribution curves are fairly similar in shape and the following model is proposed for describing cement pore size distribution :

(1) The low slope linear part above the threshold diameter represents the surface porosity of the sample and this is not interconnected to the matrix of the sample through pores of the same size.
(2) The threshold diameter is the maximum diameter for which interconnexion between pores of the same size goes deep enough into the matrix of the sample.
(3) Macroporosity represents the intergranular porosity composed of wide pores between cement grains.
(4) Mesoporosity represents interhydrates porosity : between cement grains more or less hydrated, some hydration products form and give rise to a secondary porosity.
(5) Microporosity represents the internal porosity of hydration products, mainly that of CSH gel.

. Cement pore size distribution is essentially independant of curing conditions at the thickening and setting times. At the thickening time, the hydration products have a very small internal porosity and they create only mesoporosity between each other though original macroporosity is still very large (50%). At the setting time, hydration products have filled even more intergranular space and macroporosity is decreasing sharply to the benefit of essentially mesoporosity (60%) but the hydration products are still of a low porosity by themselves (20%). When the cement hardens, macroporosity completely disappears and hydration products become microporous either through a structural change or through formation of new species.

Furthermore, trapped porosity is always composed of the largest pores present in the matrix of the cement, whatever the stage of hydration and the curing conditions.

. The valuesof threshold and modal diameters allow one to quantify the average size of free pores. It is interesting to notice that at the setting time, threshold diameter decreases when the curing pressure increases but that it starts increasing when the curing temperature exceeds 80°C. Again, for such cement slurries with a rather high water to cement ratio (44%), 80°C seems to be a transition temperature above which cement hydration proceeds differently and at a higher rate, generating larger pores. On the other hand, the modal diameters of macro and mesoporosity are not dependant on curing conditions up to the setting time. They show specific values, 0.90 microns for the macromode and 0.40 microns for the mesomode. After 24 hours of hydration, when the cement hardens, curing conditions do influence the values of these characteristic typical diameters, but curiously enough the threshold diameter decreases when temperature increases while the mesomode (which remains alone since macroporosity has disap-

VOL.
14
198

peared), increases when temperature and pressure increase. Therefore, while pores are wider, their maximum size is smaller.

CONCLUSIONS

(1) Thickening and setting times, as defined on the temperature curve of the cement, are specific stages of hydration which correspond to a given physical appearance of the cement.
(2) Cement porosity is composed of a free, well interconnected porosity, composed of tubular pores, and a trapped porosity composed of rounded pores. Mercury porosimetry allows one to obtain the "true" distribution of free pores while only the distribution of access trapped pores can be determined.
(3) Cement total porosity decreases due to the hydration process but at the same time chemical shrinkage generates new pores which increase total porosity at the time of cement setting. Pores generated by shrinkage are only free pores well interconnected between each other. Curing under pressure delays the appearance of these pores due to shrinkage.
(4) Up to cement setting, trapped porosity is solely determined by the original dispersion of cement grains in water and increases sharply during cement hardening due to the formation of hydrated species in the intergranular porosity or because of the plugging of some pores through microporous hydration products.
(5) Cement pore size distribution is characterized by a threshold diameter and three families of pores. The repartition between the three families depends on the stage of hydration, and turns from essentially intergranular porosity at the thickening time to an equal repartition between interhydrate and intra-hydrate porosities.
(6) Curing pressure influences cement pore size distribution and properties from the beginning of hydration as pressure delays the appearance of chemical shrinkage ; then cement free porosity is reduced by a large factor.
(7) Up to the setting time, the curing temperature is of little influence on cement pore size distribution except when it exceeds 80°C. Above 80°C, cement hydration proceeds at a higher rate and gives rise to larger pores. An investigation of cement pore size distribution at higher temperature (application to deep or geothermal wells) must then be carried out, in order to confirm it.

REFERENCES

(1) E.E. BODOR and al, Journal of Colloid and Interface Science, Vol. 34, n°4, p. 560-570.
(2) D.N. WINSLOW and S. DIAMOND, Journal of Materials, Vol. 5, n°3, 1970, p. 564-585.
(3) J.F. YOUNG, Proceedings of the International Symposium on Pore Structure and Properties of Materials, RILEM-IUPAC, Prague 1973, Vol. II part B, p. 205-216.
(4) S. DIAMOND, Proceedings of the International Symposium on Pore Structure and Properties of Materials, RILEM-IUPAC, Prague 1973, Vol. I part B, p. 73-88.
(5) J.F. YOUNG, Powder Technology, Vol. 9, 1974, p. 173-179
(6) A.B. AUSKERN, and W.H. HORN, Journal of the American Ceramic Society, Vol. 59, n° 1-2, 1976, p. 29-33.
(7) G.C. BUE and G.O. CHIGBO, Journal of Applied Chemistry and Biotechnology Vol. 27, 1977, p. 48-54.
(8) J.J. BEAUDOIN JCCR, Vol. 9, 1979, p. 771-781.
(9) A. BENTUR, Journal of the American Ceramic Society, Vol. 63, n° 7-8, 1980 p. 381-386
(10) F.M. PELLERIN, Bull. Liaison LCPC, n° 106, 1980, p. 105-117.
(11) P. PARCEVAUX, Thesis Docteur Ingénieur, Paris, 1980.

(12) N.M. ALFORD and A.A. RAHMAN, Journal of Materials Science, Vol. 16, 1981 p. 3105-3114.
(13) J.D. BIRCHALL, A.J. HOWARD and K. KENDALL, Nature, Vol. 289, 1981, p. 388-390.
(14) B.K. NYAME and J.M. ILLSTON, Magazine of Concrete Research, Vol. 33, n° 116, 1981, p. 139-146.
(15) R. SIERRA, Bulletin Liaison LCPC, n° 117, 1982, p. 77-81
(16) R.W. SMITHWICK, Powder Technology, Vol. 33, 1982, p. 55-64
(17) R.W. SMITHWICK, Powder Technology, Vol. 33, 1982, p. 201-209

VOL.
14
1984

CEMENT and CONCRETE RESEARCH. Vol. 14, pp. 431-436, 1984. Printed in the USA.
0008-8846/84 $3.00+00. Copyright (c) 1984 Pergamon Press, Ltd.

THE EFFECT OF SPECIMEN SIZE ON THE FRACTURE ENERGY OF CONCRETE

Sidney Mindess
Department of Civil Engineering
University of British Columbia
Vancouver, British Columbia, Canada

(Communicated by F.H. Wittmann)
(Received Nov. 9, 1983)

OL.
14
984

ABSTRACT

The effect of specimen size on the fracture energy of concrete was studied for 3-point bend tests on notched beams. Specimen sizes ranged from 100x100x840 mm to 400x400x3360 mm. It was concluded that the values for both fracture energy (G_F) and K_{IC} increased considerably for the largest beams tested. However, including the self-weight of the beams in the calculations made very little difference to the calculated values of G_F.

Introduction

The fracture energy (G_F) of concrete may be defined as the energy required to create one unit of crack area. Petersson (1-3) has described in detail how G_F may be determined from 3-point bend tests on notched beams. Recently, work at the Lund Institute of Technology (4,5) has culminated in a proposed RILEM recommendation for a test to measure G_F for mortar and concrete. Briefly, this proposal (5) involves a 3-point bend test on a notched beam. The beam dimensions are 100x100x840 mm, tested on an 800 mm span; the beam is notched at midspan to one-half the depth of the beam. The fracture energy is then calculated as

$$G_F = \frac{W_o + mg\delta_o}{A_{lig}} \qquad (1)$$

where W_o = the energy represented by the area under the load-deformation curve
m = the mass of the beam between the supports
g = the acceleration due to gravity
δ_o = maximum deflection of the beam at failure
A_{lig} = area of the uncracked ligament

Note that $mg\delta_o$ represents the energy supplied by the weight of the beam itself.

The energy terms of Equation 1 can be described graphically by looking at an idealized load-deflection curve, as shown in Figure 1. Here, W_o represents the area under the measured load-deflection curve. However, the weight of the beam also contributes energy to the system, and this is represented by W_1, W_2 and W_3. W_1 is equal to $mg\delta_o/2$, and it has been shown by Petersson (1) that $W_2 \cong W_1$, leading to Equation 1. W_3 is so small that it may be neglected. When $W_o/(W_o + W_1 + W_2) < 0.3\text{-}0.4$, Equation 1 is not applicable (5).

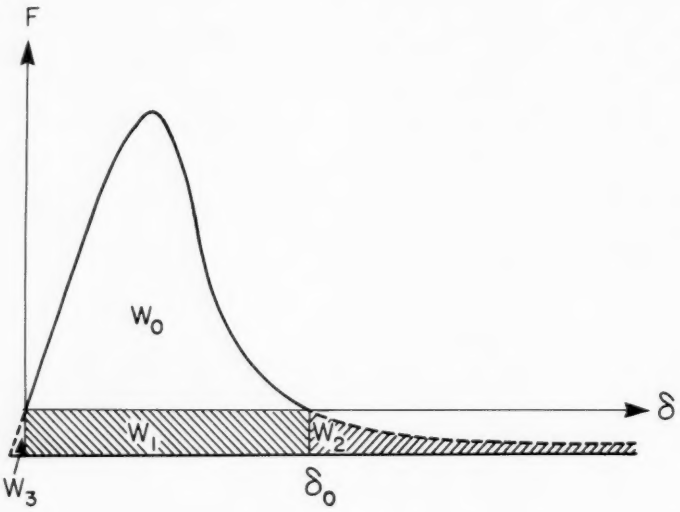

FIG. 1

Load-deflection curve for notched beam in bending when the weight of the beam is not compensated for.

This formulation is based on the assumption that all of the fracture energy is consumed in the very narrow fracture zone which develops in front of the notch as the crack propagates through the beam. However, it neglects any contribution to the microcracking process from the stresses due to the dead weight of the beam itself. While this contribution is undoubtedly negligible for reasonably small beams, it may be significant for very large specimens. It is the purpose of this paper to examine the effect of changing the size (but not the relative dimensions) of the specimens on the fracture parameters.

Experimental Procedures

Test Specimens

Test specimens of three different sizes were cast. Their dimensions were (width x depth x length):

i) 100x100x840 mm, tested on an 800 mm span
ii) 200x200x1680 mm, tested on a 1600 mm span
iii) 400x400x3360 mm, tested on a 3200 mm span

The concrete, with the mix design shown in Table 1, was delivered in a single batch by a commercial ready-mix truck. It was vibrated into the plywood forms using an immersion vibrator. The specimens were all prepared with a cast-in notch, formed by placing a piece of 4 mm thick fibre-board of the appropriate size at the bottom centre of each form. The ratio of notch depth to specimen depth was about 0.5 in all cases. For the 400x400x3360 mm

VOL. 14 1984

TABLE 1

Concrete Mix Design

Type 10* normal portland cement	460 kg/m^3
Water	174 kg/m^3
Coarse aggregate (13 mm maximum size)	1295 kg/m^3
Sand	565 kg/m^3
Water reducer and retarder	1430 mℓ/in^3
Air content	3 ± 1%
Slump	~ 75 mm
38-day compressive strength	48.5 MPa

*ASTM Type I

beams, to prevent cracking during handling, a 25 mm reinforcing bar, about 600 mm long, was cast in across the preformed notch. This bar was then cut with a torch at the preformed notch once the specimen was in place in the testing machine.

Three specimens of each size were cast. The forms were covered with wet burlap for the first two days; the specimens were then cured in the ambient laboratory environment for a further 34 to 36 days until they were tested. Three companion 150x300 mm cylinders were also cast, and subjected to the same curing. They were tested at an age of 38 days, yielding an average compressive strength of 48.5 MPa.

Test Procedure

The concrete beams were tested in a large mechanical testing machine, as shown in Figure 2, following the procedures outlined in the proposed RILEM recommendation (4). The load was applied at an approximately constant deformation rate of 0.01 mm/sec, with failure occurring about 1 minute after the start of the test. The deformation of the beam during the test was measured using an LVDT (linear variable differential transformer), placed on the top of the beam as near as possible to the centre. The load-deflection (P-δ) curves were plotted with an x-y recorder, and the areas under these P-δ curves were obtained by the method of counting squares.

Because of the substantial weight of the larger beams, it was decided to try to determine the deflections of these beams due to their own weight, to see what contribution the energy supplied by the weight of the beam might make to the fracture process. Since it was not possible to measure these dead-weight deflections directly, they were determined analytically by means of a finite element program which could calculate the deflected shape of the notched beams from the measured concrete properties. It was noted that, for the 100x100x840 beams, the dead load deflections were only about 0.6% of the deflection due to the applied load. For the 200x200x1680 mm beams, the dead load deflections were about 2.5% of the live load deflections, while for the 400x400x3360 mm beams, the dead load deflections were about 10% of the live load deflections.

Experimental Results

Due to limitations of both time and money, only 9 specimens were tested. This is far less than the recommended number of samples (8 for each size), leading to a considerable amount of scatter in the results (4). Nonetheless, the results for all of the beams tested are given in Table 2.

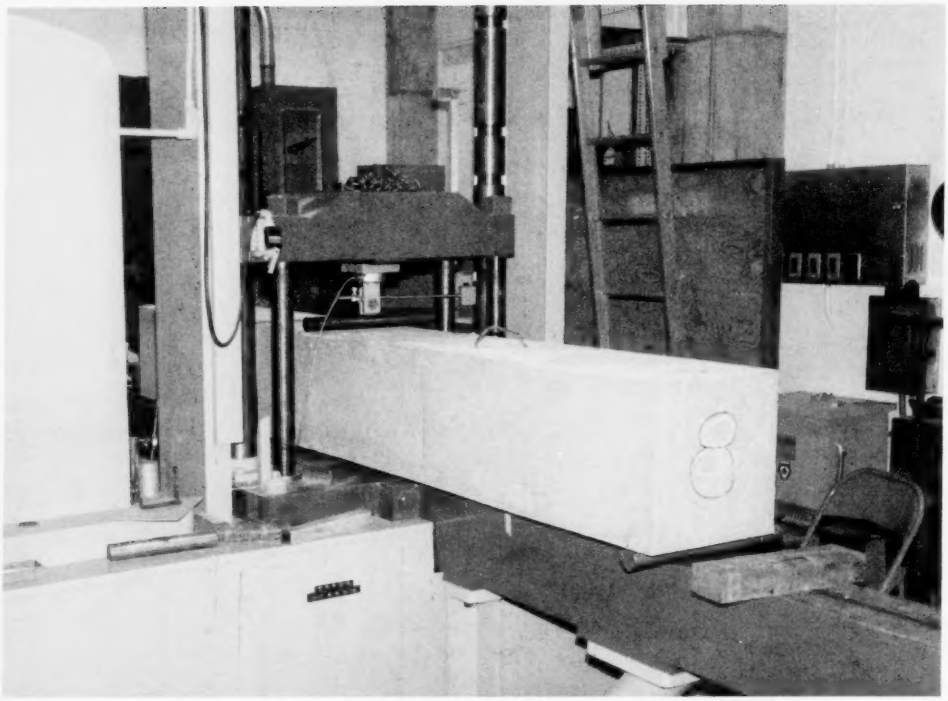

FIG. 2

Testing of a notched 400x400x3360 mm beam in 3-point bending.

In addition to the calculation of the fracture energy by Equation 1, two other calculations are presented. The first introduces an additional term into Equation 1, to include the energy from the dead-weight deflection of the beam. According to this formulation,

$$G_F^* = \frac{W_o + mg\delta_o + 0.29mg\delta_1}{A_o} \qquad (2)$$

where δ_1 is the dead weight deflection of the beam at mid-span. The term $0.29mg\delta_1$ then represents the strain energy stored in the beam due to its dead-weight deflection, based on the calculated deflected shape of the beam. For the small beams, of course, this term is negligible, but for the largest beam it is significant.

The other calculation is of the fracture toughness of the concrete, K_{IC}. Unfortunately, there is no analytical solution in the literature for K_{IC} for a notched beam under a uniformly distributed load (i.e. under its own weight). Therefore, K_{IC} for the beams in question was calculated by summing together the standard solution of Brown and Srawley (6) for a notched beam in 3-point bending, and the solution (7) for a notched beam with a constant bending moment. While this second term is only an approximation to the loading system in question, it should be sufficiently accurate for the present purposes. The results of all 3 calculations are given in Table 2.

TABLE 2

Summary of Test Results

Specimen No.	Specimen Size (mm)	P_{max} (N)	A_{lig} (m^2)	δ_o (m)	δ_1 (m)	W_{beam} (kg)	$mg\delta_o$ (Nm)	$mg\delta_1$ (Nm)	W_o (Nm)	G_F (N/m)	G_F^* (N/m)	K_{IC} $MNm^{-3/2}$
1	100x100x840	623	4.93×10^{-3}	0.76×10^{-3}	6×10^{-6}	18.43	0.137	0.001	0.251	78.	78.8	
2	"	623	4.85×10^{-3}	1.00×10^{-3}	"	18.42	0.181	0.001	0.325	104.3	104.4	
3	"	356	4.78×10^{-3}	0.89×10^{-3}	"	17.48	0.153	0.001	0.128	58.8	58.9	
								Average		80.6	80.7	0.42
4	200x200x1680	712	1.97×10^{-2}	0.64×10^{-3}	24×10^{-6}	147.7	0.927	0.035	0.238	59.1	59.7	
5	"	1560	1.95×10^{-2}	1.00×10^{-3}	"	147.0	1.442	0.035	0.836	116.8	117.3	
6	"	712	1.95×10^{-2}	0.76×10^{-3}	"	147.9	1.103	0.035	0.298	71.8	72.4	
								Average		82.6	83.1	0.41
7	400x400x3360	1710	7.73×10^{-2}	0.41×10^{-3}	98×10^{-6}	1198.1	4.819	1.152	0.582	64.9	74.2	
8	"	1000	7.82×10^{-2}	$0.64\text{-}10^{-3}$	"	1193.8	7.495	1.148	0.241	98.9	103.2	
9	"	2110	7.86×10^{-2}	1.1×10^{-3}	"	1181.9	12.754	1.136	1.168	177.1	181.3	
								Average		115.3	119.6	0.61

VOL. 14 1984

Discussion

It may be seen that, for the two smaller beam sizes, the values of G_F are essentially the same, and the corrections for the self-weight of the beams (included in G_F^*) are negligible. For the largest beams tested, G_F is about 40% higher than for the smaller beams. This is similar to the data of Sorensen (1), who found that increasing the beam depth from 50 mm to 200 mm increased G_F by about 20%. Even here, however, the correction for the self-weight of the beams adds only about 4% to the value of G_F. Hillerborg (8) has argued that the dead weight deflection of the beams should not be included separately in the calculation of G_F since it is already included in the $mg\delta_0$ term. However, this can only be an approximation, since the stresses due to the weight of the beam must somehow be accouted for explicitly in calculating the fracture energy. Nevertheless, it is clear from Table 2 that ignoring the dead weight of the beams in practice would make little difference to the results obtained.

Moreover, for the beams larger than the recommended size of 100x100x840 mm, W_o is significantly less than 0.3-0.4 of the total energy. On average, for the smallest beams, $W_o/(W_o + mg\delta_o) = 0.6$; for the medium sized beams, $W_o/(W_o + mg\delta_o) = 0.28$; for the largest beams, $W_o/(W_o + mg\delta_o) = 0.07$. Therefore, by the criterion of the proposed recommendation, the values obtained from the two larger sets of beams would be considered invalid.

The values of K_{IC} shown in Table 2 are based on the assumption that linear elastic fracture mechanics applies to concrete beams in this size range. Again, there is no difference between the values of K_{IC} calculated for the 100 mm deep and 200 mm deep beams. For the 400 mm deep beams, however, K_{IC} appears to increase by about 50% compared to the smaller beams.

However, these results are all questionable, since it has been argued that, before LEFM can be applied to concrete, very large beams must be used (9).

Conclusions

1. While for 100x100x840 mm and 200x200x1680 mm beams the values of G_F and K_{IC} appear to be independent of specimen size, these values increase considerably for the 400x400x3360 mm beams.
2. However, the proposed recommendation (4) indicates that for specimens with aggregate particles larger than 32 mm, the specimen dimensions should be increased uniformly. The results of the present tests suggest that for this may lead to rather high values of G_F, and to difficulty in meeting the requirement that W_o/total energy < 0.3-0.4. Perhaps, as Hillerborg (8) has suggested, the length of beams larger than the recommended size should only be increased by the square root of the scale factor by which the other dimensions are increased. The weight of the beam itself would then have about the same influence for any size of beam.
3. Including the self-weight of the beams in the calculations makes little difference to the calculated values of G_F, even for the largest beams tested.

Acknowledgements

The author wishes to thank undergraduate students Albert Shing, William Szto, David Woo, Simon Wu, and John Yuen, who carried out the experimental work as part of the requirements for the course C.E. 356, Engineering Materials. Some financial assistance was provided by the Natural Sciences and Engineering Research Council of Canada.

References

1. P.-E. Petersson, Report TVBM-1006, Division of Building Materials, Lund Institute of Technology, Lund, Sweden, (1981).
2. P.-E. Petersson, Cem. Concr. Res. 10, 78 (1980).
3. P.-E. Petersson, Cem. Concr. Res. 10, 91 (1980).
4. Proposed RILEM recommendation, (29 January, 1982; revised version June 1982), Determination of the Fracture Energy of Mortar and Concrete by Means of Three-Point Bend Tests on Notched Beams, Division of Building Materials, Lund Institute of Technology, Lund, Sweden, (1982).
5. P.-E. Petersson, Report TVBM-3011, Division of Building Materials, Lund Institute of Technology, Lund, Sweden, (1982).
6. W.F. Brown, Jr., and J.E. Srawley, ASTM STP 410, American Society for Testing and Materials (1967).
7. D.P. Rooke and D.J. Cartwright, Stress Intensity Factors, HMSO, London, (1976).
8. A. Hillerborg, Private Communication (1983).
9. S. Mindess, in F.H. Wittmann (ed.), Fracture Mechanics of Concrete, pp. 22-24, Elsevier Scientific Publishing Company, Amsterdam (1983).

VOL
14
198

CEMENT and CONCRETE RESEARCH. Vol. 14, pp. 437-438, 1984. Printed in the USA.
0008-8846/84 $3.00+00. Copyright (c) 1984 Pergamon Press, Ltd.

NOTES

LOW TEMPERATURE OPC-TYPE CEMENT CONTAINING SUPERHYDRAULIC C_2S PHASE

S.N. Ghosh, V.K. Mathur, and S.K. Chopra
Cement Research Institute of India
M-10, NDSE-II, New Delhi-110049, India

The earlier works on reactive belite phase have been covered recently in our review article (1). The latest studies are those reported by Suzuki, et al (2) and Stark et al (3). The former's work relates to high early strength development of C_2S phase (made from laboratory chemicals at temperatures 1360°C and above) and in the latter's work, the existence of active belite phase has been referred to giving rise to high early strength development which apears to be primarily dependent on high rate of quenching of clinker.

Through this note the above authors wish to report the development of low temperature OPC-type cement containing superhydraulic C_2S phase by adopting the normal process of cement manufacture but with the added advantage that the clinkering temperature is lower by about 100°C and yet the clinker is well formed with minimum of free lime, around 0.6%. The clinkers were obtained at 1365°C with 20 minutes of retention by firing nodules of raw meal in a laboratory furnace and subsequent air-quenching. The XRD studies reveal that C_2S phase in this clinker is a mixture of polymorphs of β-C_2S and a reactive form similar to α' phase. The clinker did not show any dusting indicating little transformation to γ phase. This had been achieved with a suitable adjustment in the moduli value of the raw mix composition, control of alkalies at a suitable level, optimization of clinkering temperature and retention time and without resorting to water quenching. However, a certain amount ($\sim$ 20%) of alite phase has been designed in this optimum composition.

The cement made out of the above clinker with 5% gypsum had a true density of 3.23 g/cc and when ground to the usual fineness of about 3000 cm^2/g (Blaine) and tested for the compressive strength in terms of standard mortar specimen as per IS: 269-1976 was found to give strength of 232 (3 days), 366 (7 days) against the minimun specified of 160 and 220 kg/cm^2 respectively. The gain in strength from 7 to 28 days was about 30% showing thereby that OPC-type clinker can be produced from industrial grade raw materials with equivalent or better performance but at significantly lower clinkering temperatures implying thereby substantial savings in energy. Further work including the effects of quenching techniques and conditions is in progress in the Cement Research Institute of India.

As per the present indication it appears that further lowering of lime content in raw mix may also be possible and this could lead to the utilization of inferior grade raw materials which is of great importance to India and several other countries not endowed with good quality limestone.

References

1. S.N. Ghosh, P.B. Rao, A.K. Paul and K. Raina, J. Mater. Sci. 14, 1554 (1979).
2. J. Stark, A. Mueller, R. Schrader, et al., Silikattechnik 31, 168 (1980).
3. K. Suzuki, S. Ito, S. Shibata and N. Fugii, 7th ICCC, Paris II, II-47 (1980).

VOL
14
198

CEMENT and CONCRETE RESEARCH. Vol. 14, pp. 439-442, 1984. Printed in the USA.
0008-8846/84 $3.00+00. Copyright (c) 1984 Pergamon Press, Ltd.

APPLICATION OF GPC FOR THE ANALYSIS OF THE OLIGOMER DISTRIBUTION OF NAPHTHALENE-BASED SUPERPLASTICIZERS

D.M. Roy
Materials Research Laboratory
The Pennsylvania State University
University Park, PA 16802 USA

G. Váradi, F.D. Tamás and G. Pályi
University of Veszprém
H-8201 Veszprém, P.O. Box 158, Hungary

B. Bartha
Egyesült Vegyimüvek
H-1657 Budapest, P.O. Box 2, Hungary

VOL.
14
984

(Received June 20, 1983)
(Refereed)

ABSTRACT

A gel permeation chromatographic method was developed for the fractionation of superplasticizer agents prepared from naphthalene sulfonic acid and formaldehyde.

Introduction

Naphthalene sulfonic acid based superplasticizers are widely used in concrete technology (1). Their effectiveness is believed to be strongly influenced by the molecular weight distribution of the product (2). In spite of the great importance of this factor surprisingly little is known about the molecular composition of the preparations used practically.

Some chromatographic efforts were already reported [PC (3), LC (4,5), HPLC (6), GPC (7,8)] but the results are often contradictory and the assignments uncertain.

A gel permeation chromatographic method, using two different types of gels was found to provide a promising entry to this problem. We report here on preliminary tests.

Experimental

Chromatography: Biogel P-4 (Bio Rad Labs.) 2x32 cm column (bed volume 100.5 cm^3); exclusion limit 3600 dalton; W_r = 2.4 g H_2O/g xerogel; V_d= 5.8 cm^3/g xerogel. Flow rate: 16.0 cm^3/h; fraction vol: 5.4 cm^3; sample vol: 1.0 cm^3;

$V_{external}$ = 39.8 ± 2.9 (7) cm^3; $V_{total, meas.}$ = 142.7 ± 8.3 (6) cm^3; $V_{internal}$ = 103.8 cm^3. Calibration: naphthalene-2-sulfonic acid (MW 207), naphthyl-di-and tripeptides (MW: 329,604,882), C-8, -9 and -11 hem peptides (MW: 1744, 1890, 2123). The volumetric partition coefficient (K_d) was calculated from $K_d = (V_{elution} - V_{external})/V_{internal}$. K_d vs. MW plots gave acceptable linearity (S > 80%). Eluent buffer: 50 mM K/PO_4 + 200 mM KCl (pH 7) which eluted 60-80% of the introduced material.

Sephadex G-75 (Superfine, Pharmacia, Uppsala, Sweden) 2.5 x 54 cm column (bed volume 265.1 cm^3); exclusion limit: 45000 dalton W_r = 7.5 g H_2O/g xerogel; V_d = 12-14 cm^3/g xerogel. Flow rate: 24.8 cm^3/h; sample vol: 2 cm^3; fraction vol. 6.2 or 8.2 cm^3; $V_{external}$ = 91.3 cm^3; $V_{total, meas.}$ = 315.4 cm^3; $V_{internal}$ = 224.1 cm^3. Calibration: Pharmacia Low MW Calibration Kit (α-lactalbumine 14400, tripsine inhibitor 20100, carbonic anhydrase 30000, ovalbumine 43000, albumine 67000, phosphorylase B 94000) At MW ≤ 43000 $\ln K_d$ vs. MW near to, linear, at MW 43000 exclusion. Eluent buffer: 50 mM K/PO_4 + 400 mM KCl (pH 7), about 80% of the introduced sample could be recovered.

Instrumentation: Radirac Fraction Collector Type 3402 B, 3403 B. Detector (UV, 280 nm): Uvicord 4701 A control unit, 4701 A optical unit; plotter 6250 A; peristaltic pump: Varioperpe X (all from LKB AB, Stockholm, Sweden).

The UV detector was calibrated with naphthalene-2-sulfonic acid (ε_{280} = 1.79 x 10^5 cm^2/g, determined with UNICAM SP 1805, 1 cm cell width, recording in the range 190-320 nm. The use of this extinction coefficient implied the supposition that the same ε can be used for the condensed naphthalene moieties too.

Preparation of the Plasticizer Sample: 208 g Naphthalene-2-sulfonic acid was reacted in a 3 L vessel (equipped with thermometer, mechanical stirrer and reflux condenser) with 40 g freshly distilled 56% aqueous formaldehyde solution which was added dropwise during 30 minutes at 100°C. After addition of the formaldehyde, 25 cm^3 H_2O was added and the reaction mixture stirred for 2 hours at 100-110°C. Then 20 g 36% aqueous formaldehyde was diluted with 25 cm^3 H_2O and slowly added to the reaction mixture (20-24 min.) at 100°C which was followed by further 2 hours stirring at 100°C. The product was neutralized with 40% aqueous NaOH which was added dropwise at 90-100°C until pH 8 was reached (140 g NaOH solution was consumed). The product was cooled to room temperature and diluted to reach 20% active substance concentration.

Testing of the Plasticizer: Concrete was made by using 300 kg/m^3 cement and 0.40 water/cement ratio. 20 cm^3 plasticizer/kg cement was added. The flow table spread was 161.5%; strength (28 days) was 21.7 MPa (101.4%).

Results and Discussion

The results of the gel permeation chromatography of the plasticizer samples are summarized in Table 1, permitting some preliminary considerations and conclusions.

Table 1

Results of GPC analysis of a naphthalene-2-sulfonic acid (NS) formaldehyde condensate

Column	Fract.	Weight of act.subst. (mg)	NS equivalent (mg)	NS equivalent (mM)	NS distribution (%)	X_i	Average MW
Biogel P-4	A	36.8	9.1	4.1×10^{-2}	34.2	0.097	562
	B	2.0	0.5	0.2×10^{-2}	1.9	0.021	
	C	21.7	5.4	2.4×10^{-2}	20.3	0.507	
	D	46.8	11.6	5.3×10^{-2}	43.6	0.374	
Sephadex G-75	A	88.3	22.0	9.9×10^{-2}	37.2	0.014	583
	B	120.7	30.0	13.6×10^{-2}	50.8	0.671	
	C	28.6	7.1	3.2×10^{-2}	12.0	0.315	

(i) GPC is of optimal efficiency and reliability if spherical particles are analyzed, which is not to be expected with naphthalene sulfonic acid/formaldehyde condensates. Thus some exaggeration of the apparent MW can be expected.

(ii) The active substance of the plasticizer contains both aromatic and ionic groups which might favor adsorption and ion exchange interaction with the gel. In this work it was attempted to avoid this effect by using high ionic strength in the eluent (200 or 400 mM KCl) which increased significantly the amount of the eluted material (from 8-20% to 60-80%). Assuming identical specific adsorption and exchange coefficients for the particular oligocondensates, a negative (diminishing) error in the measured MW cannot be fully excluded.

(iii) The calibration of the Biogel P-4 could be performed by linear, and that of the Sephadex G-75 by globular molecules, which favor the reliability of the data obtained with the former with respect to the present problem.

Taking into regard all these considerations, surprisingly good agreement was obtained between the average MW data obtained with the two gel types. The agreement between these two MW measurements excludes also the possibility of eventual irregularities in the elution order as it has been observed with other gels (7). The numerical MW values show that the oligocondensate is dimer in average.

These results indicate that the method can be used for the analysis of naphthalene sulfonic acid based superplasticizers. Of course, some refinement is necessary, especially in the preparation of more suitable calibration substances; possibly obtaining individual oligomers with a preparative variant of the method reported in this paper. Further experimental work is in course to achieve this aim.

References

1. Some leading references are:
   (a) U.S. Patent, 643,740 (1932).
   (b) V.S. Ramachandran, Cem. Res. Progs. (Cem. Div. Amer. Ceram. Soc.) 107 (1982 publ. 1983).

VOL. 14 1984

(c) Admixtures [Proc. Internat. Congr.], Constr. Press, Hornby (England) (1980).
(d) K. Asaga and D.M. Roy, Cem. Concr. Res. 10, 287 (1980).

2. (a) Canadian Patent, 961,866 (1975).
(b) M.R. Rixom, Chemical Admixtures for Concrete, p. 11, Halstad Press, New York (1978).
(c) M. Collepardi, M. Corradi and M. Valente, Developments in the Use of Superplasticizers (V.M. Malhotra, ed.), p. 485. Publ. SP-68, American Concrete Institute, Detroit (1981).

3. K. Hattori and Y. Tanino, Kogyio Kagaku Zasshi, 66, 55, 59, 65 (1963); 67, 1576 (1964).
4. S. Fudano and K. Konishi, J. Chromatogs., 56, 51 (1971).
5. J. Pomares, AQEIC Bol. Tec. 27,(5), 123 (1976).
6. H. Uchikawa and R. Furuta, Yogyo Kyokaishi, 87 (2), 115 (1979).
7. M.J. Gravey and T.F. Tadros, Kolloid-Z., Z. Polymere 250, 967 (1972).
8. M.H. Simatupand, Zement-Kalk Gips 28, 427 (1975).

Acknowledgement

This work was carried out under Grant NSF INT-8011922.

VOL
14
198

CEMENT and CONCRETE RESEARCH. Vol. 14, p. 443, 1984. Printed in the USA.
0008-8846/84 $3.00+00. Copyright (c) 1984 Pergamon Press, Ltd.

DISCUSSION

A DISCUSSION OF THE PAPER "ON THE VARIATION OF NEUTRAL-AXIS POSITION IN MORTAR BEAMS" BY O.A. KAYYALI"*

S.C. Kheok and C.F. Leung
Department of Civil Engineering
National University of Singapore
Kent Ridge, Singapore 0511

VOL. 14 1984

The writers would like to commend the author for a very interesting paper which contains a study on the variation of the neutral-axis in mortar beams.

Some of the author's conclusions agree with results obtained by the writers. Typical results of one of the concrete beams tested is shown in Fig. 1. Details of the tests are given in (1).

It can be seen in Fig. 1, that the neutral axis position started well away from the centroidal axis and progresses with increasing load towards the geometrical centroid. Such observation agrees with one of the author's conclusions. In view of the difference in the tensile and compressive deformation, an equation to calculate σ, the maximum tensile stress at the extreme fibre, has been proposed (1) for a rectangular beam.

$$\sigma = \frac{3M\ (\varepsilon_t + \varepsilon_c)}{bh^2\ \varepsilon_t}$$

where M = applied moment at the section,
b = width of the beam
h = height of the beam
ε_c = maximum compressive strain at the extreme fibre, and
ε_t = maximum tensile strain at the extreme fibre

However, Fig. 1 indicates that the neutral axis tends to start on the tensile half of the beam section. This deviates from the observation of the author where the neutral axis starts on the compressive side.

Reference

1. S.C. Kheok and C.F. Leung, "Role of Crack Initiation in Flexural Test for Tensile Strength," Indian Geotechnical Conference, India, Dec. 1983.

---

* CCR 13, 575-579 (1983).

VOL
14
1984

CEMENT and CONCRETE RESEARCH. Vol. 14, p. 445-446, 1984. Printed in the USA.
0008-8846/84 $3.00+00. Copyright (c) 1984 Pergamon Press, Ltd.

A REPLY TO A DISCUSSION BY S.C. KHEOK AND C.F. LEUNG OF THE PAPER "ON THE VARIATION OF NEUTRAL-AXIS POSITION IN MORTAR BEAMS"*

O.A. Kayyali
Department of Civil Engineering
University of Kuwait
P.O. Box 5969
Kuwait

VOL.
14
984

The author very much appreciates the interest in his paper as expressed by the discussants and is pleased that they have adopted an approach similar to his. It is evident that Kheok and Leung found this study important for further research concerning fracture characterisitcs of concrete. The author fully agrees with them in this respect. However, the author would like to make the following comments:

1) In Fig. 1 which represents results obtained by the discussants, it is observed that the plane section before bending has experienced inproportional strains during loading. The fact that the beams were concrete beams and thus less homogeneous than the mortar beams which were used by the author may contribute to the explanation of this effect. However, the author still finds it intriguing that the position of the neutral-axis in the case of concrete beams was nearer to the tensile side. In his opinion, it is expected that microcracks within the area of concrete under tension will be more numerous than in the area under compression. Thus the summation of forces for static equilibrium at the section would require greater area on the tension side than it would on the compression side.

2) The author has applied the formula proposed by the discussants to data from his tests. He obtained results which he believes to underestimate the maximum tensile stress at the extreme fibre by 11% and 23%.

Finally, the author would like to draw attention to a draftsman error in Fig. 4 of his paper. The value of 1.0 kN should have appeared on the second inclined line instead of the value of 3.0 kN.

*CCR 13, 575-579 (1983).

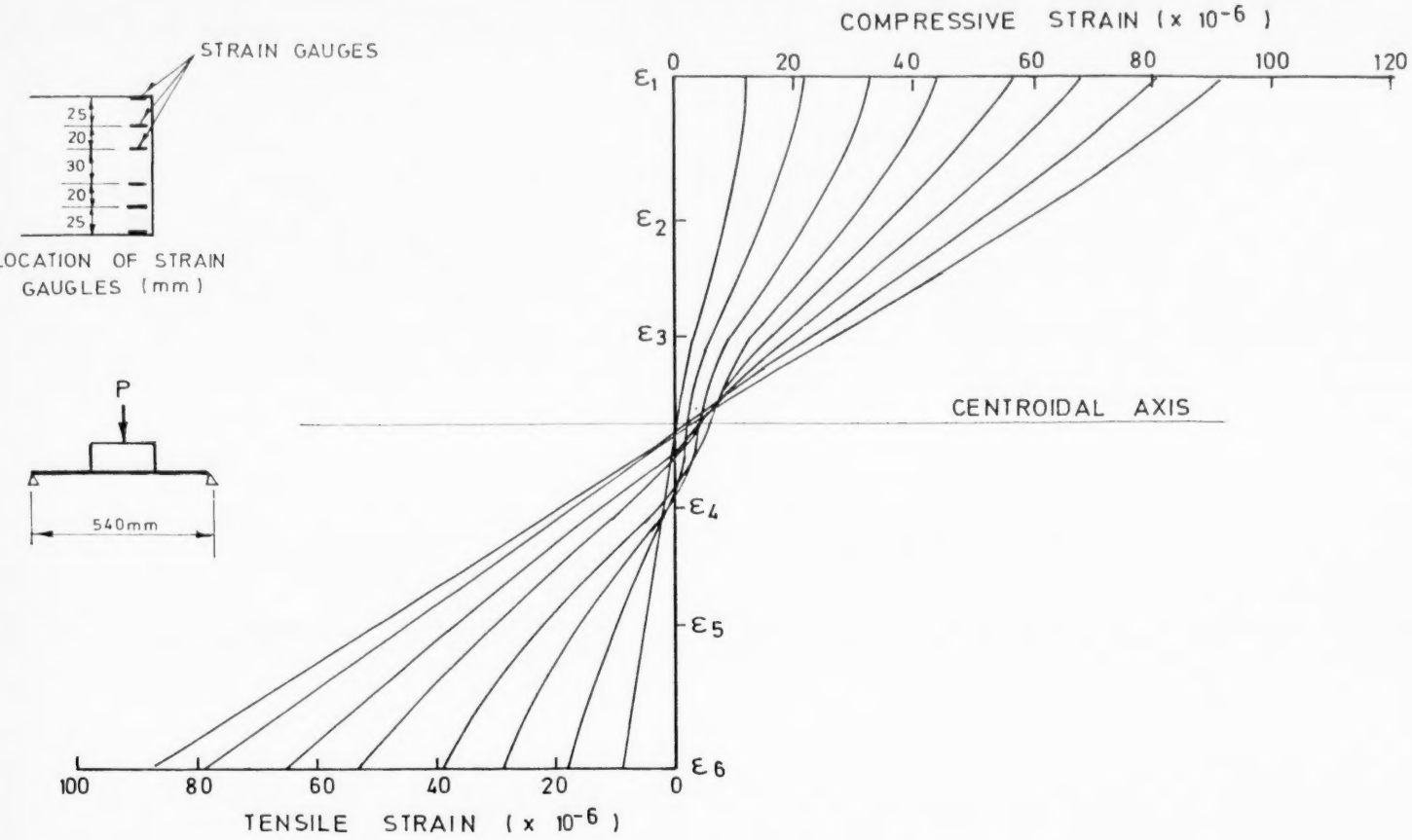

FIG. 1

Strain Profiles of Concrete Beam at Different Stages of Loading

VOL. 14, 1984

CEMENT and CONCRETE RESEARCH. Vol. 14, pp. 447-448, 1984. Printed in the USA.
0008-8846/84 $3.00+00. Copyright (c) 1984 Pergamon Press, Ltd.

NEW BOOKS

CREEP AND SHRINKAGE IN CONCRETE STRUCTURES. Edited by Z.P. Bazant and F.H. Wittmann. John Wiley & Sons, Ltd., 1982 (363 pp).

The contents of this book are based on the subject matter of ten invited lectures presented in the 1980 International Symposium on Fundamental Research on Creep and Shrinkage of Concrete. The Symposium was held at the Swiss Institute of Technology in Lausanne, under the co-sponsorship of Northwestern University and the U.S. National Science Foundation. The significant topics in the area are covered thoroughly by the distinguished researchers from various disciplines. The approaches taken for solving the problems related to the complicated phenomenon reflect the state-of-the-art knowledge in Material Sciences and Structural Mechanics. Sophisticated models developed for accurate computerized structural analysis have taken the realistic material behavior into consideration; the mechanisms identified for explaining the behavior are emphasized on the macro-level, the meso-level as well as the micro-level of the material; microstructural characteristics for the components of the hardened cement paste are based on the measurements utilizing modern techniques such as X-ray diffractions. Many fruitful research results are collected in this book.

VOL.
14
984

The book is divided into three parts. Part I consists of four chapters authored by J.F. Young, J.W. Dougill, E. Cinlar and S.E. Pihlajavaara, respectively. The fundamentals and general aspects related to concrete creep and shrinkage are viewed by the researchers in the area of Materials Sciences, Engineering Mechanics, Mathematics, and Structural Engineering. Chapter 1 deals with the microstructural characteristics of the significant components in the hardened cement paste system. Chapter 2 deals with the behavior of the composites based on methods used in classical mechanics. Chapter 3 introduces the thinking process of the probabilistic approach. Chapter 4 emphasizes the engineering features of concrete drying effects. Part II of this book, consisting of three chapters authored by C.D. Pomeroy, F.H. Wittmann and Z.P. Bazant, respectively, deals with the measurements and modeling of the material behavior. Chapter 5 describes the experimental techniques and results; chapter 6 covers the real and apparent mechanisms for creep and shrinkage phenomenon; chapter 7 presents linear and non-linear models for expressing the effects in the structures. The important parameters, including the environmental factors, are all considered in the models. Part III of this book consists of three chapters written by C.A. Anderson, W.H. Dilger and H.G. Russel, B.L. Meyers and M.A. Daye. Structural analysis with finite element approach, the methods of creep analysis and behavior from observations on full-scale structures are treated in these chapters.

The book contains a wealth of information. It will be an excellent reference not only to the researcher but to the structural engineer who is, or should be, interested in the subject.

Spencer T. Wu
Center for Building Technology
National Bureau of Standards

NEW BOOKS

ZEMENT-TASCHENBUCH. 48. Ausgabe (1984). 584 Seiten mit zahlreichen Abbildungen und Tabellen. Bauverlag GmbH, Wiesbaden und Berlin. DM 28.--.

Die jetzt erschienene Neuauflage des Zement-Taschenbuches erscheint ungefähr 4 Jahre nach der 47. Ausgabe. Wesentliche Teile der früheren Ausgaben wurden traditionsgemäss wieder übernommen. In den vergagenen Jahren ist die Beständigkeit des Betons und der Stahlbetonkonstruktionen nicht zuletzt wegen einiger spektakulärer Schadensfälle in den mittelpunkt des Interesses gerückt. Diese Tatsache wurde bei der Aufnahme von neuen Beiträgen berücksichtigt:

(1) "Beton für Aussenbauteile" von H. Weigler,

(2) "Imprägnierungen, Anstriche und Beschichtungen von Beton" von H. Klopfer, und

(3) "Hydraulisch gebundene Tragschichten" von H. Schmidt.

Zusätzlich wurde die "Richtlinie zur Verbesserung der Dauerhaftigkeit von Assenbauteilen aus Stahlbeton, März 1983", sie ist eine ergänzende Bestimmung zu DIN 1045, in das Zement-Taschenbuch aufgenommen.

F.H. Wittmann
Ecole Polytechnique Federale
de Lausanne, Switzerland

VOL.
14
1984

FUNDAMENTALS OF PORTLAND CEMENT CONCRETE: A QUANTITATIVE APPROACH. Vol. I: FRESH CONCRETE. Sándor Popovics, John Wiley & Sons, New York, 1982.

The emphasis of this book on fresh concrete is to provide a quantitative approach offering formulas acceptable for laboratory or practical use, providing input for automation and computer usage to provide better controls upon concrete quality. Different views are presented on major topics with an attempt to critically evaluate the views. Because concrete is such a complex material, the task of recommending the best quantification methods is a difficult one, and options are offered. Workability is treated thoroughly, beginning with rheology of fresh paste, through consistency, workability and rheology of fresh concrete, to dealing with the factors affecting concrete consistency. Testing of fresh concrete is considered as are the pumping, placement and vibration for different methods of placing. The principles, as well as methods are considered.

Adequately referenced and edited, the text includes many tables which provide dual listings of SI(metric) and customary English units, for broad applicability. Besides drawing from ASTM and ACI sources, Cement and Concrete Association (VK) and RILEM publications are widely quoted, as are other international sources. While the book is aimed primarily at the practitioner, laboratory workers and theoreticians will also find very useful information and compilations.

Della M. Roy

CEMENT and CONCRETE RESEARCH. Vol. 14, pp. 449-451, 1984. Printed in the USA.
0008-8846/84 $3.00+00. Copyright (c) 1984 Pergamon Press, Ltd.

OL.
14
984

NEWS ITEMS

International Conference on CONCRETE UNDER MULTIAXIAL CONDITIONS, Université Paul Sabatier, Toulouse, France. Information: M. Lorrain, Conference Secretariat, I.N.S.A., Département de Génie Civil, 31077 Toulouse Cedex, France. — May 22-24, 1984

A Symposium on BLENDED CEMENTS, sponsored by Committee C-1 Cement, of ASTM, in Denver. CO. Information: Kathy Greene, ASTM, 1916 Race Street, Philadelphia, PA 19103 USA. — June 1984

Third ASTM/CIB/RILEM International Conference on DURABILITY OF BUILDING MATERIALS AND COMPONENTS, Espoo, Finland. Information: Anneli Kaaresalo, Technical Research of Finland, Division of Building Technology, SF-02150 Espoo 15, Finland. — Aug. 12-15, 1984

International Symposia on CONCRETE PRESSURE AND STORAGE VESSELS, SEA STRUCTURES IN ARCTIC REGIONS, AND PREFABRICATION, Federation Internationale de la Procontrainte (FIP), Canadian Prestressed Concrete Institute, Calgary, Alberta, Canada. Information: FIP, c/o Genstar Structures, Ltd., 1000-1520 Fourth St., S.W., Calgary, Alberta T2R 1H5 Canada. — Aug. 25-31, 1984

Fourth International Congress on POLYMERS IN CONCRETE, Technische Holchschule Darmstadt, West Germany. Information: Prof. H. Schulz, Technische Hochschule Darmstadt, Kennwort; ICPIC 1984, Petersenstrasse 30, D-6100 Darmstadt, West Germany. — Sept. 19-21, 1984

International Conference on IN SITU/NONDESTRUCTIVE TESTING OF CONCRETE, by ACI, CANMET, National Bureau of Standards and the Canadian Society for Civil Engineering, Westin Hotel, Ottawa, Canada. Information: Harry S. Wilson, CANMET, 405 Rochester St., Ottawa, Ontario, Canada K1A 0G1. — Oct. 2-5, 1984

International Conference on TALL BUILDINGS, Shangri-la Hotel, Singapore, sponsored by the Council of the Institution of Engineers, Singapore. Information: The Chairman, ICTBS 84, 10, Anson Road, #14-06, International Plaza, Republic of Singapore (0207). — Oct. 22-26, 1984

ACI Convention, Grand Hyatt, New York, NY. Information: Ann K. Bruttel, Convention and Meetings Manager, ACI, P.O. Box 19140, Detroit, MI 48219 USA. — Oct. 28 - Nov. 2, 1984

NEWS ITEMS

CALL FOR PAPERS

Materials Research Society Symposium, M, dealing with **COAL COMBUSTION AND CONVERSION WASTES: CHARACTERIZATION, UTILIZATION AND DISPOSAL** will be held in Boston, MA 26-30 November 1984. This symposium is the 2nd in a series dealing with the characterization and utilization of industrial solid wastes. This year's symposium will concentrate on coal combusion wastes.

There are three options for dealing with the solid wastes from combustion of coal or from its conversion into gas or liquid fuels: (1) direct disposal by burial; (2) utilization in such applications as cement replacement, soil stabilization, mineral wool, structural ceramics and mine road construction; (3) extraction of valuable metals with disposal of the residues.

While the three options are coupled in various ways, especially with regard to environmental concerns, rarely do researchers dealing with the options interact. This symposium will provide a forum for such interactions, with the unifying factors being the characterization of the ash or fabricated materials, measurement of their properties and elucidation of their aqueous reactions during processing or after disposal. The symposium schedule will be designed to mesh with another MRS Symposium, J, on very high strength concrete (a major option for utilization of fly ash). (see below)

The following topic areas are representative of the content that is being solicited as oral and written presentations: phase characterization of combustion wastes; trace element partitioning in combustion waste; leachabilities (kinetics and mechanisms) of trace elements in combustion wastes; recovery from ash; utilization of ash.

Abstracts and one- to two-page summaries must be received by Dr. Turgut Demirel, Iowa State University, Dept. of Civil Engineering, Ames, IA 50011, Dr. Barry E. Scheetz, Materials Research Laboratory, The Pennsylvania State University, University Park, PA 16802, or Dr. Gregory McCarthy, North Dakota State University, Dept. of Chemistry, Fargo, ND 58105 by June 15, 1984. Papers will be selected by the sumposium co-chairman and authors will be notified of acceptance by July 30, 1984. Accepted papers will be published in appropriate refereed Journals.

Materials Research Society Symposium, J, dealing with **THE POTENTIAL FOR VERY HIGH STRENGTH CEMENT-BASED MATERIALS** will also be held in Boston, MA, 26-30 November, 1984. The fourth in a series devoted to cementitious materials, it is concerned with the concretes with strengths in excess of 10,000 psi (70 MPa). The two-day symposium will have two sessions dealing with the fundamentals of achieving very high strength cement-based matrices. A further two sessions will be devoted to applications, both in civil engineering areas where cement and concrete have traditionally been used, and in new areas where formerly ceramics, metals, or reinforced plastics have been used. It is the aim of the symposium to explore the limits to high strength and examine the transition from a traditional structural material to a low temperature ceramic-type material. Both invited and contributed papers will be presented.

Papers are solicited for the following areas: 1) Microstructure - influence of hydration products, aggregates, and other solid phases on properties; 2) Porosity and pore size distributions - influence on properties; 3) Fracture - application of fracture theories, improvement of ductility; 4) Civil engineering applications - new processes, applications, concrete properties; and 6) Novel applications in areas not traditionally associated with cements and concretes - e.g. replacements for ceramics, metals, or plastics.

VOL 14 198

NEWS ITEMS

Abstracts and one- to two-page summaries must be received by Dr. J. Francis Young, 3209 Newmark Civil Engineering Laboratory, University of Illinois, 208 North Romine, Urbana, IL 61801, by June 15, 1984. Papers will be selected by the sumposium co-chairman and authors will be notified of acceptance by July 30, 1984. Accepted papers will be published in full in a sumposium volume, after being refereed. Authors must send two copies of the complete text to reach Dr. Young by Nov. 1, 1984 in order to have their paper included in the Proceedings. Write to Dr. Young to obtain the formats for the abstracts and for any additional information.

REPORT

An IUTAM Symposium on "Mechanics of Geomaterials: Rocks, Concretes, Soils," dedicated to the memory of William Prager, was held at Northwestern University, September 11-15, 1983, under NSF sponsorship (and chaired by Z.P. Bazant). The primary objective of the Symposium was to promote interdisciplinary cooperation by bringing together mechanics specialists from various professional fields, such as structural and geotechnical engineering, geophysics, mining, nuclear reactor safety, and ocean engineering, which abound with problems that are similar from the mechanics viewpoint. After IUTAM President D.C. Drucker's opening lecture outlining Prager's impact on the evolution of inelastic continuum mechanics, 8 sessions introduced by 15 principal lectures addressed a wide range of timely topics selected by an International Scientific Committee co-chaired by Bazant and Rice. Dougill and Gudehus reviewed constitutive modeling and Grady discussed the behavior of solids with a system of cracks, Ruina, Evans and Wong treated shear localization in rocks, faulting and frictional slip, and Ingraffea and Bazant analyzed fracture propagation in rock and concrete. Subsequently, Rudnicki and Horrigmoe treated pore fluid effects in rock and concrete, Anderson and Wittmann examined creep and shrinkage and aging of concrete, Zienkiewicz, Baron and Sandler reviewed numerical modeling and dynamic analysis, and finally Mroz explored modern trends and new directions. Discussers' reports, prepared by Chen, Ehrlacher, Rice, Cleary, Pister and Bergan, critically examined the principal lectures and stimulated lively general discussions, to which more than half of the time was devoted. The questions of strain-softening, progressive fracture and damage, as well as stability, uniqueness and continuity in constitutive modeling, provoked the most intense and spirited debates. The questions of measurement and identification of material parameters, better design of experiments, and micro-mechanics of crack systems, also received much attention. Eagerness to discuss was aided by a 664 page Preprint Volume (deposited with NTIS), which was distributed in advance to all registrants. Various new results were reported in 20 short contributions. Symposium proceedings, featuring substantially revised, updated and expanded principal lectures and discussers' reports, are planned to be published by J. Wiley, London (edited by Z.P. Bazant) by the end of the summer of 1984. The book will also contain brief summaries of the main ideas, opinions and criticisms that transpired in the discussions, as recorded by Dafalias, Holcomb, Teufel, Ouchterlony, Cowin, Cedolin, Prevost and Sture.

VOL.
14
1984

CEMENT and CONCRETE RESEARCH. Vol. 14, pp.I-III, 1984. Printed in the USA.
0008-8846/84 $3.00 + .00 Copyright (c) 1984 Pergamon Press, Ltd.

SOFTWARE SURVEY SECTION

It is planned to introduce a new Software Survey Section to CEMENT and CONCRETE RESEARCH to encourage the open exchange of information on software programs unique to our professional field. With the rapid penetration of computers into academic and industrial institutions has come a parallel increase in the number of scientists and researchers designing their own software. The existence of much of this software remains unknown to even those of us who could most benefit from its use. We believe that it is of vital importance to our readers that such information be made available. We believe also that a professional journal is the best place to share such information. Your contribution would be most welcome.

VOL.
14
1984

The questionnaire on the following pages is designed to assist you in reporting on software that you may have developed or be in the process of developing. By completing this form, your information will reach thousands of your colleagues who may benefit from your work and may possibly offer suggestions for further enhancements to your software. Please complete the enclosed form and return it to:

Kathleen S. Mourant
Assistant Editor
CEMENT and CONCRETE RESEARCH
Materials Research Laboratory
University Park, PA 16802 USA

We do not intend to review or comment on the contents of the questionnaire. It will be published as is in order to expedite the information cycle process. We welcome any comments you may have.

CEMENT and CONCRETE RESEARCH. Vol. 14, pp. 453-454, 1984. Printed in the USA.
0008-8846/84 $3.00+00. Copyright (c) 1984 Pergamon Press, Ltd.

OL.
14
984

CHARACTERIZATION AND UTILIZATION OF THE BY-PRODUCTS OF COAL COMBUSTION AND GASIFICATION

PREFACE

The characterization of fly ash and its utilization as a cement replacement in concrete are well known to readers of this journal. The collection of papers in the first half of this issue highlights these topics. They are based on selected presentations in Symposium K* at the 1983 Annual Meeting of the Materials Research Society. Also included are several papers dealing with the characterization and utilization of coal gasification ash, steelmaking slag and utility boiler slag and bottom ash. By-products such as these have found limited uses in such materials as concrete aggregate, blended cement and mineral wool. The potential for utilization of all of these solid wastes is much greater. Increased utilization would contribute toward meeting the often stated long-range goal of a materials economy based heavily on recycling of wastes. Additionally, much of the cost of waste disposal could be avoided if such materials were recycled.

This collection of papers opens with contributions by Sidney Diamond and Gunnar M. Idorn in which the utilization of fly ash in the US and the state-of-the art in its utilization in concrete are described.

While many of the barriers to increased utilization of the solid by-products from coal combustion and conversion involve economics, transportation and geography, others derive from uncertainty about the nature and reproducibility of these materials and how they behave chemically and physically in various applications. The papers from the two North Dakota Universities on fly ash from the Western United States and on low-rank coal gasification ash focus on the application of materials characterization to determination of crystalline phases in two types of coal by-products. The contributions from Penn State and from Imperial College and the CCA in the UK increase our understanding of the hydration mechanisms and phase formation in cements incorporating fly ash. The Iowa State group uses chemical modelling and x-ray diffraction characterization to examine the Lime Pozzolanic Activity Test and questions its applicability as presently written to high-calcium Western US fly ashes. As noted by Sidney Diamond, the two chief applications of coal ash utilization are blended cement and soil (roadbed) stabilization. Scott Schlorholtz and Turgut Demirel have used XRD to explore the reactions

---

*"Materials Characterization Applied to Utilization, Immobilization and Disposal of Solid Wastes," held November 16-17, 1984 in Boston MA.

that lower the effectiveness of soil stabilization by lime and, by inference, by high-lime fly ash.

Oscar Manz points out that ash is not limited to these two applications. In his paper, engineering-scale demonstrations and testing of four other products that utilize coal by-products are described. Materials characterization applied to incorporation in concrete of another industrial solid waste, metallurgical slag, is the subject of a second report from Penn State.

A symposium entitled "Coal Combustion and Conversion Wastes: Characterization, Utilization and Disposal" will be held in conjunction with a symposium on "The Potential for Very High Strength Cement-Based Materials" at the 1984 MRS Annual Meeting in Boston on 26-30 November, 1984. Information on the former symposium can be obtained from me at the Department of Chemistry, North Dakota State University, Fargo, ND, 58105, USA. J. F. Young (University of Illinois, Urbana) and Sidney Mindess (University of British Columbia, Vancouver) are Co-Chairman of the latter symposium.

Gregory J. McCarthy
Guest Editor

VOL.
14
1984

CEMENT and CONCRETE RESEARCH. Vol. 14, pp. 455-462, 1984. Printed in the USA.
0008-8846/84 $3.00+00. Copyright (c) 1984 Pergamon Press, Ltd.

THE UTILIZATION OF FLYASH

Sidney Diamond
School of Civil Engineering
Purdue University, West Lafayette, IN 47907, U.S.A.

(Communicated by D.M. Roy)
(Received Dec. 5, 1983)

OL.
14
984

ABSTRACT

An informal overview is provided of the present status of the utilization of flyash, with special reference to the situation in the U.S. Approximately 48 million tons per year are produced, of which approximately 8 million tons are utilized, almost half by utilities themselves. Of the 4.5 million tons sold for external utilization, approximately 60% is used in concrete-related uses, mostly as a mineral admixture. A brief summary of typical properties of low-calcium and high-calcium flyashes is provided, with special reference to differences in potential utilization.

Introduction

This paper was prepared as a keynote talk for a symposium session on the utilization of flyash with primary focus on the current American situation. Despite the concentration on U.S. practice, it is hoped that the information and ideas presented will be of some interest to the international cement and concrete research community.

Flyash Production and Utilization Statistics

It is generally known that the volume of flyash produced in most countries exceeds the volume that can be utilized productively by a large margin, but statistics are not generally available. A RILEM committee (Technical Committee 73-SBC, under the chairmanship of P. K. Mehta) is in the process of attempting to secure and analyze such information on a world-wide basis. Table 1, used by permission, is the Committee's compilation of estimated 1982 flyash production in a number of countries. Statistics for the Soviet Union, a major producer, and for other Eastern European countries are generally unavailable.

In the United States, annual statistics on flyash production and utilization are compiled by the National Ash Association (1). These statistics

Table 1.
Estimated 1982 Flyash Production

Country	Production (tonnes)
U.S.A.	43,600,000
China	31,000,000
United Kingdom*	16,000,000
India	10,000,000
South Africa	10,000,000
France**	4,000,000
Canada	2,000,000
Denmark	1,000,000

*1980 **1981

consequence, annual flyash production has been essentially constant since 1977, with the single exception of 1979.

A similar historical prospective on the utilization of flyash in the U.S. is provided in Fig. 2. The utilization figures are somewhat more variable year-by-year than the production figures, as might be expected. The annual usage figures do not show a clear upward trend, as might have been expected from the surge of current interest in flyash in the concrete literature. Rather, the annual usage is seen to have fluctuated around an average of about 8 million tons since 1977.

are kept in avoirdupois tons, rather than in metric tonnes or SI units, and for convenience will be discussed in terms of the original units.

Fig. 1 provides a historical prospective on flyash production in the United States from 1976 to 1982, the last full year for which statistics are available. It is apparent that 1979 was a year of high flyash production. Predictions of substantial annual increases in flyash production made by many observers at that time failed to materialize because of the general industrial recession. In

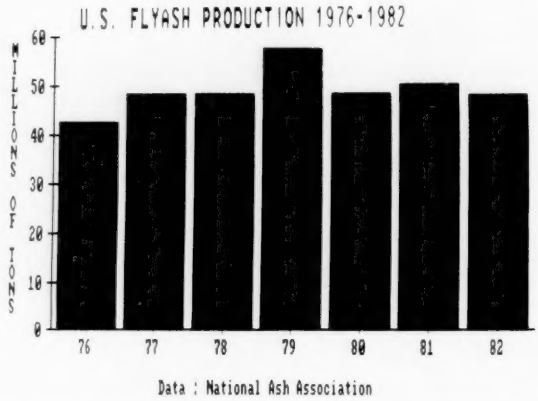

FIG. 1. Annual Production of Flyash in the U.S. 1976 - 1982.

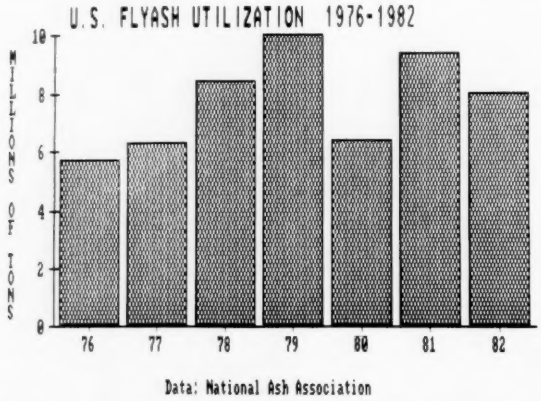

FIG. 2. Annual Utilization of Flyash in the U.S. 1976 - 1982

Statistics are available to provide a more detailed picture of the current state of U.S. ash production and utilization, as of 1982. The total production of coal burning utility plant solid wastes in 1982, including flyash, bottom ash, and boiler slag (wet bottom ash), amounted to some 65 million

VOL. 14 1984

tons. Of this total, it is obvious that the 48 million tons of flyash is predominant. Of the flyash, as previously indicated, approximately 8 million tons, or 17%, was utilized in some way and 40 million tons were dumped, usually in wet lagoon storage dumps. The prospect of trace element contamination of ground water from these storage sites has concerned environmentalists for many years.

Of the approximately 8 million tons of flyash utilized in 1982, the National Ash Association statistics indicate that close to half, 3.5 million tons, was used by the utility companies themselves. The major cited use was for structural landfill, but a large share of the total usage was designated as "miscellaneous". The writer suspects that much of this was used to help solidify liquid flue gas desulfurization scrubber sludge to permit handling the large volumes of fluid involved. Indeed, he has recently been informed that in some areas certain utilities find themselves in the anomalous position of having to purchase flyash on the open market for this use. Should stringent measures against "acid rain" difficulties be invoked in the future, it is possible that this usage may increase tremendously, especially in the Midwestern region of the U.S.

In 1982, the statistics indicate that approximately 4.5 million tons of flyash were sold by utilities, either directly or through flyash brokers. The major uses to which this flyash was applied are summarized in Table 2.

OL.
14
984

Table 2. Details of Flyash Utilization in U.S., 1982

End Use	Usage, Millions of Tons
Cement and concrete	2.7
Structural fill	0.4
Grouting	0.3
Highway base courses	0.2
Filler in asphalt mixes	0.1
Coal mining applications	0.1
Miscellaneous uses	0.7

About 60% of the flyash sold for external use in 1982 was used in the cement and concrete industry. It is thus easy to understand the extent of concern of flyash-producing utilities and flyash brokers with the concrete industry and the place of flyash in concrete technology. The next four specified uses, structural fill, grouting, highway base courses, and filler in asphalt mixes, also involve aspects of civil engineering practice. It is thus apparent that the main market for flyash sales is the civil engineering or construction segment of the economy.

Undoubtedly the details differ by country around the world, but the author believes that the same general picture prevails in most countries.

It is instructive to further examine the specific uses of flyash within the cement and concrete field. There are basically three different uses encompassed here: flyash as a cement manufacturing raw mix component, flyash as a blending or intergrinding component in portland-flyash blended cements (in the U.S. designated "portland-pozzolan" or "pozzolan-modified portland" cements), and flyash as a mineral admixture added separately to a concrete mix, with some of the cement usually being withheld.

The relative trends among these separate components of the cement and concrete market for flyash are instructive. According to National Ash Association statistics, of the almost 1.5 million tons of flyash used in the industry in 1977, almost half was used as cement plant raw mix, and only a small portion was used as a mineral admixture in concrete. The situation had changed drastically by 1979, the year of highest flyash utilization in the U.S. By 1979 cement and concrete utilization had almost doubled, to

2.7 million tons, but the proportion of it representing cement plant raw mix had halved, and the proportion representing use in blended cements had been reduced even more. In contrast, the proportion representing direct admixture usage in concrete increased dramatically, to almost 3/4 of the whole.

Between 1977 and 1979 there was a local shortage of portland cement in some regions of the U.S. It appears that many concrete producers were induced to use flyash simply to stretch out their available supplies of portland cement. Once accustomed to such use, and to its consequent economic and processing advantages, it appears that a large number of these producers have continued to incorporate flyash in their concrete, even though an oversupply of portland cement is now available.

The National Ash Association unfortunately discontinued its breakdown of cement and concrete usage of flyash into these separate components after 1979, and for succeeding years on the total usage is known. However, the writer is of the opinion that the present usage is substantially similar to that shown to exist in 1979, and that if anything, the proportion used as an admixture in concrete is growing.

This pattern of use may vary considerably from country to country, depending on local supplies of cement raw mix components and on the customary usage of blended cements. In many European countries it appears that blended cements, many containing flyash, dominate the market for portland cement, and the use of flyash as a mineral admixture is much less widespread.

Properties of Flyashes in Relation to Utilization

The several distinct end uses for flyash differ considerably among themselves in the stringency of the properties required in the flyash for successful use.

The success of flyash in structural fill applications rests primarily on the ability of the material to be compacted to a reasonably strong layer of low unit weight. This is a function primarily of particle size distribution, and to some extent of the content of spherical particles. The chemical characteristics of the flyash are secondary, although the post-compaction cementation provided by some high-calcium flyashes is likely to prove beneficial.

Grouting applications and the use of flyash as a filler in asphalt mixes and in other systems also depend primarily on the physical characteristics of the flyash - again, particle size distribution and sphericity.

With highway bases chemical considerations come into play, although not in an important way. Stabilization of some base courses (and stabilized subgrades) may rest on lime-flyash chemical reactions, i.e. the classical "pozzolanic" reaction with lime added for the purpose. Low-calcium flyashes may be entirely satisfactory or even preferred, especially where sufficient time is available for these slow reactions to take place. The only real chemical requirement is that the flyash have a sufficient content of glass that eventually will react with added lime. Some road base applications of flyash depend on the physical effects of flyash incorporation rather than its reaction with lime.

The cement and concrete end-use areas are by far the most demanding of the flyash in terms of adherence to strict criteria and requirements. However, the requirements differ considerably depending on the specific end use involved.

Flyash for use as a raw material in cement manufacture is sold and used primarily on the basis of its chemical composition, as expressed in the usual oxide convention. Such factors as glass content, the type of crystalline matter present, size distribution, etc., are relatively immaterial. Even high carbon content, which may be limiting in most other end uses, may actually be beneficial in cement raw material use, since it provides a definite (although modest) proportion of the fuel needed. Uniformity and chemical consistency from day to day and week to week is the prime necessity.

Flyash for use as a blended cement component shares some of the requirements for both raw material and direct concrete admixture use. Since such flyash eventually is incorporated in concrete, its chemical and physical characteristics must be suitable for that purpose. However, since little or no adjustment can be provided at the concrete mixing stage, flyash for use in blended cements must be of consistent and uniform chemical and physical characteristics, the consistency and predictability being as important as the numerical values of the various parameters involved. Since the blended cement manufacturer has little control over the concurrent use of chemical admixtures or of mixing and curing conditions, the flyash used should be relatively insensitive to such variations. Especially to be considered here are rheological effects, strength development characteristics, and possibilities for developing efflorescence. The color of the ash and its effect on the color of the final concrete to be produced by the blended cement may also be of importance.

OL.
14
984

Flyash for use as a mineral admixture is subject to certain standard requirements in the U.S. as it is in most countries, but the requirements are not unduly restrictive. The physical and chemical characteristics that govern its behavior in concrete are only beginning to be understood in detail. They include such parameters as the nature and amount of the glass present, the specific crystalline components buried within or deposited on the glass spheres and whether or not they are reactive, the nature and solubility of the alkalies and sulfate present, etc. These are in addition to the well-understood concern with total chemical composition, particle size distribution (especially of the coarsest fraction), carbon content as determined by ignition loss, and possible tendency toward unsoundness or inadequate resistance to sulfate attack.

Specific Characteristics of Flyashes Related to Utilization in Concrete

Up to this point, the writer has deliberately avoided drawing attention to the very considerable dichotomy that exists in concrete-related characteristics of flyashes between typical low-calcium and typical high-calcium flyashes. However, it is not possible to discuss flyash utilization in concrete in any detail without considering the wide disparity in properties and behavior of the two varieties of flyash.

Low-calcium flyashes are roughly coincident with what present ASTM specifications call "Class F" flyashes, and high-calcium flyashes with ASTM "Class C" flyashes, but the formal basis for the distinction in the present specification is anomalous. Most of the Class F flyashes are from bituminous coal, in the United States mined mostly in the East. The high calcium flyashes are produced by burning coals with high limestone (and sometimes gypsum) contents. These are primarily lignite and to some extent sub-bituminous coals, in the United States mined mostly in the West. To some extent the sub-bituminous derived flyashes are transitional between the other groups, depending on their calcium contents.

Despite the importance of the distinction in concrete applications, no separate statistics are kept by the National Ash Association on either production or utilization of the two kinds. It appears to the writer that both production and utilization of high-calcium flyashes are increasing.

An idea of the differences in chemical composition between the two types of ash can be obtained from the data of Table 3, derived from a recent presentation by Cook (2). While the values refer specifically to two individual flyashes and are not general averages for each type, they do serve to illustrate reasonable examples of low-calcium and high-calcium flyash composition, respectively.

Table 3.
Illustrative Flyash Compositions

	Low Calcium ("Class F")	High Calcium (Class "C")
SiO_2	42	34
Al_2O_3	22	19
Fe_2O_3	28	6
CaO	2	29
MgO	1	5
SO_3	1	3
K_2O	1.3	0.3
Na_2O	0.3	2.1

The silica contents of high-calcium flyashes are somewhat variable, and may be as high as those of some low-calcium ashes. Alumina contents may not be as variable. Iron oxide contents of high-calcium flyashes are usually lower than those of the Class F ashes, even though the iron oxide contents of Class F ashes are mostly not as high as the one illustrated in Table 3.

The major distinction between the two groups is CaO content. The 29% CaO content for the specific Class C flyash shown is not unusually high for a lignite-derived flyash, although flyash of intermediate CaO contents, often derived from sub-bituminous coals, are also found.

The remaining elements are often considered to be of less importance, but this is not necessarily so. Again, differences between most low-calcium and most high-calcium flyashes occur.

For example, the MgO contents of high-calcium flyashes are usually quite high, the 5% figure for the high-calcium flyash in the table being by no means atypical. Geochemically, Mg is a natural and expected associate of Ca, and many of the lignite-based flyashes are likely derived from dolomitic limestones contained within the coals. Analytical MgO usually includes both MgO in the glass phase and crystalline periclase.

The typically higher SO_3 contents of high-calcium flyashes may reflect either readily-soluble alkali sulfates (primarily sodium), or calcium sulfate (anhydrite), or both; $C_4A_3\bar{S}$ is sometimes reported as well. Some high-calcium flyashes, derived presumably from coal with substantial gypsiferous content, may have SO_3 contents as high as 10% or more.

The alkali contents and activities of low-calcium flyashes and high calcium flyashes seem to differ substantially. Many low-calcium flyashes have substantially more K_2O than Na_2O, and the K_2O seems to be primarily a constituent of the glass, and not readily soluble or available. On the other hand, many high-calcium flyashes have much more Na_2O than K_2O, and the Na_2O is often as readily-soluble sulfate.

VOL
14
198

The table above does not include values for percent loss-on-ignition. This value is obviously a reflection of the efficiency of the combustion process rather than an intrinsic characteristic of flyash that can be traced to coal chemistry. Values for modern high-calcium flyashes are usually very low, of the order of 1%, primarily because these are commonly produced by newer power plants operating with commendable efficiency on low-rank but quite uniform coals. Low-calcium flyashes produced in modern plants may have equally low carbon contents, but low-calcium flyashes produced by older and more-inefficient plants are also common, and may have carbon contents up to 10% or more.

Chemical analysis results are of substantial importance in characterizing flyashes for use in concrete, but other characteristics reflecting certain physical properties may be equally important. Table 4, also derived from data provided by Cook (2) summarizes some of these properties for the two illustrative flyashes whose compositions were given in Fig. 3.

Table 4.
Properties of Illustrative Flyashes

	Low Calcium ("Class F")	High Calcium ("Class C")
% Retained on No. 325 Sieve	28	16
Specific Gravity	2.61	2.67
Pozzolanic Activity Index (% of control strength at 28 days)	88%	101%
Water Requirement (% of control)	100%	92%

As suggested by the first entry in Table 4, the content of coarse particles is often substantially lower in high-calcium than in low-calcium flyashes. Often the entire size distribution is finer as well.

The measured specific gravity is often somewhat higher, perhaps indicative of lesser contents of hollow spheres (cenospheres and plerospheres). The pozzolanic activity index, as measured with cement after 28 days of curing at slightly elevated temperature, is almost always substantially higher for high-calcium than for low-calcium flyashes, and indeed the strengths at this time often exceed those of the reference cement paste, as it does for the flyash illustrated.

There are often differences in water requirement, i.e. water reducing effect, between low-calcium and high-calcium flyashes, usually favoring the latter. Perhaps this is a reflection of reduced contents of oversized, often non-spherical particles in the high-calcium materials. Some exceptionally coarse low-calcium flyashes may actually increase water demand in concrete.

Conclusions

Flyash utilization in the U.S. currently is at a level of about 8 million tons per year, representing about 17% of current production. Nearly half the utilization is by the utilities themselves. About 60% of the 4 1/2 million tons per year sold externally is used by the cement and concrete industry, most of it as "mineral admixture" rather than as a blended cement component or cement raw material. Other major uses are mostly civil engineering related, and include structural fills, grouting, and highway bases.

OL.
14
984

Mineral admixture (or "cement replacement") usage tends to be more demanding of the chemical and to some extent physical characteristics of the flyash than are most other uses.

A distinct dichotomy exists between the chemical and technological properties of low-calcium and high-calcium flyashes, considerably affecting their behavior in concrete and to some extent, in other uses as well. The relative amounts of the two types currently being produced are not currently being monitored, but it appears that utilization of the high-calcium flyashes is increasing rapidly. Overall utilization of flyash in the U.S. does not seem to have increased significantly in the last few years.

References

1. National Ash Association, "Ash Production and Utilization", Issued Annually by National Ash Association, Washington, D.C.

2. J. E. Cook, "High Strength Concrete Case History No. 1", presented at Annual Convention, American Concrete Institute, Los Angeles, CA March 1983.

VOL
14
198

CEMENT and CONCRETE RESEARCH. Vol. 14, pp. 463-470, 1984. Printed in the USA.
0008-8846/84 $3.00+00. Copyright (c) 1984 Pergamon Press, Ltd.

STATE OF THE ART FOR FLY ASH USES IN CONCRETE

G.M. Idorn
G.M. Idorn Consult ApS
2850 Nærum, DK

K.R. Henriksen
Kampsax A/S
Dagmarhus, 1553 Copenhagen V, DK

(Communicated by D.M. Roy)
(Received April 9, 1984)

ABSTRACT

An overview of accomplishments in recent research and of attractive further work for improvements of the uses of fly ash in concrete is presented.

Improved workability of fresh concrete, reduction of peak curing temperatures and increase of the denseness of hardened concrete are being recognized as attainable advantages in practice. Also pozzolanic reactivity as protection against reactions with alkali-susceptible aggregates is of increasing interest.

There is in research a trend towards more work about the characterisation of fly ashes in relation to chemical composition and mineralogy structure. Also their impact on the rheology of fresh cement paste, on the energetics of the hydrating system and on the microstructure of hardened cement paste is increasingly being studied. More interaction with other branches of materials science is still desirable.

The practice-research relations are demonstrated by experience with use of fly ash in the concrete of a major bridge construction in Denmark.

Coherent research and development efforts are found commendable.

Introduction

A formidable amount of research on fly ash utilization in concrete has been carried out since the commencement of the energy crisis. It seems justified to assume that the R&D investments in percentage of sales of fly ashes must by far have exceeded the general expenditure to R&D on cement and concrete in percentage of sales of these commodities. This latter expenditure was less than 0.03% of gross sales in the US cement industry and less than 0.01% in the concrete producing industry in 1978, (1), and not significantly different in most countries abroad. Numerous large conferences have been arranged for presentation of research results regarding fly ash utilization during the last ten years. The two preceding annual meetings of the Materials Research Society have provided a forum for basic research and technology development problems for the use of fly ashes as supplementary cementitious material in concrete (2), (3).

The societal background for the broad support to the R&D regarding fly ashes uses in concrete is clear enough. World production of fly ash is approaching 400m tons per year, which is about 50% of the global cement production. A general 20% substitution of cement by fly ash would represent a potential of about 10% replacement of cement production in the world, at no fuel costs. In some

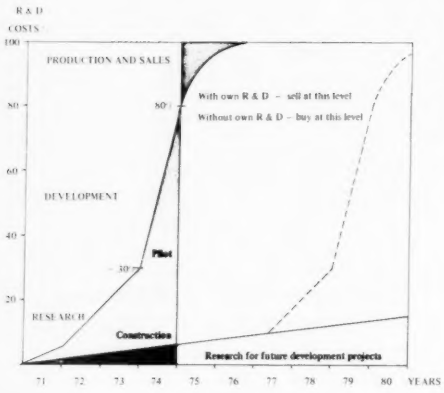

Fig.1.

R&D in a typical industry innovation program commencing 1971. The initial basic research represents max. about 5% of the total development costs. New cycles of development are envisaged about each five years. As a whole R&D form part of the industry management.

parts of the world, fly ash is not available, whereas the feasibility in other regions is enhanced by the production of excessive quantities, and by problems with disposal arrangements.
Geographic and social aspects of the fly ash issues have probably stimulated universities and funding agencies to take much interest in the research. The easy access for universities to disseminate research results through the education represents a higher rate of communication from basic research to engineering practice, than the general low tide for cement and concrete research has allowed for a long while.
However, despite the intensity of research the utilization of fly ashes in concrete is still far from approaching exhaustion of the resources.
The production of fly ashes in the US was about 48 million tons (short) in 1982. 8 million tons were used. 2.68 million tons were used for cement and concrete products (4), while the potential ought to be between 10 and 20 million tons or more

The Influence of the R&D Structure

Figure 1 displays the general system approach to R&D which industries other than cement and concrete, and familiar to several branches of the Materials Research Society, are accustomed to operate. In fact, within the high-technology areas basic research is becoming more and more an integrated part of even short-term industry innovation. And the high-technology education is coming under continuous impact of "backfiring" from research achievements for renovation of courses, projects and textbook-modules. This happens largely through university-industry cooperation.

In the comparable, conventional approach to the development of concrete technology, the research is not coherent or comprehensive, and the transfer from research to technology must overcome institutional and organisational barriers. The development is also delayed by fragmentation of the profits from innovative undertakings, which makes it difficult to find sponsors with incentives for concentration of research investments. These circumstances are also delaying the incorporation of new research in the engineering and research educations.
It is also a factor of deferment for renovation of the education in the fields of utilisation of fly ashes with cement that an analytical approach prevails in the design/construction engineering disciplines, also towards technology. Structural design theory is in its entirety applied mathematics, and the tendency is strong to request technology to be simplified to numerical limits and criteria. Over the years this tendency has pushed the technology research to become overly

analytical oriented.
The R&D for fly ash utilization requires a renovation of descriptive and conceptual approaches so as to provide model-true physico/chemical knowledge as basis for technology. Almost a decade of research communications about fly ash utilizations show that many results are mutually incompatible because their validity are confined by special testing circumstances, remote from the conditions for field concrete works, and without theoretical clarifications.
Even in the two previous MRS proceedings for the symposia N and M (2), (3) there is a considerable gap between empiric engineering-orientated and basic science-orientated presentations, whereas both types of the research show a clear preference for analytical rather than conceptual studies. This state of the art does not depreciate the progress of knowledge per se, but demonstrates that industrially required congruence and integration of basic research and technology is an issue worthwhile to discuss.

The Concrete Technology Issues

In concrete engineering the technology operations and evaluations are categorized in:

- o Materials as purchased.
- o Processing of concrete.
  - Mixing and placing.
  - Curing.
- o Performance of product, structure or building

Transformed into technology issues these categories can be keyworded:

(1) Characterisation and classification of fly ashes and of the cement with which they are to be used.
(2) Assessment of the impact of fly ashes in concrete on the rheology during mixing and dormancy(transport and placement).
(3) Determination of the mutual influence of fly ashes and cement on the heat/strength development and the structure formation of the cement paste during early curing.
(4) Elucidation of the characteristics of hardened concrete with fly ashes during long-term performance, i.e. the strength and deflections and chemical resistance, or: the long-term evolution of denseness (porosity, permeability, diffusivity) until ageing and degradation begins when full hydration is reached.

Characterisation of Fly Ashes

There are two ways in which the engineering community approaches the characterisation of fly ashes: by direct assessment of their basic materials' properties, and by simplified performance model tests.
The direct assessment of the properties of fly ashes has been much stimulated by recent research studies, see e.g. (5), 6), 7), (8) and others. These studies have in particular dealt with the chemical and mineralogical compositions of fly ashes. More studies in cooperation with the industry about the opportunities and problems by manipulating the fly ash properties seem desirable.
Chemical composition. Two "species" of fly ash have emerged from chemical analyses and characterisation of origin: The ASTM class C (lime-rich), and class F (lime-poor).
Class C fly ashes are readily activated by their own lime-content and/or by the calcium hydroxide released during the portland cement hydration.
Class F fly ashes are readily activated, at first by the alkalis released by the

portland cement after mixing and during early hydration - as demonstrated by the ability of class F fly ashes to prevent alkali-aggregate reactions in concrete - and subsequently they may be activated by the calcium hydroxide released during the portland cement hydration, as suggested by the long-time growth of strength of concrete made with class F fly ashes.

The primary distinction between the class C and class F reactivity must apparently be related both to the Ca/SiO_2 ratio of the composition and to the Ca/alkali concentration in the liquid phase of the reacting system.

There is evidence, (9), (10), (11) that the alumina-phases in the fly ashes also play a role for the hydration. Likewise, sulfates in the liquid phase are activators and create secondary complex, hydrated phases.

Altogether, the complexity of the reacting systems with fly ashes, portland cements and water is still generally characterised by regulatory simplifications which may suffice for large scale comparative characterisations of the fly ash types. However, for evaluation of their effects in concrete more work, which simulates the activating circumstances, is required.

Mineral composition and structure. While portland cement hydration primarily depends upon the chemical composition of its crystalline compounds, it is generally assumed that the reactivity of fly ash, in particular of class F, depends upon a high content of glass and only a minor content of crystalline constituents. Apparently the level of calcium content has an influence, for granulated blast-furnace slag, with a chemical composition between class C and class F fly ashes, is generally designated a "latent hydraulic material" (or "cementitious") for which a high glass content is considered favourable. Class F fly ash is in contrast often designated "pozzolanic", as being of a lower degree of hydraulicity and requiring an activator (which calcium hydroxide is considered to be), even when of high glass content.

There are many recent studies with information which is useful for further clarification of the chemistry/mineralogy issues of fly ash reactivity in a portland cement system. A conceptual approach based on thermodynamics might be useful for research aiming at concrete technology development.

Particle size distribution. The particle size distribution of fly ashes is also generally recognized as a parameter for their reactivity, just like the particle size distribution of portland cements is recognized as a parameter for their rates of hydration and strength development. Nevertheless, more quantitative characterisation of the particle size distributions for both components of a cement with fly ash would add to the value of many research studies, and would also be advantageous to learn for design and monitoring of the uses of fly ashes in engineering practice (12).

The effects of the chemical composition, the mineral composition and the particle size distribution of the fly ashes and portland cement in mixes determine together the energetics of the reacting system, and in engineering technology: the hydration products, their morphology and strength, pore characteristics and resistance to external aggressivity, as well as the rate of development of their properties during concrete production.

Rheology of Fresh Concrete

Recent research, (13), (14), (15), (16) and others suggests that basic theory concerning the mechanics of the rheology and surface chemistry of cement paste need to be applied for proper assessment of the impact on the workability of concrete with slag and fly ashes. In many cases in practice improvement of the workability has been ascribed to the addition of fly ash to particular cements, and the present paper is mentioning one such case. Chemical admixtures are also now commonly used in major construction works in order to obtain special qualities. The effects of addition of fly ash can therefore not be evaluated as separate from the effects of other admixtures and of the cement characteristics. The research should be aware that in this variety of opportunities for refinements

VOL
14
198

of concrete making in practice the savings in materials and labour costs are already operating incentives for engineering endeavours. Applicable research for manipulation of the properties of fresh concrete by fly ash is thus promising of attractive returns on the investments.

Curing of Concrete

Also research on the concrete curing process has been intensified in recent years. The applicability of the maturity concept was demonstrated at the 7ICCC, (17), at which conference it was also reported that the activation energy for blended cement with blast-furnace slag (65% slag) was about 10% higher than for pure portland cement, (18), (19).
Numerous authors have in past and recent research observed that additions of fly ash are likely to cause reduction of peak curing temperatures during curing of cement paste and concrete. In the absence of calorimetric measurements these findings must be considered qualitative evidence that the heat released by the initial hydration of portland cement functions as activator of the early hydration of fly ash together with the immediately dissolved alkalis from cement and fly ash. A subsequent, long-term hydration of fly ash continues with calcium hydroxide as activator as long as the portland cement continues to hydrate. More studies of this complex course of the hydration of cement with fly ash at realistic curing conditions are wanted for providing input data to curing technology programs.

VOL.
14
1984

Structure and Resistance of Hardened Concrete

Several workers, (20), (21), (22) have shown that remarkable reductions of porosity and of the larger fraction of pore-sizes in hardened cement paste can be attained by blending fly ash (or blast-furnace slag) with portland cement. This effect of the mineral admixtures corroborates that by their hydration they supply supplementary pore-filling and thereby densifying compounds, akin to the C-S-H initially formed by the portland cement hydration. Concurrently, at first the alkalis and subsequently calcium hydroxide are incorporated as solids in the basic C-S-H morphology. The densification at the same time accounts for the long-term strength increase which is typical of well designed and cured concrete with fly ash.
The described conception of fly ash hydration may seem to be contradicted by thin section and scanning-electron-microscope observations of cement paste and concrete in many papers, showing numerous unhydrated fly ash particles.
Considering the quantity of fly ash particles in mixes with portland cement one must assume that all degrees of hydration as well as different modes of the reactivity, type of bond morphology etc. may easily be present in even small experimental or case-study specimens (23). This may be explained with preference for internal solution of the fly ash mass and migration and precipitation of hydrates out in ambient paste or with strong bond force creation from the particle surface inwards. Incidentally, a significant amount of unhydrated cement is usually found in cement paste by microscopic examination even of old concrete, (19), (24).
Altogether, cement paste in concrete ought to be considered a "microconcrete", and to possess its strength and resistance:

- not due to a near to 100% ultimate degree of hydration and thereby full utilization of the chemical energy inherent in the cementitious constituents,

- but rather to the creation of a subtle "microconcrete system" consisting of co-existing "aggregate particles" of partially or unhydrated clinker fragments and fly ash particles in the C-S-H matrix incorporating the hydrates from the fly ash.

The "microconcrete" system is also in the course of time prone to:

(1) increase denseness, and
(2) decrease contents of the fragile, metastable calcium hydroxide,

without sacrificing the advantages by constituting an aggregate-matrix morphology in the microscale.
The "microconcrete" conception was adopted to explain the superior strength potential of the "MDF" (macro-defect-free) cement paste, in particular as far as tensile and flexural strength is concerned (25). Besides low porosity also the elimination of microsize flaws in the matrix was found important and this was attained by obtaining a dense package of cement particles at maintained low degree of hydration. A high range water reducing agent was applied to ensure adequate dispersion, and excessive strength was obtained by addition of a suitable organic monomer.
Less exotic though still significant improvements of ordinary concrete strength and resistance may be attainable by exploitation of the "microconcrete" conception with mixtures of portland cement and refined fly ash, suitable dispersion agents and monitored curing procedures.

An Example of Practice-Research Communication

The Faroe Bridges constitute the largest bridge work carried out in Denmark up to this date. They are two bridges between Zealand and Faroe and between Faroe and Falster, with lengths 1596 m and 1727 m respectively.
The substructure for the bridges, and the two large pylons (cable towers), is constructed in concrete and comprises more than 45,000 cub.meters of reinforced concrete.

Fly ash has been used primarily in order to attain:

- Improved workability of fresh concrete.
- Reduction of peak curing temperature.

In addition to that, protection against deleterious reactions with alkali-susceptible aggregates is recognized as a must for durability reasons. Application of fly ash in this respect is considered as an assurance of durability of the concrete structure.

Workability. The following precautions have been taken to secure the proper quality of the concrete as to strength and durability:

1) The grading curve of sand indicates a uni-sized material. In Denmark it is difficult to find fine aggregates (particle size less than 4 mm) with the required low content of alkali-reactive particles. Only one location has up till now been discovered. Consequently, the unsuitable grading is accepted.

2) The cement is a special low-alkali sulphate resistant and lowheat cement.

When using the sand and cement, a bleeding effect and a tendency towards segregation of the concrete was noted, during the casting of concrete.
40 kg fly ash per cub.m. was therefore added to the 330 kg cement/m^3, as a remedy.
Special requirements to workability and cohesiveness were specified for the underwater concrete.
It is general practice to specify a content of at least 400 kg/m^3 for underwater concrete to secure a sufficiently cohesive concrete. For the Faroe bridges a maximum temperature of 70°C in solid parts of the structures was, however,

also specified. This made 400 kg/m^3 of low-heat cement the absolute upper limit, and that suggested also that a part of the cement content should be substituted by fly ash.
The concrete mix for underwater concrete was therefore specified to be composed of 330 kg cement and 100 kg fly ash.

Curing Technology System. An advanced Curing Technology System was applied for planning and monitoring the concrete curing process. The application of fly ash fits well into the curing procedures.
During curing of concrete the contractor should ensure that

o no thermo-cracks occurred on the surface or in the concrete body.

o maximum concrete temperature during the curing phase should keep below 60°C. (In mass concrete 70°C).

It has been shown that temperatures beyond 70-80°C will result in changes of the cement paste and in loss of strength, and a temperature difference above 20°C across a concrete section is likely to produce thermo-cracks.
As a consequence hereof the "thermo-crack requirement" was:

> "temperature differences of maximum 20°C between the interior and the surface of the cross section are acceptable. If it is not possible to meet this requirement, a calculation of the thermo-stresses is required."

A specific problem arises from differences in temperatures between solid concrete bodies cast at different times. Thermal contraction may cause cracking if exceeding the ultimate tensile strength developed at early ages(26).
If the difference between the average temperatures in the concrete being cured and in the adjoining concrete structures exceeds 20°C, a separate study of the tensile stresses in the area on both sides of the joint is therefore necessary.
Studies of this problem have been an integrated item of the quality assurance of the concrete works at Faroe. It has been important to know the rate of heat of hydration in the concrete so that the stress development during curing of the concrete could be calculated under the given circumstances.
The rate of heat evolution by cement hydration for the concrete mix in question has occasionally been controlled by adiabatic calorimetry.
The heat of hydration and the 28 days compressive strength of the concrete with fly ash amounted to 60-80% of what was obtained with pure portland cement. However, 56 days tests showed equal or higher compressive strength with the fly ash substitution.
For the monitoring of the curing process it was on some occasions necessary to cool the fresh concrete in addition to substituting fly ash for cement. This was done by adding liquid nitrogen to the concrete during mixing, (27).

Conclusions

1. A vast quantity of data and evaluations about the effects of fly ashes in concrete has been produced by research in recent years. Less fragmentation and more convergence towards technology innovations, like in most other industries, would facilitate application of the research and its planning for effective utilization of the hydraulic energy in the fly ashes.
2. Chemical research deserves a high priority in such a context of an energy conscious R&D policy. Effective transfer of research into university education need support.
3. There is progress in the research for characterisation of the fly ashes: chemical and mineralogical compositions and particle size distributions.
4. The engineering requirements: improvements of the workability of fresh con-

crete, of curing procedures and of the resistance of hardened concrete by addition of fly ashes provide guidelines for research planning.
5.More basic research than as yet applied is by now appearing about the potential impact of fly ash upon:

- o the basic rheology of cement paste
- o the energetics of the hydration of cement paste and the interactions of cement and fly ash hydration
- o the densification of hardening cement paste by incorporation of the hydrates originating from the fly ashes, and therewith long term increase of strength and resistance.

6. The utilization of fly ash at the Faroe Bridges in Denmark is mentioned to show that civil engineering, when facing problems with concrete workability and high curing temperatures in concrete, can use fly ash with satisfactory results based upon current knowledge.

References

1. Roy, D.M. (editor). NMAB-361., 105 p (1980).
2. Diamond, S. (editor). Proc. MRS Symp.N., 331 p (1981).
3. Skalny, J. (editor). Proc. MRS Symp.M., 233 p (1982).
4. Ash at Work, VV, No 6, 4 p (1983).
5. Diamond,S. EPRI CS-2616-SR, 4, p. 34-44 (1982).
6. Diamond, S. Proc. MRS Symp.N., p. 12-33 (1981)
7. Scheetz, B.E., Strickler, D.W., Grutzek, M.W. and Roy, D.M. Proc. MRS Symp.N., p. 24-33 (1981).
8. Wesche, K. and vom Berg, W., Proc. MRS Symp.N., p. 45-52 (1981).
9. Farrauto, R.J. and Haynes, W.L., Am.Cer.Soc. Bull.52:3, p. 276-79 (1973).
10. Komarneni, S. and Roy, D.M., Cem. and Concr. Res. 12, p. 773-80 (1982).
11. Roy, D.M. Proc. Alkalis in Concr. DBF, Copenhagen (1984), 532 pp.
12. Idorn, G.M. Proc. Alkalis in Concr. DBF, Copenhagen (1984), 532 pp.
13. Young, J.F. Proc. MRS, Symp.M., p. 120-38 (1982).
14. Roy, D.M., Skalny, J. and Diamond, S., Proc. MRS, Symp.M., p. 152-173 (1982).
15. Regourd, M. Phil.Trans.R.Soc. Lond. A 310, p.85-91 (1983).
16. Ottewill, R.H.S., Phil.Trans.R.Soc. Lond. A.310, p. 67-78 (1983).
17. Owens, P.L. and Buttler, F.G., 7ICCC, Paris, Vol.IV, p. 811-16 (1980).
18. Regourd, M., Mortureux, B., Gautier, E., Hornain, H. and Volant, J., 7ICCC, Paris, Vol.II, p.105-111. (1980).
19. Roy, D.M. and Idorn, G.M., Journal ACI, 79-43, P. 444-457. (1982).
20. Feldman, R.F., Proc. MRS Symp.M., p. 124-133 (1981).
21. Mehta, P.K., ACI SP-79, Vol.I, p. 1-46 (1983).
22. Roy, D.M. and Parker, K.M., ACI, SP-79, p. 397-414 (1983).
23. Idorn, G.M., Proc. MRS Symp. M., p. 244-59 (1981).
24. Idorn, G.M. and Thaulow, N., Cem. and Concr. Res. 13, p. 739-43 (1983).
25. Birchall, J.D., Phil.Trans., Lond. A310, p. 31-39 (1983).
26. Kasai and Okamula, Proc. Int.Conf.Mech. Behaviour, IV, p. 288 ff. (1972).
27. Henriksen, K.R., Nord. Betong (Repr.), 11 pp (1983).

VOL
14
198

CEMENT and CONCRETE RESEARCH. Vol. 14, pp. 471-478, 1984. Printed in the USA.
0008-8846/84 $3.00+00. Copyright (c) 1984 Pergamon Press, Ltd.

MINERALOGY OF WESTERN FLY ASH

Gregory J. McCarthy, Kevin D. Swanson, Lindsay P. Keller and Walter C. Blatter
Departments of Chemistry and Geology, North Dakota State University
Fargo ND, 58105

(Communicated by S. Diamond)
(Received Feb. 17, 1983)

VOL.
14
1984

ABSTRACT

Twenty-six fly ash specimens from North Dakota, Wyoming and Montana lignite and sub-bituminous source coals have been studied in detail by x-ray diffraction. Chemically, these western fly ashes are characterized by higher $CaO+MgO+SO_3$ contents and lower $Al_2O_3+SiO_2$ contents than eastern bituminous fly ashes. These western fly ashes have greater proportions of crystalline material. The characteristic phases are quartz, lime, periclase, anhydrite, ferrite spinel, tricalcium aluminate, merwinite and melilite. Alkali sulfates, a sodalite structure phase and hematite also occur in some fly ashes.

Introduction

Over the last several decades North Dakota has become a major exporter of electricity generated in large part by mine-mouth power plants located in the lignite coal fields near the Missouri River. Fly ash, one of the solid waste products from these plants, constitutes a disposal problem for the power plant and in many cases for the adjacent mine when this is used as the disposal site. In semi-arid western states, buried fly ash has the potential to degrade the quality of aquifers by release of soluble salts and trace metals. Utilization of fly ash for such applications as a cement replacement in concrete and as a ceramic raw material has the double benefit of eliminating the costs of disposal and lowering the cost of the concrete or manufactured product. The University of North Dakota and North Dakota State University have been conducting joint research on the characterization, utilization and disposal of fly ash and other utility wastes for a number of years. This report describes one component of this research, the mineralogy of western fly ash as studied by x-ray powder diffraction.

By "western" fly ash we mean ash produced from combustion of low-rank western coals mined in North Dakota, Wyoming and Montana. In describing the ash from coal combustion and conversion, the term "mineralogy" conventionally refers to the phases (crystalline and noncrystalline) present in the ash. In a recent review of fly ash characterization, Diamond (1) has pointed out that

the high-calcium (Class C) fly ash produced from western lignite and subbituminous coals is characterized chemically by higher CaO, MgO and SO_3 and lower Al_2O_3 and SiO_2 content than ash from bituminous coal (Class F fly ash). Mineralogically, the the higher CaO, MgO and SO_3 contents of western fly ashes usually result in crystalline lime, periclase, calcium aluminate and calcium sulfate in addition to the dominant glassy phase. The mineralogy of Class C fly ash can play an important role in its behavior as a cement replacement because the lime when hydrated can activate a self-pozzolanic behavior in the ash itself and the two calcium phases can react with water in cementitious reactions such as ettringite formation (1,2). Indeed, one product marketed as "pozzocrete" in the upper midwest has up to 80% fly ash replacement of cement in concrete.

We recently completed a literature review on the mineralogy of all fly ashes (3). The review indicated that the majority of previous work has focussed on Class F fly ashes where the nature of the crystalline phases is of little consequence to ash behavior because the dominant crystalline phases (quartz, mullite, magnetite and hematite) are largely inert during cement-water and ash-water reactions involving the glassy phase(s). In the relatively small number of studies on high calcium fly ashes, general agreement exists on the common mineralogy, as listed above. X-ray diffraction (XRD) has played a pivotal role in the characterization of these more crystalline ashes. Because of the greater importance of the mineralogy in western fly ash utilization (and disposal), an XRD survey of the mineralogy in a moderately large number of specimens was undertaken. We report here the results of this survey of twenty-seven fly ash specimens (from twenty-two power plants) for which chemical data were available. Several dozen additional ashes (including some from the same twenty-two plants but sampled on different dates) were studied but, because chemical data on these specimens were not available, the results are not included here. However, in all cases, the crystalline phases identified in these additional ashes corresponded to the phases reported here, which encourages us to believe that the mineralogy observed in our survey is representative of all western fly ashes.

Experimental

The fly ash specimens were obtained from the Coal By-products Utilization Instutute (CBUI) at the University of North Dakota. The chemical data on these ashes were also made available by the CBUI. The analyses were made by atomic absorption spectrometry. The specific components reported are those necessary for ASTM fly ash specifications.

Fly ash specimens were ground in an agate mortar and mounted on glass microscope slides. Diffraction data were obtained with a Philips diffractometer equipped with a copper tube, theta-compensating slit, diffracted beam monochromator, proportional detector, solid state electronics and strip chart recorder. The usual scan conditions were 40KV/20ma, 250 cts full scale, and 2°/min scan speed. Phases were identified by reference to the JCPDS Mineral and Inorganic Powder Diffraction Files.

Several treatments of the fly ash specimens were performed as an aid in phase identification or to add support to a tentative identification. In one experiment, ash was mixed with distilled water in order to extract the readily soluble salts. The water to solid ratio was 100:1 and the mixture was stirred for two hours at room temperature. The residual fly ash, the solution and the solid residue from evaporation of the solution were characterized by XRD. In a second experiment, selective dissolution treatments developed by L. D.

VOL
14
198

Hulett et al. (4) were applied to a number of ash specimens to see whether any previously undetected minor components would remain in the solid residue. Ash samples were etched in a one percent HF solution for 16 hours followed by washings with HNO_3, HCl, EDTA and NH_4OH solutions. In both solution experiments, a magnetic ferrite spinel phase stuck to the stir bar so a fraction enriched in this phase could easily be obtained. In other experiments aimed at confirming the identification of tricalcium aluminate (C_3A), mixtures of ash with water and with water plus gypsum having a w/s ratio of 0.28 were allowed to set. They were then examined by XRD for residual C_3A and/or the formation of ettringite.

Results and Discussion

The available chemical analysis data for the twenty-seven fly ashes and the results of XRD characterization are collected in Table I. Also included in Table I is the coal type from which the ash is derived for cases where this information was available. The analyses usually sum to less than 100% because of components not analyzed (e.g. TiO_2, P_2O_5, alkali oxides, CO_2), unburned coal and H_2O. The analyses are ordered by silica content of the fly ash. Lignitic ashes generally fall toward the top of the table. The two lignitic ashes located near the center of the list in silica content (14 and 17) are from central North Dakota coals. Their low alumina contents are typical of the lignites, so the excess SiO_2 may be due to more than normal amounts of quartz in the coal. One bituminous coal fly ash was included in the study and fell near the bottom of the table. Actual analyses for alkali oxides (A_2O = Na_2O+K_2O) were available for only half of the ashes. The chemical trends summarized by Diamond (1,2) are evident from the table.

Fly ash 4 did not originate in a power plant but was synthesized at UND's Energy Research Center in a test combustor from Beulah-Zap North Dakota lignite. Fly ash 2 originated from the same coal in an actual power plant.

We will discuss the individual crystalline phases observed in the ash samples and provide comments on some apparent relationships between chemical composition of the ashes and crystalline phase formation.

Quartz (Qz)

Alpha quartz was observed in all fly ashes. It almost certainly results from quartz in the original coal that survives combustion. Where more than one ash from the same coal and plant was available, quartz reflections were found to have substantial variations in intensity in the diffractograms. This is probably a result of varying quartz content in the source coal.

Lime (Lm)

Crystalline CaO was observed in the diffractograms of all but two of the ashes listed in Table I. Tests with lime-synthetic ash mixtures indicated that as little as 0.5 wt% could be detected with the instrumental conditions used. Based on quantitative analyses of several of the ashes (by the standard additions method), it is estimated that the range of lime compositions varies from 0.5 to 8-10 wt%. Thus, no more than about one-third of the CaO listed in the bulk chemical analysis of any particular ash is true "free lime."

The crystalline lime concentration can be important for several reasons. It can react with water to yield self-pozzolonic reactions in the ash. However, if it is in a highly sintered ("dead burned") state with large grain

Table I

Chemistry and Mineralogy of Western Fly Ash

Phase[a]	General Composition	Crystal Data[b]
	"Primary" Crystalline Phases	
Melilite (Ml)	$(Ca,Na)(Mg,Al,Fe)(Al,Si,Fe)_2O_7$	Tetragonal: a = 7.783(3) c = 5.025(3)
Ferrite Spinel (Sp)	$(Mg,Fe)(Fe,Mg)_2O_4$	Cubic:[c] a = 8.364(2)
Merwinite (Mw)	$Ca_3Mg(SiO_4)_2$	Monoclinic:[d] a = 13.35(2) b = 5.31(1) c = 9.36(2) β = 91.4°
Bredigite (Bd)	Ca_2SiO_4	Orthohombric: a = 10.92(1) b = 18.35(2) c = 6.762(4)
Nepheline (Ne)	$NaAlSiO_4$	Hexagonal: a = 10.004(8) c = 8.395(10)
Periclase (Pc)	MgO	Cubic: a = 4.241(3)
Hematite (Hm)	Fe_2O_3	- - -
Carnegieite (Cg)	$NaAlSiO_4$	Pseudocubic: a_0 = 7.291
Plagioclase (Pg)	$(Ca,Na)(Al,Si)_4O_8$	- - -
Pyroxene (Px)	$(Ca,Na)(Mg,Fe,Al),Si,Al)_2O_6$	- - -
Cristobalite (Cb)	SiO_2	- - -
	"Secondary" Crystalline Phases	
Calcite (Cc)	$CaCO_3$	
Portlandite (Pl)	$Ca(OH)_2$	
Brucite (Bc)	$Mg(OH)_2$	
Gypsum (Gp)	$CaSO_4 \cdot 2H_2O$	
Thenardite (Tn)	Na_2SO_4	
Ettringite (Et)	$Ca_6Al_2(SO_4)_3(OH)_{12} \cdot 25H_2O$	
Goethite (Gt)	FeOOH	
	Other Crystalline Phases	
Serpentine (St) ?	$Mg_6Si_4O_{10}(OH)_8$	
Talc (Tc) ?	$Mg_3Si_4O_{10}(OH)_2$	

a. Abbreviation used in Part II in parenthesis; the first seven phases are listed in estimated decreasing order of abundance in the bulk ground ash.
b. Cell parameters in Å; standard error on the least significant figure in parenthesis.
c. SEM/EMA indicated a range of Sp compositions (see Part II); end member cell parameters: Fe_3O_4, 8.3967; $MgAl_2O_4$, 8.0831; $MgFe_2O_4$, 8.397(high), 8.375(low) [Data the JCPDS Mineral Powder Diffraction File].
d. Few unique reflections were available for merwinite.

VOL. 14 1984

sizes, lime can cause a fly ash to fail the ASTM autocalve expansion test. In one example that came to our attention recently, a commercially valuable fly ash that had been used for years as a cement replacement suddenly began to fail autoclave expansion tests and the use of this ash for various purposes in Minnesota was curtailed. Chemical analysis indicated that the ash composition had changed because a different seam was being mined at the coal source. The change was only about 2% greater CaO and 2% less SiO_2. Also, the power plant had changed its coal grinding parameters somewhat after an overhaul of the grinding equipment. Mineralogical analysis indicated a significant increase in crystalline lime in the more recent specimens, especially in the fraction of ash retained on a 325 mesh sieve. In tests at the CBUI, the -325 fraction of the ash passed the autoclave expansion test while the +325 fraction that was greatly enriched in lime failed the test dramatically. The excess lime in the coarser grains was apparantly not reactive during the initial setting of the cement. It is only during the treatment with supercritical steam that the lime hydrates to portlandite with the accompanying volume expansion that causes the autoclave test failure. The role of lime in the autoclave expansion test has been previously described by Schlorholtz (5).

Periclase (Pc)

Periclase was detected in all but three of the fly ashes highest in $SiO_2+Al_2O_3$. In some diffractograms (those from ashes having more than about 5.5% MgO) periclase reflections were among the most intense. Based on quantitative analysis of several of the ashes, we estimate a range of periclase contents from 0.4 to 4 wt% in the ashes in Table I where periclase is reported, and that about half of the MgO content of a typical ash is present as periclase. During the various water extraction tests, it was noted that the intensity of the periclase reflections did not decrease in the residues. We have observed no brucite ($Mg(OH)_2$) in fresh or water-treated ashes. Thus, we can add support to previous observations that the periclase in western fly ash is generally unreactive to basic solutions at normal temperatures and pressures (1,5).

Anhydrite (Ah)

With the high CaO and SO_3 contents of western fly ashes it is not surprising to observe $CaSO_4$ in the fly ash. The ash with its free lime is acting as a built-in "scrubber" for SO_3. The availablility of $CaSO_4$ and C_3A in these ashes promotes the self-pozzolanic reactions such as ettringite formation that cause the stored ash to set-up upon contact with water. We have observed substantial ettringite in diffractograms of ash stored outdoors as well as in ash hydrated in the laboratory.

Ferrite Spinel (Sp)

Most ashes contained a spinel structure oxide with an x-ray pattern very similar to that of magnetite. This phase is easily enriched in a magnetically separated fraction. The unit cell parameter averages 8.37 Å compared to 8.39 Å for pure magnetite. Electron microprobe analyses of ferrite spinels formed in ash gasified from the same lignite coal formation as ashes 2 and 4 in Table I indicated that spinels had substantial Mg and Al substitution (7). Aluminum substitution in fly ash spinels has been noted previously (8). Lauf (9) found that certain trace elements that were partitioned into pyrite in the coal remain partitioned in the ferrite spinel phase in fly ash. Scheetz et al. (10) reported a Mn-rich spinel structure phase in one fly ash they studied.

C_3A (CA) and Merwinite (Mw)

Several authors have reported the presence of C_3A in western fly ashes (1,2,5,11,12), and the rapid formation of ettringite in hydrated ash is certainly consistent with the presence of reactive C_3A. A weak to occasionally moderate intensity reflection at about 32.2° two-theta was noted in the diffractograms of almost all of the ashes studied. This is the position of the strongest reflection of C_3A. However, confirming reflections of moderate intensity for C_3A are usually missing (too weak to be observed?) or are overlapped by stronger reflections attributable to other phases. An exhustive search of the Powder Diffraction File for any other phases with one of three strongest lines at 32.2° yielded only merwinite, $Ca_3Mg(SiO_4)_2$, as a possibility. The strongest reflection of merwinite occurs at this angle and several additional reflections of merwinite overlap those of C_3A. In several ashes, confirming reflections of merwinite were definitly present. Similarly, C_3A was certainly present in several other ashes. In most other ashes, both appear to be present.

Merwinite is commonly observed in metallurgical slags and is especially prominant as an early metastable devitrification phase. High calcium fly ash can have compositions approaching that of some slags and merwinite would seem to be a reasonable phase to observe in such ashes. We have also observed merwinite in lignite coal gasification ash (7).

Experiments designed to monitor the C_3A component of fly ash reacted with water and with gypsum plus water showed that only part of the intensity of the characteristic C_3A reflections disappeared while the unreactive merwinite remained after several hours through weeks of setting.

Because of these overlapping reflections and because we believe that virtually all western fly ashes contain at least small amounts of both phases, we have designated these phases as CA/Mw in Table I. Grain sizes are too small for the available SEM/electron microbrobe to provide analyses of individual grains that would confirm these phase identifications. Analytical transmission electron microscopy will be necessary to determine the compositions and structure types of these two phases.

Alkali Sulfates (AS)

Some of the lignite fly ashes contained in excess of 15 wt% A_2O+SO_3 and in these, alkali sulfates were observed in the diffractograms. The most common phase was thenardite, Na_2SO_4-V, but Na_2SO_4-III and aphthitilite ($(Na,K)_2SO_4$) were also observed. Concrete having partial replacement of cement with these fly ashes may show salt efflorescence unless it is covered with plastic during setting.

On some of the more AS-rich ashes, a water extraction experiment was performed to selectively remove the AS reflections from the diffractograms. Analysis of the solutions showed high concentrations of Na, Ca and SO_4 plus some K. When the solutions were frozen, thenardite, gypsum and a small amount of ettringite were formed. When the solutions were evaporated to dryness at 110°, the residual salts were Na_2SO_4-III, bassanite ($CaSO_4.1/2H_2O$), thenardite and minor aphthitilite.

Melilite (Ml)

Weak reflections of a melilite structure phase were observed in about

half of the fly ash specimens. Melilite is a mineral structural group term for the minerals akermanite ($Ca_2MgSi_2O_7$), gehlenite ($Ca_2Al_2SiO_7$) and Na-melilite ($NaCaAlSi_2O_7$). Iron commonly substitutes in part for both Mg or Al. A melilite structure solid solution having a composition intermediate to the three end members is the dominant phase in the lignite gasification ash described elsewhere in this symposium (6,7). Melilite is also a prominant phase obtained by devitrification of the lignite fly ashes at temperatures above 700°C. The small amount observed in western fly ash may be a result of insipient devitrification as the glassy phase was cooling.

Mullite (Mu)

Mullite, $Al_6Si_2O_{13}$, is a common phase in Class F fly ash (1,2). It was observed in about half of the fly ashes studied. With one exception, mullite was not observed in ashes whose $Al_2O_3+SiO_2$ contents were less than 60% and whose Al_2O_3 was less than about 17%. Note the composition of ash 17 where the values are 61.1% and 15.5 respectively. This ash, from a North Dakota lignite, nad no mullite.

Mullite can be hard to identify, if it is present in only small amounts, because its strongest reflections are close to the strongest reflection of quartz. The HF selective dissolution was applied to seven ash specimens and with the glass phase removed, the quartz and mullite reflections were sufficiently intense and resolved to enhance mullite detection.

Sodalite (So)

The mineral sodalite is a chloride-containing sodium aluminosilicate that gives its name to a group of isostructural phases. The two phases relevant here are nosean, $Na_8Al_6Si_6O_{24}SO_4$, and hauyne, $Ca_2Na_6Al_6Si_6O_{24}(SO_4)_2$. The relationship of the cement clinker phase, $C_4A_3\bar{S}$, to these sodalite structure phases can be seen if the stoichiometry is written as $Ca_2Ca_6Al_6Al_6O_{24}(SO_4)_2$. A minor phase with the strongest reflections of a sodalite was observed in the diffractograms of seven fly ashes. This phase is probably close to $C_4A_3\bar{S}$ in composition, but we prefer to designate it by its general group name until enough individual grains can be analyzed by microprobe to establish its composition. In devitrification studies on all of these fly ashes now underway, a sodalite structure phase is commonly observed as a major devitrification product (along with hematite and melilite, pyroxene and plagioclase solid solution phases). The mechanism of sodalite phase formation here appears to be the reaction of Na and Ca sulfates with the aluminosilicate glass. In this case, the composition is probably closer to nosean-hauyne.

Hematite (Hm)

Hematite was evident in only a few of the more silica-rich diffractograms of bulk ash. However, after magnetic separation of a ferrite spinel rich fraction, the diffractogram usually showed some hematite, present perhaps as an oxidized coating. Hematite was also brought to detectable amounts in the residues of five of the seven ashes subjected to the selective dissolution experiment. Thus, we estimate that more than half of the ashes have at least small amounts of hematite.

Other Phases

Several other minor phases have been detected or are strongly suspected as being present in some of the fly ashes. Dicalcium silicate (C_2S) is one of

these. The strongest reflections of the various C_2S phases are folded into the region of the diffractogram where lime, melilite, alkali sulfates, anhydrite and merwinite also have strong reflections. It is possible that perhaps 1 wt% of one or more C_2S phases are present in ten or so specimens, but we were not able to make an umambiguous identification. Traces of calcite were occasionally observed and acid effervescence corroborated its presence.

We made many efforts to identify additional phases reported by other investigators who have studied similar fly ashes. We did not detect kalsilite ($KAlSiO_4$), arcanite (K_2SO_4) or kappa-alumina as reported by Diamond and Lopez-Flores (1) or brownmillerite and C_3S as reported by Scheetz et al. (10). With these exceptions, our results correspond in all major respects with the most comprehensive reports of XRD studies on Class C fly ashes in the literature (references 1,2,5,11 and 12) and taken together these appear to be sufficient to say that the mineralogy of western fly ash is now well understood.

Acknowledgments

This research was supported by the ND Water Resources Research Institute and the ND Mining and Mineral Resources Research Institute. The cooperation of Oscar Manz of the Coal By-products Utilization Institute and David Hassett of the Fuels Analysis Laboratory at UND, William Collins and Mark Strawn of National Minerals Corporation, Fargo, William Grosz of Basin Electric Cooperative, Bismarck, Philip Richmond of Minnkota Power Cooperative and Michael Schlosser of Cooperative Power Assocation in supplying specimens and chemical analyses is greatfully acknowldeged.

References

1. S. Diamond, in Effects of Flyash Incorporation in Cement and Concrete, MRS Proceedings, Symposium N, Nov., 1981, pp. 12-23.
2. S. Diamond and F. Lopez-Flores, ibid. pp. 34-44.
3. G. J. McCarthy, K. D. Swanson, P. J. Schields and G. H. Groenewold, "Mineralogical Controls on Toxic Element Tontamination of Groundwater from Buried Electrical Utility Solid Wastes. I Solid Waste Mineralogy. II. Literature Review of Fly Ash Mineralogy," ND Water Resources Research Institute, Contract A-078-NDAK, Final Report, 59 pp., July, 1983.
4. L. D. Hulett, A. J. Weinberger, M. Ferguson, K. J. Northcutt and W. S. Lyon, "Trace Elements and Phase Relations in Fly Ash," EA-1822 Research Project 1061, EPRI Final Report, May 1981.
5. S. M. Schlorholtz, M.S. Thesis, Iowa State University, 1982.
6. R. J. Stevenson, this symposium.
7. G. J. McCarthy, L. P. Keller, P. J. Schields, M. P. Elless and K. C. Galbreath, this symposium.
8. L. D. Hulett, A. J. Weinberger, A. J. Northcutt and M. Ferguson, Science, 210, 1356 (1980).
9. R. J. Lauf, ORNL/TM-7663, 71 pp., August, 1981.
10. B. E. Scheetz, D. W. Strictler, M.W. Grutzeck and D. M. Roy, ibid. ref. 1.
11. M. L. Mings, S. M. Schlorholtz, J. M. Pitt and T. Demirel, Personal Communication, June, 1983.
12. J. M. Pitt, M. L. Mings, S. M. Schlorholtz, ibid.

VOL
14
198

CEMENT and CONCRETE RESEARCH. Vol. 14, pp. 479-484, 1984. Printed in the USA.
0008-8846/84 $3.00+00. Copyright (c) 1984 Pergamon Press, Ltd.

MINERALOGICAL CHARACTERIZATION OF A LIGNITE GASIFICATION ASH FROM A LOW-BTU FIXED-BED GASIFIER I. X-RAY PHASE ANALYSIS

Gregory J. McCarthy, Lindsay P. Keller, Paul J. Schields,
Mark P. Elless and Keven C. Galbreath
Department of Chemistry, North Dakota State University, Fargo, ND 58105

(Communicated by S. Diamond)
(Received Nov. 17, 1983)

ABSTRACT

A lignite coal ash produced in a low-Btu atmospheric pressure gasifier has been studied by x-ray diffraction. The ash was dominantly crystalline and consisted of CaO-MgO-Na_2O-silicates (melilite, merwinite, Ca_2SiO_4-bredigite, nepheline/carnegieite), oxides (ferrite spinel, quartz, periclase, hematite), phases formed by reaction with water or precipitation from solutions used in ash handling (calcite, portlandite, brucite, thenardite, ettringite, gypsum, goethite) and several additional trace phases (plagioclase, pyroxene, cristobalite, serpentine and talc).

Introduction

The long term viability of the gas industry will depend increasingly on the production of synthetic natural gas from the gasification of coal. Coal gasification produces large amounts of ash which must be disposed of properly. It is estimated that the first commercial coal gasification plant in the US, the Great Plains Plant in Beulah ND, will produce 2.4 million Kg (2600 tons) of ash per day. The overall expense of environmentally safe disposal would be eliminated if direct utilization of the ash in the fabrication of construction and road building materials were technically and economically attractive. Alternatively, the expense could be lowered if metals such as iron, aluminum or trace elements could be extracted from the ash prior to disposal. Characterization of the chemistry and "mineralogy" (phases present in the ash) is fundamental science underlying the various utilization and extraction options.

An ash from gasification of Beulah-Zap lignite coal (the same coal to be used at the Great Plains Plant) was obtained from American Natural Resources of Detroit, MI. The ash was produced in 1980 in the low-Btu dry-ash Wellman-Galusha (W-G) gasifier located at the Twin Cities Metallurgy Center of the US Bureau of Mines in Minneapolis, MN. A description of this gasifier and of its operation with lignite coal has been given by Kilpatrick et al.(1) The W-G

gasifier differs from the commercial-scale Lurgi gasifiers to be used at Great Plains in that it operates at atmospheric pressure and with a steam-air rather than with a steam-oxygen atmosphere. The estimated gasification temperatures (900-1050°C) and residence time (15-30 min) are similar to those in a Lurgi gasifier, and it is these two factors, along with the redox conditions, that exert dominant control over the mineralogy of the ash from a given coal.

The objective of the present report is to describe the mineralogy of this ash with x-ray powder diffraction and scanning electron microscopy-electron microprobe analysis. Part I describes the x-ray phase identification and Part II the electron microscopy. While this ash was not produced under all of the same conditions to be found in a state-of-the-art Lurgi type gasifier, it did provide initial experience with low-rank coal ash mineralogy, morphology and chemistry that will form the basis of future studies of coal gasification ash.

Experimental

More than 200 Kg of ash was available. Agglomerates of up to 4 cm in diameter were present in the as-received ash. After splitting, several Kg were ground to -100 mesh in a ball mill. A representative portion of this bulk ground ash was used for elemental analysis by atomic absorption spectrometry (AAS) and energy dispersive x-ray spectrometry. The bulk ground ash and individual grains painstakingly picked according to color, habit, luster etc. under a binocular microscope were studied. The latter procedure proved to be essential for phase identification as only eight of the crystalline phases could have been identified with reasonable certainty in the bulk ground ash.

Bulk ground ash or hand-picked grains were ground further in an agate mortar and mounted on glass microscope slides. Diffraction data were obtained with a Philips diffractometer equipped with a copper tube, theta-compensating slit, diffracted beam monochromator, proportional detector, solid state electronics and strip chart recorder. Phases were identified with the JCPDS Mineral and Inorganic Powder Diffraction Files. Crystal data were obtained for some of the solid solution phases as further verification that the phase had been properly identified. Using grains that were enriched in a particular phase, a data set was collected from 1/2°/min diffractograms and computer refined using a least squares procedure.

Results and Discussion

A chemical analysis for 20 constituents of bulk ground ash is given in Table I. The relatively low $SiO_2+Al_2O_3$ and high $CaO+MgO+SO_3$ are characteristic of ash from western lignite coals (2). The concentrations of iron oxides (shown only as Fe_2O_3 in this table), Na_2O and SO_3 are also notable. The 3.2% moisture content (determined by drying at 107°C) suggested that, in addition to adsorbed water, phases containing molecular water were present. Loss of CO_2 from carbonates, H_2O from hydroxides and carbon from oxidation of residual coal gave a 4.5% loss on ignition (LOI) at 750-800°C.

Crystalline phases identified in the Wellman-Galusha ash are listed in Table II. The compositions listed incorporate insights from the electron microprobe analyses described in Part II.

Analysis of the bulk x-ray diffractogram revealed that the ash was dominantly crystalline because there was no prominant diffuse scattering

Table I

Chemical Analysis of Lignite Gasification Ash

Oxide	Wt %	Oxide	Wt %	Element	mg/kg	Element	mg/kg
SiO_2	24.9	Na_2O	8.1	Sr	2970	Cl	90
Al_2O_3	10.5	K_2O	0.5	Mn	1200	Zn	77
Fe_2O_3	15.2	TiO_2	0.8	Sr	175	Cu	71
CaO	20.1	P_2O_5	0.5	Ni	147	As	61
MgO	6.8	SO_3	4.9	Cr	117	Y	35

Loss on ignition = 3.2% Moisture = 4.5%

maximum under the large number of relatively sharp reflections. Only a few phases could be identified with certainty in the bulk diffractogram. Good matches were easily obtained with melilite group minerals (akermanite, gehlenite and Na-melilite) and magnetite (Fe_3O_4) patterns in the JCPDS Powder Diffraction File. After consideration of the high Ca-Mg content of the ash and the presence of melilite, the possibility of merwinite, $Ca_3Mg(SiO_4)_2$, was postulated and confirmed. The association (melilite+merwinite) suggested an analogy to metallurgical slags. Except for a higher CaO and lower Fe_2O_3 content in the slags, the ash composition was similar in many respects to blast furnace slags. Another phase to be expected from the analogy to slags was Ca_2SiO_4. Several reflections in the ash diffractogram were consistent with one or more of the six polymorphs of Ca_2SiO_4, but due to overlaps no positive identification could be made. Acid effervescence of the ash suggested the presence of calcite and this was confirmed by noting the strongest reflection of calcite in the diffractogram. Finally, previous work with lignite combustion ashes led us to consider quartz, hematite and periclase as likely phases and, as with calcite, there was at least one unique reflection in the diffractogram that was consistent with the presence of each of these phases.

These eight phases accounted for most of the intensity in the bulk diffractogram, but considerably more effort was required to account for the remaining reflections. Several methods were used to obtain portions of the ash that were enriched in one or more phases. Magnetic separations yielded a ferrite spinel-rich portion. Sieving the ash led to fractions richer in several phases. For example, the -325 mesh fraction was enriched in calcite and ettringite. But, it was in selecting grains (with the aid of a binocular microscope) containing only a few phases that each of the phases listed in Table II was definitely identified. In cases where there were enough unambiguously indexed reflections, unit cell parameters were obtained using the observed reflections in a least squares computer refinement. In this manner, the Ca_2SiO_4 phase was identified as the orthorhombic a_L' polymorph by analogy to the unit cell, chemical substitutions (determined with the electron microprobe) and x-ray powder pattern of the mineral bredigite. Another phase close in composition to Ca_2SiO_4 is discussed in Part II of this paper.

The phases in Table II are divided into "primary" and "secondary" according to our estimates of whether the phase formed during gasification or later after contact with water and CO_2. With regard to the proposed primary phases, it is likely that quartz and the small amounts of plagioclase and

Table II

Crystalline Phases Identified in Lignite Gasification Ash

FLY ASH NUMBER	CHEMISTRY (wt %)								MINERALOGY[b]	COAL TYPE[c]
	SiO_2	$A\ell_2O_3$	Fe_2O_3	CaO	MgO	A_2O[a]	SO_3	Total		
1	26.9	9.1	3.6	19.2	5.8	8.6	16.60	89.8	Pc, Ah, AS, Lm, Qz, CA/Mw[d]	L
2	27.5	10.2	7.2	22.3	7.2	12.3	9.50	96.20	Pc, Lm, Ah, Sp, Mw, AS, Mℓ, Qz	L
3	27.9	10.7	9.9	21.6	5.5	10.3	12.27	98.2	Qz, Ah, Pc, Sp, Lm, So, AS	L
4	28.9	11.1	11.0	18.9	6.0	8.9	6.83	91.63	Sp, Pc, Qz, Lm, Mw, Ah, Mℓ, Qz	L
5	30.2	12.5	4.6	23.6	7.9	5.24	9.60	93.6	Pc, Ah, Qz, Sp, So, Lm, Mℓ, AS	L
6	36.4	17.4	6.8	27.6	4.8		3.00	96.0	Qz, CA/Mw, Pc, Lm, Ah, Sp	S
7	36.5	18.9	5.7	28.8	3.9	1.7	1.88	97.4	Qz, CA/Mw, Lm, Pc, Ah, So	S
8	36.7	20.5	5.7	28.2	5.4	1.49	2.80	100.8	Qz, CA/Mw, Pc, Lm, Ah, Mℓ, Sp	S
9A	39.0	17.3	6.1	27.0	4.6		2.28	96.3	Qz, CA/Mw, Pc, Lm, Ah, Mℓ, Sp	S
B	42.4	16.5	5.9	27.3	2.20		2.21	96.5	Qz, CA/Mw, Pc, Lm, Ah, Mℓ, Sp	S
10	40.0	17.6	5.6	25.0	6.8	0.78	0.56	96.3	Qz, Pc, Lm, CA/Mw, Sp, Ah	S
11A	40.5	16.0	5.8	25.7	4.7		3.30	96.0	Qz, CA/Mw, Pc, Lm, Ah, So, Sp, Mℓ	S
B	41.4	14.2	6.6	25.6	4.80		3.50	96.1	Qz, CA/Mw, Pc, Lm, Ah, Sp, Mℓ	S
C	41.8	16.7	5.7	24.4	4.6		2.75	96.0	Qz, CA/Mw, Pc, Lm, Ah, Sp, So, Mℓ	S
12A	41.2	18.4	5.5	24.8	4.0		1.83	95.7	Qz, CA/Mw, Pc, Lm, Mu, Ah, Mℓ	S
B	41.9	17.1	6.5	24.2	4.3		1.99	96.0	Qz, CA/Mw, Pc, Lm, Ah, Mu, So, Sp	S
13A	41.4	21.1	6.9	20.1	4.3		2.63	96.4	Qz, CA/Mw, Pc, Mu, Ah, Lm, Sp, Mℓ, So	
B	43.0	22.5	6.1	18.8	4.0		2.12	96.5	Qz, CA/Mw, Pc, Mu, Ah, Lm, Sp	
14	42.1	12.0	8.1	18.5	5.0	3.92	4.07	93.7	Qz, AS, Pc, CA/Mw, Sp, Lm, Ah	L
15	43.0	18.2	5.4	17.7	3.9	1.24	1.75	91.2	Qz, CA/Mw, Pc, Lm, Ah, Sp, So, Mu	S
16	45.6	19.3	9.7	16.2	3.6		1.91	96.3	Qz, Lm, Pc, Mu, Ah, CA/Mw, Sp	
17	45.6	15.5	7.3	20.3	5.0	2.7	1.88	98.3	Qz, Pc, CA/Mw, Ah, Lm, Sp	L
18	45.7	21.0	5.3	19.0	4.0		1.30	96.3	Qz, Lm, Mu, Sp, Pc, Ah	S
19	49.6	18.2	21.1	4.1	0.8		1.62	95.4	Qz, Sp, Hm, Mu	
20	50.9	19.2	16.5	6.2	1.12		1.10	95.0	Qz, Sp, Mu, Lm	
21	54.7	29.9	4.5	1.1	0.80		0.27	91.3	Qz, Mu, Sp	B
22	56.3	17.2	5.2	12.9	2.8	0.46	1.27	96.1	Qz, Lm, Sp, CA/Mw, Mu, Pc	S

a. A_2O = Alkali oxide ($Na_2O + K_2O$).

b. Listed in order of intensity of the strongest reflection of each phases in the X-ray diffractogram;
Pc = Periclase
Ah = Anhydrite
AS = Alkali Sulfate
Lm = Lime
Qz = Quartz
Ca/Mw = $C_3A(Ca_3A\ell_2O_6)$ and Merwinite
Sp = Ferrite spinel
Mℓ = Melilite solid solution
So = Sodalite Structure ($C_4A_3\bar{S}$)
Mu = Mullite

c. L = Lignite S = Subbituminous B = Bituminous

d. Ca/Mw = tricalcium aluminate (C_3A) + merwinite overlapping reflections

VOL. 14 1984

pyroxene phases were present in the original lignite and survived the gasification treatment. Melilite, merwinite, and bredigite indicate considerable reaction among the inorganic constitutents of the lignite during gasification. The two polymorphs of $NaAlSiO_4$, nepheline and carnegieite could have formed by the reaction of Na-vapor species and clays from the coal. Ferrite spinel and hematite probably formed from the oxidation of pyrite and reaction of the resulting iron oxides with other spinel-forming oxides. The minor cristobalite could have formed from crystallization of noncrystalline silica in the lignite. It is possible that calcite should be included with the primary phases also. Lime (CaO) and CO_2 could have reacted to form calcite directly during gasification.

The secondary phases apparently result from reactions of the ash with the water used to sluice the ash into storage. Portlandite, brucite, goethite and gypsum would form by hydration of their anhydrous oxides and anhydrite ($CaSO_4$), respectively. Thenardite, calcite and gypsum could have crystallized from the solutions evaporating in the ash storage bins. One explanation for ettringite formation would be reaction of calcium aluminates and sulfate in the presence of water similar to the reactions that form ettringite in hydraulic cements.

The appearance of small amounts of serpentine and talc has no ready explanation because their common occurrence is in rocks where water vapor pressures of formation are considerably higher than would be expected in an atmospheric pressure gasifier. The diffractograms of both of these phases indicated low crystallinity.

OL.
14
984

During the hand-picking operations, fractions that proved to be x-ray amorphous were occasionally noted. These noncrystalline phases will be discussed in Part II of this report. Also, individual grains with chemical analyses attributable to such phases as apatite, pyrrhotite and barite that were not isolated in any of the x-ray diffraction studies, along with intergranular glass, were noted during the electron microprobe examination. It was not possible to estimate the glass content of the ash in the X-ray diffraction studies.

In summary, the W-G lignite gasification ash is dominantly crystalline and contains a large number of individual phases. Approximately ten of these were present in sufficient concentration (more than 1-2 wt%) to be verifiable in a diffractogram of the bulk ground ash. The ash contained phases indicative of contact or reaction with water during handling subsequent to gasification.

Acknowledgments

Chemical analyses were made by the Fuels Analysis Laboratory and the Energy Research Center at the University of North Dakota. This research is supported by the Gas Research Institute (J. M. Evans, GRI Project Officer).

Reference

1. M. P. Kilpatrick, R. A. Magee, T. E. Emmel and G. C. Page, EPA-600/7-80-97, May, 1980.

2. G. J. McCarthy, K. D. Swanson, L. P. Keller and W. C. Blatter, Mineralogy of Western Fly Ash, Cement and Concrete Research (this volume).

LEGAL NOTICE: This report was prepared by the North Dakota Mining and Mineral Resources Research Institute as an account of work sponsored by the Gas Research Instutute (GRI). Neither GRI, members of GRI, nor any person on behalf of either: (a) makes any warranty or representation, expressed or implied, with respect to the accruacy, completeness, or usefulness of the information contained in this report, or that the use of any apparatus, method, or process disclosed in this report may not infringe privately owned rights; or (b) assumes any liability with respect to the use of, or for damages resulting from the use of, any information, apparatus, method, or process disclosed in this report.

VOL
14
198

CEMENT and CONCRETE RESEARCH. Vol. 14, pp. 485-490, 1984. Printed in the USA.
0008-8846/84 $3.00+00. Copyright (c) 1984 Pergamon Press, Ltd.

MINERALOGICAL CHARACTERIZATION OF A LIGNITE GASIFICATION ASH FROM A LOW-BTU FIXED-BED GASIFIER
II. SCANNING ELECTRON MICROSCOPE PHASE ANALYSIS

Robert J. Stevenson
Natural Materials Analytical Laboratory
Mining and Mineral Resources Research Institute
University of North Dakota
Grand Forks, North Dakota 58202

(Refereed)
(Received Nov. 17, 1983)

VOL. 14 1984

ABSTRACT

A lignite coal ash produced in a low-BTU fixed-bed atmospheric pressure gasifier has been studied by scanning electron microscopy using both imaging and chemical analytical techniques. The primary phases of the dominantly crystalline ash are Ca-Mg-Na-Al-silicates (melilite, merwinite, two C_2S phases including bredigite, and nepheline/carnegieite) and oxides (ferrite spinel, quartz, periclase, and hematite). Additional secondary phases (calcite, portlandite, brucite, thenardite, ettrigite, gypsum, and goethite) apparently formed by reaction with water or precipitation from solutions used in ash handling. The individual grains of ash proved to be variable in bulk composition and mineralogic content.

Introduction

A variety of utilization and extraction options for gasifier ash cannot be examined thoroughly without a knowledge of the bulk chemistry, mineralogy, and phase chemistry. This information on the mineralogy of the ash is collected using x-ray diffraction (Part I) and scanning electron microscopy (SEM) (Part II). Results from x-ray diffraction (the presence of particular phases) can be extended to determine actual phase compositions and phase assemblages as well as observation of glass and trace phases using SEM. This type of multiple instrument approach has been successfully applied to fly ash by Lauf (1).

Experimental

A split of the -100 mesh as received material was embedded in epoxy and polished blocks of the epoxy and ash mixture were studied in the scanning electron microscope (SEM). Epoxy embedded samples were also prepared from grains ground with an agate mortar. These hand-picked grains were first observed with x-ray diffraction and selected on the basis of their mineralogy for further study with the SEM.

The SEM is used to collect data that falls into two classifications. The first classification of data is related to the morphology of the grains and

their constituent phases. Photographs were taken of secondary electron images (SEI), backscatter electron images, and characteristic element x-ray map images. The second type of data classification is related to chemical analysis. Analyses were completed on over 850 points and areas of grains to determine the overall chemical makeup of the sample, the range of composition of the solid-solution phases, and to identify and correlate phases identified by x-ray diffraction (Part I).

Results and Discussion

Ettringite, glass and the dominant silicate phases, nepheline/carnieite, melilite, merwinite and two C_2S phases are shown in Table I. These analyses are based on a number of points on differing grains. The number of analyses are shown in parentheses under the abbreviation of the phase (ettringite, Et; nepheline, Ne; melilite, Ml; merwinite, Mw; bredigite, $C_2S(1)$; another C_2S phase, $C_2S(2)$; and glass, G). The minor elemental oxide amounts shown are generally above one standard deviation for the analyses that comprise the average. Cation proportions are also shown in Table I.

Melilite (Table I) and ferrite spinel are examples of minerals that are part of a solid solution series, whereas the compositions of nepheline and ettringite are nearly the same in all grains. This is shown by the relatively small standard deviations associated with the oxide weight percentages.

Figures 1, 2, and 3 illustrate the solid solution nature of melilite and ferrite spinel. Figures 1 and 2 are plots of CaO versus Na_2O and Al_2O_3 versus MgO. The negative slope of the grouping of analysis points indicates the substitution of Na for Ca and the partial substitution of Al for Mg. Al also substitutes for Si in the melilite structure, but in this study the dominant substitution is for Mg. The elemental substitution in the ferrite spinels (Figure 3) is Al and Mg for Fe. The two end members that dominate the chemistry of the ferrite spinels in the Wellman-Galusha ash are magnetite (Fe_3O_4) and spinel ($MgAl_2O_4$). There is a minor component of magnesioferrite ($MgFe_2O_4$) also present in the ferrite spinel.

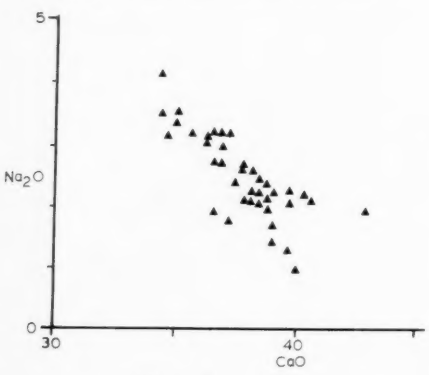

Fig. 1
CaO-Na_2O oxide plot of melilite showing Ca-Na substitution in Wellman-Galusha ash.

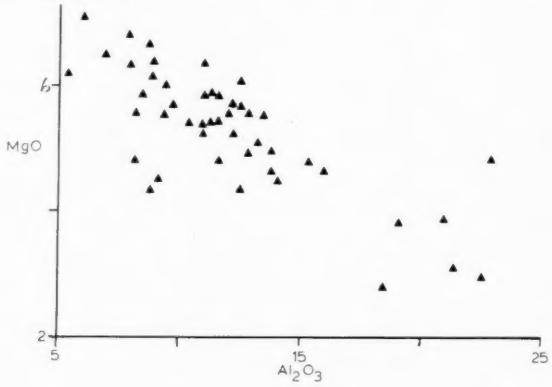

Fig. 2
Al_2O_3-MgO oxide plot of melilite showing Al-Mg substitution in Wellman-Galusha ash.

Figures 4, 5, and 6 illustrate the morphology of ettringite and the dominant primary phases. Figure 4 shows ettringite filling a cavity in the ash surrounded by bredigite and glass. Figure 5 shows the well-defined crystal

Table I
Compositions of selected phases of Wellman-Galusha ash.

	Et (5)*	Ne (12)	Ml (48)	Mw (47)	$C_2S(1)$ (12)	$C_2S(2)$ (13)	G (32)
SiO_2	1.15 (.58)**	40.64 (.51)	38.16 (3.89)	33.70 (.78)	31.61 (.86)	30.85 (1.16)	40.15 (6.18)
Al_2O_3	15.68 (1.55)	32.58 (.60)	12.09 (4.09)	0.68 (.57)	0.88 (.62)	1.32 (.86)	22.63 (7.42)
FeO	2.82 (1.45)	2.09 (.41)	3.88 (2.07)	2.93 (1.03)	1.47 (1.20)	0.45 (.40)	6.88 (4.18)
MgO	0.43 (.09)	0.70 (.17)	5.33 (.98)	7.95 (.43)	4.07 (.40)	0.58 (.60)	3.52 (1.48)
CaO	41.86 (4.30)	0.96 (.25)	37.97 (1.73)	50.34 (1.43)	56.60 (1.61)	62.38 (4.00)	12.85 (8.64)
Na_2O	1.67 (.97)	17.52 (.37)	2.43 (.59)	2.05 (.56)	2.70 (.32)	0.91 (.45)	10.39 (3.88)
K_2O	-	5.41 (.61)	-	-	-	-	0.89 (.99)
TiO_2	-	-	0.14 (.18)	0.22 (.18)	1.04 (.33)	0.27 (.30)	0.47 (.52)
P_2O_5	-	-	-	1.84 (.81)	1.29 (.84)	1.63 (1.75)	0.55 (1.01)
MnO	-	-	-	-	-	-	0.06 (.10)
SO_3	36.38 (1.51)	-	-	0.28 (.17)	0.34 (.27)	1.61 (.51)	1.61 (2.03)
O	18	4	7	8	4	4	
Si	0.129	0.994	1.755	1.876	0.901	0.878	
Al	2.061	0.942	0.652	0.044	0.029	0.044	
Fe	0.263	0.043	0.153	0.136	0.035	0.011	
Mg	0.072	0.025	0.368	0.661	0.173	0.025	
Ca	5.001	0.025	1.867	3.003	1.728	1.903	
Na	0.362	0.831	0.228	0.221	0.149	0.050	
K	-	0.170	-	-	-	-	
Ti	-	-	0.005	0.010	0.022	0.006	
P	-	-	-	0.086	0.031	0.039	
Mn	-	-	-	-	-	-	
S	3.045	-	-	0.012	0.007	0.034	
TOTAL	10.933	3.030	5.028	6.049	3.075	2.991	

* Number of point analyses
** Standard deviation shown in parentheses

outline of merwinite and spinel with nepheline-like glass filling the space between the crystals. Figure 6 is of the form melilite usually takes. Also present are spinel and nepheline-like glass.

The average of 98 grain area analyses is shown in Table II. Shown with the average based on the SEM results is the analysis of the bulk ash done by other spectroscopies (Table I, Part I). Close agreement is shown for most of the oxides. The difference in Na_2O and SO_3 is likely due to the water soluble minerals present in the bulk ash but washed out in the SEM mounts because of the polishing step. The Al_2O_3 difference is of unknown origin, although it may be related to the residual polishing compound. The large range of compositions for individual grain areas illustrates the heterogeniety of the Wellman-Galusha

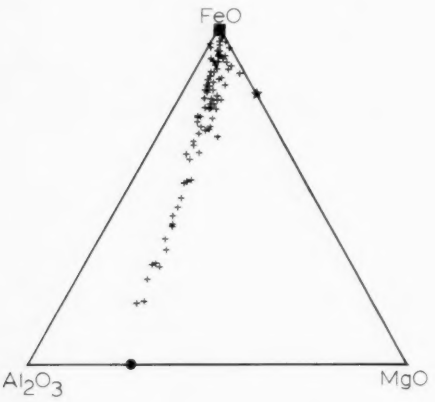

Fig. 3
Al_2O_3-FeO-MgO oxide weight percent plot of ferrite spinel in Wellman-Galusha ash. Also shown are the compositions for spinel (●), magnesioferrite (★) and magnetite (■).

Fig. 4
SEI of ettringite (Et) in cavity surrounded by bredigite and glass in Wellman-Galusha ash. Bar is 10.0 micrometers long.

Table II
Comparison of SEM and other spectroscopic analyses of Wellman-Galusha ash.

	Bulk Ash Analysis*	SEM Grain Analysis** Average	Minimum	Maximum
SiO_2	27.4	27.66	0.52	68.28
Al_2O_3	11.6	14.71	0.42	45.46
FeO	15.1	14.27	0.43	91.73
MgO	7.5	7.10	0.28	47.03
CaO	22.1	24.58	1.46	57.28
Na_2O	8.9	5.73	0.0	16.23
K_2O	0.6	0.77	0.0	11.22
TiO_2	0.9	0.76	0.0	1.99
P_2O_5	0.6	0.59	0.0	5.37
MnO	-	0.11	0.0	1.18
SO_3	5.4	3.72	0.0	66.57

*By AAS and EDXRF and normalized.
** Analysis of 98 individual grains.

ash. This heterogeniety was used to advantage in Part I in the hand-picking and subsequent x-ray diffraction work in identifying the minor minerals.

In summary, the major primary minerals are either members of a solid solution system or a defined composition. The structural formulae based on the average compositions of the major silicates and ettrigite are shown in Table III in comparison with their ideal formulae. Additionally, the compositions of

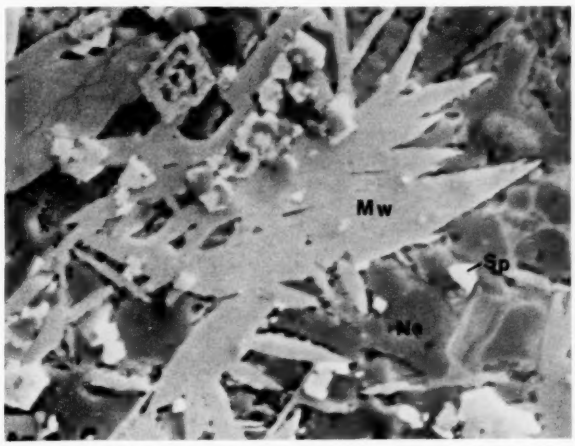

Fig. 5

SEI of merwinite (Mw), ferrite spinel (Sp), and nepheline-like glass (Ne) in Wellman-Galusha ash. Bar is 10.0 micrometers long.

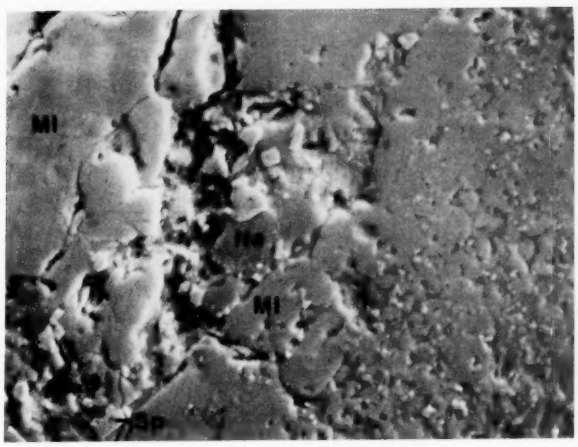

Fig. 6

SEI of melilite (Ml), ferrite spinel (Sp), and nepheline-like glass (Ne) in Wellman-Galusha ash. Bar is 10.0 micrometers long.

the grains in the ash are heterogeneous although generally the same major minerals are present in the grains.

Acknowledgements

Chemical analyses were made by the Coal By-Products Utilization Institute and the Energy Research Center at the University of North Dakota. This research is supported by the Gas Research Institute (J.M. Evans, GRI Project Officer.)

References

1. R.J. Lauf, ORNL/TM-7663, Oak Ridge National Laboratory (1981).
2. S.N. Ghosh, P. Bhaskara, A.K. Paul, and K. Raina; J. Materials Sci., v. 14 (1979).

VOL.
14
984

Table III
Structural formulae of selected phases of Wellman-Galusha ash

Melilite (Ml)

Akermanite: Ca_2 Mg Si_2 O_7

Gehlenite: Ca_2 Mg AlSi O_7

$(Ca_{1.87}Na_{0.13})(Al_{0.41}Fe_{0.15}Mg_{0.37}Na_{0.10})(Al_{0.24}Si_{1.76})O_7$

Merwinite (Mw)

Ideal: Ca_3 Mg Si_2 O_8

$Ca_{3.00}(Mg_{0.66}Na_{0.22}Fe_{0.14})(Si_{1.88}Al_{0.04}Ti_{0.01}P_{0.09}S_{0.01})O_8$

Nepheline (Ne)/Carnegieite (Cg)

Ideal: Na Al Si O_4

$(Na_{0.83}K_{0.17}Ca_{0.02}Mg_{0.02})(Al_{0.93}Fe_{0.04})(Si_{0.99}Al_{0.01})O_4$

$C_2S(1)$ - Bredigite (Bd)

Ideal: Ca_2 Si O_4

$(Ca_{1.73}Na_{0.15}Fe_{0.04}Mg_{0.17})(Si_{0.90}Al_{0.03}Ti_{0.02}P_{0.03}S_{0.04})O_4$

$C_2S(2)$

Ideal: Ca_2 Si O_4

$(Ca_{1.90}Na_{0.05}Fe_{0.01}Mg_{0.02})(Si_{0.88}Al_{0.04}Ti_{0.01}P_{0.04}S_{0.03})O_4$

Ettringite (Et)

Ideal: Ca_6 Al_2 $(SO_4)_3$ $(OH)_{12} \cdot 25\ H_2O$

$(Ca_{5.00}Na_{0.36}Fe_{0.26}Mg_{0.07})\ Al_{2.06}\ (S_{3.04}Si_{0.13})\ O_{12}\ (OH)_{12} \cdot 25\ H_2O$

GRI Disclaimer

LEGAL NOTICE This report was prepared by the North Dakota Mining and Mineral Resources Research Institute as an account of work sponsored by the Gas Research Institute (GRI). Neither GRI, members of GRI, nor any person acting on behalf of either:

a. Makes any warranty or representation, express or implied, with respect to the accuracy, completeness, or usefulness of the information contained in this report, or that the use of any apparatus, method, or process disclosed in this report may not infringe privately owned rights; or

b. Assumes any liability with respect to the use of, or for damages resulting from the use of, any information, apparatus, method, or process disclosed in this report.

VOL 14 198

CEMENT and CONCRETE RESEARCH. Vol. 14, pp. 491-498, 1984. Printed in the USA.
0008-8846/84 $3.00+00. Copyright (c) 1984 Pergamon Press, Ltd.

DEVELOPMENT OF MICROSTRUCTURE AND OTHER PROPERTIES IN FLYASH OPC SYSTEMS

Y. Halse and P. L. Pratt
Department of Metallurgy & Materials Science,
Imperial College, Prince Consort Road, London SW7 2BP, UK

and

J. A. Dalziel and W. A. Gutteridge
Cement & Concrete Association, Wexham Springs,
Slough SL3 6PL, UK.

(Refereed)
(Received Nov. 17, 1983)

VOL. 14 1984

ABSTRACT

Ordinary Portland cements and flyash blend cements containing 30% of flyash were cast at room temperature with a w/s ratio of 0.45-0.47. The $Ca(OH)_2$ content and compressive strength were measured at several ages. In the flyash-cement systems the $Ca(OH)_2$ content reached a maximum value after 7-14 days thereafter decreasing as a result of pozzolanic reaction. This decrease in $Ca(OH)_2$ content followed dissolution of the flyash surfaces and the augmentation of strength by the flyash.

Introduction

In a recent review (1), Mehta concluded that low calcium flyash does not show a large enough pozzolanic activity in OPC to affect strength until about two weeks after hydration. In previous papers (2,3) we have related changes in the early hydration of OPC caused by low calcium flyash, as measured by conduction calorimetry and XRD, to features observed in the microstructure. In this paper we compare the development of microstructure and of strength for different OP cements with similar low calcium flyashes.

Experimental Materials

Details of the two OP cements and the flyashes are given in Table 1:

TABLE 1. CHEMICAL COMPOSITIONS (%) AND SPECIFIC SURFACE AREAS

Species	SiO_2	Al_2O_3	Fe_2O_3	CaO	MgO	Na_2O	K_2O	SO_3	Free lime	Area m^2/kg
Cements										
D44	20.3	5.2	3.1	64.7	1.1	0.19	0.34	2.8	0.7	290
H	19.84	5.45	1.92	65.09	-	0.13	0.70	2.45	1.81	385
Flyashes									LOI	
FF	44.6	25.0	11.8	3.39	1.67	0.38	3.47	0.62	3.16	370
WB	47.74	25.96	9.10	1.67	1.33	1.35	3.43	0.84	5.84	375

The phase composition of the cements, given in Table 2, reveals the lower alite and the higher C_3A content of H, although Table 1 shows that H has a higher specific surface area. Measurement of the particle size distribution for the two cements confirmed this difference in surface area.

TABLE 2. CEMENT PHASES (%) BY QXRD

	D44	H
C_3S (alite)	69.0	57.7
β-C_2S (belite)	22.0	16.3
α'-C_2S	-	3.3
C_3A	5.5	13.8
C_4AF	3.0	4.0
Anhydrite	-	0.6
Hemihydrate	2.0	0.8

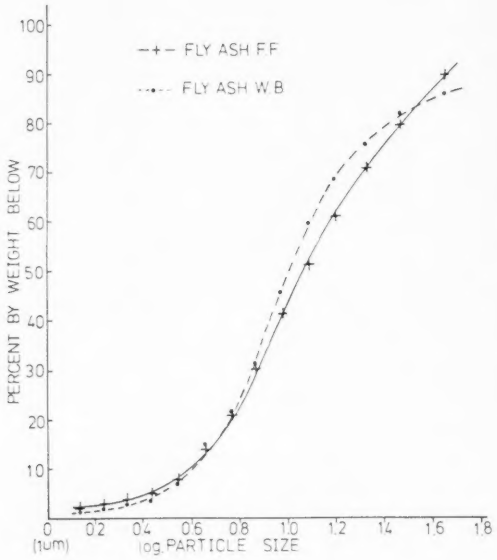

FIG.1. Particle size distributions of flyashes FF and WB

The low calcium flyashes came from Fiddlers Ferry (FF) and from West Burton (WB) power stations in the UK. The particle size distributions, measured with a Malvern Instruments particle sizer, are shown in Fig.1, confirming their similarity in specific surface area. On the Diamond classification (4), the lime content, loss on ignition, soluble alkali and SO_3 content are low while the silica glass contents at 80% (FF) and 81.2% (WB) are high. The crystalline contents are 8.8% mullite, 7.4% magnetite and 3.8% quartz for FF with 8.4%, 5.7% and 4.4% for WB.

Experimental Methods

The pastes for all experiments were mixed at w/s = 0.45-0.47. The flyash cements contained 30% by weight of p.f.a. The mixes were cast in cylindrical moulds or in flat prisms, sealed and cured at room temperature. The hydration of the D44 and FF mixes was stopped by freeze-drying while solvent replacement was used for the H and WB mixes.

The heat of hydration was measured using a conduction calorimeter at 20°C, with a paste made by shearing the mixture by hand for 2 mins. The microstructure was examined with a scanning electron microscope (SEM), and the calcium hydroxide content was measured by thermogravimetric analysis (TGA). The samples for the SEM were produced by fracturing a dried sample followed by coating with gold and for the TGA by grinding in an agate mill for 10 mins. The analyses were performed between 20°C and 800°C in a nitrogen atmosphere; the amount of $Ca(OH)_2$ was calculated from the water loss from the CH phase.

VOL
14
198

Strength was measured in compression on small cubes either 50.8 mm or 8 mm in size. Quantitative X-ray diffractometry, using the standards and software developed at C & CA, was used to characterise the materials and to follow the hydration reactions.

Experimental Results

Calorimetry

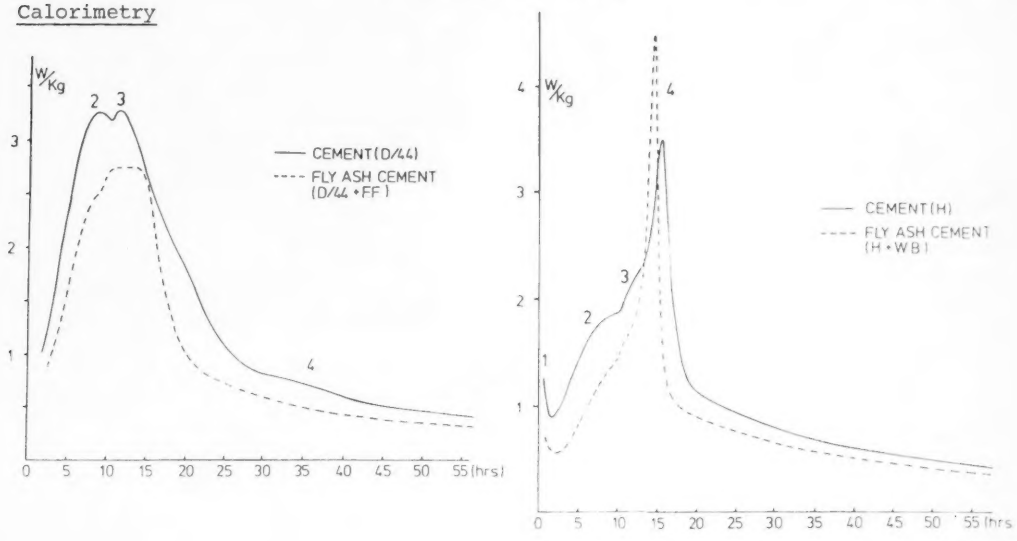

FIG.2. Rate of heat output for D44, D44/FF, H and H/WB pastes at 20°C.

The rate of heat output for the cements and the flyash blend cements is shown in Fig.2. 20 gm samples were used in all cases so that the figures for the neat cement should be decreased by 30% for comparison with the blends. For D44, the flyash increases the rate of heat output per gm of cement by about 10% for peak 2 and 20% for peak 3. Peak 2 is slightly retarded and peak 3 slightly advanced in time. Peak 4 is both increased and advanced from 35 hours to 15 hours into an extension of peak 3. Cement H appears to show air-set, with some 2.5% CH and 2.5% calcite before hydration. The rate of heat output due to alite in peak 2 is low compared to that of C_3A in peak 3. The addition of flyash advances and increases peak 3 considerably. Peak 4, associated with C_4AF, is barely detectable, perhaps due to the competition from the large amount of C_3A in this cement.

Thermogravimetry and microstructure

The formation and absorption of CH per gm of cement are shown in Fig.3. D44 is clearly much more reactive than cement H at all ages, but especially in the first few days. The addition of flyash leads to a maximum in the CH content after 7 days for D44 and after 14 days for H. In both cases there is a reduced amount of CH at very early ages, but this is quickly followed by an enhanced rate of formation of CH. This enhancement is accompanied by the precipitation and growth of C-S-H and CH on the surface of the flyash particles. Fig.4 shows this for D44/FF blends after 1 day.

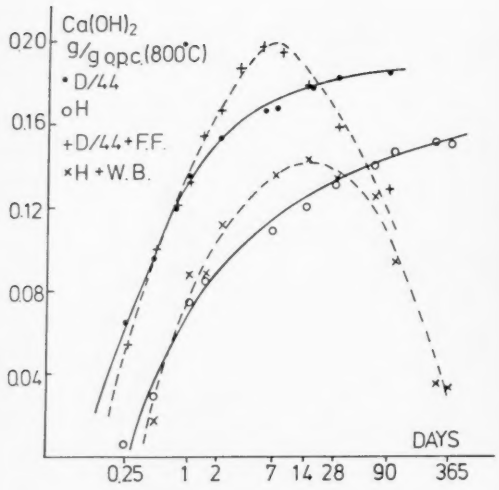

FIG.3. Calcium hydroxide content for the cements and flyash blends.

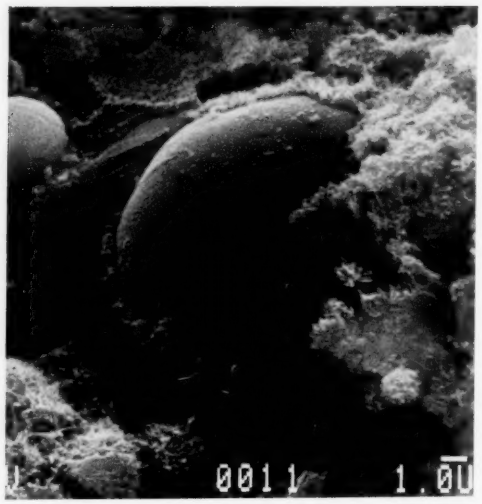

FIG.4. Growth of C-S-H and CH on surface of FF flyash particles after 1 day. SEM.

The pozzolanic reaction of the flyash with CH is shown in Fig.5, using the TG data as shown in Fig.3. For D44 with FF, the reaction appears to start within 2-3 days, whereas the less reactive cement H requires at least 7-10 days. The flyash particles in the D44/FF blend are heavily etched after 7 days, with a clear space between the particles and the shell of hydration products, Fig.6, left by the dissolution of the outer layers of glass. Many of the finer particles of flyash up to 1-2 μm in size are still visible at 7 days, but are consumed completely by 28 days in the D44/FF blends.

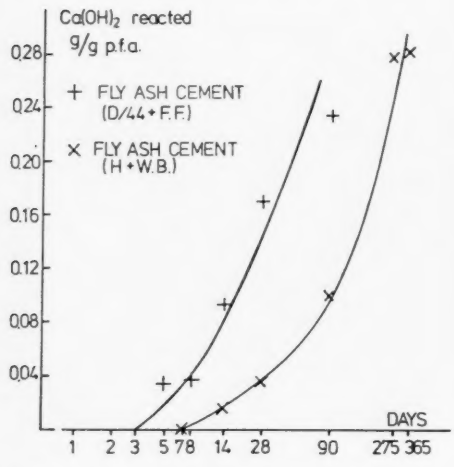

FIG.5. Pozzolanic reaction of fly-ashes with CH.

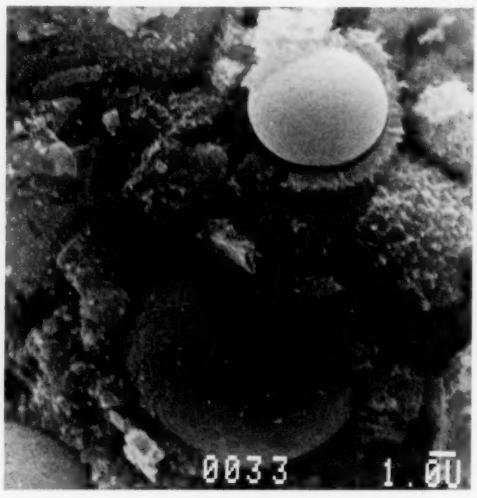

FIG.6. Dissolution of glassy layer on surface of FF flyash after 7 days. SEM.

The mean particle size from Fig.1 for the flyashes is 10-12 μm. A few of these particles were mainly quartz, carried through as incombustible material from the pulverised coal; others were mainly dendritic magnetite formed by the decomposition and oxidation of pyrites. The commonest resulted from the fusion and decomposition of kaolin leading to the formation of mullite and quartz. Fig.7 shows the appearance of acicular crystals of mullite and smaller crystals of quartz from within the glass as the pozzolanic reaction progresses from 15 days to 275 days. These particles are 10-15 μm in diameter with the mullite and quartz crystals in the glassy shell outside an inner core of much finer unreactive crystalline material. By 275 days the crystals in the dissolved shell have become absorbed in the surrounding layers of C-S-H.

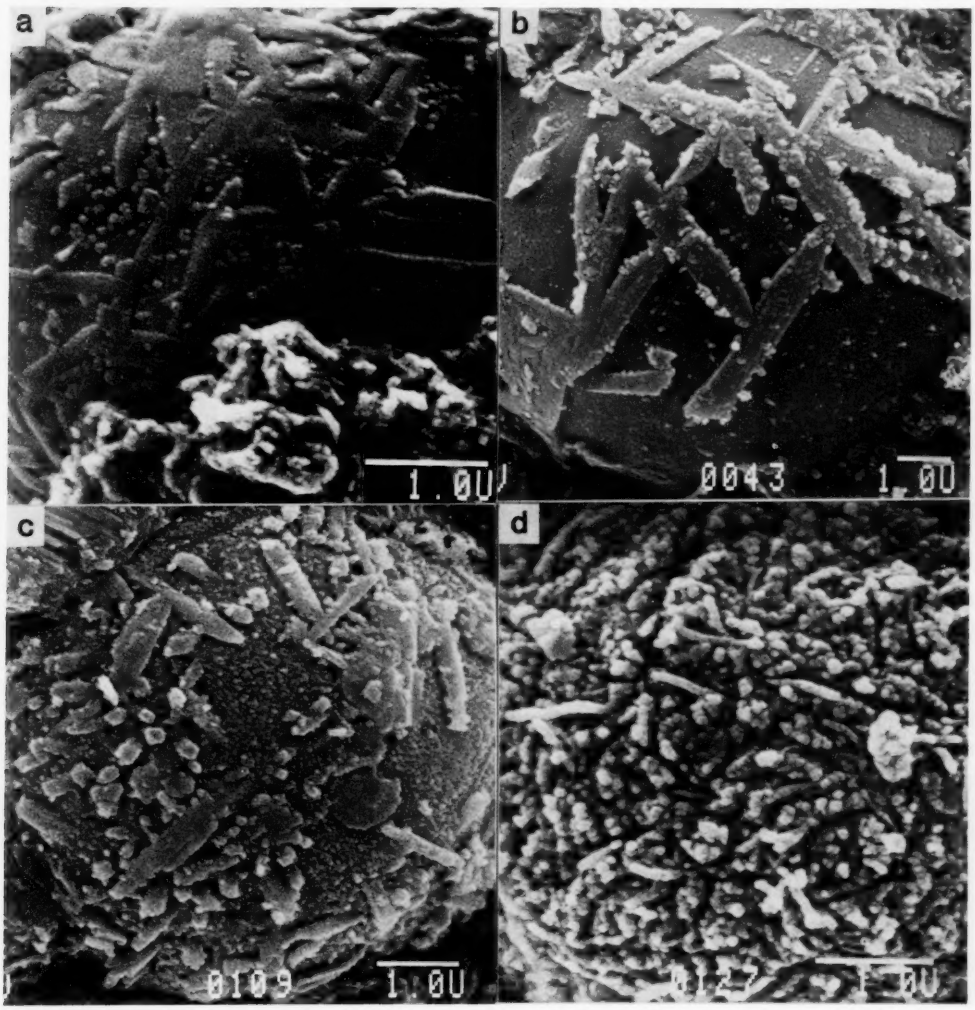

FIG.7. Mullite and quartz revealed by dissolution of the glassy phase of FF flyashes after (a) 15, (b) 28, (c) 90 and (d) 275 days. SEM.

Fig.8 shows the second common type of flyash particle of limited reactivity which contains short radial crystals with a hexagonal shape embedded in a very fine matrix beneath the glassy layer. As in Fig.8(c) there may be some long mullite crystals in the glassy layer of these particles. After 275 days the local matrix containing the hexagonal crystals has dissolved and the crystals appear to have been absorbed into the surrounding C-S-H.

Development of mechanical properties

The development of early strength in neat cement pastes of D44 is much faster than in those of H, Fig.9, although the 28 day strengths are equal. With the addition of 30% flyash, the D44/FF blends exceed the strength of neat

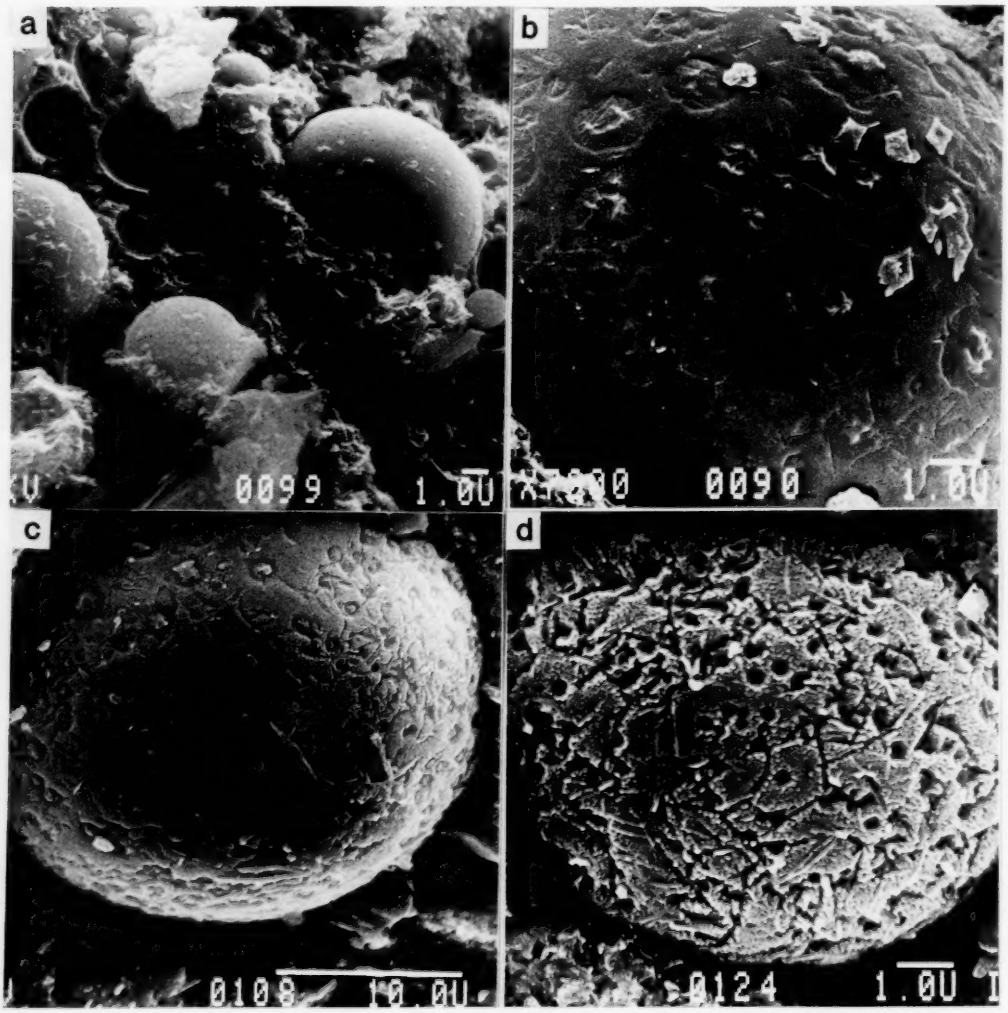

FIG.8. Radial hexagonal crystals revealed by dissolution of the glassy phase of FF flyashes after (a) 15, (b) 28, (c) 90 and (d) 275 days. SEM.

cement by 90 days whereas the H/WB blends required 365 days. In Fig.10 the contribution of the flyash to the strength of the blend starts after 2-3 days for the former but only after 7-14 days for the latter. This later development of strength for the H/WB blend parallels the later onset of the pozzolanic reaction noted in Fig.5 for these blends.

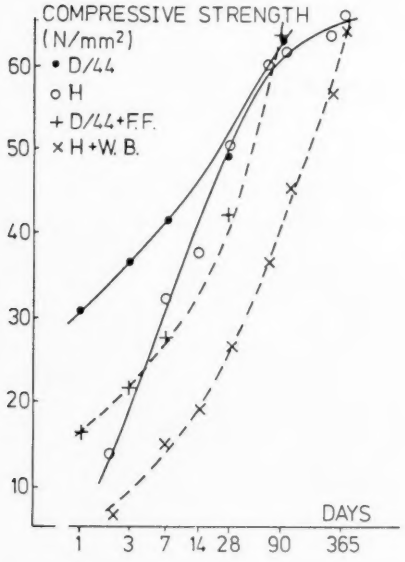

FIG.9. Development of strength in cements and flyash blends.

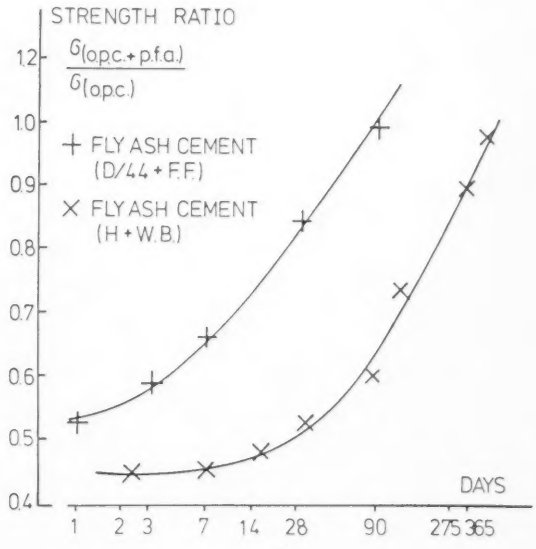

FIG.10. Contribution of flyash to the strength of D44/FF and H/WB blends.

Discussion

Hydration of the cement phases

The hydration of D44 resembles that of the Northfleet cement studied previously (2,3). The early hydration of alite, slightly retarded by the presence of aluminate ions from the flyash, is enhanced once the concentration of Ca^{2+} is high enough to nucleate CH and C-S-H on the surface of the flyash particles. The increased rate of hydration of C_3A and C_4AF in peak 3 suggests that the amount of CH in solution is reduced as early as 10-15 hours.

The calorimeter output for cement H suggests that surface hydration of the alite has taken place during storage and this is confirmed by the amounts of CH and calcite detected before hydration. No microscopy has been carried out on this cement at present, but the assignment of the peaks in Fig.2 is believed to be correct. The prominent peak 3 behaves in the way expected for C_3A while peak 4 is largely suppressed.

The pozzolanic reaction and the development of strength

The two flyashes used in these experiments were chosen for their similarity of chemical composition and particle size distribution, but their behaviour with the two cements is very different. In agreement with Mehta (1), H/WB blends contribute to the strength after 7-14 days, whereas D44/FF blends

start to contribute after only 2-3 days, more like blends containing high lime flyashes or condensed silica fume (3). This early development of reactivity and of strength appears at the moment to be unique to D44 cement with Fiddlers Ferry flyash. Previous workers using the same ash and a different Portland cement at 20°C (5) found no sign of reaction of the spheres even after 13 weeks, although at 40°C reaction was well-defined after 6 weeks. Comparing our cements D44 and H, the increased alite content of D44 must help to account for its increased reactivity, but it has a smaller specific surface area of 290 m^2/kg as against 385 m^2/kg for H.

In our previous work comparing Ironbridge and Drax flyashes using the same cement (3), we concluded that the greater reactivity of Ironbridge ash was due to its larger specific surface area (375 m^2/kg) and smaller particle size. Both Fiddlers Ferry and West Burton ashes have similar specific surface areas to Ironbridge, with higher glass contents, so that they too would be expected to have a high pozzolanic reactivity. The present results emphasise the importance of choosing a cement with a high rate of formation of CH in the first few days so as to exploit the reactivity of such a flyash. In keeping with the experiments of Sellevold et al (6) on silica fume blends, a finely ground white cement with 80% C_3S might give an even earlier contribution to strength than D44 with Fiddlers Ferry flyash. Their Danish white cement produced 0.3 gm of CH per gm of cement after 14 days compared with 0.18 gm for D44 and 0.12 gm for H.

References

1. P. Kumar Mehta, Proc. CANMET/ACI 1st Int. Conf. on The Use of Flyash, Silica Fume, Slag and Other Mineral By-Products in Concrete, Montebello, vol.1, 1 (1983).
2. A. Ghose and P. L. Pratt, MRS, Proc. N, Effects of Flyash Incorporation in Cement and Concrete, Boston, 82 (1981).
3. Y. Halse and P. L. Pratt, presented at 1st Int. Conf. on the Use of Flyash, Silica Fume, Slag and Other Mineral By-Products in Concrete, Montebello, (1983).
4. S. Diamond, 1st Int. Symp. on The Use of PFA in Concrete, Leeds (1982) vol.2.
5. D. G. Montgomery, D. C. Hughes and R. I. T. Williams, Cement & Concr. Res., 11, 4, 591 (1981).
6. E. J. Sellevold, D. H. Bager, E. Klitgaard Jensen and T. Knudsen, Nordic Research Seminar, Report BML 82.610, Condensed Silica Fume in Concrete, Trondheim, 19 (1982).

Acknowledgements

All of the materials used at Imperial College were provided by the Cement & Concrete Association. We are grateful to the Department of Mineral Resources Engineering for use of the particle sizer and TG apparatus and to SERC for a research studentship to support Y.H.

VOL
14
198

CEMENT and CONCRETE RESEARCH. Vol. 14, pp. 499-504, 1984. Printed in the USA.
0008-8846/84 $3.00+00. Copyright (c) 1984 Pergamon Press, Ltd.

AN EXAMINATION OF THE ASTM LIME POZZOLANIC ACTIVITY TEST FOR CLASS C FLY ASHES

S. Schlorholtz, T. Demirel and J. M. Pitt
Department of Civil Engineering
Iowa State University, Ames, Iowa 50011 USA

(Refereed)
(Received Nov. 17, 1983)

ABSTRACT

The role of the type of calcium hydroxide ("lime") used in the ASTM C 311-81 Lime Pozzolanic Activity Test (LPAT) has been studied. Three types of lime (reagent grade $Ca(OH)_2$, a commercial lime and a mixture of the reagent grade lime and MgO) were used with four fly ashes (three Class C and one Class F) in the LPAT. The same four fly ashes were used in the ASTM Cement Pozzolanic Activity Test. The formation of crystalline reaction products in the lime test was monitored by x-ray powder diffraction. All three Class C fly ashes failed to meet the LPAT seven-day 800 psi compressive strength criterion when the reagent grade lime was used but all three passed the test when the other two types of lime were used. X-ray diffractograms of pastes cured for three days at 55°C showed different reaction products formed from the pastes containing reagent grade lime compared to the other two lime sources. It is proposed that impurities in the commercial lime play a key role in determining the pozzolanic activity of Class C fly ashes.

VOL.
14
984

Introduction

Class C fly ashes often fail to meet the ASTM C 311-81 Section 34 Lime Pozzolanic Activity Test (LPAT) (1). When the same fly ashes are tested with the ASTM C 618 Cement Pozzolanic Test, they usually pass easily. It has been suggested that the LPAT is not appropriate for testing Class C fly ash for use in structural concrete (2). It has been found in our laboratory that a given Class C fly ash may pass the LPAT when commercial sources of lime are used but the same ash will fail when the ASTM-specified reagent grade calcium hydroxide ("lime") is used. Suspecting that the explanation for this behavior may be in the nature of impurities usually found in commercial limes we designed experiments that would incorporate three types of lime with and without impurities common in commercial limes and four Iowa fly ashes (three Class C and one Class F) in the ASTM LPAT. The formation of crystalline reaction products was monitored with x-ray diffraction (XRD).

Experimental

Reagent grade calcium hydroxide (lime) obtained from Fisher Scientific Company was used as "pure lime". A Type N commercial lime with a brand name

of Snowflake was used for the second type of lime. Since one of the many impurities commonly found in commercial limes is MgO a third lime (or "pseudo-lime") was prepared by mixing 95% (by weight) of reagent grade lime with 5% of reagent grade magnesium oxide. X-ray diffraction analysis (XRD) showed that the reagent grade lime was pure and showed no carbonation. XRD analysis on the commercial lime indicated that the major impurity was calcium carbonate. Other minor contaminants were not clearly identifiable but several small broad peaks observed in the diffractogram suggested the presence of some dicalcium silicate. XRD analysis of the pure lime-MgO mixture also showed that the major impurity was calcium carbonate which probably formed during the mixing procedure. Wet chemical analyses of the reagent grade and commercial limes are presented in Table 1. Due to the amount of silica measured in the commercial lime one could predict that this lime may contain small amounts of calcium silicates as impurities.

Four common Iowa fly ashes were used in this study. Three were classified as ASTM Class C (Neal 4, Council Bluffs and Ottumwa) while one (Neal 2) was a Class F. Chemical analyses, obtained by x-ray fluorescence spectrometry, are given in Table 2. Physical properties obtained using ASTM C 618 procedures are also given in Table 2. Compressive strength cylinders were prepared, cured and tested in accordance with ASTM procedures.

X-ray diffraction was used to follow the hydration of lime-fly ash pastes. The various constituents of the pastes were proportioned, sealed in plastic vials and then cured as described for the lime pozzolan test (1). A small amount of SiC (about 9% by total dry weight) was added to the diffraction samples to serve as an internal standard. The instrument used was a Siemens D 500 diffractometer equipped with a diffracted beam monochromator utilizing Cu Kα radiation. The generator was operated at 50 kV and 25 mA.

VOL
14
198

Results and Discussion

Table 2 gives the results of chemical analyses and physical tests performed on the four fly ashes. All of the fly ashes meet the ASTM requirement for the Cement Pozzolanic Activity Test (minimum strength of 90% of the control). Figure 1 shows the results of the LPAT on each of these fly ashes. A line is drawn at 800 psi, the compressive strength value that must be attained in order for the fly ash to pass this test. The Neal 2 Class F fly ash passed the test no matter which type of lime was used. When the reagent grade lime was used, as is required by ASTM C 311, all three Class C fly ashes failed the test. However, when either the commerical lime or the pseudo-lime (lime-MgO) mixture was used, the Class C ashes passed the test. This is evidence for a critical role of impurities in the lime-pozzolanic reactions of Class C fly ashes.

Figure 2 shows the XRD traces of the four fly ashes. The major peaks of crystalline phases are marked. The position of the broad maximum in the background is quite different for the two classes of fly ashes, as noted previously by Diamond (3). Figures 3 and 4 show XRD traces for fly ash-lime pastes after three days of curing at 55°C. Several general observations can be made from these figures. First, the crystalline hydration products for pastes containing Neal 4 or Neal 2 fly ash and reagent grade lime (see Figures 3a and 4a) are similar to each other. The major reaction product, denoted as RP in Figures 3 and 4, appears to be $Ca_3AlFe(SiO_4)(OH)_8$ (see JCPDS file No. 32-147). The major difference between Figures 3a and 4a is in the reaction products with d-spacings of 7 to 10 Å. The peaks in this range are much more intense for pastes containing Neal 2 (Class F) fly ash than they are for pastes containing Neal 4 (Class C) fly ash. This may reflect the quality of the binding properties of the mixtures, with Neal 2 being superior to Neal 4 or any of the Class C fly ashes. The remaining diffraction traces (Figures 3b,c and 4b,c) are very

Table 1.

Chemical analyses of limes.

	Reagent grade	Commercial
SiO_2	0.59	3.08
MgO	0.35	0.23
CaO	70.2	66.5

Table 2.

Chemical and physical analyses of fly ashes.

	Fly Ash			
	Neal 4	Neal 2	Council Bluffs	Ottumwa
SiO_2[a]	34.10	51.70	30.64	33.06
Al_2O_3	16.05	19.96	17.27	20.08
Fe_2O_3	6.30	6.43	4.93	5.41
CaO	26.49	16.57	27.80	24.72
MgO	6.32	3.91	6.47	4.94
SO_3	2.95	1.51	2.65	1.47
K_2O	0.24	1.63	0.31	0.37
Na_2O	1.96	0.32	1.70	1.78
Available alkali	1.39	0.27	1.18	1.15
% loss on ignition	0.2	0.3	0.2	0.2
Fineness	9.9	19.0	18.0	11.7
Specific gravity	2.69	2.35	2.69	2.62
Cement pozzolanic activity (% control)	100	101	94	108
% Autoclave expansion	0.09	0.12	0.12	0.06

[a]Elemental composition was determined by X-ray fluorescence and then expressed in terms of oxides. The method used for analysis is described in reference 4.

similar to one another and they do not contain the major hydration product that was observed in Figures 3a and 4a. Yet, the strengths observed in the lime pozzolan test with commercial lime and the psuedo-lime were superior compared to the mixes made with reagent grade lime. So again the reaction products in the 7 to 10 Å range appear to be dominating the cementing properties of the mixtures. Comparing Figures 3a, 3b and 3c makes it obvious that the impure limes (commercial lime and psuedo-lime) drastically accelerate the formation of hydration products with d-spacings in the range of 7 to 10 Å in pastes made with Neal 4 fly ash. Diffraction traces of the pastes prepared with the other two Class C ashes used in this experiment exhibited similar behavior with differences only in relative intensities. On the contrary, Figure 4 shows that the various types of lime have little influence on the formation of reaction products in the 7 to 10 Å range in pastes containing Neal 2 fly ash.

It is clear from both the LPAT and the XRD results that impurities in lime play an important role in the lime-pozzolanic reactions of Class C fly

VOL. 14 1984

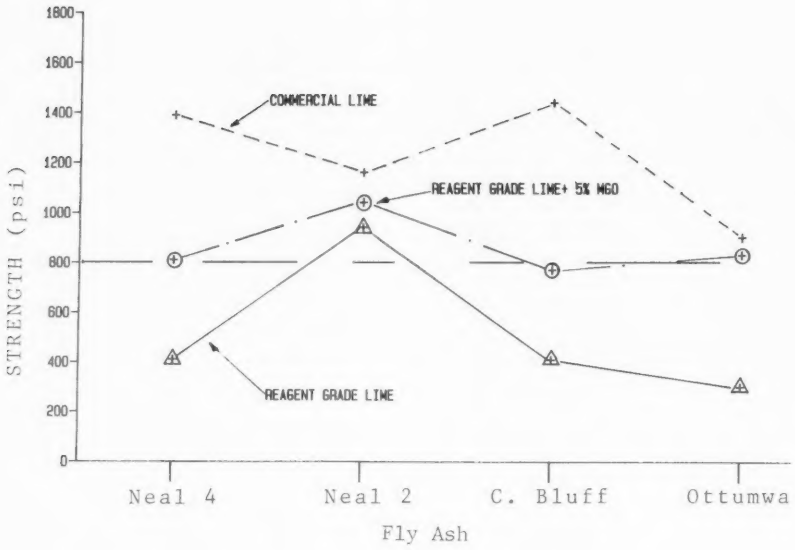

Fig. 1. Results of the LPAT with the three types of lime and the four fly ashes.

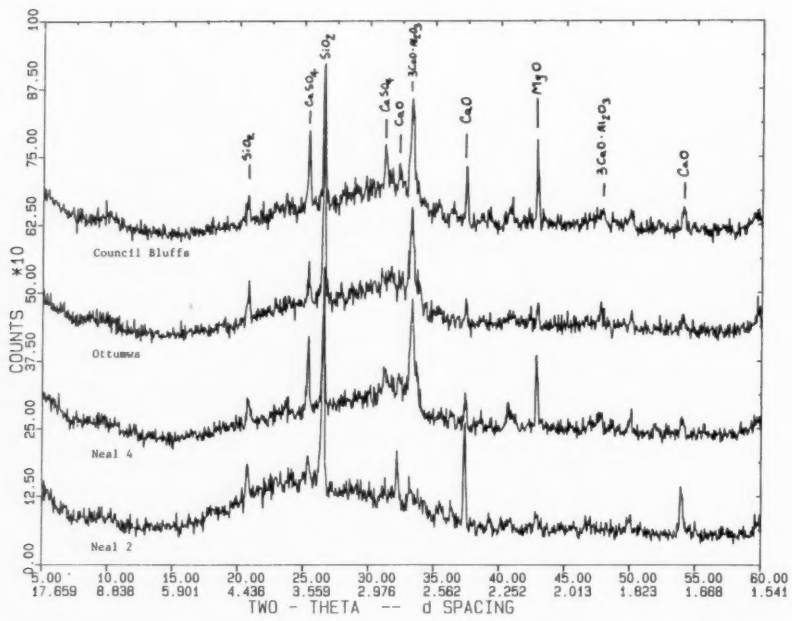

Fig. 2. XRD traces for the four fly ashes.

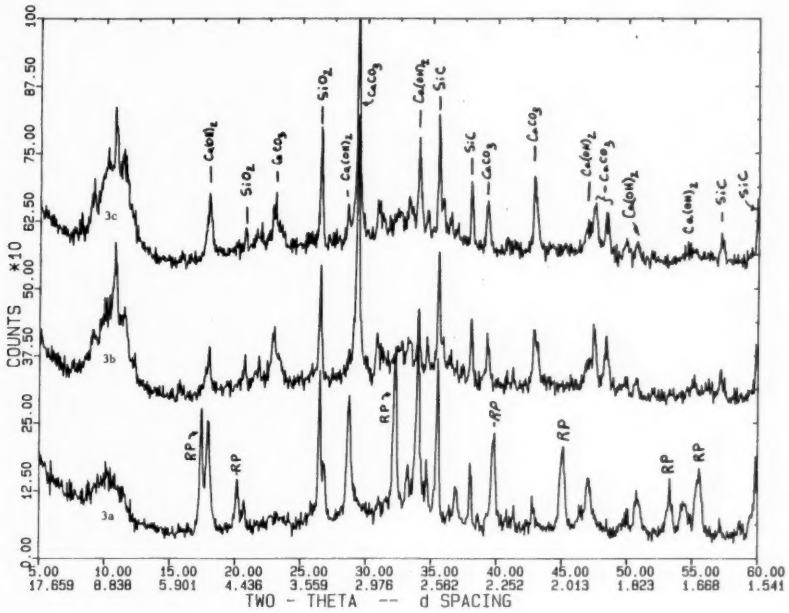

Fig. 3. Neal 4 (Class C) - lime pastes after three days curing at 55°C: (a) reagent grade lime; (b) commercial lime; (c) reagent lime + 5% MgO.

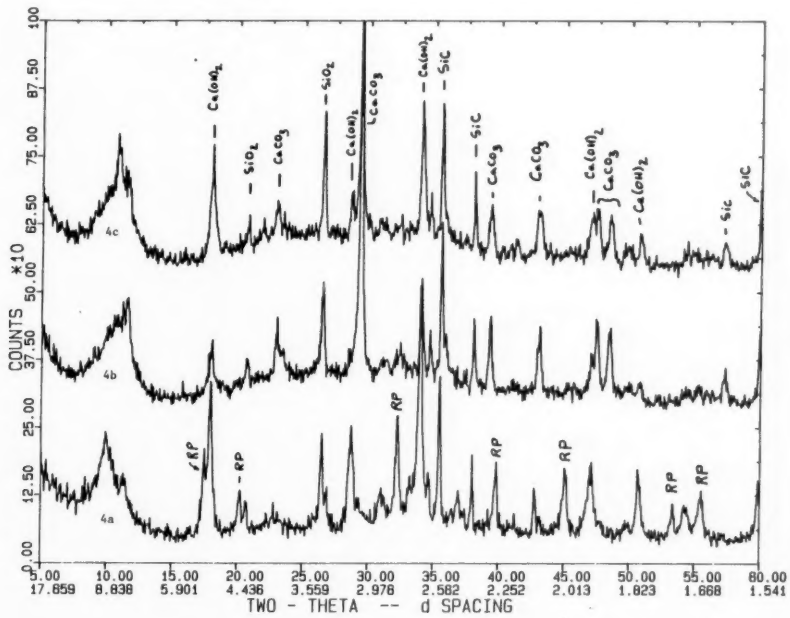

Fig. 4. Neal 2 (Class F) - lime pastes after three days curing at 55°C: (a) reagent grade lime; (b) commercial lime; (c) reagent lime + 5% MgO.

ash. In the case of the commercial lime, the active impurities may have been present in the form of poorly crystallized cementitions calcium silicates. A silica content of 3.08 wt% is equivalent to 8.8 wt% C_2S or 11.7 wt% C_3S if the silica is present in the commercial lime as these silicates.

The original premise in our experiments was that the active impurity was Mg and thus the experiments with the pseudo-lime were performed. Later, when the chemical analyses were done, it was found that the reagent grade and commercial limes had about the same level of Mg impurity. It is interesting that the pseudo-lime with its much greater level of Mg impurity did result in strength increases when used in the LPAT with Class C fly ashes. We suggest that the reaction of the Mg in solution with the glass component of the fly ashes may account for the difference in behavior of Class C and F fly ashes. As noted above, the structure of the glass in a high-calcium fly ash is obviously different from that of low-calcium ash as evidenced by the very different broad maximum in the x-ray traces (see Figure 2). The noncrystalline phases in fly ash, chiefly the glass, are responsible for this broad maximum. The glass in a high-calcium Class C ash may be calcium saturated and thus may be less affected by the Ca in solution than is the low-calcium glass of Class F fly ash. The Mg thus would be the active component of the solutions in promoting the pozzolanic reactions. On the other hand, crystalline calcium silicate impurities that may be present in the commercial lime could promote further crystallization of calcium silicate hydrates by seeding. Further studies needed to clarify and prove this hypothesis are in progress. Also, the role of calcium carbonate in the lime-fly ash system needs to be investigated.

Conclusions

Experiments have been performed that indicate that impurities in commercial lime may be an important factor in the Lime Pozzolanic Activity Test. Three different Class C fly ashes pass the LPAT when lime containing impurities is used but not when pure lime is used. It is suggested here that the impurities in the pore solutions promote the pozzolanic reactions with the Class C ashes where the glasses have high-calcium contents. Also, it is apparent that the lime pozzolan test (described in ASTM C 311-81) is biased against Class C fly ashes when reagent grade calcium hydroxide is used.

Acknowledgements

This research was supported by the Engineering Research Institute Materials Analysis and Research Laboratory at Iowa State University. We thank Prof. G. J. McCarthy of North Dakota State University for helpful suggestions and assistance in editing this manuscript.

References

1.) ASTM. 1981 Annual Book of Standards. Part 13, Philadelphia: ASTM, 1981.
2.) W. B. Butler. Cement, Concrete and Aggregates, 4[2], Winter 1982, pp. 68-72.
3.) S. Diamond. Cement and Concrete Research, 13[4], 1983, pp. 459-464.
4.) S. Schlorholtz and M. Boybay, "Quantitative X-ray Fluorescence for Fly Ashes," submitted for publication at 32nd Annual X-ray Conference, August 1-5, 1983.

VOL
14
198

CEMENT and CONCRETE RESEARCH. Vol. 14, pp. 505-512, 1984. Printed in the USA.
0008-8846/84 $3.00+00. Copyright (c) 1984 Pergamon Press, Ltd.

HYDRATION OF FLY ASH-PORTLAND CEMENTS

He Jun-yuan,* Barry E. Scheetz and Della M. Roy
Materials Research Laboratory, The Pennsylvania State University
University Park, PA 16802

(Communicated by G.M. Idorn)
(Received Nov. 17, 1983)

ABSTRACT

Hydration products of fly ash-portland cements were studied with x-ray diffraction (XRD), differential thermal analysis (DTA) and scanning electron microscopy (SEM) as part of a continuing research effort to understand the pozzolanic activity of fly ashes. It was found that the amount of calcium hydroxide crystals in the cement pastes is diminished due to the addition of fly ash to the cement. Ettringite was produced in the early age, and the consumption of sulfate by the formation of ettringite was accelerated by the addition of fly ash. A partial conversion of ettringite to monosulfate within the first 7 days of hydration was observed in the fly ash-portland cement pastes, but the formation of ettringite continued to form up to at least 28 days of hydration in the pastes without fly ash. Examination of the fly ash bearing pastes showed, in all cases, varying amounts of calcium hydroxide and unreacted portland cement, with minor quartz and gehlenite hydrate. It appears that hydration reactions actually occur in the fly ash cement pastes more or less on a particle-by-particle basis.

VOL.
14
984

Introduction

The utilization of fly ashes in cementitious bodies as a replacement for cement, an extender or as a reactive aggregate has been practiced in the United States for 46 years (1) and has received wide acceptance by the U.S. Corps of Engineers for the past twenty-five years (2). Many recent studies in the area of hydration of fly ash-portland cement have been reported (3-8). Reactivity of fly ashes has been investigated, and calcium and alkali hydroxides, and temperature are known to be the main activators of glassy phase hydration reactions as in fy ash (8). However, the hydration process and its mechanisms have not been comprehended to the degree necessary to support more extensive fly ash utilization; which suggested the need for further studies. In the first part of this two-part study (9), the pozzolanic activity index of several fly ashes, the rate of hydration heat evolution and the rate of development of hydration products for fly ash-cement pastes were determined, and the reactivity compared with that of a natural pozzolan, tuff. In this initial study, the pozzolanic activity index of the high-lime fly ash used in this present investigation was found to be larger (92.87 vs. 81.07) than the low-lime fly ash. The presence of fly ash in the pastes retarded the hydra-

*Permanent address: South China Institute of Technology, Guangzhou, China.

Table 1. Chemical Analyses of Starting Materials (percent by weight).

Compounds	Portland Cement P	Fly ash H (B 15)
SiO_2	21.00	36.80
Al_2O_3	4.02	18.10
Fe_2O_3	3.33	6.21
CaO	63.12	27.83
MgO	3.86	4.74
SO_3	2.52	1.90
Na_2O	0.23	1.22
K_2O	0.44	0.41
TiO_2	0.35	1.55
P_2O_5	0.10	0.94
MnO	0.03	0.04
SrO	0.08	0.30
BaO	0.02	0.60
L.O.I.	1.06	0.55
Totals	100.16	101.19

tion, as determined by the centroid of the second exotherm, by up to 10 hours when contrasted to the control pastes. Further, the strengths of these pastes containing fly ash were somewhat lower than the control but developed with time in a subparallel manner to the control pastes. The compressive strengths continued to increase until at 90 days of curing they were equal to or greater than the control paste without fly ash. The reasons for these differences in behavior were still not fully clear; therefore, in order to acquire a better understanding of the hydration process and its mechanism for fly ash-bearing cement, hydration products and microstructures were studied using XRD, DTA and SEM techniques.

VOL. 14 1984

Materials and Methods

The starting materials for this study included a Type I/II portland cement supplied by the Atlantic Cement Co. and two types of fly ash. The results reported here are for one Class C fly ash, supplied by DePaw Construction Co. Characterization of the starting materials was described in detail previously (3,9). The high calcium fly ash contained several crystalline phases, and a glassy phase with its broad band diffraction peaking at a smaller d-spacing than in the high-silica fly ashes (3). The chemical analyses and the physical properties for the starting materials are provided in Table 1 and Table 2 respectively.

Table 2. Physical Properties of Starting Materials.

Properties	Portland Cement P	Fly ash H
Density (g/cm^3)	3.15	2.61
Fineness		
% Residue on No. 200 (75 μm) Sieve	3.32	7.94
Specific Surface Area, Blaine (m^2/Kg)	340	354

All samples used in this study were prepared as pastes. In the test mix, 35% of the absolute volume of the cement used in the control mix was replaced

by an equal volume of fly ash. Deionized water was used to mix all samples and to prepare the saturated limewater solution which was used to immerse the specimens during curing. All samples were cured for the requisite time at 20±1°C. The water to solid (w/s) ratio was 0.43 and 0.40 for the blended cement and pure portland cement, respectively. At appropriate times, the hydration process was stopped by washing the fractured samples with acetone and vacuum drying for 24 hours or drying in an oven at about 65°C for 6 hours. The formulations of the samples are given in Table 3.

Table 3. Formulation of the Pastes With and Without Fly ash.

Number of Sample	Portland Cement P (grams)	Fly ash H (grams)	Deionized Water	w/s
P	300	--	120	0.40
FH	162	73	100	0.43

Phase compositions of hydration products were determined by DTA and XRD methods. DTA studies were carried out using a Harrop Laboratory DTA unit which utilizes α-Al_2O_3 as a control material; the rate of temperature increase was 10°C/min. XRD studies were carried out on a GE X-ray diffractometer that utilized a CuK_α radiation source with a graphite monochromator in the diffracted beam. All scan rates were equivalent to 2° 2θ/min. The microstructures and morphologies of the hydration products were investigated with an ISI DS-130 or an ISI Super IIIA scanning electron microscope. Samples used were sputter coated with approximately 250 to 300Å of gold prior to observation in the SEM.

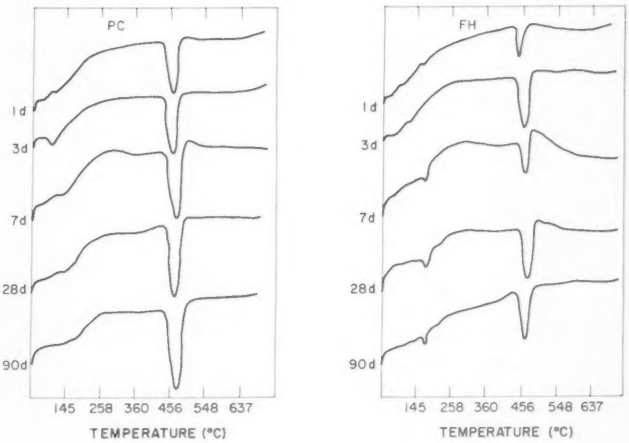

Fig. 1. DTA Curves of the Pastes. (PC = portland cement; FH = fly ash)

Experimental Results and Discussion

DTA

Figure 1(a,b) shows the DTA curves of the cement pastes after different hydration times. The content of calcium hydroxide (475° peak) in the pastes with fly ash was found to be lower than that in the pastes without additive. This result is as expected since it coincided with the data estimated by thermogravimetric analysis in the previous study (9). It was found that in

the early stages of hydration (1, 3 and 7 days), the conversion of the calcium trisulfoaluminate hydrate) ettringite to the monosulfate took place in the fly ash-bearing pastes, but its conversion in the portland cement pastes was delayed to 28 days.

Abdul-maula and Odler (4) reported that conversion of ettringite to monosulfate was observed only in cement with low SO_3 content in the fly ash. It is believed that the formation of monosulfate in the pastes containing fly ash used in this study was attributed to the low SO_3 content of the fly ash and due to the dilution effect of the addition of flyash to the cement so as to decrease the SO_4^{2-} concentration in the pore fluid.

XRD

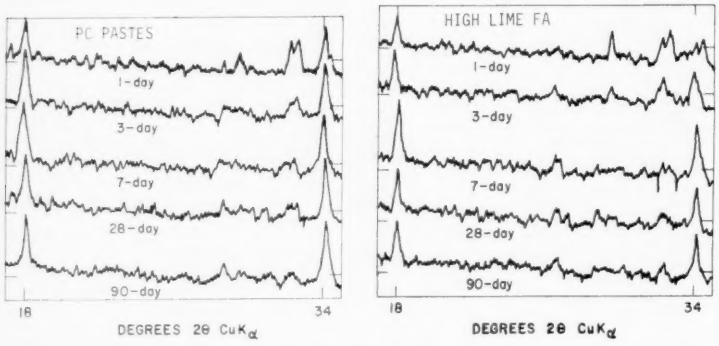

Fig. 2. Portions of the X-ray Diffraction Patterns for Cement Pastes.

Figure 2(a,b) shows the portions of the x-ray diffraction patterns for cement pastes with and without fly ash. In analyzing the patterns, it was shown that calcium hydroxide, C-S-H, and unreacted clinker phases were often present throughout the hydration history of all the cement pastes studied. Ettringite was detected, converting to monosulfate at early hydration stages in the fly ash-bearing pastes and at later stages in the control pastes without fly ash. Small amounts of quartz and gehlenite hydrate (also seen in the DTA) were also found in the pastes with fly ash, which are attributed to the starting minerals present in the fly ash, or their hydration products.

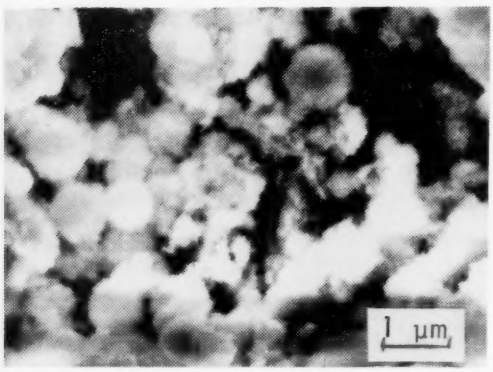

Fig. 3. SEM of Fly Ash Cement Paste Hydrated for 1 Day.

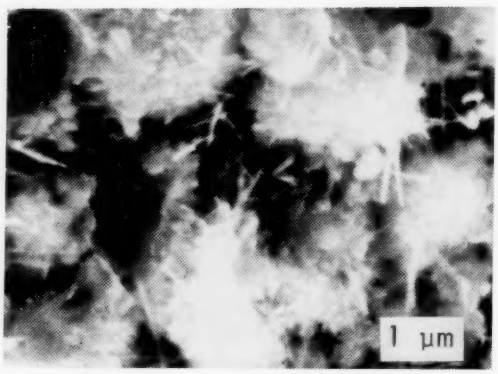

Fig. 4. SEM of Fly Ash Cement Paste Hydrated for 3 Days.

SEM

In this study, the microstructures of the hardened cement pastes and those containing high lime fly ash were monitored from 1 day to 90 days. In 1-day-old specimens of fly ash cement paste (Figure 3), some of the fly ash spheres were found to be coated by the hydration products which were due to surface hydration or precipitation from the drying of pore solution. Agglomeration of the fly ash particles was also observed. Between 3 and 7 days, ettringite needles and other reaction products had developed (Figures 4 and 5). By 28 days, the structure had become denser and stronger (Figure 6) in agreement with observations reported by Ogawa (10). Ettringite needles were no longer seen, probably being converted to monosulfate resulting in the densification of the microstructure. In general, the fly ash spheres were encapsulated by the hydration products, but some of them were separated from the matrix, remaining relatively unaltered (Figures 6 and 7). The appearance

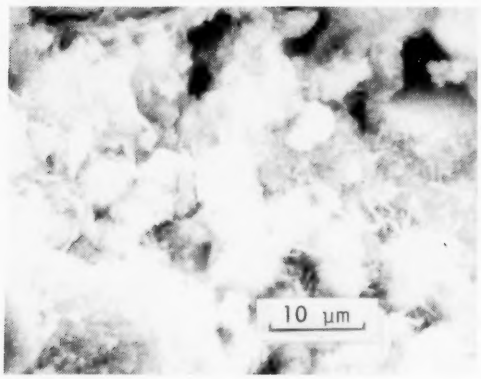

Fig. 5. SEM of Fly Ash Cement Paste Hydrated for 7 Days.

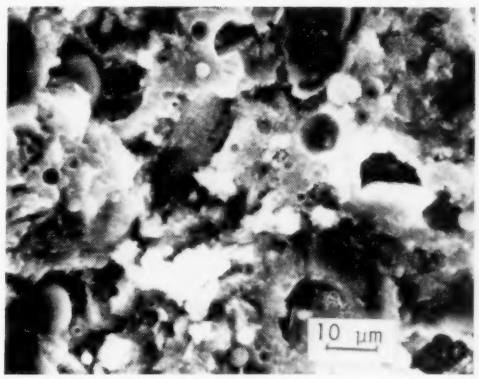

Fig. 6. SEM of Fly Ash Cement Paste Hydrated for 28 Days.

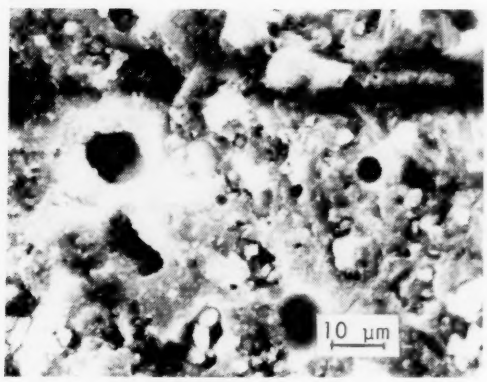

Fig. 7. SEM of Fly Ash Cement Paste Hydrated for 90 Days.

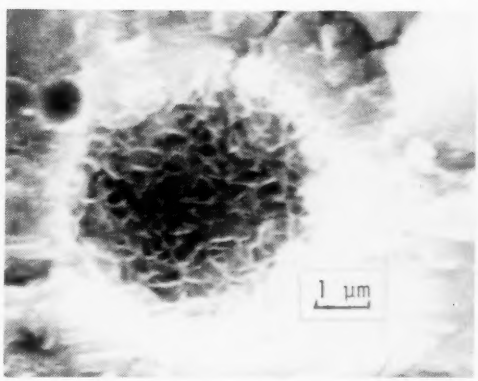

Fig. 8. SEM of Fly Ash Cement Paste Hydrated for 90 Days, Shows a Hydrated Fly Ash Sphere.

of these seemingly unaltered spheres may be related to the fracture process during preparation of the sample where failure occurred through a zone of weakness between the hydration product and the unaltered cenosphere rim. Figure 8 shows a fly ash sphere that has been completely hydrated in the 90-day-old specimen. This observation indicates that the pozzolanic reaction in the fly ash sphere had taken place. Nevertheless, many fly ash spheres had not been entirely hydrated even by 90 days of curing because the pozzolanic reaction is a slow process, and also because some of the crystalline components are unreactive.

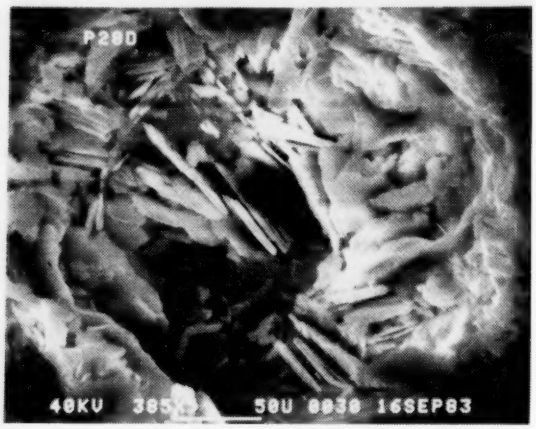

Fig. 9. SEM of Portland Cement Paste Hydrated for 28 Days, Shows a Void Filled Calcium Hydroxide.

Comparing the microstructure of pastes with and without fly ash, it is found that although the primary hydration products exhibit no significant differences, there is more crystalline calcium hydroxide generally formed in voids, for the cement pastes. Figure 9 shows just such a void formed from a cenosphere that was subsequently filled with calcium hydroxide crystals. It is attributed to the high concentration of $Ca(OH)_2$ in the solution of the paste during hydration. So, causticity of the hydration products in the portland cement paste would be higher than that in the fly ash-cement paste. Table 4 presents some results of topochemical analyses attained by an energy dispersive x-ray analyzer for 28-day-old pastes with and without fly ash. It is shown that the ratio of CaO to (SiO_2 + Al_2O_3 + Fe_2O_3) for the matrix nearby a void in the portland cement paste is 4.42 contrasted to the ratio obtained from the cement matrix adjacent to a fly ash

Table 4. Topochemical Analyses of Hydration Products in 28-Day Old Pastes With and Without Fly ash.

Position of Analysis Point		Nearby A Void	On Surface of a Fly ash Sphere	Nearby a Fly ash Sphere
Sample #/Wt.%		P28d	FH28d	FH28d
Chemical Analyses (% by Weight)	CaO	76.78	13.57	65.87
	SiO_2	14.83	26.13	13.97
	Al_2O_3	2.54	50.50	5.53
	Fe_2O_3	5.95	9.80	11.53
Molecular Ratio $CaO/(SiO_2 + Al_2O_3 Fe_2O_3)$		4.42	0.34	3.20

sphere, in the fly ash-portland cement paste, which was determined to be only 3.20. These results are not quantitative, but indicative of trends.

Sometimes ettringite needles are seen in the 28-day-old specimen of portland cement paste, suggesting that the conversion of ettringite to monosulfate in the pure cement paste occurs later than in the fly ash cement paste.

Conclusions

The experimental results reported above have shown that the content of crystalline calcium hydroxide in the fly ash-portland cement pastes is decreased as a result of the addition of fly ash, most likely resulting from the additional reaction of the calcium with alumina and silica from the fly ash to form additional C-S-H. Additional findings support the conversion of ettringite to the monosulfate at an earlier curing age in the fly ash-blended pastes than in the control pastes. This conversion was observed to be accompanied by an increase in the density of the microstructure which is manifested in the physical properties that was reported previously by the authors (3). Finally, pozzolanic reaction was observed to occur readily in the fly ash-containing pastes with the hydration of the fly ash spheres occurring on a more or less particle-by-particle basis governed primarily by the particle chemistry. These results, along with those from recent previous studies, further elucidate the complexities of the reactions of fly ash with portland cement, and support the observations that the development of properties of cementitious mixtures containing them are equivalent to or in some cases superior to those of mixtures with portland cement alone.

VOL.
14
984

Acknowledgment

The authors acknowledge the financial support of NSF Grant CPE-8219396, and the experimental support of Drs. P.H. Licastro and D. Strickler.

References

1. Manz, Oscar, E., Proceedings of the CANMET/ACI First International Conference on the Use of Fly Ash, Silica Fume, Slag and Other Mineral By-Products in Concrete, V.M. Malhotra, Ed., American Concrete Institute, SP79-8, Detroit, Michigan, 187-195 (1983).
2. Lamond, Joseph F., Proceedings of the CANMET/ACI First International Conference on the Use of Fly Ash, Silica Fume, Slag and Other Mineral By-Products in Concrete, V.M. Malhotra, Ed., American Concrete Institute, SP79-8, Detroit, Michigan, 47-70 (1983).
3. Grutzeck, M.W., D.M. Roy and B.E. Scheetz, Effects of Fly Ash Incorporation in Concrete, Ed., S. Diamond (Proceedings of Symposium N), Materials Research Society, 102 M.R.L., University Park, PA, 92-101 (1981).
4. S. Abdul-maula and Ivan Odler, Effects of Fly Ash Incorporation in Concrete, Ed., S. Diamond (Proceedings of Symposium N), Materials Research Society, 102 M.R.L., University Park, PA, 102-112 (1981).
5. Takemoto, K. and H. Uchikawa, Proc. 7th Intl. Congr. on the Chemistry of Cement, Vol. I, IV-2/1-IV2/29, Septima, Paris (1980).
6. Massazza, F., Proc. 7th Intl. Congr. on the Chemistry of Cement, Vol. IV, 85-91, Septima, Paris (1980).
7. Roy, D.M., J.P. Skalny, and S. Diamond, Concrete Rheology, Ed., J. Skalny (Proceedings, Symposium N), Materials Research Society, 102 M.R.L., University Park, PA, 152-173 (1982).

8. Roy, D., Long-Range R+D for Fly Ash Cements, Workshop Proceedings: Research and Development Needs for Use of Fly Ash in Cement and Concrete, EPRI CS-2616-SR, Spec. Rept., 501-506 (Sept. 1982).
9. He Jun-yuan, Barry E. Scheetz and Della M. Roy, Bull. Am. Ceramic Soc. (1983) in press.
10. Ogawa, K. and D.M. Roy, Cem. Concr. Res. 12 (2), 247-256 (1982).

VOL
14
198

CEMENT and CONCRETE RESEARCH. Vol. 14, pp. 513-520, 1984. Printed in the USA.
0008-8846/84 $3.00+00. Copyright (c) 1984 Pergamon Press, Ltd.

UTILIZATION OF BY-PRODUCTS FROM WESTERN COAL COMBUSTION IN THE MANUFACTURE OF MINERAL WOOL AND OTHER CERAMIC MATERIALS

Oscar E. Manz
Coal By-Products Utilization Institute and
Department of Civil Engineering

University of North Dakota
Grand Forks, North Dakota 58202

(Refereed)
(Received Nov. 17, 1983)

VOL.
14
1984

ABSTRACT

The ash by-products from combustion or gasification of western U.S. coals have chemical and mineralogical characteristics that lend themselves to utilization in ceramic materials. Laboratory and pilot-scale fabrication of four such materials has been studied. Cyclone slag from four lignite-fired power plants and a dry scrubber ash have been fabricated into mineral wool insulation in a pilot-scale cupola. Extruded and fired mixtures of fly ash, clay and ground glass have produced ceramics with extraordinary high flexural strength. Ceramic glazed wall tile that utilize fly ash in place of clay have been prepared and shown to meet most specifications for fired clay tile. Both fired and unfired dry-pressed brick containing 100% western fly ash have met ASTM specifications for fired clay brick.

Introduction

This paper concerns the utilization of solid by-products from the combustion and gasification of western coal. As discussed by Diamond (1) in these proceedings, virtually all of the fly ash produced in the United States that is not disposed of directly is utilized in cement and concrete and in soil stabilization. Yet, only about 20% of the available ash is being used at this time (1). Power plants produce other forms of ash and slag that presently have no commercial markets. The first commercial gasification ash will be generated at the Great Plains Gasification Plant in Beulah, North Dakota, in late 1984. There is also, as yet, no commercial market for this ash and it is planned to dispose of it by burial at the nearby mine site. Utilization of these various coal by-products would yield the double benefit of having a relatively inexpensive and steady source of raw materials along with elimination of disposal costs.

The chemical and mineralogical characteristics of western coal fly ashes and lignite gasification ash are discussed by McCarthy et al. (2,3) in these proceedings. These characteristics make it possible to utilize western coal

in a variety of useful ceramic materials. Among these materials are mineral wool, high flexural strength ceramics, ceramic tile and brick. The mineral wool is used in insulation and ceiling tile. The high flexural strength ceramics have been explored as a replacement for wood in areas of severe environments and in power line poles, while the ceramic tile and brick have many conventional applications. Over the last 20 years, various projects aimed at utilization of these coal by-products have been carried out at the University of North Dakota (UND). Highlights from these studies are summarized below.

Mineral Wool

Mineral wool can be fabricated from any form of coal gasification or combustion ash as long as the ash composition falls within certain limits. Workers at the University of West Virginia (4,5) and the Tennessee Valley Authority (6) have demonstrated the production of mineral wool from bituminous coal ash slag. We describe here several pilot scale experiments on mineral wool production from lignite coal slag and fly ash aimed at exploring the feasibility of mineral wool production from lignite slag, gasification ash and fly ash.

In North Dakota and South Dakota there are four lignite-fired electrical power plants that utilize cyclone boilers. This type of boiler converts the majority of the lignite ash into molten slag that collects at the bottom of the boiler and is quenched from a temperature of approximately 2600°F (1427°C) into water to form a coarse frit. This fritted slag could form the raw material for a mineral wool production furnace. Alternatively, the mineral wool could be fabricated directly from the stream of molten slag at the power plant site.

In our experiments, slag or ash is melted in an outdoor cupola (Figure 1) using coke as the fuel. The ground slag or ash in the form of balls is interlayered with coke. Temperature, measured with an optical pyrometer, is controlled by varying the supply of air and coke. A typical temperature range for melting a lignite ash is 2600-3000°F (1427-1649°C). To fiberize the molten slag, compressed air at 140 psi supplied to a blow cap which consists of a 2-in. plumbing pipe cap having a pattern of 1/8 in. holes drilled in the shape of a V (Figure 2) was used. A second method of fiberizing the molten slag, a spinning disk apparatus (similar to a cotton candy machine) was also explored. However, because of the need to study many disk configurations and spin rate variables before using the spinning disk apparatus optimally, most effect to date has concentrated on blowing mineral wool.

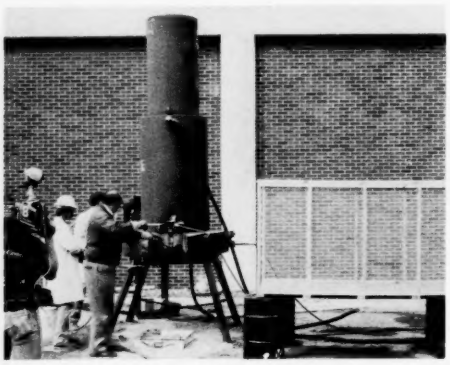

Fig. 1 Cupola Used in the Fabrication of Mineral Wood

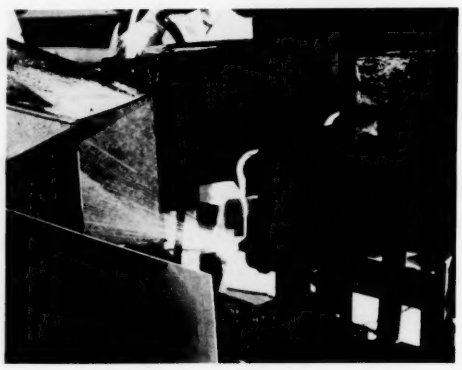

Fig. 2. Mineral Wood is Blown Using A Cap With Holes In the Form of a V.

VOL
14
198

Cyclone slag from each of the four power plants was evaluated. Compositional data for each slag are given in Table 1. The chief variable used by the industry in deciding on the suitability (melting range and viscosity) of raw materials for mineral wool production is the "acid/base ratio" (7), which is also shown in Table 1. Alkali and iron oxides are not usually included among the bases in this ratio, but we have done so because of the substantial alkali and iron contents of most lignite ashes and the important effects of these components on melting and viscosity. Iron can be present in both divalent or trivalent states in glass, but under the reducing conditions in the coke-fired cupola, the oxidation state of iron is dominantly divalent and thus it has been included with the bases. For commercial mineral wool, it is usually stated that the acid/base ratio should be in the range 0.8 to 1.2 for proper melt flow and fiberization. The Big Stone, Coyote and Milton Young slags fell within this range while the Leland Olds did not and was distinctly more difficult to fabricate into wool.

Also shown in Table 1 are the two parameters used to measure the quality of the mineral wool product. According to one manufacturer (Conwed, Inc., in Red Wing, Minnesota), for commercial mineral wool, the fiber diameter should fall within the range 4 to 7 micrometers. The wool made from Coyote and Milton Young slags do fall within this range while those from Big Stone and Leland Olds slags do not. The "shot" content (residual glass beads) is another parameter used in evaluating mineral wool. Shot content should be between 50 and 57%. The wools made from all the slags failed to meet this criterion. See Reference 8 for further details on the processing and testing of mineral wool from cyclone slags. No further work is planned with the cyclone boiler slags.

OL.
14
984

Our current work is focussed on the use of fly ash or scrubber ash as the raw material for mineral wool production. In one recent test, scrubber ash from the Antelope Valley Station in Beulah, North Dakota, has been fabricated into mineral wool. This ash is produced in a dry scrubber in which lime and the fly ash are the basic materials used to remove SO_2 from the flue gas. Fly ash still constitutes about 90% of the material. The ash is cementitious and was easily formed into balls to charge the cupola by the addition of water and hand working. The melting and fiberization characteristics resulted in greater ease of fabrication than was the case with any of the four cyclone slags, probably because of the low acid/base ratio. The product from this run is now being evaluated by a commercial mineral wool manufacturer.

High Flexural Strength Ceramics

Ceramics are inherently brittle materials with relatively low flexural strength (refer to Figure 3). In 1979, Williams and Ali (9) reported the fabrication of ceramic power poles from a mixture of fly ash, crushed scrap glass and clay. Their work used a subbituminous coal fly ash. Some exploratory work was done to see whether the ceramics could also be fabricated using a lignite coal fly ash and to optimize the ratio of ash to glass for maximum flexural strength.

Table 2 lists the compositions of the fly ash, glass and clay used in our tests. The ash was obtained from a North Dakota power plant burning lignite. The glass was beverage bottles ground to -100 mesh and the clay was a western North Dakota sandy kaolinite known as Golden Valley Clay. Also given in Table 2 are the corresponding compositions used by Williams and Ali (9). After weighing the mixture of glass, clay and fly ash, adding water and mixing, the green material was extruded using either a 1 in. diameter laboratory extruder or a 2.5 in. pilot-scale model loaned by a brick company. Considerable effort was required in adjusting water content, amount of vacuum, speed of extrusion and power requirement in order to obtain the highest density product. After

Table 1

Mineral Wool Composition, Melting and Product Data

Raw Material	Average Composition (wt%) SiO_2	Al_2O_3	CaO	MgO	Fe_2O_3	A_2O[a]	Acid/Base Ratio[b]	Melting Temperature (°F)	Fiber Diameter(μm)	% Shot
Cyclone Slag										
Big Stone (SD)	37.0	11.1	29.4	7.7	11.8	1.4	0.96	2850 (1566°C)	3.53	66.8
Coyote (ND)	33.8	15.6	25.9	6.8	14.7	3.3	0.97	2750 (1510°C)	5.53	65.7
Leland Olds (ND)	47.8	12.8	18.4	4.4	10.4	4.0	1.63	3000 (1649°C)	10.30	77.9
Milton Young (ND)	39.4	13.6	22.4	5.4	14.4	2.8	1.18	2950 (1621°C)	6.43	79.7
Scrubber Ash										
Antelope Valley (ND)	21.2	9.4	27.6	5.6	4.8	9.3	0.65	2500 (1371°C)	3.23	77.3
Commercial Mineral Wool	43.5	22.3	14.2	4.2	16.3	NA	1.90	2600 (1427°C)	5.50	50.0

[a] $A_2O = Na_2O + K_2O$ (chiefly Na_2O).

[b] $$\frac{SiO_2 + Al_2O_3}{CaO + MgO + Fe_2O_3 + A_2O}$$

drying the green material in air and in an oven, the material was fired according to the following schedule: heat to 1900°F (1038°C) and soak for 30 min., cool to 1400°F (760°C) and annealled for 1 hr. and slowly cooled in the kiln.

The apparatus for determination of flexural strength employed a Riehle universal testing machine using a three point loading. A specimen undergoing testing is shown in Figure 3. Figure 4 gives the flexural strength as a function of the ratio of fly ash to ground glass. The amount of clay was held at 10% of the dry weight of the fly ash plus glass mixture. A maximum mean value of 7903 psi was obtained when the mix ratio was 65% fly ash to 35% glass. Williams and Ali (9) reported a maximum in flexural strength of 5646 with a 50% fly ash to 50% glass mixture. A typical flexural strength for a ceramic of this configuration is 1000 psi.

Table 2

Chemical Analyses of Fly Ash, Glass and Clay

	Fly Ash (Williams and Ali (9))	Glass	Clay	Fly Ash (this study)	Glass	Clay
SiO_2	49.5	71.6	52.1	46.7	72.2	71.6
Al_2O_3	25.0	1.2	31.2	13.4	2.1	16.1
Fe_2O_3	1.1	0.7	0.8	7.5	0.1	3.2
CaO	12.2	7.6	0.4	16.8	11.2	0.5
MgO	2.1	2.6	0.3	5.0	.04	1.0
Na_2O	1.9	14.7	0.3	10.5	13.2	0.4
K_2O	0.6	0.1	1.0	0.11	1.0	1.6
TiO_2	5.4	0.2	1.6			

VOL 14 198

Additional tests were performed on these ceramics. Absorption value is the weight percent of water absorbed after the ceramic is immersed in water for 24 hrs. An absorption value less than 0.3% for unglazed ceramics is required for most applications. Our values of 0.2 to 0.4% were quite low and were comparable to those reported by Williams and Ali (9). Apparently, the partial melting of the glass components of the material results in little open porosity. Impact strength was also measured. Our maximum value for impact strength was also obtained with the 65/35 fly ash to glass ratio mix. Electrical breakdown strength was also tested, but this ware failed these tests due to the presence of sodium sulfate salt on its surfaces. This particular fly ash was unusually rich in sodium sulfate.

Although limited in scope, these results demonstrate that a useful ceramic material can be produced using very inexpensive raw materials, a fly ash that would otherwise have no value in cement/concrete applications (because of its high sodium content), used container glass and a small amount of clay.

Ceramic Glazed Wall Tile

Ceramic wall tile are made from relatively expensive raw materials such as kaolin and talc. Several years ago a small study was performed for the Saskatchewan Power Corporation to explore the use of their Boundary Dam lignite fly ash as the raw material for ceramic tile. The composition of this fly ash is given in Table 3.

Trial batches consisting of 0.9 lbs. of fly ash and 0.11 lbs. of water were mixed and pressed into 4.25 in. square tile in a steel mold using a pressure of 4500 psi. The tile were allowed to air-dry for 24 hrs. After oven drying at 212°F (100°C) for several hours, the tile were fired to a temperature of 1970°F (1077°C) (Cone 01). Glazes were then applied and the tile were refired to 1670°F (910°C) (Cone 08).

The tile were tested to the Canadian Government and ASTM specifications. Tests for warping, wedging, crazing and thermal shock were passed by the fly ash tile. Table 4 gives the results of four tests and the corresponding specifications. A typical breaking strength of ordinary tile is about 82 lbs. The tile met all specifications except for water adsorption. Apparently, there was too much open porosity with the unglazed surfaces of the tile which readily admitted water. Additional work now underway with North Dakota lig-

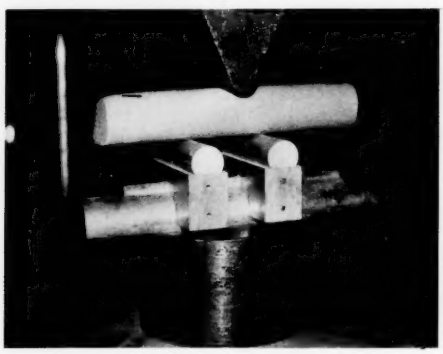

Fig. 3. Flexural Strength Testing Apparatus

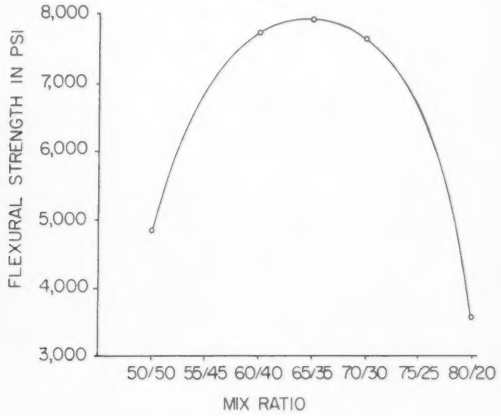

Fig. 4. Flexural Strength as a Function of the Fly Ash/Glass Ratio.

nite fly ash and gasification ash includes special attention to this water adsorption specification.

Dry Pressed Ash Brick

Another potential large-scale market for fly ash that we have explored during the last two decades is construction brick. (10) A conventional brick is largely clay. Our objective is to replace these raw materials with fly ash and other coal by-products. We report here on work performed for the Otter Tail Power Company, Fergus Falls, Minnesota, in the 1960's. This research has recently been reactivated and is now focussed on the by-products from the Great Plains Gasification Plant in Beulah, North Dakota.

Table 3

Compositions of Raw Materials for Ceramic Tile and Brick

	Boundary Dam Fly Ash	Ottertail Power Fly Ash	Ottertail Power Bottom Ash
SiO_2	41.2	25.7	31.9
Al_2O_3	22.0	13.2	13.1
Fe_2O_3	4.8	14.7	15.9
CaO	17.1	27.1	21.6
MgO	4.7	9.0	7.3
Na_2O	6.2	4.2	4.0
K_2O	0.5	0.3	0.5
SO_3	1.0	6.2	2.3

Two approaches have been tried. The first used a formulation, developed by the Coal Research Bureau of West Virginia University (11), of fly ash, cyclone slag and small amounts of sodium silicate. The fly ash and cyclone slag were from Otter Tail's Number 2 Unit in Fergus Falls, Minnesota, which burns a North Dakota lignite. A typical composition for this fly ash is given in Table 3. After several tests, it was found that greater strengths were obtained without the sodium silicate additive and this was eliminated. A mixture of 55% fly ash and 45% cyclone slag (ground to -16 mesh) was found to be optimum. This batch, combined with about 12.5% water, was mixed and pressed into bricks at 3000 psi in a steel mold. After drying at 212°F (100°C), the brick was fired at 2106°F (1154°C) (Cone 3) in an electric kiln.

The cementitious behavior exhibited by many CaO-rich western fly ashes (see reference 2) was the basis of the second approach. In such an ash the firing step can be eliminated. The bricks are simply pressed and dried at 212°F (100°C). They harden from their own self-pozzolanic reactions.

Table 5 presents the results of standard ASTM tests on the two types of fly ash brick along with the ASTM specifications for brick. Both types of brick meet the specifications. It is remarkable that the unfired brick achieved compressive strengths in the range of 2700 to 3100 psi. The ability to eliminate the energy intensive high temperature firing step is especially attractive in this coal by-product utilization option. Brick panels were made from both types of brick and have been exposed to the elements for nearly 16 years. Over this period of time the bricks have showed little deterioration.

Conclusions

We have described four means of utilizing fly ash and other by-products from western coals. These applications go beyond the familiar blended cement and soil stabilization options that account for most of the commercial utilization of fly ash. Mineral wool that meets most industry specifications has been fabricated from remelted cyclone slag or melted fly ash. Firing a mixture of fly ash, ground scrap glass and clay has yielded ceramics with extraordinary flexural strength. It has been shown that glazed ceramic wall tile can be fabricated from pure fly ash. These tile met all Canadian government specifications with the exception that their water absorption was somewhat high. Finally, brick has been fabricated from a mixture of two coal by-products, fly ash and coarsely ground cyclone slag. Whether fired at high temperature or not, the brick met all ASTM specifications. The ability to make satisfactory brick from waste materials and without high temperature firings offers the possibility of great savings in raw materials and energy costs.

Table 4

Properties of Ceramic Tile Made From Fly Ash

	Fly Ash Tile	Specifications[a]
Warpage along edges, %	0.25 convex	0.5 convex, % max 0.2 concave, % max
Warpage along diagonals, %	0.17 convex	0.35 convex, % max 0.15 concave, % max
Wedging, %	0.02	0.5 % max
Water Absorption, %	21.6	7-18%
Breaking Strength, lb.[b]	86	

[a]"Standard for Tile: Ceramic, Floor, Wall and Trim Units," Publ. 75-GP-Ib, Canadian Government Specifications Board.

[b]ASTM C648-71.

Table 5

Properties of Dry Pressed Ash Brick

	Fired Brick[a] 2106°F	Dried Brick[a] 212°F	Specification[b]
Boiling Water Absorption (%)	10.9	10.1	20.0 max
Saturation Coefficient	0.76	0.76	0.80 max
Compressive Strength (psi)	5168	3086	2500 min.

[a]55% fly ash/45% cyclone slag.

[b]ASTM for Grade SW brick.

VOL. 14 1984

Acknowledgements

This research was supported by the Department of Energy, Saskatchewan Power Corporation, National Minerals Corporation, Basin Electric Cooperative, Otter Tail Corporation and the Gas Research Institute. G. J. McCarthy of North Dakota State University is thanked for helpful discussions and editorial assistance with this manuscript.

References

1. S. Diamond, "Utilization of Fly Ash", Cement and Concrete Research (this volume).
2. G. J. McCarthy, K. E. Swanson, L. P. Keller and W. C. Blatter, Minerology of Western Fly Ash, Cement and Concrete Research (this volume).
3. G. J. McCarthy, L. P. Keller, P. J. Schields, M. P. Elless and K. C. Galbreath, Mineralogical Characterization of a Lignite Gasification Ash from a Low-BTU Fixed-Bed Gasifier, Cement and Concrete Research (this volume).
4. William F. Lawrence, "Mineral Wood Production From Coal Ash - A Progress Report, #38", Coal Research Bureau, West Virginia University, 1969.
5. "Production of Mineral Wool from Coal Ash Slag", Final Report - U.S. Bureau of Mines, Solid Waste Disposal Program, West Virginia University School of Mines, 1969.
6. F. G. Parker and T. L. McDaniel, "Production of Mineral Wool from Coal Slag", Tennessee Valley Authority, Chattanooga, Tennessee, 1978.
7. K. K. Humphreys and W. F. Lawrence, "Producing Mineral Wool from By-Products", Minerals Processing, March 1970.
8. O. E. Manz and L. C. Eaton, "Production of Mineral Wool from Lignite Coal Slags", Coal By-Products Utilization Insitute, University of North Dakota, Final Report, March 16, 1983.
9. T. D. Williams and A. Ali, "Development of Power Poles from Fly Ash, Phase II", Electric Power Research Institute, Project 851-1, September 1979.
10. O. E. Manz, "Ash from Lignite", Bureau of Mines Information Circular #8488, March 1970.
11. C. W. Turner, "The Status of Fly Ash Brick", Brick & Clay Record, June 1967, pp. 55-57.

VOL
14
198

CEMENT and CONCRETE RESEARCH. Vol. 14, pp. 521-528, 1984. Printed in the USA.
0008-8846/84 $3.00+00. Copyright (c) 1984 Pergamon Press, Ltd.

SLAG CEMENT UTILIZATION: RHEOLOGICAL PROPERTIES AND RELATED CHARACTERIZATION

Wu Xuequan and Della M. Roy
Materials Research Laboratory, The Pennsylvania State University
University Park, PA 16802

(Communicated by G.M. Idorn)
(Received Nov. 17, 1984)

VOL. 14 1984

ABSTRACT

Mortars prepared from slag-cement blends have been shown to exceed or equal the strengths of portland cement mortars at 7 to 28 days. Such cements have further potential advantages in their performance with regard to durability, and in their early stage properties which govern workability. The early stage rheological properties including mortar flow, yield stress, and viscosity were investigated, combined with zeta potential measurements, and used to explain the excellent workability. The working time of slag cement may be extended to later ages compared with portland cements through use of superplasticizers.

Introduction

Slags constitute an important mineral by-product resource (1) whose optimal utilization as cementitious materials is important to the concrete industry (2). This study is a part of investigations to determine the relationship between slag characteristics, their hydration behavior, and their performance in concrete (2-5).

The rheological behavior of fresh concrete is obviously important during the mixing, transporting, placing, consolidating and finishing operations, but also controls in part the properties of hardened concrete. This paper seeks to contribute to an understanding of the properties of cementitious materials in which major portions of the matrix consist of granulated blast furnace slag. Comparisons have been made between the properties of cements containing three different slags, two different portland cements, and two different admixtures.

Rheological behavior, including mortar flow, yield stress and viscosity were studied to provide a sensitive measure of the structural aggregation in suspension (6). Flow curves, furthermore have been commonly used to examine the effect of admixtures on the flow behavior of cement paste (7). High range water-reducers are widely used in the cement and concrete industry to reduce the required amount of mixing water and generate lower porosity cementitious

materials. Their mechanisms of action have been studied by a number of authors, and the zeta potential of cement particles was shown to play a major role (8). Qualitatively similar effects were found in type I cements to those in sulfate-resistant cements, but the former had somewhat larger (negative) zeta potentials (8). The significantly different chemistry and structure of slags from that of portland cements might be expected to contribute to differences in rheological behavior of slag-containing cements (2). Previously (9), we found that the negative magnitudes of the zeta potentials for high slag content cements, especially those containing a high-range water reducer (superplasticizer) are generally greater than those for portland cement, causing better particle dispersion and higher fluidity of the cementitious mixtures which changes with processing time and admixture concentration.

Therefore, the current studies were undertaken to compare the rheologic properties of slag cement mixtures with those containing portland cement, and to elucidate the behavior as reflected in comparison of slump and other measurements (1).

Experimental

The measured viscosities of cement pastes are affected by both material and experimental parameters: chemical composition, particle size distribution or specific surface area of the cement, water-to-cement ratio, hydration time, curing temperature, mixing time and intensity, admixture type and concentration, and the geometry, general characteristics and operating procedure of the viscometer, so that the results reported by various authors are different and even sometimes apparently contradictory (6,10,11). Hydration reactions are known to cause a change in flow behavior with time because of the consequent agglomeration of cement particles. However, agitation strongly affects the flow, causing a breakdown of aggregated structure. Continuous high shear agitation is not a normal state in most concrete production; therefore for best reproducibility, such agitation is generally avoided during the measurement of time-dependent flow behavior, except for mixing just prior to the measurement, which is necessary to assure a homogeneous slurry. In order to assure comparable results in the current measurements, identical experimental conditions were maintained in all the tests.

Samples of slag cement pastes SC-I, SC-II and SC-III were prepared by blending 1:1 weight ratio mixtures of a type I/II portland cement (code II-02) and three kinds of granulated slag, codes B19, B47 and B63, respectively, with the cement-to-slag ratio (1:1). The compositions of these materials were described in (9) and (12). The Blaine specific surface areas were, respectively, 559, 508, and 555 m^2/Kg for the B19, B47, and B63; and 368 for II-02. Flow table tests and compressive strength measurements were made according to ASTM C 109. The apparatus used for yield stress and viscosity measurement was a coaxial cylinder type viscometer HAAKE RV3. In order to measure high viscosity during initial setting periods, an MK500 measuring head was used, which is available in the torque range of -4.9 NM (500 cm.g). The sensor system used was MVIIP, which consists of rotor (bob) with grooves on the surface, and stator (cup). The diameters of the bob and cup were 18.4 mm and 21 mm, respectively. The immersion length was 60 mm.

The admixtures used were sulfonated naphthalene formaldehyde condensate high range water reducers (superplasticizers) A3 and A4, which contained 43% solid; A4 also contained an additional retarding component. The admixture (0.5 a/c wt.%) was dissolved in deionized water before mixing with cement. The concentration used was limited, since sedimentation was found to occur during viscometric experiments in cement slurries with superplasticizer concentrations greater than 0.5%, which could give rise to large errors. The water-to-cement ratios (w/c) used were 0.4.

VOL
14
198

A 600g sample was mixed by hand with 240g admixture-containing solution for 1 minute, followed by a 1.5 minute rest, then agitated at 3500 rpm and 9000 rpm for 15 seconds and 45 seconds, respectively, in a high speed blender. Thus, an identical (homogeneous agitated) slurry was produced in each case. The slurry was not additionally agitated until the required processing time approached. Prior to each measurement, the slurry was agitated by hand for 1 minute with a spatula. About 12 oz. of slurry was placed into the cup. The measurement determined the shear stress during cycles in which the shear rate was first increased and then decreased, at a speed of 100 rpm/minute, up to the maximum of 600 rpm. The cycle time was 12 minutes. The apparent viscosity data were calculated at 300 rpm on the down flow curve, according to the equation, η_a (apparent viscosity) = G·S/n, where G is an instrument constant, S is proportional to the shear stress, and n to the shear rate. All the viscosity measurements were made at 38°C, utilizing a constant temperature bath.

Results and Discussion

The compressive strengths of mortar cubes (23°C cure) of a control type I portland cement are shown in Fig. 1, which shows that 7-day compressive strengths of the 35 cement:65 slag (Newcem) are equal to that of the control, while 28-day strengths of all the blends exceed that of the control. Specimens cured at 38°C (more typical of temperatures reached in much field concrete) reached equal strength at 3 days. Results similar to Fig. 1 were found previously with blends of granulated slag with a type II/I portland cement.

Figures 2 through 5 show the viscometric curves used for the measurement of apparent viscosity and yield stress, for slag-cements and portland cement with and without superplasticizer. The portland cement (Fig. 2) showed thixotropic* behavior except in the lower shear rate range after 4.75 hours, while all the mixes with 0.5% A4 (Fig. 3) showed thixotropic behavior, and generally lower yield stresses and viscosities. The 'down' flow curves were found to be almost linear, especially in the high shear rate regions, thus, the apparent vis-

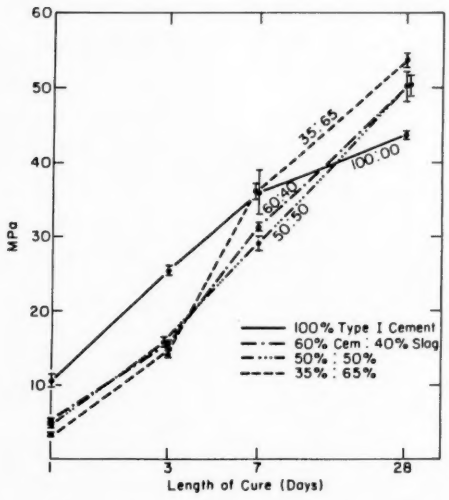

Fig. 1. Mortar cube strength (ASTM C 109) of portland and slag cements.

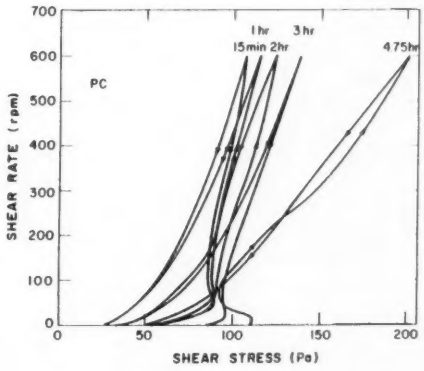

Fig. 2. Viscometric curves of 0.4 w/c portland cement paste.

*As discussed previously (13), this is really pseudothixotropic behavior.

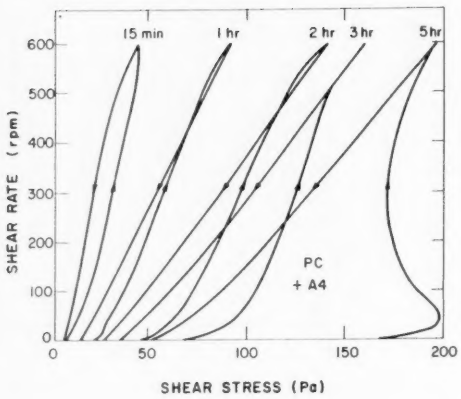

Fig. 3. Flow curves of the portland cement paste with 0.5% admixture A4.

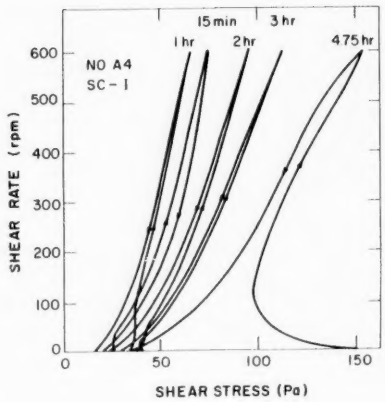

Fig. 4. Flow curves of 0.4 w/c slag cement (SC-I) paste.

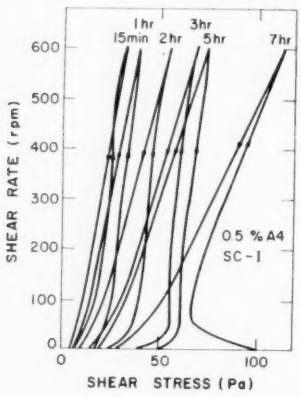

Fig. 5. Flow curve of 0.4 w/c slag cement (SC-I) paste with 0.5% A4.

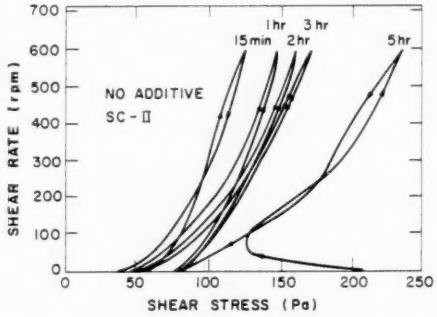

Fig. 6. Flow curves of 0.4 slag cement SC-II pastes.

cosities were calculated from the 300 rpm shear rate measurement on the decreasing shear rate curves. Slag cement SC-I (Fig. 4) showed thixotropic behavior except the measurement after 15 minutes hydration. The shear stress or viscosity after 15 minutes was higher than that after 1 hour, suggesting a slight false setting phenomenon, which disappeared upon the addition of admixture to the sample (Fig. 5). The slag cement SC-II (Fig. 6) exhibited behavior similar to that of SC-I but with normal thixotropic flow in all measurements. The addition of superplasticizer markedly lowered the yield stress (Fig. 7). Slag cement SC-III behaved somewhat differently. It exhibited significant yield stresses in the absence of admixture; while the measurements after 15 minutes and 1 hour showed antithixotropic behavior. The up and down curves crossed and double, even triple, loops occurred after 2 and 3 hours. The maximum shear stress was up to 271 Pa at 600 rpm shear rate after 3 hours, which was much higher than the other samples. However, with the addition of 0.5% admixture A4, it only required less than 50 Pa maximum shear stress at 600 rpm. This indicates that the superplasticizer affects all the slag cements beneficially, particularly SC-III, prolonging their working period.

Figure 8 contrasts the mortar flow table measurements of portland and slag cements; the flow values of cements changed with the concentration of admixture A3. It was concluded that the flow values for slag cement are higher than that for portland cement and follow the order of SC–III > SC–I > SC–II, which is the same order as that of the zeta potentials measured for those slag cements (5), i.e., the higher the negative zeta potential the higher the flow. The optimum concentration of A3 for both portland and slag cements appeared to be about 1.5% admixture-to-cement ratio, which may also be identified from the results of the zeta potential measurements. However, it was found that 0.5% superplasticizer (liquid) significantly improved (increased) the flow.

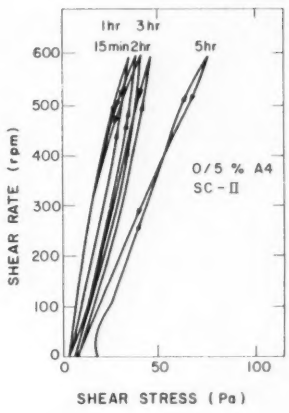

Fig. 7. Flow curve of 0.4 slag cement (SC–II) pastes with with 0.5% A4.

Figure 9 shows the changes in apparent viscosity (measured from the viscometric curves) with processing time. The viscosity trends are generally the opposite of the flow, as expected. It is obvious that viscosities for all the cements increase in magnitude with time and undergo significant changes within a certain period, corresponding approximately to the initial setting period of the cement paste; it is also correlated generally with the phenomenon of zeta potential change (7,9). The upper four curves represent those samples containing 0.5% A4. The superplasticizer A4 strongly decreases the viscosity and may slightly delay the setting. This may be explained by the increased negative zeta potentials of the cement particles with superplasticizer, giving rise to a better particle dispersion and consequently a higher fluidity of cement paste. The viscosities of the above cements with admixture A4 followed the sequence PC > SC–I > SC–II > SC–III, which corresponds roughly to the inverse sequence of negative zeta potential (9). However, in the case of those cements without admixture, the behavior was slightly more complex. The viscosities of SC–III and SC–II appear to be higher than that for portland cement, which is not easily explained from the zeta potential concept. This may be related to other effects, however, such as the higher specific surface areas of the ground slags compared with the portland cement components.

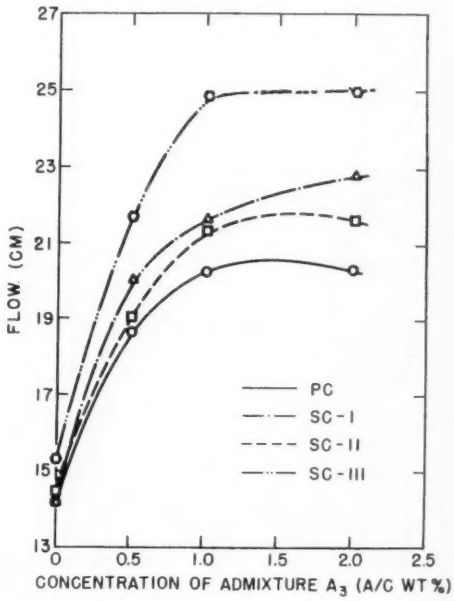

Fig. 8. Mortar flow of cement slurry vs. amount of admixture A_3.

Figure 10 shows the changes in yield stress with processing time. The results of yield stress change were similar to those of viscosity. It is noted that superplasticizer A4 significantly decreases the yield stress almost down to zero, and maintains a low yield stress until 3-4 hours or longer. The

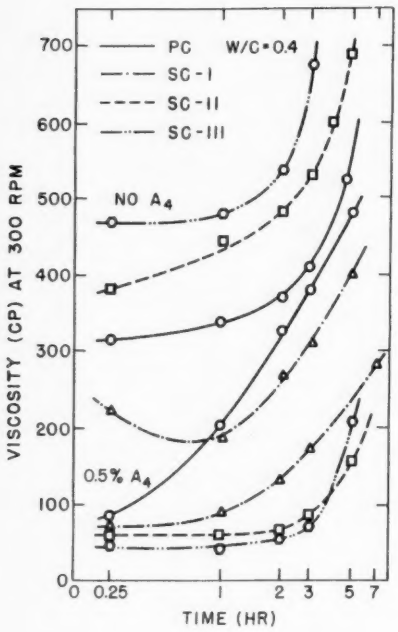

Fig. 9. Changes in apparent viscosity with processing time.

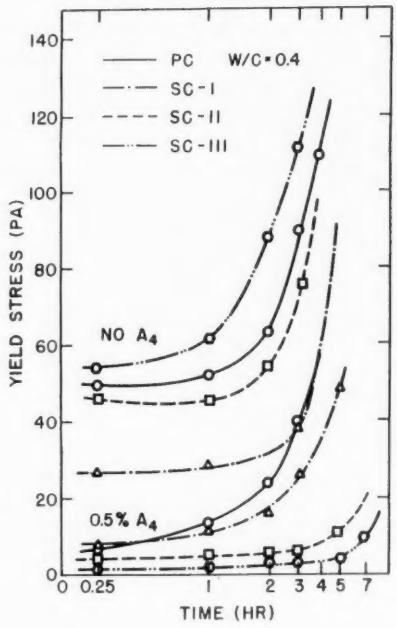

Fig. 10. Changes in yield stress with processing time.

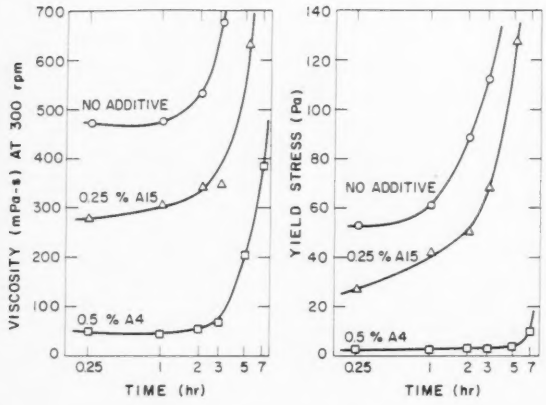

Fig. 11. The effects of different admixtures on yield stress and viscosity of slag cement SC-III (A15 = lignosulfonate).

decrease in yield stress is generally greater in the slag cements than in the portland cement.

Additional comparisons were made between the effects of a common water reducing admixture (lignosulfonate,A15) and the superplasticizer. Figure 11 compares the effects upon slag cement SC-III. The use of 0.25%* of A15 lowered the viscosity and yield stress, but did not have as pronounced an effect, nor did it remain effective as long as the superplasticizer. The effects upon the yield stress and viscosity are compared in Fig. 12. The same slag, B63, was used in all mixtures. It is noted that the effect of 0.5% superplasticizer A4 on slag cement with type I cement (code I-09) is less pronounced than that with type II cement (code II-04) and

*This concentration was recommended by the manufacturer.

also did not remain effective as long. In the absence of admixture, the viscosity and yield stress of slag cement with type I cement were lower than that with type II cement in the earlier stage. However, the trend reversed after about 3 hours. The former fact may be related to the higher negative zeta potential found for a type I cement as indicated previously (8), while the latter fact may be explained by the higher C_3A content of type I cement, which results in faster hydration.

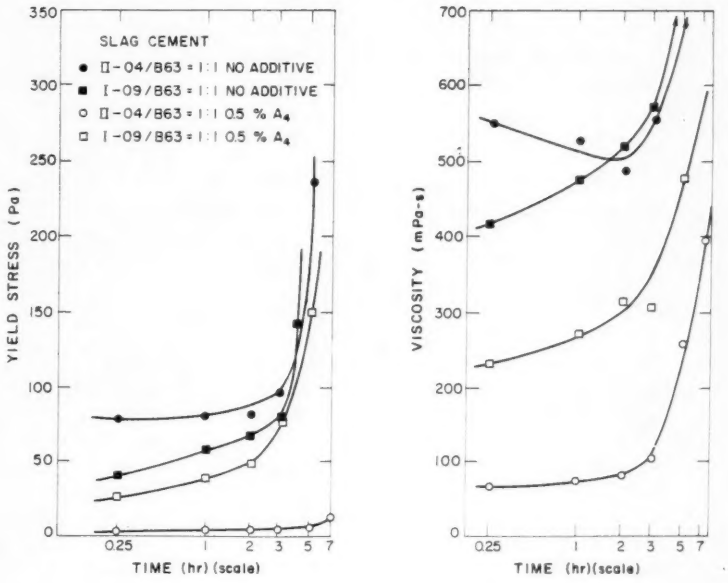

Fig. 12. Yield stress and viscosity of 50:50 blends of slag with type I and type II cements.

Discussion and Conclusions

The rheological behavior of fresh cement pastes and mortars has been compared with the behavior of mixtures (1:1 weight blends) of portland cement with granulated slag. Adequate workability is obviously related to the achievement of satisfactory long-term performances of concrete (1-5). The materials studied showed increased strength in mortar cube tests of the slag blends, over those of the portland cement controls beyond 7 days (or beyond 3 days at elevated temperatures). The higher slump imparted to concrete mixtures by granulated slags (1) is reflected in the somewhat lower viscosities and yield stress values for the slag cement pastes. A substantially greater benefit from additions of water reducers or superplasticizers is realized for the rheological properties of slag cements, than for portland cements. The same phenomena have been observed in zeta potential measurements(9), which show the higher negative surface charge developed on slag particle surfaces, providing a mechanism for generating better dispersion and hence better workability. Part of the explanation for the greater effectiveness may be related to the lower basicity for slag cement (9). High range water reducers were observed to react in part with dissolving species from hydrating portland cement (16); so that in contrast, the superplasticizer effects may be realized more fully in the slag-cement mixtures than with portland cement alone.

The flow behavior of high surface area slag-containing cement mortars was found to be relatively similar to that of lower surface area portland cements. The use of high range water reducers (superplasticizers, ~0.23% of cement) accentuated the differences, causing all the slag mixtures to exhibit greater

flow than the comparable portland cement mixtures. Similar effects to the above (2) were produced by addition of lignosulfonate-type water-reducing admixtures, only the effects were much less pronounced. The viscosity and yield stress of all cement slurries generally increase with processing time and undergo significant change within a certain period, which is related to the time dependence of the zeta potential. However, slag cement workability periods can generally be extended beyond those of portland cement.

Acknowledgement

We acknowledge the assistance of R. Prave in part of the measurements. Financial support was provided by NSF grant CPE-8112821, the Atlantic Cement Co. and Lohja Corporation. W.X. was a visiting scientist from Nanjing Institute of Chemical Engineering, Nanjing, The People's Republic of China.

References

1. J.W. Meusel and J.H. Rose, Proc. CANMET/ACI First Intl. Conf. on Use of Fly Ash, Silica Fume, Slag and Other Mineral By-Products in Concrete, Vol. I, 397-414. ACI SP-79, V.M. Malhotra, Ed., ACT, Detroit (1983).
2. D.M. Roy and G.M. Idorn, ACI Journal 79-43, 444-457 (1982).
3. G.M. Idorn and D.M. Roy, Factors Affecting the Durability of Concrete Using Blast-Furnace Slag Cement, ASTM (in press).
4. R.I.A. Malek and D.M. Roy, Effect of Slag Cement and Aggregate Type on Alkali-Aggregate Reaction and its Mechanisms, 6th Intl. Conf. on Alkalis in Concretes, Research and Practice, Copenhagen (1983, in press).
5. D.M. Roy and K.M. Parker, Proc. CANMET/ACI First Intl. Conf. on Use of Fly Ash, Silica Fume, Slag and Other Mineral By-Products in Concrete, Vol. I. ACI SP-79, V.M. Malhotra, Ed., ACT, Detroit (1983).
6. D.M. Roy and K. Asaga, Cem. Concr. Res. 9, 731 (1979).
7. Yasufe Otsubo, Seiichi Miyai, and Kaoru Umeya, Cem. Concr. Res. 10, 631 (1980).
8. D.M. Roy, M. Daimon, and K. Asaga, 7th Intl. Congress on the Chemistry of Cement, 1980, Paris, Vol. I, Theme II-242-246.
9. X. Wu and D.M. Roy, Cement Rheology, pp. 215-223 (Proc., Symp. M, Materials Research Society, 1982), J. Skalny, Ed. (1983).
10. D.M. Roy, S. Diamond, and J.P. Skalny, Cement Rheology, pp. 152-173 (Proc., Symp. M, Materials Research Society, 1982), J. Skalny, Ed. (1983).
11. W. Von Berg, Mag. Concr. Res. 31, 211 (1979).
12. X. Wu and D.M. Roy, Cem. Concr. Res. 13, 277-286 (1983).
13. E.L. White and D.M. Roy, Cement Rheology, pp. 108-119 (Proc., Symp. M, Materials Research Society, 1982), J. Skalny, Ed. (1983).
14. M. Pigeon and M. Regourd, Proc. CANMET/ACI First Intl. Conf. on Use of Fly Ash, Silica Fume, Slag and Other Mineral By-Products in Concrete, Vol. I, 979-998. ACI SP-79, V.M. Malhotra, Ed., ACT, Detroit (1983).
15. D.M. Roy, E.L. White, and Z. Nakagawa, ASTM (in press).
16. M. Daimon and D.M. Roy, Cem. Concr. Res. 8, 753-764 (1978).

VOL
14
198

CEMENT and CONCRETE RESEARCH. Vol. 14, pp. 529-532, 1984. Printed in the USA.
0008-8846/84 $3.00+00. Copyright (c) 1984 Pergamon Press, Ltd.

QUICK LIME-GYPSUM INTERACTIONS IN STABILIZED SOIL BASES FOR CONCRETE HIGHWAYS

S. Schlorholtz and T. Demirel
Department of Civil Engineering
Iowa State University, Ames, Iowa 50011 USA

(Communicated by D.M. Roy)
(Received Nov. 17, 1983)

VOL.
14
984

ABSTRACT

Lime stabilization of clayey soils is very common throughout many parts of the world. Typically if heaving is observed after quick lime (CaO) stabilization, then one may think that insufficient lime and/or poor slaking and mixing techniques may be the root of the problem. Actually, there are several other reasons for the observed heaving. One explanation is that the lime may have been hard burnt, thus rendering the lime inactive until months later. Another explanation is due to the interaction of the quick lime with gypsum ($CaSO_4 \cdot 2H_2O$) in the soil to be stabilized.

One may conclude that lime, Type I portland cement, or Class C fly ash stabilization of high gypsum bearing soils would at best produce poor results because of the possibility of expansion due to the formation of ettringite.

Introduction

Sulfate attack is probably the most common form of chemical attack experienced by portland cement concrete. The purpose of this paper is to present comments on the nature of sulfate attack in lime stabilized soils. A portion of the paper includes the presentation of data and conclusions obtained from an actual construction project that experienced detrimental subbase heaving due to sulfate attack.

The Nature of Sulfate Attack

Sulfate attack in portland cement concrete is typically represented by equation 1 (1) although there are several combinations of reactants that may produce the same product (i.e., ettringite).

$$\underset{\text{(monosulfoaluminate)}}{3CaO.Al_2O_3.CaSO_4.12H_2O} + \underset{\text{(gypsum)}}{2CaSO_4.2H_2O} + \underset{\text{(water)}}{18H_2O} \rightarrow \underset{\text{(ettringite)}}{3CaO.Al_2O_3.3CaSO_4.32H_2O} \quad (1)$$

Actually the reaction may be much more complex than shown above and at least one author claims that this equation alone does not explain all the expansion problems normally associated with sulfate attack (2,3,4,5). In this paper we will follow a slightly different mode of thinking since the subject under investigation is sulfate attack in stabilized soils rather than sulfate attack

in concrete. Assume we can idealize a lime-clay system as denoted in equation 2, where the vague term "clay" simply refers to an alumino-silicate of high specific surface that has no self-cementitious properties. This reaction is pozzolanic in nature and thus is a fairly slow reaction:

$$CaO + H_2O + \text{excess clay} \rightarrow Ca_aAl_b.cH_2O + Ca_xSi_y.zH_2O + \text{clay} \quad (2)$$

where a, b, c, x, y and z are variables that are dependent on temperature, pressure and the molar ratios of reactants. If gypsum is added to the system and a fairly high moisture content is maintained then reaction 3 may occur.

$$Ca_aAl_b.cH_2O + CaSO_4.2H_2O \rightarrow 3CaO.Al_2O_3.3CaSO_4.32H_2O + \ldots \quad (3)$$

If reaction 3 took place in a soil that had been compacted to a high density (90 to 95% standard proctor density) then detrimental expansion may take place due to the formation of ettringite. The reactions that have been listed above are only very simplistic models, the real nature of the soil-lime-gypsum interaction is much more complex, depending heavily on soil properties, lime activity, and the soil moisture content.

A Case History

Figure 1 illustrates what appears to be the influence of sulfate attack on a lime stabilized soil. The soil samples were taken from borings made at several different locations in a road construction project. The project was located in the southern United States and the borings were made after localized heaving was reported to the consulting engineers (approximately eight months after the project was completed). The consulting engineers ruled out the possibility of freeze-thaw heaving.

Ettringite Reaction

Figure 1a shows a X-ray diffraction (XRD) trace of the virgin soil (i.e., not treated with lime). Figure 1b shows the XRD trace of a soil taken from a borehole in a zone that was stabilized with quick lime (CaO) and showed no measurable heaving. Figure 1c shows a soil sample that was taken from a borehole located in a zone that was treated with CaO and showed severe heaving. All XRD traces were made using a Siemens D 500 diffractometer with copper K_α radiation. The diffractometer is equipped with a graphite monochromator.

The obvious difference between the virgin soil (Figure 1a) and the treated soils (Figures 1b,c) is the presence of gypsum in the latter. The consulting engineer acknowledged that gypsum rock was present in portions of the construction project. The gypsum rock was probably inadvertently pulverized and incorporated into the subgrade during the mixing phase of the project. The sample taken from the heaving zone (see Figure 1c) also shows that a considerable amount of ettringite had formed. A sample taken from the zone that did not experience heaving (see Figure 1b) may also show the presence of ettringite but if it is present then it is in much smaller quantities. Apparently, the formation of ettringite in the highly compacted subbase caused the heaving because no expanding clay minerals were evident in the diffraction traces. A point of major concern to the owner of the project would be how to attempt to eliminate further heaving without having to tear up the pavement and then remove and/or restabilize the subbase soil. Any attempt to restabilize the existing subgrade with lime or Type I portland cement would be very questionable since the soil still contains large quantities of gypsum. Actually, due to the current lack of knowledge of the mechanism of this type of chemical attack in soils it is impossible to predict how much (if any) future expansion may take place.

VOL. 14 1984

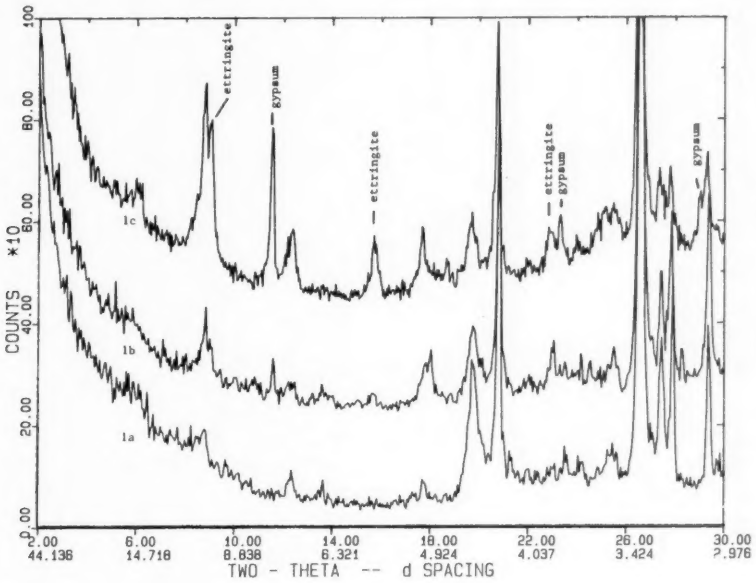

Fig. 1.

Formation of ettringite in a soil containing gypsum: (a) virgin soil; (b) soil from zone showing no heaving; (c) soil from heaving zone.

Other Possible Reactions

One interesting aspect of equation 2 is the rate at which it proceeds. As mentioned earlier typically it is assumed that this reaction proceeds slowly (measured in terms of days) so one may speculate on the types of reactions that may occur in a quick lime-gypsum system before the clay-lime (pozzolanic) reaction. If, for example, insufficient water was used to slake the quick lime then reaction 4 is thermodynamically possible since the Gibbs free energy of formation (ΔG°_{298}) is -37 k-cal/reaction. Reaction 4

$$3CaO + 2CaSO_4.2H_2O \rightarrow 3Ca(OH)_2 + 2CaSO_4.\tfrac{1}{2}H_2O \qquad (4)$$

could then be followed by a subsequent reaction in which the gypsum hemi-hydrate would react with water from the environment to form gypsum (dihydrate). Both of these reactions result in a positive volume change (i.e., expansion). The end products of the reactions would be gypsum and calcium hydroxide (assuming total hydration occurs) and thus the pozzolanic reaction is still possible and as described earlier it could be followed by the formation of ettringite (see reaction 3).

Reaction 4 is possible and it does occur in gypsum-quick lime mixtures stored at 55 $\pm$ 5°C. However, the reaction is quite slow and requires several weeks for completion (see Figure 2). Figure 2a shows the gypsum-lime mixture after one day at 55°C. Figure 2b shows the same mixture after 18 days at 55°C; conversion from $CaSO_4.2H_2O$ to $CaSO_4.\frac{1}{2}H_2O$ is complete and the free water is readily used to convert CaO to $Ca(OH)_2$. Since the reaction is so slow it need not be considered further.

Stabilization of soils with Class C fly ash may also create a system containing calcium oxide, calcium sulfate (anhydrite), and tricalcium

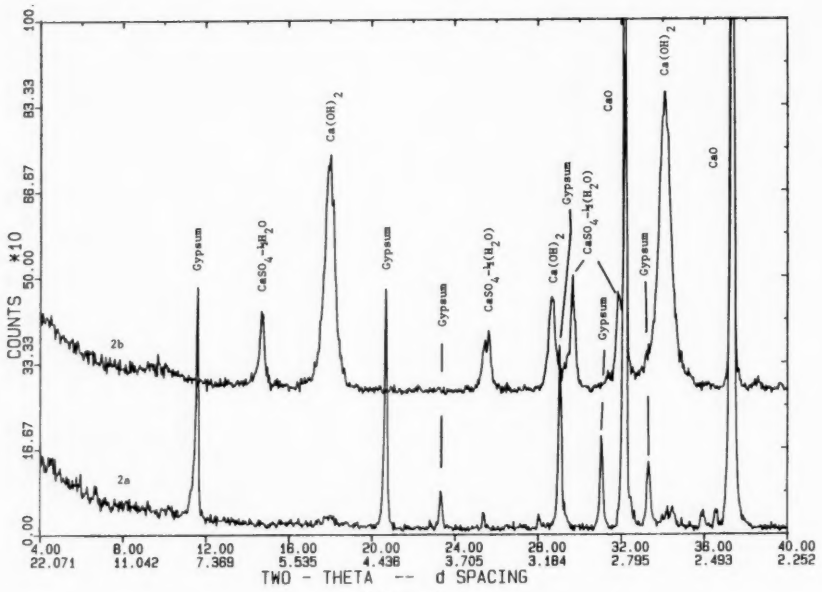

Fig. 2.

Gypsum-quick lime interaction: (a) 2.5:1 lime to gypsum mixture after one day @ 55°C; (b) same mixture after 18 days @ 55°C.

aluminate since these three compounds are often found in Class C fly ashes. The formation of ettringite is commonly the major reaction that occurs in the early stages of hydration of Class C fly ashes, whether or not this could lead to detrimental future expansion in the presence of excess gypsum is presently not known. Also, the free lime present in some fly ashes does not appear to hydrate readily, an indication of some type of inactivity in the calcium oxide that may lead to future problems (6).

Summary and Conclusions

In summary, it has been shown that sulfate attack can occur in stabilized soil bases if the proper conditions are met. The sulfate attack which appears to result in the formation of ettringite may cause detrimental expansion in subbases that are compacted to high densities. Several other reactions were considered which may contribute to expansion in construction projects when quick lime and/or Class C fly ash are used for the stabilizing agent and a free source of gypsum is available.

References

1.) S. Mindness and J. F. Young. Concrete. Prentice-Hall: Englewood Cliffs, N.J., 1981.
2.) S. Chatterji and J. W. Jeffery. Mag. Conc. Res., 15[44], pp. 83-86, 1963.
3.) P. K. Mehta. Amer. Ceram. Soc., 15[4], pp. 204-208, 1967.
4.) P. K. Mehta. Cem. & Conc. Res., 3[1], pp. 1-6, 1973.
5.) P. K. Mehta. Cem. & Conc. Res., 13[3], pp. 401-406, 1983.
6.) S. Schlorholtz. Unpublished M.S. Thesis, Iowa State University, 1983.

CEMENT and CONCRETE RESEARCH. Vol. 14, pp. 533-538, 1984. Printed in the USA.
0008-8846/84 $3.00+00. Copyright (c) 1984 Pergamon Press, Ltd.

BENDING STRENGTH OF PULP CEMENT BOARD COMPOSED OF SEPARATED PULP FROM MUNICIPAL SOLID WASTE

T. Kitamura, R. Matsuo, Y. Kobayashi, and S. Katoh
Government Industrial Research Institute, Shikoku
2-3-3 Hananomiya, 761 Takamatsu, Japan

(Communicated by D.M. Roy)
(Received Oct. 29, 1982; in final form Jan. 3, 1984)

OL.
14
984

ABSTRACT

The relation between bending strength and X-ray diffraction intensity for pulp cement board composed of separated pulp from municipal solid waste was studied. Higher bending strength was observed for the boards with higher diffraction intensity of $Ca(OH)_2$. Lower bending strength at the same diffraction intensity was observed for the boards from coarsely separated pulps than those from other pulps used. This difference in bending strength was discussed in relation to the differences in the strength of pulp and the amount of fine fraction in pulp.

Introduction

Reclamation of municipal solid waste has successfully been promoted (1-3) in the demand for saving natural resources. Separated pulp, which should be reclamated at high production rates in the future from municipal solid waste, demands establishing a way to be utilized. At first, making paper from the pulp was tried. In the trial, paper with enough quality for toilet roll was made (3) from the pulp, which was obtained after a fine separating process.

Utilization of the pulp as a raw material for pulp cement board should be promising, in that the requirement for brightness and strength of pulp is not as severe as for paper. This mild requirement would make it possible to utilize the pulp from a coarse separating process, which have a higher yield and lower costs than that from the fine separating process.

In preceding papers (4,6), a survey for the preparation of pulp cement board was reported. In the survey it was clear that the mixture of raw materials which contain coarse separated pulp, should be diluted to about 8% consistency and mixed more than 30 minutes to get the boards, which surpass the JIS level of bending strength; or the pulp should be treated with alkaline before the preparation procedure to attain a much higher strength.

In this report the bending strength of the pulp cement board is investigated in relation to its X-ray diffraction property to get insight into the factors which affect the bending strength of the board, and to get a diagnostic criterion

for the formation of the pulp cement board. The criterion is necessary regarding the possible fluctuations of pulp properties from municipal solid waste.

Experimental

Materials

A fresh bag of commercially available portland cement was used. Serpentine from Tanoura in Kumamoto prefecture in Japan was crushed to powder. The size distribution was measured by an image analyser Luzex 500 of NIRECO equipped with an optical microscope. Maximum size distribution was observed at 3-4 μm for the serpentine. Above 95% of the particles were of diameters below 20 μm.

Two kinds of separated pulps were used. One, which was named R.P., was sampled after a rough separation process from municipal solid waste, and the other, named B.P., was sampled in the bleaching process, which is situated before the fine separation process in the pilot plant of "Star dust 80" for reclamation of resources from municipal solid waste. Pulp from filter paper (F.P.) and thermomechanical pulp of red pine (T.P.) were used for comparison. The asbestos used was commercially available crysotile M-6-40.

Procedure

A composition of raw materials after JIS A-5414 for pulp cement board was used. Various mixing conditions and diluting conditions of the mixture were employed to control the formation of the board (4). The mixture was sucked into the forming machine on a filter, and pressed between copper nets of 80 meshes per sq. inch to get boards with a bulk density of 1.0 to 0.3 g/cm^2 and a thickness of 6.3 mm. The board was cured in a polyethylene film for a determined period. All the procedures above were carried out at a room temperature of 25°C. After the curing the board was dried in an oven for 2 hours at 60°C and after that for 22 hours at 105°C.

Measurement

Bending strength was measured by a strain meter of Toyo Boldwin Tensilon UTM-4LH. The span for the test piece was 10 cm and the width 5 cm. Other conditions were selected after JIS K-6911. The zero span strength of the pulp sheets was measured by the strain meter equipped with parts after TAPPI 231-sm-58. X-ray powder diffraction pattern of the boards and raw materials were measured with a rigakudenki X-ray diffractometer RAD-II at 40 kV and 30 mA for Cu target with a graphite monochrometer. Slits were 1°-1°--0.15 mm with step width 0.02° and preset time 1 s/step. Zeta potentials of pulps and cement were measured with a streaming potentiometer Shimazu ZP-10B. A screening test of the pulp was made after JIS P-8207.

Results and Discussion

One of the typical X-ray diffraction patterns of the pulp cement boards formed from the separated pulps is shown in Figure 1. Those peaks at 2θ = 12.2° and 24.6° were assigned to serpentine, and those peaks at 32.2° and 32.6° are both common to belite and alite of unhydrated cement components. Those peaks at 34.4° and 18.06° are assigned to $Ca(OH)_2$, which resulted from the hydration reaction (5) of cement. Intensity of peaks for alite and belite decreased substantially during the starring process of the cement, which occurred immediately after mixing with water, and a slow decrease of the peak height followed during the hardening process for more than three weeks. For most of the boards the peak height for alite and belite approached to some values in a narrow range of variation as shown in Fig. 2. On the other hand the peak height of $Ca(OH)_2$ at

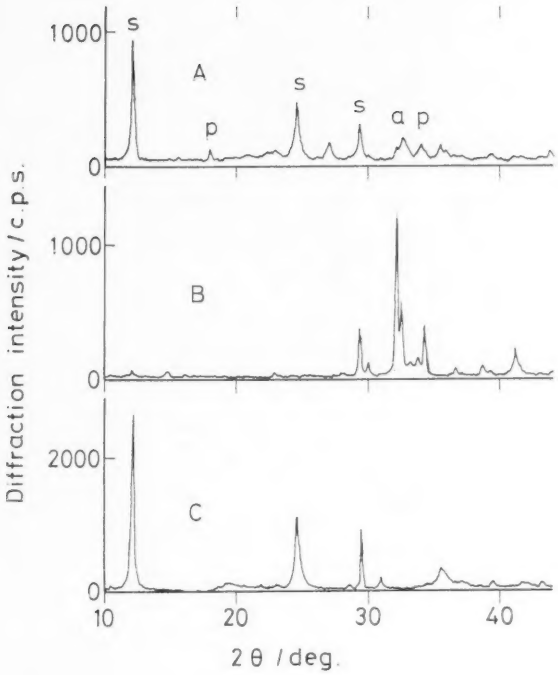

FIG. 1
Characteristic X-ray patterns.
A: Pulp cement board
B: Portland cement
C: Serpentine

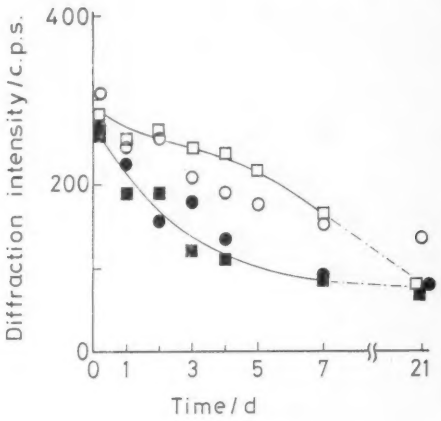

FIG. 2
Diffraction intensity for alite at $2\theta = 32.6°$ during the curing.
○ □ : Board from R.P.
● ■ : Board from B.P.

$2\theta = 18.06°$, which was not observed until 6 hours after mixing with water, increased during the curing preparation conditions. Plots of X-ray diffraction intensity at $2\theta = 18.06°$, which was the strongest diffraction for $Ca(OH)_2$ in the cement board, and the bending strength of the board vs. the curing period are shown in Fig. 3. From the plots it is known that diffraction by $Ca(OH)_2$ is first observed after one day of curing with the board from B.P., whereas in the case of R.P. the diffraction peak was not observed until 2 days after mixing. Also, the diffraction intensity after 3 weeks was higher for boards from B.P. than from R.P. It was also noticed that an increase in bending strength of the boards was observed at the time of curing period, when the diffraction intensity of $Ca(OH)_2$ increased. These facts show that hardening of cement in the board is closely related to crystallization of $Ca(OH)_2$, and the inhibition of the hardening reaction of cement is observed with the use of R.P. Accordingly, the bending strength of the boards from R.P. is lower than that from B.P. This consideration leads to the idea of taking diffraction intensity at $2\theta = 18.06°$ as a diagnostic criterion, by which it should be possible to expect the manifestation of bending strength at the early stage of curing. Bending strength of the board is plotted in Fig. 4 against diffraction intensity at $2\theta = 18.06°$ for all kinds of pulp used. The results show that higher bending strength was observed for the boards with higher diffraction intensity. This shows that hardening of cement in the board is one of the most important factors which affect the bending strength.

Existence of other factors which dominate the bending strength of the boards, could be inferred by comparing the bending strength at the same diffraction intensity of $Ca(OH)_2$. The plots of bending strength vs. diffraction intensity for the boards from F.P., T.P., B.P., and R.P. are shown in Figs. 5 and 6. From the plots it is known that bending strength at a diffraction intensity of

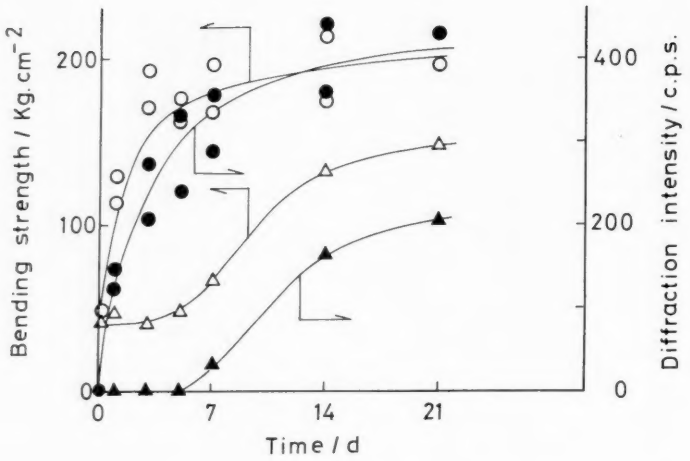

FIG. 3
Diffraction intensity for $Ca(OH)_2$ at 2θ = 18.06° and bending strength during the curing.

△ ▲ : Board from R.P.

○ ● : Board from B.P.

$Ca(OH)_2$ for the boards from R.P. is a little lower than that from F.P. and T.P., whereas that from B.P. is not. These facts suggest the existence of another influencing factor, which give lower strength for the boards from R.P.

Deduction of the influencing factor was made from the result of the tensile test of the board. Different stress-strain curves were obtained (see Fig. 7) for boards with low and high strength. A slow decrease in stress was observed after the yield point for the boards with low strength, whereas a sudden decrease was observed for the boards with high strength board. In accordance with this result, the broken face of the test piece showed a fracture of the cement and pluck out of pulp for the boards with low strength, and cut off the pulp for the boards with high strength as shown in Fig. 8. These features of fracture suggest that tensile strength of the pulp is the second factor for the boards with high strength, whereas for the boards with low strength the second factor can be that which affect the ease of plucking out, namely the fine fraction of pulp, because too short a pulp can not be expected to resist against plucking out, or the adhesive property between pulp and cement.

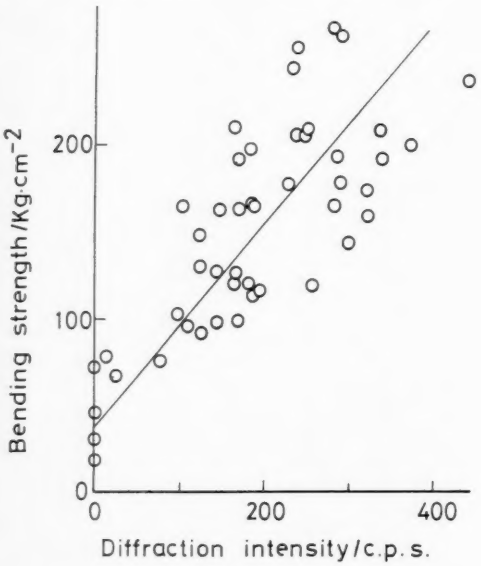

FIG. 4
Diffraction intensity of $Ca(OH)_2$ and bending strength of the board.

The second factor to be discussed as a measure of tensile strength of pulp, is the zero span breaking length of the sheet form from the pulp, be-

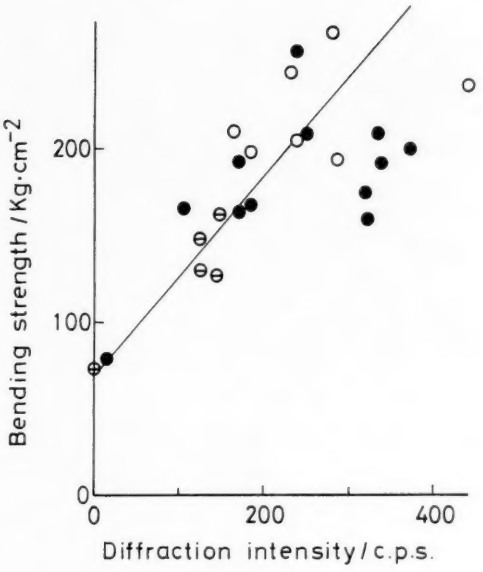

FIG. 5
Diffraction intensity at 2θ = 18.06° and bending strength.
○ F.P., ⊖ T.P., ● B.P.

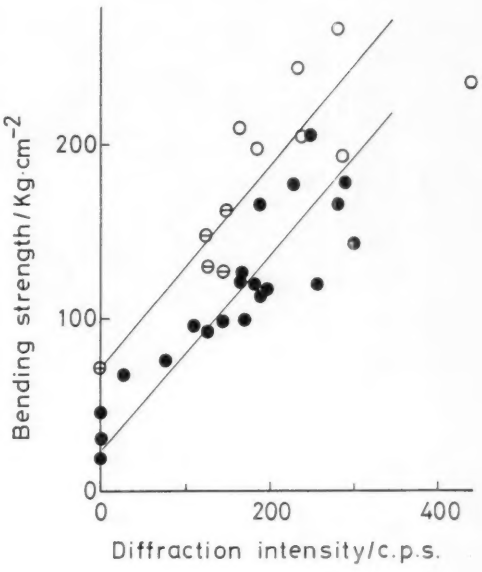

FIG. 6
Diffraction intensity at 2θ = 18.06° and bending strength.
○ F.P., ⊖ T.P., ● R.P.

cause the situation of pulling in regard to the contribution by fiber strength and fine fraction of pulp is similar to tensile test of the pulp cement board. The result of the zero span breaking length test is given in Table 1. The result, in order of strength F.P. > B.P. > R.P. agrees with that of the board at the high diffraction intensity region of $Ca(OH)_2$.

The factor at the low strength region could be discussed by taking as a measure of strength against plucking out the fine fraction (150 meshes pass) of pulp, and as a measure of adhesive property the zeta potential of pulp and cement. The results biven in Table 2 show that fines content of pulps are in reverse order to that of bending strength and that the order of zeta potential is not in a simple relation with that of strength. This result suggests that fines content of pulp is related to the strength of the board at low strength region.

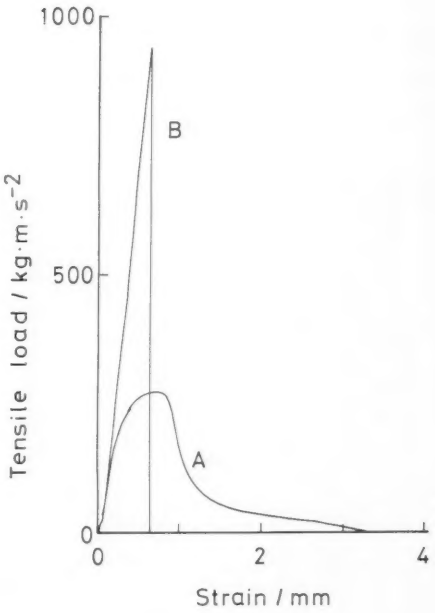

FIG. 7
Tensile test of the board.
A: Curing 2h, strength 49 Kg.cm^{-2}
B: Curing 7d, strength 196 Kg.cm^{-2}

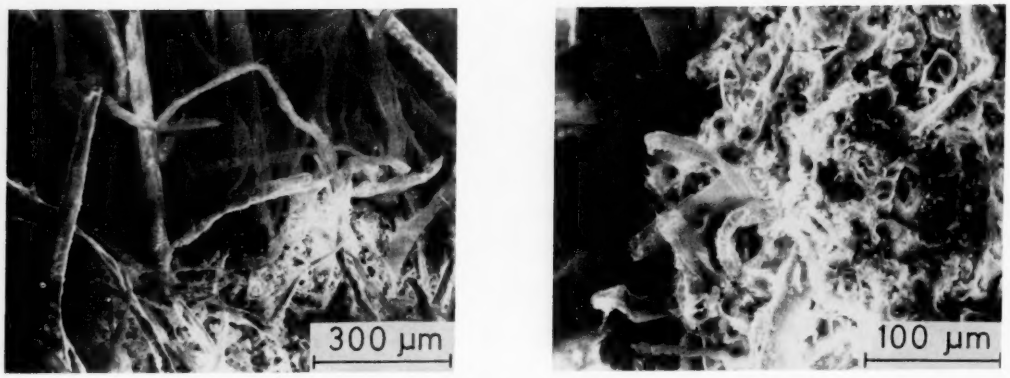

A FIG. 8 B
Fractured section of the boards prepared from B.P.
A: Curing 2h, strength 49 $Kg.cm^{-2}$
B: Curing 7d, strength 196 $Kg.cm^{-2}$

Conclusion

The most important factor which affects the bending strength of the pulp cement board composed of selected pulp from municipal solid waste, is the extent of hardening of cement in the board.

X-ray diffraction intensity of the board for $Ca(OH)_2$ was shown to relate closely to the extent of hardening of cement, and it can be used as a rough criterion for the formation of bending strength of the board at the early stage of curing.

The second factor deduced was the strength of pulp determined by zero span strength of sheet, especially in the high strength region of the board.

Table 1
Zero span breaking length of sheet

Pulp	Zero span breaking length (km)	Coefficient of variation (%)
F.P.	4.72	6
T.P.	4.55	10
R.P.	4.03	7
B.P.	4.81	8

Table 2
Fine fracture and zeta potential of pulp

Pulp	Fine fraction (%)	Zeta potential (mV)
F.P.	18.8	-8.5
T.P.	26.0	-21.1
R.P.	42.1	-4.9
B.P.	22.9	-11.2

References

1. H. Takamatsu, Kogyogijutsu, 20, 52 (1979).
2. T. Sakiyama and H. Nishizaki, Pulp and Paper Engineering 22, 23 (1979).
3. K. Itoh (to Ebara Manufacturing Ind. Co. Ltd.), Japanese Patent Publication 50-136402 (4.10.1974).
4. R. Matsuo, Y. Kobayashi, T. Kitamura, S. Katoh, M. Hirajima, and M. Koga, JAPAN TAPPI 36, 557 (1982).
5. M. Kusunoki, K. Aikawa, and N. Akiyama, J. Asbestos Cement Sheets Soc. Jpn. 22, 26 (1979).
6. M. Hirajima, M. Koga, Y. Kobayashi, and R. Matsuo, JAPAN TAPPI 36, 733 (1982).

VOL. 14 1984

CEMENT and CONCRETE RESEARCH. Vol. 14, pp. 539-545, 1984. Printed in the USA.
0008-8846/84 $3.00+00. Copyright (c) 1984 Pergamon Press, Ltd.

HARDENED PORTLAND CEMENT PASTES, MODELISATION OF THE MICRO-STRUCTURE AND EVOLUTION LAWS OF MECHANICAL PROPERTIES III - ELASTIC MODULUS

J.L. Granju and J.C. Maso
Laboratoire de Génie Civil
de l'Institut National des Sciences Appliquées
et de l'Université Paul Sabatier de Toulouse
(équipe de recherche associée au C.N.R.S. n°998)

(Communicated by M. Regourd)
(Received July 18, 1983)

OL.
14
984

ABSTRACT

This paper is the last one of a series of three (1)(2). It proves that the difference in the evolution laws of the compressive strength R_c and of the elastic modulus E is just apparent. Indeed, on the one hand the micro-structure model developed regarding R_c evolution allows to account for E evolution, its validity is thus strengthened, on the other hand R_c and E both obey laws of the same type, $R_c = R_o e^{-An}$ and $E = E_o e^{-A'n}$.

We show that this dual behaviour is due to the fact that E_o and A' are much more sensitive than R_o and A to the hardening time or the hydration degree. This allows us to forsee the possibility of a selective altering of E and R_c.

Introduction

The elastic modulus E and the compressive strength R_c of Portland cement pastes evoluate differently (see figures 1 and 2).

The physical model of the micro-structure proposed in the first paper of this series (1) and confirmed in the second paper (2) was developed regarding the evolution of the compressive strength. If it also allows to account for the different evolution of the modulus E its validity and its generality will then be definitively proved.

This will be done by showing that, on the contrary of what it looks like, the elastic modulus obeys the law $E = E_o e^{-A'n}$ or $E = \frac{E_o}{e^{A'}} e^{A'K\Gamma}$ of the same type as the strength law $R_c = R_o e^{-An}$ or $R_c = \frac{R_o}{e^A} e^{AK\Gamma}$. The differences between the respective evolutions of E and R_c will be explained.

The notations of these above formulas are the ones of the previous papers (1)(2) of this series or are directly transposed from them, we will just briefly remind them.

- R_c and E : respectively compressive strength and elastic modulus

- n : capillary porosity = 1 - KΓ, K being the swelling of the hydrated grains associated with hydration and Γ being a coefficient characterizing the initial cement-water ratio of the paste.

- A and A' : coefficient characterizing the nature and quality of the contacts between grains participating in, respectivley, the strength R_c and the modulus E.

- R_o and E_o : respectively the compressive strength and the elastic modulus of a, theoretical, zero capillary porosity paste. As R_o is roughly constant, E_o varies in a wide range (3), from the modulus E_a of the anhydrous part of the hydrated grain to the modulus E_g of the hydrated part, so called gel, ($E_a >> E_g$). The higher is the hydration degree, the lower is E_o.

Results

This paper is based on the use of the results of two different series of tests. On one hand on the series of tests dealt with in the first paper (1) (figures 1 and 2) giving the values of R_c and E. These were measured simultaneously and the comparison of their evolution is pertinent. On the other hand on the tests dealt with in the second paper (2) giving the value of the hydration degree m versus Γ and the hydration time (figure 3).

These two series of tests having been performed on pastes of the same cement, molded and cured in the same conditions, we admitted that the hydration degrees measured in the second series were a good approximation of what they were in the first series. The hydration degrees so accounted for allow to calculate the corresponding values K of the swelling. That for, we use the relation $K = m(K_g - 1) + 1$ in which K_g, actual swelling of the hydrated matter, is constant as soon as the hardening time exceeds a few days (with the cement concerned $K_g \simeq 2.15$)

Discussion

The most striking difference between the evolutions of R_c and E is that the separation of pastes into two groups of separate behaviour (1), manifest on the graphs $R_c = f(\Gamma)$ and $\text{Log } R_c = f(\Gamma)$ is invisible on the graphs $E = f(\Gamma)$ and $\text{Log } E = f(\Gamma)$ (figures 1 and 2).

The case of pastes hardened for an infinite time was dealt with in a previous paper (3). We showed that the modulus E_a of the anhydrous part of hydrated grains is much higher than the modulus E_g of gel ; hence the modulus E_o of the hydrated grain increases as the hydration degree decreases.

The pastes of $\Gamma \geq \Gamma_p$ have a constant capillary porosity, equal to zero. Their strength R_c is constant but, Γ increasing, their hydration degree decreases (figure 3) and E_o increases. This is consistent with the noticed increase of E and the proposed law $E = E_o\, e^{-A'n}$. On another hand, after infinite hardening time, the nature and efficiency of the contacts from grains to grains being expected constant and characterized by the minimum values of A and A', this increase of E must be attributed only to the variation of E_o. The measured values of E_a and E_g show that this is possible. The value of E_o is linked to E_a et E_g by a relation of the following type : $E_o = \dfrac{E_a V_a + E_g V_g}{V_a + V_g}$

V_a and V_g being the respective volumes of anhydrous material and of gel.

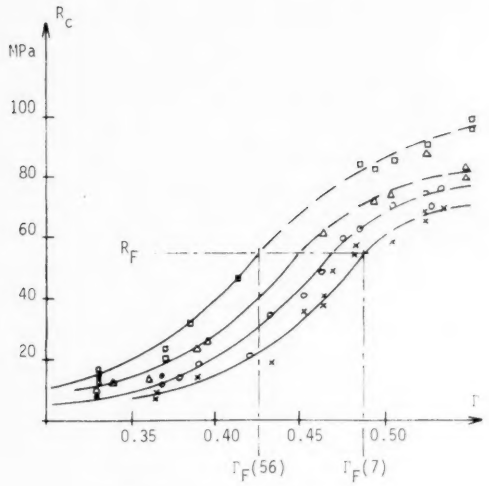

a - compressive strength R_c versus cement-water contents Γ.

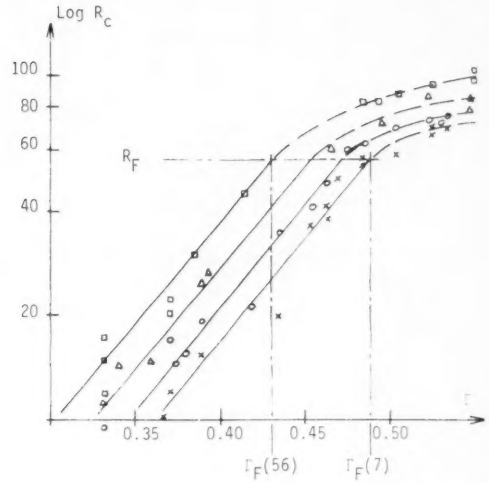

b - Log of compressive strength R_c versus cement-water contents Γ.

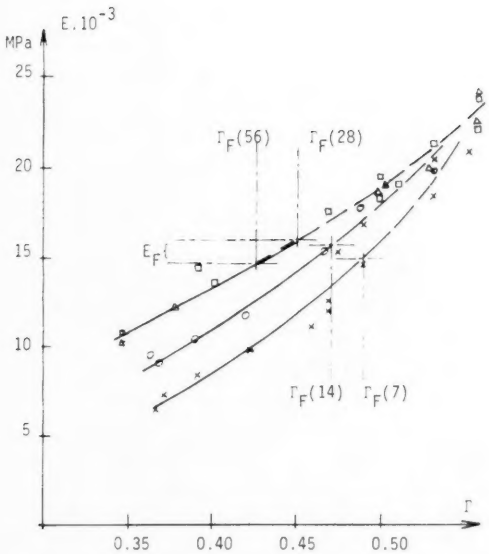

a - elastic modulus E verus cement-water contents Γ.

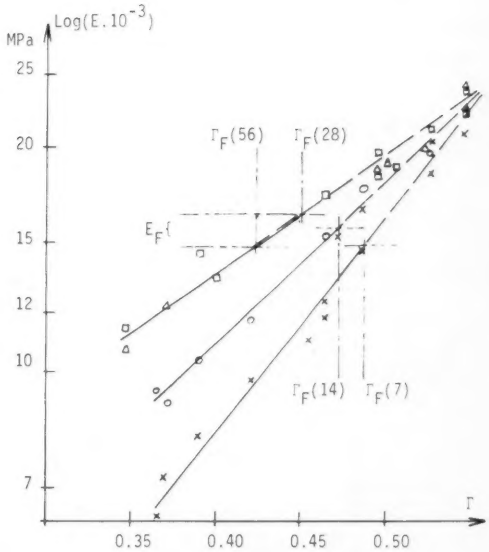

b - Log of elastic modulus E versus cement-water contents Γ.

hardening times : × 7days ○ 14 days △ 28 days □ 56 days

FIG.1
Compared evolutions of R_c and E, finite hardening times

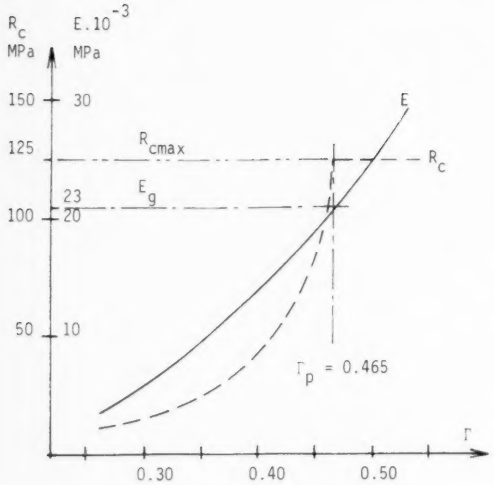

compressive strength R_c and elastic modulus E versus cement-water contents Γ.

FIG.2
Compared evolutions of R_c and E, infinite hardening time

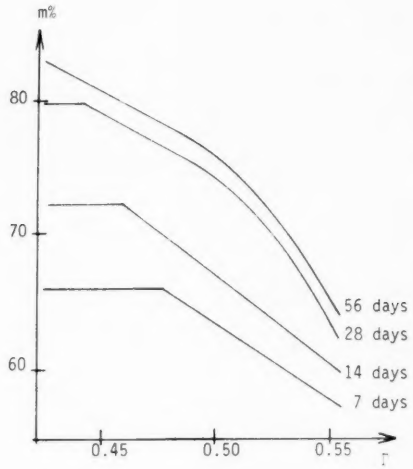

hydration degree m versus cement-water contents Γ.

FIG.3
Hydration degrees accounted for

For an initial anhydrous volume = 1 it follows $V_a = 1 - m$, $V_g = m.K_g$ and at last $E_o = [(1 - m)\ E_a + mK_g\ E_g] / [m\ (K_g - 1) + 1]$

The case of pastes hardened for finite times is more complex, E_o and A' vary together. We will isolate the relative incidence of the variations of E_o and A' upon the value of E and prove the pertinence of the law $E = E_o e^{-A'n}$ and of the model of the micro-structure derived from the compressive strength study.

Value of E at the boundary between the first and the second group

This boundary is invisible on the graphs $E = f(\Gamma)$ and $\text{Log } E = f(\Gamma)$, for each hardening time considered the corresponding value $\Gamma_F(t)$ of Γ is read on the graphs $R_c = f(\Gamma)$ (figure 1), (1). Besides, the curves $m = f(\Gamma)$ of the figure 3 show that the corresponding hydration degree increases from ≃ 65% at 7 days to ≃ 83% at 56 days. With that it must be associated a noticeable decrease of E_o which must at its turn have effects on the value of E ; for the infinite hardening time, the hydration degree varying from 72% to 90% (as Γ decreases from 0,55 to 0,49) and at constant porosity (n = 0), the modulus E decreases from ≃ 31.10^3 MPa to ≃ 23.10^3 MPa (figure 2).

This boundary between the first and the second group corresponds to a unique value n_F of the capillary porosity. If the variation law expected for E is pertinent, the corresponding value is $E_F = E_o\ e^{-A'n_F}$; at constant porosity ($n = n_F$) the decrease of E_o as hardening time increases must lead to a noticeable decrease of E.

On the figures 1 and 2 one notes that it is not the case. For the considered hardening times E_F is roughly constant.

This can be explained by a large variation of A' compensating the effects of E_o variation. Indeed the curves Log E = f(Γ) of figure 2 show that the product A'K decreases as the hardening time increases.

Hence, as considering the strength R_c one can write AK = Ct = J, considering the modulus E the product A'K is no longer constant ; the hardening time increasing, A' decreases drastically, at a much higher rate than K increases. That may explain the apparent steadiness of E_F.

Curves Log E = f(KΓ) (figure 4)

The proposed variation law can be written as well Log E = (Log E_o-A')+A'.(KΓ). The separation into the first and the second groups then is clearly visible, but, on the other hand these curves are not arranged in accordance with the increasing hardening times.

In the first group

These curves are straight lines. This implies that, for each hardening time considered, A' and E_o are constant, they can be labelled A'(t) and E_o(t). According to our previous study of the strength R_c, we know that, in the first group and for each hardening time the nature and efficiency of the contacts from grains to grains is constant, hence A and A' = Ct, as well as the hydration degree m is constant and, extrapolating the results obtained for infinite hardening time we note that $E_o \simeq \frac{(1-m)\ E_a + m\ K_g\ E_g}{m\ (K_g-1) + 1}$ = Ct. The fact that these last conclusions are consistent with the experimental results implies that, on one hand the law $E = E_o\ e^{-A'n}$ is applicable to the first group pastes, on the other hand, for a given cement and for the hardening times considered here, E_o varies only with the hydration degree.

The variation law being applicable, these straight curves are such as their slope is A'(t) and their ordonate at the absciss KΓ = 1 is E_o(t). These values so read confirm that A'(t) and E_o(t) decrease strongly when hardening time increases.

In the second group

The curves show a strong concavity turned towards the positive values of E. For each hardening time, the hydration degree decreasing as Γ increases (figure 3), E_o and consequently E increase. This, nevertheless is not enough to state that in the second group the noticed evolution of E is due only to the variation of E_o. Concurrently A' may vary as well and have a noticeable influence.

Curves Log $E_{corrected}$ = f(KΓ) (figure 5)

$E_{corrected}$ is fictitious, it represents what the elastic modulus would be if E_o was constant. By this artifice the curves Log $E_{corrected}$ = f(KΓ) are turned unconnected with the variations of E_o, they are then much appropriate to show the variations of A'.

To draw these curves we chose E_o = Ct = E_g of 100% hydrated pastes, i.e. E_o = Ct = E_g. For a given value of KΓ, and consequently of n, one can write, according to the variation law $E = E_o e^{-A'n}$ and according to its definition $E_{corrected} = E_g e^{-A'n} \simeq E.\frac{E_g}{E_o}$. Lacking more precise information the calculation of E_o was based on the relation proposed for infinite hardening time and

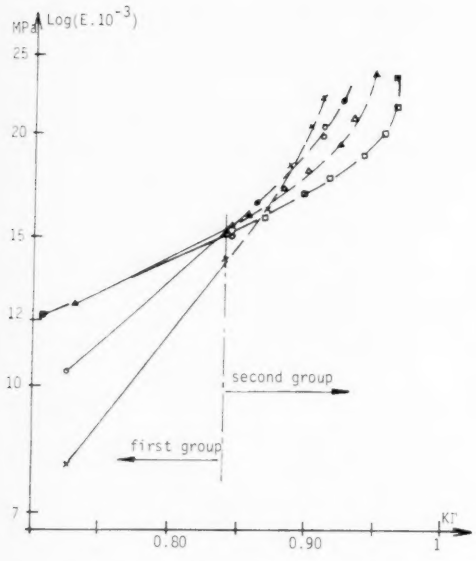

FIG.4
Log of elastic modulus E versus KΓ (KΓ equals 1 - capillary porosity).

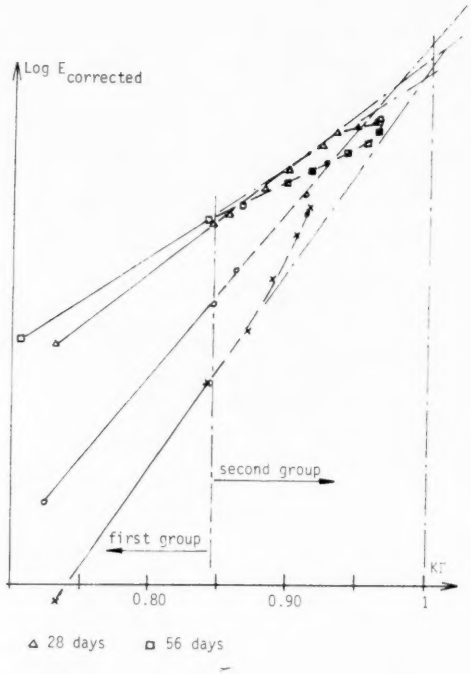

FIG.5
Log of corrected elastic modulus versus KΓ

on the associated values of E_a and E_g : $E_a \simeq 90.10^3$ MPa and $E_g \simeq 21.10^3$MPa
One notes that the curves $E_{corrected} = f(K\Gamma)$, built as explained above, are perfectly arranged according to the increasing hardening times.

In the first group

The curves are straigth lines, the continuation of which being nearly concurrent at the absciss KΓ = 1. This confirms with no doubt the validity of the evolution law $E = E_o e^{-A'n}$ or $E = \frac{E_o}{e^{A'}} e^{A'K\Gamma}$ associated with the fact that, for a given cement, E_o varies only with the hydration degree m. The good arrangement of the curves is a consequence of both that fact and the already confirmed evolution of A'.

In the second group

The strong increase of E is no longer visible. Therefore the variation of E_o with hydration degree is the main cause of the sharp curvature of the curves Log E = f(KΓ) in the second group. The large uncertainty affecting the values of $E_{corrected}$, due to the incertainties effecting the value of m, the characteristics of the actual relation $E_o = f(E_a, E_g)$ and the values of E_a and E_g, does not allow us to enter into further details.

Conclusion

The model proposed for the micro-structure of APC pastes allows to account for the much different evolutions of their compressive strength and of their elastic modulus, it is definitively confirmed. As generally accredited for other porous materials the elastic modulus and the compressive strength of pastes obey evolution laws of the same type. They are respectively written

$E = E_0 e^{-A'n}$ and $R_c = R_0 e^{-An}$.

Here finishes the analogy. As R_0 = Ct, E_0 sharply decreases when the hydration degree increases. Although A and A', characterizing the nature and the efficiency of contacts from grains to grains, both decrease when hardening time increases, A varies very little and can often be considered as steady, the large variation of A' has a major influence upon the evolution of E.

That has an important incidence on practice. Comparing two pastes of the same capillary porosity, they have compressive strengths of the same order of magnitude, on the contrary their elastic moduli have no reason to be alike. This is clearly illustrated on the graphs Log E = f(KΓ) of figure 4, the pastes of equal capillary porosity being characterized by an equal value of KΓ. The converse is still more important. Two pastes showing equal values of modulus E have no reason to have strengths of the same magnitude.

Consequently, in the case of hardened Portland cement pastes, any indirect measurement, through the measure of the elastic modulus or through a measure depending on the value of the elastic modulus, intending to give an information about the strength R_c or only its evolution is reliable only in a strictly bounded field, often quite narrow. The evolution of E reflects that of R_c only when E_0 and A' remain constant, i.e. in the case of the first group pastes for a given hardening time and a given curing mode.

This study shows as well that the elastic modulus is much more sensitive than the compressive strength to the hydration degree and the nature of contacts from grains to grains. This allows us to foresee the possibility of a selective altering of E and R_c, in order to improve the mechanical response of the paste in the desired way.

References

1. J.L. Granju and J.C. Maso. Cem. Conc. Res. 14, 249-256 (1984).
2. J.L. Granju and J.C. Maso. Cem. Conc. Res. 14, 303-310 (1984).
3. J.L. Granju and J.C. Maso. Cem. Conc. Res. 10, 731-738 (1980).

VOL. 14 1984

CEMENT and CONCRETE RESEARCH. Vol. 14, pp. 546-558, 1984. Printed in the USA.
0008-8846/84 $3.00+00. Copyright (c) 1984 Pergamon Press, Ltd.

THE PENETRATION OF CHLORIDES INTO HARDENED CEMENT PASTES

H G Midgley and J M Illston
Concrete Research Laboratory, Civil Engineering Division
The Hatfield Polytechnic, Hatfield, Herts, U K

(Communicated by C.D. Pomeroy)
(Received Sept. 19, 1983)

ABSTRACT

The penetration of chloride ions into hardened cement pastes (hcp) has been measured by chemical analysis, X Ray diffraction and thermal analysis. The penetration of chloride depends on the permeability; thus the greater the w/c ratio the greater is the penetration.
The concentration of chloride in the hcp is dependent on the concentration of the surrounding solution.
The chloride ions react with the anhydrous tricalcium aluminate in the unhydrated cement left in the hcp but not with the complex hydrated calcium aluminate salts including ettringite.
Calcium mono-chloroaluminate hydrate is formed, but not all the chloride which penetrates reacts to form this mineral. The quantity of chloroaluminate formed is independent of the chloride concentration in the hcp.
From a study of the pore size distribution of the hcp by mercury intrusion porosimetry it is deduced that the penetrating chloride reduces the sizes of the small pores thus reducing the permeability.

VOL
14
198

Introduction

Calleja (1) in his principal report to the Paris Congress on the Chemistry of Cement on the durability of concrete discussed the attack by chlorides on cement paste, especially added calcium chloride or sodium chloride as de-icing salts. He reported that the action of concentrated chloride solutions altered the physical structure of the hardened cement paste (hcp) by lowering the evaporable water contents by osmotic pressure action with a concomitant increase in strength, and additionally by a chemical change in which the calcium monochloroaluminate hydrate $C_3A\ CaCl_2 10H_2O$ is formed.

Collepardi et al (2) reported that the attack of chlorides proceeds by ionic penetration, that it follows Fick's diffusion law, and that it is independent of chloride concentration.

Gjorv and Vennesland (3) showed that for ordinary Portland cements time is the governing factor for the chloride penetration although the w/c ratio also influences the surface layer penetration.

Ushiyama et al and Page et al (4,5,6) determined the relative diffusion coefficients of sodium, potassium, lithium and chloride ions through hcp and found that the diffusion coefficient of chloride anions is much greater than the values for the cations, indicating the electropositive character of the hcp when considered as a semipermeable membrane.

Richartz (7) reported that during the hydration of Portland cement in the presence of chlorides ettringite is always formed first, until all the gypsum is used up, then the calcium monochloroaluminate hydrate is formed; so ettringite is the more stable phase.

Regourd et al (8) found that when chloride ions penetrate hcp the initially fibrous C-S-H is changed to a reticulated morphology.

Verbeck (9) found a considerable difference in behaviour of different cement pastes when exposed to sea water attack. He found that for reinforced concrete specimens subjected to long term tests in sea water, an increase in the C_3A content reduced the level of cracking observed. He also found that sulphate resisting Portland cements with C_3A contents between 2 and 5% are 5 times as vulnerable to cracking due to steel rusting as cements with 8 to 11% C_3A.

No detailed study has been reported on the changes in the microstructure of hcp produced as a result of sodium chloride penetration. This report investigates the rate of penetration of chloride ions, the effects on the minerals and on the micropore structure.

Experimental

Samples of hardened cement pastes (hcp) were made using a cement of potential compound composition C_3S 64, C_2S 13, C_3A 6.8, C_4AF 7.3, $CaSO_4$ 3.6% and a fineness of 348 m^2/kg. Water:cement ratios (w/c) of 0.23, 0.47 and 0.71 were used; the cement and distilled water were weighed and hand mixed before rotating in a glass pot for times of between 2 hours for the specimens of w/c 0.23 to 6 hours for the specimens of w/c 0.71. When the samples were homogenised they were introduced into plastic tubes 23 mm diameter by 70 mm high. The tubes were then rotated at about 1 rev. per sec. for a further 24 hours at a temperature of $21 \pm 1^{o}C$, then demoulded and stored for 1 month in a saturated solution of $Ca(OH)_2$ also kept at $21 \pm 1^{o}C$.

After this initial conditioning the cylinders were removed from the $Ca(OH)_2$ storage and forced into undersized rubber tubes of 20 mm diameter; one end of the sheath was sealed with a rubber bung and further sealed with silicone rubber. The free end was lightly ground to remove calcium hydroxide bloom.

Three cylinders of the hcp of each w/c ratio were placed in one of the following conditions, all at $21 \pm 1^{o}C$: (i) a fresh solution of $Ca(OH)_2$, designated W; (ii) a solution of sodium chloride containing 30g/litre NaCl, equivalent to sea water concentration, designated S; and (iii) a solution containing 150g/litre NaCl designated 5S. These solutions were replenished at 6 months.

At 6 months and 1 year one of the appropriate cylinders was removed from storage, demoulded and split into five approximately equal minicylinders, each 14mm high designated 1 to 5, top to bottom. At 6 months no special precautions against carbonation were taken, at 1 year all the handling took place in a CO_2 free glove box.

The thermal analyses were carried out on a Stanton-Redcroft Derivative Thermogravimetric Analyser (TG750). About 20mg of the ground hcp was used as the sample. Two techniques were used, firstly normal DTG heating at

20°C/min. from 2° to 1005°C and secondly semi-isothermal DTG (10) where on reaching a peak maximum the heating was switched from programmed heating at 20°C/min. to isothermal and held there until the derivative trace had returned to the base line. The presence of calcium hydroxide, calcium carbonate, C_4AH_{13}, C_2AH_8, $C_3A.CaSO_4 12H_2O$ and C_3AH_6 were detected by the semi-isothermal method. Where possible the apparatus was calibrated by runs with synthetic preparations. For quantitative estimates of those minerals it has been assumed that they are present in the pure form and that the weight loss as recorded on the T.G. is that which is present as water of crystallisation, hydroxyl or carbonate in the empirical formula. No specific peak temperatures for each compound were found but the order in which the responses occurred were for C_4AH_{13} (and carbonated species), $C_3A.CaSO_4 12H_2O$, C_2AH_8, C_3AH_6, $Ca(OH)_2$ and $CaCO_3$.

No reasonable method is available for the determination of the quantity of C-S-H present in an hcp, so some semi-quantitative estimate has been attempted. It was observed that, both for synthetic C-S-H and natural plombierite from Scawt Hill, after the initial weight loss due to adsorbed water at less than 110°C, there was a gradual weight loss up to 1000°C. This continuous weight loss had been noted by Taylor (11).

To make an estimate of the quantity of the calcium hydrosilicate in the hcp the residual weight loss between 3° and 1000°C, after accounting for the known crystalline phases, and adsorbed and capillary water occurring at temperatures below 100°C, was assigned to the calcium hydrosilicate. The weight of this phase was calculated from a composition of $1CaO\ 1SiO_2 2.5H_2O$. This method although fraught with inaccuracies is the best estimate available and will represent differences between samples with some degree of reliability.

Calcium hydroxide, calcium carbonate and 'dry weight' were all determined from the weight losses at about 500, 950°C, and the total weight loss at 1000°C. The X-ray diffraction data were obtained on a photographic film Guinier focussing camera using Copper K alpha radiation generated at 40Kv and 40ma. The diffraction maxima were measured from densitometric traces obtained from a Joyce-Lobel Chromoscan.

The Chung (12) technique for QXRD was used, with calcium hydroxide from the hcp as the internal standard. Calibration mixtures of hcp with added synthetic $3CaO.Al_2O_3\ 3CaSO_4\ 32H_2O$ and $3CaO.Al_2O_3.\ CaCl_2 12H_2O$ were used with characteristic reflections at 9.7 and 8.9Å.

The chemical analysis for chloride content was by means of Quantab (TM) chloride titrators. An appropriate weight of the ground hcp (0.5 to 1g) was dissolved in 50ml of $0.1NHNO_3$, the solution neutralised with anhydrous sodium carbonate to a pH greater than 8 and then tested for chloride content. The titrators were calibrated with solutions containing 0.5708 and 1.007g NaCl per 1000ml. The results agreed with the calibration tables supplied by the manufacturers to ± 0.001% NaCl. The experimental variability was estimated by repeating the determination eight times with the solution of NaCl containing 0.5708g/1000ml. This estimate gave an average result of 0.5725g/1000ml, with a standard deviation of 0.0012 giving a coefficient of variation of 2%.

In this report the quantity of chloride found is given to ± 0.005%, well within the experimental variability.

The pore size distributions in the range 75,000 to 40 Å pore radii were determined using a mercury intrusion porosimeter (Carlo Erba Series 200). All the samples were predried in vacuum at 105°C.

VOL. 14 198

The pore radii were calculated from the Washburn equation $r = 2\gamma \cos\theta/P$, where r is equivalent radius in Å, P is pressure in Kg/cm^2, θ the contact angle for mercury, here taken as 140° (see (14)), and γ the surface tension of $0.48N/mm^2$. Using these values for θ and γ the relationship for r reduces to $r = 75{,}000/P$.

To plot the pore size distribution, differences in pore volume per unit weight (dv/g) were determined for equal differences of unity in log radius (d ln r).

The small pores were measured using nitrogen adsorption and desorption isotherms obtained from a Carlo-Erba Sorptomatic 2000 apparatus. The specimens were dried in a similar manner to that used for mercury intrusion porosimetry.

The pore size distribution was obtained from the desorption branch of the isotherm using the relationships

$$R_p = (R_k + t)$$

where

$$t = \sqrt[3]{\frac{-172.6}{\log P/Po}} \quad \text{and} \quad R_k = -4.14/\log P/Po$$

and P/Po = desorption relative pressure, R_k = apparent pore radius and t = thickness of multimolecular layer of nitrogen proportional to P/Po.

Results

Mineralogy

The quantities of calcium hydrosilicate and calcium hydroxide varied little with chloride penetration but did vary with w/c ratio and age of curing. Table 1 gives a summary of the results. Calcium carbonate did vary since at 6 months no protection against CO_2 was provided while at 1 year all samples were handled in a CO_2 free environment.

The dry weight % of the complex calcium aluminate hydrate salts other than ettringite or the chloroaluminate salt are given in Table 2, from which it may be seen that the penetration of chloride has no effect on the quantities of those compounds. The average standard deviation of the determination was 0.5.

The results of the determination of ettringite are given in Fig.1.

It can be seen that storage in sodium chloride solution has no effect on the quantity of ettringite present.

The quantities of the monochloroaluminate hydrate $C_3A.CaCl_2.12H_2O$ formed by storage in sodium chloride solution are given in Fig 2. As would be

TABLE 1

Average dry weight % of calcium hydrosilicate, $Ca(OH)_2$ and $CaCO_3$ for hcps of different w/c ratio at 6m and 1y, for specimens stored in water, top 14 mm

w/c	age	calcium hydrosilicate	$Ca(OH)_2$	$CaCO_3$
0.71	6m	26.7	29.6	11.6
0.71	1y	39.4	30.5	0.3
0.47	6m	29.8	23.7	7.9
0.47	1y	32.8	24.6	0.0
0.23	6m	27.5	12.8	3.6
0.23	1y	26.6	15.0	0.0

VOL.
14
984

TABLE 2

Dry weight percentage of calcium aluminate hydrates in hcp wt % of mineral for specimens with w/c ratios 0.71, 0.47 stored in water, " sea water" and "5 times sea water", top 14 mm

hcp mark	C_4AH_{13}	$C_3A.CaSO_4 12H_2O$	C_2AH_8	C_3AH_6
0.71/W	2.6	3.2	2.3	2.6
0.71/S	1.9	2.8	2.5	3.4
0.71/5S	2.2	3.0	2.5	5.2
0.47/W	2.9	2.7	2.5	3.6
0.47/S	2.7	3.6	2.8	3.5
0.47/5S	2.5	3.4	3.6	3.9

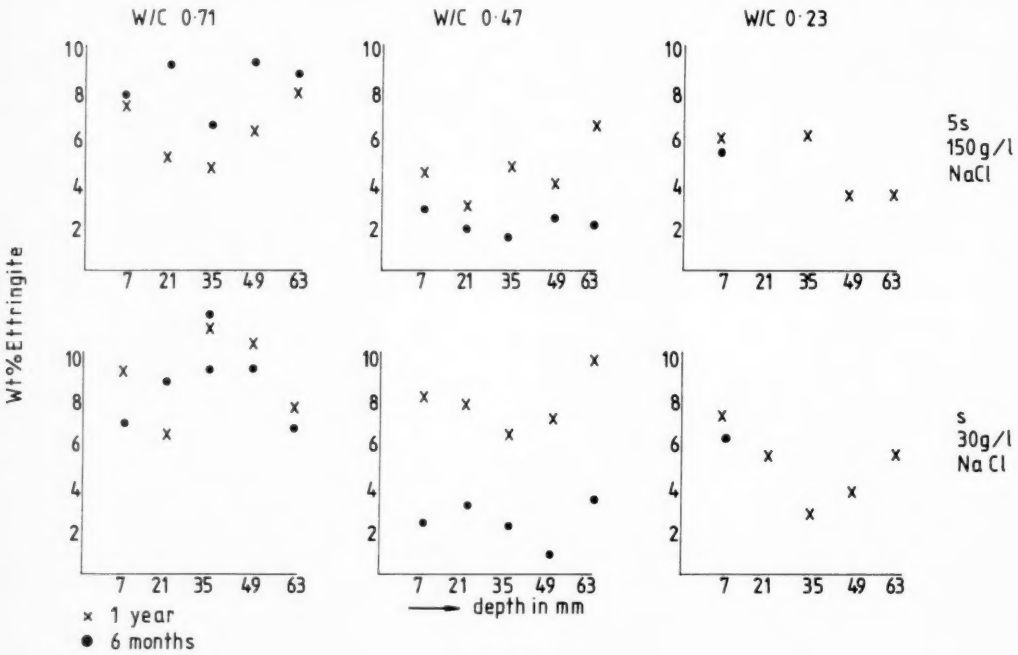

FIG 1

Quantity of ettringite in hcp of various w/c ratios at different depths of cylinder when exposed to sodium chloride solutions.

expected the quantity of the chloroaluminate decreases with depth of penetration of the chloride ions. It is also seen that as the permeability increases with increasing w/c ratio more chloroaluminate is formed. However the concentration of the solution in contact with the hcp has little or no effect on the quantity of chloroaluminate formed. From this it is suggested that the governing factors in chloroaluminate formation are the mineral composition of the cement used and its physical structure.

The evaporable water content i.e. the wt per cent loss at less than 105°C has been determined for the specimens stored for 1 year and are given in Table 3.

VOL 14 198

TABLE 3

Evaporable water content of hcp specimens at 1 year for specimens w/c 0.23, 0.47 and 0.71, stored in water, "sea water" and "5 times sea water", top 14mm

Mark	Average wt loss
0.23/W	9.94
0.23/S	11.64
0.23/5S	10.09
0.47/W	22.22
0.47/S	22.44
0.47/5S	21.88
0.71/W	36.45
0.71/S	34.27
0.71/5S	35.10

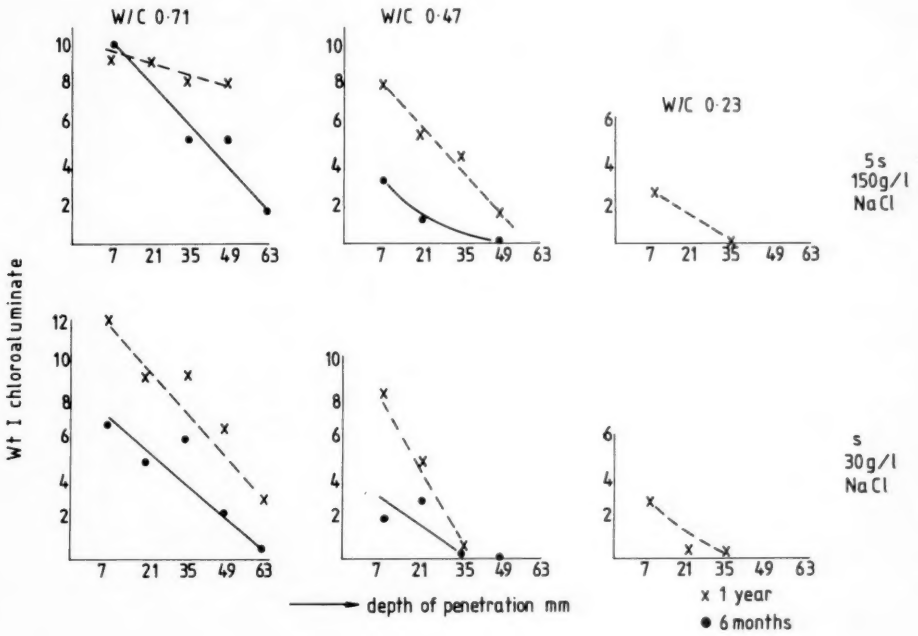

FIG 2

Quantity of calcium monochloroaluminate in hcp of various w/c ratios at different depths of cylinder when exposed to sodium chloride solutions

It can be seen that chloride penetration does not alter the evaporable water contents, in contradistinction to the effects observed by Calleja (1) when using chlorides in the mixing water.

Chemical Analyses

The analyses for total chloride in hcps are summarised in Fig 3. The penetration of total chloride is exponential with depth and the concentration may be represented by the equation $C = kd^{-m}$, where d is distance (mm) into the cylinder, k a constant reflecting the depth of penetration and m the slope of the curve.

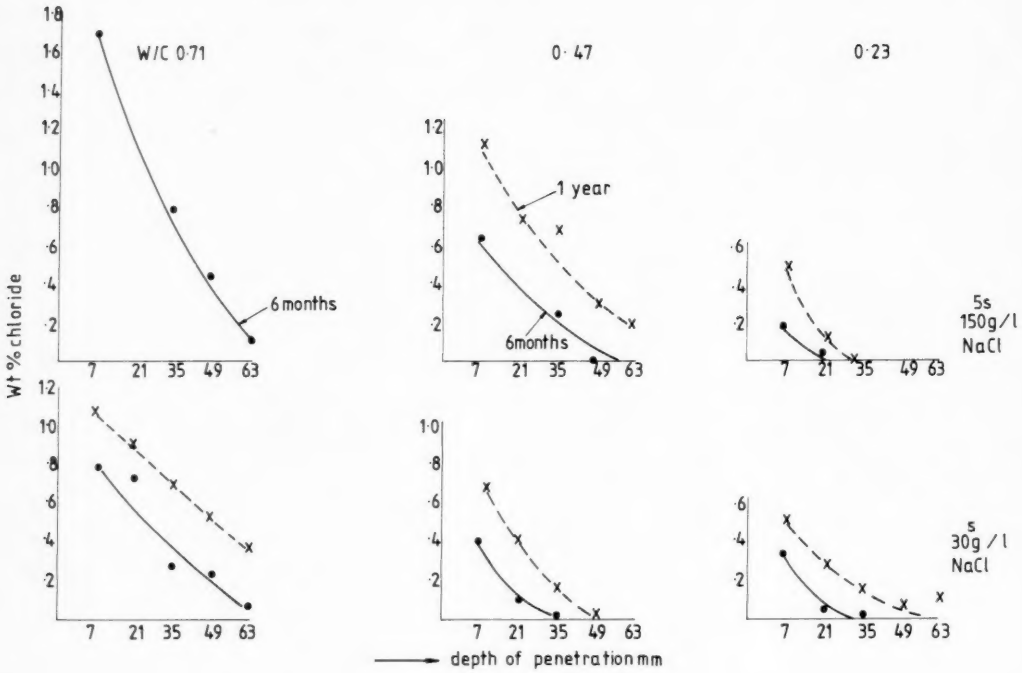

FIG 3

Quantity of chloride found in hcps of various w/c ratios at various depths after exposure to chloride solutions

Table 4 gives the data for the specimens at 6m and 1 year. The average correlation coefficient was 0.81.

TABLE 4

Penetration of chloride ions into hcp

	at 6m		at 1y	
Mark	k	m	k	m
0.23/S	17.3	0.08	6.07	0.09
0.23/5S	22.4	0.10	12.70	0.02
0.47/S	27.6	0.68	17.50	0.09
0.47/5S	27.6	0.42	13.29	1.09
0.71/S	27.6	0.75	15.84	1.02
0.71/5S	27.6	0.65	+	+

+ data unreliable - seal at bottom of cylinder sheath breached.

The diffusion coefficients, Table 5, may be calculated from the quantity of chloride ions present at the distance of penetration and the relationship:-

$$D_{C1} = -\frac{1}{2t} \cdot \frac{dx}{dc} \int_0^{C_1} x\,dC$$

where D_{C1} is the diffusion coefficient at the maximum concentration, x is the distance (mm) from the boundary, and t is the time in seconds. $\frac{dx}{dc}$ is

calculated from the tangent of the slope of the plot of chloride concentration v distance and $\int_0^{C_1} x\,dC$ from the area under the same curve.

TABLE 5

Diffusion coefficients ($cm^2/sec \times 10^{-8}$) for chloride ions into hcp

Mark	6 months	1 year
0.23/S	0.12	0.56
0.23/5S	0.38	0.65
0.47/S	0.68	0.85
0.47/5S	1.17	2.30
0.71/S	2.31	2.17
0.71/5S	7.32	2.70*

* data unreliable due to breach of seal at bottom of specimen

VOL. 14 984

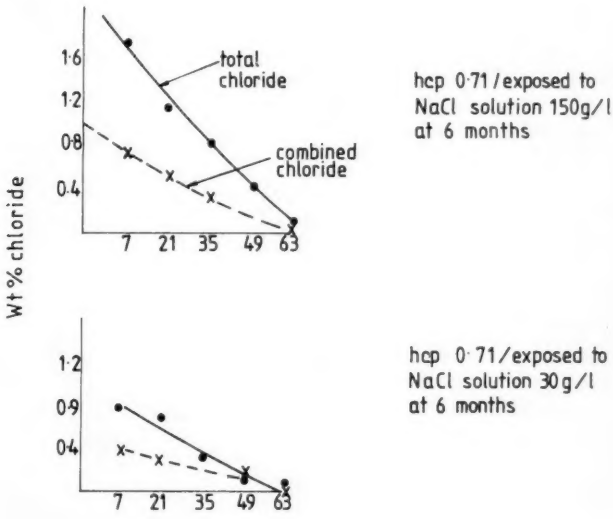

FIG 4

Quantities of total and combined chlorides for various depths in hcp w/c 0.71.

Two types of chloride were found; (a) bound in the monochloroaluminate and (b) free, given by the difference between the total chloride (Fig 3) and that calculated from the stoichometry of the chloroaluminate. It was found that there was always free chloride present, Fig 4. From these curves it can be seen that the quantities vary sympathetically indicating that the quantity of chloride reacting is concentration dependent.

Pore size distribution

The pore size distributions for all the specimens of hcp were determined by mercury intrusion porosimetry; the results in the range 100 - 1000Å pore radii are given in Figs 5 a,b,c and 6 a,b,c, for the top 14mm of the cylinders.

As previously stated, the specimens used for mercury intrusion porosimetry (mip) were prepared by drying in vacuum at 105°C. It is realised that this method may alter some of the pores but from the work reported earlier by the authors (14) it is considered that the method of drying has little or no effect on pores of radii greater than 100Å. It is also realised that mip

FIG 5

Pore size distribution in top 14 mm of cylinder of hcp after 6m curing in water w and sodium chloride solutions (S and 5S)

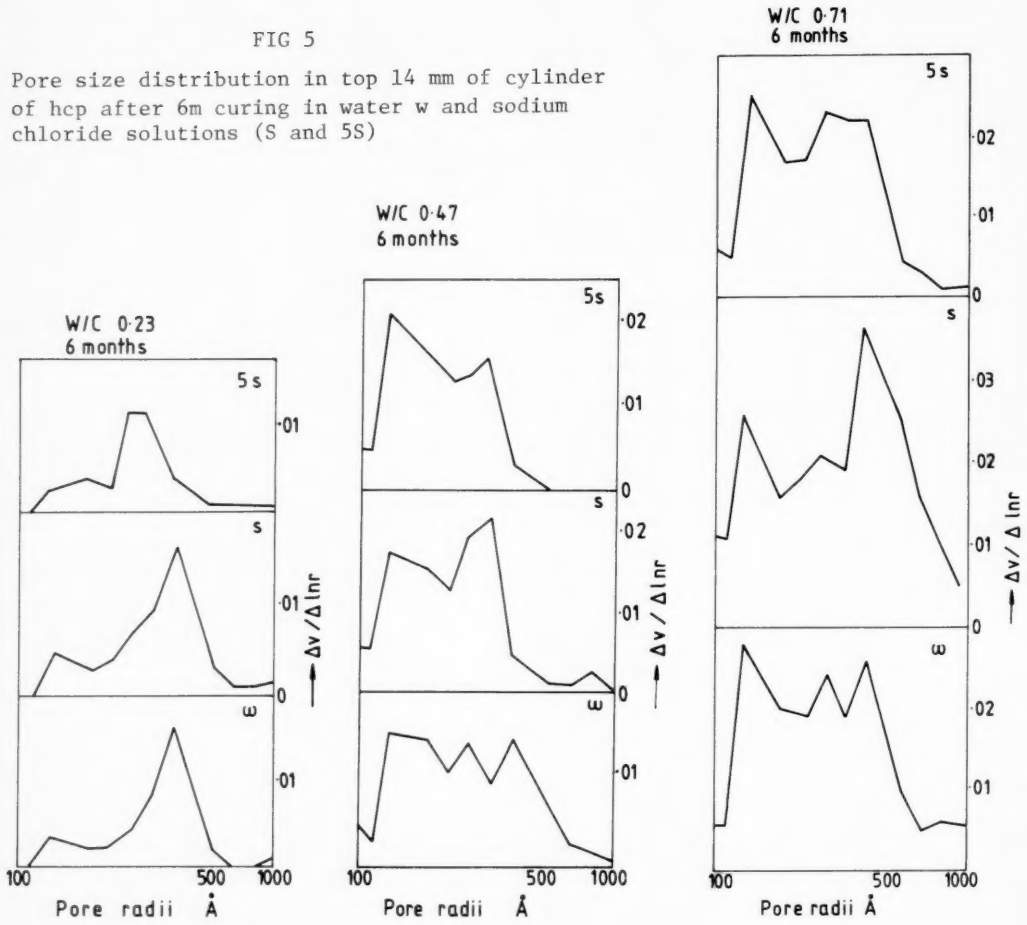

may or may not measure the true diameter of a spherical void but may measure the diameter of the entrance radius; however some allowance is made for this effect by the delay introduced automatically in the method of measuring the intruded value at any pressure. As differences are considered here and not absolute sizes it is thought that the methods employed provide reliable data to support the changes suggested resulting from the chloride penetration of hcp.

The pores in the range 10 to 1000Å were measured by nitrogen adsorption porosimetry for three samples of hcp as shown in Fig 7. The results seem to indicate a very large increase in the 20Å pores with chloride penetration, although the total porosity in this range changes only from 51.8 to 53.8m^2/g. Since there is a considerable change in the surface area with pores of 20Å pore radii there must be a compensating diminution of pores in the region 30 - 1000Å radii; however mercury intrusion porosimetry, Fig 6(c) does not show such a change in this region. The authors have shown (14) that in this region the two methods give comparable results for specimens treated in the way reported here. It is therefore concluded that there must be another effect altering the pore distribution at 20Å as found in the nitrogen adsorption technique. It is suggested that something is interfering with the monolayer of nitrogen being formed and so with the interpretation of the

FIG 6

Pore size distribution in top 14 mm of cylinder of hcp after 1 year curing in water w and sodium chloride solutions (S and 5S)

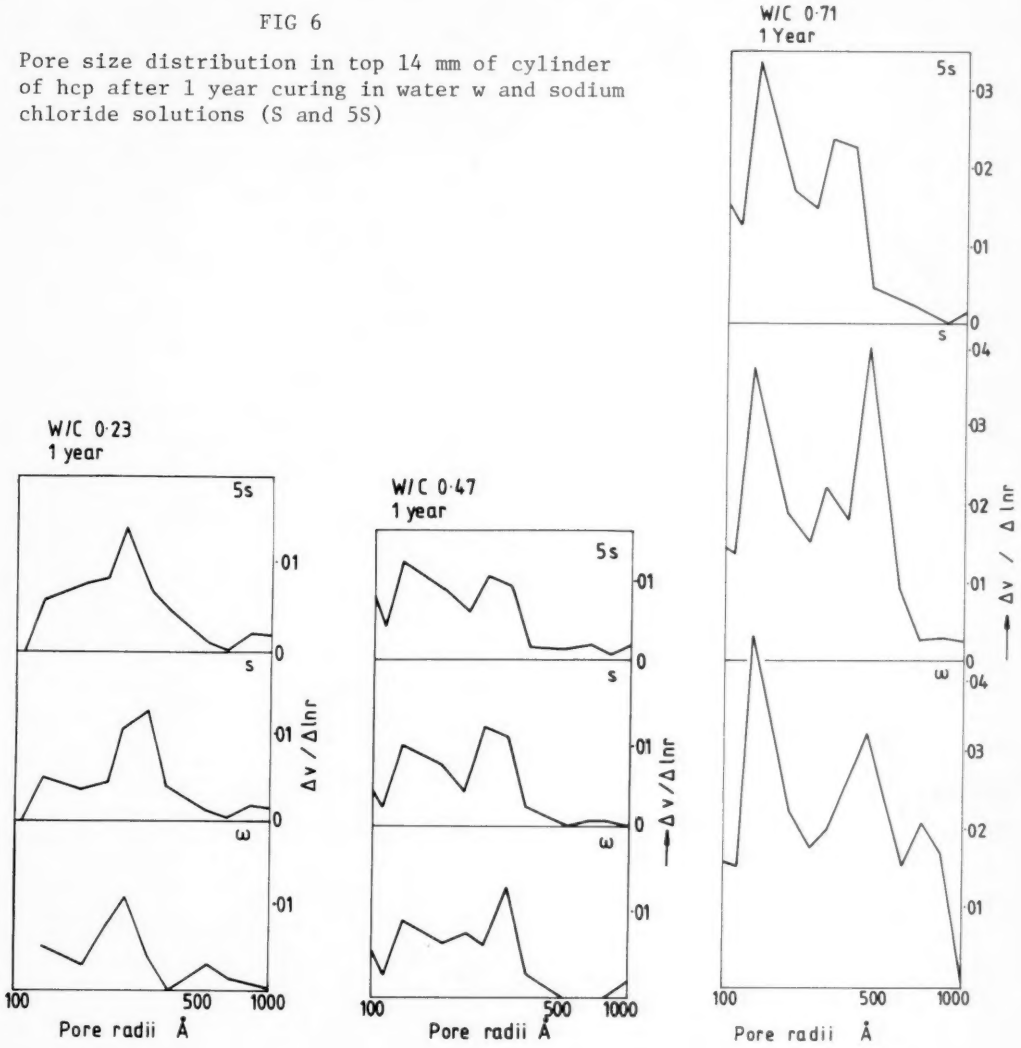

desorption isotherm. It is already known that chloride ions are adsorbed on to the surface of C-S-H. Gregg and Sing (15) have noted that changes in the chemical nature of the surface may influence the nitrogen isotherms since the nitrogen molecule contains an electrical quadrapole qhich interacts with any changes in the surface conditions. The authors are of the opinion that with the probable adsorption of free chloride on to the paste particle surface, the use of nitrogen adsorption for the measurement of surface area or pore size distribution is suspect; it has therefore not been used more fully.

Discussion

The mineralogical examinations of the hcp specimens show that the penetration of chloride ions does not affect the quantities of the complex calcium aluminate salt hydrates C_4AH_{13}, C_2AH_8, C_3AH_6, $C_3A.CaSO_4 12H_2O$ or ettringite. However, chloride ions which penetrate the hcp to form the monochloroaluminate

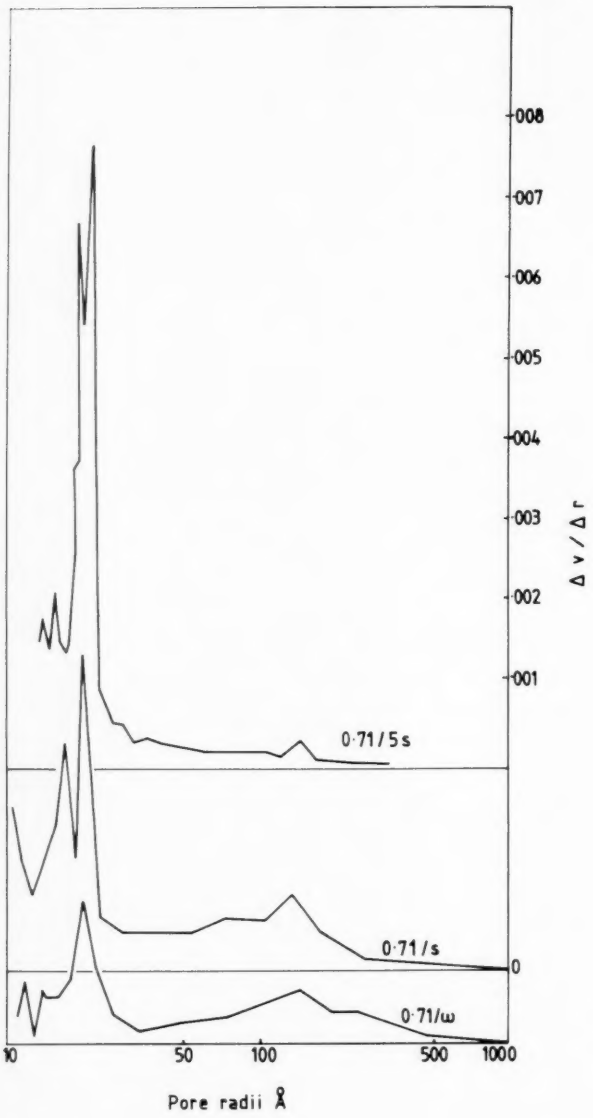

FIG 7

Pore size distribution by nitrogen desorption isotherm for top 14 mm of hcp 0.71 w/c after curing for 1 year in water, and in sodium chloride solutions.

VOL. 14 1984

hydrate $C_3A.CaCl_2.12H_2O$, which will normally result from reaction with the unhydrated C_3A still present in the hcp.

The results of the determination of calcium hydrosilicate in the hcp specimens are less clear although there is some evidence that storage in sodium chloride solutions may slightly increase the quantity although this difference may vanish with completion of hydration by 1 year.

The penetration of chlorides into hcp follows a power relationship

$$C = kd^{-m}$$

where c = concentration of chloride, d is distance into the hcp and k and m are constants depending on time and permeability of the paste.

The results clearly show that the amount of chloride ions penetrating is time dependent; at low w/c ratio (0.23) the concentration of total chloride ions at 1 year is independent of the concentration of the surrounding solution, although at 6 months the higher sodium chloride concentration produces a surface penetration twice that of the lower concentration. At w/c ratios of 0.47 and 0.71 for both 6 months and 1 year storage the chloride content at the surface is for the higher sodium chloride concentration (150g/l) roughly 1½ times that of the lower sodium chloride concentration (30g/l).

The quantities of monochloroaluminate formed are independent of the concentration of the storage solutions.

The conclusion from this data is that the total chloride penetration is dependent in time, concentration of chlorides in surrounding solution, and on the permeability of the hcp (as shown by the w/c ratio of original paste). The amount of the calcium monochloroaluminate hydrate formed is dependent on time and permeability but not on the concentration of the chloride in the storage solution. It follows that from the mineralogical changes observed in the hcps it is the composition of the original cement, i.e. the C_3A contents which govern the amount of monochloroaluminate formed.

The investigations into the micropore distributions of the hcps, bearing in mind the limitations of the method of analysis, show that at the low w/c ratio (0.23) at 6 months storage in water there is a maximum in the frequency of occurrence of pore spaces of radii about 400Å; penetration of chloride ions reduce the pore maxima to about 270 and 250Å. At one year all specimens of hcp both in water and sodium chloride solutions have a pore size maxima at about 270Å pore radius. This leads to the conclusion that either the chlorides are reacting to form extra material such as $CaCl_2$, or the surface binding of chloride ions on to the C-S-H surface fill in the pores, or it is affecting the rate of formation of C-S-H or its morphology to reduce the inter solid pores. From the mineralogical data no significant change in the quantity of the hydrates could be measured, so it is suggested that the reduction in pore size is due to the formation of calcium chloride on the surface of the C-S-H.

OL.
14
984

At the higher w/c ratios the differences are similar but are not so clear; nevertheless there is a reduction in the pore sizes associated with chloride penetration.

The total porosity is less affected by chloride penetration but there is a slight reduction with the highest solution concentrations. However as Illston and Nyame (16) have shown, the permeability of hcp is not directly related to porosity but rather to a continuous pore radius and it follows that the permeability of hcps with be reduced as the chlorides penetrate, irrespective of the quantity of chloride bound in the calcium monochloro-aluminate hydrate.

Conclusions

1. Chloride ions penetrate hcp, the greater the w/c ratio the greater the distance of penetration.
2. The concentration of chloride ions in the hcp is dependent on concentration of the surrounding solution.
3. The chloride ions react with the anhydrous tricalcium aluminate in the remaining unhydrated cement in the hcp but not with the complex hydrated calcium aluminate salts (including ettringite) already formed in the hcp.
4. The monochloroaluminate hydrate $C_3A.CaCl_2 12H_2O$ is formed, but not all the chlorides so react. The quantity of monochloroaluminate hydrate is

independent of the chloride concentrations and so must be dependent on the C_3A present in the unhydrated cement particles remaining in the hcp.

5. At the highest w/c ratio (0.71) used more C-S-H is produced in the presence of sodium chloride.

6. Chloride ion penetration into hcp alters the pore size distribution, the greater the chloride present the smaller the pores found.

7. The higher the C_3A content of the cement the greater will be resistance of the concrete to reinforcement rusting in the presence of permeating chlorides, because less free chloride ions will be left following the formation of the chloroaluminate.

8. Since the pore sizes found in the presence of chlorides are smaller than for non chloride environments the permeability to water will be reduced.

Acknowledgements

The authors would like to thank their colleagues, Mr D S Oxley, Mr M Harmer and Miss L Hamlyn for their considerable help with the experimental work. They would also like to thank the Science Research Council of the UK for their support of this research programme.

References

1. J. Calleja, "Durability," Principal Report VII, 2, 7th International Congress on the Chemistry of Cement, Paris 1980.
2. M. Collepardi, A. Marcials and R. Turrizani, Il Cemento 67, (4), 157-163.
3. O.E. Gjorv and O. Vennesland, Cem. Concr. Res. 9 (2), 229-238 (1979).
4. S. Ushiyama and S. Goto, "Diffusion of Various Ions in Hardened Cement Pastes," Proc. VI ICCC, Mosco Sec. 11. 1974.
5. C.L. Page, N.R. Short and A. Eltarras, Cem. Concr. Res. 11, 395-405 (1981).
6. H. Ushiyama, H.I. Wakura and T. Fukinega, "Diffusion of Sulphate Ion in Hardened Portland Cement." Rev. 30th Gen. Meeting Cam. Assoc. Japan, p. 47-49, 1969.
7. W. Richartz, Zement-Kalk-Gips 22 (10), 447-456 (1969).
8. M. Regourd, H. Hornain and B. Montureux, "Microstructure of Concrete in Agressive Environments," 1st Int. Conf. on Durability of Building Materials and Components. Nat. Res. Council Canada, Ottawa, 1978.
9. G.J. Verbeck, "Field and Laboratory Studies of the Sulphate Resistance of Concrete." Performance of Concrete, Ed., E.G. Swenson. Canadian Building Series, University of Toronto Press, 113-124, 1968.
10. B. El-Jazari and J.M. Illston, Cem. Concr. Res. 7, 247-258 (1977).
11. H.F. Taylor, "The Chemistry of Cement Hydration," Prac. 7th Conf. Silicat Ind. Budapest, 199-220, 1965.
12. F.H. Chung, J. Appl. Crystall. 1, 526 (1974).
13. H.G. Midgley and J.M. Illston, "Effect of Chloride Penetration on the Properties of Hardened Cement Pastes." Communication VII, 101, 7th Int. Cong. Chem. Cement, Vol. III, Paris 1980.
14. H.G. Midgley and J.M. Illston, Cem. Concr. Res. 13, 197-206 (1983).
15. S.J. Gregg and K.S.W. Sing, "The Adsorption of Gases on Porous Solids," Surface and Colloidal Science, vol.9, Ed., E. Matyeric, New York, 1976.
16. B.K. Nyame and J.M. Illston, "Capillary Pore Structure and Permeability of Hardened Cement Paste," Communication VI, 181, 7th Int. Cong. Chem. Cement, Vol. III, Paris 1980.

VOL 14 198

CEMENT and CONCRETE RESEARCH. Vol. 14, pp. 559-564, 1984. Printed in the USA.
0008-8846/84 $3.00+00. Copyright (c) 1984 Pergamon Press, Ltd.

DEVICES TO IMPROVING THE TECHNIQUES OF PREPARING PIC

A. Zuk, M. Wejchan-Judek and L. Balewski
Institute of Chemical Technology
Politechnika Poznańska, Poznań
Poland

(Communicated by F. Massazza)
(Received Nov. 14, 1983; in final form April 2, 1984)

ABSTRACT

New polymerization techniques were applied in the production of PIC. In the first experiment, the polymerization was carried out in liquid medium, water or oil, containing active additives. In the second one, an addition of ethylene glycol dimethacrylate (EGDM) was applied in production of PIC by impregnation with methyl methacrylate. In both cases a high polymerization yields were achieved. Typical properties of the PIC obtained were investigated. The morphology of the PIC obtained with EGDM was characterized on the basis of electron micrographs.

Introduction

Polymer impregnated concrete is recognized as a superior construction material with higher durability and strength than plain concrete. PIC is much less permeable to water and is more resistant to freeze-thaw damage than plain concrete. PIC is made by impregnating dried concrete with a monomer - methyl methacrylate containing benzoyl peroxide as an effective initiator and polymerization by increasing the temperature of the monomer containing concrete. Methyl methacrylate is a volatile liquid which under the polymerization conditions tends to evaporate. In the papers published up to the present moment this phenomenon was prevented only by physical means (1,2). The impregnated details were covered with coatings of paints or coatings obtained from prepolymer. Wrapping in aluminium and polyethylene foils and polymerization in a liquid medium were used.

From the studies undertaken in the Institute of Chemical Technology, it appears that the best effects are obtained by connecting the physical method with the chemical one, which is based on inserting an additional, effective initiator or accelerator to the polymerization medium. The method accelerates polymerization in the layer close to the surface and in this way makes monomer loss from the impregnated concrete difficult. Methyl methacrylate is a monomer most freqeuntly used for PIC preparation. It is possible to link the linear polymeric chains through the use of crosslinking agents. Such agents are polyfunctional molecules (3,4) which have more than one site available for polymerization reactions. Crosslinking increases the mechanical properties of the

polymer, increases its resistance to the action of aggressive media and increases its thermal stability.

In this paper we present our results on PIC obtained by polymerization of methyl methacrylate (MM) containing di-functional cross-linking agent - ethylene glycol dimethacryalte (EGDM) and benzoyl peroxide as initiator. EGDM (5,6) is very reactive and polymerizes with high thermal effect. Thus co-polymerization can take place at lower temperature. We have studied its influence on MM polymerization route. It is shown in Figure 1.

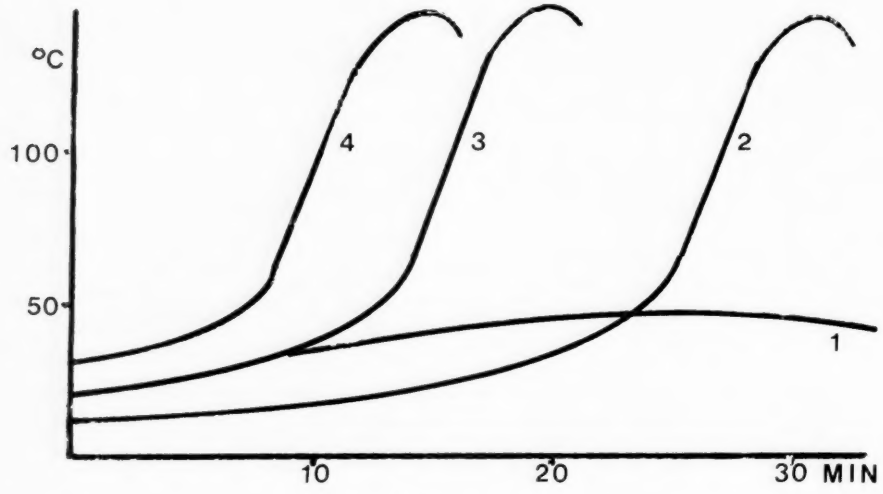

FIG. 1

Thermal route of MM polymerization in the presence of:

1 - 1% benzoyl peroxide, 0.1% N,N-dimethylaniline;
2 - 10% EGDM, 2% benzoyl peroxide, 0.4% N,N-dimethylaniline - initial temperature 10°C;
3 - 10% EGDM, 2% benzoyl peroxide, 0.4% N.N-dimethylaniline - initial temperature 20°C;
4 - 10% EGDM, 2% benzoyl peroxide, 0.4% N,N-dimethylaniline - initial temperature 30°C.

Experimental

Preparation of Specimens

We have used samples in the form of cubes 10x10x10 cm (Table 1) or cylinders 8x8 xm (Table 2). The specimens were prepared from Portland cement "250" by water-to-cement ratio = 0.5. Before impregnation, the specimens were dried at 120°C to weight constant (ca 24 hours).

Impregnation

The specimens which were to be polymerized in medium with active additives were impregnated by submerging them in MM containing 1% benzoyl peroxide for 24 hours. The specimens polymerized with EGDM were immersed for 24 hours in the bath consisting of 90 parts MM, 10 parts EGDM, and 2 parts benzoyl peroxide.

VOL. 14 1984

Polymerization

In the first experiment, the polymerization was carried out as a two-step process. The impregnated specimens were heated for 6 hours at 60-90°C in polymerization media. After that time polymerization was finished in the air at 80-100°C in 18 hours. The following media of polymerization were used:

W - water
W2 - water containing 2% ammonium persulphate
W3 - water containing 3% ammonium persulphate
LT - oil containing 0.1% N,N-dimethyl-p-toluidine
LAT- oil containing 0.4% N,N-dimethyl aniline and 0.4% N,N-dimethyl-p-toluidine

In the second experiment, the polymerization was carried out in water or mineral oil medium at temperature 75-80°C, during 1-3 hours.

Results

Table I
Properties of PIC prepared in an active polymerization medium

W	V	MM	med	PMM	f	Wp	k	P	Pr
%	%	%	-	%	%	%	-	MPa	-
			series 1	d = 2.20 kg/l					
5.6	12.3	4.0	W3	3.2	78	0.3	20	50	1.6
5.5	12.3	-	N	-	-	-	-	32	1.0
			series 2	d = 2.17 kg/l					
7.5	16.3	5.2	W3	4.7	90	0.2	40	43	2.4
7.6	16.3	5.3	W2	4.5	73	0.3	25	44	2.4
7.5	16.3	5.5	W	4.0	74	0.4	20	44	2.4
7.4	16.1	-	N	-	-	-	-	18	1.0
			series 3	d = 2.13 kg/l					
7.4	15.6	5.4	W3	4.4	81	0.6	12	27	2.3
7.3	15.5	-	N	-	-	-	-	12	1.0
			series 4	d = 2.02 kg/l					
8.7	17.7	6.6	W3	5.4	81	1.0	9	25	2.8
8.9	17.9	-	N	-	-	-	-	9	1.0
			series 5	d = 2.23 kg/l					
5.4	12.2	4.2	LAT	3.9	92	0.1	55	58	1.8
5.6	12.3	4.4	LT	4.0	91	0.2	40	72	2.2
5.5	12.3	-	N	-	-	-	-	32	1.0

W-water absorption; V-porosity; MM-methyl methacrylate absorption; med-polymerization medium (N-nonpolymerized); PMM-poly (methyl methacrylate) content; f-polymerization efficiency; Wp-water absorption of PIC; k-coefficient of water absorption decrease (k=W/Wp); P-compressive strength; PR-relative compressive strength ($Pr-P/P_{nonpolymerized}$)

Table II
Properties of PIC prepared with addition of ethylene glycol dimethacrylate

Polymerization			Properties			
MM	med	tech	PMM	Wp	cond	P
%	-	-	%	%	-	MPa
	nonpolymerized *			6.5	n	35.7
				7.0	H_2O	27.5
				7.1	+/-	19.7
5.3	w	2h80	5.3	0.5	n	83.7
5.7	w	1h80	5.7	0.5	n	76.5
5.7	w	2h75	5.2	0.5	n	98.2
5.0	ol	2h75	5.0	0.5	n	83.7
4.3	ol	2h75	4.3	0.5	n	73.1
5.3	ol	2h75	5.3	0.5	H_2O	126.0
3.5	ol	3h75	3.5	0.5	H_2O	56.2
3.5	ol	3h75	3.5	0.5	H_2O	62.1
3.5	ol	3h75	3.5	0.8	H_2O	50.4
6.0	w	2h75	5.3	0.4	+/-	94.5
4.7	ol	2h75	4.7	0.4	+/-	111.6
3.3	ol	3h85	3.3	0.4	+/-	42.3
3.3	ol	3h85	3.3	0.7	+/-	45.4

* density - 2.24 kg/l; porosity - 14.0%

MM-methyl methacrylate absorption; med-polymerization medium; w-water, ol-mineral oil; tech-time (h) and polymerization temperature (°C); PMM-poly(methyl methacrylate) content; Wp-water absorption of PIC; cond-testing conditions: n-moist cured 28 days at 20°C, H_2O-immersed in water (20°C) during 6 weeks, +/- -25 cycles of freezing (-20°C) and thawing (20°C, 24h) in water; P-compressive strength.

Discussion

The above results indicate that in both experiments high yields of polymerization were achieved, i.e. that the monomer loss was small. Insertion of amine or persulphate to the polymerization medium causes a characteristic distribution of the polymer in the specimens (Fig. 2), i.e. there is a core of non-polymerized concrete with a 2.0cm layer of PIC. The following mechanism is possible. An application of amine or persulphate creates good conditions for the initiation of polymerization in the layer close to the specimen surface. The heat conveyed and the polymerization heat enlarges the pressure of methyl methacrylate vapors in the concrete. However, the layer close to the surface which was earlier polymerized under the influence of additives forms a barrier for the monomer and in the deeper layers, polymerization occurs with maximal filling of voids and pores. It is reflected by the fact that the polymer is distributed in ca 85% of the specimen's volume.

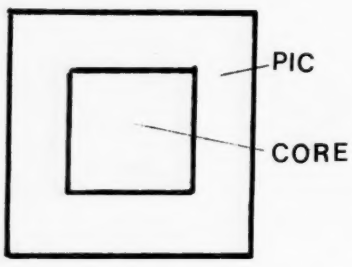

FIG. 2
Profile of PIC specimen.

Such distribution of polymer in the specimen manifests itself by an increase of compressive strength and significant decrease of water absorption in relation to non-polymerized specimens.

The addition of EGDM to impregnation of concrete with methyl methacrylate causes an increase of compressive strength of ca 30 MPa in relation to specimens impregnated with methyl methacrylate without additives. Water absorption was significantly decreased (to ca 0.5%). In consequence, its resistance to hydrolize and freeze-thaw resistance increased. The samples of PIC subjected to freeze-thaw resistance examination posses only slightly diminished compressive strength. It is close to the value of compressive strength of PIC samples seasoned in water. It indicates a good tightening of the concrete surface with polymer. It is revealed by electron micrographs (Fig. 3). On the fracture's picture near the surface of the sample where the most advantageous polymerization conditions occur, a smooth, cast coat on concrete grains is observed ("b"). On micrograph "c", it is seen how concrete grains coated with polymer stick together. On micrograph "d", the layer of polymer appears as a brighter surround-

OL.
14
984

a

b

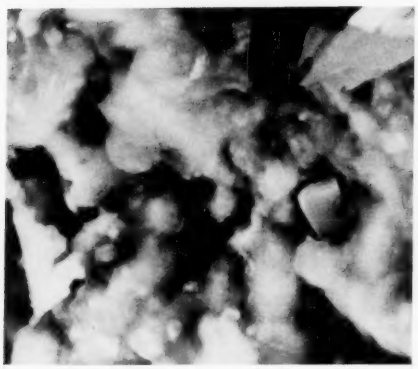

c

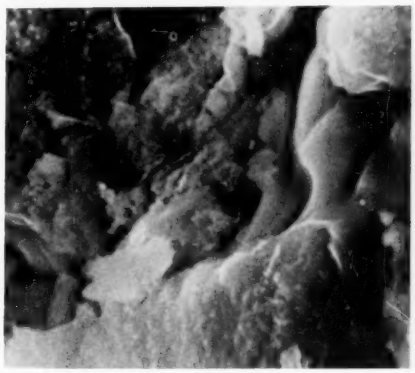

d

FIG. 3

Electron micrographs of fractures: a - unimpregnated concrete; b,c,d - PIC

ing of the fracture of concrete grain. Observersation of micrographs indicates a good adhesion of a chosen polymer to concrete.

Conclusions

1. The insertion of active additives to liquid polymerization medium makes it possible to produce PIC showing big compaction of polymer in the layer close to the surface without using high-pressure polymerization.

2. The application of methyl methacrylate crosslinked with ethylene glycol dimethacrylate to PIC significantly increases compressive strength, freeze-thaw durability and resistance to water attack simultaneously decreasing water absorption. The used polymer shows high adhesion to concrete.

3. Both of the polymerization techniques presented above guarantee high polymerization yield - small losses of monomers.

References

1. U. Bumm, G. W. Topilskij, Z. Prikl. Chim. XLIX (7), 1462 (1976).
2. Pat. France 2124870 (1982).
3. Terashita, Masanichi, Kyushu Shika Gakkai Zasshi 30 (4), 562 (1976).
4. C.J. Slop, Plastica 4, 92 (1977).
5. F.N. Bondaruk, M.A. Korszunow, W.A. Kisielew, I.G. Sumin, Z. Prikl. Chim. XLV (11), 2500 (1972).
6. E.A. Frolowa, T.P. Erszkowa, E.F. Ustawczikow, W.A. Kisielew, Z. Prikl. Chim. LI (10), 2366 (1978).

Acknowledgements

The efficient technical assistance of Karol Jóźwiak in making the micrographs is acknowledged by the authors.

VOL. 14 1984

CEMENT and CONCRETE RESEARCH. Vol. 14, pp. 565-573, 1984. Printed in the USA.
0008-8846/84 $3.00+00. Pergamon Press, Ltd.

AN ELECTRON MICROPROBE STUDY OF A MATURE CEMENT PASTE

H.F.W. Taylor* and D.E. Newbury
National Bureau of Standards
Washington, DC 20234, USA

(Communicated by J.P. Skalny)
(Received Nov. 28, 1983)

OL.
14
984

ABSTRACT

A portland cement paste 23 years old, and essentially fully hydrated, was studied by electron probe microanalysis. X-ray images indicated that the shapes of the original, largely polymineralic cement grains, and those of the regions occupied by the individual phases within them, are substantially preserved in the hydrated material. This was shown especially clearly by the Mg and Fe images, probably because these elements do not readily migrate in the alkaline medium. Estimation of individual phase compositions is rendered uncertain because of possible admixture of phases on or below a micrometer scale, but the atomic ratios relative to Ca are, approximately: Mg 0.03, Al 0.08, Si 0.60, S 0.03 and Fe 0.015 (Ca:Si 1.67) for the C-S-H, and Al 0.40, Si 0.33 and Fe 0.27 for the hydrogarnet.

Introduction

In a previous paper (1), we reported an electron probe microanalysis (EPMA) study of mature tricalcium silicate (C_3S) and β-dicalcium silicate (C_2S) pastes; the present paper describes an extension of this work to a mature portland cement paste. Several previous studies of cement pastes by EPMA or scanning electron microscope-energy dispersive X-ray (SEM-EDX) analysis (2,3) or analytical electron microscopy (4,5) have been reported. In the most recent EPMA study, Rayment and Majumdar (3) reported that, in young pastes, the calcium silicate hydrate (C-S-H) compositions vary as between inner and outer products, but that in pastes some years old, a single composition predominates. For these mature pastes, they reported Ca:Si ratios of 1.82 - 2.7, partly dependent on the ratio of water to solids (w:s), with minor contents of other elements. The ratios of (Ca + Mg) to (Si + Al + Fe + S) were less variable than those of Ca to Si, or other comparable ratios, and they concluded that Mg can replace Ca, and that Al, Fe and S can replace Si in the C-S-H structure.

*Present Address: Department of Chemistry, University of Aberdeen, Old Aberdeen AB9 2UE, Scotland, UK

None of the previous investigations has provided any detailed information on the distribution of calcium hydroxide (CH) or of the hydrated aluminate and ferrite phases, and in the present work these aspects were investigated.

Experimental

The specimen (6) was a paste prepared from a Type I portland cement at the Portland Cement Association Research and Development Laboratories (PCA designation C7OA-4525), and was 23 years old when examined. It had w:s = 0.45 and had been stored moist at 25°C. The original cement (6; PCA designation LTS12) had a Blaine specific surface of 328 m^2kg^{-1} and chemical composition (weight percent) SiO_2, 21.4; Al_2O_3, 5.8; Fe_2O_3, 2.4; Mn_2O_3, 0.11; TiO_2, 0.24; CaO, 63.6; MgO, 3.0, Na_2O, 0.28; K_2O, 0.40; SO_3, 1.6; P_2O_5, 0.24; Insoluble Residue, 0.11; Ignition Loss, 0.6 (Total 99.8); Free CaO 0.1. The Bogue composition was C_3S, 45.0; C_2S, 28.0; $Ca_3Al_2O_6$ (C_3A), 12.6; Ca_2AlFeO_5 (C_4AF), 7.3; $CaSO_4$, 2.7. X-ray diffraction of the paste showed as the only clearly detectable phases CH, very poorly crystalline C-S-H, a hydrogarnet with a = 1.24 nm, which is compatible with a composition near $Ca_3AlFeSiO_{12}H_8$, and very weak indications of AFm ("aluminum iron mono") phases from peaks at 0.89 and 0.77 nm.

The most satisfactory method of specimen preparation was found to be cutting with a diamond micro saw followed directly by gentle polishing with 1 μm diamond paste on cloth, using xylene as lubricant throughout. The analytical techniques were as described in the previous paper (1).

Results and Discussion

X-Ray Area Scans

X-ray area scans were obtained for Mg, Al, Si, S, Ca and Fe, in three separate areas. The resolution was relatively low in the first area studied, but much higher in the other two, because a better polishing technique had had been found. Fig. 1 gives results for one of these latter areas; those for the other were similar.

Fig. 1a is the Mg image. The most interesting feature is the pattern of angular or rounded regions of low Mg content on a background of very low or zero Mg content. These regions are up to approximately 50 μm in largest dimension, and their size and shape distributions suggest that they are relicts of the original cement grains. Within them, the Mg contents are distinctly variable. At one extreme, there are areas in which Mg is very low or absent, but which are surrounded by rims of higher Mg content. At the other extreme, there are areas of very high Mg content, as at MM. These latter areas are up to approximately 10 μm in size, and contain little or no Ca, Si, Fe, Al or S. Subsequent spot analyses confirmed that they were either unreacted MgO or, less probably in view of their shapes, MgO that had hydrated to give $Mg(OH)_2$.

The above interpretation of the Mg image is consistent with the fact that all the anhydrous clinker phases can contain this element, though in varying amounts; because of its low solubility in the alkaline pore fluid, one would not expect Mg to migrate readily. The Mg image may thus be used to distinguish inner from outer hydrate for cement grains above a few μm in size, even when, as in the present case, there is no other way of doing this.

The Ca image (Fig. 1b) is relatively uniform, but shows discontinuous regions of higher Ca content (e.g., at CC). These are fairly sharply defined, irregular in shape, and up to approximately 50 μm in largest dimension. They occur largely or wholly in the outer product, and constitute

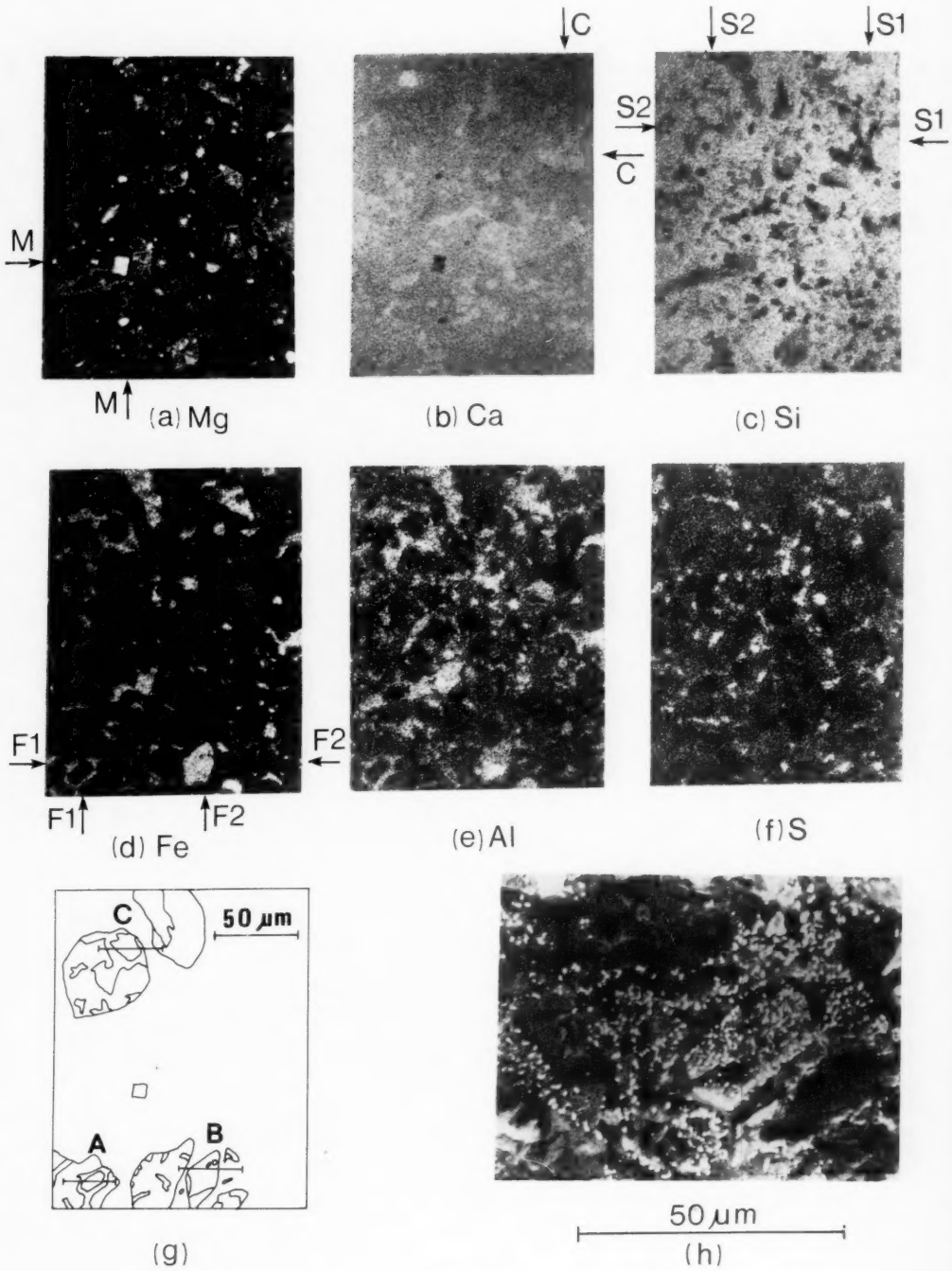

FIG. 1

(a) - (f): X-ray images. A light area denotes a high concentration of the specified element. (g): Locations of Traverses A-C. (a) - (g) are of the same area. (h): Secondary electron image of the area containing Traverse A.

20-25 percent of the total area. In general, the contents of the other elements are low in these regions, which are thus, largely at least, ones of calcium hydroxide.

The Si image (Fig. 1c) shows discontinuous regions low in Si on a background high in Si. Many of the low-Si regions (e.g., at S1S1) correspond to the regions described above as being of CH, MgO or $Mg(OH)_2$. Those that are not tend to be in the inner product (e.g., at S2S2). The high-Si regions occur in inner and outer products alike, and no differences in Si content at the presumed boundaries of the original cement grains are detectable from the area scans. These high-Si regions are presumed to consist essentially of C-S-H.

The Fe image (Fig. 1d) shows sharply defined, discontinuous regions relatively high in Fe (e.g., at F1F1 and F2F2) on a background very low in Fe. The high-Fe regions are relatively low in Si and occur almost wholly in the inner product; the Fe, like the Mg, is of low solubility in the alkaline pore fluid, and would not be expected to migrate readily.

The Al image (Fig. 1e) is less sharply differentiated. There are regions of higher and lower Al content, but their boundaries are somewhat diffuse. The regions high in Fe are, probably without exception, also high in Al, but the reverse is not true. The regions high in Al but not in Fe occur in both inner and outer products. The only regions in which Al is very low or absent are probably those described earlier as being of $Ca(OH)_2$, MgO or $Mg(OH)_2$. One would expect Al to migrate more easily than Fe in the alkaline medium, on account of its higher solubility.

The results for Si, Fe and Al give a clear indication of the composite or polymineralic nature of at least many of the larger cement grains originally present. The area near the upper left hand corner, for instance, shows a matrix of material high in Fe and Al, which partially encloses regions high in Si (Fig. 1c, S2S2). It is presumed that the regions high in Si are relicts of alite or belite crystals, and that those high in Al and Fe are relicts of the interstitial C_3A or C_4AF; the calcium silicates have been replaced by C-S-H, and the interstitial material largely by hydrated phases high in Al and Fe, shown later to be mainly hydrogarnet. The relict interstitial material is also frequently high in Mg. This element is known to occur preferentially in the interstitial material, either as periclase or as a substituent in the C_4AF (7,8). Other relict cement grains show features similar to that just described; for instance, one near the lower left hand corner includes a pseudohexagonal feature that could be the relict of an alite crystal. Fig. 1h shows a secondary electron image of this area at a higher magnification. On the other hand, the prominent grain to its right appears to consist mainly of hydrated phases high in Al and Fe (Fig.1d, F2F2), and is presumably the relict of a grain that consisted largely of interstitial material.

The S image (Fig. 1f) shows relatively little differentiation, but there are regions of higher S content up to approximately 10 μm in largest dimension and others, somewhat larger, of very low S content. The regions high in S are largely or wholly in the outer product, and possibly tend to ring the edges of the relict cement grains. They tend to be of high Al content. A possible explanation is that, in the first hours of hydration, ettringite forms rapidly and deposits on the surfaces of the larger cement grains; the ettringite later decomposes, but the ions thus released tend to remain in place. The phase nature of these high-S regions was not established.

VOL
14
198

Spot Analyses

In all, 275 spot analyses were made, in 6 traverses at 1 μm intervals, one 2 μm x 2 μm grid scan and some additional points. Some of the regions analyzed were chosen to investigate particular features indicated by the X-ray area scans, and others in an attempt to obtain representative coverage. Of the 275 analyses, 22 lying in regions of MgO or $Mg(OH)_2$ were excluded as non-representative; the remaining 253 were normalized to anhydrous oxide sums of unity, and mean weight fractions of each element were calculated. Comparison of the results thus obtained with the analysis of the original cement (6; Table 1) shows that the analyses are moderately representative of the entire material, though it appears that regions of calcium hydroxide are under- and those of phases high in Al and Fe over-represented.

TABLE 1

Comparison of Mean Weight Fractions of Elements in the Paste with Those in the Original Cement

	Mg	Al	Si	P	S	Ca	Fe
Paste*	0.018	0.043	0.113	0.001	0.010	0.423	0.028
Cement	0.018	0.031	0.100	0.001	0.006	0.455	0.017

* Means from 253 analyses normalized to anhydrous oxide sums of unity.

Fig. 2 gives a general impression of the distribution of compositions. The atom ratios of (Al + Fe) to Ca are plotted against those of Si to Ca, and an indication of S:Ca and Mg:Ca ratios is provided. Because of the uncertainty regarding possible replacement of Ca by Mg, analyses with Mg:Ca > 0.2 should be interpreted with particular care. Most of the analyses shown could be of C-S-H, calcium hydroxide, hydrogarnet, or mixtures of two or all three of these phases. This conclusion is compatible with the X-ray diffraction (XRD) evidence.

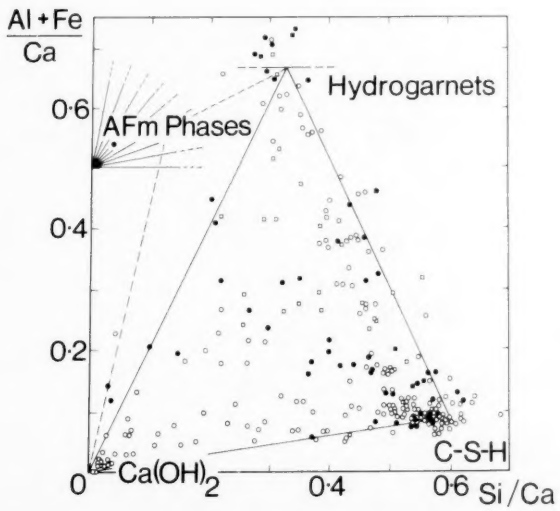

FIG. 2

Results of electron probe spot analyses, expressed on a plot of (Al + Fe):Ca against Si:Ca atom ratios.

S:Ca	Mg:Ca
< 0.04	< 0.2
⩾ 0.04	< 0.2
< 0.04	⩾ 0.2
⩾ 0.04	⩾ 0.2

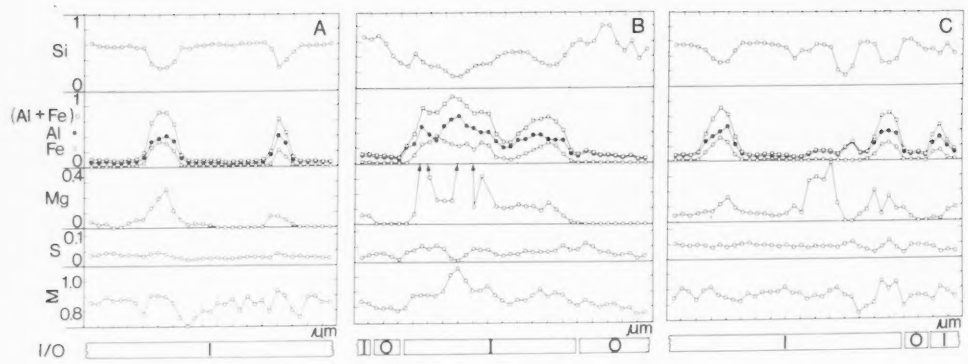

FIG. 3

Electron probe microanalysis results for the three traverses shown on Fig. 1g, expressed as atom ratios relative to Ca. Σ denotes the anhydrous oxide sums. I and O denote, respectively, analyses falling in regions considered to be inner and outer product.

Fig. 3 gives results for three of the traverses, the approximate locations of which are shown on Fig. 1g. Traverse A probably lies entirely within a single relict cement grain. It includes three regions consisting substantially of C-S-H, and two of relict interstitial material. As noted earlier, the central part is probably a relict alite crystal. Traverse B is centered on an area of relict interstitial material; both ends are located on material consisting substantially of C-S-H, which probably includes both inner and outer products. Traverse C lies largely within a single relict grain, within which it includes two regions consisting largely of C-S-H and two of relict interstitial material. Its right hand end appears to cross a region of outer product, to finish on a second relict grain.

Compositions of Individual Phases

Based on Fig. 2, three compositional regions were chosen for more detailed investigation. Their definitions, which are arbitrary, are given in Table 2. Within the traverses or grid scans, the longest unbroken sequences of spot analyses in each group were 13 μm for the compositions high in C-S-H, 8 μm for those high in calcium hydroxide and 10 μm for those high in Al and Fe. These results are compatible with those of the area scans.

TABLE 2

Definitions of Compositional Regions

Si:Ca	(Al + Fe):Ca	Mg:Ca	No. of Analyses	Description
≥ 0.4	< 0.2	< 0.2	108	High in C-S-H
< 0.1	< 0.1	< 0.2	20	High in CH
< 0.5	≥ 0.2	< 0.2	62	High in Al and Fe

C-S-H Composition

Table 3, col. 1, gives the results for the 108 analyses in the group high in C-S-H, expressed as means of atom ratios. Estimation of the true C-S-H composition is rendered uncertain by the likelihood that many of the analyses are of C-S-H mixed with other phases on or below a sub-micrometer scale. If it is assumed that this is the principal reason for the variation within this group, the best estimates of the ratios of Si to Ca and of (Al + Fe) to Ca are approximately those represented by the appropriate corner of the triangle in Fig. 2. Based on these ratios, and on those for Mg, Al, S and Fe to Ca given in cols. 1 - 4, the most probable estimate of the mean C-S-H composition is that given in Table 3, col. 5.

TABLE 3

EPMA Analyses of Samples High in C-S-H*

Atom Ratios	1 All	2 Traverse A (Inner)	3 Traverse C (Inner)	4 Travs. B and C (Outer)	5 Estimated C-S-H Composition
Mg:Ca	0.03(3)	0.02(2)	0.05(1)	0.00(0)	0.03
Al:Ca	0.09(3)	0.08(2)	0.05(1)	0.10(2)	0.08
Si:Ca	0.55(7)	0.59(3)	0.55(2)	0.59(11)	0.60
S :Ca	0.03(1)	0.03(1)	0.05(0)	0.03(1)	0.03
Fe:Ca	0.02(1)	0.02(1)	0.01(1)	0.01(1)	0.015
(Al+Fe):Ca	0.11(3)	0.09(3)	0.09(2)	0.11(3)	0.09
A	0.69(7)	0.71(3)	0.69(3)	0.73(13)	0.72
B	0.67(7)	0.70(3)	0.65(2)	0.73(13)	0.70
Ca:Si	1.86(23)	1.71(8)	1.82(7)	1.74(31)	1.67
Anhydrous Oxide Sum	0.88(12)	0.84(5)	0.87(3)	0.81(3)	0.85
No. of Analyses	108	27	11	13	-

* "All" defined by Si:Ca $\geq$ 0.4, (Al + Fe):Ca < 0.2, Mg:Ca < 0.2.
A = (Si + Al + Fe + S):Ca. B = (Si + Al + Fe + S):(Ca + Mg).
Ratios and sums in cols. 1-4 are means with standard deviations on final digit(s) in parentheses.

An attempt was made to determine whether there was any significant compositional difference between the C-S-H in the inner and outer products. Cols. 2 and 3, Table 3, give mean results for the inner product C-S-H of Traverses A and C, respectively, while col. 4 gives those for what was probably outer product C-S-H in Traverses B and C. The Mg:Ca ratios were consistently low (< 0.01) in the outer product C-S-H, but very variable in the inner product C-S-H (0. 00-0.08). The variation within the inner product may reflect variations in the Mg contents both between and within the alite and belite crystals originally present. There were were no other statistically significant differences, except possibly in the Al:Ca ratios, which were higher (p = 0.01) in the outer product C-S-H.

The anhydrous oxide sums for the C-S-H were typically around 0.85 (Table 3); assuming the deficiency to be water, this corresponds to an H_2O:SiO_2 ratio near 1.0. This ratio is about what would be expected for C-S-H dehydrated in a high vacuum, and contrasts markedly with the lower values of 0.6 to 0.8 found for the C-S-H in calcium silicate pastes (1).

The Al:Ca, Fe:Ca and S:Ca ratios found in the present work are close to those found in some other mature portland cement pastes by analytical electron microscopy (4,5), which, however, gave lower Ca:Si ratios of 1.5-1.6. The present results may also be compared with those of Rayment and Majumdar (3) for the C-S-H of three cement pastes and three concrete samples aged 2.5-10 years. These workers reported contents of elements as atoms per 10 atoms of oxygen. The ratios of these contents to those of Ca on the same basis were Si, 0.43-0.60; Al, 0.06-0.16; Fe, 0.02-0.05 and S, 0.01-0.16; the Ca:Si ratios were 1.82-2.7. The low values for Si, and the high ones for Al, Fe and Ca:Si suggest that many of these analyses must relate to C-S-H mixed with other phases.

The standard deviations on the ratios Si:Ca, (Si + Al + Fe + S) : Ca and (Si + Al + Fe + S) : (Ca + Mg) given in Table 3 are almost identical. This neither supports nor disproves Rayment and Majumdar's conclusion that Mg can replace Ca and that Al, Fe and S can replace Ca in the C-S-H structure; their conclusion does, however, receive limited support from the fact that the Si:Ca ratio of 0.60 given in Table 3, col. 5, is below that of 0.67 suggested for the C-S-H of calcium silicate pastes (1), though the (Si + Al + Fe + S) : (Ca + Mg) ratio is distinctly higher. In a material so poorly ordered as C-S-H, ionic replacement should not necessarily be understood in the strict sense that applies to crystalline compounds. It could have a more general meaning involving replacement of one ion by another occupying approximately the same amount of space but not necessarily in the same position.

VOL. 14 198

Calcium Hydroxide

The mean atom ratios relative to Ca in the 20 analyses in the group of compositions high in calcium hydroxide (Table 2) were Mg, 0.01(1); Al, 0.03 (2); Si, 0.04(2); P, 0.001(3); S, 0.004(5) and Fe, 0.01(1); the parentheses enclose standard deviations on the final digits. These results agree broadly with those of Rayment and Majumdar (3) and with those found using analytical electron microscopy (4,5). It is not clear whether the extraneous elements occur as inclusions or as substituents in the calcium hydroxide structure.

Hydrogarnet and Other Phases

Table 4, col. 1, gives mean atom ratios for the 62 analyses in the group of compositions high in Al and Fe (Table 2). These results, supported by those in Fig. 2, are compatible with the observation that the main phase high in these elements and detectable by XRD is a hydrogarnet. To obtain a more exact estimate of its composition, mean atom ratios were calculated from 19 analyses with (Al + Fe):Ca $\geq$ 0.5, Si:Ca $\geq$ 0.2 and Mg:Ca < 0.2 (Table 4, col. 1). Most of these analyses were from regions of relict interstitial material in Traverses A, B and C (Fig. 3). The results, like those of the area scans, show that the Fe tends to concentrate in the hydrogarnet, which has a composition near $Ca_3Al_{1.2}Fe_{0.8}SiO_{12}H_8$. More detailed discussion of the hydrogarnet composition would be unjustified because of uncertainty concerning the extent to which it is mixed with other phases.

The XRD results showed the presence of small proportions of AFm phases. One EPMA analysis (Table 4, col. 3) corresponded quite closely to the monosulfate, $Ca_4Al_2(OH)_{12}(SO_4).6H_2O$, and others could be attributed to mixtures of this or other AFm phases with C-S-H, or more rarely with calcium hydroxide (Fig. 2). Many of these analyses are distinguished by relatively high S:Ca ratios, which tended to increase as the AFm compositions were approached.

Some of the analyses in Traverse B gave very high values for (Al + Fe):Ca of 0.8-0.9 and very high anhydrous oxide sums of 1.0-1.1 (Fig. 3). These

TABLE 4

EPMA Analyses of Samples High in Al and Fe

Atom Ratios	1 All	2 Hydrogarnet	3 AFm Phase
Mg:Ca	0.08(6)	0.11(5)	0.00
Al:Ca	0.32(13)	0.36(9)	0.55
Si:Ca	0.34(11)	0.32(5)	0.04
S :Ca	0.04(4)	0.04(1)	0.24
Fe:Ca	0.14(11)	0.26(10)	0.00
(Al + Fe):Ca	0.47(19)	0.63(6)	0.55
Anhydrous Oxide Sum	0.89(9)	0.90(4)	0.79
No. of Analyses	62	19	1

* Ratios and sums in cols. 1 and 2 are means with standard deviations on final digit(s) in parentheses. "All" is defined by (Al + Fe):Ca $\geq$ 0.2, Si:Ca < 0.5, Mg:Ca < 0.2 and hydrogarnet by (Al + Fe):Ca $\geq$ 0.5, Si:Ca $\geq$ 0.2, Mg:Ca < 0.2.

results suggest that a little unreacted C_4AF may have remained, although it was not detected by XRD.

The analyses as a whole show that the Mg tends to associate with the Al and Fe; this is indicated both by the EPMA traverses in Fig. 3 and by the Mg : Ca ratios in Tables 3 and 4, and is attributable to the fact that, in the clinker, this element tends to be concentrated in the interstitial material, especially in the ferrite phase and as periclase. In the mature paste, part of this Mg occurs as unhydrated periclase or $Mg(OH)_2$, as is shown by the X-ray images (Fig. 1) and by the high Mg contents (up to 13 weight percent) indicated by some of the analyses in Traverses B and C (Fig. 3); also part may substitute for Ca in the hydrogarnet and AFm phases. The Mg that was initially present in the alite or belite probably passes into the C-S-H.

Acknowledgments

One of us (H.F.W.T.) thanks the National Bureau of Standards, and more particularly Dr. G. Frohnsdorff (Building Materials Division, Center for Building Technology) and Dr. P.W. Brown (Cement Hydration Group), for the funding of this work and of the visits to NBS during which it was done, and for their interest and much helpful discussion. We thank also the Portland Cement Association for the specimen and Dr. C. Robbins for an XRD analysis.

References

1. H.F.W. Taylor and D.E. Newbury, Cem. Concr. Res.
2. M.S. Stucke and A.J. Majumdar, "Hydraulic Cement Pastes - Their Structure and Properties", Cement and Concrete Assoc., Slough, p.2 (1976).
3. D.L. Rayment and A.J. Majumdar, Cem. Concr. Res. 12, 753 (1982).
4. E.E. Lachowski, K. Mohan, H.F.W. Taylor and A.E. Moore, J. Amer. Ceram. Soc. 63, 447 (1980).
5. E.E. Lachowski, K. Mohan, H.F.W. Taylor, C.D. Lawrence and A.E. Moore, J. Amer. Ceram. Soc. 64, 319 (1981).
6. W. Lerch and C.L. Ford, J. Amer. Concr. Inst. 19, 745 (1948); L.S. Brown, ibid. p.877.
7. M. Regourd and A. Guinier, Proc. 6th. Int. Congr. Chem. Cement, Moscow, 1974, 1, 25 (1976).
8. A. Ghose and P. Barnes, Cem. Concr. Res. 9, 747 (1979).

CEMENT and CONCRETE RESEARCH. Vol. 14, pp. 574-584, 1984. Printed in the USA.
0008-8846/84 $3.00+00. Copyright (c) 1984 Pergamon Press, Ltd.

COMMENTS ON ELECTROCHEMICAL MEASUREMENTS OF THE RATE OF CORROSION OF STEEL IN CONCRETE

Carolyn M. Hansson
The Danish Corrosion Centre
Park Alle 345, DK-2600 Glostrup
Denmark

(Communicated by D.M. Roy)
(Received Dec. 16, 1983)

ABSTRACT

The electrochemical processes involved in the corrosion of steel are briefly described in terms of their thermodynamics and kinetics. The purpose is to explain and discuss the currently used laboratory techniques of corrosion rate measurements of reinforcement steel in concrete.

VOL
14
198

Introduction

Good quality concrete provides excellent protection for steel reinforcement. Chemical protection is provided by the concrete's high alkalinity and physical protection by the concrete acting as a barrier which impedes the access of aggressive species. Nevertheless, corrosion of steel reinforcement is becoming the most common cause of failure in concrete structures. In such structures as bridges and parking garages, this fact may be attributed, in large part, to the use of deicing salts. In other structures, carbonation of the concrete cover or salt penetration from sea spray, for example, may be responsible. The unexpected rapidity of these effects may, in turn, be due to incorrect specifications or to lack of control in mixing or placing of the concrete. They may also be due to incorrect use or inadequate knowledge concerning the use of the many cement additives and replacement materials which have become available in recent years.

All too often concrete is specified only on the basis of its (28 day) strength which gives little, if any, information about its durability. Thus, it is becoming more and more apparent that quantitative information is required on the effect of a range of concrete parameters (the water/cement ratio, the cement binder content, the curing conditions) together with the effects of cement additives and replacements on the durability of concrete from the viewpoint of reinforcement corrosion. Unfortunately, while one can predict whether or not corrosion is thermodynamically possible, one cannot predict the rate of corrosion theoretically and this must be determined

empirically. The only practical way in which this information can be obtained and documented in a reasonable time is by laboratory measurements of actual corrosion rates under specified and controlled conditions.

Until recently, corrosion of steel in concrete was most frequently studied by exposing samples to known environments for long periods of time, then removing the concrete cover and either weighing or measuring the steel to determine the amount of material corroded. Such experiments take many years to complete and are, obviously, destructive in nature. In recent years, however, electrochemical techniques have come to be used in the study of reinforcing steel. There are several major advantages of these methods. Firstly, they can give an estimate of the actual corrosion rate existing at the time of the experiment, not just the accumulated amount of corrosion over a long period of time. Consequently, it is not necessary to expose samples to a given environment for long periods. Secondly, the techniques are extremely sensitive, enabling measurement of corrosion rates as low as 0.01 μm/year. Thirdly, they are not destructive and, therefore, measurements can be repeated on the same samples, for example, after exposure to different environments

Electrochemical techniques are currently being used in a few laboratories around the world to gather the relevant information concerning the effect of concrete and environmental parameters on the corrosion of reinforcement but there seems to be a language barrier between the concrete community and the corrosion community which hinders the transfer of this information from the laboratory to the "real world". The purpose of this article is, thus, to describe the principles underlying the electrochemical techniques used in the laboratory to measure corrosion rates of steel in concrete. Electrochemical inspection and monitoring of actual structures will be discussed in a subsequent article[1].

VOL.
14
984

Corrosion as an Electrochemical Process

Corrosion is an electrochemical process. In other words, it is a chemical reaction involving the transfer of charge (electrons) from one species to another. For an electrochemical reaction to occur (in the absence of an external electrical source) there must be two half cell reactions: one capable of producing electrons (the anodic reaction) and one capable of consuming electrons (the cathodic reaction). Moreover, the rates of production and consumption must be equal in order to satisfy a charge balance. Because there is no net current, it is not possible to measure the current due to corrosion directly but it can be determined indirectly as described later.

For steel embedded in concrete, the anodic reactions of interest are:

$$3Fe + 4H_2O \rightarrow Fe_3O_4 + 8H^+ + 8e^- \qquad \langle 1a \rangle$$

$$2Fe + 3H_2O \rightarrow Fe_2O_3 + 6H^+ + 6e^- \qquad \langle 1b \rangle$$

$$Fe + 2H_2O \rightarrow HFeO_2^- + 3H^+ + 2e^- \qquad \langle 1c \rangle$$

$$Fe \rightarrow Fe^{++} + 2e^- \qquad \langle 1d \rangle$$

The possible cathodic reactions depend on the availability of O_2 and on the pH in the vicinty of the steel surface. The most likely reactions are:

$$2H_2O + O_2 + 4e^- \rightarrow 4OH^- \qquad \langle 2 \rangle$$

$$2H^+ + 2e^- \rightarrow H_2 \qquad \langle 3 \rangle$$

The Reactions 1a-d represent the dissolution or oxidation of iron and, as described below, for good quality concrete, in which the pH is normally of the order of 13.5, Reactions 1a and 1b are of primary interest. In the absence of other factors, the oxides Fe_3O_4 and Fe_2O_3 will form as a very thin, protective layer on the surface (a passive layer), as indicated schematically in Fig.1. If the pH is reduced. eg. by carbonation, then the same oxides will be produced as a non-protective layer, ie. as rust, and in much greater quantities. This has two detrimental effects: it reduces the cross section of the steel and, thereby, its load bearing capability and, because the rust has a volume several times greater than the iron from which it is produced, it also results in cracking and spalling of the concrete cover. Alternatively, there may be local corrosion attack resulting in pits in the steel, also indicated in Fig.1. In this case, the steel may be completely perforated with little or no visible damage to the concrete cover. As described below, the most common cause of this type of corrosion is breakdown of the passive film by chloride ions.

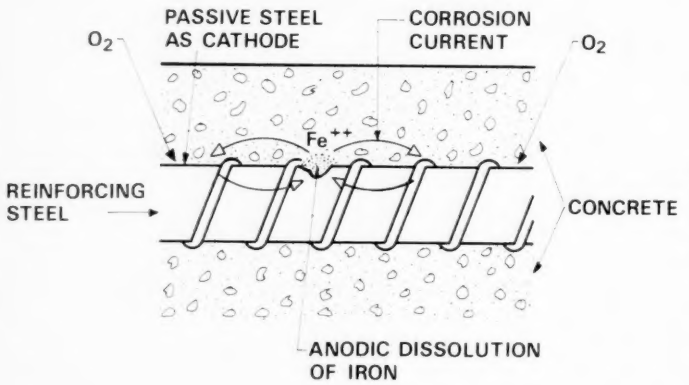

FIG. 1

Schematic illustration of the corrosion of reinforcement steel in concrete.

In order for corrosion to proceed, there must be a complete "electrical circuit" between anodic and cathodic areas of the steel. The flow of electrons and ions between these areas - the corrosion current - is indicated in Fig. 1. The magnitude of the corrosion current is a direct measure of the rate of corrosion of the steel. Thus, a corrosion current (determined per unit area of reinforcement) of 1 A/m^2 is equivalent to an average oxidation or dissolution of 1.16 mm per year from the surface of the steel. As in any other electrical circuit, the corrosion current is limited by the resistance of the circuit. In this case, the important factor is the electrical resistance of the concrete.

While the electrical resistance of the concrete is one of the factors controlling how fast corrosion can occur (ie. the reaction kinetics), the parameters determining whether or not corrosion is actually possible (the reaction thermodynamics) are the pH of the concrete pore solution and the electrochemical potential existing at the steel surface.[§] One can determine theoretically[2] whether or not the reactions are thermodynamically possible

---

[§]**The electrochemical potential** is a measure of the ease of electron charge transfer between the steel and the cement pore water solution and is, thus, a property of the steel/concrete interface, not of the steel itself. It is not possible to determine the absolute value of the potential and, therefore, the potential difference between the steel surface and a reference electrode

and values of E as a function of pH for which the above reactions are in equilibrium can easily be calculated and are available in graphical form[3] as illustrated in Fig. 2.

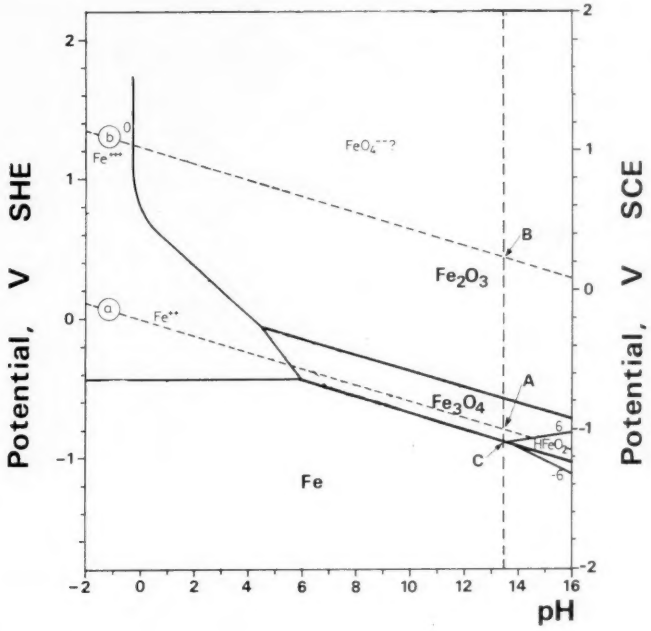

FIG. 2

A simplified version of diagram given in Ref 3, of the equilibrium phases of iron in aqueous solutions as a function of pH and electrochemical potential.

At pH 13.5 (typical of OPC), iron is in equilibrium with Fe_3O_4 at E = -1125 mV SCE (-881 mV SHE), point "C" in Fig. 2. At potentials lower than this, iron is the stable phase and, therefore, corrosion cannot occur. At higher values of the potential, Fe_3O_4 or Fe_2O_3 is the stable phase and corrosion (or oxidation) can occur. In theory, the more positive the potential, the higher will be the corrosion rate. However, at high pH (>9) in the presence of O_2, the oxide forms a passive film on the surface of the iron. This film acts as a protective coating but is not completely protective. Thus, corrosion is not stopped but the rate of corrosion is reduced to an insignificant level.

A second effect of this passive film is that there is no unique value of the corrosion potential. Its highest possible value is determined by the equilibrium potential of O_2, the dashed line in Fig.2. In aerated concrete of pH 13.5, the highest potential of the steel would thus be +175 mV SCE (point "B" in Fig. 2). The lowest potential at which the passive film has been experi-

---

(for example, a standard hydrogen electrode, "SHE", or a saturated calomel electrode,"SCE") is taken as a measure of the actual potential and is quoted as volts (or more commonly , millivolts) relative the electrode used, eg. as V SHE or V SCE. That value of the potential existing in a freely corroding system (ie. without any impressed potential from an external source) is known variously as the corrosion potential, the open circuit potential or the reversible potential and is often given the symbol E_R.

mentally found to be stable at this pH is -594 mV SCE[4]. In practice, the steel can adopt any potential within this range and still be passivated.

On the basis of the above, one can envisage the following sequence of events when fresh concrete is poured around steel reinforcement:

1. As the steel is coated with wet cement, it will rapidly develop a passive surface film due to the high pH of the cement pore water and the availability of oxygen. The potential of the steel will lie anywhere between +175 and -594 mV SCE (these limits are pH dependent); it may or may not be uniform over the surface of the steel and it may be stable or fluctuate with time. In the absence of aggressive chemicals, such as chloride ions, the corrosion current will be negligible, probably of the order of 10^{-4} to 10^{-3} A/m^2 equivalent to 0.1 - 1.0 μm/year.

2. The maintenance of the passive film requires both a high pH and access of oxygen. The greater the availability of oxygen, the thicker will be the passive film and the higher (more positive) will be the corrosion potential, E_R.

3. If the concrete is allowed to dry out, the potential can be expected to be high because of the easy access of oxygen. However, the corrosion rate will be limited by the passivity of the steel (in concrete that is not carbonated) and by the availability of water (in carbonated concrete). This is because water is required both for the corrosion process (Reactions 1 and 2) and for transport of the charge within the concrete.

4. If the concrete is buried under moist ground or is in deep water, the corrosion rate will be limited by the availability of oxygen. Eventually, all the oxygen in the concrete will be reduced and the potential will drop to a level at which the passive film is not stable and the film itself will be reduced, leaving bare steel in an "active" state. The actual corrosion rate under these circumstances is , however, not much higher than that in the passive state and will be determined by (i) the potential E_R, (ii) the diffusion rates of the reactants and the corrosion products in the concrete and (iii) the electrical resistivity of the concrete. In theory, the potential could fall to a level sufficiently low for hydrogen to be evolved by Reaction 3 (point "A" in Fig. 2) but such low values have not been measured in practice as yet.

5. Unacceptably high corrosion rates which lead to cracking and spalling of the concrete are usually caused by carbonation or chloride ion attack. Carbonation is the reaction between CO_2 from the atmosphere and (primarily) the $Ca(OH)_2$ in the cement. Penetration of the gaseous CO_2 into the concrete occurs most rapidly at low humidities but the chemical reaction takes place in the pore water solution and so occurs most rapidly in saturated concrete. Therefore, net result is that, in practice, carbonation provides the biggest problem at intermediate humidities. There is some disagreement in the literature as to the optimum humidity for the maximum carbonation rate but that is probably because it is also affected by concrete parameters such as cement type, w/c ratio and age. The effect of carbonation is to reduce the pH of the cement pore solution to a level at which the passive film is not stable. As in the case of deaerated concrete, the passive film will dissolve and active corrosion will occur over all the depassivated steel. However, in contrast to the situation described in (4) above in which the concrete is water saturated but deaerated, oxygen is generally readily available in carbonated concrete and a high rate of corrosion (possibly >1 A/m^2 or >1 mm/yr) can be maintained.

VOL
14
198

6. Chloride ions can also initiate active and rapid corrosion but by a different means. The Cl^- can cause local breakdown of the passive film even at high pH, thereby exposing the steel to active dissolution and allowing pits to develop. Galvanic corrosion[§] is then established with the local pits acting as anode and the large, unaffected areas of passivated steel acting as cathode. Since cathodic and anodic currents must be equal, extremely high anodic current densities can develop and pits can rapidly penetrate the thickness of the reinforcement. Furthermore, the acid produced by the corrosion reaction can dissolve the adjacent cement, thereby, removing the local diffusion barriers. There is no unique threshold value of chloride concentration in the concrete for the initiating of pitting: the higher the electrochemical potential and the lower the pH, the less chloride is needed for corrosion to start. Moreover, the type of cement and the w/c ratio play a role in determining how much of the chloride is available in the pore water and how much is chemically bound in the cement.

7. Carbon dioxide and chloride ions can act synergistically in that the carbonation reaction can lower the pH of the pore water allowing chloride attack to occur at lower chloride concentrations than are necessary for corrosion in the uncarbonated concrete.

Electrochemical Kinetic Measurements

As mentioned above, the possibility of a corrosion reaction occurring can be predicted theoretically but the kinetics of the reaction, ie, the rate at which it proceeds, can only be determined empirically. Yet it is the rate at which the steel corrodes which is of interest to the engineer and is, thus, of greatest importance.

Electrochemical kinetic measurements are standard and very common procedures in the study of the corrosion of metals in aqueous solutions. However, they have not been widely used for steel in concrete because of the experimental difficulties involved with (i) the very low current densities, (ii) the high electrical resistance of the concrete and (iii) the long experimental times involved. However, such measurements can be used to give both an estimate of the corrosion rate occurring at the time of the investigation, and an idea of how the corrosion rate will change if the corrosion potential were to change due, for example, to environmental changes. Electrochemistry can also be used to detect the onset of corrosion due to carbonation or to chloride penetration and can give a measure of the magnitude of these effects in different environments or different concretes.

Figure 3 gives a schematic representation of the currents due to (ie. the rates of) the Reactions 1a, 2 and 3 as a function of electrochemical potential. The equilibrium potentials (at which the net current for each reaction is zero) are given as E^O_{Fe}, E^O_O and E^O_H, respectively. At equilibrium in an aerated solution of high pH, the potential at the steel interface will attain that value ($E_{R(Fe/O)}$) at which the cathodic current, i_c, due to oxygen reduction (line (b)) is equal to the anodic current, i_a, due to iron dissolution or oxidation (line (c)) and the corresponding corrosion rate will be $i_{R(Fe/O)}$. In deaerated solutions, on the other hand, the corrosion potential

---

[§]**Galvanic corrosion** is the term applied to the acceleration in the rate of corrosion of one metal due to contact with a dissimilar metal and is due to the difference in electrochemical potential of the two metals. In the present case, the two "dissimilar" metals are the areas of actively corroding steel and the remaining passivated steel.

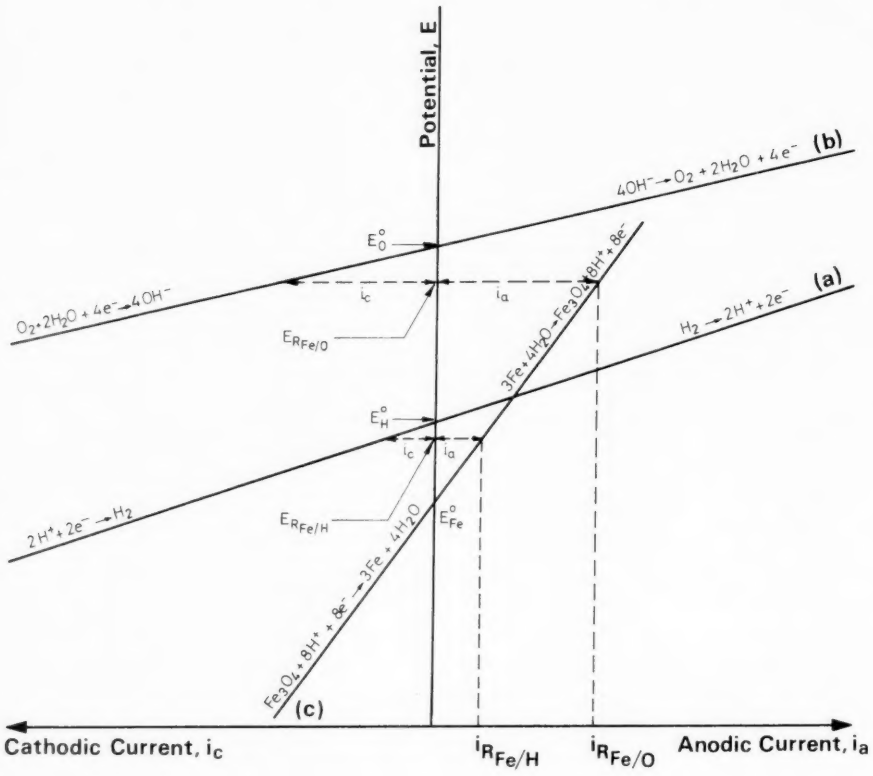

FIG. 3.

The potential/current relationship for Equations 1a, 2 and 3

and corrosion current will attain lower values, $E_{R(Fe/H)}$ and $i_{R(Fe/H)}$, respectively, corresponding to the values at which the rate of hydrogen evolution (line (a)) is equal to the rate of iron oxidation.

Because of the large range of current values often involved, the currents are usually plotted on a logarithmic scale with anodic and cathodic currents plotted in the same direction, as illustrated schematically in Fig. 4.

In practice, it is not possible to determine the actual corrosion rate (as the corrosion current, i_R), directly. This is because, during actual corrosion, the rate of emission of electrons by the iron is exactly equal to their rate of consumption by the oxygen and/or hydrogen ions and, therefore, there is no measurable net current. In order to obtain an estimate of the current, i_R, it is necessary to shift the potential away from the equilibrium value, E_R, measure the resultant net current and extrapolate the data back to E_R.

Experimentally, this can be accomplished as illustrated schematically in Fig. 5. A steel rod is embedded in the cement paste, mortar or concrete of interest and, after appropriate curing, the sample is immersed in water. The corrosion potential, E_R, of the steel is measured relative to a reference electrode and then, by means of a potentiostat, the potential of the embedded steel is shifted away from E_R. The resulting current flowing between the embedded steel (the working electrode) and an external steel plate (the

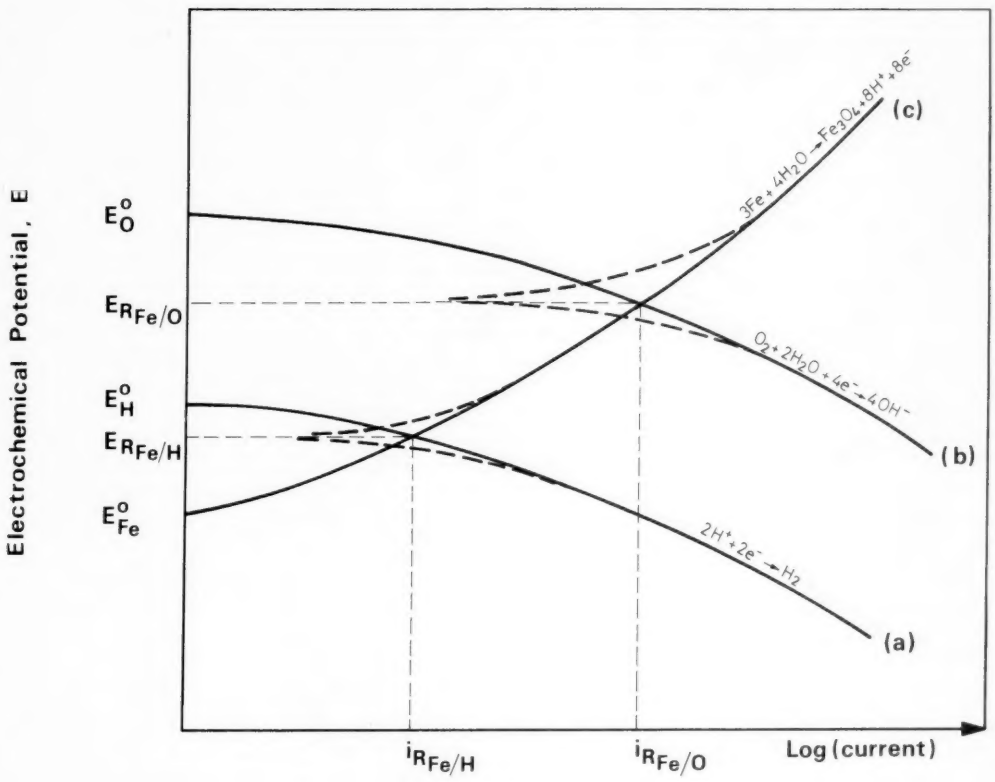

FIG.4.

The potential/log(current) relationship for Equations 1a, 2 and 3

counter electrode) is then measured. What one actually measures is the net current (i_a - i_c) which is shown as the heavy dashed lines in Fig. 4.

Potentiostatic Polarization Curves

One electrochemical method of studying corrosion of reinforcement steel embedded in concrete or mortar, is to determine a "complete" polarization curve. This may be accomplished either potentiodynamically or potentiostatically. The former, which the is most common in the study of metals in aqueous solutions, involves sweeping the potential from E_R in a positive direction a few hundred millivolts while simultaneously determining the current, then reversing the potential sweep to a few hundred millivolts more negative than E_R and so back again to E_R. The potentiostatic technique is similar except that the potential is applied in steps and the system allowed to come (more or less) to equilibrium at each step before the current is measured. For steel embedded in concrete, in which diffusion and migration processes are slow, the latter technique is considered (by the author!) to be the more appropriate.

The shape of the polarization curve for passivated steel in concrete is shown schematically in Fig.6, in which the various reactions are indicated. Fig. 7 shows experimental curves[6] obtained potentiostatically for steel in OPC

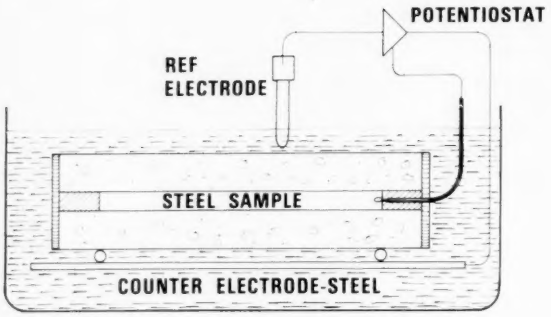

FIG. 5

Schematic illustration of potentiostatic measurements

mortar (a) in the passive state and (b) after it was exposed to chloride solution for a few weeks and had begun to corrode. By extrapolating the data from higher potentials to E_R, it is clear that the corrosion rate of the passive steel is only 10^{-4} A/m^2 or ~0.1 μm/year whereas that which has been attacked by chloride ions is corroding at a rate of 10^{-1} A/m^2 or ~0.1 mm/year. The current, however, is averaged over the whole bar and, in the case of chloride attack, the corrosion is a local phenomenon and covers only a small fraction of the total area of the steel. By removing the concrete and measuring the area of corrosion, the actual corrosion rate was found to be, in fact, 1 mm/year.

Because the data were obtained potentiostatically and the samples allowed to come to steady state at each value of applied potential, the polarization curves also give an indication of the maximum rate of corrosion of the steel if the potential should be raised. Potentiodynamic measurements do not allow the system to come to steady state and on cannot, therefore, infer anything from current values at different potentials.

Determination of a complete potentiostatic polarization curve can take up to a month of experimental measurements. However, a large number of samples can be connected in parallel and examined simultaneously. In concrete, where there are numerous variables to investigate and samples vary with age, this ability to measure, simultaneously, a number of samples which were cast at the same time and, for example, then exposed to different conditions, can be a significant advantage. There are, of course, also some disadvantages of the technique and there has been doubt expressed[7] concerning the long term effects on the samples of applying overpotentials of several hundred millivolts. Such effects are currently under investigation but preliminary results suggest that there is as short term effect but not a long term one[8].

Linear Polarization or Polarization Resistance

This technique, also known as the "Stearn-Geary" method [9], involves much smaller polarization of the steel. The current is measured for applied potentials up to +10 mV from E_R and the slope of the curve through zero applied potential, as shown in Fig. 8, is determined as the "polarization resistance", R. The actual current is then calculated from the relationship:

$$i_{corr} = B/R$$

where B is an empirical constant normally determined from the full polarization curve. While this is an easy and quick technique, the value of B has not been determined accurately for steel in concrete and the value used is generally that obtained for steel in alkaline aqueous solutions. A second

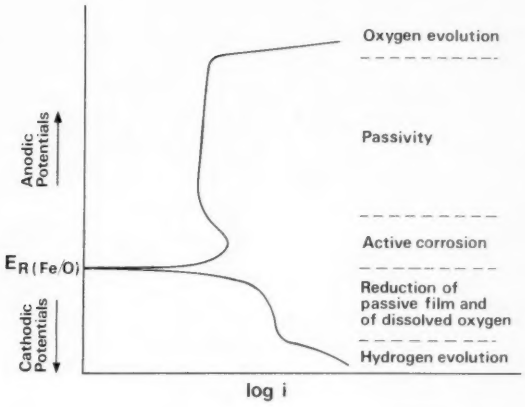

FIG. 6

Schematic polarization curve for passivated steel in dearated concrete.

disadvantage is that at such small overpotentials, the net current for steel that is not actively corroding is extremely small giving rise to measuring difficulties. Thus, the technique is appropriate for actively corroding steel but less so for passivated steel. Moreover, because each sample will have a different value of E_R, all samples must be measured individually.

Determination of the Onset of Corrosion

A fairly simple method of determining the onset of corrosion under given environmental conditions is to apply a constant positive potential of a few hundred millivolt to the steel embedded in concrete and periodically measure

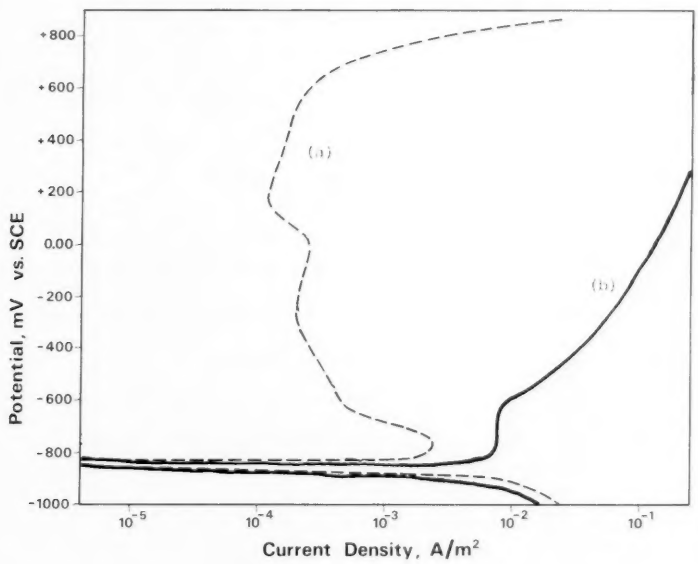

FIG. 7

Experimental potentiostatic polarization curves for steel in OPC mortar (w/c = 0.5) at 22°C. Curve (a) is for passivated steel and curve (b) for corroding steel due to chloride ion attack.

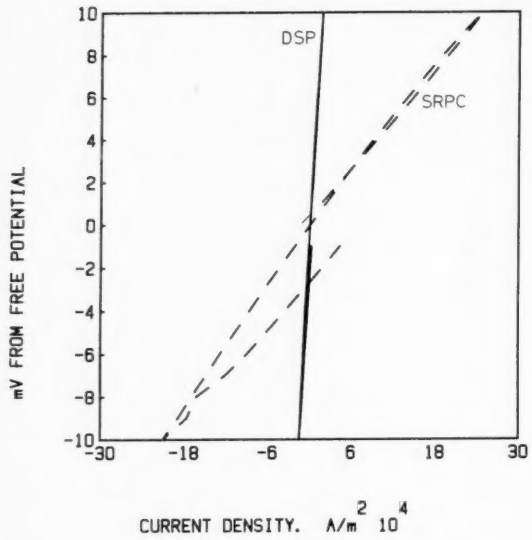

FIG. 8

Experimental polarization resistance curves for passive steel in dense silica-cement mortar (DSP) and actively corroding steel in Cl^--containing OPC mortar.

the current flowing from the steel to an external electrode. For example, samples can be immersed in salt water, be subjected to an impressed anodic potential and the current monitored daily until a signifiant increase in current is noticed, corresponding to the onset of chloride ion attack. This technique is particularly useful for comparing different cement types, or different concrete qualities.

VOL.
14
198

Acknowledgments

The author would like to express her appreciation of the financial support for this work provided by the Danish Council for Scientific and Industrial Research. She would also like to thank Dr. I.L.H. Hansson and Mr. H.H. Bache for their valuable comments on the manuscript.

References

1. F.O. Grønvold, The Danish Corrosion Centre, to be published.
2. See for example: J.C. Scully, "The Fundamentals of Corrosion", 2nd. edition, Pergamon Press, Oxford, 1975.
3. M. Pourbaix, "Atlas of Electrochemical Equilibria in Aqueous Solutions", Pergamon Press, Oxford, 1966.
4. M. Pourbaix, Corrosion Science 14, 25 (1974).
5. See for example: J.O'M. Bockris and D. Drazic, "Electrochemical Science", Taylor and Francis Ltd., London, 1972.
6. C.M. Preece, H. Arup and T. Frølund, Proc. 1st. Int. Conf. on the Use of Fly Ash, Slag, Silica Fume and Other Mineral By-products in Cement, Montebello, Canada, 1983.
7. C.L. Page and K.W.J. Treadaway, Nature, 297, 109 (1982).
8. C.M. Hansson, The Danish Corrosion Centre, to be published.
9. M. Stearn and A.L. Geary, J. Electrochem. Soc. 104, 56-63 (1957).

CEMENT and CONCRETE RESEARCH. Vol. 14, pp. 585-594, 1984. Printed in the USA.
0008-8846/84 $3.00+00. Copyright (c) 1984 Pergamon Press, Ltd.

DRYING SHRINKAGE OF PORTLAND CEMENT PASTES
I. MICROCRACKING DURING DRYING

C.-L. Hwang* and J. F. Young
Department of Civil Engineering
University of Illinois
Urbana, Illinois 61801

(Refereed)
(Received Oct. 31, 1983; in final form April 19, 1984)

ABSTRACT

The occurrence of microcracking of portland cement pastes during drying has been studied by comparing the effects of specimen thickness on shrinkage and cracking using light microscopy. Increases in specimen thickness tended to impede drying and wetting, but there were only slight changes (less than experimental errors) in total and reversible shrinkage once equilibrium was attained. Although microcracking occurred at the beginning of drying whenever the thin specimen (thickness <2mm) was suddenly exposed to low relative humidity (~50%), the cracks eventually closed up. It was concluded that no matter whether or not this microcracking happened, the shrinkage of the specimen after reaching equilibrium was unrestrained.

OL.
14
984

Introduction

Wittman (1) has pointed out that shrinkage mechanisms can only be deduced from measurements of total deformation of drying specimens when unrestrained shrinkage occurs. This does not happen in mortar or concrete specimens (2-4) because moisture gradients cause tensile cracking (4), and carbonation shrinkage may also occur (3). There is a possibility that cement paste specimens, often used to explore shrinkage mechanisms, may undergo similar microcracking. The fact that the permeability coefficient of a dried paste was found to be 70-fold greater than that of an undried paste (5) has been explained as the effect of microcracking (6,7). Bazant and Raftshoel (7) determined that microcracking will occur even in a specimen 1 mm thick if it is suddenly exposed to a lower rh. Microcracking may even occur at high relative humidities as a result of shrinkage stresses developed in the vicinity of CH crystals (9), and may offset drying shrinkage (7) (although this mechanism was not thought (10) to have a strong influence).

Chatterji (6) concluded that drying shrinkage of cement paste is not a material parameter because of microcrack formation, but Bentur et al. (11) claimed that such cracking is a result of moisture gradients and will not occur in thin specimens. Both specimen thickness (12) and drying rate (12,13) apparently have

*Associate Professor of Construction Engineering and Technology, National Taiwan Institute of Technology, Taiwan, ROC.

no effect on the magnitude of shrinkage when specimens are dried to an equilibrium condition. Actually, the size and shape of a paste specimen will affect the rate of drying (8), but the ultimate irreversible, reversible, and total shrinkages are not greatly affected (12,13). Day and Illston (12), therefore, concluded that miniature specimens can be used to measure the unrestrained response of the material as long as equilibrium conditions are met.

Experimental

Pastes of a Type I portland cement were prepared at 0.4 w/s (water/solid) ratio, using procedures similar to those described by Helmuth and Turk (14) (see Figure 1). Specimen thicknesses for measuring the effect of geometry on shrinkage were 1 and 3 mm, and less than 1 mm for direct observation of microcracking. Gauge lengths were about 100 mm.

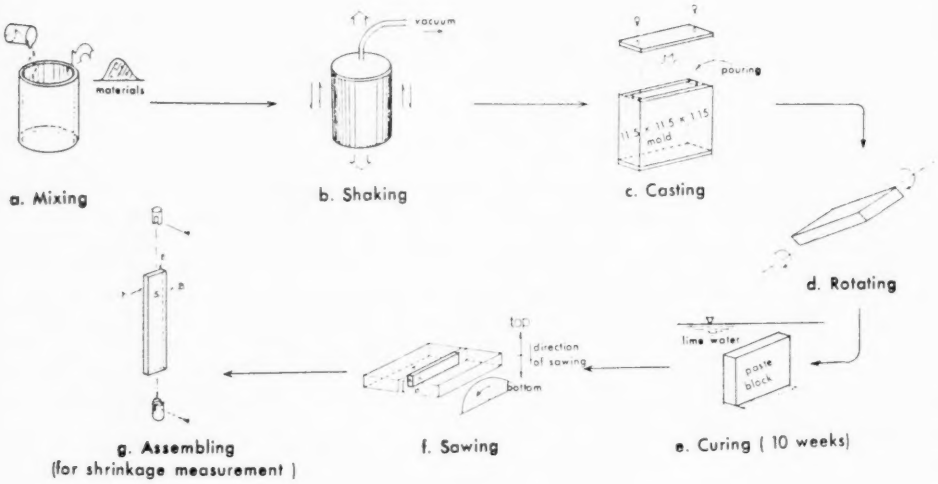

Figure 1. Flow chart of specimen preparation.

Shrinkage and Weight Change Measurement

The original dimensions of the specimens were measured using a vernier caliper under water. Then the free water on the specimen surface was quickly wiped off with a paper towel, and the specimen was put into a clean plastic tube with lids on both sides. The virgin weight of the specimen in the saturated surface dry (SSD) state was then measured on an analytical balance, (Ainsworth, Model 24N) which was readable to 0.01 mg. The original reference weight of the specimen was determined with two 1/4-in stainless steel grips (which were machined with either a 1.2 mm or 3.2 mm slot in the center which resembled a U-shaped notch), two plastic plates, and four 3/32-in OD stainless steel bolts. The hardware formed the gauge points and, after weighing, the specimen was assembled under water with two grips on the longitudinal sides as shown in Figure 1 (procedure g). The original reference length reading was measured with a frame-type dial gauge comparator (15), which was zeroed using a 5-in long stainless steel rod. The specimen was then transferred to a desiccator at 100% relative humidity, which was kept free of carbon dioxide, until shrinkage and weight change measurements were begun. Shrinkage measurements were reproducible to $\pm$ 5 x 10^{-6} mm/mm.

Drying was accomplished with the aid of vacuum desiccators that contained an appropriate saturated salt solution (15,16). The reliability of this humidity-controlling method has been found to be satisfactory (16); the sorption characteristics of a vycor glass obtained using this method coincided with those obtained using aqueous sulfuric acid solutions (17), and is similar to other data (18). In order to insure that air was completely removed from the system, the use of slow pumping for a few minutes was necessary.

Since the moisture within a specimen diffused out fairly rapidly due to the specimen's small thickness, it was necessary to measure the specimen several times on the first day of drying. Rewetting was needed in order to get the true profile of shrinkage versus weight change. After drying for 30 days at four different relative humidities specimens were transferred to a dessicator at 100% rh. As in the case of the drying process, the rewetting was monitored several times within the first day of rewetting. Finally, the specimens were resaturated with water under vacuum to insure that no entrapped air bubbles impeded the filling of the pores.

Light Microscopy

To detect the presence and onset of microcracking during drying a 1-2 mm thick specimen was moved directly from 100% rh to room rh (about 50%) on the specimen stage of a Carl Zeiss photomicroscope. Microcracks can be observed easily by the off-centered, bright-field illuminating technique (19) at a magnification of 740x or higher. Dark-field illuminating was also used at a magnification of 350x or lower. In this case the specimen was periodically dyed with a solution of silver nitrate in methanol every ten minutes during the first hour after observation was started. Silver nitrate absorbed in the cracks subsequently reacted with the alkaline environment to form a silver oxide-metallic silver mixture which provided a dark stain highlighting the cracks. A resolution of less than 1 μm could be achieved by both methods.

Results and Discussion

Shrinkage and Weight Change

The influence of specimen thickness can be seen from Figure 2, and is summarized in Table 1. The thickness of the specimens tended to impede drying and wetting. Specimen thickness affects the relative weight change more than the relative length change. This is thought to be due to the fact that water in capillary pores must diffuse a greater distance to leave the specimen, while internal stresses causing shrinkage still develop quite quickly.

Microcracking Observations

The specimen was exposed to ambient relative humidity (∿50%) while being observed under off-center, bright-field illumination at 737x magnification. After about 8 minutes of drying, "ridges" were seen around CH crystals, along with some surface microcracking. It was not possible to obtain satisfactory micrographs of the ridging effect, but the microcracks can be photographed quite well at lower magnification (373x), as shown in Figure 3. The ridging around CH crystals cannot be readily distinguished in such photographs, but arrows mark two of the more prominent examples. Later, at about 15 minutes, the specimen was dyed with silver nitrate in methanol and observed by dark-field illumination at 373x magnification. The cracks at the edges, which are best observed in this manner, gradually opened up during the first day, but later closed up (to ∿1 μm), some disappearing entirely. Figure 4 illustrates this behavior. Most of the cracks are located near the edges of the specimen with only a few located near the center. Figure 5 presents schematically the

Table 1. The Effects of the Specimen Thickness on Shrinkage Behavior

Series	1 mm Nominal Thickness				3 mm Nominal Thickness			
Thickness (mm)	1.03	0.94	0.91	0.70	2.95	2.66	2.52	2.28
rh (%)	80	60	40	20	80	60	40	20
Time to reach equil.† (hrs)	75	74	70	70	75	75	103	103
Max. shrinkage rate (% length change/hr)	0.0326	0.0359	0.0633	0.1228	0.0196	0.0411	0.0413	0.0462
Max. drying rate (% water loss/hr)	1.93	2.24	4.44	9.60	0.45	0.85	1.09	1.59
Time to reach equil. at 100% rh (hrs)	100	120	150	145	86	94	146	146
Max. swelling rate (% length change/hr)	0.0265	0.0441	0.0509	0.0598	0.0183	0.0294	0.0425	0.0192
Max. wetting rate (% water gain/hr)	0.45	0.90	1.30	4.32	0.26	0.45	0.67	0.96
Total Shrinkage (%)	.1155	.2023	0.3156	0.3539	0.1108	0.1943	0.2931	0.3169
Irreversible shrinkage (%) (% of total)	.0355 (31)	.0571 (28)	2.0936 (30)	0.1008 (28)	0.0309 (28)	0.0504 (26)	0.0741 (25)	0.0804 (25)
Reversible shrinkage (%) (% of total)	.0800 (29)	.1452 (72)	0.2220 (70)	0.2531 (72)	0.0799 (72)	0.1439 (74)	0.2190 (75)	0.2365 (75)
Weight loss (%)	5.17	9.13	12.23	14.75	3.73	8.17	11.39	13.58

† Equilibrium was defined as the time when moisture change rate was less than 0.02 % per hour and strain rate was less than 0.0002 % per hour. (13)

VOL. 14 1984

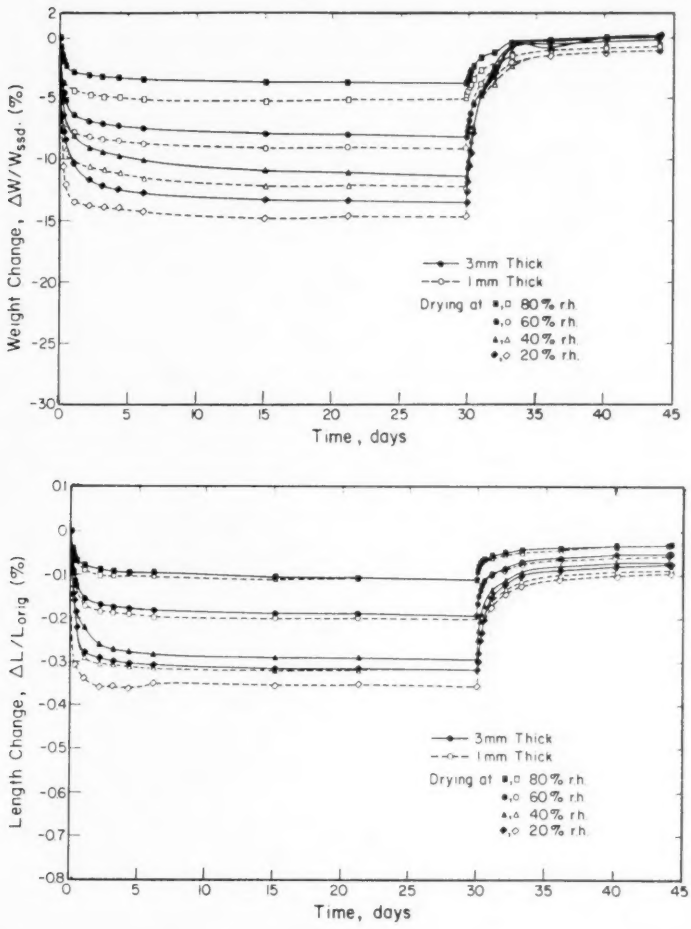

Figure 2. Effect of specimen thickness on drying at various relative humidities (a) weight change with time, (b) length change with time. (Samples rewet after 30 days drying)

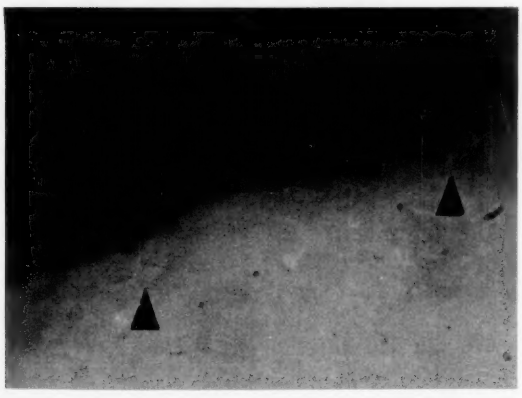

Figure 3. Micrograph (reflected light) of specimen surface cracking after 24 min. drying at 50% rh. Arrows mark examples of "ridging" around CH crystals (373x). The irregular line of contrast running across the micrograph is a surface crack caused by rapid drying at the surface.

general pattern of the cracking after two days exposure. The tensile crack pattern observed by Chatterji (7) only occurred when the specimen was warped, constrained on one side, or macrostructurally heterogeneous due to bleeding on the surface or incompatibility of the materials such as the curving area of a cylindrical specimen. A typical crack pattern is shown in Figure 6 when drying from one side under restrained conditions. The average original crack width was greater than 1 mm. Permanent microcracks were only observed on one side, where heterogeneity due to bleeding is suspected. This may have occurred in a previous study (21) of shrinkage cracking.

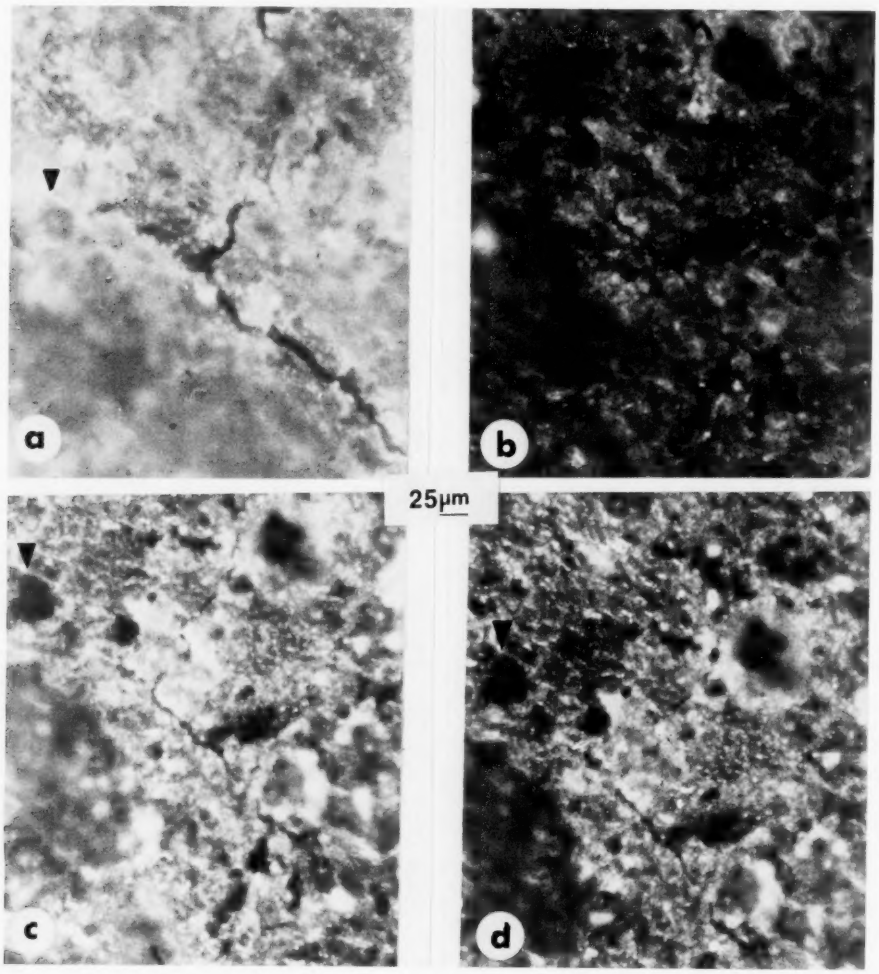

Figure 4. Light micrographs of specimen edge cracking during drying. (a) 1 day, (b) 3 days, (c) 4 days, and (d) 6 days. In (d) only the residual silver from the silver nitrate stain is seen, the cracks having closed up completely. (The arrow in each micrograph indicates the same pore, which was used as a location marking.)

VOL
14
198

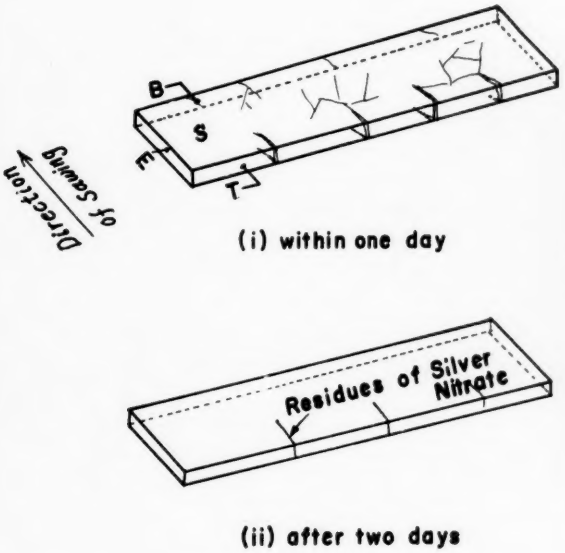

Fig. 5. Schematic view of cracking behavior in thin unrestrained specimens during drying (T and B are cast surfaces (top and bottom) while E and S are sawn surfaces

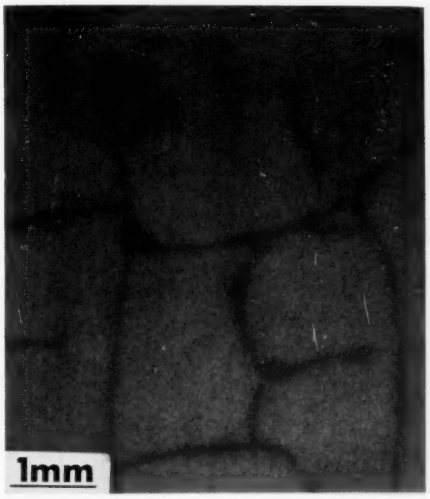

Fig. 6. Optical micrograph showing tensile cracking pattern after restrained drying for 4 hours (silver nitrate stain)

Phenomenologically, from direct observation the microcracking process can be represented schematically, as in Figure 7. Stage I is the "impact" period. At the beginning of this stage, the specimen suffers an extreme surface contraction due to sudden drying, and this might induce some microcracking due to tensile stress exceeding the tensile strength of the paste near the edge. Local ridges were observed around the CH crystals at the beginning of drying because of compression at the region of CH crystals induced by shrinkage of the C-S-H alone. Microcracks also radiate from CH boundary due to the differential contraction between CH and C-S-H phases. Kawamura (9) predicted this kind of microcrack, but not the ridging effect. The "ridging" around CH crystals is reduced after a while because the stress perpendicular to CH boundaries due to the C-S-H is reduced, but the radiating cracks due to differential contraction propagate to form randomly oriented cracks which pass around other CH boundaries but are arrested by other cracks. Once the cracks have initiated, the internal compressive stresses caused by the differential moisture gradients dissipate, and driving forces exerted inside the pores of the specimen decrease as the moisture diffuses out. Because the moisture during this stage is lost fairly rapidly, as would be expected from diffusion theory, the cracking propagates as in Stage II.

In Stage III, the cracks fully open up since the shrinkage near the edge has almost ceased due to moisture being lost more rapidly from the new cracked surfaces. However, near the center portion shrinkage is still going on, until internal tensile stress is less than the paste strength, at which time the cracks cease to propagate. After Stage III. the cracks close up gradually as the center core shrinks until fully closed, and only small traces of silver nitrate can be observed. Unless there is macroscopic heterogeneity (due to a higher w/s ratio near the edge caused by bleeding) the cracks of a cement paste

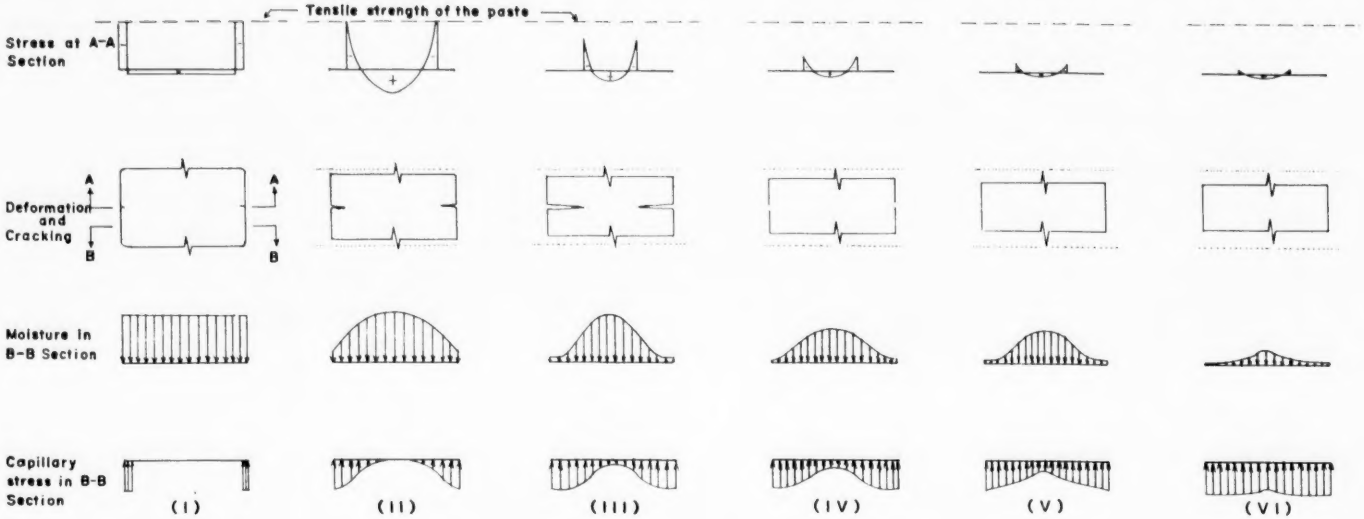

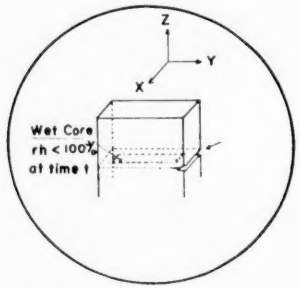

Fig. 7. Schematic Demonstration of Deformation, Crack Formation, Internal Stresses, Moisture Profile and Capillary Stresses of a Thin Specimen ($t \simeq 1mm$).
(I) 10 minutes (II) 10 minutes $\sim$ 4 hours
(III) 4 hours $\sim$ 1 day (IV) 1 $\sim$ 2 days (V) 2 $\sim$ 4 days (VI) after 4 days (almost equilibrium)

should wholly close up when the shrinkage reaches equilibrium with the given relative humidity. Equilibrium was assumed to have been reached when the weight loss rate had fallen to 0.02% per hour and the shrinkage rate to 0.0002% per hour (13).

The extent of microcracking is somewhat exaggerated in Figure 5 for clarity. The cracks at the edges only propagate to about 5% of the specimen width so that about 90% of the specimen width remains uncracked. Thus it is anticipated that the shrinkage of this specimen is largely unrestrained. This was confirmed by the absence of size effects. The "macrocracking" that occasionally occurs in thin-walled cylindrical specimens during rapid drying (11) is caused by the difference in length between the inner and outer circumferences, which leads to slightly different shrinkage strains and hence induces a circumferential stress. This type of cracking will not affect the longitudinal shrinkage behavior.

This conclusion may not contradict the observation of a higher permeability coefficient for a dried specimen (5), since, if the cracks occur at the surface, the effective thickness will be reduced and this will increase the flow rate. The apparent (but not the intrinsic), permeability coefficient may give some information of the extent of cracking, but cannot be used to deduce the true history of cracking.

Conclusions

The thickness of cement paste specimens in the range of 1 to 3 mm did not affect equilibrium shrinkage, although it did affect drying and rewetting rates. Therefore, the measured shrinkage of a thin specimen can be used to determine the shrinkage of the paste under unrestrained conditions.

Direct observation by optical microscopy also showed that, although some microcracks may form on the surfaces at the beginning of drying, only a small volume of the paste is affected. These cracks close up later and do not affect the shrinkage at the equilibrium condition.

Acknowledgments

This work forms part of a thesis by C.-L.H. in partial fulfillment of the Ph.D. degree at the University of Illinois. Partial financial support for C.-L.H. was provided by the University of Illinois Research Board. The assistance of Professor F. V. Lawrence and Dr. N. Ho with the light microscopy is gratefully acknowledged.

References

1. F. W. Wittmann, in "Creep and Shrinkage in Concrete Structures," p. 129, Ed. Z. P. Bazant and F. H. Wittmann, John Wiley & Sons, Ltd., Chichester, U.K., 1982.
2. D. Campbell-Allen and D. F. Rogers, Mater. Struct. (Paris), 8, 193 (1975).
3. D. W. Hobbs and H. R. Mears, Mag. Concr. Res., 23, 89 (1971).
4. F. H. Wittmann and P. E. Roelfstra, Cem. Concr. Res., 10, 601 (1980).
5. T. C. Powers, L. E. Copeland, J. C. Hayes, and H. M. Mann, J. Amer. Concr. Inst., 51 285 (1954).
6. S. Chatterji, Cem. Concr. Res., 6, 145-148 (1976).
7. S. Chatterji, Cem. Concr. Res., 9, 655 (1979).
8. Z. P. Bazant and W. J. Raftshoel, Cem. Concr. Res., 12, 209 (1982).
9. M. Kawamura, J. Am. Cer. Soc., 61, 281 (1978).
10. Z. P. Bazant and W. J. Raftshoel, Cem. Concr. Res., 12, 132 (1982).

VOL. 14 984

11. A. Bentur, R. L. Berger, F. V. Lawrence, N. B. Milestone, S. Mindess, and J. F. Young, Cem. Concr. Res., 9, 657 (1979).
12. R. A. Helmuth and D. H. Turk, J. Res. Develop. Lab., Portland Cem. Assoc., 9, 8 (1967).
13. R. L. Day and J. M. Illston, Cem. Concr. Res., 13, 7 (1983).
14. R. A. Helmuth and D. H. Turk, Highway Res. Bd. Spec. Rpt. 80, p. 135 (1966).
15. L. J. Parrott and J. F. Young, in "Fundamental Research on Creep and Shrinkage of Concrete," p. 550, Ed. E. H. Wittmann, Martinus Nijhoff, The Hague, Netherlands, 1983.
16. L. J. Parrott, W. Hansen, and R. L. Berger, Cem. Concr. Res., 10, 647 (1980).
17. W. Hansen, Ph.D. Thesis, University of Illinois, 1983.
18. C. H. Amberg and R. McIntosh, Canad. J. Chem., 30, 1012 (1952).
19. D. D. Higgins and J. E. Bailey, in "Hydraulic Cement Pastes: Their Structure and Properties," p. 283, Cem. Concr. Assoc., Slough, U.K. (1976).
20. S. Chatterji, Cem. Concr. Res., 12, 797 (1982).
21. S. Chatterji, N. Thaulow, and P. Christensen, Cem. Concr. Res., 11, 155 (1981).

VOL
14
198

CEMENT and CONCRETE RESEARCH. Vol. 14, pp. 595-599, 1984. Printed in the USA.
0008-8846/84 $3.00+00. Pergamon Press, Ltd.

NOTE

INTRINSIC SORPTION POTENTIAL OF CEMENT COMPONENTS FOR ^{134}Cs

R.W. Crawford, C. McCulloch, M. Angus, F.P. Glasser and A.A. Rahman
Department of Chemistry, University of Aberdeen, Meston Walk,
Old Aberdeen, AB9 2UE, Scotland U.K.

(Communicated by C.D. Pomeroy)
(Received Oct. 31, 1983)

ABSTRACT

The sorptive powers of radioactive Cs for partially or fully hydrated compounds present in cement has been determined at ~18°C for $[Cs^+] \sim 2 \times 10^{-4}$M. In CO_2-free conditions, the hydration products of the silicate, aluminate, ferrite and sulphate phases show negligible sorption, typically less than 0.3%, in experiments ranging in duration between 1h and 40d.

VOL.
14
984

Introduction

Cement-based formulations have been used in the immobilization of nuclear wastes (1). The mechanism of immobilization is, however, complex. Cements undoubtedly afford a degree of physical encapsulation. However, precipitation of some species, arising from the alkaline nature of cement environments, also occurs thereby complicating the interpretation of experimental data on the sorptive potential of cements.

A cement matrix is made by mixing finely ground anhydrous phases, termed clinker, with water. The clinker typically has a surface area of 2-5 x 10^3 cm^2g^{-1}. However, the hydration products have an even greater surface area, typically 10 - 100 m^2g^{-1} (N_2 adsorption) and 250 - 450 m^2g^{-1} (H_2O adsorption) for the calcium silicate hydrate (C-S-H) phase. The high surface area, poor crystallinity at T < 100°C, and rheological properties suggest that the silicate fraction of cement 'paste' is essentially gel-like. Other constituents, such as $Ca(OH)_2$ and calcium aluminate hydrates, are more crystalline but also exhibit high surface areas.

Cesium is difficult to immobilize in cement. It is not precipitated in alkaline solution and is known to be readily leached from set cements (2). It is therefore important to establish whether cement components exhibit significant sorption for Cs, bearing in mind that radiocesium immobilized in cement is typically present only in low concentration, $ca < 10^{-4}$M. Our approach has been to study Cs sorption of phases of cement, either singly or in combination. Data have been reported for some of these components using chemical analyses of solutions of non-radioactive Cs (3). In the present paper, the data have been obtained using spiked radio-Cs, which permits more sensitive assay, and the list of cement components studied has been extended.

Experimental

Phase-pure compounds (>98 - 99% pure) were prepared according to the methods described or referenced in Table 1. Anhydrous phases were made in Pt crucibles heated in air in electrically heated muffles, typically in 20 - 25g batches. The samples were crushed if required before hydration to cement powder fineness (2-4 x $10^3 cm^2 g^{-1}$) which was determined by the Blaine air permeability method.

TABLE 1.

Preparation of Sorbants.

Sorbant	Cement* Chemical representation	Starting Materials and Conditions of Preparation	Reference
$Ca_4Al_2Fe_2O_{10}$	C_4AF	$CaCO_3$, Al_2O_3, Fe_2O_3; 1325°C	5
$Ca_3Al_2O_6$	C_3A	$CaCO_3$, Al_2O_3; 1350°C	5
$Ca_{12}Al_{14}O_{33}$	$C_{12}A_7$	$CaCO_3$, Al_2O_3; 1200°C	12
$Ca_{12}Al_{14}O_{31}F_2$	$C_{11}A_7CaF_2$	$CaCO_3$, Al_2O_3, CaF_2; 1200°C	6
Ca_3SiO_5	C_3S	$CaCO_3$, SiO_2; 1450°C	7
βCa_2SiO_4	βC_2S	$CaCO_3$, SiO_2; 1450°C (B_2O_3 stabilized)	8
γCa_2SiO_4	γC_2S	$CaCO_3$, SiO_2; 1450°C	12
$CaSO_4 \cdot 0.5H_2O$	$C\bar{S}\frac{1}{2}H$	$CaSO_4$, $2H_2O$; 150°C	12
$Ca_6Al_2S_3O_{21} \cdot 32H_2O$	$C_6A\bar{S}_3H_{32}$	$Ca(OH)_2$, $CaSO_4$, $Ca_4Al_6SO_{17}$, H_2O <18°C	9

*Cement chemical shorthand nomenclature: C = CaO, A = Al_2O_3, F = Fe_2O_3, S = SiO_2, $\bar{S}$ = SO_3, H = H_2O. Ettringite has the approximate formula $C_6A\bar{S}_3H_{32}$.

Crystalline ettringite was prepared by reaction of C_3A with gypsum and water at or below 18°C. The synthetic C-S-H gel was made by precipitation:- by mixing, with stirring, 0.1M Na_2SiO_3 and 0.1M $Ca(NO_3)_2$ solutions. The product was aged for 7 - 10d, filtered, and washed free of nitrate ions prior to use. The hydration products of a cement made to BS 12 (similar to ASTM Type 1) were made by hydrating commercial cement at 18°C with continuous ball milling for 60d. This hydrated product, consisting of a C-S-H gel together with calcium aluminates, $Ca(OH)_2$, etc., was used for sorption studies and was always handled in a CO_2-free atmosphere. The sorptive power for Cs was determined by shaking several grams of the potential sorbate with 500 mℓ of distilled water in sealed plastic containers at 18°C for periods up to 28d. Aliquots of solution were periodically removed for analysis. The Cs source was either CsCℓ or $CsNO_3$ and sorption occurred typically from solutions having an initial Cs content of 2-3 x 10^{-4} M. Analyses for Cs by atomic absorption were not satisfactory because of the rather small changes in Cs concentrations and also because of the need to remove suspended materials prior to analyses by filtration: cellulose filtration media were found to exhibit significant Cs sorption relative to that of the cement components being tested. Therefore, radiometric analyses were used in conjunction

with centrifugation to remove suspended matter: the solution was spiked with ^{134}Cs, a γ emitter with a half-life of 2.06 yr. Precise liquid aliquots were withdrawn using an Eppendorf pipette and the solution clarified by centrifugation, during which time CO_2 was excluded by using a CO_2-free glove-box. The clear solution, free from sediment, was counted using a Tl-activated NaI scintillometer tuned to the appropriate energies; 604.7 and 795.8 keV.

Results

Table 2 records the results obtained in terms of counts (disintegrations per minute, dpm) from the start of the experiment. Some data points have been omitted; only the shortest and longest times, together with selected data obtained at intermediate times, are given. During the course of the experiment the anhydrous reactants had partially or wholly hydrated: C_3A, C_4AF and $C_{11}A_7.CaF_2$ had completely hydrated, C_3S had mostly hydrated, βC_2S had partially hydrated, while γC_2S remained largely unhydrated at the conclusion of the experiment (these abbreviations are defined in Table 1). The fine-grained gypsum remained unchanged. The results obtained show that (i) the anhydrous clinker phases present in Portland cement exhibit virtually no sorption for Cs, (ii) during the course of hydration the *in situ* development of hydrate phases does not significantly increase the sorption potential and (iii) C-S-H together with $Ca(OH)_2$, made in a separate stage and subsequently mixed with Cs-containing solution, does not develop a useful sorptive potential. Thus synthetic C-S-H and C-S-H made from hydration of commercial clinker have similar behaviour towards dilute Cs solutions, with neither exhibiting significant soprtion for radiocesium.

Discussion

It would appear from the present data that the components of cement, anhydrous and hydrous, taken either singly or in combination, do not possess significant sorption potential for Cs^+ at solution strengths $\sim 10^{-4}$ M: the sorption is less than 0.3%. The generally poor sorption potential (but not its proximate value) might have been anticipated from the high leach rates reported for Cs in previous studies (7). Hydrated cements comprise a solid with complex porosity extending to microporous regimes. Therefore ions which remain soluble during the setting process, undergoing neither crystallochemical incorporation in the structures of the solid phase nor sorption on the surfaces, are potentially liable to be leached when Cs-containing fluids in the pores can exchange with leachant.

Nevertheless, the hydration products of cement have very high surface areas, typically 10 - 100 m^2/g for C-S-H when measured by N_2 absorption, and their negligible sorption for Cs must indicate that the surfaces of the principal hydration products have no sites suitable for sorption of large positive ions. Some of the crystalline phases developed in cements, of which ettringite is the most important example, have zeolite-like structures. The crystal structure of ettringite is known to contain open channels which can collect a large range of negatively-charged particles or neutral molecules (10, 11). But, as shown, the channels clearly do not afford favourable sites for the retention of positive ions.

Conclusive proof of the low sorptive power of cement phases for Cs is important for two reasons. Firstly, leach-rate models are usually designed to include a number of parameters, including a factor for sorptive effects. It is useful to establish that, for Portland cements set under normal conditions, this factor is negligible. Secondly, the intrinsic lack of

VOL. 14 984

TABLE 2.

Sorption of Cs onto Selected Cement Components

Initial Phase Composition	C_4AF	C_3S	C_3A	βC_2S	γC_2S	$C\bar{S}$	$C_{11}A_7.CaF_2$	Ettringite	C-S-H	Ordinary Portland Cement
Cs^+ Molarity	2.92×10^{-4}	3.40×10^{-4}	2.96×10^{-4}	2.98×10^{-4}	2.85×10^{-4}	2.85×10^{-4}	2.64×10^{-4}	2.76×10^{-4}	2.83×10^{-4}	2.83×10^{-4}
Initial Count Rate† (dpm)	4211±36	4320±74	4372±26	4410±28	4219±68	4208±49	3909±63	4078±41	4227±49	4216±58
Time h d										
1	4234±35	4322±85	4436±47	4436±62	4399±68		4020±59	4020±37		
2	4185±43	4391±69	4405±41	4458±28	4399±51	4208±49		4077±38		
4	4266±81	4336±55	4386±18	4395±32	4371±41			4026±46		
6	4234±39	4412±34	4474±35	4507±23	4349±32		4011±28	4023±47		
1	4362±46	4406±53	4421±83	4469±31	4205±40	4210±54	4003±42	4040±41	4201±56	4312±43
3 - 9	4182±60	4275±41	4423±24	4430±29	4290±39	4207±46	3984±33	4018±36	4302±37	4295±61
10 - 19	4262±36	4297±13	4404±44	4221±36	4299±29	4296±36	3903±40	3996±27	4211±49	4206±32
20 - 40	4214±40	4300±25	4400±55			4292±38				

† This activity represents the bulk solution count rate prior to addition of sorbants.

VOL 14 198

sorption potential lends additional weight to improving the physical properties of cement leading to leaching, *e.g.* permeability, as well as encouraging efforts to improve the sorptive characteristics of cement-based systems by tailoring the composition, for example, by adding Cs-selective sorbants which can be shown to remain stable in the cement environment.

Finally, we note that the absence of any mechanism for the removal of radiocesium by the cement components and their hydration products enables us to follow the rate at which water is withdrawn into the hydration products, by monitoring the progressive increase in Cs^+ concentration in the remaining pore fluid. The technique and its application to cement hydration will be described more fully in a subsequent paper.

Acknowledgement

This work has been commissioned by the European Atomic Energy Community through its indirect action program and by the United Kingdom Department of the Environment as part of its radioactive waste management research programme. The results will be used in the formulation of Government policy but at this stage they do not necessarily represent Government policy.

References

1. J.A. Stone, in "Scientific Basis for Nuclear Waste Management" (G.J. McCarthy, Ed.) Vol. 1, p. 443, Plenum Press, New York (1978).
2. F.P. Glasser, A.A. Rahman, R.W. Crawford, C.E. McCulloch and M.J. Angus, "Immobilization and Leaching Mechanisms of Radwastes in Cement-based Matrices", U.K. Department of the Environment, Report DOE/RW/82.050, (1982).
3. S. Komarnerni and D.M. Roy, Cement Concrete Res., 11, 789 (1981).
4. G. Rudolph and R. Köster, in "Scientific Basis for Nuclear Waste Management" (G.J. McCarthy, Ed.) Vol. 1, p. 467, Plenum Press, New York (1978).
5. I. Jawed, S. Goto and R. Kondo, Cement Concrete Res., 6, 442, (1976).
6. H. Uchikawa and S. Uchide, Cement Concrete Res., 2, 682 (1972).
7. K. Mohan and F.P. Glasser, Cement Concrete Res., 7, 1, (1977).
8. I. Jelenic, Cement Concrete Res., 8, 173, (1978).
9. K. Ogawa and D.M. Roy, Cement Concrete Res., 11, 741, (1981).
10. A.E. Moore and H.F.W. Taylor, Nature, 218, 1048, (1968).
11. A.E. Moore and H.F.W. Taylor, Acta Crystallog., B26, 386, (1970).
12. F.M. Lea, "The Chemistry of Cement and Concrete" 3rd Edition, 18, pp 46 - 49, Edward Arnold Pub., (1970).

VOL. 14 1984

VOL
14
198

CEMENT and CONCRETE RESEARCH. Vol. 14, pp. 601-602, 1984. Printed in the USA.
0008-8846/84 $3.00+00. Copyright (c) 1984 Pergamon Press, Ltd.

DISCUSSIONS

UNE DISCUSSION DU MEMOIRE "INFLUENCE DE LA TEMPERATURE DE RECUIT SUR LA CINETIQUE DE L'HYDRATATION DU SILICATE TRICALCIQUE" PAR P. FIERENS, KABUEMA Y. ET J. TIRLOCQ*

John Bensted
Blue Circle Industries PLC,
Research and Development Division,
London Road, Greenhithe, Kent, DA9 9JQ,
Angleterre

VOL. 14 1984

J'ai lu le travail par MM. Fierens, Kabuema et Tirlocq (1) avec beaucoup d' intérêt. Ces auteurs ont montré les effets utiles de recuit du silicate tricalcique à une température comprise entre 800 et 1600°C sur sa cinétique d' hydratation, étudiée par la microcalorimétrie. Les échantillons traités à 1000 et 1200°C, qui se distinguent par une teneur élevée en chaux libre due à une décomposition thermique mais également par une courbe de thermoluminescence nettement différente, présentent une cinétique d'hydratation plus lente que celle des autres échantillons. Il semble donc que non seulement la décomposition thermique partielle mais également les characteristiques des défauts de structure du silicate tricalcique pourraient influencer la cinétique de son hydratation.

Ces idées sont compatibles avec les résultats de Maycock, Skalny et Kalyoncu (2), qui ont étudiés l'influence des défauts de structure. On a introduit ces défauts par chauffer, tremper ou moudre et la période d' induction pendant l'hydratation du silicate tricalcique a été réduite. Les auteurs ont conclu que l'existence d'une couche protecteuse hydratée sur le surface ne soit pas la cause de la période d'induction et ainsi influence le processus d'hydratation, parce qu' elle s'est formée après l'introduction des défauts de structure.

Il serait difficile à ce moment de faire une extrapolation des résultats avec le silicate tricalcique à l'alite dans les ciments portlands. L'alite n'est pas de silicate tricalcique pur. Réellement il y a un nombre infini de différents types - différentes origines et variations des matériaux crus, différentes conditions de brûler dans les fours (3). Il serait difficile à présent pour étudier les effets des

*CCR 12, 455 (1982).

défauts dans l'alite pratiquement. Les études par MM. Fierens, Kabuema et Tirlocq sont d'une importance fondamentale pour chercher les principes basiques qui déterminent l'hydratation du silicate tricalcique et ainsi la base d'application pour comprendre l'hydratation de la phase d'alite dans les ciments portlands.

Bibliographie

1. P. Fierens, Kabuema Y. et J. Tirlocq, Cement and Concrete Research 12(4), 455 (1982).
2. J.N. Maycock, J. Skalny et R. Kalyoncu, Cement and Concrete Research 4(5), 835, (1974).
3. J. Bensted et S.P. Varma, Cement Technology 5(4), 378 (1974).

VOL
14
198

CEMENT and CONCRETE RESEARCH. Vol. 14, pp. 603-609, 1984. Printed in the USA.
0008-8846/84 $3.00+00. Pergamon Press, Ltd.

A DISCUSSION OF THE PAPER "THEORIES OF EXPANSION IN SULFOALUMINATE-TYPE EXPANSIVE CEMENTS: SCHOOLS OF THOUGHT," BY M.D. COHEN*

Bryant Mather
Chief, Structures Laboratory
U.S. Army Engineer Waterways Experiment Station
Box 631, Vicksburg, Mississippi 39180 USA

VOL.
14
1984

Dr. Cohen seems to believe that when expansion results from the formation of ettringite in hardened cement paste, mortar, concrete, or grout, there are only two "schools of thought" available to describe how the ettringite formation results in an increase in the dimensions of the system.

I disagree. I do not believe the observed increases in dimensions of systems made using types M, K, and S expansive cement or of systems undergoing sulfate attack must be explained either as "crystal growth pressure" or "water-adsorption and swelling" of gel.

Polivka (1973), discussing expansion of expansive cements, wrote that "formation of (ettringite) is accompanied by a large increase in volume and is the basic mechanism of expansive cements ... Ettringite starts to form as soon as water is added to the cement ... and continues to form ... until the SO_3 or Al_2O_3 is exhausted." ACI Committee 223, in 1970, wrote (Section 2.1) "formation of ettringite is the source of the expansive force." In my discussion of that report (Mather, 1971) I noted that "The report states (Section 1.1) that 'much is yet to be learned about the mechanism and chemistry of expansive cement ...' The report also states, in the last paragraph of Section 2.6, that 'Unequivocal proof has not yet been established on the mechanism of formation of the expansive phases resulting in expansive forces. It is, however, probable that ettringite crystals when surrounded and restrained by reaction products grow in size and thereby are responsible for the development of stresses.'

"In the same issue of the Journal in which the report appears, there is also a discussion by Brown (1970) of the paper by Kalousek and Benton and the authors' closure to this discussion. These contributions concern themselves with the mechanism of ettringite formation and the origin of the expansive forces associated with that formation as this subject relates to the mechanism of seawater attack on cement paste. Anyone concerned with the explanation of how expansive cement gets to be expansive would benefit from a study of this discussion and the closure thereto.

"I believe that the expansive forces that are usefully generated when expansive cement is used in concrete can not begin to manifest themselves until after a certain degree of rigidity has been developed by setting and hardening in the concrete. It is then, I believe, that the formation of ettringite from

*CCR 13, 809-818 (1983).

anhydrous calcium aluminate, hydrated calcium aluminate, or unhydrated calcium aluminate sulfate proceeds by the in-place conversion of these aluminum-bearing substances to ettringite. The mechanism by which this development of ettringite, in situ, produces stress is regarded as entirely analogous to the mechanisms by which a balloon expands when gas is placed in it or to that by which a water-filled container tries to expand when the water in it is converted by freezing into ice (Bache and Isen, 1968); namely, there is a larger volume of substance than there is volume of space to contain it and the substance is inadequately compressible by the restraint provided by the walls of the space; therefore, the space enlarges. My inclination, therefore, would be to reword the sentences quoted from Section 2.6 of the report as follows:

"'Many details of the mechanism by which the formation of ettringite results in the development of expansive forces remain to be fully understood. It is known that the volumes of the materials that react to form ettringite occupy a greater combined volume than the volume occupied by the solid ettringite that is formed. Consequently, the mechanism of ettringite formation and concomitant development of expansive forces must involve the alteration, in situ, of a quantity of the aluminate (or aluminate sulfate) reactant to ettringite by a process that delivers the water and other reactants in solution to the reaction site and leaves elsewhere in the structure some space formerly occupied by solution that is no longer fully filled with solution. The expansive force developed by the conversion of the aluminate (or aluminate sulfate) to ettringite is related to the relative volume of the aluminate (or aluminate sulfate) reactant to that of ettringite and the restraint provided by the surrounding matrix.'"

In its closure the committee said: "While there is no objection to the suggested wording as applying qualitatively to the development of forces by the expansive solids within the porous matrix, it illustrates the difficulties of the quantitative determination of possible expansions. For instance, in a Type K expansive cement concrete having a fairly low water-solids ratio of 0.3, the stoichiometry of the reactions involving ettringite formation could be represented as shown in Table A.

"Accordingly, the increase in the volume of solids on complete hydration is:

$$\frac{2143 - (235 + 368 + 101 + 609)}{(235 + 368 + 101 + 609)} \times 100 = 63 \text{ percent}$$

"While the mix water is (610 + 1088 + 336) x 0.3 = 609, complete ettringite formation as per stoichiometry of the reaction would require (1674-609) = 1065 g of curing water. Even when larger quantities of mix water are used in the concrete, it is not accurate to consider it a part of the reactants as far

TABLE A - STOICHIOMETRY OF REACTIONS FOR ETTRINGITE FORMATION

Property	$C_4A_3\bar{S}$	+ $8C\bar{S}$	+ 6C	+ 32^*H (aq mixing)	$\xrightarrow{aq}$	$3C_6A\bar{S}_3H_{32}$
Molar/weight	610	1088	336	609		3708
Density	2.8	2.96	3.32	1		1.73
Molar volume cm^3	235	368	101	609		2143

* I believe this should be "96"

as volumetric changes from the anhydrous phase to the hydrate which actually produces expansion are concerned.

"It should be emphasized that both in the committee report and Mr. Mather's discussion, it is stated that many details of the expansive mechanisms remain to be fully understood. Considerable expansions under conditions of restraint are found when pastes containing monosulfate hydrate ($C_4A\bar{S}H_{18}$) and gypsum are converted to ettringite. Also, the question of whether development of expansive forces results from through-solution crystallization pressure in confined spaces or in-situ hydration and growth of crystals has not yet been convincingly resolved. The committee, therefore, does not feel it should reword the report as suggested by Mr. Mather. ... Thermodynamics shows that there is available a very large amount of free energy, about 55 kcal/mol of ettringite (formed from C_3A) which equals about 169,000 ft-lb of work (1.0 kcal = 3080 ft-lb).

"The potential expansive force developed in an expansive concrete may be computed from the free energy change and increase in volume. (This computation applies only to Type S cement; the free energy changes are not available for the other two types of cement, but probably are of a similar magnitude.) The following problem involves 1 cu ft of concrete (before expansion) and a linear expansion of 1 percent. It is assumed that the total increase in volume is due to ettringite crystallization in totally confined spaces and, therefore, the volume of expansion equals the volume of expansive ettringite. (It is to be understood that a substantial amount of ettringite formed in the still plastic paste and also, later, in voids without causing expansion.) The volume increase in the 1 cu ft of concrete in the problem is 55 cu in. (902 cc) which equals 1590 g (1.27 mols) of ettringite. The formation of the 1.27 mols supplied 70.4 kcal of free energy which equals 217,000 ft-lb of work acting in three directions. The work in one direction is therefore, 72,300 ft-lb/ft^2 or 492 ft-lb/in.^{2}. Force equals work/distance. The linear expansion of 1.0 percent represents 0.01 ft distance through which the potential force would have acted. Therefore, the expansive force is 49,000 psi. A similar computation, except that no assumption is needed on the volume of ettringite formed, for conversion of 1.0 cu ft of C_3A to 8 cu ft of ettringite gave a value of 47,000 psi as the potential expansive force. The 1:8 ratio of molar volumes of C_3A to ettringite is definitely known. This stress is not developed as such; it is the stress which would have to be applied triaxially to the concrete to stop the ettringite reaction. Mehta and Klein (1966) described an experiment in which the strains caused by formation of ettringite from $C_4A_3\bar{S}$ in an appropriate container was indicative of a stress of 35,000 psi. The relatively close agreement between this value and those just given, and considering the difference between the two systems and methods, appears to justify the conclusion that ettringite formation in a confined space is potentially capable of developing very high forces.

"The hypothesis of expansive force development presented in the committee report was selected because it has no apparent contradiction with laws of chemistry, particularly of thermodynamics, and physics. The other proposed hypothesis did not appear to fully meet this requirement. Another compelling reason for selection of the hypothesis was the very high lattice energies of crystalline compounds such as ettringite, possibly in the order of several hundreds kcal/mol. The ultimate source of the expansive force may be visualized as originating from the powerful electrostatic attractions existing between charges on sites of the pristine surface of an ettringite crystals and ions of opposite charge in the solution. These are Coulomb forces and vary inversely with the square of distance between the two charges. The chances for attracting an ion from solution to a site on the growing crystal against the resistance of the surrounding hydration products in intimate contact with the crystal, appear highly favorable because of the high strength of the forces of attraction oper-

ating over realtively long distances. The fundamentals of the process of attraction vs repulsion as function of distance between charges are similar to those reviewed by Phillеo (1966) in explaining the origin of concrete strength.

"Regarding the gross features of the mechanism by which ettringite formation causes expansion, it is interesting to note that both Mather and Mehta are in general agreement with the mechanism proposed earlier by Kalousek and Benton (1970). Since neither Messrs. Mather nor Mehta, however, propose an alternative explanation on the fundamental origin of the expansive force, only the feature of the mechanism appears to be controversial."

In a previous discussion of the effects of seawater on concrete (Mather, 1966) the chemical reactions involving magnesium sulfate with calcium aluminate were reviewed. In 1968 I quoted Hansen and Offutt (1962) on the volumetric relations getting from tricalcium aluminate (C_3A) plus gypsum to ettringite, as follows:

$$3CaO\cdot Al_2O_3 + 3CaSO_4\cdot 2H_2O + 25H_2O \rightarrow 3CaO\cdot Al_2O_3\cdot 3CaSO_4\cdot 31H_2O$$

88.8 222.3 450 714.7 (46.4)

1 8

The numbers in the first line below the equations are participating volumes. The number in parentheses at the right is the volume added to that on the right side of the equation to make its volume equal to the sum of those on the left; thus this reaction involves a net reduction in volume of the reactants. The second line of numbers compares the relative volume of anhydrous C_3A and the volume of calcium aluminum sulphate formed from it by sulphate reaction; the increase in volume is eightfold.

In 1969 I again reviewed these relations, again noting that "The phenomena related to the formation of hydrated sulfates in concrete, or in aggregates, cement pastes, or mortars, have been investigated for many years for a variety of purposes. The cyclic immersion of aggregate particles in solutions of sodium or magnesium sulfate, followed by drying, is the basis of one of the oldest procedures employed to develop data purported to relate to aggregate 'soundness.' The storage of mortar specimens in sulfate solutions is the basis of many tests for sulfate resistance of cements. Sulfate-resistance testing procedures in which sulfate is added to the mortar and the mortar specimens are stored in water are in widespread use. These latter procedures are similar to procedures employed in studies of expansive cements ... When an expansion occurs, it is because the hydrated sulfates that are formed ... by reactions in place, occupy a larger volume than was available and hence exert stress on their surroundings. The stress so exerted produces elastic and inelastic strains of magnitudes and proportions depending on the level of stress, the mechanical properties of the system, and the geometry of the specimen. All of the hydrated sulfates of interest are crystalline to some degree; consequently, their formation may be referred to as crystallization, and an increase in the amount that is present may be referred to as 'crystal growth.' The stresses accompanying such formation have been referred to as resulting from crystal growth even as the stresses accompanying the freezing of water have been referred to as resulting from ice crystal growth. The facts that the substances are crystalline and that an increase in the amount present involves crystal growth are of minor significance to an understanding of the mechanisms by which such formation produces stresses which induce the strains that are observed as expansions and cracking.

"If the space occupied in an aggregate particle or in a sample of mortar, cement paste, or concrete by a quantity of a hydrated sulfate after equilibra-

tion of strain had been occupied by a liquid or gas that had exerted the same stress under the same conditions of confinement, the final volumetric relations of the system in which it existed would be the same. The relevant phenomenology of the sulfate soundness test of aggregates, the various sulfate susceptibility tests for pastes, mortars, and concretes, the various expansivity tests for expansive cements, tests for resistance to freezing and thawing, tests for the potential expansivity caused by chemical reactions of alkalies and aggregates, tests for oxidation or hydration of aggregate or cement constituents or embedded corrodible metals does not primarily depend on whether the products formed are crystalline or noncrystalline. The relevant phenomenology concerns the specific volume of products formed, the amount of products formed, the compressibility of the products formed, the restraint imposed by the surroundings, and the rate of formation of the products.

In the case of ettringite, it has been observed that, if one takes the anhydrous analogue of this material ($C_4A_3\bar{S}$) plus calcium sulfate and calcium oxide and packs it tightly in a container capable of providing a very high level of volumetric restraint and then allows it to hydrate in place, the strains observed in the container can reach levels indicative of stresses of the order of 50,000 psi.

"Aroni et al (1966) note that it was Michaelis (1892) who first attributed the disruption of concrete, when attacked by aggressive waters containing sulfates, to the reaction between C_3A and sulfates to form ettringite. They note that the useful feature of this reaction to the application of expanding cement to chemical prestressing is the high energy of the expansion; i.e., its ability to perform work and expand under restraint. They also note that there is little in the literature on the basic phenomena of crystal growth under pressure. As did Schaffer (1932), they refer to the work of Becker and Day (1905), but do not appear to have rejected the hypothesis. They refer to the conclusions of Hansen (1963) and Taber (1916) and ask what the applicability of these conclusions is to expanding concrete.

"Hansen (1963) reviewed the literature relating to the phenomenon of crystal growth as a source of expansion in portland-cement concrete. He begins his review with the statement that 'portland-cement pastes expand during setting and hardening, whereas they would be expected to contract because the volumes of the hydrated phases are less than the sum of the volumes of the water and the reactants forming these phases.' He refers to the work of Becker and Day (1905) and attributes the observed ability of a growing crystal to lift a weight as a consequence of the existence of a film of solution beneath the growing crystal, the concentration differences in the solution, and the relation of solubility of the crystal to the pressure on it. He cites the conclusions of Taber (1916), both with regard to these circumstances and with regard to the relations of crystals growing in porous media having a range of pore sizes. Taber showed that crystals growing in larger pores will receive material from the solution in the smaller pores and grow at the interface between liquid and crystal. Hansen concludes that theories that attribute expansions in concrete to crystals growing from solution against one another do not appear to be realistic. He describes two conditions under which a crystal may grow and exert pressure on materials opposing its growth. One is the condition in which a weighted crystal rests on the floor of a container on a film of solution that is supersaturated with respect to the bottom face of the crystal. The other is the condition in which a single crystal fills a container that opens into another container filled with a solution supersaturated with respect to the film of solution supporting the crystal. He mentions last the rehydration of a partially dehydrated solid exposed to water vapor, noting that in this way, crystals can grow without the presence of liquid water.

"Schaffer (1932) wrote 'There is considerable doubt as to whether or not the axial growth is actually associated with a force. Correns (1926) concluded that the so-called crystallization forces, which cannot be explained by volume increase due to a change in phase, may be explained on the basis that super-saturated solution is drawn into capillary space between the crystals and the adjacent matter by surface tension forces.'

"Wellman and Wilson (1965) wrote: 'The fragmentation of rocks by the crystallization of salts ... is important in a restricted range of environments and produces distinctive topographic forms ... The chemical free energy of a given mass of solid increases with its surface area. Therefore, any system tends to reduce the area of its interfaces to a minimum, and in a system containing crystals in equilibrium with a saturated solution larger crystals will grow at the expense of the smaller. It is less obvious why, when the larger crystals entirely fill a pore space, they continue to grow against the constraint imposed by the walls of the pore, expand the pore and fragment the rock ... a large rock pore will be enlarged provided that the surface tension of the salt times the dA/dV of the micropores is greater than the mechanical strength of the rock. Thus for rocks of equal mechanical strength, those with large pores separated from each other by microporous regions will be most liable to"such internal expansion.

I conclude that when you put more than one unit volume of anything in a restrained three-dimensional space having, initially, a size of one unit volume something has to give; either the quantity added must reduce itself in amount (some leaks out) or in volume (it is compressed) or the space enlarges either elastically or inelastically without rupture or it cracks. The question of whether or not the volume of something that is placed in the space is put there intentionally as blowing up a balloon; or unintentionally as rusting of reinforcing steel in a concrete bridge deck; or whether or not the larger volume is of the same chemical composition and physical state as the smaller as liquid mercury in a thermometer at higher and lower temperature; or different in physical state but not in composition as ice and water; or crystalline as ice or non-crystalline as liquid mercury; or different in composition as C_3A and ettringite is always interesting but does not explain how the force is produced. In the case of expansive cement the expansion occurs because as water, calcium ions, and sulfate ions proceed to the reaction site through the permeable pore space in the cement paste to the C_3A particle surface replace those used in sulfating and hydrating the C_3A to ettringite, the volume of ettringite formed per unit volume of C_3A used is in the ratio of 8:1. The fact that the ettringite is crystalline or colloidal is irrelevant, hence the argument that one must choose between Dr. Cohen's two schools is not valid.

VOL
14
198

References

1. ACI Committee 223, "Expansive Cement Concretes - Present State of Knowledge," ACI Journal, Proceedings, Vol. 67, No. 8, 583-610 (August 1970).
2. ACI Committee 223, Closure to Discussion, ACI Journal, Proceedings, Vol. 68, No. 4, 295-297 (1971).
3. Samuel Aroni, Milos Polivka, and Boris Bresler, Expansive Cements and Expanding Concrete, Report No. 66-7, Structures and Materials Research, Dept. of Civil Engineering, University of California, Berkeley, CA, 74 pp. (1966).
4. Hans Henrick Bache and Jens Christian Isen, Modal Determination of Concrete Resistance to Popout Formation, Journal of the American Concrete Institute, Proceedings, Vol. 65, 445-450 (June 1968).
5. G.F. Becker and A.L. Day, The Linear Force of Growing Crystals, Washington Academy of Science, Vol. 7, p. 283 (1905).

6. Levi S. Brown, Discussion of a paper by G.L. Kalousek and E.J. Benton, "Mechanism of Seawater Attack on Cement Pastes," ACI Journal, Proceedings, Vol. 67, No. 8, 646-648 (August 1970).
7. C.W. Correns, Explanation of the So-Called Force of Crystallization, Sitzungsberichte der preussichen Akademie der Wissenschaften, pp. 10-11 and 81-88 (1926).
8. W.C. Hansen, Crystal Growth as a Source of Expansion in Portland-Cement Concrete, Proceedings, American Soc. for Testing and Materials, Vol. 63, 932-945 (1963).
9. W.C. Hansen and J.S. Offutt, Gypsum and Anhydrite in Portland Cement, U.S. Gypsum Co., Chicago, 63 pp. (1962).
10. G.L. Kalousek and E.J. Benton, Authors' closure of a paper by G.L. Kalousek and E.J. Benton, "Mechanism of Seawater Attack on Cement Pastes, ACI Journal Proceedings, Vol. 67, No. 8, 646-648 (August 1970).
11. Bryant Mather, Effects of Seawater on Concrete, Symposium on Effects of Aggressive Fluids on Concrete, Highway Research Record No. 113, pp. 33-42 (1966).
12. Bryant Mather, Field and Laboratory Studies of the Sulfate Resistance of Concrete, Performance of Concrete - Resistance of Concrete to Sulphate and Other Environmental Conditions - A Symposium in Honor of Thorbergur Thorvaldson, Canadian Building Series No. 2, University of Toronto Press, pp. 66-67 (1968).
13. Bryant Mather, "Sulfate Soundness, Sulfate Attack, and Expansive Cement in Concrete," in Proc. RILEM Int. Symp. on Durability of Concrete - 1969, Preliminary Report, Vol. 11, Academia, Prague, pp. C-209 to C-220 (1969).
14. Bryant Mather, Discussion of ACI Committee 223, 1970 Report, ACI Journal Proceedings, Vol. 68, No. 4, p. 293 (1971).
15. P.K. Mehta and Alexander Klein, "Investigations of the Hydration Products in the System $4CaO \cdot 3Al_2O_3 \cdot SO_3$ - $CaSO_4$ - CaO -H_2O," Special Report 90, Symposium on Structure of Portland Cement Paste and Concrete, Highway Research Board, Washington, DC (1966).
16. W. Michaelis, (title not available), Tonindustrie-Zeitung, Vol. 15, p. 105 (1892).
17. R.E. Philleo, "The Origin of Strength of Concrete," Highway Research Board Special Report 90, pp. 175-185 (1966).
18. Milos Polivka, Factors Influencing Expansion of Expansive Cement Concretes in ACI SP-38, pp. 239-250 (1973).
19. R.J. Schaffer, The Weathering of Natural Building Stones, Building Research Special Report No. 18, Dept. of Scientific and Industrial Research, London, 149 pp. (1932).
20. Stephen Taber, The Growth of Crystals Under External Pressure, American Journal of Science, Vol. XLI, p. 532 (1916).
21. H.W. Wellman and A.T. Wilson, Salt Weathering, a Neglected Geological Erosive Agent in Coastal and Arid Environments, Nature, Vol. 205, No. 4976, pp. 1097-1098 (March 13, 1965).

VOL. 14 984

CEMENT and CONCRETE RESEARCH. Vol. 14, pp. 610-612, 1984. Printed in the USA.
0008-8846/84 $3.00+00. Copyright (c) 1984 Pergamon Press, Ltd.

A REPLY TO A DISCUSSION BY B. MATHER OF THE PAPER "THEORIES OF EXPANSION IN SULFOALUMINATE-TYPE EXPANSIVE CEMENTS: SCHOOLS OF THOUGHT"*

M.D. Cohen
Department of Civil Engineering
Northeastern University
Boston, Massachusetts 02115

VOL 14 198

The interest and comments of Mr. Mather on my paper are appreciated. Mr. Mather seems to disagree that expansion in types K, M and S expansive cements may be explained by the Crystal Growth Theory or the Swelling Theory, both of which emphasize the crystalline characteristic of ettringite. In his discussion, Mr. Mather also suggests that it is irrelevant as to what the characteristic of ettringite is and that elucidation of the expansion on the basis of volume increase suffices. In his comments, Mr. Mather raises some important issues. However, his arguments are not substantiative.

The fact that expansion is associated with volume increase upon C_3A or $C_4A_3\overline{S}$- ettringite transformation is not disputed by either theory. However, this volume increase by itself does not completely elucidate the expansion mechanism (1). A.P. Laurie (2) in explaining the breaking up of stone by formation of calcium sulfate crystals wrote;

> "...this has been attributed to the fact that, equivalent for equivalent, the calcium sulfate crystal occupies a larger volume. But I do not think this (volume increase) is the main cause ...It is the persistent growth of the crystals in certain layers or pockets which ultimately breaks up the stone."

In view of the above statements, I would like to suggest the following equation for the total volume of ettringite produced at time t;

$$V(t) = N(t)\ L(t)\ A(t) \quad \text{.....(a)}$$

---

* CCR 13, 809-818, 1983

or simply,

$$V = N\ L\ A \quad \ldots\ldots\ldots\ldots\ldots\ldots\ldots\ldots (b)$$

where N is the total number of ettringite particles at time t, and L and A are, respectively, length and the cross-sectional area of a single ettringite particle at time t. To avoid complexity, I am assuming all ettringite particles to be identical. Differentiating (b),

$$dV = AL\ dN + NA\ dL + NL\ dA \quad \ldots\ldots\ldots\ldots\ldots\ldots (c)$$

Equation (c) indicates that volume increase of ettringite may be accompanied by increase in the number of ettringite particles dN (first term), by growth in length dL (second term) and by growth in cross-sectional area dA (third term) of a single ettringite particle. Now, which of these terms dominates and/or contributes to the expansion of the hardened paste or concrete is the major issue that differentiates between the different theories. If expansion occurs by swelling of colloidal ettringite, then the first term (AL dN) may dominate. If expansion occurs by crystal growth or crystallization pressure, the second term (NA dL), and possibly the first (AL dN) may dominate. The role of the third term (NL dA), increase in cross-sectional area, has not been discussed much in the literature. Thus, volume increase is a function of the characteristic of ettringite and any change may lead to a different amount of expansion.

The calculated volume increase from the stoichiometric equations depends primarily on the molecular weights and densities of the materials involved. The molecular weights are determined theoretically but the densities experimentally. The calculated volume increase is therefore dependent on the method used, laboratory conditions, and on the characteristic of the materials involved. For example, if a product is crystalline, it should have a larger density than its amorphous counterpart. As a result, the calculated volume increase would be smaller. Thus, contrary to Mr. Mather's assertion, expansion based on volume increase must depend on the characteristic of ettringite.

In further support of his arguments, Mr. Mather suggests that since the different tests that he mentioned do not "primarily depend on whether the products formed are crystalline or noncrystalline", then one can conclude that this characteristic is not important. This statement is invalid. None of these tests are intended to explain the mechanisms involved. Had they been, this characteristic could have been important. Moreover, presumably, the group of experts involved in designing such tests had a thorough understanding and appreciation of the importance of the crystallinity of the products formed or involved in each test.

That ettringite can impose a very high expansive stress or potential has not been disputed by the two schools of thought. The calculated value of the expansion based on the thermodynamic calculation could depend partly on the crystallinity or non-crystallinity of ettringite. The reason is that any change in this characteristic could change the values of the free energy, the volume increase, and therefore,the calculated expansive stress.

Mr. Mather has the impression that I am suggesting one has to choose one of the two theories in search of an explanation for expansion. This is not so. The purpose of my paper is indicated clearly by the title and in no way have I attempted to go beyond a review of the theories involved. In conclusion, based on the literature, I stand with my belief that expansion, thus far, has been explained by two major theories, Crystal Growth and Swelling, both of which emphasize the crystallinity of ettringite.

References

1. Cohen, M.D. "Modeling of Expansive Cements". Journal of Cement and Concrete Research. V. 13, No. 4, pp. 519-528. July 1983.

2. Laurie, A.P. "Stone Decay and the Preservation of Buildings". Journal of the Society of Chemical Industry. London. Pp. 86T-92T. February 27, 1925.

VOL. 14 198

CEMENT and CONCRETE RESEARCH. Vol. 14, pp. 613-614, 1984. Printed in the USA.
0008-8846/84 $3.00+00. Copyright (c) 1984 Pergamon Press, Ltd.

NEWS ITEMS

Third ASTM/CIB/RILEM International Conference on DURABILITY OF BUILDING MATERIALS AND COMPONENTS, Espoo, Finland. Information: Anneli Kaaresalo, Technical Research of Finland, Division of Builidng Technology, SF-02150 Espoo 15, Finland. — Aug. 12-15, 1984

International Symposia on CONCRETE PRESSURE AND STORAGE VESSELS, SEA STRUCTURES IN ARCTIC REGIONS, AND PREFABRICATION, Federation Internationale de la Procontrainte (FIP), Canadian Prestressed Concrete Institute, Calgary, Alberta, Canada. Information: FIP, c/o Genstar Structures, Ltd., 1000-1520 Fourth St., S.W., Calgary, Alberta T2R 1H5 Canada. — Aug. 25-31, 1984

Fourth International Congress on POLYMERS IN CONCRETE, Technische Holchschule Darmstadt, W. Germany. Information: Prof. H. Schulz, Technische Hochschule Darmstadt, Kennwort; ICPIC 1984, Petersenstrasse 30, D-6100 Darmstadt, W. Germany. — Sept. 19-21, 1984

International Conference on IN SITU/NONDESTRUCTIVE TESTING OF CONCRETE, by ACI, CANMET, National Bureau of Standards and the Canadian Society for Civil Engineering, Westin Hotel, Ottawa, Canada. Information: Harry S. Wilson, CANMET, 405 Rochester St., Ottawa, Ontario, Canada K1A 0G1. — Oct. 2-5, 1984

International Conference on TALL BUILDINGS, Shangri-la Hotel, Singapore, sponsored by the Council of the Institution of Engineers, Singapore. Information: The Chairman, ICTBS 84, 10, Anson Road, #14-06, International Plaza, Republic of Singapore (0207). — Oct. 22-26, 1984

ACI Convention, Grand Hyatt, New York, NY. Information: Ann K. Bruttel, Convention and Meetings Manager, ACI, P.O. Box 19140, Detroit, MI 48219 USA. — Oct. 28 - Nov. 2, 1984

Materials Research Society Symposium L, THE POTENTIAL FOR VERY HIGH STRENGTH CEMENT-BASED MATERIALS, Boston Marriott Hotel/Copley Place, Boston, MA. Information: Dr. J. Francis Young, 3209 Newmark Civil Engineering Lab., University of Illinois-UC, Urbana, IL 61801 or Dr. Sidney Mindess, Dept. of Civil Engineering, University of British Columbia, Vancouver V6T 1W5, Canada. — Nov. 26-30, 1984

Materials Research Society Symposium M, COAL COMBUSTION AND CONVERSION WASTES: CHARACTERIZATION, UTILIZATION AND DISPOSAL, Boston Marriott Hotel/Copley Place, Boston, MA. Information: — Nov. 26-30, 1984

NEWS ITEMS

Dr. Turgut Demirel, Dept. of Civil Engineering, Iowa State University, Ames, IA 50011, or Dr. Gregory McCarthy, Dept. of Chemistry, North Dakota State University, Fargo, ND 58105, or Dr. Barry E. Scheetz, Materials Research Laboratory, The Pennsylvania State University, University Park, PA 16802.

The 8th International Congress on the CHEMISTRY OF CEMENT, Rio de Janeiro, Brazil. Information: Secretaria Geral do 8° Congresso de Quinica do Cimento, Rua da Assembléia, No. 10, 40° andar, Grupo 4001-20011, Rio de Janeiro/RJ, Brazil. Late Summer 1986

CALL FOR PAPERS

The 7th International Conference on Cement & Concrete Microscopy will be held from March 25-28, 1985, at the Americana Hotel, Fort Worth, Texas, USA. The topics to be covered at this conference are:

1. Microscopic structures of building materials, including: lime, gypsum, light and heavyweight aggregates, cement, concrete, slag, flyash, silica fume, etc.
2. Microscopic structures of the different types of cement clinker products and hydration.
3. Effect of additives on the microstructure of cement and concrete and the relationship between the microstructure and concrete strength.
4. Application of different types of microscopes for the quality control of clinker, cement, concrete, etc.
5. X-ray diffraction analysis of Portland cement and related materials and the relationship between the microstructure and the mineralogical composition.

A workshop demonstrating the practical application of various microscopes will be included. An exposition of the different types of microscopes will be presented.

Authors should send abstracts, no later than November 15, 1984 to:

Arturo G. Nisperos, Material Service Corp., 901 N. Sangamon St., Chicago, IL 60622 (subjects dealing with microscopy of concrete and concrete-making materials).

James Bayles, Coplay Cement Co., Nazareth, PA 18064 or Dr. George R. Gouda, Kuwait Inst. for Scientific Research, P.O. Box 24885, Safat, Kuwait (subjects dealing with the microscopy of cement and clinkers).

The text, typed according to the instructions of ICMA is due by Jan. 31, 1985.

VOL. 14 1984

CEMENT and CONCRETE RESEARCH. Vol. 14, pp. 615-621, 1984. Printed in the USA.
0008-8846/84 $3.00+00. Copyright (c) 1984 Pergamon Press, Ltd.

WASTE CEMENT DUSTS AS ACTIVATING AGENTS FOR RUBBER COMPOUNDS

Andrzej Krysztafkiewicz and Marek Maik
Institute of Chemical and Engineering Technology
Politechnika Poznańska
60-965 Poznań, Poland

(Communicated by D.M. Roy)
(Received May 13, 1983; in final form May 29, 1984)

OL.
14
984

ABSTRACT

The possibility of substitution of an expensive zinc oxide by the waste cement dusts used in the character of the rubber compound activators were shown. The chemical constitution and the physico-chemical properties of the used cement dusts were investigated, as well as the physico-mechanical parameters of the vulcanizates which had these cement dusts, were determined. Some good strength properties were found for the vulcanizates which had the cement dusts. The results show a real possibility of the elimination of zinc oxide as an activating agent of the rubber compounds, and of substitution of one of the waste cement dusts.

Introduction

We can find more and more publications which deal with the utilization of the fine waste cement dusts instead of zinc oxide (1,2). Calcium oxide and magnesium oxide, as the components of cement dusts, are commonly believed to play the role of the inorganic accelerators of the sulphur vulcanization process of rubber compounds. The modern rubber technology uses magnesium oxide mainly for compositions based on the elastomers that contain halogens in their molecules (3). The replacement of zinc oxide with magnesium oxide, e.g. in butyl rubber compounds, leads to higher tensile strengths of vulcanizates (4). The aim of our investigations was to find out whether zinc oxide, which is comparatively expensive, could be substituted by some waste cement dusts. Moreover, the Polish steelworks zinc oxide is often a substrate which has the heterogeneous grain size distribution and a tendency to the sinter formation in rubber compounds that has a disadvantageous influence upon the properties of final vulcanizates.

The production of cement and great amounts of waste dusts are inseparable. The sources of these dusts are grinder assemblies, which grind cement, driers, cement kilns and transporters of different kinds. The use of dust collectors, which suck air or gases off installations and then separate dusts, is the efficient means of dust removal.

In this work, we examined the dusts which had been removed in "Nowiny" and "Opole" cement plants by multicyclones.

Experimental

To begin with, we examined the chemical constitutions and checked if the waste dusts were homogeneous substrates. The metal, mostly Cu, Pb and Mn ion contents which were in micro quantities in the dusts, were determined by the use of atomic absorption method. The homogenity of the waste cement dusts is a basic feature which plays a predominant role before introducing the ones to compounds based on synthetic or natural rubbers.

At the same time, the analogous examinations of zinc oxide used as the activating agent in the rubber compounds and which was substituted, partly or totally, for the examined waste cement dusts, were carried out.

pH of water extracts were determined potentiometricly after 4% dispersion of the examined samples in distilled water were made. Specific surfaces were determined by the use of chromatographic method (5). The amounts of adsorbed nitrogen were calculated from desorption peaks because of their greater symmetry. The degrees of dispersion for all the samples were examined by the use of Sartorius sedimentation scales (6). The x-ray examinations of the cement dust samples were carried out using the HZG-3 horizontal diffractometer with the TURM-62 generator.

CuKα radiation with the nickel filter was used. The dust samples were pressed before they were inserted into the apparatus. The observations of preparations under a microscope were carried out using the intermediate single-stage replica method (8,9) which is very precise in reflecting examined objects, has a high resolving power, a good transparency in an electron beam and a relatively good stability. The objects, 20-30 thousand times magnified, were filmed by the JEM-7 over-exposure electronic microscope (Jeolco - Japan).

The waste cement dusts underwent an additional operation of pulverization in a jet-circulation mill, JET MIZER 0202 model made by the USA, in order to obtain a precise homogenization of the products.

The next step was to substitute zinc oxide in rubber compounds based on the natural rubber, RSS, and the butadiene-styrene, Ker 1500, produced by Zaklady Chemiczne Oświęcim, for the prepared cement dusts. In the case of the RSS rubber, we used amounts of cement dusts which contained zinc oxide in quantity that was approximately equal to that of zinc oxide which was introduced to the rubber compounds. The rubber compounds were prepared in laboratory rolling mill at the temperature of ca 60°C and vulcanized at the temperature of 143°C and under the pressure of 150 atm. In the case of the Ker 1500 rubber, the compound ratios were in agreement with the standard (see Table 1).

The rubber vulcanizates underwent resistance tests according to appropriate standards, and the amounts of unbounded sulphur as a function of time were determined. Sulphur was determined according to the previously elaborated thin-layer chromatography method (10,11).

Results

The results of the chemical analysis of the waste cement dusts and the used zinc oxide, as well as the results of physico-chemical property tests are placed in Table 2.

The results of an additional absorption analysis of trace amounts of some metals which have a negative influence on the properties of vulcanizates are shown in Table 3.

The data of the degree of fineness analysis of the examined waste cement dusts and zinc oxide, as well as the results of the sedimentation analysis of the cement dust from the "Nowiny" cement plant, which were previously jet milled,

VOL
14
198

TABLE 1

Compound Ratios for the Usage of Waste Cement Dust Instead of Zinc Oxide

Compounds	I	II	III	IV	V	VI
Butadiene-styrene rubber, Ker 1500	100	100	100	100	100	100
Stearin	1	1	1	1	1	1
Accelerating agent	2	2	2	2	2	2
Carbon black PM-75	50	50	50	50	50	50
Zinc oxide	5	4	3	2	1	0
Waste cement dust	0	5	5	5	5	5
Sulphur	2	2	2	2	2	2

TABLE 2

Chemical Constitution and the Basic Physico-Chemical Properties of the Examined Cement Dusts and Zinc Oxide

Characteristic	"Nowiny" cement dust	"Opole" cement dust	Zinc Oxide
Chemical Constitution (%)			
CaO	57.80	58.05	-
SiO_2	24.58	22.50	-
Al_2O_3	4.58	5.71	-
$FeO + Fe_2O_3$	0.90	1.98	-
MgO	2.88	2.29	-
SO_3	0.64	0.80	-
ZnO	0.85	0.75	99.63
TiO_2	traces	0.05	-
Moisture content (%)	1.15	1.37	0.50
pH of water extract	10.2	9.9	6.3
Specific surface (m^2/g)	9.5	8.6	10.5
Specific gravity (g/cm^3)	5.42	5.33	5.27
Bulk density (g/dm^3)	634	625	521

are shown in Table 4. The electronic-microscope photograph shows a sample of cement dust, immediately after its separation in a multicyclone, magnified 30 thousand times (Fig. 1).

Physico-mechanical parameters which characterize the natural rubber vulcanizates containing the cement dusts are shown in Table 5. For the comparison reason, the table contains also vulcanizates prepared after introducing various amounts of zinc oxide.

TABLE 3

Ion Metal Contents in the Cement Dusts from the "Nowiny" Cement Plant, % by Weight

Component	Sample taken on the 1st day	Sample taken on the 2nd day	Permissible standard for a rubber compound
Cu	0.005	0.009	0.01
Pb	0.012	0.012	0.01
Mn	0.037	0.020	0.01

TABLE 4

The Degree of Fineness of the Investigated Samples According to the Sartorius Method

Sample	% by weight of a fraction (average)			
	<5 μm	5-10 μm	10-20 μm	>20 μm
Zinc oxide	72.5	11.8	7.6	8.1
"Nowiny" waste cement dust	77.2	12.8	4.2	5.8
"Opole" waste cement dust	76.7	13.2	3.8	6.3
"Nowiny" waste cement dust after jet milling	93.6	2.1	3.4	0.9

The results of the investigations of butadiene-styrene rubber compounds with carbon black filler, the total or a part amount of ZnO activator, and a constant amount of cement dust are shown in Table 6. The vulcanizations were carried out at the temperature of 143°C and during the time of 40 minutes. The amounts of the bounded sulphur as a function of the vulcanization times of the vulcanizates obtained according to the recipe shown in Table 1, are shown in Fig. 2.

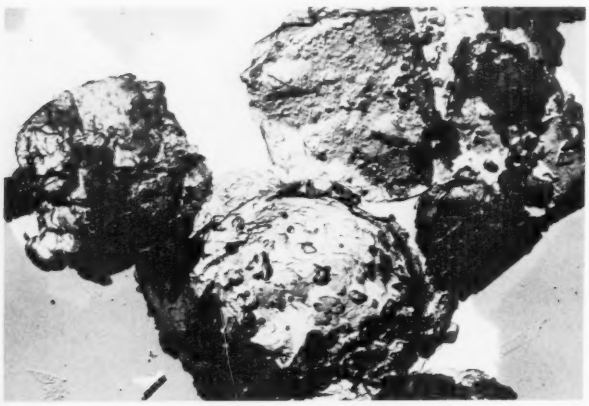

FIG. 1

The electronic-microscope photograph of the "Nowiny" cement dust. Magnification, 30 thousand times.

TABLE 5

The Physico-Mechanical Properties of Vulcanizates Based on the Natural Rubber

	Compound			
	I	II	III	IV
	% by weight			
RSS	100	100	100	100
Stearin	1	1	1	1
Accelerator M	2	2	2	2
Sulphur	2	2	2	2
Cement dust	50	100	-	-
Zinc oxide	-	-	1	5
Tensile strength (MPa)	4.5	5.9	11.3	17.2
Elongation (%)	730	650	780	700
Hardness (°Sh)	31	46	35	40

TABLE 6

The Physico-Mechanical Properties of Butadiene-Styrene Vulcanizates Containing Cement Dust

Number of Compound	H (°Sh)	M-300 (MPa)	R_r (MPa)	E (%)	E_t (%)	R_{rd} (kG/cm)	F (%)
I	63	8.7	18.0	660			
		10.6	17.9	600	12	123	36
		10.6	17.5	540	16	135	
		11.0	14.6	540			
II	63	10.4	15.9	440			
		10.0	17.1	600	20	124	38
		9.6	15.2	600	16	122	
		10.3	17.1	640			
III	57	10.3	19.6	580			
		10.1	19.6	600	16	150	42
		11.0	18.8	580	20	144	
		9.6	18.1	600			
IV	57	8.4	17.3	560			
		10.3	17.9	600	16	125	45
		10.7	17.6	580	20	133	
		10.2	17.1	580			
V	59	12.0	19.3	580			
		11.9	18.3	520	20	125	42
		10.8	17.6	600	16	134	
		10.4	17.6	580			
VI	62	10.6	16.7	540			
		10.7	17.4	580	28	129	41
		8.3	13.6	600	24	122	
		9.4	15.0	540			

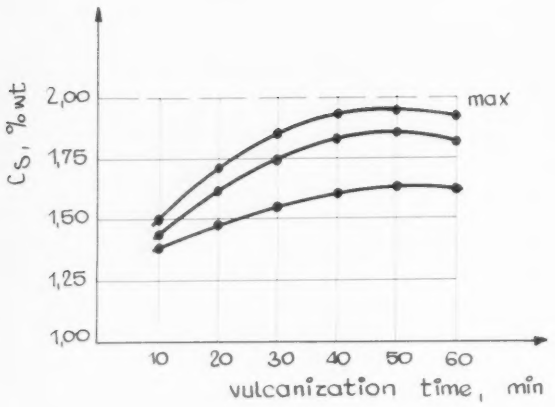

FIG. 2

The effect of vulcanization time on the bound sulphur, C_S.

Discussion

Although the external surface of the waste cement dusts is little developed, it is not smaller than the specific surface of the used zinc oxide. As the amounts of ZnO in the investigated samples of the cement dusts are small (less than 1%) and they change in a narrow range, the samples can be considered as homogenous ones in this respect. The results of chemical analysis were confirmed by x-ray investigations which showed the crystalline forms of ZnO with the admixtures of $Zn(OH)_2$ and $ZnCO_3$ in the cement dust samples. The additional, atom absorption analysis showed small amounts of copper, lead and manganese compounds in the examined samples. When amounts of the above compounds in rubber compounds or gum compounds are greater than the permissible ones in the standard, the activation and initiation of an oxidation process take place which can lead to degradation of a polymer. This degradation leads, certainly, to worse utilization qualities. From the rubber industry point of view, the most harmful impurities in cement dusts are those of the copper and manganese compounds which are usually on the surface of the dust grains. The amounts of manganese shown in Table 3, are from 2 to 4 times greater than the permissible ones, which can have a disadvantageous influence on the parameters of a produced rubber. Above all, that can effect aging properties. However, when cement dusts are used entirely as a substitute for zinc oxide, the amounts of manganese are very unlikely to be greater than the permissible standard ones.

The sedimentation analysis data show a considerable grain size homogenity of the waste cement dusts, as the amount of the 0-5 μm fraction is greater than 75%. They also show that the amount of the fraction having grain size greater than 5 μm is20-25% in which there is only 6% of those which the grain size is greater than 20 μm.

The jet mill powdering causes not only a certain de-agglomeration, but above all, improves homogenity of the cement dusts (the amount of 0-5 μm fraction exceeds considerably 90%) and diminishes the amount of the fraction which grains of a bigger size, below 1%.

The analysis of electron microscope photographs showed that the cement dusts, contrary to zinc oxide, do not easily form agglomerates. Although the shapes of grains were various, most of them were close to the spherical one and the surfaces were developed moderately or slightly.

While introducing the cement dusts into rubber compounds, no anomaly was observed and mixing of them which was carried out on mixing rolls, was quite similar to that for zinc oxide.

The data analysis (Table 5) shows a negative influence of amounts of the cement dusts on the tensile strengths. It must be stressed, however, that the natural rubber filled even with reinforcing filler, diminishes its strength parameters.

The investigations show that a small amount of zinc oxide in cement dusts makes it necessary to add a certain amount of the former one. The added amounts of cement dusts, which recompense the absence of ZnO, should not be too big so as not to play the part of inert fillers.

Table 6 shows the highest values of modulus for the vulcanizates which contain 5 parts by weight of waste cement dust and only 1 part by weight of ZnO. The samples which contain no zinc oxide have also good modulus. For example, M-300 sample has the modulus of about 10.0 MPa. The best tensile strengths distinguish III and V compounds which have 3 and 5 parts by weight of ZnO respectively and 5 parts by weight of the dust. The values of their parameters are 18-19.0 MPa which is greater than the one for the I compound, approximately 17.5 MPa, with no cement dust and 5 parts by weight of ZnO. The VI compound with no zinc oxide also has a considerable, 16.0 MPa, tensile strength.

Tensile set, E_t, is nearly the same for all of the samples but for the vulcanizate with no zinc oxide. For the last one, they are slightly higher, yet smaller than the ones in the standard.

The tearing strengths, R_{rd}, vary similarly to those of the tensile strength, with the highest values for the III and the V vulcanizates. The flexibilities, F, decrease when the amounts of cement dust increase.

Conclusions

Waste cement dusts are good substitutes for zinc oxide in rubber compounds. It is possible to eliminate entirely zinc oxide as the activating agent, from the rubber compounds based on the butadiene-styrene rubber, Ker 1500. In order to diminish the usage of ZnO and take advantage of waste cement dusts, a certain 1 part by weight of ZnO for 5 parts by weight of cement dust, is suggested to be added.

The rubbers with addded cement dusts, in the above amounts, have good strength parameters and sulphur indroduced during the rubber compound preparation process is nearly completely bound. These good results of the investigations may be explained by the presence of various metal oxides, mainly CaO and MgO, which have a positive influence on the formation of stable bonds with sulphur during a vulcanization process.

References

1. G.W. Szypina, L.I. Dewikina, W.N. Krasowskij and J.N. Gromowa, Kauczuk i riezina 7, 16 (1982).
2. L.I. Dewikina, G.W. Szypina, W.G. Korsakow and W.N. Krasowskij, Kauczuk i riezina 12, 15 (1978).
3. R.B. Kron, J.W. Palmer, Rubber World 156, 57 (1967).
4. Newalls Insulation and Chemical Co., Ltd. "Light Magnesium Oxide and its use in the Rubber Industry," Ref. 119, England 1965.
5. T. Paryjczak "Chromatografia gazowa w badaniach adsorpcji i katalizy", PWN Warszawa, 1975.
6. J. Kulka, Polimery 13, 263 (1968).
7. B.D. Cullity, "Podstawy dyfrakcji promieni rentgenowskich," PWN Warszawa, 1964.
8. D.E. Bradley, Brit. J. Appl. Phys. 5, 65 (1954).
9. A. Krysztafkiewicz, W. Wieczorek and L. Domka, Polimery 26, 221 (1981).
10. I.R. Davies and S. Thuraisingham, J. Chromatography 35, 513 (1968).
11. A. Krysztafkiewicz and L. Domka, Polimery 27, 206 (1982).

CEMENT and CONCRETE RESEARCH. Vol. 14, pp. 622-630, 1984. Printed in the USA.
0008-8846/84 $3.00+00. Copyright (c) 1984 Pergamon Press, Ltd.

THE DISPERSION MODEL FOR HYDRATION OF PORTLAND CEMENT

I. GENERAL CONCEPTS

Torben Knudsen
The Institute of Mineral Industry, Building 204,
The Technical University of Denmark,
DK-2800 Lyngby, Denmark

(Communicated by D.M. Roy)
(Received Sept. 7, 1983)

ABSTRACT

This paper introduces an analytical mathematical model for development of the hydration of Portland cement:

$$t_0 + t_1 A + t_2 A^2 = t$$

t is time, and t_0, t_1 and t_2 are time-constants depending on temperature, cement type, admixtures etc. A is the hydration ratio, i.e. the ratio of hydrated to unhydrated cement. The dispersion model has been derived on basis of the typical particle size distribution for tube-milled products. Earlier findings by us have proven the particle size distribution to be a dominant factor in the correct modelling of cement hydration. The parameterization of hydration curves, which is easily performed with the dispersion model, gives a sufficient characterization of these for purposes of practical interpretations of the effects of factors decisive for the development of hydration.

VOL.
14
1984

Introduction

This paper describes a mathematical model for the development of the hydration of Portland cements. The content of the model differs in many respects from earlier attempts to model cement hydration, but a comparison to other models is outside the scope of this paper. The model of hydration presented here is the result of our previous work with cement hydration (1,2). These works were inspired by the works of Taplin (3). He was the first to point to the importance of the particle size distribution (psd) in the modelling of cement hydration. The influence of psd on the shape of the hydration curve has in our work been brought into explicit form in the dispersion model of hydration. The model appears in a mathematical analytical form, which can easily be used for parameterizing hydration curves.

The dispersion in particle sizes in a material like cement is such, that the state of reaction of the smallest particles is significantly different from the state of reaction of the largest particles. While the smallest particles may be fully hydrated, the largest particles may have a low degree of hydration. In fact, at any time of hydration there exists a distribution of degrees of hydra-

tion, corresponding to one point on the hydration curve. Thus it may be understood, that the development of hydration of a single particle can not directly be discovered by the hydration curve. For materials with a broad psd like in cements it can be shown by numerical means, that only gross features in the kinetics governing the hydration of a single particle, may be discovered by the hydration curve. A change for instance from constant rate kinetics to surface reaction controlled kinetics, both being linear kinetics, makes no significant change in the hydration curve obtained by calculation. This important observation will be designated the "dispersion rule".

Thus the influence of psd may be considered a complexity in the study of hydration kinetics per se. On the other hand, in attempts to model the hydration development of cements it constitutes a simplifying factor. According to the dispersion rule differences within a size class in morphorlogy, chemical composition etc. can hardly be recognized in the hydration curve. The hydration curve is sensitive mainly to the psd (with the exception mentioned later), and the psd-curve for tube-milled products is smooth and simple in form.

Now what is left of kinetic information in the hydration curves?
Mainly two features:

1) When hydration curves are plotted as function of log-t, the position of the curve on this axis determines the value of the rate-constant (The situation is more complicated when 2 rate-constants govern the hydration development).

2) The two important groups: linear and parabolic kinetics, can be recognized in the hydration curves.

OL.
14
984

In order to appreciate the last point one should note that all kinetic equations leaning on the shrinking-core model contain the variables r,t and k, being the particle size, time and the rate-constant respectively, in either of two combinations:

$$\text{linear: } \frac{kt}{r} \quad ; \quad \text{parabolic: } \frac{(kt)^{\frac{1}{2}}}{r} \qquad (1)$$

This fundamental difference between linear and parabolic kinetic equations "overrides" the dispersion rule since it constitutes a difference in the way r and t enters the kinetic equations. The fact that r and t enter the kinetic equation in ratios is not a mere coincidence. It is a result of shrinking-core kinetics, and it guarantees that reaction curves belonging to different particle sizes never cross. While the dispersion rule may be said to be primarily responsible for the simplicity in modelling hydration with the dispersion model, the simplicity is also the result of a deliberate limitation in its range of validity. As can easily be verified by noting the form of the dispersion model, this model does not give a correct description of the early accelleratory part of the hydration curve, i.e. the interval 0-15% is outside the reach of the model, and should be left out in numerical work with it. The model in its presented form models this part by shifting the zero-point of time to t_0. A closer agreement in the range 0-15% can be obtained by using a more correct formula for psd (see eq.2 in ref. 1) than used in the derivation presented in this paper. But the new parameter entering the model, as a result of this modification of the formula for psd, depends only on the correct description of the finest 5% of psd, and contains no further kinetic information. Therefore we feel, that the loss of close agreement in the first 15% of the hydration curve is not a serious loss, and the primary goal with the dispersion model is a general and useful characterization of hydration curves, and not the optimal accuracy in modelling all parts of the hydration curve.

Outlines of the derivation of the dispersion model of hydration.

Due to the earlier mentioned effect of the dispersion of particle sizes the crucial point in modelling cement hydration is the transformation from single particle kinetics to the hydration of the total ensemble of particle sizes. By assuming independent reactions of particles this transformation may be represented by:

$$\alpha(t) = \int_0^\infty w(r)\ \alpha(r,t)dr \qquad (2)$$

where $\alpha(t)$ is degree of hydration of the ensemble of particle sizes, $w(r)$ is the frequency psd, and $\alpha(r,t)$ the degree of hydration of a particle of size r.

$\alpha(r,t)$

Much mathematical modelling of hydration in the literature has been concerned with theories about $\alpha(r,t)$. Comparison to experimental data has often been done by putting $r=\bar{r}$, where $\bar{r}$ is the mean particle size of the material in question. This procedure may be very misleading, if the psd of the samples are not sufficiently narrow (2). Theories involving specific assumptions as to the form of $\alpha(r,t)$ must be compared with hydration data from narrow-sized samples. The frequently referenced data presented by Kondo and Ueda in Tokyo symposium (4) is not narrow-sized as far as modelling with $r=\bar{r}$ is concerned. This was shown in ref. (2).

Taplin seems to have been the only author who earlier suggested a solution of eq.2, which was not purely numerical (5). He used a log-normal distribution for psd, and his very elegant index-of-reaction equation for $\alpha(r,t)$, but his solution is in form of a series-development, which can hardly be called analytical in the stricter sense of the word.

Some of the reason for the difficulty in suggesting analytical solutions to eq.2 lies in the form of $\alpha(r,t)$. All suggestions, so far, as to the form of $\alpha(r,t)$ has a time of termination. From that time on the $\alpha(r,t)$-curve is a straight line with $\alpha=1$. Such a curve, composed of an ascending part and a constant part, can hardly be given a simple analytical form, suitfull for the solution of eq.2.

In our case we have chosen an analytical form for $\alpha(r,t)$ with the property $\alpha(r,t)<1$ for all values of t:

$$\alpha(r,t) = \exp\left(-\frac{r}{(kt)^i}\right) \quad ; \quad i = \begin{cases} 1 \text{ for linear} \\ \frac{1}{2} \text{ for parabolic} \end{cases} \qquad (3)$$

where k is a rate-constant. This form resembles quite closely the "classical" forms up to ca. 70% of hydration, but thereafter ascends more slowly towards the asymptote $\alpha=1$. It is a convenient mathematical form for the solution of eq.2, but so far no direct physical interpretation can be given of it. A choice like this, of an $\alpha(r,t)$ which disregards a physical content, is relying on the dispersion rule, which says that the hydration curve is insensitive to the form of $\alpha(r,t)$. All, which is important, is that the independent variables should appear in the combination as given by eq.1. This is not the whole truth though! The use of the dispersion rule should be seen in the light of the convolution principle as derived in (1), but a closer evaluation of this point is outside the scope of this introductory paper.

w(r)

As to the form of w(r) appearing in the integral of eq.2 it is a lucky coincidence, that the psd of tube-milled product like cement may be modelled in 95% of its range by a form as simple as:

$$w(r) = \frac{1}{r_0} \exp(-\frac{r}{r_0}) \qquad (4)$$

where r_0 is a constant in the equation depending on fineness. This form is suited for the integration (eq.2) with $\alpha(r,t)$ given by eq.3. Its major draw-back is the lack of agreement for the finest 5% of the material. The error is such that it leads to infinite specific surfaces. This is of no serious practical consequence though, since experiments show $1/r_0$ to be directly proportional to Blaine's measure of fineness (6).

Solving the integral

By insertion of eq.3 and eq.4 into integral of eq.2 we arrive at the solution:

for linear: $$\alpha(t) = \frac{t}{t + t_1} \quad ; \quad t_1 = \frac{r_0}{k_1} \qquad (5a)$$

for parabolic: $$\alpha(t) = \frac{\sqrt{t}}{\sqrt{t} + \sqrt{t_2}} \quad ; \quad t_2 = \frac{r_0^2}{k_2} \qquad (5b)$$

Both eq. 5a and eq.5b are simple hyperbolas in t and $\sqrt{t}$ respectively. The time-dependency in eq.5a is well-known in drying shrinkage and creep, and has been suggested a few times for modelling the strenght development of concrete (7,8,9). Why it has never found wide-spread application in practice within hydration modelling may be due to two reasons. Firstly, eq.5a covers only one group of hydration curves encountered in practice. The other group obeying eq.5b is equally important. We find that hydration curves for normal Portland cement are modelled by eq.5a, whereas eq.5b should be used when modelling the hydration development of for instance white cement. Secondly, the importance of introducing the correct zero-point for time has not been recognized in much mathematical modelling of hydration (10), (Carino in ref. (9) correctly introduces t_0). The proper use of eqs.5 depends on the correct choice of zero-point. Thus the time appearing in eqs.5 is "reaction time", and should be understood as $t_m - t_0$, where t_m is the time from mixing. The reason for the introduction of t_0 in modelling of hydration is the obvious one, that the dormant period is not included in the modelling, except as a delay in the start of the hydration development. (In the equations to follow t_0 will appear explicitly and t takes on the meaning of time from mixing).

In most practical cases the use of eqs.5 is dependent on another adjustable parameter besides t_1 (or t_2) and t_0. This parameter appears in connection with the definition of α. Since very few data in the literature contain direct measurement of α (as obtained with XRD), properties like heat evolution, non-evaporable water, chemical shrinkage, etc. have to be relied on. The use of such data for the modelling of hydration require a knowledge of P_∞ (the property measured after infinitely long time) or the estimation of this parameter by adju-

sting $\alpha \equiv P/P_\infty$ until the best fit with eqs.5 is obtained. How this is done in practice will be described in the following chapter.

The final form of the dispersion model

For the purpose of arriving at the final form of the dispersion model we prefer to rewrite eqs.5:

$$\text{linear:} \qquad t_0 + t_1 A = t \tag{6a}$$

$$\text{parabolic:} \qquad t_0 + t_2 A^2 = t \tag{6b}$$

where $A \equiv \alpha/(1-\alpha) = P/(P_\infty - P)$, and t in contrast to eqs.5 take on the meaning of time from mixing, since t_0 is now explicitly entering the equations. Written in this way the designation linear and parabolic take on a direct formal meaning, besides refering to the underlying kinetics. A is called by us the hydration ratio as opposed to α the hydration degree.

Experiments in this laboratory using chemical shrinkage of Portland cement paste, with the admixture $CaCl_2$, triggered the fusion of eq.6a and eq.6b to the final form (11):

$$t_0 + t_1 A + t_2 A^2 = t \tag{7}$$

Eqs.6a and 6b are still contained as limiting cases of eq.7, when either t_1 or t_2 takes on the value 0.

The hydration experiment with additions of $CaCl_2$ showed, that by adding from 2 to 6% by weight of cement, kinetics changed from linear (eq.6a) to parabolic (eq.6b). In between none of these limiting cases could produce satisfactory fits. The combinatory eq.7 gave excellent fits for all additions: 2,4 and 6% (see fig. 1). The parameters t_1 and t_2 changed in this interval in such a way, that the ratio t_1/t_1+t_2 changed its value from approximately 100% to approximately 0%. We defined this ratio as degree of linearity:DL.

The derivation of eq.7 from first principles is not complicated, but will not be given in this paper. In brief, it considers two separate resistances depending on the linear and parabolic part, and makes series-coupling as with resistances in an electrical curcuit. This is done for kinetics of the individual particles, whereafter the transformation by means of the integral in eq.2 is performed. The fact that eq.7 comes out as a linear combination of eqs.6a and 6b is a result of the particular form assumed for linear and parabolic kinetics in eqs.3.

Concluding this chapter we find it important to stress, that although the form for eq.7 is such, that the parabolic element t_2A^2 will be governing for sufficiently long times, numerous hydration curves modelled by us could in practice be considered 100% linear. A change from linear to parabolic kinetics as pictured by eq.7 may come so late (small values of t_2) as to have no practical implication.

Parameterizing hydration curves with the model

In the following a brief description will be given of the use of the dispersion model for parameterizing hydration curves. Examples of the success of the dispersion model in modelling hydration curves for cement will not be given in this paper, except for the example presented in fig.1. Reference will be made to earlier presentations concerning the applicability of the dispersion model in the form of eqs.6 (1,2,12), and to a recent Ph.D. thesis for a more thorough documentation including the final form eq.7 (11).

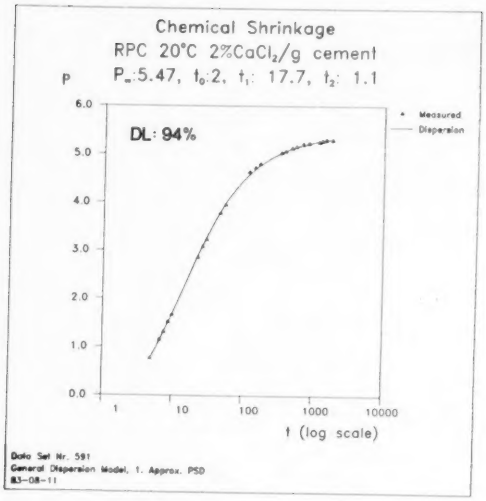

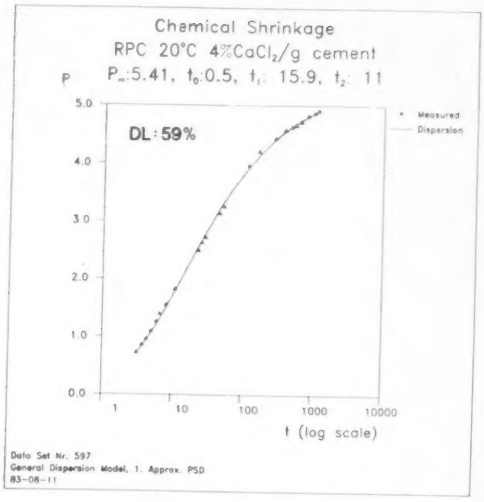

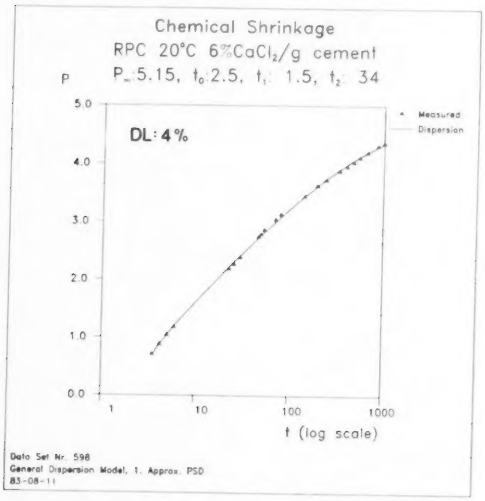

Fig.1 Measurements of chemical shrinkage of rapid hardening Portland cement (w/c=0.5), fitted by the dispersion model. The degree of linearity DL is seen to change from 94% to 4% by addition of from 2-6% $CaCl_2$ by weight of cement. Time-constants are in hours and chemical shrinkage P in ml/loo g cement.

Regression calculation

The dispersion model of hydration, as given in eq.7, presents itself as a parabola in A and t. The fitting to experimental data may therefore be performed as a simple polynomial regression, higher order than 2 being discarded. The parameter P_∞, entering the definition of A, can be determined by stepwise, repeated regression calculations until a value of P_∞ produces a minimum in the residual variation calculated at each step. As mentioned in the introduction, points belonging to the interval 0-ca. 15% in degree of hydration should not be included in the modelling.

Our experience with regression analysis using eq.7 has shown, that the correct assignment of dependent and independent variables is a crucial point in the analysis. We found, that if t is used as dependent and A as independent variables, too much emphasize is put on points with large t's on the expense of the lower part of the hydration curve. Thus for purposes of regression calculation we rewrite eq.7:

$$1 = t_0(1/t) + t_1(A/t) + t_2(A^2/t) \quad (8)$$

When this form is used in regression, approximately equal weight is put on all points.

Sometimes a visual inspection of points in the late part of the curve may prove useful. Points deviating too much from a smoothly drawn curve may be detrimental to regression in this part of the curve, and are better left out of the analysis.

A graphical method

A graphical method may be applied for the determination of the parameters t_0, t_1, t_2 and P_∞ in the dispersion model. This method uses a double-log paper and a transparent sheet. Place the sheet on top of the log-paper, and draw a smooth curve through the data points. Now translate the sheet along the log-P axis (P is the measured property) until the following equation is satisfied:

$$t_{80} = 16t_{20} - 27t_{40} + 12t_{60} \quad (9)$$

where t_{20}, t_{40}, t_{60} and t_{80} are times (as read from the curve) corresponding to 20,40,60 and 80% hydration. Now P_∞ is the value on the sheet falling at 100% on the double-log paper, and t_0, t_1 and t_2 may be calculated by:

$$\begin{aligned} t_0 &= 1.4t_{20} - .44t_{50} + .022t_{80} \\ t_1 &= -1.8t_{20} + 1.9t_{50} - .11t_{80} \\ t_2 &= .36t_{20} - .44t_{50} + .089t_{80} \end{aligned} \quad (10)$$

Inaccurate or incomplete data sets

The success of modelling with eq.7 depends on the accuracy and completeness of the data set. Data sets may often be encountered, which consist of few points or do not cover a sufficient range in α to be useful in the above mentioned methods of parameterizing. In that case it is wiser to resort to the forms given in eqs.6a and 6b. With these forms a graduated characterization of hydration curves in degree of linearity has been abolished, and substituted for an estimation in either linear or parabolic kinetics. A simple graphical procedure is to plot $1/P$ against $1/(t-t_0)$ in the linear case, and against $1/\sqrt{t-t_0}$, in the parabolic case. In both cases a straight line is produced giving $1/P_\infty$ by extrapolation to infinite time. Since t_0 is entering the variables plotted, this adjustable parameter must be determined by trial and error until the best straight line is being produced.

For data sets from hydration experiments which are not carried far enough, it is often found that plotting against $1/(t-t_0)$ or $1/\sqrt{t-t_0}$ produces equally good straight lines. In this case linear or parabolic kinetics may be selected by considering the two different values of P_∞ obtained. One may be in closer agreement with expectation than the other. If an expectation value of P_∞ is not known, it must be concluded that the data set at hand is insufficient for parameterizing.

Chemical shrinkage as a source of hydration data

Measurements of chemical shrinkage have been found by us to be an extremely valuable source of information on cements hydration. Much of our success with the use of eq.7 has depended on the completeness of data sets obtained with this method. Measurements of chemical shrinkage can easily be obtained as continous curves and can be carried out for as long as neccesary to provide the

completeness required for successful modelling. The measurement is simple, and the number of samples studied is not limited by cost or labour. By adjusting the sample-size depending on the water/cement-ratio we have found no trouble in securing unhindered suction of water into the samples and thus securing accurate measurements of hydration. A full documentation of the use of chemical shrinkage in the study of cement hydration can be found in Mette Geiker's Ph.D. thesis (11).

Discussion on the model

It is the ultimate goal of any mathematical model of hydration to be able to predict the out-come of future hydration experiments. To achieve this goal the relations between the factors decisive for the development of hydration and the parameters entering the model should be searched for. In the case of the dispersion model two important relations are built into the model. Primarily the effect of fineness is explicitly given by the model, as seen from eqs.5, and has been experimentally verified in (6), at least for the linear case. The effect of temperature on the parameters t_1 and t_2 is given in so far as its effect on the rate constants k_1 and k_2 can be assessed. The applicability of the Arrhenius eqation for this purpose has been demonstrated in ref.(12).

Concerning the effect of chemical composition of the cement and the effect of chemical admixtures we have been greatly concerned with the question of what factors determine the underlying kinetics, linear or parabolic. Our observations so far seem to indicate, that high degree of "available" Ca^{++}-ions in the beginning of the hydration favors parabolic kinetics. These Ca^{++}-ions may come from sources such as gypsum in the cement or from added $CaCl_2$ etc. Ca^{++}-ions may become "unavailable" for the hydration of the clinker particles by precipitation with C_3A in the well-known double salts of the form $C_3A(CB)_y(H_2O)_x$, (where B stands for an anion). Thus small ratios of Ca^{++}-ions to the amount of free C_3A (C_3A not bound in the interior of the clinker particle) produces linear kinetics and for large ratios we get parabolic kinetics. Many experiments (to be published later) performed in our laboratory seem to reveal this pattern. In some intermediate range of ratios we get a joint kinetics as already explained with the additions of $CaCl_2$ to Portland cement pastes. Another example is white clinker which hydrates almost linear whereas white cement is parabolic, and with additions of gypsum we experience the same gradual change from linear to parabolic kinetics with decreasing values of DL. It should be mentioned that the factors influencing the "order of kinetics" (whether linear or parabolic) influence the length of the dormant period as well, as modelled by t_0 in eq.7. Linear kinetics generally comes together with long dormant periods and vice versa.

These observations of the influence of available Ca^{++}-ions during the early period of hydration have lead us to a tentative mechanistic interpretation. According to these speculations linear kinetics is the result of a membrane highly resistant to transport of water, and which maintains its stability and resistance throughout hydration. When the membrane formed is weak (or absent!) diffusion through the inner (and probably outer) zone of hydration products becomes rate-controlling and parabolic kinetics results. The state of membrane, we believe, is highly dependent on the available Ca^{++}-ions (alkali-ions seem to have the same effect, although to a lesser extent) in the pore-solution, large amounts of Ca^{++}-ions favoring a weak membrane. Since the membrane consists of colloidal particle bound together with polar attractive forces, it is tempting to speculate that Ca^{++}-ions (in combination with available anions) substitutes the highly polar silanol groups, thus leading to weaker attractive forces between the colloidal particles. This last point is pure speculation, but might act as a contemporary model to aid in proposing further experiments to elucidate this point.

An interesting article concerning the aforementioned has appeared recently (13). N.L.Thomas et al performed experiments with EDTA in hydration of cement. Their findings and conclusions are in good agreement with our lines of thinking concerning the influence of Ca^{++}-ions on the length of the dormant period and on the C/S-ratio of the membrane.

References

1. T. Knudsen, 7th International Congress on the Chemistry of Cement, Paris 1980, I-170.
2. T. Knudsen, Engineering Foundation Conference, Henniker, New Hampshire 1982.
3. J.H. Taplin, 5th International Symposium on the Chemistry of Cement, Tokio 1968, Vol II, p. 249, p. 337 and p. 421.
4. R. Kondo and S. Ueda, ibid Vol II, p. 203.
5. J.H. Taplin, J.C.S.Faraday I, 76,2229(1980).
6. S. Bang Larsen, M.Sc. report, Danish Technical University, The Institute of Mineral Industry, 1983 (in danish).
7. C.J. Bernhardt, Rilem Symposium on Winter Concreting, 1956.
8. Chin Fung Kee, ACI Journal, March 1971.
9. N.J. Carino, International Conference on Concrete at Early Ages, Paris 1982, Vol I, p. 123.
10. T. Knudsen, Cement and Concrete Research, 9,799(1979).
11. M. Geiker, Ph.D. thesis, Danish Technical University, The Institute of Mineral Industry, 1983.
12. M. Geiker and T. Knudsen, Cement and Concrete Research, 12,603(1982).
13. N.L. Thomas and D.D. Double, Cement and Concrete Research 13,391(1983).

VOL.
14
198

CEMENT and CONCRETE RESEARCH. Vol. 14, pp. 631-638, 1984. Printed in the USA.
0008-8846/84. $3.00+00. Copyright (c) 1984 Pergamon Press, Ltd.

THE FLUIDITY OF FLY ASH-CEMENT PASTE WITH SUPERPLASTICIZER

S. Nagataki
Dept. of Civil Eng., Tokyo Institute of Technology
Ookayama, Meguroku, Tokyo, Japan

E. Sakai
Central Research Lab., Denki Kagaku Kogyo Co., Ltd., Japan

T. Takeuchi
Tsukuba Central Research Lab., Fujisawa Pharmaceutical Co., Ltd., Japan

(Communicated by M. Daimon)
(Received Oct. 31, 1983)

OL.
14
984

ABSTRACT

The influence of various fly ashes on the fluidity of fly ash-cement paste with superplasticizer was investigated in connection with the amounts of superplasticizer adsorbed on fly ashes, the change of ζ-potential and the physical properties of fly ashes. Fly ash indicates a high negative ζ-potential, and by adding superplasticizer, an even higher negative ζ-potential is indicated. However, the fluidity of fly ash paste is not improved by addition of superplasticizer as much as in the case of cement. The fluidity of fly ash-cement paste mixed with superplasticizer is influenced by the kinds of fly ashes. The bulk specific gravity of fly ash may be an index for judging the influence of fly ash on the fluidity of fly ash-cement paste.

Introduction

Coal-fired thermal power generation is being reconsidered in Japan because of the necessity to diversify energy resources, and accompanying this, it is expected that the yield of by-product coal ash will be increased. Accordingly, there is again a strong current to actively utilize fly ash making up the greater part of coal ash in concrete. However, in view of the resources situation and environmental conditions in Japan, it is assumed that the fly ash expected to increase in quantity hereafter will be considerably different qualitywise from the fly ash produced in the country in the past since overseas coal will now be used and the production of the fly ash will be under conditions of low combustion temperature. Further, when application of fly ash to high-strength concrete and superplasticized concrete using superplasticizers which have been focused on in the field of concrete in recent years is considered, it is realized that there are many points that are unclear regarding the interaction between fly ash and superplasticizer, and it is necessary for this to be studied at an early date.

The authors have already shown that manufacturing high-strength concretes

using large quantities of various kinds of fly ash produced in Japan is possible. The effect of fly ash on the fluidity of concrete is great at such times and it has been found that there are cases when water-cement ratios cannot be lowered beyond a certain level (1).

Considering the above, examinations were made in this study of the physical property values of fly ash and the phenomenon of adsorption of superplasticizer on fly ash in relation to the influence of fly ash on the fluidity of cement paste containing superplasticizers in order to clarify the effects of the physical properties of fly ash on the workability of concrete and the interaction with superplasticizer.

Experiments

Materials Used and Mix Proportions

The cement used was ordinary portland cement not containing mineral fines, while fly ash was of five varieties from three power stations. The superplasticizer was of the naphthalene type.

Water-binder ratios [water/(cement + fly ash): W/(C + F)] were 0.35, 0.41 and 0.50, fly ash replacement rates [F/(C + F)] were varied between 0 and 100%, while dosages of the superplasticizer were 0 to 0.5% solids by weight of binder.

Measurement of Coefficient of Viscosity

Coefficients of viscosity were determined by the cylinder viscometer previously reported (2) on pastes mixed using a hand mixer. Calculations of the coefficients of viscosity were made by the Buckingham-Reiner equation.

Measurement of Adsorption

The quantities of superplasticizers adsorbed at water-binder ratio of 1.0 for cement, fly ash and blends of the two were measured. The adsorbed quantities were obtained deducting the quantities remaining in the liquid phase from the quantities added, measurements of the amounts remaining in the liquid phase being made in the manner described below. To 20 g of cement or fly ash, 20 ml of superplasticizer solution of the specified concentration were added. After allowing adsorption to occur for a given length of time in a constant temperature revolving tank, centrifugal separation and filtering was done and the supernatant liquid was extracted. The extracted solution was diluted to the range of measurement for the superplasticizer. The degree of adsorption at wavelength of 228 nm on the ultraviolet adsorption spectrum was measured and the quantity of superplasticizer was calculated by a calibration curve determined in advance.

Measurement of ζ-Potential

The sample consisted of 0.2 g of a powder dispersed in 100 ml of water, and the ζ-potential was determined by electrophoresis using a Laser Zee™ Model 500 (mfd by Pen Kem). This apparatus does not require a long time for measurement while it is possible to measure average-type ζ-potentials of individual particles.

Measurement of Uncombusted Carbon in Fly Ash and Removal by Heat Treatment

Measurements of uncombusted carbon in fly ash were made by the infra red analyzer EMIA-1200 (mfd by Horiba, Ltd.) for analyzing carbon and sulfur in metal. For clarifying the interaction with superplasticizer of fly ash it-

self, uncombusted carbon in fly ash was eliminated by the following method. In order to avoid changes in surface properties of fly ash as much as possible, and moreover, to remove carbon by causing it to be completely combusted, a minimum temperature of 800°C referring to DTA and TG measurement results and a minimum combustion time of 10 minutes referring to ignition loss test results were set. It was confirmed that the fly ash after removal was not changed in shape and other properties compared with conditions before heat treatment through observations by scanning electron microscope (SEM) and results of X-ray powder diffraction.

Measurement of Bulk Specific Gravity

The bulk specific gravities of the fly ashes were measured adapting JIS Z 2504, "Method for Determining Apparent Density of Metal Powder". Fly ash was placed in the cylindrical container (volume 280 cm^3) shown in Fig. 1, thoroughly compacted by thumping through drops of a flow table (for flow measurements of mortar), and after levelling off the top surface, the weight of the contents per unit volume was taken as the bulk specific gravity.

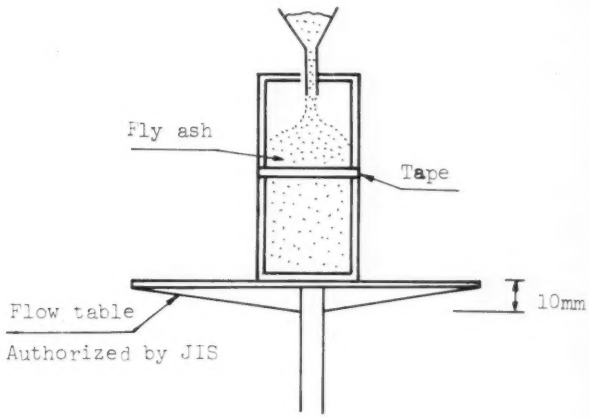

Fig. 1
Apparatus of measuring bulk specific gravity

Results and Discussions

Characterization of Fly Ash

The properties of the various fly ashes used in the experiments are shown in Table 1. The ignition losses of the fly ashes C, D and E do not satisfy the requirement of the JIS value of 5% or under, and this is thought to be due to increases in uncombusted carbon because of combustion temperatures having been lowered in recent years to satisfy NO_x regulations. The abovementioned standard value in Japan had been prescribed before NO_x regulations were initiated and it is thought necessary for it to be reconsidered.

Further, unit water content ratios normally considered as yardsticks for fluidity were all under 100%. Bulk specific gravities differed considerably according to the varieties of fly ash. An SEM photomicrograph of fly ash C is shown in Fig. 2, and that the fly ash contained particles of such poor shapes indicates that bulk specific gravity was low. Specific gravity according to JIS and the specific gravity of fly ash ground for three days in a ball mill differ considerably, indicating that air bubbles and voids in fly ash are fairly large in quantity.

Table 1
Properties of fly ashes

Fly Ash	SiO_2 (%)	Moisture Content (%)	Ig.loss (%)	C (%)	Fineness (cm^2/g)	Unit water-content ratio(%)	Compresive Strength ratio (%)		Specific Gravity		
							28days	91days	JIS	After Mill	Bulk
A	52.6	0.12	2.80	1.12	3000	95	68	107	2.22	2.58	1.40
B	52.5	0.11	2.99	1.19	2900	97	76	105	2.25	2.59	1.41
C	49.2	0.14	6.64	3.99	3300	97	83	101	2.20	2.60	1.29
D	48.2	0.24	10.29	8.36	3000	99	73	94	2.17	2.62	1.23
E	50.1	0.16	5.86	4.14	4100	98	75	102	2.25	2.56	1.38

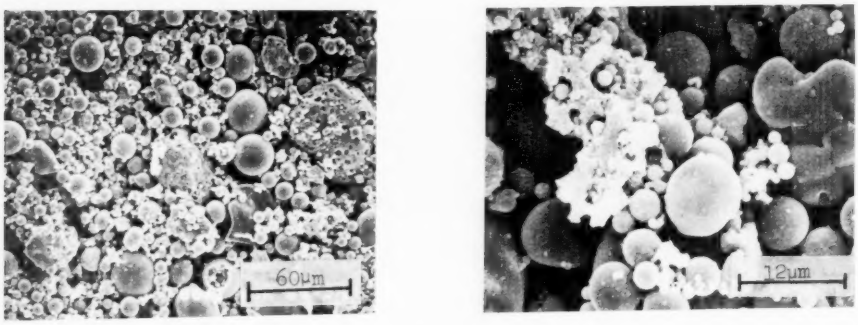

Fig. 2
SEM photographs of fly ash C

Influences of Superplasticizer and Physical Properties of Fly Ash on Fluidity of Fly Ash Paste

The rates of adsorption of the superplasticizer on cement and fly ash are as shown in Fig. 3, and in general, the rate of adsorption on fly ash is higher than in case of cement. Both have more or less reached equilibrium at one hour of adsorption. The adsorption isotherms after one hour of adsorption are shown in Fig. 4. Langmuir isotherms are seen for both cement and fly ash. Fly ash reaches saturation adsorption at a low equilibrium concentration, while there are cases of greater amounts of adsorption than with cement, the amounts differing considerably according to the variety of fly ash. However, when adsorption quantities are determined for fly ashes with carbon removed by heat treatment, practically no difference is seen between fly ashes as indicated in Fig. 4, while moreover, the saturation adsorption quantity is approximately one half that in case of cement. Further, the difference between adsorption on untreated fly ash and adsorption on heat-treated fly ash, in effect, the amount of adsorption on uncombusted carbon shows almost no correlation with the carbon quantities in Table 1. This is thought to be because the adsorption capability of carbon differs considerably depending on the variety of the fly ash.

VOL.
14
1984

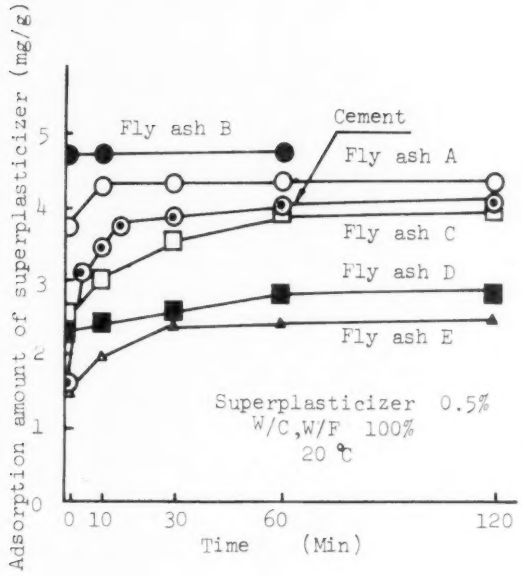

Fig. 3
Rate of adsorption of superplasticizer on fly ashes and cement

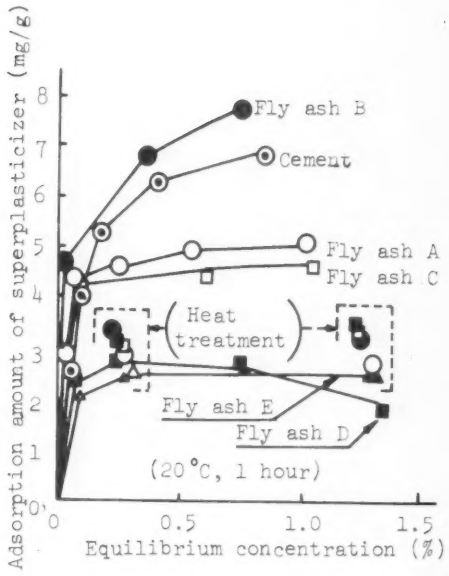

Fig. 4
Adsorption isotherm curves of superplasticizer on fly ashes and cement

The variations in ζ-potential are shown in Fig. 5. The fly ash indicates a high negative value in the first place, and with addition of superplasticizer a still higher negative value is indicated, and moreover, a negative ζ-potential higher than in the case of cement may be seen. However, as shown in Fig. 6, the fluidity of fly ash is not improved very much by the addition of superplasticizer, and rather, the influence of the fly ash itself is great. This is thought to be because the fly ash involved in ζ-potential measurements is limited to small particles, and the influence of the other larger particles on the fluidity of fly ash is great, indicating that there is a necessity to evaluate fluidity from the powder characteristics of fly ash. However, it is not that fluidity is completely unimproved by addition of superplasticizer, and improvement of fluidity by addition of such an admixture is greater for fly ash containing carbon of especially low capacity to adsorb superplasticizer (Fig. 6, E) compared with fly ashes which are not so (Fig. 6, B,C).

Figure 7 shows the relationship between bulk specific gravity measured as a characteristic value of fly ash and the coefficient of viscosity of paste. The coefficient of viscosity indicates a lower value the higher the bulk specific gravity. This bulk specific gravity is related to the shape of fly ash observed by SEM, and the bulk specific gravity becomes lower the higher the content of particles with poor shapes.

As described above, in case of fly ash the fluidity of paste is determined by the physical property values of the fly ash itself, and fluidity is not improved very much even when superplasticizer.

Fluidity of Fly Ash-Cement Paste

Figure 8 shows the influence of fly ash replacement ratio on coefficients

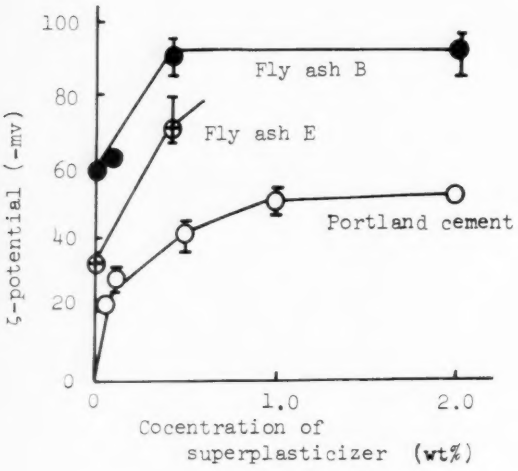

Fig. 5
The ζ-potential of fly ashes and cement in the presence of superplasticizer

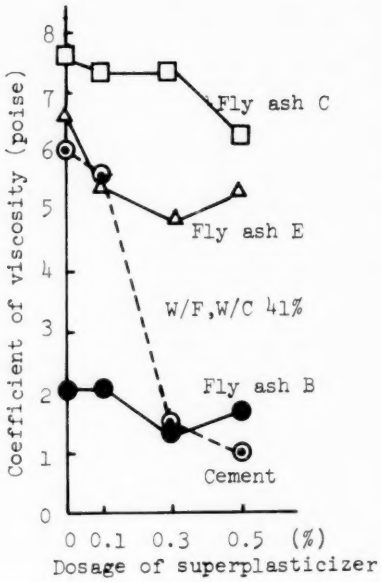

Fig. 6
Influence of superplasticizer on viscosity of fly ash or cement paste

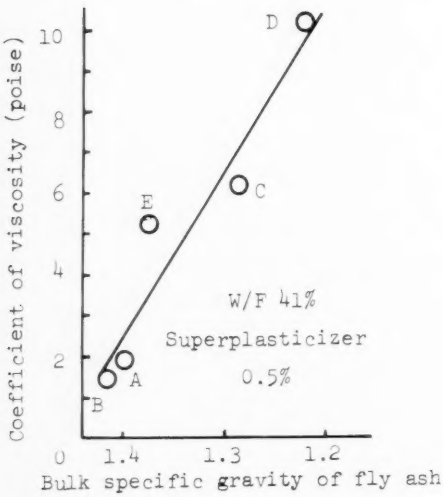

Fig. 7
Relation between the viscosity of fly ash paste and the bulk specific gravity of fly ashes

of viscosity of fly ash-cement pastes at low water-binder ratio of 0.35 and normal water-binder ratio of 0.50. At 0.50, which is a normal water-binder ratio, there are partially cases of increases in coefficients of viscosity along with replacement ratios, but others show trends of decrease to indicate that addition of fly ash is advantageous for improving fluidity of paste, and this agrees with the results on unit water content ratios shown in Table 1. However, in case water-binder ratio is made low at 0.35 by addition of superplasticizer, the differences according to the varieties of fly ash become greater with increased replacement ratios, and unlike the results of unit water content ratios, there are cases when the fluidities are not improved. As shown in Fig. 9, the influence of fly ash was especially great in case of low water-cement ratio, and coefficients of viscosity of fly ash-cement pastes had correlations with bulk specific gravities of the fly ashes at the various

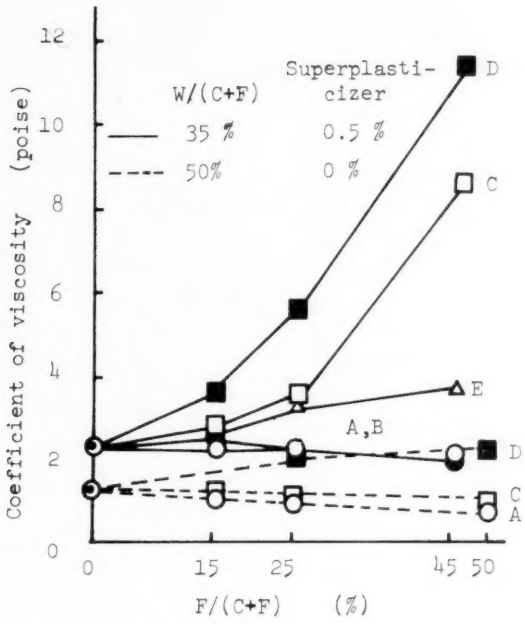

Fig. 8
Relation between the replacement ratio of fly ash and paste viscosity

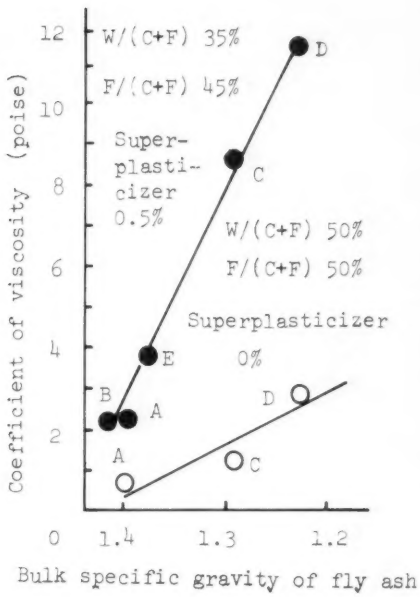

Fig. 9
The relation between bulk specific gravity of fly ashes and the viscosity of fly ash-cement paste

water-binder ratios, and this was the same even when replacement ratio was varied. Consequently, it is thought that bulk specific gravity can serve as one index for judging whether fluidity of cement paste to which fly ash has been added is good or bad.

Further, the amount of adsorption of superplasticizer on fly ash-cement is shown in Fig. 10, and at normal quantity of fly ash used it is about the same as for adsorption on cement alone. That such a result is obtained in spite of the fact the quantity of adsorption on fly ash differs considerably depending on variety of fly ash can be considered to be the situation below. In effect, adsorption on fly ash of high adsorption speed (including uncombusted carbon) is completed first, after which adsorption on cement of high adsorption quantity occurs, and there is good agreement between the measured amount of adsorption and the calculated value assumed as described above. Consequently, the dosage of superplasticizer is not changed very much in the case of fly ash-cement, either. As for variation in ζ-potential due to addition of superplasticizer, approximately the same values as for cement alone are indicated up to fly ash replacement ratio of 50%, and a high negative value as with fly ash is not indicated. This is thought to be due to a peculiar adsorption of Ca^{2+} ions released accompanying hydration of cement.

As described above, when water-cement ratio is lowered in fly ash-cement paste, the fluidity differs extremely depending on the variety of the fly ash. Since the fluidity of fly ash is not improved very mech by superplasticizer at such time, it is important to know what degree of fluidity the fly ash possesses in the first place. It is thought that the bulk specific gravity of fly ash is useful as an index of the above.

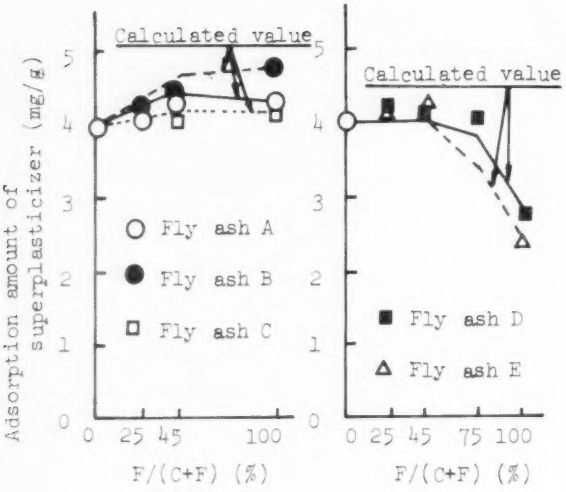

Fig. 10
Relation between the amount of superplasticizer adsorbed on fly ash cement paste and the replacement ratio of fly ash (W/(C + F) = 100%, Dosage of superplasticizer : 0.5%, at 20°C, 1 hour)

Conclusions

The results obtained within the scope of this study may be summarized as follows:

(1) The amount of adsorption of superplasticizer on fly ash differs considerably according to the variety of fly ash, whereas amounts of adsorption on fly ashes heat-treated to remove uncombusted carbon are all more or less the same and are approximately one half the adsorption on cement. It is thought the differences in amounts of adsorption on fly ash are unrelated to carbon quantity and due to differences in the adsorption capacities of the carbons.

(2) The amount of adsorption of superplasticizer on fly ash-cement at a normal replacement ratio is roughly equal to that in the case of cement only.

(3) Fly ash indicates a high negative ζ-potential, and by adding superplasticizer, an even higher negative ζ-potential is indicated. However, the fluidity of fly ash paste is not improved by addition of superplasticizer as much as in the case of cement. This is thought to be due to the influence of large particles not dispersed by superplasticizer being great.

(4) A correlation exists between bulk specific gravity of fly ash and fluidity of fly ash paste, and coefficient of viscosity is lower the higher the bulk specific gravity. It is thought the bulk specific gravity of fly ash is useful as an index for judging the influence of fly ash on the fluidity of fly ash-cement paste.

References

1. S. Nagataki, E. Sakai and M. Maeda, International Symposium, "The Use of PFA in Concrete", 201, Leeds University, England, (1982).
2. S. Nagataki and H. Kawano, 7th Int'l Cong. on the Chem. of Cement, Paris, Vol. III, VI 120, (1980).

VOL 14 198

CEMENT and CONCRETE RESEARCH. Vol. 14, pp. 639-644, 1984. Printed in the USA.
0008-8846/84 $3.00+00. Copyright (c) 1984 Pergamon Press, Ltd.

THERMAL DEFORMATION OF LOADED CONCRETE DURING THERMAL CYCLES FROM 20°C TO -165°C.

J. Planas, H. Corres, M. Elices
Department of Materials Science. ETS. Ing. Caminos
Universidad Politécnica de Madrid. Madrid-3. Spain

R. Chueca
Auxini S.A. and Dragados y Construcciones S.A.
Madrid. Spain.

(Communicated by Z.P. Bazant)
(Received Nov. 11, 1983)

VOL.
14
984

ABSTRACT

Thermal deformation of concrete samples has been measured. Unloaded water-saturated concrete exhibits a complex strain behaviour during thermal cycles, characterized by dilatation cooling and an irreversible expansion reheating. Loaded water-saturated concrete behaves in a different way. The transition region is reversed -with respect to unloaded samples- and almost dissapears, when compressive stress of 15 MPa is applied. Also an irreversible compressive deformation is bound after reheating. A qualitative explanation of such effects, assuming that microcracking is the dominant deformation mechanism in the transition range, is offered. Further research is needed along this direction.

Introduction

Concrete has been accepted, in the last years, as a desirable constituent in storage systems for refrigerated liquefied gases (RLG), especially for liquefied natural gas (LNG). Nowadays, prestressed concrete tanks for storage of LNG have significant advantages over existing systems, giving a higher level of overall safety and helping to meet the increasing stringent international safety regulations.

Among conditions to be considered in the design of cryogenic structures, the differential loads due to temperature changes during cooling and during (accidental) warming are one of the dominant factors to be taken into account. In particular, data on thermal deformation of concrete are indispensable to the designer.

Reinforcing steel exhibits an almost linear thermal deformation. Water saturated concrete, however, displays completely different behaviour (figure 1, from Reference 1). Thus, internal stresses due to these differences may arise. It is suspected that the steel may be overstressed, while the concrete may suffer an additional compression.

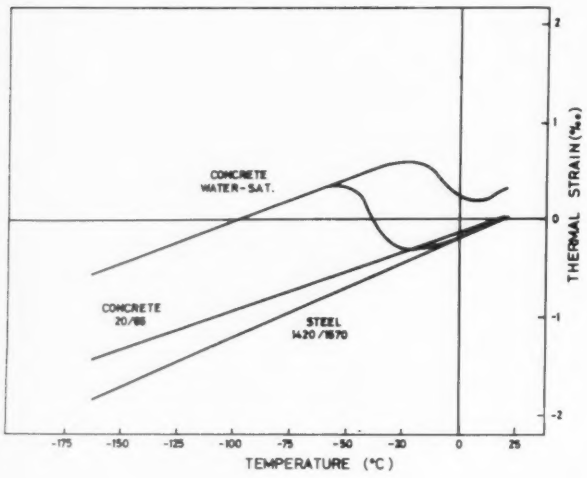

FIG. 1

Thermal strains versus temperature of prestressing steel, water-saturated and normally stored concrete (1)

The present paper reports the results of thermal deformation, under load , of water-saturated concrete during a thermal cycle; cooling from room temperature down to LNG temperature (-165°C) and warming up again. The novelty of these results is reflected in the influence of compressive loads on the non-linear part of concrete thermal strain, as well as on its irreversibility. Such effects cast some doubts on the experimental thermal strains from unloaded samples, as used in designing cryogenic structures.

Materials and Sample Preparation

1. Cement

Rapid hardening Portland cement (ASTM type III) has been used. Tests according to ASTM C 150, after 28 days, gave for compressive strength and flexure strength 50.2 MPa and 8.8 MPa, respectively.

2. Aggregates

Crushed siliceous aggregates and sand have been used in concrete. Grading of aggregate was according to Table 1.

TABLE 1
Grading of aggregates

Aggregate size (mm.)	20 - 5	5 - 1.25	less than 1.25
Percentage (%)	30	25	45

3. Concrete

A single concrete mix design, as shown in Table 2, was used throughout the study. Concrete properties are summarized in Table 3.

4. Concrete Samples

Test specimens for thermal deformation measurements were concrete cylinders of 15 cm length and 7.5 cm diameter.

TABLE 2
Proportional mixing of concrete, by weigth

Cement	Coarse aggregate (mm.) 20 - 5 - 1.25	Fine aggregate (mm.) less than 1.25	Water
1	1.38 1.15	2.07	0.45

TABLE 3
Concrete properties

Air (% by volume)	Slump (cm.)	28 day strength (MPa) compressive	tensile	Tangent modulus 28 day (MPa)
2.45	8.3	38.8	3.0	26.600

VOL. 14 984

Fresh concrete was poured into PVC cylindrical moulds with steel basis. Concrete was compacted by means of a vibrating table. After demoulding, samples were stored under water until testing time.

Some samples have been instrumented with two thermocouples, one in the core and another on the surface, in order to ascertain the temperature profile during cooling and warming. Such cylinders have been used as dummy samples during experimentation. The other concrete samples have been instrumented with two thermocouples glued on the surface.

In order to avoid moisture losses during testing, all cylinders were covered with a thin epoxy layer before testing, just after being taken out of the storage pool.

Thermal Deformation of Unloaded Concrete

A modular cooling chamber was used for cooling concrete cylinders. The cooling chamber, control and data acquisition systems are depicted in the block diagram of figure 2.

The temperature was lowered by spraying a mist of liquefied nitrogen and controlled by an electromagnetic valve. The intended thermal cycle was introduced through the temperature controller (see figure 2) and the surface temperature response, measured by two thermocouples, recorded as an output of the data acquisition system. The chosen cooling rate was 0.35°C/min., low enough to avoid significant temperature differences between two points in the specimens. For our concrete cylinders this temperature difference was less than 2°C.

Thermal strains have been measured by means of quartz glass dilatometers (Ref. 1, Sec. 4.2.2.2). The relative displacement of central points of the two opposite end faces of concrete cylinders was picked up by quartz glass rods. This displacement is transmited by one of the rods to an extensometer outside the temperature chamber. The accurancy of the extensometer was better than 0.003 mm. From this relative displacement, concrete strain is calculated in the data acquisition system and plotted as a function of temperature.

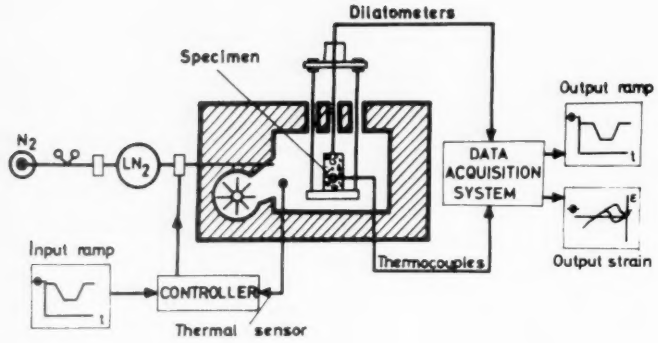

FIG. 2

Block diagram of the system used for measuring thermal strains of unloaded samples.

Figure 3 shows the evolution of thermal strains during two temperature cycles (shown schematecaly in the upper part) of water-saturated and dry concrete cylinders. These results are average values of four samples. That behaviour has already been described by Rostasy and coworkers (1, 2, 3).

Three typical ranges can be distinguished for water-saturated samples:

a. Within the first range, between +20 and -15°C, contraction occurs.

b. Between about -20 and -60°C, a pronounced expansion is observed. The behaviour in this transition range is related to the phase transition of water to ice in pores of small diameter. The expansion becomes more pronounced the greater the water content and the higher the water/cement ratio.

c. In the third region, an almost linear and completely reversible contraction again occurs.

When reheating the specimen an even greater expansion occurs in the second stage. Irreversible strains indicate internal micro-cracking as a result of frost attack. If the temperature cycle is repeated,the expansion of saturated specimens increases with each cycle and irreversible strain increases also, as depicted in figure 3.

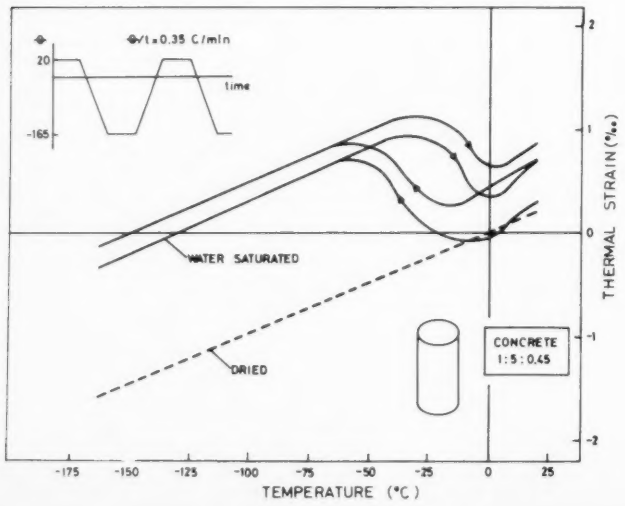

FIG. 3

Thermal strains versus temperature of unloaded samples (water-saturated and dried) along two thermal cycles.

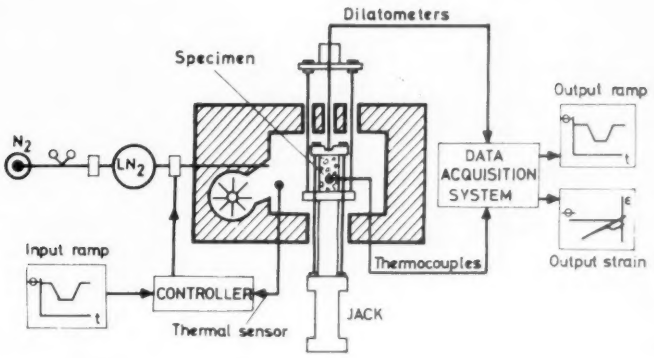

FIG. 4

Block diagram of the system used for measuring thermal strains of loaded samples.

Loaded Concrete Thermal Deformation

Tests have been performed with the modular chamber already described (figure 4) and with the same thermal history, cooling and heating at a rate of 0.35°C/min. The difference between these two experiments was the load applied to concrete during testing.

Loading of concrete cylinders was performed by means of hydraulic jacks (figure 4). The compressive stress applied to the cylinder was 15 MPa, a realistic figure for prestressed elements. Load stability was better than ± 1% of the applied load. In the first step, in order to avoid coupling between creep and thermal strains, specimens were loaded at room temperature and remained at it until creep was negligible (the relative displacement between central points of cylinder bases was less that 0.003 mm. in a 12 hours period). Afterwards, cooling started and thermal strain measurements were performed during thermal cycles.

Figure 5 shows the evolution of thermal strains along two temperature cycles (depicted in the upper part) of water saturated concrete cylinders under load. Also the thermal strains of similar unloaded samples are shown for comparative purposes. All these results are average values of four samples. It can be seen that the behaviour of loaded specimens differs significantly from that of unloaded samples.

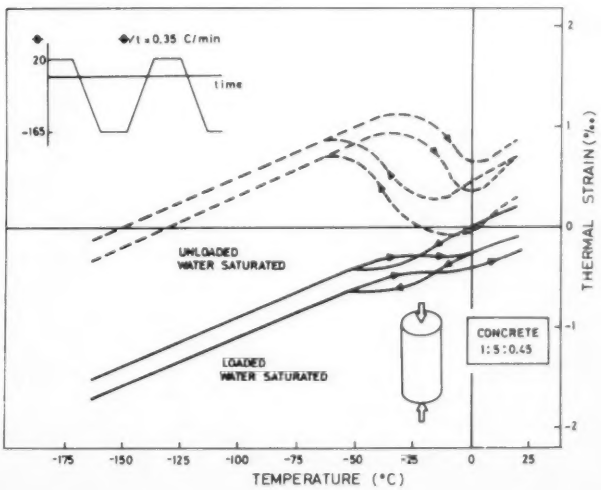

FIG. 5

Thermal strains versus temperature of loaded water-saturated samples along two thermal cycles. (Unloaded water-saturated samples are included for comparison).

The irreversible expansion exhibited by unloaded specimens after cycling turns out to be a contraction for the loaded ones. This is consistent with the assumption that pore pressure build-up during water freezing causes microcracking and, as a consequence, an overall stiffness decrease. This progressive softening may explain the residual compressive strain after cycling of loaded samples.

A second effect is the behaviour in the transition range. Although this range is more similar to unloaded dry samples than to unloaded water-saturated ones, there are some aspects that deserve further comments. When cooled, loaded specimens showed higher contraction that dried samples, followed by a relative longitudinal expansion. This behaviour can be tentatively explained in a qualitative way by assuming that, during the pore pressure build-up process, microcracking proceeds in an anisotropic way. Initially, propagation of preexisting microcracks oriented transversely to the load axis is prevented due to the compressive stress, while microcracks oriented parallel to the load axis are free to open and propagate. Water volume increase is accomodated inside open cracks and finally is manifested as a transverse expansion. The associated damage produces a loss of axial stiffness and the corresponding increase in compressive strain. When the pore pressure reaches a value high enough to overcome the effect of the external load, microcracks transverse to the load axis open first and subsequently propagate, giving rise to an axial expansion (figure 5). This very simplified explanation assumes that microcracking is the dominant deformation mechanism in the transition range. This fact has to be verified by further research.

Conclusions and Future Work

From the above mentioned results the following conclusions can be drawn:

1. Unloaded water-saturated concrete exhibits a complex strain behaviour during thermal cycles ranging from room temperature down to -70°C or lower. This behaviour is characterized by an expansion during cooling (between about -20°C and -60°C) and by an irreversible expansion during reheating. Although this type of temperature-strain curves has already been reported by Rostasy and coworkers (2, 3), other published data (4) do not show the same trend, and more experimental information is needed before a comprehensive description of the phenomenon can be done.
2. Uniaxially loaded (15 MPa) water-saturated concrete behaves quite differently from unloaded samples, presenting highly diminished non-linear effects in the transition range and a compressive irreversible strain increase.
3. Experimental results show that the superposition principle is not aplicable and that behaviour is strongly path-dependent. They also suggest that complete modeling of the thermomechanical behaviour of concrete in this temperature range will have to include pore pressure build-up description and anisotropic internal damage (microcracking).
4. This research has revealed the role of compressive loads in the thermal behaviour, of water-saturated concrete at low temperatures. Work is in progress to ascertain the behaviour of concrete under lower loads and with different amounts of freezable water. Effects of the cooling rate and the percentage of entrained air are also being investigated.

References

1. M. Elices, F.S. Rostasy, W.M. Faas and G. Wiedemann. "Cryogenic Behaviour of Materials for Prestressed Concrete." FIP state of the art report. Wexham Springs. Slough (1982).
2. F.S. Rostasy and G. Wiedemann. 1st Int. Conf. on Cryogenic Concrete. The Concrete Society (1981).
3. F.S. Rostasy, U. Schneider and G. Wiedemann. Cem. Conc. Res. 9, 365 (1979).
4. G. Tognon. 5th Int. Symp. Chemistry of Cement, 229 (1969).

VOL
14
198

CEMENT and CONCRETE RESEARCH. Vol. 14, pp. 645-656, 1984. Printed in the USA.
0008-8846/84 $3.00+00. Pergamon Press, Ltd.

INFLUENCE OF $CaSO_4 \cdot 2H_2O$, $CaSO_4 \cdot \frac{1}{2}H_2O$ AND $CaSO_4$ ON THE INITIAL HYDRATION OF CLINKER HAVING DIFFERENT BURNING DEGREE

Hiroshi UCHIKAWA, Shunichiro UCHIDA, Kenji OGAWA
and Shunsuke HANEHARA

Central Research Laboratory, Onoda Cement Co., Ltd.
1-1-7 Toyosu Koto-ku, Tokyo Japan

(Communicated by D.M. Roy)
(Received Aug. 8, 1983)

VOL.
14
1984

ABSTRACT

Relation between early hydration process and properties of fresh cement until setting was studied by using nine kinds of cements prepared from three commercial clinkers with various buring degree and three kinds of calcium sulfates, that is, natural gypsum, β-hemihydrate and anhydrite Ⅱ. $Ca(OH)_2$ and $CaSO_4$ saturation ratio in liquid phase influenced remarkably on the early hydration process of cement paste rather than the hydraulic reactivity of clinker minerals themselves. Setting time well corresponded to the period of maximum $Ca(OH)_2$ saturation ratio in liquid phase which coincided also with the period of vivid hydration of alite.
Soft burning of clinker so as to remain a little amount (0.5% level) of free lime was effective for shortening the setting time but strength at longer age was slightly inferior to that of cement from well burnt clinker. Though the setting time was shortened in the order of natural gypsum, β-hemihydrate and anhydrite Ⅱ in cement from well burnt clinker, no remarkable influence of the kind of calcium sulfate was recognized in cement from poorly burnt clinker.

焼成度が異なる工場製クリンカーと二水、β半水、Ⅱ型無水石膏とから調製した9種類のセメントを用い、それらの早期の水和反応過程と凝結に至るまでのペーストの物性との関連につき検討した。セメントの早期水和反応過程には、セメントを構成する各鉱物相の反応性の良否よりも、液相中の$Ca(OH)_2$及び$CaSO_4$の飽和比が顕著に影響する。凝結時間と液相中の$Ca(OH)_2$飽和比が極大値を示す時期とはよく対応し、これはエーライトが活発な水和を開始する時期と一致する。

凝結時間を短縮するためには、クリンカーの焼成度を若干量のf.CaOが残る程度まで低下させる事が有効であるが、長期強度の発現は若干低下する。良く焼き締められたクリンカーでは凝結時間は二水、β半水、Ⅱ型無水石膏添加の順に短かくなるが、焼き締めの悪いクリンカーでは、凝結時間に及ぼす石膏の影響は殆ど認められない。

INTRODUCTION

Properties of mortar and concrete developed in the early stage of hydration of cement such as fluidity, bleeding, setting time, change of workability with time and early strength especially in case of using admixture became very important factor in the quality of concrete as energy-saving and automatic placing technology of concrete developed. Therefore, it is necessary not only to select appropriate additive and admixture, but also to make clear the characters of cement and admixture which influence on the properties of cement paste, mortar and concrete during the early hydration.

There are two main factors which influence on the reaction during the early hydration of cement (1)(2)(3). First factor is the rate of dissolution of calcium sulfate, that is, gypsum, hemihydrate and anhydrite. Second one is reactivity of clinker minerals, especially alite, C_3A and C_4AF. The reactivity of clinker minerals is considered to be strongly influenced by burning degree of clinker.

From these standpoints, the authors studied the influence of various kinds of calcium sulfate on the initial hydration of cements prepared from clinkers with various burning degree.

SAMPLE

Clinker

Character of clinker

Practically, clinker mineral formation proceeds above alite formation temperature and reaction rate is exponentially proportional to the difference between maximum (T) and critical (To=1250°C) temperature. Therefore, burning degree F can be expressed as following equation.

$$F=at\cdot\exp[b\cdot(T-To)] \quad \cdots\cdots 1)$$

Where a and b are constant and t is retention time to keep clinker above To. Retention time and temperature difference mentioned above in equation 1) have close relation with size of belite and birefringence of alite (4). Chemical compositions of three clinkers from same rotary cement kiln used in this experiment are shown in Table 1. Content of free CaO and liter weight of clinkers, birefringence and size of alite and belite, and burning condition of clinkers estimated by microscopic observation are shown in Table 2.

Twenty eight-day compressive strength (JIS) of cement mortar prepared from clinker W, A and P was 43.1, 39.2 and 35.3 MPa, respectively.

Mineralogical compositions of clinkers calculated by modified Bogue's equation and measured by chemical separation method are also shown in Table 2. There was small difference between them except for the amount of C_3A phase.

Chemical composition of alite and aluminate phase measured by EPMA and separated ferrite phase determined by chemical analysis was shown in Table 3. It was proved that the amount of MgO, Al_2O_3 and Fe_2O_3 was increased and birefringence of alite was decreased when the burning degree was lowered.

Table 1 Chemical composition of each clinker and natural gypsum

Sample	ig. loss	in-sol	SiO_2	Al_2O_3	Fe_2O_3	CaO	MgO	Na_2O	K_2O	P_2O_5	TiO_2	SO_3	Total (%)
Clinker W	0.2	0.2	22.9	5.1	3.4	64.8	1.4	0.26	0.68	0.13	0.29	0.62	99.9
Clinker A	0.2	0.2	22.3	5.2	3.1	64.8	1.4	0.28	0.81	0.15	0.29	0.67	99.4
Clinker P	0.2	0.3	22.5	4.9	3.3	63.8	1.4	0.29	1.12	0.14	0.28	1.33	99.6
Gypsum	20.3	-	0.9	0.2	0.1	32.7	0.5	-	-	-	-	44.8	99.5

W: well burnt clinker A: averagely burnt clinker P: poorly burnt clinker

Table 2 Mineralogical composition, water soluble component and burning condition of each clinker

Clinker	Mineralogical composition (%)									Water soluble (%)		
	C_3S	C_2S	C_3S+C_2S	C_3A	C_4AF	K_2SO_4	Na_2SO_4	F.CaO	Total	Na_2O	K_2O	SO_3
W	56.2	23.2	79.4	8.4	10.3	1.3	0.1	0.17	99.7*			
			81.5	6.2	10.9	0.7	0.2	0.17	99.7**	0.08	0.39	0.18
A	56.5	21.2	77.7	9.4	9.4	1.5	-	1.11	99.1			
			79.0	6.6	11.3	0.9	0.2	1.11	99.1	0.10	0.49	0.36
P	49.7	26.8	76.5	8.3	9.9	2.1	0.7	1.64	99.1			
			78.4	8.3	8.8	1.6	0.4	1.64	99.1	0.16	0.87	0.55

	Liter weight (kg/l)	Free CaO (%)	Alite size (μm)	Alite bf.	Belite size (μm)	Belite bf.	Estimated burning condition**** Heating rate	Maximum temperature	Retention time***	Cooling rate
W	1.25	0.17	40	0.007	30	0.012	+	+++	++++	++++
A	1.15	1.11	30	0.006	20	0.015	++	++	+++	+++
P	1.10	1.64	20	0.004	10	0.018	+++	+	+	+

Note: * : Calculated from Bogue's equation
** : Measured by chemical analysis of separated phase
bf.: Birefringence, ***: Retention time above critical temperature
****: Estimated by microscopic method
++++: Excellent, +++: Good, ++: Average, +: Poor

Table 3 Chemical composition and crystallographic data of each clinker mineral

Clinker	Alite phase						Lattice constant			
	CaO (%)	SiO_2	MgO	Al_2O_3	Fe_2O_3	Crystal system	a (Å)	b	c	$(a/b)^2$	$\angle\beta$
W	71.54	25.10	0.65	0.75	0.53	M_{III}	12.254	7.054	24.98	3.018	90.03
A	71.37	24.97	0.74	0.87	0.75	M_{III}	12.239	7.054	24.99	3.010	90.01
P	70.82	24.88	0.79	0.99	0.88	M_I, M_{III}	12.241	7.053	25.00	3.012	89.99

	Aluminate phase							
	CaO	SiO_2	MgO	Al_2O_3	Fe_2O_3	Na_2O	K_2O (%)	Crystal system
W	54.57	5.45	0.94	29.66	4.47	1.95	1.48	Cubic, Orthorhombic
A	54.36	4.98	1.05	30.34	4.71	1.78	1.06	Cubic, Orthorhombic
P	56.38	5.06	0.91	31.32	3.23	1.25	0.82	Cubic

	Ferrite phase								
	CaO (%)	SiO_2	MgO	Al_2O_3	Fe_2O_3	Crystal system	Lattice constant (Å) a	b	c
W	46.91	3.28	3.12	23.09	19.64	Orthorhombic	5.32	14.50	5.54
A	46.91	3.50	3.22	23.02	19.64	Orthorhombic	5.32	14.49	5.53
P	47.89	2.90	3.22	23.69	19.64	Orthorhombic	5.32	14.48	5.53

Note: Chemical composition of alite and aluminate phase obtained by EPMA

Pure ferrite phase was obtained by dissolving the residue of salicylic acid-methanol treatment (5), with 2% HNO_3-methanol treatment (6). Though there was no remarkable difference of composition for ferrite phases in three clinkers, the quantity of SiO_2 was increased slightly and alkali was decreased with burning degree. Estimated compositions of ferrite phase calculated by both powder x-ray diffraction and wet analysis were approximately C_6A_2F (7).

The amount of water soluble Na_2O, K_2O and SO_3 was large in poorly burnt clinker as shown in Table 2. Large difference of water soluble Na_2O in spite of same Na_2O level indicates the existence of Na_2O bearing solid solution.

Lattice constants of alite calculated after Yamaguchi and Miyabe (8) and ferrite phase were shown in Table 3. Clinker P contains M_{III} and M_I modification of alite. X-ray diffraction peaks of separated interstitial phase in Fig. 1 show the existence of small amount of orthorhombic C_3A in clinker W and A indicating the formation of alkali solid solution by rapid cooling of molten phase (9). Though difference was observed in the intensity of C_3A and C_4AF solid solution, no difference could be observed in lattice constants of ferrite phase among three clinkers.

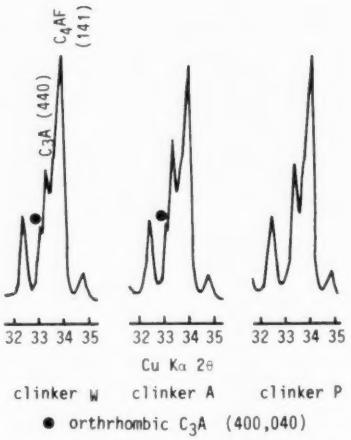

Fig. 1 X-ray diffraction profile of interstitial phase

Calcium sulfate

Character of calcium sulfate

β-hemihydrate and anhydrite Ⅱ was prepared by heating natural gypsum at 120°C for 12hrs. and at 800°C for 2hrs. respectively. They were identified by XRD and TG-DSC. Chemical composition of natural gypsum is shown in Table 1. Crystallite size of anhydrite reached to 2000 Å and was almost corresponded with that of natural anhydrite.

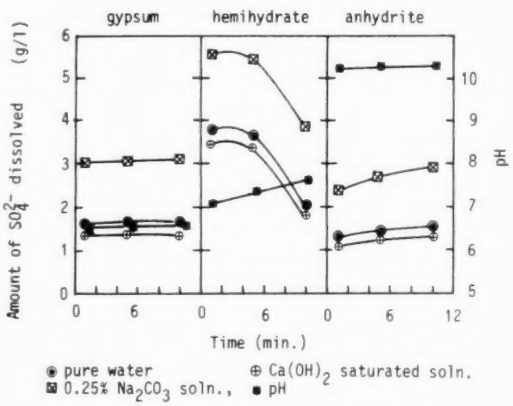

Fig. 2 The amount of SO_4^{2-} dissolved and pH of liquid phase for each calcium sulfate-water suspension

The amount of SO_4^{2-} dissolved and pH value of liquid phase of water-solid mixture for each calcium sulfate are shown in Fig. 2. In gypsum, the amount of SO_4^{2-} dissolved into pure water reached maximum value of 1.63 SO_4^{2-} g/l immediately after mixing. In hemihydrate, it was three times as large as that of gypsum but the amount of SO_4^{2-} in liquid was decreased by the precipitation of secondary gypsum. In anhydrite, it was about four fifths as large as that of gypsum and the amount of SO_4^{2-} in liquid increased with time. Amounts of SO_4^{2-} from dissolved calcium sulfate was rised in alkali solution such as Na_2CO_3 and it was lowered in the $Ca(OH)_2$ saturated solution. The pH value at 20°C of 4 g/l water solution of anhydrite, hemihydrate and gypsum was 10.2, 7.2 and 6.6, respectively.

Preparation of cement

Cements were prepared from clinker W, A and P by adding natural gypsum hemihydrate and anhydrite until total SO_3 in cement attained to 1.9%. Each mixture was interground and adjusted until Blaine specific surface area reached 3200±100cm²/g.

EXPERIMENT

Preparation of hydrated sample

Each cement was hydrated at 10°C, 20°C and 30°C with the water cement ratio of 0.3. After determined curing time, hydration was stopped by dispersing the sample in acetone. Hydrated sample was dried by two methods, that is, D-drying and drying under CO_2 free air of which relative humidity is 15% (RH 15% drying).

Determination of ionic concentration in liquid phase

Liquid phase of suspension (W/C=4.0) was obtained by the filteration after determined curing time and the concentration of Ca^{2+}, Na^+, K^+, OH^- and SO_4^{2-} in liquid phase was measured.

Measurement of heat evolution in hydration

Heat evolution of each cement paste was measured by conduction calorimetry at 10°C, 20°C and 30°C with the water cement ratio of 0.4.

Quantitative analysis of $Ca(OH)_2$ and ettringite

The amount of $Ca(OH)_2$ and ettringite in the hydrated sample dried in air of RH 15% was determined by modified TG-DSC method (10).

Measurement of specific surface area and observation of morphology of hydrates

Specific surface area of D-dryed hydrated sample was measured by BET method. Microstructure of hydrated sample was observed by scanning electron microscopy.

Measurement of setting time

Setting time of cement was measured under JIS R5201.

Flow curve measurement with rotational viscometer

Each cement was mixed with water at W/C=0.3 for 210 seconds by hand. Flow curve of the paste was obtained by coaxial rotational viscometer with double cylinders RV 12 (HAAKE Co., Ltd.) using the sensor system of MVIP(11). Paste was dispersed homogeneously on the surface of sensor system by rotating the rotor at 512 rpm for 30 seconds. The measurement was continued until noize caused by the setting of paste was observed.

RESULT AND DISCUSSION

Early hydration process

Time dependency of ionic concentration and $Ca(OH)_2$ and $CaSO_4$ saturation ratio of liquid phase

Fig. 3 shows the time dependency of concentration of ions in liquid phase of cement-water suspension. Concentration of Ca^{2+}, Na^+, K^+ and OH^- showed high level in poorly burnt clinker which contained much free CaO and alkali sulfate as shown in Fig. 3 (a)(d)(e). Ca^{2+} and SO_4^{2-} concentration was remarkably changed by the kind of calcium sulfate added with time but this change of OH^- concentration was not so large. This result coincided with the tendency shown in Fig. 2.

Fig. 4 shows the time dependency of $Ca(OH)_2$ and $CaSO_4$ saturation ratio calculated from concentration of each ion after Fujii and Kondo (12)(13). $Ca(OH)_2$ saturation ratio increased rapidly and reached the peak at an early age in cement from poorly burnt clinker. Influence of the kind of calcium sulfate was not so clear except for earlier appearence of peak in cements

containing hemihydrate, which is deduced to relate to the increase of Ca^{2+} ionic concentration.

$CaSO_4$ saturation ratio was large in the order of anhydrite, gypsum and hemihydrate added cement. Initial $CaSO_4$ saturation ratio was largest when

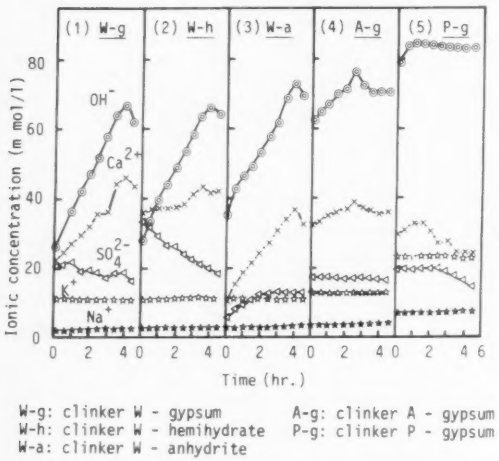

Fig. 3 Change of ionic concentration in liquid phase of cement-water suspension

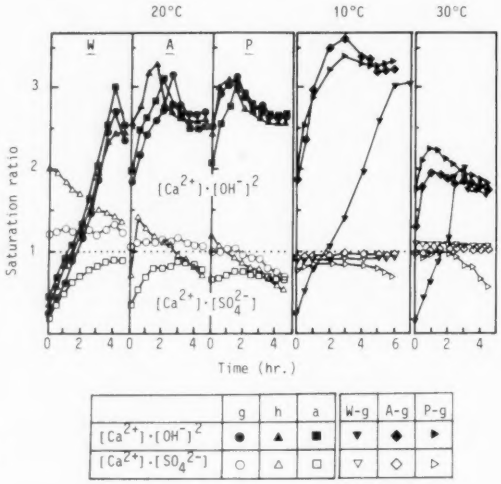

Fig. 4 Change of $[Ca^{2+}]\cdot[OH^-]^2$ and $[Ca^{2+}]\cdot[SO_4^{2-}]$ in liquid phase of cement-water suspension (saturation level=1.0)

hemihydrate was used but it was decreased rapidly by the precipitation of secondary gypsum. $CaSO_4$ saturation ratio was decreased in the cement from poorly burnt clinker and the difference among three calcium sulfates was small. Much soluble alkali sulfates in poorly burned clinker are considered to be responsible to the decrease of $CaSO_4$ saturation ratio.

At high curing temperature, $Ca(OH)_2$ saturation ratio was lowered and peak appeared earlier, while $CaSO_4$ saturation ratio rised. The effect of the kind of calcium sulfate and burning degree of clinker on both $Ca(OH)_2$ and $CaSO_4$ saturation ratio was unchanged with temperature.

Heat evolution rate

Heat evolution curves of each cement at various curing temperature are shown in Fig. 5. The position and height of the second peak which corresponded to hydration of alite were remarkably influenced by the burning degree of clinker. The second peak appeared earlier in the cement from poorly burnt clinker. The influence of the kind of added calcium sulfate on the position of second peak was small but it appeared earlier when hemihydrate was added. The position of second peak was closely related to the peak position of $Ca(OH)_2$ saturation ratio. This result indicates the vivid hydration of alite after induction period begins when $Ca(OH)_2$ saturation ratio attains to maximum value. The period of vivid hydration of alite is accelerated in cement manufactured by the intergrinding of clinker, gypsum and lime (14). Therefore, it is considered that vivid hydration of alite is strongly controlled by $Ca(OH)_2$ saturation ratio of liquid phase rather than the difference of hydraulic reactivity of alite mainly depended on crystal structure and minor constituents.

VOL 14 198

The amount of hydration products and time dependency of BET specific surface area of each cement paste

Ettringite, $Ca(OH)_2$ and C-S-H were main hydration products during initial few hours. Fig. 6 shows the change of the amount of ettringite and $Ca(OH)_2$ formed and the change of BET specific surface area of paste with

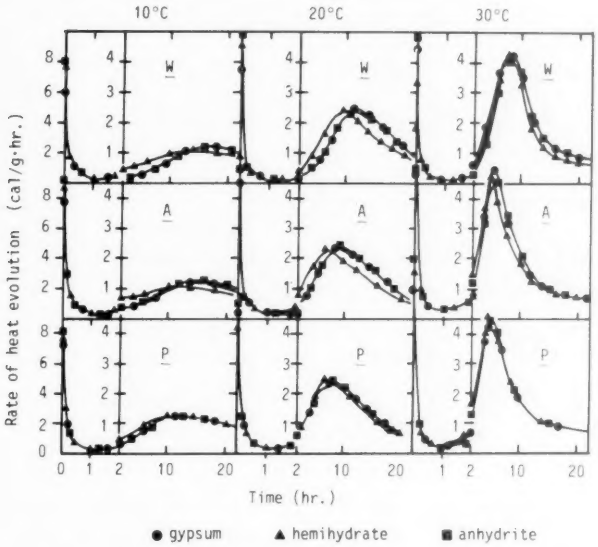

Fig. 5 Heat evolution curves of each cement at different curing temperature (same notation as in Fig. 3)

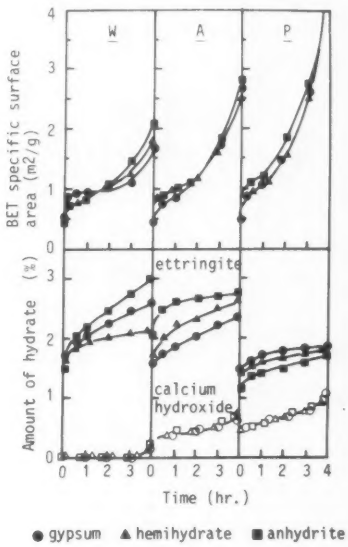

Fig. 6 Change of amount of hydrates formed and BET specific surface area of paste

time. The influence of kind of calcium sulfate on the amount of ettringite formed was changed with burning degree of clinker. The amount of ettringite formed is considered to be influenced by $Ca(OH)_2$ and $CaSO_4$ saturation ratio in liquid phase as well as hydraulic reactivity of interstitial phase itself.

Heat evolution curves of interstitial phase of each clinker separated by salicylic acid-methanol method are shown in Fig. 7. As ferrite phase had little compositional and structural difference with the difference of burning degree, hydraulic reactivity of interstitial phase seemed to depend mainly on the quantity, crystal structure and minor constituents of C_3A solid solution. Clinker P has interstitial phase of the highest reactivity. Interstitial phase of clinker W is more reactive than that of clinker A from the data in Fig. 7 The difference of hydraulic reactivity of C3A solid solution in each

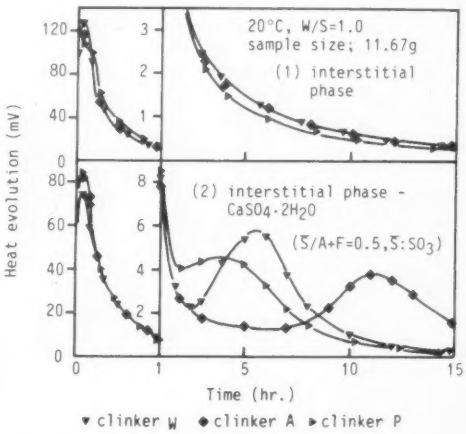

Fig. 7 Heat evolution curves of interstitial phase

clinker could be explained by the character of C_3A such as difference of modification of C_3A as reported by Regourd (15) and the amount of K_2O as impurity of C_3A solid solution (1).

The amount of ettringite formed in the cement paste from clinker P was small in spite of highest reactivity of interstitial phase. High $Ca(OH)_2$ saturation ratio in liquid phase under the presence of calcium sulfate depressed the hydration of interstitial phase. In the cement from well burnt clinker, amount of ettringite formed in the early hydration was large in the order of hemihydrate, gypsum and anhydrite added cement corresponding to $CaSO_4$ saturation ratio in liquid phase. This difference became small or the trend turned opposite in cements from clinker A and P. Depressed dissolution of calcium sulfate, precipitation of small ettringite and the formation of dense layer of ettringite on the surface of unhydrated grain in high $Ca(OH)_2$ saturation ratio in the liquid phase might be one of the reasons of the above-mentioned phenomenon observed in the cements from clinker A and P. This result suggests that the amount of ettringite formed was influenced by $Ca(OH)_2$ saturation ratio in liquid phase which has close relation to free CaO in clinker and $CaSO_4$ saturation ratio in liquid phase which is affected by the kind of added calcium sulfate rather than hydraulic reactivity of interstitial phase itself.

The amount of existed $Ca(OH)_2$, that is the difference between sum of formed $Ca(OH)_2$ by the hydration of calcium silicates and free lime and consumed $Ca(OH)_2$, measured by TG-DSC method was ranged from 0.3 to 1.1% after 4 hour hydration. Therefore, the amount of existed $Ca(OH)_2$ is not always represented the rate of hydration of alite in cement. On the contrary, the change of BET specific surface area with time shown in Fig. 6 corresponds to the rate of hydration of alite at the initial stage (16). Increase in BET specific surface area of cement from clinker P at an earlier age showed good correspondence to the second peak position in heat evolution curve.

VOL
14
198

Morphology of hydrate

Scanning electron micrographs of hydrated cement paste are shown in Fig.8. Ettringite formed partly on the surface of cement particles and it remained almost same size. Morphology of ettringite became short prismatic at high $Ca(OH)_2$ saturation ratio and became small irregular rod and equi-dimentional shape at high $CaSO_4$ saturation ratio. This effect was much more remarkable in $Ca(OH)_2$ than in $CaSO_4$ saturation ratio. The morphology of ettringite formed did not change at the initial stage within 4 hours. Precipitation of large gypsum crystal could be observed in hemihydrate added cement paste. With the descending of burning degree of clinker, the size of precipitated gypsum turned small due to the increase of $Ca(OH)_2$ and the decrease of $CaSO_4$ saturation ratio. Small hexagonal plate like $Ca(OH)_2$ was observed in cement rich in free CaO. The reason why clinker P has a large BET specific surface area at 1 hour in spite of less ettringite formation is considered that small $Ca(OH)_2$ by the hydration of free CaO and small ettringite crystal are formed under high $Ca(OH)_2$ saturation ratio. In cement paste containing anhydrite, calcium aluminate hydrate and monosulfate hydrate could not be observed in the early hydration. After 2 hours, acicular C-S-H precipitate widely around cement particles and its morphology was not changed by $CaSO_4$ and $Ca(OH)_2$ saturation ratio.

Properties of cement paste during early hydration

Setting time

Initial and final setting time of cement at each curing temperature are shown in Fig. 9. Setting time was shortened with lowering of burning degree and with rising of curing temperature. The difference of setting time with different kind of calcium sulfate was recognized clearly in well burnt clinker

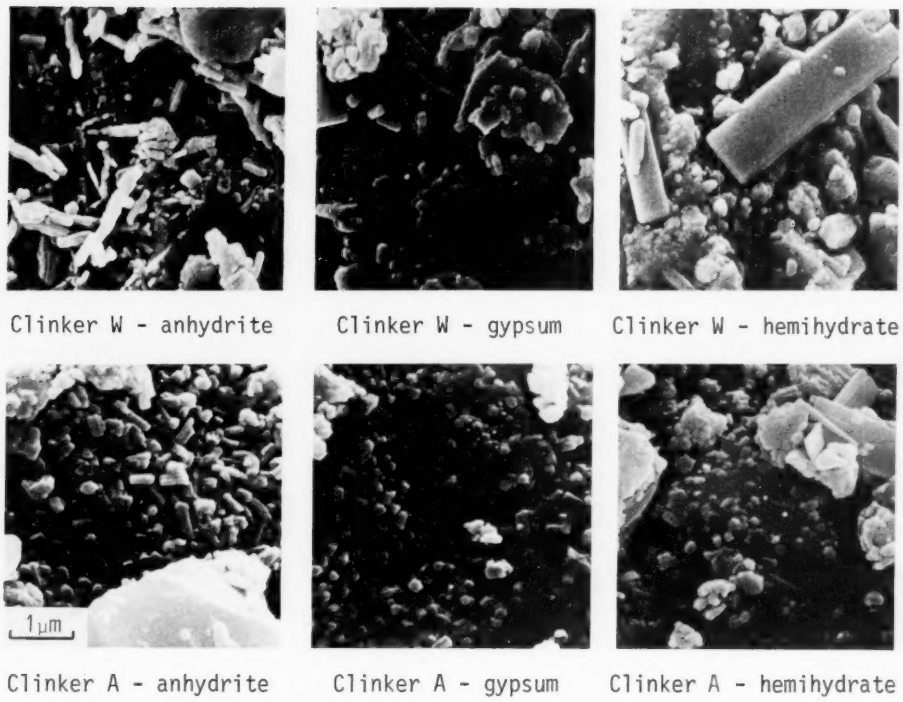

Clinker W - anhydrite Clinker W - gypsum Clinker W - hemihydrate

Clinker A - anhydrite Clinker A - gypsum Clinker A - hemihydrate

Fig. 8 Scanning electron micrograph of hydrated cement (age 30 min., at 20°C)

cured at low temperature. The setting time was the order of gypsum, hemihydrate and anhydrite containing cement from long side.

Setting of cement paste is corresponded to the process of structure formation when colloidal solution develops gel properties and it is caused by the adhesiveness of water film around cement and hydrate particles and the cohesive force between hydrates. Therefore, the increase of specific surface area and contact points of hydrates grown to needle like shape contributes to setting of cement paste. Generally, normal setting of cement paste is brought by the hydration of alite (17)(18). But Locher et al (1) have reported that normal setting occurs upon the recrystallization of ettringite rather than by the formation of new hydration products of alite.

As before mentioned, the second peak position of heat evolution vs. time curve and rising position of BET specific surface area vs. time curve coincide with the initial setting time, therefore, setting time is certainly related closely to the beginning of vivid hydration of alite. The difference of setting time by the kind of calcium sulfate may be caused by the difference of amount and morphology of ettringite depended on mainly $Ca(OH)_2$ and $CaSO_4$ saturation ratio in liquid phase.

In the cement from poorly burnt clinker, vivid hydration of alite and formation of C-S-H having large specific surface area at the initial stage much contribute to the setting time of cement paste, as the amount and shape of ettringite formed are small. On the other hand, in the cement from well burnt clinker, as ettringite formed has much amount and large acicular shape, hydration of interstitial phase more contributes to the setting time so that the effect of the kind of calcium sulfate for setting is increased.

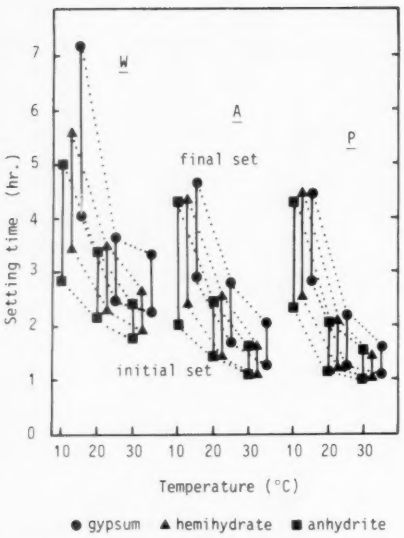

Fig. 9 Setting time of each cement at different curing temperature

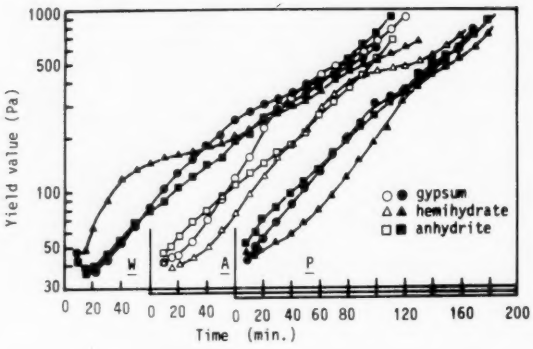

Fig. 11 The time dependency of yield value of fresh cement paste (W/C=0.30, 20°C)

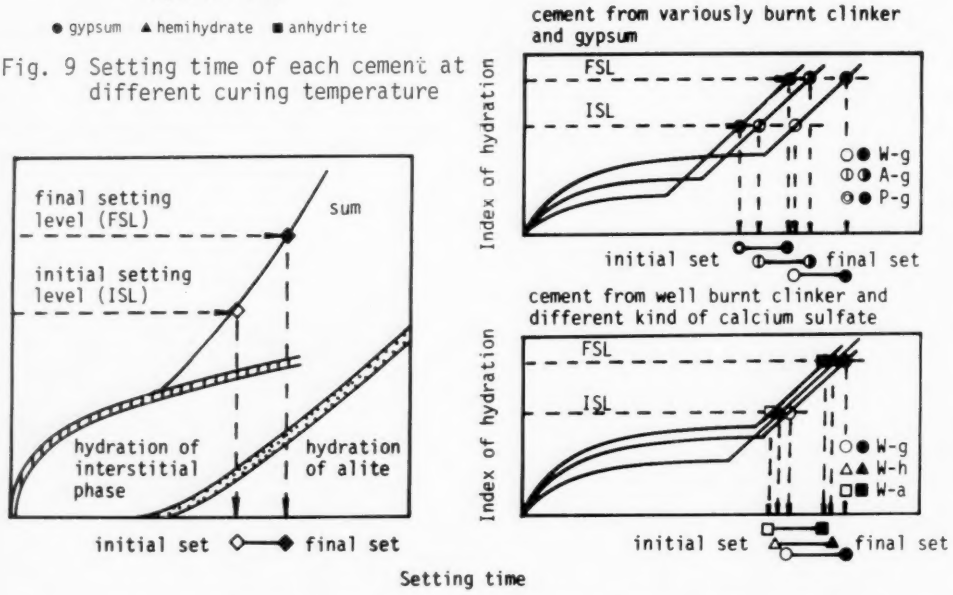

Fig. 10 Schematic explanation of relationship between index of hydration for each clinker mineral and setting time (same notation as in Fig. 3)

Time dependency of the degree of hydration for each clinker mineral until setting time was schematically explained in Fig. 10. Setting of cement paste is expressed as the summed results of hydration of calcium silicate and interstitial phase and setting occurs when the index of hydration which includes the kind, size, morphology and amount of hydrates reaches a certain level.

Change of the yield value of cement paste with time

The increase of yield value shown in Fig. 11 during initial two hours was mainly caused by crystillization of gypsum from hemihydrate and increase

of specific surface area by the formation of ettringite. Vivid hydration of alite was responsible at the most part after this period. Generally, yield value was increased more rapidly with poorly burnt clinker corresponding to its increase in specific surface area except for the cement containing hemihydrate. Increase in yield value of hemihydrate added clinker W till one hour may be caused by the crystallization of large crystal of gypsum by the hydration of hemihydrate. This result shows that influence of calcium sulfates on the fluidity of fresh cement paste at early stage is closely related to burning degree of clinker.

CONCLUSION

Following results were obtained by using the cements prepared from variously burnt clinkers with same kiln and natural gypsum, β-hemihydrate and anhydrite Ⅱ obtained by heating natural gypsum.

1. Burning degree of clinker defined as the function of temperature and retention time at burning zone shows good correspondence to the amount of free CaO and liter weight measured by conventional method, and the optical properties of clinker measured by microscopic observation.

Alite in well burnt clinker belonged to M_{III} modification. In poorly burnt clinker, M_I modification of alite was recognized and the amount of impurities such as MgO, Al_2O_3 and Fe_2O_3 in alite increased and birefringence of alite lowered. The amount of water soluble Na_2O, K_2O and SO_3 was small in well burnt clinker. Orthorhombic C_3A solid soluton containing much amount of Na_2O and K_2O was observed in rapidly cooled clinker. In the cement prepared from well burnt clinker and gypsum, the best 28-day compressive strength of mortar was obtained.

2. $Ca(OH)_2$ and $CaSO_4$ saturation ratio in liquid phase were more influential factors on the early hydration process of alite and interstitial phase than their hydraulic reactivity.

3. $CaSO_4$ saturation ratio in liquid phase of cement-water suspension was initially high in the order of anhydrite, gypsum and hemihydrate added cement from same clinker but it decreased remarkably with time in hemihydrate added cement because of the precipitation of gypsum. The difference was large in low $Ca(OH)_2$ and small in case of high $Ca(OH)_2$ saturation ratio.

4. Maximum value of $Ca(OH)_2$ saturation ratio in liquid phase of cement-water suspension was attained quickly in poorly burnt clinker and slowly in well burnt clinker regardless of the kind of added calcium sulfates. The difference was caused by the quantity of free CaO and water soluble alkali sulfate and it was reduced with the rise of curing temperature.

5. The amount of ettringite formed was roughly inversely proportional to the amount of $Ca(OH)_2$ existed in paste and alkali sulfate in cement, that is, less in the cement from poorly burnt clinker and much in the cement from well burnt clinker. In case of low $Ca(OH)_2$ saturation ratio, the amount of ettringite formed was increased with the decrease of $CaSO_4$ saturation ratio. But the influence of $CaSO_4$ saturation ratio on the amount of ettringite formed was reduced in high $Ca(OH)_2$ saturation ratio. The morphology of ettringite formed in high $Ca(OH)_2$ saturation ratio became short and prismatic. Small irregular rod and equidimentional shaped ettringite was formed in high $CaSO_4$ saturation ratio. Acicular C-S-H precipitated around the cement particle after 2 hours but its morphology was not changed by $Ca(OH)_2$ and $CaSO_4$ saturation ratio.

6. Stiffening of paste within 2 hours at 20°C is mainly caused by the crystallization of gypsum from hemihydrate (so-called plaster set) and extraordinary increase of specific surface area of ettringite. The former occurs in case of cement from well burnt clinker and hemihydrate, the latter occurs in case of cement from poorly burnt clinker and anhydrite or gypsum.

OL.
14
984

It is recognizable quantitatively by the yield value of paste measured by viscometry.

7. Normal setting time is closely related to the period of the initiation of the vivid hydration of alite which corresponds to the maximum value of $Ca(OH)_2$ saturation ratio in liquid phase of cement-water suspension and is easily observable by the peak of heat evolution curve in conduction calorimetry and the increasing point of BET specific surface area.

8. The difference of setting time with kind of calcium sulfate was recognized clearly in well burnt clinker cured at low temperature. The phenomenon was caused mainly by the difference of amount and morphology of ettringite formed.

REFERENCES

1. F.W. Locher, W. Richartz and S. Sprung, Zement-Kalk-Gips 29, 435-442 (1976); 33, 271-277 (1980); 35, 669-676 (1982).
2. L. Odler and R. Wonneman, 7th International Congress on the Chemistry of Cement (Paris), IV, 510-513 (1980).
3. J.P. Skalny and J.P. Young, 7th International Congress on the Chemistry of Cement (Paris), I, II 1/3-1/45 (1980).
4. Y. Ono, 7th International Congress on the Chemistry of Cement (Paris) II, I 206-211 (1980).
5. S. Takashima and F. Amano, Sement Gijitsu Nenpo, 13, 50-54 (1959).
6. S. Sato, Y. Tamura, K. Takahashi and H. Muto, Semento Gijitsu Nenpo, 24, 24-26 (1970).
7. E. Woermann, Th. Hahn and W. Eysel, Amer. Ceram. Soc., Bull. 44, 299 (1965).
8. G. Yamaguchi and H. Miyabe, J. Amer. Ceram. Soc. 43, 219-224 (1960).
9. K.S. Han and F.P. Glasser, Cement and Concrete Research 10, 483-489 (1980).
10. H. Uchikawa, S. Uchida and Y. Mihara, Sement Gijitsu Nenpo 34, 58-66 (1980).
11. H. Uchikawa, K. Ogawa and S. Uchida, Proc. Ann. Mtg. of Materials Research Society, M4, 4, Boston (1982).
12. W. Kondo and K. Fujii, J. Cer. Assoc. of Japan, 82(6), 333-336 (1974).
13. K. Fujii, Proc. Cement and Concrete Seminar (Private meeting).
14. H. Uchikawa, S. Uchida and K. Ogawa, in preparation.
15. M. Regourd, il Cemento, 75, 323-336 (1978).
16. R. Kondo, 5th International Symposium on the Chemistry of Cement (Tokyo), II, 203-248 (1968).
17. J. Gebauer, Zement-Kalk-Gips, 31, 302-304 (1978).
18. L.D. Adams, Cement and Concrete Research 6, 293-307 (1976).

VOL
14
198

CEMENT and CONCRETE RESEARCH. Vol. 14, pp. 657-662, 1984. Printed in the USA.
0008-8846/84 $3.00+00. Copyright (c) 1984 Pergamon Press, Ltd.

EQUILIBRIA AND NON-EQUILIBRIA IN THE FORMATION OF XONOTLITE AND TRUSCOTTITE

K. Luke and H.F.W. Taylor
Department of Chemistry, University of Aberdeen
Meston Walk, Old Aberdeen AB9 2UE, Scotland, UK

(Communicated by D.M. Roy)
(Received Oct. 17, 1983)

ABSTRACT

The conclusions of Roy and Harker (1960) regarding phase equilibria in the silica-rich part of the $CaO-SiO_2-H_2O$ system are substantially confirmed; in particular, truscottite ($C_7S_{12}H_{\sim 3}$) coexists stably with silica and aqueous solution from below 200°C to approximately 350°C at saturated steam pressures. However, non-equilibrium situations readily occur in which xonotlite (C_6S_6H) is formed when truscottite would be expected. These situations are attributed to incongruent solubilty of truscottite, coupled with extreme reluctance or inability of xonotlite to react with silica and aqueous solution to give truscottite. As a result, if xonotlite forms before truscottite it persists, and any process in which silica is effectively removed from the system, however temporarily, can cause a conversion of truscottite into xonotlite that is for practical purposes irreversible and potentially complete. Such loss of silica could occur through liquid or vapor transport, and may be brought about by temperature gradients.

Introduction

The conditions of formation and stability of the various calcium silicate hydrate phases in the presence of excess silica and aqueous solutions at elevated temperatures and pressures are relevant to the hardening and durability of some potential geothermal cements. Roy and Harker (1), Harker (2) and Roy and Johnson (3) studied phase equilibria in the $CaO-SiO_2-H_2O$ system over a wide range of temperature, pressure and composition. For saturated steam pressures in presence of excess silica, they found the stable calcium silicate hydrate phases to be gyrolite ($C_2S_3H_{\sim 2}$) below about 180°C, truscottite ($C_7S_{12}H_{\sim 3}$) from about 180°C to about 350°C, and xonotlite (C_6S_6H) above about 350°C. Buckner et al. (4) found that xonotlite decomposed to give wollastonite (β-CS) at 400±10°C under a pressure of 34.5 MPa. More recently, Langton et al. (5) have substantially confirmed these results, but reported a somewhat lower temperature (385±5°C at 68.9 MPa) for the decomposition of xonotlite.

It is nevertheless widely observed that xonotlite is more readily formed than gyrolite or truscottite over a wide range of conditions for which the latter would be expected. Gyrolite and truscottite are reported to form readily only if the starting materials include silica in a reactive form (4-8). For this or other reasons, some investigators have considered that the stability ranges of one or both of these phases are narrower than given above. Thus, for saturated steam pressures, Peppler (9) concluded that gyrolite was metastable relative to xonotlite plus silica at 180°C, and Meyer and Jaunarajs (10) concluded that truscottite was unstable relative to xonotlite plus cristobalite above about 300°C; for a pressure of 138 MPa, Juan et al. (11) concluded that truscottite became unstable relative to wollastonite plus quartz above 272°C. Further study of the formation of these calcium silicate hydrate phases under both equilibrium and non-equilibrium conditions was therefore undertaken.

Experimental

Starting Materials

CaO was prepared by heating analytical reagent grade $CaCO_3$ at 1000°C for a few hours. Quartz contained 99.9% SiO_2 and was of particle size below 10 μm. Silicic acid (Mallinckrodt 'Special Bulky') contained 85% SiO_2, with alkalies (below 0.2%) as the only significant impurities. β-C_2S, stabilized with 0.4 % Na_2O, truscottite and xonotlite were samples prepared using the above starting materials and contained no impurities detected by XRD.

Preparation and Examination of Products

Hydrothermal preparations were carried out in stainless steel pressure tubes with a capacity of about 15 cm^3 (length 110 mm, diameter 13 mm internally). The reaction mixtures were contained in silver test tubes of about 6 cm^3 capacity; these were placed inside the pressure tubes, which were heated in ovens, muffle furnaces or tube furnaces, in vertical or sloping positions. In all but a few runs, the amount of water was such as to give saturated steam pressures for temperatures up to the critical temperature of water (374°C), and a calculated pressure of about 34 MPa at 400°C. At the end of a run, the tube was quenched and the solid product filtered and dried with acetone. The products were friable or powdery unless the starting material contained β-C_2S, when they were hard and required first to be crushed. All products were examined by XRD using a Hägg type Guinier camera, and some also by analytical electron microscopy, selected area electron diffraction or bulk chemical analysis.

Results

Reaction Mixture Placed Directly in the Silver Tube

In 157 runs, the solid starting materials (0.5 - 2.0 g dry weight) were placed directly in the silver tube, and water (total volume usually 4.5 cm^3) was placed partly inside and partly outside it. In a further 61 runs, the same procedure was adopted, but the dry weight of solids was 100 mg. The starting materials were most commonly CaO plus silicic acid (113 runs), CaO plus quartz (27 runs), β-C_2S plus quartz (29 runs) or truscottite mixed with xonotlite or with xonotlite and quartz (37 runs). The temperatures were 200°-400°C, the times were from 7 hours to 84 days, and except where stated, the bulk molar Ca/Si ratio was 0.6.

The runs using CaO plus quartz gave predominantly C-S-H(I) at 200°-225°C and xonotlite at 250°-375°C, often with varying amounts of "3.15 Å Phase" (12) and traces of foshagite. At 350°-375°C, wollastonite was sometimes also formed. These observations agree with earlier results (8). The runs using

VOL 14 198

CaO plus silicic acid, or β-C_2S plus quartz, gave results broadly similar to each other. At 200°-250°C the usual products were gyrolite or truscottite or both. At 275°-350°C the results were irreproducible. The major products were always truscottite or xonotlite or both, but the relative amounts of these phases were unpredictable. They did not show any clear dependence on time, but decrease in the content of dry solids to 100 mg tended to favor formation of xonotlite. At 375°C, various combinations of xonotlite, wollastonite, pseudowollastonite, truscottite and cristobalite were obtained. The runs using mixtures containing truscottite also gave broadly similar results to the above; at 200°C no detectable changes occurred, but at higher temperatures the truscottite was in varying degrees replaced by xonotlite.

Silica Loss

Several observations indicated that the formation of xonotlite below about 350°C was, at least in part, caused by effective loss of silica from the reaction mixture. Thus, some of the reactions using β-C_2S plus quartz mentioned above gave xonotlite with no detectable unreacted quartz. In some others, films or hard deposits formed on the inner walls of the silver tubes, and were shown by XRD and chemical analysis to consist of amorphous silica. This phenomenon has been observed previously (2, 13). In yet others, analyses of samples representative of the entire product showed marked increases in Ca/Si ratio; e.g., in one run using 100 mg of a mixture of CaO plus silicic acid, the Ca/Si ratio increased from 0.6 to 0.95 and, in agreement with this, XRD showed only xonotlite. These effects were most marked in the runs using only 100 mg of solid starting materials, but were not confined to them. Some of the silica probably migrated into the space between the silver tube and the outer steel tube, but this was not positively established.

VOL.
14
984

Temperature Gradients

In some other of the runs mentioned above, the bulk Ca/Si ratio of the effective reaction mixture did not change appreciably, but segregation into regions of differing Ca/Si ratio occurred. In several runs using CaO plus silicic acid, the solid products in the top, middle and bottom parts of the silver tube were examined separately, and in some such cases, differences in chemical and phase compositions were observed; e.g., in one case, the top, middle and bottom portions had Ca/Si ratios of 0.57, 0.81 and 0.66, respectively, and XRD showed the top portion to consist of truscottite and the two other portions to be mixtures of truscottite and xonotlite. In some of these runs, thermocouples were attached to the outsides of the pressure tubes at various points. The results showed that segregation in the product was associated with temperature differences of up to 9 deg C between different points. Segregation was therefore attributed to temperature gradients within the reaction mixture.

Experiments at Lower Ca/Si Ratios

If the decomposition of truscottite and consequent formation of xonotlite is caused by effective loss of silica from the reaction mixture, it should be limited or prevented by working at lower Ca/Si ratios, and this was found to be the case. Using mixtures of CaO plus silicic acid (1 g dry weight), 11 runs were carried out at Ca/Si ratios of 0.52, temperatures of 200°-375°C and times of 3-21 days. For temperatures up to 350°C, the tendency to give xonotlite as opposed to truscottite was much reduced. In addition, 5 runs were carried out at Ca/Si ratios of 0.2-0.5 using either CaO plus silicic acid or β-C_2S plus quartz at 275 C for times of 2-28 days; in all of them, truscottite or gyrolite was the major and often the only product. A similar run at 375°C gave xonotlite.

The possibility was considered that formation of xonotlite could be caused by local inhomogeneities in the starting materials prior to heating, but experiments in which the mixing procedure was varied showed that this was not a significant effect in the present experiments.

Reaction Mixture Contained in a Capsule Surrounded by Excess Silica

In all the runs described above, the solid reactants were placed directly in the silver tube. As a further test of the hypothesis that xonotlite formation from mixtures with Ca/Si ratios around 0.6 was attributable to silica migration, runs were carried out in which the solid starting materials (50 mg dry weight) was placed in an envelope of gold foil which was tightly folded but not sealed, and then embedded in a large excess (1 g) of silicic acid, which, together with the water (4.5 cm^3) was placed in the silver tube. The latter was tightly capped and placed in the pressure tube. The starting materials were either CaO plus silicic acid (27 runs), truscottite, sometimes mixed with xonotlite and quartz (16 runs), β-C_2S plus quartz (5 runs) or CaO plus quartz (1 run). The Ca/Si ratios were nearly always close to 0.6, the times were 0.75-59 days and the temperatures were 200°-400°C. The run using CaO plus quartz (at 350°C) gave xonotlite, but with the other starting materials gyrolite or gyrolite plus truscottite was formed at 200°-225°C, truscottite was nearly always the most abundant and often the only product at 250°-375°C, and various combinations of truscottite, xonotlite, pseudowollastonite and cristobalite were formed at 385°-400°C. Cristobalite was detected as a product of some of the runs at lower temperatures, especially at or above 350°C. A few runs were also carried out in which the capsule was embedded in silica glass or quartz instead of in silicic acid. Silica glass behaved similarly to quartz, but when quartz was used, truscottite within the capsule decomposed at 350°C to give xonotlite, though it was relatively persistent at 325°C.

Attempts to Effect Reaction Between Xonotlite and Silicic Acid

Various runs were carried out using mixtures of xonotlite plus silicic acid, to find whether these phases react hydrothermally to give truscottite (13 runs). The temperatures were 200°-375°C, the times were 3-168 days, and other conditions were chosen so as to maximize the possibility of xonotlite formation. In a typical example, the sample had bulk Ca/Si = 0.2 and was contained in a gold capsule embedded in 1 g of silicic acid; the temperature was 300°C, the time was 21 days, and a little alkali was added, as this favors formation of truscottite (8). In none of these experiments was any reaction detected, other than the partial crystallization of silicic acid to cristobalite in some cases.

Discussion

To provide a basis for understanding these results, it is necessary to consider the solubilities of xonotlite and truscottite. No studies on solubilities in the CaO-SiO_2-H_2O system appear to have been published since the early work of Peppler (9), which was done at 180°C, but Kalousek and Romberger (13), in an unpublished study, found that at 274°C xonotlite dissolves congruently, whereas truscottite dissolves very incongruently, giving a solution very low in CaO and relatively high in SiO_2. Using their data and published data on silica solubilities (14), a tentative solubility diagram was constructed (Fig. 1). The relevant invariant concentrations (in mmol/l) are, approximately: a, CaO 0.1, SiO_2 0.1; b, CaO 0.01, SiO_2 5; c, SiO_2 10. From this diagram, it will be seen that if truscottite is equilibrated with a limited volume of water, most will remain undissolved, but a little will dissolve, giving xonotlite and a solution having the composition which is represented by the triple point at b.

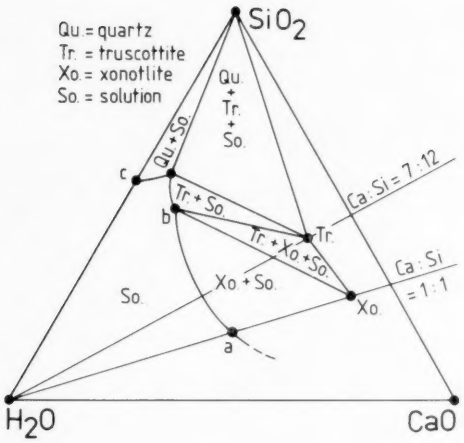

FIG. 1

Suggested solubility diagram for part of the $CaO-SiO_2-H_2O$ system at 274°C. *** Schematic and not to scale ***

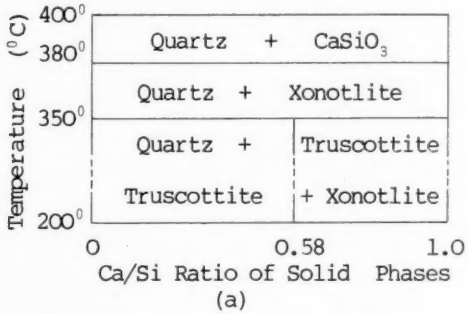

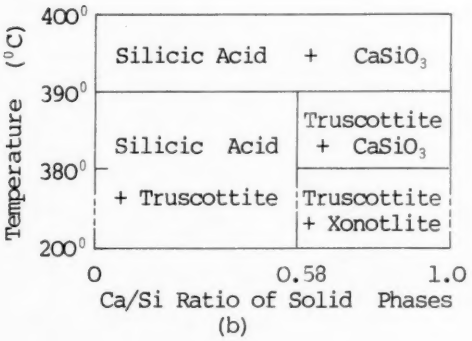

FIG. 2

Solid phases in (a) true or (b) metastable equilibrium at 200°-400°C for the pressures given in the text.

Any process that causes silica to segregate results in a decomposition of truscottite that appears to be irreversible. This irreversibility is due to the extreme reluctance or inability of xonotlite to react with silica under hydrothermal conditions. In the present experiments, silica segregation was observed to happen in two ways. One involved its physical separation from the main part of the reaction mixture, sometimes leading to the formation of a visible film or deposit; migration could occur by either liquid or vapor transport (14). The other was associated with temperature gradients, and probably depended on the fact that the solubility of silica increases markedly with temperature (14). In a hotter region, a solution relatively high in silica is formed. This migrates through convection to a cooler region, where part of the silica is deposited. The solution thus depleted in silica is recirculated to the hotter region, and more truscottite is decomposed. Other mechanisms of silica removal are doubtless possible, such as leaching in an open system by solutions of low silica content.

In the processes described above, truscottite is formed initially but later decomposes. Failure to reach equilibrium can also occur because truscottite is not formed in the first place. As shown earlier (8), this situation occurs if lime is readily available compared with silica, and thus notably if the starting materials are CaO plus quartz. The sequence of reactions then begins with C-S-H of high Ca/Si ratio, C-S-H of lower Ca/Si ratio and tobermorite (6). Tobermorite can react hydrothermally with quartz to give gyrolite (15,16), which above about 200°C is replaced by truscottite, but this reaction is slow compared with the competing reaction in which tobermorite is replaced by xonotlite; the latter does not react with quartz, and persists. The small amounts of other

phases, such as foshagite and "3.15 Å Phase", that are formed seem also not to react with quartz. If, in contrast, silica is readily available compared with lime, the reaction sequence is different, probably passing through Z-Phase (16) and gyrolite to truscottite; this situation occurs if the starting materials contain silicic acid, and especially with mixtures of the latter with β-C_2S (8).

The present results agree substantially with the equilibrium relationships given by Roy and Harker (1). Fig. 2 gives suggested stability fields for the solid phases that take into account the latters' results, as well as those of Harker (2), Roy and Johnson (3), Langton et al. (5) and the present investigation, including especially the runs in which the sample was placed in a gold capsule embedded in excess silicic acid. Fig. 2a represents the probable true equilibria, in which any silica occurs as quartz, and Fig. 2b the metastable equilibria in which it occurs as silicic acid or silica glass. Due to lack of data, the possible existence of fields for "K-Phase" (17) and "3.15 Å Phase" is ignored. The upper stability limit for truscottite is placed at approximately 350°C with quartz or 390°C with silicic acid. The much lower values suggested by Meyer and Jaunarajs (10) and Juan et al. (11) are attributed to non-equilibrium effects, possibly similar to those observed in the present work. The stable polymorph of CS under the conditions represented is probably wollastonite, the formation in some runs of pseudowollastonite being attributable to the structural relationship between the latter phase and truscottite.

Acknowledgements

We thank the US Department of Energy (Contract No. BNL/DOE 404003-S, subcontracted through the Colorado School of Mines), Dowell and the University of Aberdeen for support, Dr. G.L. Kalousek, Dr. C.A. Langton and Professor D.M. Roy for helpful discussions, and Dr. Kalousek also for the unpublished data of Ref. 13. The work was reported at the 84th Annual Meeting of the American Ceramic Society in Cincinnati, Ohio, in 1982.

References

1. D.M. Roy and R.I. Harker, Proc. 4th. Int. Symp. Chem. Cement, Washington, 1960, 1, 196 (1962).
2. R.I. Harker, J. Amer. Ceram. Soc. 47, 521 (1964).
3. D.M. Roy and A.M. Johnson, Proc. Symp. Autoclaved Calcium Silicate Building Products, London, 1965, 114 (1967).
4. D.A. Buckner, D.M. Roy and R. Roy, Amer. J. Sci. 258, 132 (1960).
5. C.A. Langton, E.L. White, M.W. Grutzeck and D.M. Roy, Proc. 8th. Int. Congr. Chem. Cements, Paris, 1980, 3, V-145 (1980).
6. G.L. Kalousek, J. Amer. Concr. Inst. 26, 989 (1955).
7. L. Števula and J. Petrovič, Silikáty 24, 341 (1980).
8. K. Luke, H.F.W. Taylor and G.L. Kalousek, Cem. Concr. Res. 11, 197 (1981).
9. R.B. Peppler, J. Res. Nat. Bur. Stands. 54, 205 (1955).
10. J.W. Meyer and K.L. Jaunarajs, Amer. Mineral. 46, 913 (1961).
11. V.C. Juan, C.-C. Youh and H.-J. Lo, Proc. Geol. Soc. China [Taiwan] (13), 34 (1970).
12. A. Bezjak, I. Jelenić and J. Jernejčič, Nature [Lond.] 248, 581 (1974).
13. G.L. Kalousek and S.B. Romberger, Private Communication from Dr. Kalousek.
14. R.K. Iler, The Chemistry of Silica, Chapter 1. John Wiley and Sons, New York (1979).
15. A. Aitken and H.F.W. Taylor, J. Appl. Chem. 10, 7 (1960).
16. G.O. Assarsson, Proc. 4th. Int. Symp. Chem. Cement, Washington, 1960, 1, 190 (1962).
17. J.A. Gard, K. Luke and H.F.W. Taylor, Cem. Concr. Res. 11, 659 (1981).

VOL
14
198

CEMENT and CONCRETE RESEARCH. Vol. 14, pp. 663-669, 1984. Printed in the USA.
0008-8846/84 $3.00+00. Copyright (c) 1984 Pergamon Press, Ltd.

OBSERVATIONS ON SILICATE GARDENS

H. Stade and W. Wieker

Zentralinstitut für Anorganische Chemie der
Akademie der Wissenschaften der DDR, 1199 Berlin, DDR

(Communicated by D.M. Roy)
(Received Sept. 13, 1983)

VOL.
14
1984

ABSTRACT

Formation, composition and properties of silicate gardens originated from solid $CaCl_2.6H_2O$ and sodium silicate solutions with Na_2O/SiO_2 = 0.5-1.5 and 0.5-2.5 moles SiO_2/l are described. In this reaction cryst. $Ca(OH)_2$ and C-S-H phases of different anion compositions are formed. The permeability of the products, covering the $CaCl_2$ crystals, with respect to water is strongly influenced by the Na_2O/SiO_2 mole ratio and the SiO_2 concentration in the sodium silicate solution.
A parallel is drawn between the membranes of the gardens and the C-S-H phase coating hydrated Ca_3SiO_5.

Introduction

The so-called silicate gardens, being formed by reaction of soluble salts of di- and trivalent cations with alkali silicate solutions have recently come to an increasing interest, because similar phases are considered to be formed in the early stages of the hydration of Ca_3SiO_5(C_3S) /1-5/. "Garden" and hydration products consist in the beginning of the reaction of thin membranes and it is assumed that such membranes cover the C_3S particles primarily giving rise to the retardation of the hydration reaction /1-6/. In the following some observations are reported, concerning the constitution and properties of the phases being formed during the growth of the silicate gardens from solid $CaCl_2$ and sodium silicate solutions. The results will be discussed in connection with the hydration of C_3S.

Results

On covering $CaCl_2.6H_2O$ crystals with sodium silicate solutions, coatings are formed at the surface of the crystals, from

which tube-like dendrites grow out. These tubes possess relatively smooth and dense but crinkled surfaces within the first 15 minutes after formation (Fig. 1), when silicate solutions with high Na_2O/SiO_2

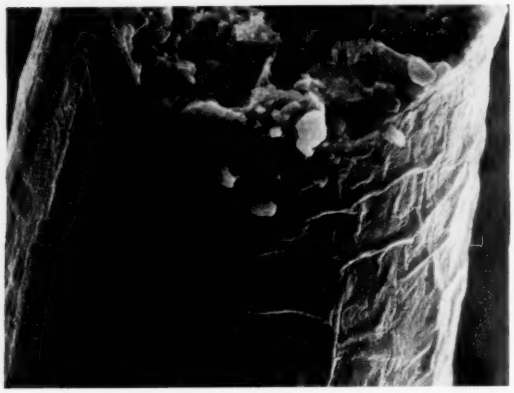

FIG. 1

Tube of a silicate garden formed from sodium silicate solution with Na_2O/SiO_2 = 1.5 after 15 minutes. SEM, magn. 1000:1

mole ratio (Na_2O/SiO_2 = 1,5) and high concentrations (> 1 mole SiO_2/l) are used, whereas those solutions with Na_2O/SiO_2 = 1.0 and the same SiO_2 concentration give after the same time products with relatively coarse pores (Fig. 2).

VOL
14
198

FIG. 2

Surface of a silicate garden tube, formed from sodium silicate solution with Na_2O/SiO_2 = 1.0 after 15 minutes. SEM, magn. 3000:1

Tubes with rough surfaces are also obtained, when the SiO_2 concentration in the sodium silicate solution is decreased to 0.5 mole SiO_2/l.

With increasing time these surfaces get coarser, which can be attributed obviously to a secondary phase, formed at the tube surface. Fig. 3 shows such a secondary phase, which has peeled off from the primarily formed surface, certainly during the specimen preparation. The main amount of new phases grow at the inner side of the membrane. These phases mostly are of irregular shape (Fig. 1), but they can also appear in a lath- or plate-like form.

The degree of condensation of the silicate anions of these phases depends on the Na_2O/SiO_2 mole ratio of the sodium silicate solutions used, as can be seen by the corresponding molybdate reaction curves (Fig. 4).

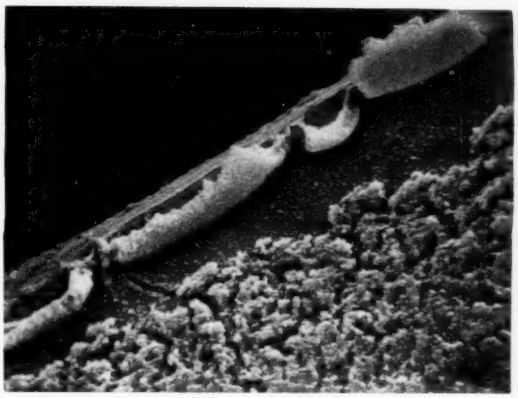

FIG. 3

Secondary phase on the surface of a tube from sodium silicate solution with Na_2O/SiO_2 = 1.5 after 3 hours. SEM, magn. 500:1

A phase formed from sodium silicate solution with 1.5 Na_2O/SiO_2 being 1 M in SiO_2 yields a molybdate reaction curve similar to that of C-S-H(di,poly) /7/. That means this phase contains low molecular silicate anions, mostly disilicate and polysilicate in nearly equal proportion.

With to Na_2O/SiO_2 = 1.0 decreasing mole ratio in the sodium silicate solution the degree of condensation of the high molecular part of the anions increases (Fig. 4, curve 4). A Further decrease to 0.5 Na_2O/SiO_2 moreover leads to a decrease of the amount of the low molecular anions (curve 5).

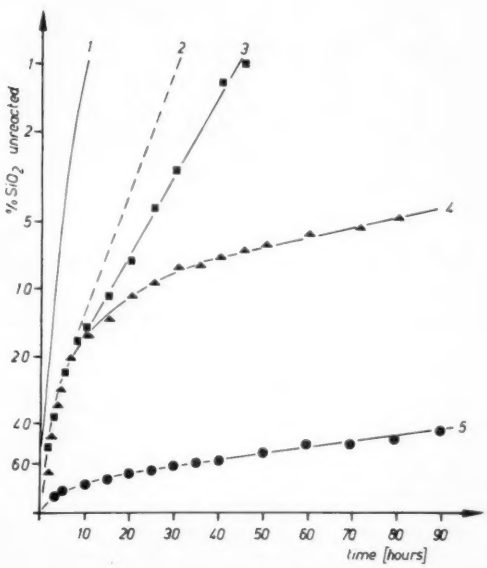

FIG. 4

Molybdate reaction curves of C-S-H phases from precipitation reactions (curves 1 and 2) and of silicate gardens (curves 3 - 5) each after 3 hours (concentration of the sodium silicate solution 1 M in SiO_2; Na_2O/SiO_2 ratio: curve 1 - 1.5, 2 - 1.0, 3 - 1.5, 4 - 1.0, 5 - 0.5).

The degree of condensation of the anions of the "gardens" is markedly higher than that of phases formed by precipitation from $CaCl_2$ solution with sodium silicate solutions of the same composition, as can be seen by comparison of the corresponding molybdate reaction curves (Fig. 4).

Differences between C-S-H phases, formed by precipitation, and silicate gardens exist also in their composition. Whereas the CaO/SiO_2 ratio in the precipitates is generally smaller than the Na_2O/SiO_2 mole ratio in the solution used for precipitation /7, 8/, it is much higher in the "gardens". For example in the garden products, formed from solution with 1 Na_2O/SiO_2, the CaO/SiO_2 mole ratio rises up to 1.9 and from solutions with 1.5 Na_2O/SiO_2 to more than 2.0.

The reason for these high CaO/SiO_2 mole ratios is that crystalline $Ca(OH)_2$ is formed already within the first 15 minutes after the beginning of the reaction, as shown by X-ray diffraction.
The formation of crystalline calcium hydroxide under the conditions described was unexpected, because precipitation of C-S-H phases from $CaCl_2$- and sodium silicate solutions results in $Ca(OH)_2$-free products, if the Na_2O/SiO_2 ratio is smaller than 1.5 in solution /7, 8/.

As shown above, the properties of the garden products depend on the conditions of their formation. Therefore it was obvious to check, whether the permeability of water across such phases is also influenced by these conditions.

To do this, $CaCl_2.6H_2O$ was molten in a glass tube and then crystallized by cooling. The relatively smooth surface of the crystallized melt was then covered with sodium silicate solutions of different concentrations and Na_2O/SiO_2 mole ratios.

At once after adding the silicate solution a membrane was formed at the boundary. Through this membrane water diffuses, dissolving the solid $CaCl_2.6H_2O$ lying underneath. The height of the so formed concentrated $CaCl_2$ solution in the tube increases with time (Fig. 5). By plotting this height in mm versus time t for sodium silicate solutions of different Na_2O/SiO_2 mole ratios at a constant SiO_2 concentration (2.5 M, Fig. 6), it can be shown that with increasing Na_2O/SiO_2 ratio the amount of $CaCl_2$ solution formed decreases. That means the diffusion rate of water through the membrane decreases.

A decrease of the diffusion rates was also observed using silicate solutions with increasing SiO_2 concentration at constant Na_2O/SiO_2 mole ratio (Fig. 7, Na_2O/SiO_2 = 1.5).

If a solution of high ion concentration, for example with a mole ratio of 1.5 Na_2O/SiO_2 and a concentration of 2.5 moles SiO_2/l, is exchanged within the first 10 minutes after formation of the boundary layer against a diluted one (0.5 moles SiO_2/l) of the same Na_2O/SiO_2 mole ratio, then the diffusion rate is actually higher (fig. 7, curve 5) than with the exchanged one (curve 1), but smaller than that in the experiment with a membrane, formed from this solution of low concentration directly (curve 4).

Discussion

DOUBLE et al. /5, 9/ interpreted the silicate gardens as mixed hydrous oxides. From the molybdate reaction curves shown above it is evident that at the very least with $CaCl_2$ in sodium silicate solutions with mole ratios higher than 0.5 Na_2O/SiO_2 C-S-H phases but not hydrous silica are formed beside crystalline $Ca(OH)_2$. The degree of condensation of the silicate anions of the C-S-H phases

VOL
14
198

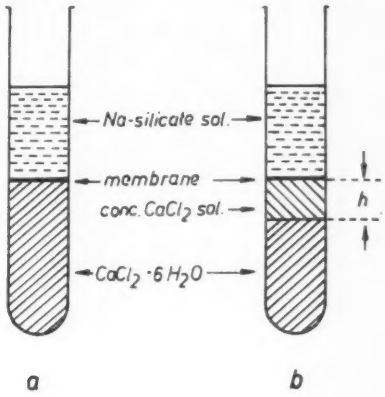

FIG. 5

Experimental procedure for determination of the diffusion rate of H_2O across C-S-H membranes. a: at once after covering the $CaCl_2.6H_2O$ with sodium silicate solution. b: after a reaction time t.

VOL. 14 1984

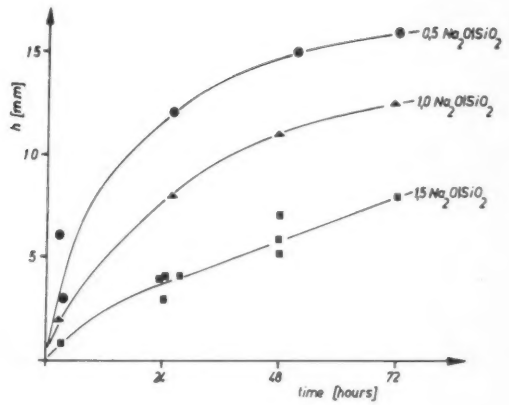

FIG. 6

Diffusion of water across a C-S-H membrane, dependent on the Na_2O/SiO_2 ratio of the sodium silicate solution ($[SiO_2]$ = 2.5 M)

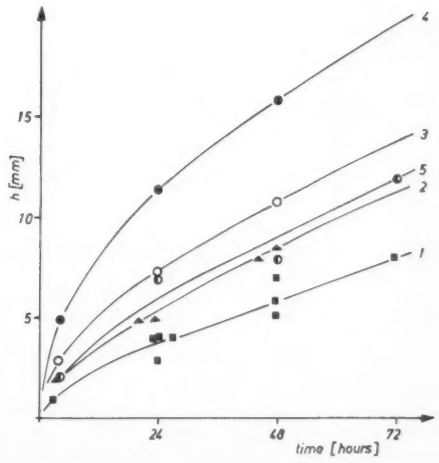

FIG. 7

Diffusion of water across a C-S-H membrane, dependent on the SiO_2 concentration of the sodium silicate solution with Na_2O/SiO_2 = 1.5 (SiO_2 concentrations: curve 1 - 2.6, 2 - 2.0, 3 - 1.0, 4 - 0.5 moles/l, 5 - 2.6 moles/l, exchanged against a solution with 0.5 moles/l).

increases with decreasing Na_2O/SiO_2 mole ratio in the sodium silicate solution (Fig. 4).

The mean degree of condensation of these phases however is higher than that of the phases produced by precipitation reaction. The reason may be that the C-S-H phase grows into the concentrated $CaCl_2$-solution. In this environment of relatively low p_H a higher degree of condensation of silicate anions is to be expected than by precipitation in strongly basic solution /7, 8/.

The appearance of crystalline $Ca(OH)_2$ in the "gardens" is explained by BIRCHALL et al. /4/ in such a way that Ca^{2+}-ions diffuse through the membrane into the alcaline silicate solution and are precipitated there as $Ca(OH)_2$. From our own results /7, 8/ it can be concluded that on contacting Ca^{2+}-ions with sodium silicate solutions C-S-H phases are formed as most sparingly soluble compounds in this system. As Fig. 3 shows, secondary formations on the outer face of the membrane appear indeed, which can be attributed to a diffusion of Ca^{2+}-ions from the $CaCl_2$ solution inside the tubes towards outside. These secondary C-S-H formations, however, appear only after longer times (> 2 h), whereas the formation of crystalline $Ca(OH)_2$ can be detected already after at least 15 minutes.
This indicates a precipitation of $Ca(OH)_2$ in the course of the membrane formation at the boundary between the calcium chloride crystals and the sodium silicate solution.

As described above the diffusion rate of water across the membranes formed at the surface of $CaCl_2.6H_2O$ crystals is dependent both on the Na_2O/SiO_2 mole ratio of the silicate solution and its SiO_2 concentration. The higher the concentration in this solution the lower is the diffusion rate of water across the membrane. This might be attributed to an osmotic driving force, depending on the difference in ion-concentration at either side of the membrane. In this case a substitution of the concentrated sodium silicate solution against a diluted one after formation of the membrane should result in a diffusion rate of water, corresponding to the concentration of the latter solution But as shown above that is not to be observed.

The diffusion rate is indeed not equal to that of the concentrated solution (Fig. 7, curve 1), but markedly smaller than that of the diluted one (curve 4 and 5, respectively).
That means not only osmotic laws control the diffusion of water. Moreover the permeability of the membrane itself is a limiting factor, depending on the composition of the C-S-H phase. The higher the CaO/SiO_2 mole ratio the smaller is its permeability.

The proved dependence of the permeability of C-S-H membranes on the conditions of formation, especially on their composition, is of highly importance on the hydration kinetics of C_3S, because in the beginning of the hydration membranes are formed, comparable to those of the silicate gardens /1-5/.

For example it gets well understandable, why the rate of hydration of C_3S in the beginning of the reaction can be altered by admixtures, influencing the $Ca(OH)_2$ concentration in the pore solution. As shown earlier /7, 8, 10, 11, 12/, the composition of C-S-H phases depends on the $Ca(OH)_2$ concentration in the solution from which they are formed. So with admixtures, able to bind $Ca(OH)_2$, like silica /13/ and ion exchangers /14/ the CaO/SiO_2 mole ratio of the C-S-H phase surrounding the hydrated C_3S grains, can be decreased. That leads, as shown above, to a higher permeability of the membrane for water molecules, resulting in a higher hydration

VOL
14
198

rate. On the other side, admixtures like $Ca(OH)_2$, able to increase the $Ca(OH)_2$ concentration around the membrane, decrease the reaction rate /15/.

The investigation of the silicate gardens have shown by this that about the permeability of the C-S-H membranes, depending on their composition, effects are well to be explained, which proceed during the hydration of C_3S, when the composition of the C-S-H coating on the C_3S grains is altered for example via the $Ca(OH)_2$ concentration in the pore solutions.

Acknowledgements

The authors gratefully acknowledge technical assistance by Mrs. B. Ködderitzsch. Thanks are also due to Mrs. R. Bimberg, Hochschule für Architektur und Bauwesen, Weimar, and Mr. J. Richter-Mendau, Zentralinstitut für Physikalische Chemie der Akademie der Wissenschaften der DDR, Berlin, for SEM investigations.

References

1. D.D. Double and A. Hellawell, Nature 261, 486, 1976
2. D.D. Double, A. Hellawell and S.J. Perry, Proc. Roy. Soc. (London), A 359, 435, 1978
3. J.D. Birchall, A.J. Howard and J.E. Bailey, Proc. Roy. Soc. (London), A 360, 445, 1978
4. D.D. Double, Silicates Ind. 43, 233, 1978
5. J.D. Birchall, A.J. Howard and D.D. Double, Cement Concr. Res. 10, 145, 1980
6. H.M. Jennings and P.L. Pratt, Cement Concrete Res. 9, 501, 1979
7. H. Stade, Z. anorg. allg. Chem. 470, 69, 1980
8. H. Stade and W. Wieker, Z. anorg. allg. Chem. 466, 55, 1980
9. R.D. Coatman, N.L. Thomas and D.D. Double, J. Mater. Sci. 15, 2017, 1980
10. H.F.W. Taylor, J. Chem. Soc. 1950, 3682
11. S.A. Greenberg and T.N. Chang, J. Phys.Chem. 69, 182, 1965
12. K. Fujii and W. Kondo, J. Chem. Soc., Dalton Transact. 1981, 645
13. H.N. Stein and J. Steevels, J. appl. Chem. 14, 338, 1964
14. Ch. Stadelmann and W. Wieker, Z. anorg. allg. Chem. in press
15. J.G.M. DeJong, H.N. Stein and J.M. Steevels, J. Appl. Chem. 17, 246, 1967

VOL. 14 984

CEMENT and CONCRETE RESEARCH. Vol. 14, pp. 670-678, 1984. Printed in the USA.
0008-8846/84 $3.00+00. Copyright (c) 1984 Pergamon Press, Ltd.

STUDIES OF LOW-POROSITY CONCRETES DESIGNED FOR BRIDGE DECK APPLICATIONS: 1. INTRODUCTORY REMARKS, MIX DESIGNS, STRENGTH DEVELOPMENT, AND RHEOLOGICAL CHARACTERISTICS

S. Ebow Coleman* and Sidney Diamond
School of Civil Engineering, Purdue University
West Lafayette, IN 47907, U.S.A.

(Communicated by J. Skalny)
(Received Dec. 16, 1983)

ABSTRACT

A major concrete problem in recent years has been premature deterioration of concrete bridge decks due to corrosion of reinforcing steel. The research reported here was designed to explore the possibility of eliminating the problem by the use of low porosity concrete. A brief review of low porosity cement systems is provided. Mix design considerations for low porosity concretes are explored. The results of laboratory trials on rheological and other features of fresh low porosity concretes are reported, and compressive strength data are provided for several different low porosity concrete systems.

VOL
14
198

Introduction

A major concrete problem in recent years has been the early deterioration of concrete bridge decks in areas where salt is routinely applied for winter de-icing. Considerable evidence now suggests that traditional reinforced concrete as ordinarily designed for concrete bridge decks is not adequate to provide satisfactory service under such exposure conditions.

The problem is triggered by penetration of chloride ions from the applied salt through the concrete and to the vicinity of the upper mat of reinforcing steel, which results in accelerated steel corrosion. Expansive pressures generated by the accumulation of corrosion products tend to lift off the relatively thin layer of concrete cover usually provided. Local delamination occurs, followed by spalling under the influence of repeated traffic impacts. In severe cases total failure of the bridge deck may be experienced in only a few years.

* Present Address: Dowell, Division of Dow Chemical USA, Tulsa OK. 74101, U.S.A.

A number of features of the concrete ordinarily placed in bridge decks tend to exacerbate the problem. High water contents are often used to insure proper placement and consolidation around the steel; often bleeding channels result, which can provide almost direct access of chloride ions to the vicinity of the steel. Once delamination starts to occur, the strength of most bridge deck concretes is is insufficient to resist the dislodging effects of repeated impacts, especially from heavy truck traffic, and progressive spalling rapidly ensues.

The use of epoxy-coated reinforcing steel is currently considered by many to provide an effective solution to the problem, the epoxy coating serving to prevent access of chloride and water to the covered steel. However, an alternate approach that might be considered is that of improving the concrete itself. In particular we have in mind the use of a self-consolidating, high slump concrete, but one capable of achieving these characteristics at a very low water content. This would limit permeability and diffusion of chloride ions, and limit the development of bleeding channels.

VOL.
14
984

In the current state of concrete technology there are several ways available to design such concrete. High-range water reducers coupled with flyash or silica fume provide one approach. Another approach is the use of so-called "low porosity" cement in appropriately-designed rich concrete mixes. This approach offers some significant advantages in terms of additional alkaline protection of the steel, and may prove to be significantly less expensive as well. The present paper and additional papers in this series describe our results with low porosity concretes investigated in the context of their specific applicability to the bridge deck durability problem.

Low Porosity Cements

Low porosity cement ("LP cement") is simply ordinary ground Porland cement clinker, usually ground somewhat finer than ordinary portland cement, to which no gypsum has been added. The appropriate range of fineness is about that of ASTM Type III cements, ca. 500 sq. m/kg. The setting and rheological characteristics of concrete made with such cement ("LP concrete") are controlled by a combination of an appropriate lignosulfonate and an alkali carbonate or bicarbonate, usally dissolved in the mix water.

LP cements were investigated extensively by Brunauer and co-workers in the late 1960's and early 1970's, and a patent was obtained by Brunauer in 1972(1). Subsequent development work was carried out by several cement companies, and a superior lignosulfonate-type admixture has been developed for the purpose by the Westvaco Corporation. U. S. patents covering various aspects of LP cement and concrete technology have been awarded to Stryker(2) and Ball, Braddon and Stryker(3) of Westvaco, and to Mills(4) of Martin Marietta Cement Co., Inc. A substantial number of research publications from various countries has appeared in recent years(5-17).

Materials Used in the Present Investigation

Low Porosity Cement

The ground clinker used in the LP concretes described here was a Type I clinker produced at the Holly Hill, S.C. plant of the Giant Portland Cement Co., and was ground to a Blaine fineness of approximately 540 sq.m/kg with no gypsum being incorporated. A plant analysis of the clinker is given in Table 1. Its chemical composition is that of an ordinary Type I portland cement clinker except that the alkali content is unusually low. This is not a necessary feature of LP cements.

Table 1.
Chemical Characteristics of the Ground Clinker Used.

1. Chemical Composition:

Oxide	%
SiO_2	22.2
Al_2O_3	6.2
Fe_2O_3	2.6
CaO	67.6
MgO	1.06
Na_2O	0.07
K_2O	0.17
SO_3	0.13
Total alkalies as equiv Na_2O	0.18
Ignition loss	0.35
Free CaO	0.69

2. Potential Compound Composition (Bogue):

Compound	%
C_3S	58.2
C_2S	19.7
C_3A	11.9
C_4AF	8.0

The specific admixture combination used in batching the LP concretes consisted of a sulfonated Kraft process pine lignin developed for LP use by Westvaco and designated "REAX-LP", and reagent grade sodium bicarbonate. The sulfonated lignin product is said to be completely free of sugars and other carbohydrates.

Aggregates

The coarse aggregate used was a hard, clean limestone from Kentland, Indiana, having a bulk specific gravity (SSD) of 2.62 and an absorption of 1.2%. The aggregate was dried and graded before use, the size separations being 3/4 to 1/2 in., 1/2 to 3/8 in., 3/8 in. to No. 4, and No. 4 to No. 8. In most of the LP concretes prepared the ratios of the amounts used were 1.5:1.2:1.0, the material passing No. 4 being discarded.

The sand used was a natural siliceous sand of fineness modulus 2.71, with a measured absorption of 2.7% and bulk specific gravity (SSD) of 2.53.

Flyash

Much of the experimental concrete was batched with a high-calcium flyash obtained from the Otter Tail Power Co. plant at Fergus Falls, MI. Analysis indicated a CaO content of approximately 30%, and an unfortunately high sulfate content in excess of 6%. The ignition loss was less than 2%, and the specific gravity was measured as 2.69. This high measured specific gravity suggests the relative absence of cenospheres and other hollow particles.

Mix Design Considerations

In exploring the behavior of concretes batched in various proportions it became apparent that relatively lean LP concretes, i.e. those batched at ca. 300 kg/cu. m (500 lbs/cu. yd) were only marginally workable at the low water contents desired (w:c ratios ca. 0.30), but were unduly sensitive to mixing conditions and to evaporative loss of water. Such concretes exhibited an obvious shortage of paste volume. It bacame clear that practical LP concrete capable of easy placement at low water:cement ratios would require cement factors on the order of 550 kg/ cu. m (about 900 lbs/cu. yd.), or else more modest cement factors supplemented by flyash. It was found that the high-calcium flyash used in these trials had a generally beneficial effect on most of the properties of the fresh LP concretes.

While a number of variations in mix design were entertained in various experimental concretes, there were two "typical" mix designs which served as the basic patterns for nearly all of the experimental concretes. One of these was a "straight" LP concrete with a cement factor of about 534 kg/cu m (900 lbs/cu.yd) and a w:c ratio of approximately 0.30, the other a flyash-bearing concrete with a cement factor of about 415 kg/cu m (700 lbs/cu. yd) supplemented with about 60 kg/cu. m (250 lbs/cu. yd.) of flyash, with the water to cement plus flyash ratio being about the same as the w:c ratio of the first mix. Typical mix designs for the two concretes are given in Table 2.

Since the LP cement system does not use interground gypsum but relies on batch-mixed lignosulfonate and alkali carbonate or bicarbonate admixtures for set control and rheological modification, the proportion of these components actually added is under the control of the concrete producer. This flexibility provides an opportunity for adjustment of dosage to fit varying circumstances, but it also may require that adjustments be made when new batches of cement with changed characteristics are introduced. Such changes, especially of lignosulfonate content, were required several times during the course of this work. Typical values of the admixtures used were about 0.6% of the lignosulfonate and 1.2% of the sodium bicarbonate, both by weight of ground clinker.

TABLE 2.
Typical Concrete Mix Designs

1. LP concretes without flyash:

Ground Clinker: 558 kg/cu. m
Coarse Aggreg: 1010 kg/cu. m
Sand: 675 kg/cu. m
Water: 156 kg/cu. m
(w:c 0.28)

2. Flyash-Bearing LP Concretes:

Ground clinker: 410 kg/cu.m
Flyash: 140 kg/cu.m
Coarse Aggr: 1010 kg/cu.m
Sand: 658 kg/cu. m
Water: 156 kg/cu. m
(w:(c+f) 0.28)

Strength Levels Attained

In previous work carried out at Purdue University (9),

compressive strengths of the order of 70 MPa (10,000 psi) were ordinarily obtained with low porosity concretes at 28 days.

In the present study compressive strengths development in several series of LP concretes were studied for ages up to 1 year. The concrete mixes actually tested for strength were somewhat leaner than the mix designs of Table 3. For these tests, carried out early in the program, the ground clinker contents of the concretes batched without flyash were approximately 475 kg/cu. m (800 lbs/cu.yd.), and the w:c ratio was 0.30. For concretes batched with flyash, the ground clinker content was 412 kg/cu. m (695 lbs/cu. yd.) and the w:(c+f) ratio was 0.30.

The concretes were cast into 3 in. x 6 in. steel molds, hand-rodded, demolded at 1 day, and cured continuously in a fog room until tested. Cylinders tested at ages of three months or less were capped; those tested at later ages were lapped at both ends using a lapping wheel. The actual compression testing was carried out in a standard concrete testing machine of 114,000 kg (250,000 lb) capacity, which was only marginally adequate for testing the stronger concrete cylinders; thus the true strengths may actually have been higher than those recorded.

Results of the testing are provided in Table 3. The relatively lean LP concretes batched without flyash achieved compressive strengths of the order of 55 MPa (8000 psi) at 7 days, 65 MPa (9500 psi) at 28 days, and 100 MPa (14,500 psi) at 1 year. These rather remarkable strength levels are customarily encountered in LP concretes.

VOL. 14 1984

Incorporation of the flyash produced concrete of strength levels only slightly lower than those cited above, at least for ages of up to 3 months. The long-term strength levels for these flyash-bearing concretes seemed to be limited to the vicinity of 70 MPa (about 10,000 psi).

TABLE 3. Compressive Strengths and Sample Standard Deviations for LP Concretes, MPa*

Age	LP Concretes Without Flyash		Flyash-Bearing LP Concretes	
7 d.	55.1 (7990)	3.8 (560)	51.9 (7520)	2.3 (340)
28 d.	65.2 (9450)	6.9 (1000)	60.6 (8790)	3.5 (510)
3 mo.	78.4 (11400)	4.2 (610)	71.2 (10600)	6.1 (880)
6 mo.	81.9 (11900)	4.5 (650)	66.7 (9670)	7.4 (1080)
1 yr.	99.8 (14500)	4.5 (650)	----------	----------

*Equivalents in psi are given in parenthesis. Strength values are averages for 3 replicate cylinders each.

One of the reasons for the lesser strength development in the flyash-bearing LP concretes may be the extra air incorporated in these mixes. The air content of the LP concretes batched without flyash is of the order of 2% or less, which is about what is

normally expected. However, the LP concretes batched with flyash appear to incorporate about 6% total air voids, presumably due to an interaction between the flyash and the lignosulfonate admixture.

Rheological Characteristics of Fresh LP Concretes

The most striking feature of LP concrete that distinguishes it from conventional concrete that might be made from the same ground clinker and aggregates is the ability to produce readily workable mixes at low water contents. This is due to the ability of the specially-designed lignosulfonate and alkali bicarbonate admixtures to provide and maintain extremely effective dispersion of the ground clinker grains in a system of very limited water content.

The rheology of such concrete mixes is sufficiently different from conventional concretes (including superplasticized concretes) that special mention of these features should be made.

We found that LP concretes batched without flyash at w:c ratios between 0.24 and 0.30 exhibited high slumps, measured values varying between 15 and 25 cm (6 and 10 in.). Despite these high slumps, the concretes were not easy to work, seeming to actively resist rapid displacement or manipulation. It was difficult to pull a trowel through the mix rapidly, although very little resistance was felt to slow movement of the same implement. This dilatant effect was, however, easily overcome by modest vibration, which rendered the system much more fluid. Alternatively, incorporation of flyash eliminated this resistance to rapid displacement, presumably by modifying the size distribution characteristics of the fines present.

The slump measurements themselves do not appear to constitute a particularly valid index to the rheological behavior of these concretes, the slump itself being a slow, continuous flow under self-weight rather than the rapid displacement normally experienced when a slump cone is removed.

A number of trials were carried out using the Vebe apparatus, which measures time to collapse under a specified vibrational input, and these seemed to provide a much more suitable relative indication of rheological behavior of the fresh LP concrete. Typical LP concretes yielded Vebe times of less than 3 seconds, indicative of the high mobility under vibration, even when static slump measurements were only of the order of 15 to 18 cm (6 or 7 in.).

In this work, we distinguished LP concretes as "fully flowing" in slump tests if they completely collapsed under their own weight in less than 30 seconds. A number of such concrets were produced, and these usually showed Vebe times of 1 second or less.

An important characteristic of fresh concrete is its tendency (or lack of it) toward segregation and excessive bleeding. Any dispersed cement system that flows freely needs to be carefully

checked for this characteristic, even at low water contents. In our observations, there was some limited tendency to segregation and excessive bleeding in leaner LP concrete mixes batched without flyash. This behavior seemed to be influenced by the dosage level of the lignosulfonate; reducing the lignosulfonate dosage level reduced the tendency toward segregation considerably, but at some cost to workability. Addition of flyash to such lean mixes or incorporation of higher contents of ground clinker resulted in LP concretes essentially free of difficulty in this regard.

One of the limiting features in the use of superplasticized concrete for field applications involving low water contents is the factor of slump loss starting relatively soon after mixing. The dispersion induced by the superplasticizer is temporary, and when the concentration of superplasticizer in the mix water is lowered sufficiently by its incorporation into the early hydration products, the dispersive effect is lost. In consequence, the slump rapidly decreases to that of a non-superplasticized concrete of the same water content. As part of the investigation carried out here, we attempted to determine the extent to which LP concretes might be subject to the same difficulty.

VOL. 14 1984

In these trials we examined the effect of elapsed time on slumps and Vebe times of a series of concretes batched at modest LP cement factor of about 445 kg/cu. m (750 lbs/cu. yd.), and others supplemented by various percentages of flyash addition. The water:(cement+flyash) ratios were typically about 0.30 to 0.32. In most of these trials, Vebe times were measured initially, and then at half hour intervals, with the concrete protected from evaporation in between, and a brief re-mixing just prior to the measurement.

Initial slumps were very high, and initial Vebe times 1 or 2 seconds, indicating fully flowing concrete. Vebe time increased to the order of 10 seconds by the first hour, and to about 18 seconds by the second hour. The data on the effects of flyash addition are somewhat conflicting, but it appeared that additions of small percentages of flyash were not beneficial in maintaining fluidity of the mix, but that larger additions, of the order of 35% by weight of cement, were moderately helpful or at least not deleterious. It may be recalled that the particular flyash used in these trials had an unusually high sulfate content, which may have influenced the system in a manner not fully typical of flyashes in general.

What systematic data are not available, mixes richer in ground clinker appear to be relatively more resistant to time-dependent changes in rheological characteristics. Further, it is clear from earlier work that the specific content of lignosulfonate influences the maintenance of fluidity appreciably. Higher dosages of lignosulfonate will prolong fluidity for long periods, but at the same time may delay set unduly.

Some miscellaneous observations on the behavior of fresh LP concretes are summarized below:

1. It appears that LP concretes that show initial slumps of 15 cm (6 in.) or more or initial Vebe times of 3 seconds or less are essentially self-consolidating, and require almost no rodding or vibration to completely eliminate honeycombs or skips even in corners of molds or other restricted spaces.

2. Such concrete will flow spontaneously on inclined surfaces of slopes greater than about 8%. This may cause some practical difficulty in concrete placement on inclined surfaces.

3. LP concretes assume mirror-like contact surfaces when cast against plastic sheets, and presumably against other smooth surfaces as well. Thus form irregularities will be well reflected in the hardened concrete.

Conclusions

Concrete that may be suitable for highway bridge decks with special characteristics helpful in preventing or delaying steel corrosion that results in premature failure can be formulated from low porosity cement. Such concrete probably requires high cement contents or moderately high cement contents supplemented by flyash. Experimental concretes mixed at water:cement ratios of the order of 0.30 show high initial slumps and Vebe times of the order of 1 second, and are self-consolidating. However they do lose fluidity with time, and show peculiar rheological characteristics that will have to be taken into account in designing concrete for bridge-deck or other field use. Strengths of the order of 70 MPa (10,000 psi) may be obtained at 28 days, with significant increases at later ages possible. The rheological behavior of flyash-bearing fresh low-porosity concrete seems superior in some respects to concrete batched without flyash, although the strength attained appears somewhat less.

Acknowledgements

This report and subsequent planned reports in this series are based in part on the Ph. D. thesis of the first named author. The research was carried out under the auspices of the Joint Highway Research Project, Purdue University, and was supported by the Federal Highway Administration, U.S. Department of Transportation and the Indiana Department of Highways. The contents reflect the views of the authors, who are responsible for the facts and the accuracy of the data presented herein, and do not reflect the official views and policies of the Federal Highway Administration.

We acknowledge with thanks the encouragement offered and the materials kindly provided by Dr. Frank J. Ball, Associate Corporate Research Director, Westvaco Corporation.

References

1. S. Brunauer, U.S. Patent No. 3,689,294 issued Sept. 1972
2. L. J. Stryker, U.S. Patent No. 3,959,294 issued May, 1976.
3. F. J. Ball, D. V. Braddon, and L. J. Stryker, U.S. Patent No.

3,960,582 issued June 1976.
4. M. H. Wills, Jr., U.S. Patent No. 4,019,918 issued Apr. 1978
5. J. Skalny, J. C. Phillips, and D. S. Cahn, CCR 3 29-40 (1973)
6. J. Skalny and I. Odler, Transp. Res. Record 564 27-38 (1976)
7. K. M. Hanna, Zement-Kalk-Gips 30 140-142 (1977) in German.
8. K. M. Hanna, ibid 293-295 (1977) in German.
9. S. Diamond and C. Gomez-Toledo, Report JHRP-77-10, Joint Highway Research Project, Purdue University (1977)
10. S. Diamond and C. Gomez-Toledo, CCR 8 613-621 (1978)
11. I. Odler, V. Duckstein, and T. Becker, CCR 8 469-480 (1978)
12. I. Odler, R. Schonfeld, and H. Dorr, CCR 8 525-538 (1978)
13 S. Diamond and C. Gomez-Toledo, Il Cemento 75 189-194 (1978)
14 S. Diamond, World Cement Techn. 116-121 April (1980)
15. M. Collepardi, S. Monosi, and G. Moriconi, CCR 10 253-262 (1980)
16. F. Skvara, K. Kolar, j. Novotny, and Z. Zadak, CCR 10 251-261 (1980)
17. F. Skvara, Z. Zadak, and K. Kolar, Silikaty XXV 251-261 (1981)

VOL.
14
1984

CEMENT and CONCRETE RESEARCH. Vol. 14, pp. 679-685, 1984. Printed in the USA.
0008-8846/84 $3.00+00. Copyright (c) 1984 Pergamon Press, Ltd.

CONDUCTIMETRIE,HYDRATATION,REACTIVITE DE L'ALUMINATE MONOCALCIQUE

P. GALTIER et B. GUILHOT
Ecole Nationale Supérieure des Mines
Laboratoire de Chimie-Physique
158,cours Fauriel
42023 St-ETIENNE Cedex(France)

(Communicated by B. Cottin)
(Received Dec. 14, 1983)

OL.
14
984

ABSTRACT

The study of calcium monoaluminate hydration by electrical conductivity reveals transient phenomena, and permits defining the mechanism of reaction. The residual parts of other aluminates (CA_2 and $C_{12}A_7$) modify CA conductivity curves, mainly when supersaturation is setting up.

L'étude, par conductimétrie électrique en milieu dilué, de l'hydratation de l'aluminate monocalcique a permis d'élucider un certain nombre de points sur les mécanismes de la réaction. Les quantités résiduelles d'autres aluminates (CA_2 et $C_{12}A_7$) présentes dans le CA modifient les courbes de conductivité notamment au niveau du "palier de sursaturation".

INTRODUCTION

L'avancement de la réaction d'hydratation de l'aluminate monocalcique peut être suivi à travers la concentration en ions de l'eau d'hydratation.

Cette méthode de suivi de l'hydratation donne lieu à l'établissement de courbes de concentration de la solution en fonction du temps(1). On effectue, à intervalles réguliers, des prélèvements

de la solution sur lesquels on procède à une analyse chimique des espèces dissoutes. On observe ainsi des paliers de sursaturation qui finissent par retomber au niveau fixé par l'équilibre de solubilité des produits finaux (2 à 5).

L'intérêt de cette méthode est de déterminer très précisément la concentration de chacune des espèces chimiques en solution et de permettre ainsi le suivi du rapport C/A en solution au cours de l'hydratation. Des auteurs ont montré (6) que ce rapport varie lors de l'hydratation de l'aluminate monocalcique. L'inconvénient majeur de cette méthode semi-continue réside dans le fait qu'elle nécessite pour chaque tracé de courbe, un nombre très important d'analyses.

Afin d'avoir une mesure en continu, il est apparu intéressant d'enregistrer la conductibilité électrique de la suspension. En suivant l'évolution de celle-ci, on compte de la même façon tous les porteurs de charge en solution, sans connaître leurs proportions relatives. Cette méthode, à la fois globale et simplifiée, sans avoir la rigueur de la précédente, peut la compléter. Il faudra bien entendu rester prudent au niveau de l'interprétation, puisque, dans le cas des aluminates de calcium, on peut obtenir la même conductivité électrique avec des rapports C/A en solution différents.

I - PREPARATION DE L'ALUMINATE MONOCALCIQUE

Nous avons préparé le CA par réaction solide-solide : c'est le mode opératoire qui a permis la découverte des différents aluminates de chaux, et le procédé qui est utilisé industriellement pour les fabriquer.

Des différentes études (8 à 13) de la réaction chaux-alumine à haute température (1400°C), il ressort qu'on ne peut synthétiser par ce moyen un CA de grande pureté. Il contient inévitablement des traces d'un des produits intermédiaires de la réaction, qui sont d'autres aluminates de composition $C_{12}A_7$ et CA_2.

Sachant cela, nous avons cherché à obtenir un degré d'avancement aussi poussé que possible en prenant un certain nombre de précautions dans la préparation de l'aluminate, notamment dans l'homogénéisation des deux réactants solides. En effet, il a été montré par ailleurs (14) que le nombre de contacts entre grains était un des paramètres les plus importants pour l'avancement des réactions solide-solide.

I - 1) - CHOIX DES REACTANTS -

Nous avons choisi (15) une alumine α RHONE POULENC Ref.LS20, à faible teneur en soude, et à température de calcination moyenne (1250°C), relativement active (16), et le carbonate de calcium R.P.E. CARLO ERBA. Après dessication préalable, ces deux produits sont pesés dans les proportions stoechiométriques désirées.

I - 2) - HOMOGENEISATION DES POUDRES -

Cette opération est à la fois très délicate et très importante, quand il s'agit comme ici de solides très finement divisés. En effet, le nombre de contacts entre les grains de chacune des deux poudres et l'homogénéité du mélange en dépendent en grande partie. Nous avons pu observer en particulier que les différents

mélanges à sec de ces deux poudres, même au moyen d'appareils performants, sont imparfaits. Pour obtenir un mélange homogène, la mise en suspension des poudres en milieu liquide est un moyen efficace.

Pour cela, nous avons utilisé l'eau, dans laquelle les réactants sont extrêmement peu solubles, et qui semble bien dissocier les agrégats entre grains d'une même poudre. Pour favoriser encore la dispersion des agrégats et le mélange intime des deux poudres, nous avons réalisé l'opération de mise en suspension dans la jarre de broyage (en carbure de tungstène) d'un broyeur planétaire, et nous avons, dans un deuxième temps, cobroyé en milieu liquide les deux réactants pendant quelques minutes. L'eau est ensuite évaporée sous agitation constante de la suspension, de façon à éviter d'éventuelles ségrégations par décantation. Ce mode opératoire en milieu liquide réalise un bon contact entre les deux poudres et élimine tout collage sur les parois avant l'opération de mélange proprement dite.

Ce mélange par mise en suspension en milieu liquide s'apparente au procédé industriel dit "par voie humide".

I - 3) - DECARBONATATION + PASTILLAGE -
Après décarbonatation atmosphérique à 1000°C pendant 1 h 30, la poudre est pastillée sous une pression de 2,5 T/cm^2, de manière à assurer pour la cuisson le plus grand nombre possible de contacts entre grains des deux réactants (14).

I - 4) - CUISSON -
La pastille, placée dans une nacelle en platine, est portée en environ 2 heures, à haute température (1450°C), sous air, et est maintenue à cette température durant environ 6 heures. A l'issue de cette cuisson, la pastille se refroidit à la vitesse naturelle du four.

En suivant ce protocole opératoire, nous avons obtenu diverses préparations de CA, et différents aluminates en faisant varier les proportions relatives de chaux et d'alumine. Ces composés ont ensuite été utilisés pour nos essais d'hydratation en calorimétrie et en conductimétrie.

II - NON-REPRODUCTIBILITE DES ESSAIS D'HYDRATATION EN CALORIMETRIE.

Au cours de notre étude, nous nous sommes heurtés à des difficultés de reproductibilité des essais d'hydratation en calorimétrie isotherme, difficultés signalées aussi par LONGUET (15,13) ce qui est d'autant plus surprenant que, dans les mêmes conditions, la cinétique d'hydratation du sulfate de calcium est, elle, bien reproductible (7).

Après de nombreuses recherches (16), nous avons établi que la répartition granulométrique de la poudre est la cause principale de la plus ou moins bonne reproductibilité de l'hydratation "en pâte pure". En effet, cette mauvaise reproductibilité est liée à la présence de très fines particules et n'est plus observée, après un tamisage efficace de la poudre, permettant d'avoir des grains calibrés, donc des espaces intergranulaires relativement bien réguliers.

Ceci montre que, dans les conditions de l'hydratation en pâte, les paramètres fixant la géométrie du système réactionnel ont

une grande importance sur la réactivité d'une poudre.

III - ESSAIS DE CONDUCTIMETRIE -

Nous avons été amenés à utiliser cette autre technique expérimentale de suivi de l'hydratation de l'aluminate monocalcique qu'est la conductimétrie électrique, du fait de la non-reproductibilité des essais de calorimétrie, et surtout en raison du grand intérêt de cette deuxième méthode.

III - 1) - OBSERVATIONS PRELIMINAIRES -
Il faut dire cependant que, malgré toutes les précautions prises, nous n'avons pas obtenu une bonne reproductibilité dans les conditions des essais de conductimétrie. Cependant, le manque de reproductibilité, moins important que dans les essais de calorimétrie, autorise un certain nombre de conclusions. La cause de ce phénomène semble être ici la formation aléatoire d'une fine pellicule de particules ultrafines qu'on observe à l'interface liquide-air, et dans laquelle semble s'amorcer l'hydratation(16).

La conductibilité électrique de la solution au cours de l'hydratation du CA est d'environ 3 mS/cm. Quelle que soit l'origine de l'aluminate, nous n'avons jamais observé de véritables paliers de sursaturation, il s'agit plutôt d'un maximum fortement aplati. Une analyse des phases solides, présentes, juste après la chute de la conductibilité électrique de la solution, montre que l'anhydre initial n'est pas hydraté en totalité à cette échéance.

Un certain nombre d'"irrégularités" (qui se retrouvent pour toutes les prises d'essai d'une même préparation - cf Figure 2a) apparaissent quelquefois, d'une manière reproductible, sur les courbes d'hydratation, notamment au début et à la fin du palier de sursaturation.

III - 2) - REACTIVITE DE L'ALUMINATE MONOCALCIQUE -
Le principal facteur de la réactivité semble être la composition minéralogique du matériau de départ : la réactivité dépend en premier lieu de la présence à l'état de traces, d'aluminates autres que CA. On observe en effet quand la préparation de CA contient des traces de CA_2 une augmentation de la durée d'hydratation. En relation avec celle-ci, la conductibilité électrique de la solution atteint des niveaux de plus en plus bas. Inversement la présence de $C_{12}A_7$ diminue la durée d'hydratation et augmente la conductivité électrique (cf. Figure 1).

III - 3) - EFFET ACCELERATEUR DES AJOUTS DE $C_{12}A_7$ -
Dans les essais d'hydratation en calorimétrie, il est bien connu que des ajouts en proportion croissante de $C_{12}A_7$ raccourcissent chaque fois un peu plus le temps d'hydratation d'une préparation de CA.
Dans les essais de conductimétrie, le même effet accélérateur par le $C_{12}A_7$ peut être observé pour des ajouts de ce composé inférieurs à 1% en poids (cf. Figure 2a)

L'évolution des courbes de conductimétrie, en fonction de la proportion de $C_{12}A_7$ ajoutée en mélange, est similaire à celle obtenue pour des préparations de CA comportant des quantités croissantes de $C_{12}A_7$ formées au cours de leur synthèse (comparaison des Figures 2a et 1). Toutefois dans le cas des mélanges,

VOL. 14 1984

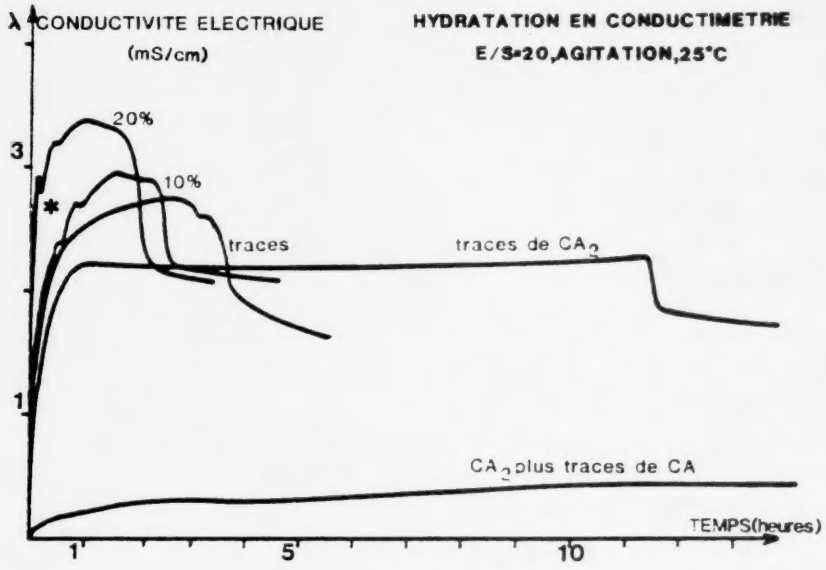

FIG. 1

Reactivite de differentes preparations de Ca Plus X% de $C_{12}A_7$

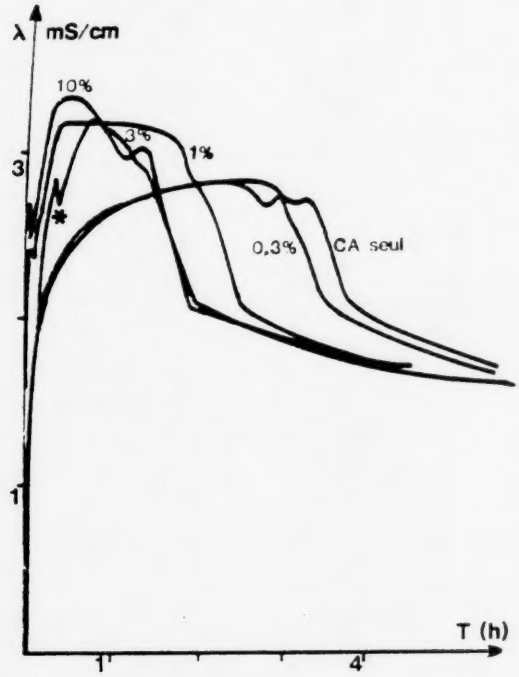

FIG. 2a

Ajouts de $C_{12}A_7$

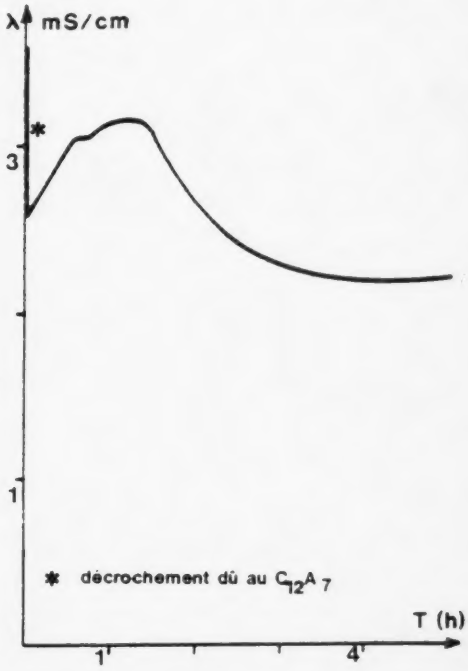

FIG. 2b

Hydratation du $C_{12}A_7$

ces effets se manifestent pour des proportions bien plus faibles de $C_{12}A_7$ ajouté.
En particulier, le décrochement dans la première partie fortement croissante de la courbe de conductivité, d'autant plus prononcé que la proportion de $C_{12}A_7$ est importante, apparaît ici, dans le cas des mélanges, pour des additions de $C_{12}A_7$ inférieures à 1%. Ceci prouve que cette "irrégularité" est bien due à la présence dans le CA de $C_{12}A_7$ résiduel.

Ce décrochement est encore plus important lors de l'hydratation de $C_{12}A_7$ pratiquement pur (cf. Figure 2b).

Cette brusque retombée de la conductivité électrique, associée à la concentration des espèces ioniques en solution, ne peut être attribuée qu'à la précipitation à cet instant d'un produit d'hydratation.
Cette observation corrobore la mise en évidence de C_2AH_8 et de gel d'alumine dès le début de la période athermique, dans les conditions d'hydratation de la calorimétrie (17).

Cette précipitation, peu après le contact avec l'eau n'empêche pas pour autant l'établissement d'un palier de sursaturation qui peut se maintenir pendant plusieurs heures. La sursaturation se maintient donc en présence de quantités notables de produits hydratés, si l'on en juge par l'amplitude du décrochement que provoque leur apparition.

Il paraît logique alors de considérer que ces paliers sont le résultat d'une compétition entre la précipitation continue de ces produits d'hydratation et la dissolution du CA. Ces paliers sont d'ailleurs d'autant plus hauts, que la dissolution de la préparation considérée est plus rapide. La nature cinétique de ces paliers est encore confirmée par leur forme de maximum aplati que nous observons au cours de ces mesures en continu.

Il semble donc que la conception du mécanisme d'hydratation proposé (7) pour le sulfate de calcium puisse s'appliquer dans ses grandes lignes à l'aluminate monocalcique.

L'adjonction de chaux vive CaO (6,16) provoque des effets analogues à l'ajout de $C_{12}A_7$ (bien que pour des quantités différentes), ce qui peut laisser supposer que le rôle accélérateur du $C_{12}A_7$ dans l'hydratation du CA est dû au passage préférentiel du $C_{12}A_7$ en solution. En particulier, le phénomène transitoire (d'amplitude très marquée) que le $C_{12}A_7$ présente lorsqu'il est pur, dès son premier contact avec l'eau (cf. Figure 2b) pourrait s'expliquer précisément par un rapport stoechiométrique en solution chaux/alumine nettement supérieur à 1.

CONCLUSION GENERALE

L'introduction de la technique expérimentale de conductimétrie en tant que méthode de suivi de la réaction d'hydratation permet de progresser dans la connaissance du mécanisme d'hydratation de l'aluminate monocalcique. La réactivité des préparations d'aluminate monocalcique dépend essentiellement de leur composition minéralogique ; c'est à dire des quantités résiduelles des autres aluminates CA_2 ou $C_{12}A_7$ qu'elles contiennent. Avec les prises d'essais contenant du $C_{12}A_7$ (soit qu'il ait été formé lors de la synthèse, soit qu'il ait été ajouté), on observe sur les courbes

VOL. 14 1984

de conductivité, un décrochement avant l'établissement du palier de sursaturation. Cette "irrégularité" met en évidence, là encore, la précipitation d'un hydrate dès les premiers instants de la réaction d'hydratation. L'établissement postérieur du palier de sursaturation laisse penser que ce dernier est lui-même dû à la compétition entre la précipitation de ces produits d'hydratation et la dissolution de l'anhydre. La nature cinétique de ces paliers est confirmée par l'allure des courbes de conductivité pour des préparations d'aluminate monocalcique de réactivité croissante. Une augmentation de la cinétique de dissolution entraîne une élévation de la conductivité de la solution et un raccourcissement de la durée du palier de sursaturation.

La conception du mécanisme d'hydratation proposé pour le sulfate de calcium (7) s'applique donc, dans ses grandes lignes, à l'hydratation de l'aluminate monocalcique.

BIBLIOGRAPHIE

1. L.S.WELLS, E.T.CARLSON, J.Res.Nat.Bur.Stand.,57,6,R.P.2723(1956)

2. D.MENETRIER, Thèse, Dijon (1977)

3. D.BERTRANDIE, Thèse, Dijon (1977)

4. P.BARRET,D.MENETRIER,D.BERTRANDIE, Cem.Concret.Res.4,545,(1974)

5. P.BARRET,D.MENETRIER,D.BERTRANDIE, Cem.Concret.Res.,4,723,(1974)

6. P.BARRET,D.BERTRANDIE,C.R.Acad.Sc.Paris, 288, 106, 291(1979)

7. P.GALTIER,M.SOUSTELLE,B.GUILHOT, Cem.Concret.Res. 13, 703(1983)

8. P.J.BALDOCK,A.PARKER,I.SLADDIN,J.Appl.Cryst.3,188,(1970)

9. W.HÖRKNER,H.K.MÜLLER-BUSCHBAUM,J.Inorg.Nucl.Chem.38,983,(1976)

10. B.AUDOUZE,Thèse Clermont-Ferrand (1958)

11. W.DE KEYSER,Bull.Soc.Chim.Belg.60,516, (1951)

12. E.CALVET,H.PRAT,"Récents Progrès en Microcalorimétrie", Monographie DUNOD N°6 (1956)

13. M.DE TOURNADRE, Thèse, Marseille (1964)

14. M. COURNIL, Thèse, Grenoble, 1980

15. P.LONGUET, Communication au XXIVe Congrès International de Chimie Industrielle, Bruxelles (1952)

16. P.GALTIER, Thèse, St-Etienne, 1981

17. P.GALTIER, B.GUILHOT,M.MURAT,A.BACHIORRINI,A.NEGRO,7e Congrès International de Chimie des Ciments, Paris, 1980, Septima, vol II, pII-214

OL.
14
984

CEMENT and CONCRETE RESEARCH. Vol. 14, pp. 686-692, 1984. Printed in the USA.
0008/8846/84 $3.00+00. Copyright (C) 1984 Pergamon Press, Ltd.

EFFECT OF SO_3 ON FORMATION AND HYDRAULIC REACTIVITY OF BELITE

B. Ziemer and B. Altrichter
Central Institute of Inorganic Chemistry
Academy of Sciences of the GDR
1199 Berlin, Rudower Chaussee 5, Czechoslovakia

V. Jesenak
Chair of Chemical Technology of Silicates
TH Bratislava, CS-81243 Bratislava, Janska 1,

(Communicated by W. Wieker)
(Received Dec. 19, 1983; in final form May 23, 1984)

VOL. 14 1984

ABSTRACT

SO_3 accelerates the formation of belite between 1100 and 1300°C. Its efficiency rests on the permanent generation of CaO in statu nascendi by the equilibria $CaSO_4 \rightleftarrows CaO + SO_3$ and $SO_3 \rightleftarrows SO_2 + 1/2\ O_2$. Via the gaseous phase this CaO is transported to SiO_2 and reacts there to belite. Only 0.5 - 1.5% SO_3 are dissolved in belite stabilizing its β-modification, but without increasing the hydraulic reactivity markedly.

Introduction

In the past ten years various investigations have been carried out using SO_3 as a mineralizing agent for clinker burning and as an ingredient for producing new types of cement. Odler and Abdul-Maula (1) studied the effect of SO_3 on lime conversion and found an acceleration up to 1300°C. Wächtler (2) observed a decreased oil consumption when SO_3 is present in quantities adapted to the alkali content.

Starting from iron-rich raw materials and $CaSO_4$ ($C\bar{S}$), Metha (3) invented a hydraulic cement of the approximate phase composition of 35% belite, 30% C_4AF, 20% $C_4A_3\bar{S}$ and 15% $C\bar{S}$ (belite = C_2S containing foreign oxides in solid solution). Although alite is missing, the attainable strength parameters are comparable to those of portland cement. Alite is also missing in porsal cement developed by Viswanathan et al. (4), which has a phase composition of 50-60% belite, 10-20% $C_4A_3\bar{S}$, 5-20% CA and 0-20% $C_{12}A_7$. The good hardening properties of this cement are accompanied by a high sulfate resistance.

Because belite is the main constituent in these two cements and in the active belite cement proposed by Stark, et al. (5), we thought it would be useful to study the influence of SO_3 on the formation and the hydraulic reactivity of belite without other phases being present.

Formation of Belite

Specimens of four different series were burnt:

A : without $C\bar{S}$ in the raw mixture and in a normal atmosphere,
A' : without $C\bar{S}$ in the raw mixture and in a stream of dried air,
B : with 5% $C\bar{S}$ in the raw mixture and in a normal atmosphere,
C : without $C\bar{S}$ in the raw mixture and in a dried stream of 99 vol.% air and 1 vol.% SO_2.

The raw mixture prepared from calcite, aerosil, boehmite, goethite, periclase, orthoclase and albite had the composition of the average belite in portland cement clinker $Ca_{87}MgAlFeNa_{1/2}K_{1/2}(Al_3Si_4O_{18})$ analysed by Yamaguchi (6). After burning the pressed mixtures at 1000-1400°C for various times, the degree of reaction was determined from the CaO conversion (series A and B) or from the SiO_2 conversion (series A' and C).

Figures 1-3 show the mineralizing effect of SO_3. The DTA curves in Fig. 4 express it also by shifting the belite formation peak I from 1320 down to 1200°C. The DTG curve B reveals a mass loss beginning above 1100°C. This indicates the decomposition of $C\bar{S}$ and the transition of SO_3 into the gaseous phase. It is remarkable that beginning from this temperature, a higher reaction degree of series B compared to series A becomes visible in Fig. 1.

From high temperature Guinier photographs of samples during heating up to 1200°C and from Guinier photographs of samples quenched after heating, it could be seen that in addition to the major phase belite, other phases were also formed:

A : CS (950-1100°C),
B : CS (950-1100°C, $C_5S_2\bar{S}$ (1050-1250°C), $C_4A_3\bar{S}$ (1050-1350°C) and remaining $C\bar{S}$ (up to 1300°C),
C : CS and $C\bar{S}$ (both up to 1300°C) and $C_4A_3\bar{S}$ (up to 1350°C).

In the series C, the $C\bar{S}$ contents varied with temperature, e.g. from nearly 15% at 1177°C to only traces at 1300°C, and $C_5S_2\bar{S}$ was not surely detected. The latter might be explained by the dry atmosphere, in which the samples were burnt and in which, according to Pliego-Cuervo and Glasser (7), no $C_5S_2\bar{S}$ will be formed,

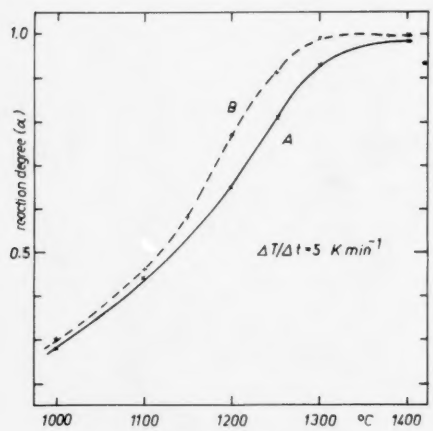

FIG. 1

SO_3-effect as f(T), A : without $C\bar{S}$, B : with $C\bar{S}$, D(raw) = 2.35Mg/m^3

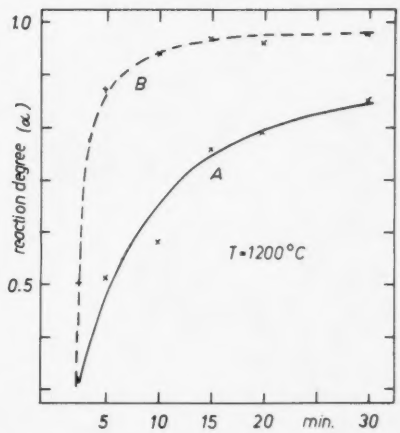

FIG. 2

SO_3-effect at 1200°C, A : without $C\bar{S}$, B : with $C\bar{S}$, D(raw) = 2.35 Mg/m^3

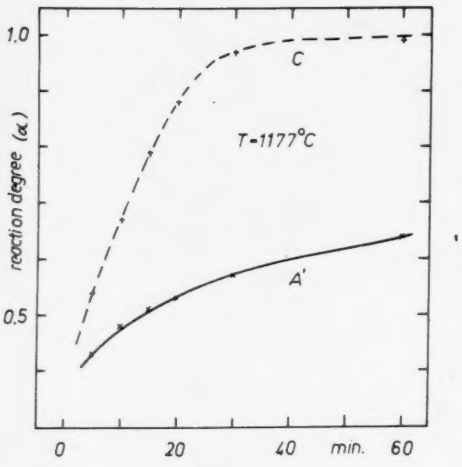

FIG. 3

SO_3-effect at 1177°C, A' : without SO_2, C : with SO_2, D(raw) = 1.72Mg/m^3

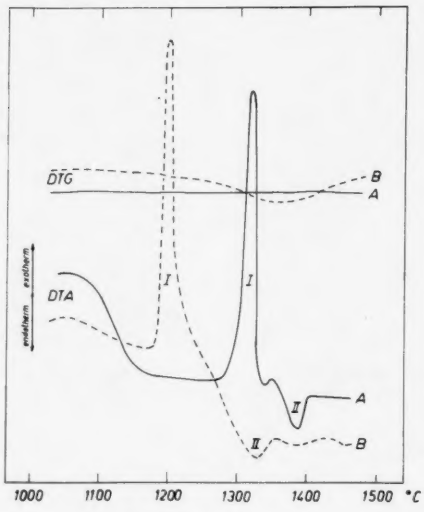

FIG. 4

DTA/DTG curves of the raw mixtures A and B.

VOL. 14 1984

but C_2S and $C\bar{S}$ are co-existing under these conditions. In order to elucidate the action mechanism of the SO_3 mineralizer, a test developed by Sharp, et al. (8) was applied. This tests decides whether the diffusion of the reactants to each other, D(α), the phase boundary reaction, R(α), or the nucleation and the growing of the product phase, A(α), is the rate controlling step in a solid state reaction. For all α-values of Fig. 2, the reduced times $t/t_{0.5}$ ($t_{0.5}$ is the time for 50% reaction) were calculated and faced to Sharp's theoretical values in Table 1.

Table 1

Experimental Data of α and $t/t_{0.5}$ Opposed to the Theoretical Values of D(α), R(α) and A(α)

α	$t/t_{0.5}$-values of				
	series A (without SO_3)	series B (with SO_3)	D(α) (theoretical values)	R(α)	A(α)
0.40	0.68	n.d.	0.60	0.76	0.90
0.50	1.0	1.0	1.0	1.0	1.0
0.60	1.50	1.17	1.54	1.28	1.10
0.70	2.23	1.33	2.30	1.61	1.20
0.80	3.59	1.61	3.38	2.01	1.32
0.85	5.63	1.80	4.12	2.27	1.40
0.90	n.d.	2.70	5.03	2.60	1.49
0.95	n.d.	4.60	6.30	3.06	1.63

A comparison of the columns "series A" and "D(α)" indicates that the belite formation reaction is a diffusion controlled one. From this, it follows that the rate increasing effect of SO_3 must rest on the acceleration of the transport of the major reactants CaO and SiO_2 to each other (for discussing "series B", see later).

Two ideas about the action mechanism of SO_3 arose from the preceding results which had to be examined by further experiments:

1. This mechanism is based on the decomposition of $C\bar{S}$ above 1100°C. After decomposition, SO_3 might be incorporated into the lattice of the growing Ca_2SiO_4 crystals. When $(SiO_4)^{4-}$ units are partially substituted by $(SO_4)^{2-}$, vacancies in the Ca sublattice result, which makes the Ca^{2+} diffusion through the reaction layer easier. That SO_3 is really incorporated could be guessed from the downwards shift of the $\alpha' \rightarrow \alpha$ transition peak II in Fig. 4, and it was finally detected by electron probe micro analysis (EPMA). The measured SO_3 contents given in Fig. 5 indicate that 0.6% is taken up by α'-C_2S, i.e. in the effective temperature range of SO_3, only 0.6% vacant sites are created in the Ca sublattice. Because this small ratio of vacancies cannot explain the intense SO_3 effect satisfactorily, another mechanism was looked for.

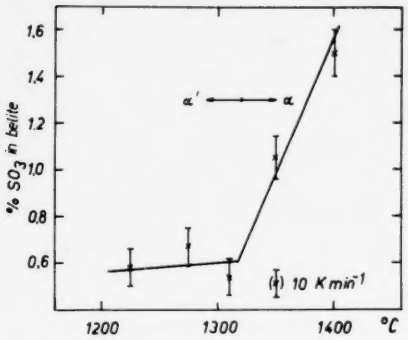

FIG. 5

SO_3 contents in quenched belites; the "10K min^{-1}" value stands for a slowly cooled belite.

2. This mechanism bases on the simultaneous decomposition and formation of $C\bar{S}$ between 1100 and 1300°C. From this, it follows that between those temperatures all reactants of the equilibria $CaSO_4 \rightleftarrows CaO + SO_3$ and $SO_3 \rightleftarrows SO_2 + 1/2\ O_2$ are present, which means a permanent formation of CaO in statu nascendi. This CaO might easily evaporate and react with SiO_2. This assumption was tested by a simple experiment. The two pairs, $CaCO_3$-tablet/quartz-disc, and ($3CaCO_3$ + $1CaSO_4$)-tablet/quartz-disc, were slowly (and simultaneously) heated up to 1300°C. The partners in both pairs were separated by a 250 µm thick platinum sheet with a 1 mm hole in its center. The succeeding EPMA revealed that only in the presence of $C\bar{S}$, calcium silicates are formed on the quartz surface, cf. Fig. 6.

Including CaO, which comes from the decomposition of $CaCO_3$ and SiO_2, the SO_3 effect for the formation of Ca_2SiO_4 can be summarized by the following reaction scheme:

$$CaCO_3 \xrightarrow{<1000°C} CaO_{solid} + CO_2$$

$$SO_2 + 1/2\ O_2 \rightleftarrows SO_3 \rightarrow CaSO_4 \xrightarrow{>1100°C} SO_3 + CaO_{vapour}$$

$$1/2\ SiO_2 \longrightarrow 1/2\ Ca_2SiO_4$$

By assuming a CaO vapour pressure of 1.0 Pa at 1200°C, an estimation according to equation (k) in Schäfer (9) makes evident that all the CaO in our samples is transported along a distance of 25 µm during half an hour. From this estimation and the good accordance with the results of Odler and Abdul-Maula, this action mechanism of SO_3 seems more likely than the first one. Another aspect which supports this mechanism is that the values of series B in Table 1 deviate distinctly from those of series A and $D(\alpha)$. This possibly indicates a shift of the Jander-reaction type towards a more complex one (an overlapping of $A(\alpha)$ below α=0.8 and $D(\alpha)$ above α=0.8) due to the change from a "through solid phases" reaction to a "via gaseous phase" reaction.

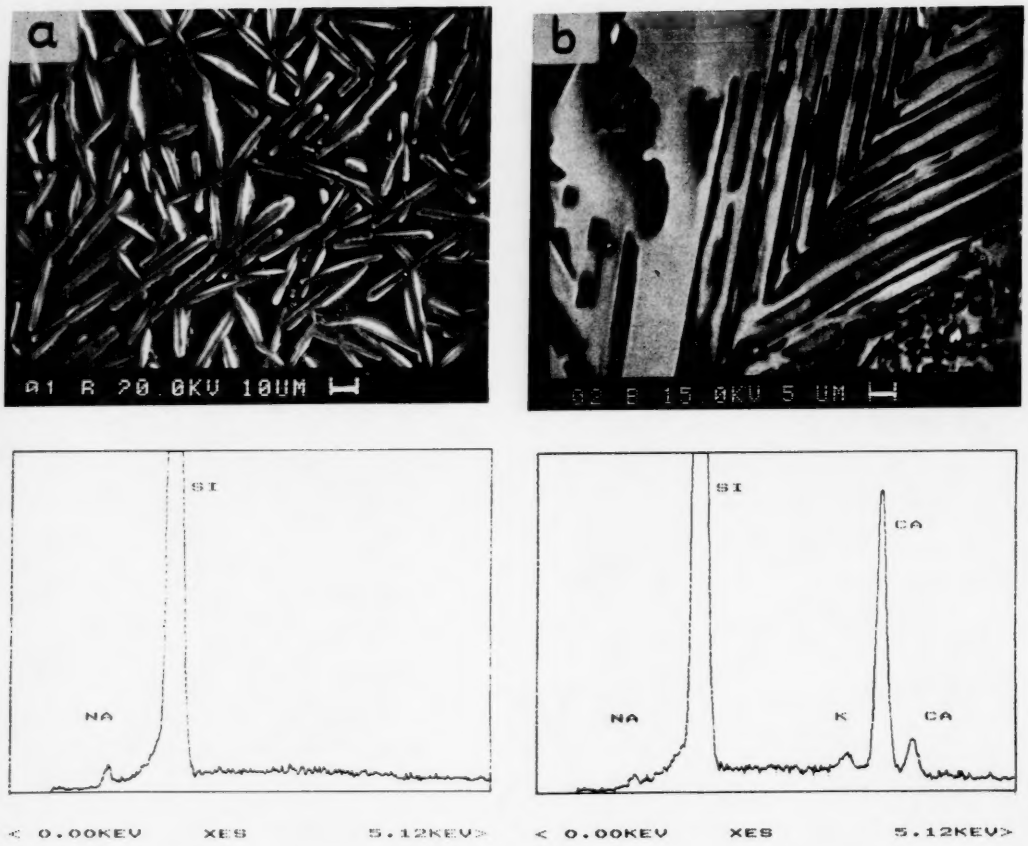

FIG. 6

The reaction of CaO with SiO_2

a) without SO_3: only formation of cristobalite (top) takes place on quartz, Ca is not detectable in EDS (bottom)

b) with SO_3: formation of calcium silicates (top, bright areas) takes place on quartz, Ca is detectable in EDS (bottom)

Na and K come from pollutions in $CaCO_3$ and $CaSO_4$, respectively.

Hydraulic Reactivity of Belite

All belites studied were synthesized in the stability range of the α-C_2S modification. The addition of $C\bar{S}$ to the raw mixture, the burning in a SO_2 containing atmosphere or the quenching of the samples alone keep the belites stable in the β-modification after cooling down to room temperature. But slowly cooled belites without SO_3 in solid solution dust to inactive γ-C_2S and lie, thus, outside of any consideration with respect to hydraulic reactivity. The other specimens were ground to a specific surface of 300 m^2/kg, mixed with alite for blends of 75% belite + 25% alite and were hydrated in pastes with w/c = 0.5 at 20°C.

During the first three days the heat of hydration was measured by means of differential calorimetry (10). After ten days the hydration was stopped by treating the samples with isopropanole and acetone, and the degree of hydration

VOL. 14 1984

Table 2

Data of Hydraulic Reactivity

phase	burning temperature in °C	cooling rate in K/min	heat of hydration in J/g after 1	24	72h	degree of hydration after 10d
β-belite	1430	1000	14	39	135	0.09
β-belite (1.0% SO_3)	1350	1000	23	38	74	0.28
β-belite (0.5% SO_3)	1350	20	27	57	71	0.20
alite, MII	1430	1000	12 (3)	176 (44)	300 (75)	0.96

The chemical composition of alite corresponds to the average alite analysed by Yamaguchi (6). The values in parentheses represent the alite portion of the heat of hydration.
The relatively high heat of hydration after one hour hydration time in the SO_3-containing specimens might be caused by the small amount of $C_4A_3\bar{S}$.

was determined by X-ray diffraction from the unreacted parts of belite and alite. The obtained values are summarized in Table 2.

From Table 2, it can be seen that

- alite hydrates much more rapidly than belite corresponding to the analogue results published by Odler and Schüppstuhl (11) who studied the combined hydration of C_3S and β-C_2S.
- belite with SO_3 in solid solution is maintained as β-C_2S at room temperature independent on the cooling rate. In the cements developed by Metha (3) and Viswanathan et al. (4), belite is also found to be in the β-modification.
- SO_3 retards the belite hydration during the first three days, but accelerates it slightly after that period.
- a rapid cooling increases the hydraulic reactivity. But this effect is less significant here, than for active belite cement (5) or for BaO-containing C_2S (12), where the α'-modification was maintained after rapid cooling.

From these results it can be concluded that belite is not the dominant phase which makes those special cements (3,4) so reactive, but rather phases such as $C_4A_3\bar{S}$, $C\bar{S}$, CA, $C_{12}A_7$ and C_4AF or their combined hydration including belite.

Acknowledgement

We are indebted to Z. Hrabe and K.H. Jost for helpful discussions, and thank Z. Hrabe, M. Dubik and G. Oliew for their assistance during the experimental works.

References

1. I. Odler and S. Abdul-Maula, Zement-Kalk-Gips 33, 132 (1980).
2. H.J. Wächtler, Silikattechnik 31, 7 (1980).
3. K. Metha, U.S. Patent 4,036,657 (1977) C04B 7/02.
4. V.N. Viswanathan, S.J. Raina and A.K. Chatterjee, World Cement Technology 9, 109 (1978).

5. J. Stark, A. Müller, R. Schrader, K. Rümpler and B. Dahm, Silikattechnik 30, 357 (1979).
6. G. Yamaguchi and S. Takagi, Proceedings Vth Int. Symp. Cement Chemistry, Tokyo 1968, Part I, p. 181.
7. Y.B. Pliego-Cuervo and F.P. Glasser, Cem. Concr. Res. 8, 455 (1978).
8. H.J. Sharp, G.W. Brindley and B.N. Achar, J. Am. Ceram. Soc. 49, 379 (1966).
9. H. Schäfer, Chemische Transportreaktionen, p. 29, Verlag Chemie, Weinheim (1962).
10. G. Oliew and W. Wieker, Silikattechnik 32, 152 (1981).
11. I. Odler and J. Schüppstuhl, Cem. Concr. Res. 12, 13 (1982).
12. B. Ziemer and G. Oliew, Silikattechnik 33, 176 (1982).

VOL.
14
1984

CEMENT and CONCRETE RESEARCH. Vol. 14, pp. 693-704, 1984. Printed in the USA.
0008-8846/84 $3.00+00. Copyright (c) 1984 Pergamon Press, Ltd.

HIGH STRENGTH MORTARS CONTAINING CONDENSED SILICA FUME

M.Buil, A.M.Paillère, B.Roussel
Laboratoire Central des Ponts et Chaussées
58, Bd Lefebvre 75015 PARIS, France

(Communicated by M. Regourd)
(Received Dec. 15, 1983)

ABSTRACT

A silica fume and a superplasticizer have been added to an ordinary easily flowing mortar composition. The optimal amounts of those constituents have been determined in order to obtain the maximum compressive strength for a constant workability. Large contents of silica fume and superplasticizer are needed (silica/cement=0.40 and superplasticizer/cement=2.4% in dry weights). The compressive strengths are approximately twice higher at 2,7 and 28 days as compared to the reference mortar. The drying shrinkage is slightly increased and the hydration kinetics is highly modified.

Introduction

The use of condensed silica fume has been the subject of several recent studies, in particular in the nordic countries which are important producers of this industrial by-product (1-6). It has led to the definition of a new technique for achieving high strength concretes, given by Bache (2). An amount of ultrafine particles, for example ten to a hundred times smaller than the average size of the cement particles, is added to the concrete mix in order to fill the spaces between the cement grains. The water/cement ratio is thus decreased, resulting in large mechanical strength increases. Condensed silica fumes seem very well suited for this purpose owing to their very small size (B.E.T. specific surface= 10 to 25 m^2/g) and their spherical shape.

In practice, it is necessary to prevent the coagulation of the silica particles by the calcium ions released by the cement. Superplasticizers appeared to be effective dispersing agents for the silica fume-cement system (2). A supplementary effect for strength improvement comes from the generally high pozzolanicity of silica fume (1,4,7-10). So the use of large quantities of silica fume added to the concrete mix with a superplasticizer has allowed the achievement of easily flowing concretes of low water/cement ratios (0.20 to 0.30) and very high strengths (110 to 160 MPa in compressive tests on cast cylinders 10 cm x 20 cm at 28 days with ordinary aggregates (2)).

The first aim of the present work was to evaluate the highest strength increase attainable with an easily flowing mortar using ordinary sand and cement by addition of a silica fume and a superplasticizer. It was also decided

to evaluate the possible shrinkage increases that we could expect owing to the shrinkage increase generally observed either by fine particles addition or by superplasticizing admixtures addition. A second aim was to get more informations about the physico-chemical interactions in the cement-silica fume-superplasticizer system.

Experimental

Experimental program

In order to limit the extent of the experimental work, only one type of each constituent of the mortars has been used i.e. : one silica fume (noted SF), one superplasticizer (SP) and one ordinary composition of mortar were choosen. Silica fume and superplasticizer were simply added to the mortar mix, without any modification of the other contents. This provided a basis for testing the hypothesis according which the principal granular effect of silica fume is a filling of the spaces between the cement grains. The optimal amounts of SF and SP were determined using a workability test in order to obtain the lowest W/C at constant workability (15s $\pm$ 5s = easily flowing mortar). The strengths of themortars containing SF and SP were compared to the reference mortar. The hydration kinetics of the cement-SF-SP system was studied by isothermal calorimetry.

Materials

a) Cement. The cement used is an ordinary Portland cement. BSS=3000 cm^2/g, the chemical analysis and the Bogue potential composition are shown in table 1 and table 2.

TABLE 1

Chemical analysis of cement (%)

CaO	SiO_2	Al_2O_3	Fe_2O_3	MgO	Na_2O	K_2O	SO_3	L.O.I.
63.60	20.40	5.28	1.81	0.75	0.10	0.40	3.36	0.90

TABLE 2

Bogue potential composition (%)

C_3S	C_2S	C_3A	C_4AF	$C\bar{S}.2H$	$CaCO_3$	free lime
44.9	24.6	IO.9	5.5	7.2	2.0	1.7

b) Condensed silica fume (SF). The silica used is a by-product of the zirconia fabrication.

The chemical analysis is shown in table 3.

FIG. 1 shows the granulometric curve obtained by sedimentometry in water. The silica suspension was dispersed by ultra-sound and measurements were made with a Sedigraph 5000 from Micromeritics.

c) Superplasticizer (SP). The admixture choosen for this study is a sodium naphtalene sulfonate formaldehyde condensate in aqueous solution (dry weight : 41 %). The amounts of this admixture are given in dry weight in this study,

VOL. 14 1984

TABLE 3

Chemical analysis of silica fume (%)

SiO_2	Fe_2O_3	ZrO_2	Al_2O_3	Na_2O	CaO	L.O.I.	humidity
94.5	0.25	1.30	3.40	0.16	0.10	0.40	0.22

B.E.T. specific surface : 17.0 ± 0.3 m^2/g

FIG. 1

Granulometric curve of silica fume

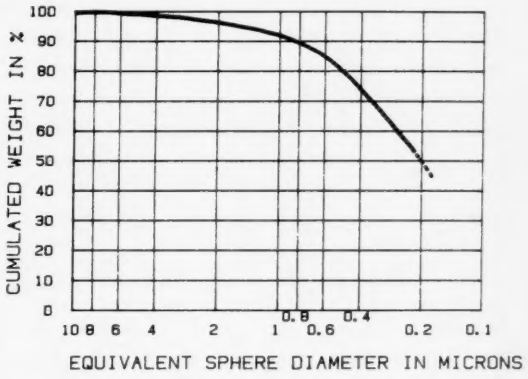

the water content of the superplaticizer is taken into account in the total water content of the mortars. The superplasticizer was added to the water before mixing the mortars.

d) Sand. Siliceous sand, granularity according to the french standard P 15-403.

TABLE 4

Equivalent diameter (mm)	› 0.08	› 0.16	› 0.50	› 1.00	› 1.60	› 2.00
%	98 ± 2	88 ± 5	67 ± 5	33 ± 5	5 ± 5	0

e) Mortars. A standard sand to cement ratio of 3 was choosen. The mixing procedure was in conformity with the standards P 15-403 and P 15-411 excepted for the mixing time increased from 2 x 2 mn to 3 x 2 mn at high speed. Silica fume was added premixed with the cement.

Mechanical tests

a) Workability measurements were performed with a "maniabilimetre LCL" described in the standard P 18-452. This device measures the flow time between two reference marks for a mortar sample flowing in a vibrating box.

b) Compressive and flexural strengths were measured on 4 x 4 x 16 cm prisms kept at 20° c ± 1°c and 90 % ± 5 RH until testing (standard P 15-451).

c) Drying shrinkage was measured on 4 x 4 x 16 cm prisms kept at 20°c ± 1°c and 50 % ± 5 R.H. (P 15-433).

Physico-chemical tests

a) Adsorption measurements. Suspensions of SF (5g/l) in aqueous solutions of superplasticizer (0.04 to 0.40 g/l) and lime (I g/l) were stirred during 1 hour at 20° C. The suspensions were centrifugated and the amount of adsorbed superplasticizer was determined by measuring the concentration remaining in solution by UV spectrophotometry.

b) Isothermal calorimetry. The heat evolutions of pastes during hydration were recorded with an isothermal conduction calorimeter (designed by CERILH, (11)). The cells contain 40 g of cement ; water is injected into the cells when complete thermal equilibrium is reached. A mixing device permits a short mixing inside the cells.

Results and discussion

Determination of the optimal SP and SF contents

a) Adsorption of SP by SF.

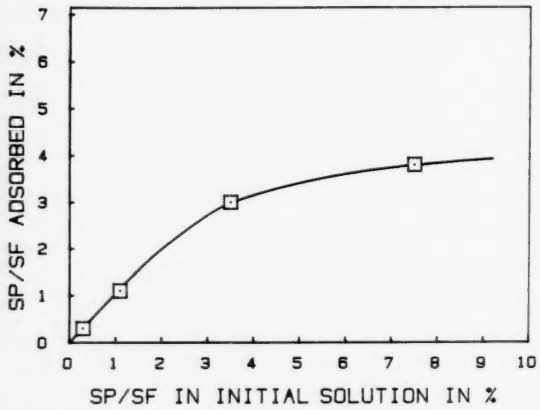

FIG.2

Adsorption of SP by SF

FIG.2 shows the quantities of SP adsorbed by SF dispersed in lime water (1 g/l) as a function of the quantities of SP in solution before adsorption.

SF is saturated at approximately SP/SF = 4 %. This value is not far from a rough estimate of the weight of a monomolecular film covering the surface of the particles. Taking for SP a density d = I.7, a molecular weight MW : 1 700 g (according to the manufacturer) and a specific surface SS : I7.0 $m^2.g^{-1}$, assuming a cubic elementary volume, the weight of the monomolecular layer of SP is, for I g of silica :

$$1.7.\left\{\frac{1.700}{1.7.\ 10^3.\ 6.023.\ 10^{23}}\right\}^{\frac{1}{3}}.\ 17.0.10^3 = 23.10^{-5}\text{kg/g silica}$$

$$= 0.034\ \text{g/g silica}$$

or $\frac{SP}{SF} = 3.4\ \%$

b) Determination of the SP content by the workability test. Two sets of workability measurements were carried out with two silica/cement ratios SF/C : 0.30 and 0.40. The water to cement ratio was determined as a function of the ratio SP/SF (from 0 % to I0 %) with a constant workability of 15 s

VOL. 14 1984

± 5 s. The results are on Fig 3. When the SP/SF ratio increases until approximately 6 %, the W/C ratio decreases sharply. Beyond 6 %, this decrease is much less significant. This figure was taken as the optimal value for SP/SF. It is higher than the saturating amount of SP determined in a) (4 %). We may suppose that the difference (SP/SF = 2 %) is adsorbed on the cement particles.

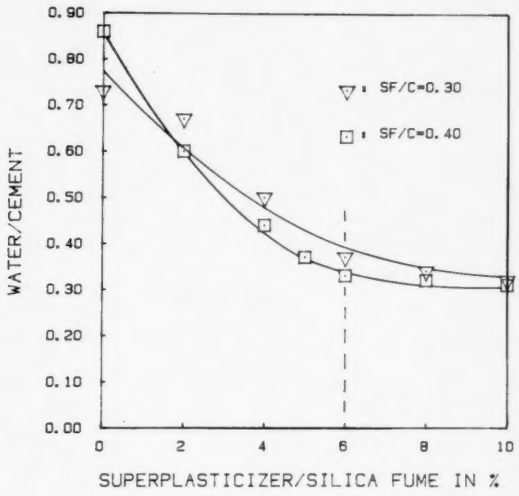

FIG.3

W/C vs. SP/SF at constant workability (15 s ± 5 s) and SF/C=0.30 and 0.40

c) Determination of the SF content. Another set of workability measurements was made at a constant SP/SF = 6 % and varying SF/C (from 0.20 to 0.60). Fig 4 shows the W/C versus the SF/C at constant workability of 15 s ± 5 s. A minimum appears for approximately SF/C = 0.40, this has been taken as the optimum ratio.

In conclusion, the optimal composition was assumed to be : SF/C = 0.40, SP/SF = 0.06 giving W/C = 0.34 for a workability of 15 s.

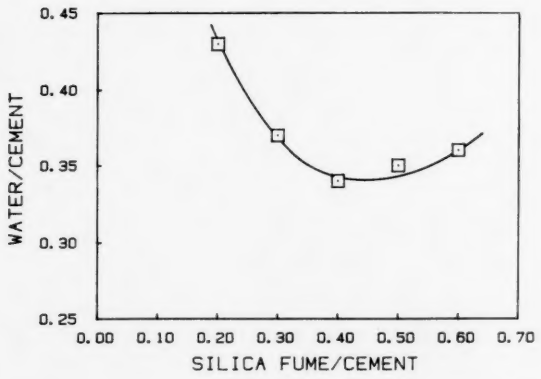

FIG. 4

W/C versus SF/C at constant workability (15 s ± 5 s)

This water reduction does not fit with the water reduction that we should have attained if the cement intergranular spaces of the reference mortar were simply filled with SF. As a matter of fact, the total volume of wa-

ter+silica + air ($V_W + V_{SF} + V_A$) should be equal to the volume of water + air ($V'_W + V'_A$) of the reference mortar. On the basis of the results previously given, we may assume that 2 % out of the 6 % SP/SF ratio is adsorbed by the cement, therefore we should consider a reference mortar containing SP with a ratio SP/C = 2 x 0.4 = 0.8 %. For a workability of 15 s ± 5 s, the W/C ratio of this reference mortar is 0.41. Air content measurements showed no difference between the optimal mortar and this reference mortar (air entrained = 5 %). So we can calculate a partial porosity

$$p' = \frac{V_W + V_{SF}}{C} = 0.52 \text{ cm}^3.\text{g}^{-1}$$ to be compared to $$p'r = \frac{V'_W}{C} = 0.41 \text{ cm}^3.\text{g}^{-1}$$

for the reference. This discrepancy could be explained partially by the fact that the ultrafine particles increase the viscosity of the interstitial phase filling the cement intergranular spaces, thus at constant workability we could expect an increase of the water content in comparison with the quantity just needed by a partial replacement of water by ultrafine particles. But we can also suggest an interference effect between the biggest silica particles and the smallest cement particles. We cannot assess the relative importance of those two effects.

Mechanical properties of the mortars.

a) Strength measurements. Two series of strength measurements were made at constant workability (15 s ± 5 s) :

1) at constant SF/C (0.40) and varying SP/SF (from 0 to 10 %, Fig. 5)

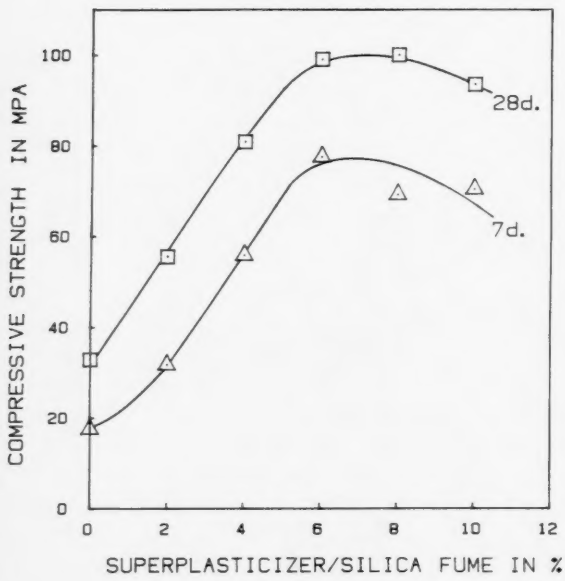

FIG. 5

Compressive strength vs. SP/SF at 7 days and 28 days.

2) at constant SP/SF (6 %) and varying SF/C (0.20 to 0.60, Fig. 6)

The results confirmed that the composition designed for obtained the lowest W/C ratio at constant workability (SF/C : 0.40, SP/SF : 6 %) gives also the highest strengths. Table 5 shows the different mortar compositions prepared for comparison with the optimal composition (n° 1).

VOL. 14 1984

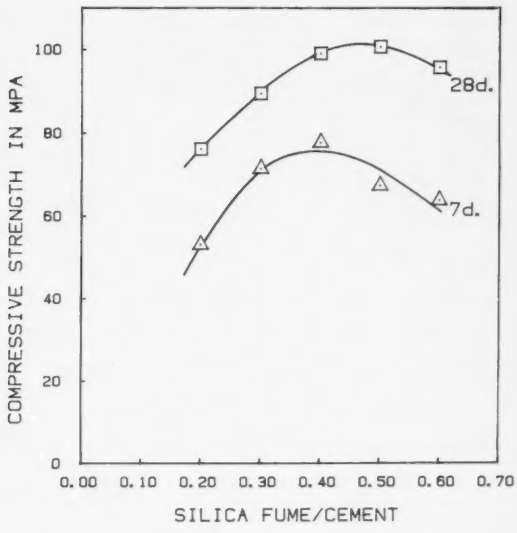

FIG. 6

Compressive strength vs. SF/C at 7 days and 28 days

TABLE 5

Characteristics of the mortars prepared for mechanical tests

mortar number	SP/C (%)	SF/C	W/C
1	2.4	0.40	0.34
2	2.4	0	0.37
3	2.4	0.40	0.37
4	0.8	0	0.41
5	2.4	0.40	0.41
6	0	0	0.485

The sample n° 2 contains the same SP/C ratio as n° 1 with no SF and a W/C giving the same workability as n° 1. Sample n° 3 contains the same SP/C and SF/C as the optimal composition and the same W/C as n° 2 in order to get a comparison at constant W/C with and without SF. Sample n° 4 contains no SF and a SP/C equivalent to the ratio assumed to be adsorbed by the cement in sample n° 1 (see section III : I.a). Sample n° 5 contains SF and has the same W/C as n° 4. Sample n° 6 is the reference sample without SP nor SF with a W/C giving a workability of 15 s.

Table 6 gives the results of the compressive and flexural tests at 2, 7 and 28 days.

We notice a very large compressive strength increase for mortar 1 compared to reference 6 : approximately 100 % for the three hydration times (2 d, 7 d, 28 d). The comparison between mortars 2 and 3 and between 4 and 5 shows the existence of a supplementary effect of strength increase, not due to the water reduction brought by SF and possibly explained by the pozzolanic effect of SF (this point should be assessed by more precise porosity studies). The flexural strengths are improved in a lesser amount by SF addition.

TABLE 6

Flexural and compressive strengths (S_f and S_c) in MPa

mortar number	2 days		7 days		28 days	
	S_f	S_c	S_f	S_c	S_f	S_c
1	8.9	46.8	11.2	77.5	14.5	99.0
2	7.5	38.1	10.0	53.6	9.4	63.0
3	-	-	11.3	72.5	12.6	91.8
4	-	-	7.6	46.7	9.6	52.4
5	-	-	8.4	58.7	11.2	80.7
6	5.8	24.9	7.3	39.1	7.6	50.0

b) Drying shrinkage. Fig. 7 gives the drying shrinkage of the mortar compositions n° 1 - 2 - 6 of table 1.

We observe only a slight increase of the shrinkage of the mortar containing SF and SP (n° 1) compared to the reference mortar n° 6. But this shrinkage is much smaller than that induced by the addition of SP alone (n°2).

Isothermal calorimetry

The different mixes prepared for the heat evolution measurements are given in table 7. The tests were made at 25.0°C.

Fig. 8 shows the heat evolution of the cement - SF mixes (samples C1-C2-C3-C4). We observe an increase of the height of the second peak (C_3S peak) and an acceleration and a sharp increase of the third peak (C_3A peak) as the percentage of silica increases. DTA carried out on the hydration products has shown that the silica used in our study is highly pozzolanic, so the increase of the maximum C_3S hydration rate is certainly due to this pozzolanic effect as it has already been observed on other pozzolanic materials (12).

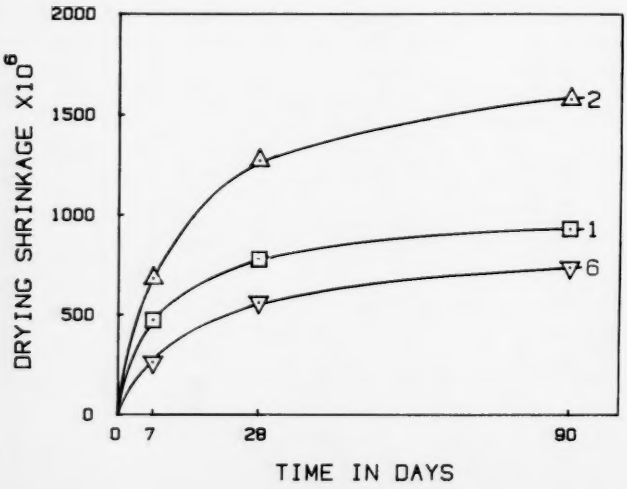

FIG. 7

Drying shrinkage vs. time for mortar compositions 1,2 and 6.

VOL. 14 1984

TABLE 7

Characteristics of cement - SF - SP mixes prepared for isothermal calorimetry

Sample		SF/C	SP/C (%)	W/C
(reference)	C1	0	0	1.00
Cement + SF	C2	0.05	0	1.00 *
	C3	0.10	0	1.00
	C4	0.40	0	1.00
(reference)	C5	0	0	0.50
Cement + SP	C6	0	0.8	0.50 *
	C7	0	1.2	0.50
	C8	0	1.6	0.50
	C9	0	2.4	0.50
	C10	0	3.2	0.50
Cement + SF + SP	C11	0.40	0.8	1.00
	C12	0.40	1.6	1.00
	C13	0.40	2.4	1.00
	C14	0.40	3.2	1.00

* higher W/C (1.00 instead of 0,50) were necessary for a homogeneous mixing inside the calorimeter cells when using cement - SF mixes.

The acceleration of the third peak may be attributed to an acceleration of the rate of formation of ettringite caused by a decrease of the calcium hydroxide concentration. Such an effect has already been reported for amorphous silica - Portland cement mixes (13) and also for pure components systems (C_3A, gypsum, lime) (14).

Fig.9 gives the heat evolution of the cement for different SP percentages (C5-C6-C7-C8-C9-C10). We observe a reduction and a retardation of the

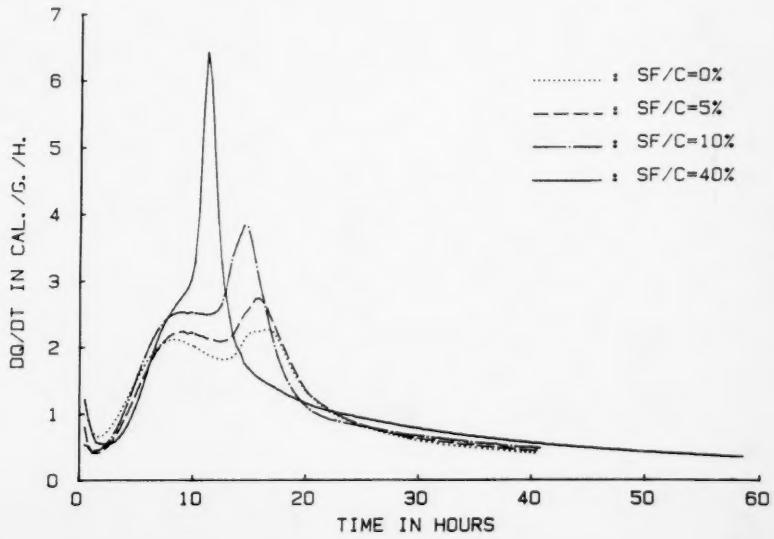

FIG. 8

Heat evolution curves of samples C1-C2-C3-C4.

C_3S peak and also a retardation of the C_3A peak but to a lesser extent so that the two peaks are getting closer to each other as the SP amount increases.

Fig.10 shows the combined effect of SF and SP (C11-C12-C13-C14) for a constant ratio SF/C : 0,40 and varying amounts of SP.

The transformation of the heat curve of the cement-SF mix for increasing amounts of SP seems to be qualitatively the same as in the case of the cement alone : we observe a retardation of the C_3S and C_3A peaks, but to a lesser extent for the C_3A peak so that the two peaks are superimposed for a ratio SP/C higher than 1.6 %.

An interesting point appears concerning the length of this retardation : for the same SP/C ratios, the retardation of the principal peak of the cement-SF mix becomes very significantly increased as compared to the cement alone, when the ratio SP/C is higher than 1.6 %. We suggest an hypothesis for explaining this increased C_3S retardation on the basis of few preliminary chemical tests which have shown that calcium ions and SP form a complex in aqueous solution thus increasing the calcium hydroxide solubility, and that this complex is adsorbed on SF. Thus,in the case of the cement-SF-SP mixes, we have the superimposition of those two effects : an adsorption on SF of the calcium ions released by the cement particles and an increased solubility of calcium hydroxide (when the SP content is higher than the saturating amount for complete coverage of the SF surface so that SP is also present in solution). This could explain,for high SP percentages, an increase of the length of the induction period of the C_3S hydration in the cement-SP-SF mix as compared to the cement-SP mix by increasing the amount of calcium ions released by C_3S before reaching the critical supersaturation degree in calcium hydroxide of the interstitial solution.

Conclusion

1. This study has shown that the addition of silica fume in large quantities in mortars (SF/C=0.40) needs a large amount of superplasticizer (SP/SF = 6 % in dry weight) in order to achieve very high strengths.

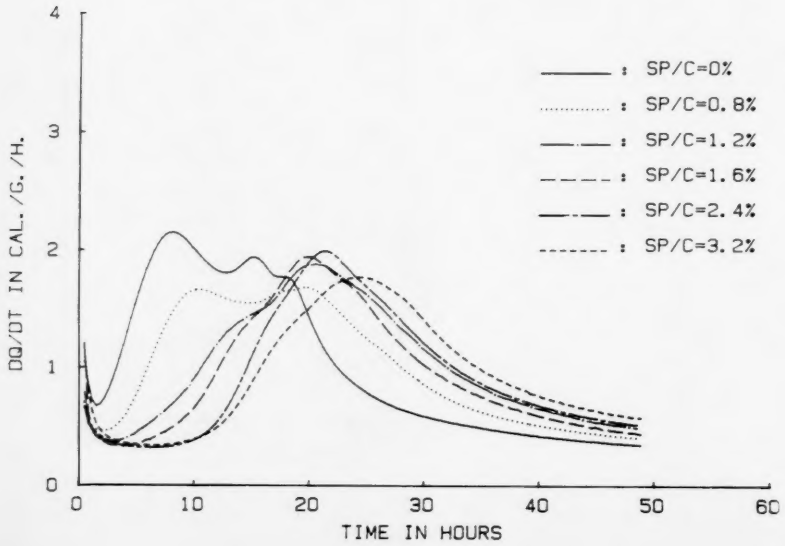

FIG. 9

Heat evolution curves of samples C5-C6-C7-C8-C9-C10-

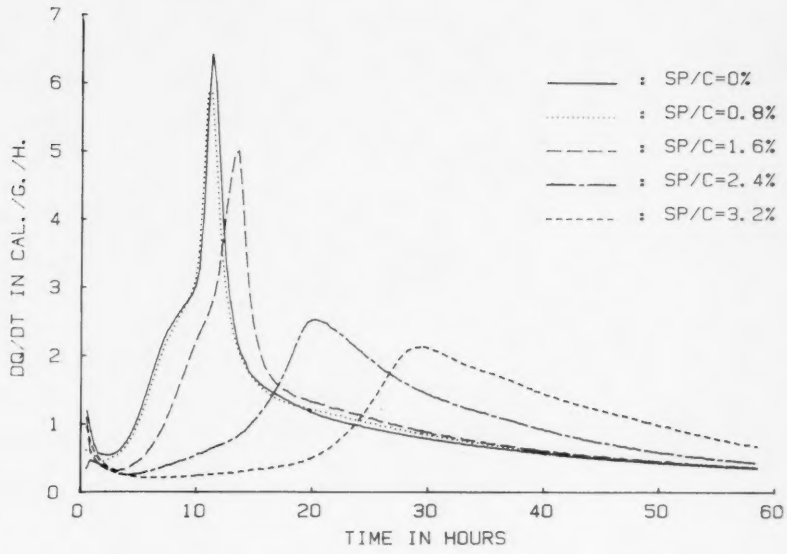

FIG.10

Heat evolution curves of samples C11-C12-C13-C14-

2. The compressive strengths are very significantly increased (about twice higher at 2,7,28 d) for ordinary easily flowing mortars.

3. The drying shrinkage is only slightly increased.

4. The hydration kinetics of the cement is highly modified by the addition of the silica fume and superplasticizer used in this study (retardation of the principal peak in isothermal calorimetry). More studies are needed on that subject, in particular the influence of temperature and nature of the components : cement, silica fume, superplasticizer. The interference effect between the respective granulometries of cement and silica should also clearly be assessed in order to define the most suited characteristics of the cement for this type of mix.

In view of pratical applications, date are needed on the influence of the mixing procedures and the aging of silica fume (for example in a premix composition with cement).

Acknowledgements

The authors are indebted to P. WITIER and M. DETREZ for helpful suggestions and assistance concerning the chemical aspects of this study.

References

1. A. Traetteberg, Il Cemento 3, 369-375 (1978).
2. H.H. Bache, Proc. 2nd Int. Conf. on Superplasticizers in Concrete, Ottawa, June 1981.
3. P.C. Aitcin, P. Pinsonneault, G. Rau, Mater. Res. Soc., annual meeting, Boston, Nov. 1981.
4. E.J. Sellevold, D.H. Bager, E. Klitgaard, T. Knudsen, Nordisk Miniseminar on silica in concrete, Dec. 1981.
5. K.E. Loland, O.E. Gjorv, Nordisk Betong, 6, 5-10 (1981).
6. L. Hjorth, Nordic Concrete Research publ. n° 1, Oslo, Dec. 1982.
7. H. Asgeirsson, G. Gudmunsson, Cem. Concr. Res. 9, 249-252 (1979).
8. M. Regourd, B. Mortureux, E. Gautier, 5th Int. Symp. on Concrete Technology, Monterrey, Mexico, March 1981.

9. V.M. Malhotra, G.G. Carette, Construction, 27, n° 5, 443-6 (1982).
10. E. Gautier, Revue des Matér., 677, 17-27 (1973).
11. M. W. Grutzeck, D.M. Roy, D. Wolfe-Confer, Proc. 4th Int. Conf. on Cement Microscopy, Las Vegas, March 28-April 1, 1982.
12. K. Takemoto, H. Uchikawa, Proc. 7th Int. Symp. on Chemistry of Cement, Paris, Vol. I, IV.2 (1980).
13. H.N. Stein, J.M. Stevels, J. Appl. Chem., 14, 338-356 (1964).
14. A. Bonin, G. Cariou, Proc. 7th Int. Symp. on Chemistry of Cement, Paris, Vol. III, V-158 (1980).

VOL.
14
1984

CEMENT and CONCRETE RESEARCH. Vol. 14, pp. 705-716, 1984. Printed in the USA.
0008-8846/84 $3.00+00. Copyright (c) 1984 Pergamon Press, Ltd.

ASSESSMENT OF ELASTIC MODULUS OF CONCRETE AND ITS INFLUENCE ON STRUCTURAL DESIGN

G. Pascale and A. Di Leo
Institute of Scienza delle Costruzioni
University of Bologna (Italy)

(Communicated by F. Massazza)
(Received Jan. 10, 1984)

ABSTRACT

The present work reports the results of an experimental research on the correlation between the modulus of elasticity and the compressive stregth of concrete, which considerably disagrees with the indications provided for by some bodies of rules. The influence on structural design is then assessed by means of simple examples.

Signification of fundamental symbols used

R_c, f_c = cubic and cylindric compressive strength $N \cdot mm^{-2}$;
$\bar{R}_c$ = mean value of R_c;
R_{ck}, f_{ck} = characteristic values of R_c and f_c respectively;
E_c = modulus of elasticity $N \cdot mm^{-2}$;
E_o, E_d, E_s = initial tengent, dynamic and static modulus of elasticity respectively $N \cdot mm^{-2}$;
$\bar{E}_s$ = mean value of E_s;
s = standard deviation;
C_v = coefficient of variation;
f = frequency density;
e = percent error of experimental results with regard to the proposed correlation;
d = deflection of mideline cross-section mm;
g_σ = critical load $N \cdot m^{-1}$;
σ_s = normal stress for steel $N \cdot mm^{-2}$.

Introduction

The definition of the elastic modulus for concretes is not univocal, since concrete has a mainly visco-elastic behaviour. The experimental procedures existing in the different countries provide for the determination of both the initial tangent modulus of the stress-strain diagram E_o and the secant modulus E_s. The former can be determined by means of vibration methods [1, 2], the latter by tests with compressive static loading on the basis of test methods, according to which

unloading and reloading cycles between pre-established stress levels are carried out in order to remove the viscous component from the strain measure [3, 4].

For design purposes, the static modulus E_s is to be considered in order to estimate the strain and displacement elastic components of reinforced and prestressed concrete structures, as provided for by the different national codes. In accordance with these codes, on the other hand, it is possible to estimate the value of the modulus to be assumed in computations on the basis of correlations with the cubic R_c or cylindrical f_c compressive strengths.

On principle, a correlation between these two quantities is not justified by the existence of a physical connection, the former being an elastic parameter, the latter a crushing parameter. The effort to determine empiric correlations is due to purely technical needs by structural designers, who demand a prediction criterion of the value of the elastic modulus with an approximation suitable for the purpose. At present, several proposals for the form of the most suitable correlation have been advanced [6, 8, 12]. Apart from the ambiguity due to the introduction of strenght mean or characteristic values into such correlations, they are generally of the linear type with the square root of the compressive strength: the proportionality coefficient proposed is generally comprised between 5600 and 6600 for quantities expressed in $N \cdot mm^{-2}$. According to many investigators [5, 6], such correlations lead to estimate the value of the modulus upwards, so that one may think that they refer to the tangent modulus E_0 instead of the secant modulus E_s. The Italian Technical Specifications currently in force (M.D. 26/3/1980), for instance, in accordance with the Specifications CEB/FIP 1972, suggest the use of the relation:

$$E_c = 5700\sqrt{R_{ck}} \tag{1}$$

The most recent Model Code CEB/FIP 1978 reports the relation:

$$E_c = 9500\,(f_{ck} + 8)^{1/3} \cong 8820\,(R_{ck} + 10)^{1/3}\ ;\quad R_{ck} = 1.25\,f_{ck} \tag{2}$$

which differs from the previous one not only in the form, but also because it leads to considerably lower values (Fig. 3). The relations similar to Eq. (1) are generally based on the acceptance of the characteristic stress-strain diagram provided for by the above-mentioned specifications CEB/FIP 1972. The following relation is similar in the form to Eq. (1), but is based on experience [7]:

$$E_c = 4700\sqrt{f_c} \cong 4200\sqrt{R_c}\ ;\quad R_c = 1.25\,f_c \tag{3}$$

It is proposed by the ACI Building Code 1971 [8]. This relation, however, cannot be directly compared with the previous ones, since it contains the mean value of the compressive strength instead of the characteristic value. The use of the different correlations proposed implies assessments of the static modulus of elasticity which remarkably differ one another, a fact that may be quite important for design purposes.

The aim of this work is to check the reliability of the correlations proposed as well as to assess the influence of a wrong choice of the value of the elastic modulus on structural design by means of simple examples. On the basis of the indications provided by a previous work [9], the investigation has also been extended to thermally-treated concretes, since some national codes do not allow the above-mentioned relations to be used in the case of steam-cured concretes.

Experimental programme

The concrete used to cast the specimens was taken from casts performed in a precasting factory producing pieces of prestressed concrete. The nominal mix proportions per cubic metre were as follows: 187 kg of fine sand (10 per cent), 561 kg of coarse sand (32 per cent), 468 kg of crushed limestone 6 ÷ 9 mm (26 per cent), 561 kg of crushed limestone 12 ÷ 17 mm (32 per cent), 200 l of water, 400 kg of Portland cement 525 and superplasticizer admixture (1.5 per cent).

VOL. 14 1984

These mix proportions were kept constant in all samples, apart from the variations typical of the concrete mixing plant and supplies. This choice, if on one hand has meant to work only with one kind of concrete, on the other hand has made it possible to consider all the causes of variability existing when using concrete. Moreover, it should be kept in mind that, in order to assess the characteristic and mean values of the quantities in exam, a sufficiently sized sampling of homogeneous material is required, so that extending the investigation to other kinds of concrete would have meant making the experimental programme too onerous. It should be noted, on the other hand, that the characteristics of the concrete used are substantially similar to those of the concretes generally used when casting prestressed pieces.

36 samples were drawn in about one year and a half. Each of them was composed of 12 prismatic specimens (15 x 15 x 45 cm) and 24 cubic specimens (15 x 15 x 15). Half of them underwent a heat treatment together with the structural elements realized with the same cast. They were then, together with the others, air-cured, i.e. treated by exposure to air at an even temperature and humidity inside the laboratory. The tests, for both types of curing, were carried out at the ages of 14 and 28 days, 3 and 6 months, 1 and 2 years. The quantities experimentally assessed are:

- cubic compressive strength R_c according to UNI 6132-72;
- secant static modulus of elasticity of concrete in compression E_s and prismatic compressive strength R_p according to UNI 6556-76;
- longitudinal velocity of ultrasonic pulses V_L according to BS 4408: Part 5: 1974 and relative dynamic modulus of elasticity E_d according to the indications provided for by the Recommendation RILEM [10].

On the basis of some preliminary tests, it was possible to ascertain that the values of the static modulus determined according to the test methods proposed by UNI 6556-76, practically coincide with those determined according to the Recommendation RILEM CPC 8-1975.

Analysis and discussion of the experimental results

In the Table 1 the test results relative to the quantities measured R_c, E_s and E_d are summarized. The statistical parameters are reported for each set of data. On the basis of the table, it is possible to have an idea of both the changes in time and the distribution of the quantities represented. It is to be noted that, although the characteristic strength is defined only for tests carried out on specimens 28 day aged, in this work the characteristic strength was calculated also for other ages, in order to correlate it with the elastic modulus at different ages (Model Code CEB/FIP, 2.5.2). The values of the coefficient of variation C_v of the compressive strength, about 10 per cent, reflect the substantial homogeneity of the concrete used, thus justifying the statistical processing performed. A comparison between the values of the coefficient of variation of the elastic modulus points out a remarkable difference between the values C_v for the static modulus and those for the dynamic one: the values of the latter are approximately half as high as those of the former. This is a consequence of the fact that the dynamic modulus was assessed on the basis of the velocity of ultrasonic pulses which reveals a remarkably lower dispersion with respect to the mechanical properties which can be correlated to it, that is the compressive strength and the modulus of elasticity. It is also influenced by parameters different from those which most contribute to change the mechanical characteristics. This is further pointed out by the curves of Fig. 1, which were obtained by fitting the points representing the mean values of the quantities measured at different ages with respect to the correspondig points after 28 days of curing. The considerable decrease in time concerning the dynamic modulus thus determined, in accordance with the results obtained by other authors [11], can be imputed to the influence of the loss of water on the velocity of ultrasonic

Table 1
Statistic parameters of R_s, E_s and E_d

		AIR CURING						STEAM CURING					
	AGE [days]	14	28	90	180	365	730	14	28	90	180	365	730
Cubic compressive strength	n	36	36	35	36	36	36	36	36	35	36	36	36
	R_c [N · mm^{-2}]	49.3	52.6	56.6	58.1	58.6	58.2	47.8	51.8	55.1	57.9	58.0	58.9
	s [N · mm^{-2}]	4.9	4.8	6.1	5.3	5.8	5.8	5.7	5.3	5.3	6.0	6.3	6.4
	R_{ck} [N · mm^{-2}]	41.2	44.8	46.6	49.4	49.0	48.6	38.5	43.0	46.4	48.0	47.9	48.4
	C_v [%]	10.0	9.2	10.8	9.1	10.0	10.0	11.8	10.3	9.6	10.4	10.6	10.8
Static modulus of elasticity	n	35	35	35	36	36	35	35	35	34	36	36	36
	E_s [N · mm^{-2}]	26125	27086	28518	29315	29263	29449	25438	26811	27841	28675	28998	28694
	s [N · mm^{-2}]	2824	3285	2716	3219	3295	3118	2765	2844	2736	2775	3207	2785
	C_v [%]	10.8	12.1	9.5	11.0	11.2	10.6	10.9	10.6	9.8	9.7	11.0	9.7
Dynamic modulus of elasticity	n	28	29	34	35	35	34	28	29	33	35	35	35
	E_d [N · mm^{-2}]	38114	38688	38609	38360	37106	35478	36024	36575	36754	36624	36223	34027
	s [N · mm^{-2}]	2054	2118	2221	2267	2594	2016	2094	2462	2549	2641	2574	2228
	C_v [%]	5.4	5.5	5.8	5.9	7.0	5.7	5.8	6.7	6.9	7.2	7.1	6.5

VOL. 14 1984

pulses. The relative decrement of the steam-cured specimens is lower, and this may be explained by the fact that, for such specimens, a more considerable loss of water takes place already during the cooling phase of the thermal cycle, as can be seen by comparing the values shown in Table 1. This influence, on the other hand, is not exerted on the values of the static modulus (Fig. 1).

The static modulus of elasticity E_s and the compressive strength R_c, on the contrary, can be correlated, as it can be deduced from the curves of the figure 1. On the basis of the experimental results obtained, the most suitable correlations have proved to be those of the form $E_s = K\sqrt{R_c}$ or $E_s = a(R_c + b)^{1/3}$, which, on the other hand, provide similar evaluations.

By the relations (1), (2) and (3) it may be noted that the mean value of the elastic modulus is related either to the mean value of the strength or to the characteristic value. The results of the present work have been analyzed so as to obtain information on both procedures. The value of the numerical coefficient K of the relation between the mean values of the elastic modulus and the compressive strength has been assessed at each age of curing for both steam curing and air curing (Table 2) by regression according to the method of least squares.

Considering that the values of K remain substantially constant, a global re-processing of the data available was decided. The correlation obtained is represented in Fig. 2, together with the corresponding confidence limits at 90 per cent, and is compared with Eq. (3), homogeneous in the form, of the A.C.I. Building Code - 1971. In Table 2 the values of the coefficient K′ of the correlation between the mean value of the elastic modulus and the characteristic value of the compressive strength are also reported. Such values have been fitted (Fig. 3) on the basis of a correlation of the form of Eq. (1). By way of comparison, in Fig. 3 are also reported Eq. (1) and (2). As far as the latter is concerned, the best-fit curve, to which it is formally homogeneous, of the experimental data obtained was also assessed. An analysis of the data reported in Table 2 and in Fig. 2 and 3 leads to the following considerations:

a) in Fig. 3 it is shown that the experimental vaues of the elastic modulus are considerably lower than those assessable on the basis of relations (1) and (2), with differences which cannot be accepted at time of design, as illustrated in the following paragraph;

b) from the same figure, it may be noted that such differences are not due to the form of the

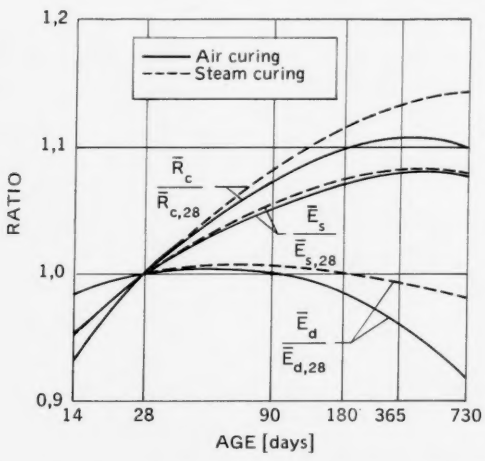

Fig. 1 - Ratio of the mechanical properties versus time.

Table 2

Values of the coefficients K and K′ of the correlations between the mean value of the static modulus of elasticity and the mean and characteristic values of the square root of the compressive strength.

$E_s = K\sqrt{R_c}$		$\bar{E}_s = K'\sqrt{R_{ck}}$		
AGE	AIR CURING		STEAM CURING	
days	k	k′	k	k′
14	3724	4071	3706	4098
28	3727	4046	3732	4086
90	3797	4178	3754	4088
180	3855	4208	3781	4136
365	3827	4179	3822	4192
730	3854	4223	3747	4123

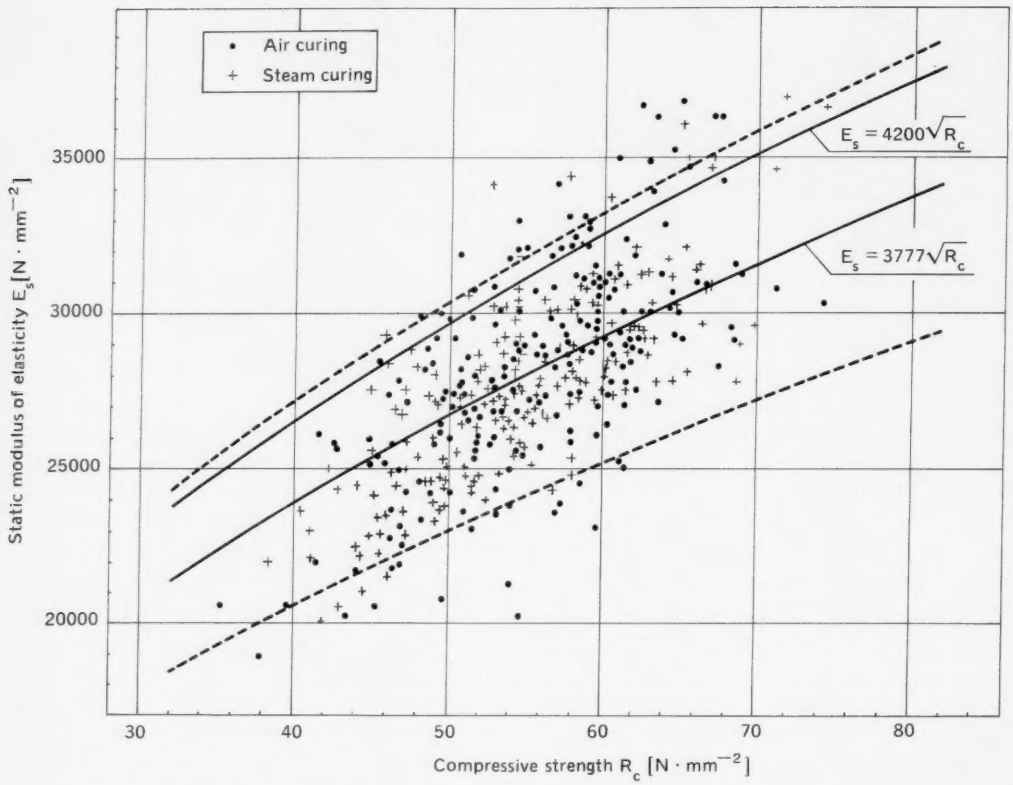

Fig. 2 - Correlation obtained and corresponding confidence limits at 90 per cent compared with the one proposed by the A.C.I. Building Code 1971.

correlation, but rather to the values of the numerical constants contained in Eq. (1) and (2);
c) in Fig. 2, on the contrary, it is shown that the values of the modulus obtained with the present research can be compared with those assessable on the basis of Eq. (3) for technical purposes. A comparison with the results recently obtained by other investigators [5, 20] would lead to the same considerations;

d) on the basis of the results of this research together with the results obtained by other authors [5, 7] who have worked on concretes with different mix proportions and in other strength ranges, it may be adfirmed that the assumption of a value of $K \simeq 4000$ is suitable for tecnical purposes, admitting a difference of about ± 15 per cent in the real value with regard to the estimated value (Fig. 4). This may be true for concretes which, as for mix proportions and maximum size of the aggregate, can be considered normal concretes;

e) on the basis of the results obtained, we disagree with the discrimination done by some bodies of rules in adopting a correlation between the elastic modulus and the compressive strength for steam-cured concretes. In this regard, the only condition to be verified is that all the phases of the thermal cycle are suitably designed, so as not to damage the concrete structure [9].

VOL. 14 1984

Influence of the value of the elastic modulus of concrete on structural design

As a completion of the present work, some significant examples are reported in this paragraph in order to point out the importance of a suitable assessment of the elastic modulus of concrete to be considered in structural design. We don't mean by this to treat the subject in an exhaustive way, which would deserve to be treated separately. Anyway, even without referring to complicated examples, however widely studied in several treatises [13, 14], the analysis of simple structural problems recurring in applied engineering may here suffice.

Generally speaking, it may be adfirmed that a suitable assumption of the value of the elastic modulus of concrete is very important when it is of technical interest to predict displacements

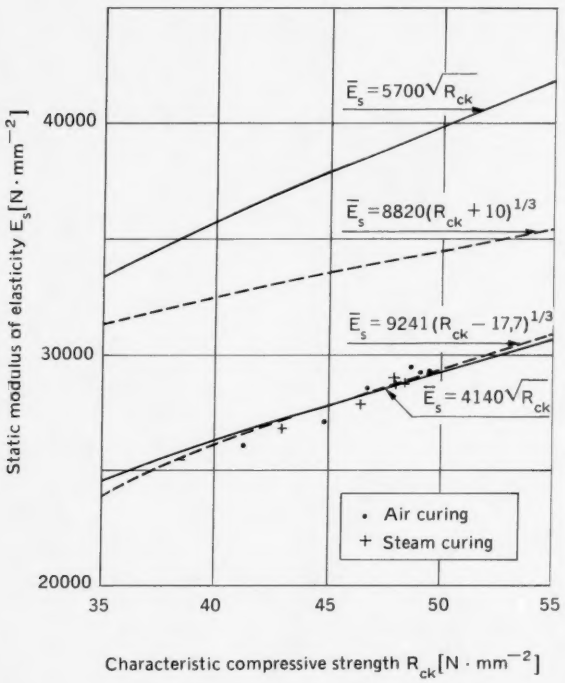

Fig. 3 - Correlations proposed by the M.D. 26/3/80 and by the Model Codel CEB/FIP 1978 in comparison with the formally analogous ones fitting the experimental values.

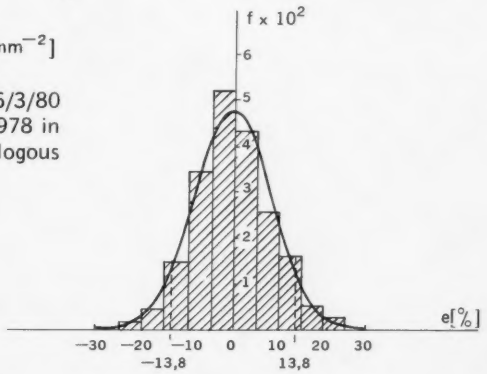

Fig. 4 - Histogram and normal distribution function of the frequency density of the error of the experimental data with regard to the correlation of Fig. 2 and corresponding confidence interval at 90 per cent.

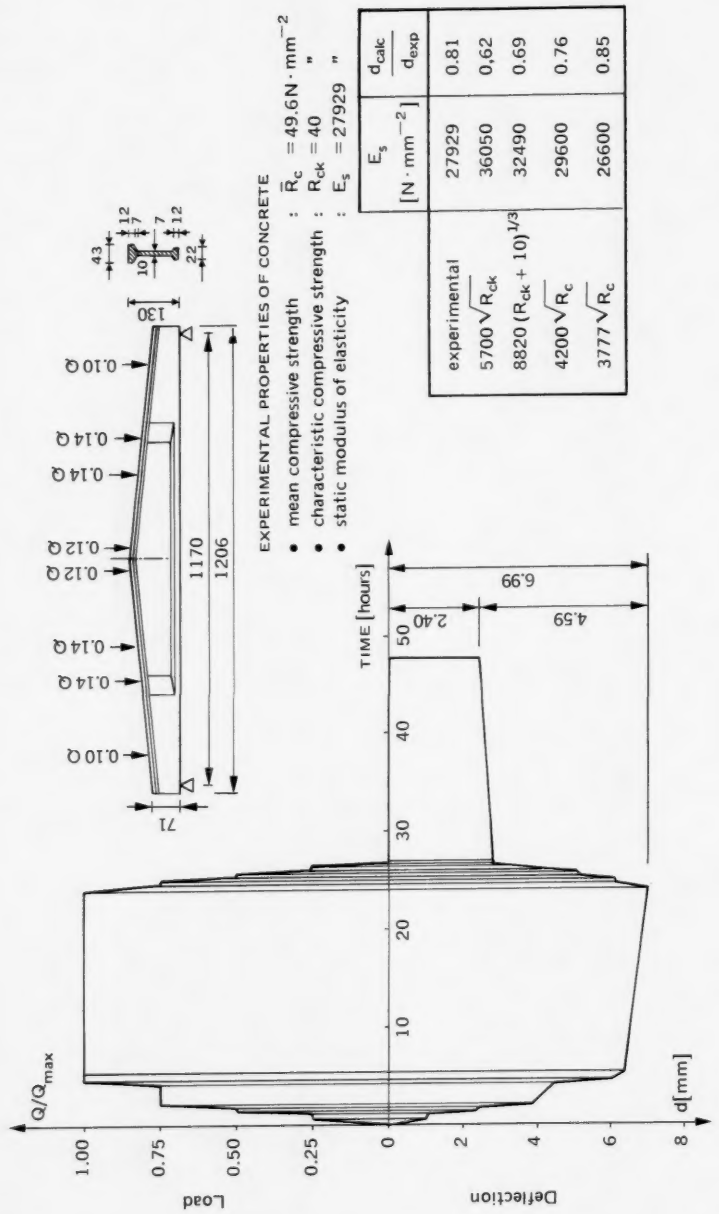

Fig. 5 - Loading test on a reinforced concrete double tafered beam.

VOL. 14 1984

and/or strains so as to carry out compliance, stability and strength tests. To this purpose, three structural examples are reported in the following. The first one refers to the load-deflection link of a reinforced concrete precast double lean-to beam and is intended to check the experimental results obtained by means of a load test. The other two examples, the former referring to a combined torsional and flexural buckling, the latter to a strength test, aim at pointing out the consequences of an unsuitable assessment of the elastic modulus of concrete.

1st example: reinforced concrete double lean-to beam (Fig. 5).

The example refers to a load test carried out according to the static arrangement illustrated in the figure and in conformity with the methods provided for by the Temporary Specification RILEM proposed by the 20-TBS Committee Testing Building Structures In Situ [15]. The mechanical properties of concrete determined on samples drawn when casting the beam are also reported in the figure. The maximum value Q_{max} of the test load rechead corresponds to that of the service load. The table reported, together with the figure, permits us to compare the value of the elastic modulus determined experimentally with the values assessable by means of the relations reported in the table. On the basis of such values, we have reported the ratio of the corresponding calculated values of the mideline deflection to the value determined experimentally - from which the downward displacements at the supports have already been eliminated-which can be deduced from the diagram obtained.

By comparing the values of the elastic modulus, it may be noted that the value of the modulus of the concrete of which the beam is made (27929 $N \cdot mm^{-2}$) is substantially consistent with the values assessed on the basis of the relations proposed by A.C.I. (29600 $N \cdot mm^{-2}$) and by the authors (26600 $N \cdot mm^{-2}$): the variations are included in the estimate ranges reported in Fig. 2. The assessment upwards consequent to the indication provided for by the M.D. 26/3/80 (36050 $N \cdot mm^{-2}$), which is not acceptable for design purposes, is confirmed. Consequently, a comparison between the expected compliances leads to the same considerations.

2nd example: prestressed concrete bridge beam being temporarily lifted (Fig. 6).

For this kind of structural elements, considering their limited stiffness to lateral deflection, a combined torsional and flexural stability test should be carried out during the lifting and transport phases, during which the beam, which is subject to its own weight, is hooked by means of a suitable equalizing rocker arm in two symmetrical points, generally next to the extrados. The critical load can assessed [6] by the relation:

$$g_{cr} = \frac{1}{\alpha} \frac{EI_y}{\ell^4} e$$

e being the eccentricity, i.e. the distance of the lifting point from the centre of gravity G of the cross-section (in this case, e = 83 cm), and α a coefficient depending on the parameter c. As for the case in exam, ℓ = 16.25 m, we have reported in the graph of Fig. 6 the link between the critical load and the static modulus of elasticity with regard to two lifting configurations including the ones generally used. The most delicate phase is obviously the lifting of the form to be taken to the storage place, where concrete is left to cure for a period lower than 24 hours. As far as this phase is concerned, the mechanical characteristics of the concrete of which the beam was made were the following ones [16, 17]: $R_c = 39.8\ N \cdot mm^{-2}$ and $R_{ck} = 35.7\ N \cdot mm^{-2}$ assessed during the current production. Corrispondingly, the modulus of elasticity can be assessed according to the relation provided for by the Model Code CEB/FIP ($E_s = 8820\ (R_{ck} + 10)^{1/3} = 31534\ N \cdot mm^{-2}$) and the one proposed by the authors ($E_s = 3777 \sqrt{R_c} = 23828\ N \cdot mm^{-2}$). The values of g_{cr} for both configurations considered are reported in the graph of Fig. 6. Comparing the first relation with the second one, a considerable reduction ($\simeq$ 25 per cent) in the safety factor g_{cr}/g may be noted, g being equal, in this case, to 8300 $N \cdot m^{-1}$, up to values lower than 2.

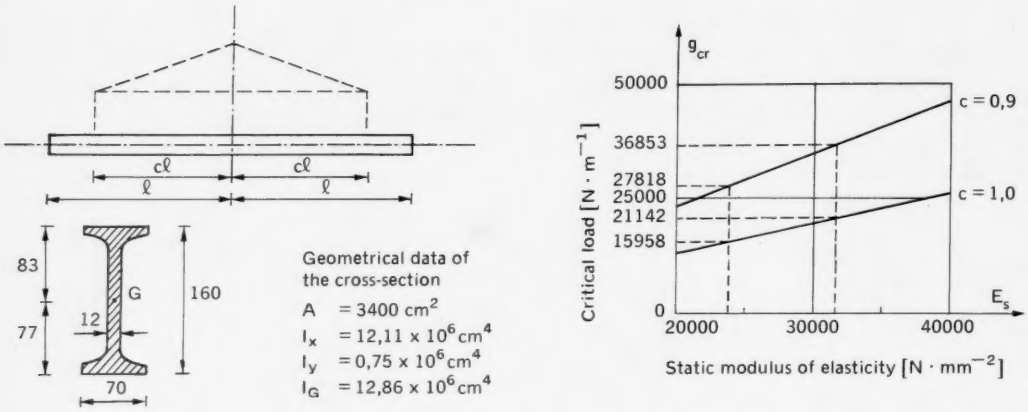

Fig. 6 - Prestressed concrete bridge beam being lifted

3rd example: steel-concrete bridge beam (Fig. 7).

The safety check of such beams can be carried out, provided that the sections remain plane, by means of the homogenized section method [13, 14], with regard to the initial time $t = t_0$ and the final time $t = \infty$ [18, 19]. Referring to the section of Fig. 7, the stress state according to the values of the elastic modulus of concrete assessed on the basis of the value $R_{ck} = 30\ N \cdot mm^{-2}$ using the relation provided for by the Model Code CEB/FIP and the one proposed by the authors, was calculated. In order to compute the stresses at time $t = \infty$, a coefficient of viscosity $\varphi(t_\infty, t_0) = 3$ was adopted. The comparison points out the non-verification of steel stresses in the stressed region using the value of the modulus assessed by the authors ($\sigma_s = -161.8\ N \cdot mm^{-2}$) as against the positive result ($\sigma_s = -132.0\ N \cdot mm^{-2}$) on the basis of the indications of the Model Code CEB/FIP.

Final considerations

The main results obtained with this research consist in pointing out, first of all, that the correlations between modulus of elasticity and compressive strength of concrete provided for by

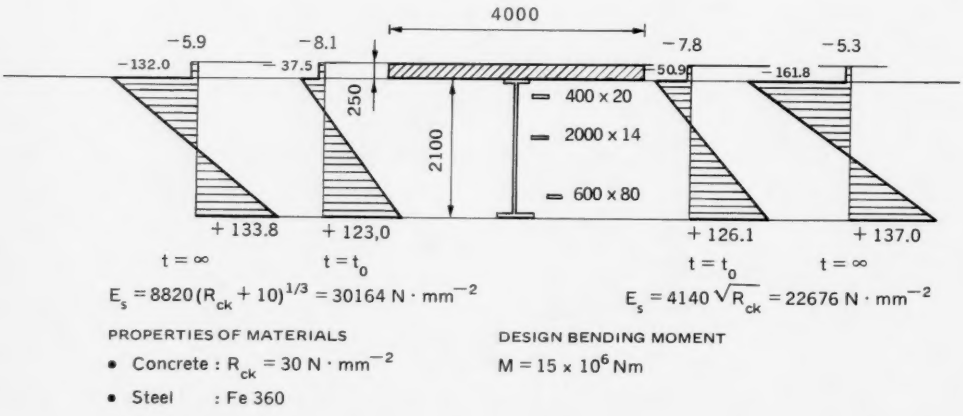

Fig. 7 - Safety check of a steel-concrete section subject to bending moment.

VOL. 14 1984

some European bodies of rules lead to an estimate upwards of the value of the elastic modulus at least as far as the concretes made up of crushed limestone are concerned. This fact has a considerable influence on the structural design. Moreover, the exclusion of steam-cured concretes from the use of a correlation between modulus of elasticity and compressive strength is not justified. The substantial agreement of the results obtained with those published by other authors suggests the use of a generalized correlation of the kind $E_s = 4000 \sqrt{R_c}$ at least for the most used concretes in non-massive structural elements, in which the maximum aggregate size is small.

Acknowledgments - The experimental programme realized for this research and carried out over three years was made possible thanks to the collaboration of the "Cooperativa Muratori e Cementisti" of Ravenna as far as the casting and supply of specimens were concerned. The financial support of the Italian Research National Council (C.N.R.) is also gratefully acnowledged.

References

[1] V. Hermann, J.W. Weber, K. Wesche, The dynamic modulus of elasticity as an equivalent for the initial tangent modulus of static testing — Rilem, Proceedings of 2nd International Symposium on "New Developments in Non-Destructive Testing of Non-Metallic Materials", Constanta (Rumania), 4 ÷ 7 September 1974.

[2] A. Di Leo, La determinazione delle proprietà elastiche dei calcestruzzi con i metodi vibrazionali — INARCOS, No 415, gennaio/febbraio 1981.

[3] K. Wesche, W. Manns, Evaluation of an international inquiry to determine the modulus of elasticity of concrete under static compression — Materials and Structures (RILEM), Vol. 3, No 15, May/June 1970.

[4] G. Pascale, Le prove di compressione e di modulo statico di elasticità del calcestruzzo — INARCOS, No 408, maggio 1980.

[5] M. Collepardi, M. Corradi, G. Moriconi, Calcestruzzi ultraresistenti ed affidabili per strutture antisismiche — La Prefabbricazione, No 4, aprile 1978.

[6] F. Martinez y Cabrera, Problemi di stabilità dell'equilibrio elastico nelle fasi transitorie — ITEC/La prefabbricazione Ed., Quaderno N. 5 C.T.E., 1981.

[7] A. Pauw, Static modulus of elasticity of concrete as affected by density — A.C.I. Journal, No 12, December 1960.

[8] A. M. Neville, Properties of concrete — Pitman Ed., London, 1973.

[9] P. Matildi, A. Di Leo, G. Pascale, Il modulo di elasticità dei calcestruzzi maturati a vapore: un'analisi delle conoscenze attuali — La Prefabbricazione, N. 10, ottobre 1981.

[10] Recommandation de la RILEM, Les essais sur béton par la méthode de l'auscultation dynamique — Annales I.T.B.T.P., N. 309 - 310, Septembre/Octobre 1973.

[11] R. L'Hermite, G. Dawance, J. Chefdeville, L'auscultation dynamique du béton: méhtode vibratoire de mesure du module d'élasticité des bétons en oeuvre et sur éprouvettes — Annales I.T.B.T.P., N. 207 - 208, Mars/Avril 1965.

[12] M.Collepardi, Scienza e tecnologia del calcestruzzo — Ed. U. Hoepli, Milano, 1980.

[13] P. Pozzati, Teoria e tecnica delle strutture — UTET Ed., 1977.

[14] P. Matildi, M. Mele, Impalcati a piastra ortotropa ed in sistema misto acciaio-calcestruzzo — ITALSIDER s.p.a., 1971.

[15] D. Szöke, General recommendation for loading tests of load-bearing structures in-situ — Materials and Structures, Vol. 9, No 53, 1976.

[16] P. Matildi, G. Pascale, Risultati di esperienze sulla maturazione a vapore dei calcestruzzi — La Prefabbricazione, N. 10, ottobre 1978.

[17] P. Matildi, G. Pascale, Ancora sulla stagionatura a vapore dei calcestruzzi — La Prefabbricazione, N. 11, novembre 1980.

[18] P. Matildi, Influenza della viscosità e del ritiro dei calcestruzzi giovani sul comportamento delle strutture miste in acciaio-calcestruzzo — Corso di Perfezionamento per le costruzioni in cemento armato del Politecnico di Milano, Vol. XVI, 1962.

[19] P. Matildi, M. Bufalini, Contributo al calcolo dei sistemi misti in acciaio-calcestruzzo — Costruzioni Metalliche, N. 4, 1963.

[20] G. Toniolo, F. Morisi, A. Vai, E. Rigoldi, Risultati di un ciclo di sperimentazione su calcestruzzi maturati a vapore — Atti del Congresso C.T.E. 1982 sulla Industrializzazione Edilizia, Verona 11 - 14 novembre 1982.

VOL.
14
1984

CEMENT and CONCRETE RESEARCH. Vol. 14, pp. 717-728, 1984. Printed in the USA.
0008-8846/84 $3.00+00. Copyright (c) 1984 Pergamon Press, Ltd.

IMPROVEMENT OF THE DURABILITY OF GLASS FIBER REINFORCED CEMENT USING BLENDED CEMENT MATRIX

S. Leonard and A. Bentur
Building Research Station - Faculty of Civil Engineering
Technion, Haifa, Israel

(Refereed)
(Received Nov. 28, 1983; in final form July 10, 1984)

ABSTRACT

Blended cements prepared with two fly ashes were used as matrices in glass fiber reinforced cement (GRC) composites in an attempt to improve their durability. The hydrated matrices from the two blended cements investigated here had similar strength and composition. Both fly ashes reduced the $Ca(OH)_2$ content to the same extent but in both cases the pH level was only slightly reduced compared to the portland cement matrix. In spite of these similarities, the GRC prepared with one fly ash showed considerable improvement in durability while the other one had only a small positive effect. SEM observations indicated that the improved durability in one case was associated with modification in the microstructure of the hydration products deposited in between the glass filaments, resulting in a much more open structure compared to that of portland cement matrix or the other blended cement. It is therefore suggested that the potential of the blended cement matrix to improve the durability of GRC is associated with its ability to modify the microstructure of the paste at the glass interface. This characteristic is not necessarily related to the overall composition of the blended cement matrix and to the reactivity of fly ash with $Ca(OH)_2$.

Introduction

Cements pastes and mortars can be reinforced with glass fiber strands to produce a composite with high tensile strength and ductility. The improved mechanical properties of the glass fiber reinforced cement (GRC) composite and the manufacturing technologies developed make it a suitable material for production of thin elements with variable shapes (1)(2). However, one of the limitations of this composite is the degradation in mechanical properties on aging, especially in humid environments, which results in embrittlement and loss in tensile strength. This durability problem is the result of chemical attack on the glass by the alkaline cement environment (3)(4). It has also been suggested that growth of hydration products, mainly CH*, in between the filaments in the strand can result in reduction of the strain capacity of the

*Cement chemistry notation is used: C = CaO; S = SiO_2; A = Al_2O_3; F = Fe_2O_3; H = H_2O

composite and can also lead to its embrittlement (3)(5)(6). A special type of high zirconia glass, known as alkali resistant (AR) was developed and it has a better resistance to alkaline environment. However, tests of glass fiber strands of this kind (7)(8) as well as GRC composites prepared with this glass (9) have indicated that it is not immune to aging effects although it can substantially reduce the rates of loss of mechanical properties of the composite.

In view of these limitations, attempts have been made to improve the durability of GRC by modifying the cementitious matrix, to reduce its high alkalinity and CH content which are believed to be the main causes for the aging problem. Various works have been reported using portland cements belnded with fly ash (10), pozzolans (11) and blast furnace slag (12), carbonated portland cement (13) and non-portland cement matrices like alumina cement (14)(15) and supersulphated cement (16). In some of these systems improvements in the durability characteristics of GRC could be observed while in others no advantages were gained by the modified matrix. From the results of such reports no general conclusions can be drawn with regard to the correlations between matrix composition and aging of GRC. Therefore, they provide no basis for predicting the durability performance of GRC from the composition of the matrix.

In the present work, the durability of GRC produced with blended cements of two different fly ash specimens was studied. The two fly ash specimens had a similar influence on the composition and mechanical properties of the blended cement matrices, but they were considerably different in their effect on the aging of the composite. The conclusions drawn from the similarities and differences in these systems may be helpful in resolving some of the complex characteristics of GRC composites prepared with modified cementitious matrices.

VOL. 14 1984

Experimental

Materials

The composition and physical properties of the portland cement (OPC) and the two fly ash specimens (pfa A and pfa B) studied in this work are given in Table 1. The x-ray diffraction (XRD) patterns of the fly ash speciemns are given in Fig. 1. They were obtained with CuK_α radiation at a scanning speed of $2^o 2\theta$/min. The two fly ash specimens have hardly any soluble alkalies but they are different in their CaO and SiO_2 contents: pfa A has a higher content of CaO but is lower in SiO_2 content. The XRD patterns indicate that both fly ashes have similar peaks of crystalline compounds and that fly ash B seems to have a greater content of glassy material.

Particle size distribution of the two fly ash specimens were determined by the hydrometer procedure of ASTM D422-63. The results are presented in Fig. 2. The curves in Fig. 2 and the Blaine fineness values in Table 1 indicate that fly ash A consisted of much finer particles.

The glass fiber strands used in the present work were Cem-FIL 1 produced by Pilkington Brothers Ltd., Great Britain.

Mix Composition

The matrices in the present work were prepared from pastes of blends containing 15, 25 and 35% by weight of fly ash. The pastes were of similar consistencies and their water to solids ratio was in the range of 0.32 to 0.36. Control mixes of OPC pastes were prepared at water cement ratios in this range.

Table 1
Composition and physical properties of fly ash specimens and portland cement

	OPC	pfa A	pfa B
CaO	63.48%	7.1%	1.0%
SiO_2	21.14	41.6	52.0
Al_2O_3	5.91	28.4	30.4
Fe_2O_3	2.85	5.9	7.2
TiO_2		1.4	1.4
MgO	1.56	2.1	0.37
Na_2O	0.34	0.6	0.3
K_2O	0.36	0.35	0.38
Soluble Alkalies		0.031	0.013
P_2O_5		1.2	1.0
SO_3	2.56	2.0	0.24
L.O.I.	2.04	10.2	6.6
Fineness, Blaine	3200	7100	3600
Density, g/cm^3	3.09	2.22	1.98

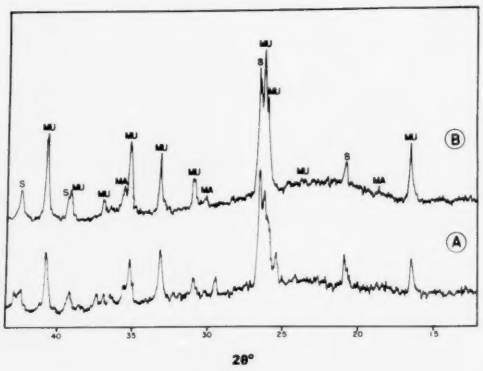

FIG. 1
X-ray diffraction patterns of the two fly ash specimens. (MU-Mullite, MA-Magnetite, S-Quartz)

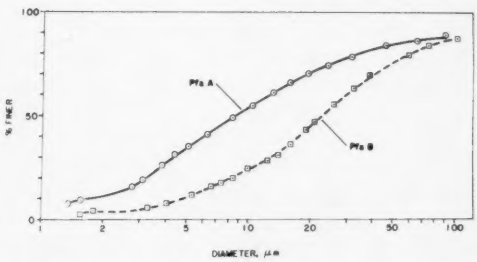

FIG. 2
Particle size distribution of the two fly ash specimens.

Specimens

The GRC specimens consisted of two layers of oriented continuous glass fiber strands which were placed between three, 3 mm thick layers of paste (Fig. 3). A special mold was constructed for this purpose and with the aid of spacers, the glass fiber strands could be accurately positioned. The glass fiber strands content was 1.1% by volume. The specimens produced were 210 x 180 x 10 mm plates. Preliminary tests indicated that such specimens could be easily produced in the laboratory and their mechanical testing indicated that

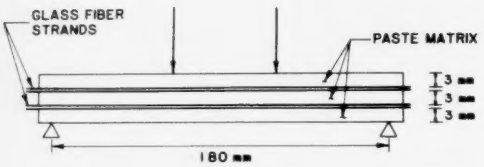

FIG. 3
Schmetic description of GRC specimen and loading arrangement.

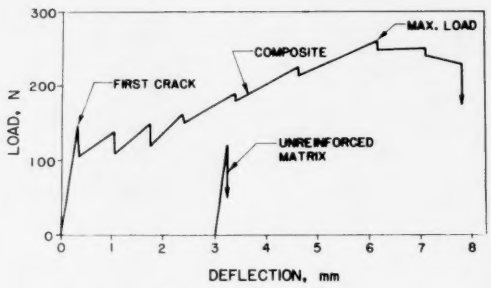

FIG. 4
Load-deflection curves of reinforced and unreinforced specimens prepared from OPC paste, after 28 days of water curing.

their properties were similar in nature to commercial boards produced by the spray technique. In addition to that, the variability in the properties of the laboratory specimens was relatively small.

Companion, unreinforced specimens were prepared in the same mold, and also as 25 mm cubes.

Curing and Tests

The specimens were demolded after one day and then kept continuously in lime water at 20°C, up to one year. At different ages, the plates were cut into strips of 25 mm width parallel to the fiber direction. These were tested in saturated surface dry conditions in flexure, by third point loading over a span of 180 mm, as shown schematically in Fig. 3. Table model Instron was used for that purpose with cross head speed of 0.5 mm/min. Load-deflection curves were recorded and typical ones are given in Fig. 4, for reinforced and unreinforced specimens. The characteristics of GRC composite can be clearly observed in this figure. The load-deflection curve is linear up to the first crack load (the first discontinuity in the curve) and from there on multiple cracking takes place, which is characterized by discontinuities in the curve. In this region, the load is gradually transferred to the glass fiber strands and the increase in load over the first crack load is the result of the greater load capacity of the glass fiber strands. The higher load and larger deflections of the reinforced composite, as compared to the unreinforced matrix, reflect the important advantages gained by the glass fiber strands reinforcement: increase in tensile strength, toughness and ductility. In the present work, the apparent modulus of rupture (M.O.R.) was calculated from the beam theory, using the value of maximum load for this calculation. The toughness was estimated by calculating the area under the load-deflection curve, which will be called work to fracture (W.F.). The coefficients of variation of M.O.R. and W.F. were usually smaller than 10% and 20%, respectively. The results are the average of at least six specimens.

The unreinforced specimens were also tested at the same age to determine M.O.R. and compressive strength. Some of these specimens were ground, dried and analyzed by thermo gravimetric method to determine the CH content, using Perkin Elmer TGS-2. Non-evaporable water content was determined by weight loss on heating to 1050°C. CH content values were calculated as percent weight of the cementing material (portland cement or portland cement + fly ash) in the unhydrated paste.

VOL. 14 1984

An indication for the pH level of the different matrices was obtained by measuring the pH of a solution prepared with equal weights of ground hydrated paste and deionized water. Obviously, such a test will not yield the actual pH level of the pore solution of the paste, but it is useful for comparative purposes, to determine whether the fly ash in the blended cement had any effect on the pH of the matrix.

SEM observations of the composites were carried out on the fractured surface perpendicular to the strand orientation and also on the surface exposed when the specimens were split in the plane of the strands.

Results

Properties and composition of the matrices.

The effect of duration of curing on the CH content of pastes of OPC and blended cements with 35% fly ash A and B are shown in Fig. 5. The CH content of the OPC paste increased continuously with time, with a rapid rate during the first 10 days and a slower one later on. The curves for the two blended cements were practically the same and their CH content was considerably smaller than that of the OPC. There is a rapid increase in their CH content during the first 10 days, and afterwards it remained constant for a while and then started to decrease slightly with time. The differences between the CH curves of OPC and the blended cements can be readily interpreted if a curve is drawn for a hypothetical case of a blend of OPC with 35% inert filler (Fig. 5). The CH content values in this curve are 65% of the values of the OPC curve. Up to about 10 days, the curves for the fly ash blends and the inert filler blend are practically identical, indicating that the fly ash in the blend is behaving as an inert filler. From this stage on, the differences between the 35% inert filler curve and the fly ash blends curves increase continuously with time, indicating that the fly ash is reacting to reduce the CH content liberated in the portland cement hydration. From these results it can be concluded that the reactivity of both fly ash specimens is similar, and at the age of 150 days they reacted with approximately 35% of the CH formed in the portland cement hydration.

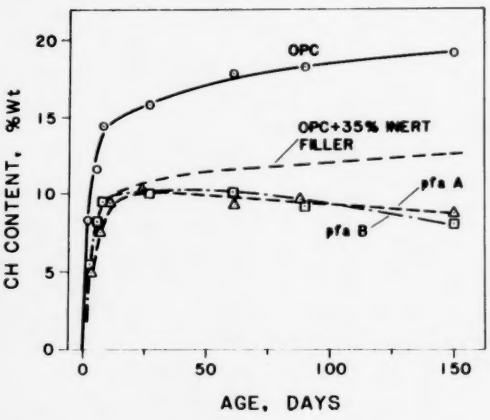

FIG. 5
The effect of duration of curing in water at 20°C on the CH content of pastes of OPC and blended cements with 35% fly ash.

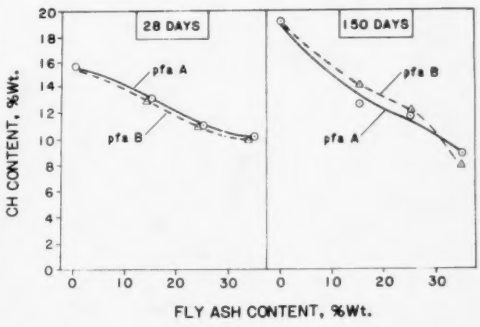

FIG. 6
The effect of fly ash content in the blended cements on the CH content of pastes hydrated for 28 and 150 days.

The CH content-time curves for the 15% and 25% blends also indicated that the two fly ash specimens had similar reactivity with CH. This is also evident in Fig. 6 which shows the effect of fly ash content on the CH content after 28 and 150 days of curing: the curves for the two fly ash specimens are very similar. The increase in CH content with decrease in fly ash content is expected, since there is less fly ash to react and reduce the content of CH liberated in the portland cement hydration.

The pH values at 28 days and 150 days are given in Table 2. They indicate that the addition of fly ash resulted in a slight reduction in pH level (about 0.1 and 0.2 at 28 and 150 days, respectively, for the 35% blends). The pH levels of the blended cements with the two different fly ash specimens were practically the same. The only small effects of blending with fly ash on the pH level could be explained on the basis of the work reported by Diamond (17) who showed that addition of 30% fly ash resulted in only a small reduction in the calculated pH level (≈0.2 at 80 days). It was explained in that work, that since the concentration of OH^- (and therefore the pH level) is controlled by the concentrations of Na^+ and K^+ in the pore solution, it would be expected that, for fly ash specimens that do not remove or add Na^+ and K^+ to the solution, the pH would reduce only slightly and the fly ash could be considered as an inert filler, having a diluting effect only. The trends with the fly ash specimens tested in the present work can be explained in this way.

Table 2

pH values of pastes of OPC and blended cements hydrated for 28 and 150 days.

Fly ash content (% wt.)	pH values			
	28 days		150 days	
	pfa A	pfa B	pfa A	pfa B
0	13.02	13.02	12.97	12.97
15	12.92	12.97	12.90	12.90
25	12.94	12.96	12.83	12.79
35	12.93	12.91	12.76	12.72

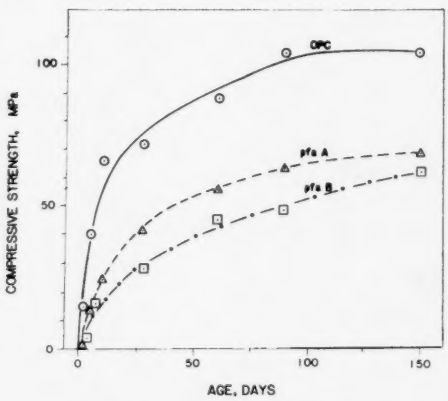

FIG. 7
Compressive strength development of pastes of OPC and blended cements with 35% fly ash, cured in water.

The mechanical properties of the matrices, as estimated from compressive strength, indicated that the strength of the blended cement with fly ash A was somewhat higher than that of the blended cement with fly ash B, but the differences were not big and they tended to become very small at 150 days. This is demonstrated for the 35% blends in Fig. 7. The strength of the blended cements was always lower than that of OPC, and the differences were greater for higher fly ash contents.

Mechanical properties of the GRC composites

The effects of duration of aging on the M.O.R. and W.F. of GRC composites

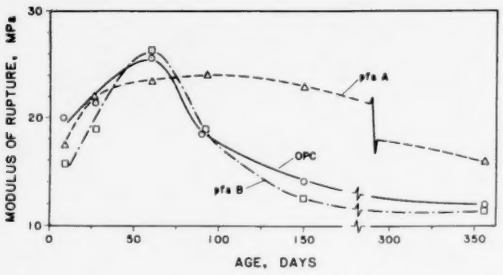

FIG. 8
Effect of aging in water at 20°C on the M.O.R. of GRC composites prepared from matrices of OPC and blended cements with 35% fly ash.

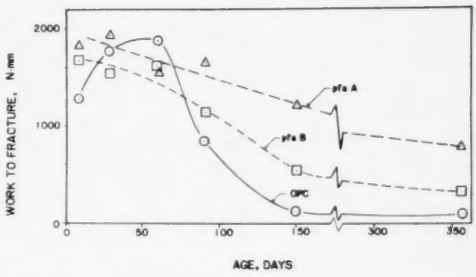

FIG. 9
Effect of aging in water at 20°C on the W.F. of GRC composites prepared from matrices of OPC and blended cements with 35% fly ash.

with matrices of OPC and blended cements with 35% fly ash are shown in Figs. 8 and 9. It can be clearly seen that the GRC with OPC matrix lost approximately 50% of its M.O.R. and almost all of its W.F. after 150 days of water storage, and it became brittle at this age. The composite with blended cement matrix of fly ash A showed much better durability characteristics and the rate of loss of its M.O.R. and W.F. was much smaller; at one year it still retained 50% of its original W.F. value and it was still considerably ductile. The GRC with blended cement of fly ash B showed some improvement in durability over the GRC with OPC matrix, but this improvement was considerably smaller than that obtained with the blended cement of fly ash A.

The effects of fly ash content in the blended cements on the M.O.R. and W.F. of the GRC composites are shown in Figs. 10 and 11 for 150 days and 1 year of aging in water at 20°C. These figures also demonstrate the considerable improvement in properties that could be obtained with the blended cements of fly ash A. In this system the properties improved with increase in fly ash content, but the 1 year results (Fig. 11) indicated that the addditional ad-

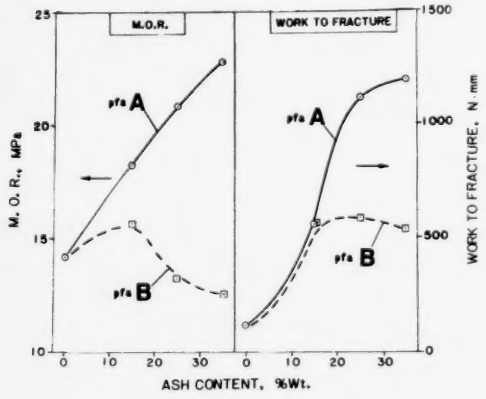

FIG. 10
Effect of fly ash content on the M.O.R. and W.F. values of GRC composites aged in water at 20°C for 150 days.

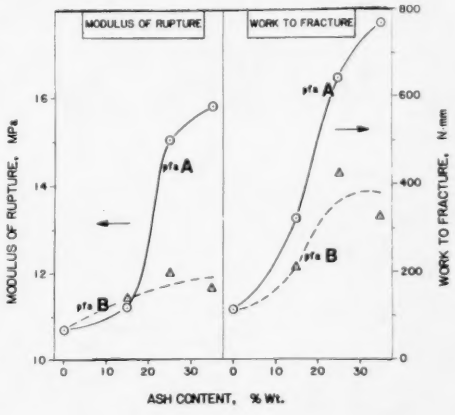

FIG. 11
Effect of fly ash content on the M.O.R. and W.F. values of GRC composites aged in water at 20°C for 1 year.

vantage gained by increasing the fly ash content from 25% to 35% was relatively small. The improvements gained by using blended cement with fly ash B were much smaller.

SEM Observations

Many broken filaments could be observed on the fractured surface of the GRC composite with OPC matrix that was aged for 150 days (Fig. 12a). The spaces between the filaments were filled with hydration products. Only a small portion of the filaments in the strand were pulled out and hydration products could be seen sticking to their surface (Fig. 12b). Observations of the specimens split in the plane of the strand (Fig. 12c) showed that in some zones a large portion of the spaces between the filaments was filled with hydration products that could form a dense packing (mainly CH) around the filaments.

Observations of the fractured surface of the GRC composite prepared from matrix with blended cement of fly ash A and aged for 150 days in water at 20°C indicated that, in most of the cases, the filaments in the strands were pulled out and no hydration products were sticking to their surface (Fig. 13a). The spaces between the filaments were usually free of any hydration products (Fig. 13b) and in the few cases where hydrating material was deposited in between the filaments, it was seen to be porous and not well crystallized (Fig. 13c).

VOL. 14 1984

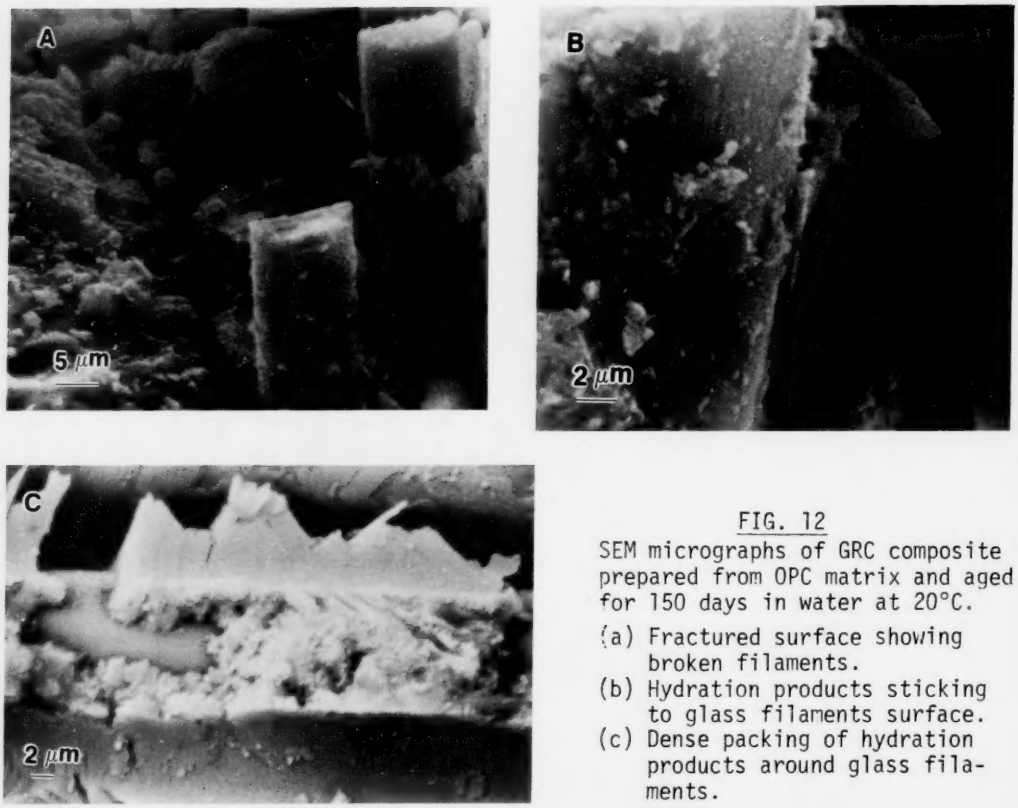

FIG. 12
SEM micrographs of GRC composite prepared from OPC matrix and aged for 150 days in water at 20°C.
(a) Fractured surface showing broken filaments.
(b) Hydration products sticking to glass filaments surface.
(c) Dense packing of hydration products around glass filaments.

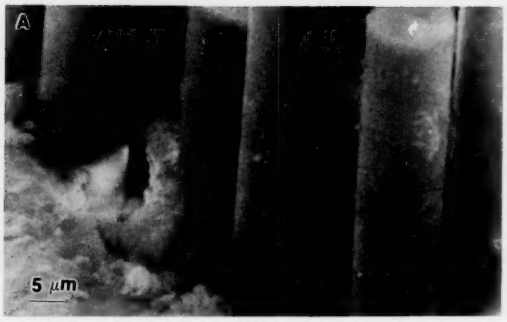

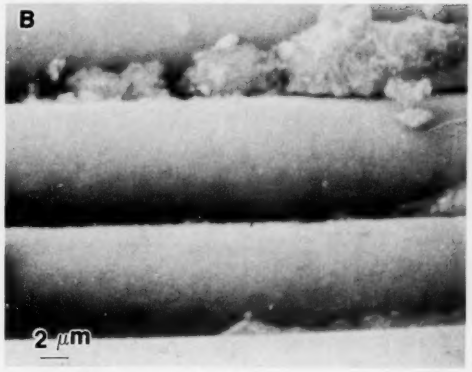

FIG. 13

SEM micrographs of GRC composites prepared from blended cement matrix (25% fly ash A) aged for 150 days in water at 20°C.

(a) Fractured surface showing pulled out filaments.
(b) Spaces between filaments, free of hydration products.
(c) Spaces between filaments in which porous and poorly crystalline hydration products were deposited.

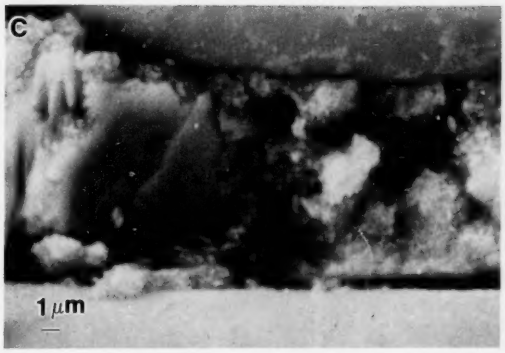

The SEM observations of GRC composite prepared from matrix with blended cement of fly ash B and aged for 150 days in water at 20°C tended to be more similar to those prepared with OPC matrix, but it seemed to have a somewhat greater portion of pulled out filaments. Formation of crystalline CH enveloping the filaments could also be observed in certain zones (Fig. 14).

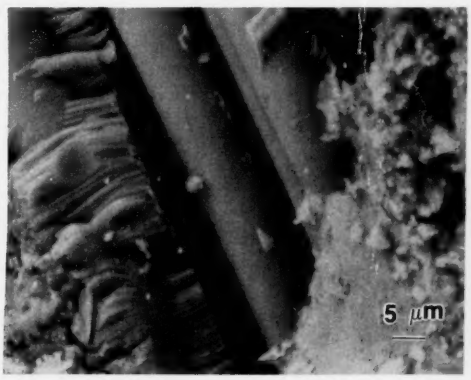

FIG. 14

SEM micrograph of GRC composite prepared from blended cement matrix (25% fly ash B) aged for 150 days in water at 20°C.

Discussion

The results presented in the previous sections indicated that the two fly ashes were equally reactive and reduced,to the same extent, the CH liberated in the cement hydration. They had a similar effect on the pH level and strength of the blended cement matrix. However, they were markedly different in their influence on the durability of the composite: one of them (pfa A) improved it significantly while the other (pfa B) resulted in only a very limited improvement. SEM observations indicated that the composites prepared from blended cements of the two fly ash specimens were different in the paste microstructure in the vicinity of the filaments and in between them. This difference may account for the differences in the aging characteristics: the blended cement with pfa B produced a composite in which the spaces between the filaments had a greater tendency to be filled with hydration products, some of them quite dense, while with the pfa A, the microstructure of the paste around the filaments was much more open. Thus, with pfa A the microstructure of the paste around the glass filaments was modified while with pfa B it remained more similar to that of GRC with OPC matrix. Since the growth of hydration products in between filaments in the strand has been suggested to be one of the causes for embrittlement (5)(6), the modification in the microstructure in this zone which was induced by the presence of fly ash A in the blended cement may account for the superior behavior of the GRC prepared with this matrix. At present we do not have a satisfactory explanation to the observation that one fly ash could cause such a change and improve the durability while the effect of the other was very small, in spite of the fact that both of them were equally reactive with CH liberated in the cement hydration. It should not be ruled out that the differences in particle size distribution was associated with the difference in the performance of the two. The fly ash which consisted of finer particles (pfa A) performed better in the GRC composite. The much higher content of particles smaller than 3 μm in pfa A (~20% in pfa A and ~6% in pfa B) may turn out to be crucial, since particles in this size range may better penetrate into the spaces between the filaments and may therefore be more effective in modifying the paste microstructure at the glass filament-cement matrix interface. The spaces between the filaments in the strand are usually smaller than 3 μm.

The results discussed here indicate that the aging performance of GRC with different matrices can not be adequately predicted from the overall composition of the matrix, since it is probably the effect of the matrix on the microstructure at the interface which is of prime importance. Therefore, the reactivity of the fly ash is not by itself a suitable parameter for predicting the durability of GRC prepared with blended cement matrix. Some other factors that at present are not resolved, but which probably affect the interface microstructure and not the overall matrix composition should be taken into account.

It is of interest to note that in spite of the fact that the different matrices had similar pH levels, their durability characteristics were considerably different. Since the extent of chemical degradation of the glass filaments is expected to be a function of the pH level, these trends suggest that at least during the first year of aging in water, the effect of chemical degradation is limited. At this stage, changes in the microstructure of the hydration products in the spaces between the filaments play an important role in controlling the embrittlement of GRC. It is possible that the surface treatment given to the newer generation of AR glass (for example Cem-FIL-2 (4))affects not only the chemical durability of the glass but the nature of the hydration products which develop in its vicinity.

VOL. 14 1984

Conclusions

1. The results of the present study indicate that matrices which are similar in the composition of their hydration products and have practically the same pH levels can yield GRC composites which show considerable difference in their aging behavior. The matrices which resulted in improved durability were the ones in which growth of CH in between the filaments was largely prevented. It seems that for the first year of aging in water, the microstructural changes of the paste near the glass - cement interface are crucial in controlling the durability and that chemical degradation, which is pH controlled, is less important, at least at this stage of aging.

2. The use of matrices of portland cement blended with fly ash can sometimes result in improvement in the durability of GRC. This occurs when the modified matrix can influence the microstructure and extent of growth of hydration products in the spaces between the filaments. The fly ash that inhibited the growth of CH in these spaces was the one that improved the durability.

3. The reactivity of the fly ash as estimated from the reduction in CH content in the blended cement matrix can not serve as an adequate criterion for its effectiveness in improving the durability of GRC. The reduction in CH content does not necessarily result in sufficient reduction of growth of CH in the spaces in between the filaments.

Acknowledgement

This work is based on the M.Sc thesis of one of the authors (S.L) supervised by the other (A.B).

References

1. A. J. Majumdar and V. Laws, Composites, 10, 17, (1979).
2. B. A. Proctor, pp. 69-86 in "Fibrous Concrete," Proc. Symp. on Fibrous Concrete, London, The Construction Press, (1980).
3. A. J. Majumdar, pp. 37-60 in "Advances in Cement-Matrix Composites", D. M. Roy, A. J. Majumdar, S. P. Shah and J. A. Manson (Eds.), Materials Research Society, (1980).
4. B. A. Proctor, D. R. Oakley and K. L. Litherland, Composites, 13, 173, (1982).
5. M. J. Stucke and A. J. Majumdar, J. Mater. Sci., 11, 1019, (1976).
6. E. B. Cohen and S. Diamond, pp. 315-325 in Proc. RILEM Symp. "Fibre Reinforced Cement and Concrete", A. Neville (Ed), The Construction Press, (1975).
7. A. J. Majumdar, "The Role of the Interface in Glass Fibre Reinforced Cement", Current Paper CP 57/74, Building Research Establishment, London, (1974).
8. A. J. Majumdar, J. M. West and L. J. Larner, "Properties of Glass Fibre in Cement Environment", Current Paper CP 24/77, Building Research Establishment, London, (1977).
9. Building Research Establishment, "A Study of the Properties of Cem FIL/OPC Composites", Current Paper CP 38/76, Building Research Establishment, London, (1976).
10. A. J. Majumdar, pp. 48-68 in Proc. RILEM Symp. "Fibre Reinforced Cement and Concrete", A. Neville (Ed.), The Construction Press, (1975).
11. B. Singh and A. J. Majumdar, Int. J. Cement Composites and Lightweight Concrete, 3, 93, (1981).

12. R. H. Mills, Cem. Concr. Res. 11, 421, (1981).
13. A. Bentur, Durability of Building Materials, 1, 313, (1983).
14. A. J. Majumdar and R. W. Nurse, "Glass Fibre Reinforced Cement", Current Paper CP 79/74, Building Research Establishment, London, (1974).
15. W. A. Patterson and H. C. Chan, J. Mater. Sci., 6, 342, (1971).
16. A. J. Majumdar, B. Singh and T. J. Evans, Composites, 12, 177, (1981).
17. S. Diamond, Cem. Concr. Res., 11, 383, (1981).

VOL.
14
1984

CEMENT and CONCRETE RESEARCH. Vol. 14, pp. 729-740, 1984. Printed in the USA.
0008-8846/84 $3.00+00. Copyright (c) 1984 Pergamon Press, Ltd.

PRELIMINARY DATA ON QXRD ANALYSIS OF PORTLAND CEMENT AND CLINKER USING CeO_2 AS THE INTERNAL STANDARD

Bret H. Howard
Martin Marietta Laboratories
1450 S. Rolling Road
Baltimore, Maryland 21227

(Communicated by D.M. Roy)
(Received Jan. 5, 1984)

ABSTRACT

A procedure for the quantitative determination of C_3S, β-C_2S, and periclase in portland cement and clinker by x-ray diffraction is described. This procedure utilizes CeO_2 as the internal standard and is based on peak height ratios of analyte to internal standard. Data from the comparison of CeO_2 and Si as internal standards are also presented.

Introduction

The most common method for the quantitative x-ray diffraction analysis (QXRD) of portland cement and clinker involves the addition of a known amount of an internal standard of a controlled particle size. The purpose of this internal standard is to help correct for matrix effects between samples and time-dependent changes in x-ray intensity. It is therefore vital that there be no changes in the intensity of the x-rays diffracted from the standard due to effects related to its chemical and physical nature. Silicon is probably the most common internal standard in use today.

In this paper, other possible compounds for use as internal standards will be evaluated in an attempt to find one having comparable chemical and physical properties to silicon, but more reproducible diffraction intensity. A QXRD procedure for analysis of C_3S, β-C_2S and periclase in portland cement and clinker using CeO_2 as the internal standard will also be described.

Instrumentation

A Philips APD 3600/02 automated x-ray powder diffractometer with the following features was used:

Detector: Scintillation
Tube: Copper, 1800 watts; operating 40KV, 35 mA
Monochromator: Graphite crystal
Goniometer: Philips, 6° take-off angle, stepping motor driven, automatic sample changer
Slits: theta compensating divergent, 0.2° receiving
Data collection, storage and display: Data General Nova 4 computer, 64K core memory; dual 5 megabyte firm disks; single 1/3 megabyte floppy; two Tektronix CRT terminals; Tektronix hard copy unit.

TABLE 1

Compounds Considered for Internal Standard Use (2,3,4,5,6)

Compound and JCPDS Pattern Number	d-Spacing of peak to be used	Properties	Reason for Rejection Evaluation
Si 5-565	3.138	MP-1410°C, insoluble in water, cubic hard, easily obtainable	None
CaF_2 (fluorite) 4-864	3.153	H=4, MP-1423°C, slightly soluble in water, cubic, perfect cleavage on several planes, possible overlap with C_3S/C_2S at 28.10°2θ, chemically stable	None
TiO_2 (rutile) 21-1276	3.247	H=6 - 6 1/2, MP-1830-1850°C, insoluble in water, tetragonal, overlap with C_3S/C_2S at 27.40°2θ, stable, easily obtainable	Overlap
ZnS (sphalerite) 5-566	3.123	H=3 1/2 - 4, essentially insoluble in water, transition at 1020°C, can slowly oxidize in air to sulfate on contact with water, cubic	Difficult to obtain pure polymorph of correct particle size.
B-MnO_2 (pyrolusite) 24-735	3.110	H=6 - 6 1/2, loss of -O at 535°C, insoluble in water, strong oxidizer, tetragonal, overlaps 42.9° MgO peak	Overlap, reactive
Be_2SiO_4 (phenazite) 9-431	3.119	Hexagonal, overlaps 42.9° MgO peak, not easily obtainable in pure form	Overlap, availability
CdF_2 23-864	3.112	MP-1100°C, soluble in water, poisonous cubic	Toxicity, solubility
CeO_2 4-593	3.124	MP-2600°C, insoluble in water, cubic	None
GeO_2 9-379	3.11	MP-1086°C, insoluble in water, tetragonal, overlaps 42.9° MgO peak	Overlap
AgF_2 19-1134	3.14	MP-690°C, decomposes in water, very hygroscopic highly toxic, very reactive, orthorhombic	Toxicity, reactivity

VOL. 14 1984

Internal Standard Selection

Past experience has indicated that there may be significant variations in the peak heights measured for silicon in duplicate samples. These variations caused errors of unacceptable magnitude in the analyses of cements and clinkers. The most probable cause is excessive particle size or variations in particle size (1). There may be preferred orientation due to the angular shape of the particles (to be shown by SEM later in this paper). There may also be problems associated with sample preparation using silicon (e.g., its hardness).

Several important factors were considered in the selection of suitable internal standards to replace silicon. Materials were selected initially that had a high intensity peak in the region of 27°2θ to 29°2θ -- approximately the same location as the 100% peak of silicon. Rutile (TiO_2) was also considered, although it does not fall in this range. The candidates must have a pattern that has no peaks that overlap with the peaks to be measured in the cement phase. A compound with a cubic structure is preferred due to the simplicity of its pattern. The compound should be chemically unreactive, especially with respect to selective dissolution techniques. It should also be physically stable such that moderate heating and grinding do not change its structure. Its toxicity was also considered since it must be handled repeatedly by the operator. The compounds considered, some of their physical and chemical characteristics, and the reasons for their selection or rejection are shown in Table 1.

Three compounds were selected for further study: silicon (control), CaF_2 and CeO_2. The silicon used was Sargent Welch -200 mesh (SC14626). It was ground by hand and sieved to -400 mesh. An XRD pattern is shown in Figure 1.

The CaF_2 used was Baker reagent grade. The XRD pattern indicates that the particle size of the "as-received" CaF_2 was too small. It was increased by fusing the CaF_2 at 1500°C in a platinum crucible and cooling slowly to room temperature. The CaF_2 appeared to have a blue tint after fusing, possibly due to an impurity. It was then broken up and ground to -200 mesh. The XRD scan (Figure 1) shows CaF_2 of a suitable particle size; however, a trace of CaO and an unidentified compound was present. The CaO was removed by ethylene glycol, but the unidentified compound could not be removed (7). Repeating the procedure gave the same results.

The CeO_2 used was Alpha Products 99.9% pure that was ground for five minutes in a Spex tungsten carbide ball mill with freon. After grinding, the CeO_2 was found to be suitable for use. The XRD scan (Figure 1) shows pure CeO_2 of good particle size.

The silicon, CaF_2, and CeO_2 particle shapes were determined by SEM examination (Figure 2). The silicon and CaF_2 were very angular, possibly causing preferred orientation problems and although sieved there was also a large variation in particle size. The CeO_2 was slightly less angular and had a much smaller, more uniform particle size. The sample used was not sieved. The unground CeO_2 appeared to consist of spherical conglomerates of very small crystals.

Since these compounds may be exposed to extraction solutions, their solubilities in these solutions must be determined. The solutions tested were salicylic acid in methanol (7,8), maleic acid in methanol (9), hot ethylene glycol (7), and potassium hydroxide and sugar in water (7). The CaF_2 extraction solutions were analyzed by ion-selective electrode for F^-. No F^- could be detected in any of the filtrates showing that CaF_2 is sufficiently

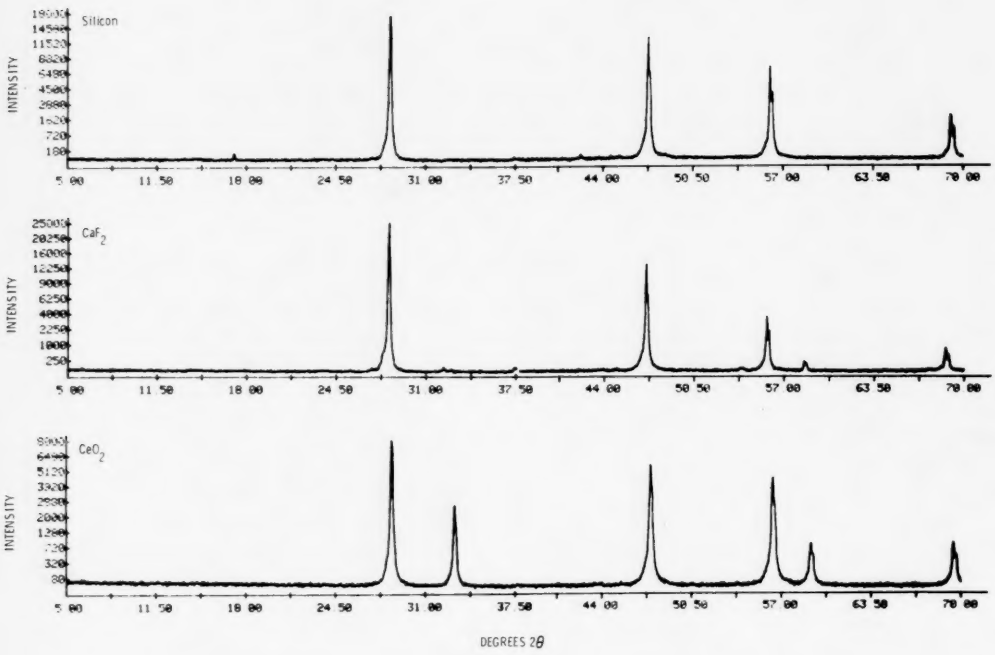

FIG. 1
XRD scans of internal standards (as received).

insoluble. The filtrates from the CeO_2 extractions were analyzed by ICP for cerium. The cerium concentration in the filtrates was <10 ppm, showing that CeO_2 also is sufficiently insoluble to be used as an internal standard. Silicon was not tested since it is already known to be resistant to these solutions (10).

Silicon, CaF_2 and CeO_2 were then compared by a suitable method to determine their actual performance as internal standards. The method used was based on the comparison of repeated scans of identically prepared samples to obtain information on the reproducibility of the peak intensities. The samples were prepared in the same way as those used for the calibration curves.

A standard production clinker was selected to provide a matrix for the internal standard. The clinker was prepared for use by grinding in a Bleuhler mill for five minutes. No extractions were made since the clinker is to be used for comparison only. An XRD scan of the clinker showed the expected clinker minerals.

The samples for comparison were prepared by weighing 1.0000 grams of the clinker into a Spex mixer mill along with a given amount of one of the internal standards prepared as previously described. The Spex mixer mill contained sixty 1/16-inch ball bearings. The samples were mixed for ten minutes with freon. The freon was then evaporated and the sample was transferred to a labeled vial for use later that day. Three pellets were pressed from each sample using a constant procedure.

VOL. 14 1984

The samples were scanned from 26°2θ to 32°2θ at several scanning speeds and each pellet was scanned three times. The peak intensities were measured by determining the peak heights and backgrounds using the APD 3600 graphics.

The first CaF_2 samples indicated that its unsuitable for use in this procedure as an internal standard because of the great reduction in particle size during the ten-minute mixing step. This size reduction, which probably is due to the softness and clevage of CaF_2, caused the CaF_2 peak to broaden to such an extent that its height could not be accurately measured due to overlap with cement mineral peaks. Therefore, CaF_2 was not considered further.

To compare the reproducibility of the intensity measurements, the ratios of the C_3S/β-C_2S peak at 29.4°2θ, the C_3S peak at 30°2θ and the β-C_2S peak at 31°2θ to the internal standard were calculated and graphed (Figure 3) and the standard deviations were calculated (Table 2). The graphs consist of the coded sample identification on the x-axis and the ratio measurement on the y-axis. Five sample mixtures were prepared, three pellets were pressed from each mixture and each pellet was scanned three times. Perfect intensity reproduction will produce a straight line parallel to the x-axis.

Comparison of internal standard results indicated that CeO_2 should make a better internal standard in this procedure than silicon because it appeared to have much better reproducibility. For the worst case, β-C_2S at 31°2θ, the reproducibility of CeO_2 was twice as good as that of silicon. As a result of this comparison, CeO_2 was used as the internal standard in the following QXRD procedure.

TABLE 2

Means and Standard Deviations of Internal Standard Comparison Ratios

CeO_2		2θ angle	
Peak Ratio	29.4°	30°	31°
Mean	0.591	0.192	0.031
Standard Deviation	0.021	0.009	0.003
Si		2θ angle	
Peak Ratio	29.4°	30°	31°
Mean	1.023	0.334	0.047
Standard Deviation	0.179	0.056	0.009

Preparation of calibration curves

Calibration curves were prepared using synthetic cement minerals and commercially available compounds. C_3S and β-C_2S were synthesized with lattice impurities in an attempt to match those occuring in actual clinker. C_3A and C_4AF were "pure" compounds and were used only in matrix preparation. Periclase was synthesized from Fisher reagent grade MgO.

C_3S was prepared by mixing enough excess CaO as $CaCO_3$ with an average production clinker to convert all β-C_2S to C_3S. The approximate amount of

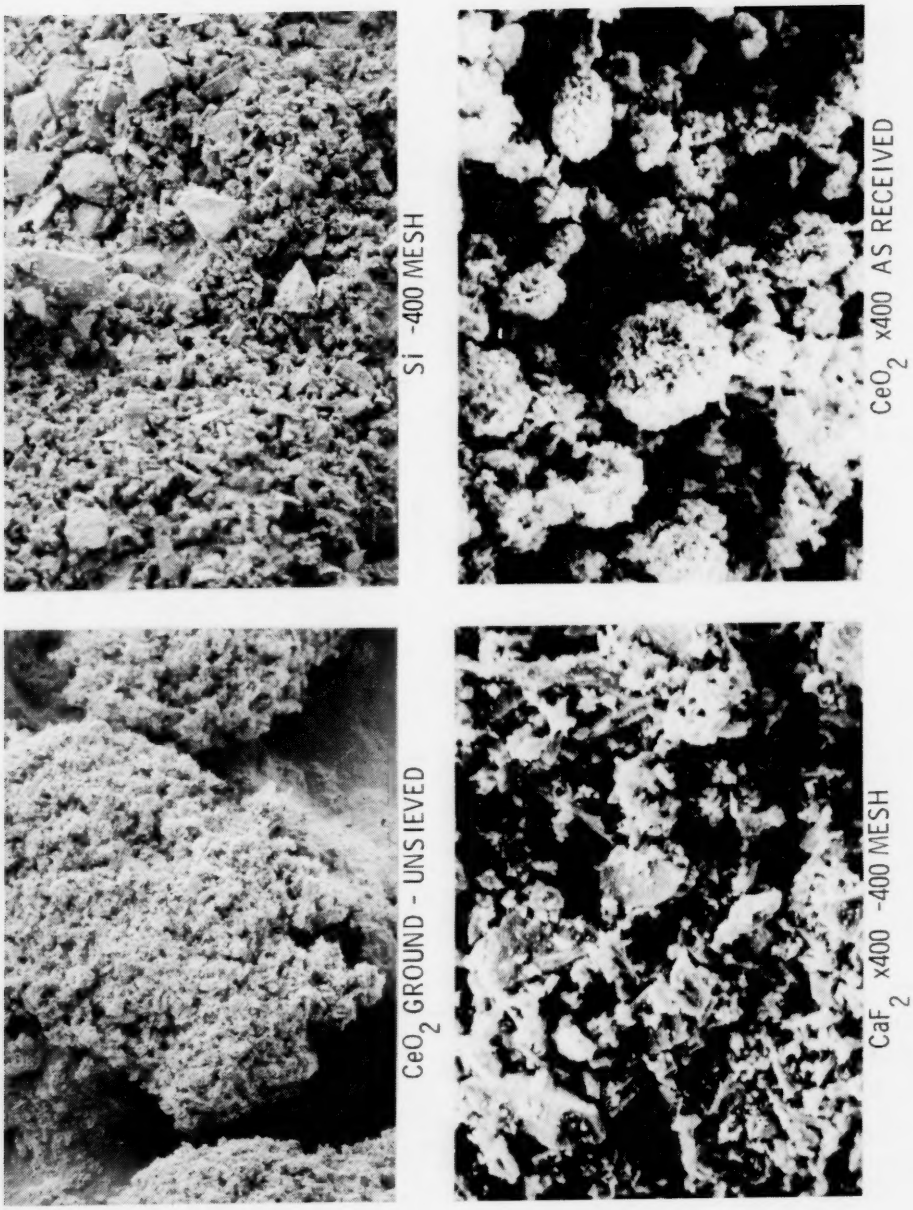

FIG. 2
SEM photographs of silicon, CaF_2 and CeO_2.

VOL. 14 1984

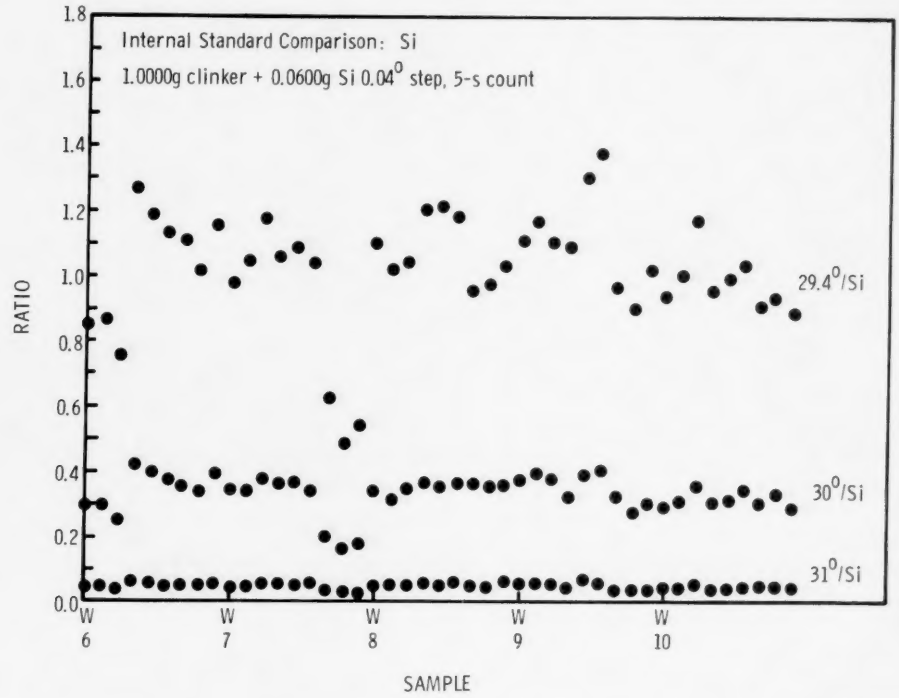

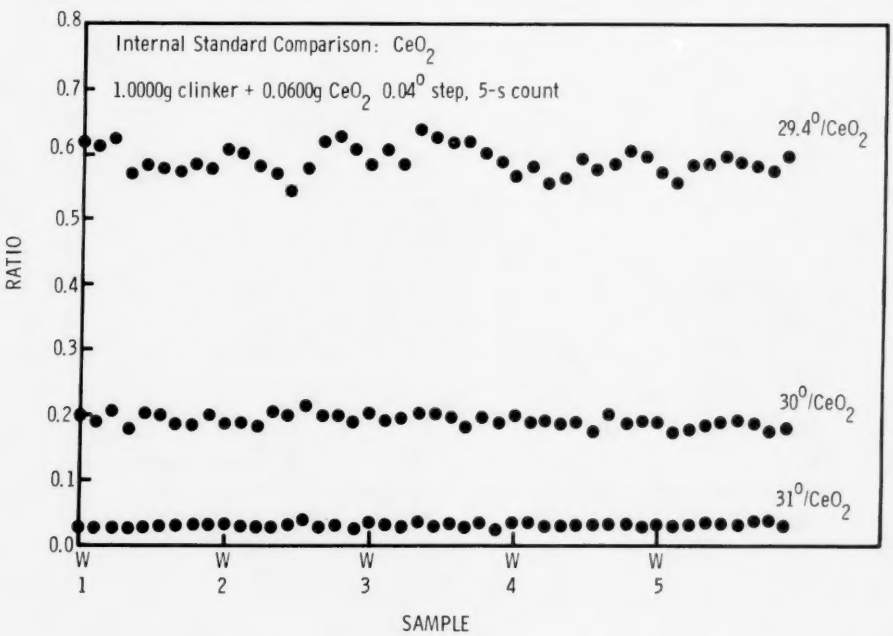

FIG. 3

Intensity reproducibility comparisons

$CaCO_3$ was calculated from the Bogue value obtained by XRF analysis. The mixture was ignited at 1500°C for 90 minutes in a platinum crucible and was ground after cooling. The ignition and grinding steps were done twice to ensure a complete reaction. The interstitial minerals were removed by potassium hydroxide-sugar extraction and the excess CaO was removed by a hot ethylene glycol extraction. The residue was then ground for 5 minutes in a Spex tungsten carbide mill with freon to prepare it for calibration use. XRD analysis showed only C_3S (11).

β-C_2S was prepared from the following reagent-grade chemicals: $CaCO_3$ (calcite) and SiO_2 (quartz) with sodium tartrate, potassium hydrogen phthalate, MgO, and Fe_2O_3 to stabilize the lattice. These compounds were mixed together in a Bleuhler mill and ignited at 1500°C for 90 minutes in a platinum crucible. The sample was then quenched in air and ground. The above heating, grinding and quenching sequence was repeated to ensure complete reaction. The sample was then extracted with KOH-sugar to remove any interstitial minerals formed. The sample was ground for 5 minutes in a Spex tungsten carbide mill to prepare it for calibration use. XRD analysis shows pure β-C_2S (11).

Several unsuccessful β-C_2S synthesis attempts were made in which the β-C_2S converted to γ-C_2S on cooling. Also, during the KOH-sugar extraction a trace of black magnetic particles was noted; most were removed magnetically. These particles probably were Fe_3O_4, formed during heating from Fe_2O_3. No Fe_3O_4 was detected by XRD so it was believed that the amount remaining was so minor that it would not interfere with the calibration.

A 50% C_3A/50% C_4AF matrix was prepared using the pure commercial compounds. Equal amounts of each were mixed in a Spex mixer mill with freon for 10 minutes.

Periclase was prepared from Fisher reagent-grade MgO. Five grams were ignited in a platinum crucible at 1500°C for 90 minutes, cooled and then ground in a Spex tungsten carbide mill for 5 minutes. XRD shows pure periclase suitable for calibration use.

Calibration curve preparation for C_3S and β-C_2S:

The calibration curves for C_3S and β-C_2S were prepared using the synthetic minerals previously described. Each calibration mixture contains the appropriate amount of C_3S, β-C_2S, matrix, and CeO_2. The C_3S percentage ranged from 10% to 80% and the C_2S from 0% to 70%.

The components of each mixture were weighed on an analytical balance and placed directly into the Spex mixing chambers. The mixtures were then ground for 10 minutes with freon, evaporated and transferred to a labeled vial. The calibration samples were run on the same day as prepared.

The computer was programmed to run a fast scan on each pellet from 5° to 70°2θ to detect contamination or other problems. Calibration data was collected from 26° to 32°2θ with a step size of 0.04°2θ and a count time of 5 seconds. Three pellets were run from each calibration mixture and each pellet was scanned three times. All data were stored on a computer disk for peak measurement at a convenient time.

The peaks measured for the calibration curves were 30°2θ for C_3S, 31°2θ for β-C_2S and 28.5°2θ for CeO_2. Peak heights and backgrounds were determined using the APD 3600 graphics and C_3S:CeO_2 and β-C_2S:CeO_2 ratios were calculated. The ratios for the nine data points for each calibration mixture were averaged and graphed to produce a calibration curve. A least squares program was used to determine the linear equation for the graphs. The calibration curves are shown in Figure 4.

VOL. 14 1984

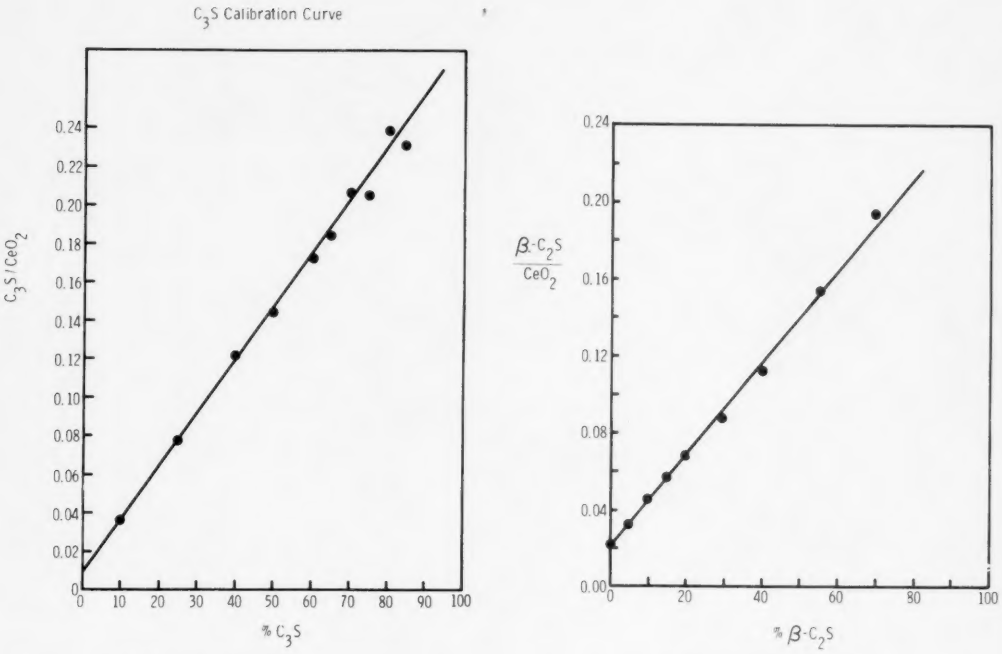

C_3S calibration curve

C_2S calibration curve

FIG. 4

Calibration curve for periclase:

The calibration curve for periclase was prepared using the synthetic periclase, matrix, and CeO_2 previously described. The calibration mixtures were made to approximate the salicylic acid residues of cements and clinkers and ranged from 0% to 5% periclase.

The calibration mixtures were prepared in essentially the same way as for C_3S and β-C_2S so the procedure will not be described in detail. The components were weighed and mixed in the Spex mixer mill and the pellets were prepared as before. Three pellets were prepared and each was scanned three times from 19° to 29°2θ for the CeO_2 peak and from 40° to 44°2θ for the MgO peak at the same scanning speed used for C_3S and β-C_2S. Scanning from 19° to 29°2θ will allow gypsum at 20.8°2θ and anhydrite at 24.5°2θ to be determined from the same scan in the future.

The data were collected and stored for later use. The periclase to CeO_2 ratios were calculated, averaged, and graphed. The linear equation was calculated using a least squares program. The calibration curve is shown in Figure 5.

Cement and clinker analyses

C_3S and β-C_2S analysis:

Five grams of the cement or clinker to be analyzed were preground in a Spex tungsten carbide mill for 5 minutes with freon. 1.0000 grams of sample and 0.0600 grams of CeO_2 were then weighed and placed directly in the Spex mixer mill and mixed for 10 minutes with freon.

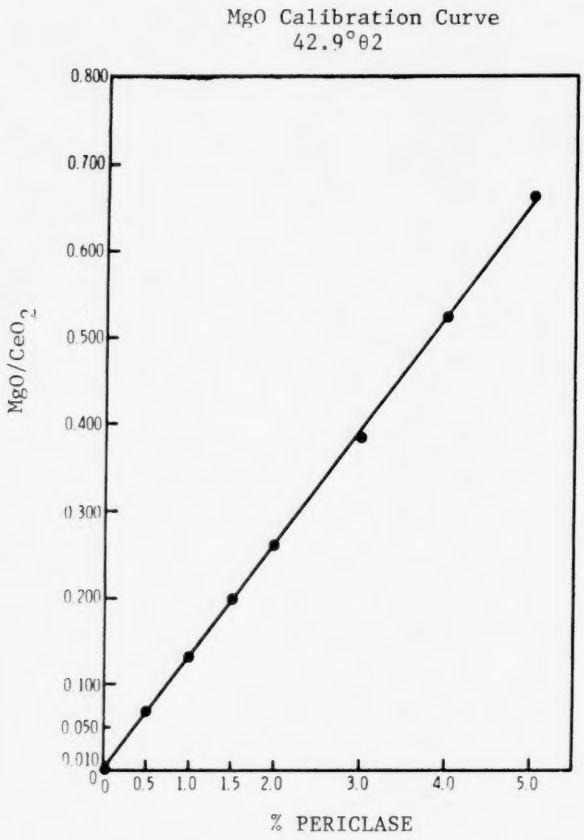

FIG. 5
Periclase calibration curve

Three pellets were pressed from each sample and each pellet was scanned three times using the conditions described for the calibration curve. The peak heights were measured, the ratios were calculated, and the average was used to determine the percentage of C_3S and β-C_2S by direct reading from the graph or calculation using the calibration equation.

Periclase analysis:

2.0000 grams of the 5.0 grams preground sample were weighed and placed into the Spex mixer mill along with 0.0600 grams CeO_2. The sample was then ground with freon for 10 minutes and extracted with salicylic acid to remove calcium silicates (7,8). The residue was removed by vacuum filtration and dried in a dessicator.

The pellets were prepared in the same way and run under the same conditions as used in the periclase calibration curve. A fast scan from 5° to 70°2θ was also run to qualitatively determine other phases present. The average periclase to CeO_2 ratio is then used to determine the percent periclase in the unextracted sample.

VOL. 14 1984

Analysis of six cement samples:

Six previously analyzed cements, Incas samples E1 through E6, were re-analyzed in an attempt to evaluate the accuracy and usefulness of the described procedure. These samples have been studied extensively by Aldridge and have been quantitatively analyzed by several laboratories by XRD. Our and Aldridge's results are listed in Table 3 (12).

TABLE 3

Results of QXRD analysis of Incas samples

Results	Experimental [a]		Aldridge [b] (12)		Bogue Values (13)	
Sample	%C_3S	%C_2S	%C_3S	%C_2S	%C_3S	%C_2S
E1	74.6 (5.2)	8.5 (1.7)	69 (5)	15 (4)	66.5	12.4
E2	69.1 (3.9)	3.8 (1.8)	72 (8)	12 (5)	73.0	8.7
E3	59.4 (3.0)	10.1 (1.3)	62 (7)	19 (5)	59.3	17.2
E4	44.2 (1.1)	26.1 (2.3)	49 (5)	31 (5)	43.9	33.6
E5	55.5 (2.0)	8.6 (1.4)	59 (10)	21 (8)	58.3	15.2
E6	60.0 (4.8)	22.3 (2.0)	61 (6)	26 (6)	54.3	27.0

(a) Standard deviations of results for nine pieces of data from three pellets three scans per pellet.

(b) Standard deviations from the laboratories that submitted analysis results to Aldridge are shown in brackets.

Results and Conclusions

The C_3S analysis results fell within one standard deviation of Aldridge's with the exception of E1 which was slightly more. The β-C_2S analysis results fell significantly lower than Aldridge's values. The reason for the low β-C_2S results is unknown. It may be related to the minerology or particle size of the Incas samples, the synthetic β-C_2S used in the calibration, or to interstitial overlap of the measured peaks.

Although the procedure produced adequate and relatively rapid results for the comparison of cements and clinkers, there is some doubt as to their absolute accuracy. The improvements needed include recalibration using integrated peak areas, better data collection and reduction procedures, the use of a rotating sample holder, as well as calibrations for CSH_2, $CSH_{1/2}$, CS, C_4AF, and C_3A. The further automation of data collection and reduction will increase the speed of the analysis by reducing the time-consuming manual manipulation of data. Also, using a KOH-sugar extraction for the removal of interstitial minerals which may overlap C_3S and β-C_2S peaks should improve the results significantly be decreasing overlap related errors. This extraction will lengthen the procedure somewhat, however, the improvement in the results should justify the additional time.

This work shows that CeO_2 is an acceptable internal standard for cement and clinker analysis. It has some advantages over silicon, such as less of a tendency for preferred orientation and better intensity reproducibility as measured by peak height. It is also physically and chemically stable under these analytical conditions.

The results reported in this paper are only preliminary. More work is planned to improve this technique. However, even with the present data the advantages of CeO_2 over Si have been established.

Acknowledgements

I would like to express my thanks for the invaluable discussions, comments and technical assistance provided by J. Skalny, I. Jawed and J. Epp. I would especially like to thank L. Struble for her advice and assistance in the calibration portion of this procedure. Her previous work was the foundation on which the calibration portion was based. Support for this work was provided by The Martin Marietta Corporation, Cement division.

References

1. Klug and Alexander, X-ray Diffraction Procedures for Polycrystalline and Amorphous Materials, John Wiley and Sons, New York, Second Edition, p.p. 536-552 (1974).
2. JCPDS Powder Diffraction File, Inorganic Phases, Search Manual, JCPDS International Centre for Diffraction Data, Swarthmore, PA (1981).
3. JCPDS card file, Inorganic Phases, JCPDS International Centre for Diffraction Data, Swarthmore, PA (1981).
4. Palache, Berman, Froudel, Dana's System of Mineralogy, John Wiley & Sons, Inc., New York, Seventh Edition, Volumes 1,2 & 3 (1944).
5. Weast, Handbook of Chemistry and Physics, 62nd edition, CRC Press, Inc., (1981).
6. The Merck Index, Merck & Co., Inc., Ninth Edition (1976).
7. Klemm, W. and Skalny, J., Selective Dissolution of Clinker Minerals and Its Applications, Martin Marietta Laboratories, Baltimore, MD, (1980) Technical Report 77-32, p. 12.
8. Moore, A. Cement Technology 7 85-94 (1976).
9. Tabikh, A. and Weht, R. Cement and Concrete Research 1, 317-328 (1971).
10. Struble, L., Martin Marietta Laboratories, Baltimore, MD, (1982). Private communication.
11. Struble, L., Martin Marietta Laboratories, Baltimore, MD, (1982). Quantitative X-ray Diffraction Progress Reports, No. 1 (MML TR 80-22) and No. 2 (MML TR 80-45).
12. Aldridge, L.P., International Cement Analysis Study, Part 3, Quantitative X-ray Diffraction Analysis of Cements, Department of Scientific and Industrial Research, New Zealand, 1975.
13. Aldridge, L.P., International Cement Analysis Study, Part 4, Comparison of Results, Department of Scientific and Industrial Research, New Zealand, 1978.

VOL. 14 1984

CEMENT and CONCRETE RESEARCH. Vol. 14, pp. 741-748, 1984. Printed in the USA.
0008-8846/84 $3.00+00. Copyright (c) 1984 Pergamon Press, Ltd.

Hydrothermal Study in the System Na_2O-CaO-SiO_2-H_2O at 300°C

Yaozhong Xi[1] and L.S. Dent Glasser

Department of Chemistry, University of Aberdeen
Meston Walk, Old Aberdeen AB9 2UE, Scotland UK.

(Communicated by D.M. Roy)
(Received Jan. 30, 1984)

ABSTRACT

Using silicic acid, fused quartz, CaO, NaOH, α-CS, NS, NC_2S_3, N_2CS_3 (2) as starting materials, reaction products are pectolite, β-NS_2, xonotlite, foshagite, NC_2S_2H, CH, $C_6S_2H_3$, quartz and NS. Pectolite is the predominent phase; its formation requires a minimum amount of water as solvent. Pectolite and NC_2S_2H are the only two quaternary products in the system. The reactivity of the starting materials, conditions of formation and the importance of the aqueous phase, including the way it is added, are discussed.

Introduction

The system Na_2O-CaO-SiO_2-H_2O at 25°C was first studied by Kalousek (1). Pectolite (NC_4S_6H), the predominent phase in the system, had been synthesised earlier by Clark and Bunn (2), by treating a mixture of lime, precipitated silica and sodium hydroxide at 100°C for 3.5 days. A further quaternary phase, $CaNaHSiO_4$ (NC_2S_2H) was first produced by Thilo, Funk and Wichmann (3), who autoclaved NCS at 100°C. Recent interest in the system has centred on

---

1) Permanent address: Research Institute of Building Materials, Guanzhung, East Suburb, Beijing, The People's Republic of China.

2) The following abbreviations are used in this paper:

P = pectolite (NC_4S_6H), F = foshagite (C_4S_3H), T = truscottite ($C_7S_{12}H_3$), Q = Quartz, sa = silicic acid, fq = fused quartz, w/s = water:solid ratio.

the effect of NaOH on hydrothermal reactions in the system $CaO-SiO_2-H_2O$ at 100°C (4) and at 300 - 650°C (5), and on the development of geothermal well cements and deep oil-well cements (6,7,8).

The aim of the present work was to find whether any new phases could be prepared in this system at 300°C. A thorough survey (110 runs) detected no new phases under the conditions used, but the data obtained do further characterise the phase relations in the system at elevated temperatures, and reveal that the phase NC_2S_2H can be prepared from a wider range of compositions than was formerly believed.

Experimental

AnalaR grade materials were used except as noted. CaO was made by burning $CaCO_3$ at 1050°C for 6 hours. Soda was introduced as sodium hydroxide pellets. Fused quartz (Spectrasil) had 0.02% total impurity, fineness 100 mesh. Silicic acid (Mallinkrodt Inc.) contained 85.4% SiO_2, 0.015% max. Al.

NS, NC_2S_3, N_2CS_3 and α-CS were prepared by heating stoichiometric mixtures of Na_2CO_3, $CaCO_3$ and fused quartz; all were decarbonated at 850°C and the reaction completed at 1350, 1200, 1060-1160 and 700-850°C respectively. Each product was reheated and reground three times or more until the X-ray powder pattern showed only the pure crystalline phase with no free CaO.

Hydrothermal preparations were carried out in standard Morey bombs of 15 mℓ capacity with silver tube inserts of 6 mℓ capacity. For each run about 0.1-0.4 g of solid starting materials were weighed directly into the silver inserts and 0.1-8.0 mℓ of water added. The bombs were held at 300 ± 10°C for 1-10 days and the reaction products were examined using a Hägg Guinier camera with $CuK_{\alpha 1}$ radiation.

Throughout the work, special care was taken to avoid contamination by atmospheric carbon dioxide; the water added to the bombs was always free of CO_2.

RESULTS AND DISCUSSION

Hydrothermal Products

Representative runs are listed in Table 1, 2, and 3 and plotted on Fig. 1. This figure is not an equilibrium diagram, but attempts to show the products of runs of different starting compositions, indicated by open circles. Solid lines connect these starting compositions to the products detected at the end of the run. This method of plotting shows very clearly that very few runs gave a single-phase product, and also that the products were almost always poorer in soda than the starting composition, indicating that another phase, a sodium-rich solution, was almost invariably present. Figure 2 shows very rough fields for the formation of different products, based on the data in Fig. 1 and the tables.

Crystalline products detected included pectolite, β-NS_2, xonotlite, foshagite, $C_6S_2H_3$, NC_2S_2H, CH, quartz and NS, all of which have previously been found in the system; these are indicated by full circles in Fig. 1. The most commonly encountered phase was pectolite; this and NC_2S_2H were the only quarternary phases detected. No new phase containing both Na and Ca was found; tobermorite did not appear: β-NS_2 was present near the siliceous corner.

VOL. 14 1984

Table 1

Hydrothermal products with 2 mℓ water in bombs at 300°C for 2-4 days

No.	Starting Materials 0.1 - 0.4 g	Mole percentage N	C	S	Products Detected
1	NS + C + sa	2.8	42.2	55.0	X + Q
2	N_2CS_3 + fg	8.3	4.2	87.5	Q + β-NS_2 + P
3	NS + C	8.5	83.5	8.5	CH
4	NC_2S_3 + sa	9.9	19.8	70.3	P + Q
5	NS + C + sa	12.2	11.3	76.5	Q + P
6	NS + C	13.1	73.9	13.1	CH + $C_6S_2H_3$ + F
7	NC_2S_3 + sa	13.3	26.6	60.2	P + Q
8	NC_2S_3 + sa	14.9	29.7	55.4	P
9	NS + C	15.7	68.5	15.7	$C_6S_2H_3$ + CH + F
10	NC_2S_3 + sa	16.0	32.0	52.0	P
11	NS + C + sa	18.0	19.7	62.3	P + β-NS_2
12	N_2CS_3 + sa	19.8	9.9	70.3	Q + P + β-NS_2
13	N_2CS_3 + fg	25.0	12.5	62.5	P + β-NS_2 + Q
14	NS + C	30.0	40.0	30.0	CH + P + NC_2S_2H
15	NS + C + sa	30.4	4.3	65.3	P + β-NS_2
16	NS + C + sa	32.0	2.1	65.9	β-NS_2 + Q + p
17	N_2CS_3 + sa	32.0	16.0	52.0	P
18	NS + C + sa	33.7	53.6	12.6	CH + NC_2S_2H
19	NS + C	36.7	26.6	36.7	P
20	NS + C	37.1	25.7	37.1	P
21	NaOH + C + sa	42.2	23.6	34.1	P + NC_2S_2H
22	NaOH + C + sa	44.0	39.0	17.0	CH + NC_2S_2H
23	NaOH + C + sa	60.7	19.6	19.6	P
24	NaOH + C + sa	69.3	15.7	15.1	NS
25	NaOH + C + sa	78.6	10.0	11.4	Solution

Table 2

No.	Starting Materials	Mole percentage N	C	S	Water (mℓ)	time (h)	Temp (°C)	Products detected
26	NS + C + sa	24.0	26.0	50.0	2	3	300	P + β-NS_2
27	N_2CS_3 + α-CS	16.7	33.3	50.0	1	48	300	P + α-CS
28	N_2CS_3 + α-CS	16.7	33.3	50.0	4	48	300	P + α-CS
29	α-CS	0	50.0	50.0	2	6 d	400	α-CS
30	NaOH + α-CS	12.0	35.2	52.9	2	10 d	300	P + α-CS
31	NaOH + C + sa	16.7	33.3	50.0	2	46	300	P
32	NaOH + C + fq	16.7	33.3	50.0	2	46	300	P + CH + Q
33	NaOH + C + fq	16.7	33.3	50.0	8	46	300	P
34	NC_2S_3 + sa	9.9	19.8	70.3	2	49	300	P + Q
35	N_2CS_3 + sa	26.5	13.3	60.2	2	48	300	P + β-NS_2
36	N_2CS_3 + sa	29.9	15.0	55.1	2	48	300	P + β-NS_2
37	N_2CS_3 + sa	26.5	13.3	60.2	2	7 d	200	P + β-NS_2
38	N_2CS_3 + sa	29.9	15.0	55.1	2	7 d	200	P + β-NS_2

Abbreviation : d = days

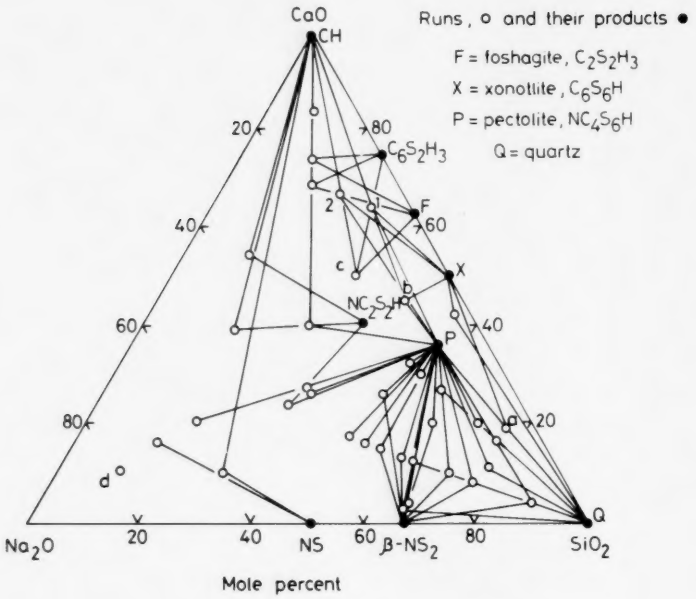

FIG. 1

Hydrothermal products in the system Na_2O-CaO-SiO_2-H_2O at 300°C Runs were for 2 - 4 days, 2 mℓ water added, with silicic acid, NS, NC_2S_3 or N_2CS_3 as source of silica. Composition of runs is shown by open circles; they are connected by solid lines to the products formed, which are shown as full circles.

Incomplete lines indicate that the product did not form from the run in question. For example, composition 1 gave CH, X and P, connected to it by complete lines, but not F or $C_6S_2H_3$ as shown by the gaps in the lines. Similarly, composition 2 gives P, X and CH, but not F. These two compositions, and those labelled a, b, and c, correspond to the compositions in Table 4. The run marked d gave no crystalline product, being mainly soluble.

NC_2S_2H occurred in a few runs with excess water (w/s about 10), which is surprising, since previous syntheses (3,4) used very little water. This condition does not however seem to be necessary. Xonotlite was formed in runs containing about 10 mole or less Na_2O.

Reactivity of Starting Materials

Table 2 and 3 enable the reactivity of different starting materials to be compared. NS, silicic acid, NC_2S_3, and N_2CS_3 all react rapidly. Comparing sample 31 with 32 (Table 2), shows that fused quartz is less reactive than silicic acid, because of its coarseness and high density, and because the silicic acid has a high content of silanol groups. α-CS reacts very slowly with water, remaining unchanged after 6 days at 400°C (run 29, Table 2), although it partly reacted with NaOH in 10 days at 300°C (run 30, Table 2) to form pectolite. Using the more reactive starting materials, pectolite forms at 300°C in a matter of hours (run 26): at 200°C (runs 37, 38) pectolite forms after 7 days. It can therefore appear over a range of temperatures (4,8).

VOL. 14 1984

Table 3

Effect of varying quantities of water added to bombs at 300°C
(Starting materials 0.1 - 0.4 g)

No.	N:C:S	Starting Materials	Water (mℓ)	time (h)	Products detected
39	1 2 3	NC_2S_3	0.1	66	NC_2S_3
40	1 2 3	NC_2S_3	0.2	50	P + NC_2S_3
41	1 2 3	NC_2S_3	0.5	48	P
42	1 2 3	NC_2S_3	0.8	50	P
43	1 2 3	NC_2S_3	1.0	66	P
44	1 2 3	NC_2S_3	1.5	24	P
45	1 2 3	NC_2S_3	2.0	48	P
46	1 2 3	NC_2S_3	2.5	24	P
47	1 2 3	NC_2S_3	4.0	24	P
48	1 2 3	NC_2S_3	8.0	48	P
49	1 2 3	NC_2S_3	2.0(1)	67	NC_2S_3
50	2 1 3	N_2CS_3	0.1	66	N_2CS_3
51	2 1 3	N_2CS_3	0.2	47.5	NC_2S_3 + NS + P
52	2 1 3	N_2CS_3	0.5	47.5	P + NS
53	2 1 3	N_2CS_3	0.8	48	P
54	2 1 3	N_2CS_3	1.0	66	P
55	2 1 3	N_2CS_3	2.0	49	P
56	2 1 3	N_2CS_3	4.0	24	P
57	2 1 3	N_2CS_3	8.0	48	P
58	2 1 3	NaOH+C+sa	0.2	47.5	NC_2S_3 + NS + P
59	2 1 3	NaOH+C+sa	0.5	47.5	P + NS + β-NS_2

(1) Water was added into the bomb outside the silver tube. Water was added into silver tubes in all the other runs.

Function of Water

The water added to a run fulfils three functions:

(i) generation of pressure,

(ii) provision of structural water,

(iii) solvent action.

With regard to (i), calculation using Van der Waals' equation* indicates that about 0.6 mℓ H_2O should be sufficient to produce saturated steam in a bomb of 15 mℓ capacity; the exact pressure generated is somewhat indeterminate, because the composition of the soda-rich solution is not known.

For the provision of structural water, (ii), very little is needed; about 1 μℓ provides enough to form pectolite from 0.1 - 0.4 g starting materials.

The solvent action, (iii), is plainly important; it has already been remarked that Fig. 1 shows that the crystalline phases produced are almost always poorer in soda than the starting materials. Further evidence about this is provided by comparison of the products formed when water is added in physically distinct parts of the system, as discussed below.

Table 3 shows the effect of varying the amount of water added. Runs 39 - 48 show what happens to NC_2S_3 as the amount of water added into the silver tube is varied. When 0.1 mℓ is added, there is no reaction; presumably all the water departs into the vapour phase before reaction has a chance to proceed; 0.2 mℓ produces some pectolite - perhaps in the presence of liquid water while the temperature is rising, which takes about 2 hours from room temperature to 300°C - but much unchanged starting material remains; for 0.5 mℓ or more (roughly corresponding to the 0.6 mℓ calculated to be needed to give saturated steam) identical products form, independently of the actual quantity added, provided that it is added into the silver tube insert.

Surprisingly, it does seem to matter where the water is added; in run 49, 2.0 mℓ water were added to the bomb outside the tube, whose contents were left dry. Under these conditions, no pectolite formed even after nearly

*Van der Waals' equation: $(P + \frac{a_o}{V^2})(V - b_o)\,RT$, $a_o = 5.46$, $b_o = 3.05 \times 10^{-2}$

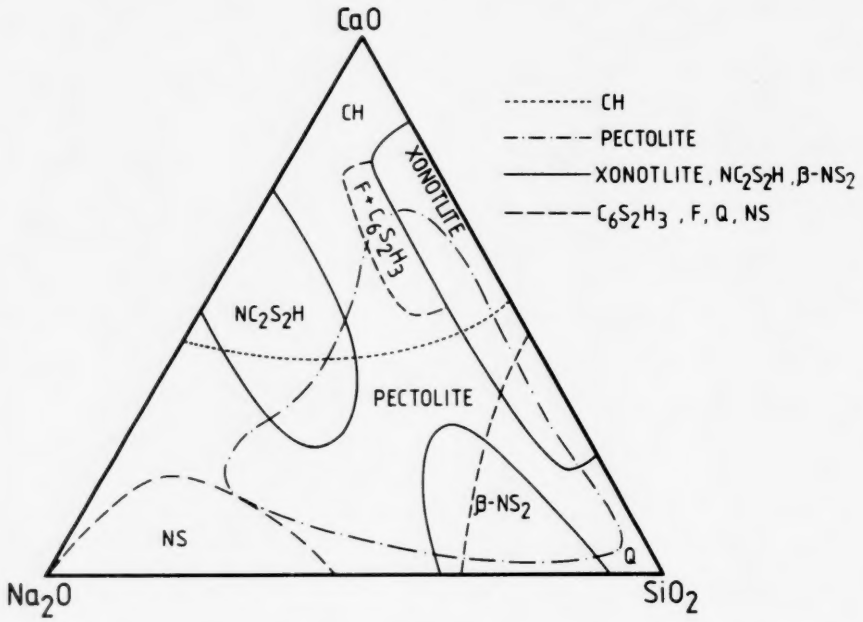

Fig. 2

Possible formation fields for products in the system Na_2O-CaO-SiO_2-H_2O at 300°C. The areas are based on Fig. 1, and are the minimum needed to account for the results therein; the true areas could be larger.

three days. One would have intuitively expected that in the course of that time, the water would have redistributed itself around the physical space available to it; indeed, the presence of soluble material in the charge within the silver tube should (through lowering of the vapour pressure) encourage the condensation of liquid water within the tube. This does not however, appear to happen, and the observation helps to explain discrepancies between different studies, as discussed in the next section.

With more soda-rich starting materials (runs 50 - 59), variation of products with water content was again observed. As before, with very small quantities there is no reaction; with slightly larger quantities, a sodium silicate phase is found; with still larger quantities, the latter disappears because of its relatively high solubility.

Formation of Pectolite

De Vynck (5), using quite similar conditions of temperature and pressure to the present work (Table 4), did not observe the formation of pectolite. He used an autoclave vessel kept under saturated steam pressure at 300°C; we used Morey bombs at 300°C: the pressure in them would have been slightly lower than that calculated for pure water because of the dissolved sodium silicates (about 0.1 N) but probably not significantly so. The principal difference between the two sets of experiments is in the physical location of the water at the start of the runs.

De Vynck's reaction mixture was thick paste and the pressure was

VOL. 14 1984

Table 4

Comparison of some runs in present study with those by De Vynck (5) at 300°C.

mole ratio N	C	S	present study[1] (w/s ∿ 10)		De Vynck[2] (thick paste)
0.25	1	4	X + little p + Q	(a)[3]	T + gel
0.25	1	1	p + CH + X	(b)	F + T
0.5	1.5	1	$C_6S_2H_3$ + CH + F	(c)	F + NC_2S_2H
0.25	2	1	P + CH + X	(1)	F
0.5	3	1	P + CH + X	(2)	CH + F + NC_2S_2H

1) In Morey bombs, 0.2 - 0.3 g starting material was used. NS, CaO, silicic acid were starting materials.

2) 50 cc thick paste, made of NaOH, CH, pure silica gel and little water, was placed in a pure iron crucible with a pure iron lid. Crucibles were kept in a 50 cc autoclave with saturated steam pressure (87 kg/cm²) at 300°C.

3) Letters (a) (b) (c) and (1) and (2) refer to points on Figure 1.

generated by water outside the iron crucible that contained it. In his runs, therefore, less water was in direct contact with the reactants than in the present study, when water was added directly to the reactants in the silver tube. (As already pointed out, the products are different if the reactants are left dry, and the water addded to the bomb outside; if the water is not in direct contact with the starting material but serves only to generate pressure, there is no reaction.) It seems that in order for pectolite to form, sufficient water must be in direct contact with the starting materials, and this in turns seems to indicate that the reaction must go through solution. This explains the differences between our results and De Vynck's; obviously care is needed in comparing the results of different workers if the details of the experimental techniques are not fully known.

This is most interesting, since it implies that physical equilibrium (let alone chemical equilibrium) is not always reached in closed systems. Since the partial vapour pressure of the solvent in a solution is lower than that in a pure solvent, water added outside the reaction vessel ought, in theory, to distil into it; in practice, this apparently does not happen, at least not in the course of the first few days. It seems likely that other seeming inconsistencies in the literature could be attributable to this.

Pectolite, usually accompanied by xonotlite, truscottite, foshagite, tobermorite or sodium silicates, is the most frequently encountered phase in the system. It shows high strength and impressive resistance to corrosion by geothermal brines, and its possible use as a binder in the geothermal environment has been investigated (6,7). Pectolite, forming as it does at relatively low temperature (>180°C) could be a desirable component of ordinary hydrothermal products that, while being basically calcium silicates, utilise raw materials that contain relatively high amounts of sodium.

Summary

1) Using Morey bombs at 300°C, the hydrothermal products starting from a variety of starting materials at w/s ∿10 are pectolite, β-NS_2, xonotlite, foshagite, NC_2S_2H, CH, $C_6S_2H_3$, quartz and NS. No new quaternary phases were detected. NC_2S_2H can appear not only under restricted water conditions, but also in the presence of excess water.

2) Pectolite readily forms from most compositions in the system, provided sufficient water is present. It appears to form by reaction through solution.

3) As starting materials, NS, NC_2S_3, N_2CS_3 and silicic acid are very reactive, fused quartz less so and α-CS is quite inert.

4) The physical region in which the water is added to the system is important. Water added outside the reactant container serves to produce vapour pressure, but in some cases at least, may not be available as a component in the reaction. Physical equilibrium may not be reached in the course of a few days.

Acknowledgement

We thank the Chinese Government for travel and living support to Mr. Xi, which allowed him to work in Aberdeen. This work was presented at the 85th Annual Meeting of the American Ceramic Society in Chicago, 1983.

VOL. 14 1984

References

1. G.L. Kalousek, J. Res. Natl. Bur. Stand., 32, 285 (1944).
2. L.M. Clark, C.W. Bunn, J. Soc. Chem. Ind. 59, 155 (1940).
3. E. Thilo, H. Funk and E.M. Wichmann. Abhandl. deut. Akad. Wiss. Berlin, Klasse Math. allg. Naturw. 4 (1951).
4. E.A. Blakeman, J.A. Gard, C.G. Ramsay and H.F.W. Taylor, J. appl. chem. Biotechnol. 24, 239 (1974).
5. I. De Vynck, Bull. Soc. Chim. Belg., 89, 715 (1980).
6. E.B. Nelson and G.L. Kalousek, Cem. Concr. Res. 7, 687 (1977).
7. E.B. Nelson, L.H. Eilers and G.L. Kalousek, Cem. Concr. Res. 11, 371 (1981).
8. C.A. Langton, E.L. White, M.W. Grutzeck and D.M. Roy, 7th Int. Cong. Chem. Cement, Paris, 3, V-145 (1980).

CEMENT and CONCRETE RESEARCH. Vol. 14, pp. 749-753, 1984. Printed in the USA.
0008-8846/84 $3.00+00. Copyright (c) 1984 Pergamon Press, Ltd.

A PLEA FOR RECOGNITION OF THE IMPACT OF CHEMISTRY ON THE DURABILITY OF CONCRETE

G.M. Idorn, D. Sc.
G.M. Idorn Consult ApS, Naerum, Denmark

(Communicated by J. Skalny)
(Received Nov. 14, 1983; in final form Jan. 18, 1984)

ABSTRACT

The European organizations CEB and RILEM arranged a workshop on the durability on concrete in May 1983 at the Technical University in Lyngby, Denmark. The background was increasing public concern the last few years about soaring costs for rehabilitation of deteriorating concrete used in housing, roads, bridges, and other applications that closely affect all levels of society. Presented at the workshop, the present paper is an attempt to view the problem beyond an assessment of the technical issues, and to propose solutions. Based on experience from research since 1953 and from numerous investigations of the deterioration of modern concrete and the durability of older concrete, the writer points out essential requirements for updating concrete technology, and emphasizes the need to apply and incorporate adequate chemical knowledge in concrete technology education.

Introduction

The cement industry has learned through intensive research to apply inorganic chemistry for effective monitoring of the cement manufacturing processes. However, concrete structural design and construction are still largely carried out without application of chemical knowledge for monitoring concrete's remarkable sensitivity to workability, curing, and exposure to harmful elements in the environment.

The most essential feature in present day concrete technology is that the technical and industrial development during the last 30-40 years has made concrete a chemically reactive system throughout its phases: 1) as fresh concrete, 2) during curing, and 3) during performance. This is due to the integral effects of many kinds related to factors such as:

- Chemical admixtures
- Mineral substitution materials
- Strength capability of cement
- Rates of concrete production
- Demands on structural capability
- Aggressive environments.

Altogether these developments have greatly improved the ability of concrete to serve general social development as a foundation for housing, industrial production, and infrastructure functions. This can with justification be considered a great civil engineering feat.

However, the general "public voice" is now speaking with increasing concern, frequently raising to anger, against the deplorable ways in which concrete is malfunctioning. This is because a high degree of performance capability of concrete in service now shows an unexpected price tag of defective performance reliability. Corrosion of reinforcement and alkali-silica reactions have been pinpointed as the major deleterious mechanisms. One of the contributions to the discussions of the CEB-RILEM workshop emphasized that engineering, in contrast to research, needs to be a decision-making business. Unfortunately then the workshop must be considered a consequence of an increasing impact of wrong engineering decisions, which have made concrete durability the most controversial issue of civil engineering at the present time.

Under these circumstances, it is somewhat peculiar that the workshop seemed to demonstrate practically complete agreement between delegates regarding the various issues under discussion. This could imply either that the delegates constituted the supreme elite of the situation, ready to formulate and implement the solutions to the problems, or that the discussions were not based on actual practice.

VOL. 14 1984

The Role of Research

The research community ought to be aware that the impact of the dissatisfaction with concrete falls upon the civil engineering community, while the research people are sheltered by the "modelwalls" between themselves and engineering practice. Therefore, research is still, in principle, supporting technology conceptions that largely treat field concrete as a "static" material - in the fresh state characterized by the slump test, in the hardened state by its compressive strength at room temperature curing.

Meanwhile, the inorganic chemists have at their disposal advanced knowledge on reaction kinetics and thermodynamics to explain the energy and mass transfer in concrete during its modern manufacture. This data cannot, with modern cements and rates of production, be boiled down to simple fragmentary, regulatory acceptance figures for the civil engineering design and site control, as in the past days of craft-predominated concrete making.

Fresh concrete with the compositions and fineness of modern cements, including slag, fly ash, or silica fume and with one or another of the many available chemical admixtures, is a reacting colloid system from the very moment of mixing, and the workability of concrete is time/temperature dependent during its processing.

Curing of modern concrete is on the one hand a heat preservation process meant to take advantage of rapid strength development. On the other hand, if not monitored, it is a source of lasting flaws, high porosity and microcracking in the hardening concrete, and can soon damage long-term resistance of the hardened concrete. By application of Arrhenius' and Fourier's laws, curing is however a process that now can be perfectly well designed and monitored on-line during concrete production.

Despite the general reliance on conventional technology concepts, hardened concrete is increasingly exposed to deleterious physico-chemical processes, which are only nominally treated by research. Most frequently, this area of chemistry is taught and applied as if adequately modelled by room-temperature stoichiometric equations. However, the real chemical processes in concrete are to a large extent colloidal, never reach equilibrium stages, and are utterly dependent upon humidity, temperature, and on the availability of reactants. Investigations of concrete deterioration therefore usually lead to findings different from the generally accepted laboratory models.

The Importance of Concrete Chemistry

The neglect of concrete chemistry is remarkable considering the spectacular development of instrumentation and methodology for micro and submicro studies of the morphology and structure of concrete; for instance, using optical petrography, X-ray diffractometry, DTA-DTG, and electron microscopy. These new developments have occurred during the same era in which concrete deterioration has grown to a problem on the societal level of importance.

Yet, very few countries have more than a handful of skilled petrographers, and much research still explains hydration of cement on the basis of room temperature experiments far removed from the conditions to which contemporary concrete hardening is exposed.

L.
4
84

Likewise, despite the routine application in modern concrete production of chemical and mineral admixtures and energy-intensive concrete processing technology, the majority of research still relies on the obsolete static slump test, and has not produced adequate up-to-date rheology-monitoring instrumentation. Colloid chemistry plays only an obscure role in concrete research at the present time, and therefore does not attract funding sponsorships for long-term work.

During the workshop, several speakers have stressed the importance of concrete permeability - referring to a dependence on w/c, quoted from experimental work by T.C. Powers back in 1949. That has but little application as a generalization to concrete in 1983. Also, the influence of C_3A in cement has been touched upon in general terms, without regard for the simultaneous influence on the durability of varying C_4AF and C_3S contents.

Furthermore, curing has been discussed without clear identification of the deleterious impact of flaws and increase of porosity/permeability, which are characteristic consequences of overheating of modern concrete during the early phase of hardening.

Proposed Solutions

A Fundamental Educational Approach

Having been faced for a number of years with neglect of concrete chemistry in contemporary engineering technology, the writer identifies education as the most fundamental issue for the improvement of concrete durability. Universities must provide updated courses on concrete chemistry to stu-

dents of concrete technology. This is not a request impossible to comply with since most universities and technology education centers possess elaborate, empirical, civil engineering-based technology courses. However, the presently increasing deterioration of concrete shows that the content of these courses does not suffice for modern practice.

At the same time, most of the same educational institutions do possess chemical departments with the needed knowledge available. It is therefore feasible to establish integrated physico-chemical courses in most countries, and these ought to be initiated with the help of outstanding member of the research community.

A Realistic Approach

Because of the controversial nature of the problem, it may be useful to adopt a realistic approach that might improve the concrete durability situation in the broad, international theatre.

First, one must realize that there is not much which can be done with noticeable effects within a short time period. The revenues in consulting and contracting engineering have plunged now for a number of years, and competition has taken heavy tolls in profitability and generally drawn attention to priorities other than alteration of the concrete technology. Simultaneously, the funding of research, public and private, has shrunk, and much research has itself become contaminated by commercial necessity. This has caused sudden media and political attention to "bad" concrete to gain an exaggerated governing influence on the research planning and policies, beyond more valuable analyses of durability problems.

VOL. 14 1984

Those presently engaged - within CEB-RILEM and elsewhere - in action planning to solve the problems must therefore rely upon undivided dedication if significant progress is to be made in the state of the art.

A Concept for Action-Planning

The best advice to CEB-RILEM is that these organizations strengthen cooperative efforts, with:

- An analysis of research and education needs in basic scientific and application-orientated education. Implementation of the necessary chemically-based research requires that knowledge of chemistry be incorporated in the study of concrete technology engineering.
- Adequate attention paid to both concrete processing and concrete behavior. The processing of fresh concrete ought to be emphasized as a neglected area because conventional concrete-making historically has developed as a craft, which is no longer valid, neither in the industrialized countries nor in developing regions.

Any CEB-RILEM or other organizational approach should consider both short-term and long-term activities. At present, under the pressure of apparently insurmountable short-term problems and limited resources, attention becomes exclusively directed toward immediate needs and conventional views. This situation easily enhanses reinforcement of obsolete conceptions and neglects the importance of concrete chemistry.

The major short-term need is to apply adequate chemical knowledge in concrete manufacture. The long-term strategy is to develop a reliable basis for education of new concrete technology engineers who can learn to regain the broad public confidence that is required to make concrete serve its indispensable social functions.

As an immediate action, CEB-RILEM ought to arrange for disseminating information to university and engineering schools about desirable themes for integrated concrete chemistry-engineering technology courses both for undergraduate and graduate students. Presumably, an undertaking in that direction would stimulate present CEB-RILEM involvement in the issue of concrete durability. To promote innovations in practice and progress of science and research.

Concluding Remarks

It is striking that the CEB-RILEM cooperative work is exclusively civil-engineering orientated. Most chemistry applied so far has been presented and used in simplified models feasible for adaption in concrete specifications and convenient testing procedures. Consequently, scientists with a basis in chemistry have either adopted exaggerated popularisation in their communications or confined themselves to communicate with other chemists rather than with civil engineers.

This hegemony of civil engineering in concrete technology was advantageous in the classic engineering era up to about 1950-1960, when concrete durability was still assumed, and when civil engineers had basic courses in chemistry.

Today, things are different. The chemistry in concrete manufacture and use is becoming an increasingly expensive barrier against urgent progress of the civil engineering art. This is essentially why CEB-RILEM is advised to do something to change the present course.

CEMENT and CONCRETE RESEARCH. Vol. 14, pp. 754-756, 1984. Printed in the USA.
0008-8846/84 $3.00+00. Copyright (c) 1984 Pergamon Press, Ltd.

NOTES

EFFECT OF SUPERPLASTICIZING ADMIXTURES ON CEMENT HYDRATION

A. Mor and P. K. Mehta
Department of Civil Engineering
University of California, Berkeley, CA 94720

(Communicated by D.M. Roy)
(Received Jan. 17, 1984)

VOL.
14
1984

Since the advent of superplasticizing admixtures (ASTM Class F, high range water-reducers), many investigators have reported water reductions of the order of 15 to 25 percent by incorporation of these admixtures in concrete. The corresponding increase in concrete strength has, generally, been attributed to the reduced water-cement ratio.

Johnston et al (1) found that even when the water-cement ratio was kept constant the superplasticized concrete showed higher compressive strengths at early ages than the reference concrete, however, at later ages the difference in strengths was negligible. For instance, in a concrete mixture containing a naphthalene-condensate type admixture, at 0.5 water-cement ratio it was found that the 7-day compressive strength of the superplasticized concrete was about 20 percent higher than the reference concrete, but at 365 days the strength difference was reduced to less than 5 percent. Johnston et al speculated that this increase in early strength of concrete in the presence of a superplasticizer was probably due to the higher rate of cement hydration. However, contrary results are reported by Gu Dezhen et al (2) who found that, compared to a reference cement paste made with 0.25 water-cement ratio, the superplasticized pastes including one containing a naphthalene-condensate had less water of hydration (combined or nonevaporable water) at 1, 3, 7, and 28 days.

The authors carried out a preliminary investigation to clarify the issue. Concrete mixtures of constant water-cement ratio were made with ASTM Type I portland cement and two types of superplasticizers, namely a naphthalene formaldehyde condensate and a melamine formaldehyde condensate. The amount of superplasticizer in concrete was 1, 2, or 3 percent by weight of cement. Compared to reference concrete, the 7 and 28-day compressive strengths of superplasticized concrete were higher by 5 to 10 percent, however, tests on the 7 months old specimens showed that the strength advantage had disappeared by then. A parallel investigation was carried out on a neat cement paste hydrated with water corresponding to 0.28 water-cement ratio, and both with or

without 1 percent of either of the two superplasticizers by weight of cement. The pastes were moist-cured at normal temperature for 28 days, then the hydration was stopped by acetone washing and vacuum drying at 70°C for 24 hours. The dried specimens were tested for the combined or non-evaporable water content by ignition to constant weight at 900°C. A portion of the dried specimens was investigated for pore size distribution by Mercury Intrusion Porosimetry.

The ignition losses of the reference cement paste, the cement paste containing the melamine-condensate, and the cement paste containing the naphthalene-condensate were found to be 11.4, 13.35, and 13.60 percent, respectively. Accordingly, it can be calculated that the superplasticized cement pastes showed 17 and 19 percent higher degree of hydration, respectively, than the reference cement paste. The data of this investigation, therefore, confirm the hypothesis of Johnston et al (1) that the rate of cement hydration increases in the presence of superplasticizers.

Further affirmation of the conclusion reached above was provided by the results of pore size distribution analyses shown in the Figure. Since the pore size distributions for the cement pastes containing the superplasticizing admixtures were similar, only one plot is shown in addition to the data for the reference paste.

Mehta and Manmohan (3) suggested that, from standpoint of compressive strength, the capillary pore volume in a hydrated cement paste may be divided into harmful pores (e.g. pores larger than 1000Å) and harmless pores (e.g. pores smaller than 1000Å). The total cumulative volume of all capillary pores (i.e. pores >45 Å, as limited by the instrumental capacity), small capillary pores (45 to 1000Å), large capillary pores (>1000Å), and percentage of both large and small capillary pores present in the three cement pastes are shown in the following Table:

	CAPILLARY PORE VOLUME, cm^3/g			Pores, %	
	Total Volume	Small Pores	Large Pores	Large	Small
Reference Paste	0.0720	0.0433	0.0287	40	60
Paste Containing Melamine-condensate	0.0860	0.0663	0.0197	23	77
Paste Containing Naphthalene-condensate	0.0870	0.0692	0.0178	20	80

It is obvious from the tabulated data that percentage of large capillary pores in the 28-day old reference cement paste is almost twice than in the superplasticized cement pastes. At a given water-cement ratio the higher compressive strength of superplasticized concrete can, therefore, be directly associated with the lower amount of large capillary pores present in the superplasticized cement paste than the reference cement paste. Everything else remaining the same, a superplasticized cement paste, with a better dis-

persion of anhydrous cement particles, is expected to show a higher overall rate of hydration and, accordingly, a faster rate of segmentation of the large capillary spaces present in the original paste. Interestingly, Gu Dezhen et al (2) also observed an appreciable decrease in large pores, and increase in harmless pores (<250Å) in the superplasticized cement pastes.

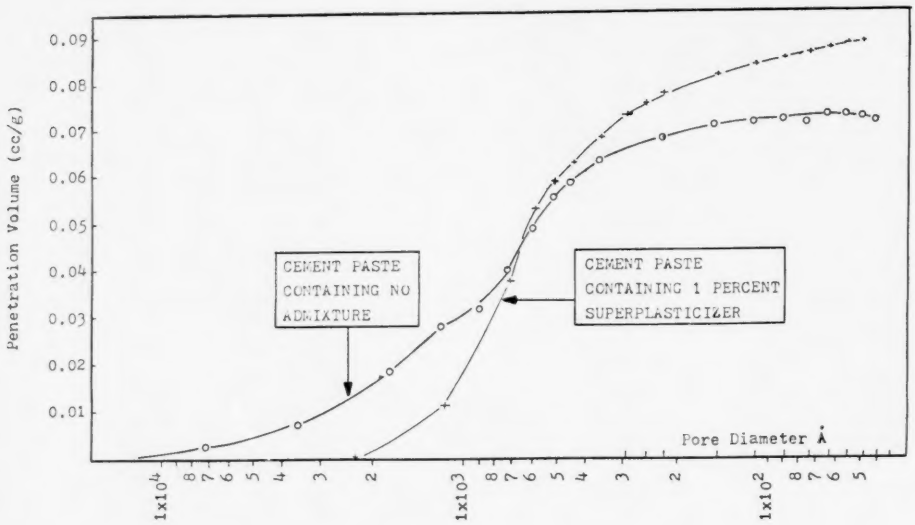

FIG. PORE SIZE DISTRIBUTION PLOTS FOR THE CEMENT PASTES

VOL. 14 1984

References

1. C. D. Johnston, B. R. Gamble, and V. M. Malhotra, "Effect of Superplasticizers on Properties of Fresh and Hardened Concrete," Proc. TRB Symp. Superplast. in Concrete, Transp. Res. Record No. 720, Washington D.C.,1979.

2. Gu Dezhen, Xiong Dayu, and Lu Zhang, "Model of Mechanism for Naphthalene Series Water-Reducing Agents," ACI Jour., V. 79, No. 5, pp. 378, 1982.

3. P. K. Mehta and D. Manmohan, "Pore Size Distribution and Permeability of Hardened Cement Pastes," Proc. 7th Intl. Congress on Chemistry of Cements, V. 3, pp. VII 1-5, 1980.

CEMENT and CONCRETE RESEARCH. Vol. 14, pp. 757-758, 1984. Printed in the USA.
0008-8846/84 $3.00+00. Copyright (c) 1984 Pergamon Press, Ltd.

THE SPACING FACTOR IN ENTRAINED AIR-BUBBLES. HAS IT ANY SIGNIFICANCE?

S. Chatterji
Teknologisk Institut
2630 Taastrup. Denmark

(Communicated by D.M. Roy)
(Received Feb. 1, 1984)

L.
4
84

It has now generally been accepted that the performance of a concrete sample in a freeze-thaw environment improves, if it contains a fine air-bubble system. Soon after the original emperical observation, Powers proposed a saturated flow hydraulic pressure hypothesis to explain the observed improvement (1). According to this hypothesis when a saturated concrete sample is in a freezing environment, ice crystals start to form in water-filled cavities of the paste. This ice formation forces some water out of the cavities, through narrow capillaries, to the air-bubbles, and it also generates the high hydraulic pressure which is necessary for the water-flow. If the hydraulic pressure is higher than the tensile strength of the paste, a rapture occurs. An entrainment of a fine air-bubble system in concrete, by reducing the path length of water-flow, limits the possibility of generation of a high hydraulic pressure. Thus in the context of the saturated flow hydraulic pressure hypothesis, the average inter-bubble distance has a definite fundamental significance. Based upon assumptions that all air-bubbles in a sample are equal-sized spheres arranged in a simple cubic lattice throughout the paste, Powers calculated a characteristic length called "the spacing factor" (2), which is related to the average inter-bubble distance. The spacing factor is used extensively to define the performance of concrete samples both in research and in practice (3, 4). In some countries, a maximum value of the spacing factor is required for all concrete structures that are to be exposed to freeze-thaw environments.

Powers' assumptions of equal-sized air-bubbles and their arrangement in a simple cubic lattice are seldom satisfied in practice. A more realistic value of the spacing factor may be obtained by an auto-correlation analysis of the data collected to obtain the air content by the modified point-count method (5).

The above uncertainty is of minor importance. The major uncertainty about the "spacing factor" arises from the refutation of

the saturated flow hydraulic pressure hypothesis itself. Powers and Helmuth have shown that the saturated flow hydraulic pressure mechanism plays a minor role in breakdown of concrete samples in freezing environments (6). Helmuth has further concluded that the water-flow to the air-bubbles is always unsaturated (7). In the case of unsaturated flow, the hydraulic pressure is independent of the path length of water-flow. In this case the spacing factor loses all its physical and scientific relevance.

If above is correct, then the present-day emphasis on the spacing factor is hampering the development of other more meaningful measures by drawing attention away from the real needs. I wonder if other workers have any views on this subject.

It should be understood that I am not trying to cast doubt on the beneficial effect of air entrainment; I accept that as proven beyond doubt. The only purpose of this discussion is to ascertain if the spacing factor is still a relevant measure.

References

1. Powers - Proc. Am. Conc. Inst. 41, 245-272, 1945.
2. Powers - Highway Research Board, 29, 184-202, 1949.
3. Litvan - Advances in Colloid and Interface Sci. 9, 253-302, 1978.
4. Helmuth - Proc. 4th Intern. Symp. Chem. of Cement. Vol. III, 855-869. Washington, 1960.
5. ASTM C 457 - 71.
6. Powers and Helmuth - Proc. Highway Res. Board, 32, 285-297, 1953.
7. Helmuth - Proc. 4th Intern. Symp. Chem. of Cement. Vol. III, 829-833. Washington, 1960.

VOL. 14 1984

CEMENT and CONCRETE RESEARCH. Vol. 14, pp. 759-760, 1984. Printed in the USA.
0008-8846/84 $3.00+00. Copyright (c) 1984 Pergamon Press, Ltd.

DISCUSSIONS

A DISCUSSION OF THE PAPER

"THE RETARDING ACTION OF SUGARS ON CEMENT HYDRATION"
BY N.L. THOMAS AND D.J. BIRCHALL*

S. Chatterji
Teknologisk Institut
2630 Taastrup.Denmark

In this paper the authors have reported some rather unexpected and interesting results without much comments. Some clarifications by the authors of the following points will be of interest.

1) From Fig. 4 and Fig. 5 it can be seen that after 300 minutes Ca-ion level in the aqueous phase was 125 mM, that of OH-ion was 250 mM and Si was 22 mM. Fe and Al levels were above about 7 and 5 mM, respectively. A OH/Ca mole ratio of 2 means that their charges were balanced. This raises the question about the states of Si, Fe and Al. Were these present in ionic or in neutral state? Their presence in ionic states will require some negative ions to balance their charge. The presence of neutral Si in such a highly alkaline solution will also be somewhat anomalous.

2) The authors seem to be proposing that sucrose-calcium adduct inhibits the nucleation and growth of $Ca(OH)_2$ and CSH. In that case sucrose will act as a set-retarder, but not as a hydration-retarder of Portland cement. The continued increase in ion concentrations, as shown in Figs. 4 and 5, tells against sucrose being a hydration-retarder and indicates an unabated hydration of cement. Will it not be desirable to make a distinction between a set-retarder and a hydration-retarder?

3) The continued hydration of cement in its turn will require a Ca/Si mole ratio of about 3 i.e. that of anhydrous cement, if all dissolved Ca and Si were in solution. However, from Figs. 4 and 5 it can be seen that the aqueous phase after 300 minutes had a Ca/Si mole ratio of about 6, i.e. approximately half of the dissolved Si is missing. Obviously sucrose is not very efficient in keeping Si in solution. But what has happened to the missing Si?

*CCR 13, 830-842 (1983).

4) All commercial Portland cements contain some water soluble alkali salts. These alkali salts tend to get causticized fairly early during cement hydration. If the analyses shown in Figs. 4 and 5 are total analyses of the aqueous phase at different time intervals, then it will appear that sucrose has somehow made the alkali salts either insoluble or reduced the rates of solution drastically.

VOL.
14
1984

CEMENT and CONCRETE RESEARCH. Vol. 14, pp. 761-762, 1984. Printed in the USA.
0008-8846/84 $3.00+00. Copyright (c) 1984 Pergamon Press, Ltd.

A REPLY TO A DISCUSSION BY S CHATTERJI OF "THE RETARDING ACTION OF SUGARS ON CEMENT HYDRATION" BY N L THOMAS AND J D BIRCHALL*

N L Thomas and J D Birchall
Imperial Chemical Industries, New Science Group,
PO Box No 11, Runcorn, Cheshire, UK

The authors would like to thank Dr Chatterji for his discussion of their paper (1) and wish to make the following comments in reply.

1) The analyses shown in Fig 4 were of Ca^{2+} obtained by titration with EDTA and 'nominal' OH^- obtained by titration with HCl. Fig 5 shows the levels of Si, Fe and Al found in the same solutions. No attempt was made to analyse for other species in solution such as Na^+, K^+ and SO_4^{2-} of which it is well known that there are significant amounts present (2, 3). Note also that 50 mM sucrose solution was added to the paste and since sucrose is a weak acid with a pKa value of 12.6 (4) it will be at least partially ionized at the pH of these solutions - which was pH 12.7. Hence sucrose anions will contribute to the charge balance in solution and hence to the 'nominal' OH^- concentration measured.

The authors are under no misapprehension that Si, Fe and Al are present as neutral species in the aqueous phase of these cement pastes and certainly do not hold Dr Chatterji's apparent view that these species could be positively charged ions. At pH 12.7 Si exists as the monomer ions $H_3SiO_4^-$ and $H_2SiO_4^{2-}$ and also as the dimer $H_4Si_2O_7^{2-}$ (5). Al and Fe are amphoteric and will be present as $Al(OH)_4^-$ and $Fe(OH)_6^{3-}$. Depending on the pK values of all the anions present they too will contribute to the nominal OH^- concentration measured. However, since we did not attempt to measure all the species present in solution it would seem unfruitful to speculate on the charge balance of only a part of what was present. Instead we want to draw attention to the large increase in calcium concentration and the dramatic increases in Si, Al and Fe found in the aqueous phase of cement pastes mixed with sucrose.

2) Sucrose certainly does increase the concentration of ions in solution as shown clearly in Figs 4 and 5. Investigations using isothermal calorimetry (6) show that addition of sucrose to a cement paste not only extends the dormant period, indicating a retarded setting process, but also gives rise to a lower second heat evolution peak. This latter effect is indicative of a hydration-retarder. Hence, although it is easy to agree that sucrose is a set-retarder it appears to be a matter of semantics as to whether or not it is a hydration-retarder.

*CCR 13, 830-842 (1983).

3) Typical values for C/S ratios in cement filtrates reported in the literature are greater than 100 and mostly around a value of 1000 (7). When OPC is mixed with 50 mM sucrose solution it is found that the C/S ratio drops continuously with time as more OPC is apparently solubilized. These results, taken from Figs 4 and 5, are tabulated below.

TABLE 1

Decrease in C/S Ratio with time for cement paste mixed with 50 mM Sucrose

C/S Ratio	Mixing Time
250	20 secs
114	1 min
93	5 mins
90	10 mins
19	30 mins
10	70 mins
8.5	120 mins
6.2	210 mins
5.9	300 mins

After 300 minutes both Ca^{2+} and Si levels continue to rise showing dissolution is still occurring, ie the system has not yet reached equilibrium. The theoretical C/S ratio in solution if the OPC were to dissolve congruently would be 3.5 (from the Bogue Analysis) and with time the C/S ratio in these sucrose systems would be expected to approach this value. What is very remarkable is that the C/S ratio has dropped from a value of 1000 found in control cement pastes down to a value of about 6 after 300 minutes stirring in 50 mM sucrose. It is evident that sucrose (or rather the 1:1 calcium-sucrose adduct) has a remarkable ability to prevent the precipitation of CSH gel, and that it is very efficient in keeping Si in solution. Further work on this topic will be published in ref 8.

VOL. 14 1984

References

1. N. L. Thomas and J. D. Birchall, Cem. Concr. Res. 13, 830 (1983)
2. C. D. Lawrence, Symp. Structure of Portland Cement Paste & Concrete, Highway Research Board Special Report 90, Washington DC, 378 (1966).
3. N. L. Thomas, D. A. Jameson and D. D. Double, Cem. Concr. Res. 11, 143 (1981).
4. B. Capon and W. G. Overend, Adv. Carbo. Chem. 15, 32 (1960).
5. R. K. Iler, 'The Chemistry of Silica' chap. 2. John Wiley & Sons, New York (1979).
6. D. D. Double, Phil. Trans. R.Soc. Lond. A310, 53 (1983).
7. N. L. Thomas and D. D. Double Cem. Concr. Res. 11, 675 (1981).
8. J. D. Birchall and N. L. Thomas. Proc. Brit Ceram. Soc. Special Ed. Conf. Chemistry and Chemically-Related Properties of Cement. London April 1984.

CEMENT and CONCRETE RESEARCH. Vol. 14, p. 763, 1984. Printed in the USA.
0008-8846/84 $3.00+00. Copyright (c) 1984 Pergamon Press, Ltd.

A DISCUSSION OF THE PAPER "A CLASSIFICATION OF INORGANIC AND ORGANIC ADMIXTURES BY CONDUCTION CALORIMETRY" BY C.R. WILDING, A. WALTER AND D.D. DOUBLE*

W.B. Butler
Monier Resources Research
P.O. Box 7, Villawood, N.S.W. 2163, Australia

In detailing their procedures, the authors mention that two samples of cement, of differing Bogue composition, but both ordinary Portland Cement from one works, were used in the trials.

However, no mention is made in the results in regard to differences in performance with the two samples used. A strong note of warning must be sounded to those who might try to apply the results of this work broadly and without confirmatory tests. In our experience, the relative performance of admixtures generally is strongly influenced by cement chemistry. Particularly when more than one admixture is present, it is a brave man who predicts the setting performance of the concrete without testing the mixture.

The comments of the authors would be appreciated.

*CCR 14, 185-194 (1984).

CEMENT and CONCRETE RESEARCH. Vol. 14, p. 764, 1984. Printed in the USA.
0008-8846/84 $3.00+00. Copyright (c) 1984 Pergamon Press, Ltd.

A REPLY TO A DISCUSSION OF "A CLASSIFICATION OF INORGANIC AND ORGANIC ADMIXTURES BY CONDUCTION CALORIMETRY"* BY W.B. BUTLER

by C.R. Wilding, A. Walter and D.D. Double
Dept. of Metallurgy and Science of Materials
University of Oxford, Oxford OX1 3PH, U.K.

VOL. 14 1984

The results presented were part of a chemical study of the effect of admixtures on the hydration of Portland cement in order to understand how these admixtures might work. Although two different batches of ordinary Portland cement were used, tests showed that they gave comparable results in the calorimetric experiments. The aims of the research were stated in the final paragraph of the introduction. It was not advocated that the results could be directly transferred to the setting and hardening of bulk concrete where many other factors, apart from hydration chemistry, are involved.

*CCR 14, 185-194 (1984).

CEMENT and CONCRETE RESEARCH. Vol. 14, pp. 765-766, 1984. Printed in the USA.
0008-8846/84 $3.00+00. Copyright (c) 1984 Pergamon Press, Ltd.

NEWS ITEMS

Fourth International Congress on POLYMERS IN CONCRETE, Technische Holchschule Darmstadt, W. Germany. Information: Prof. H. Schulz, Technische Hochschule Darmstadt, Kennwort, ICPIC 1984, Petersenstrasse 30, D-6100 Darmstadt, W. Germany. — Sept. 19-21, 1984

International Conference on IN SITU/NONDESTRUCTIVE TESTING OF CONCRETE, by ACI, CANMET, National Bureau of Standards and the Canadian Society for Civil Engineering, Westin Hotel, Ottawa, Canada. Information: Harry S. Wilson, CANMET, 405 Rochester St., Ottawa, Ontario, Canada K1A 0G1. — Oct. 2-5, 1984

International Conference on TALL BUILDINGS, Shangri-la Hotel, Singapore, sponsored by the Council of the Institution of Engineers, Singapore. Information: The Chairman, ICTBS 84, 10, Anson Road, #14-06, International Plaza, Republic of Singapore (0207). — Oct. 22-26, 1984

ACI Convention, Grand Hyatt, New York, NY. Information: Ann K. Bruttel, Convention and Meetings Manager, ACI, P.O. Box 19140, Detroit, MI 48219 USA. — Oct. 28 - Nov. 2, 1984

Materials Research Society Symposium L, THE POTENTIAL FOR VERY HIGH STRENGTH CEMENT-BASED MATERIALS, Boston Marriott Hotel/Copley Place, Boston, MA. Information: Dr. J. Francis Young, 3209 Newmark Civil Engineering Lab., University of Illinois-UC, Urbana, IL 61801 or Dr. Sidney Mindess, Dept. of Civil Engineering, University of British Columbia, Vancouver V6T 1W5, Canada. — Nov. 26-30, 1984

Materials Research Society Symposium M, COAL COMBUSTION AND CONVERSION WASTES: CHARACTERIZATION, UTILIZATION AND DISPOSAL, Boston Marriott Hotel/Copley Place, Boston, MA. Information: Dr. Turgut Demirel, Dept. of Civil Engineering, Iowa State University, Ames, IA 50011, or Dr. Gregory McCarthy, Dept. of Chemistry, North Dakota State University, Fargo, ND 58105, or Dr. Barry E. Scheetz, Materials Research Laboratory, The Pennsylvania State University, University Park, PA 16802. — Nov. 26-30, 1984

Annual Convention of the AMERICAN CONCRETE INSTITUTE, Denver, CO. Information: Ann K. Bruttell, Convention and Meetings Manager, ACI, P.O. Box 19150, Detroit, MI, USA. — March 1985

The 8th International Congress on the CHEMISTRY OF CEMENT, Rio de Janeiro, Brazil. Information: Secretaria Geral do 8° Congresso de Quinica do Cimento, Rua da Assembléia, No. 10, 40° andar, Grupo 5001-20011, Rio de Janeiro/RJ, Brazil. — Late Summer 1986

NEWS ITEMS

CALL FOR PAPERS

The 7th International Conference on CEMENT & CONCRETE MICROSCOPY will be held from March 25-28, 1985, at the Americana Hotel, Fort Worth, TX, USA. The topics to be covered are: (1) Microscopic structures of building materials, including lime, gypsum, light and heavyweight aggregates, cement, concrete, slag, flyash, silica fume, etc.; (2) Microscopic structures of the different types of cement clinker products and hydration; (3) Effect of additives on the microstructure of cement and concrete and the relationship between the microstructure and concrete strength; (4) Application of different types of microscopes for the quality control of clinker, cement, concrete, etc.; (5) X-ray diffraction analysis of Portland cement and related materials and the relationship between the microstructure and the mineralogical composition.

Authors should send abstracts by November 15, 1984 to: Arturo G. Nisperos, Material Service Corp., 901 N. Sangamon St., Chicago, IL 60622 (subjects dealing with microscopy of concrete and concrete-making materials); or to James Bayles, Coplay Cement Co., Nazareth, PA 18064 or Dr. George R. Gouda, Kuwait Inst. for Scientific Research, P.O. Box 24885, Safat, Kuwait (subjects dealing with the microscopy of cement and clinkers). Final text is due by Jan. 31, 1985.

A Symposium on EVALUATION OF FIRE DAMAGE OF CONCRETE AND REPAIR OF DAMAGE will be held during the ACI fall convention in Chicago, IL, October 1985, sponsored by Committee 215, Fire Resistance and Fire Protection of Structures. Papers on a variety of topics which comply with the general theme of the symposium are solicited.

Authors should send Paper title, 300 word abstract and author(s) name, title, organization, and address, by Oct. 31, 1984, to T.Z. Harmathy, Committee 216 Chairman, National Research Council of Canada, Division of Building Research, Ottawa, Ontario, K1A OR6, Canada; or F.Ray Vollert, Rockwell Hanford Operations, P.O. Box 800, Richland, WA 99352.

An International Symposium on CONSOLIDATION OF CONCRETE will be held during the ACI annual convention in San Francisco, CA, March 1986, sponsored by Committee 309, Consolidation of Concrete. Topics include, but are not limited to: effect of mix properties, concrete materials; methods of consolidation, selection of vibrator equipment; equipment for vibration, new developments; theoretical aspects regarding consolidation; test methods for judging adequacy of consolidation in fresh concrete; methods for measuring vibrator efficiency, frequency, amplitude, force; procedure of vibration, internal and external; revibration, timing, extent, benefits; design of form equipment and placing vibrator on forms, size, spacing, form requirements; consideration of construction details, reinforcement spacing, concrete workability; mass concrete, roller compaction; structural concrete, pavements, slabs, precast products, block, pipes; special concretes, lightweight, heavyweight; quality control, consolidation of test specimens; field preformance, discussion of experiences of properly and improperly consolidated concrete.

Authors should send Paper title, 200 word abstracts, and author(s) name, title, organization, and address by Dec. 31, 1984 to Steven H. Gebler, Construction Technology Laboratories, Portland Cement Association, 5420 Old Orchard Road, Skokie, IL 60077. Final papers are due June 30, 1985.

VOL. 14 1984

CEMENT and CONCRETE RESEARCH. Vol. 14, pp. 767-775, 1984. Printed in the USA.
0008-8846/84 $3.00+00. Copyright (c) 1984 Pergamon Press, Ltd.

THE INFLUENCE OF FLY ASH CENOSPHERES ON THE DETAILS OF CRACKING IN FLYASH-BEARING CEMENT PASTES

Denis Montgomery
Department of Civil and Mining Engineering, University of Wollongong
Wollongong, NSW 2500, Australia

Sidney Diamond
School of Civil Engineering, Purdue University
West Lafayette, IN 47907, U.S.A.

(Communicated by G. Frohnsdorff)
(Received Jan. 10, 1984)

L.
4
84

ABSTRACT

Compact tension specimens were prepared from a cement-flyash paste with an especially-high content of cenospheres, to permit examination of the details of the influence of cenospheres on the cracking pattern obtained on loading such specimens in the SEM. It was found that even after extensive aging, the advancing crack typically went around the cenosphere-paste interface rather than cleaving through the cenosphere itself. Branching of the crack on its path around the cenosphere perimeter was commonly observed. Thus, cenospheres in flyash-cement systems appear to act as energy-dissipating inclusions in fracture and do not necessarily weaken the system.

Introduction

In recent years work has been carried out at Purdue University (1-3) aimed at documenting the details of crack initiation and propagation in various cement systems. These observations have been made using specimens loaded and observed within the specimen chamber of a scanning electron microscope (SEM), so that crack initiation and propagation paths could be directly visualized. Cracking induced by both tension and compression loadings have been studied.

The use of flyash as a component of blended cements or as a mineral admixture in concrete has become commonplace in recent years. Among the more interesting features of many flyashes is a small but conspicuous proportion of cenospheres, relatively large thin-walled hollow particles produced during flyash formation by evolution of gas trapped in a viscous molten glass matrix. While the content of such particles in most flyashes is likely less than 1% by weight, occasional flyashes have higher proportions present. In any event, the proportion of cenospheres by volume

is obviously greater than the weight proportion, and given the hollow character of the particles and the thinness of their shells, some effect of the presence of these particles on crack propagation might be evidenced. The work described here is the result of a brief investigation to explore this possibility.

Experimental Details

The cement pastes studied were prepared using a blend of 70 percent by weight of an ordinary ASTM Type I portland cement and 30 percent by weight of a fraction of an ASTM Class F low-calcium flyash separated so as to be highly enriched in cenospheres. The flyash was obtained from the Stout station of the Indianapolis Power and Light Co., and is a fairly typical bituminous coal flyash. As such, it is not particularly rich in cenospheres but does contain enough cenosphere particles that it can serve as a source for such material.

To obtain a flyash fraction enriched in cenospheres, small amounts of flyash were stirred vigorously in deionized water for a few minutes, and then the bulk of the ash was permitted to settle. The supernatant suspension was then siphoned off and passed through a Whatman No. 42 filter paper, leaving behind a residue which was dried and then ignited at 750 degrees C to remove residual carbon. As indicated in Fig. 1, the flyash material recovered consisted of a mixture of large cenospheres averaging about 60 micrometers in diameter and very much smaller solid flyash spheres of the order of perhaps 1 to 8 micrometers in diameter. No attempt was made to assess the proportions of the two classes of particles.

VOL. 14 1984

Pastes having a water:solids ratio of 0.35 were prepared using a 70% cement - 30% cenosphere-enriched flyash blend. Mixing was carried out under vacuum in a special chamber designed to minimize the entrapment of air in the paste. The paste was then cast into molds to produce compact tension specimens of a type previously described (1), light vibration being used to facilitate the casting operation. This is necessary since the specimens are cast around a prepositioned thin blade element so as to produce the preformed notch necessary in loading a compact tension specimen. The specimens were stored over water for 24 hours, demolded, and then cured under saturated limewater for various periods.

Prior to testing, each compact tension specimen was polished using successively No. 240, No. 800, and No. 1200 aluminum oxide grits. This procedure removed the paste film which had formed against the mold and exposed the cenospheres that were lying in the plane of the new surface produced, slicing many of them open and exposing their hollow centers. Unfortunately, the procedure also resulted in the collection and entrapment of some grit and ground residue particles within these shells, which were not removed despite extensive washing. It is not considered that the presence of such material influenced the cracking pattern being investigated.

The specimens were then loaded in the testing device within the SEM chamber, in the saturated surface dry condition. The technique used is that recently described (4), in which the secondary electron detector of the SEM is replaced with a Robinson backscattered electron detector. The specimen chamber is kept effectively saturated with water vapor by air drawn through a wet gas bubbler system. In this way the specimen can be maintained at the modest vacuum required (approximately 0.7 torr) while also being kept in a wet environment to prevent excessive drying and shrinkage cracking. No cracking prior to mechanical loading was detected.

Loading was applied by advancing a wedge in the manner customary for compact tension systems, until a crack was produced. After study and photographic recording of the details of the initial crack, the loading was renewed until the crack ran completely through the specimen, fracturing it into two pieces. Both halves were then removed from the SEM, dried, mounted on an SEM stub, and sputter-coated with a thin gold-palladium layer to permit observation at higher resolution. Both the polished surface and the surface formed by the crack itself were then examined with the secondary electron detector, the Robinson detector being disconnected.

Observations

As indicated in Fig. 1, the cenosphere enriched flyash component of the blended cement used consisted of large and easily recognized cenospheres and large numbers of much finer solid particles. The cenospheres ranged in size from about 25 μm to about 150 μm, with the mean being about 60 μm. Examination of broken cenospheres indicated a mean wall thickness of about 4 μm. It is obvious that such particles are easily recognizable on a polished surface, and the trace of a crack intersecting such a particle is relatively easy to define.

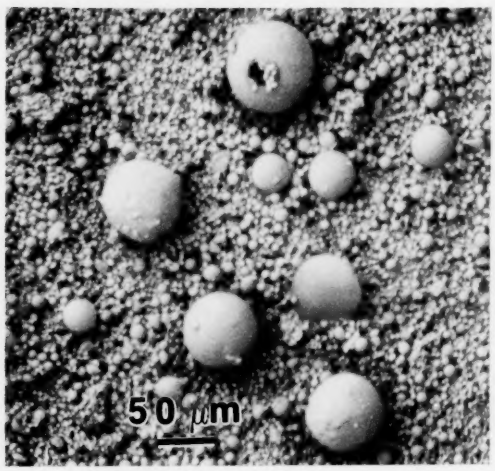

FIG. 1
Recovered flyash material consisting of large cenospheres and small solid spheres.
Original magnification: 170x.

Illustrations of typical cracking patterns for these specimens are shown in Figs. 2a and 2b. In general, the fracture path pattern resembles that previously observed for ordinary portland cement pastes (2). The path of the advancing crack is generally in the forward direction ahead of the notch, as expected; this is the upward direction in most of the micrographs below. The actual path is tortuous and made up of short segments which mark successive small changes in direction as seen in Fig. 2a. The other feature commonly observed in ordinary cement pastes is occasional branching of the main crack, throwing off one or more subsidiary cracks (2). In the present work, the cenosphere-enriched flyash cement pastes show occasional branching when the crack advances around the periphery of a cenosphere, as well as occasionally in the "bulk" paste matrix. Fig. 2b provides an illustration of each type, marked "A" and "B", respectively.

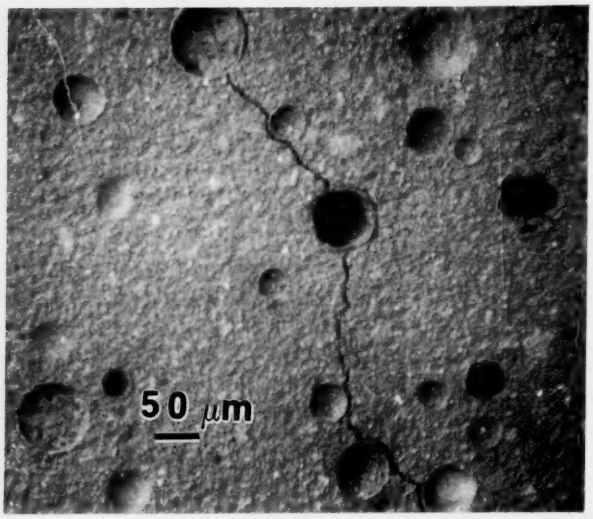

FIG. 2a
Typical cracking pattern for cenosphere-enriched flyash-cement paste showing crack path around boundaries of the cenospheres.
Original magnification: 140x.

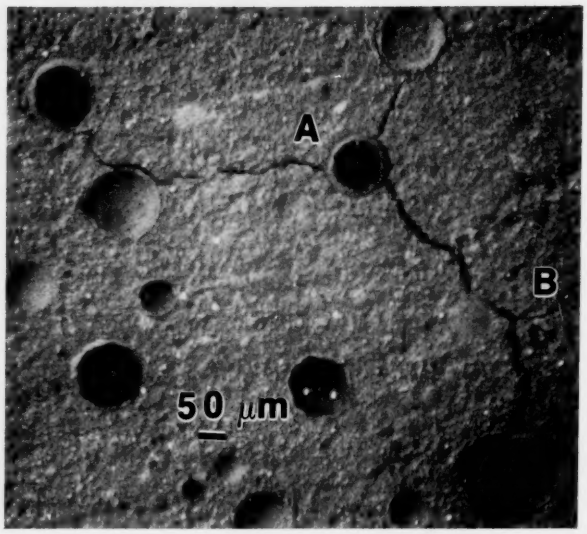

FIG. 2b
Cracking pattern showing branching at cenosphere, designated A, and in bulk paste, designated B.
Original magnification: 80x.

VOL. 14 1984

The predominant feature observed to occur when the advancing crack encountered a cenosphere was a partial encircling of the cenosphere by the crack, with the crack following a path along the interface between the circumference of the sphere and the surrounding paste matrix. This behavior is exhibited in 10 of the 11 intersections of the crack with cenospheres in Figs. 2a and 2b.

Subsequent examination of the actual surface of fracture produced by the crack (after the two halves of the specimen had been dried and coated) indicated that generally a lime-rich layer had formed in contact with the cenosphere, and that the crack had separated this layer cleanly from the outside surface of the cenosphere. This is indicated in Fig. 3, which shows the actual crack-created surface, marked "F" (for fracture) in the micrograph. The original polished surface, approximately at right angles to the crack-created fracture surface, appears at the very top of the

micrograph, and is designated "P". The upper right portion of the micrograph shows the sliced-open top of the truncated cenosphere, with the original top removed in the grinding process; the partial shell remaining seems to be full of grit and polishing debris. The lime-rich layer just outside of the cenosphere boundary and separated from it by the advancing crack is marked "L" in the micrograph.

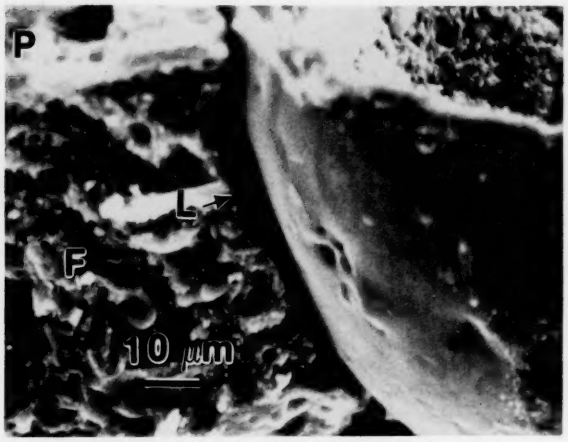

FIG. 3
Micrograph showing separation between cenosphere and cement paste matrix caused by advancing crack. P is original polished surface, F is a fracture surface created by the crack, L is the lime-rich boundary. Original magnification: 1000x.

In some instances local features exposed at the crack intersection with a cenosphere are more complex. An illustration of one such occurrence is provided in Fig. 4. In this micrograph the polished surface is again indicated by "P" and the fracture surface created by the main advancing crack by "F". The 10 μm-wide crack shown extending downward from the polished surface is the trace of a branch crack. In this illustration the cenosphere happened to lay along the intersection of the main crack and a branch crack, at a distance of about 40 μm below the polished surface. It is seen that in this case the main crack has passed directly through the cenosphere, creating the exposed opening. The branch crack, in contrast, has gone around the interface of the cenosphere, resulting in a clean separation of the sphere from the matrix.

FIG. 4
Cenosphere found at intersection of main crack and a branch crack. P is the original polished surface, F is the fracture surface created by the main crack. Original magnification: 500x.

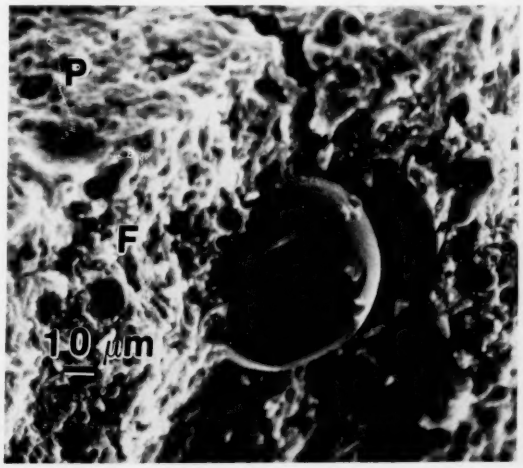

It was found that very few of the cenospheres were actually broken during the fracturing process. Even for specimens cured in limewater for 50 days at ambient temperature and then cured an additional 10 days at 50°C to accelerate additional hydration, examination indicated that fewer than 10 percent of the cenospheres exposed on the polished surface and intersected by an advancing crack suffered any visible damage. This result was confirmed after subsequent separation and mounting of the two halves of the fractured specimen. Examination of the newly-created surfaces indicated a preponderance of unfractured cenospheres partially bound to the cement paste matrix, along with a considerable number of sockets where cenospheres had pulled out and adhered to the other half of the original specimen. Comparatively few fractured cenospheres were observed.

One illustration of a crack running through, rather than around a cenosphere has already been provided. In Fig. 2b the crack intersecting the large cenosphere at the bottom right-hand edge of the figure has passed directly through the cenosphere. Fig. 5 provides another illustration, in a 50-day old paste. The general surface exposed is that of the polished surface. The 25 μm-wide crack depicted is the trace of the main crack, which has passed through the cenosphere and produced a major disruption to the local structure. This particular cenosphere seems to have been almost filled with grit and polishing debris when the polished surface was created.

Cenospheres incorporated in cement paste systems provide an illustration of a class of thin-walled spherical inclusions. While the walls are thin with respect to the diameter of the particles, it is obvious that they are thick enough to provide a crack-path modifying effect. To provide an illustration of "infinitely thin" spherical inclusions and their effects on the crack path, an air-entrained portland cement paste was made in which air bubbles of sizes comparable to those of the cenospheres were incorporated within the matrix. Testing these specimens in the same apparatus produced crack patterns and branching similar to those of pastes containing cenospheres. However, the air bubbles provide no resistance to the advancing crack, and as indicated in Fig. 6, the crack passed directly through all of the air bubbles encountered on its path.

Finally, while the main concern of this work was with details of the fracturing process, the opportunity was taken to observe the surfaces of the cenospheres separated from the paste matrix by the passage of a crack for

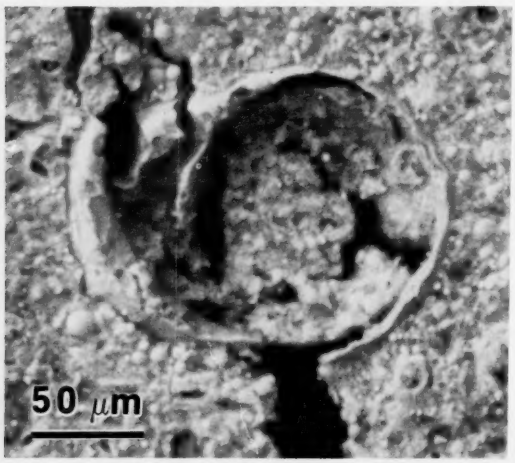

FIG. 5
Cenosphere on polished surface disrupted by advancing crack. Original magnification: 400x.

VOL. 14 1984

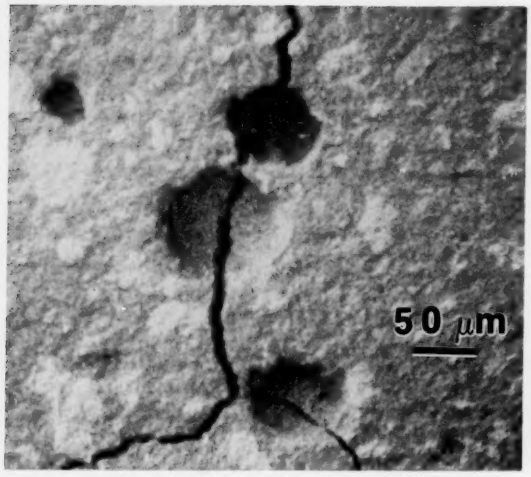

FIG. 6
Micrograph showing advancing crack penetration directly through air voids in deliberately air-entrained cement paste.
Original magnification: 200x.

visual evidence of reaction with the cement paste. Fig. 7a shows a typical cenosphere surface region exposed by the advance of a crack in a specimen cured for 14 days. There is no visual indication of physical or chemical

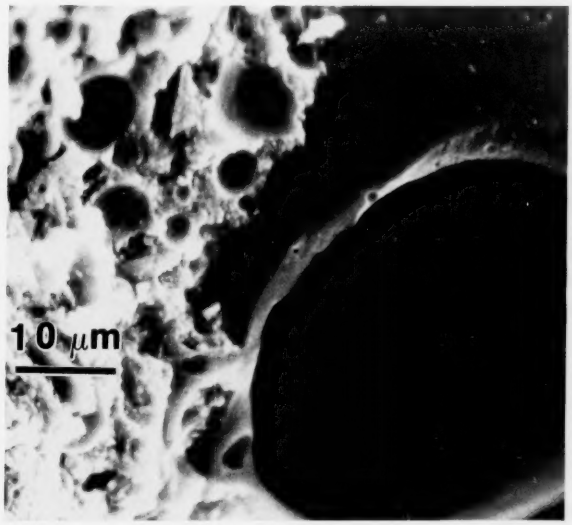

FIG 7a
Micrograph showing cenosphere surface exposed by advancing crack in 14-day old specimen; no visual evidence of reaction can be seen.
Original magnification: 1500x.

interaction having taken place between the surrounding cement paste matrix and the outer surface of the cenosphere. In contrast, after 50 days of ambient-temperature curing followed by 10 days at 50°C, a number of spheres exposed by passage of a crack did show signs of reaction. Fig. 7b provides an illustration of this, in the form of faint but distinguishable etching away of the glass of the exposed surface. In the area marked "A" faint outlines of embedded laminar crystals, probably mullite, are exposed by the start of this chemical etching reaction process. The removal of the top portion of the cenosphere in Fig. 7b was the result of the surface polishing procedure and was not due to fracture.

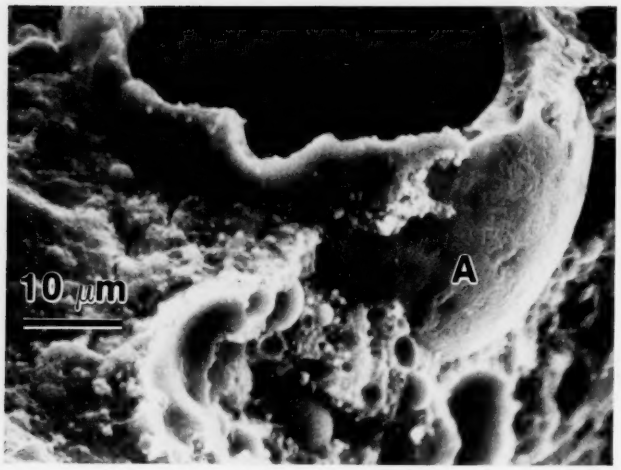

FIG. 7b
Micrograph showing cenosphere surface exposed by advancing crack in specimen cured for 50 days at room temperature and for 10 additional days at 50°C. A indicates exposed surface exhibiting definite indications of etching of glass. Original magnification: 1500x.

Conclusions

Cement-flyash pastes incorporating cenospheres develop the usual tortuous and branched crack pattern when loaded in the compact tension device, but show certain specific features peculiar to the intersection of the advancing crack with the cenospheres. The predominant interaction is a boundary layer separation of the cenosphere outer surface from the surrounding cement paste matrix as the crack passes around, rather than through the cenosphere. Sometimes the crack branches while traversing around a cenosphere. The separation appears clean, even in well-aged specimens, and seems to be due to the limited adhesion developed between the cenosphere and the calcium hydroxide-rich layer that develops around it. Interactions in which the advancing crack goes through, rather than around, the cenosphere occur in less than 10 percent of the observed contracts, even after the specimens had been cured at an elevated temperature.

The increase in crack length and tortuousity induced by the presence of the cenospheres appears to constitute an energy-dissipating mechanism that should act to decrease the tendency toward fracture of a loaded cenosphere-containing specimen as compared to one that does not contain such inclusions. Whether such an effect is of any quantitative significance remains to be seen.

Observation of cenosphere surfaces parted from the cement paste matrix by passage of a crack showed little indication of chemical reaction even after almost two months of room-temperature curing in limewater. However, after ten days of additional curing at 50°C, some evidence of surface etching of the outer glass surface was detected.

VOL. 14 1984

Acknowledgements

The work reported here was carried out at Purdue University while the first-named author was on a study leave from the University of Wollongong. Appreciation is due to Janet Lovell and to Arnon Bentur for advice and technical assistance during the course of this work.

References

1. S. Diamond and S. Mindess, Proc. 7th Intl. Congr. Chem. Cement, V. III, pp. VI-114 to VI-119 (1980).
2. S. Mindess and S. Diamond, Cem. Concr. Res. 10 (4) 509-519 (1980).
3. S. Mindess and S. Diamond, Cem. Concr. Res. 12 (5) 569-576 (1982).
4. S. Diamond, S. Mindess and J. Lovell, Cem. Concr. Res. 13 (1) 107-113 (1983).

L.
4
84

CEMENT and CONCRETE RESEARCH. Vol. 14, pp. 776-784, 1984. Printed in the USA.
0008-8846/84 $3.00+00. Copyright (c) 1984 Pergamon Press, Ltd.

WASTE CEMENT DUSTS AS FILLERS FOR RUBBER COMPOUNDS

Andrzej Krysztafkiewicz and Marek Maik
Institute of Chemical and Engineering Technology
Politechnika Poznańska
60-965 Poznań, Poland

(Communicated by D.M. Roy)
(Received May 13, 1983; in final form March 15, 1984)

ABSTRACT

The possibility of substitution of expensive active fillers, e.g. carbon black, for the waste products which can play the role of these filllers, e.g. the waste cement dusts or the waste post-HF silica, were investigated. The physico-chemical properties of the investigated waste cement dusts and the waste post-HF silica, as well as the strength properties of the rubber compounds containing these as fillers, were determined. To increase the activity and chemical affinity with the rubber, the waste cement dusts and the waste post-HF silica were modified by the use of adhesion promoters, that is alkoxysilanes. It was found that it would be possible to partly substitute carbon black for the waste cement dusts and the waste post-HF silica. The mixture ratio of a compound which had these wastes and showed the optimum strength properties was proposed.

VOL. 14 1984

Introduction

The world energy crisis forces a deep and precise analysis of used fillers upon the producers of rubber. These analysis should not be restricted to the prices of plastics, rubbers and fillers, but they must consider energy consumption and wearing out of processing machines. Kinds of fillers and methods of their application are usually kept secret by the producers and for this reason, the information on fillers are very often not precise.

There are four basic phases which can coexist in cements. These are: $3CaO \cdot SiO_2$, $2CaO \cdot SiO_2$, $3CaO \cdot Al_2O_3$ and $4CaO \cdot Al_2O_3 \cdot Fe_2O_3$. It is the calcium silicates that can influence the application of cement as the fillers of rubber compounds. The increase of chemical affinity of the investigated cement dust to polymer chains of rubber networks is of great importance, and at present, the investigation of this increase towards more plastics, before their plasticization, is thoroughly carried out. The mixing of cement with styrene-butadiene latex is of considerable importance in the preparation of some new types of building materials. To achieve that, the anionic surface-active agents are used which are introduced in order to obtain the desired dispersion and emulsification for the preparation of a co-polymer, as well as non-ionic surface active agents which are added in order to stabilize a polymer in a cement composition.

The surface of cement dusts can be modified by the use of polyorganosiloxane compounds (1), as well as alkoxysilane (2-6) and organotitanate (7,8) adhesion promoters. In our investigations, we partly used the silane coupling agents to increase chemical affinity of cement dusts towards a polymer (rubber).

Experimental

The investigations of the waste cement dusts, dedusted by multicyclones in "Nowiny" cement plant, together with the investigations of the pretreated waste silica coming from the production of hydrofluoric acid (post-HF silica), were carried out. The latter was used with the former as fillers in rubber compounds. PM-75 commercially pure carbon black, produced in the USSR, was also used as a substitute for silica.

The chemical constitution of the investigated samples, the pH of water extracts and moisture content were determined. Specific surfaces were measured chromatographically (10).

The whiteness degree of the waste cement dusts and silica were determined leucometrically. The Zeiss leucometer, with a 6V and 30W mercury lamp as a light source, and blue, 459 mμ, as well as red, 614 mμ, were used. As a standard we used a freshly roasted barium sulphate.

The activity of cement dust and waste silica were regulated through a change of hydrophilic surfaces, partly or totally, for hydrophobic ones. To do this, some silanes were used to modify surfaces of these fillers. The modifications were carried out in the semi-commercial scale by the use of a mixer of our own construction, which had the capacity of 3.5 dm^3 (11). The following silanes, as the modifiers, produced by Union Carbide Corporation (4), were used:

A-189 gamma-mercaptopropyltrimethoxysilane
A-172 vinyl-tris(beta-methoxyethoxy)silane
A-1100 gamma-aminopropyltriethoxysilane

The silanes were added in the amounts of 0.5 - 3.0 parts by weight for a 100 parts by weight of filler. Because of the low efficiency of silane as a modifer of waste cement dusts, we tried to mix cement with the post-HF waste silica, which is characterized by a considerably greater degree of interaction with the silane alkoxy groups.

The choice of this silica was dictated by its physico-chemical parameters, mainly particle diameters and specific surfaces, which are similar to those of cement dust. Bulk density and packing density were determined by the use of a WE-5 electromagnetic volume indicator (12). Shaking down coefficient as packing density and bulk density, the ratio of a loosely poured material was also calculated.

To obtain a fuller characteristic of the investigated fillers, the water and dibutylpthalate absorbing capacities were determined. The amount of absorbed water depends on the surface development and on the degree of agglomeration of a filler. The end point of the investigated water absorbing capacity was taken the one in which one drop of water causes a clear fluxing of the formed paste. In terms of dibutylpthalate, the end point was chosen as the one in which the consistency of paste changes rapidly and makes it stick to a glass plate.

Heat of immersion was determined in a KRM differential calorimeter (13), using the electric method of the calorimeter capacity determination. Water and benzene immersion heat of modified and non-modified samples of waste silica and cement dust were measured. The observations of samples were carried out by the use of the intermediate single-stage replica method (14) and a JEM-7A (Jeolco-

Japan) over-exposure electron microscope. The next step was to investigate the Ker 1500 butadiene-styrene rubber compounds which contained waste cement dust. The mixture ratio is shown in Table 1.

TABLE 1

Mixture Ratio of the Ker 1500 Rubber Compound Based on Cement Dust

Ingredient	Compound		
	A	B	C
	(part by weight)		
Ker 1500	100	100	100
Stearin	1	1	1
Accelerant M	2	2	2
Sulphur	2	2	2
Cement dust	100	100	100
Zinc oxide	-	1	2

Within each of the above A, B, and C compounds, the following samples of cement dust were introduced: (0) non-modified cement dust; (1) cement dust + 2 parts by weight of A-1100 silane; (2) cement dust + 2 parts by weight of A-189 silane; and (3) cement dust + 2 parts by weight of A-172 silane. Cement dusts were also used to substitute, partly or totally, some reinforcing or semi-reinforcing fillers such as the PM-75 commercial carbon black and the waste post-HF silica. The compound ratio was as follows:

Ker 1500	100 parts by weight
Stearin	2 parts by weight
Cement	0-50 parts by weight
Carbon black or silica	0-50 parts by weight
Zinc oxide	5 parts by weight
Benzothiazole disulphide	2.2 parts by weight
Diphenyloguanidine	1.4 parts by weight
Sulphur	2 parts by weight

The strength tests of the rubber vuncanizates were carried out. In this paper, we show the results of them for the vulcanization at 143°C for 30 minutes.

Results

Table 2 illustrates the chemical analysis results of the "Nowiny" cement dust and the waste post-HF silica.

Table 3 shows some physico-chemical properties data of the non-modified fillers.

The results of immersion heat tests are shown in Table 4. It shows that data for silica and cement dust modified by 3 parts by weight of the used silanes. The comparison of water and benzene immersion heat of the investigated filler samples modified by the A-189 silane, is shown in Figure 1.

Figure 2 shows the electron microscope photograph of cement dust, post-HF silica and the 1:1 mixture of them. The strength test results of the compounds in Table 1, filled with non-modified and alkoxysilane modified cement dusts, are shown in Table 5.

Physico-mechanical indexes for the Ker 1500 rubbers, which have various amounts of the cement dust and the waste silica, are given in Table 6. Table 7 shows the same indexes for the Ker 1500 rubbers containing various amounts of

VOL. 14 1984

TABLE 2

Chemical Constitution of the Investigated Cement Dusts and Semi-Reinforcing Post-HF Silica (average % by weight)

Ingredient	"Nowiny" waste cement dust	Dried waste post-HF silica
SiO_2	24.58	88.42
Al_2O_3	4.58	2.20
CaO	57.80	1.63
$FeO+Fe_2O_3$	0.90	0.45
MgO	2.88	-
F^-	-	2.42
moisture	1.15	2.30

TABLE 3

Physico-Chemical Properties Data of the "Nowiny" Cement Dust and the Waste Post-HF Silica

Property	"Nowiny" cement dust	Waste post-HF silica
Water suspension pH	10.2	6.2
Specific gravity (g/cm^3)	5.42	2.05
Bulk density (g/dm^3)	634	245
Packing density (g/dm^3)	865	380
Shaking down coefficient	1.36	1.55
Water absorption (g/100g)	-	100
Dibutyl pthalate absorption (g/100g)	62	90
Whiteness degree (%)	32.1	70.7
Specific surface (m^2/g)	10.5	42.1

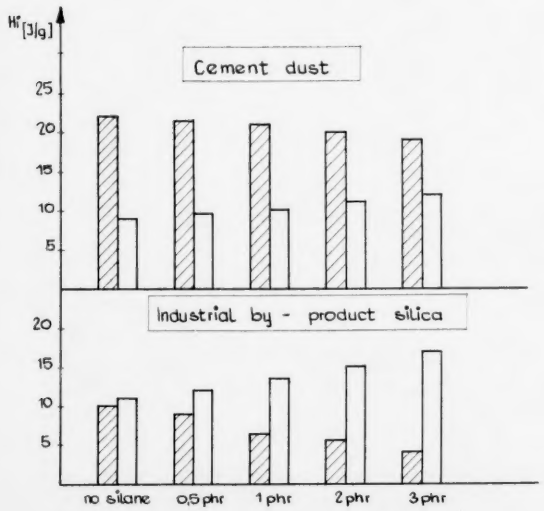

FIG. 1

The influence of A-189 mercapto-silane quantity upon the immersion heat of modified waste silica and cement dust.

Water immersion heat

Bezene immersion heat

TABLE 4

Water and Benzene Immersion Heat of Cement Dust and Waste Post-HF Silica

Kind of Sample	Water Immersion Heat		Benzene Immersion Heat	
	cal/g	J/g	cal/g	J/g
Waste post-HF silica	2.42	10.13	2.45	10.23
Waste post-HF silica + 3 parts by weight of A-189	1.03	4.31	3.80	15.89
Waste post-HF silica + 3 parts by weight of A-1100	2.86	11.95	3.40	14.31
Waste cement dust	5.63	23.52	1.94	8.13
Waste cement dust + 3 parts by weight of A-189	4.55	19.02	2.25	9.41
Waste cement dust + 3 parts by weight of A-1100	5.80	24.24	2.15	8.99

VOL. 14 1984

TABLE 5

Physico-Mechanical Properties of the Ker 1500 Rubber Vulcanizates Filled with Non-Modified and Alkoxysilane Modified Cement Dusts

Compound	Tensile strength (MPa)	Relative elongation (%)	Tensile set (%)	Hardness (°Sh)
A/0	2.72	680	40	61
A/1	3.24	720	44	60
A/2	4.14	760	36	68
A/3	3.80	520	32	67
B/0	3.30	580	24	66
B/1	4.25	600	24	65
B/2	4.58	540	28	68
B/3	4.45	540	28	65
C/0	3.67	550	28	65
C/1	4.80	600	28	65
C/2	5.73	560	28	65
C/3	5.30	420	28	65

the dust and the PM-75 commercial carbon black. Figure 3 shows the tensile strengths for rubbers filled with 1:1 mixture of the cement dust and the post-HF silica modified by various silanes as a function of the silane amounts.

Discussion

Cement dust and post-HF silica have badly developed surfaces and as a result of this they belong to little active fillers. In order to increase their

(a)

(b)

(c)

FIG. 2

Electron-microscope photograph of the investigated fillers. Magnification x 30.000. (a) cement dust; (b) post-HF silica; (c) 1:1 mixture of cement dust and post-HF silica.

TABLE 6

Physico-Mechanical Indexes for the Ker 1500 Rubbers Containing Various Amounts of the Non-Modified Cement Dust and the Post-HF Silica. Vulcanization Parameters: Time - 30 minutes; Temperature - 143°C.

Index	Amount of cement dust (parts by weight)					
	0	10	20	30	40	50
	Amount of waste silica (parts by weight)					
	50	40	30	20	10	0
Tensile strength (MPa)	5.6	5.0	4.2	3.9	3.4	2.8
Relative elongation (%)	310	330	400	400	520	540
Tensile set (%)	10	12	12	18	24	26
Modulus 300 (MPa)	4.8	4.5	3.6	3.4	2.9	2.3

TABLE 7

Physico-Mechanical Indexes for the Ker 1500 Rubbers Containing Non-Modified Cement Dust and PM-75 Commercial Carbon Black. Vulcanization Parameters: Time - 30 minutes; Temperature - 143°C.

Filler	Tensile strength (MPa)	Relative elongation (%)	Tensile set (%)	Flexibility (%)
Commercial Carbon black (50 parts by weight)	18.4	460	8	50
Carbon black + cement dust (10 parts by weight)	16.2	540	12	50
Carbon black (25 parts by weight) + cement dust (25 parts by weight)	13.4	620	16	50

VOL. 14 1984

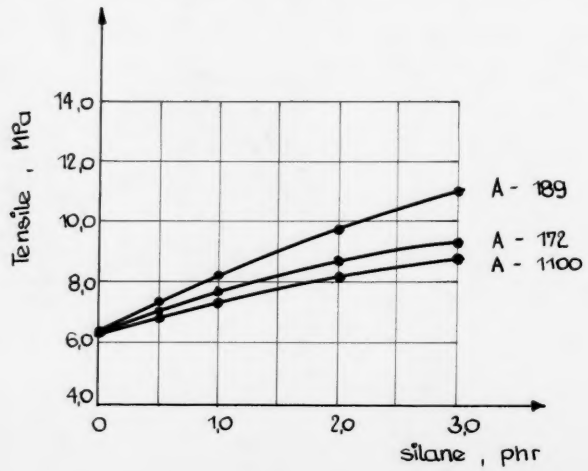

FIG. 3

The influence of the amount of silanes upon the tensile strength of rubbers filled with the 1:1 mixture of cement dust and post-HF silica.

activity and chemical affinity towards rubbers, it is necessary to modify their surfaces. In our investigations, we used alkoxysilane adhesion promoters. We found that cement dusts undergo the influence of these silanes only slightly, so we mixed them with silica which can be modified by the silanes very easily. When choosing the appropriate silica, we took into account particle sizes, so that the difference between the dust ones and the silica ones would be the smallest. For this reason, we used the post-HF silica, which is the waste silica from the HF production. Figure 3 confirms the similarity of the particle sizes and shows that the dust and the silica were as thoroughly mixed as possible.

Cement dusts are characterized by a low, slightly about 30% whiteness degree. Silica, also, because of its impurities, e.g. AlF_3, CaF_2, obtained during the production process, has a low, ca 70%, whiteness degree.

The bulk density of cement dusts is high, over 600 g/dm^3, while that of silica is lower and amounts to about 250 g/dm^3. The high values of bulk densities are the result of considerably larger particle sizes which are, on the average, 80-100 nm and 100-150 nm for the silica and the dust, respectively. They are also the result, as can be seen in the photographs, of badly developed external surfaces.

The water and the dibutyl pthalate absorbing capacity is very low for both the cement dust and the waste silica. In terms of the dust, the water absorbing capacity can not be measured because of the cement setting. The dibutyl pthalate absorbing capacity of the dust and of the silica are 62 g/100g and 90 g/100g, respectively. It must be said here that the dibutyl pthalate absorbing capacity values for the generally used silica and slicate fillers, in most cases exceed 200 g/100g and 300 g/100g. The very low dibutyl pthalate absorbing capacities prove once more the necessity of modification by the use of substances which increase the chemical affinity towards hydrocarbon chains of a rubber.

The hydrophobic properties of the investigated preparations can be calculated from the heat of the immersion results obtained by the KRM differential calorimeter method. The above data show that the water immersion heats decrease and the benzene immersion heats increase, when the dust and the silica surfaces are immersed in the A-189 mercaptosilane, as shown in Table 4. It must be stressed that the modified cement dusts, contrary to the silica, change their water and benzene immersion heats only slightly, which can be explained by a very weak interaction between silanes and the surface groups of cement dusts. Although the A-1100 aminosilane modification of the surfaces causes an increase of the water immersion heat, the benzene immersion heat is close to that of a surface modified by the use of A-189 silane. The increase of the water immersion heat is caused by the creation of hydrogen bonds between amine groups of the introduced silane and water molecules.

The low immersion heat values of cement dust surfaces, even after their modification by the use of silanes, show the passive character of this rubber filler and confirms the proper usage of the waste silica together with the dust, as the rubber compound fillers. While introducing the waste cement dust and post-HF silica into the examined rubbers and mixing them on mixing rolls, no anomaly was observed.

The physico-mechanical properties of the vulcanizates, first of all, depend on the size of the dust and the silica particles, as well as the specific surfaces and the bulk densities of the dust and the silica. The character of a surface also exerts a considerable influence. Chemical affinity, and what comes out of it, strength parameters, depend to a great degree upon the hydrophobic properties. In the Ker 1500 butadiene-styrene rubber vulcanizates, using an appropriate modification and a constant of 50 parts by weight, contents of a

filler, the following average tensile strengths were obtained:

Kind of Filler	R_r(MPa)
Rubber industry limit	90 - 100
Ker 1500 rubber without fillers (with all the other components)	20
Non-modified cement dust	40
Cement dust + 2 parts by weight of A-1100	60
Cement dust + post-HF silica (3:1)	60
Cement dust + post-HF silica (1:1)	70
Cement dust + post-HF silica (1:1) + 3 parts by weight of A-189	110
Cement dust + PM-75 carbon black (1:1)	135

The above data prove the advantage of the last two systems which can, to a certain extent, eliminate carbon black.

Conclusions

The investigations proved that cement dust can be a cheap, low-active filler and can be recommended, partly, as a substitute for commercial carbon black and silica in the recipe for the Ker 1500 butadiene-styrene rubber compounds.

The system consisting of 25 parts by weight of the post-HF silica and 25 parts by weight of the dust modified, in terms of the butadiene-styrene rubbers, by A-189 mercaptosilane, or even a better one consisting of 25 parts by weight of the dust and 25 parts by weight of commercial carbon black, can be proposed. The later one allows eliminating the high energy-consuming carbon black by up to 50%.

Apart from the satisfying results of tensile strengths and modulus, the above investigations proved nearly the same values of tension set for both samples and only slight increase of their elasticity.

VOL. 14 1984

References

1. R. Bode, H. Ferch and H. Tvatzscher, Kautschuk und Gummi 20, 578 (1967).
2. M. Kranz, L. Domka, A. Krysztafkiewicz and M. Maik, Polimery 24, 86 (1979).
3. F. Thurn and S. Wolff, Kaut. u. Gum. Kunstst. 28, 733 (1975).
4. Union Carbide-Akzo-Symp. "Stomil" Zakopane, 1974 (Poland).
5. Wacker Silanes für industrielle Anwendungen, München, July 1975.
6. Chwan-Hwa Chiang, Nan-I-liu and J.L. Koenig, J. Colloid Inter.Sci. 86, 26 (1982).
7. S.J. Monte, "Coupling Agents-Titanate" Modern Plastics Encyclopedia, October 1977, Vol. 54, Number 10 A.
8. S.J. Monte, G. Sugerman and D.J. Seeman, "Titanate Coupling Agents - Current Applications," Kenrich Petrochemicals, Inc., American Chemical Society, Rubber Division, Chicago, May 1977.
9. A. Krysztafkiewicz, L. Domka and W. Wieczorek, Polimery 26, 221 (1981).
10. T. Paryjczak "Chromatografia gazowa w badaniach adsorpcji i katalizy" PWN Warszawa, 1975.
11. L. Domka and A. Krysztafkiewicz, Polish pat. 119 358 (1982).
12. Polish pat. 45 878 20-IV (1957).
13. W. Zielenkiewicz and K. Kurek, Przem. Chem. 45, 247 (1966).
14. D.E. Bradley, Brit. J. Appl. Phys. 5, 65 (1954).

CEMENT and CONCRETE RESEARCH. Vol. 14, pp. 785-792, 1984. Printed in the USA.
0008-8846/84 $3.00+00. Copyright (c) 1984 Pergamon Press, Ltd.

MECHANICAL PROPERTIES OF POLYMER IMPREGNATED CEMENT SYSTEMS AND THE EFFECT OF MOISTURE ON THEIR DIMENSIONAL STABILITY

R.F. Feldman and J.J. Beaudoin
Division of Building Research
National Research Council Canada
Ottawa, Canada K1A 0R6

(Communicated by F.H. Wittmann)
(Received Feb. 1, 1984)

L.
4
84

ABSTRACT

Cement matrices were prepared by autoclaving portland cement-silica mixtures having various percentages by weight of silica, with water-to-cement ratios of from 0.22 to 0.45. Normal cement paste samples were also made for comparison. Samples were heated to 100°C in vacuum for 24 h before impregnation with methyl methacrylate monomer (MMA), which was then polymerized; impregnation was repeated for complete impregnation.

Young's modulus and microhardness were measured as a function of volume fraction of PMMA and results compared with those obtained from similar samples conditioned to 11% RH.

Autoclaved impregnated and unimpregnated specimens and room-temperature-cured cement paste specimens at both conditions were exposed to 100% RH and their length changes measured for up to four years.

Permeation to water vapour in the impregnated specimens, although decreased, still occurs and impregnation increased long-term expansion on exposure. Expansion on exposure to 100% RH is much larger for D-dried than for 11% RH-conditioned matrices; the latter produced stronger bodies on impregnation.

Introduction

The mechanical property values of porous cement systems can be increased by several hundred percent by impregnation. Impregnation also results in large decreases in water permeability (1-3). Earlier work with sulphur as an impregnant showed that these large increases can be accounted for using equations based on a Reuss' mixing rule (4). However, exposure of some sulphur-impregnated matrices, especially those with high surface areas, to 100% RH results in dimensional changes, often leading to destruction and extrusion of sulphur (5).

Studies on cement-based matrices impregnated with methyl methacrylate (MMA) have shown that increases in microhardness over the unimpregnated state

are greater than for those with sulphur, for the same volume fraction of impregnant (6). These studies indicated that polymethyl methacrylate (PMMA) in micro-pores forms a better bond with the matrix than sulphur and that the properties of PMMA in the micro-pores of cement paste are different from those for PMMA in large pores. The rate of expansion of MMA-impregnated cement systems exposed to 100% RH might, therefore, be significantly different than the rate of expansion of sulphur-impregnated cement systems. It has been observed that MMA-impregnated porous glass, when exposed to 100% RH, remains stable, although some expansion does occur, and this may be partly due to gradual absorption of water by the polymers (7).

This work is a continuation of the study on MMA-impregnated porous glass. The extent to which water can enter (on long-time exposure) cement systems impregnated with MMA, and the factors controlling their durability, are determined. Autoclaved cement-silica mixtures were selected to obtain matrices having a wide range of properties. For example, varying silica content from 0 to 65% by weight gives hydration products having significantly different pore structure, density, and chemical composition. Properties of D-dried MMA-impregnated cement systems are compared with similar systems conditioned only to 11% RH before impregnation. (At 11% RH many of the interlayer positions in the cement hydrate are occupied by water.) These comparisons are based on the mechanical properties of the composites and the length-change response on exposure to 100% RH.

Experimental

Specimens used were thin discs, 32 mm in diameter and 1.3 mm thick, in order to facilitate complete and homogeneous impregnation. Samples used were the same type used in previous work (8): a series of 36 autoclaved (216°C, 2.04 MPa) portland cement-silica mixtures, having 5, 10, 20, 30, 50 and 65% by weight of silica, were prepared with water-to-cement ratios of 0.22, 0.26, 0.30, 0.35, 0.40 and 0.45. Samples of cement paste, prepared at water-to-cement ratios of 0.45, 0.70 and 1.10 and hydrated at room temperature for eight years, were also used. All samples were heated in vacuum for 24 h at 100°C before impregnation.

Methods

Porosity Determination

Porosity was determined before and after impregnation by measuring solid volume by helium comparison pycnometry, as described previously (4). The apparent volume was determined by weighing in methanol, samples saturated with methanol.

Mechanical Properties

Young's modulus and microhardness of the samples were determined before and after impregnation, using techniques described in reference 4. The modulus values given are average values for five discs, and the hardness values are the average of ten measurements made on each of three discs.

Impregnation

Discs conditioned in vacuum at 100°C for 24 h were vacuum-saturated with methyl methacrylate monomer in a vacuum vessel; specimens were contained in a metal basket. After saturation the samples were raised above the excess monomer and, in the presence of its vapour, exposed to cobalt radiation (41.7 rad/s) for 17 h. After the mechanical properties and porosity were measured, the samples were re-impregnated and re-exposed to the radiation (6) to reduce porosity due to shrinkage occurring during polymerization.

Exposure to 100% RH

Thirty by ten millimetre prisms were cut from the discs, both before and

VOL. 14 1984

after impregnation, and used for length-change measurements; they were mounted on 25-mm gauge length extensometers with sensitivity of 1×10^{-4} mm/25 mm. These systems were enclosed in vacuum chambers and exposed to 100% RH. Although autoclaved specimens were prepared at several w/s ratios, only those specimens prepared at w/s of 0.45 and the room-temperature-cured paste at w/c of 0.70 were selected for exposure to 100% RH (5). The w/c = 0.70 specimen was used since it has a porosity similar to the autoclaved specimens at w/c of 0.45.

Results

Mechanical Properties

As in the previous paper (samples preconditioned at 11% RH), modulus of elasticity and microhardness of the D-dried samples were plotted against the volume fraction of polymer (6). The regression lines are shown in Figs. 1 and 2. The volume fraction of polymer is derived from the initial porosity minus the residual porosity; most of the residual porosities are less than one percent.

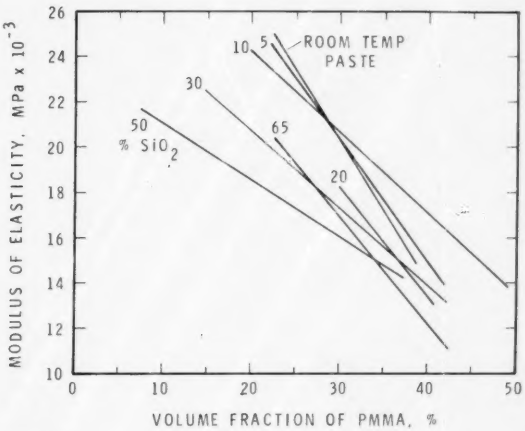

FIG. 1

Modulus of elasticity vs volume fraction of PMMA for autoclaved cement-silica mixtures D-dried prior to impregnation.

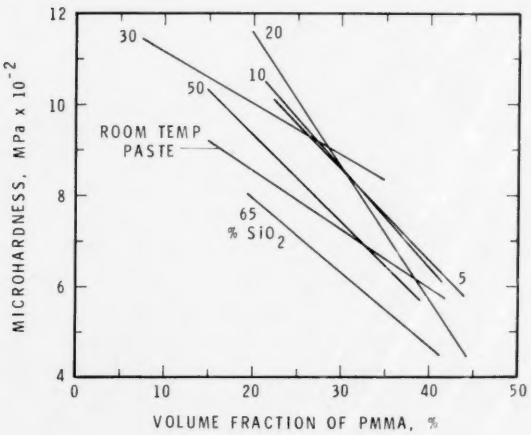

FIG. 2

Microhardness vs volume fraction of PMMA for autoclaved cement-silica mixtures D-dried prior to impregnation.

Although the modulus of elasticity, and microhardness vs polymer volume fraction curves for D-dried and 11% RH-conditioned specimens show similar trends, (i.e., the relative position of the curves with respect to each silica content is similar) the values at any volume fraction of polymer for a given

silica content are generally about 20% less for D-dried specimens than for the specimens conditioned at 11% RH. The maximum ratio of modulus of elasticity of impregnated samples to that of unimpregnated, for D-dried specimens, is 2.5 as compared to 3.5 for specimens conditioned at 11% RH; corresponding ratios for microhardness are 5.5 and 7.5.

The data for Young's modulus and microhardness grouped in water/solids ratios are plotted against the original silica content of the mix (Figs. 3A and 3B). As was observed in earlier work with samples conditioned at 11% RH, the maximum values of Young's modulus for D-dried specimens are at the low-silica end of the curves (6). In the case of microhardness there is a maximum at 20% silica content for most ratios.

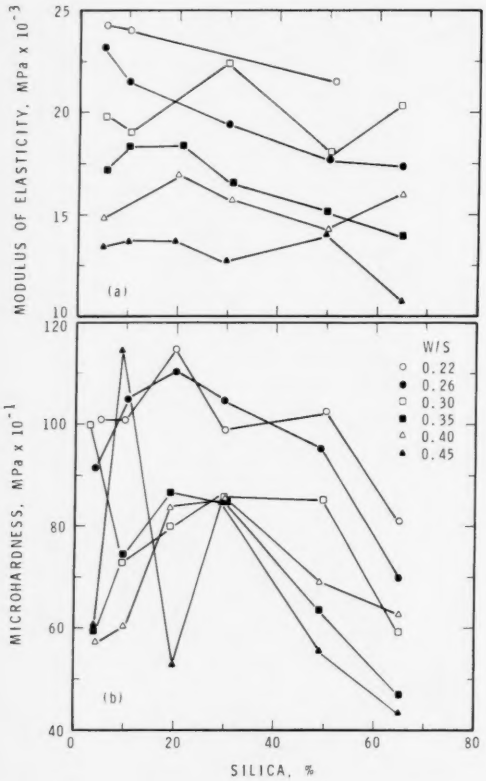

FIG. 3

Dependence of modulus of elasticity and microhardness on silica content of MMA-impregnated autoclaved cement-silica mixtures D-dried prior to impregnation

Length Change on Exposure to 100% RH

The results for unimpregnated specimens conditioned at 11% RH are presented in Fig. 4. The rate of expansion for most of the unimpregnated specimens decreased considerably after one-day exposure and is lowest for the 5 and 10% silica preparation.

For the impregnated samples conditioned at 11% RH prior to impregnation, (Fig. 5) the rate of expansion is lower than for the unimpregnated bodies for all the specimens up to a maximum of about seven days; after 75 days exposure the impregnated samples have all expanded more than twice the amount of the unimpregnated specimens. The expansion continued in the period measured from 100 to 1450 days without termination. It is greatest for the room-temperature paste. The amount of expansion

VOL. 14 1984

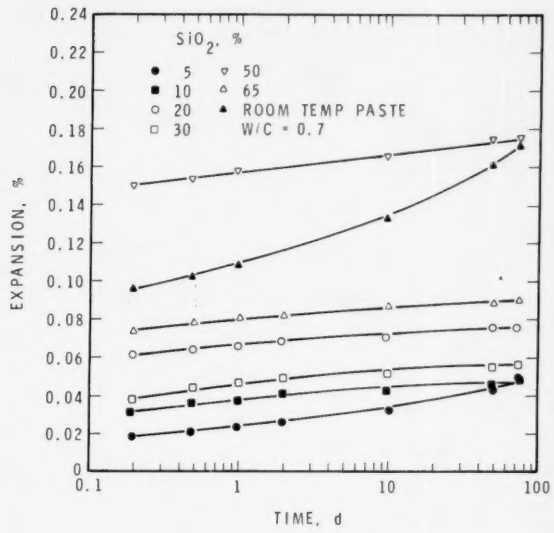

FIG. 4

Expansion of unimpregnated autoclaved cement-silica mixtures (w/s = 0.45) exposed to 100% RH after equilibration at 11% RH.

approximately conforms to observations made for sulphur-impregnated bodies, where higher surface-area materials had greater expansion (5).

The results for exposure of the D-dried specimens to 100% RH are presented in Fig. 6 (unimpregnated) and Fig. 7 (impregnated). The unimpregnated samples were all still expanding at 1450 days, even though the rate of expansion decreased with time throughout. The expansion was greatest for the 0.70 w/c paste and least for the 5 and 10% SiO_2 preparations; the expansion for most of the preparations is about four times that of the specimens conditioned to 11% RH.

The D-dried impregnated specimens show similar characteristics to those conditioned at 11% RH in that they exceeded the expansion of the unimpregnated specimens at 3-11 days exposure. After 920 days of exposure they all exceeded the values of the unimpregnated specimens by about 40 to 100% and the rate of expansion at the termination of measurement was considerably in excess of those for the unimpregnated bodies. It was also slightly greater than the rate for the impregnated specimens conditioned at 11% RH in the period between 200 and 1000 days of exposure.

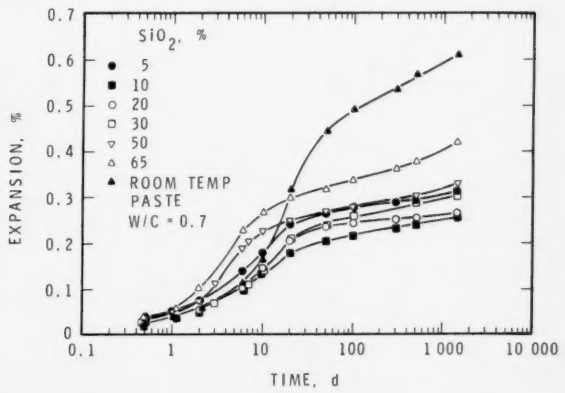

FIG. 5

Expansion of MMA-impregnated autoclaved cement-silica mixtures (w/s = 0.45) exposed to 100% RH after equilibration at 11% RH.

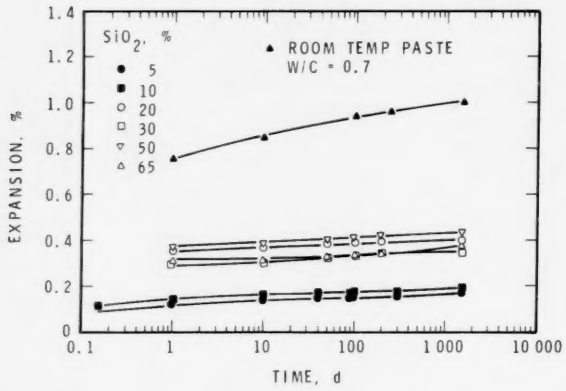

FIG. 6

Expansion of unimpregnated autoclaved cement-silica mixtures (w/s = 0.45) exposed to 100% RH after D-drying.

All the autoclaved cement-silica specimens conformed approximately to the observation that the greater the specific surface area of the matrix material, the greater the expansion on exposure to water vapour.

A comparison of length-change results on exposure to 100% RH for the 0.70 w/c paste specimens with four different treatments is presented in Fig. 8. The increased length change due to D-drying, as opposed to conditioning at 11% RH, is evident. Expansion of impregnated samples is greater than that of unimpregnated samples after 20 days.

VOL. 14 1984

Discussion

D-dried portland cement systems containing polymerized MMA have greatly-increased mechanical properties. These increases, however, are not as high as those for systems pre-dried to only 11% RH prior to impregnation; in that case, they are probably partly due to the presence of interlayer water. This factor may not be as important with regard to durability as the increased shrinkage of D-dried bodies during drying over the 11% RH condition or as the

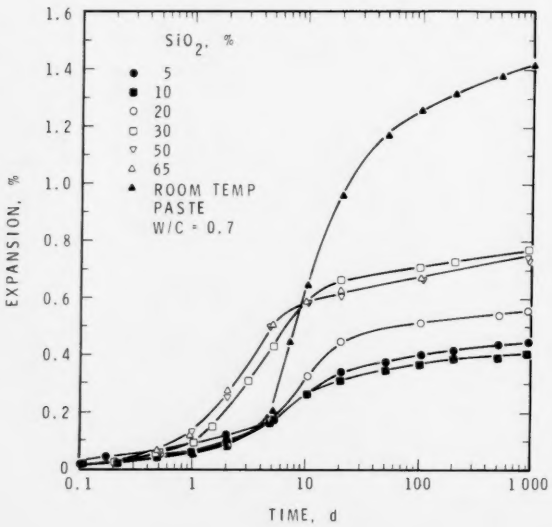

FIG. 7

Expansion of MMA-impregnated autoclaved cement-silica mixtures (w/s = 0.45) exposed to 100% RH after D-drying.

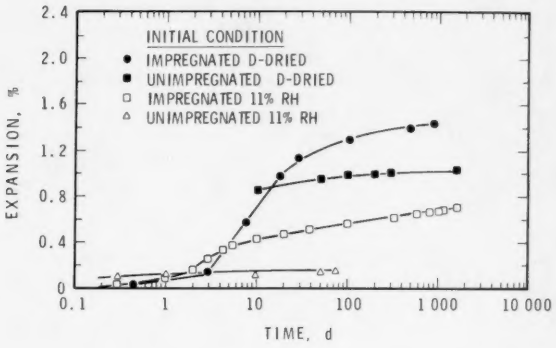

FIG. 8

Expansion of room temperature hydrated MMA-impregnated cement paste (w/c = 0.70) exposed to 100% RH.

resultant larger expansion of D-dried bodies that may occur when the impregnated body is exposed to high humidities. It is clear that impregnation does not completely seal the pores from water vapour; not only does the water vapour re-enter the pores and adsorb on some of the cement matrix interface, as was shown previously for porous glass (7), but it also re-enters the vacated interlayer spaces of the D-dried specimen. This is apparent from the magnitude of the expansion. However, the expansion is somewhat retarded by the presence of polymerized MMA in the pores. This result also suggests that little MMA enters the interlayer spaces in the time available before polymerization.

The expansion of the impregnated D-dried and 11% RH-conditioned specimens is considerably greater than of similar specimens not impregnated. The rate of expansion after 100 days exposure is of the same order as a normal creep rate for cement paste. Beyond ten days exposure, some of the expansion may be due to creep of the matrix brought on by pressure created within the pores by swelling of polymerized MMA due to absorption of water. This explanation is supported by the observation that in this region the expansion increases with surface area of the matrix, which generally increases with silica content (5).

The difference between sulphur-impregnated and MMA-impregnated cement systems (where the sulphur-impregnated matrices of larger surface areas are totally destroyed on exposure to water vapour) is in the interaction between the impregnant and the matrix. In the case of the MMA as impregnant, an interaction seems to occur with the matrix at the interface, although it is not clear whether it is chemical or purely physical (9); PMMA acts as a good stress modifier and reinforces the matrix, despite the fact that it provides the forces which cause the matrix to creep.

The above phenomena will undoubtedly take place in impregnated concrete, although slowly. The specimens used in this study were thin (about 1 mm) and measurements were carried out over a period of four years. In sulphur-impregnated systems, paste was destroyed in 24 hours and concrete in a few years (5). The present study would indicate that polymer-impregnated concrete will probably not be destroyed even over long periods of exposure. However, it would be beneficial to avoid the extreme D-drying that normally is done prior to impregnation.

Conclusions

1. PMMA-impregnated cement matrices have improved mechanical properties over unimpregnated material.
2. Permeability to water vapour is decreased by impregnation but water can

still permeate the body at a slower rate.
3. Water vapour enters both the pores and the layered structure of the C-S-H material after impregnation.
4. Expansion on exposure to 100% RH is larger for D-dried matrices than for matrices conditioned at 11% RH before impregnation.
5. Expansion on exposure to 100% RH is increased by impregnation for both D-dried and 11% RH-conditioned material.
6. Stresses in the pores of impregnated material are caused by absorption of water in PMMA in the pores. This appears to cause long-term creep expansion.
7. Concrete conditioned to 11% RH can be successfully impregnated and is more stable to water exposure than the D-dried material.

Acknowledgement

The authors wish to acknowledge with thanks the work of G. Harts, A. Charron and G. Chan in performing most of the experiments. This paper is a contribution from the Division of Building Research, National Research Council Canada, and is published with the approval of the Director of the Division.

References

1. Int. Symp. on New Uses for Sulphur and Pyrites, Madrid, May 1976. The Sulphur Institute, UK.
2. Proc. 1st Int. Congress on Polymer Concretes, London, May 1975. Ed. The Concrete Society. Construction Press, London, (1976).
3. M. Steinberg, L.E. Kukachka, P. Colombo and B. Nanowitz, In Multi-component Polymer Systems, Ed. R.F. Gould. Advances in Chemistry Series No. 99, Am. Chem. Soc., Washington, DC (1971).
4. R.F. Feldman and J.J. Beaudoin, Cem. Concr. Res. 7, 19 (1977).
5. R.F. Feldman and J.J. Beaudoin, Cem. Concr. Res. 8, 273 (1978).
6. R.F. Feldman and J.J. Beaudoin, Cem. Concr. Res. 8, 425 (1978).
7. G.G. Litvan, R.F. Feldman and P.E. Grattan-Bellew, Cem. Concr. Res. 12, 649 (1982).
8. J.J. Beaudoin and R.F. Feldman, Cem. Concr. Res. 5, 103 (1975).
9. V.S. Ramachandran and P.J. Sereda, Thermochimica Acta 5, 443 (1973).

VOL. 14 1984

CEMENT and CONCRETE RESEARCH. Vol. 14, pp. 793-806, 1984. Printed in the USA.
0008-8846/84 $3.00+00. Copyright (c) 1984 Pergamon Press, Ltd.

DOUBLE-POWER LOGARITHMIC LAW FOR CONCRETE CREEP

Zdeněk P. Bažant[1] and Jenn-Chuan Chern[2]
Center for Concrete and Geomaterials
The Technological Institute,
Northwestern University
Evanston, Illinois 60201, U.S.A.

(Communicated by F.H. Wittmann)
(Received Feb. 17, 1984)

ABSTRACT

An improvement of the double-power law for creep at constant temperature and moisture content is proposed. Comparisons with available test data indicate that the final slopes of long-term creep curves, as indicated by the double-power law, are predominantly on the high side. This is remedied by introducing a transition to a straight line in the logarithmic scale of load duration. The strain at the transition as well as the slope of the straight line are the same for all ages at loading. The strain and the slope at the transition point are continuous, while the curvature is discontinuous. The new law is also found to significantly limit the occurrence of divergence of the creep curves and of negative values at the ends of the relaxation curves calculated by the superposition principle. Extensive statistical comparisons with test data from the literature justify the proposed law.

Introduction

Although the double-power law [2,3] provides a relatively good description of the existing test data and the creep of concrete at constant temperature and water content, called the basic creep, one can detect some deviations which seem to be systematic rather than random. In particular, the final slope of the curves of strain versus the logarithm of load duration appears to be somewhat too steep when long-term tests are considered. This study examines whether this can be remedied by introducing a transition to a logarithmic law for long times.

Review of Double-Power Law

The basic creep of concrete may be relatively well described by the double-power law [1,2,3,7]:

$$J(t,t') = \frac{1}{E_0} + \frac{\phi_1}{E_0}\,(t'^{-m} + \alpha)(t - t')^n \qquad (1)$$

[1]Professor of Civil Engineering and Center Director

[2]Graduate Research Assistant

in which $J(t,t')$ is the compliance function (also called the creep function), which represents the strain at age t caused by a unit uniaxial constant stress acting since age t'; E_0 is the asymptotic modulus, which may be visualized as the left-hand side asymptotic value of the curve of $J(t,t')$ versus $\log(t-t')$, and n, m, α, and ϕ_1 are material parameters. Their typical values are $n \simeq 1/8$, $m \simeq 1/3$, and if t and t' are in days then $\alpha \simeq 0.05$ and $\phi_1 = 3$ to 6. Also, $E_0 \simeq 1.5E_{28}$ where E_{28} is the conventional elastic modulus at age 28 days. Since $(t-t')^n = \exp[n \ln(t-t')]$, the plots of $J(t,t')$ versus $\log(t-t')$ at constant t' have the shape of exponentials.

Eq. 1 has a remarkably broad range of applicability. It yields acceptable values for ages at loading from about 1 day to many years, and for load durations from 1 second to several decades. It also yields acceptable compliance values for rapidly (dynamically) applied loads, and the dynamic modulus is approximately obtained from Eq. 1 as the value of $1/J(t'+\Delta,t')$ for $\Delta \simeq 10^{-7}$ day, whereas the conventional (static) elastic modulus is obtained as the value of $1/J(t'+\Delta,t')$ for $\Delta \simeq 0.1$ day [24]. Since four parameters, namely E_0, ϕ_1, m and α are required to describe the age dependence of the elastic modulus we see that only one additional parameter, n, is needed to describe all creep.

Extensive statistical regression analyses of practically all test data available in the literature revealed that the double-power law exhibits, on the whole, smaller errors than other formulas for concrete creep proposed before [4,5,6,1,2,3,7]. The power function of load duration $t-t'$, involved in Eq. 1, was first introduced by Straub [8] and Shank [25]. Wittmann et al. [12] gave supporting arguments for the power function based on the activation energy theory, and Cinlar, Bažant and Osman [26] gave other supporting arguments based on a certain reasonable hypothesis for the stochastic nature of the physical mechanism of creep. Others, e.g. Branson [9,10], introduced a power function of age t'.

It has often been commented that a power function of $t-t'$ predicts too much creep for longer durations, exceeding 1 month. These critical comments were, however, incorrect since they resulted from using the power function to describe only that part of the creep strain that is in addition to the conventional short-time strain, approximately the strain for load duration 0.1 day [2]. With this approach, the horizontal asymptotic value in Fig. 1 is obtained too high, and in order to fit the test data for medium load durations (1 day to 30 days) one needs to introduce a relatively high curvature by using a high value for exponent n, about $n \simeq 1/3$. This then inevitably causes the power curve to shoot above the data points for longer load durations. Recently it has been discovered [2], however, that the applicability range becomes much broader if the power function is used to describe the entire creep strain including that which occurs for very short load durations (from 10^{-6} second to 0.1 day). This represents a fundamental difference from the earlier use of the power function, and invalidates the aforementioned critical comments. Since the left-hand asymptote (given by $1/E_0$) is much lower than considered in the classical studies (Fig. 1), exponent n required to fit the creep data between 1 and 30 day durations is much smaller, roughly 1/8. This then causes that the power curve has a much smaller positive curvature in the log-time plot, and thus does not overshoot the test data for long creep durations. (There remains, however, an overshoot for very long creep durations, and that is what we try to improve here.)

Note also that another advantage of including the entire creep strain in the power law is that $1/E_0$ can be considered age-independent, while the earlier approach in which only the creep strain after approximately 0.1 day was

VOL. 14 1984

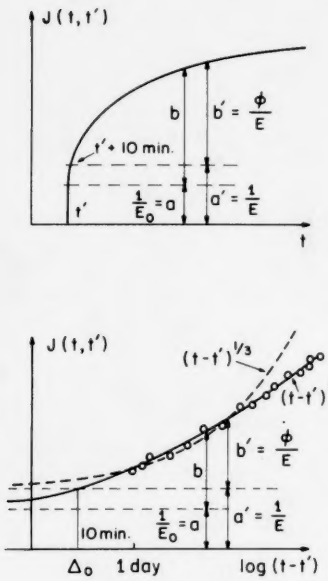

FIG. 1. Creep Curves in Actual and Log Time Scales (a = true elastic deformation, b = true creep, a' = conventional elastic deformation, b' = conventional creep).

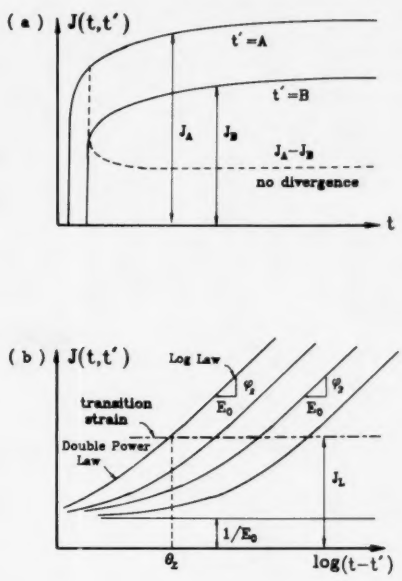

FIG. 2. (a) Theoretical Recovery Curve Obtained by Principle of Superposition, Showing No Divergence; (b) Typical Curves of Double-Power Logarithmic Law.

described by the power function, required considering an age-dependent elastic modulus E(t').

Although the double-power law is intended to describe only the basic creep it may be used as an approximation for creep in drying environment provided the cross section is relatively massive, with a thickness over about 30 cm. For such cross sections, the average creep deformation in the cross section is closer to that of a sealed cylinder than to that of a standard six-inch cylinder exposed to a drying environment.

Proposed Formulation

When the compliance values J(t,t') are plotted against log(t - t') for various constant values of h at constant t', it is found that for longer durations (over several years) the double-power law yields in most cases predictions that are somewhat on the high side. Especially, the final slope appears to be in most cases higher than the measured one (Fig. 1). A remedy can be achieved by introducing a transition to straight lines in the log-time scale at a certain creep duration θ_L. This may be accomplished by the following formulas

$$J(t,t') = \frac{1}{E_0} + \frac{\phi_1}{E_0}(t'^{-m} + \alpha)(t - t')^n \quad \text{for } t - t' \le \theta_L \text{ (double-power law)}$$

$$= \frac{n\phi_L}{E_0} \ln \frac{t - t'}{\theta_L} + \frac{1 + \phi_L}{E_0} \quad \text{for } t - t' \ge \theta_L \text{ (log-law)} \qquad (2)$$

in which $$\theta_L = \left(\frac{\phi_L}{\phi_1 (t'^{-m} + \alpha)}\right)^{1/n}. \quad (3)$$

According to these formulas, which may be called the Double-Power Logarithmic Law, the slope at the transition times θ_L (in log-time scale) is the same for all ages t' at loading, and the value of J(t,t') at which the transition occurs is also the same. So, the ranges of validity of the double-power law and of the logarithmic law are separated by a horizontal line (see Fig. 2b); for longer t' the transition occurs at longer creep duration. For very high ages at loading, the double-power law is valid throughout the entire lifetime.

Divergence of Creep Curves

If the principle of superposition is used, as a crude approximation, to calculate the creep recovery curves from the creep curves for various ages at loading, the recovery curves can be either monotonic, with a monotonic decay to an asymptotic value, or nonmonotonic, with a minimum followed by a monotonic rise up to a certain asymptotic value. Nonmonotonic recovery curves are thermodynamically impossible for a non-aging material, however, they are thermodynamically admissible in case of aging [11,30]. With some exceptions, which might be due to statistical scatter or the effect of drying, most test data show a monotonic decay [11,12,31]. Thus, although recovery cannot in fact be accurately predicted using the linear principle of superposition [12], it seems preferable to use compliance functions that cannot yield nonmonotonic recovery curves upon superposition. This condition is verified when, for the same age t, the creep curve for a higher age at loading t' has a higher slope, i.e. $\partial[\partial J(t,t')/\partial t]/\partial t' \geq 0$ or [11]

$$\frac{\partial^2 J(t,t')}{\partial t \partial t'} \geq 0. \quad (4)$$

It may be readily verified that the logarithmic law in Eq. 2 never violates the inequality in Eq. 4 (Fig. 2a). On the other hand, the double-power law (Eq. 2) violates this inequality beginning with a certain creep duration. It is possible to always satisfy with Eq. 2 the inequality in Eq. 4 if the following condition is verified

$$\phi_L \leq \phi_1 \left(\frac{1-n}{m f_{max}}\right)^n \quad (5)$$

in which

$$f_{max} = \text{Max}\left[t'^{\frac{m-n}{n}} (1 + \alpha t'^m)^{-\frac{n+1}{n}}\right]. \quad (6)$$

Comparison With Test Data

Same as the double-power law, Eq. 2 should be applied only to creep at constant water content, called the basic creep. Only under such conditions the creep represents a constitutive property of the material. The creep observed on drying specimens is not a constitutive property but an average property of the specimen as a whole, since the drying causes in the specimen a highly nonuniform distribution of water content and of stress, produces microcracking, and leads to great differences in creep at various points. An empirical description of the mean creep of drying specimens requires, therefore, much more complicated formulas.

Eq. 2 has six material parameters, E_0, n, m, α, ϕ_0, ϕ_L, which have to be

VOL. 14 1984

determined from test data. Similarly to previous works [2,3], this may be accomplished by minimizing the sum of squared deviations Δ of Eq. 2 from the given data. When all six material parameters are considered as unknown, the optimization problem is a nonlinear one. The optimum fits have been obtained by Marquardt-Levenberg algorithm, for which an efficient library subroutine exists. The test data used in optimization have been extracted from a computerized data bank set up at Northwestern University. Since most experimentalists did not take their readings at times uniformly spaced in the logarithmic time scale, the raw data as reported are biased in that some readings are crowded at certain times and others are too sparse. For this reason, the test data from the literature have been smoothed visually by hand. At the same time, the hand smoothing approximately achieves elimination of the measurement error, which needs to be done since structures do not feel this error. The hand-smoothed curves were characterized by data points placed at regular intervals in the $\log(t - t')$ scale, using two points per decade.

The deviations of Eq. 2 from test data have been characterized by the coefficient of variation defined [3,7, 31] as:

$$\bar{\omega} = \left(\frac{1}{N}\sum_{j=1}^{N}\omega_j^2\right)^{1/2}, \quad \omega_j = \frac{1}{\bar{J}_j}\left(\frac{1}{n-1}\sum_{i=1}^{n}\Delta_{ij}^2\right)^{1/2}, \quad \bar{J}_j = \frac{1}{n}\sum_{i=1}^{n}\tilde{J}_{ij} \tag{7}$$

in which $\tilde{J}_{ij}$ $(i = 1,\ldots,n)$ are the characteristic points of the data set number j (placed at regular spacing in log-time scale) on the creep curves reported in the data set; n = number of all data points on all curves within the data set, Δ_{ij} = vertical deviations of Eq. 2 from these data points, $\bar{J}_j$ = mean ordinate of all data points from the data set number j, ω_j = coefficient of variation for data set number j, $\bar{\omega}$ = the overall coefficient of variation for all data sets combined $(j = 1,\ldots,N)$.

Fig. 3 shows the optimum fits of the data sets reported in Refs. 15, 16, 17, 18, 19, 20, 21 and 23. For comparison, Fig. 3 shows the optimal fits previously achieved with the double-power law [2,3]. The coefficients of variation are summarized in Table 1a. The overall coefficient of variation for the fits by the double-power law is $\bar{\omega} = 5.45\%$ [2], and for the present Eq. 2 we achieve $\bar{\omega} = 3.9\%$. We see that some improvement is achieved by Eq. 2.

More importantly, we may note that the final slopes achieved with Eq. 2 are better. This is important for extrapolation to longer times. Therefore, we determine for all creep curves the final slope, which we draw graphically as illustrated in Fig. 3 by the dashed lines, and we compare these experimental slopes with the value of $\partial J(t,t')/\partial \log(t - t')$ according to Eq. 2 for the last sampling time of each curve. The combined coefficient of variation for the deviations from the measured final slopes for all data tests, $\bar{\omega}_f$, is found to be 34% for the optimum fits by the double-power law, and 29% for Eq. 2; see Fig. 3 and Table 1b. Thus, we see that the present formulation achieves an appreciable improvement in the representation of the final slopes of the creep curves, and therefore also in the extrapolation to longer times.

The foregoing fits of test data (Fig. 3) have been obtained without the nondivergence restriction (Eqs. 4 - 6). If this restriction is imposed in data fitting, the optimum fits must obviously get worse. Such fits are shown in Fig. 4, and the corresponding coefficient of variation for all data sets is found to be $\bar{\omega} = 5.54\%$, while for the double-power law it is $\bar{\omega} = 5.45\%$. Although here there is no improvement, one finds now a significant improvement for the final slopes of creep curves, as is shown in Fig. 4, in which case $\bar{\omega}_f = 22\%$, as compared to $\bar{\omega}_f = 34\%$ for the double-power law.

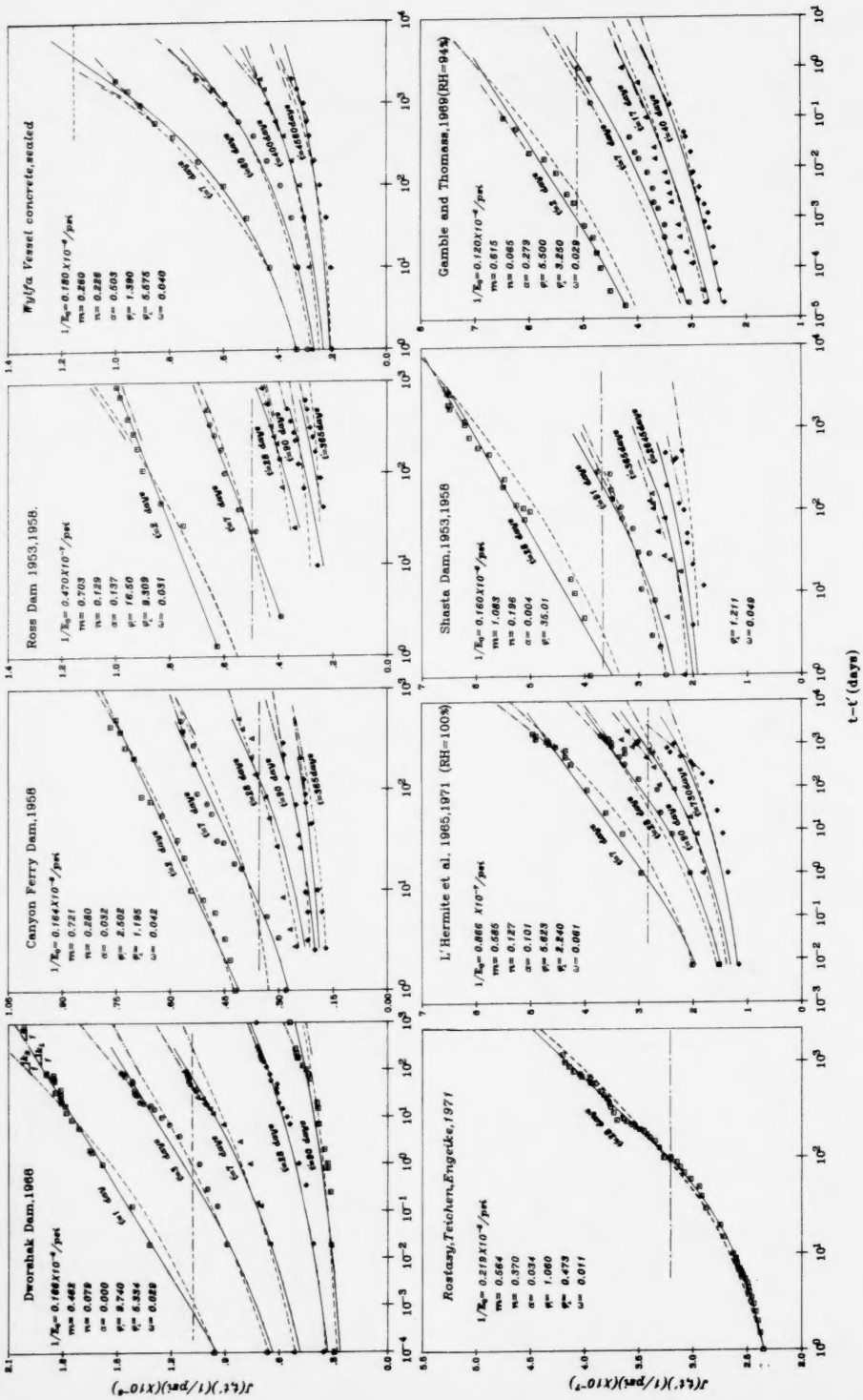

FIG. 3. Optimum Fits of Test Data by Double-Power Logarithmic Law without the Nondivergence Restriction.

VOL. 14 1984

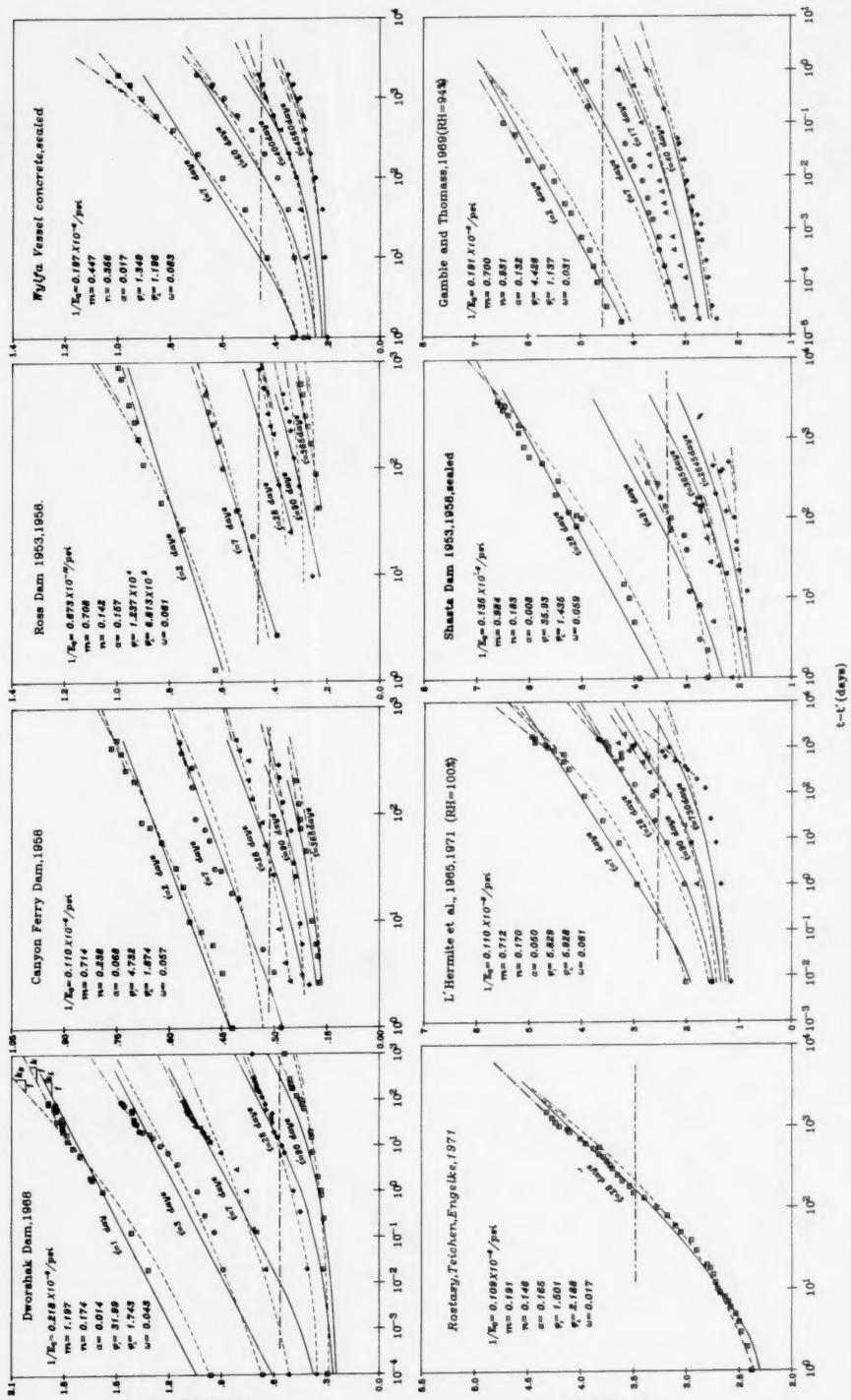

FIG. 4. Optimum Fits of Test Data by Double-Power Logarithmic Law with the Nondivergence Restriction.

Due to the nonlinearity of the optimization problem, it is hard to carry out a more refined statistical analysis which would indicate the increase of error as a function of the distance from the centroid of measured data. To obtain information on this aspect, it is necessary to linearize Eq. 2 so that linear regression statistics can be applied. For this purpose we may introduce the notations

$$y = E_0 J(t,t') - 1, \quad x = \phi_1 (t'^{-m} + \alpha)(t-t')^n \quad \text{for } (t-t') \le \theta_L$$
$$x = (n+1)\phi_L \ln \frac{t-t'}{\theta_L} \quad \text{for } (t-t') \ge \theta_L \tag{8}$$

This allows writing Eq. 2 as $y = c_0 + c_1 x$, in which c_0 and c_1 are coefficients to be found by linear regression analysis. Variable y may be regarded as the creep coefficient relative to instantaneous value $1/E_0$. If Eq. 2 represented the test data perfectly, then c_1 would be 1 and c_0 would be 0. The deviations of c_1 from 1 and of c_0 from 0 characterize the errors. Statistical regression analysis yields not only the mean values of c_1 and c_0, but also their coefficients of variation, as well as the confidence intervals for the values of y and for the mean of y.

Using the material parameters found before, the test data from the literature, used in Fig. 3, can be all plotted in one regression diagram; see Fig. 5. The regression line is shown as a solid line. Furthermore, the hyperbolas representing the 95% confidence intervals, are shown as the dashed lines. We may note the widening of the confidence interval with the distance from the centroid of the test data. The values of c_1 and c_0 found from the linear regression analysis may be interpreted as corrections to the values of ϕ_1 and of $1/E_0$. Comparing the statistical regressions in Figs. 5a and 5b for the present formulation and the double-power law, we again see very little difference. As we already showed, an appreciable improvement is achieved only in the final slopes to which the linear regression does not apply.

VOL. 14 1984

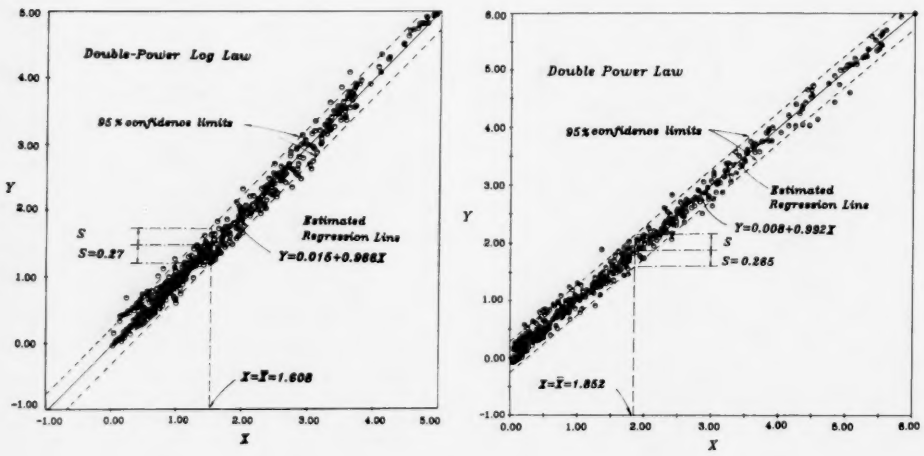

FIG. 5
Regression Plots for Double-Power Logarithmic Law and Double-Power Law.

Prediction of Creep

The capability of close fitting the available test data is an indication of the correctness of the mathematical formula for creep. It is, however, another matter to predict creep of a given concrete if no measurements were taken. The prediction is notoriously far more uncertain. Due to the very large uncertainty in predicting the parameters E_0, m, n, α, ϕ_1 and ϕ_L from concrete strength and composition, hardly any improvement can be achieved with the present formulation (Eq. 2) compared to the double-power law, and therefore the prediction formulas in Eqs. 16, 17, 18, 15 and 19 from Ref. 3 (or Eqs. 9a-9e from Ref. 7) are recommended to be also used with the present formulation. An additional formula is needed for parameter ϕ_L, for which the following expression may be recommended

$$\phi_L = \frac{\phi_1}{1.53 - 0.06\ f'_c} \tag{9}$$

with f'_c in ksi (1 ksi = 6.895 MPa); see Fig. 6. This equation does not guarantee nondivergence, in general. Nevertheless, the increase in the separation of any two adjacent creep curves for adjacent ages at loading is quite small, much smaller than that obtained with the double-power law.

Table 1 shows the coefficient of variation for all data sets and Fig. 7 gives the predictions of creep curves. When all parameters are predicted (for the concretes considered) on the basis of the aforementioned formulas, $\bar{\omega}$ is 21.3%, as compared to 24.1% for the double-power law. We see that the prediction of final slope is greatly improved by double-power logarithmic law. For final slopes of creep curves, as shown in Table 1b, $\bar{\omega}$ = 34% as compared with 61% for double-power law!

As has been shown before, the predictions of creep are drastically improved if the initial elastic value of deformation is measured. From such an initial value, one can determine one material parameter, E_0. The uncertainty of predicting creep when the initial elastic deformation is known may be illustrated by comparing the formula predictions obtained for these data under the condition that the value of E_0 is optimized. Such statistical comparisons are shown in Table 1.

Stress Relaxation Predictions

Unlike creep recovery, the stress relaxation at constant strain may be rather closely predicted on the basis of the principle of superposition. This is confirmed by relaxation measurements, although measurements of very long

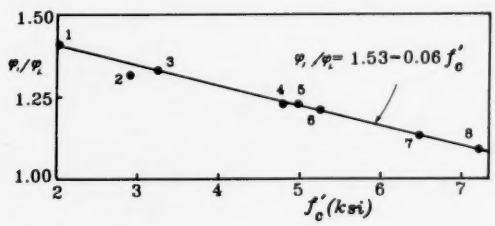

FIG. 6

ϕ_1/ϕ_L Versus the 28 Day Cylinder Strength f'_c. (1. Dworshak Dam, 2. Canyon Ferry Dam, 3. Shasta Dam, 4. Gamble and Thomass, 5. Ross Dam, 6. L'Hermite et al., 7. Rostasy et al., 8. Wylfa Vessel).

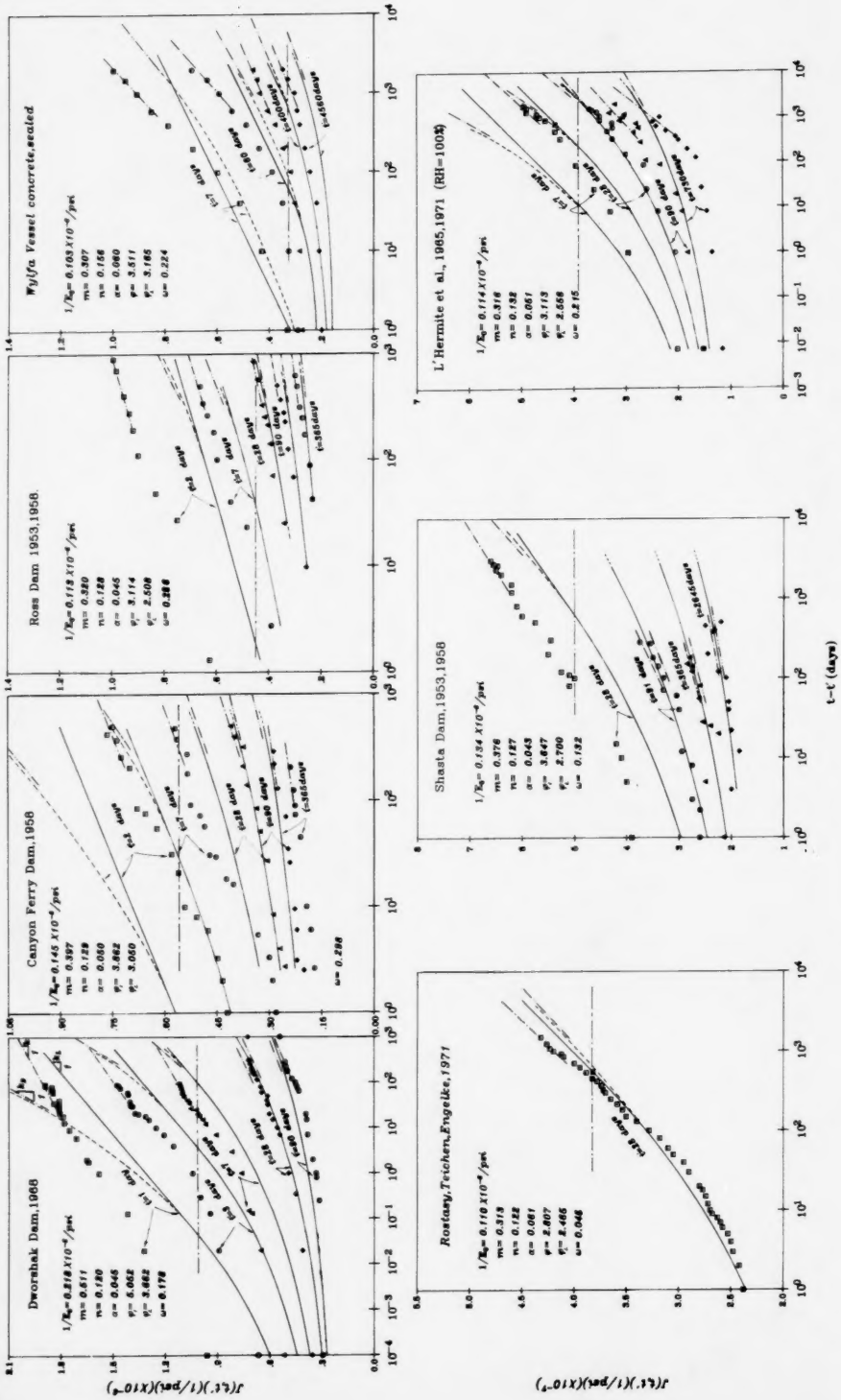

FIG. 7. Fits of Test Data by Prediction Formulas.

VOL. 14 1984

TABLE 1. Coefficient of Variation for Test Data

TABLE 1a. For sampling points (in percent)

j	data set \ creep law	Optimum Fits DPL [3]	DPL [2]	DPLL	DPLL*	Prediction Formula DPL [3]	DPLL	DPLL**
1	Canyon Ferry Dam [15,16]	4.60	5.58	5.70	4.20	39.6	29.8	6.20
2	Ross Dam [15,16]	3.50	7.00	6.10	3.09	27.7	28.6	16.5
3	Dworshak Dam [17]	5.46	5.63	4.80	2.90	21.2	17.8	11.1
4	Rostasy et al. [22]	1.00	1.20	1.70	1.12	5.10	4.50	3.50
5	L'Hermite et al. [18]	4.90	6.28	6.11	6.10	25.2	21.5	7.30
6	Shasta Dam [15,16]	4.10	5.37	5.90	4.90	13.6	13.2	8.80
7	Wylfa Vessel [19,20,21]	4.14	4.15	8.30	4.00	21.0	22.4	9.50
8	Gamble-Thomass [23]	2.82	6.20	3.10	2.90	-	-	-
	$\bar{\omega}$	4.03	5.45	5.54	3.91	24.12	21.30	9.72

TABLE 1b. Final Slopes

Data Sets	t'	Optimum Fits DPL[2] Δ_D	DPLL Δ_L	DPLL* Δ_L	Prediction Formulas DPL[3] Δ_D	DPLL Δ_L
1	2	0.38	0.0	0.0	1.20	0.08
	7	0.17	0.30	0.20	0.85	0.0
	28	0.0	0.30	0.30	0.0	0.0
	90	0.40	0.45	0.40	0.10	0.10
	365	0.32	0.50	0.10	0.20	0.20
2	2	0.70	0.0	0.0	1.00	0.0
	7	0.0	0.0	0.0	0.50	0.24
	28	0.26	0.65	0.30	0.0	0.0
	90	0.50	0.30	0.05	0.50	0.50
	365	0.60	0.40	0.0	0.40	0.40
3	1	0.60	0.0	0.0	1.64	0.62
	3	0.05	0.31	0.0	1.00	0.30
	7	0.20	0.0	0.0	0.80	0.60
	28	0.0	0.22	0.0	0.0	0.0
	90	0.50	0.10	0.50	0.30	0.30
4	28	0.25	0.0	0.0	0.11	0.08
5	7	0.04	0.41	0.35	0.54	0.20
	28	0.17	0.32	0.17	0.50	0.05
	90	0.17	0.0	0.0	0.25	0.20
	730	0.60	0.53	0.50	0.60	0.60
6	28	0.39	0.0	0.0	0.35	0.05
	91	0.0	0.0	0.12	0.08	0.10
	365	0.0	0.24	0.0	0.10	0.10
	2645	0.50	0.15	0.25	0.10	0.10
7	7	0.39	0.30	0.35	0.20	0.56
	60	0.17	0.25	0.17	0.40	0.43
	400	0.05	0.41	0.05	0.30	0.20
	4560	0.29	0.15	0.35	0.15	0.15
8	2	0.20	0.14	0.05	1.0	0.70
	7	0.0	0.0	0.0	0.80	0.80
	17	0.0	0.10	0.05	0.60	0.60
	40	0.28	0.24	0.20	0.15	0.15
	$\bar{\omega}_f$ †	0.34	0.29	0.22	0.61	0.34

Note: Δ_D, Δ_L are normalized errors of final slopes for curves of double-power law (k_D) and Double-Power Logarithmic Law (k_L) in comparisons with the final slopes of test data (k) and defined as $|k_D/k - 1|$, $|k_L/k - 1|$, respectively.

* Double-Power Logarithmic Law without the nondivergence restriction.

**Double-Power Logarithmic Law with optimum E_0.

† $\bar{\omega}_f = \left[\frac{1}{n-1}\sum_{i=1}^{n} \Delta_{D_i}^2\right]^{1/2}$ or $\left[\frac{1}{n-1}\sum_{i=1}^{n} \Delta_{L_i}^2\right]^{1/2}$.

durations (over 10 years) are lacking. It has been noted before that, for small ages at the instant of initial straining, the stress relaxation curves cross into negative stress values at very long times (over 10 years) when they are calculated by the principle of superposition from the double-power law. The same thing happens when the calculation is done by the principle of superposition directly from certain measured creep curves. From the thermodynamic viewpoint [30], there exists no fundamental prohibition against such negative values when one deals with an aging material. Nevertheless, it is not clear whether the negative values at the end of early-age relaxation curves are not caused merely by the choice of the creep formula or by an experimental error in creep measurements.

To examine this aspect, the creep data for Dworshak Dam [17] and for Canyon Ferry Dam [15,16] were optimally fitted by the double-power law and by the present formulation (Eq. 2), and for both cases the stress relaxation curves were calculated on the basis of the superposition principle using a highly accurate step-by-step algorithm [13,14]. The results of the calculation are shown in Fig. 8 by the solid curves for the present formulation and by the dashed curves for the double-power law. We see that the present formulation limits the occurrence of negative stress values at the end of early-age relaxation curves, which seems to be a desirable feature.

Conclusions

1. The double-power law yields for the creep curves plotted in log-time final slopes that are predominantly on the high side when compared with long-time measurements. This may be remedied by a creep law which exhibits a transition from the double-power law to a straight line in the logarithmic scale of creep duration at a certain transition time. The straight line has the same slope for all ages at loading and the transition occurs later for an older concrete.

2. The aforementioned improvement in the representation of the final slope of the creep curves should allow a better extrapolation of creep data into very long times.

VOL. 14 1984

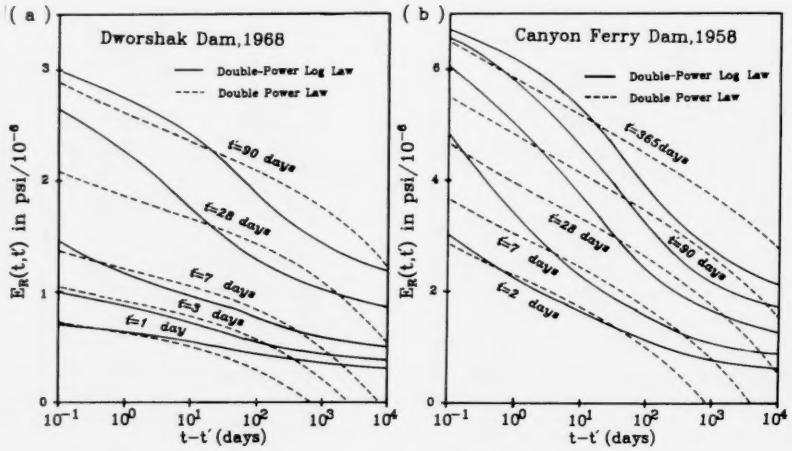

FIG. 8
Comparisons of Stress Relaxation Predictions for Dworshak Dam [17] and Canyon Ferry Dam [15,16].

3. The new formulation reduces the occurrence of divergence of creep curves. Although the divergence could be eliminated, for certain values of material parameters, completely, the representation of existing test data would be impaired.

4. The new law also greatly reduces the possibility that the relaxation curves calculated on the basis of the superposition principle would cross at very long times into negative values.

Acknowledgment - Support by the U.S. National Science Foundation under Grant No. CEE-8303148 to Northwestern University is gratefully acknowledged.

References

1. Z.P. Bažant, Mechanics Today, 2, 1 (1975) (J. Wiley, New York).
2. Z.P. Bažant, E. Osman, Materials and Structures (RILEM, Paris), 9, No. 49, 3 (1976).
3. Z.P. Bažant, L. Panula, Materials and Structures, Parts I and II: 11, No. 65, 307(1978), Parts III and IV: 11, No. 66, 415(1978), Parts V and VI: 12, No. 69, 169(1979).
4. F.H. Wittmann, M. Setzer, Cem. Concr. Res., 1, 679(1971).
5. Z.P. Bažant, E. Osman, Cem. Concr. Res. 7, 119 (1977).
6. Z.P. Bažant, W. Thonguthai, Materials and Structures (RILEM, Paris), 9, 91 (1976).
7. Z.P. Bažant, L. Panula, J. PCI, May-June, 86 (1980).
8. H. Straub, Proc. Am. Soc. Civil Engng., 56, 49 (1930).
9. D.E. Branson, B.L. Meyers, K.M. Kripamarayaman, Highway Research Record, No. 324, 15 (1970).
10. D.E. Branson, Deformation of Concrete Structures, McGraw-Hill, New York (1977).
11. Z.P. Bažant, S.S. Kim, Cem. Concr. Res., 8, 601 (1978).
12. Z.P. Bažant, "Mathematical Models for Creep and Shrinkage of Concrete," Chapter 7 in Creep and Shrinkage in Concrete Structures, edited by Z.P. Bažant and F.H. Wittmann, John Wiley & Sons (1982).
13. Z.P. Bažant, ASCE Comm. on Finite Element Analysis of R.C. Structures, Report on Finite Element Analysis of Reinf. Concrete Structures, Chapter 6, on Time-Dependent Effects, ASCE Special Publication, New York (1982).
14. Z.P. Bažant, Materials and Structures (RILEM, Paris) 15, No. 88, 283(1982).
15. J.A. Hanson, Concrete Lab., Report No. Sp-38, U.S. Dept. of the Interior, Bureau of Reclamation, Denver, Colorado, July 1953.
16. E.M. Harboe et al., Concrete Lab. Report No. C-854, Div. of Engng. Lab., U.S. Dept. of the Interior, Bureau of Reclamation, Denver, Colorado, March 1958.
17. D. Pirtz, Report No. 65-2, Structural Engng. Lab., Univ. of California, Berkeley, October 1968.
18. R.G. L'Hermite, M. Mamillan, C. Lefèvre, Annales de l'Institut Techn. du Bâtiment et des Travaux Publics, 18, No. 207-208, 323 (1965). (See also Int. Conf. on the Structure of Concrete, Cement and Concrete Assoc., London, 423 (1968).)
19. R.D. Browne, R. Blundell, Materials and Structures (RILEM, Paris) 2, 133 (1969).
20. R.D. Browne, R.E.D. Burrow, in "Structure, Solid Mechanics and Engineering Design," Civil Engng. Materials Conf. held in Southampton 1969, Ed. by M. Te'eni, Wiley Interscience, 1343 (1971).
21. R.D. Browne, P.P. Bamforth, Third Int. Conf. on Struct. Mech. in Reactor Technology, Paper H 1/8, London, Sept. 1975.
22. F.S. Rostasy, K.T. Teichen, H. Engelke, Amtliche Forschungs-und Material-

prüfungsanstalt für das Bauwesen, Otto-Graf-Institut, Universität Stuttgart, Strassenbau und Strassenverkehrstechnik, Heft 139 (1972).
23. B.R. Gamble, L.H. Thomass, Proc. of the Australian Conf. on the Mech. of Structures and Materials, Adelaide, Australia, Paper No. 24, (Aug. 1969).
24. Z.P. Bažant, B. Oh, J. Eng. Mech. Div., ASCE, 108, 764 (1982).
25. J.R. Shank, Ohio State Univ. Eng. Exp. Stn., Bull. No. 91, (1935).
26. E. Cinlar, Z.P. Bažant, and E. Osman, J. Eng. Mech. Div., ASCE, 103, No. EM6, Proc. Paper 13447, 1069-88 (1977).
27. Z.P. Bažant, E. Osman, W. Thonguthai, Material and Structures (RILEM, Paris) 9, No. 54, 395(1976).
28. "Prediction of Creep, Shrinkage and Temperature Effects in Concrete Structures," Report No. ACI 209 R-82 by ACI Committee 209, Subcommittee II, chaired by D.J. Carreira, in ACI Special Publication SP-76, "Designing for the Effects of Creep, Shrinkage and Temperature," (Proc. of A. Pauw Symp. held at ACI Conv., Houston, 1978), Am. Concr. Institute Detroit, 193-300 (1982).
29. Z.P. Bažant, J. Eng. Mech. Div., ASCE, 102, 1049 (1977).
30. Z.P. Bažant, J. Eng. Mech. Div., ASCE, 105, 933 (1979).
31. Z.P. Bažant, S. Zebich, Cem. Concr. Res., 13, 869 (1983).

VOL. 14 1984

CEMENT and CONCRETE RESEARCH. Vol. 14, pp. 807-815, 1984. Printed in the USA.
0008-8846/84 $3.00+00. Copyright (c) 1984 Pergamon Press, Ltd.

MIKROKALORIMETRISCHE STUDIE ÜBER DIE EISBILDUNG IN CHLORIDHALTIGEM ZEMENTSTEIN

H. W. Dorner

Lehrstuhl für Baustoffkunde und Werkstoffprüfung

Technische Universität München, Baumbachstraße 7,
8000 München 60

(Communicated by F.H. Wittmann)
(Received Feb. 6, 1984)

ABSTRACT

Differential scanning calorimetry (DSC) of wet porous materials in the temperature range between + 20°C and - 60°C is a sensitive tool to investigate phase transitions and supercooling of pore water. Storage of hydrated cement paste (hcp) in water containing 5 % chloride at an age of 8 months after freeze drying leads to an increase of the enthalpy change between - 10°C and - 25°C (phase transition of free water in capillary pores with r_H > 10 nm) and to a strong reduction of the enthalpy change between - 43°C and - 52°C (phase transition of water in the medium gel pores with 3 nm < r_H < 10 nm) in comparison to hcp without addition of chloride.

ZUSAMMENFASSUNG

Mit der Differential-Scanning-Kalorimetrie (DSC) können in feuchten, porösen Stoffen im Temperaturbereich zwischen + 20°C und - 60°C Phasenübergänge und Unterkühlungseffekte von Porenwasser auf empfindliche Weise nachgewiesen werden. Die Lagerung von 8 Monate alten, gefriergetrockneten Zementsteinproben in 5%iger Chloridlösung führte zu einer gesteigerten Wärmefreisetzung zwischen - 10°C und - 25°C (Phasenübergang des freien Wassers in Kapillarporen mit r_H > 10 nm) und zu einer stark verminderten Wärmeabgabe zwischen - 43°C und - 52°C (Phasenübergang des Wassers in den mittleren Gelporen mit 3 nm < r_H < 10 nm). Zementstein ohne Chloridzugabe zeigte diese Effekte nicht.

Einleitung

Das Gefrieren von Porenwasser in porösen, keramischen Stoffen, wie dem Zementstein, wird durch Oberflächenkräfte stark verändert. Die Veränderung ist umso größer, je kleiner die Poren sind und je näher das Porenwasser der Festkörperoberfläche ist. Eine thermodynamische Beschreibung dieses Phänomens wurde von Setzer (1) gegeben. Zur direkten Untersuchung des Phasenüberganges Wasser/Eis können mikrokalorimetrische Messungen (DSC) im Tieftemperaturbereich herangezogen werden (2, 3, 4). In Kombination mit gravimetrischen Bestimmungen lassen sich Erstarrungswärmen und die beim jeweiligen Phasenübergang gefrierende Menge Wasser bestimmen (5). In (4) wurde zudem die Lage der DSC-Signale dem Gefrieren von Wasser in bestimmten Poren zugeordnet.

Über das Gefrieren von chloridhaltigem Porenwasser in Zementstein wurde erstmals von Litvan (6) ausführlicher berichtet. Er lagerte feuchte Zementsteinprobekörper (d = 1,27 mm) in wäßrigen NaCl-Lösungen unterschiedlicher Konzentration. Bei der mikrokalorimetrischen Untersuchung der Probekörper (Kühlrate: 0,33 °C/min) registrierte er bis zu hohen Cl^--Konzentrationen (ca. 11 %) 2 exotherme Peaks zwischen ca. - 10°C und - 30°C. Meier (7) untersuchte mikrokalorimetrisch den Einfluß von 14 und 31%igen, wäßrigen $CaCl_2$-Lösungen auf die Unterkühlbarkeit von Porenwasser in wassergesättigten Zementsteinzylindern (d = h = 4 mm). Unabhängig von der angewandten $CaCl_2$-Konzentration erfolgte nach seinen Angaben der Phasenübergang Wasser/Eis stets bei - 16°C.

Hier wird über mikrokalorimetrische Untersuchungen von chloridhaltigem Zementstein im Temperaturbereich + 20°C bis - 60°C berichtet, bei denen die Auswirkungen der unterschiedlichen Chloridbindung im Zementgel und der Kationenart auf die Eisbildung studiert wurden.

Experimentelle Durchführung

Verwendete Zemente

Es wurden ein Portlandzement PZ 35 F und ein Hochofenzement HOZ 35 L NW/HS mit mind. 70 % Hüttensand eines süddeutschen Werkes verwendet. Beide Zemente waren aus demselben Klinker hergestellt worden. Vom Werk wurden uns folgende Durchschnittsanalysen für den Klinker und den Hochofenzement mitgeteilt (siehe Tabelle 1).

Herstellung und Lagerung der Proben

Aus beiden Zementen wurden Leime mit und ohne Chloridzugabe und einem Wasserzementwert ω = 0,50 hergestellt. Die Chlorid-

VOL. 14 1984

Tabelle 1: Oxid- und Chloridgehalte der verwendeten Zemente

	Klinker (%)	HOZ 35 L NW/HS (%)
SiO_2	20,39	24,80
Al_2O_3	6,03	15,07
Fe_2O_3	3,46	1,62
CaO	65,29	49,15
MgO	2,11	1,67
SO_3	0,93	3,52
K_2O	1,64	0,90
Cl^- *	0,06	0,03
Glühverlust	0,20	1,70
Unlösliches	0,10	0,20

Nachträglich am PZ 35 F und HOZ 35 L NW/HS bestimmt.

Die rechnerischen Werte der Phasenzusammensetzung des Klinkers (nach Bogue) betrugen: C_3S = 61 %; C_2S = 13 %; C_3A = 10 % und C_4AF = 11 %.

zugabe erfolgte durch Lösen von NaCl und $CaCl_2 \cdot 2H_2O$ im Anmachwasser, wobei 2,5 % Chlorid, bezogen auf den Zement, eingewogen wurden. Die Verunreinigungen in beiden chloridhaltigen Salzen betrugen höchstens 0,5 %.

Die Leime wurden in eine spezielle Schalung (d = 4 mm, h = 100 mm) eingerüttelt. Danach wurde die Schalung gasdicht verschlossen und in einer Wendemaschine 24 h gedreht. Im Alter von 1 d wurden die Zementsteinstäbchen entschalt und daraufhin im Exsikkator bei 20°C zwei Monate über Wasser in Gegenwart von gasförmigem Stickstoff (Reinheit: 99,999 Vol.-%) hydratisiert.

Anschließend wurden aus den Zementsteinstäbchen mit Hilfe einer diamantbesetzten Säge unter Kühlung mit kaltem, gasförmigen Stickstoff ca. 1,5 mm dicke Tabletten herausgesägt. Die Masse der feuchten Zementsteintabletten lag im Mittel bei 38 mg (HOZ) bzw. 41 mg (PZ).

Die Tabletten wurden unterschiedlich gelagert:

Probekörper ohne Chloridzugabe (Reihe a)

Tabletten aus 2 Monate altem Zementstein wurden weitere 2 - 6 Monate bei 20°C im Exsikkator über Wasser in N_2-Gas gelagert.

Probekörper ohne Chloridzugabe (Reihe b)

Tabletten aus 2 Monate altem Zementstein wurden weitere 6 Monate bei 20°C im Exsikkator über Wasser in N_2-Gas gelagert, anschließend 2 d gefriergetrocknet (Wasserdampfdruck 0,76 µm Hg) und dann 7 d bei 20°C unter bidestilliertem Wasser aufbewahrt.

Probekörper ohne Chloridzugabe (Reihe c)

Tabletten aus 2 Monate altem Zementstein wurden weitere 6 Monate bei 20°C im Exsikkator über Wasser in N_2-Gas gelagert, anschließend 2 d gefriergetrocknet und dann 7 d bei 20°C in 8,24%iger NaCl- bzw. 10,36%iger $CaCl_2 \cdot 2H_2O$-Lösung (das entspricht einer 5%igen Chloridlösung) gelagert.

Bei dieser Lagerungsart wurden von den Tabletten unabhängig vom verwendeten Zement rd. 5 % Chlorid, bezogen auf die bei 105°C getrocknete Probe, aufgenommen.

Probekörper mit Chloridzugabe (Reihe d)

Tabletten aus 2 Monate altem Zementstein wurden weitere 6 Monate im Exsikkator bei 20°C über Wasser in N_2-Gas gelagert. Danach wurde ein Teil der Tabletten 2 d gefriergetrocknet und anschließend bei 20°C und 58 %, 90 % sowie 100 % r. F. wieder befeuchtet.

Meßmethoden

Die Zementsteintabletten wurden in Aluminiumtiegeln (V = 40 µl) gasdicht verschweißt. Mit der Thermoanalyseanlage (TA 2000 B, Fa. Mettler) wurden die Proben im Temperaturbereich von + 20°C bis - 60°C in verschiedenen Meßbereichen (50 - 500 µV) bei einer Kühlrate von 2 K/min untersucht. Das Meßverfahren ist in (5) genauer beschrieben worden.

Die durch Gefriertrocknung verdampfbare Menge Wasser (W_e) und die nach Lagerung gefriergetrockneter Proben im Klima 20/58 bis zum Gleichgewicht von der Probe aufgenommene Wassermenge W_{ng} in g/g Trockenmasse des Zementsteines (m_o) wurde gravimetrisch mit einer Mikrowaage (Meßbereich 10^{-6} g) ermittelt. Als Trockenmasse m_o wird die Summe aus Zementmasse (m_z) und der Masse des nicht verdampfbaren Wassers (m_n) bezeichnet.

Ergebnisse und Diskussion

Tabletten ohne und mit Chloridzugabe, die 2 Monate bei 20°C über Wasser in N_2-Gas gelagert worden waren (Reihen a und d), ergaben bei der mikrokalorimetrischen Untersuchung charakteristische Abkühlungskurven, siehe Bilder 1 und 2. Je nach Temperaturbereich wurden unterschiedliche Thermospannungen ΔU, die dem jeweiligen Temperaturunterschied zwischen Meßprobe und Referenzprobe proportional sind, registriert. Diese Temperaturunterschiede wurden durch gefrierendes Porenwasser in der Meßprobe verursacht. Es wurden drei Phasenübergänge beobachtet.

VOL. 14 1984

Ein plötzlich einsetzender Phasenübergang sehr hoher Intensität bei ca. - 20°C gefolgt von einem intensitätsschwachen Phasenübergang zwischen - 20°C und - 30°C und einem Phasenübergang mittlerer bis hoher Intensität im Temperaturbereich von - 40°C bis - 50°C.

Der Phasenübergang bei ca. - 20°C wird nach (4) durch das Gefrieren von ungestörtem, freiem Wasser (bulk water) verursacht, welches sich in Poren mit r_H größer 10 nm befindet. In (5) wurde gezeigt, daß der Phasenübergang mit Maximum bei ca. - 43°C dem Gefrieren des Wassers in den mittleren Gelporen ($3\ nm < r_H < 10\ nm$) zugeordnet werden kann. Der dritte, intensitätsschwächste Phasenübergang konnte bisher noch nicht eindeutig zugeordnet werden. Er trat bei calciumchloridhaltigem Zementstein nicht auf.

Während der Phasenübergang des Wassers in den mittleren Gelporen bei Tabletten der Reihe a ziemlich konstant bei T_o = - 43°C erfolgte, trat bei gleich altem und wie in Reihe a gelagertem Zementstein der Reihe d je nach verwendetem Salz meist eine Verschiebung des Kurvenmaximums nach tieferen Temperaturen auf. Die NaCl-Zugabe führte hierbei zu der größten Gefrierpunktserniedrigung.

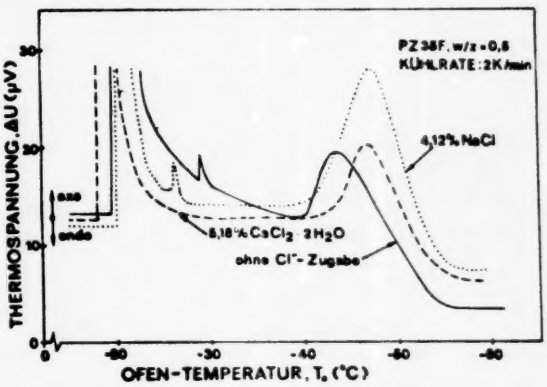

Bild 1: Phasenübergänge des Porenwassers in 4 Monate altem, wassergesättigtem Portlandzementstein

Im Vergleich zur jeweiligen Zementsteinprobe ohne Chloridzusatz führte der Natrium- und Calciumchloridzusatz zu Phasenübergängen des Wassers in den Gelporen von etwa gleicher Intensität. Lediglich beim Zementstein aus PZ 35 F mit NaCl-Zugabe wurde ein intensitätsstärkerer Phasenübergang registriert.

Im Vergleich zu Portlandzementstein fällt die bei Hochofenzementstein wesentlich größere Peakfläche des DSC-Signals bei T_o zwischen - 40 und - 50°C auf.

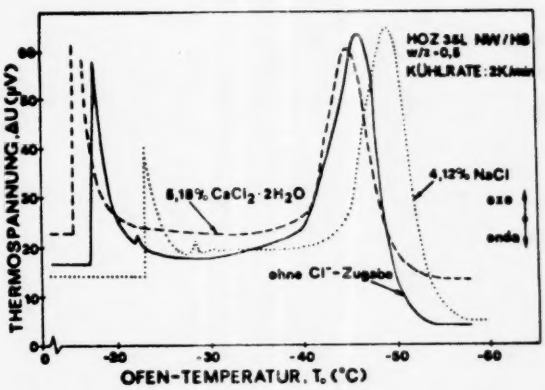

Bild 2: Phasenübergänge des Porenwassers in 4 Monate altem, wassergesättigtem Hochofenzementstein

Proben, die das Chlorid erst bei der Lagerung aufgenommen hatten (Reihe c), ergaben im Vergleich

zu den Proben der Reihe b stark veränderte Abkühlungskurven (vgl. Bilder 3 und 4). Der Phasenübergang des Gelwassers (Kurvenmaximum) wurde gegenüber demjenigen der Probe ohne Chloridzusatz auf T_o-Werte tiefer als - 50°C verschoben. Die Peakintensität, die der Umwandlungsenthalpie proportional ist, war je nach Salzart um ca. 90 - 95 % (PZ) bzw. um ca. 42 - 56 % (HOZ) geringer als diejenige von Probekörpern ohne Chloridzusatz etwa gleicher Masse. Umgekehrt lagen die Verhältnisse beim Phasenübergang des Wassers in den Kapillarporen. Die Peakintensität war je nach Salzart und bezogen auf die Probe ohne Chloridzusatz um ca. 100 - 170 % (PZ) bzw. um 155 - 250 % (HOZ) höher, wobei für NaCl enthaltende Probekörper die größten Zunahmen gemessen wurden.

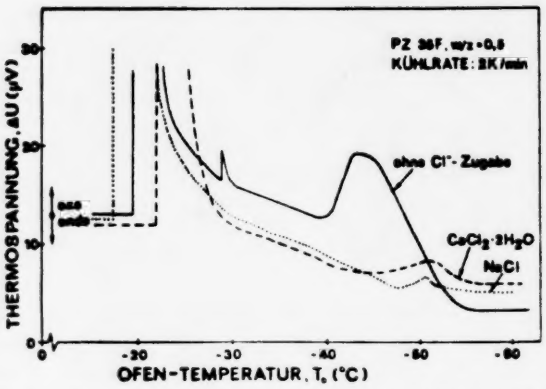

Bild 3: Phasenübergänge des Porenwassers in 8 Monate altem, wassergesättigtem Portlandzementstein

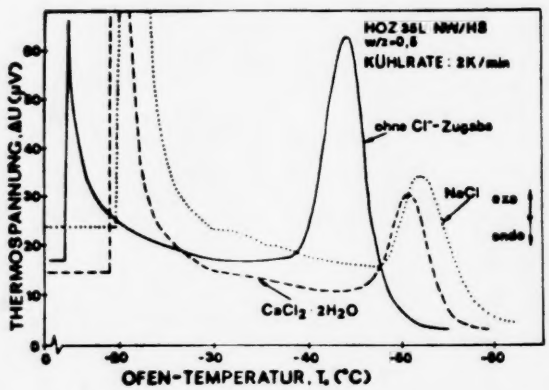

Bild 4: Phasenübergänge des Porenwassers in 8 Monate altem, wassergesättigtem Hochofenzementstein

Da die gemessenen Umwandlungsenthalpien dem Anteil gefrorenen Wassers in den verschiedenen Poren des Zementsteins proportional sind, wurden neben den mikrokalorimetrischen Messungen auch gravimetrische Messungen durchgeführt. Mit Hilfe der bekannten Schmelzenthalpie des freien Wassers mit 334 J/g sowie den mikrokalorimetrisch und gravimetrisch erhaltenen Meßdaten an unterschiedlich befeuchteten, gefriergetrockneten Zementsteinprobekörpern wurden nach (5), die bei unterschiedlichen Temperaturen gefrierenden Porenwasseranteile bzw. das nicht gefrierende Porenwasser rechnerisch ermittelt.
In feuchtem Zementstein können demnach folgende Wasseranteile unterschieden werden:

W_n: Gravimetrisch bestimmbare, chemisch gebundene Wassermenge in g/g geglühter Substanz.

W_e: Gravimetrisch bestimmbare, verdampfbare Wassermenge in g/g Trockenmasse (m_o). W_e hängt dabei von der angewandten Trockenmethode ab.

VOL. 14 1984

W_{ng}: Gravimetrisch bestimmbare, adsorbierte Wassermenge in Zementstein nach Lagerung desselben bei 20°C und bei rel. Feuchtigkeiten bis ca. 60 %.

W_{f1}: Mikrokalorimetrisch bestimmbare Eis- bzw. Wassermenge beim Phasenübergang zwischen ca. - 10 bis - 25°C (Temperatur T_o) (freies Wasser)

W_{f2}: Mikrokalorimetrisch bestimmbare Eis- bzw. Wassermenge beim Phasenübergang zwischen - 40°C und - 55°C (T_o) (Gelwasser)

Näherungsweise ergibt sich folgende Wasserbilanz:

$$W_e = W_{ng} + W_{f1} + W_{f2} \qquad (1)$$

Die Tabellen 1 und 2 enthalten die Werte für W_e, W_{f1} und W_{f2} der Tabletten aus Reihe c. Zum Vergleich enthalten beide Tabellen auch die entsprechenden Werte für die 7 Tage in bidestilliertem Wasser gelagerten Proben ohne Chloridzusatz (Reihe b).

Die Tabellen 1 und 2 bestätigen die Ergebnisse der mikrokalorimetrischen Messungen: Die Lagerung in den Chloridlösungen führt bei Zementstein aus beiden Zementen zu einem Gefrieren von mehr Porenwasser zwischen - 10 und - 25°C. In diesem Temperaturbereich erleidet freies Wasser einen Phasenübergang. Nach Lagerung in den Chloridlösungen weisen Proben aus Portlandzementstein rund 12 % mehr verdampfbares Wasser auf. Bei Proben aus Hochofenzementstein führt die Lagerung in den Chloridlösungen zu einer Zunahme von W_e um ca. 7 % (NaCl) bzw. ca. 1 % ($CaCl_2 \cdot 2H_2O$).

Die Menge des verdampfbaren Wassers (W_e) in wassergesättigtem Zementstein hängt von dessen Porosität ab. Trotz sorgfältiger Präparation waren einheitliche Porositätsverhältnisse in jedem Teilvolumen der Zementsteinstäbchen nicht erreichbar. Die herausgesägten Zementsteintabletten wiesen demzufolge schwankende W_e-Werte auf. Die an 18 Tabletten aus einem Zementsteinstäbchen (Reihe a) ermittelte Standardabweichung (s_{We}) des verdampfbaren Wassers betrug zum Beispiel 0,024 g/g (PZ) bzw. 0,019 g/g (HOZ). Bei einmaliger Abkühlung feuchter Tabletten derselben Serie auf - 60°C betrug die Standardabweichung s_{Wf1} (18 Tabletten) des freien Wassers 0,016 g/g (PZ) bzw. 0,011 g/g (HOZ).

Tabelle 1

Verdampfbares und gefrierbares Porenwasser in Portlandzementstein (Reihe c) nach Lagerung in Natrium- bzw. Calciumchloridlösung

	W_e (g/g)	W_{f1} (g/g)	W_{f2} (g/g)
PZ/H_2O	0,319	0,074	0,162
PZ/NaCl	0,357	0,113	0,160
PZ/$CaCl_2$	0,354	0,092	0,182

Tabelle 2

Verdampfbares und gefrierbares Porenwasser in Hochofenzementstein (Reihe c) nach Lagerung in Natrium- bzw. Calciumchloridlösung

	W_e (g/g)	W_{f1} (g/g)	W_{f2} (g/g)
HOZ/H_2O	0,385	0,035	0,271
HOZ/NaCl	0,413	0,089	0,235
HOZ/$CaCl_2$	0,389	0,061	0,248

Die unterschiedlichen W_e-Werte, ermittelt an Tabletten aus Reihe c (vgl. Tabellen 1 und 2), könnten somit im Extremfall durch Porositätsschwankungen in den Tabletten bedingt sein. Die daneben angegebenen Werte für W_{f1} und W_{f2} sind hauptsächlich von der Zementart sowie von der Zahl der Abkühlungszyklen und Gefriertrocknungsvorgänge abhängig. Die Streuungen für W_e, W_{f1} und W_{f2} in Tabletten der Reihe c wurden bisher noch nicht ermittelt.

Die Tabellen 1 und 2 zeigen, daß sich der Anteil freien Wassers (W_{f1}) in den Tabletten nach Lagerung in Chloridlösung deutlich erhöht. Der nach Gleichung (1) ermittelte Gelwasseranteil dürfte hingegen auch nach der Cl^--Lagerung annähernd konstant geblieben sein, obwohl die Intensität des Phasenübergangs zwischen - 40°C und - 50°C deutlich zurückgeht (vgl. Bilder 3 und 4).

Tabelle 3
Umwandlungswärme des Gelwassers in Portlandzementstein (Reihe c) nach Lagerung in Chloridlösung

	m_o (g)	W_{f2} (g/g)	ΔH_{Wf2} (J/g)
PZ/H_2O	0,02726	0,162	46
PZ/NaCl	0,03187	0,160	2
PZ/$CaCl_2$	0,03266	0,182	3

Tabelle 4
Umwandlungswärme des Gelwassers in Hochofenzementstein (Reihe c) nach Lagerung in Chloridlösung

	m_o (g)	W_{f2} (g/g)	ΔH_{Wf2} (J/g)
HOZ/H_2O	0,029378	0,271	91
HOZ/NaCl	0,029928	0,235	53
HOZ/$CaCl_2$	0,030469	0,248	40

Die mikrokalorimetrische Bestimmung der Umwandlungswärme ΔH_{Wf2} des Wassers in den Gelporen zeigt, daß ΔH_{Wf2} nach der Lagerung der Tabletten in Chloridlösung, stark abfällt (vgl. Tabellen 3 und 4). Im Gegensatz dazu weisen Zementsteintabletten der Reihe d, mit 2,5 % Chlorid, bezogen auf Zement, eine ähnliche Umwandlungswärme auf, wie die 7 Tage unter Wasser gelagerten Zementsteintabletten ohne Chloridzusatz (vgl. Tab. 5).

Als Grund für die z. T. drastisch reduzierte Umwandlungswärme des Wassers in den Gelporen des Zementsteins werden die durch Chloride des Natriums und Calciums geänderten Grenzflächenverhältnisse zwischen der inneren Zementsteinoberfläche und dem adsorbierten Wasserfilm angesehen. Durch Adsorption von Chlorid-, Natrium- und Calciumionen am getrockneten Zementstein entsteht wahrscheinlich eine noch stärker strukturierte, oberflächennahe Wasserschicht. In ihr dürften vormals von Wassermolekülen eingenommene Plätze teilweise von Na^+-, Ca^{++} und Cl^--Ionen besetzt worden sein, so daß die verdrängten Wassermoleküle nunmehr geringeren Oberflächenkräften ausgesetzt sind als vorher.

Tabelle 5
Verdampfbares und gefrierbares Porenwasser sowie Umwandlungswärme des Gelporenwassers in Portland- und Hochofenzementstein (Reihe d)

	W_e (g/g)	W_{f1} (g/g)	W_{f2} (g/g)	ΔH_{Wf2}
PZ (NaCl)	0,320	0,067	0,172	42
PZ ($CaCl_2$)	0,314	0,075	0,159	39
HOZ (NaCl)	0,365	0,035	0,250	89
HOZ ($CaCl_2$)	0,349	0,037	0,23	95

VOL. 14 1984

Dank
====

Herrn Prof. Dr. techn. R. Springenschmid und Herrn Prof. Dr.-Ing. habil. Dr. rer. nat. M. J. Setzer danke ich für die wertvollen Anregungen bei der Durchführung dieser Arbeit.
Mein Dank gilt ferner Frl. H. Schlee, Herrn R. Holzmann und Herrn H. Gottmann für die Probenpräparation und die durchgeführten Messungen.
Der Deutschen Forschungsgemeinschaft danke ich besonders für die finanzielle Unterstützung dieser Forschungsarbeit.

Literaturangaben
================

1. M. J. Setzer, DAfStb. Heft 280, S. 45 (1977)
2. C. Fontenay, E. J. Sellevold, Proceldings ASTM Spec. Tech. Pub. Series 691 (1981) 1. Intern. Conf. on Durability of Building Mat. and Components, Ottawa 1978
3. G. G. Litvan, Adv. Coll. Sc., 9, 253 (1978)
4. N. Stockhausen, H. W. Dorner, B. Zech und M. J. Setzer, CCR, 9, 783-794 (1979)
5. H. W. Dorner und M. J. Setzer, CCR, 10, 403-411 (1980)
6. G. G. Litvan, J. Am. Ceram. Soc. 58, 26 (1975)
7. U. G. Meier und A. B. Harnik, CCR, 8, 545-552 (1978)

CEMENT and CONCRETE RESEARCH. Vol. 14, pp. 816-818, 1984. Printed in the USA.
0008-8846/84 $3.00+00. Copyright (c) 1984 Pergamon Press, Ltd.

PREVENTION OF ALKALI-SILICA EXPANSION BY USING SLAG-PORTLAND CEMENT

S. Chatterji and N.F. Clausson-Kaas
Teknologisk Institut
2630 Taastrup Denmark

(Communicated by G.M. Idorn)
(Received Feb. 13, 1984)

ABSTRACT

A previously postulated hypothesis that concrete or mortar prisms devoid of free $Ca(OH)_2$ will not suffer from alkali-silica expansion has been tested. In this investigation high slag-Portland cements were used to make mortar prisms with a reactive sand. Storage of these prisms in a saturated NaCl bath at 50°C caused no expansion. At the end of the storage period in NaCl bath, the prisms were found to be free of $Ca(OH)_2$. The results are consistent with the proposed hypothesis.

VOL. 14 1984

In a recent paper one of the authors (SC) has suggested that the presence of free $Ca(OH)_2$ is a pre-requisite for the development of expansive alkali-silica reaction; it has also been suggested that the removal of free $Ca(OH)_2$ from a mortar or concrete specimen will stop alkali-silica reaction expansion even in the presence of excess alkali salts (1). In this paper the results of work done to test this hypothesis are reported.

One of the ways to produce mortar or concrete specimens free of $Ca(OH)_2$ is to use slag-Portland cement. It is known that powdered granulated blast furnace slag consumes $Ca(OH)_2$ during its hydration (2). By adjusting the proportions of granulated slag and Portland cement it is possible to produce a slag-Portland cement which will be free or nearly free of $Ca(OH)_2$ after 28 days hydration. Mortar prisms made with such a slag-Portland cement and a reactive sand will aslo be free of $Ca(OH)_2$ from 28 days onwards. These prisms may then be used to test the proposed hypothesis. This is what has been done in this investigation.

Materials and Experimental Techniques

Two slag-Portland cements of German origin and an ordinary Portland cement of Danish origin were used in this investigation. Each of the slag-Portland cements contains about 65% granulated

blast furnace slag. 0/4 mm sand from one of the most reactive sand sources in Denmark was used to make 1:3::cement:sand mortar with each of the above cement types. The water/cement ratio of the mortar mixes was 0.5. Several 40x40x160 mm prisms were cast from each of the mortars. The rpisms were cured in a humid atmosphere for first 24 hours and thereafter under water for 27 days. The expansivity of the mortar prisms were then tested using the warm saturated NaCl bath technique (3). Expansion measurements were carried out for 8 weeks. At the end of the expansion measurement period, one prism from each of the mortar types was used to detect the presence of free $Ca(OH)_2$ by X-ray diffraction technique.

TABLE I.

Mean expansion of Mortar Bars made with different Cements.

No. of weeks / Cement Type	% Expansion							
	1	2	3	4	5	6	7	8
Ordinary Portland	0.038	0.253	0.471	0.622	0.632	0.640	0.647	0.644
H.O.Z.-35 LNW-HS 80/2430	0.005	-0.017	-0.019	-0.019	-0.029	-0.032	-0.032	-0.039
H.O.Z.-35 GEWB 80/2431	0.015	-0.007	-0.015	-0.015	-0.022	-0.024	-0.024	-0.024

Results and Discussion

Prior to the selection of the two slag-Portland cements, a preliminary screening was carried out on a number of slag-Portland cements. In this preliminary test 28 days old paste specimens from each of the slag-Portland cements were examined by X-ray diffraction technique to determine their $Ca(OH)_2$ contents. The two slag-Portland cements which liberated only traces of $Ca(OH)_2$ were chosen for this investigation.

The results of the expansion measurements are shown in Table 1. Table 1 shows that the prisms made with the ordinary Portland cement expanded from the second week onwards, whereas those made with the slag-Portland cements showed slight contractions.

The X-ray diffraction examination of the mortar prisms showed that the prisms made with the ordinary Portland cement had abundant amounts of $Ca(OH)_2$ crystals in them, whereas those made with the slag-Portland cements had none. The X-ray diffraction results also showed that in all three samples significant amounts of monochloroaluminate hydrate have formed. In view of the fact that the prisms were stored in a saturated NaCl bath at 50°C for 8 weeks it is not very surprising that significant amounts of monochloroaluminate hydrate have formed in these samples. It will thus appear that the lack of expansion in the cases of slag-Portland cement mortars could not be attributed to a lack of penetration of

NaCl in them. Neither the absence of expansion could be attributed to a lack of OH-ions. All three sets of prisms were stored in the same bath along with other prisms made with Portland cement. A typical pH of this type of baths is 13 or higher. Furthermore, the formation of monochloroaluminate hydrate is itself a OH-ion liberating process.

The results of this investigation are thus consistant with the hypothesis which states that expansion due to alkali-silica reaction can be controlled by removing free $Ca(OH)_2$ from the specimen. If other workers can confirm this relationship between the absences of free $Ca(OH)_2$ and alkali-silica expansion, then it opens a rational way of avoiding the expansion. Further tests of the above hypothesis are in progress and the results will be reported at a later date.

We are aware of the previous claims of the reduction of alkali-silica expansion by using slag cement. There are some difference between the present and previous investigations. In all previous investigations the alkali contents were limited to those of the cements, in the present investigation, however, the alkali contents were effectively unlimited. In other words, the improvement in performance could not be attributed to a higher alkali-binding capacity of slag-Portland cements than ordinary Portland cements, any absorption will be compensated by a migration from the bath (see the X-ray diffraction results). Moreover none of the previous workers has drawn any relationship between the presence of calcium hydroxide and alkali-silica expansion.

VOL. 14 1984

Acknowledgements

The authors would like to thank Prof. F. Locher and Dr. Smolczyk for the slag-Portland cement samples. This work was partly supported by a grant from the Danish Council for Technical Research (S.T.V.F.). The authors are grateful for this grant.

References

1. S. Chatterji - Cement & Con. Res. 9, 185, 1979.
2. R.W. Nurse - in The Chemistry of Cements. Ed. Taylor. Academic Press. London 1964, pp. 51-52.
3. S. Chatterji - Cement & Con. Res. 8, 647, 1978.

CEMENT and CONCRETE RESEARCH. Vol. 14, pp. 819-832, 1984. Printed in the USA.
0008-8846/84 $3.00+00. Copyright (c) 1984 Pergamon Press, Ltd.

GENERALIZED AGE-ADJUSTED EFFECTIVE MODULUS METHOD FOR CREEP IN COMPOSITE BEAM STRUCTURES. PART I - THEORY

Jakov D. Lazić[1] and Vera B. Lazić[2]
Faculty of Civil Engineering and
Faculty of Transport and Traffic Engineering, respectively
University of Belgrade, Belgrade, Yugoslavia

(Refereed)
(Received Feb. 17, 1984)

ABSTRACT

The age-adjusted effective modulus method for approximate analysis of structures exhibiting linear aging creep law and underlying Bažant's theorem is generalized to a form which is more accurate for composite beam structures in flexure. A rigorous derivation of a linear algebraic relationship between the internal force histories and the deformation histories of the beam is given using the integral operator symbolics.

Introduction

The age-adjusted effective modulus method, developed in 1971 [1], has been recognized during the last few years to represent the most efficient and accurate method of approximate analyis of creep and shrinkage effects in concrete structures under the assumption of a linear creep law. As shown by Bažant [1], this method is based on the property that if the strain history represents a linear combination of the compliance function (or the creep coefficient), then the stress history represents a linear combination of the relaxation function. The practical usefulness of this property (Bažant's theorem) is due to the fact that in many situations the time variations of stresses and strains may be rather closely approximated by such linear combinations.

In the analysis of composite cross sections, however, one may encounter some situations in which the accuracy of this method is not very high since the time histories of stresses and strains are not very close to the aforementioned linear combinations. Nevertheless, since the formulation of the creep problem for a composite beam in flexure remains linear, a similar linearity property may be expected to hold in a generalized sense for the matrix of all internal forces in the cross section and the associated deformation variables (the curvature and axial extension).

---

[1]Professor, Dr.sc.techn.; Effective Member of RILEM.
[2]Associate Professor, Dr.sc.techn.

Development of such a generalization of the age-adjusted effective modulus method for the flexure of composite beam structures is the objective of the present paper.

The mathematical formulation can be effectively carried out only with the help of integral operators. For reader's convenience, a brief review of this topic is included in the Appendix. A detailed exposition cannot be, however, included because of space limitations, and reference should be made to appropriate mathematical texts.

Integral Operator Formulation

Basic Equations

The equations governing the stresses in composite and prestressed beam structures with uncracked cross sections consist of (1) the stress-strain relations for concrete and for steel; (2) Bernoulli's assumption of plain cross sections which represents at the same time the compatibility conditions of the composite cross section; and (3) the equilibrium equations of the cross section.

As explained in the Appendix (Eq. A.11), the integral type stress-strain relation for concrete (c) may be symbolically written in the form:

$$\sigma_c = E_{co}\tilde{R}'(\varepsilon - \varepsilon_s), \qquad (\tau = t_o) \tag{1}$$

in which $\sigma = \sigma(t,t_o)$ is the stress, $\varepsilon = \varepsilon(t,t_o)$ is the strain, $\varepsilon_s = \varepsilon_s(t,t_o)$ is the shrinkage strain, $E_{co} = E_c(t_o)$ represents the instantaneous elastic modulus, t or τ is the time in days from casting of concrete, t_o is the time at first load application in days, and $\tilde{R}'$ is the linear integral operator (see Appendix). In what follows, the shrinkage is omitted because it can be treated separately.

The relaxation of prestressing steel (p) is also taken into account. As a sufficiently accurate approximation, it may be supposed that the nondimensional relaxation function, $R_p^* = R_p^*(t,\tau)$, in interval (τ,t) depends linearly on the nondimensional concrete relaxation function, $R^* = R^*(t,\tau)$ [3]:

$$R_p^* = \rho' 1^* + \rho R^*, \quad \rho = \frac{\zeta_p}{1 - R^*}, \quad \rho' = 1 - \rho, \quad (\tau = t_o) \tag{2}$$

in which ρ = constant for a given pair (t_o,t) and for the initial stress σ_{po} in prestressing steel, ζ_p is the prestessing steel relaxation corresponding to the time interval (t_o,t) and to the initial stress σ_{po}. The stress-strain relation for prestressing steel may be also written in the operator formulation:

$$\sigma_p = E_p\tilde{R}'_p\,\varepsilon, \qquad (\tau = t_o) \tag{3}$$

in which E is the elastic modulus, and $\tilde{R}'_p$ is the linear integral operator (see Appendix). In the special case of $\rho = 0$ $(\zeta_p = 0)$, Eq. (3) characterizes an elastic material.

Steel parts (n) and reinforcing steel (m) follow Hooke's law:

$$\sigma_k = E_k\,\varepsilon, \qquad (k = n,m). \tag{4}$$

VOL. 14 1984

The special case when a composite cross section does not contain any steel part represents a homogeneous cross section.

Bernoulli's assumption of plain cross sections provides:

$$\varepsilon = \eta + \kappa y \tag{5}$$

in which $\eta = \eta(x,t,t_o)$ is the normal strain and $\kappa = \kappa(x,t,t_o)$ is the change in the curvature of the beam axis.

When strain ε at a general point and stresses σ_k $(k = n,m,p,c)$ are eliminated from the equilibrium equations and from Eqs. (1), (3) and (4), the basic equations which apply to an arbitrary composite cross section are obtained [4]:

$$E_u A_i \tilde{R}'_{11}\,\eta + E_u S_i \tilde{R}'_{12}\,\kappa = N,$$

$$E_u S_i \tilde{R}'_{21}\,\eta + E_u J_i \tilde{R}'_{22}\,\kappa = M, \qquad (\tau = t_o) \tag{6}$$

in which A_i, S_i, and J_i are the cross section geometrical properties (Ref. 4 Appendix 2)[3], E_u is the elastic modulus arbitrary chosen, and $\tilde{R}'_{hl}$ $(h,l = 1,2)$ are the linear integral operators (see Appendix); $N = N(x,t,t_o)$ is the axial force, and $M = M(x,t,t_o)$ is the bending moment. These equations represent a system of two inhomogeneous integral equations.

Basic Functions

The individual forms $\tilde{R}'_h$ $(h = 1,2)$ of the operator matrix of system (6) may be written as:

$$\tilde{R}'_h = \gamma'_h \tilde{1}' + \gamma_h \tilde{R}' , \qquad \gamma'_h = 1 - \gamma_h, \qquad (h = 1,2) \tag{7}$$

where γ_h = coefficients (see Appendix). Their inverse operators, denoted as $\tilde{F}'_h$ $(h = 1,2)$, satisfy the relation:

$$\tilde{R}'_h \tilde{F}'_h = \tilde{1}' , \qquad (h = 1,2). \tag{8}$$

The solution of basic equations (6) may be expressed through inverse operators $\tilde{F}'_h$:

$$\eta = \frac{1}{E_u \Delta\gamma}\left[(\delta\gamma_2 \tilde{F}'_1 + \delta\gamma_1 \tilde{F}'_2)\,\frac{N}{A_i} + \gamma_{12}\,\frac{S_i}{A_i}\,(\tilde{F}'_1 - \tilde{F}'_2)\,\frac{M}{J_i}\right],$$

$$\kappa = \frac{1}{E_u \Delta\gamma}\left[\gamma_{21}\,\frac{S_i}{J_i}\,(\tilde{F}'_1 - \tilde{F}'_2)\,\frac{N}{A_i} + (\delta\gamma_1 \tilde{F}'_1 + \delta\gamma_2 \tilde{F}'_2)\,\frac{M}{J_i}\right] \tag{9}$$

where $\tau = t_o$.

Further it is convenient to introduce operators:

$$\tilde{B}'_h = \tilde{R}' \tilde{F}'_h , \qquad \tilde{K}'_h = \tilde{R}'_h \tilde{F}' , \qquad (h = 1,2) \tag{10}$$

which are inverse to each other, i.e.

$$\tilde{B}'_h \tilde{K}'_h = \tilde{1}' , \qquad (h = 1,2). \tag{11}$$

[3] see also Notations

It is also necessary to introduce the following functions:

$$R_h^* = R_h^*(\gamma_h,t,\tau) = \tilde{R}_h' 1^* = \gamma_h' 1^* + \gamma_h R^* \ , \tag{12}$$

and $F_h^*(\gamma_h,t,\tau)$, $K_h^*(\gamma_h,t,\tau)$, $B_h^*(\gamma_h,t,\tau)$, (for $\tau \geqslant t_o$ and $h = 1,2$). They are the integrals of the functions R_h', F_h', K_h' and B_h', respectively, Eq. (A.3). It may be shown that the functions K_h^* linearly depend on the concrete compliance function F^*:

$$K_h^* = \gamma_h 1^* + \gamma_h' F^* = \left[\frac{\gamma_h'}{e(\tau)} + \gamma_h \right] 1^* + \frac{\gamma_h'}{e(\tau)} \varphi(t,\tau) \tag{13}$$

where $\tau \geqslant t_o$ $(h = 1,2)$, and that functions B_h^* linearly depend on functions F_h^*:

$$B_h^* = \frac{1}{\gamma_h} (1^* - \gamma_h' F_h^*) \ , \qquad (\tau \geqslant t_o, \quad h = 1,2). \tag{14}$$

Developing the operator relation (A.14) and using Eqs. (A.5), (A.2) and (A.8), we arrive at the inhomogeneous integral equation:

$$F^*(t,t)\ R^*(t,\tau) - \int_\tau^t \frac{\partial F^*(t,\theta)}{\partial \theta} R^*(\theta,\tau)\ d\theta = 1, \quad (\tau \geqslant t_o). \tag{15}$$

Similarly, developing the operator relations (A.15), we arrive at two independent inhomogeneous integral equations:

$$K_h^*(\gamma_h,t,t)\ B_h^*(\gamma_h,t,\tau) - \int_\tau^t \frac{\partial K_h^*(\gamma_h,t,\theta)}{\partial \theta} B_h^*(\gamma_h,\theta,\tau)\ d\theta = 1 \tag{16}$$

where $\tau \geqslant t_o$, $h = 1,2$.

Keeping in mind relations (13), we may notice that functions B_h^*, as well as the concrete relaxation function R^*, are determined from the concrete compliance function F^*, as solutions of inhomogeneous integral equations. Functions B_h^* are called the basic functions.

For any particular compliance function, two functions R_h^* (i.e. F_h^*), or K_h^* (i.e., the basic functions B_h^*, $h = 1,2$), correspond to any given composite cross section. They are different for different cross sections because, through coefficients γ_h, they depend on the material properties of all the types of steel in the cross section, on the concrete elastic modulus at $t = t_o$, and on the cross section geometrical properties (see Appendix 2 in Ref. 4 and Notations).

Note that by introducing $\gamma_h' = 1$ we arrive at the special case (Eq. A.17) in which the integral equations (16) reduce to the well known relation between functions F^* and R^* for concrete, given by Eq. 15.

Determination of the Stresses

Theorem I. If in a composite cross section the axial force and the bending moment depend linearly on functions R_1^* and R_2^*,

VOL. 14 1984

i.e.

$$N = N_1 R_1^* + N_2 R_2^* + N_3 1^* ,$$
$$M = M_1 R_1^* + M_2 R_2^* + M_3 1^* , \tag{17}$$

$N_1,\ldots,M_3$ being arbitrary constants, then functions η and κ, determining the deformation of the composite cross section, depend linearly on functions F_1^* and F_2^*, i.e.

$$\eta = \eta_1 F_1^* + \eta_2 F_2^* + \eta_3 1^* ,$$
$$\kappa = \kappa_1 F_1^* + \kappa_2 F_2^* + \kappa_3 1^* \tag{18}$$

in which the corresponding operators $\tilde{R}_h'$ and $\tilde{F}_h'$ $(h = 1,2)$ are inverse, and $\eta_1,\ldots,\kappa_3$ are time-independent.

This theorem represents a generalization of Bažant's theorem [1,8]. The proof of this theorem is given in Ref. 4, Appendix 3.

Function R_h^* and F_h^* $(h = 1,2)$ are related to the composite cross section. The special case when $\gamma_1 = \gamma_2 = 1$, they reduce to concrete relaxation function R^* and concrete compliance function F^*, respectively (Eq. A.16). This applies to the case of a homogeneous cross section. Under these conditions, the special case of Theorem I, equivalent to Bažant's theorem, reads: If the axial force and the bending moment in the homogeneous cross section depend linearly on the concrete relaxation function, i.e.

$$N = N_1^o R^* + N_2^o 1^* , \qquad M = M_1^o R^* + M_2^o 1^* , \tag{19}$$

$N_1^o,\ldots,M_2^o$ being arbitrary constants, then functions η and κ depend linearly on the concrete compliance function, i.e.

$$\eta = \frac{1}{E_{co}} \left(\frac{N_1^o}{A_c} 1^* + \frac{N_2^o}{A_c} F^* \right), \quad \kappa = \frac{1}{E_{co}} \left(\frac{M_1^o}{J_c} 1^* + \frac{M_2^o}{J_c} F^* \right) \tag{20}$$

in which the corresponding operators $\tilde{R}'$ and $\tilde{F}'$ are inverse (for a homogeneous cross section, A_c is its area and J_c is its centroidal moment of inertia).

Theorem II. If in a composite cross section the axial force and the bending moment depend linearly on the concrete relaxation function, R^*, i.e.

$$N = N_4 R^* + N_5 1^* , \qquad M = M_4 R^* + M_5 1^* , \tag{21}$$

$N_4,\ldots,M_5$ being arbitrary constants, then the stresses in part k $(k = n,m,p,c)$ of the cross section depend linearly on the concrete relaxation function, R^*, and the basic functions, B_h^*, i.e.

$$\sigma_k = \nu_k \left(U_k 1^* + V_k R^* + \sum_{h=1}^{2} W_{hk} B_h^* \right) \tag{22}$$

in which U_k, V_k and W_{hk} $(h = 1,2)$ are time-independent (Ref. 4, paragraph 3).

Using Eqs. (12), the law in Eq. 21 may be represented as a linear combination of the functions R_1^* and R_2^* (Eq. 17), and using Eqs. (14), the law of stress variations (Eq. 22) represents a linear combination of the functions R^* and F_h^* ($h = 1,2$). In such a form, this theorem is easier to understand because the corresponding operators $\tilde{R}_h'$ and $\tilde{F}_h'$ are inverse. The form in which Theorem II is given is, however, more suitable, since the functions R^* and B_h^* are determined directly from the concrete compliance function, F^*, as the solution of an inhomogeneous integral equation (Eq. 16).

In the special case when $\gamma_1 = \gamma_2 = 1$, Theorem II refers to the homogeneous cross section: Under the conditions (21) the stress depends linearly on the concrete relaxation function, R^*. This follows from Eqs. (14). In view of Theorems I and II referring to the homogeneous cross section, and of expression (5), we may conclude: If the strain, ε, at a general point of a homogeneous cross section depends linearly on the concrete compliance function, F^*, i.e.

$$\varepsilon = \varepsilon_1^o F^* + \varepsilon_2^o 1^* \tag{23}$$

in which ε_1^o and ε_2^o are constants, then the stresses vary linearly with the concrete relaxation function, R^*, i.e.

$$\sigma_c = E_{co}(\varepsilon_1^o 1^* + \varepsilon_2^o R^*). \tag{24}$$

This statement represents Bažant's theorem formulated for aging linear creep law for concrete in Ref. 1.

Albegraic Relations Between Deformations and Internal Forces

We may start from the equations which determine the stresses in composite and prestressed beam structures with uncracked cross sections. The following algebraic stress-strain relation for concrete may be adopted:

$$\sigma_c = E_{co}\,\zeta_c'(\varepsilon - \varepsilon_s) - \rho_c\sigma_{co}\,, \quad \sigma_{co} = \sigma_c(t_o,t_o). \tag{25}$$

In similarity to the original age-adjusted effective modulus method [1] (AAEM method) it is convenient to introduce:

$$\zeta_c' = \frac{1}{1+\chi_F\varphi}\,, \quad \rho_c = \frac{\chi_F'\varphi}{1+\chi_F\varphi}\,, \quad \chi_F' = 1-\chi_F\,, \quad \zeta_c = 1-\zeta_c' \tag{26}$$

where χ_F is a certain parameter. Later on it will be shown which factors influence the selection of χ_F-values. The special case when this parameter becomes identical to the aging coefficient χ [1] Eq. (25) represents the well known AAEM method. When $\chi_F = 1$ the same equation represents the well known effective modulus method (EM method).

The stress-strain relation for prestressing steel is algebraic to begin with, and may be written as:

$$\sigma_p = E_p\zeta_p'\varepsilon, \qquad \zeta_p' = 1-\zeta_p\,. \tag{27}$$

For a given prestressing steel relaxation ζ_p, this relationship implies the largest possible creep deformation. Thereby the effects of prestressing steel relaxation are overestimated.

VOL. 14 1984

The basic equations in the algebraic formulation are:

$$E_u A_{i\zeta}\,\eta + E_u S_{i\zeta}\,\kappa = N + \rho_c\,(N_o\,\frac{A_{cr}}{A_i} + M_o\,\frac{S_{cr}}{J_i})\ ,$$
$$E_u S_{i\zeta}\,\eta + E_u J_{i\zeta}\,\kappa = M + \rho_c\,[\,y_c(N_o\,\frac{A_{cr}}{A_i} + M_o\,\frac{S_{cr}}{J_i}) + M_o\,\frac{I_{cr}}{J_i}\,]\ . \qquad (28)$$

These equations and the used notations are given in Ref. 4, paragraph 2.2 (see also Notations).

The algebraic expressions for stresses are obtained by incorporating the solutions of these basic equations into (5), (25), (27), and (4). Parameter χ_F appears by means of ρ_c and of the cross section geometrical properties $A_{i\zeta}$, $S_{i\zeta}$, and $J_{i\zeta}$ in expressions σ_k $(k = n,m,p,c)$.

The solutions of the basic equations for special case of homogeneous cross section (Ref. 4. paragraph 3) are:

$$E_{co}\,\eta = \frac{1}{\zeta'_c}\,(\frac{N}{A_c} + \rho_c\,\frac{N_o}{A_c}),\quad E_{co}\,\kappa = \frac{1}{\zeta'_c}\,(\frac{M}{J_c} + \rho_c\,\frac{M_o}{J_c})\ . \qquad (29)$$

Corrected Aging Coefficients

In algebraic expressions (29), parameter χ_F appears through coefficients ζ'_c and ρ_c. When its value is determined from the condition that, for N and M according to law (19), the value of η (i.e. κ) should be the same as that ensuing from the accurate expressions (20), we obtain (Ref. 4, paragraph 3):

$$\chi_F = \chi = \frac{1}{1-R^*} - \frac{1}{\varphi}\ . \qquad (30)$$

This is the well known aging coefficient of the AAEM method [1].

From Eqs. (A.15), (13) for $\tau = t_o$, and (A.5), we obtain:

$$\tilde{B}'_h K^*_h = 1^*\ ,\quad \text{i.e.}\quad \tilde{B}'_h(1^* + \gamma'_h\varphi) = 1^*,\quad (h = 1,2)\ , \qquad (31)$$

and from Eqs. (A.14) and (A.6) for $\tau = t_o$ we obtain:

$$\tilde{R}'F^* = 1^*,\quad \text{i.e.}\quad \tilde{R}'(1^* + \varphi) = 1^*. \qquad (32)$$

On the basis of Eq. (30) and of the analogy of expressions (31) with (32), we may define the coefficients:

$$\chi_{\gamma h} = \frac{1}{1-B^*_h} - \frac{1}{\gamma'_h\varphi}\ ,\quad (h = 1,2). \qquad (33)$$

Through a formal introduction of $\gamma'_h = 1$, i.e. $B^*_h \equiv R^*$ (Eq. A.17), these expressions reduce to Eq. (30). The classical aging coefficient χ which refers to concrete [1] is a special case of coefficients $\chi_{\gamma h}$ referring to the composite cross section.

For any special creep function and any given pair (t_o,t) two coefficients $\chi_{\gamma h}$ correspond to each given composite cross section. They depend on the material properties of all materials interacting within the composite cross section, and on the cross section geometrical properties. They may be called the corrected aging coefficients.

To achieve an insight into the influence of γ_h on these coefficients, Figure 1 shows a comparison of the $\chi_{\gamma h}$ values for $\gamma_h' = 0.1$, 0.5, and 1. These coefficients correspond to the ACI creep prediction model for structural concrete [5] and to the CEB-FIP creep prediction model [6]. Solid lines indicate the CEB-FIP creep model, dry environment $\varphi_{fl} = 3.0$, $h_o = 20$ cm , $t_o = 7$ days. Dashed lines indicate the ACI creep model, $t_o = 7$ days, $\phi(\infty,7) = 4.152$. (The last value is obtained from the condition that for $t_o = 7$ days, and $t - t_o = 10^4$ days the ACI and CEB-FIP compliance functions have the same value).

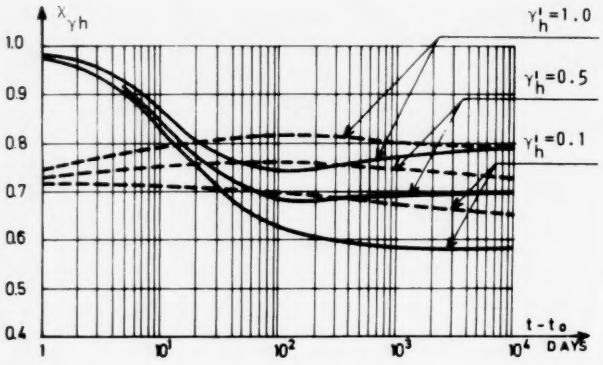

FIG. 1
Corrected Aging Coefficients $\chi_{\gamma h}$

For a given pair (t_o,t), lower values $\chi_{\gamma h}$ correspond to lower values of γ_h'. For $\gamma_h' = 1$, their highest values are obtained, which are, in fact, the aging coefficients χ.

Numerical evaluations show that the compliance function recommended by ACI [5] leads to considerably smaller differences between the values $\chi_{\gamma h}$ for $\gamma_h' = 0.1$ and $\gamma_h' = 1$ than does the function recommended by CEB-FIP [6]. This conclusion agree with the fact that the original AAEM method was found to agree quite well, for ACI compliance function, with the exact solutions of composite cross sections [9].

Summary and Conclusions

The presented integral operator formulation of the problem of bending of composite and prestressed beam structures leads to functions, relations and laws corresponding to the composite cross section. Functions R_h^* (i.e. F_h^*), or K_h^* (i.e. B_h^*) $(h = 1,2)$ describe the properties of the composite cross section. For a given concrete compliance function, F^*, they depend, through the coefficients γ_h, on the material properties of all types of steel contained in the cross section, on the concrete elastic modulus at $t = t_o$, and on the cross section geometrical properties. For certain special values of coefficients γ_h, the functions R_h^*, F_h^* (i.e. B_h^*, K_h^*) reduce to the concrete relaxation function, R^*, and the concrete compliance function, F^*.

The integral relations between functions B_h^* and K_h^* for the composite cross section are established. As a special case, they

reduce to the well known relation between R^* and F^* for concrete. For a given time variation of the axial force and the bending moment, Theorems I and II establishe the time variation of the deformation and the stresses in the composite cross section. As a special case, they reduce to the well known Bažant's theorem [1].

In analogy to the aging coefficient χ of the AAEM method for concrete, corrected aging coefficients $\chi_{\gamma h}$ ($h = 1, 2$) for a composite cross section are defined. For any given compliance function, they depend on coefficients γ_h characterizing the given composite cross section. As a special case, the corrected aging coefficients $\chi_{\gamma h}$ reduce to the well known aging coefficient χ which depends solely on the material properties of concrete.

Appendix - Linear Integral Operators for Aging Creep

The linear integral operator $\tilde{G}$, is associated to a function of two arguments, $G = G(t,\tau)$, which satisfies the condition $G(t,\tau) \equiv \equiv 0$ for $t < \tau$. Operator $\tilde{G}$ is defined for any function $U = U(t,\tau)$, $\tau \geqslant t_o$, by the following expression:

$$I = I(t,\tau) = \int_{\tau}^{t} G(t,\theta)U(\theta,\tau)d\theta = \tilde{G}U \ . \tag{A.1}$$

In functions I and U, the second argument is a parameter if $\tau = t_o$.

For linear integral operators, the laws of algebra of ordinary numbers are valid, except for the commutative law which in the general case does not hold. However, all the operators defined in the present problem have the commutative property.

The following notations are introduced:

$$G' = G'(t,\tau) = \frac{\partial G(t,\tau)}{\partial \tau} \ , \quad 1' = 1'(t,\tau) = \delta(\tau - t),$$

$$1^* = 1^*(t,\tau) = H(t-\tau) = \begin{cases} 1 \text{ for } t > \tau \\ 0 \text{ for } t \leqslant \tau \end{cases} \quad (\tau \geqslant t_o)$$

where $\delta(\tau - t) = \delta(t - \tau)$ is the Dirac function [7] and $H(t-\tau)$ is the Heaviside function.

The operator $1'$ associated to the Dirac function $1'$ is the unity operator. The following is valid for it:

$$\tilde{1}'U = \int_{\tau}^{t} \delta(\theta - t)U(\theta,\tau)\, d\theta = U(t,\tau) = U \ . \tag{A.2}$$

If G' is substituted for G ($G \neq 1'$) and 1^* for U in Eq. (A.1) we get:

$$G^* = G^*(t,\tau) = \tilde{G}'1^* = \int_{\tau}^{t} \frac{\partial G(t,\theta)}{\partial \theta} H(\theta - \tau)\, d\theta =$$

$$= G(t,t) - G(t,\tau), \quad G' \neq 1', \quad (\tau \geqslant t_o). \tag{A.3}$$

The function G* is called the integral of the function G'. In particular, the integral of the Dirac function 1' is the Heaviside function:

$$\tilde{1}'1^* = \int_{\tau}^{t} \delta(\theta - t)H(\theta - \tau)\, d\theta = H(t - \tau) = 1^* \ . \qquad (A.4)$$

The nondimensional concrete compliance function is:

$$F^* = F^*(t, \tau) = \frac{1}{e(t)}\, 1^* + f^*(t, \tau) \ , \quad (\tau \geq t_o)$$

where

$$\frac{1}{e} = \frac{1}{e(t)} = F^*(t, t) = \frac{E_{co}}{E_c(t)} \ ; \quad e(t_o) = 1 \ ; \quad f^*(\tau, \tau) = 0 \ , \qquad (A.5)$$

for $\tau \geq t_o$. This function may be also represented in the following way:

$$F^* = F^*(t, \tau) = \frac{1}{e(\tau)}\, [1 + \varphi(t, \tau)] \ , \qquad (\tau \geq t_o) \qquad (A.6)$$

where $\varphi(t, \tau)$ is the creep coefficient:

$$\varphi = \varphi(t, \tau) = \frac{e(\tau)}{e(t)} - 1 + e(\tau) f^*(t, \tau) \ , \ (\tau \geq t_o).$$

The uniaxial creep law may be expressed in the following form:

$$\varepsilon(t,t_o) - \varepsilon_S(t,t_o) = \frac{1}{E_{co}} \int_{t_o}^{t} F^*(t,\theta)\, d\sigma_c(\theta,t_o) \ .$$

Applying integration by parts, and introducing (A.5), we get:

$$\varepsilon(t,t_o) - \varepsilon_S(t,t_o) = \frac{1}{E_{co}} \Big[\frac{1}{e(t)}\, \sigma_c(t,t_o) + \int_{t_o}^{t} \frac{\partial f(t,\theta)}{\partial \theta}\, \sigma_c(\theta,t_o)\, d\theta \Big] \ , \qquad (A.7)$$

where $\sigma_c(t_o,t_o) = 0$ and

$$f' = f'(t, \theta) = -\frac{\partial F^*(t,\theta)}{\partial \theta}, \qquad (t \geq \theta > t_o) \ . \qquad (A.8)$$

When $U \equiv \sigma_c$ and $G \equiv F'$, the expression

$$F' = \frac{1}{e}\, 1' + f' \ , \qquad (A.9)$$

may be introduced in Eq. (A.1) and when expression (A.2) is used, the operator formulation of integral equation (A.7) becomes:

$$\varepsilon - \varepsilon_S = \frac{1}{E_{co}}\, \tilde{F}'\sigma_c \ , \qquad (\tau \geq t_o). \qquad (A.10)$$

The integral of function F' is the nondimensional concrete compliance function, F*;

VOL. 14 1984

$$\tilde{F}'1^* = (\frac{1}{e}\,\tilde{1}' + \tilde{f}')1^* = F^*(t,\tau) = F^* \ , \qquad (\tau \geq t_o) .$$

This relation is obtained by using Eqs. (A.5), (A.4), (A.8), and (A.3).

Applying a similar procedure to the form of the creep law based on the ralaxation function,

$$\sigma_c(t,t_o) = E_{co} \int_{t_o}^{t} R^*(t,\theta)\, d[\varepsilon(\theta,t_o) - \varepsilon_s(\theta,t_o)] \ ,$$

we arrive at the operator formulation:

$$\sigma_c = E_{co}\tilde{R}'(\varepsilon - \varepsilon_s) \ , \qquad (\tau \geq t_o) \qquad (A.11)$$

where:

$$\tilde{R}' = \frac{1}{h}\,\tilde{1}' - \tilde{\Psi}' .$$

The integral of function R′ represents the nondimensional concrete relaxation function:

$$R^* = R^*(t,\tau) = \tilde{R}'1^* = \frac{1}{h}\,1^* - \Psi^* \ , \quad (\tau \geq t_o) \qquad (A.12)$$

where:

$$\Psi' = \Psi'(t,\theta) = \frac{\partial R^*(t,\theta)}{\partial \theta} \ , \qquad (t \geq \theta > t_o) .$$

By means of algebraic elimination of σ_c (i.e. $\varepsilon - \varepsilon_s$) from Eqs. (A.11) and (A.10), the following operator expressions, valid for inverse operators, are obtained:

$$\tilde{F}'\tilde{R}' = \tilde{1}' \quad \text{and} \quad \tilde{F}'\tilde{R}' = \tilde{R}'\tilde{F}' . \qquad (A.13)$$

Integrating these expressions, we get:

$$\tilde{F}'R^* = (\frac{1}{e}\,\tilde{1}' + \tilde{f}')R^* = 1^*, \quad \text{and} \quad \tilde{F}'R^* = \tilde{R}'F^* . \qquad (A.14)$$

The first expression represents an operator formulation of the relation between functions F^* and R^*, the integral form of which was given by expression (15).

From Eqs. (A.14), (A.12), (A.5), and (15) for $\tau = t$ we obtain:

$$\frac{1}{h} = \frac{1}{h(t)} = R^*(t,t) = \frac{1}{F^*(t,t)} = e(t), \ \Psi^*(\tau,\tau) = 0, \ (\tau > t_o) .$$

In setting up the basic equations (6), the following operators are introduced:

$$\tilde{R}'_{hl} = e_{hl}\tilde{1}' - \gamma_{hl}\tilde{\Psi}' \ , \quad \tilde{R}'_{12} = \tilde{R}'_{21} \ , \quad (h,l = 1,2)$$

$$e_{hl} = \delta_{hl} + \gamma_{hl}(e - 1) \ , \quad \delta_{hl} = \begin{cases} 1 \text{ for } h = l \\ 0 \text{ for } h \neq l \end{cases}$$

where γ_{hl} = coefficients depending on the reduced geometrical cross

section properties and on the prestressing steel relaxation characterized by ρ (Eq. 2). The individual values of symmetric matrix $\|\gamma_{hl}\|_{2,2}$ are γ_h ($h = 1,2$, see Appendix 2 in Ref. 4 and Notations).

System of equations (6) may be formally solved as a system of algebraic linear equations by applying Cramer's rule.

When the operator relation (8) is multiplied by (A.13) and when operators $\tilde{B}'_h$ and $\tilde{K}'_h$ (Eq. 10) are introduced, it may be shown that these operators are the inverse operators, and so Eqs. (11) are obtained. Integrating these equations we get:

$$\tilde{K}'_h B^*_h = 1^*, \qquad \tilde{K}'_h B^*_h = \tilde{B}'_h K^*_h \ , \qquad (h = 1,2). \tag{A.15}$$

By setting $\gamma_1 = \gamma_2 = 1$ ($\gamma_{11} = \gamma_{22} = 1$, $\gamma_{12} = \gamma_{21} = 0$, see Appendix 2 in Ref. 4) we obtain the special case of the homogeneous cross section. Then, from Eq. (7), and comparing relation (8) with (A.13), we get:

$$\tilde{R}'_h \equiv \tilde{R}' \ , \quad \tilde{F}'_h \equiv \tilde{F}' \qquad \text{i.e.} \qquad R^*_h \equiv R^* \ , \quad F^*_h \equiv F^*. \tag{A.16}$$

Functions R^*_h, F^*_h and the corresponding operators $\tilde{R}'_h$, $\tilde{F}'_h$ ($h = 1,2$) relevant to the composite cross section reduce in this special case to the concrete relaxation function, R^*, the concrete compliance function, F^*, and the corresponding operators $\tilde{R}'$, $\tilde{F}'$. However, by introducing $\gamma'_h = 1$ from Eq. (13) and comparing relations (A.14) and (A.15), we can obtain:

$$\tilde{K}'_h \equiv \tilde{F}' \ , \quad \tilde{B}'_h \equiv \tilde{R}' \ , \quad \text{i.e.} \quad K^*_h \equiv F^*, \quad B^*_h \equiv R^*. \tag{A.17}$$

The nondimensional prestressing steel relaxation function R^*_p is represented by the integral:

$$R^*_p = \tilde{R}'_p 1^*, \qquad \tilde{R}'_p = \rho' \tilde{1} + \rho \tilde{R}'. \tag{A.18}$$

Notations

Subscripts:

n,m,p,c = for steel parts, reiforcing steel, prestressing steel and concrete.

The following symbols are also used in this paper:

A_k, I_k = area and inertia moment of part k (k=n,m,p,c) of composite cross section;

E_j, E_{co}, E_u = Young's moduli: of part j (j=n,m,p), of concrete at time t_o, and arbitrary chosen;

ν_j, ν_c = reducing factors: $\nu_j = E_j/E_u$ (j=n,m,p) and $\nu_c = E_{co}/E_u$;

A_{kr}, I_{kr} = reduced area $A_{kr} = \nu_k A_k$, and reduced inertia moment $I_{kr} = \nu_k I_k$ of part k (k=n,m,p,c) of composite cross section;

A_i = transformed cross section area $A_i = \sum_k A_{kr}$;

VOL. 14 1984

y_k = ordinate of centroid of A_k (k=n,m,p,c) refering to centroid of A_i;

S_{kr} = first moment of A_{kr}, $S_{kr}=y_k A_{kr}$ (k=n,m,p,c); $\sum_k S_{kr}=0$;

J_i = moment of inertia of transformed cross section $J_i = \sum_k J_{kr}$, where $J_{kr} = I_{kr} + y_k^2 A_{kr}$, (k=n,m,p,c);

S_i = $\sqrt{A_i J_i}$;

ρ = defined by Eq. (2);

γ_{hl} = coefficients (h,l=1,2): $\gamma_{11} = \frac{A_{cr}}{A_i} + \rho \frac{A_{pr}}{A_i}$,

$$\gamma_{12} = \gamma_{21} = \frac{S_{cr}}{S_i} + \rho \frac{S_{pr}}{S_i}, \quad \gamma_{22} = \frac{J_{cr}}{J_i} + \rho \frac{J_{cr}}{J_i};$$

ζ_c = defined by Eq. (26);

ζ_p = defined by Eqs. (2), (27);

$A_{i\zeta}, S_{i\zeta}, J_{i\zeta}$ = area, first moment and inertia moment of creep transformed cross section: $A_{i\zeta} = A_i - \zeta_c A_{cr} - \zeta_p A_{pr}$, $S_{i\zeta} = -\zeta_c S_{cr} - \zeta_p S_{pr}$, $J_{i\zeta} = J_i - \zeta_c J_{cr} - \zeta_p J_{pr}$;

N_o, M_o = axial force and bending moment at time t_o.

Remarks

The bases of the mathematical theory for aging concrete of the linear creep law was given independently by Maslov (Ref. 14 in Part II) and McHenry (Ref. 15 in Part II). They have applied the principle of superposition due to Volterra (Ref. 16 in Part II). The way of solving the creep problems, on a wide scale, was opened by Mandel (Ref. 17 in Part II) and Huet (Ref. 18 in Part II), who introduced the integro-differential operators. By means of these operators it is possible to solve the problem symbolically, indicating the number of mathematical operations. The application of the linear integral operators, used in the present and in other authors' papers (Ref. 3, 4 and Ref. 12 in Part II) was inspired by the works of Mandel and Huet. Such linear integral operators are more convenient because they lead to the simple stress and displacement expressions for composite beam structures. Some solutions of the same problem for particular compliance functions were given (e.g. Fröhlich, Ref. 19 in Part II and Arutyunian, Ref. 20 in Part II). Also, for an arbitrary comliance function (Mola, Appendix L in Ref. 2), such cases were solved when it was possible to use the analogy with the stress determination if the strain depends linearly on the concrete compliance function.

Acknowledgment

The present paper belongs to a research project which has been supported by the Office of Scientific Research of Serbia.

References

1. Z. P. Bažant, "Prediction of Concrete Creep Effects Using Age-Adjusted Effective Modulus Method", Am. Concrete Inst. J., 69, 1972, pp. 212-217.

2. CEB Design Manual, "Structural Effects of Time-Dependent Behaviour of Concrete", M. A. Chiorino, Chmn., Comité Euro - International du Béton, Bulletin d'Information Nº 136, Juillet 1980, Paris, pp. 107-121, 226-244.

3. V. B. Lazić, J. D. Lazić, "Les contraintes et les pertes de précontrainte dans les structures précontraintes", Annales de l'Institut Technique du Bâtiment et des Travaux Publics, Nº 355, Novembre 1977, TMC Nº 211, pp. 34-55.

4. J. D. Lazić, V. B. Lazić, "Prévision des effets du fluage du béton dans les structures mixtes et précontraintes", Annales de l'Institut Technique du Bâtiment et des Travaux Publics, Nº 399, Novembre 1981, TMC Nº 246, pp. 26-52.

5. ACI Committee 209, Subcommittee 2, "Prediction of Creep, Shrinkage and Temperature Effects in Concrete Structures", SP - 27, American Concrete Institute, Detroit, 1971, pp. 51-93.

6. "Model Code for Concrete Structures", Comité Euro - International du Béton - Fédération Internationale de la Précontrainte, Bulletin d'Information Nº 124/125 E, Vol. 2, Appendix e, April 1978, Paris.

7. G. F. Roach, "Green's Functions", Van Nostrand Reinhold Comp., London, (1970), pp. 141-145.

8. Z. P. Bažant, "Mathematical Models for Creep and Shrinkage of Concrete", Chapter 7 in "Creep and Shrinkage in Concrete Structures", eds. Z. P. Bažant and F. H. Wittmann, J. Wiley, London, (1982).

9. Z. P. Bažant, L. J. Najjar, "Comparison of Approximate Linear Methods for Concrete Creep", J. of the Struc. Div., ASCE, Vol. 99, No. ST9, Proc. Paper 10006, September, 1973, pp. 1851-1874.

VOL. 14 1984

CEMENT and CONCRETE RESEARCH. Vol. 14, pp. 833-838, 1984. Printed in the USA.
0008-8846/84 $3.00+00. Copyright (c) 1984 Pergamon Press, Ltd.

KINETIC ANALYSIS OF EXTRACTION OF CALCIUM SILICATES WITH METHANOLIC SOLUTION OF SALICYLIC ACID. II. EXTRACTION OF DICALCIUM SILICATES

V. Runje and A. Bezjak

Department of Chemistry, Faculty of Pharmacy and
Biochemistry, University of Zagreb, Zagreb, Yugoslavia

(Communicated by Z. Šauman)
(Received Feb. 17, 1984)

ABSTRACT

By applying the methods described in Part I. of the article, kinetic analysis for extractions of γ-, β- and α'-modifications of Ca_2SiO_4 by methanolic solution of salicylic acid was carried out. According to the obtained results, surface interaction is the rate-determining process in all the three cases, and the values of the rate constants increase in the following order: β-, γ-, α'-modification. The rate constants of the reaction were assessed for three temperatures, which made it possible to calculate the activation energy.

Introduction

In our previous work (1) the procedure was worked out for the determination of kinetic parameters of the extraction of solid phases from polysize systems containing particles which can be approximated to spheres. The application of the developed theory was illustrated on the system γ-Ca_2SiO_4 -methanolic solution of salicylic acid. In the present work various Ca_2SiO_4 polymorphs, i.e. α'-, β - and γ-modifications were used with the aim to find conditions for their selective extraction. Like in the case of γ-Ca_2SiO_4 extraction, β-Ca_2SiO_4 particles were also approximated to spheres and, consequently, the relationships developed in Part I. were applied for kinetic analysis of the extraction of β-Ca_2SiO_4. α'-Ca_2SiO_4 particles, however, could not be approximated to spheres but to thin cylinders, and for that case the theory was modified accordingly.

Theoretical Part

In a polysize system containing particles which can be approximated to spheres the rate of extraction is defined by the expression:

$$\frac{d\alpha}{dt} = K_I C_o (1 - \varkappa \alpha) \cdot \sum w_i \cdot F (R_i, \alpha_i) \qquad (1)$$

which gives:

$$\bar{G}(\alpha) = \int_0^{\alpha} \frac{d\alpha}{(1 - \varkappa \alpha) \Sigma w_i \cdot F (R_i, \alpha_i)} = K_I C_o t \qquad (2)$$

where $\alpha = \Sigma w_i \cdot \alpha_i$, $\varkappa = m_o/m_g$. m_o is the initial mass of the solid phase depending on the initial concentration of reactant C_o. In the above equations $1/F(R_i, \alpha_i)$ is the sum of two resistances: the resistance to surface interaction and the resistance to diffusion through solution, i.e.:

$$1/F(R_i, \alpha_i) = \frac{R_i}{(1- \alpha_i)^{2/3}} + \frac{R_i^{3/2} \left[1 + 2(1 - \alpha_i)^{1/2} \right]}{3 K_{ID} R_o^{1/2} (1 - \alpha_i)^{1/2}} \qquad (3)$$

In the above equation K_{ID} includes the ratio of rate constants for diffusion and interaction and also the thickness of the diffusion layer (1). R_o belongs to the particles of the referential radius and has been introduced in order to define the extraction degree of particles with radius R_i in relation to the extraction degree of particles with the referential radius according to:

$$\int_0^{\alpha_i} \frac{d\alpha_i}{F(R_i, \alpha_i)} = \int_0^{\alpha_o} \frac{d\alpha_o}{F(R_o, \alpha_o)} \qquad (4)$$

As explained previously (1), expression (2) is applied for calculating $\bar{G}(\alpha)$ values by using the given particle size distribution and the selected set of K_{ID} and $\varkappa$ values. If the set has been correctly chosen, the result is a linear dependence between $\bar{G}(\alpha)$ and t. When, however, particles are not approximated to spheres but by thin cylinders, expression (2) takes another form:

$$- \ln (1- \varkappa \alpha) = K_I \varkappa C_o \left(\sum \frac{w_i}{R_i} \right) t \qquad (5)$$

Expression (5) is obtained on the assumption that (i) the thickness of a particle is proportional to the radius of the cylinder base, (ii) in the course of the dissolution the thickness of a particle diminishes, with the radius of the base remaining constant, and (iii) surface interaction is the rate-determining step.

Experimental Part

Preparation of Ca_2SiO_4 Samples

All the three polymorphous modifications of dicalcium silicate were obtained by burning a stoichiometric mixture of quartz and $CaCO_3$ at 1450 °C. α'- form was stabilized by addition of 3% B_2O_3, and β -form by addition of 1% B_2O_3. The synthetised samples were ground in an agate ball mill. The

VOL. 14 1984

granulometric analysis was carried out by applying Coulter counter method, the obtained results being shown in Table 1.

Table 1.

Particle Size Distribution for α'-, β- and γ-Ca_2SiO_4

R_i (μm)	w_i (α')	w_i (β)	w_i (γ)
0.25	0.025	0.010	0.010
0.75	0.045	0.015	0.010
1.25	0.050	0.035	0.010
1.75	0.040	0.020	0.020
2.50	0.060	0.040	0.050
3.50	0.080	0.070	0.095
4.50	0.065	0.060	0.100
5.50	0.075	0.070	0.110
7.00	0.105	0.135	0.125
9.00	0.135	0.175	0.120
11.00	0.150	0.150	0.105
13.00	0.065	0.125	0.060
15.00	0.050	0.080	0.050
17.00	0.060	0.015	0.040
20.00	-	-	0.040
22.50	-	-	0.030
25.00	-	-	0.025

Extraction of Samples

The concentration of salicylic acid was 0.05 mole/l for extracting α'- and β-Ca_2SiO_4, and 0.10 mole/l for γ-Ca_2SiO_4. Experiments were performed by stirring samples with a magnetic stirrer (350 rpm) at constant temperatures, as indicated in Table 2. where also the applied solid-to-liquid ratios are given.

Table 2.

Experimental Conditions of Extraction

Modification	α'-	β-	γ-
sol.- liq. (g cm^{-3})	1/300	1/300	1/200
Temperature (^oC)	13	18	20
	18	23	25
	23	30	30

The obtained α -t interdependences are represented in Figs. 1, 2 and 3.

Results and Discussion

As already shown in Part I., two sets of data are required for the determination of kinetic parameters of extraction of dicalcium silicates. They are (i) particle size distribution of the original sample and (ii) degrees of reaction α for consecutive time intervals t. The previous work has also shown that surface interaction manifests itself as rate-determining step in the extraction process and therefore $\bar{G}(\alpha)$-t interdependences should be calculated by using relatively high K_{ID} values (K_{ID} = 250). In calculating $\bar{G}(\alpha)$, $\varkappa$ = 1.160 was taken for γ-Ca_2SiO_4 from Part I. For α'- and β-Ca_2SiO_4 the value was obtained from data given in the present work. The ratio of moles of Ca^{2+} ions to those of salicylic acid at the applied solid-to-liquid ratio, which was the same for both modifications, indicates that with both α'- and β-Ca_2SiO_4 the limiting value of the degree of reaction amounts to 0.645. This has been determined experimentally also for α'-modification. It is obvious from Fig. 1 that the value was obtained after 90 min. at 23 °C; the belonging $\varkappa$ value amounts to 1.550. After setting and K_{ID} values, $\bar{G}(\alpha)$ -t interdependences were calculated by applying Eqs. (2) and (3). The obtained results are represented in Figs. 4, 5 and 6a which show that, regardless of the applied temperatures, straight lines were obtained by plotting $\bar{G}(\alpha)$ versus time for β - and γ - modifications. For α'-Ca_2SiO_4, however, non-linear interdependences resulted at all the three temperatures (Fig. 6a). This finding is in accordance with TEM observations, according to which Ca_2SiO_4 particles are not spherical; in one direction they are much thinner that in the other two (2) and consequently their surface area can be expressed in a more satisfactory way if they are approximated to thin cylinders. In that

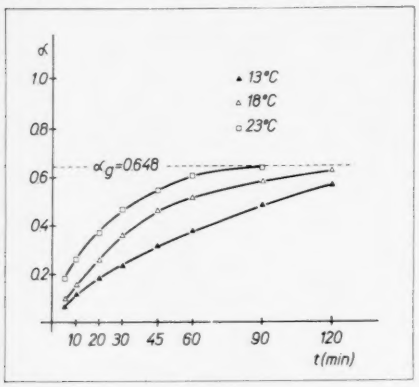

Fig. 1
α-t interdependence for α'-Ca_2SiO_4

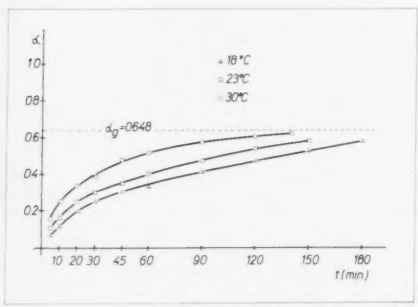

Fig. 2
α-t interdependence for β-Ca_2SiO_4

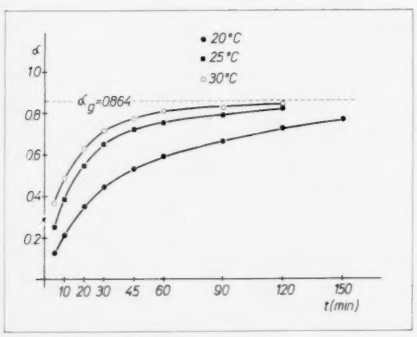

Fig. 3
α-t interdependence for γ-Ca_2SiO_4

VOL. 14 1984

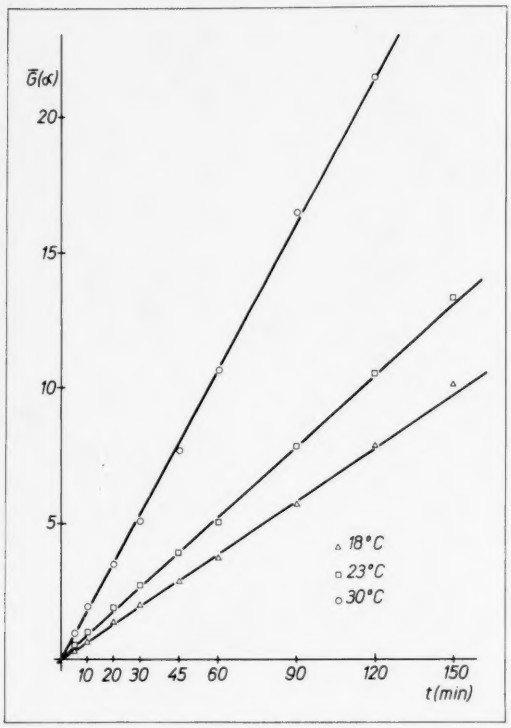

Fig. 4
Calculated $\bar{G}(\alpha)$-t interdependence for β-Ca_2SiO_4

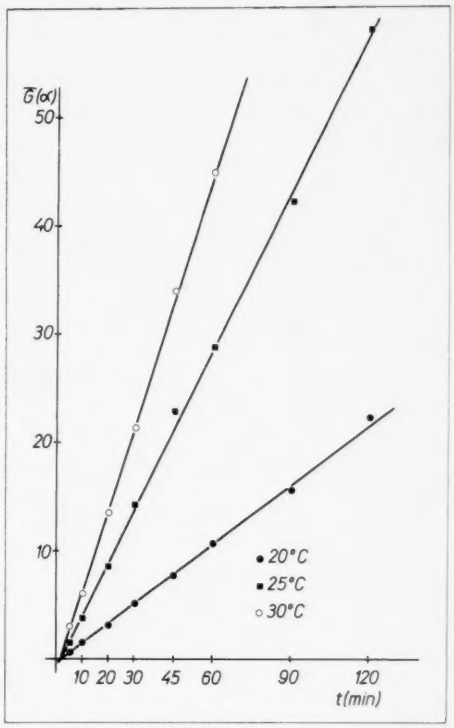

Fig. 5
Calculated $\bar{G}(\alpha)$-t interdependence for γ-Ca_2SiO_4

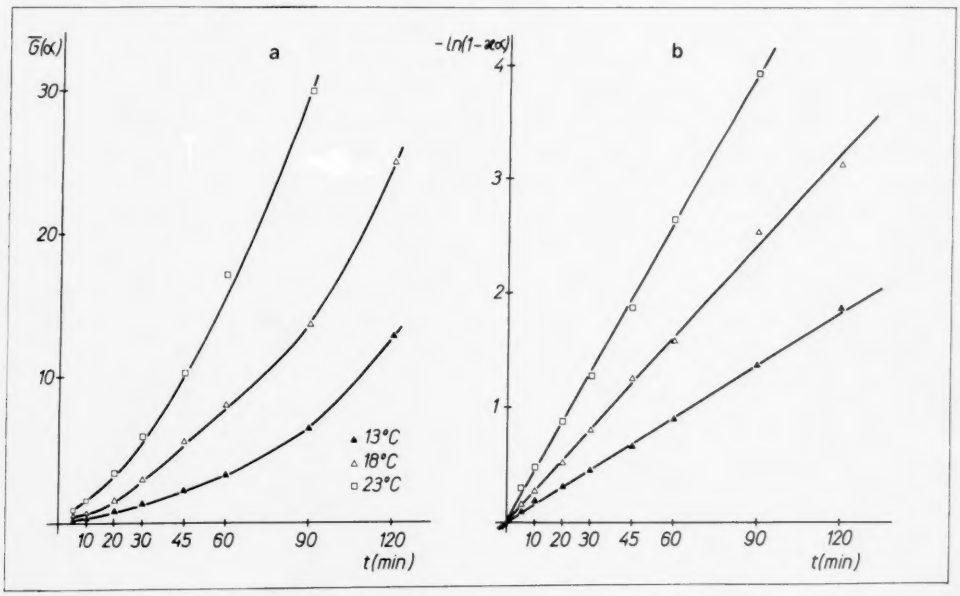

Fig. 6
Calculated $\bar{G}(\alpha)$-t interdependence for α'-Ca_2SiO_4

Table 3.

Rate Constants for Extraction of Ca_2SiO_4-modifications in Methanolic Solutions of Salicylic Acid

Modif.	t(°C)	K_I(μm l $mol^{-1}min^{-1}$)
α'	13	3.00
	18	5.50
	23	8.00
β	18	1.24
	23	1.74
	30	3.04
γ	20	1.90
	25	4.85
	30	6.60

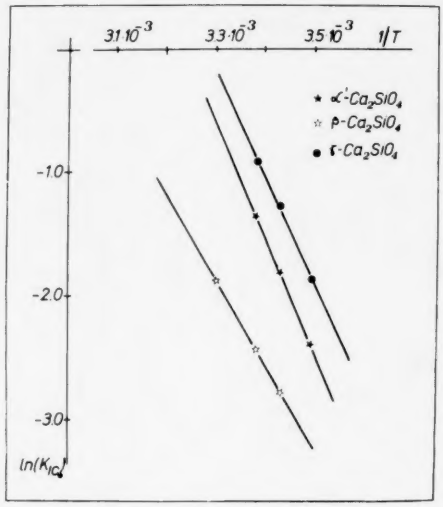

Fig. 7
$\ln K_I - \frac{1}{T}$ interdependences for extraction of Ca_2SiO_4-modifications in methanolic solution of salicylic acid

VOL. 14 1984

case the surface area of particles does not change considerably in the course of extraction. Assuming that the particles are cylindrical, i. e. by applying Eq. (5), linear relationships have been obtained in the case of α'-Ca_2SiO_4 modification (Fig. 6b) as well.

The rate constants for surface interaction as determined from the slope of the lines and the belonging C_o concentration are listed in Table 3. It is a well known fact that the rate of dissolution for processes controlled by surface interaction increases about three to four times if the temperature increases by about 10 °C. Thus the ratio of constants obtained at different temperatures also confirms the results of kinetic analysis according to which surface interaction is the rate-determining step in extraction of dicalcium silicates by methanolic solution of salicylic acid.

Using the data for the reaction rate constants at different temperatures the activation energy of extraction has been determined from Arrhenius plot (Fig. 7). It amounts to 72.3 $KJmol^{-1}$ for α'- modification, 57.3 $KJmol^{-1}$ for β-modification and 70.5 $KJmol^{-1}$ for γ-modification of Ca_2SiO_4.

References

1. A. Bezjak, V. Runje, Cement and Concrete Research 13, No. 2, 186 (1983)

2. I. Jelenić, A. Bezjak, X Technical Meeting of Yugoslav Association of Cement Producers, Lukavac 1982, Communication I/a-13

CEMENT and CONCRETE RESEARCH. Vol. 14, pp. 839-842, 1984. Printed in the USA.
0008-8846/84 $3.00+00. Copyright (c) 1984 Pergamon Press, Ltd.

FORMATION OF SOLUBLE ANHYDRITE BY SALICYLIC ACID EXTRACTION OF CALCIUM SILICOSULFATE

F. J. Tang and E. M. Gartner
Chemical/Physical Research Department
Portland Cement Association, Skokie, IL 60077 USA

(Communicated by J.P. Skalny)
(Received Feb. 28, 1984)

ABSTRACT

Calcium silicosulfate and anhydrite were subjected to extraction by salicylic acid in methanol. Only calcium silicosulfate was affected, leaving a residue which was identified as "soluble anhydrite." The fraction of residue produced was close to that expected for stoichiometric precipitation of sulfate as $CaSO_4$. It is suggested that soluble anhydrite found in cement clinker residues after salicylic acid extraction may form in a similar manner from sulfate ions dissolved in belite or alite.

Background

A solution of salicylic acid in anhydrous methanol is commonly used to extract the calcium silicate phases from portland cements and clinkers in order to facilitate XRD analysis of the interstitial phases. In performing such extractions on certain high-sulfur clinkers (1), we noted the presence of broad X-ray reflections at 14.6, 25.6, 29.6, 31.8 and 53.9°2θ (CuKα) corresponding to "soluble anhydrite" or γ-$CaSO_4$ (JCPDS File 26-0329). Since this phase is unstable at clinkering temperatures, it was concluded that it must have formed during the salicylic acid extraction, either from hydration of "natural" anhydrite or by precipitation of sulfate ions dissolved in the extracted calcium silicate phases. In order to test these hypotheses, it was decided to conduct salicylic acid extractions of carefully prepared samples of calcium silicosulfate [$Ca_5(SiO_4)_2(SO_4)$] and natural anhydrite.

Experimental

Calcium silicosulfate was prepared by heating a mixture of γ-C_2S* and reagent-grade gypsum in a 2:1 molar ratio; the γ-C_2S was prepared previously by burning a mixture of high purity carbonate and silica. The homogenized mixture was burned in a loosely covered platinum dish in an electric muffle furnace at 1200°C for 3-1/2 hours. The product was analyzed for sulfate content by acid dissolution and ion chromatography. It showed slightly less than the theoretical sulfate content, presumably due to some volatilization of sulfur during heating. Nevertheless, it gave an X-ray diffraction pattern very similar to that reported by Gutt and Smith (2), with no evidence of any uncombined calcium silicate.

Anhydrite was prepared by igniting reagent-grade gypsum at 900°C for 2 hours. The X-ray diffraction pattern of the ignited product was identical to that given in JCPDS File 6-0226 for natural anhydrite.

Samples of these materials were ground to pass a 200-mesh screen. Five grams of each powder were stirred with a solution of 60 g salicylic acid (reagent grade) in 400 ml absolute (reagent grade) methanol for 1 hr at 23°C. The residues were filtered on a glass filter paper, air dried, and weighed. They were then dried in an oven at 300°C and reweighed. In the case of anhydrite, the air dried residue amounted to over 99% by weight of the starting material. This residue gave an XRD pattern identical to that of the original sample before treatment. In the case of the calcium silicosulfate only, the filtrate was evaporated to dryness, ignited at 900°C, and the residue analyzed for sulfur by the Leco furnace method; typical results are given in Table 1.

VOL. 14 1984

TABLE 1

Materials Balance (mass %)

Nominal composition of starting material:	$Ca_5(SiO_4)_2SO_4$
Theoretical SO_3 content	16.7
SO_3 content by ion chromatography	16.0
Actual residue after extraction and ignition at 300°C	26.7
Expected residue if all SO_3 in starting material were precipitated as $CaSO_4$	
$16.0 \times \frac{136.14}{80.06}$	27.2
SO_3 content of dried filtrate after ignition at 900°C	0.05

*Cement Chemists' Notation: C=CaO, S=SiO_2, A=Al_2O_3, F=Fe_2O_3

Discussion

As shown in Table 1, the ignited residue from the calcium silicosulfate extraction accounted for over 98% of the sulfate contained in the original sample. This, together with the very low solubility of the anhydrite sample, implies that the solubility of $CaSO_4$ in the salicylic acid/methanol solution was not more than about 0.06 g/L methanol. The very low sulfur content of the ignited filtrate suggests a much lower solubility, but there is a possibility of sulfur loss during ignition due to the presence of a reductant (salicylic acid).

In one case, the whole extraction and filtration procedure was carried out under an atmosphere of dry nitrogen, and the residue was examined directly by XRD under the dry atmosphere. The resulting diffraction pattern revealed broad reflections, apparently indicating a very poor crystalline form of soluble anhydrite (Fig. 1).

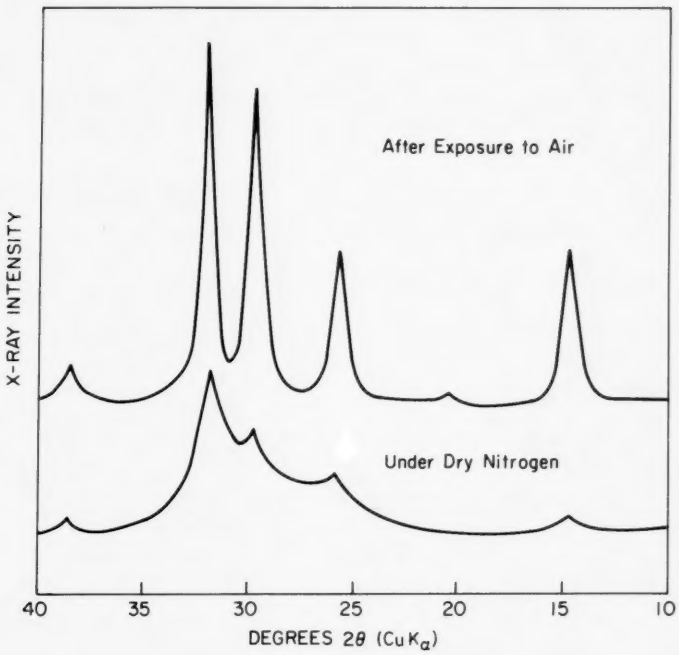

FIG. 1

X-ray diffraction patterns of extraction residues from calcium silicosulfate

Also shown in the figure is the diffraction pattern obtained on the same residue after it had been allowed to stand in air for a few hours. The marked sharpening and intensification of the soluble anhydrite lines indicate an increase in crystallinity, presumably resulting from uptake of atmospheric moisture. At later ages, gypsum lines appeared in the pattern.

Ignition losses determined at 300°C for residues which had been filtered and dried in air were always in excess of 6.2%, indicating that uptake of the first 0.5 mole water/mole $CaSO_4$ was rapid. For this reason, we were not able to determine the

amount of water contained in the dry residue immediately after precipitation under dry nitrogen. However, it is reported that soluble anhydrite can vary in composition all the way from hemihydrate, with 0.5 mole water, down to γ-$CaSO_4$, which may contain as little as 0.001 mole water/mole $CaSO_4$ (3). Thus, it is quite possible for soluble anhydrite to have formed under almost completely anhydrous conditions.

The exact nature of the soluble salicylate complexes formed by calcium or silicate ions in methanol is not known to us, but it appears from our results that calcium ions bind to sulfate strongly enough to inhibit formation of a salicylate complex. Presumably, precipitation of $CaSO_4$ during the extraction is very rapid and thus leads to the formation of a poorly crystalline form of soluble anhydrite. This is consistent with our observation of soluble anhydrite in the salicylic acid extraction residue of certain portland cement clinkers which contained high sulfate contents in a non-water-soluble form. Formation of soluble anhydrite under these circumstances appears to be a good indication of high sulfate contents in solid solution in the calcium silicate phases in these clinkers, as has been confirmed by microprobe analysis (1). In many cases, "natural" anhydrite is also present in clinker but is easily distinguished from the soluble anhydrite precipitated during the extraction.

VOL. 14 1984

References

1. E. M. Gartner and F. J. Tang, to be published.

2. W. Gutt and M. A. Smith, Nature 210 (5034) 408 (1966).

3. J. Bensted, il Cemento 72 (3) 139 (1975).

CEMENT and CONCRETE RESEARCH. Vol. 14, pp. 843-846, 1984. Printed in the USA.
0008-8846/84 $3.00+00. Pergamon Press, Ltd.

THE RATE OF CALCIUM HYDROXIDE PRECIPITATION MEASURED BY ELECTRICAL CONDUCTANCE

Paul Wencil Brown, Kevin Galuk, Geoffrey Frohnsdorff
Center for Building Technology, National Bureau of Standards,
Washington, DC 20234

(Communicated by J.P. Skalny)
(Received Feb. 28, 1984)

ABSTRACT

The rates of calcium hydroxide precipitation from supersaturated solutions were measured. The times of onset of precipitation were shorter for the solutions seeded with $Ca(OH)_2$ or with C-S-H, than for unseeded solutions. Calorimetric measurements indicated the presence of solid $Ca(OH)_2$ added at the time of mixing to be ineffective in promoting the onset of the acceleratory period of C_3S hydration. This suggests that $Ca(OH)_2$ precipitation is not the principal factor which determines the end of the induction period in C_3S hydration.

Introduction

Understanding the factors affecting the precipitation of calcium hydroxide during the hydration of tricalcium silicate is important to the development of a more complete understanding of the hydration process. Generally, the onset of $Ca(OH)_2$ precipitation roughly coincides with the onset of the acceleratory period of C_3S hydration. It has, therefore, been argued that it is this precipitation process which allows hydration to accelerate by relieving the high degree of supersaturation in the solution [1]. In opposition to this casual argument, the alternative view is that $Ca(OH)_2$ precipitation is an effect of the onset of acceleratory period. This view contends that the onset of rapid C_3S hydration causes the concentration of calcium hydroxide in solution to exceed a critical degree of supersaturation which results in its precipitation.

The objectives of this investigation were to measure the time of onset of $Ca(OH)_2$ hydroxide precipitation as function of the degree of supersaturation, to investigate the effects of the presence of solid $Ca(OH)_2$ or C-S-H on these times and to determine whether the presence of solid $Ca(OH)_2$ promotes the onset of the acceleratory period of C_3S hydration.

Experimental

Supersaturated $Ca(OH)_2$ solutions were prepared by hydrating C_3S (330 m^2/kg) at various water-to-solids ratios for approximately 2 hours. This yielded solutions whose calcium ion concentrations ranged from 1.4 to 1.9 g/ℓ as CaO. Test solutions were prepared by filtration through 0.2 μm filters to remove solids. Supersaturated $Ca(OH)_2$ solutions prepared in this manner avoid the

presence of various ions, such as sodium or chloride, while containing small amounts of dissolved silica. Therefore, solutions prepared in this way tend to be more representative of those in contact with hydrating C_3S pastes than are solutions prepared by other means. The solutions were prepared in amounts sufficient to allow three electrical conductance experiments to be performed simultaneously. After filtration, the solution was partitioned into three polyethylene bottles, conductance cells inserted, and measurements initiated. The solution preparation and the conductance measurements were carried out in a glove box to minimize exposure to carbon dioxide. The solution temperatures were 29±1°C and the solutions were stirred throughout the course of each experiment. Solution conductivities were measured every 60 seconds by recording the readings from the conductance meters using a data acquistion system interfaced with a minicomputer.

The rates of $Ca(OH)_2$ precipitation were measured in unseeded solutions, in solutions seeded with C-S-H, and in solutions seeded with solid $Ca(OH)_2$. C-S-H seeds were prepared by reacting 0.33g of C_3S in a liter of water for 7 days. This solution was decanted in order to concentrate the C-S-H so that after stirring, 10 ml of this solution contained approximately 8 mg of C-S-H assuming its stoichiometry to be $C_3S_2H_3$. Calcium hydroxide seeds were prepared by filtering a hydrating C_3S solution whose calcium ion concentration was 1.74 g/ℓ as CaO and allowing $Ca(OH)_2$ to precipitate. Ten ml of this solution contained approximately 8 mg of solid $Ca(OH)_2$. No attempt was made to determine the surface areas of the seeding materials.

VOL. 14 1984

Results

Fig. 1 compares the precipitation rate of $Ca(OH)_2$ from an unseeded solution with those from the same solution when seeded with solid $Ca(OH)_2$ or with C-S-H. In this figure, the normalized changes in conductance are plotted as a percent reaction against time. The conductance of the supersaturated solution, having a calcium ion concentration of 1.76 g/ℓ as CaO, is represented as 0 percent reaction. The conductance of the saturated solution after $Ca(OH)_2$ precipitation was complete is represented as 100 percent reaction. In this instance, the calcium ion concentration in solution was 1.15 g/ℓ as CaO. This concentration was reached regardless of whether the solutions were seeded with C-S-H or $Ca(OH)_2$ or were unseeded.

Compared to the unseeded solution, the addition of 8 mg of solid $Ca(OH)_2$ significantly decreased the time required for the initiation of precipitation. The addition of a similar mass of C-S-H also promoted $Ca(OH)_2$ precipitation. However, the C-S-H was a far less effective nucleating agent than $Ca(OH)_2$ itself. The unseeded solution remained supersaturated for an extended period. The length of time required for precipitation to initiate from unseeded solutions was observed to correlate with the degree of supersaturation as shown in Table 1. This table shows that even highly supersaturated solutions require lengths of time well in excess of the induction period for the initiation of precipitation in the absence of nucleating agents.

Isothermal calorimetry was used to assess the effects of the presence of solid $Ca(OH)_2$ on the rate of heat liberation during early C_3S hydration. Simultaneous calorimetric determinations were performed at 25°C at a solution-to-solids ratio of 0.58 using a multicelled microcalorimeter [2]. In this experiment, both mix solutions used were saturated with respect to calcium hydroxide; however, solid $Ca(OH)_2$ was also present in one of the solutions. The results of this experiment are shown in Fig. 2. This figure indicates that the presence of solid $Ca(OH)_2$ at the start of C_3S hydration did not decrease the length of the induction period.

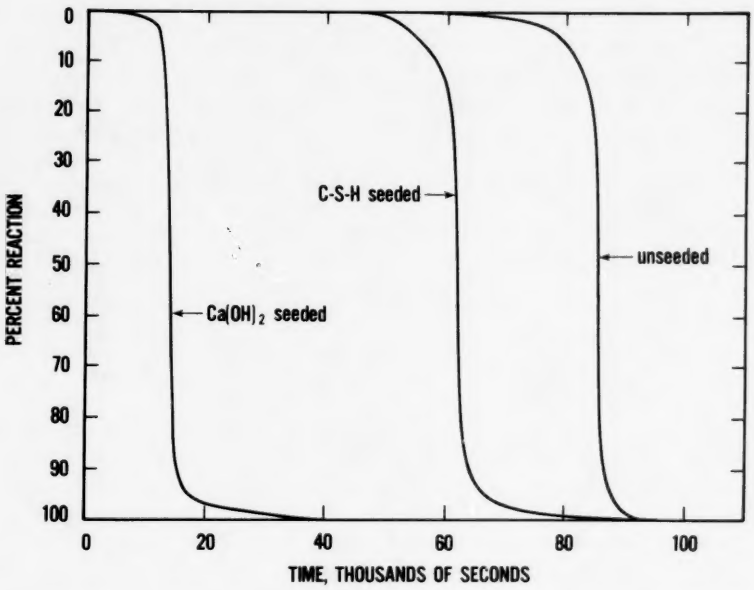

Figure 1. The rates of precipitation of $Ca(OH)_2$ from a solution seeded with solid $Ca(OH)_2$, a solution seeded with C-S-H, and from an unseeded solution.

L.
4
84

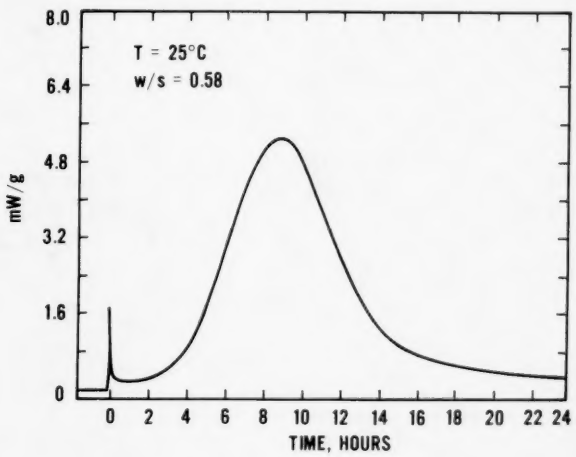

Figure 2. Calorimetric curves for C_3S hydrated in saturated $Ca(OH)_2$ solution or in saturated $Ca(OH)_2$ solution containing solid $Ca(OH)_2$ The two curves are indistinguishable.

Table 1. Effect of Calcium Ion Concentrations on the Time of Initiation of $Ca(OH)_2$ Precipitation from Unseeded Solutions

Calcium Ion Concentration, g/ℓ as CaO	Onset Time, sec
1.977	5,700
1.889	17,000
1.760	54,000
1.650	160,000
1.475	>360,000

Discussion

Odler [3] showed that the addition of partially hydrated C_3S to freshly mixed C_3S paste accelerated hydration, whereas, the addition of solid $Ca(OH)_2$ did not. The latter result is consistent with the present findings. Alternatively, it has been suggested that the precise effect of admixed $Ca(OH)_2$ is dependent on its morphology [4]. Accordingly, the $Ca(OH)_2$ seeds used in the present investigation were obtained by precipitation from a filtered supersaturated solution achieved by hydrating C_3S. This was done in order to simulate the conditions under which $Ca(OH)_2$ precipitates during C_3S hydration.

The onset of precipitation from the calcium hydroxide seeded solution was not instantaneous, Fig. 1. This is in contrast with the data of Tadros, et al. [5] who observed immediate $Ca(OH)_2$ precipitation from solution under generally similar experimental conditions. The retardation of the initiation of precipitation in the present case may result from the presence of silica in solution. Silica has been reported to retard the nucleation of calcium hydroxide [1], most probably as a result of adsorption on growth surfaces.

A comparison of the conductivity data in Fig. 1 with the calorimetric data in Fig. 2 indicates that, while the addition of solid $Ca(OH)_2$ promotes precipitation, the presence of solid $Ca(OH)_2$ does not decrease the length of the induction period during C_3S hydration. This suggests that the onset of the acceleratory period is not controlled by the onset of $Ca(OH)_2$ precipitation.

References

1. J. Skalny and J. F. Young, VII Intl. Cong. Chem. Cement I, II-1/3, Paris, 1980.
2. E. J. Prosen, P. W. Brown, and G. Frohnsdorff, to be published.
3. I. Odler and H. Dörr, Cem. Concr. Res. 9(3), 277 (1979).
4. N. R. Greening, private communication.
5. M. E. Tadros, J. Skalny, and R. S. Kalyoncu, J. Coll Interface Sci. 55, 20, (1976).

VOL. 14 1984

CEMENT and CONCRETE RESEARCH. Vol. 14, pp. 847-854, 1984. Printed in the USA.
0008-8846/84 $3.00+00. Copyright (c) 1984 Pergamon Press, Ltd.

PARAMETRIC ANALYSIS OF THE HEAT EVOLUTION DURING HYDRATION OF A CEMENTITIOUS PLUG IN A BOREHOLE

C. Gotsis and D.M. Roy
Materials Research Laboratory, The Pennsylvania State University
University Park, PA 16802, USA

(Communicated by G.M. Idorn)
(Received March 1; in final form Sept. 15, 1984)

ABSTRACT

Parametric analysis by the computer program ATHENAN of the hydration of a cementitious plug in the borehole of a test rock, showed that the temperature rise within the plug is most sensitive to the size of the plug and moderately sensitive to the conductivities of the plug and the rock followed by less sensitive to the diffusivities of the plug and the rock and the heat transfer coefficient between the rock and the surrounding air. For a given heat of hydration of a mixture, a critical plug size exists given the environmental conditions.

Introduction

It is well known that a few mathematical models have been developed or applied to the hydration of portland cement with varied success (1). Such a model would be useful in predicting the kinetics of the reactions that take place during the course of hydration and therefore the rate of heat liberation so that cracks due to either thermal stresses or drying shrinkage could be avoided by properly choosing the materials and emplacement conditions, namely initial temperature, size of individual pours, and total size, among other factors.

To improve the calculation accuracy of the temperature distributions during the course of hydration of cementitious mixtures a nonlinear finite difference computer program called ATHENAN was developed by Gotsis (2). ATHENAN calculates the temperature distribution in axisymetric cylindrical domains that may react exothermally, like the hydration of cements, radioactive waste canisters and other solid state exothermal reactions. The development of ATHENAN was made in part to support the geologic disposal of radioactive wastes.

Sealing of the boreholes that connect the biosphere with the repository surroundings is necessary in order to prevent radionuclide transport to the biosphere with a rate not higher than that through the host rock. This is to be achieved by natural fillers or manmade grouts or other cementitious materials (3). Several cementitious mixtures were investigated and the mixture with a suitable combination of physical and mechanical properties was

selected for study in a simulated laboratory scale plugging of a drilled granite cylinder by experimental measurements and computer simulations.

The objectives of these studies were to develop a means for determining whether the selected cementitious mixture could be used for plugging boreholes without developing excessive maximum temperatures or temperature differentials that could cause development of cracks, to validate the computer model ATHENAN, and then to use the computer model for assessing the applicability of the selected cementitious mixtures in different geometries and types of rocks. The model would apply to concretes in any cylindrical configuration.

In the present paper the applicability will be discussed, while the experimental measurements and the validation of the computer model ATHENAN have been presented elsewhere (4).

Geometry and Heat of Hydration

A cylindrical granite specimen with a height of 30 cm and a diameter of 39.37 cm was used. The cylinder had a borehole of 20.32 cm diameter and 18.75 cm height (Figure 1). Because of the homogeneity of the materials and the existence of an axis of revolution, it is necessary to examine only a meridional cross-sectional area consisting of the semi-plane which includes the axis of revolution.

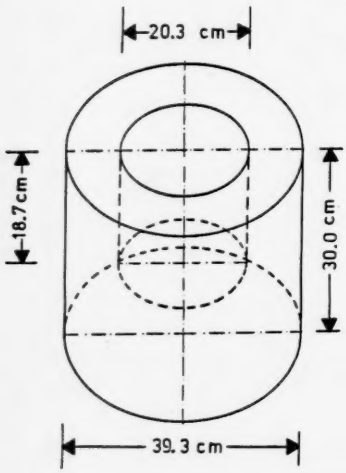

Fig. 1. Granite specimen geometry before thermocouple holes were drilled.

Small cylindrical holes were drilled in order to accommodate thermocouple wires for temperature measurement. Figure 2 shows the grid of the finite difference computer model ATHENAN overlayed on the meridional cross-sectional area of the specimen. Materials 2 and 3 are the

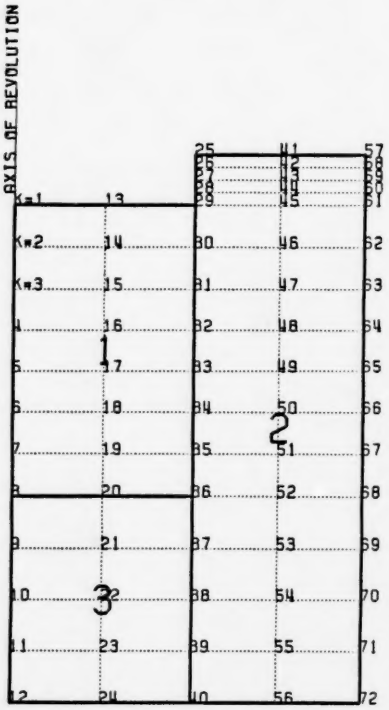

Fig. 2. The meridional cross-sectional area and the overlay of the finite difference grid of the program ATHENAN.

VOL. 14 1984

granite and material 1 is the cement plug. The nodes of the grid are numbered K = 1, 2, tious mixture was the PSU number 82-022 (2), the composition of which is shown in Tables 1 and 2.

The rate of heat evolution from hydration of the mixture PSU 82-022 which was used to plug the granite borehole was measured at 34.5, 50, and 60.5 degrees Celsius, respectively, using the SEEBECK type envelope calorimeters, model C-1245-2-E, Thermometics Corporation, San Diego, California. The recordings were made with SOLTEC recorders; both the rate and the cumulative heat liberated were plotted versus time (Figures 3 and 4).

For use with the program ATHENAN, the rates of hydration were stored in computer files in digital form. A subroutine was written for the program ATHENAN in order to interpolate by the trapezoidal rule between times and temperatures and obtain the rate of heat of hydration for any node at any given time and temperature.

Table 1. The cementitious mixture PSU 82-022.

*MRL code	component	percent by weight
Z-47	shrinkage-compensating cement, type K	33.82
E01	distilled water	15.895
B51	volatilized silica fume	7.29
B25	flyash	8.18
C57	sand ASTM C-109	33.82
A36	superplasticizer	0.99
A27	defoamer D-47	0.005

*MRL = Materials Research Laboratory at The Pennsylvania State University

Table 2. Chemical and spectrochemical analyses of components of PSU 82-022.

chemical component	% by weight cement	fly ash	silica fume
SiO_2	20.1	50.2	96.0
Al_2O_3	4.11	27.0	0.10
TiO_2	0.22	1.40	<0.1
Fe_2O_3	3.19	13.8	<0.1
MgO	4.18	0.84	0.13
CaO	62.26	1.82	0.12
MnO	0.05	0.034	0.010
Na_2O	0.14	0.24	0.1
K_2O	0.45	2.45	0.45
P_2O_5	0.12	0.49	0.07
SrO	0.05	900 ppm	
BaO	0.05	1250 ppm	
SO_3	4.59		
L.O.I. (1000°C)	2.04		
TOTALS	101.45	98.27	96.86

The heat transfer number used in the program ATHENAN to simulate the hydration of the cementitious mixture in the granite borehole was estimated for natural convection between the granite and the air above the plug for vertical and horizontal surfaces to be 4.0 $W/K/m^2$ (5).

Using the experimental values for the cementitious plug thermal conductivity 0.8 W/m/K, granite conductivity 2.25 W/m/K, calculated cement diffusivity 6×10^{-7} m^2/s, and granite diffusivity 18.3×10^{-7} m^2/s into the

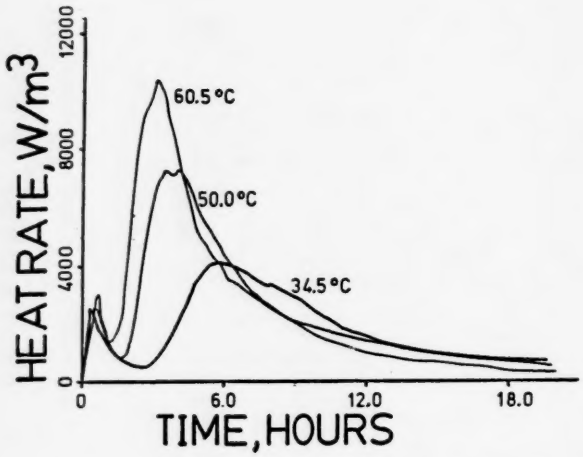

Fig. 3. The rate of hydration versus time for the PSU 82-022 cement mix. The numbers indicate temperature of the jackpot surrounding the calorimeter.

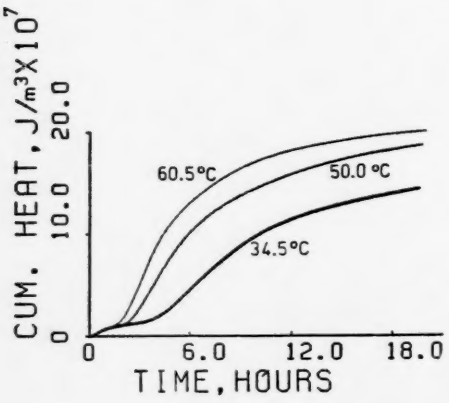

Fig. 4. The cumulative heat of hydration versus time for the PSU 82-022 cement mix. The numbers indicate temperature of the jackpot surrounding the calorimeter.

computer program ATHENAN the simulated temperature history was in good agreement with the thermocouple measurements (2,4). The initial condition was at 34°C and the surrounding air was at 90% humidity and 34°C.

Parametric Analysis

A parametric analysis was performed to study the influence of the values of the thermal properties and the geometry used as input for the calculation of the temperature history by the computer program ATHENAN of a plug made of the cementitious mixture PSU 82-022 within the granite borehole. The parameters varied were the conductivity and the diffusivity of the cementitious plug and the granite, the heat transfer coefficients between the granite and the surrounding air, and the size of the granitic specimen keeping the geometric proportions constant. Three different values were used for each parameter by the program ATHENAN, while the other parameters were kept constant at their experimental values as in the previous section. The results of these three calculations, namely the temperature versus time for nodal points 5 (near the center of the plug) and 50 (near the center of the granite mass) were plotted in two separate graphs and are shown in Figure 5. The variation of the magnitude of the thermal effects caused by the variation of the borehole diameter is shown in Figure 6. It can be seen that the lower the conductivity and the heat transfer coefficient, the higher the diffusivity and the larger the size, the greater the temperature rise.

It is obvious that by decreasing the heat transfer coefficient, the heat loss to the air surrounding the granite decreases, thus increasing the temperature of the borehole plug and the granite. Increase of the initial temperature of the cement further increases the heat production as shown in Figures 3 and 4, which consequently further increases the temperature rise.

VOL. 14 1984

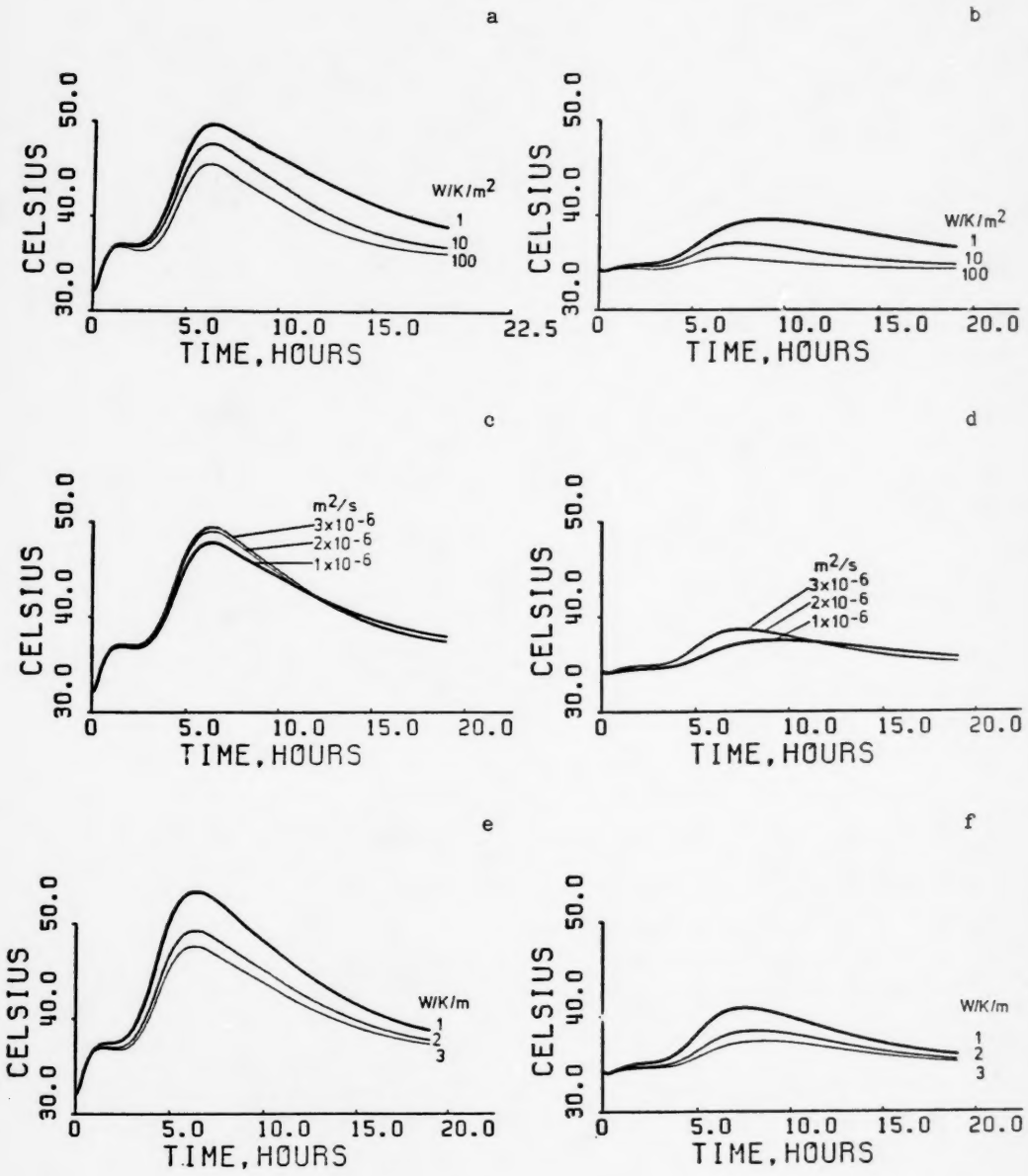

Fig. 5. Sensitivity analysis of the effects of conductivity and diffusivity of the cement mix PSU 82-022 and granite and of the heat transfer coefficient between the granite and the surrounding air (nodes 5 or 50) by the program ATHENAN. (a) Variation of the heat transfer coefficient, node 5. (b) Variation of the heat transfer coefficient, node 50. (c) Variation of the granite diffusivity, node 5. (d) Variation of the granite diffusivity, node 50. (e) Variation of the granite conductivity, node 5. (f) Variation of the granite conductivity, node 50.

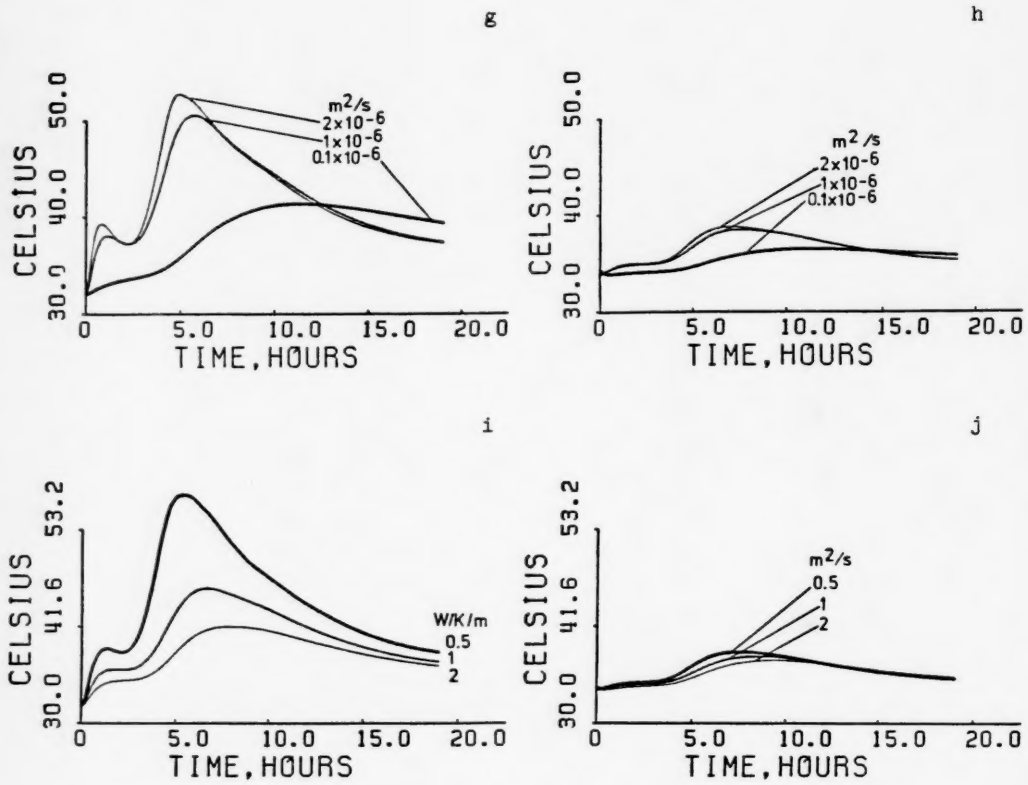

Fig. 5. (continued). (g) Variation of the cement diffusivity, node 5. (h) Variation of the cement diffusivity, node 50. (i) Variation of the cement conductivity, node 5. (j) Variation of the cement conductivity, node 50.

By increasing the diffusivity of the granite (while keeping the conductivity constant), the heat capacity is decreased which means that the rate of temperature rise within the granite is increased, given the same amount of heat, thus, creating higher temperatures within the granite. Higher temperatures within the granite means lower losses of heat from the plug to the granite; this increases the temperature of the plug which consequently further accelerates the heat production and elevates the temperature.

By increasing the diffusivity of the cementitious plug (while keeping the conductivity constant) higher temperatures are created within the plug, using the same argument as before; higher temperatures within the cementitious plug cause higher rate of heat production and therefore higher temperatures.

By decreasing the conductivity of the granite, conditions closer to adiabatic are created for the cementitious plug, thus increasing the temperature of the cement which consequently further increases the heat production. By decreasing the conductivity of the plug the heat flow is decreased and therefore also the losses from the cementitious plug. This increases the temperature of the cement which produces more heat thus raising

VOL. 14 1984

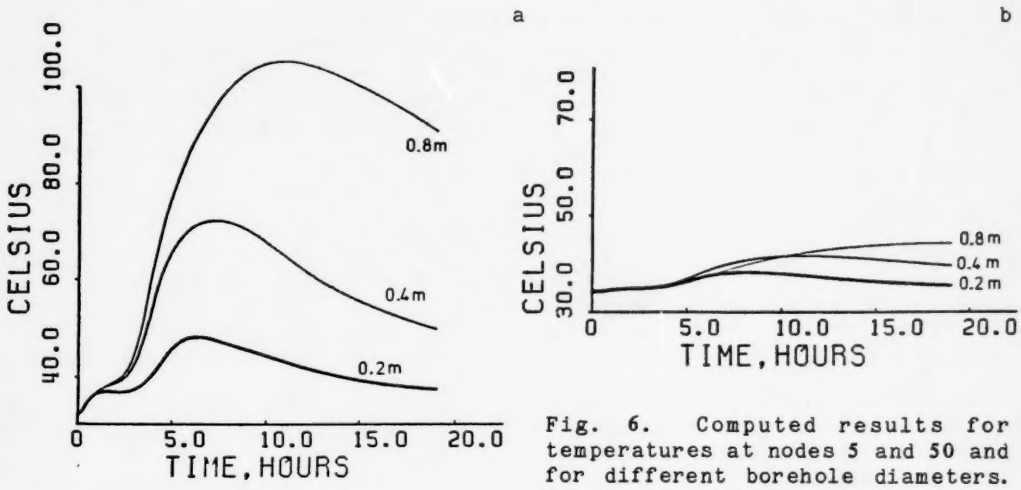

Fig. 6. Computed results for temperatures at nodes 5 and 50 and for different borehole diameters. (a) Node 5. (b) Node 50.

the temperature of the cement even more while the temperature of the granite varies a little.

By increasing the size, the ratio of the heat production to the heat loss of the cylindrical cementitious plug is generally increased, which can otherwise be expressed as the ratio of the volume to the area which increases linearly with the height or the diameter since the proportions remain constant. This increase in size or borehole diameter increases the heat production rate and decreases the losses of the cementitious plug which raises its temperature.

Of the parameters studied, the size of the borehole is possibly the most significant. It is obvious that for the given proportions of the granite and the initial conditions given in the previous section, the critical borehole diameter appears to be less than 0.8 m (Figure 6a), where the temperature at the center of the plug reaches about 100 degrees Celsius, which could cause cracking of the plug, if not adequately confined (6). Practically, it will be less than this, depending upon the stresses developed, and differential thermal expansion effects at the interface. It is obvious that with lower initial temperatures, the rate of temperature rise will be lower and the critical size could be increased. Lowering of the initial temperature of the cementitious mixture may be most easily achieved by lowering the temperature of its components before mixing. In critical areas cooling with liquid nitrogen has actually been used to maintain satisfactorily low temperature (7,8) when emplaced. The authors have stated elsewhere that a maximum acceptable temperature difference between the interior (hottest) and exterior (coolest) and a maximum of 10–20°C between new and old concrete are acceptable.

Of the other parameters the thermal conductivity of the cementitious plug is the most important followed by the conductivity of the rock and the diffusivity of the plug. For the given geometry of the borehole, thermal stresses developed during the course of hydration of the cementitious mixture may be reduced if the conductivity of the rock is higher, or by increasing the conductivity and the heat capacity (which decreases the diffusivity) of the

cementitious plug. Increase of the conductivity and the heat capacity may be achieved by decreasing the proportion of portland cement, increasing fly ash or slag components and more conductive and denser ingredients (inert components) such as quartz (9), or by decreasing the porosity of the hydrating paste. Use of cements with larger amounts of gypsum and aluminate phase which produce more ettringite to generate a positive expansion, producing better interfacial contact, and enhancing the conductivity (10).

Conclusions

It has been shown by using the program ATHENAN, that the most sensitive parameter (aside from the heat of hydration) for the temperature rise during the hydration of concrete cylindrical forms, or specifically of a cementitious plug in a borehole was the size of the hydrating cementitious mixture, and of lesser importance the thermal conductivities and diffusivities and the heat transfer coefficient. For the cementitious material PSU 82-022, a critical value for the diameter of 0.8 m was found for the given relative geometry and single lift emplacement conditions with an ambient temperature of 34°C so as to not generate temperatures above 100°C. The ATHENAN computer program can therefore be used to calculate the temperature history and the emplacement conditions of cementitious plugs. Studies in progress are considering the stress development and will be reported elsewhere.

Acknowledgements

This research was supported in part by the Office of Nuclear Waste Isolation and Sandia National Laboratory in studies performed for the isolation of commercial radioactive wastes.

VOL. 14 1984

References

1. J. Pommersheim and J.R. Clifton, Cements Research Progress, published by the American Ceramic Society, Columbus, OH, Ch. 13, 281 (1979).
2. C. Gotsis, ATHENAN: Axisymetric Thermal Nonlinear Analysis--A Computer Program for Cements and Other Chemically Reactive Cylindrical Domains and Associated Computer Graphics Algorithms, Doctoral Dissertation, The Pennsylvania State University, May (1984).
3. D.M. Roy, B.E. Scheetz, C.A. Langton, and M.W. Grutzeck, Selection and Durability of Seal Materials for a Basalt Repository. Preliminary Studies. MRL-C/PSU-022, Materials Research Laboratory, The Pennsylvania State University, University Park (1982).
4. C. Gotsis, H.A. McKinstry, and D.M. Roy, Axisymetric Thermal Nonlinear Analysis in Chemically Reactive Cylindrical Domains by the Computer Program ATHENAN, submitted for publication (1984).
5. J.R. Welty, C.E. Wicks, and J.E. Wilson, Fundamentals of Momentum, Heat and Mass Transfer, John Wiley and Sons (1976).
6. L.A. Emelity, Los Alamos Scientific Laboratory, Los Alamos, New Mexico, personal communication (April 13, 1981).
7. K. Roger Henriksen, Avoidance of Cracking at Construction Joints Between Solid Concrete Sections, Nordisk Betons, Vol. 1, 3-11 (1983).
8. G.M. Idorn and K.R. Henriksen, Cem. Concr. Res. 14 (4), 463 (1984).
9. A.A. Rousan and D.M. Roy, A Thermal Comparator Method for Measuring Thermal Conductivity of Cementitious Materials, Ind. Eng. Chem. Prod. Res. Dev., Vol. 22, No. 2 (1983).
10. M.W. Grutzeck and D.M. Roy, Experimental Characterization of Salt and Non-Salt Containing Grouts and Mortars, Office of Nuclear Waste Isolation, Battelle Memorial Institute, Columbus, OH (1984).

CEMENT and CONCRETE RESEARCH. Vol. 14, pp. 855-865, 1984. Printed in the USA.
0008-8846/84 $3.00+00. Copyright (c) 1984 Pergamon Press, Ltd.

EIN VERFAHREN ZUR BERECHNUNG DER BETONFESTIGKEIT UNTER SCHWELLENDEN BELASTUNGEN

Dr.-Ing. Kazimierz Furtak
Technische Hochschule Kraków, Polen
In der Zeit vom 30.12.82 bis 30.09.83 als Stipendiat des Deutschen Akademischen Austauschdienstes bei Prof.Dr.-Ing. E. Grasser; Institut für Bauingenieurwesen III, Fachgebiet Massivbau, TU München

(Communicated by F.H. Wittmann)
(Received March 1, 1984)

ABSTRACT

The paper gives a method to determine the fatigue compressive strength of concrete at a given number of cyclic loads, β_{Ni}. A parameter D is introduced, which takes into account microcrack development in concrete, depending on the critical stresses. The influence of the loading frequency on the fatigue strength is taken into account.

Einführung und Problemstellung

Wiederholte Belastungen führen bei Baustoffen zu den bekannten Ermüdungserscheinungen, die im allgemeinen auf Strukturveränderungen im Mikrobereich zurückzuführen sind. Aufgrund seines extrem inhomogenen Aufbaues weist der Beton lokale Spannungs- und Verformungsspitzen auf, welche schon vor der Erstbelastung ein beachtliches Ausmaß, bis hin zur Mikrorißbildung, annehmen können (1, 2).

Die in der Literatur bekannten Gleichungen zur Ermittlung der Ermüdungsfestigkeit des Betons berücksichtigen diese Strukturveränderungen nicht. Die Formeln beschreiben nur empirisch die Ergebnisse von Untersuchungen und können nicht auf spezielle Betonarten (z.B. Faserbeton) oder auf extreme Bedingungen (Temperatureinflüsse) übertragen werden, da sie den Einfluß der betontechnologischen Faktoren nicht berücksichtigen. Diese angesprochenen Faktoren beinflussen aber die unterschiedlichen Verläufe der Strukturzerstörung, d. h. die Entstehung und Entwicklung von Mikrorissen im Betongefüge. Die Bildung von Mikrorissen wiederum beeinflußt entscheidend die Ermüdungsfestigkeit β_N in Abhängigkeit von der Anzahl der wiederholten Belastungen N.

Im folgenden werden die kritischen Spannungen σ_I und σ_{II} definiert. Sie sind in Abhängigkeit von der Betonzusammensetzung (3, 4) und den Randbedingungen des Erhärtungsprozesses (3, 4, 5) logische Grenzwerte bei der Bestimmung der Ermüdungsfestigkeit.

Als σ_I wird diejenige Spannung definiert, bei welcher die vor der Belastung bestehende Anzahl von Mikrorissen noch nahezu unverändert bleibt bzw. deren Länge und Klaffung sich nur unbeträchtlich vergrößert. Das Überschreiten dieser Spannung verursacht eine stetige, aber stabile Entwicklung der Mikrorisse.

Die kritische Spannung σ_{II} verursacht ein Verbinden der Mikrorisse zu zusammenhängenden Ketten, welche durch den Zementstein, manchmal auch durch die Körner des Zuschlagstoffes, meistens aber entlang deren Berührungszonen verlaufen. Ab dieser Spannung entwickeln sich die Mikrorisse und Risse bis zur völligen Zerstörung des Betons, und zwar unabhängig davon, ob die Belastung sich vergrößert oder nicht. Die Betonzerstörung ist dann nur noch von der Einwirkungszeit der Belastung abhängig.

Die so definierten kritischen Spannungen können als die Meßgrößen des Strukturzustandes (1, 3, 6) angesehen und unter anderem durch die Messung der Quer- und Längsverformungen bestimmt werden. Dabei sollten u.a. die in Bild 1 vorgestellten Kriterien angewandt werden.

In dieser Arbeit wird ein Vorschlag für die Berechnung der Betonfestigkeit nach beliebigen Lastspielen $N_i < N$ vorgestellt. Die Berücksichtigung der Geschwindigkeit von Belastungsveränderungen ist möglich. Die angegebenen Lösungen werden durch die Ergebnisse von fremden und eigenen Untersuchungen bestätigt.

VOL. 14 1984

Die Ermüdungsfestigkeit des Betons

Grundlage für die Beschreibung der Ermüdungsfestigkeit des Betons ist der von J.L.van Ornum und anderen Forschern festgestellte nichtlineare Zusammenhang von β_N - logN. Es wurde die exponentielle Kurve

$$\beta_N/\beta_c = CN^{-A}(1 + BR \log N)\, C_f \qquad (1)$$

mit $R = \sigma_{min}/\sigma_{max}$ angenommen.

Der Faktor C berücksichtigt hierin die erhöhte Betonfestigkeit unter dynamischer Belastung im Vergleich zur statischen Belastung. Nach (7) kann C = 1,16 angenommen werden.

Durch den Faktor C_f wird der Einfluß der Belastungsgeschwindigkeit berücksichtigt. Dieser wird im allgemeinen wie folgt berechnet:

$$C_f = 1 + a(1 - bR) \log f \qquad (2)$$

Dabei ist f die Belastungsfrequenz [Hz], a und b sind konstante Koeffizienten. Mit a = 0,07 und b = 1,00 ergibt sich der Faktor C_f zu

$$C_f = 1 + 0{,}07(1 - R) \log f \qquad (3)$$

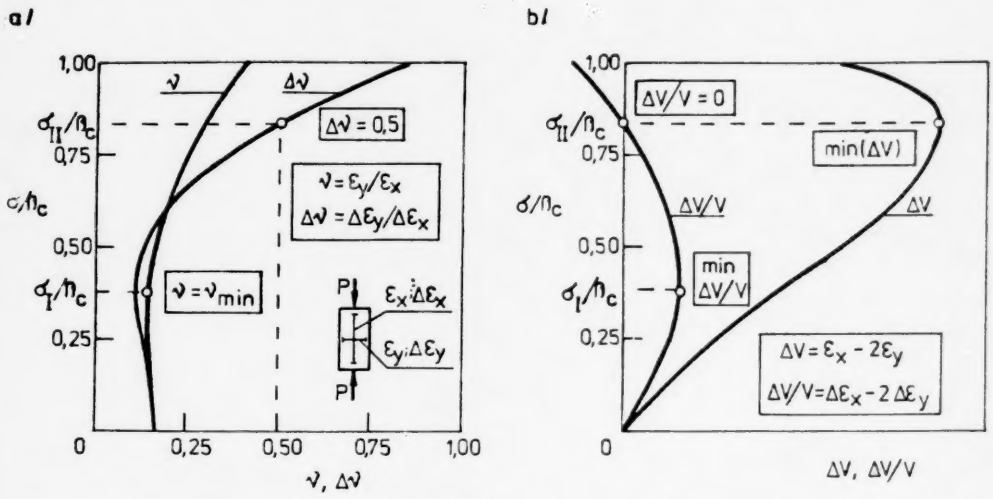

Bild 1

Kriterien zur Ermittlung der kritischen Spannungen

Die Werte a und b wurden so festgelegt, daß bei einer Würfeldruckprüfung $C \cdot C_f = 1$ ist.

Nach (8, 9, 10) wird mit t = 10 Jahren eine maßgebliche Zeitgrenze gesetzt, ab der bei konstanter Belastung keine Strukturveränderungen des Betongefüges mehr zu erwarten sind. Mit der Grundfrequenz von f = 1Hz errechnen sich damit $N = 3{,}15 \cdot 10^9$ Lastwechsel (logN = 9,5).

Die Variablen A und B werden durch die kritischen Spannungen beschrieben. Setzt man die Ermüdungsfestigkeit β_N(R = 0, f = 1Hz, logN = 9,5) gleich der kritischen Spannung σ_I und die Dauerfestigkeit β_N(R ≃ 1, logN = 9,5) gleich der kritischen Spannung σ_{II}, dann ergibt sich

$$A = 0{,}008 - 0{,}118 \log(\sigma_I/\beta_c) \qquad (4)$$

$$B = 0{,}118(\sigma_{II}/\sigma_I - 1) \qquad (5)$$

Hierbei ist β_c die statische Betonfestigkeit.

Nach (3) bis (6) und (9) ist $\sigma_I = (0{,}35 \div 0{,}55)\beta_c$ und $\sigma_{II} = (0{,}70 \div 0{,}90)\beta_c$. Dabei ergeben die Mittelwerte $\sigma_I = 0{,}45\beta_c$ und $\sigma_{II} = 0{,}80\beta_c$ gute Näherungswerte. In den eigenen Untersuchungen (3, 4) wurden die Mittelwerte $\sigma_I = 0{,}453\beta_c$ und $\sigma_{II} = 0{,}790$ beobachtet. Die Untersuchungen wurden an Betonzylindern (Ø 15 cm, h = 30 cm) der Festigkeitsklasse B 25 (Mittelwert $\beta_c = 27{,}0$ MN/m^2) durchgeführt.

Die ausführliche Analyse der Untersuchungsergebnisse ergab eine nichtlineare Abhängigkeit β_N - R. Die Annahme einer linearen Beziehung β_N - R in Gleichung (1) bewirkt jedoch nur einen vernachlässigbaren Fehler.

Der Verlauf der Strukturzerstörung im Beton

Nach (6) kann die Rißentwicklung im Beton durch die Veränderung des Querdehnungskoeffizienten $\Delta\nu$ beschrieben werden ($\Delta\nu = \Delta\varepsilon_y/\Delta\varepsilon_x$; $\Delta\varepsilon_x$ und $\Delta\varepsilon_y$ sind die Längs- und Querverformungsänderungen bei einem Kraftzuwachs von ΔP). Die Abhängigkeit $\Delta\nu$ von der Spannung σ wird im Bild 2 dargestellt.

Im Bereich $\sigma = 0$ bis $\sigma = \sigma_I$ nimmt $\Delta\nu$ in etwa den konstanten Wert $\Delta\nu_I$ an. Zwischen σ_I und σ_{II} vergrößert sich auch $\Delta\nu$ von $\Delta\nu_I$ auf $\Delta\nu_{II}$. Der Spannung σ_o ($\sigma_I < \sigma_o < \sigma_{II}$) entspricht $\Delta\nu = \Delta\nu_o$. Für σ_{II} gilt definitionsgemäß immer $\Delta\nu = \Delta\nu_{II} = 0{,}5$. Der Wert $\Delta\nu = \Delta\nu_k$ wird bei der Bruchlast erreicht. Nach (11) ist $\Delta\nu_k = 1{,}0$. Eine genaue Berechnung ist nach Formel (9) möglich.

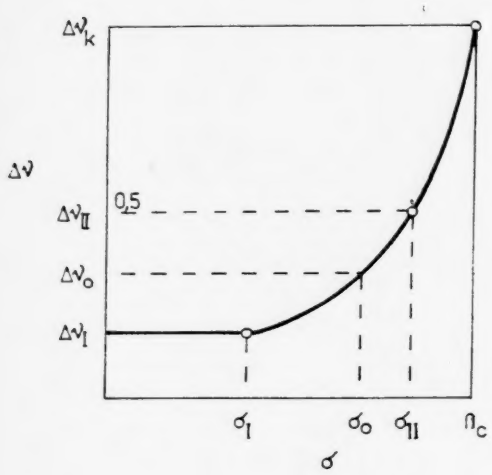

Bild 2 Abhängigkeit zwischen $\Delta\nu$ und σ

Die mit der Schwingungsobergrenze $\sigma_{max} = \sigma_o$ wiederholten Belastungen bewirken eine Vergrößerung des Wertes $\Delta\nu$ von $\Delta\nu_o$ bis zum Wert $\Delta\nu_k$, welcher nicht nur bei der Bruchlast unter statischer Belastung, sondern auch nach N Lastwechseln erreicht wird. Nach (11) wird angenommen, daß der Zuwachs $\Delta\nu$ um $d\Delta\nu$ proportional zu $\Delta\nu$ und dN ist:

$$d\Delta\nu = B_1\, \Delta\nu\, dN \qquad (6)$$

Durch Lösung der Gleichung (6) und nach Einsetzen der Bedingungen $\Delta\nu = \Delta\nu_o$ für $N_i = 1$ und $\Delta\nu = \Delta\nu_k$ mit N_i und N errechnet sich

$$\Delta\nu = \Delta\nu_o (\Delta\nu_k/\Delta\nu_o)^{N_i/N} \qquad (7)$$

Der Wert $\Delta\nu_o$ in Gleichung (7) kann in Abhängigkeit von dem Spannungswert σ_o folgendermaßen bestimmt werden:

Die exponentielle Abhängigkeit für den Spannungszuwachs von σ_I auf σ_{II} sei in der Form

$$\Delta\nu = B_2\, \Delta\nu_I\, e^{B_3\sigma} \qquad (8)$$

gegeben. Mit den Bedingungen $\Delta\nu = \Delta\nu_I$ für $\sigma_o = \sigma_I$ und $\Delta\nu = \Delta\nu_{II}$ für $\sigma_o = \sigma_{II}$ erhält man:

$$\Delta\nu_o = \Delta\nu_I (\Delta\nu_{II}/\Delta\nu_I)^{\gamma} \qquad (9)$$

worin

$$\gamma = \frac{\sigma_o - \sigma_I}{\sigma_{II} - \sigma_I} \qquad (10)$$

ist.

VOL. 14 1984

Der Grenzwert der Lastwechsel N kann mit Hilfe der Gleichung (1) berechnet werden.

Für die Abschätzung der Rißentwicklung ist es zweckmäßig, D quasi als Maß dieser Strukturzerstörung einzuführen. D wird durch die Gleichung

$$D = \frac{\Delta\nu - \Delta\nu_I}{\Delta\nu_k - \Delta\nu_I} \tag{11}$$

definiert und erfüllt folgende Bedingungen:
Für $N_i = 1$ und $\sigma = \sigma_I$ ist $\Delta\nu = \Delta\nu_I$ und $D = O$,
für $N_i = N$ ist $\Delta\nu = \Delta\nu_k$ und $D = 1$.

Dadurch ergibt sich die Möglichkeit, die Größe D als Kenngröße für die irreversible Rißstruktur des Betons unter konstanten oder veränderlichen Belastungen zu benutzen.

Durch Einsetzen von (7) und (9) in (11) erhält man die Gleichung

$$D = (D_1 + d_a)\ (\Delta\nu_k/\Delta\nu_o)^{N_i/N} - d_a \tag{13}$$

mit

$$d_a = \frac{\Delta\nu_I}{\Delta\nu_k - \Delta\nu_I} \tag{14}$$

Nimmt man die Gültigkeit der Gleichung (9) auch für den Spannungszuwachs im Bereich $\sigma_{II} < \sigma_o < \beta_c$ an, so ergibt sich

$$d_a = \frac{1}{(\Delta\nu_{II}/\Delta\nu_I)^{\gamma} - 1} \tag{15}$$

Der Exponent wird dabei nach Gleichung (10) mit $\sigma_o = \beta_c$ berechnet. Die gegebenen Lösungen sind für den Spannungszuwachs $O \leq \sigma_o < \sigma_I$ nicht exakt. Bei derart niedrigen Spannungen wird angenommen, daß auch häufige Lastwechsel keine nennenswerte Mikrorißentwicklung hervorrufen.

Die Betonfestigkeit nach beliebigen Lastwechseln

Die Entstehung und die Entwicklung der Strukturstörungen bei wiederholten Belastungen bewirken einen stetigen Verlust der effektiven Betonfläche und damit die Abnahme seiner Festigkeit. Diese Abnahme ist, ähnlich wie der Zuwachs $d\Delta\nu$, proportional der Anfangsfläche zum Zuwachs der Lastwechsel. Im einfachsten Fall der linearen Abhängigkeit der Betonfestigkeit β_{N_i} (mit Lastwechsel N_i) von D ergibt sich

$$\beta_{N_i} = k\ D + m \tag{16}$$

Nach Erfüllung der Randbedingungen:
$\beta_{N_i} = \beta_c$ für $D = O$,
$\beta_{N_i} = \beta_N = \sigma_{max}$ für $D = 1$ $(N_i = N)$
bekommt man

$$\beta_{N_i}/\beta_c = \beta_c - \sigma_{max}) \; D \tag{17}$$

oder

$$\beta_{N_i}/\beta_c = 1 - (1 - \kappa) \; D \tag{18}$$

Die Abnahme der Festigkeit des Betons nach dem N_i-ten Lastwechsel ist gleich

$$\Delta\beta_c = (\beta_c - \sigma_{max}) \; D \tag{19}$$

oder

$$\Delta\beta_c/\beta_c = (1 - \kappa) \; D \tag{20}$$

Untersuchungen mit den angegebenen Lösungen

Die Ermüdungsfestigkeit

Die angegebenen Lösungen werden anhand fremder und auch eigener Versuche in den Bildern 3 bis 12 dargestellt. Die Faktoren A und B errechneten sich mit $\sigma_I = 0{,}45\beta_c$ und $\sigma_{II} = 0{,}80\beta_c$ zu A = 0,049 und B = 0,092.

Im folgenden sind die wichtigsten Daten zu den eigenen Versuchen aufgeführt: Betonfestigkeitsklasse B 25; $\beta_c = 26{,}19 MN/m^2$; W/Z = 0,5; κ = 0,60 und 0,75; R = 0,3; f = 6,67 und 15,00 Hz.

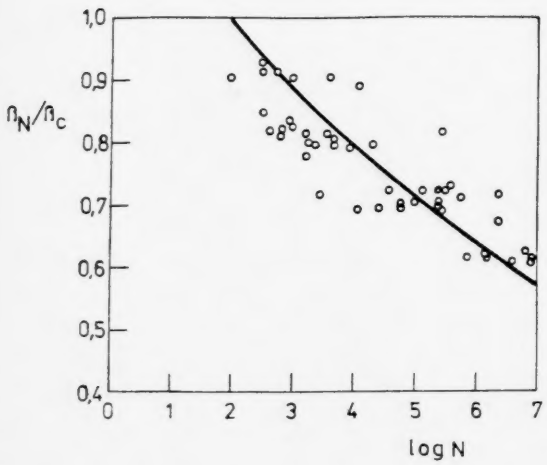

Bild 3

Untersuchungsergebnisse nach Antrim und McLaughlin (13)

Die Werte der kritischen Spannungen wurden durch Messung der Quer- und Längsverformungen an Betonzylindern (Ø 15 cm, h = 30 cm) bestimmt:
- Für den bei geringer Temperatur erhärteten Beton (-3° C - +2°C) ist $\sigma_I = 0{,}23 \; \beta_c$ und $\sigma_{II} = 0{,}72 \; \beta_c$,
- für den thermisch beeinflußten Beton ist $\sigma_I = 0{,}34 \; \beta_c$ und $\sigma_{II} = 0{,}76 \; \beta_c$.

Ausgedehnte Erkenntnisse über den Einfluß geringer Temperaturen während der Erhärtungsphase auf die Werte der kritischen Spannungen können aus den Untersuchungsergebnissen von M. Rybiański gewonnen werden. Für den unter Frost (-1° C) erhärteten Beton erhielt er $\sigma_I = 0{,}185\beta_c$ und $\sigma_{II} = 0{,}750 \; \beta_c$.

VOL. 14 1984

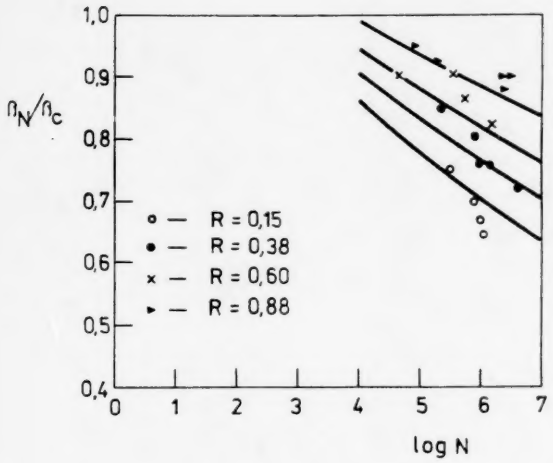

Bild 4

Untersuchungsergebnisse nach Assimacopoulos, Warner und Ekberg (14)

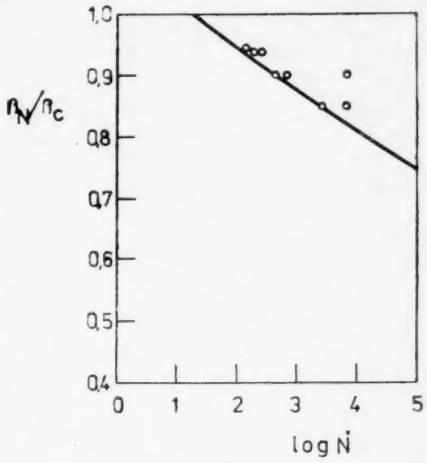

Bild 5

Untersuchungsergebnisse nach Awad und Hilsdorf (15)

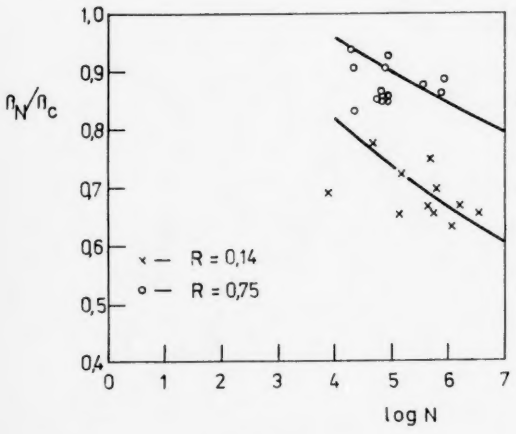

Bild 6

Untersuchungsergebnisse nach Gaede (16)

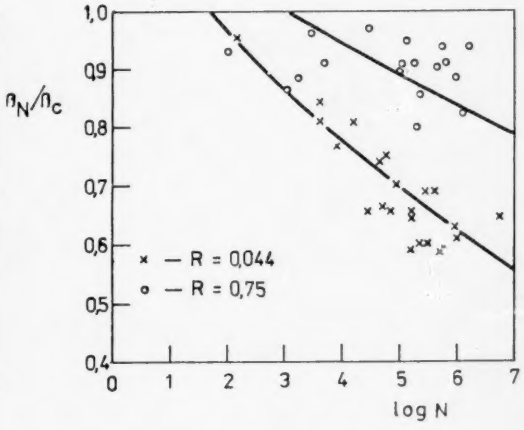

Bild 7

Untersuchungsergebnisse nach Graf und Brenner (12)

Untersuchungen über den Einfluß von thermischer Beeinflussung sind dem Verfasser nicht bekannt.

Die Ergebnisse der eigenen Untersuchungen werden in den Bildern 10 und 11 dargestellt. Die nicht aufgrund der Dauerschwellbelastung zerstörten Versuchskörper sind mit einem Pfeil gekennzeichnet. Zum Vergleich ist auch die Kurve für Beton, der unter normalen Bedingungen erhärtet ist, eingezeichnet.

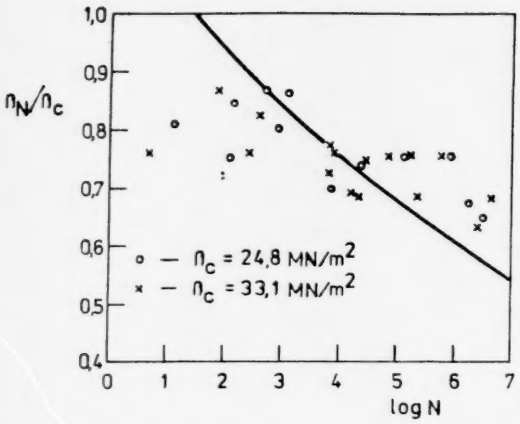

Bild 8

Untersuchungsergebnisse nach Kesler (17)

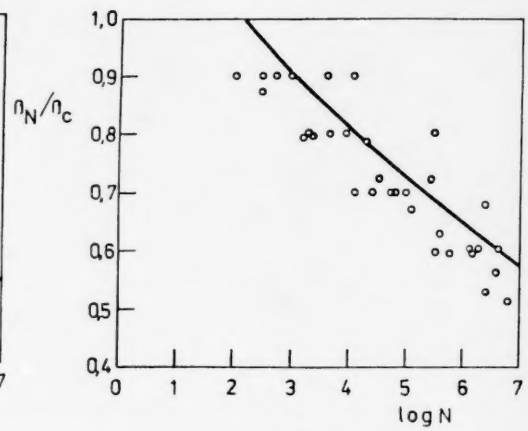

Bild 9

Untersuchungsergebnisse nach Korcynskij und Bieczeniewa (7)

Die in Bild 11 dargestellten Versuchsergebnisse zeigen eindeutig, daß die Temperatur während der Betonerhärtungsphase einen Einfluß auf die Ermüdungsfestigkeit hat. So ergeben die bei niedrigen Temperaturen erhärteten Versuchskörper auch die kleinsten Werte der kritischen Spannungen σ_I und σ_{II}.

Eine deutliche Steigerung der Ermüdungsfestigkeit für Faserbeton beobachtete S. Sasiadek (18) bei seinen Untersuchungen. Diese bestätigen die Abhängigkeit zwischen β_N und den kritischen Spannungen. Für diese Betonart sind σ_I und σ_{II} höher als für den

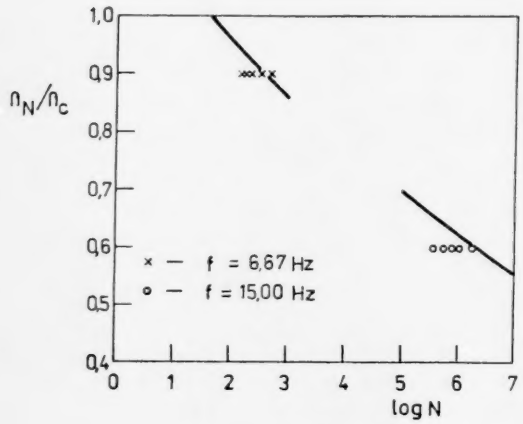

Bild 10

Eigene Untersuchungsergebnisse der Ermüdungsfestigkeit des Betons

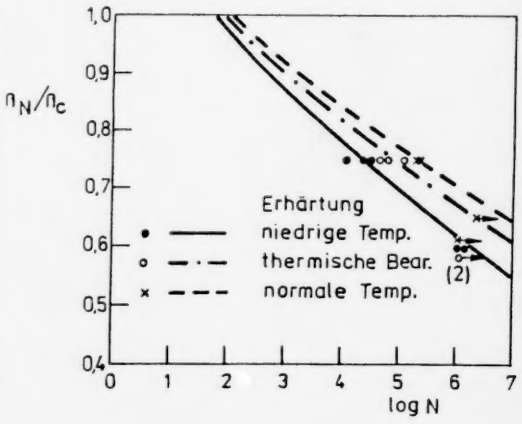

Bild 11

Untersuchungsergebnisse der Ermüdungsfestigkeit des bei niedrigen Temperaturen erhärteten oder thermisch beeinflußten Betons

VOL. 14 1984

normalen Beton, da die fein verteilten Stahlfasern die Entstehung, vor allem aber die Entwicklung von Mikrorissen und Rissen in der Betonstruktur behindern. W. Freitag hat in seiner Arbeit (19) festgestellt, daß die Ermüdungsfestigkeit von der Betonfestigkeit abhängt. Eine Zunahme der Betonfestigkeit führt auch zu einer Zunahme der bezogenen Ermüdungsfestigkeit. Eine ähnliche Tendenz wurde früher für die kritischen Spannungen bemerkt (6).

Versuche zur Ermittlung der Betonfestigkeit nach beliebigen Lastwechseln

Auf diesem Gebiet wurde ein Vergleich der Theorie mit Versuchsergebnissen anhand eigener Untersuchungen vorgenommen. Die Versuchskörper waren Betonwürfel (a = 15cm) mit einer Festigkeit von 24,74 MN/m^2 bis 31,89 MN/m^2. In Bild 12 sind die Ergebnisse dargestellt. Die theoretische Kurve wurde für f = 6,67 Hz gezeichnet.

Die in Bild 12 dargestellten theoretischen Kurvenverläufe stehen im Einklang mit den Untersuchungsergebnissen. Eingezeichnet wurde dabei für $N \geq 10^6$ jedes Ergebnis, für $N = 5 \cdot 10^5$ der Mittelwert aus 4 Versuchen und für $N = 10^5$ der Mittelwert aus 6 Versuchen.

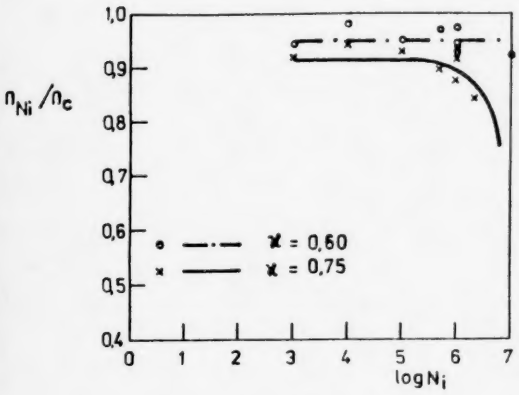

Bild 12

Festigkeit des Betons nach beliebigen Lastwechseln N_i

Bemerkungen und Schlußbetrachtungen

In der Arbeit wurden Möglichkeiten zur Beschreibung der Ermüdungsfestigkeit des Beton $ß_N$ und der Betonfestigkeit $ß_{Ni}$ nach beliebigen Lastwechslen N_i angegeben. Mit dem Wert D wurde ein Kriterium zur Berücksichtigung der Rißentwicklung eingeführt, für das ebenso wie für die Betonfestigkeitswerte $ß_N$ und $ß_{Ni}$ ein Zusammenhang mit den kritischen Grenzspannungen besteht. Es wurde auch der Einfluß der Belastungsfrequenz f berücksichtigt.

Die angegebenen Lösungen wurden mit fremden und eigenen Versuchen verglichen. Wie die Bilder 3 bis 12 zeigen, stehen die theoretischen Kurven in gutem Einklang mit den Versuchsergebnissen. Dies trifft auch für Untersuchungen an Beton zu, der während der Erhärtung niedrigen Temperaturen unterworfen war.

Der Verfasser dankt Herrn Dipl.-Stat. W. Kruse und Herrn Dipl.-Ing. I. Nissen für die Hilfe bei der Übersetzung herzlich.

Literatur

1. S.P. Shah und O.F. Slate, Internal microcracking, mortar aggregate bond and the stress-strain curve of concrete, Proc. of an Inter. Conf., The Structure of Concrete, London, Sept. 1965.
2. M. Dantu, Etude des contraintes dans les milieux heterogenes. Application an Beton, Annales de l'Inst. Techn. du Batiment et des Travaux Publics, No 121, Janvier 1958.
3. K. Flage und K. Furtak, Significance of technological factors in the course of stress destruction in concrete, Third national conf. with inter. participation on "Mechanics and Technology of Composite Materials", Warna 1982.
4. K. Furtak, Wpływ mikrodefektów strukturalnych w betonie na pracę mostowych belek żelbetowych (Einfluß struktureller Mikrorisse im Beton auf die Verformung der Stahlbetonbrückenbalken), Diss., Kraków 1979.
5. M. Rybiański, Wytrzymałość i odkształcalność betonu poddanego oddziaływaniu obniżonych temperatur (Festigkeit und Verformbarkeit des unter geringen Temperaturen erhärteten Betons), Diss. Wrocław 1976.
6. O.J. Berg, Fizyczeskije osnowy teorii procznosti bietona i żelezobietona (Physikalische Grundlage der Theorie der Festigkeit des Betons und des Stahlbetons), Gosstrojizdat, Moskwa 1961.
7. J.L. Korczynskij und G.W. Bieczeniewa, Procznost stroitielnych materiałow pri dinamiczeskich nagruženijach (Festigkeit von Baumaterialien unter dynamischen Belastungen), Literatura po stroitielstwu, Moskwa 1966.
8. T.T.C. Hsu, Fatigue of Plain Concrete, ACI Journal, Vol.78, July-August 1981.
9. P. Desayi und C.S. Viswanatha, True Ultimate Strength of Plain Concrete, Bulletin RILEM, 36/1976.
10. H. Rüsch, Physikalische Fragen der Betonprüfung. Zement-Kalk-Gips, 1/1959.
11. W.P. Czirkow, Uczet niesimmietricznych cikłow pri rasczetie resursa żelezobietonnych bałok niebolszich proletow (Berücksichtigung unsymmetrischer Belastungszylklen für die Ermittlung der Lebensdauer von Stahlbetonbalken), Trudy MIIT, wypusk 430, Moskwa 1973.
12. O. Graf und E. Brenner, Versuche zur Ermittlung der Widerstandsfähigkeit von Beton gegen oftmals wiederholte Druckbelastung, Deutscher Ausschuß für Eisenbeton, H. 76/1934 und H. 83/1936.
13. J. deC. Antrim und J.F. Mc Laughlin, Fatigue Study of Air-Entrained Concrete, ACI Journal, Vol. 55, May 1959.
14. B.M. Assimacopoulos, R.F. Warner und C.E. Ekberg, High Speed Fatigue Tests on Small Specimens of Plain Concrete, Prestressed Concrete Institute, Journal, Vol. 4, No. 2, Sept. 1959.

VOL. 14 1984

15. M.E. Awad und H.K. Hilsdorf, Strength and Deformation Characteristics of Plain Concrete Subjected to High Repeated and Sustained Load. Civil Engineering Studies, Structural Research Series, No. 372, Department of Civil Engineering, University of Illinois, Urbana, Febr. 1971.

16. K. Gaede, Versuche über die Festigkeit und die Verformung von Beton bei Druck- Schwellbeanspruchung, Deutscher Ausschuß für Stahlbeton, H. 144/1962.

17. C.E. Kesler, Effect of Speed of Testing on Flexural Fatigue Strength of Plain Concrete, Proc., Highway Research Board, Vol. 32, 1953.

18. S. Sasiadek, Odporność zmęczeniowa betonu drobnoziarnistego z dodatkiem włókien stalowych (Ermüdungswiderstand des Faserbetons) Diss., Kraków 1980.

19. W. Freitag, Das Ermüdungsverhalten des Betons, Stand der Kenntnisse und der Forschung, Beton, 5/1970.

L.
4
84

CEMENT and CONCRETE RESEARCH. Vol. 14, pp. 866-872, 1984. Printed in the USA.
0008-8846/84 $3.00+00. Copyright (c) 1984 Pergamon Press, Ltd.

STUDY OF THE SYSTEM $CaO-SiO_2-CO_2-H_2O$ IN RELATION TO SCAWTITE UNDER HYDROTHERMAL CONDITIONS

I. Kaprálik, L. Števula, J. Petrovič, and F. Hanic
Institute of Inorganic Chemistry
Centre of the Chemical Research, Slovak Academy of Sciences,
Dúbravská cesta, 842 36 Bratislava, Czechoslovakia

(Communicated by Z. Šauman)
(Received Feb. 17; in final form Sept. 4, 1984)

ABSTRACT

Hydrothermal studies showed the location of scawtite in the narrow internal tetrahedron foshagite-xonotlite-CO_2-H_2O of the system $CaO-SiO_2-CO_2-H_2O$ and its compatibility with the calcium silicate hydrates in the 4-phase assemblages. The phase assemblages in this region involve scawtite, foshagite, xonotlite, tobermorite, hillebrandite, calcite and silica. The carbonation series of the 4-phase assemblages were determined in the sections $C_4S_3-CO_2-H_2O$ ($C_4S_3 = 4CaO.3SiO_2$), $C_7S_6-CO_2-H_2O$ and $C_6S_6-CO_2-H_2O$ at 473 K and saturated steam pressure in dependence on the CO_2 content. The carbonating influence of CO_2 takes place in the volume of the $CaO-SiO_2-CO_2-H_2O$ system up to the CO_2 concentration limited by the calcite-silica-H_2O triangle. Above this CO_2 content, carbon dioxide appears in a gaseous form together with gaseous H_2O in the 4-phase assemblage calcite-silica-CO_2H_2O. The instability of scawtite under the CO_2 excess ($CO_2/C_7S_6 > 1$) is influenced by its structural arrangement. The present channels enable penetration of CO_2 molecules into the structure and formation of carbonated phases.

VOL. 14 1984

Introduction

Scawtite, $7CaO.6SiO_2.CO_2.2H_2O$, is the only known quarternary phase in the system $CaO-SiO_2-CO_2-H_2O$. For a long time, the formula $CaO.SiO_2.H_2O$ was proposed for this compound (1), later described as CSH(A) (2). McConnel (3) and Mudroch (4) suggested from crystallographic examination, that CSH(A) is very similar to the natural mineral, scawtite. Buckner, et al. (5), established the identity of the phase CSH(A) occuring in the system $CaO-SiO_2-CO_2-H_2O$ at low partial pressures of CO_2 with scawtite. Harker (6) confirmed the previous report (5) by successful synthesis of the compound of composition $7CaO.6SiO_2.CO_2.2H_2O$ ($C_7S_6CO_2H_2$). He localized the scawtite composition in the section wollastonite-calcite-H_2O and he established the existence of scawtite in the phase assemblages of the system $CaO-SiO_2-CO_2-H_2O$. The formation of scawtite in the system $CaO-SiO_2-CO_2-H_2O$ under hydrothermal conditions, is treated in several papers (7-12). The compound has been studied widely because of its potential influence on hydration reactions.

This work studies the influence of CO_2 on the formation of scawtite and its

phase relations within the system $CaO-SiO_2-H_2O-CO_2$ at 493 K and staurated steam pressures.

Experimental

The samples of stoichiometric composition were prepared in the form of water suspensions (1:10) from SiO_2 (natural mineral from Brazil, SiO_2 99.8 wt.%), NH_4HCO_3 (analytical grade) and CaO (from $CaCO_3$, analytical grade, by decarbonation at 1273 K for 3 h). The homogenized mixtures were placed in the teflon capsules which were then enclosed in the hermetic pressure cylinder. The hydrothermal synthesis ran for 7 days at 413-473 K.

The crystalline products of the hydrothermal syntheses were identified by X-ray phase analysis. The powder diffraction records were taken on a powder diffractometer Philips 1540 using CuKα radiation and goniometer rate 1° 2θ/min.

Hydrothermal synthesis of scawtite in the section $7CaO.6SiO_2-CO_2-H_2O$ of the system $CaO-SiO_2-CO_2-H_2O$ at 413-573 K

Harker (6) synthetized scawtite from the mixture of silica and CaO in the proportions required for $7CaO.6SiO_2.2CO_2$, $7CaO.6SiO_2.CO_2$, or $7CaO.6SiO_2$ at elevated temperatures and pressures for varying times up to four weeks. He found that total pressure had little effect on the formation of scawtite whose formation was restricted to temperatures between 413 and 573 K. Pure scawtite could only be prepared by using $Ca(OH)_2$, silica and stoichiometric amount of CO_2 dissolved in the excess water. At lower temperatures, tobermorite and calcite appeared to be stable parts of the assemblages, and at higher temperatures, xonotlite and calcite (or wollastonite and calcite) were produced.

The present paper contains an account of studies on hydrothermal synthesis of scawtite from water suspensions of CaO, silica and CO_2 (from NH_4HCO_3), a mix of stoichiometric composition equivalent to $7CaO.6SiO_2.CO_2$ (molar ratio $CO_2/C_7S_6 = 1$) at temperatures between 413 and 573 K for 7 days according to the reaction scheme:

$$7CaO + 6SiO_2 + CO_2 + 2H_2O \rightarrow 7CaO.6SiO_2.CO_2.2H_2O \quad (1)$$

The products of reaction (1) identified by X-ray phase analysis are summarized in Table 1.

Table 1
Formation of the intermediate phases at the hydrothermal synthesis of scawtite at 413 - 473 K

Molar ratio CO_2 / C_7S_6	Heat treatment		X-ray analysis
	Temperature (K)	Time (days)	
1.0	413	7	T, CT, Q in trace quantities
1.0	433	7	Sc, T, CT
1.0	453	7	Sc, with some T
1.0	473	7	Sc

C = CaO, S = silica, T = tobermorite, CT = calcite, Q = quartz, and Sc = scawtite

The results given in Table 1 give evidence that scawtite is formed through the intermediate products, tobermorite and calcite, and the rate of reaction (1) depends only on temperature. Table 1 shows that pure scawtite could be prepared at temperatures 453 - 473 K.

Tobermorite, xonotlite and foshagite are the phases compatible with scawtite in the phase assemblages of the section $C_7S_6CO_2$-H_2O containing also the scawtite composition. These phases were synthetized at the same hydrothermal conditions (time, temperature) as scawtite. All three compounds were formed after 7 days heat treatment at 473 K. Tobermorite and xonotlite were produced most rapidly. Foshagite always was accompanied by a small amount of xonotlite. Tobermorite was identified as a metastable phase (in agreement with (13)), according to its slow transition to the stable xonotlite phase at temperatures above 423 K. The phase assemblages containing tobermorite may be therefore suggested as metastable systems at 473 K (14-18).

Section $7CaO.6SiO_2$-CO_2-H_2O at 473 K and saturated steam pressure

The composition of scawtite (6) is delimited within the section C_7S_6-CO_2-H_2O of the system CaO-SiO_2-CO_2-H_2O (Fig. 1). Harker (6) found that both synthetic and natural scawtites decomposed into calcite and amorphous SiO_2 when they were stirred in water solution saturated with CO_2 at 294 K. This result shows that scawtite is unstable in the presence of excessive CO_2.

In this connection, we investigated the phase equilibria in the water suspensions containing increasing ratio CO_2/C_7S_6 at 473 K and saturated steam pressure. The results of the X-ray phase analysis of the solid products are summarized in Table 2.

The results in Table 2 show that with increasing molar ratio CO_2/C_7S_6 from 1 to 7 at the excess of H_2O, there exist in the section C_7S_6-CO_2-H_2O carbonated series of the four compatible quarternary assemblages (Sc + Fo + Xo + H), (Sc + T + CT + H), (T + CT + S + H) and (CT + S + CO_2 + H) (Sc = scawtite, Fo = foshagite, Xo = xonotlite, H = H_2O, T = tobermorite, CT = calcite, S = silica). These phase assemblages are compatible with excess of H_2O in the apex of the phase triangle C_7S_6-CO_2-H_2O. Their stability fields are delimited by solid lines in Fig. 2, determined by scawtite composition and by three binary assemblages (T + 2CT), (7CT + 6S) and 2Fo + Xo). These three assemblages were determined from phase analysis of the products of hydrothermal reactions:

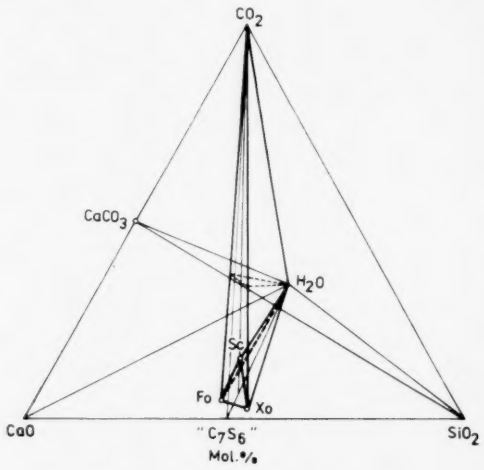

FIG. 1
System CaO-SiO_2-CO_2-H_2O showing location of scawtite in the internal region Fo-Xo-CO_2-H_2O. Fo - foshagite, Xo = xonotlite, Sc = scawtite.

$$C_7S_6H_2(CO_2) + CO_2 + 3H_2O \rightarrow C_5S_6H_5 + 2CaCO_3 \quad (2)$$

$$C_7S_6H_2(CO_2) + 6CO_2 + nH_2O \rightarrow 7CaCO_3 + SiO_2\ (colloid) \quad (3)$$

$$2C_7S_6 + 3H_2O \rightarrow 2C_4S_3H + C_6S_6H \quad (4)$$

as well as reaction (1). Reactions (2) and (3) agree with the known fact that scawtite is unstable in excess of CO_2 ($CO_2/C_7S_6 \geq 2$). The stability field of scawtite between the quarternary assemblages (Fig. 2) is therefore quite narrow. The content of calcium silicate hydrate phases decreases and the portion of car-

VOL. 14 1984

Table 2
Phase equilibrium data for the section C_7S_6-CO_2-H_2O in an excess of water

Molar ratio CO_2 / C_7S_6	Hydrotheral synthesis Temperature (K)	Time (days)	X-ray analysis
< 1	473	7	Sc, Fo, Xo
1	473	7	Sc
1 - 2	473	7	Sc, T, CT
2	473	7	T, CT
2 - 7	473	7	T, CT, S
7	473	7	CT, S
> 7	473	7	CT, S

C_7S_6 = $7CaO.6SiO_2$, Sc = scawtite, Fo = foshagite, Xo - xonotlite, T = tobermorite, CT = calcite, S = silica.

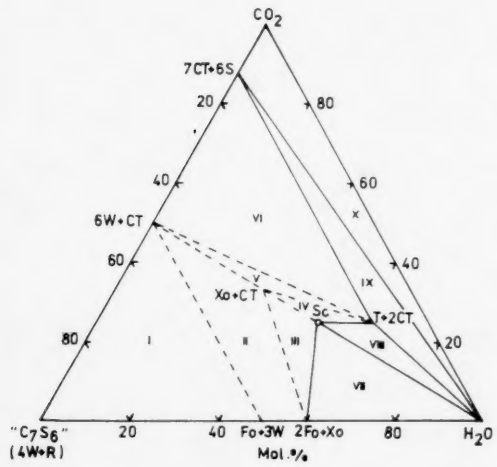

FIG. 2
Diagram of the section C_7S_6-CO_2-H_2O of the system CaO-SiO_2-CO_2-H_2O including the scawtite composition and 4-phase assemblages. The assemblages outlined with solid lines (VII - X) are those which were determined experimentally. The assemblages outlined with dashed lines (I - VI) were established from the hydration series (2) - (4).

W = wollastonite, R = rankinite, CT = calcite, Fo = foshagite, Xo = xonotlite, T = tobermorite, H = H_2O, S = silica.

(I) W + R + CT + Fo; (II) W + CT + Fo + Xo; (III) Sc + CT + Xo + Fo; (IV) W + CT + S + T; (V) W + CT + Xo + T; (VI) Sc + CT + Xo + T; (VII) Sc + Fo + Xo + H; (VIII) Sc + CT + T + H; (IX T + CT + S + H; (X) CT + S + CO_2 + H.

bonated phases (scawtite and calcite) increases with the increasing molar ratio CO_2/C_7S_6. At ratio $CO_2/C_7S_6 \geq 7$, there exists the only phase assemblage (CT + S + H) in the system CaO-SiO_2-CO_2-H_2O compatible with CO_2.

Fast hydrothermal conversion of scawtite into different carbonated phases controlled by excess of CO_2 has its origin in the structural arrangement. Scawtite has a layer structure. Layers of CaO_6 octahedra alternate with layers containing Si_6O_{18} rings and CO_3^{2-} groups (19). They are oriented parallel with (101). Holes in the cyclic $Si_6O_{18}^{12-}$ groups (Fig. 3) overlap with holes in layers containing CaO_6 polyhedra. There arise channels enabling penetration of the linear CO_2 molecules inwards the structure and reaction of these molecules with the CaO_6 polyhedra. In the same time, water molecules belonging to the calcium-oxygen octahedra cannot escape from the structure at normal temperature due to the bent form and molecular dimensions. Similar penetration of CO_2 was

observed in the case of cordierite structure containing six-member $Al_2Si_4O_{18}$ rings (20).

The positions of another three binary phase assemblages (6W + CT), (Xo + CT) and (Fo + 3W) (W = wollastonite), together with the above mentioned three binary assemblages and scawtite composition, delimitate in the section C_7S_6-CO_2-H_2O (Fig. 2) further six possible quarternary phase assemblages: (W + CT + R + Fo), (W + CT + Fo + Xo), (W + CT + Xo + T), (W + CT + S + T), (Sc + CT + Xo + Fo) and (Sc + CT + Xo + T). Their stability fields are separated by dashed lines in Fig. 2.

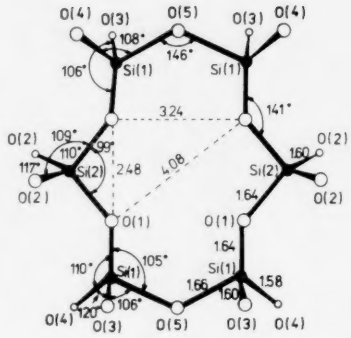

FIG. 3
Geometry of the $Si_6O_{18}^{12-}$ ring in the scawtite structure. Interatomic distances are given in $[10^{-10}m]$.

The existence of the assemblage (6W + CT) on the binary join C_7S_6-CO_2 is suggested according to the equilibrium P_{CO_2}-T curve for the univariant reactions (21, 22): calcite + quartz $\rightleftarrows$ wollastonite + CO_2 and $3CaCO_3 + 2CaSiO_3 \rightleftarrows 2Ca_2SiO_4.CaCO_3 + CO_2$. The assemblage (Xo + CT) appears as an intermediate product in the hydration series along the join (6W + CT)-H_2O (Fig. 2) according to the scheme:

$$(6W + CT \xrightarrow{H_2O} (Xo + CT) \xrightarrow{H_2O} C_7S_6H_2(CO_2) \qquad (5)$$

The assemblage (Fo + 3W) appears as an intermediate product in the hydration series along the join C_7S_6-H_2O (Fig. 2):

$$2C_7S_6 \xrightarrow{2H_2O} 2(Fo + 3W) \xrightarrow{H_2O} (2Fo + Xo) \qquad (6)$$

We verified the formation of the stable phase assemblages (Sc + H_2O) and (2Fo + Xo + H_2O) according to the reaction schemes (5) and (6) by hydrothermal reactions of the water suspensions (6W + CT), (Xo + CT) and (7CaO + $6SiO_2$).

The hydration series (5) and (6) show that the existence of three binary assemblages (6W + CT), (Xo + CT) and (2Fo + Xo) and six 4-phase assemblages I - VI in the section C_7S_6-CO_2-H_2O (Fig. 2) is only possible at water contents which correspond to the stoichiometric hydrated compounds. When the water content exceeds the stoichiometric amount, the hydration process proceeds under formation of the phase associations compatible with H_2O appear very slowly. This is demonstrated by the presence of the metastable tobermorite phase in the phase associations in the section C_7S_6-CO_2-H_2O (Fig. 2). All phase assemblages including tobermorite are metastable under given hydrothermal conditions.

The hydrothermal experiments indicate that the hydration process proceeds through several transition phases and the combination of phases in the phase assemblages may be significantly influenced by experimental conditions (14-18).

Conclusions

The results of the phase analysis of the system C_7S_6-CO_2-H_2O have confirmed that the join (7CT + 6S)-H_2O represents a section in the subsystem CT-S-H which limits concentration of CO_2 fixed stoichiometrically in calcite. The CO_2 excess appeared in form of gaseous phase together with the H_2O vapour in the 4-phase assemblage (CT + S + CO_2 + H_2O). The mixtures deficient in CO_2 always reacted with CaO to give carbonized series of compounds in the 4-phase assemblages involving scawtite and distinct calcium silicate hydrates or scawtite and calcite.

VOL. 14 1984

The composition of the calcium silicate hydrates depended on the molar ratio C/S in the system.

The formation of scawtite in the system $CaO-SiO_2-CO_2-H_2O$ shows that the small amount of CO_2 can bind considerable quantity of CaO and SiO_2 in the compound $C_7S_6H_2(CO_2)$ reducing in such a way the content of calcium silicate hydrates in the phase assemblages. With increasing amount of CO_2, the content of calcium silicate hydrates strongly decreases (Fig. 4). The occurrence of calcium silicate hydrates and carbonated calcium silicate hydrates is limited to the CO_2 concentration corresponding to the concentration triangle CT-S-H. Above this CO_2 content, carbon dioxide appears in the gaseous form together with gaseous H_2O in the 4-phase assemblage CT-S-CO_2-H_2O.

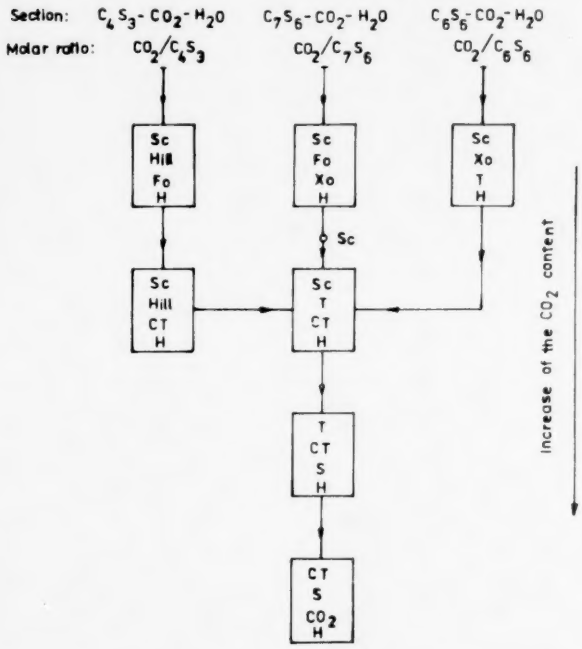

FIG. 4
Schematic representation showing carbonation series of the 4-phase assemblages of the sections C_4S_3-CO_2-H_2O, C_7S_6-CO_2-H_2O and C_6S_6-CO_2-H_2O of the system $CaO-SiO_2-CO_2-H_2O$ at 473 K and saturated steam pressure.

Hill = hillebrandite.

The scheme in Fig. 4 involves 4-phase assemblages occuring in the system $CaO-SiO_2-CO_2-H_2O$ at saturated steam pressure for definite molar ratios CO_2/C_4S_3, CO_2/C_4S_3, CO_2/C_6S_6 in the sections: C_4S_3-CO_2-H_2O, C_7S_6-CO_2-H_2O and C_6S_6-CO_2-H_2O. The compositions C_4S_3, C_7S_6 and C_6S_6 on the join $CaO-SiO_2$ correspond to the molar ratios C/S in the compounds C_4S_3H (foshagite), $C_7S_6H_2(CO_2)$ (scawtite) and C_6S_6H (xonotlite). The composition of scawtite takes place in the subsystem Fo-Xo-CO_2-H_2O (Fig. 1). The scawtite composition divides this subsystem into 4-phase assemblages in which scawtite coexists with foshagite, xonotlite, hillebrandite or tobermorite. The composition of hillebrandite and tobermorite is to be found outside the tetrahedron Fo-Xo-CO_2-H_2O. The formation of the 4-phase assemblages at increasing CO_2 content and the change of the phase composition in dependence on the molar ratio C/S was discussed above and it is seen on the scheme in Fig. 4. This scheme is in a close relation to the technological processes in which hydration and carbonation of calcium silicates proceeds under hydrothermal conditions.

References

1. E.P. Flint, H.F. McMurdie and L.S. Wells, J. Res. National Bureau of Standards, 21, 617 (1938).
2. R.H. Bogue, Mag. Concr. Res., No. 14, 87 (1953).

3. J.D.C. McConnell, Amer. Min., 40, 510 (1955).
4. J. Murdoch, Amer. Min., 40, 505 (1955).
5. A.A. Buckner, D.M. Roy and R. Roy, Amer. J. Sci., 258, 132 (1960).
6. R.I. Harker, Min. Mag., 34, 232 (1965).
7. J.F. Young, R.L. Berger and J. Breese, J. Amer. Cer. Soc., 57, 394 (1974).
8. Z. Šauman, Cem. Concr. Res., 1, 645 (1971).
9. J.N. Maycock and J. Skalny, Cem. Concr. Res., 4, 69 (1974).
10. G.L. Kalousek and E.B. Nelson, Cem. Concr. Res., 8, 283 (1978).
11. H. Mortel and K. Piper, Tonindustrie-Ztg., 102, 513 (1978).
12. L. Stevula and J. Petrovic, Cem. Concr. Res., 11, 549 (1981).
13. H.F.W. Taylor, The Chemistry of Cement, Academic Press, London 1964, p. 189.
14. L. Heller and H.F.W. Taylor, J. Chem. Soc., 2535 (1952).
15. R.B. Peppler, J. Res. National Bureau of Standards 54, 205 (1955).
16. G.L. Kalousek, Proc. Amer. Concr. Inst. 51, 989 (1955).
17. G.O. Assarson, J. Phys. Chem., 62, 223 (1958).
18. R.I. Harker, J. Amer. Ceram. Soc., 47, 521 (1964).
19. J.J. Pluth and J.V. Smith, Acta Crystallogr., B 29, 73 (1973).
20. T. Armbruster and F.D. Bloss, Amer. Min., 67, 284 (1982).
21. R.I. Harker and O.F. Tuttle, Amer. J. Sci., 254, 249 (1956).
22. O.F. Tuttle and R.I. Harker, Amer. J. Sci., 255, 228 (1957).

VOL.
14
1984

CEMENT and CONCRETE RESEARCH. Vol. 14, pp. 873-883, 1984. Printed in the USA.
0008-8846/84 $3.00+00. Copyright (c) 1984 Pergamon Press, Ltd.

THE QUANTITATIVE DETERMINATION OF GLASS IN SLAG BY INFRARED SPECTROSCOPY

A.R.N. Eberendu and K.E. Daugherty
Department of Chemistry
North Texas State University
Denton, Texas 76203

(Refereed)
(Received March 12, 1984)

ABSTRACT

Determinations of the glass content of synthetic and blast furnace slags by infrared absorption spectroscopy are described. A linear relationship exists between the calculated infrared absorption R-values and the percentage glass determined by optical microscopy count. The use of an internal standard and a constant grinding time for the slag sample are crucial to obtaining an accurate and reproducible result. The technique is simple, inexpensive, and minimizes time consuming sample preparations such as washings and particle sizings common in the optical microscopy method.

Introduction

Some slags increase the hydraulic activity of portland cement when admixed in the correct proportions. The hydraulic and cementitious properties of slags are related among other factors to the glass content (1-3). The glassiness of slag, and hence the hydraulicity, is presently determined by various methods which include optical microscopy (4), x-ray diffraction (5) and luminescence spectroscopy (6). However, some of these methods are either limited in their applications (7) or change the physical and chemical properties of the sample.

The major components of slags are oxides such as lime, silica, alumina and magnesia. The chemical compositions and the percentages of these oxides may differ from slag to slag and from country to country. They are however reasonably constant for a particular source (8).

Slag exists in two phases, the glassy and/or the crystalline phases. The chemical components and the quenching technique adopted during the cooling of the molten slag determine the predominant phase (1). If the oxides that form slag are basic (net-work breakers), or amphoteric and acidic (net-work formers), the predominance of one form of the oxides over the other may be crucial in the formation of the glass phase.

Since silica is a major component of slag and forms strong tetrahedral

net work bonds, the O-Si-O bending vibration absorption band of silicates in the slag is selected for the measurements among the bands in the spectrum. Moreover, in the presence of the acidic oxide silica, lime, magnesia and possibly alumina may not form strong net work bonds.

Infrared absorption spectroscopy has been effectively applied in the qualitative identification and elucidation of the structure of glass and crystalline materials (9, 10). The quantitative application of infrared spectroscopy for solid materials using alkali halides has not fared well because of the problems of particle size of the sample (11, 12) and physicochemical interaction between the substance and the dispersing medium (13). However, the detection and determination of the crystalline and amorphous absorption bands are possible from investigations of infrared bands (14). It is observed that the infrared absorption band spectra of crystalline and glassy slags are different in their shapes and sizes under identical sample treatment. These differences are utilized to determine the glass content by developing an empirical function called R-value (Ratio-value).

Infrared Absorption R-values. (Ratio-values).

Theoretically, quantitative analysis by infrared absorption ideally uses the area under the peak of a selected band to determine the concentration of the desired substance. This procedure may not be applicable to slags since the concentration of the vibrating species is the same in both the crystalline and glassy form of the slag. However, since the glassy form was observed to produce a broad and short absorption silicate band, while the crystalline slag appeared to produce a narrower and taller band, a technique of an R-value calculation was empirically developed to fit the observation.

$$\text{R-value} = \frac{\dfrac{\text{Peak height of 475 cm}^{-1}\text{ of unknown slag}}{\text{Peak width at 475 cm}^{-1}\text{ of unknown slag at 1/2 height}}}{\dfrac{\text{Peak height at 1400 cm}^{-1}\text{ of internal standard}}{\text{Peak width at 1400 cm}^{-1}\text{ of internal standard at 1/2 height}}}$$

In arriving at this definition, some assumptions were empirically made.

1. The base line of the internal standard at peak maximum was chosen as the baseline of the analytical sample absorption peak.
2. A triangle was drawn over the absorption peak comprising the already defined baseline and the best lines that touch most of the analytical absorption peak to form a triangle.
3. The triangle may not be isoceles but can follow the shape of the absorption band.
4. The peak height of the absorption band was measured from the base of the resulting triangle to the apex and the width at half height was similarly determined.

All the lengths were measured using a ruler calibrated in millimeter units. However, any other convenient units may be used. Experimental data demonstrated that one can easily quantitatively determine glass content to within $\pm$5% accuracy.

Experimental

In order to simulate commercial slags, a range of synthetic slags were prepared in 20 gram lots. Starting materials were American Chemical Society reagent grade calcium carbonate powder, Mallinckrodt Chemical Works national formulary magnesium carbonate powder, aluminum hydroxide powder purified from

VOL. 14 1984

Matheson, Coleman and Bell, and -240 mesh silicon dioxide (floated) powder from Fisher Scientific Company. The calcined materials were fused homogeneously in a Lindberg furnace.

A series of base to acid B/A = $\frac{(CaO + MgO)}{(Al_2O_3 + SiO_2)}$ ratios were homogeneously prepared to final slag composition ranging from 0.80-1.30 (Table 1). The samples with varying B/A ratios were individually prepared and weighed into platinum crucibles.

TABLE 1

SYNTHETIC SLAG CHEMICAL COMPOSITION

B/A Ratio	Grams of $CaCo_3$	Grams of $MgCO_3$	Grams of $Al(OH)_3$	Grams of SiO_2
0.80	11.8985	4.6484	3.4000	8.8889
0.85	12.3004	4.8055	3.3081	8.6486
0.90	12.6813	4.9542	3.2211	8.4211
0.95	13.0426	5.0954	3.1385	8.2051
1.00	13.3858	5.2295	3.0600	8.0000
1.05	13.7128	5.3570	2.9854	7.8049
1.10	14.0232	5.4785	2.9143	7.6190
1.15	14.3197	5.5943	2.8465	7.4419
1.20	14.6027	5.7049	2.7818	7.2727
1.25	14.8731	5.8105	2.7200	7.1111
1.30	15.1318	5.9116	2.6609	6.9565

Each B/A ratio was prepared in duplicate. The two crucibles, each containing the same B/A ratio composition were placed in a Lindberg furnace stabilized at 500 deg. C. which was then slowly increased to 1475 deg. C. (15). Duplicate samples of the given B/A ratio composition were left at this temperature for 8 hours or until completely molten. One of the duplicate crucibles with the contents was quenched in liquid nitrogen in order to produce a high glass content. The other duplicate sample was left in the furnace and allowed to cool slowly to 1050 deg. C. in order to anneal. After 6-7 hours at 1050°C, the sample was slowly cooled to room temperature in order to produce a slag of high crystalline content.

Another set of duplicate replicas of B/A ratios was similarly prepared. However, in order to produce high glass slag, one of the duplicate samples was chilled in ice-water mixture in place of liquid nitrogen. The other duplicate was annealed and slow-cooled as previously described. X-ray diffraction analysis revealed that the major minerals formed were akermanite/gehlenite.

Particle Size Reduction and Infrared Scan

Both the slow-cooled, the liquid nitrogen and the ice-water quenched slags were ground with mortar and pestle and separated to different mesh sizes. The +325 particle size was reduced further by a Perkin-Elmer vibrating mill for 4 minutes. An appropriate quantity of the sample was mixed with preground potassium bromide-ammonium chloride mixture to a final homogenous material of two percent sample and two-tenths percent ammonium chloride as internal standard. Approximately 150 mg of this mixture was pressed into a transparent disc in a Carver Press at 30,000 pounds per square inch for 10 seconds without

TABLE II

STANDARD CALIBRATION TABLE FOR SYNTHETIC SLAG (B/A = .90)

	Internal Standard			Standard Sample Mixes				
Percent	Peak Height (mm)	Width at 1/2 Height (mm)	Peak Height / Width at 1/2 Height	Peak Height (mm)	Width at 1/2 Height (mm)	Peak Height / Width at 1/2 Height	R-value	Mean R-value ±RSD
100	87.0	7.0	12	45.0	38.0	1.18	.098	.097
	81.0	7.1	11	38.0	35.5	1.07	.097	±1.5%
	85.0	7.3	12	41.5	36.5	1.14	.095	
90	84.0	7.0	12	51.0	29.0	1.76	.15	.16
	81.0	7.3	11	52.0	29.0	1.79	.16	±3.6%
	80.0	7.0	11	48.5	28.0	1.73	.16	
80	84.6	7.2	12	57.0	24.5	2.33	.19	.20
	80.0	7.5	11	53.5	22.5	2.38	.22	±7.6%
	83.0	7.1	12	60.0	25.5	2.35	.20	
60	84.0	7.2	12	72.0	17.9	4.02	.34	.35
	86.0	7.5	11	76.0	19.2	3.96	.36	±3.2%
	83.0	7.1	12	70.0	17.0	4.12	.34	
40	89.0	7.2	12	78.0	14.0	5.57	.46	.45
	87.0	7.8	11	84.0	17.0	4.94	.45	±2.2%
	95.0	8.0	12	96.0	18.0	5.33	.44	
20	71.0	7.0	10	85.0	15.0	5.67	.56	.56
	76.0	7.0	11	96.0	15.0	6.00	.54	±2.7%
	79.0	7.6	10	96.5	17.0	5.68	.57	
10	84.0	7.0	12	101	13.6	7.43	.62	.62
	79.0	7.0	11	101	14.5	6.96	.63	± .93%
	77.0	7.0	11	102	15.0	6.80	.62	
0	82.0	7.5	11	111	15.0	7.40	.67	.67
	75.0	7.0	11	102	14.0	7.28	.66	±1.5%
	81.0	7.5	11	109	14.6	7.46	.68	

VOL. 14 1984

vacuum. Clear and acceptable discs were produced 95% of the time using this procedure.

The discs were scanned in a Perkin-Elmer Infrared Spectrometer - 1330. The spectrometer was a double beam optical null instrument with microprocessor controlled abscissa function having t/5 filter grating and capable of scanning full frequency range 4000-200 reciprocal centimeters in a scan time of 12 minutes. The gain was set at normal with a narrow slit program. Each sample was run in triplicate by using different discs and the mean used in the calculation and determination of glass content.

Calibration Using Internal Standard Method

An internal standard, ammonium chloride, was thoroughly mixed with powdered potassium bromide by grinding the mixture for one minute in a vibrating mill to produce a mixture containing 0.2% by weight ammonium chloride. A series of spectra were run of various pre-calculated mixtures of slow-cooled synthetic slag designated as 0% glass, and ice-water quenched duplicate, designated as 100% glass in discs prepared from the potassium bromide - ammonium chloride standard matrix. A triangle was drawn over the absorption peak between 500 - 462 wave numbers of the O-Si-O bending vibration using the ammonium chloride baseline as the reference.

The Ratio-values (R-values) were calculated as defined. For each sample mixture, three discs were scanned to obtain the ratio-values. A linear regression analysis with percent glass as the independent variable and the ratios as the dependent variables (Table II) gave the calibration curve (see fig. 1) with a correlation of 0.9982. Using the same potassium bromide - ammonium chloride mixture as standard disc material, the percent glass of any slag may be determined.

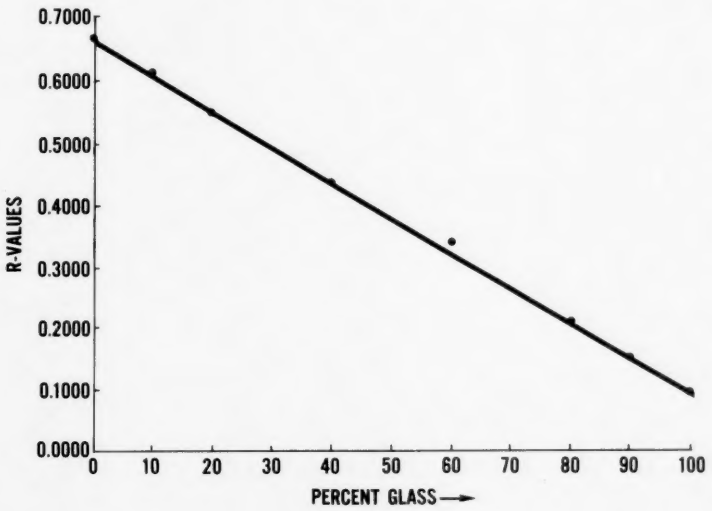

FIG. 1

Standard calibration plot of R-values as a function of the percentage of glass.

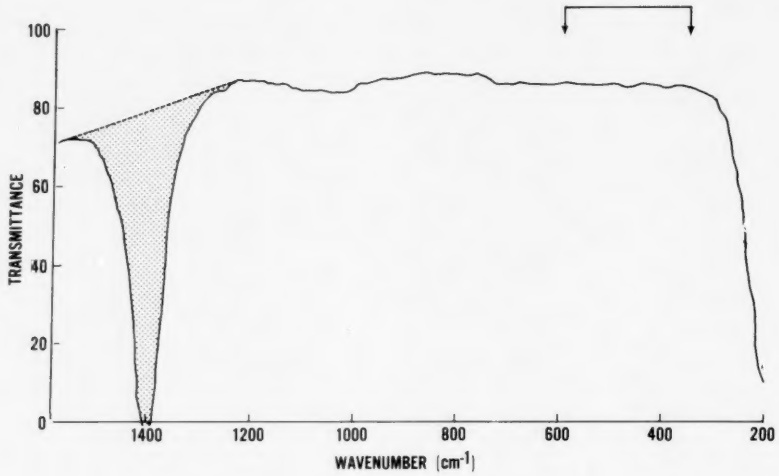

FIG. 2

Infrared absorption spectrum of a 0.5% ammonium chloride in potassium bromide

VOL. 14 1984

Results and Discussion

Figure 2 illustrates the infrared absorption spectrum of 0.5% ammonium chloride.

It is transparent below 1390^{cm-1} making it an ideal choice as the internal standard for slags. Figure 3 illustrates the spectra of a synthetic slag and blast furnace slag. They are qualitatively similar. The major mineral present in slow-cooled synthetic slag as well as devitrified blast furnace slags is melilite, a solid solution of akermanite ($2CaO \cdot MgO \cdot 2SiO_2$) and gehlenite ($2CaO \cdot Al_2O_3 \cdot SiO_2$), as confirmed by their powder x-ray diffraction patterns.

In vitrified slag, the glassy structure is mostly melilite. Infrared absorption bands of glassy slags are broad due to non-uniform structures while crystalline forms have relatively sharp, tall and narrow band peaks (see Fig.4). Four prominent strong absorption bands are distinguished and have been successfully assigned (16,9). The absorption band around 480-462 cm-1 due to O-Si-O bending vibration (9) is strong and is used as the analytical absorption band in this study. In the glass form, the absorption band is broad and may incorporate Si-O-Al(VI) band found within 580-500 cm-1.

From the data in Table III, Figure 5 is constructed. The linear regression plot of the infrared absrption R-values as a function of the optical microscopy glass count shows a good correlation coefficient (0.9989). The trend is very good if we take into consideration errors that may occur during sample washings as a prerequisite for microscopy glass count.

The chemical composition of a slag material has an important role to play in the glass content (17,1). Decreased base to acid ratio results in higher glass formation, perhaps due to the increase in glass forming cations such as silicon (18). However, the method of quenching the slag contributes to its degree of glassiness. An ice-water mixture appears to be more efficient in producing glass than liquid nitrogen if the platinum crucible with the contents

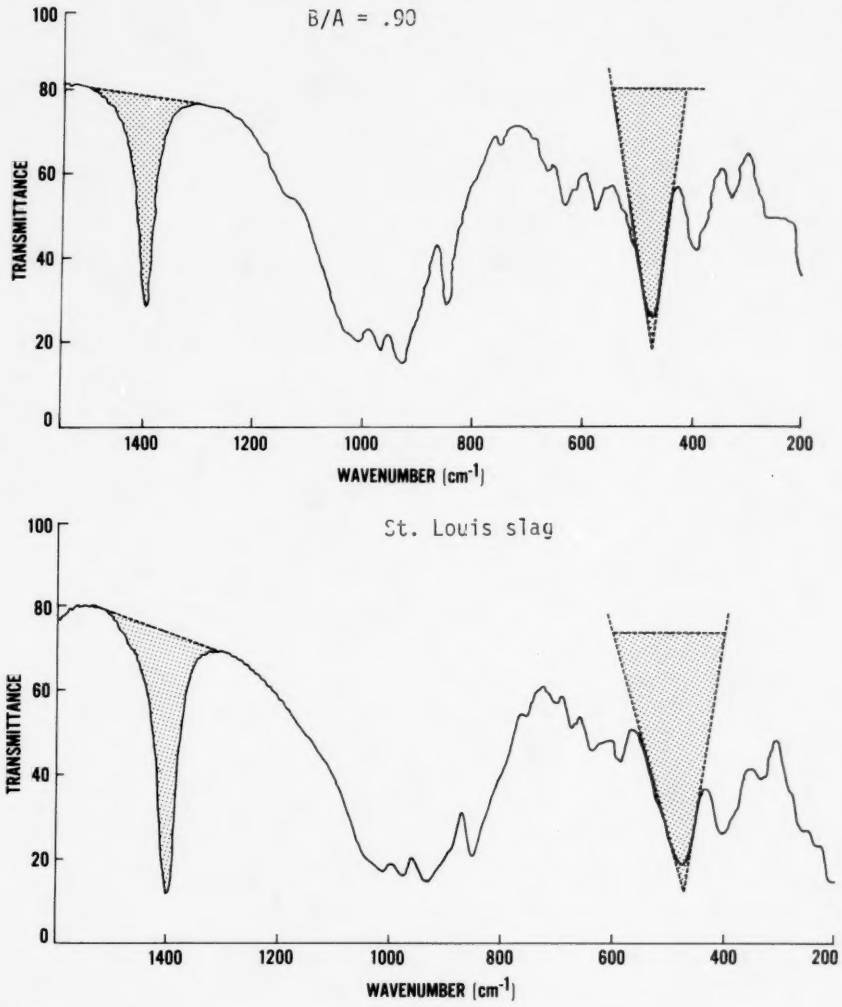

FIG. 3

Infrared absorption spectra of slow cooled synthetic slag and St. Louis slow cooled slag.

is thrown into the liquid. Figure 6 constructed from Table IV illustrates this behavior.

The most important factor in obtaining accurate results of glass determination by infrared spectroscopy appears to be the control of particle size of the slag sample and the matrix. The slag sample must be ground separately for at least 4 minutes using stainless steel vibrating mill before mixing with the preground potassium bromide-ammonium chloride standard mixture. An example of grind study of synthetic slag (B/A =.90) is shown in figure 7 from Table V. Ammonium chloride especially is very sensitive to grinding time and should be controlled by ginding in a mixture of potassium bromide for one minute as a standard matrix material.

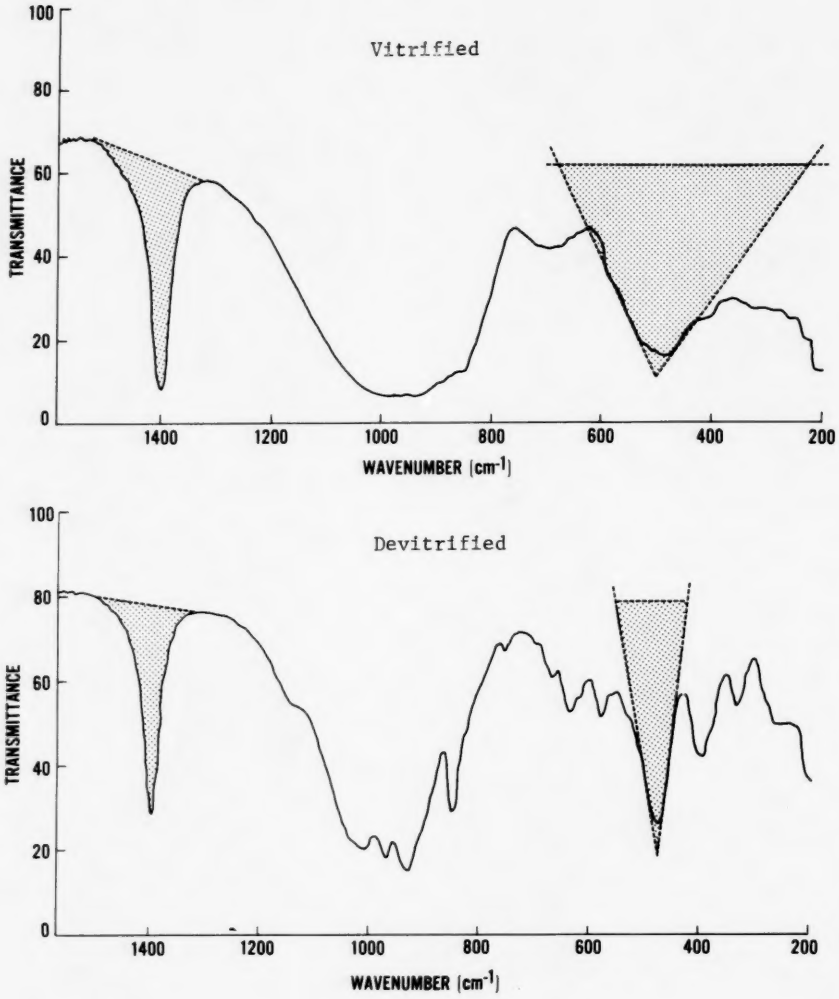

FIG. 4

Infrared absorption spectra of vitrifies and devitified
Synthetic slag of the same chemical composition

VOL. 14 1984

Conclusions

The glass content of slags can be determined inexpensively with this method. It is simple and can be performed in any laboratory equipped with an infrared spectrometer capable of scanning down to 400 wavenumbers.

It minimizes time consuming sample preparations, such as sample particle sizings and washings, common in optical microscopy methods. The direct analysis of a slag sample is more attractive, since the quality of the sample as a function of its hydraulic activity is not modified by washings and particle sizings. Elemental impurities in blast furnace slags which affect the glass content determinations in luminescence and ultraviolet methods are absent or minimal using this infrared spectroscopy technique.

TABLE III.

INFRARED ABSORPTION R-VALUES AND THE CORRESPONDING MICROSCOPY GLASS COUNT OF SOME COMMERCIAL SLAGS.

Commercial Slag Source	Percent Glass by Microscopy	Mean R-values RSD
Hamilton Slag	36.4	.37 ± .27%
St. Louis Slag	5.47	.51 ± .28%
Yawata Slag	92.1	.085 ± .75%
Levy Slag	38.1	.37 ± .57%
"Crystalline" Slag	3.85	.52 ± .60%

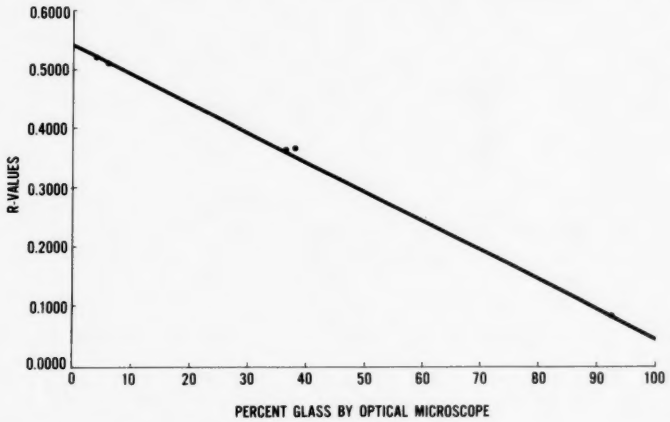

Fig. 5
Infrared absorption R-values as a function of the corresponding microscopy glass count for some blast furnace slags.

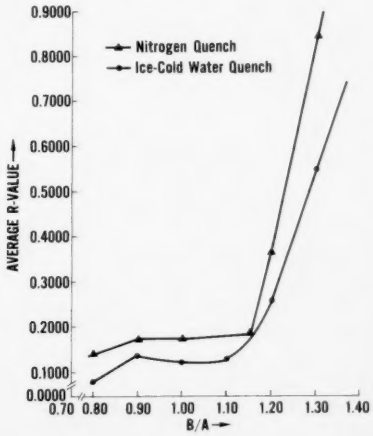

FIG. 6

Infrared absorption R-value as a function of B/A ratio.

TABLE IV.
Comparison of Quenching Techinique
Glass Content (R-value)

Base/Acid Ratio	Mean R-value N_2 Quench	Mean R-value Ice-Water Quench
0.80	.14	.082
0.90	.17	.14
1.00	.17	.12
1.10	N/A	.13
1.15	.18	N/A
1.20	.37	.26
1.30	.85	.55

VOL. 14 1984

TABLE V

EFFECT OF TIME OF GRINDING ON INFRARED
R-VALUES OF B/A =.90

Time of grinding (minutes)	Mean R-value ± S. D.
0	0.23 ± .002
0.5	0.47 ± .004
1.0	0.54 ± .003
2.0	0.58 ± .001
4.0	0.61 ± .012
6.0	0.67 ± .004

The correlation between microscopy determination of glass and infrared absorption R-values supports the use of the infrared spectroscopy in quantitating the glass content of slags. The present technique eliminates bias usually experienced during glass counting by optical microscopy and offers a good substitute for the high cost of maintaining and operating an x-ray diffraction unit. The method may be more accurate than optical microscopy. However, this is difficult to determine because the standards used to develop the infrared procedure were calibrated by optical microscopy.

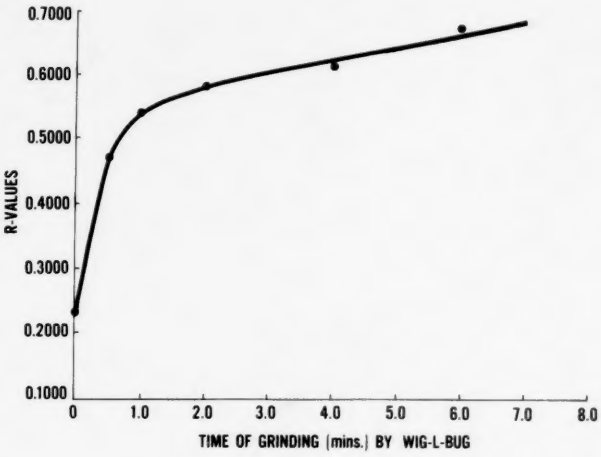

FIG.7

Infrared absorption R-value as a function of the grinding time

L.
4
84

Acknowledgements

The authors would like to thank the Robert A. Welch Foundation and the St. Louis Slag Products Company for support of this investigation.

References

1. Daugherty, K. E., B. Saad, C. Weirich and A. Eberendu, Silicates Industriels, XLVIII, 107-110 (1983).
2. Locher, F. W., Proceedings of the Fourth International Symposium on the on the Chemistry of Cement, Washington, D. C. 267-275 (1960).
3. Watt, J. D. and D. J. Thorn J. Appl. Chem.;15, 594-595 (1965).
4. Fulton, F. S., Portland Cement Institute Monograph, Johannesburgh, South Africa (1974).
5. Ohlberg, S. M. and D. W. Strikler, J. Am. Ceramic Soc. 45, 170 (1962).
6. Kreidl, N. J., Opt. Soc. Am. 35, 252 (1945).
7. Weyl, W. A. and E. Thumen, Sprechsaal, 67, 95 (1934).
8. Lee, A. R., Blast Furnace and Steel Slag-Production Properties and Uses, New York, Academic Press (1963).
9. Mackenzie, K. J. D., J. Am. Ceramic Soc. 55, 68 (1972).
10. Furukawa, T., A. Brawer and W. B. White, J. Am. Ceramic Soc. 62, 351 (1979).
11. Lejeune, R. and G. Duyckaerts, Spectrochim ACTA 6, 194 (1954).
12. Henry, R. L., J. Opt. Soc. Am. 38, 775 (1948).
13. Farmer, V. C. Spectrochim ACTA 8, 374 (1957).
14. Ihibashi, M. Polymer Letters 1, 529 (1963).
15. Automobile Glass Science Research Institute konstantinouka. Translated from Zhurnal Prikjkhimic 49, 757 (1976).
16. Delbert, E. D. and E. R. Guy, J. Am. Ceramic Soc. 45, 480 (1962).
17. Visser, S., J. E. Kruger, Van Aardt and M. P. Brandt, National Building Research Institute's Council for Scientific and Industrial Research, Pretoria, S. Africa, ISBN 0798808101 (1975).
18. Kreidl, N. J., J. Opt. Soc. Am. 35, 252 (1945).

CEMENT and CONCRETE RESEARCH. Vol. 14, pp. 884-886, 1984. Printed in the USA.
0008-8846/84 $3.00+00. Copyright (c) 1984 Pergamon Press, Ltd.

NOTES

THE DETERMINATION OF SETTING TIME OF PORTLAND CEMENT BY THE VICAT TEST

I. Soroka
Professor, Building Research Station, Faculty of Civil Engineering,
Technion - Israel Institute of Technology, Haifa 32000

(Communicated by J.P. Skalny)
(Received Feb. 24, 1984)

ABSTRACT

In quick-setting cements, setting may occur, wholly or partly, within the four minutes of the specified mixing time. The resulting structure, however, is broken by the mixing operation and the cements exhibit a normal, or near normal, setting. Hence, the use of the Vicat test (BS 4550: Part 3) for determining setting times of quick setting cements is not always adequate and may give misleading results.

VOL. 14 1984

Introduction

The use of the Vicat for determining the setting times of cements involves a simple procedure which has been universally employed and specified (1-4) for many years. Under normal conditions, i.e. when cements of normal setting times are concerned, the Vicat test is quite satisfactory for all practical purposes. It should be point out, however, that under certain conditions, i.e. when initial setting times of the order of a few minutes are involved, the Vicat test ceases to be adequate and may give misleading results. This limitation of the Vicat test which, again, is relevant to quick-setting cements only, became apparent in a series of tests which are briefly discussed here.

Testing Procedure and Results

In the tests involved, the water consistence and setting times were determined in cements of different gypsum content in accordance with BS 4550: Part 3 (5). The cements in question were prepared from two ordinary Portland cement clinkers (Table 1) by grinding together the clinker and the gypsum to the fineness of 330m^2/kg when determined by the air permeability method (6). The gypsum used was phosphogypsum containing 2.1% and 1.1% P_2O_5 and F respectively, and the amound added, expressed as SO_3, varied from 0 to 3% with respect to the weight of the clinker. Results are presented in Fig. 1, in which the standard consistence is presented as the amount of water required to produce a paste of a standard consistence, expressed as percentage of the weight of the cement.

Table 1

Chemical Composition of the Clinkers (percent by wt)

Clinker	CaO	SiO_2	Al_2O_3	Fe_2O_3	SO_3	MgO	Na_2O	K_2O	Insol.	L.O.I.
A	65.98	22.00	5.96	3.04	0.30	1.60	0.36	0.34	0.63	0.30
B	65.86	23.36	5.86	2.44	0.40	1.28	0.25	0.30	0.40	0.26

Discussion

Gypsum is added to the cement in order to retard its setting and, in most cases, Portland cements exhibit quick setting without such, or a similar, retardation. The retarding effect depends on the type of gypsum involved and the amount added. Generally speaking, for a given type of gypsum, the setting time increases with the increase in the added amount up to a certain SO_3 concentration (7).

In the light of the preceding discussion, the data of Fig. 1 are partly unexpected and warrant a suitable explanation. It may be erroneously concluded that the setting times of both clinkers tested complied with the relevant requirements of the standards, namely a minimum initial setting time of 45 minutes and a maximum final setting time of 600 minutes (1). Furthermore, it is indicated that the addition of small amounts of gypsum, i.e. some 0.5% of SO_3, actually accelerated, rather than retarded, the setting of the cements in question. It is known, of course, that some clinkers do not exhibit quick setting without added gypsum and it may be argued that this was also the case under conditions at hand. The accelerated effect of the gypsum, however, has not been observed and is, indeed, rather difficult, if not impossible, to explain on the basis of present knowledge.

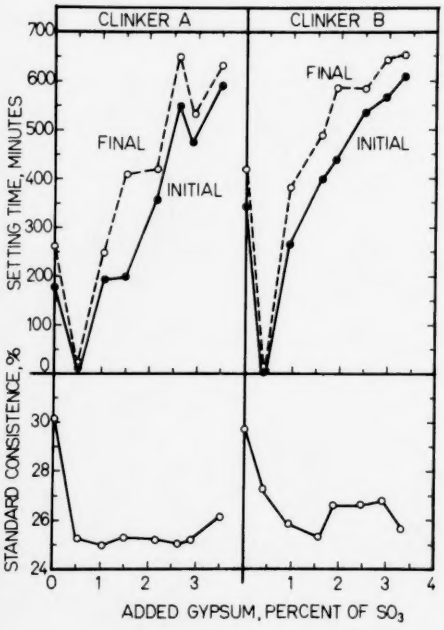

FIG. 1
Effect of gypsum on setting times and standard consistence

In the manufacture of Portland cement, the gypsum is interground with the clinker, and the temperature may rise high enough for the gypsum to partially dehydrate to hemihydrate. On the addition of water, the hemihydrate re-hydrates quickly back to gypsum and brings about the stiffening of the cement paste, i.e. false set takes place. Under conditions at hand, however, the apparent accelerating effect of the small addition of gypsum cannot be attributed to false set, because if this were the case, such a set would have occurred in all the cements, and not only in those containing small amounts of gypsum. In fact, the false set would have been more pronounced in the cements containing the higher amount of gypsum rather than in those containing a low amount of gypsum. Moreover, the very same apparent effect on setting time was observed in another study (8)

where the gypsum was mixed, and not interground with the cement, i.e. where the possible formation of hemihydrate could not be considered any more. It is quite reasonable to exclude, therefore, the possibility of false set to explain apparent accelerating effect of small additions of gypsum on setting times under conditions at hand.

BS 4550 requires to prepare the paste for testing by "vigorously" mixing the water and the cement for 240 ± 5 s (5). It follows that if setting occurs, partly or wholly, within the four minutes of the mixing, the set is broken and the paste may exhibit an apparent normal or near normal setting. If this is the case, and setting takes place during the mixing operation, some of the water is chemically combined with the cement, and a greater amount of mixing water will be required to produce the standard consistence. It can be seen that, indeed, the two cements without any added gypsum, and the one from clinker B containing only 0.4% of added SO_3, required a significantly greater amount of mixing water in order to reach the standard consistence. Moreover, when the same cements were mixed with water for only 30 s, stiffening became apparent within a few minutes and the resulting pastes became brittle and unworkable.

In view of the preceding discussion, the following may be concluded with respect to mechanism involved. In the cements with no added gypsum, the aluminates react with water immediately, but no setting occurs because the resulting structure is broken by the mechanical effect of the mixing operation. At the end of the four minutes, when mixing is completed, the paste contains hardly any unhydrated aluminates and setting is brought about mainly by the hyration of the calcium-silicates after some time, i.e. "normal" setting takes place with the resulting setting times being similar to those of a properly retarded cement. However, when only a small amount of gypsum is added to the cement, only part of the aluminates hydrates while the other part remains unhydrated in the paste when mixing is completed. In the absence of sufficient amounts of $SO_4^{=}$, however, the remaining aluminates hydrate within a short time. Hence, the rather short setting times characterizing the cements in which the added gypsum content was equivalent to about 0.5% of SO_3.

VOL. 14 1984

Summary of Conclusions

In quick setting cements setting may occur, partly or wholly, during mixing. The resulting structure, however, is broken by the mixing operation and the cements, when tested by the Vicat needle, exhibit an apparent normal, or near normal, initial setting times. This limitation of the Vicat test is relevant to the special case of quick setting cements, whereas for normal cements, the Vicat test should be considered satisfactory for all practical purposes.

References

1. BS 12: 1978, "Ordinary and Rapid-Hardening Portland Cement."
2. ASTM C150-81, "Portland Cement," 1982 Annual Book of ASTM Standards, Part 13, pp. 153-159.
3. DIN 1164 (Nov. 1978), "Portland-Hochofen-und Trasszement," Blatt 1:Begriffe, Bestaudteile, Anforderungen, Lieferung.
4. "Cement Standards of the World," Cembureau Paris, Beton Verlag, Dusseldorf, 1968.
5. BS 4550: 1978, "Methods of Testing Cement," Part 3: Physical tests, Section 3.6 Test for setting times.
6. ASTM C204-81, "Test for Fineness of Portland Cement by Air Permeability Apparatus," 1982 Annual Book of ASTM Standards, Part 13, pp. 207-213.
7. F.M. Lea, "The Chemistry of Portland Cement," Edward Arnold Ltd., London, 1970, p. 298.
8. MikyasAbayneh, "Effect of Gypsum on Properties and Internal Structure of Portland Cement Paste," Ph.D. Thesis, Faculty of Civil Engineering, Technion - Israel Institute of Technology, Haifa, 1983.

CEMENT and CONCRETE RESEARCH. Vol. 14, pp. 887-890, 1984. Printed in the USA.
0008-8846/84 $3.00+00. Pergamon Press, Ltd.

THE GLASS IN LOW-CALCIUM FLY ASH

Bryant Mather
Structures Laboratory
U.S. Army Engineer Waterways Experiment Station
P.O. Box 631
Vicksburg, Mississippi 39180 USA

(Refereed)
(Received March 7, 1984)

Among the 16 materials studied in the Corps. of Engineers investigation of pozzolans and slags (Mather, 1958) were four fly ashes, all collected in the eastern part of the United States, all from power plants burning bituminous coal. They were designated AD-3 (Chicago), AD-7 (Detroit), AD-8 (Philadelphia) and AD-9 (Baltimore). The CaO, by chemical analysis, was between 2.3 and 5.3 percent. Mather (1958) gave some data on these including the following:

	AD-3	AD-7	AD-8	AD-9
SiO_2	47.2	47.4	38.2	44.9
Al_2O_3	19.5	34.0	25.7	34.0
Fe_2O_3	18.2	9.0	16.3	6.5
CaO	5.3	2.3	3.9	2.3
Loss on Ignition	0.8	3.9	12.2	7.9
Carbon	0.43	3.17	11.13	7.22
Finer than 75-μm sieve	95.5	92.8	93.6	85.1
Finer than 45-μm sieve	93.5	81.7	85.8	81.5

The values for silica content plotted in Fig. 2, recalculated omitting the carbon and Fe_2O_3, are 58.0, 54.0, 52.6, and 52.0 respectively. Some quartz was noted but did not make up as much as 3% by mass of any sample based either on microscope or XRD evaluation.

The discussions by Diamond (1983, 1984) and Idorn (1984) on the glass in fly ash suggested that data on the glass in these four ashes might desirably be recorded. These data are taken from a manuscript report prepared by Katharine Mather from data developed by D.M. Hausen and A.D. Buck.

Transparent isotropic particles were recorded as glass. Glass content was determined as weighted average by particle counts in sieve-size groups.

Most of the glass particles are spheres in the 1-20 μm range. The index of refraction of the colored glass was higher than that of the colorless glass

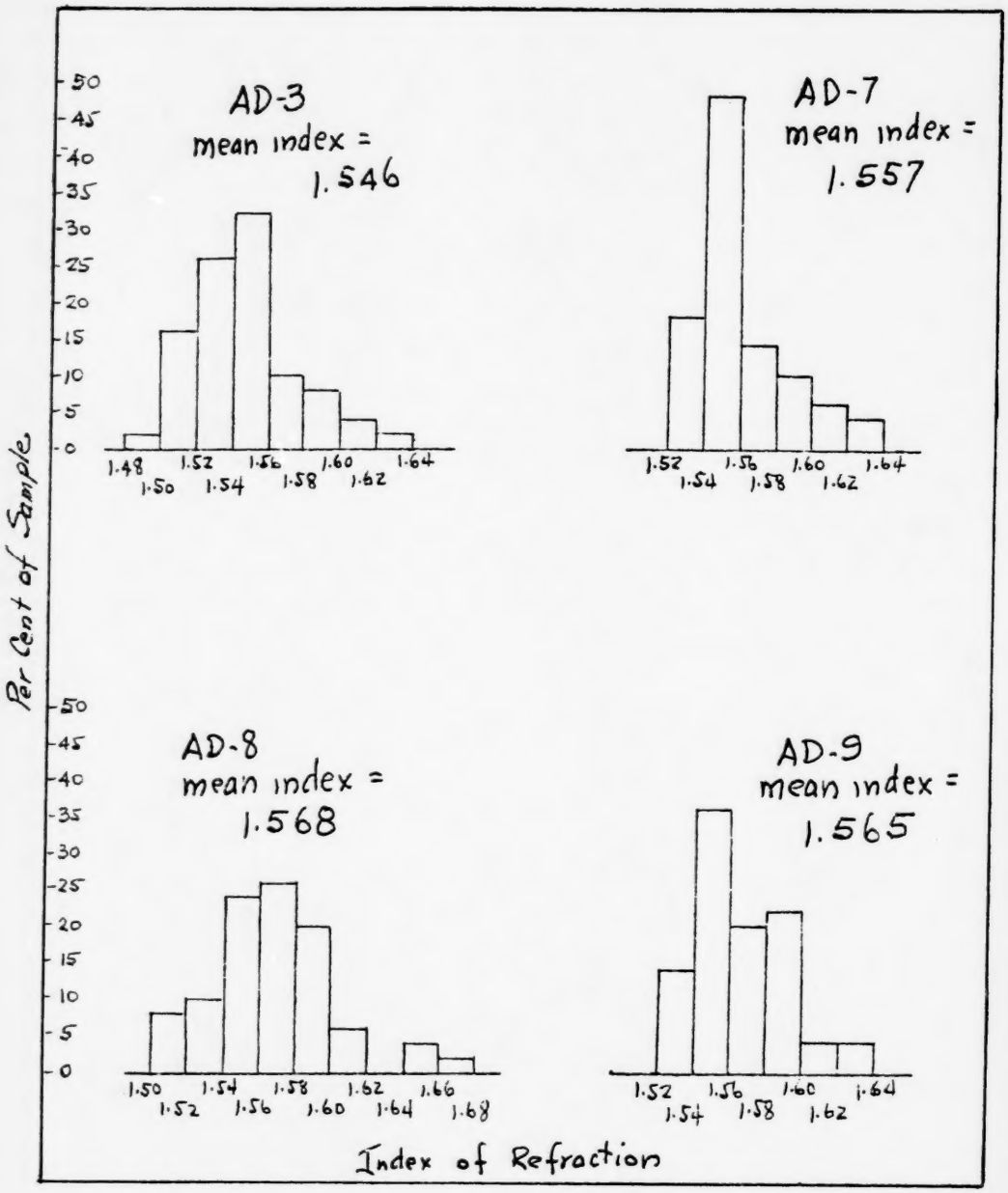

FIG. 1

Histograms of the distributions of indices of refraction of of glassy particles in four fly ashes.

VOL. 14 1984

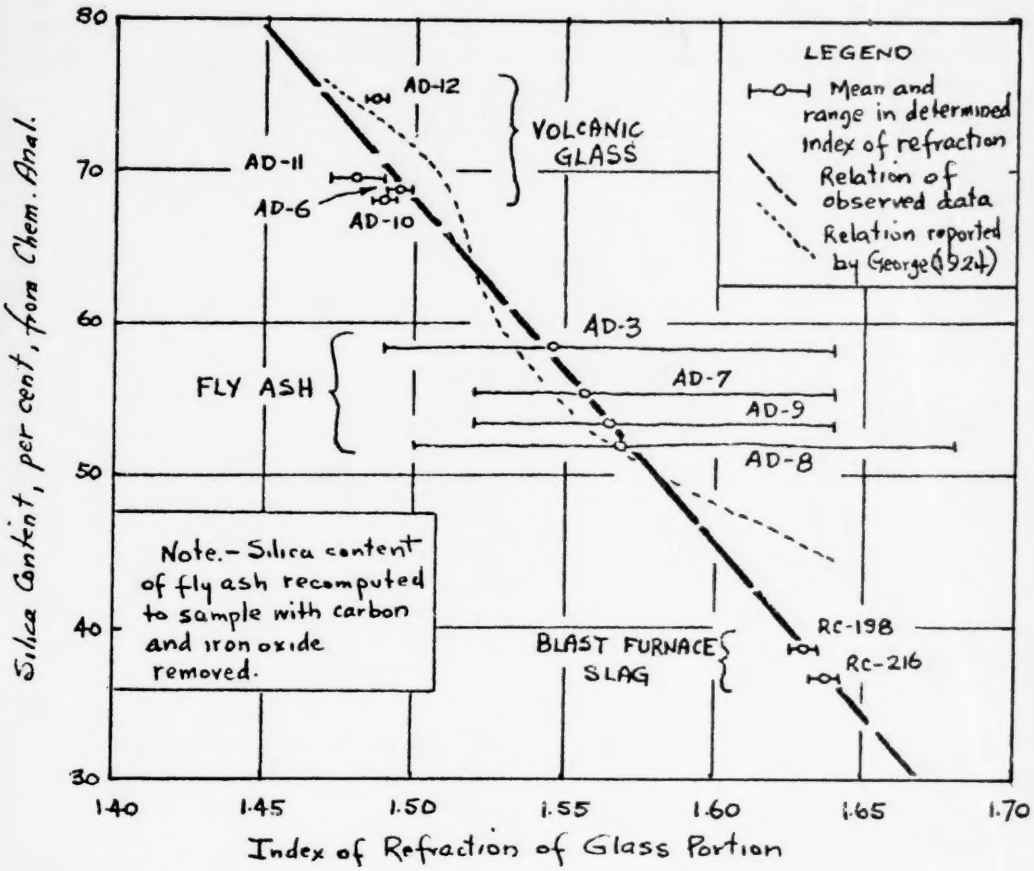

FIG. 2

A simple inverse linear relationship has been found to exist between silica content and mean index of refraction of glass portion of glassy admixtures

	AD-3	AD-7	AD-8	AD-9
Glass, %	81	75	51	70
Size range, μm	1-10	3-13	4-20	3-14
Mean indes of refraction	1.546	1.557	1.568	1.565
% glass in				
150 to 75-μm size	60	55	35	60
size finer than 75 μm	82	76	52	72

but there was a range of indices in each case. About 10 percent of the glass particles contained crystalline inclusions; mullite needles were more common in yellowish-green glass of higher index. The silica content of the glass can be

estimated from the index of refraction (George, 1924). Fifty glass particles in each of several samples of each fly ash were recorded as having an index of refraction above or below that of the immersion medium. The media used had indices of from 1.480 to 1.680 in steps of 0.020. The examination was made using white light at a magnification of 420X. The data are presented in Fig. 1 as histograms. The data as mean and range are indicated in Fig. 2 on which also are shown the index of refraction of the glass in other materials containing glass used in the study partially reported by Mather (1958).

References

S. Diamond, Cement and Concrete Research 13, 459 (1983).
S. Diamond, Cement and Concrete Research 14, 146 (1984).
W.O. George, J. of Geology 32, 353-372 (1924).
G.M. Idorn, Cement and Concrete Research 14, 145 (1984).
B. Mather, The Partial Replacement of Cement in Concrete, Am. Soc. Testing Materials, Sp. Tech. Publ. No. 205, Philadelphia, PA, pp. 37-73, 1958.

VOL.
14
1984

CEMENT and CONCRETE RESEARCH. Vol. 14, pp. 891-893, 1984. Printed in the USA.
0008-8846/84 $3.00+00. Pergamon Press, Ltd.

DISCUSSIONS

A DISCUSSION OF THE PAPER "STUDIES OF ALKALI-SILICA REACTION - PART II. EFFECT OF AIR ENTRAINMENT ON EXPANSION," BY A.D. JENSEN, S. CHATTERJI, P. CHRISTENSEN, AND N. THAULOW*

Bryant Mather
Structures Laboratory
Waterways Experiment Station
Vicksburg, Mississippi 39180, USA

The authors interpret the results they found, which included a 40 % expansion reduction associated with an increase of air content of mortar from about 5 % to 9 % as due to the 4 % added air produced by use of an air-entraining admixture. They also speculate that the "general suspicion in Denmark" that "an entrained air-void system is not as effective" in preventing damage due to freezing and thawing "as has been claimed by workers of other countries" may be, in part, due to partial filling of the air voids with products of alkali-silica reaction.

Vivian (1947, 1950) studied the effect of void space in mortar on expansion due to alkali-silica reaction. He did not use an air-entraining admixture but rather caused percentage of void space to vary by altering the water-cement ratio, or the aggregate content. One of his conclusions (Vivian, 1947) was "Entrainment of air in mortar may prevent serious expansion, provided the number and volume of individual air voids are sufficiently large. Unless voids of greater volume than that of the reaction product are situated close to each reactive aggregate particle, the mortar will be cracked and expanded to some extent."

The relationships revealed by Vivian's studies (1947) are indicated in Figures 1, 2, and 4 from his paper. These were not reproduced in the summary of that paper that was published in the USA (Vivian, 1950). In the summary, Vivian expressed his findings in these words: "... when the amount of void space in the mortar exceeded 7-8 percent by volume, the mortar was not expanded abnormally"; when it was less than this, "expansion was abnormally large." This suggests that it is the total amount of distributed voids that is effective and it is not required that the increase in volume be produced specifically by the use of an air-entraining admixture.

As to the role of air-void filling by deposition of reaction products on effectiveness of the air-void system in playing its role in contributing to making water-saturated concrete immune to the effects of freezing and thawing, there are several relevant points. A proper air-void system with a bubble-spacing factor ($\bar{L}$) less than 0.20 mm (0.008 in.) is absolutely necessary but is never sufficient. The concrete will be immune only if it also is made with

*CCR 14, 311-314 (1984).

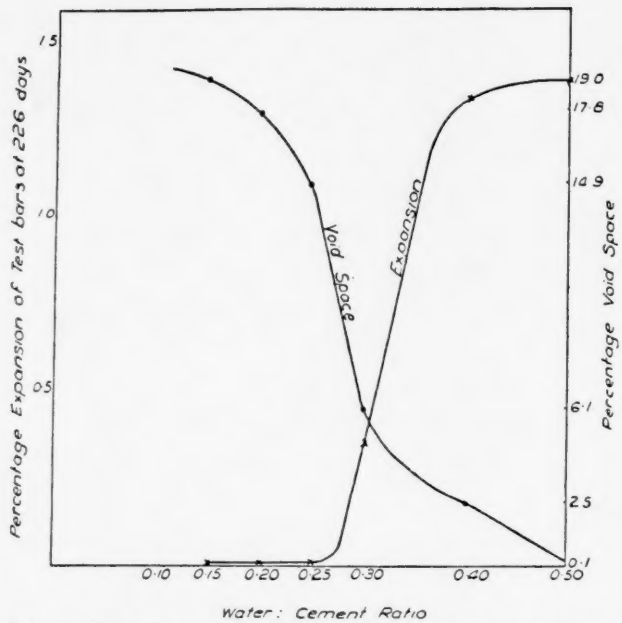

FIG. 1.—Showing correlation between expansion and void space of mortar test bars made with a uniform cement: aggregate ratio (1 : 2) and water: cement ratios as shown.

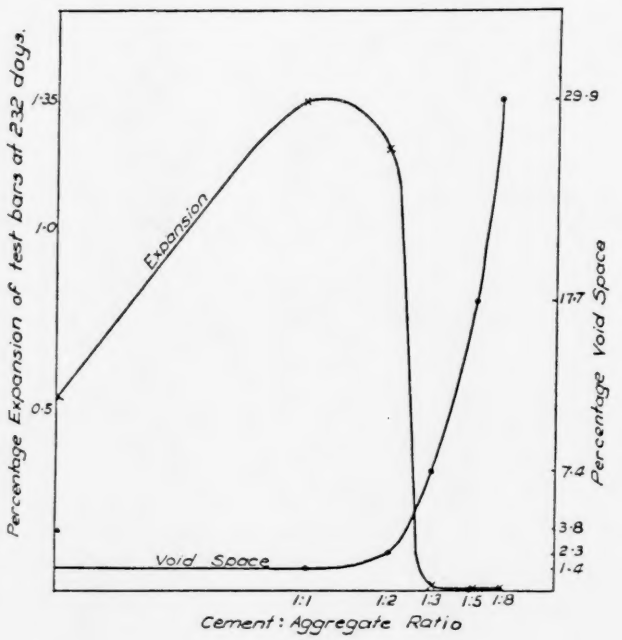

FIG. 2.—Showing correlation between expansion and void space of mortars with given cement: aggregate ratios. A uniform water: cement ratio (0·50 : 1) was used with each mortar.

VOL. 14 1984

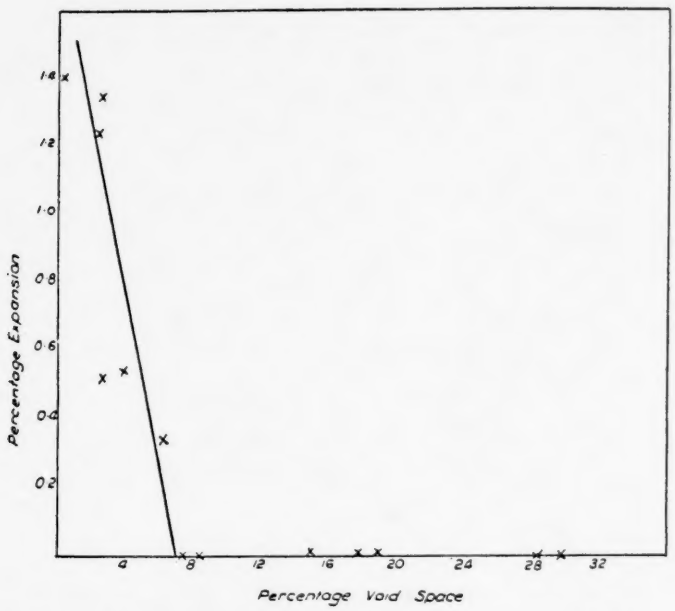

FIG. 4.—Showing the relationship between mortar expansion at 226 or 232 days and void space.

sound aggregate and if it is allowed to mature so as to reduce its fractional volume of freezable water at saturation to a sufficiently low value so that the air-void system can accommodate the increase in that volume on freezing. Such maturity will be achieved when the concrete has a compressive strength of about 25 MPa (3500 psi). If all of these criteria are met, the concrete will be immune to harm by freezing and thawing even if saturated, by natural processes when frozen.

The air voids can be significantly reduced in volume without comparable reduction in their effectiveness since the volume of air required to achieve $\bar{L} < 0.20$ mm is much greater than 9 % of the fractional volume of freezable water at saturation of concrete of the stipulated minimum maturity to be frost resistant. The 9 % of the volume of the mortar fraction of the concrete that is normally required to be air-void space in order to achieve the $\bar{L} < 0.20$ mm is, typically, about 10 times the increase in volume of the freezable water on freezing. I doubt that deposition of reaction product in voids has rendered air-entrained concrete less effective in providing frost resistance in Denmark than it has been elsewhere. I expect that air entrainment has been less effective in Denmark than other places because, since those who tried it didn't really believe in it, they didn't give it a fair trial. They did not insure that, in the hardened concrete, in service, there really was, at least 95% of the time in the "air-entrained" concrete an air bubble not further away than 0.20 mm from any point in the cement paste. All the concrete that we have ever seen that has been damaged by freezing and thawing while critically saturated either had $\bar{L} > 0.20$ mm (the usual case) or unsound aggregate, or was frozen while immature (strength < 3500 psi).

References

1. H.E. Vivian, Studies in Cement Aggregate Reaction, III. The Effect of Void Space on Mortar Expansion, Bull. 229, Council for Scientific and Industrial Research, Melbourne, pp. 55-67 (1947).
2. H.E. Vivian, Some Australian Studies on Cement-Aggregate Reaction in Mortar, J. Amer. Conc. Inst. Proc. 46, 617-621 (1950).

CEMENT and CONCRETE RESEARCH. Vol. 14, p. 894, 1984. Printed in the USA.
0008-8846/84 $3.00+00. Copyright (c) 1984 Pergamon Press, Ltd.

REPLY TO MATHER'S DISCUSSION OF "STUDIES OF ALKALI-SILICA REACTION - PART II ETC."*

A.D. Jensen, S. Chatterji,
P. Christensen and N. Thaulow
Teknologisk Institut, Denmark

First of all we would like to thank Dr. Mather for his interest in our paper and especially for sending us copies of Vivian's papers, for which we are grateful.

Dr. Mather's discussion may be divided into two parts. The first part deals with the priority of the observation that an incorporation of air-voids decreases the alkali-silica expansion. Without any question Vivian has the priority. Until recently we were unaware of these important papers and wonder why they have been forgotten by most workers and no attempt has been made in recent years to counteract or at least reduce alkali-silica expansion by incorporating air-voids. Let us hope that in the future the above observation will be utilized.

VOL. 14 1984

The second part of the discussion deals with frost damage. Actually Dr. Mather has raised two points:

(a) Characteristics of air-voids in hardened concrete structures: Until recently characterization of air-voids in hardened concrete structures was a time-consuming and expensive operation, and as a result was seldom used in day-to-day quality control. Specifications mostly demanded use of an approved air-entraining agent and about 5% by volume of air in fresh mixes. As this worked in other countries, it should have worked in Denmark as well.

(b) Volume of air required to ensure frost resistance: Dr. Mather has already noted that the requirement of $\bar{L}$ less than 0.20 mm can be satisfied by concrete samples containing much less air than the customary demand of 5%. A concrete sample containing about 3% air or less may easily satisfy the demand of $\bar{L}$ less than 0.20 mm; however it is a general belief that such a concrete sample will not be frost resistant. It would appear that a further criterion of about 5% air-void has to be added to those listed by Dr. Mather Now let us consider the case of a concrete sample which contained 5% air at the beginning, but 2% air-void has been subsequently filled up by reaction products. Obviously this sample will be more prone to frost damage than a comparison sample where no filling up occurred. We drew attention to this state.

---

*CCR 14, 311-314 (1984).

CEMENT and CONCRETE RESEARCH. Vol. 14, pp. 895-896, 1984. Printed in the USA.
0008-8846/84 $3.00+00. Copyright (c) 1984 Pergamon Press, Ltd.

NEWS ITEMS

Annual Convention of the AMERICAN CONCRETE INSTITUTE, Denver, CO. Information: Ann K. Burttell, Convention and Meetings Manager, ACI, P.O. Box 19150, Detroit, MI USA. — March 1985

Seminar on TECHNOLOGY OF CONCRETE WHEN POZZOLANS, SLAGS, AND CHEMICAL ADMIXTURES ARE USED, sponsored by Universidad Autonoma de Neuvo Leon, Monterrey, N.L., Mexico and co-sponsored by ACI and RILEM. Information: Raymundo Rivera-Villarreal, Apartado Postal No. 17, Sue "B," San Nicolas de Los Garza, N.L. Mexico, 64000. — March 1985

7th International Conference on CEMENT & CONCRETE MICROSCOPY, Americana Hotel, Fort Worth, TX, USA. Information: Arturo G. Nisperos, Material Service Corp., 901 N. Sangamon St., Chicago, IL 60622. — March 25-28, 1985

1st International Conference on DEMOLITION AND RECYCLING OF CONCRETE, Rotterdam Hilton Hotel in the Netherlands. Sponsored by the European Demolition Assoc., and the Technical Committee 37-DRC of the RILEM. Information: Mr. R.C. Basart, 44 Benoordenhoutseweg, 2596 BC DEN HAAG, The Netherlands, or Prof. T.C. Hansen, Building Materials Laboratory, Technical University of Denmark, 2800 Lyngby, Denmark. — May 31 - June 3, 1985

Symposium on EVALUATION OF FIRE DAMAGE OF CONCRETE AND REPAIR OF DAMAGE during the ACI fall convention in Chicago. Information: T.Z. Harmathy, National Research Council of Canada, Division of Building Research, Ottawa, Ontario K1A OR6, Canada, or F. Ray Vollert, Rockwell Hanford Operations, P.O. Box 800, Richland, WA 99352. — October 1985

The 8th International Congress on the CHEMISTRY OF CEMENT, Rio de Janeiro, Brazil. Information: Secretaria Geral do 8° Congresso de Quinica do Cimento, Rua da Assembleia, No. 10, 40° andar, Grupo 5001-20011, Rio de Janeiro/RJ, Brazil. — Late Summer 1986

ANNOUNCEMENT OF A SYMPOSIUM

The 2nd International Symposium on HYDROTHERMAL REACTIONS will be held at The Pennsylvania State University, University Park, PA, August 12-14, 1985. The conference continues the traditions of the first symposium which was held in Japan in 1982 and the Nobel Symposium on "The Chemistry and Geochemistry of Solutions at High Temperatures and Pressures" held in Sweden in 1979. The purpose of the conference will be to bring together scientists active in research

on high pressure aqueous and related chemical systems. Included will be applications to hydrothermal geochemistry, reactions used to prepare electronic materials and ceramics, hydrothermal crystal growth, near- and supercritical separations, corrosion chemistry, and the physical chemistry of fluids at high pressures and temperatures.

The conference co-chairmen are Prof. H.L. Barnes of The Pennsylvania State University, and Dr. R.A. Laudise at AT&T Bell Laboratories. Further information may be obtained by writing: Second International Symposium on Hydrothermal Reactions, The Pennsylvania State University, Keller Conference Center, University Park, PA 16802 USA.

CALL FOR PAPERS

An International Symposium on CONSOLIDATION OF CONCRETE will be held during the ACI annual convention in San Francisco, CA, March 1986, sponsored by Committee 309, Consolidation of Concrete. Topics include, but are not limited to: effect of mix properties, concrete materials; methods of consolidation, selection of vibrator equipment; equipment for vibration, new developments; theoretical aspects regarding consolidation; test methods for judging adequacy of consolidation in fresh concrete; methods for measuring vibrator efficiency, frequincy, amplitude, force; procedure of vibration, internal and external; revibration, timing, extent, benefits; design of form equipment and placing vibrator on forms, size, spacing, form requirements; consideration of construction details, reinforcement spacing, concrete workability; mass concrete, roller compaction; structural concrete, pavements, slabs, precast products, block, pipes; special concretes, lightweight, heavyweight; quality control, consolidation of test specimens; field performance, discussion of experiences of properly and improperly consolidated concrete.

Authors should send Paper title, 200 word abstracts, and author(s) name, title, organization, and address by Dec. 31, 1984 to Steven H. Gebler, Construction Technology Laboratories, Portland Cement Association, 5420 Old Orchard Road, Skokie, IL 60077. Final papers are due June 30, 1985.

VOL. 14 1984

OBITUARY

Sir Frederick Lea, CB, CBE, FRSC, died on July 7 at the age of 84. He was Director of Building Research at the Department of Scientific and Industrial Research from 1946 to 1965, where he served for forty years, making major contributions to the chemistry of cement, and to fostering building research in post-war Britain, the Commonwealth and internationally. Lea developed the technology of cements and pozzolanas, work leading to the economic utilization of industrial wastes like blast-furnace slag and later pulverized fuel from coal-burning power stations. The author of many papers, his textbook "The Chemistry of Cements and Concrete" is a standard work of reference, now in Third Edition.

In 1964 he was awarded the Walter C. Voss Award by the ASTM, the first occasion the award was made outside North America. He was a founding member of CIB, the International Council for Building Research, Studies and Documentation (President, 1955-57), and of RILEM, the International Union of Testing and Research Laboratories for Materials and Structures (President, 1957-58). He also chaired the Concrete Committee of the International Congress on Large Dams from 1953-1959.

CEMENT AND CONCRETE RESEARCH, Vol. 14, pp. I-III, 1984
0008-8846/84 $3.00 + .00 Printed in the USA
Copyright (c) 1984 Pergamon Press Ltd. All rights reserved

EDITORIAL:
SOFTWARE SURVEY SECTION

It is planned to introduce a new Software Survey Section to CEMENT AND CONCRETE RESEARCH to encourage the open exchange of information on software programs unique to our professional field. With the rapid penetration of computers into academic and industrial institutions has come a parallel increase in the number of scientists and researchers designing their own software. The existence of much of this software remains unknown to even those of us who could most benefit from its use. We believe that it is of vital importance to our readers that such information be made available. We believe also that a professional journal is the best place to share such information. Your contribution would be most welcome.

The questionnaire on the following pages is designed to assist you in reporting on software that you may have developed or be in the process of developing. By completing this form, your information will reach thousands of your colleagues who may benefit from your work and may possibly offer suggestions for further enhancements to your software. Please complete the enclosed form and return it to:

Kathleen S. Mourant
Assistant Editor
CEMENT AND CONCRETE RESEARCH
202 Materials Research Laboratory
Pennsylvania State University
University Park, PA 16802 USA

We do not intend to review or comment on the contents of the questionnaire. It will be published as is in order to expedite the information cycle process. I would welcome any comments you may have.

II Software Survey Section

NAME OF JOURNAL CEMENT AND CONCRETE RESEARCH

P E R G A M O N P R E S S
SOFTWARE DESCRIPTION FORM

Title of software package: _____

_____

_____

It Is: [ ]Application program [ ]Utility [ ]Other_____

Specific area _____
(e.g. Thermodynamics, Inventory Control)

Software developed for [name of computer(s)] _____
in [language(s)] _____
to run under [operating system] _____
and is available in the following media:
[ ]Floppy disk/diskette. Specify:
Size _____ Density _____ [ ]Single-sided [ ]Dual-sided
[ ]Magnetic tape. Specify:
Size _____ Density _____ Character set _____

Distributed by:_____

Minimum hardware configuration required: _____

Required memory: _____ User training required: [ ]Yes [ ]No

Documentation: [ ]None [ ]Minimal [ ]Self-documenting
[ ]Extensive external documentation

Source code available: [ ]Yes [ ]No

Level of development: [ ]Design complete [ ]Coding complete
[ ]Fully operational [ ]Collaboration would be welcomed

Is software being used currently? [ ]Yes [ ]No
If yes, how long? _____ If yes, how many sites? _____

Contributor is available for user inquiries: [ ]Yes [ ]No

Return completed forms to:

Kathleen S. Mourant, Assistant Editor
CEMENT AND CONCRETE RESEARCH
202 Materials Research Laboratory
Pennsylvania State University
University Park, PA 16802 USA

(continued)

[This Software Description Form may be photocopied without permission]

VOL. 14 1984

Description of what software does [200 words]:

OL.
14
984

Potential users: _____

Fields of interest: _____

# # # # # # #

Name of
contributor: _____

Institution: _____

Address: _____

_____

Telephone number: _____

# # # # # # #

Reference No. [Assigned by Journal Editor] _____

- -

[The information below is not for publication.]

Would you like to have your program:

Reviewed? [ ]Yes [ ]No [ ]Not at this time

Marketed and distributed? [ ]Yes [ ]No [ ]Not at this time

[This Software Description Form may be photocopied without permission]